

Indoor air Quality and Its Effects on Health in Urban Houses of Indonesia: A case study of Surabaya

TETSU KUBOTA¹, HANIEF ARIEFMAN SANI¹, USEP SURAHMAN², SOPHIA HILDEBRANDT³,
HAMIDIE RONALD DANIEL RAY², BETA PARAMITA²

¹Graduate School for International Development and Cooperation, Hiroshima University, Higashi-Hiroshima, Japan

²Universitas Pendidikan Indonesia (UPI), Bandung, Indonesia

³Institute for Infrastructure and Resources Management, Leipzig University, Leipzig, Germany

ABSTRACT: *There is a possibility that the sick building syndrome has already spread widely among the newly constructed apartments in major cities of Indonesia. This study investigates the current conditions of indoor air quality, focusing especially on formaldehyde and TVOC, and their effects on health among occupants in the urban houses located in the city of Surabaya. A total of 471 respondents were interviewed and 82 rooms were measured from September 2017 to January 2018. The results indicated that around 50% of the respondents in the apartments showed some degrees of chemical sensitivity risk. More than 60% of the measured formaldehyde levels in the apartments exceeded the WHO standard, 0.08 ppm. The respondents living in rooms with higher mean formaldehyde values tended to have higher multiple chemical sensitivity risk scores.*

KEYWORDS: *Indoor air quality, Sick building syndrome, QEESI, Formaldehyde, Developing countries*

1. INTRODUCTION

Indoor air quality (IAQ) and its effects on health of occupants have been studied in many parts of the world over the last several decades [1]. In developing countries, however, most of the IAQ studies focused on the issues of exposure to biomass combustion, and thus there are relatively few studies investigating IAQ in urban houses [2]. Nevertheless, in response to rapid population growth and urbanization, the construction of urban houses using modern building materials is thriving in developing countries – but without sufficient standards or regulations for the building materials as well as minimum ventilation rates. This study investigates the current conditions of IAQ, focusing especially on formaldehyde and TVOCs, and their effects on health among occupants in urban houses of Indonesia. This paper presents the results of a case study conducted in the city of Surabaya in 2017-2018.

2. METHODOLOGY

Field investigations consisting of face-to-face interviews and measurements were conducted in five high-rise apartments, including low-medium cost apartments and condominiums, and five unplanned residential neighbourhoods, the so-called Kampongs from September 2017 to January 2018 (Table 1). This period includes part of dry season (Sep to Oct) and wet season (Nov to Jan). A total of 471 respondents were interviewed and 82 rooms were measured. The Kampongs comprise dense unplanned landed houses (approximately 11-53 years old) without proper urban

Table 1: Number of samples

	Kampongs	Apartment	Total
Questionnaire	298 (63%)	173 (37%)	471
IAQ measurement	42	40	82
Spirometer test	46	21	67



Figure 1: Views of (a) Kampongs and (b) apartment

infrastructure, whereas the apartments are high-rise buildings of about 20-storey or more (Fig. 1). These apartments were newly constructed since 2010 (see Table 4).

The interviews were conducted using a questionnaire form comprising the Quick Environmental Exposure and Sensitivity Inventory (QEESI[®]) developed by Miller & Prihoda [3] and several additional questions, amongst others: cleaning habits, window-opening behaviour and socio-economic factors. Formaldehyde (FMM-MD, Shinyei) and TVOCs (ToxiRAE Pro, RAE Systems) were measured on top of air temperature and RH for approximately three days in master bedroom and living room of respective houses. The interval time of measurement was 1 min for TVOC and 30 min for the other parameters. In addition, lung capacity of occupants was measured by the spirometer test.

PLEA 2018 HONG KONG

Smart and Healthy within the City

Table 2: MCS risk criteria [3]

Degree to which MCS is suggested	Symptom Severity Score	Chemical Intolerance Score	Masking Score
Very suggestive	≥ 40	≥ 40	≥ 4
Very suggestive	≥ 40	≥ 40	< 4
Somewhat suggestive	≥ 40	< 40	≥ 4
Not suggestive	≥ 40	< 40	< 4
Problematic	< 40	≥ 40	≥ 4
Problematic	< 40	≥ 40	< 4
Not suggestive	< 40	< 40	≥ 4
Not suggestive	< 40	< 40	< 4

Multiple chemical sensitivity (MCS), which was recommended to replace idiopathic environmental intolerance (IEI) in the World Health Organization/International Programme on Chemical Safety (WHO/IPCS) workshop, is defined as an acquired disorder with multiple recurrent symptoms, as being associated with diverse environmental factors tolerated by the majority of people, and as not being explainable by any known medical or psychiatric disorder [4]. Miller & Prihoda [3] developed the QEESI to differentiate between chemically sensitive people and normal people.

The QEESI consists of the following five scales [3]: chemical intolerance (to what extent certain odor or exposures make one sick); other intolerances (to what extent a variety of other exposures make one sick); the severity of symptoms (to what extent one experiences certain symptoms); the masking index (whether there is ongoing exposure from routinely used products); and life impact (to what extent the sensitivity affects certain aspects of life). Each scale is composed of ten questions, and each question is scored from 0-10, except for the masking index, which is scored as 'yes: 1' or 'no: 0'. Miller & Prihoda [3] suggested ranges for the scales and interpretation guidelines. The criteria for the risk criteria (degree to which MCS is suggested) are shown in Table 2.

3. RESULTS AND DISCUSSION

3.1 Multiple chemical sensitivity (MCS) risk

The final calculated results of MCS were analysed by respective housing types (Fig. 2). As shown, only 21.9% of respondents show some degrees of intolerances in Kampongs, but the percentage of problematic respondents is significantly higher in the apartments, which is 48.8% ($p < 0.01$). The percentage of problematic and very suggestive respondents in the apartments are more than twice than Kampongs. Fig. 3 shows the detailed results from QEESI. As illustrated in Fig. 3a, the respondents show high degrees of intolerance particularly to tobacco, diesel/gas, insecticide and paint. Overall, the magnitudes of intolerance in the apartments are significantly higher than those in Kampongs in most kinds of chemicals ($p < 0.01$). Nevertheless, if only problematic respondents of which MCS risks range from 'problematic' to 'very suggestive' are analysed

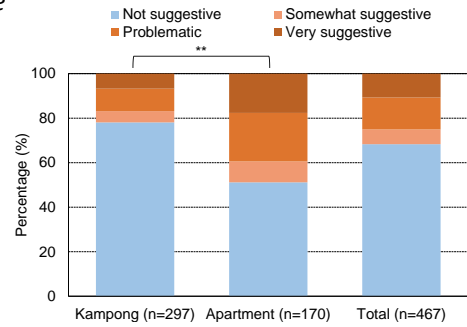


Figure 2: Results of MCS risk

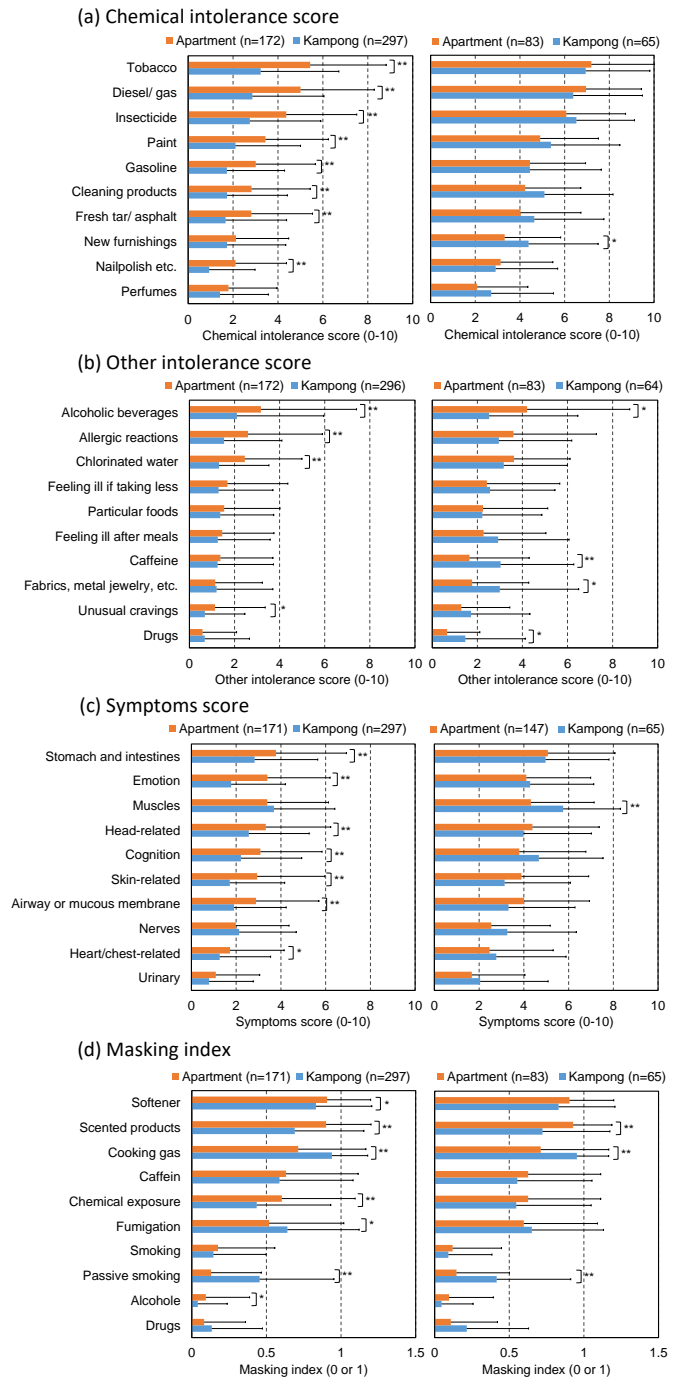


Figure 3: Results of QEESI. The left figure shows those of all samples and the right indicates those of only problematic respondents (MCS risk: 'Problematic' to 'Very suggestive'). The error bar indicates a standard deviation, and, hereafter, * shows 1% significant level, whereas ** indicates at 5% level.

PLEA 2018 HONG KONG

Smart and Healthy within the 2-degree Limit

(i.e. the right figures of Fig. 3), the magnitudes of intolerance in the apartments are not higher than those of Kampongs (Fig. 3a). Rather, the intolerance to new furnishings is higher in Kampongs than that in the apartments. Meanwhile, the degrees of intolerance to other chemicals are not as high as previous items, and some of them, including alcoholic beverages, allergic reactions and chlorinated water, present significant differences between Kampongs and apartment (Fig. 3b).

On average, symptoms scores (Kampongs/apartments) are high in terms of stomach and intestines (2.8/3.8), emotion (1.8/3.4), muscles (3.7/3.4), head-related (2.6/3.3), cognition (2.2/3.1), skin-related (1.7/2.9) and airway or mucous membrane (1.9/2.9). Significant differences between the two groups can be seen in most of the items, except for muscles. The average symptoms score for the muscles in Kampongs is significantly higher than that of apartments even among the problematic respondents ($p < 0.01$).

As described before, the masking index assesses whether there is ongoing exposure from routinely used products [3]. Among the problematic respondents, the average index score for scented products in the apartments is higher than that of Kampongs, whereas those for cooking gas and passive smoking in Kampongs are higher than the apartments (Fig. 3d).

The above results imply that although most of the factors affecting MCS risk are similar among problematic respondents of both Kampongs and apartments, a few different factors also can be seen in the two groups, such as intolerance to new furnishings, symptoms on muscles, masking factors of scented products, cooking gas and passive smoking.

3.2 Factors affecting MCS risk

We conducted correlation analyses to identify the factors affecting MCS risk scores in Kampongs and apartments respectively using the Spearman's test or Chi-square test depending on types of variable. Table 3 summarises the surveyed personal attribute variables and their relations to the MCS risk scores respectively. First, it is found that the female respondents tend to obtain higher MCS risk scores in the apartments ($p < 0.05$). In contrast, the increases in age and household income tend to increase the MCS risk in Kampongs ($p < 0.05$, $p < 0.01$). Second, the occupation of respondents has significant relationship with MCS in Kampongs: in particular, government officers and retired respondents tend to have higher MCS risk scores. The increase in stress level increases MCS risk scores in both groups. Meanwhile, those who have a medical history of asthma, eczema and other kinds of allergy tend to have higher MCS risk scores in Kampongs.

Table 3: Personal attributes and their relations to MCS risk

Variables	Kam- pongs	p	Apart- ment	p	Total	p
Gender [%]		.474		.032		.146
Male	35.5		42.1		37.9	
Female	64.5		57.9		62.1	
Age [%]		.068		.809		.115
<20	14.3		16.0		14.9	
20-29	13.0		68.0		33.1	
30-39	17.7		5.9		13.4	
40-49	27.0		4.7		18.8	
>50	28.0		5.3		19.7	
Income [%]		.000		.496		.000
<150US\$	24.8		10.5		18.3	
150-450	56.4		49.2		53.1	
450-750	9.4		14.5		12.1	
>750	9.4		25.8		16.5	
Occupation [%]		.001		.778		.001
Government	4.0		7.0		5.1	
Private	21.9		14.5		19.2	
Entrepreneur	21.5		6.4		16.0	
Student	19.2		66.3		36.5	
Housewife	24.6		3.5		16.8	
Retired	6.7		0.6		4.5	
Others	2.0		1.7		1.9	
Stress [0-10]	2.1	.000	4.3	.004	2.9	.000
Asthma [%]	12.8	.041	17.4	.740	14.5	.080
Eczema [%]	25.3	.000	36.0	.055	29.3	.000
Allergy [%]	31.6	.031	36.5	.117	33.4	.007

Table 4: Building attributes and their relations to MCS risk

Variables	Kam- pongs	p	Apart- ment	p	Total	p
Age of building [years]	31.7	.146	4.5	.750	25.2	.880
Duration of living [years]	25.3	.405	1.9	.474	15.2	.000
No. of windows in bedroom [%]		.004		.924		.049
0	12.5		7.0		10.1	
1	67.7		73.4		70.1	
>1	19.8		19.6		19.7	
No. of windows in living room [%]		.000		.280		.000
0	3.0		5.3		3.8	
1	75.9		47.4		65.6	
>1	21.2		47.4		30.6	
Duration of opening windows [hrs/day]						
Bedroom	13.6	.416	6.5	.141	9.9	.000
Living room	12.8	.773	7.3	.853	10.5	.008
HVAC ownership [%]						
Air-conditioner	20.9	.007	99.2	.608	57.6	.000
Fan	99.3	.509	29.5	.526	66.9	.001
Exhaust fan	10.6	.888	51.6	.133	29.9	.085
Modification [%]	71.1	.017	25.2	.987	50.2	.394
Water leakage [%]	69.8	.387	27.6	.143	50.4	.065
Furniture [mean units]		.003		.322		.087
Living room	3.8		5.1		4.4	
Bedroom	3.1		3.3		3.2	
Cleaning rooms [%]		.006		.626		.016
1/month or less						
Every 2-3 weeks	0.0		5.4		2.5	
Every week	0.0		6.2		2.8	
Every 2-5 days	2.6		32.3		16.3	
Everyday	7.8		27.7		17.0	
Cleaning	89.6		28.5		61.4	
Cleaning bathrooms [%]		.689		.061		.011
1/month or less	2.4		17.4		9.3	
Every 2-3 weeks	9.8		13.8		11.6	
Every week	36.9		43.7		40.1	
Every 2-5 days	28.6		18.6		23.9	
Everyday	22.3		6.6		15.0	

PLEA 2018 HONG KONG

Smart and Healthy within the 2-degree Limit

Table 4 presents the surveyed building attribute variables and their relations to the MCS risk scores. As shown, overall, the duration of living in the present houses has a significant relationship with MCS risk ($p < 0.01$), but the relationships are seen neither in each of the groups. Meanwhile, the increases in number of windows in both master bedroom and living room increase the MCS risk in Kampongs ($p < 0.01$). Nevertheless, the duration of opening windows obtains a significant relationship with MCS risk only for all samples ($p < 0.01$). Furthermore, in Kampongs, the ownership level of air-conditioning ($p < 0.01$), the history of modification ($p < 0.05$), the number of furniture in the living room ($p < 0.05$) and the frequency of cleaning rooms ($p < 0.05$) have significant relationships with MCS risk.

Table 5 indicates the surveyed indoor air quality sensations and their relations to the MCS risk scores. As shown, those who feel some smell and mold growth in their houses of Kampongs tend to obtain higher MCS risk scores ($p < 0.05$).

3.3 Indoor air quality (IAQ) measurement

Outdoor weather conditions differed between dry and wet seasons. As shown in Fig. 4, during the dry season, the outdoor air temperature ranges from 25.1-36.3°C with an average temperature of 29.9°C, whereas the RH ranges from 34-86% with an average of 64%. Meanwhile, the average outdoor temperature dropped to 28.1°C while the average RH increased up to 77% during the wet season.

In the dry season, the measured indoor air temperatures range from approximately 29-32°C in Kampongs, while those in apartments ranges from 27-31°C. As shown, air-conditioning was used in most of the rooms in the apartments unlike in Kampongs. The indoor RH does not exceed 70% even in Kampongs during most of the period in the dry season partially due to the increased indoor air temperatures. In

Table 5: Indoor air quality and their relations to MCS risk

Variables	Kampongs	p	Apartment	p	Total	p
Smell/Odor [%]	51.0	.024	60.5	.160	55.4	.064
IAQ [%]		.893		.056		.324
(Rather) Clean	42.1		42.3		42.2	
Neutral	46.7		43.8		45.4	
(Rather) Dirty	11.2		13.8		12.4	
OAQ [%]		.089		.148		.027
(Rather) Clean	38.8		33.8		36.5	
Neutral	43.4		54.6		48.6	
(Rather) Dirty	17.8		11.5		14.9	
Humidity [%]		.051		.128		.307
(Rather) Dry	31.3		30.7		31.0	
Neutral	42.7		48.0		45.1	
(Rather) Humid	26.0		21.3		23.8	
Mold [%]	42.4	.005	37.0	.660	39.9	.296
Mite [%]	6.0	.921	18.1	.107	11.5	.007

contrast, indoor RH maintained very high values, up to 87% in Kampongs during the wet season, while the indoor air temperatures were decreased to approximately 27-29°C.

The mean and maximum formaldehyde and TVOCs during the measurement periods were illustrated respectively in Fig. 5. These values were calculated based on the measured 30 min temporal average values, and therefore even the maximum values over the measurement period can be comparable with major international/domestic standards on IAQ. Overall, the average values of both formaldehyde and TVOCs are higher in the apartments than those in Kampongs except for the average maximum values of TVOCs, although a significant difference is found only for the mean values of formaldehyde ($p < 0.01$). For example, the maximum values of formaldehyde range up to approximately 0.172 ppm with an average of 0.081 ppm in Kampongs, while those in the apartments range from approximately 0.048-0.183 ppm with an average of 0.115 ppm, which is higher than the WHO standard, 0.08 ppm. Meanwhile, the maximum values of TVOCs range up to approximately 5.21 mg/m³ with an average of 2.59 mg/m³ in Kampongs, while those in apartments range up to

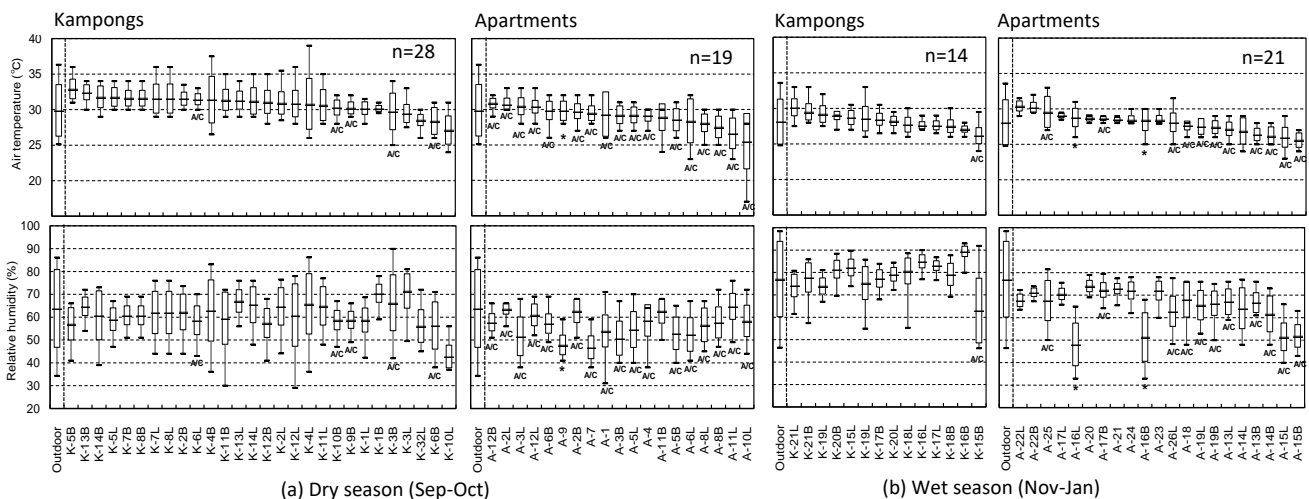


Figure 4: Statistical summary of outdoor and indoor air temperature and RH. 'AC' indicates rooms equipped with air-conditioning and * shows unknown. Hereafter, the box charts indicate the mean, the mean \pm standard deviation and the maximum/minimum values.

PLEA 2018 HONG KONG

Smart and Healthy W.

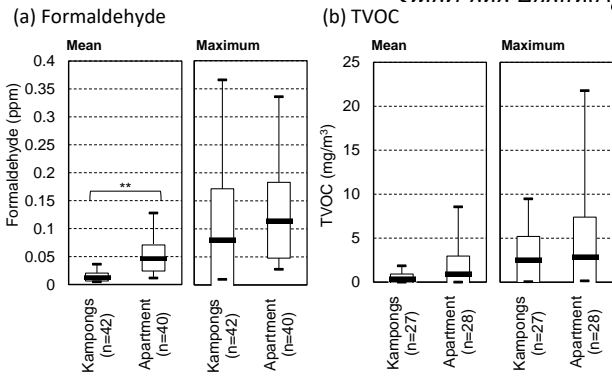


Figure 5: Statistical summary of IAQ measurement results.

approximately 7.40 mg/m^3 with an average of 2.90 mg/m^3 .

Figs. 6-7 present cumulative frequencies of formaldehyde and TVOCs respectively. As shown in Fig. 6, overall, the formaldehyde concentrations are higher in the apartments than those of Kampongs especially in terms of mean values. It should be noted that extremely high maximum values of formaldehyde were, however, obtained in both groups (Fig. 6b). This means that the background formaldehyde concentrations are apparently higher in the apartments than Kampongs as expected, but there are some exceptional cases even in Kampongs in which the formaldehyde levels are intermittently very high. Nevertheless, the result indicates that a large proportion of occupants in the apartments are routinely exposed to a high concentration of formaldehyde. As shown in Fig. 6b, more than 60% of the measured formaldehyde levels in the apartments exceed the WHO standard, whereas about 20% exceed the standard in Kampongs.

As shown in Fig. 7, the measured TVOC levels are not so different between Kampongs and apartments. Overall, the measured TVOC levels are divided into two opposites. Although approximately 60% of the rooms obtain relatively low TVOC levels with mean values of less than $400 \text{ }\mu\text{g/m}^3$, the rest of the rooms obtain high values, up to $8,000 \text{ }\mu\text{g/m}^3$ on average. Both Kampongs and apartments contain several extreme cases in which the maximum values range from $8,000$ up to $21,800 \text{ }\mu\text{g/m}^3$.

3.4 Influence of IAQ levels on MCS risk

We analysed the differences of mean values of formaldehyde and TVOCs respectively between the two different MCS risk groups: 'not suggestive' and 'suggestive' to 'very suggestive' (Figs. 8-9). As shown in Fig. 8, significant differences are found in terms of formaldehyde in both Kampongs and apartments for mean and maximum values respectively. As expected, the respondents living in rooms with higher formaldehyde values tend to have higher MCS risk scores. Nevertheless, the opposite tendency can be seen for the maximum formaldehyde values in Kampongs. This is probably because there were some

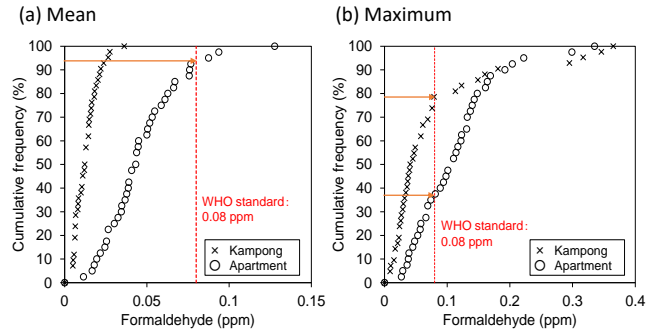


Figure 6: Cumulative frequency of the measured formaldehyde.

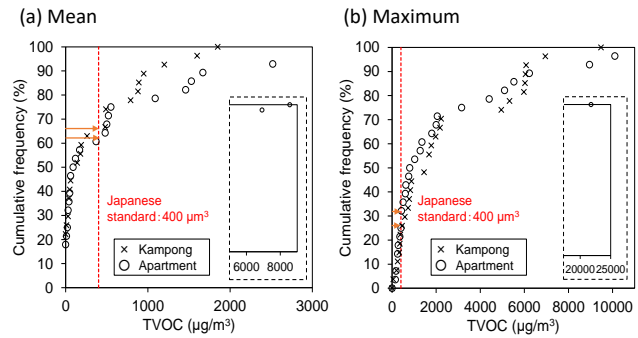


Figure 7: Cumulative frequency of the measured TVOCs.

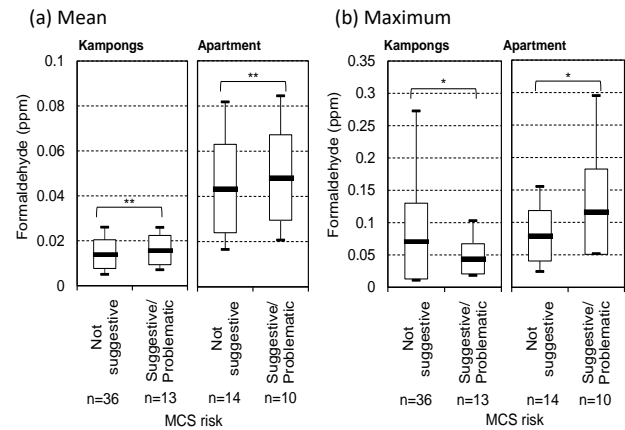


Figure 8: Formaldehyde levels by different MCS risk groups.

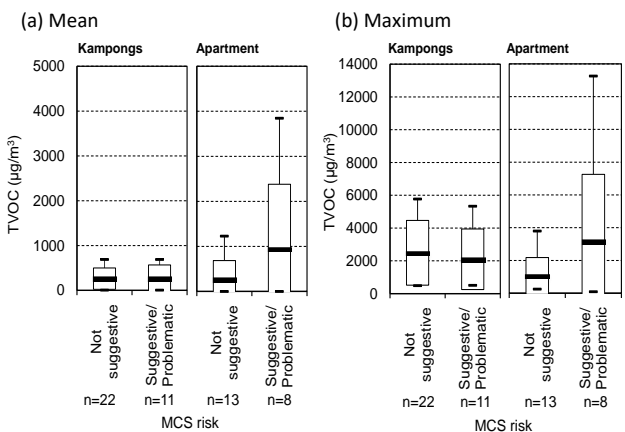


Figure 9: TVOC levels by different MCS risk groups.

exceptional cases in Kampongs in which the formaldehyde levels were intermittently very high as discussed before. In other words, this result implies that the long-term routinely exposure to formaldehyde would be more influential to the

PLEA 2018 HONG KONG

Smart and Healthy within the 2-degree Limit

occupants' chemical intolerance than by the intermittent but high exposures.

In contrast, significant differences cannot be seen in the TVOC results (Fig. 9). However, basically, the higher TVOC level is the higher the MCS scores would be, except for the maximum values in Kampongs.

3.5 Results of spirometer test

The FEV1% values were calculated based on the measured force expiration volume over a second (FEV1) compared with Indonesian standard values proposed in [5]. The above standard values are determined depending on the respondent's age and gender [5]. The FEV1%, which assesses the respondent's FEV1 levels compared with the required standard values in percentage, is an important measure of pulmonary function. As shown in Fig. 10, more than 55% of the respondents in Kampongs are considered less than normal respiratory conditions, while more than 85% in the apartments are considered the same. A significant difference was not found in mean values between the two groups ($p=0.108$), but overall, the respondents in the apartments show further worse conditions than Kampongs. Further analysis is needed to identify the factors causing these worse respiratory conditions in both groups.

4. CONCLUSIONS

This research is probably the first attempt to assess the IAQ conditions and their effects on health in urban houses of Indonesia. The key findings from the case study of Surabaya are as follows:

(1) There was a significant difference in mean values of MCS risk between Kampongs and the newly constructed apartments. Around 50% of the respondents in the apartments showed some degrees of chemical sensitivity risk, indicating possible spread of sick building syndrome.

(2) On the other hand, significant differences were not found in the results of TVOC measurement as well as spirometer tests between Kampongs and apartments. This implies that there are other IAQ problems even in Kampongs, which cannot be measured by the degree of chemical intolerance.

(3) Although most of the factors affecting MCS risk were similar among the problematic respondents of both two groups, there were a few different factors on the other hand. The chemical intolerance to new furnishings, symptoms on muscles, masking factors of cooking gas and passive smoking were higher in Kampongs, whereas the masking factor of scented products was higher in the apartments instead.

(4) Various kinds of personal and building attributes were found to affect MCS risk scores, but the influential factors were quite different between Kampongs and apartments, except for the degree of stress. For example, in Kampongs, the increases in age and household income increased MCS risk scores.

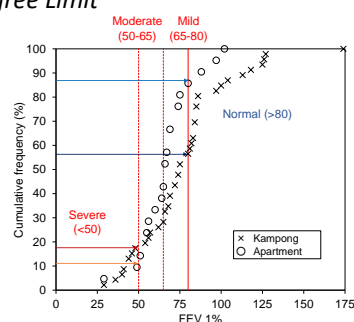


Figure 10: Cumulative frequency of FEV1%.

Moreover, those who have a history of allergic diseases tended to record higher MCS risk. In contrast, in the apartments, the female respondents tended to obtain higher MCS risk. In Kampongs, more factors are associated with personal and building attributes than the apartments.

(5) The average maximum values of formaldehyde were 0.081 ppm in Kampongs and 0.115 ppm in the apartments, which are higher than the WHO standard, 0.08 ppm. It was found that the background formaldehyde levels were apparently higher in the apartments than Kampongs, but there were some exceptional cases even in Kampongs in which the formaldehyde levels were intermittently very high. On the other hand, the measured TVOC levels were not so different between the two groups, ranging very widely up to 22 mg/m³ in maximum value.

(6) The respondents living in rooms with higher mean formaldehyde values tended to have higher MCS risk scores. It was suggested that the long-term routinely exposure to formaldehyde would be more influential to the occupants' chemical intolerance, which was particularly seen in the apartments, than by the intermittent but high exposures.

ACKNOWLEDGEMENTS

This research was supported by a grant from Panasonic Corporation and KAKENHI (JP15KK0210). We also would like to thank Dr. I Gusti Ngurah Antaryama and Dr. Sri Nastiti of Institut Teknologi 10 Nopember Surabaya (ITS) and the students who kindly supported our survey.

REFERENCES

1. Tham, K.W., (2016). Indoor air quality and its effects on humans-A review of challenges and developments in the last 30 years. *Energy and Buildings*, 130: p. 637-650.
2. Joshi, S.M., (2008). The sick building syndrome. *Indian J. of Occupational and Environmental Medicine*, 12: pp. 61-64.
3. Miller, C.S., Prihoda, T.J., (1999). The environmental exposure and sensitivity Inventory (EESI): a standardized approach for measuring chemical intolerances for research and clinical applications. *Toxicology and Industrial Health* 15: pp. 370-385.
4. Heo, Y., Kim, S.H., Lee, S.K., Kim, H.A., (2017). Factors contributing to the self-reported prevalence of multiple chemical sensitivity in public facility workers and the general population of Korea. *J. of UOEH*, 39(4): pp. 249-258.

PLEA 2018 HONG KONG

Smart and Healthy within the 2-degree Limit

5. Alsagaff, H., Mangunegoro, H., (1993). Nilai normal faal paru orang Indonesia pada usia sekolah dan pekerja dewasa berdasarkan rekomendasi. *American Thoracic Society (ATS) 1987*. Surabaya: Airlangga University Press. pp. 26-122.

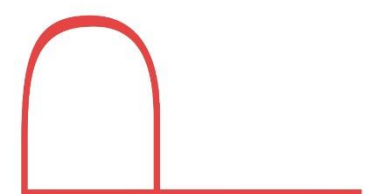
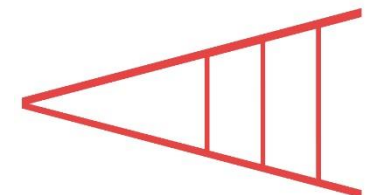
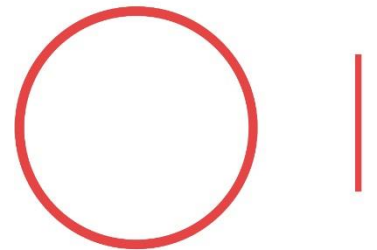
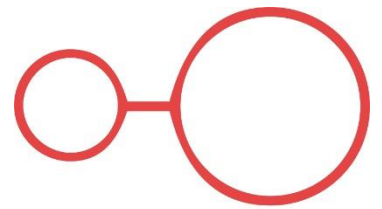
VOLUME 1

34th International Conference on
Passive and Low Energy Architecture

Smart and Healthy
Within the Two-Degree Limit

Edited by:

Edward Ng, Square Fong, Chao Ren



PLEA 2018:

Smart and Healthy Within the Two-Degree Limit

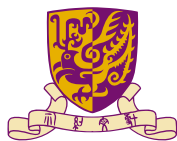
Proceedings of the 34th International Conference on

Passive and Low Energy Architecture;

Dec 10-12, 2018

Hong Kong, China

Organised by:



香港中文大學

The Chinese University of Hong Kong



香港中文大學環境、
能源及可持續發展研究所
Institute of Environment,
Energy and Sustainability, CUHK



PLEA

Conference Chair:

Edward Ng,

Yao Ling Sun Professor of Architecture,

School of Architecture,

The Chinese University of Hong Kong

Conference Proceedings Edited by:

Edward Ng, Squire Fong, Chao Ren

School of Architecture

The Chinese University of Hong Kong

AIT Building

Shatin, New Territories

Hong Kong SAR, China

Copyright of the individual papers remains with the Authors.

Portions of this proceedings may be reproduced only with proper credit to the authors and the conference proceedings.

This book was prepared from the input files supplied by the authors. The editors and the publisher do not accept any responsibility for the content of the papers herein published.

Electronic version as:

ISBN: 978-962-8272-35-8

©Copyright: PLEA 2018 Hong Kong

PLEA 2018

PLEA stands for Passive and Low Energy Architecture. It is an organisation engaged in a worldwide discourse on sustainable architecture and urban design through its annual international conference, workshops and publications. It commits to the development, documentation and diffusion of the principles of bioclimatic design and the application of natural and innovative techniques for sustainable architecture and urban design.

PLEA is an autonomous, non-profit association of individuals sharing the art, science, planning and design of the built environment. PLEA pursues its objectives through international conferences and workshops; expert group meetings and consultancies; scientific and technical publications; and architectural competitions and exhibitions. Since 1982, PLEA has organised conferences and events across the globe. The annual conference of PLEA is regarded, attracting academics and practicing architects in equal numbers. Past conferences have taken place in United States, Europe, South America, Asia, Africa and Australia.

It is the first time that the PLEA conference comes to Hong Kong in 2018. The juxtaposition of Hong Kong's compact and high-density living and scenic countryside makes it an intriguing case of urban sustainability and climate resilience. The urban and built environment represents both challenges and opportunities amid climate change. As the world approaches the 2-degree limit, living smart and healthy has become a priority in urban development. Smart cities are driven by science and technology but are meaningless without consideration for the people and community.

Design and practice are essential in implementation, while education and training stimulate innovation and empower professionals and laymen alike. With the theme "Smart and Healthy within the 2-degree Limit", the conference strives to address the different facets of smart and healthy living and aims to bring together designers, academics, researchers, students, and professionals in the building industry in the pursuit of a better and more sustainable urban and built environment.

Edward Ng
Conference Chair

INTERNATIONAL ADVISORY COMMITTEE

Dr. Heide Schuster, BLAUSTUDIO - Sustainability in Architecture and Urban Design, Germany

Dr. Simos Yannas, Architectural Association School of Architecture, UK

Dr. Joana Carla Soares Gonçalves, The University of São Paulo, Brazil

Prof. Rajat Gupta, Oxford Brookes University, UK

Dr. Sanda Lenzholzer, Wageningen University, The Netherlands

Prof. Pablo La Roche, Cal Poly Pomona, United States

Arch. Mario Cucinella, Mario Cucinella Architects S.R.L., Italy

Prof. Sue Roaf, Retired, Centre of Excellence in Sustainable Building Design, Heriot-Watt University, UK

Prof. Alfredo Fernández-González, University of Nevada, United States

Dr. Paula Cadima, Architectural Association School of Architecture, UK

Prof. Brian Ford, Natural Cooling Ltd, UK

Prof. Christopher Webster, University of Hong Kong, Hong Kong, China

ORGANISING COMMITTEE

Prof. Edward Ng, The Chinese University of Hong Kong, Hong Kong, China [Chairman]

Dr. Tin-Tai Chow, City University of Hong Kong

Prof. Jimmy Fung, Hong Kong University of Science and Technology

Prof. Yuguo Li, The University of Hong Kong

Dr. Shengwei Wang, The Hong Kong Polytechnic University

Mr. Tang Man Bun, Hong Kong Institute of Urban Design

Dr. Raymond Yau, Swire Properties

Mr. John Ng, The University of Hong Kong

Mr. M.K. Leung, Ronald Lu & Partners (Hong Kong) Ltd.

Technical Sub-committee

Dr. Chao Ren, The University of Hong Kong

Dr. Kevin Lau, The Chinese University of Hong Kong

Dr. Chad McKee, The University of Hong Kong

Dr. Sunliang Cao, The Hong Kong Polytechnic University

Dr. Fong Kwong Fai, City University of Hong Kong

Mr. Tony Ip, Tony Ip Green Architects Ltd.

Mr. Ricky Li, Ove Arup & Partners (HK) Ltd.

SCIENTIFIC COMMITTEE

Dr. Amal Abuzeinab
Dr. Timothy Oluseun Adekunle
Dr. Rajendra Singh Adhikari
Dr. Avlokita Agrawal
Prof. Sanyogita Manu Agrawala
Prof. Khandaker Shabbir Ahmed
Dr. Sura Al-Maiyah
Prof. Jose Manuel Almodovar
Dr. Hector Altamirano
Prof. Hasim Altan
Prof. Sergio Altomonte
Prof. Servando Alvarez
Prof. Massimo Angrilli
Ms. Carmen Antuna Rozado
Dr. Rigoberto Arambula Lara
Dr. Michele arch. Manigrasso
Prof. Shady Attia
Dr. Rahman Azari
Prof. George Baird
Prof. Adolfo F. L. Baratta
Mr. Enrico Baschieri
Dr. Liliana Olga Beltran
Dr. Umberto Berardi
Prof. Susana Biondi
Dr. Sahera Bleibleh
Prof. Terri M Boake
Dr. Paola Boarin
Prof. Andrea Boeri
Prof. Martha Christine Bohm
Mr. Mehrdad Borna
Dr. Helena Camara Lace Brandao
Dr. Luisa Brotas
Prof. Gian Luca Brunetti
Dr. Neil Keith Burford
Prof. Waldo E. Bustamante
Dr. Paula San Payo Cadima
Dr. Francesca Calarco
Prof. Eliana Cangelli
Dr. Gustavo Alexandre Cardoso Cantuaria
Prof. Guedi Capeluto
Prof. Paola Caputo
Mr. Paul John Carew
Dr. Kate Carter
Dr. Szu-cheng Chien
Dr. Joon-Ho Choi
Dr. Roberta Cocci Grifoni
Dr. Raphael Compagnon
Prof. Manuel de Arriaga Brito Correia-Guedes
Prof. Courtney Crosson
Prof. Rolando-Arturo Cubillos Gonzalez
Dr. Marwa Dabaieh
Prof. Francesca De Filippi
Prof. Robert Mark DeKay
Prof. Claude Demers
Prof. Gokay Deveci
Prof. Branka Dimitrijevic
Dr. Silvia Domingo-Irigoyen
Dr. Samuel Dominguez-Amarillo
Dr. Jiangtao Du
Dr. Denise Helena Silva Duarte
Dr. Meshack O Efeoma
Prof. Soofia Tahira Elias-Ozkan
Dr. Heba Elsharkawy

Dr. Ihab Elzeyadi
Prof. Rohinton Emmanuel
Prof. Evyatar Erell
Dr. Carlos Javier Esparza Lopez
Dr. Kristian Fabbri
Prof. Enrico Fabrizio
Dr. Honey Fadaie Tamidjanie
Dr. Juliana Felkner
Ms. Jessica Fernandez Aguera
Dr. Nisha A. Fernando
Prof. Anderson Targino da Silva Ferreira
Mr. Isak Worre Foged
Prof. Brian Ford
Mr. Andrea Fornasiero
Prof. Robert Fryer
Dr. Khaled Galal Ahmed
Prof. Paola Gallo
Prof. Susanne Gampfer
Dr. Yun Gao
Dr. Jose Roberto Garcia Chavez
Dr. Veronica Garcia-Hansen
Prof. Jacopo Gaspari
Dr. Stephanie Gauthier
Ms. Marjan Ghobad
Prof. Aymeric Alain Girard
Dr. Gabriel Gomez-Azpeitia
Dr. Mehreen Saleem Gul
Ms. Nidhi Gupta
Prof. Rajat Gupta
Ms. Mary Guzowski
Prof. Emanuele Habib
Prof. Annette Hafner
Prof. Bruce T Haglund
Dr. Muhannad J. A. Haj Hussein
Prof. S Robert Hastings
Mr. Navid Hatefnia
Prof. Runa T. Hellwig
Dr. Daniel Herrera
Dr. Christina Hopfe
Prof. Michaela Hoppe
Dr. Nina Amor Hormazabal-Poblete
Dr. Lingjiang Huang
Dr. Guadalupe Huelsz
Dr. Mehlika Inanici
Dr. Vicky Ingram
Dr. Saiful Islam
Dr. Stoyanka Marinova Ivanova
Prof. Usha Iyer-Raniga
Dr. Beverley Lorraine James
Ms. Gloria Cecilia Jimenez Dianderas
Dr. Mohammad Arif Kamal
Dr. Genku Kayo
Prof. Greg Keeffe
Dr. Inji Kenawy
Prof. Nikolaus Knebel
Dr. Roberta Consentino Kronka Mulfarth
Prof. Alison Kwok
Ms. Mili Kyropoulou
Dr. Pablo Miguel La Roche
Prof. Werner Xaver Lang
Mr. Ping Hang (Benson) Lau
Dr. Sanda Lenzholzer
Dr. Fabrizio Leonforte

Prof. J Owen Lewis
Mr. Florian Lichtblau
Dr. Maria Lopez de Asiain Alberich
Mr. Richard Lorch
Dr. Yujie Lu
Prof. Elena Lucchi
Dr. Atefe Makhmalbaf
Ms. Valentina Marincioni
Mr. Keith McAllister
Prof. Shannon Sanders McDonald
Dr. Lori Barbara McElroy
Dr. Grainne Marie McGill
Prof. Christopher M. Meek
Dr. Isaac A. Meir
Ms. Rosalie Menon
Ms. Ranny Loureiro Xavier Nascimento Michalski
Dr. Mahta Mirmoghtadaee
Ms. Anamika Vachaspati Mishra
Prof. Jitka Mohelnikova
Dr. Mahsan Mohsenin
Dr. Marta Molina-Huelva
Dr. Sameh Monna
Dr. Azadeh Montazami
Prof. Circe Maria Gama Monteiro
Prof. Leonardo Marques Monteiro
Mr. Martin Morelli
Dr. Filbert Musau
Prof. Emanuele Naboni
Prof. Zoltan Nagy
Prof. Leticia de Oliveira Neves
Mr. Amir Nezamdoost
Prof. Marialena Nikolopoulou
Ms. Sarah O Dwyer
Dr. Sonja Oliveira
Dr. Mark Raphael Owor Olweny
Ms. Sara Omrani
Ms. Federica Ottone
Dr. Massimo Palme
Dr. Beta Paramita
Prof. Ulrike Passe
Mr. Nimish Bhupendra Patel
Mr. Mic Patterson
Prof. David Pearlmutter
Dr. Sofie Pelsmakers
Prof. Fernando Ruttkay Pereira
Prof. Troy Nolan Peters
Dr. Gloria Pignatta
Prof. Adrian Pitts
Dr. Andre Potvin
Dr. Ash Ragheb
Dr. Upendra Rajapaksha
Mr. Bardhyl Rama
Prof. Rajan Rawal
Ms. Dana Raydan
Dr. Andras Reith
Ms. Valentina Resente
Dr. Lucelia Taranto Rodrigues
Dr. Jorge Rodriguez-Alvarez
Prof. Jean-Francois RogerFrance
Ms. Rosa Romano
Mr. Flavio Rosa

Prof. Matthias Rudolph
Dr. Masoud Sajjadian
Prof. Marco Sala
Prof. Ashraf Salama
Dr. Aizaz Samuel
Dr. Paola Sassi
Dr. Kay Saville-Smith
Dr. Rosa Schiano-Phan
Prof. Marc Eugene Schiler
Dr. Heide G. Schuster
Prof. Subhashini Selvaraj
Prof. Kelly Shannon
Dr. Adil Sharag-Eldin
Prof. Tim Sharpe
Prof. Masanori Shukuya
Prof. Cesarina Siddi
Dr. Matthias Sieveke
Dr. Joana Carla Soares Goncalves
Ms. Maria Spastri
Dr. Alessandro Speccher
Prof. Malini Srivastava
Dr. Thanos N Stasinopoulos
Prof. Fionn Stevenson
Prof. Vera A Straka
Ms. Sadia Subrina
Dr. Jae Yong Suk
Dr. Tiziana Susca
Prof. Kheira Anissa Tabet Aoul
Dr. Abel Tablada
Ms. Tasneem Tariq
Ms. Leena Thomas
Mr. Andrew Robert Toland
Prof. Chiara Tonelli
Dr. Eleni Tracada
Dr. Maureen Eileen Trebilcock
Dr. Antonella Trombadore
Ms. Janine Tuechsen
Ms. Samina Mazumder Tuli
Prof. Brenda Vale
Dr. Fan Wang
Dr. Julian (Jialiang) Wang
Dr. Yupeng Wang
Dr. Paulina Wegertseder
Dr. Andrea Wheeler
Mr. Christopher James Whitman
Dr. Jan Wienold
Dr. Jin Woo
Dr. Feng Yang
Dr. Simos Yannas
Dr. Fatih Yazicioglu
Prof. Roshni Udyavar Yehuda
Dr. Dongwoo Yeom
Dr. Grace Yepez-Salmon
Mr. Aram Krikor Yeretian
Prof. Abraham Yezioro
Dr. Chanikam Yimprayoon
Dr. Chao Yuan
Dr. Gökçen Firdevs Yücel
Dr. Sahar Zahiri
Prof. Nouredine Zemmouri

SPONSORS & SUPPORTING ORGANISATIONS



Funding Support:

Q:

A: Social Science/CUHK

Wood Sponsor:

L&O
ARCHITECTS

Bamboo Sponsors:

AD+RG
architecture design and research group ltd
建築設計及研究所有限公司

 **SWIRE PROPERTIES**

Sole Sponsor of Student Design Colloquium:

 **RONALD LU
& PARTNERS**

Supporting Partners:



Supporting Organisations:

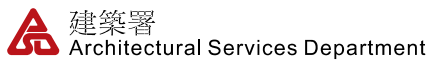


TABLE OF CONTENTS

Volume 1 – Long Paper (Science and Technology)

Volume 2 – Long Paper (Design and Practice, People and Community, Education and Training)

Volume 3 – Short Paper

Volume 1 – Long Paper

SCIENCE AND TECHNOLOGY

1100	Calibrated Urban Systems Design: A Simulation-based Design Workflow using Measured Data Clustering to Calibrate Urban Building Energy Models (UBEMs)	2
1105	Convenience Store: The Unintended Large Energy Consumers In Urban Taiwan	8
1114	Do energy performance certifications matter in housing selection? Evidence from choice experiments in Barcelona	13
1126	Quantification of Airflow Patterns in a Naturally Ventilated Building Simulated in a Water Table Apparatus	19
1140	Impact of Inlet Water Temperature on Cooling from Misting Fans:	25
1275	The International Style in Israel	31
1146	Environmental Benefits when Reusing Load-Bearing Components in Office Buildings: A case study.	37
1150	New Framework For Quantifying Outer Luminous Variation Through Dynamic Methods	43
1171	Optimal Design of Urban Thermal Environment Using 3D City Models and Numerical Simulation	49
1211	Summertime thermal comfort and adaptive behaviours in mixed-mode office buildings in Harbin, China	55
1214	Passive Downdraft Cooling Towers Performance Evaluation	61
1217	Neutral global warming potential target of electricity storage as threshold for greenhouse gas emission mitigation in buildings	67
1237	Assessing the Adaptability of the Saudi Residential Building's Energy Code for Future Climate Change Scenarios	73
1245	Green Roofs for Cooling	79
1247	Potential Wind Power Utilization in Diverging Passages Between Two High-Rise Buildings	85
1254	3DFOGTECH® Portable Fog Water Station for Water-stressed Environments	91

1255	An Analysis of a Handful of Solar Decathlon Europe 2014 Prototypes	97
1257	Building Energy Models in the Operational Phase: Automation of the Model Calibration Process	103
1258	Building-integrated carbon capturing 2.0	109
1264	Statistical Analysis of Architectural Features Effects on Indoor Environmental Conditions in A Plus Energy House Prototype	115
1268	Reducing Thermal Stress in Philippine Classrooms	121
1271	Physical Monitoring of Replacement Infill Panels for Historic Timber-Framed Buildings in the UK:	128
1275	Embodied Carbon Benefits of Reusing Structural Components in the Built Environment: A Medium-rise Office Building Case Study	132
1276	Findings from a Survey on the Current Use of Life-Cycle Assessment in Building Design	138
1294	Passive Cooling with Phase Change Materials	144
1295	Optimization of Intensive Daylight Simulations	150
1297	Dynamic Microclimate Modelling for Urban China	156
1299	Artificial Neural Network Based Smart Forecast Models	163
1338	Experimental Study on an Air-Phase-Change-Material Unit for Summer Thermal Comfort in a Naturally Ventilated Building	169
1342	Investigation of the Implications of Future Bioclimatic Potential on Annual Heating And Cooling Energy Load In Residential Buildings In India	175
1345	Evaluation of soil-cement blocks	182
1350	Development of an Energetic Profile of Buildings: From Current Status to Achievable Improvement	187
1354	Shadowing windows with BIPV blinds	194
1355	Downscaling Climate Models: Running Nested Simulations In The Microclimate Model ENVI-met	200
1373	Variations of Microclimatic Conditions in Residential Neighbourhoods in Ho Chi Minh City	206
1375	Predicting Changes in Spatial Planning Using Artificial Neural Networks on the Basis of Satellite Images: Examples of selected cities in Lodz agglomeration (Poland)	212
1392	Sizing Natural Ventilation Systems for Cooling: The potential of NV systems to deliver thermal comfort while reducing energy demands of multi-storey residential buildings in India.	218
1400	Vehicular Anthropogenic Heat in the Physical Parameters of An Urban Canyon for Warm Humid Climate	225
1409	Smart and Healthy Buildings Factor of Reality	231
1412	Effects of Urban Space Opening Layouts on Pedestrian-level Wind Conditions	237
1418	Reducing Building Waste through Light Timber Frame Design	244

1424	Unmanned Aerial System (UAS) Applications in Energy Audits	250
1430	Enhancement of the WUDAPT Portal Tool WUDAPT2ENVI-met	256
1439	A Parametric Study to Optimize the Thermal Performance of Mongolian Self-built Houses in Terms of Energy Efficiency: Towards a cleaner environment for Ulaanbaatar	262
1452	Sensitivity of Passive Design Strategies to Climate Change	268
1455	Heat Stress Pattern of Air-Conditioned Buildings with Shallow Plan Forms and Single Skin Facades	274
1459	Simplified Sensing and In-situ Measuring Approach for Building Window Properties	280
1464	Experimental Biases in Discomfort Glare Evaluations	287
1481	Investigating the Impact of Architectural Form and Wind Direction on the Performance of a Passive Draught Evaporative Cooling Tower in Saudi Arabia	294
1491	Improving Louvers With Indirect Evaporative Cooling As Heat Exchanger:	300
1494	The Partial replacement of Ordinary Portland Cement with Rice Husk Ash to Stabilize Compressed Earth Blocks for Affordable Building Materials	306
1496	Summertime Overheating and Heat Stress in Multi-Family Colonial Revival Style Timber-Frame Buildings	311
1497	Retrofitting Strategies for Social Housing Buildings in Different Climate Conditions.	318
1499	Vegetation as a Potential Tool for Improving Thermal Comfort and Exposure to Solar Radiation in the Streets of Quito	324
1510	Two-Phases Evaporative Cooling for Better Outdoor Thermal Comfort in High-Density Tropical Cities	329
1518	CFD Analysis on Irregular Breezeway Patterns in High-Density Asian Urban Areas	335
1545	Integration of LCA tools in BIM toward a regenerative design.	341
1547	Assessment of the Building-Integrated Photovoltaic Potential in Urban Renewal Processes in the Swiss Context:	347
1548	Development of an Adaptive Passive Façade:	353
1551	Influence of Office Building Height in Urban Areas on Surrounding Microclimate and Building Performance	359
1556	Study on Firewood Consumption Patterns in Dhading District of Nepal	366
1564	Passive Down-Draught Evaporative Cooling Applicability and Performance in Single Family Houses	372
1573	Daylighting in Sacred Buildings: Application of dynamic brightness balance and contrast in divine luminous environment for energy saving and visual comfort	378
1575	Urban Microclimate and Energy Performance: An integrated simulation method	384
1582	Evaluating Computer Aided Design Tools for Building Performance: Trusting and Defining the Predetermined Automated Inputs	390

1586	Indoor air Quality and Its Effects on Health in Urban Houses of Indonesia	396
1598	Study on the Thermal Performance of Office Spaces in the Tropics	403
1602	Estimating Impact of Green-Blue Infrastructure on Air Temperature Using Remote Sensing	409
1607	Development of the Adaptive Thermal Comfort Model for Sustainable Housing Design in Japan	414
1620	Development of an Affordable Sensing and Monitoring System for Post-Occupancy Building Performance Evaluation	421
1624	An Empirical Investigation of the Link between Indoor Environment and Workplace Productivity in a UK Office Building	427
1631	The Impact of Urban Form on Summer Time Air Temperature and Energy Demand: A Case Study at Dhaka, Bangladesh	434
1653	Effect of Intra-Climate Variation in Thermal Performance of Public Housing in a Composite Climate Of India	440
1654	Assessing the Glare Potential of Complex Fenestration Systems:	446
1692	A Comparative Study of Hygrothermal Simulations for a Bamboo Wall System with Natural Wool Insulation	452
1696	Particulate Concentrations in Bedrooms in Airtight Dwellings	459
1701	Impact of Apartment Room Layout in Reducing Unwanted Temperature-Rise in Rooms Adjacent to Kitchen	466
1729	Breaking the Glass Box: Strategies to reduce the Energy Consumption in 24/7 IT Offices in Delhi NCR	472
1732	Integrating Hydroponics into Office Buildings	478
1761	Recycled Materials Impact on Thermal Comfort of Low-Cost Housing in Latin America	485
0132	Innovative RES Solutions for Isolated Territories	490



Volume 1

Long Paper

Science and Technology

SCIENCE AND TECHNOLOGY

Science and Technology has a central role in innovation for better urban living. This track explores the latest scientific and technological research that improves our understanding of the environment and brings changes to future urban development, for example:

- low energy building performance and simulation technology
- renewable energies and energy technology
- material technology and zero waste construction
- the sciences of urban heat island, urban design and adaptation to climate change

Calibrated Urban Systems Design

A Simulation-based Design Workflow using Measured Data Clustering to Calibrate Urban Building Energy Models (UBEMs)

Tarek Rakha and Rawad El Kontar

School of Architecture, Syracuse University, Syracuse, NY, United States

ABSTRACT: This paper presents a workflow that informs urban design decisions using measured data clustering to calibrate Urban Building Energy Models (UBEMs). The method's goal is to support urban design in terms of form, building systems configurations, as well as influencing user behaviour aspects in the built environment through a systemic analysis of measured data to develop reliable future-case design scenario energy models. Detailed data on appliance-level electricity use were employed via data clustering to calibrate a UBEM for the Mueller community in Austin, TX, USA. The data were collected by the Pecan Street Institute for a year in 2014 from consumers in Austin and other cities. Firstly, collected energy data was restructured and cleaned from corrupt and missing information. Secondly, in order to identify common energy use patterns, a model-based clustering algorithm for functional data was applied. Behavioural/usage profiles were determined through clustering and translated into usage schedules and behaviours. As a result, a UBEM built in the urban modelling interface (umi) was calibrated, with fully calibrated and semi calibrated buildings, within a maximum error margin of 14%. Finally, an illustration of calibrated-UBEM design case scenarios is presented, and implications on community energy potential effects are discussed.

KEYWORDS: Measured Data, Urban Building Energy Modelling (UBEM), Simulation, Data Clustering, Occupancy

1. INTRODUCTION

People currently live in cities more than ever before in human history; 55% of the world's population lives in urban areas and expected to increase to 68% by 2050 [1]. Cities are built and continue to grow at an unprecedented rate, along with a myriad of negative effects linked to urban living that include building energy inefficiency, consequent increase in carbon emissions and its effect on climate change exacerbation [2]. Buildings account for 40% of carbon production in the U.S. [3], and the role urban design plays in mitigating built environment impacts is critical. There is an urgent need to improve energy efficiency and integrate renewable electricity sources, while enhancing the lives of individuals and communities that consume, and in some cases, produce energy. To improve the energy performance of buildings, multiple validated, open-source simulation engines have been developed over the past decades [4]. Conversely, urban environmental analysis praxis lack several key capabilities it needs to comprehensively evaluate the environmental performance of districts and communities. This stems from a deficiency of validated computational tools to measure critical performance aspects at the urban scale. As a result, Urban Building Energy Models (UBEMs) emerged as a nascent field that simulates various built environment performance measures, and predicts various future trajectories of neighbourhoods, societies and cities. [5,6].

UBEMs in practice simulate multiple performance metrics, including operational energy, to inform design decisions and energy policies. In order to accurately

represent the effects of actual user behaviour and urban context on building energy demand, UBEMs should be calibrated based on measured energy data. Various approaches were previously implemented to calibrate energy models at the building scale, including meta-modelling, optimization and Bayesian calibration [7,8]; where Bayesian calibration was further represented as the method best-equipped to address uncertainty scenarios in UBEMs [9]. When measured data is provided from energy utility companies and/or installed sensors, individual building energy model automation workflows are needed to make UBEMs an effective tool for real applications [10]. However, excessive computational effort, required high level expertise and significant labour time associated with such calibration methods renders this task less-than-practical for better informed urban design activities in practice.

In an attempt to accelerate UBEMs calibration processes, data clustering techniques may be used as a pre-processing step for energy model inputs. This can include identifying archetypes [11], summarizing key clusters for subsequent simulation analysis [12,13], assessing clusters for particular behaviours and opportunities [14,15] or identifying key patterns from high-frequency data [16-20]. In addition, multivariate analysis can be applied to measure operating performance in building systems and types [19,20]. Clustering methods include heuristic algorithms such as K-means, K-modes, hierarchical, fuzzy or model-based robust approaches such as cluster-wise regression and mixture models. Based on multiple approaches reviewed in the literature, there are inherent trade-offs when comparing clustering

methods. Therefore, defining a clear analytical purpose aids in choosing an appropriate clustering method [21]. This research aims to address a gap in the literature on calibrating UBEMs, where the goal is to develop a novel simulation-based design analytics framework that focuses on calibration as a tool for urban systems design in terms of form, building systems configurations, as well as influencing user behaviour aspects in the built environment. This is achieved through systemic analysis of measured data to develop reliable future-case design scenario energy models. In this paper, the authors developed a calibrated UBEM workflow as a method to inform neighbourhood-scale urban design decisions. Detailed data on appliance-level electricity use is employed via data clustering to calibrate a UBEM for the Mueller community in Austin, TX, USA. Firstly, collected energy data is pre-processed to extract build a database. Secondly, in order to identify common energy use patterns, a model-based clustering algorithm for functional data is used, which was previously proposed in [22]. The method is applied to cluster 45 building's data for heating, cooling, lighting and equipment measured for a year (8760 hours). Thirdly, a UBEM for the Mueller community is developed using umi [23] plug-in for Rhino3D CAD software, with initial inputs from existing construction and assumptions for human behaviour. The UBEM is then calibrated for representative operational energy performance through a distance-based measure comparison with clustered energy data. Finally, the calibrated UBEM is discussed as a design tool by creating multiple scenarios and comparing future performance of the analysed neighbourhood. The investigation concludes by speculating the value of calibrated UBEMs to inform energy efficient urban design decisions in practice.

collected from sensors and reorganised into hourly energy consumption from 1:00 till 24:00 for each household. The hourly data are grouped into the following categories: Lighting, equipment, heating, and cooling. This process reduces the dimension of the data and allows users to analyse each variable separately.

2.2 Functional Clustering

Knowing that data measures are collected from m different houses. The history of observed energy use data for the n th house is represented as $y_n = \{y_n(t_{n1}), \dots, y_n(t_{nS_n})\}^T$; S_n represents the number of observations for unit n and $\{t_{nh}, h = 1, \dots, S_n\} \subset \mathcal{R}$ represents the observation time points for unit n . The observation time points represent the time at which energy use is measured. For instance, $t \in \{1:00, \dots, 24:00\}$ may represent the daily energy consumption structured into hourly use for each household. According to these m data signals functional clustering, which was proposed by Bouveyron et al [22], is applied to group energy use behaviours. This approach is based on recovering the functional nature of the data through a finite basis expansion, and then a functional Gaussian mixture model is utilized for clustering of the time series data in a discriminative functional subspace. The optimal number of clusters K is selected using a Bayesian Information Criterion (BIC). This method is applied to cluster 45 building's data for heating, cooling, lighting and equipment measured for a year (8760 hours). In this clustering analysis each function represents the behaviour of a building over the entire season. Hourly data of each building is first plotted as a continuous function. Then smoothing the data is applied using functional Principal Component Analysis (PCA). The data functions are then clustered and a mean behavioural profile with confidence intervals is plotted as a representation of each cluster. Clustering is then applied to lighting, cooling, heating and equipment energy use and behavioural profiles of each clustering applications are derived. These behavioural profiles are then analysed and translated into inputs to calibrate a UBEM behavioural inputs on a seasonal and daily basis. They are also used as a reference baseline to identify the performance of a future design iterations by comparing simulated results with the existing behavioural profiles.

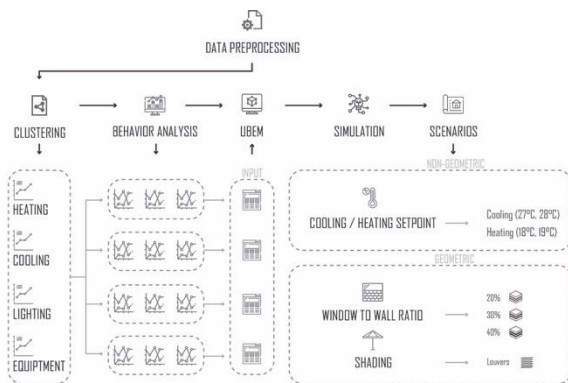


Figure 1: Research method framework.

2. METHODOLOGY

Fig. 1 illustrates the methodology process.

2.1 Data Pre-processing

The data is restructured and cleaned from corrupt and missing information. Energy use measured data are

2.3 UBEM Development

Each of the resultant profiles from the clustering analysis is translated into energy usage schedules and intensities. The translation of behavioural energy use profile is achieved using Equation (1).

$$F_c(t_1, t_2) = \int_{t_1}^{t_2} y_{vc}(t).dt / \text{Max Load} \quad (1)$$

Let $F_c(t_1, t_2)$ be the fraction to be applied to a load between time instances t_1 and t_2 for a specific variable

PLEA 2018 HONG KONG

Smart and Healthy within the 2-degree Limit

cluster vc , where $v \in \{l, e, c, h\}$ where l, e, c, h are lighting, equipment, cooling, and heating respectively.

While manipulating schedule settings aim to more accurately represent energy use behaviours on an hourly basis; illuminance targets and heating/cooling setpoints also have a significant effect on defining the overall intensity of the consequent lighting, cooling, and heating energy use. The authors defined a range of setpoints based on the ASHRAE 90.1 standard, then parametrized inputs for energy efficiency. Using this range of setpoints each behavioural profile will be assigned a setpoint or illuminance target that correspond to its energy use intensity. In UBEMs inputs can be in form of template libraries, therefore energy usage schedules and behaviours are formatted in a template library. Finally, each template is assigned to its corresponding building ID or cluster of buildings in the UBEM. In this process calibration of the model is achieved by utilizing the generated inputs which summarize the energy load patterns and behaviours of the neighbourhood more accurately.

Developing an UBEM is achieved in three steps, characterization, generation and simulation. First, modelling characterization includes acquiring weather information, building and context geometry, as well as non-geometric building information. Geometric building information, construction and material properties are acquired through construction audits or from maps and information from municipality departments. Each cluster of buildings in the model is assigned to its corresponding template that represent its specific energy use behaviour. The user can use the UBEM to simulate different design iterations of the built environment. These iterations can include geometric changes as urban layouts and different orientations or non-geometric studies such as testing different setpoint effects on the urban energy usage.

3. RESULTS

A residential community in Austin, TX, where measured energy use data is extracted from smart meters, is used as a case study to demonstrate the methodology. After pre-processing the dataset, behavioural/usage profiles were determined by applying functional clustering analysis to cluster each of the variables on a seasonal and daily basis. Figure 2 and 3 show the clustering process of cooling energy use throughout a day and a season; according to the BIC vs K graph the optimal number of clusters K was determined to be 3 and 4 respectively. Afterward results were derived from seasonal and daily clustering analysis of each variable. Figure 4 shows the seasonal clustering analysis of cooling energy use.

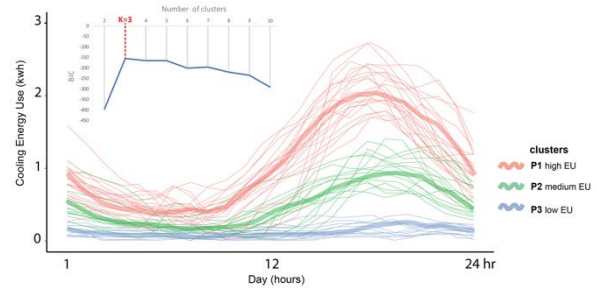


Figure 2- Daily clustering analysis for cooling energy use

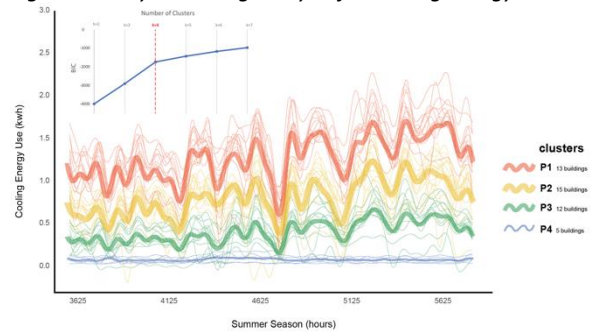


Figure 3- Seasonal clustering analysis for cooling energy use

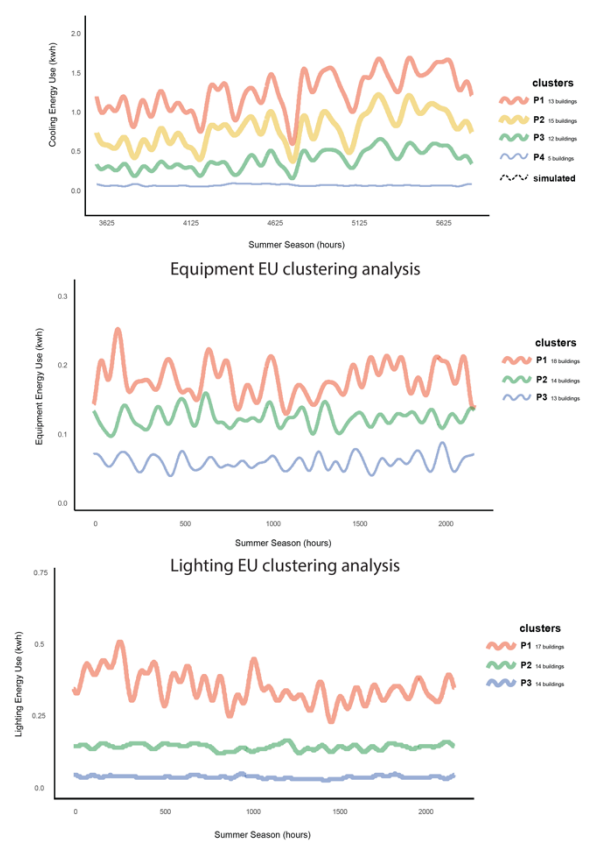


Figure 4- Seasonal clustering analysis results for cooling, equipment, and lighting energy use.

PLEA 2018 HONG KONG

Smart and Healthy within the 2-degree Limit

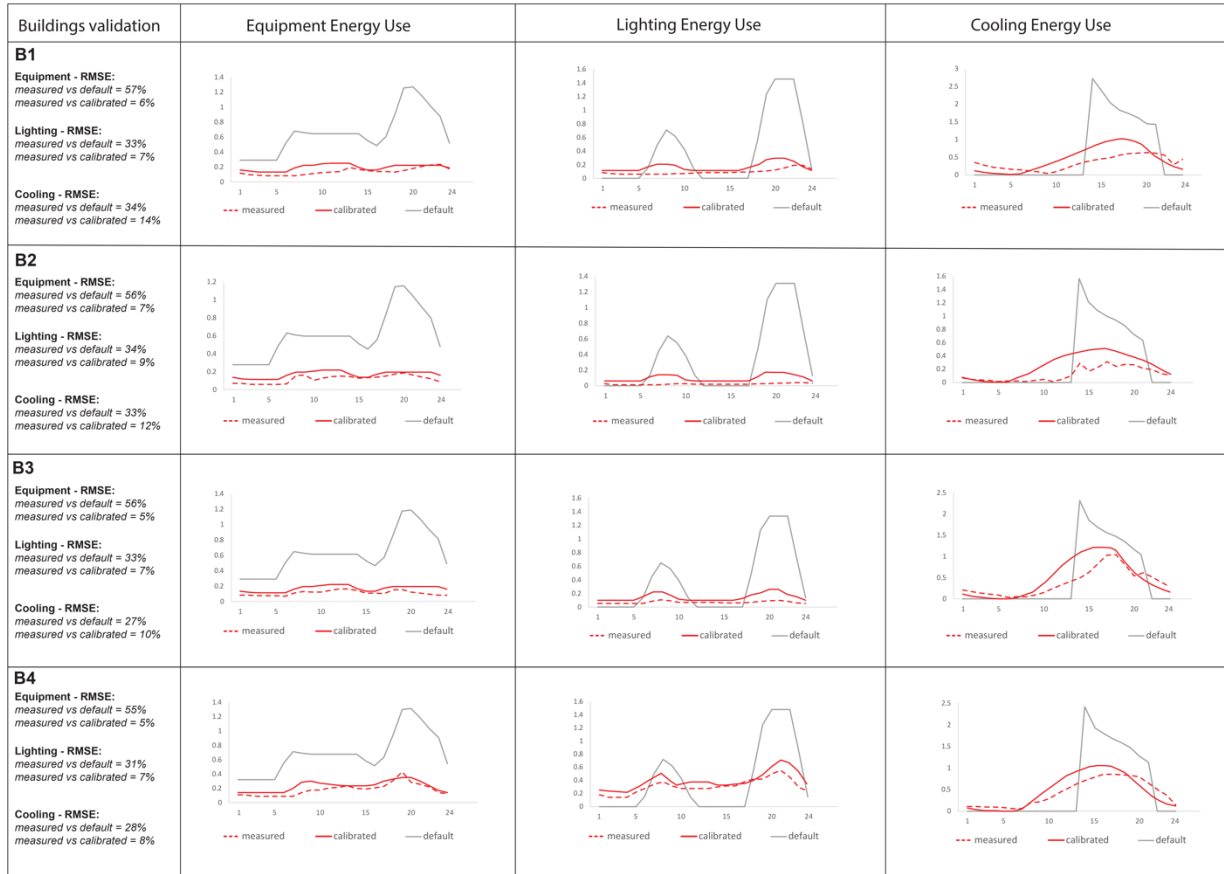


Figure 5. Comparison between baseline, calibrated simulation and measured data, validated using RMSE.

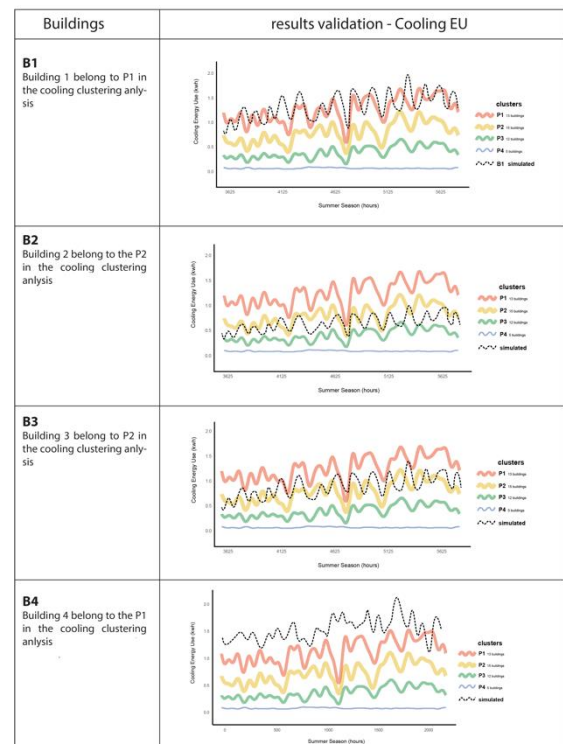
A baseline UBE model for this case study was developed using the umi plugin for Rhino3D CAD software. The model used Austin-amp-Mabry Actual Meteorological Year (AMY) weather file, where full year historical data from 2014 was used for the study. Inputs for building geometric data, constructions and material were defined by extracting information from the existing constructions, with reasonable assumptions.

Both baseline and calibrated simulation results were extracted and plotted against measured data (Fig. 5). Simulated profiles (denoted as y_s) in all variables were notably closer to the measured data (denoted as y_m) as compared to the baseline model results. The simulated patterns in cooling, equipment and lighting energy use were notably closer to measured data (within a 14% margin of error) as compared to the default model results. These results were validated through the Root Mean Square Error (RMSE) which is a statistical measure to describe the similarity of two data sets. It characterizes the average variance of the elements of the simulated profile with respect to the measured profile. It is defined as:

$$rel. RMSE = \frac{1}{24} \sqrt{\sum_{i=1}^{n=24} \frac{(y_{s,i} - y_{m,i})^2}{y_{m,i}}} \quad (2)$$

According to the RMSE and by comparing the results of the default model and calibrated model with the

measured data, the outcomes validated results on a daily basis and identified the improvement of the calibration method. Heating energy use was disregarded, since heating energy is negligible in this climate setting.



PLEA 2018 HONG KONG

Smart and Healthy within the 2-degree Limit

Figure 6- Example validation of four buildings' cooling use.

In order to validate the clustering analysis results at a seasonal basis simulated results were plotted from the calibrated model against the clustered seasonal profiles (Fig. 6).

4. DISCUSSION

The primary advantage of the presented method is that it explicitly models the functional nature of the data and takes advantage of data temporal dynamics. Furthermore, the comparably lower computational complexity and efficient visualization of the clustered systems adds practicality in case of real urban design applications. To demonstrate this, four design scenarios were developed to showcase the effect design parameters has on calibrated UBEMs Energy Use Intensity (EUI) variations, showcased in Fig. 7.

Higher Window-to-Wall Ratio (WWR) of 40% demonstrated an overall increase in EUI, which showed that savings from decreased lighting energy did not offset increase in cooling energy in the Austin TX climate. Following the same logic, 10% WWR showed significant decrease in EUI. The addition of shading had a varying and insignificant effect due to its ineffectiveness in certain orientations. Increasing the cooling setpoint had a significant decrease in energy use in all simulated buildings of the calibrated UBEM.

ways, other effects on lighting and equipment should be studied and further demonstrated.

5. CONCLUSION

The young field of UBEMs is growing and the need to rely on validated community-scale models is essential. Misrepresentation of urban energy flows can significantly hinder the use of simulation tools to support built environment research and practice, as simulation faults at the urban scale would have a critical and possible exponential negative effect. In this paper the authors demonstrated how the use of measured data can calibrate UBEMs that especially help in creating design cases that demonstrated the effectiveness of the proposed workflow. Its potential lies in the ability to aid designers in exploratory research without relying on excessive computational power, extraordinary level of expertise or substantial labour time. The impact of the proposed framework is demonstrated through the use of functional data clustering that create behaviour-based inputs which calibrated buildings within the UBEMs within a 14% maximum margin of error. Future research should investigate the various operational energy use trends in beyond cooling and into lighting and equipment, as well as demonstrating calibration at the multiple building scale, rather than limited number of examples. Such calibrated UBEMs can inform members of the community on design and behaviour alterations that will decrease their environmental impact and increase their energy efficiency and consequent sustainability.

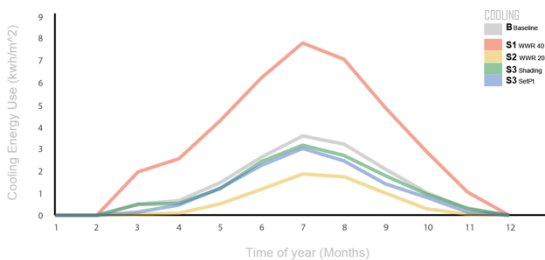


Figure 8- Example cooling EUI design scenario variations.

Fig. 8 showcases the effect design parameters have on one building example from the UBEM in terms of cooling EUI. Although these parameters effect cooling in various

ACKNOWLEDGEMENTS

This publication is based on work funded in part by the National Science Foundation (NSF), under the Smart and Connected Communities program grant 1737550, and the Syracuse Center of Excellence Faculty Fellows program. The authors would like to thank the Pecan Street Institute for providing access to measured energy data for the Mueller community in Austin, Texas. The authors are also grateful for the work that students Elena Echarri, Yu Qian Wang, and Rutuja Ganoo provided to

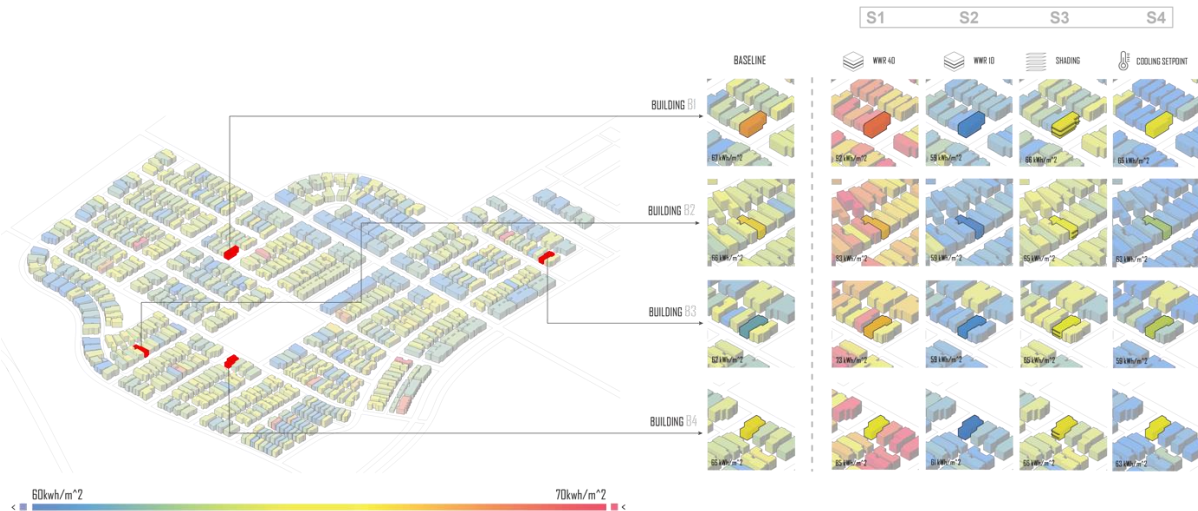


Figure 7- Design case scenario for the calibrated UBEM, showcasing four example buildings' EUI performance.

PLEA 2018 HONG KONG

Smart and Healthy within the 2-degree Limit

support this manuscript.

REFERENCES

1. United Nations. World urbanization prospects: the 2018 revision. United Nations, Department of Economic and Social Affairs (DESA), Population Division, New York, 2018.
2. Rosenzweig, Cynthia, William D. Solecki, Patricia Romero-Lankao, Shagun Mehrotra, Shobhakar Dhakal, and Somayya Ali Ibrahim, eds. *Climate Change and Cities: Second Assessment Report of the Urban Climate Change Research Network*. Cambridge University Press, 2018.
3. U.S. Energy Information Administration, How much energy is consumed in U.S. residential and commercial buildings? [Online]. Retrieved from: <https://www.eia.gov/tools/faqs/faq.php?id=86&t=1>, (2017), Accessed date: 31 May 2018.
4. Crawley, Drury B., Jon W. Hand, Michaël Kummert, and Brent T. Griffith. "Contrasting the capabilities of building energy performance simulation programs." *Building and Environment* 43, no. 4 (2008): 661-673.
5. Reinhart, Christoph F., and Carlos Cerezo Davila. "Urban building energy modeling—A review of a nascent field." *Building and Environment* 97 (2016): 196-202.
6. Bourdic, Loëiz, and Serge Salat. "Building energy models and assessment systems at the district and city scales: a review." *Building Research & Information* 40, no. 4 (2012): 518-526.
7. Coakley, Daniel, Paul Raftery, and Marcus Keane. "A review of methods to match building energy simulation models to measured data." *Renewable and Sustainable Energy Reviews* 37 (2014): 123-141.
8. Fabrizio, Enrico, and Valentina Monetti. "Methodologies and advancements in the calibration of building energy models." *Energies* 8, no. 4 (2015): 2548-2574.
9. Sokol, Julia, Carlos Cerezo Davila, and Christoph F. Reinhart. "Validation of a Bayesian-based method for defining residential archetypes in urban building energy models." *Energy and Buildings* 134 (2017): 11-24.
10. Davila, Carlos Cerezo, Christoph F. Reinhart, and Jamie L. Bemis. "Modeling Boston: A workflow for the efficient generation and maintenance of urban building energy models from existing geospatial datasets." *Energy* 117 (2016): 237-250.
11. Famuyibo, Adesoji Albert, Aidan Duffy, and Paul Strachan. "Developing archetypes for domestic dwellings—An Irish case study." *Energy and Buildings* 50 (2012): 150-157.
12. Santamouris, M., G. Mihalakakou, P. Patargias, N. Gaitani, K. Sfakianaki, M. Papaglastra, C. Pavlou et al. "Using intelligent clustering techniques to classify the energy performance of school buildings." *Energy and buildings* 39, no. 1 (2007): 45-51.
13. Booth, A. T., R. Choudhary, and D. J. Spiegelhalter. "Handling uncertainty in housing stock models." *Building and Environment* 48 (2012): 35-47.
14. Yu, Zhun, Benjamin CM Fung, Fariborz Haghighat, Hiroshi Yoshino, and Edward Morofsky. "A systematic procedure to study the influence of occupant behavior on building energy consumption." *Energy and Buildings* 43, no. 6 (2011): 1409-1417.
15. Petcharat, Siriwarin, Supachart Chungpaibulpatana, and Pattana Rakkwamsuk. "Assessment of potential energy saving using cluster analysis: A case study of lighting systems in buildings." *Energy and Buildings* 52 (2012): 145-152.
16. Seem, John E. "Pattern recognition algorithm for determining days of the week with similar energy consumption profiles." *Energy and Buildings* 37, no. 2 (2005): 127-139.
17. Domínguez-Muñoz, Fernando, José M. Cejudo-López, Antonio Carrillo-Andrés, and Manuel Gallardo-Salazar. "Selection of typical demand days for CHP optimization." *Energy and buildings* 43, no. 11 (2011): 3036-3043.
18. Kiluk, Sebastian. "Algorithmic acquisition of diagnostic patterns in district heating billing system." *Applied energy* 91, no. 1 (2012): 146-155.
19. Lam, Joseph C., Kevin KW Wan, and K. L. Cheung. "An analysis of climatic influences on chiller plant electricity consumption." *Applied Energy* 86, no. 6 (2009): 933-940.
20. Räsänen, Teemu, Dimitrios Voukantsis, Harri Niska, Kostas Karatzas, and Mikko Kolehmainen. "Data-based method for creating electricity use load profiles using large amount of customer-specific hourly measured electricity use data." *Applied Energy* 87, no. 11 (2010): 3538-3545.
21. Hsu, David. "Comparison of integrated clustering methods for accurate and stable prediction of building energy consumption data." *Applied energy* 160 (2015): 153-163.
22. Bouveyron, Charles, Etienne Côme, and Julien Jacques. "The discriminative functional mixture model for a comparative analysis of bike sharing systems." *The Annals of Applied Statistics* 9, no. 4 (2015): 1726-1760.
23. Reinhart, C F., Dogan, T., Jakubiec J.A., Rakha, T. and Sang, A., 2013. "Umi - an urban simulation environment for building energy use, daylighting and walkability," In *Proceedings of Building Simulation 2013*, 25 -28 August, Chambéry: France.
- [24] Bouveyron, Charles, Etienne Côme, and Julien Jacques. "The discriminative functional mixture model for a comparative analysis of bike sharing systems." *The Annals of Applied Statistics* 9, no. 4 (2015): 1726-1760.

Convenience Store: The Unintended Large Energy Consumers In Urban Taiwan

CHEN-YU HUNG¹, NEVEEN HAMZA¹

¹Newcastle University, Newcastle upon Tyne, United Kingdom.

Abstract: In Taiwan, the average of convenient store's Energy Use Intensity (EUI) is high at a 1501 (kWh/m²/year) which is 3 times higher than department stores, 7times higher than central air conditioning office buildings and 38times higher than housing due to operational hours, internal loads and a poorly designed building envelope. Unexpectedly, communities use convenience stores as thermal comfort refuges during summer. This study utilised a dataset of 251 convenience stores in Taiwan from the largest leading retailer to obtain data on the physical, construction elements, energy use and siting of convenience stores. Sample analysis results analysed the architectural features and main locations, urban setting of the convenience store for a base case design. The dynamic software IES-VE (2016) is used to simulate different envelope improvement techniques to understand cooling demand and indoor thermal performance in relation to an urban setting. The dataset energy loads were used to validate the simulation results. The simulation results show that the most efficient building envelope improvement type is an insulation roof with shading. It saves 17% of cooling load in arterial roads while saving up to 18% of cooling load in residential areas.

Keywords: Convenience store, Energy consumption, Building envelopes.

1. INTRODUCTION

In Taiwan, the average of convenient store's Energy Use Intensity (EUI) is 1501 to 2346 (kWh/m²/ year) [1, 2] which is 3 times higher than department stores, 7 times higher than central air conditioning office buildings and 38 times higher than housing. Taiwan is a country that possesses a significant density of convenience stores. There were 10,199 convenience stores serving 23 million people in Taiwan (Statistical information obtained at the end of 2016), which means there is one store for every 2,304 person. This study aims to investigate the energy consumption of stand-alone convenience stores in Taiwan in two different urban settings. It seeks to investigate and propose energy reduction strategies for new development and refurbished convenience stores. Nowadays, retailers develop their stores with more space to provide more facilities to increase consumers' footfall. According to the retailer's annual report (2016) the convenience stores with a designated seating plan and coffee shop incur better sales.

Currently, retailers tend to construct and refurbish existing shops to increase the visual connection between outside and the inside of shops and leading to an all glazed facade regardless of urban setting orientation (Fig. 1). However, this change of building envelope influences the indoor atmosphere and energy consumption. Researchers note that the indoor atmosphere can change occupants' behaviours and energy performance. [3,4]. Heat loads on building envelopes due to the intensity of solar radiation and less temperature fluctuations and a high level of humidity in the Taiwanese hot humid climate contributes as one of the major

factors that have a direct impact on indoor thermal comfort.



Figure 1: Convenience store façade.

2. CONVENIENCE STORE IN TAIWAN

As convenience stores continued to penetrate the Taiwanese market and competition increased, the existing stores designed ways to ensure their survival. The stores offered a wide range of convenient products that met customers' specific needs. To manage the high competition, Taiwanese convenience stores developed strategies that led to the introduction of hybrid convenience stores that provides other facilities such as neighbourhood meeting places, toilets and seating areas [5]. While these stores offered fast foods, they appreciated the need for dining furniture and facilities that enabled customers to enjoy the services and products and an extended stay indoors.

2.1 Convenience store buildings in Taiwan

A new convenience store design introduced to Taiwan's customer in 2012. The new convenience stores with a designated seating plan and coffee shop incur better sales. The stand-alone convenience store has more space than others and has developed into the fundamental convenience store architectural type in Taiwan. It is an ongoing challenge to improve a building's energy

PLEA 2018 HONG KONG

Smart and Healthy within the 2-degree Limit

efficiency without compromising its indoor environmental quality. Nowadays, a convenience store is not only a place for shopping but also a community place for the neighbourhood.

The light steel buildings are palpable in Taiwan and are deemed desirable due to the inexpensive construction; the building fabric is constructed of reusable and recyclable fast to build materials. However, the light steel buildings lack insulation, which causes the indoor temperature to reach 40°C in the summertime [5]. To counter such temperatures, air conditioning systems are used to improve the indoor thermal environment, which leads to a heightened consumption of energy.

2.2 The influence of store design on user

Shopping is not just about retrieving items from shelves according to one's needs; it is an experience that one desires to enjoy. The retail store atmosphere can influence emotional responses, such as pleasure, arousal and dominance [6]. The importance of the time spent in the shop relates to a comfortable or an enjoyable experience. The significant element of retail environment is the ambient condition, such as lighting, temperature and noise [7]. However, thermal comfort is the condition of mind that expresses satisfaction with the thermal environment; therefore, it is strongly related to psychology [8].

3. METHODS

The largest leading retailer provided a dataset of 1,416 stores. The following sources were included: region, address, operation type, electricity number, district type, dimension of the store (total dimension, business area and storehouse), annual power expense, monthly customer flow, equipment type and equipment quantities. The obtained information was organised into a spreadsheet database and the chief facilities engineer was consulted. After examining the retailer's database, there were 251 stand-alone convenience stores with complete data. A previous study was used Google Maps to determinate convenience store building types in Taiwan [1]. This study used Google Maps street view to understand convenience store's architectural feature such as window's orientation, structure, urban street settings, determining the road classification, adjacent and surrounding building's height. Sample analysis results provide the architectural features and main locations, urban setting of convenience store for base case design. The dataset analysis shows over 82% of stand-alone convenience stores were located in the arterial road and residential area and 98% of 251 stand-alone convenience stores were steel roof and steel construction with single glazing buildings. The dynamic software (IES-VE) is used to simulate different envelope improvement techniques to understand the cooling

demand and indoor thermal performance in relation to urban setting.

4. STAND-ALONE CONVENIENCE STORE ENERGY CONSUMPTION

Convenience stores in Taiwan tend to use the large floor to ceiling single glazing as buildings' façade to visually attract people and to display products. However, the large single glazing areas can increase heat gain during the summertime. Table 1 shows the results of statistical tests of two sided and three sided window convenience store. Generally, the two sided window stores have marginally larger store sizes, which lead to lower EUI. Table 1 indicates that the three side window convenience stores can attract more customers than two side window stores but it also increases annual store electricity consumption. However, the three side window stores tend to have more customers and higher EUI and energy consumption than two side window stores.

Table 1: Comparison of two sided and three sided windows stores information.

Number Of windows	Store size (m ²)	Annual power consumption (kWh)	Customer	EUI (kWh/m ² /year)
Two-sided	138.1	175,211	319,290	1,344.0
Three-sided	128.6	176,164	339,494	1,432.0

The database indicates variations of architectural shading overhangs of the convenience stores. Stores varied in the provision of overhangs that provides a space for customers to rest and a smoking area for smokers without optimization of its dimensions to deal with the onslaught of direct solar radiation. Table 2 shows that stores with three sides overhang have the highest EUI due to smaller store size. The one side overhang stores have the lowest EUI because it tend to be adjacent to other buildings, which causes less heat gain.

Table 2: Energy consumption comparison of store with shading.

Overhang	Store Size (m ²)	Energy consumption (kWh)	Customers	EUI (kWh/m ² /year)
Without	140.7	176,618.9	346,038	1,363.9
One side	135.0	169,945.1	318,399	1,323.9
Two side	139.2	175,784.5	321,135	1,339.9
Three side	131.1	176,442.0	355,196	1,418.8

The thermal environment of the store and its surrounding largely influences the energy consumption of respective appliances. For instance, during summer, the electricity consumption of air conditioning, and freezing and refrigeration appliances increases during summer. The energy measurement data shows that the cooling energy consumption in summer is six times higher than winter. Table 3 shows the building's

PLEA 2018 HONG KONG

Smart and Healthy within the 2-degree Limit

envelope setting detail and Table 4 shows the internal gain equipment list of the base model.

Table 3: Information of simulation base case.

Built up area	105m ²
Entrance	East
Window orientation	East and south
Number of Storeys	1
Floor to Floor Height	3.5m
External Walls	Tile + Brick wall+ 15 mm of timber board
Internal Walls	Brick wall + 15 mm of timer board
Glazing	8 mm single glass
Roof	1mm metal cladding+ 15mm timber board
Ceiling	15 mm Plasterboard
Infiltration rate	4.5 m ³ /h/m ²
Lighting	2272w
Occupancy	7
Cooling set point	26°C

Table 4: Internal gain equipment list.

Equipment	Wattage	Quantities
Microwave	1800	2
Hotdog machine	900	1
Oden machine	900	2
Coffee machine	3080	2
Tea eggs cooker	800	2
Water dispenser	2800	1
Computer and POS system	500	2
ATM	4300	1
Copy machine and multiple media kiosk	200	1

The existing store's roof only uses metal cladding and adds a timber panel in inner surface to reduce the noise from raining seasons. The store has a large configuration of glazing. There is no possibility of opening windows at the convenience store as they are all sealed for security, air quality and reduction of outdoor sound.

During the examination of the surfaces of the envelope, various aspects will be signified during the process of simulation. These include internal gain, occupation and equipment, and lighting. In cooling mode, the key focus is placed on sensible heat; the impact of latent heat is so low that it is insignificant. All effective parameters in the assessment of the building envelope are considered in connection with the Hsinchu City climate.

According to monitored data, during the summertime, the highest indoor temperature in non air cooled space can reach 46.1°C at 14:00 in the summertime. The simulation base case result shows that the highest temperature in the summertime was 48.59°C, which was over estimated the indoor temperature by 2.5°C, but creates a standard base case for comparison. The existing building simulation result shows that the mean percentage of people dissatisfied is 80.89%

The study simulates two most common stand-alone convenience store urban settings: arterial road and residential area. Each urban setting simulation includes four types store exposure: one side, two side, three side and four side exposure (Fig. 3).

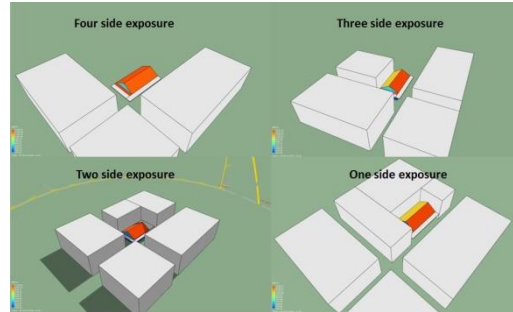


Figure 3: IES-VE modelled view of the building exposure.

5. STORE'S ENVELOPE IMPROVEMENT

The base case is a stand-alone convenience store (in what urban setting) for simulation as it present over 80% of existing convenience stores condition such as structure, store size and architectural form (two side windows with veranda or shading) and can use it to validate with simulation work (Fig. 4). This study simulates two urban settings: arterial road and residential area. The arterial road stores were surrounded by 3.2m low rise buildings and 2.8m width roads while the residential area stores were surrounded by 12m height buildings and 4.5m width road.

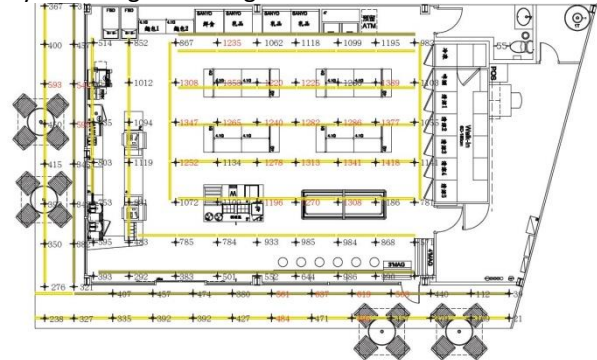


Figure 4: Base case store floor plan.

5.1 Roof insulation improvement simulation

This section presents the simulation result of the insulated roof. as the convenience store buildings are not subject to compliance with building thermal performance regulations in Taiwan, the existing building roofs are; 1 mm metal cladding, 15mm timber board and 15 mm plasterboard without any insulation.

The simulation model added two types common insulation material between the metal cladding and timber board. First, insulation material is a 50 mm insulation board, and second is 30 mm of polystyrene foam (see Table 5). Those insulation materials are widely used for roof insulation on buildings in Taiwan, such as resident buildings, office buildings and schools.

PLEA 2018 HONG KONG

Smart and Healthy within the 2-degree Limit

Table 5: The construction template of insulation roof.

External Walls	Tile + brick wall+ 15 mm of timer board
Internal Walls	Brick wall + 15 mm of timer board
Glazing	8 mm single glass 1mm metal cladding + 50mm
Roof	insulation board + 30mm polystyrene foam+ 15mm timer board
Ceiling	15 mm Plasterboard

Table 6 shows that the roof insulation significantly reduced indoor temperature. In general, the mean temperature can significantly reduce from 33.51°C to 27.9°C. Moreover, the mean number of people dissatisfied also reduced from 80.89% to 52.87%. The store with insulation roof can save cooling load up to 13%.

Table 6: The simulation result of insulation roof in arterial road.

Exposure	Four sides	Three sides	Two sides	One side
Mean temperature (°C)	27.9	27.93	27.92	27.93
Mean people dissatisfied (%)	52.87	53.1	53.03	53.1
Cooling load(kWh)				

Table 7 shows that the insulation material adds on a residential urban setting can significantly reduce mean temperature from 33.51°C to 27.79°C. Moreover, the mean number of people dissatisfied also reduced from 80.89% to 51.75%. It save cooling energy consumption up to 15%.

Table 7: The simulation result of insulation roof in residential area.

Exposure	Four sides	Three sides	Two sides	One side
Mean temperature (°C)	27.8	27.92	27.79	27.92
Mean people dissatisfied (%)	51.89	53.02	51.75	53.03

5.2 Optimizing the wall sections environmental performance

The shading device is an economic technique to reduce the solar gain. Most of convenience stores have the shading device. However, the designer placed the shading device too high and it cannot shade the ceiling to floor glazing properly (Fig. 5). This study simulated insulation roof with shading device. The louver shading device is placed at 2.3m above ground allows for airflow to reduce thermal stratification on the façade (Fig. 6).



Figure 5: Shading device of convenience store.

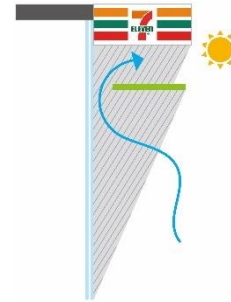


Figure 6: Louver shading device.

Generally, the mean temperature in arterial road store can decline from 33.51°C to 25.22°C and the mean people dissatisfied also reduce from 80.89% to 39.18% (Table 8). It save cooling load about 17%.

Table 8: The simulation result of optimizing the wall sections environment in arterial road.

Exposure	Four sides	Three sides	Two sides	One side
Mean temperature (°C)	26.84	26.91	25.82	25.22
Mean people dissatisfied (%)	42.39	43.14	39.56	39.18

Table 9 presents that the mean temperature of store in residential area can decline from 33.51°C to 25.87°C and the mean people dissatisfied also reduce from 80.89% to 39.14%. The insulation roof with louver shading device can save cooling energy up to 18% in residential area.

Table 9: The simulation result of optimizing the wall sections environment in residential area.

Exposure	Four sides	Three sides	Two sides	One side
Mean temperature (°C)	26.13	26.85	25.94	25.87
Mean people dissatisfied (%)	40.77	42.56	39.62	39.14

5.3 Double glazing performance

The large configuration of glazing makes convenience stores brighter and transparent but also increases the heat gain. According to the previous studies [9, 10] double glazing can keep the building transparent, but reduce the heat gain and improve the indoor thermal environment. This study changed the existing 8 mm

PLEA 2018 HONG KONG

Smart and Healthy within the 2-degree Limit

single glass to 8 mm reflective glass with 10mm argon cavity between two glazing. Table 10 shows the simulation result of store added double-glazing on an arterial road urban setting. The mean temperature can significantly reduce from 33.51°C to 27.94°C. Table 11 shows the simulation result of double glazing in an arterial road urban setting. The mean temperature can significantly reduce from 33.51°C to 27.92°C. The double glazing envelope improvement can save cooling energy consumption up to 11% in both urban settings.

Table 10: The simulation result of double glazing in arterial road.

Exposure	Four sides	Three sides	Two sides	One side
Mean temperature (°C)	28.03	28.07	27.94	28.07
Mean people dissatisfied (%)	54.19	54.52	53.22	54.52

Table 11: The simulation result of double glazing in residential area.

Exposure	Four sides	Three sides	Two sides	One side
Mean temperature (°C)	28.02	28.05	27.92	28.05
Mean people dissatisfied (%)	54.02	54.34	53.04	54.34

6. CONCLUSION

Statistical analysis shows that the three sided window stores tend to attract more customers and higher EUI and energy consumption than two sided window stores. It can be concluded that three sided window stores can increase perceptions of spaciousness by linking interior and exterior visually for customers, which results in attracting more customers. About one in six of convenience stores in Taiwan are standalone convenience store. The store's envelope improvement can save energy up to 2,033kWh/year at a stand-alone convenience store which means saving 3,429,000 kWh per year in Taiwan. Provision of overhangs and insulated

roofs proves to be the preferred architectural configuration to save energy while keeping the glazed areas. This study however didn't find using double glazing to provide substantial energy savings, indicating that for economies of scale the single glazing is a viable option to maintain connectedness of indoors and outdoors visually.

REFERENCES

- Cho, C. (2013). Energy Consumption and Use the Characteristics of Convenience store. Master dissertation. Chaoyang University of Technology.
- Chou, D., Chang, C. and Hsu, Y. (2016). Investigation and analysis of power consumption in convenience stores in Taiwan. *Energy and Buildings*, 133, pp.670-687.
- Kotler, P. (1973). Atmospherics as a marketing tool. *Journal of Retailing*, 49(4), pp.48-64.
- Michon, R., Chebat, J. and Turley, L. (2005). Mall atmospherics: the interaction effects of the mall environment on shopping behaviour. *Journal of Business Research*, 58(5), pp.576-583.
- Hsueh, C. and Hsu, J. (2010). Taiwan Convenience Stores 2010. USDA GAIN reports.
- Donovan, R. and Rossiter, J. (1982). Store Atmosphere: An Environmental Psychology Approach. *Journal of Retailing*, 58 (Spring), pp.34-57.
- Underhill, P., (2009). *Why we buy: The science of shopping*. Simon and Schuster Paperbacks.
- Chen, P., (2008). A Study on the Influence of Regulating Indoor Temperature of the Working Environment on Human Responses. Master dissertation. National Cheng Kung University.
- Hamza, N. (2004). The performance of double skin facades in office building refurbishment in hot arid areas. PhD. Newcastle University.
- Chan, A., Chow, T., Fong, K. and Lin, Z. (2009). Investigation on energy performance of double skin façade in Hong Kong. *Energy and Buildings*, 41(11), pp.1135-1142.

Do Energy Performance Certifications Matter in Housing Selection?

Evidence from choice experiments in Barcelona

CARLOS MARMOLEJO-DUARTE¹, ANDRÉS AMPUDIA-FARIAS¹

¹Centre for Land Policy and Valuations, ETS Architecture of Barcelona, Technical University of Catalonia

ABSTRACT: Energy Performance Certificates have been implemented in Spain just in the moment of the largest real estate recession, such situation does not allow to observe consumers' preferences on energy efficient homes. This paper uses choice experiment to study the relative importance of energy efficiency in relation to other functional and quality attributes. In order to evaluate the role of framework information in the formation of household preferences the sample has been split into 2 sets and informed on the economic and environmental implications of energy efficiency using technical and illustrative units. Results suggest that households do give importance to energy efficiency mainly when they are informed in an easy-to understand way. This latter finding has important implications for the design of energy policy.

KEYWORDS: Energy efficiency, choice experiments, Energy-performance-certificates

1. INTRODUCTION

Fifteen years ago the EU introduced the energy performance certifications (EPC) to give universal energy transparency to the real estate market. The aim of such policy is to foster energy-efficiency informed purchasing and letting decisions. Under the hypothesis that an increased utility coming from energy bill savings and the preservation of environment might transform into explicit preferences for efficient real estate. Such utility can capitalise on higher prices and preference of efficient buildings. Empirical evidence, coming from different EU countries has found a market premium for EPC efficient residential and commercial buildings (see Mudgal et al. 2013). In the case of Spain, such evidence is scarce (Marmolejo, 2016), and the few existing studies do report market premiums that are quite below in relation to other countries. One of the reason is the very recent transposition of the Energy Performance of Buildings Directive by means of the Real Decree 235/2013, that has it made mandatory to include the energy label as of the 1st of June of 2013. The second reason is that such transposition came into force in the worst real estate recession which does not allow to observe consumers' preferences for energy efficient homes.

This paper tries to fill this gap by means of 2 clearly different objectives:

To identify the relative importance of energy performance certifications in relation to other housing attributes in choice selection

To study whether such importance, if any, is different in the event that housing consumers are informed on the economic and environmental implications of energy efficiency using easy-to-understand units, instead of the technical units legally established. Previous research has

strengthened the importance of information background on the preference formation for efficient homes (Marmolejo, et al., 2017).

In order to achieve such objectives a family of choice based experiments have been done in order to identify the implicit preferences of a sample of potential multifamily users in Barcelona. In order to quantify the marginal utility of the assessed housing attributes, a conventional logistic regression has been implemented.

2. EMPIRICAL EVIDENCE ON ENERGY EFFICIENCY PREFERENCES

An important number of studies uses hedonic pricing to estimate the marginal price of green labels including EPC (Marmolejo & Bravi, 2017). The pioneering work of Brounen and Kok (2011) in The Netherlands found that there is 3.6% transaction market premium from green dwellings, comparing to inefficient dwellings: improving energy EPC ranking from D to A (the more efficient rank) or from G (the most inefficient rank) to D, increase 10% or 5% housing prices respectively. Mudgal et al. (2013) have performed a study comprising a number of European cities which details that the impact of different levels of the EPC on selling prices is varied, ranging from only 0.4%, for each rank, in Oxford up to 10.5% in Vienna. Fuerst et al. (2015) report for the analysis of selling prices in England that a G->D improvement implies a 7% price increase, at the time that the improvement D->B implies a market premium on 5%. In Spain Marmolejo (2016) report an increase of only 5.11% for improving the EPC rank from G to A (it is to say only 0.8% for each rank). This latter finding may come from the late adoption of EPC policy but also different climatic conditions and environmental concerns perspectives. The above-stated conclusions do not shed light on consumers' preferences

PLEA 2018 HONG KONG

Smart and Healthy within the 2-degree Limit

when other architectural attributes are present. For that reason, an increasing number of studies use choice experiments to uncover the preference structure, just as it is done in this paper.

In the literature, the use of stated preferences is well established. In such family, choice experiments (CE) have proven to be a powerful technique to study consumer's preferences. In relation to other declared preferences (Marmolejo & Ruiz, 2013). CE approach portrays 3 main advantages:

It is robust to strategic/complacency bias since respondents are not directly questioned to state the preference for a concrete attribute (e.g. energy efficiency) It is familiar to respondents since it emulates exactly the same elicitation process that they use when acquiring products in the market

It allows to identify trade-offs of utility since the election of the preferred alternative implies the rejection of the remaining of the offered options.

In the Netherlands, Poortinga et al. (2013) used a paper-based on conjoint analysis where respondents declared the acceptability level of some energy-saving measures in a Likert scale. In this way, the authors identified the trade-off between energy-saving appliances and willingness to change consumption behaviour. In a similar line, Sadler [9] used two paper-based choice experiments to assess preferences for home renovations and heating systems in Canada. Each "choice set" was formed by alternative heating systems already available in the market; and the choice of home renovation with and without energy retrofits. Her results highlight that households prefer energy-efficient renovation over renovations without energy retrofits. In Switzerland, Banfi et al. (2008) used telephone-based choice experiments to determine willingness to pay for energy-saving measures in residential buildings. Each choice task consisted of reading a card that listed the features of the actual house and those of another dwelling and having to choose the one which was preferred out of the two alternatives. Offered improvements included air renewal systems and insulation of windows and facades. Their analysis indicates that consumers significantly value green attributes, due to the energy savings and environmental benefits they bring along; even though other attributes, such as thermal comfort, air quality and noise protection, are considered. Achtnicht (2014) uses face-to-face computer-assisted choice experiments to assess the consumers' energy preferences in renovations with energy retrofits resulting from insulation and heating systems. An important novelty in his study is the inclusion of the actual economic savings and CO₂ emissions, as well as professional energy consultancy services. The respondents were provided with two hypothetical measures of upgrade regarding their

heating supply and usage respectively, from which they could choose.

The research reported here is different since it explores the trade-offs between the EPC ranking and other residential attributes while selecting a standard urban apartment and taking into consideration that energy efficiency is enclosed in the EPC scheme. Moreover, it explores whether the respondents do give a different importance to energy efficiency when they are informed on the economic and environmental implications using technical units (i.e kWh/sq.m of non-renewable primary energy) versus illustrative ones (Euro/month savings in the energy bill).

3. METHOD, DATA AND CASE STUDY

We use choice based experiments (CE) to achieve the 2 objectives of the paper. CEs consist in submitting a group of individuals to a task in which they are faced with choosing, within a set of alternatives, the preferred option (usually a product or service). These alternatives are usually named "the choice set" and, from the cognitive point of view, their comparison (followed by the final choice) represents the task that the respondent is called to accomplish. The observed component of utility associated with different alternatives is usually defined as a function involving a simple linear combination of attributes and parameters estimates. The partial utility of each attribute is calculated by means of a discrete choice model.

The detractors of state preferences methods argue that the actual behaviour of people tends to be different from that stated in surveys. Such a gap is known as the hypothetical bias (HB). Nonetheless, researchers have found (List, 2001; Fifer et al., 2014) that HB tends to be smaller when: 1) goods assessed are private, as opposed to public; 2) experiments are realistic (i.e. payment vehicles are familiar and people rely on the feasibility to provide the attributes of the assessed goods); and 3) individuals are carefully selected so as to ensure convenient experience and appropriate demographics.

All these reasons support the use of CEs in this work, in absence of data about actual transactions, since: 1) usually, people choose between a finite set of alternatives when looking for a new apartment; 2) houses are private goods and people are used to paying a price according to their attributes; 3) the EPC ranking is usually declared in the actual market offers; 4) a clear and realistic payment vehicle has been designed and the amount is in keeping both with monthly mortgage and rent payments, with which people are already familiar, and 5) respondents were carefully selected so as to ensure the necessary cognitive resources to perform the task.

The implementation of the CE of this study consisted of: Determination of the attributes and levels of each attribute

PLEA 2018 HONG KONG

Smart and Healthy within the 2-degree Limit

Design of a comprehensive survey where the CE were framed

Identification of the relevant population and sample size

Implementation of surveys

Analysis of the data using discrete choice models

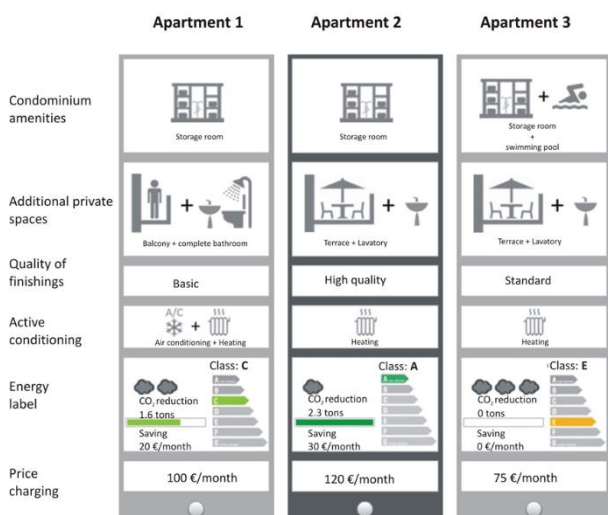


Figure 1: Example of the computer assisted choice set

In this research the selected attributes come from a specific research on typology and advertisement of new housing developments in Barcelona. The attributes/levels used in the CE are as follows:

Condominium amenities. Two levels: storage room or storage room plus swimming pool. It is common that new developments in Barcelona do include such attributes even when they are targeted at medium- and medium-low income population segments.

Additional private spaces. Two levels: terrace and restroom; or balcony plus complete additional bathroom. In general, new developments with three bedrooms do include two complete bathrooms; nevertheless, a trade-off between the spaces “additional bathroom/restroom” and “balcony/terrace” could be present. Due climatic reasons, privately-used open spaces, such as balconies and mainly terraces, are important in multifamily markets in Barcelona.

Quality of finishings. Three levels: basic, standard and high quality. For each level, a description was given regarding the kind of material used in walls, floors and kitchen.

Active conditioning. Two levels: (radiant) heating and heating plus air conditioning (heating pump).

Energy label. Three levels: “E” (the minimum EPC level, according to the current building regulation in Spain), “C” and “A”. Half of the participants were informed on the economic and environmental implications of energy efficiency in two different ways as further discussed.

Price charging. Respondents were informed about the fact that using high-quality finishings and energy-efficient attributes (i.e. wall/ window insulation)

increases the construction cost of the building. For that reason, a price charging up to 130 € would be added to the monthly payment of rent or mortgage. The price charge has been calculated by adding production and development costs for different levels of finishes and energy classes. To transform these marginal increases into monthly payments a direct capitalization has been used with a 4 % yield (which is the usual standard in Barcelona for this kind of apartments). The price charge allocation is, thus, conditional to the finishings, thus avoiding the possibility to present an unrealistic combination of low-quality apartment with high prices. The assumption is that respondents value the trade-off between price charge (marginal price) and the overall benefits derived from different apartment attributes.

The CE was incorporated into a survey applied to residents of the Barcelona’s area older than 18 years which participate in the main decision-making of their household. It is to say the sample is formed by actual owners and tenants of homes in the study area. In order to assure the representativeness of income and demographics, the respondents were recruited along the different neighbours of the city and neighbouring municipalities up to cover all the income levels as well as the age cohorts. The survey was made part face to face and part using an online platform. In total the sample consists of 2,000 CE coming from 500 participants after discarding 166 incomplete or unreliable surveys according to the under-average duration of the answering time.

The survey itself consisted of the following structure:

Contextualization. The goal of this section is to understand the previous knowledge of respondents about the EPC scheme, as well as their energy consumption and sustainable habits and their satisfaction about the status-quo option.

Choice experiment. Each respondent was asked to perform four choice tasks after being clearly informed about each of the attributes and levels used in the different apartment alternatives included in choice sets. In doing so, complementary graphic material was used in order to visualize the quality of the finishings.

Socio-economic profile. In order to test whether preferences depend on individuals’ heterogeneity, socio-economic characteristics (SECs) such as gender, age, income, professional status and educational level were controlled.

After being informed on the attributes and levels than a recently completed apartment may have, respondents were asked to indicate the preferred one in the event that they have to move to another apartment. An example of the choice task is illustrated in Fig 1.

Two different experiments were applied to each half of the sample. In the first one (EVP1) the economic and environmental implications of energy efficiency were stated using the technical legal units (kWh/sq. m/annum

PLEA 2018 HONG KONG

Smart and Healthy within the 2-degree Limit

of primary non-renewable energy and tons of CO₂). In the second experiment (EVP2), illustrative easy-to-understand units were used: monthly savings in energy bills expressed in Euro; and the emissions equivalent in terms of car mileage. In order to avoid a selection bias the participants were randomly assigned to the 2 choice experiments.

4. RESULTS

Fig. 2 contains the sociodemographics of the 500 participants. As seen, the cohort of 18-30 comprises half of the sample, which although does not exactly correspond to the general age distribution provides important insights on preferences of young households most in a tenant tenure.

Age		Household net disposable income	
Year		Euro/month	
18-30	50%	<600	3%
31-45	20%	600-1200	11%
46-65	26%	1201-1800	15%
>65	4%	1801-2400	17%
		2400-3000	16%
Completed studies		3001-3600	15%
		3601-4200	10%
Primary	1%	4201-4800	6%
Secondary	1%	>4800	8%
Technical High School	7%		
High School	17%	Sex	
1st University degree	19%	Women	49%
Bachelor	34%	Men	51%
Postgraduated	20%		

Source: Own elaboration

Figure 2: Sociodemographic data from the sample

Fig. 3 contains the results of the discrete choice models calibration for the 2 choice experiments carried out (EVP1 and EVP3). Broadly, the outcomings for the 2 experiments are the same, despite the fact that respondents were different as it has been said. Such results suggest that respondents are attracted more for the swimming pool rather than only having a storage room. As well, they do prefer apartments with a terrace instead of a balcony, despite that this latter option includes an additional bathroom. This finding strength the importance of open spaces over additional interior spaces in the Mediterranean climate. Regarding the quality of finishings clearly the high-quality option is the less popular among respondents, since the additional price to be paid for the apartment as a leasehold or mortgage payment was correlated with the quality. So the larger the quality, the larger the price.

Interestingly, the basic quality of finishings does not represent the most desired alternative, but the standard one. In other words, people declare to prefer standard qualities but not expensive ones. For that reason, developers in Spain even when apartments are targeted

to the upper demand segment do exhibit medium-high quality finishings allowing in this way a further customisation.

On the active conditioning systems, respondents were clearly attracted by the flats portraying air conditioning and heating, instead of having only heating. This finding is important since in Mediterranean countries the summer tends to be very hot.

Coming to the energy efficiency, clearly the respondents rejected the alternatives containing the worst of the EPC class "E" and prioritized those including class "A", the most efficient one. Regarding the price, as expected the coefficient is negative, which suggest that larger prices do represent a loss of utility for consumers. This trend is common in all choice experiments regardless its thematic application.

	EVP1 MOD 1			EVP3 MOD 1		
	Efecto	Std Err	T ratio	Efecto	Std Err	T ratio
Model adjustment						
rh	0.42139			0.42041		
Log-likelihood model	- 853			- 854		
Log-likelihood null model	- 1,099			- 1,099		
Dif	246			244		
Certainty percentatge	22			0		
Consisten Akaike Info Criteri	18			1,772		
Chi sq	5			489		
Chi sq relative	55			61		
Condominium amenities						
Storage room	- 0.14	0.04	- 3.55	- 0.14	0.04	- 3.63
Storage room + swimming pool	0.14	0.04	3.55	0.14	0.04	3.63
Additional private spaces						
Balcony + complete bathroom	- 0.13	0.04	- 3.20	- 0.20	0.04	- 5.01
Terrace + lavatory	0.13	0.04	3.20	0.20	0.04	5.01
Quality of finishings						
Basic	0.41	0.06	7.40	0.38	0.06	6.95
Standard	0.98	0.06	7.06	0.30	0.06	5.39
High quality	- 0.80	0.07	- 12.20	- 0.68	0.06	- 10.59
Active conditioning						
Heating	- 0.27	0.04	- 6.74	- 0.25	0.04	- 6.29
Air conditioning + Heating	0.27	0.04	6.74	0.25	0.04	6.29
Energy class						
Class E	- 0.84	0.07	- 12.64	- 0.95	0.07	- 13.70
Class C	0.07	0.06	1.27	0.18	0.06	3.25
Class A	0.77	0.05	14.08	0.77	0.06	13.98
Additional price						
Lineal	- 0.15693	0.04909	- 3.19664	- 0.19618	0.04828	- 4.06297

Source: Own elaboration

Figure 3: Discrete choice models results

Figure 4 depicts the relative importance of each attribute. Clearly Energy class is the most important attribute in both of the choice experiments. The second attribute in importance is the quality of finishings concomitant with price (thus it can be read as the importance of price on apartment choice), followed by the active temperature conditioning, the private spaces and condo amenities.

PLEA 2018 HONG KONG

Smart and Healthy within the 2-degree Limit

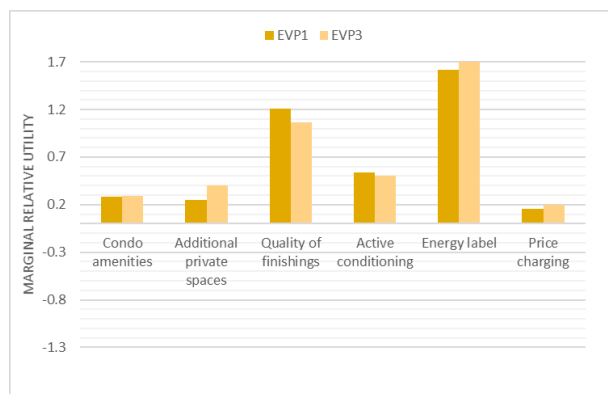


Figure 4: Relative marginal utilities coming from logit model

This latter figure also allows comparing the different importance that respondents gave to the attributes when were informed in different ways on energy efficiency implications. As said before EVP1 experiment informed using technical/legal units, it is to say kWh/sq. m²/year and CO₂ tons; conversely in EVP3 respondents were informed using illustrative units, it is to say Euro/month of energy savings and the reduction of CO₂ in equivalent car mileage. As it is clear household do clearly prime more the energy efficiency of the offered apartment in the latter case when the economic and environmental implications are showed in meaningful terms. Such larger importance seems to be in detriment of the quality of the finishings which relative marginal utility decays in EVP3 sample in relation to EVP1.

5. CONCLUSIONS

Energy efficiency is a multidimensional housing attribute coming from different active and passive measures. For most of the consumers such attribute is opaque due to cognitive limitations and information asymmetry. All in all, represents a barrier for the diffusion of energy efficient homes. In order to broke down such opacity using an easy-to-understand energy-efficiency indicator, the European Union released the Energy Performance of Buildings Directive which makes it mandatory to include an Energy Performance Certificate when a property is transacted in the leasing and selling market. So as for 1st of June of 2013 almost all properties being transacted have to include the EPC class in Spain.

Nonetheless, it is not clear the relative importance of Energy Efficiency in relation to other residential attributes when choosing a property for leasing or buying. For that reason, in this paper we use choice experiments to assess the importance of this residential attribute in relation to other which are preminent in the marketing of apartments in Barcelona such as condominium amenities, private space arrangements, quality of finishings and active thermal conditioners.

In order to test whether information framework might influence household decisions the implications of energy

efficiency in economic and environmental terms were informed using technical and illustrative units.

The results suggest that respondents do positively appreciate energy efficiency in relation to the other attributes. Such preference is larger when they are informed using easy-to-understand illustrative units instead that the technical ones contained in the normative. This latter finding has an important implication for energy policy and suggests that more attention has to be placed in the design of the communication of energy efficiency, since most of the residential consumers are not experts in this field. So, the easier such implications are stated in the Energy Performance Certificates, the larger the efficacy of such policy. Of the the main criticism to the EPC labels in Spain is the completely lack of information about the scheme. The RD 235/2013 has given for granted that people are aware of what is exactly measured by the energy certificates and the implications for household economy and environmental welfare. Such assumption is far to be realistic and more attention need to be paid in the recasting of the Directive and its national transposition.

ACKNOWLEDGEMENTS

This paper is part of the EnerValor project MINECO/FEDER BIA-2015-63606-R. Authors thank all the volunteers involved in gathering the empirical data.

REFERENCES

- Achtnticht, M.; Madlener, R. Factors influencing German house owners' preferences on energy retrofits. *Energy Policy*, 2014, 68, 254-263
- Banfi, S.; Farsi, M.; Filippini, M.; Jakob, M. Willingness to pay for energy-saving measures in residential buildings. *Energy Economics*, 2008, 30, 503-516.
- Brounen, D., & Kok, N. (2011). On the economics of energy labels in the housing market. *Journal of Environmental Economics and Management*, 62(2): 166-179.
- Fifer, S.; Rose, J.; Greaves, S. Hypothetical bias in stated choice experiments: is it a problem? And if so, how do we deal with it? *Transportation Research Part A*, 2014, 61, 164-177
- Fuerst, F., McAllister, P., Nanda, A., & Wyatt, P. (2015). Does energy efficiency matter to home-buyers? An investigation of EPC ratings and transaction prices in England. *Energy economics*, 48: 145-156.
- List, J.; Gallet, C. What Experimental protocol influence disparities between actual and hypothetical stated values? Evidence from a meta-analysis. *Environmental and Resource Economics*, 2001, 20, 241-254
- Mudgal, S., Lyons, L., Cohen, F., Lyons, R., & Fedrigo-Fazio, D. (2013). *Energy performance certificates in buildings and their impact on transaction prices and rents in selected EU countries*. European Commission (DG Energy): Paris, France.
- Marmolejo, C. (2016). La incidencia de la calificación energética sobre los valores residenciales: un análisis para el mercado plurifamiliar en Barcelona. *Informes de la Construcción*, 68 (543): 156.

PLEA 2018 HONG KONG

Smart and Healthy within the 2-degree Limit

Marmolejo, C.; Bravi, M. (2017). Does the Energy Label (EL) Matter in the Residential Market? A Stated Preference Analysis in Barcelona, *Buildings*, 7 (53).

Marmolejo, C.; García-Hooghuis, A.; Garcia-Masia, A. (2017) ¿Cuánto nos importa la clase energética de nuestras viviendas? Un análisis del nivel de comprensión de los Energy Performance Certificates, disposición y motivos de pago en Barcelona, *Habitat Sustentable*, 7 (1)

Marmolejo, C.; Ruiz, M. (2013). Using choice-based-experiments to support real estate design decisions, *Journal of European Real Estate Research*, 6 (1).

Poortinga, W.; Steg, L.; Vlek, C.; Wiersma, G. Household preferences for energy-saving measures: A conjoint analysis. *Journal of Economic Psychology*, 2013, 24, 49-64.

Quantification of Airflow Patterns in a Naturally Ventilated Building Simulated in a Water Table Apparatus

POOJA MUNDHE¹, RASHMIN MOHAN DAMLE¹, PRASAD VAIDYA¹, MICHAEL G. APTE¹

¹CEPT University, Ahmedabad, India

ABSTRACT: Today, most of the people spend 80-90% of the time indoors either in the office or at home. Indoor air is contaminated by human activities and building materials which emit volatile organic compounds. Exposure to these compounds has a short and long-term impact on health. It is therefore important to provide a healthy and productive indoor environment. Acceptable indoor air quality can be maintained by operating a building in natural ventilation, and this can also reduce energy consumption. The water table is an inexpensive, easily accessible apparatus that helps to analyze natural ventilation in buildings due to wind effect and provides instantaneous two-dimensional results of airflow patterns in and around the building. This paper provides and tests a methodology to objectively quantify the images from the water table simulations and calculate results for ventilation metrics like percentage of dead spots, absolute ventilation efficiency, air changes per hour, dose and room mean age of air that quantifies air movement within a physical building model simulated in the apparatus. The quantitative method will help for comparative analysis between design options and make design decisions in terms of opening sizes, orientation, and appropriate positioning of openings optimized for wind-driven naturally ventilated buildings.

KEYWORDS: Natural ventilation, water table apparatus, indoor air quality, ventilation metrics, image processing

1. INTRODUCTION

Strategies like natural or hybrid ventilation decrease the dependence on air-conditioning, which in turn reducing the primary energy consumption [1]. On average, people spend 80-90% of the time indoors [2] either in the office or at home. Indoor air is contaminated by human activities and release of pollutants from materials used in buildings [3]. It is therefore of vital importance to provide a good indoor environment, as it has an impact on the health and productivity of people [4]. Predicting the performance of naturally ventilated buildings is complex, as the parameters governing the airflow, such as temperature and wind, are highly variable over time. The varying airflow path and ventilation rate also results in varying energy consumption.

The different methods available for analysis of natural ventilation designs include the following:

Analytical and empirical models

Scale modelling using a wind tunnel, smoke chamber, salt bath and water table

Full-scale prototypes

Simulation: Computational Fluid Dynamics modelling

Out of these types, the water table apparatus is inexpensive, easily accessible and provides instantaneous results. It helps analyze natural airflow through buildings due to wind action. It is an apparatus as seen in (Fig. 1), wherein dyed (Potassium permanganate) solution is introduced from one side (left side, i.e. windward side) of the input tank and passes through the working zone (central portion). First, a scale building model made out of white Poly Vinyl Chloride (PVC) foam board having a base of transparent acrylic

sheet is immersed in clear water [5] in the working zone and then the dyed water flows towards and past the model. As the dye solution passes through the apertures in the model, its movement is evident in the water, providing a scaled simulation of air movement in a building of the same geometry [6].

There are only a few studies available where methods like the water table apparatus have been used to visualize airflow in and around physical building models. In one of the studies [7] showed using the water table results that the Architects prediction of the airflow pattern in a naturally ventilated building is not correct. Previous experiments using the water table approach largely relied on qualitative and visual analysis of flow patterns. Royan [5] quantified airflow and access to ventilation using simple image processing filters with threshold values of pixels that were subjectively assumed to be adequate levels of ventilation. Since such subjective analysis lack consistency, it does not lend itself to objective quantified comparative analysis. There is a need to objectively quantify the airflow patterns and access to ventilation using industry standard methods of measuring ventilation. This paper summarizes how existing ventilation metrics have been incorporated in quantifying airflow images of a water table apparatus.



PLEA 2018 HONG KONG

Smart and Healthy within the 2-degree Limit

Figure 1: View of the Water table apparatus with dye solution flowing towards the building model

2. METHODOLOGY

To quantify the airflow pattern observed in the water table experiment, initially, a physical building model is simulated in the water table apparatus. The photographic data recorded from the water table experiment are converted to ventilation metrics. Finally, these metrics are verified for a complex geometry 3-bedroom apartment by comparing the quantitative results with the visual airflow patterns.

2.1 Simulating an apartment in water table apparatus

The apartment selected for this study was a 3-bedroom physical building model of scale 1:50 and the details are shown in (Fig. 2) and (Table 1).

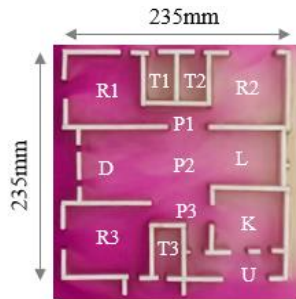


Figure 2: 3-bedroom apartment floor plan with dye movement resembling air flow patterns

Table 1: 3-bedroom apartment room nomenclature

Abbreviations	Room Name	Abbreviations	Room Name
R1	Room 1	L	Living
T1	Toilet 1	R3	Room 3
T2	Toilet 2	T3	Toilet 3
R2	Room 2	P3	Passage 3
P1	Passage 1	K	Kitchen
D	Dining	U	Utility
P2	Passage 2		

2.2 Photographic data to ventilation metrics

The image obtained from the water table as seen in (Fig. 2), consists of gradation of dye that represents air movement in a space. Therefore, to convert the photographic data to ventilation metrics following steps were carried out.

2.2.1 Extracting images as per desired time frames

Initially, the images from the experiment video were extracted. To extract an image from the video, it is important to crop the interior portion of each room excluding walls of the model. This was done to avoid the contribution of white (255-pixel value) PVC foam board walls in the metric calculation. Pixel values represent the darkness or brightness of an image and in this case, it represents the optical density of dye. The value ranges

from 0 to 255, where 0 is the darkest point and 255 is the brightest point. Further, VLC software [8] was used for taking snapshots from the video at any time frame. This helped in taking the snapshots of the cropped video and saving it in PNG (Portable Network Graphics) format. The images obtained from the above process at every second were further post-processed for their pixel values.

2.2.2 Extracting pixel values

For ease of obtaining pixel values, visualization, and reducing computing time, the RGB (Red, Green, Blue) image obtained from the water table experiment was then converted into a grayscale using MATLAB (Matrix Laboratory) [9]. The pixel values were then extracted from this grayscale image. By doing this, only one value was obtained for each pixel, i.e., a weighted sum of RGB values.

2.2.3 Establishing the relation between pixel and concentration values

In this work, the metrics are derived based on the relative difference in concentration values. To identify the relation between pixel values and dye concentration a calibration curve was developed, as illustrated in (Fig. 3). This helps to calculate the dye concentration based on the pixel value and can be used for calculations using "Equation (1)". Once the concentration values are available the ventilation metrics were calculated.

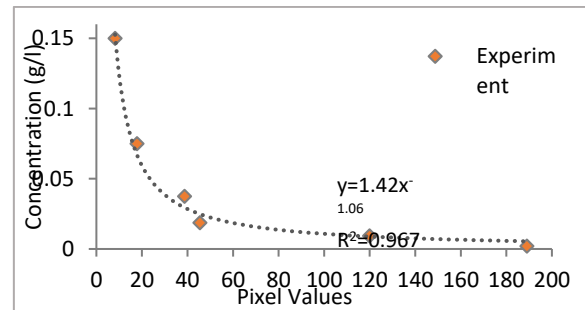


Figure 3: Relation between pixel values and dye concentration

$$C = 1.42 * Px^{-1.06} \quad (1)$$

where C – concentration of dye (g/l);

Px – pixel value.

2.3 Ventilation Metrics

The conditions in the water table experiment represent the conditions in a room. Before starting the experiment, there is only clear water inside the room model i.e., zero dye concentration (0 g/l). This value keeps on increasing as the dyed water enters the room. Thus, the initial clear water condition resembles to be a room filled with stale / contaminated air and infiltration of dye is the fresh air coming inside the room. For a given room, pixel values were extracted and converted to concentration values using the calibration curve as shown in (Fig. 3). The

PLEA 2018 HONG KONG

Smart and Healthy within the 2-degree Limit

relative spatial concentrations were used to evaluate five metrics as follows.

2.3.1 Percentage of Dead Spots

Dead spots mean the air is stagnant, and little/no mixing up of incoming fresh air. This will be seen as a zone with low dye concentration with no movement of air. It is a metric that determines the percentage of dead spots (%DS) in a room which is not adequately ventilated [5] and is calculated using "Equation (2)".

$$\% DS = \frac{C_{max} - C}{C_{max}} \quad (2)$$

where %DS – Percentage of dead spots (%);

C_{max} – maximum concentration in room(g/l);
 C – concentration in room after t, s (g/l).

2.3.2 Absolute Ventilation Efficiency

Absolute ventilation efficiency (AVE) is a metric that helps to determine the ability of the system to decrease contaminant concentration in a room. This can be calculated based on "Equation (3)" [10]. The system is said to be most effective if the value is 1 and least effective when it is 0.

$$Ea = \frac{(C_o - C)}{(C_o - C_s)} \quad (3)$$

where Ea – Absolute Ventilation Efficiency;

C_o - initial concentration in the room (g/l);
 C – concentration in the room after t, s (g/l);
 C_s – concentration in the outdoor supply (g/l).

2.3.3 Air Changes per Hour

Air changes per hour (ACH) is the number of times the air within the room is renovated. It is calculated by using the mass balance "Equation (4)" [11]. This equation considers the inside and outside concentration over the evaluation period.

$$dc = P * ACH * C_s * dt + \frac{S}{V} dt - (ACH + k)C_i * dt \quad (4)$$

where dc - change in inside room concentration (g/l);

P - penetration factor (unitless);
 ACH – air changes per hour (h^{-1});
 C_s – concentration in the outdoor supply (g/l);
 dt - time frame (h);
 C_i - inside room concentration (g/l);
 S - indoor source emission rate (ml/h);
 V - indoor volume (m^3);
 k - reactivity rate (h^{-1}).

This metric is calculated when there are well-mixed conditions inside the room. To do this, the average concentration values at a given time frame are used. The outside concentration (C_s) is averaged near the window

and inside concentration (C_i) is the average room concentration as shown in (Fig. 4).

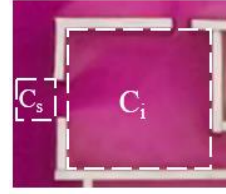


Figure 4: Visual representation of ACH parameters for room 1 of a 3-bedroom apartment

The ACH in case of the water table is dependent on the velocity, density, viscosity of water, characteristic length, area of the window and volume of the room i.e. $ACH = f(v, \rho, \mu, d, A, V)$. Thus, to identify the relation of ACH in the air to that of ACH calculated from the water, a dimensional analysis is carried out which results in "Equation (5)".

$$(ACH)_{air} = \left(\frac{ACH * d}{v} \right)_{water} * \left(\frac{v}{d} \right)_{air} \quad (5)$$

where, ACH – air changes per hour (h^{-1});

d - characteristic length of building (m);

v - velocity of fluid (m/s).

2.3.4 Dose

The dose is a measure of the mass of the pollutant collected at a particular spatial location [12]. It is a function of time and inside pollutant concentration, therefore, as the concentration of pollutants in a room increases, the dose increases. To calculate the dose for each room, "Equation (6)" is used, which is the time integral of the concentration. To solve this integral, trapezoidal rule specified in "Equation (7)" [13] is used. The calculation considers the area under the curve, which is the dose.

$$dose = \int_0^t C(t) dt \quad (6)$$

where $C(t)$ – inside room concentration at t, s (g/l).

$$\int_a^b f(x) dx = \frac{h}{2} (f_0 + f_n + 2 * \sum_{i=1}^{n-1} f_i) \quad (7)$$

where h - time step, (s);

f_0 - Initial concentration in room (g/l);

f_n - concentration in room at the end, t, s (g/l);

f_i - concentration in room after t, s (g/l).

2.3.5 Room Mean Age of Air

The room mean age of air (RMA) determines the time required by the fresh air to reach any room from the inlet point. Lesser age suggests the fast provision of supply air in that room and vice versa. In case of the water table, it is assumed that the room is fully contaminated and the

incoming dye to be the fresh air. In this study, because the dyed water comes in, the concentration inside the room increases, that is why it is similar to a step-up experiment. It can be calculated using "Equation (8)" [14].

$$t_{age,P} = \frac{\int_0^{\infty} t \left[1 - \frac{C_p(t)}{C_p(\infty)} \right] dt}{\int_0^{\infty} \left[1 - \frac{C_p(t)}{C_p(\infty)} \right] dt} \quad (8)$$

where $t_{age,P}$ - Room mean age of air (s);
 $C_p(\infty)$ -maximum concentration in room (g/l);
 $C_p(t)$ - concentration in room after t, s (g/l);
 t – time frame (s).

3. RESULTS AND DISCUSSION

In this study, the dyed water that is entering the room represents air. Therefore, for ease of understanding flow development and explanation of metrics, the incoming dyed water is referred to as air. The flow patterns for 3-bedroom apartment were documented and analysed and then the five above metrics were calculated for each room. The calculations were done considering the average outside and inside room concentration as shown in (Fig. 4). Moreover, understanding the airflow patterns for different rooms helped to relate the quantitative metric results.

3.1 Visual flow pattern analysis

The flow patterns along with the line diagrams observed for a 3-bedroom apartment are presented in (Fig. 5). The first frame is after 1 minute, which is the time when the air enters the room. Initially, it can be observed in (Fig. 5) that the flow patterns are similar in R1 and R3 as the number of windows, size and positions are same, except that R3 side window has a wing wall. However, after 1 minute due to this wing wall, the air does not enter from the side window as that of R1, where the air also enters from the side window. As the air in R1 and R3 flows out from the side window and door, eddies are formed at the corners near the window on the windward side as seen in (Fig. 5b). For the dining, as there are two windows on the windward side and no barrier on opposite side, the air flows straight towards the living room. Because of this straight flow, eddies are formed between the area near the windows on the windward side, and at the left top/bottom corners of this room, as seen in (Fig. 5b). In R2, the air enters from the door and the window which is parallel to the flow direction so there is an eddy motion. Further, K gets ventilated due to the air coming from the P2 and P3, which leaves towards the windows in the utility room(U). For toilets (T1, T2, T3), windows are parallel to the direction of the flow and the doors are closed, so it takes longer time for air to reach these rooms.

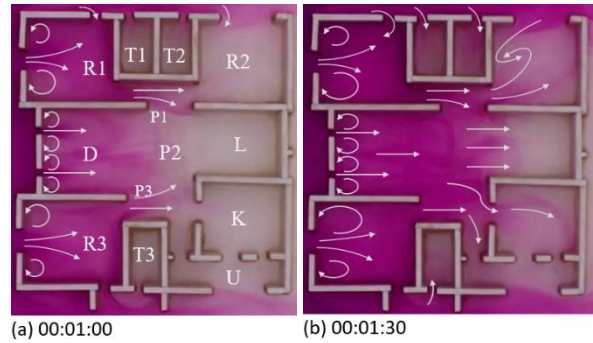


Figure 5: Flow patterns observed in a 3-bedroom apartment at the end of two time frames

3.2 Percentage of Dead Spots

The % DS goes on decreasing in all the rooms as the time proceeds. It can be observed in (Fig. 6a), that the %DS after 1min are maximum in R2, L, K, and U, as the fresh air has not reached these rooms. Whereas, the rooms which are in front get ventilated, diluting the contaminated air. The room D, despite having two windows has more % DS (91.7%) as compared to R1 (88.7%) and R3 (90.3%), as there is no barrier on the opposite side which will stop the fresh air. Therefore, these straight flows creating eddies result in more %DS as shown in (Fig. 5). In case of R2, due to eddies as seen in (Fig. 5b), the %DS are higher (91%) than L (89.5%) which lacks cross ventilation.

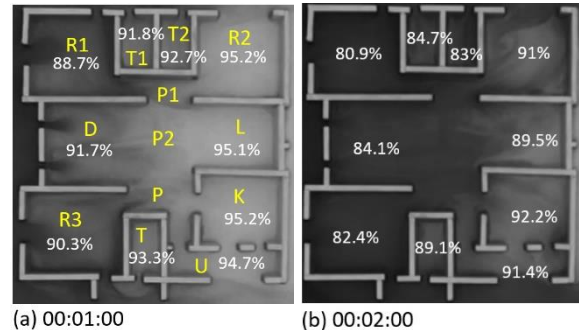


Figure 6: Percentage dead spots in all the rooms at the end of two time frames

Further, if we consider that the outdoor air quality is good, then the rooms that have good indoor air quality (IAQ) are R1, D, and R3. This is because fresh air replaces the maximum contaminated air in these rooms. Whereas, the IAQ is poor in U because the air accumulating the contaminated air from R3, P3, and K is passed into this room.

3.3 Absolute Ventilation Efficiency

AVE is maximum in the rooms which have window perpendicular to the direction of the airflow. It is maximum in the rooms which are on the windward side, i.e., R1, D, and R3, and same, i.e., 0.05 for R3, L, K and U after 1min, as seen in (Fig. 7a). As, these rooms are on the other side of the main source of fresh air supply,

PLEA 2018 HONG KONG

Smart and Healthy within the 2-degree Limit

which can be seen in (Fig. 7a). In R2, due to recirculation, the efficiency is less (0.09) as compared to L (0.10) as seen in (Fig. 7b).

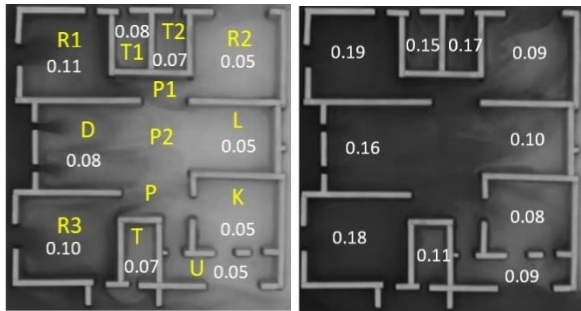


Figure 7: Absolute ventilation efficiency in all the rooms at the end of two time frames

Furthermore, the efficiency is very less, i.e., 0.05% for U until the air enters this room. Once, it reaches this room, i.e., at the end of 2 minutes, due to maximum windows the efficiency increases by 40%, as seen in (Fig. 7b). Moreover, as the area is small as compared to other rooms, it achieves maximum efficiency in a shorter period. Thus, the efficiency increases and pollutant concentration decreases, as the infiltration of fresh air increases. Finally, it can be observed that windows on the windward side are more efficient in reducing the pollutant concentration. This is because of effective delivery of fresh air throughout the room.

3.4 Air Changes per Hour

The ACH is calculated for various rooms in the apartment having windows perpendicular, (i.e., R1, R2, K), and parallel (i.e., T1, T2, T3) to the direction of the flow. ACH for R1, R3, and K are different, as the supply conditions vary as explained in (Fig. 5). Further, it can be observed in (Table 2) that the ACH is nearly half for R1 than R3. The difference is more due to the varying outside supply concentration. For toilets, the ACH in water and air is maximum in T2 due to a maximum fresh air supply, whereas it is less in T1 and T3 as shown in (Table 2). The difference between the ACH for T1 and T3 is less, this is because the supply air concentration near the window is affected by the air coming out from the side window of R1 and R2 respectively.

Table 2: ACH in water and air for different rooms of a 3-bedroom apartment

Rooms	ACH in water(h ⁻¹)	ACH in air(h ⁻¹)
R1	13.7	0.33
R3	24	0.63
K	54.1	0.4
T1	65.8	0.52
T2	113.2	0.5
T3	17	0.85

3.5 Dose

In this case, it is considered that the incoming dye is polluted outdoor air which is undesirable and is trying to penetrate inside the room through the windows. It can be observed in (Fig. 8a), that after 1 min, as the polluted air has only reached R1, D, and R3 the dose is more, as compared to the rooms away from the source, i.e., rooms R2, L, K and U. As this polluted outside air starts penetrating inside the rooms dose increases and can be seen in (Fig. 8b). The dose is less where maximum eddies are formed as in case of R2, as explained in (Fig. 5b). It is also less when this polluted air is not able to uniformly spread in a room. If the room area is small and is exposed for a longer period, then the dose will be higher. This is the case for rooms T1, T2, T3 as seen in (Fig. 8b).

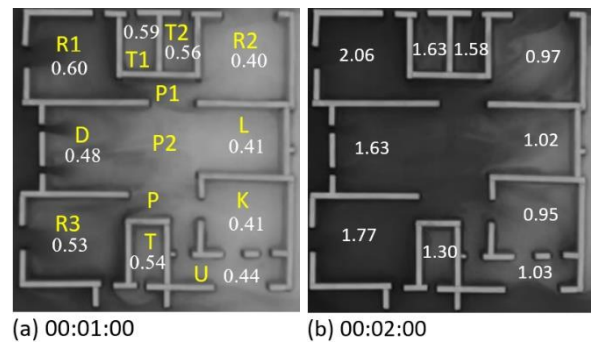


Figure 8: Dose in all rooms at the end of two time frames

Dose is a function of time and indoor polluted air concentration, so as the concentration increases, as seen in (Fig. 9), the dose increases. Thus, at the end of the experiment, i.e., maximum exposure time, the dose is maximum in R1, D, R3 as the polluted indoor air concentration is maximum, as seen in (Fig. 9).

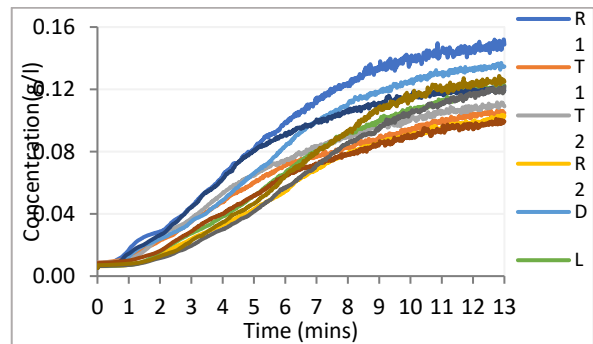


Figure 9: Rise in polluted indoor air concentration due to rise in outdoor polluted air concentration with time

3.6 Room Mean Age of Air

The results of RMA are presented in (Fig. 10). As RMA depends on the time required for fresh air to reach a room from the inlet point (i.e., a window on windward side), the concentration (i.e., fresh air) inside a room needs to be observed. Therefore, if we observe in (Fig. 10), the age is less in the rooms like R1, D, and R3. This is because the rooms are near to the inlet point, receiving

PLEA 2018 HONG KONG

Smart and Healthy within the 2-degree Limit

maximum fresh air supply. Whereas, rooms like R2, L, K, and U are away from the windows on the windward side and will require more time to achieve uniform supply of fresh air. In case of R2, the age is more due to eddies formed in the room as seen in (Fig. 5b). The age is also more in toilets as their windows are parallel to the direction of the flow, taking more time for the room to achieve uniform supply of fresh air. Thus, lesser the RMA in a room, more is the supply of fresh and vice versa. This means that the contaminant concentration will reduce quickly in R1, D, and R3 as compared to the other rooms away from the inlet point.

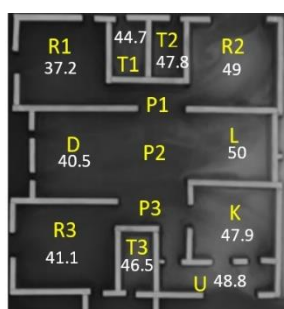


Figure 10: Room mean age of air in all the rooms at the end of 2 minutes

4. CONCLUSION

The water table is a simple and relatively inexpensive apparatus for visualizing the flow patterns in and around the buildings. In this paper, a methodology has been developed to quantify the flow patterns that are generated in water table apparatus in terms of existing ventilation metrics. A detailed methodology is developed for quantifying these metrics with the help of image processing data. This will be of utility for educational purposes, serving architects, energy consultants and practicing engineers.

When the case of a 3BHK apartment was tested, the rooms which are near to the window on the windward side have the least percentage of dead spots, room mean age of air and higher air changes per hour as compared to the ones away from it. These rooms also have good indoor air quality due to the direct supply of fresh air. The air changes per hour are maximum in the rooms which are smaller in the area. However, the dose in these rooms is higher as the rooms are exposed to the incoming polluted outdoor air from the window for a longer period. Finally, it is concluded that the derivation of ventilation metrics with the current methodology gives physically realistic results, that agree with visual observation in the water table.

Water table analysis can be used for two-dimensional airflow, as in case of high rise apartment buildings, where the air movement is through windows at the same level. It cannot be used when the level/ height of the windows varies within the room, or the model, or for large size

windows where significant stack effect occurs within the window itself, or within the room.

REFERENCES

1. Omer, A. M. (2008). Energy, environment and sustainable development. *Renewable and Sustainable Energy Reviews*, 12(9), 2265–2300. <https://doi.org/10.1016/j.rser.2007.05.001>
2. Jomehzadeh, F., Nejat, P., Calautit, J. K., Yusof, M. B. M., Zaki, S. A., Hughes, B. R., & Yazid, M. N. A. W. M. (2017). A review on windcatcher for passive cooling and natural ventilation in buildings, Part 1: Indoor air quality and thermal comfort assessment. *Renewable and Sustainable Energy Reviews*, 70(November), 736–756. <https://doi.org/10.1016/j.rser.2016.11.254>
3. Sundell, J. (2004). On the history of indoor air quality and health. *Indoor Air*, 14(7), 51–58. <https://doi.org/10.1111/j.1600-0668.2004.00273.x>
4. Tham, K. W. (2016). Indoor air quality and its effects on humans—A review of challenges and developments in the last 30 years. *Energy and Buildings*, 130, 637–650. <https://doi.org/10.1016/j.enbuild.2016.08.071>
5. Royan, M. (2017). Simulating Natural Ventilation in Residential Building using Water Table apparatus. CEPT University.
6. Norbert, L. (2015). *Heating, Cooling, Lighting: Sustainable Design Methods for Architects*. Wiley (Fourth).
7. Toledo, A., & Pereira, F. (2005). Natural Ventilation due to wind action: practice knowledge against experimental airflow visualisation. *International Conference “Passive and Low Energy Cooling for the Built Environment,”* 1(May), 1109. Retrieved from http://www.inive.org/members_area/medias/pdf/Inive%5Cpa_lenc%5C2005%5CToledo.pdf
8. VLC (Version 3.0.1). (2018).
9. MathWorks. MATLAB (Version 9.3.US). (2017).
10. Awbi, H. (1991). *Ventilation of Buildings* (First). E & FN SPON.
11. Dockery, D. W., & Spengler, J. D. (1981). Indoor-outdoor relationships of respirable sulfates and particles. *Atmospheric Environment* (1967), 15(3), 335–343. [https://doi.org/10.1016/0004-6981\(81\)90036-6](https://doi.org/10.1016/0004-6981(81)90036-6)
12. Hainsohn, R. J., & Cimbala, J. M. (2003). *Indoor Air Quality Engineering: Environmental Health and Control of Indoor Pollutants*. New York: Marcel Dekker.
13. Chapra, S. C., & Canale, R. P. (1990). *Numerical Methods For Engineers*. (A. T. Brown & S. Tenney, Eds.) (Second). Singapore: McGraw-Hill International Editions.
14. Kwon, K. S., Lee, I. B., Han, H. T., Shin, C. Y., Hwang, H. S., Hong, S. W., ... Han, C. P. (2011). Analysing ventilation efficiency in a test chamber using age-of-air concept and CFD technology. *Biosystems Engineering*, 110(4), 421–433. <https://doi.org/10.1016/j.biosystemseng.2011.08.013>

Impact of Inlet Water Temperature on Cooling from Misting Fans: A CFD Simulation Study

KAI ZHENG¹, NYUK HIEN WONG¹

¹Department of Building, National University of Singapore

ABSTRACT: Non-atomizing misting systems have typically been employed to alleviate the problem of thermal heat stress among occupants and have been shown to be effective especially in temperate countries. However, its impact in tropical countries is not widely studied and it is the same for the impact of the water temperature on reducing air and skin temperature. Using CFD simulation models, this paper seeks to address these gaps. A Lagrangian-Eulerian approach is adopted using the Steady K-Epsilon turbulence model and Discrete Phase Model in Ansys Fluent software. Inputs for misting spray and modelling human skin are adopted from other published papers, and Grid Independence studies are also conducted. The results show that Misting sprays can cool the air temperature by up to 4.5°C, based on a hot afternoon condition in Singapore and there is an almost linear relationship between water temperature and cooling effect. At 3m downstream from nozzle, a 45°C water temperature leads to neither decrease nor increase in air temperature. Skin temperatures can also be reduced by a maximum of 3°C. Due to thermal properties of water, even 95°C water temperature only increases air temperature by less than 4°C.

KEYWORDS: Evaporative cooling, Misting fan, Water temperature, Skin temperature, Urban Heat Island

1. INTRODUCTION

Singapore is a tropical country with high temperatures and humidity throughout the year. Being a densely populated city with a population of 5.4 million housed on a small land area of 719.1 km², the Urban Heat Island (UHI) effect has been prevalent. The UHI effect is a phenomenon where urban areas tend to be warmer than their rural surroundings due to the replacement of building infrastructure over existing open land and vegetation [1]. Air-conditioning has been the most popular method to provide thermal comfort to the local population. However, air-conditioners have been found to consume large amounts of energy and are not environmentally friendly due to the use of refrigerants. This has led to the search of alternative means of countering the rise in temperatures, among which the use of misting sprays is one of them.

The use of misting sprays for cooling the environment taps on the principle of evaporative cooling, where water absorbs heat when it evaporates due to its latent heat of vaporization. Such systems have been adopted primarily in temperate countries where there is greater wet bulb depressions and thus greater potential for evaporative cooling, including Japan [2] and India [3]. Satisfactory results have also been derived in environments with high humidity [4]. The misting spray systems consume less energy than typical air-conditioners and do not use environmentally aggressive refrigerants [5]. Other benefits include lower installation and operating costs. Different parameters that affect the degree of evaporative cooling from such systems, like nozzle size and pressure, have been studied in other papers [6][7]. However, the impact of the inlet water temperature has

only been mildly explored [16], and there is a research gap on how extreme water temperatures affect cooling. This study seeks to address this gap based on the impacts on the outlet Dry Bulb Temperature (DBT) and the temperature on the human skin, based on a Computational Fluid Dynamics (CFD) study.

2. METHODOLOGY

Many variables from the air, water and system-side play a role in determining the cooling effects of a misting fan. These variables include inlet air velocity, water pressure, and other factors. This paper will focus on studying the inlet water temperature (T_{inlet}) and its impact on ambient air temperature, using computational fluid dynamics (CFD) simulations.

2.1 CFD

This study uses the commercial CFD software, FLUENT version 18.2, and is set up in a Lagrangian-Eulerian frame. A steady Reynolds-averaged Navier-Stokes (RANS) turbulence model is employed for the wind flow in Lagrangian frame, with unsteady particles introduced into the domain through the Discrete Phase Model (DPM) for the Eulerian frame. A steady-state simulation assumes that the solution is non-time-dependent, and the two-equation realizable K-Epsilon model with standard wall function is adopted for the turbulence model for its economic approach in computing complex turbulent flows. The realizable model differs from the standard model in that the turbulent viscosity is now a variable, and a new transport equation is adopted for the dissipation rate. The K-Epsilon model has been shown to be inaccurate for flows that separate under adverse

pressure gradients, which is not the case in this study. Further, the standard wall function is adopted since near-wall treatments are not as critical in this study. In addition, the species transport model is used, carrying a mixture template of water-vapor, oxygen and nitrogen. Since no chemical reactions are studied for this paper, all other options are not adopted.

2.2 Modelled Room

This study assumes a simple 10m by 10m room for its boundary condition and is 3m in height. No furniture or other objects are modelled that may obstruct wind flows, except for a human head which is modelled as a sphere as shown in Figure 1. The sphere measures 20cm in radius, and its thermal properties are typical to that of human skin so that cooling effects on skin temperatures can also be studied. The thermal properties are shown in Table 1 below.

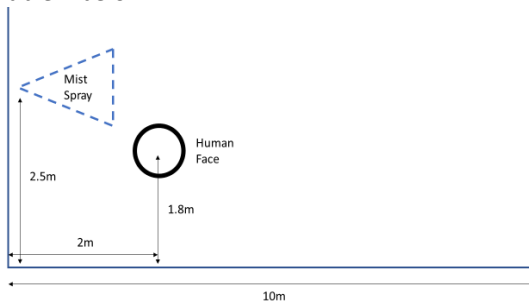


Figure 1: Schematic of CFD model

Table 1: Thermal Properties of Human

Property	Value	Reference
Skin Conductivity	0.293 W/(m-K)	[8]
Specific Heat	3470 J/(kg°C)	[9]
Mass of human head	4.5 kg	[10]

The room is modelled to have 0.2m thick aluminium sides and top with a ‘temperature’ thermal condition, having a default value of 26.85°C, and a ‘reflect’ DPM condition with particle-wall heat exchange turned on. The ground is set to have an ‘escape’ DPM condition that is reminiscent of a previous study [3] where fins are placed to allow unevaporated water to drain out of the room rather than form puddles of water on the floor.

Wind flow is in the x-direction, measuring 0.5 m/s wind speeds and 5% turbulent intensity from the inlet boundary. The environmental conditions in the room are 30°C and 58% RH - values which are typical of hot afternoons in Singapore. An ‘escape’ DPM condition is also used for the ‘outlet’ boundary.

Finally, a ‘coupled’ thermal condition is used for the solid face and face shadow, with wall thickness of 0.2m and ‘human skin’ material as set out in Table 1. The ‘coupled’ option calculates heat transfer directly from the solution in the adjacent cells, so no further conditions need to be inputted. The DPM condition is set to ‘reflect’ as it resembles the actual conditions where water

droplets reflect off human hair and skin, with particle-wall heat exchange turned on.

2.3 Mist Spray

Like mentioned above, the DPM model is used for modelling the misting spray. Wind flow is first run to convergence without the introduction of the spray, before DPM is turned on and updated at every 10 iteration intervals with unsteady particle tracking. The particle time step size is chosen to be 0.05s, a value sufficiently small to advance the particles accurately; and the number of time steps chosen as ‘1’ so that droplets do not penetrate the domain too quickly. Stochastic collision, coalescence and breakup models are all turned on since these processes are largely dominant in a typical misting spray.

For the injection, a single hollow cone spray is placed in the room at coordinates (0, 5, 2.5), spraying in the x-axis direction. The material used in the spray is water liquid, and its diameter distribution follows that of the Rosin-Rammler distribution [11]. The range of droplet sizes is divided into several discrete intervals, each represented by a mean diameter to calculate the droplet trajectory. The Rosin-Rammler distribution assumes an exponential relationship exists between droplet diameter and mass fraction of droplets with diameter greater than d , and is given by

$$Y_d = e - (d/\bar{d})^n \quad (1)$$

Where,

Y_d = mass fraction of droplets diameter greater than d

\bar{d} = size constant

n = size distribution parameter

In this study, the inputs for the water droplets are set forth in Table 2 and is based on a previous study [3]. The velocity of the water jet is set as 10 m/s, with cone angle 15 degrees, and the mass flow rate is set as 0.05 kg/s. There are 20 diameters and 300 streams – both values recommended by another CFD study [6]. The vaporization model adopted is the convection/diffusion-controlled one, that is suitable for high vaporization rates where the convective flow becomes important. This contrasts with the diffusion-controlled model where the vaporization rate is slow and hugely governed by gradient diffusion.

For the physical models, a Dynamic-drag model is used for Drag law. Since the Weber number in this study is large, the droplet shape is likely to distort and resemble more closely to that of a disc than a sphere, having significantly higher drag. The dynamic drag model is used in this study since it accounts for droplet distortion. Likewise, since this study is a high Weber number flow, the ‘Wave’ breakup model is used. The children particles are considered in the same tracking step.

PLEA 2018 HONG KONG

Smart and Healthy within the 2-degree Limit

Table 2: Droplet properties for Rosin-Rammler distribution

Property	Value
Min. Diameter	7.4 e-5 (m)
Max. Diameter	5.18 e-4 (m)
Mean Diameter	3.69 e-4 (m)
Spread Parameter	3.67

2.4 Grid Independence

In all CFD simulations, it is good practice to conduct grid independence studies to ensure that the solution does not change as the mesh resolution changes. For this study, three grids were generated through a grid refinement process, where the first grid consisted of 700k cells (Coarse), the second grid with 1.3 million cells (Medium) and the third grid with 2.27 million cells (Fine). For all three grids, a local mesh sizing is adopted to provide a maximum 0.1m element size at the 'face' area, while a cut-cell assembly meshing is used for the other areas. For consistent reporting of the grid-independence results, the grid-convergence index (GCI) that is based on generalized Richardson Extrapolation is used for this study [12].

Richardson Extrapolation assumes discrete solutions f to have a series representation, in grid spacing h . By combining two separate discrete solutions, f_1 and f_2 , a more accurate estimate of f can be derived. Where a grid doubling is conducted, the grid refinement ratio is 2 and this allows a simplified equation where:

$$f[\text{exact}] = 4/3f_1 - 1/3f_2 \quad (2)$$

However, to use Equation 2, the values of f_1 and f_2 must be taken from the same points. In this study, the points are taken from three scenarios – at 3m downstream, 9m downstream and for the front and back of the face. The error in a fine grid solution, f_1 , is then approximated by comparing to a coarse grid f_2 , and is defined as

$$E_1^{\text{fine}} = \mathcal{E} / (1-r^p) \quad (3)$$

$$GCI = F_s E_1^{\text{fine}} \quad (4)$$

Where,

$\mathcal{E} = f_2 - f_1$

$r =$ refinement factor

$p =$ formal order of accuracy of algorithm

$F_s =$ Factor of safety (1.25 in this study)

The order of accuracy, p , can be calculated using three solutions with constant r , as below:

$$P = \ln ((f_3-f_2)/(f_2-f_1)) / \ln (r) \quad (5)$$

Finally, by comparing two GCI values over three grids, the asymptotic range of convergence can also be computed as follows:

$$GCI_{23} = r^p GCI_{12} \quad (6)$$

Using the above equations (2-6) and air temperature values taken from centre point of 9m downstream contour, the grid convergence results can be summarized as shown in Table 3:

Table 3: Values for calculating GCI and Asymptotic Range

F ₁	F ₂	F ₃	p
28.96	28.85	28.94	0.2895
GCI ₁₂		GCI ₂₃	Asymptotic Range
2.6213		2.1380	0.997

Since the asymptotic value is approximately one, this indicates that the solutions are well within asymptotic range of convergence and we can say the cooled air temperature has an error band of 2.62%. The Coarse grid of 700k cells is thus adopted for this study.

2.5 Experimental Measurements

The study seeks to establish the impact of water temperature on evaporative cooling, and thus the water temperature is varied from 10°C to 95°C, at 5°C intervals. Three main sets of results are then extracted for the study – at 3m downstream, 5m downstream and front/back face temperatures. For the 3m and 5m downstream profiles, five points of measurement are taken at equivalent distances from each other and this is represented in Figure 2 as an example. For the modelled face, only one measurement point is taken per side, at the centre-point, as shown in Figure 3.

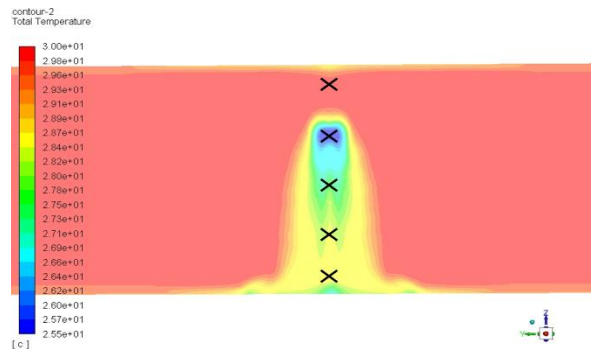


Figure 2: Points of measurement for cooled air temperature

PLEA 2018 HONG KONG

Smart and Healthy within the 2-degree Limit

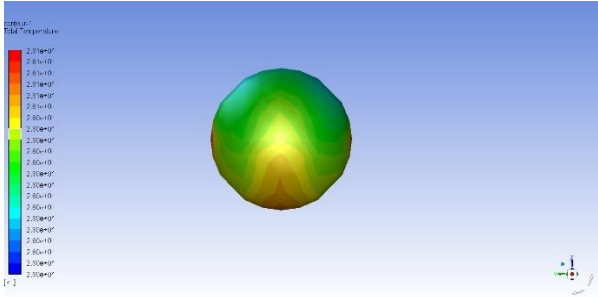


Figure 3: Temperature profile for modelled face

3. RESULTS AND DISCUSSION

3.1 Air Temperature

The impact of different water temperatures on the resultant air temperatures are shown in Figures 4 & 5, separated by whether the water temperatures are above or below the inlet air temperature. The temperatures are plotted against the height position like marked in Figure 2. As seen from Figure 4, the main area of cooling occurs between 2m and 2.5m height, with the greatest cooling of about 4.5°C occurring for the 10°C water temperature case. Even when the water temperature is the same as the inlet air temperature, an approximate 1.3°C reduction in temperature is still achieved. In fact, as seen in Figure 5, even a water temperature 5°C higher than inlet air temperature can produce a 0.5°C cooling. Interesting to note from Figure 5 is that even water temperatures as high as 95°C only increases the air temperatures by less than 4°C.

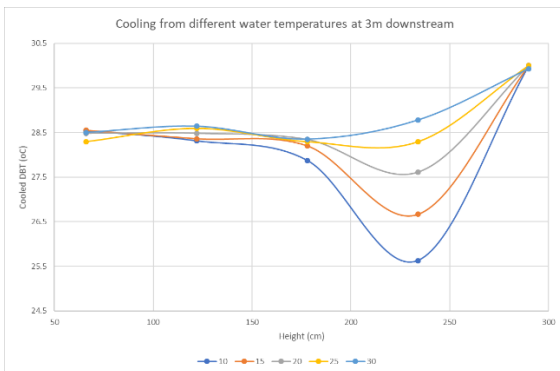


Figure 4: Temperature Contour for 3m downstream (Water Temp values below Air temp)

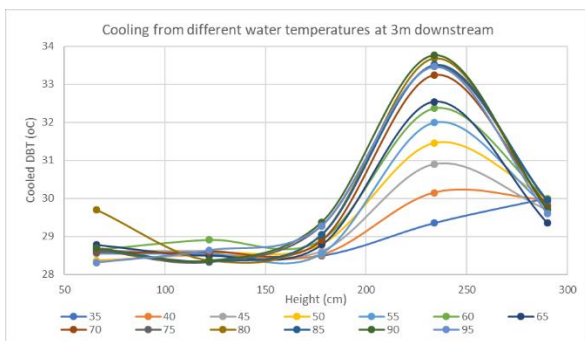


Figure 5: Temperature Profile for 3m downstream (Water Temp values above Air Temp)

Similar results can be seen even at 5m downstream from the nozzle, and the results are shown in Figures 6 & 7. Likewise, the rise in air temperature is only about 2°C even with the hottest water temperature. The main difference, however, is at the height where cooling occurs, where it is now at 1m to 1.5m due to gravitational effects. Further, the degree of cooling is expectedly less at 5m downstream than 3m. This can be explained by looking at the remaining mass of water droplets where more evaporation would have happened upstream, and the available mass of droplets is less at 5m downstream and thus, less heat transfer will take place. This is evident from the equation from the latent heat of vaporization:

$$Q = mL \quad (7)$$

Where,

Q = heat absorbed/released (J)

M = mass of water droplets (kg)

L = latent heat of vaporization (22.6×10^5 J/kg)

As the mass of water droplets decrease, the amount of heat absorbed subsequently also decreases since the latent heat of vaporization does not change.

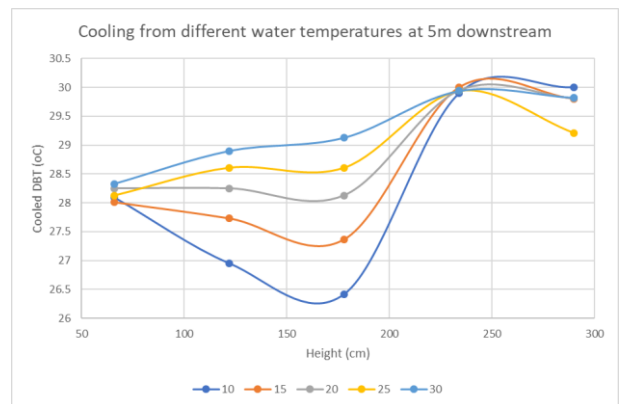


Figure 6: Temperature Profile at 5m downstream (Water Temp below Air Temp)

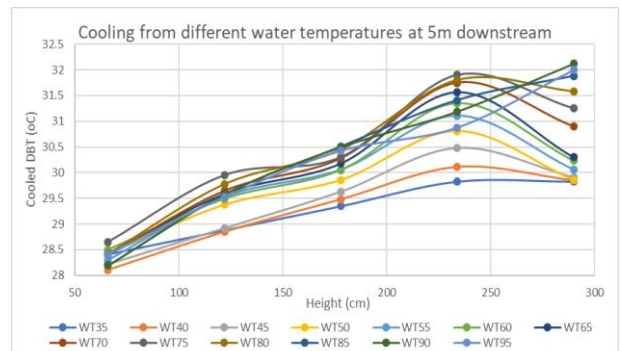


Figure 7: Temperature Profile at 5m downstream (Water Temp above Air Temp)

PLEA 2018 HONG KONG

Smart and Healthy within the 2-degree Limit

Figure 8 shows the relationship between the reduction in DBT and the inlet water temperature, taken from the centre point, 1.25m height, from 3m downstream. Even at such high-water temperatures, cooling still exists possibly due to the significantly larger heat absorbed from the latent heat of vaporization compared to the sensible heat exchange [13]. Understandably, the amount of cooling decreases with increasing water temperature, and this is shown in Figure 8 as having an almost linear relationship with a R^2 value of about 0.92. Closer to human height, the reduction in DBT plotted in Figure 9 is taken from a height of 1.8m, likewise at 3m downstream. A similarly linear relationship exists with a R^2 of about 0.93. A negative drop in DBT as shown in Figure 9 means that the DBT increases from the sensible heat exchange between water droplets and air.

These results can prove useful for urban planners in determining the appropriate water temperatures to use. Like air-conditioning cooling towers, the spraying of water can pose diseases like Legionella, and a higher water temperature can potentially alleviate this problem at the expense of decreased cooling. This study can be used as a guide to strike that balance. For non-atomizing nozzle sprays, this study can also provide insights to balance energy use with the degree of cooling in DBT. For example, looking at Figure 8, cooling the inlet water temperature from 30°C to 20°C provides only a 0.1°C DBT reduction, and it is thus unwise to adopt such a measure since it is a relative waste of energy. It should be noted, however, that these results will differ from other atomizing sprays where water droplets are significantly smaller in size, since the evaporation rate is significantly quicker, and the mass flow is typically much lower to achieve those sizes.

3.2 Human Skin Temperature

Like mentioned in section 2.2, the human face is modelled as a sphere in this study, with the heat conductivity value like human skin. Thus, it should be noted that the temperature values are more typical of skin temperature rather than the human body core temperature. This temperature is plotted against the different water temperatures and shown in Figure 10. The 'front' is defined as the side of the sphere that is facing the nozzle, and the 'back' is otherwise. In this case, the difference in temperatures are not significantly differently, and even at high water temperatures, the skin temperature never rises above the inlet air temperature of 30°C. Adapting conditions in Singapore, the average tap water temperature is about 25°C and this indicates a face temperature of about 28.4°C.

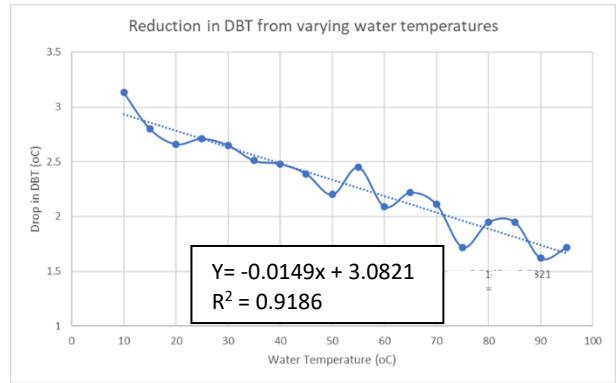


Figure 8: Reduction in DBT plotted against different water temperatures at 3m downstream

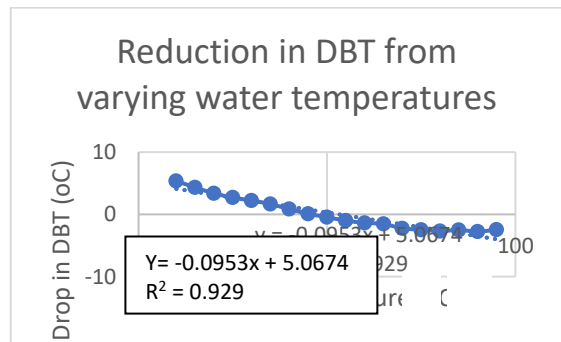


Figure 9 Reduction in DBT with varying water temperatures at 1.8m height 3m downstream

The modelling of skin temperature can potentially aid in more accurate evaluations of thermal sensation and thermal comfort, by relating both variables to the mean skin temperature (T_{sk}). The mean skin temperature is shown in Equation 8 [14]:

$$T_{sk} = 0.06t_{forehead} + 0.08t_{upperarm} + 0.06t_{elbow} + 0.05t_{hand} + 0.12t_{back} + 0.12t_{chest} + 0.12t_{abdomen} + 0.19t_{thigh} + 0.13t_{calf} + 0.07t_{root} \quad (8)$$

A clear correlation has also been established in prior study relating T_{sk} to thermal comfort levels [15]. However, it should be noted that the study was conducted in China in an indoor environment under sleeping conditions and is vastly different from this paper that studies outdoor environments in street canyons. Further, only the face temperature is modelled in this study, and future studies can seek to measure skin temperature at more measurement points and derive a more comprehensive mean skin temperature.

PLEA 2018 HONG KONG

Smart and Healthy within the 2-degree Limit

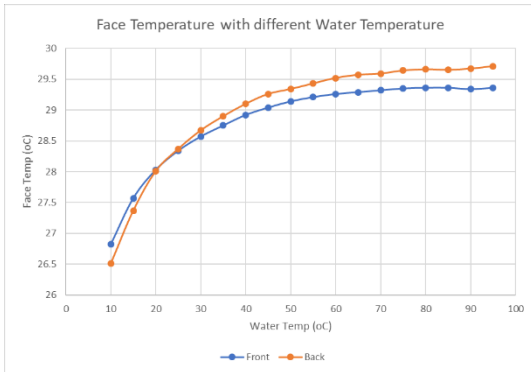


Figure 10: Change in face temperature with varying water temperature

4. CONCLUSION

Using CFD simulations, this paper has studied the impact of changing the inlet water temperature on the reduction in air temperature and human face skin temperature. A wide range of water temperatures were studied, from 10°C to 95°C, and results have shown that there is a linear relationship with the change in DBT. As water temperature gets cooler, more cooling in the DBT is expected, but only at a relatively low rate depending on the points of measurement. Even at its greatest cooling, the difference in DBT cooling between using 20°C water and 30°C water is only about 1°C, due to the thermal conductivity properties of water. Relatedly, even extremely hot water temperatures only warm the DBT by less than 4°C. Thus, this paper can provide guidelines for urban planners to balance cooling or warming the water temperature for greater cooling or alleviating the problem of legionella. The mean skin temperature is also a good indicator for thermal comfort, and this paper has provided insights to how the face temperature changes with different water temperatures.

Future studies should seek to model the whole human body to provide more comprehensive insights into the mean skin temperature change and its relevance to thermal sensation and comfort. In addition, similar methodologies can be conducted for atomizing sprays that do not produce 'wetness' upon contact with human skin since such sprays are significantly different from the sprays used in this paper.

REFERENCES

- [1] US EPA, "Heat Islands," 11 January 2017. [Online]. Available: <https://www.epa.gov/heat-islands/learn-about-heat-islands>. [Accessed 2 April 2018].
- [2] G. Yoon, H. Yamada and M. Okumiya, "Study on Cooling System with using Water Mist-Control Strategy for Water Mist System," in *Renewable Energy*, Yokohama, Japan, 2010.
- [3] R. Sureshkumar, S. Kale and P. Dhar, "Heat and Mass Transfer Processes between a Water Spray and Ambient Air - I. Experimental Data," *Applied Thermal Engineering*, vol. 28, pp. 349-360, 2008.
- [4] A. Haeussermann, E. Hartung, T. Jungbluth, E. Vranken, J.-M. Aerts and D. Berckmans, "Cooling Effects and Evaporation Characteristics of Fogging Systems in an Experimental Piggery," *Biosystems Engineering*, vol. 97, pp. 395-405, 2007.
- [5] N. H. Wong and A. Z. Chong, "Performance evaluation of misting fans in hot and humid climate," *Building and Environment*, vol. 45, pp. 2666-2678, 2010.
- [6] H. Montazeri, B. Blocken and J. L. Hensen, "CFD Analysis of the Impact of Physical Parameters on Evaporative Cooling by a Mist Spray System," *Applied Thermal Engineering*, vol. 75, pp. 608-622, 2015.
- [7] R. Sureshkumar, S. Kale and P. Dhar, "Heat and Mass Transfer Processes between a Water Spray and Ambient Air - II. Simulations," *Applied Thermal Engineering*, vol. 28, pp. 361-371, 2008.
- [8] M. L. Cohen, "Measurement of the Thermal Properties of Human Skin- A Review," *The Journal of Investigative Dermatology*, vol. 69, no. 3, pp. 333-338, 1977.
- [9] Engineering Toolbox, "Human Body and Specific Heat," 2003. [Online]. Available: https://www.engineeringtoolbox.com/human-body-specific-heat-d_393.html. [Accessed 3 April 2018].
- [10] P. Brindza, How Many Atoms are in the Human Head?, Newport News, VA: Jefferson Lab, 2006.
- [11] P. A. Vesilind, "The Rosin-Rammler Particle Size Distribution," *Resource Recovery and Conservation*, vol. 5, pp. 275-277, 1980.
- [12] P. Roache, "Quantification of uncertainty in Computational Fluid Dynamics," *Annual Review of Fluid Mechanics*, vol. 29, pp. 123-160, 1997.
- [13] C. Farnham, K. Emura and T. Mizuno, "Evaluation of cooling effects: outdoor water mist fan," *Building Research & Information*, vol. 43, no. 3, pp. 334-345, 2015.
- [14] J. Colin, J. Timbal, Y. Houdas, C. Boutelier and J. Guieu, "Computation of mean body temperature from rectal and skin temperatures," *Journal of Applied Physiology*, vol. 31, pp. 484-489, 1971.
- [15] W. Liu, Z. Lian and Q. Deng, "Use of mean skin temperature in evaluation of individual thermal comfort for a person in a sleeping posture under steady thermal environment," *Indoor and Built Environment*, vol. 24, no. 4, pp. 489-499, 2015.
- [16] K. Zheng, M. Ichinose and N. H. Wong, "Parametric study on the cooling effects from dry mists in a controlled environment," *Building and Environment*, vol. 141, pp. 61-70, 2018.

The International Style in Israel

Spatial Comfort Performance of Residential Buildings in Tel-Aviv on the 1930's

YEZIORO ABRAHAM¹, NICOLA SABA¹

¹ Faculty of Architecture and Town Planning. Technion - Israel Institute of Technology, Haifa, Israel

ABSTRACT: In 1930's, the Jewish modernist architects, who travelled to Europe to study returned to the country. They discussed the influence of local climate on the building design. The climatic adaptation of these buildings was based merely on the Architecture itself. Environmental aspects, such as natural ventilation and shading, were a significant part in the architectural discourse and practice. The solutions provided sometimes were based on research and sometimes on common sense. Despite the efforts, these solutions have been never properly evaluated to confirm if they are indeed performing as expected. Lack of strict testing has been due to the absence of methods and tools to carry out these tests, especially spatial tools. However, today we can assess the thermal performance of the building by using novel computer models, and presenting the results on the space itself through spatial maps. This study will focus on the climatic performance of residential buildings in the 1930's, which were built in Tel-Aviv in the International style. It will examine these buildings in terms of their ability to achieve thermal comfort. It will also question the intentions of the architects and the effectiveness of their architectural solutions in order to maintain comfortable conditions in the buildings.

KEYWORDS: Thermal Comfort, Adaptive Thermal Maps, the International style.

1. INTRODUCTION

The paper assess whether the architectural solutions, guidelines and guidance, which architects and professionals set, wrote and hypothesized in 1930's, provide a comfortable internal environment on buildings built during the International style movement in Tel-Aviv. At that time, the leading modernist architects discussed the subject of adaptation to local climate conditions and its influence on the building design [1]. This adaptation was based merely on architectural features, since there were no mechanical systems to improve thermal comfort conditions in the buildings. Despite the original intentions and statements, the buildings themselves have been never properly evaluated in order to understand if they indeed were comfortable for the residents. Today the option of field measurements and monitoring is not possible because of the changes these buildings have undergone over the years, mainly by the introduction of AC systems. However, today we have novel computer models, which can provide spatial mapping of thermal comfort conditions. These tools allow us to recognize the different behaviour of each part of the space, especially when it comes to passive building. Using these models will make possible to understand the relation between architectural features and the Thermal Autonomy (TA) achieved in the building [2]. TA results of two buildings will be presented. They show that the buildings performance is more oriented towards summer time (80%-100% TA) and less on the winter (12%-45% TA) (Tables 1 and 2).

2. BACKGROUND

In the early 1930's, many Jewish architects who have gained their academic degrees in Europe have returned to the country. They were deeply influenced by the modern architectural movement [3]. At that time, the population of Tel Aviv grew due to the large waves of migration, which have increased the level of the construction industry in the city. The International style and the principles of the modern movement were reflected by most of the buildings built in Tel Aviv at the time [1].

In those years, the International style began to spread throughout the world as a global movement. This led the modernist architects in general to show interests in local building and climate conditions. In the country the architects wrote about the need to adapt the International style to the local climate conditions. They suggested solutions, hypotheses and rules of thumb about the way architecture should deal with those adaptations. This knowledge was only an approach when the discourse begun. The architects mainly focused on natural ventilation and shading as strategies to deal with the heat stress, while winter time was less considered an issue to deal with. From the building perspective and its envelope, the buildings were built of the most common materials of the period, concrete and silicate bricks (Uvalues for wall and roof are 2.1 and 3.2 W/m²K respectively). Lacking insulation materials, which can improve the thermal performance of the buildings, architects implemented mainly shading and natural

PLEA 2018 HONG KONG

Smart and Healthy within the 2-degree Limit

crossed ventilation as main strategies to deal with climate issues. They used concrete awnings, reduced the number of openings and oriented the windows to the West (prevailing winds) and balcony balustrades (Fig. 1). The most popular element is the sun balcony, which had played an important role, both climatically and socially [1, 4].

In terms of the residential unit, the architects tend to locate the apartment rooms in the west and the bedrooms in the east to maximize their exposure to the sun [5]. They also divided the apartment into two areas according to the prevailing wind direction to improve their ventilation conditions: bedrooms and toilets to the east and kitchen, living room and balcony to the west (Fig. 2).



Figure 1: Shading and Ventilation, 1934 [6].

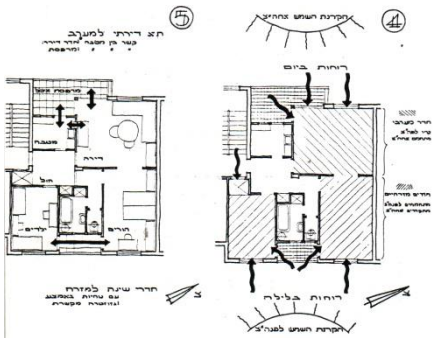


Figure 2: Function and Ventilation, 1937 [7].

2.1 Existing literature

The residential buildings of the International style have been studied extensively from various aspects as part of the architectural practice in the country: historical, ideological and national meanings, analysis of architectural elements, and even the adaptation of the style to local climatic conditions [1, 4]. Moreover, also investigating the climate performance of the International style buildings through computational analysis of energy consumption [5, 8]. Despite of the wide historical knowledge, essential information is still missing which is related to the thermal performance of these buildings and the thermal comfort of their passive environments.

2.2 Adaptive comfort model

This paper refers essentially to two fields, history and sustainability. The research is based on examination of building's thermal performance, and how the local climate had impacts on the style and on the practice of architecture in a time where the use of active mechanical systems was absent. It uses innovative tools to examine

the sustainability of historical buildings. It is based on the Adaptive Comfort Model (ACM), which gives us the ability to examine passive and natural ventilated buildings [2, 9] (Fig. 3).

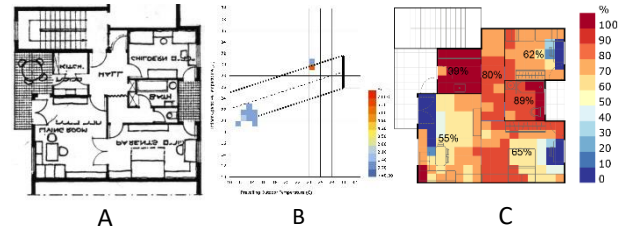


Figure 3: Adaptive Comfort Model. A: Original Plan; B: Current Adaptive Comfort Graph Representation; C: Whole Space Adaptive Comfort Map.

The ACM is based on studies that examined the thermal comfort of occupants within their natural, passive environment. One of the aspects that distinguish this method is its reliance on the fact that the user has the ability to control and change the conditions of the space. The ACM is influenced by two main variables, the operative temperature and the average external temperature. In addition, it takes into account the physical, cultural and personal factors, and also the expectation of the occupants [10, 11].

This study uses advanced and contemporary methods of spatial mapping that present the results on the space itself and enable to assess quantitative and qualitative the climatic performance of the residential unit. Current representation methods (Fig. 3B) display a value of just one point in space, without giving a good indication of the whole space performance. A spatial representation method, on the contrary, allows to fully understand the performance of the whole area and then, differentiate its potential and flaws (Fig. 3C) [10].

3. METHODOLOGY

This study focused on the examination of the TA in residential units. Two residential buildings are presented as case studies. The study explored the architects' considerations of the climatic conditions in the design process of the residential buildings. Each building stresses different characteristics. Several apartments were selected from each building for testing their TA by computerized simulation tools, and presenting the results though spatial maps. For each case study and their closed environment, a schematic three-dimensional model has been built in the software Rhino, using the Ladybug + Honeybee (LB+HB) extensions to the Grasshopper environment [12]. The simulation engine of the model is the robust hourly dynamic model EnergyPlus developed by the US Department of Energy [13].

PLEA 2018 HONG KONG

Smart and Healthy within the 2-degree Limit

The evaluation process is divided into three stages: 1) Building geometry modelling and properties definitions (Fig. 4). The stage includes defining thermal zones (rooms) that compose each representative apartment, and specifying the construction materials for each thermal zone. Various properties regarding issues like infiltration, loads, schedules for opening or closing windows and shutters, number of persons by apartment area, hours of operation, etc. are defined at this stage as well. These properties were defined according to the common conditions of the period. 2) Energy simulation based on the local climate file. In this part, the adaptive and spatial calculations are performed by LB+HB. 3) Creation of the spatial maps for evaluating the TA for each space and apartment. For reducing the amount of maps and in order to create representative maps of the major seasons of the year, the research focuses on the typical hot week (26.09-02.10) and the typical cold week (08.03-14.03).

The TA spatial map of this study represents the **percent of time** when space meets or exceeds passive requirements and criteria. The criteria refer to the European standard EN 15251, comfort class 2 ($\pm 3^{\circ}\text{C}$). From this map, the climatic performance of the apartment can be quantitatively and qualitatively assessed. It is possible to quantify the adaptive comfort of the room, by the comfort percentage. But also, by the colour scale, to discern which parts of the room are more or less comfortable for the occupants, such as in an area close to the window or away from the envelope (Fig. 5). The same color range scale was used for both seasons in order to compare between winter and summer thermal maps.

These outcomes enable us to understand the relationship between the comfort percentages, according to their spread in the unit areas and the architectural elements of the building.

3.1 Case Studies

The two buildings which will be presented represent two ideological approaches: public housing (Meonot HOD), and private residential building (Engel House). The first, Meonot HOD (Figs. 6-9), by Sharon (1933-1934). The chosen building is part of a cluster of three buildings (Figs. 6, 7-building O'). The architectural characteristics related to climate adaptation are expressed in two aspects: The layout, which allows better ventilation and sun exposure and the residential units themselves, which mainly refer to the internal organization according to the desired direction of the wind. The apartments are organized, mainly suggesting that the bedrooms need to be placed

in the east and the living rooms to the west according to the prevailing wind, while recommending a balcony on the west side for shading.

Three representative apartments were chosen from this building for evaluation. One is a typical Western unit (O1). Its internal organization is based on the general trend, apartment rooms in the west and bedrooms in the east, with an emphasis on creating connections and openings between the eastern and western directions for cross ventilation. The other two apartments, are southern oriented (O2 and O3) (Figs. 7-8). O2 is located in the northern part and O3 in the southern part of the building. Both have the same internal organization but mirrored and with different treatment of the envelope.

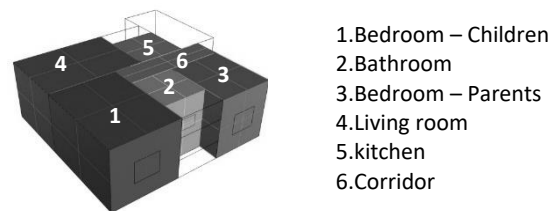


Figure 4: Typical geometry model according to spaces which also represent thermal zones.

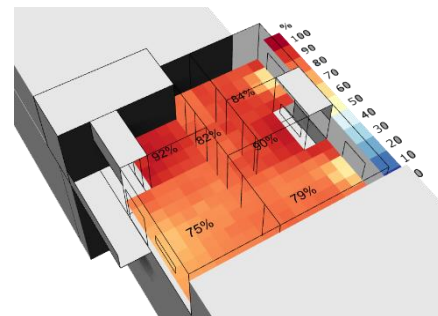


Figure 5: Thermal Autonomy map for an apartment in the Meonot HOD Building.

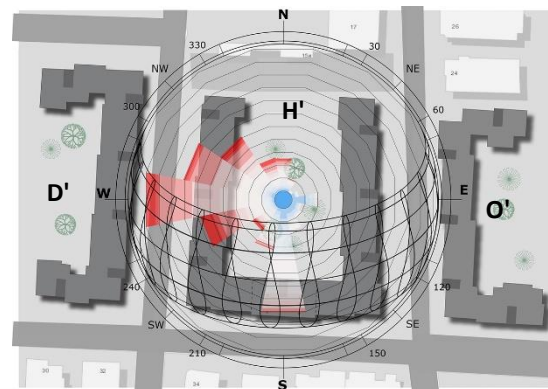


Figure 6: Meonot HOD cluster.

PLEA 2018 HONG KONG

Smart and Healthy within the 2-degree Limit

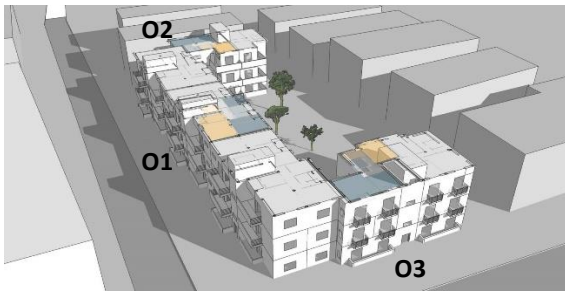


Figure 7: Meonot HOD, Building O'.

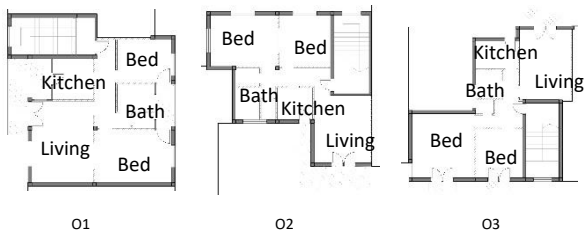


Figure 8: Meonot HOD. Apartments selected for evaluation.



Figure 9: Meonot HOD. A- O1, west deep balcony [14]. B- O2, south deep balcony. C- O3, south narrow balcony.

The second building, Engel house (Figs. 10-12), by Rechter (1933). It represents the construction on pilots that was very common at the time. In addition to the stylistic influence of Le Corbusier, there are also climatic considerations regarding two aspects: natural ventilation, achieved on the western wing of the building, and strong use of shading elements, bumps around the windows for shading and to emphasize the horizontal lines on the front. Two representative apartments were selected in this building (Figs. 10-11). One, a Western unit (E1), was chosen because of its typical orientation, as was customary at that time. The second, a southern unit (E2), that presents a different orientation, south-north. Unit E1 is larger in size than E2, as well as it has three facades (East, South and West), whereas E2 has only two (North and South). The internal organization is not based on the trends applied at that time.

4. RESULTS

The three apartments of Meonot HOD, produce a comfortable internal environment in summer time and a less comfortable winter environment. This is consistent with the intentions of the architects at the time, who were mainly engaged towards the summer. In many cases, the difference in the thermal performance of the units in both seasons is due to the treatment of the

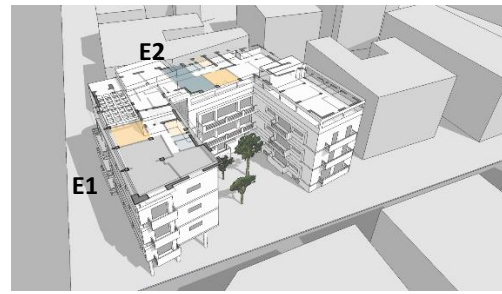


Figure 10: Engel House Building.

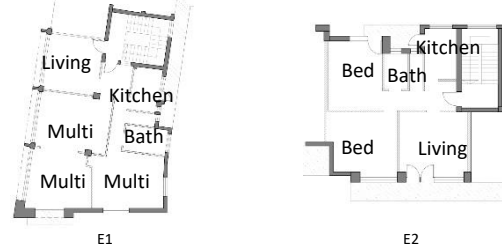


Figure 11: Engel House. Apartments selected for evaluation.

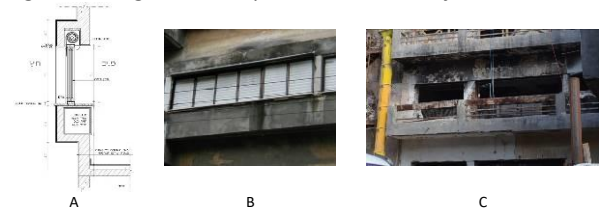


Figure 12: Engel House. A- E1, west thick wall & E2, south thick wall [15]. B- E1, film windows [14]. C- E2, Wide openings and deep balcony.

envelope that contributed to the summer performance but impaired its function in the winter. For instance, the west deep balcony (Fig. 8, 9-A) of unit O1 blocks the direct radiation, and improved the conditions of the internal environment especially of the kitchen in the summer but prevented passive solar heating in the winter that led to uncomfortable environment (Fig. 13).

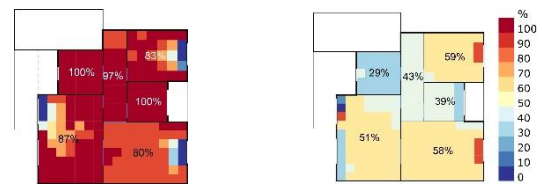


Figure 13: Meonot HOD, Unit O1, 13:00. Left: summer, Right: winter.

The way the architect treated the envelope and especially the different types of balconies in the south façade of the two southern units (O2, O3) have led to different TA results mostly in the winter (12%, 32%), (Table 1). As the narrow balconies of unit O3 (Fig. 9-C) allows the sun's rays to increase the temperature of the bedrooms in the south, the deep balcony of unit O2 (Fig. 9-B) blocks the direct radiation from heating the kitchen and the living room. The deep balcony of O2 led to more comfortable conditions in summer at the southern

PLEA 2018 HONG KONG

Smart and Healthy within the 2-degree Limit

rooms, than those of O3 especially at the areas near the windows (Table 1). It can be seen that the western unit (O1), which is directed and organized according to the general assumptions of the architects, does not show the highest comfort rates in the typical hot week compared to the other two southern units (O2 and O3) (Table 1). But it works best in the cold typical week with the highest comfort percentage. This shows that the architects'

Table 1: TA maps for summer and winter, whole day. Three units of Meonot HOD, O1-west, O2-south, O3-south.

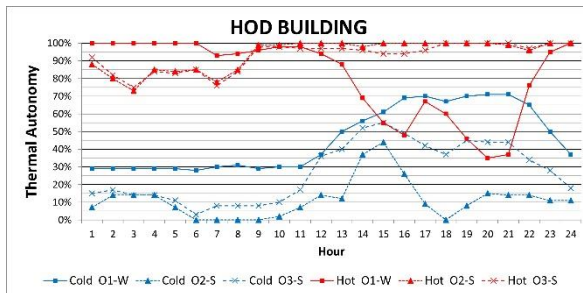
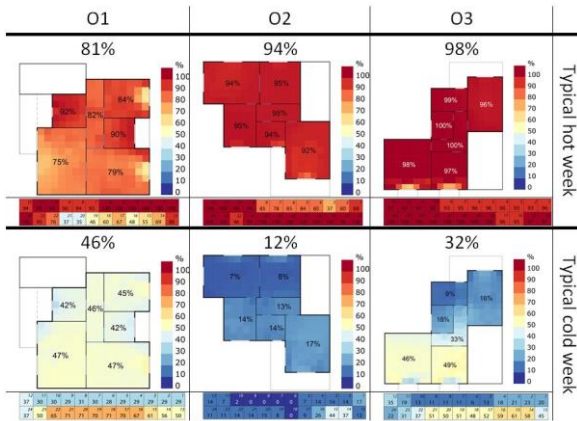


Figure 14: Meonot HOD Building. Thermal Autonomy (TA) Summary.

O1, O2 and O3 perform differently in summer (Fig. 14). In the early morning hours until 9:00, O2 and O3 units indicate lower TA conditions than O1. From 11:00 AM, O1's TA conditions are declining (under 40%) while O2 and O3 apartments show high TA percentages. In the winter, the three apartments perform similarly. The early morning hours are less comfortable and from noon there is an improvement in the TA percentage. When O1 is the most comfortable unit, O2 is the least comfortable unit and O3 describes a moderate state. This stems mainly from the orientation, but also from the architectural elements through which the architect handled the various orientations.

The two apartments of Engel house produce a comfortable indoor environment in the summer in general, and a less comfortable in winter, as the intentions of the architects at the time. Such as, the thick wall and the type of the openings in the west façade, the

assumptions regarding the West-East orientation are not unequivocal. In other words, even though the TA of the Western unit is good most of the day, the South oriented apartments show a better performance in summer. However, in winter time the West oriented apartment performs better than the other two (Table 1).

Table 2: TA maps for summer and winter, during a whole day. Two units of Engel House, E1-west, E2-south.

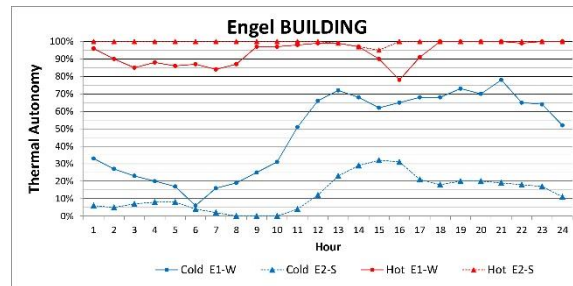
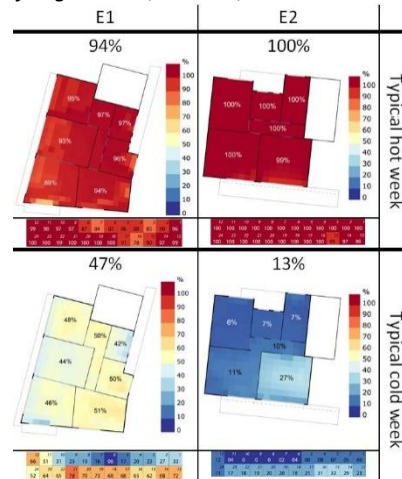


Figure 15: Engel Building. Thermal Autonomy (TA) Summary.

architect used film windows (narrow long windows) that are shaded by bumps around them as thick wall (Fig. 12-A, B). Though, they do not block the direct radiation in the summer, which increases the temperature in the space and then decreasing the comfort, especially in areas close to the windows (Table 2). In contrast, this treatment of the western facade improves the thermal comfort conditions in the winter, when the film windows allow direct light to reach the space and the thick wall improves the thermal mass and its ability to gain heat during the day and to release it during the night, thus improving the comfort percentage which led to a more comfortable environment. But the thick wall at the south façade of unit E2 combined with a deep balcony and wide windows (Fig. 12-C) caused, on the one hand very high TA in the summer (100%) by blocking the direct radiation and improving the thermal mass function through delay the heat transfer, but it caused very low TA in the winter (13%). The deep balcony and the thick wall created an

PLEA 2018 HONG KONG

Smart and Healthy within the 2-degree Limit

isolated area that prevented the unit rooms to gain heat and thus to an uncomfortable environment (Table 2). It can be seen that the western unit (E1), which is directed and organized according to the architects' general assumption (although it does function well in the summer), does not indicate the highest TA in the hot typical week compared with the southern unit E2. But it has the best performance in the typical cold week with relatively high comfort percentages (E1-47%, E2-13%). This shows that the architects' assumptions about the Western reference are not unequivocal, and especially towards the season they aimed at.

The two units E1 and E2 describe a different situation in the summer. While the southern E2 unit maintains an almost uniform and very high TA, the western E1 describes a more variable behavior. In the early hours of the morning, until 9:00, E1 points to lower TA percentage (about 85%), which is due to a lower operative temperature than the comfort zone. Between 9:00 and 14:00 the unit indicates higher percentages. From 14:00 until 16:00, the values decrease. This is due to operative temperature above the comfort zone due to the direct radiation that enters the space through the film windows on the western side. In the evening the comfort percentages are on the rise and this is probably due to the release of heat from the mass and the purge night ventilation. In the winter season, the two units describe similar behavior. The morning hours are less comfortable, and from 10:00 the TA improves. Unit E1 is being the most comfortable and E2 less comfortable with large differences especially in the afternoon and evening hours (Fig. 15). This stems mainly from the orientation, but also from the architectural elements through which the architect uses for each front.

5. CONCLUSION

In general, it can be seen that architects in the 1930's were, in most cases, able to produce residential units with comfortable interior environments during the summer season. Nevertheless, they were less comfortable during the winter. This statement suite the architects' discourse, directed mainly to the hot season. The architectural elements play an important role and affect the way the unit performs. Units having the same orientation but different treatment of their envelope have indicated different TA performance. In most cases the architectural elements, as balconies and openings etc. that were useful in the summer have harmed the unit's thermal performance in the winter. It can be concluded that architects who used architectural elements to protect residential units from the sun did that in a very strict way. In many cases these considerations led to very high comfort percentages during the summer but it produced cold and uncomfortable environments in the winter.

The recommended orientation by most of the architects (east-west) achieve lower TA percentages relative to south-north units, especially in the summer. However, in the winter it indicated the highest comfort rates.

The proposed methodology and results obtained provide an additional layer of knowledge in the understanding of the history of the Israeli-architecture and understanding of the climatic performance of the buildings as an integral part of their research and documentation process.

ACKNOWLEDGEMENTS

Thanks to the Technion - Israel Institute of Technology and to the PBC program for outstanding master students from minority groups for the scholarship.

REFERENCES

1. Metzger-Szmuk, N., (1994). Houses from the Sand. International Style in Tel-Aviv 1931-1948. Tel-Aviv: The Yehoshua Rabinovich Foundation for the Arts, (Hebrew).
2. ASHRAE. (2004). Standard 55-2004. Thermal Environmental Conditions for Human Occupancy. American Society of Heating, Refrigerating and Air-Conditioning Engineers: (ASHRAE).
3. Kallus, R., (1997). Patrick Geddes and the Evolution of a Housing Type in Tel-Aviv, *Planning Perspectives*, 12:3, 281-320.
4. Betser, A. (1984). Apartment Houses in Tel-Aviv in the Thirties – their Development, Concept and Design. Master's degree in Science, Department of Architecture and Town Planning, Technion (Hebrew).
5. Aleksandrowicz, O. (2015). Architecture's Unwanted Child: Building Climatology in Israel, 1940-1977. Thesis for Dr. Techn. Vienna: Technical University.
6. Adler, L. (1934). Why? Official New Immigrant, "The Building in the Near East", May, 11 (Hebrew).
7. Sharon, a. (1937). Planning of Condominiums. "The Building" - *Journal of Architecture and Town Building*, August, 1-4 (Hebrew).
8. BBSR. (2015). Tel Aviv White City: Modernist buildings in Israel and Germany. Germany: the Federal Office for Building and Regional Planning.
9. Nicol, F., M. Humphreys and S. Roaf, (2012). Adaptive Thermal Comfort, Principles and Practice. Routledge Publishing House.
10. Mackey, C., (2015). Pan Climatic Humans, Shaping Thermal Habits in an Unconditioned Society. M.Arch & M.Sc, MIT.
11. Webb, A. (2012). Mapping Comfort: An Analysis Method for Understanding Diversity in the Thermal Environment. M.Sc.: Submitted to the Department of Architecture MIT.
12. Sadeghipour Roudsari, M., M. Pak, (2013). Ladybug: a parametric environmental plugin for grasshopper to help designers create an environmentally-conscious design. In: Proceedings of the 13th International IBPSA Conference, Lyon, France.
13. US Department of Energy, [Online], Available: <https://energyplus.net/> [August 2018].
14. Eyal, T. (2014). Pre- Documentation File - Meonot HOD. The Municipality of Tel Aviv (Hebrew).
15. Bar Or, A. (2012). The Engel House Documentation File. Tel Aviv (Hebrew).

Environmental Benefits when Reusing Load-Bearing Components in Office Buildings: A case study.

ENDRIT HOXHA^{1,2}, CORENTIN FIVET¹

¹Structural Xploration Lab, École Polytechnique Fédérale de Lausanne (EPFL) & smart living lab, Switzerland

²Epoka University, Faculty of Architecture and Engineering, Department of Civil Engineering, Tirana, Albania

ABSTRACT: This case study applies life-cycle assessment methods to the preliminary design of an office building in order to quantify the benefits achieved when reusing its load-bearing components. Results show that the production of the load-bearing system would account for 40% of the global warming potential indicator. The slabs are responsible for 65% of the environmental impacts among all structural elements and should be considered for reuse first. Compared to traditional constructions built from first-use material, a fictitious reuse of undamaged load-bearing components over three consecutive use cycles would reduce the global warming potential indicator by 25%. The global warming potential of reuse is eventually computed according to three repartition methods, highlighting the need to separate the life-cycle footprints related to production, use, and end-of-life more systematically.

KEYWORDS: Building life cycle assessment, Net zero energy building, Reuse.

1. INTRODUCTION

The reduction of the environmental footprint of buildings is of great importance because they are responsible for 42% of final energy demand and 35% of greenhouse gases emissions [0].

The prevalent strategy consists in minimizing the environmental impact of the operational phase of the building. Design parameters and active or passive solutions are optimized to reduce the scale and the impacts of the energy demand for heating, cooling, ventilation, domestic hot water, lighting, and appliances [0-0]. Another strategy consists in minimizing the impacts of the construction and the end-of-life of the building by replacing detrimental components [0-0] with components of lower impacts [0]. This second strategy not only reduces greenhouse gases emissions. It also responds to the exhaustion of raw materials and to waste management issues, which includes land use and pollution considerations. The building industry is the heaviest and most voluminous waste streams in the European Union [0].

Counteracting the systematic landfilling of construction components, end-of-life solutions have been developed to recover the embodied energy in those components, to recycle them in new ones, or to reuse them as they are. Energy recovery and recycling are two largely implemented approaches [0-0] with a real potential to reduce the environmental impact and the quantity of waste produced by building industry [0-0]. Still, recycling requires additional energy for transforming the components even though recycled components are usually of lower value than their sourced components. More importantly, energy recovery and recycling are in most cases applied before the actual obsolescence of the building component, which forces its premature

replacement. Reuse is regarded as a more efficient solution [0].

The reuse of building components has been the object of numerous applications in practice [0-0]. Authors have also assessed the environmental benefits of reusing building components. Most of them consider that reused components have zero impact. Converging in quasi-similar results, they conclude that reuse reduces embodied energy and resources by 30% compared to traditional scenarios [0-0].

Other authors have assessed the environmental benefits of building projects whose components are designed to be reused in consecutive life cycle stages. According to Aye et al. [0], such option reduces embodied energy by 81%, 32% and 70% respectively for constructions in steel, concrete and timber. Akbarnezhad, et al. [0] show that designing to reuse structural elements in future building lifecycles reduce the embodied energy and carbon emissions respectively by 35% and 38%.

We believe that not only literature contains a limited number of studies but also that their results are not uniform even though such cases are of crucial importance in both scientific and practical terms. Non-uniformity is due to various reasons, mainly related to the choice of functional unit, boundary of the study, hypothesis and assumptions, environmental product declaration's database or building project considered in the evaluations.

Looking forward to more rigorous evaluations, this paper discusses the assessment of the environmental impacts of a building designed to be reused, through a complete cradle-to-cradle cycle. We produce a time-dependent comparison of scenarios reusing and not reusing load bearing systems. Discrepancies of three methods to allocate the benefits of reuse are eventually introduced.

PLEA 2018 HONG KONG

Smart and Healthy within the 2-degree Limit

2. METHOD

Environmental impacts are here assessed according to the European standard [0], which breaks down the building in its life stages: production (A1-A3), construction (A4 & A5), use (B1-B7), end-of-life (C1-C4) and benefits (D). Based on this standard, the production phase (A1-A3) considers the environmental impacts associated to the production of building material and components. The impacts related to the transport of components from their production factory to the building site and all the impacts and processes for the construction of building are considered in the construction phase (A4-A5). The impacts related to maintenance, repair, replacement, the refurbishment of components and energy and water use during the operation phase are included in the use phase (B1-B7). The impacts related to the demolition or deconstruction of the building, to the transport of its components to the waste site, and to their elimination are taken into account in the end-of-life phase (C1-C4). Module D considers all probable benefits resulting from the recovery, recycling or reuse of building components.

As the main objective of this work is the evaluation of the reuse of building components, energy and water use during the operational phase is not considered into the boundary of the study. The impacts of these stages are anyway minor in low or net zero energy buildings [0].

The reference study period of the building is assumed as equal to 60 years and the chosen functional unit is a square meter of floor area per year. Regarding the transport of components from factory to the building site and the processes linked with the construction phase, assumptions are similar to those considered in [0]. For simplification reasons, it is assumed that the renovation of the building happens after 30 years of its use and only comprises the replacement of the technical installations, windows, and doors. The KBOB database is used for the evaluation of impacts as it is found as the most pertinent for the Swiss context. This database relies largely on Ecoinvent [0] and contains information about the environmental impacts of building materials and components, which are evaluated in accordance with the CEN standard [0].

The cumulative energy demand, non-renewable energy and global warming potential indicators are assessed as they are considered as the most important according “2000-watt society vision” [0].

Finally, the problematic of the allocation of the benefits of reused is tackled while reviewing the various methods proposed in [0].

3. CASE STUDY

The office building that is used as case study is described in [0] and illustrated on Figure 1. It is a preliminary design that has been specifically developed to estimate the

future performance values of a yet-to-be-designed building in Fribourg, Switzerland. This upcoming building is meant to be representative of the future buildings' trends, according to the directives of the Council of the European Parliament, which requires all new buildings to be NZEBs by the end of 2020 [0]. Responding to this requirement the building has a very low environmental impact during its operational phase due to a well-insulated envelope ($0.1 \text{ W/m}^2\cdot\text{K}$) and the implementation of a district heating system, solar panels, and photovoltaics panels, for covering heating, cooling and electricity demands. With an energy reference area of 6035 m^2 mostly for office purposes, the load-bearing structure is supposed to be reversible and without any strong link with other non-structural components and systems.

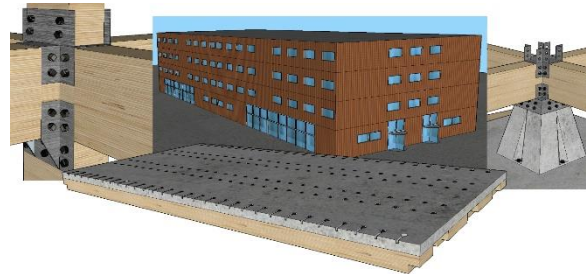


Figure 11: Conceptual design and some connectors.

The reinforced concrete foundation is connected to wooden beams and columns through steel connectors. Reversibility of the connections is everywhere ensured thanks to the use of bolts. The $3 \times 6 \text{ m}$ -slab consists in a 0.1 m -reinforced concrete layer bolted to $6 \times 0.6 \times 0.18 \text{ m}$ wooden beams. Following an approach similar to [0], we have assumed that a 40 t crane would lift the components during construction process and that a 1000-watt drill would tighten the bolts. The duration for lifting a slab or a wall is assumed equal to 30 minute. The duration for drilling each bolt is assumed equal to 30 seconds.

PLEA 2018 HONG KONG

Smart and Healthy within the 2-degree Limit

4. RESULTS

The results obtained for the cumulative energy demand (CED), non-renewable energy (CEDnr) and global warming potential (GWP) indicators are presented on Figure 2.

assumes that all elements are reused, meaning that the new versions of the building are exactly similar and that all reused components have a longer lifespan than at least three times that of the building.

The results for the cumulative energy demand (black),

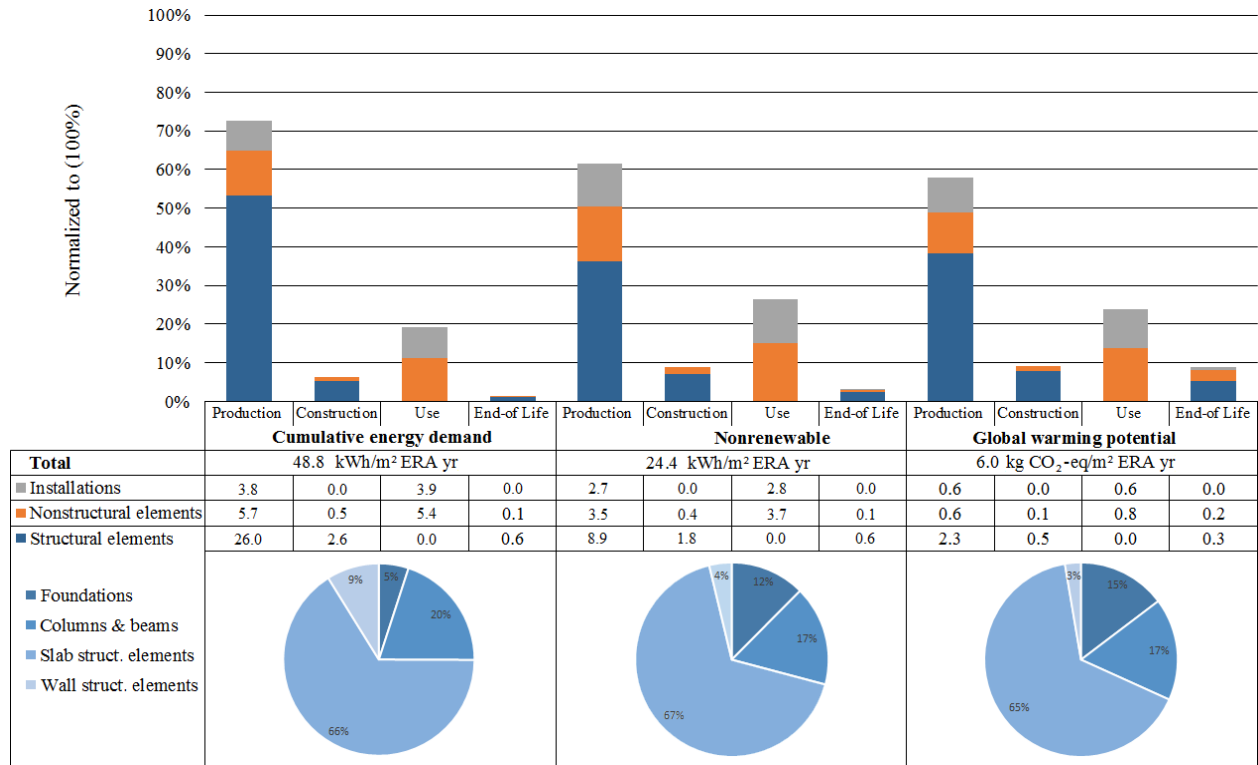


Figure 2: Environmental impacts.

A comparison of these impacts with the 2050 intermediate targets of the “2000-watt society vision” [0] – i.e. respectively 42 kWh/m² ERA yr, 36.1 kWh/m² ERA yr and 10 kg CO₂-eq/m² ERA yr [30-32] shows that only the non-renewable energy and global warming potential criteria are fulfilled. A more-detailed analysis is required to understand what changes are needed in order to satisfy the CED criteria. To that purpose, the bottom of figure 2 details the relative contribution of each construction elements to the overall environmental impacts of the building.

For all indicators the production phase is the biggest responsible with 72%, 60% and 58% respectively regarding the CED, CEDnr and GWP indicators. Moreover, the production of the structural elements and in particular the production of the slabs accounts for the highest impacts. Their reuse is therefore greatly encouraged. Figure 3 presents the distribution of impacts over time when columns, beams, slabs, and walls are reused over three consecutive use phases. This scenario is ideal since each transition to a new use phase assumes no damage due to deconstruction, transport, storage or reconstruction. Moreover, this scenario implicitly

non-renewable (red) and global warming potential (blue) indicators are compared for both the reuse scenario (solid line) and the traditional scenario (dashed line). The study shows that reuse can be a pertinent solution for significantly reducing the environmental impacts of buildings. For instance, the global warming potential indicator is 43% lower when the chosen structural components are used over three phases. The reduction of impacts is approximately 48% for renewable energy and 43% for non-renewable energy. These large numbers are not representative of conventional constructions since they are mainly due to the comparably very low operational energy demands.

Under reuse assumptions, the global impacts of the building eventually reach the 2150’ future targets [0].

PLEA 2018 HONG KONG

Smart and Healthy within the 2-degree Limit

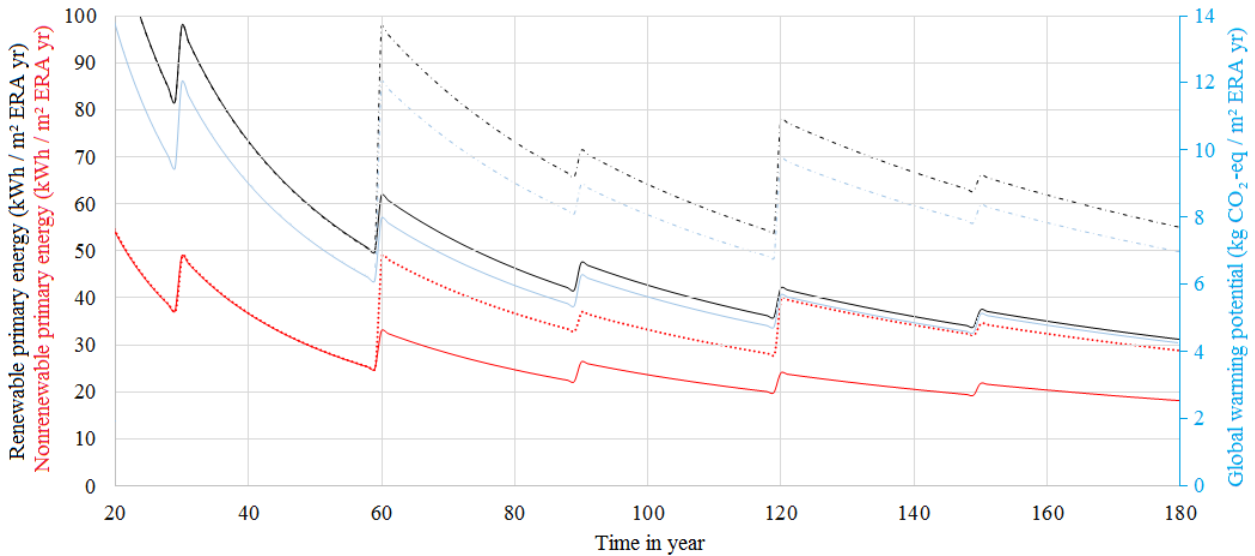


Figure 3: Dynamic analysis of the environmental impacts of the building with and without reuse of its load-bearing components.

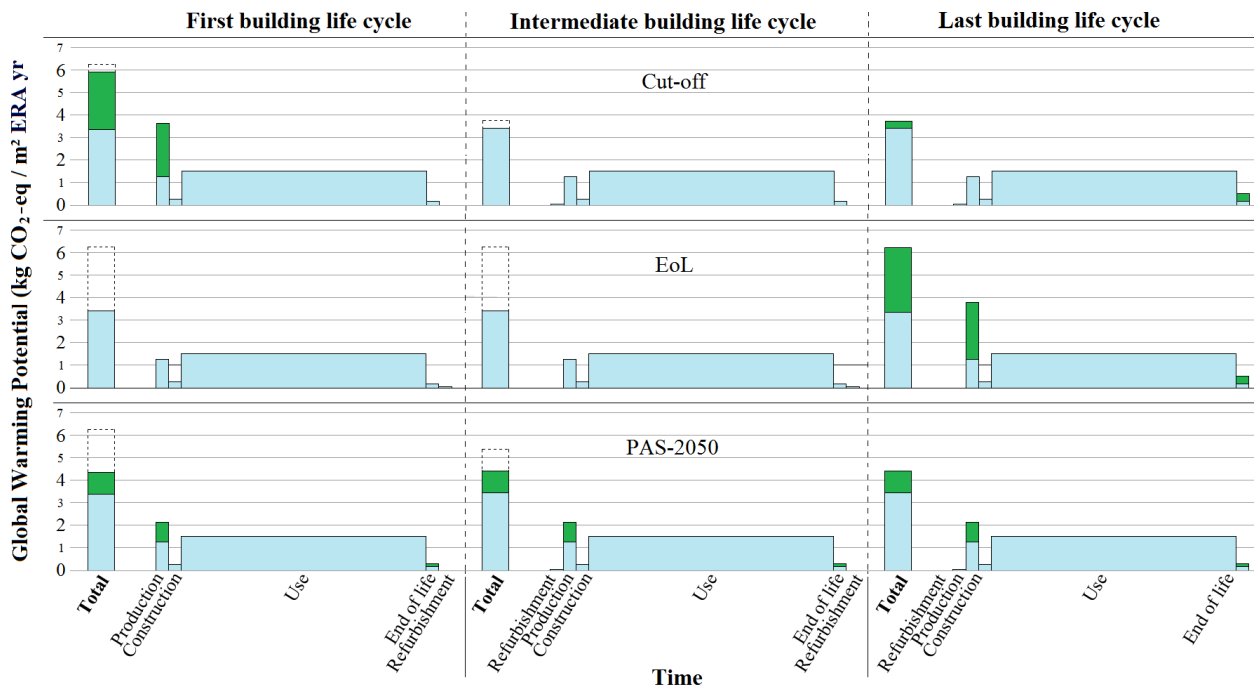


Figure 4: Allocation of impacts for three different methods of distributions, and according to the three representative types of life cycles.

Although this case study emphasizes the need for reusing load-bearing components, its practical implementation is undermined by the lack of consistent LCA indicators to encourage both the construction of reusable components and their reuse. Indeed, the way the LCA benefits are allocated to the various building actors highly influences their motivation to implement reuse. Figure 4 presents three possible distributions of the environmental impacts generated after reuse, as introduced in [0]. We here present them according to three representative types of life cycle: the first cycle,

which includes the manufacture of the component; all intermediary cycles, and the last cycle, which includes the end-of-life treatment of the component. This subdivision displays the discrepancy between the three aforementioned distribution methods.

According to the first method, i.e. the Cut-off method, the impacts of the production of the reused components are attributed to the first life cycle. According to the second method, i.e. the End-of-life (EoL) method, the impacts are attributed to the last life cycle. According to

PLEA 2018 HONG KONG

Smart and Healthy within the 2-degree Limit

the third method, i.e. the PAS-2050, impacts are distributed proportionally over all use cycles.

Let us first consider the impact of those distribution methods over their incentives to reuse. If one applies the cut-off method, the producer is not rewarded for producing components that can be reused. However, contractors who reuse the same components do not account for any impact related to those components.

The exact opposite behaviour stems from the EoL method. While producers are encouraged to build reusable components, building contractors take a high risk when reusing them. They are responsible for all environmental impacts if the components can no longer be reused.

The PAS-2050 rewards everyone in the same way and may therefore appear as ideal to promote reuse.

However, the above conclusion is different if the distribution methods are compared according to the degree of reliability of their calculated results. Indeed, the PAS-2050 method presents the largest uncertainties because the number of use cycles of a component is unknown before the component reaches its end of life. The EoL method also calculates unreliable results since the probability of reusing the building components elements after the current cycle is never 100%. Only the cut-off method provides results that can be considered as reliable because the method does not depend on future uses. From this point of view, we identified the Cut-off method as most reliable.

In conclusion, there is an impossibility to allocate the benefits of reuse in such a way that all actors are rewarded with reliable values. A direction of future research therefore consists in assigning reuse probabilities to every type of components, according to their potential uses, to the way they can be assembled and disassembled, and to the probable market demands. The resulting life-cycle assessment would then include an analysis of uncertainties.

5. CONCLUSION

This paper addressed the environmental benefits of reusing load-bearing components over multiple use cycles. The evaluation of the benefits is applied to a case study that considers the preliminary design of a state-of-the-art building to be constructed in the upcoming years. Results show that the impacts of the production of the load-bearing system would account for 38% of the global warming potential (GWP) indicator, and for 53% and 37% of the cumulative demand of renewable (CED) and non-renewable (CEDnr) energy respectively. Within the structural system, the slabs account for the largest impacts (66%) and would therefore be considered for reuse firstly.

Compared to traditional constructions built from raw material, a fictitious reuse of undamaged load-bearing components over three consecutive use cycles would

reduce the GWP indicator by 39% and the CED and CEDnr indicators by 43% and 36% respectively. These high numbers, although pumped up by very low operational energy demands, call for reversible structural systems and for the assessment of further case studies.

The paper concludes with a comparison of three methods to distribute the impacts of reuse between the various life cycles: the cut-off method, the end-of-life method, and the PAS-2050 method. This comparison highlights the impossibility to reward every reuse actor in a reliable way. Future research in the field shall focus on defining probabilities of reuse within uncertainty analyses.

REFERENCES

- European Commission, 2016. *Buildings-Energy*. Energy URL <https://ec.europa.eu/energy/en/topics/energy-efficiency/buildings>. (accessed : 14/05/2018).
- Perez-Lombard, L., Ortiz, J., Pout, C., 2008. A review on buildings energy consumption information. *Energy Build.* 40 (3), 394e398. <http://dx.doi.org/10.1016/j.enbuild.2007.03.007>.
- Ruiz, R., Bertagnolio, S., Lemort, V. (2012). Global sensitivity analysis applied to total energy use in buildings. *International High-Performance Buildings Conference*. Paper 78.
- Lasvaux, S., Lebert, A., Achim F., Grannec, F., Hoxha, E., Nibel, S., Schiopu, N., Chevalier, J. (2017). Towards guidance values for the environmental performance of buildings: application to the statistical analysis of 40 low-energy single-family houses' LCA in France. *The International Journal of Life Cycle Assessment* 22-5, 657-674.
- Häfliger, I.F., John, V., Passer, A., Lasvaux, S., Hoxha, E., Saade, M.R.M. and Habert, G., (2017). Buildings environmental impacts' sensitivity related to LCA modelling choices of construction materials. *Journal of Cleaner Production*, 156, pp.805-816.
- Hoxha, E., Habert, G., Lasvaux, S., Chevalier, J. and Le Roy, R. (2017). Influence of construction material uncertainties on residential building LCA reliability. *Journal of Cleaner Production*, 144, pp.33-47.
- Iribarren, D., Marvuglia, A., Hild, P., Guiton, M., Popovici, E., Benetto, E. (2015). Life cycle assessment and data envelopment analysis approach for the selection of building components according to their environmental impact efficiency: a case study for external walls. *J. Clean. Prod.* 87, 707e716. <http://dx.doi.org/10.1016/j.jclepro.2014.10.073>.
- European Commission (2016). Waste. Waste URL http://ec.europa.eu/environment/waste/construction_demolition.htm. (accessed : 14/05/2018).
- Guignot, S., Touzé, S., von der Weid, F., Ménard, Y., Villeneuve, J. (2015). Recycling construction and demolition waste as building materials. *Journal of Industrial Ecology*, 9, 6.
- Sullens, W., Hooper, B., Lent, T., Geiger, C., Vallette, J. (2015). Optimizing recycling: Criteria for comparing and improving recycled feedstocks in building products.
- Gao, W., Ariyama, T., Ojima, T., Meier, A. (2001). Energy impacts of recycling disassembly material in residential buildings. *Energy and Buildings* 33, 553-562.
- Blengini, A. (2009). Life cycle of buildings, demolition and recycling potential: A case study in Turin Italy. *Building and Environment* 44, 319-330.

PLEA 2018 HONG KONG

Smart and Healthy within the 2-degree Limit

- Commission to the European Parliament, the Council, the European Economic and Social Committee and the Committee of the Regions (2015). *Closing the loop - An EU action plan for the Circular Economy*, European Commission, Brussels.
- Falk, B., Guy, B. (2007). *Unbuilding: Salvaging the Architectural Treasures of Unwanted*. Taunton Press. ISBN-10: 1561588253.
- Gorgolewski, M. (2008). Designing with reused building components: some challenges. *Building Research & Information* 36:2, 175-188.
- Keller, J. (2011). Housing reclaimed. Sustainable homes for next to nothing. *New Society*. ISBN: 9780865716964.
- Thormark, C. (2000). Environmental analysis of a building with reused building materials. *International Journal of Low Energy and sustainability buildings*.
- Thormark, C. (2002). A low energy building in a life cycle-its embodied energy, energy need for operation and recycling potential. *Building and Environment* 37: 429-435.
- Diyamandoglu, V., Fortuna, L.M. (2015). Deconstruction of wood-framed houses: Material recovery and environmental impact. *Resources, Conservation and Recycling*, 100: 21-30.
- Aye, L., Ngo, T., Crawford, R. H., Gammampila, R., Mendis, P. (2012). Life cycle greenhouse gas emissions and energy analysis of prefabricated reusable building modules. *Energy and Buildings*, 47, 159-168.
- Akbarnezhad, A., Ong, K.C.G. Chandra, L.R. (2014). Economic and environmental assessment of deconstruction strategies using building information modeling. *Automation in Construction*, 37, 131-144.
- European Committee for Standardization (CEN) (2011). *Sustainability of construction works-assessment of environmental performance of buildings-calculation method*. FprEN 15978:2011.
- Hoxha, E. and Jusselme, T. (2017). On the necessity of improving the environmental impacts of furniture and appliances in net-zero energy buildings. *Science of The Total Environment*, 596, pp.405-416.
- Hoxha, E., Jusselme, T., Andersen, M., Rey, E. (2016). Introduction of a dynamic interpretation of building LCA results: the case of the smart living building in Fribourg, Switzerland. *Sustainable Built Environment (SBE)*. Zurich, Switzerland.
- Frischknecht, R., Friedli, R., Gugerli, H. (2013). The Swiss platform of life cycle assessment data in the building sector-connecting industry, administration, builders and research. *The 6th International Conference on Life Cycle Management in Gothenburg*.
- EN-15804, *Sustainability of Construction Works. Environmental Product Declarations. Core Rules for the Product Category of Construction Products*, European Committee for Standardization (CEN), 2012, ISBN: 9780580822322.
- SIA 2040, 2011. *Path to Energy Efficiency* (in French) Society of Engineers and Architects, Switzerland.
- BSI, PAS 2050 – Assessing the life cycle greenhouse gas emissions of goods and services. The British Standard Institute, 2008.
- Jusselme, T., Brambilla, A., Hoxha, E., Jiang, Y., Vuarnoz, D., Cozza, S. (2015). Building 2050-Scientific concept and transition to the experimental phase (No. EPFL-REPORT-214874).
- Glias, A. (2013). *The "Donor Skelet" Designing with reused structural concrete elements*. Master thesis. TUDelft university of technology. The Netherlands.
- Kellenberger, D. Ménard, M. Schneider, S. Org, M. Victor, K. Lenel, S., (2012). Réhabiliter des friches industrielles pour réaliser la société à 2000 watts. Guide et exemples, Projet conjoint de Stadt Zürich, Zürich ewz, Confédération Suisse, Switzerland.
- Hoxha, E., Jusselme, T., Brambilla, A., Cozza, S., Andersen, M., Rey, E. 2016. Impact targets as guidelines towards low carbon buildings: A preliminary concept. *PLEA 2016*. Los Angeles, USA.

New Framework For Quantifying Outer Luminous Variation Through Dynamic Methods

FRANCISCA RODRIGUEZ^{1,2}, VERONICA GARCIA-HANSEN¹, ALICIA ALLAN¹, GILLIAN ISOARDI¹

¹Queensland University of Technology, Brisbane, Australia
²Universidad Tecnica Federico Santa Maria, Valparaiso, Chile

ABSTRACT: Providing access to a view out is fundamental for ensuring healthy living conditions in indoor spaces; however, there are no procedures for capturing luminous variations of a view over time. The study introduces a dynamic method for quantifying such variables through HDR time-lapse photography and digital image-processing techniques. Two series with analogous contextual features portrayed three consistent luminous variability conditions. Local luminous variation suggests the highest potential to influence visual response. Finally, the paper discusses design implications and future refinements to the methodology.

KEYWORDS: View, Dynamic Methods, Lightness, Time-Lapse, Image-Processing.

1. INTRODUCTION

Developing methods for evaluating health and wellbeing is one of the major interests of researchers in the daylighting field, as time spent indoors increases while the exposure to direct sunlight and environmental variables decreases [1]. Along with daylight, providing access to a view out is one of the most important factors for ensuring healthy living conditions in indoor spaces [2], to the point that it has been suggested that having a view out might be even more important than letting daylight in [3]. A view establishes a sense of connectedness to the outer environment that stimulates general wellbeing in the long term [4]. It also provides cues for estimating relevant contextual information through constant changes in luminous conditions. Nevertheless, there are currently no procedures for capturing these environmental luminous variations in view over time, which limits the ability to examine the impact of such variation on health and wellbeing. The lack of a validated framework for evaluating the dynamic character of the outer environment constitutes a major gap in research, especially when compared to the well-established dynamic daylight evaluation methods, currently in use [5-7]. View out has been examined from multiple perspectives, including building sciences, environmental psychology, and with an interdisciplinary approach.

1.1 View evaluation: building sciences

From the perspective of building sciences, view out is generally assessed through simulations, as it is considered a natural effect of window design [8]. From a similar performance-driven approach, some authors in the field have addressed the study of view by analysing external obstructions in relation to acceptable unobstructed visual areas and visual openness [9-10], by implementing graphic representations and simulations in

the context of high-density cities for urban planning purposes.

Researchers in the architectural field, on the other hand, have emphasised how occupants perceive a view by examining how windows induce aesthetic delight, visual interest and an overall sense of connectedness to the outer environment, as depicted in static imagery [11-12]. In search for design patterns, architectural researchers enumerated design parameters and view characteristics with potential to convey positive effects to the viewers in terms of wellbeing [13-14]. As an example, Markus [14] outlined various principles for view-satisfactory window design in buildings, and information content (i.e., the extent of sky, city or landscape, and ground that a view out contains as seen from a static position) is the most relatable approach for analysing the quality of a view out. The information content analysis of static view imagery has become the most implemented approach to evaluating the quality of a view out within the field, although there have been further adaptations in terms of composition and character [15].

1.2 View evaluation: environmental psychology

With a focus on evaluating compositional attributes with the potential for enhancing people's lives, the environmental psychology field has largely discussed the benefits of accessing a view out for improving health and wellbeing. Based on precursor studies conducted for evaluating the influence of nature on preference [16], researchers in the field examined the exposure to natural features in different settings, suggesting consistent results. A view out that provides such information can have a positive impact on hospital patients –by shortening time of recovery [17]; office workers –by improving job satisfaction [18] and relieving physical and physiological symptoms of discomfort [19]; and school

PLEA 2018 HONG KONG

Smart and Healthy within the 2-degree Limit

students – by supporting scoring in tests [20-21] and directed attention restoration [21]-. In recent years, the scope of these studies has extended to the evaluation of different urban features in view scenes, providing interesting findings that suggest a clear relationship between familiarity and visual preference [22].

Similar to the methods adopted in building sciences, the environmental psychology field rely on qualitative descriptors of static imagery to evaluate view out. Most of these studies based their findings on a combination of surveys with the qualification of static imagery or naturalistic observations of a view out at specific moments [23]. However, researchers in the field have pointed the importance of continuous exposure to environmental view for receiving its full restorative potential [16]. Therefore, there is a need for approaches implementing a dynamic evaluation of view.

1.3 View evaluation: interdisciplinary approach

Recent interdisciplinary studies have proposed new approaches to assessing the benefits of a view out, combining dynamic methods for daylight evaluation with view preference conditions outlined by environmental psychology research [16]. By integrating dynamic evaluative methods and theoretical knowledge from different disciplines, researchers suggested that a complex view out would diminish the perception of glare reported by building occupants [24]. Similarly, researchers established a new approach for integrating dynamic daylight and view out, by quantifying daylight gain over time -illuminance levels- from windows previously weighed in terms of view preference through surveys [25].

The exposed studies provide critical contributions to our understanding of view; however, a comprehensive study focused on evaluating dynamic luminous variations in view would provide a better comprehension of such conditions on health and wellbeing. Furthermore, the assessment of view over time could facilitate the development of an integrated dynamic daylight and view framework, in order to establish a comprehensive evaluation of indoor luminous conditions for health and wellbeing in buildings.

1.4 View evaluation: proposed framework

Implemented by computer vision, digital image-processing techniques have developed dramatically in recent years [26]. Recently, researchers in building sciences started utilising such methods for depicting luminous information from HDR imagery, both from naturalistic photographs and computer-generated imagery [27-30]. The employment of new techniques refreshes the existing toolkit available for dynamic representation of static scenes, as is the case of time-lapse photography. Enabling an accurate depiction of variations over time, time-lapse photography is a

technique consistently used for the study of movement [31].

In search for new methodologies to examine environmental variation, the present study proposes a method for the dynamic evaluation of outer luminous variations, using HDR time-lapse photography and applying digital image-processing techniques. This technique will be used to create a framework for quantifying outer luminous variations in view scenes over time. This approach could be used to assess how a view can contribute to health and wellbeing in building occupants in future experiments and field studies.

2. RESEARCH QUESTION, AIMS AND OBJECTIVES

By implementing a protocol for data collection of HDR time-lapse photography over time, to be tested through digital image-processing techniques, the present study aims to explore ways to illustrate, describe and analyse outer luminous variations across the day. In particular, this study aims to delve into different types of luminous variability conditions with the potential to influence visual response over time, by establishing preliminary thresholds within prospective categories. Finally, the present study aims to infer view scene characteristics that might influence luminous variations in future experiments, by comparing outcomes between different view series.

3. METHODOLOGY AND METHODS

3.1 Light attributes

Previous studies outlined luminous attributes that can assist with the description of indoor visual and perceived conditions [32-33]. Due to its potential to depict the subjective visual experience of a view out, the present study focused on quantifying variability of *lightness* in outer environments. The authors acknowledge that chromatic attributes -such as colour rendering and colour appearance- may also influence in the dynamic study of view out; hence, it is expected that future stages of this research will take such attributes into consideration.

3.2 Related variables

A large number of additional variables are likely to influence both the extent to which view luminous conditions vary, and human perception of a view out. To take these into consideration, the authors implemented a preliminary categorisation of variables to structure the collection of data.

3.2.1 View features

According to literature, three independent features are potentially relevant to the characterisation of luminous variations in view [2, 5]: visual features (i.e., *nature* and *urban*); proximity (i.e., *near* and *distant*); and orientation (i.e., view facing *north*, *south*, *east* or *west*). Although

PLEA 2018 HONG KONG

Smart and Healthy within the 2-degree Limit

examining a range of view types combinations would be ideal, the core aim of the present study is to assess a method for capturing outer luminous variability rather than to evaluate visual preference among people. Hence, this study will focus on evaluating luminous variations in view over time from two series with the following visual features: *urban*; proximity: *near*; and orientation: *south*.

3.2.2 Sky conditions

With an average of 113 days per year with clear sky conditions [34], the city of Brisbane (Queensland, Australia) is a good location for collecting naturalistic time-lapse HDR imagery under clear sky conditions, as it conveys luminous dynamism at a surface level. At the same time, intermittent sky is also a good source of variation. For this study, the authors considered both clear and intermittent sky models.

3.3 Data collection and analysis

3.3.1 Series collection

As a data collection protocol, the authors gathered a series of representative view scenes through time-lapse photography using 30-minute interval between photos. Previous calibration also considered time intervals of 15, 30 and 60 minutes, however the 30-minute interval was chosen to have an appropriate sensitivity to lighting changes. An intervalometer controlled the collection of photographs. To create HDR images, multiple exposure photographs were taken with a Canon EOS 550D camera fixed on a tripod, and a Canon 18-55 mm f1:3.5-5.6 IS lens. Next, the authors processed the collected multiple exposure photographs with the assistance of HDR software.

Due to the broad availability of view scenes with different contextual information, the authors collected data at Queensland University of Technology, Gardens Point Campus during the month of May 2018. The collection consisted of eight time-lapse HDR image series, processed according to the series (Series 01: Clear sky conditions; Series 02: Intermittent sky conditions). As discussed in section 3.2.1, this paper presents two series with specific contextual characteristics (Fig. 1).

3.3.2 Processing protocol

The authors developed two routines in MATLAB software. The first routine consisted of collecting lightness information from each image by converting the series of HDR time-lapse photography into CIE L*a*b* colour space matrices, and extracting per-pixel lightness values

from L* channel -where values range from the darkest L*=0 to the brightest L*=100 (Fig.2)-. This action facilitated a preliminary evaluation of lightness distribution, and provided inputs for the following routines. The second routine consisted on calculating the absolute difference between two consecutive matrices depicting lightness values from L*channel, and iterating this routine until completing the series. According to the Commission Internationale de l'Eclairage (2004), lightness differences between two samples could be described as absolute differences, which can be used for the study of lightness variability as follows (Equation 1):

$$\text{Lightness Variability } (\Delta L^*) = |NL^* - ML^*| \quad (1)$$

, where M and N are two consecutive matrices depicting absolute difference values from L*channel after two consecutive images were converted into CIE L*a*b* colour space.

4. ANALYSIS AND RESULTS

4.1 Lightness variability evaluation within the series

After processing the collected HDR time-lapse series, three different types of luminous variation emerged from this study:

No luminous variation, described as time intervals where luminous conditions remained unaltered, or Lightness Variability <20,

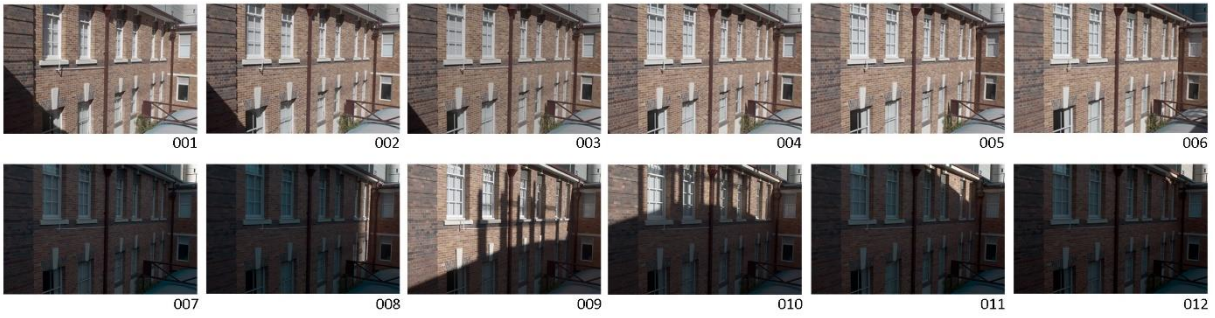
Global luminous variation, described as variations in luminous conditions over time following predictable movement of lightness paths within the series, with Lightness Variability ranging from 30-60. In some circumstances, higher Lightness Variability ranges (60-80) applied; however, the predictability of lightness paths' movement remained unaltered, *Local luminous variation*, described as Lightness Variability peaks (>80) at specific time intervals within the series that are difficult to predict.

The abovementioned luminous conditions appeared within Series 01 and Series 02: *No luminous variation* (e.g., Series 01, time intervals 005-004; Series 02, time intervals 011-010) barely appears in Series 01, which is probably due to the absence of lightness variability values from the sky, and direct solar incidence on the building surface creating shadows. In opposition, this condition clearly appears in Series 02 over several time intervals under intermittent sky and without direct solar incidence on the building surface (Fig.3).

PLEA 2018 HONG KONG

Smart and Healthy within the 2-degree Limit

Series 01



Series 02

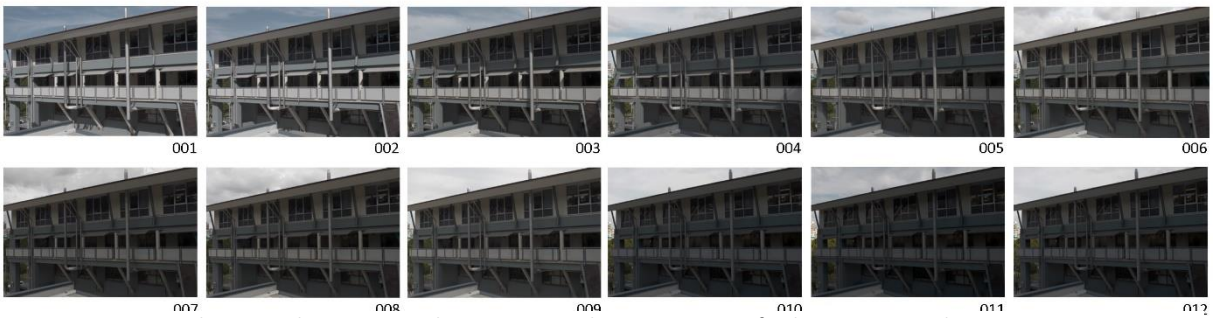
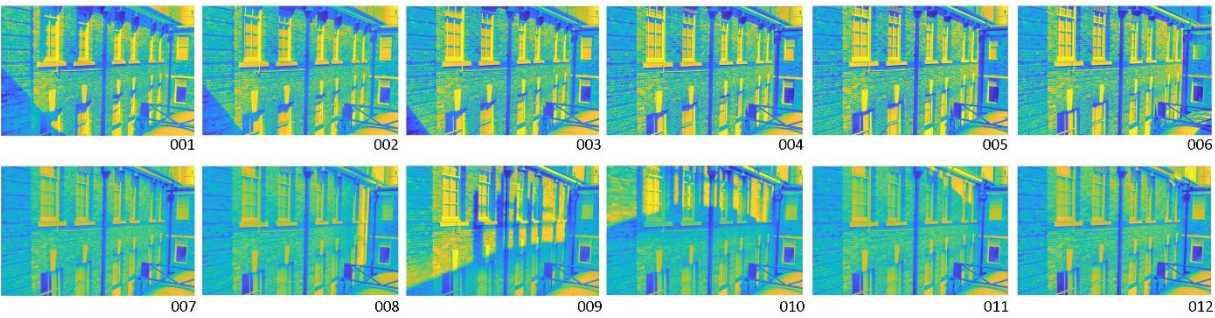


Figure 1: Series 01 and 02, time-lapse images depicting naturalistic sequences of Urban, Near, South View Scenes.

Series 01



Series 02

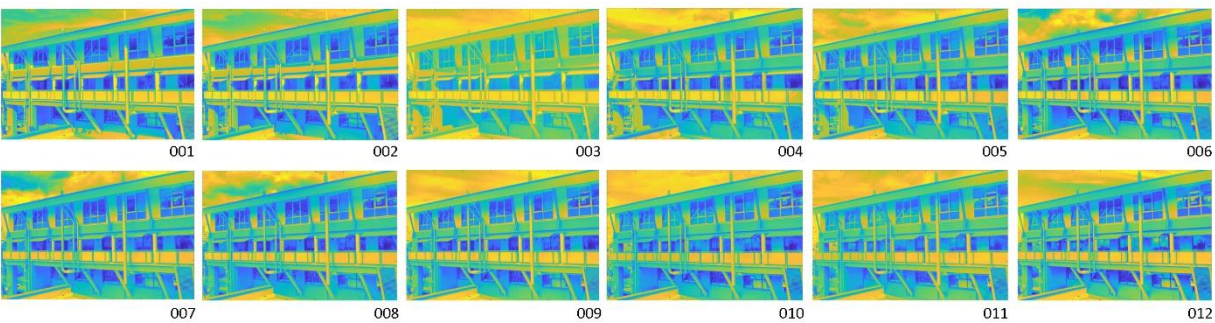


Figure 2: Series 01 and 02, time-lapse images depicting lightness values (L^*) of Urban, Near, South View Scenes

Global luminous variation (e.g., Series 01, time intervals 002-001 and 003-002; Series 02, time intervals 002-001 and 005-004) appears constantly in Series 01, due to changes of the solar angle projecting shadows over the building surface (Fig.4). Lightness paths' movements are predictable, and clearly portrayed in 30 minutes time intervals. In Series 02, this condition is difficult to notice, as sky intermittences makes lightness paths' movements difficult to predict on the building surface.

Local luminous variation (e.g., Series 01, time intervals 008-007, 009-008 and 011-010) clearly appears in Series 01, that is, under clear sky conditions (Fig.5), and is not noticeable in Series 02, that is, under intermittent sky conditions. The authors noticed that, apart from its unpredictability, this condition has a higher variability speed than *Global luminous variation*, which may influence visual interest and visual response. This condition suggests great potential for the purposes of

PLEA 2018 HONG KONG

Smart and Healthy within the 2-degree Limit

evaluating the impact of environmental luminous variations on health and wellbeing. It is therefore necessary to refine the collection methodology in order to assess variability speed issues from this condition in future stages of this research.



Figure 3: Series 02, time intervals i11-i10, depicting No luminous variation.

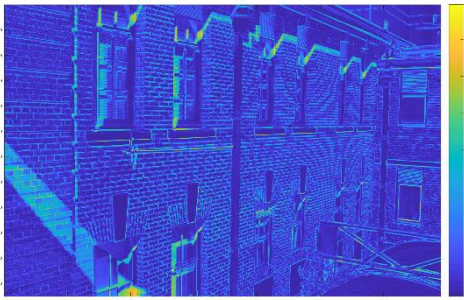


Figure 4: Series 01, time intervals i2-i1, depicting Global luminous variation.



Figure 5: Series 01, time intervals i9-i8, depicting Local luminous variation.

4.2 Lightness variability evaluation between the series

As discussed in section 3.2, the series presented in this study depicted equivalent scene information (i.e., visual features: *urban*; proximity: *near*; and orientation: *south*) and different sky conditions (Series 01: Clear sky conditions; Series 02: Intermittent sky conditions). For this sample, quantitative differences in lightness values are clear, particularly concerning minimum and maximum lightness values and its distribution across the day. The authors acknowledge that such differences correspond to individual attributes of the settings, as the reflectance values and characteristics of each setting will

differ; nevertheless, observations on the morphology of a view out may also provide explanations on such differences. As an example, the rotation angle of the exposed features in relation to the point of view that may influence the exposure to direct sunlight, as well as non-portrayed features that may generate unexpected shadows over a view scene are inherent conditions of the urban scenery and may inform further stages of this study.

5. DISCUSSION

The present study introduced a dynamic method for quantifying environmental luminous variations in view scenes over time, using HDR time-lapse photography and applying digital image-processing techniques. Overall, this study provides new insights with the potential to contribute to the dynamic evaluation of outer luminous conditions.

The observation of lightness values across the day permitted the characterisation of three types of luminous variability showing potential to influence visual interest and visual response. In the future, the study of luminous variability should also assess chromatic attributes as depicted in view scenes, aiming to portray an accurate representation of view out [4], and to determine thresholds that would help understand how different attributes influence visual response in building occupants over time.

In this study, luminous variability was considered in a limited type of view scenes under two different sky conditions. The categorisation of previous theoretical findings in literature [2-5] facilitated the comparison of similar view scenes. Future stages of this study would include other features from view scenes, aiming to establish a broader sample for examining environmental luminous variations in view.

Finally, the study outlined future adjustments to the methodology, aiming to provide a more complete depiction of luminous variation in view scenes. First, a control study among a small group of participants would help establishing clearer thresholds within different luminous conditions and examining the implications of other attributes of luminous variation (e.g. colour) and view configuration (e.g. number of depth layers) on visual response towards the exterior. Second, the collection of a diverse range of view scenes would facilitate the comparison between variability conditions among different types of urban, natural and combined settings. Lastly, a measurement protocol for collecting lightness and chromatic variability data would facilitate the calibration of the framework, and encourage new experiments and field studies in the future.

ACKNOWLEDGEMENTS

The first author acknowledges the Faculty of Creative Industries, Queensland University of Technology (QUT)

PLEA 2018 HONG KONG

Smart and Healthy within the 2-degree Limit

for supporting this PhD research through a Postgraduate Research Award, and the Department of Architecture, Universidad Tecnica Federico Santa Maria (UTFSM) for continuous financial sponsorship.

REFERENCES

1. Klepeis, N. E., Nelson, W. C., Ott, W. R., Robinson, J. P., Tsang, A. M., Switzer, P., Engelmann, W. H. (2001). The National Human Activity Pattern Survey (NHAPS): a resource for assessing exposure to environmental pollutants. *Journal of Exposure Science and Environmental Epidemiology*, 11(3), 231.
2. Kaplan, R. (2001). The nature of the view from home: Psychological benefits. *Environ Behav*, 33(4), 507-542.
3. Boyce, P., Hunter, C., & Howlett, O. (2003). *The benefits of daylight through windows*. New York: LRC.
4. Granzier, J. J., & Valsecchi, M. (2014). Variations in daylight as a contextual cue for estimating season, time of day, and weather conditions. *J Vision*, 14(1), 22-22.
5. Reinhart, C. F., Mardaljevic, J., & Rogers, Z. (2006). Dynamic daylight performance metrics for sustainable building design. *Leukos*, 3(1), 7-31.
6. Andersen, M. (2015). Unweaving the human response in daylighting design. *Build Environ*, 91, 101-117.
7. Konis, K. (2017). A novel circadian daylight metric for building design and evaluation. *Build Environ*, 113, 22-38.
8. Van Den Wymelenberg, K. G. (2014). Visual comfort, discomfort glare, and occupant fenestration control: developing a research agenda. *Leukos*, 10(4), 207-221.
9. Ng, E. (2010). Designing for Daylighting. In Ng, E. (Ed.), *Designing high-density cities: for social and environmental sustainability* (pp. 181-194). New York, NY; Earthscan.
10. Shach-Pinsly, D., Fisher-Gewirtzman, D., & Burt, M. (2011). Visual exposure and visual openness: an integrated approach and comparative evaluation. *Journal of Urban Design*, 16(2), 233-256.
11. Steane, M. A. (2004). Environmental diversity and natural lighting strategies. In K. Steemers & M. A. Steane (Eds.), *Environmental Diversity in Architecture* (pp. 159-178). New York, NY; London, England: Spon Press.
12. Jacobs, J. M., Cairns, S., & Strelbel, I. (2012). Materialising vision: Performing a high-rise view. In D. P. Tolia-Kelly & G. Rose (Eds.), *Visibility/materiality: Images, objects and practices* (pp. 133-152). Burlington, VT; Farnham, Surrey, England: Ashgate Publishing, Ltd.
13. Alexander, C., Ishikawa, S., Silverstein, M., i Ramió, J. R., Jacobson, M., & Fiksdahl-King, I. (1977). *A pattern language*. Barcelona: GG.
14. Markus, T. A. (1967). The function of windows—a reappraisal. *Building Science*, 2(2), 97-121.
15. Matusiak, B. S., & Klöckner, C. A. (2016). How we evaluate the view out through the window. *Architectural Science Review*, 59(3), 203-211.
16. Kaplan, R., & Kaplan, S. (1989). *The experience of nature: A psychological perspective*. Cambridge: CUP Archive.
17. Benedetti, F., Colombo, C., Barbini, B., Campori, E., & Smeraldi, E. (2001). Morning sunlight reduces length of hospitalization in bipolar depression. *Journal of affective disorders*, 62(3), 221-223.
18. Farley, K. M., & Veitch, J. A. (2001). A room with a view: A review of the effects of windows on work and well-being.
19. Aries, M. B., Veitch, J. A., & Newsham, G. R. (2010). Windows, view, and office characteristics predict physical and psychological discomfort. *Journal of Environmental Psychology*, 30(4), 533-541.
20. Heschong, L., Wright, R. L., & Okura, S. (2002). Daylighting impacts on human performance in school. *Journal of the Illuminating Engineering Society*, 31(2), 101-114.
21. Tennessen, C. M., & Cimprich, B. (1995). Views to nature: Effects on attention. *Journal of Environmental Psychology*, 15(1), 77-85.
22. Herzog, T. R., & Shier, R. L. (2000). Complexity, age, and building preference. *Environ Behav*, 32(4), 557-575. Herzog and Schier 2000
23. Mirza, L. (2015). *Windowscapes: A Study of Landscape Preferences in an Urban Situation*. Doctoral dissertation, ResearchSpace@ Auckland.
24. Tuaycharoen, N., & Tregenza, P. (2007). View and discomfort glare from windows. *Lighting Research & Technology*, 39(2), 185-200.
25. Hellinga, H. (2013). *Daylight and view: the influence of windows on the visual quality of indoor spaces*. Doctoral dissertation, TU Delft, Delft University of Technology.
26. Gonzalez, R. C., Woods, R. E., & Eddins, S. L. (2009). *Digital Image Processing Using MATLAB®*: Gatesmark Publishing.
27. Sadeghi Nahrkhalaji, R. (2017). *Study of Building Surrounding Luminous Environment using High Dynamic Range Image-Based Lighting Model*. Doctoral dissertation, The Pennsylvania State University.
28. Rockcastle, S., & Andersen, M. (2014). Measuring the dynamics of contrast & daylight variability in architecture: A proof-of-concept methodology. *Building and Environment*, 81, 320-333.
29. Jakubiec, J. A., Van Den Wymelenberg, K., Inanici, M., & Mahic, A. (2016). *Improving the accuracy of measurements in daylit interior scenes using high dynamic range photography*. Paper presented at the Proceedings of the 32nd PLEA Conference, Los Angeles, CA, USA.
30. Cauwerts, C., & Piderit, M. B. (2018). Application of High-Dynamic Range Imaging Techniques in Architecture: A Step toward High-Quality Daylit Interiors? *Journal of Imaging*, 4(1), 19.
31. Weston, C. (2016). *Spanning time the essential guide to time-lapse photography*. New York : Focal Press.
32. Liljefors, A. (1999). *Lighting—visually and physically*. *Lighting Department, Arkitekturskolan, KTH, Stockholm*.
33. Cauwerts, C. (2013). *Influence of presentation modes on visual perceptions of daylit spaces*. Doctoral dissertation, Université catholique de Louvain (UCL), Louvain-la-Neuve, Belgium.
34. Bureau of Meteorology, Australian Government. Climate statistics for Australian locations. http://www.bom.gov.au/climate/averages/tables/cw_040214.shtml. Accessed on May 2018.

Optimal Design of Urban Thermal Environment Using 3D City Models and Numerical Simulation: A Case Study of a Historical District in China

YANWEN LUO¹, JIANG HE¹, JUNMU QIU¹, NANXIONG HUANG¹

¹Architecture and Urban Planning Department, Civil Engineering & Architecture College, Guangxi University, Nanning, China

ABSTRACT: It is becoming more and more important to create a comfortable thermal environment in cities. In order to increase consideration of the thermal environment in the planning and design process, this study proposed a method to combine rule-based rapid modelling with thermal environment simulation. This method can realize the flexible and visualized presentation of landscape and the thermal environment effect. Meanwhile economic cost of design elements was also taken into consideration. The proposed method can support the designers to evaluate the trade-offs among landscape, thermal environment and cost and then choose a better scheme. A historic district in China was taken as a case study object in this paper. Three optimization plans were made by changing building height, greening space and area of water-permeable pavements. Through visual analysis of 3D landscape models and thermal simulations, it was found that the green space and water-permeable pavements had an obvious effect on the improvement of the thermal environment, but control of building height had negative thermal improving effect. The proposed method also effectively improved public understanding of reconstruction design and thermal environment formation.

KEYWORDS: Urban reconstruction, Historical district, Rule-based modelling, Thermal environment, Trade-offs analysis

1. INTRODUCTION

The thermal environment in many cities of China has deteriorated as a result of rapid economic development, industrialization, and accelerating urban development. Thus the built thermal environment has become a hot research issue [1-2]. Though many studies have used numerical simulations to explore the relationship between characteristics of the built environment and the urban thermal environment, there is still a significant room for applying these findings to city design. For example, many studies indicate that increasing tree coverage and water area could improve the thermal environment. However, seldom have explained the trade-offs among landscape, thermal effect and costs under consideration of increase of trees and water areas [3-4]. Furthermore, the existing research is lack of look at thermal environments in urban historical districts. Understanding the factors that can produce a good urban thermal environment in historic districts could support city reconstruction and preserve historical heritage [5-6]. If 3D city models of a historical district could be combined with thermal evaluation index based on numerical simulation, it would be more visualized for planners to analyze the trade-offs among different factors. In order to fill this gap in the literature, this study proposed an integrated approach of rule-based 3D city modelling and numerical simulation to identify landscape design factors that could improve the thermal environment in historical districts. A case study was conducted for a historical district in a southern city of China, Nanning.

2. METHODOLOGY

2.1 Research concept

The principal methodology of this study was to use rule-based city 3D modelling to efficiently build 3D city models for different design schemes and then conduct numerical simulation to evaluate the thermal environment for the schemes. Through changing the landscape design conditions for each scheme and making cost estimation of the optimized schemes, we established relationship among the landscape, thermal environment and cost. This analysis assisted planners to have a visual understanding of the trade-offs among scenery, thermal environment and cost. Moreover, as the result was visualized, it can improve public understanding of the effect from optimization design. Fig.1 shows the research framework.

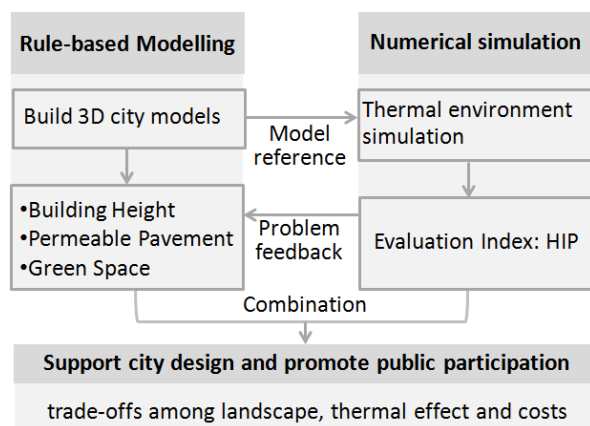


Figure 1: Research framework

PLEA 2018 HONG KONG

Smart and Healthy within the 2-degree Limit

Firstly, 3D models for the study district were built using the rule-based modelling method. The thermal environment in the study district was simulated and the simulation results were used to identify thermally uncomfortable locations. Secondly, the following design factors for improving the thermal environment in uncomfortable locations were considered: building height, water-permeable pavements and green space. Thermal simulations for each optimized design were also conducted. Thirdly, 3D models were combined with thermal simulation and improvement cost to support city design and promote public participation.

2.2 Rule-based modelling method

Most of popular interactive modelling methods such as AutoCAD and SketchUp, have limited capability in large and medium-scale 3D city modelling as mentioned in Reference[5]. Against this background, a rule-based modelling method was gradually applied in the field of city modelling. For city model generation, a rule means using computer languages to describe and determine how to generate the models [5]. Nowadays, there is computer software using the rule-based idea to build models, such as CityEngine (CE), City Gen, OL-system. Because CE is focused on city construction and is fully functional, it is selected to be used to build 3D city models in this study.

The modelling principle of CE is to describe how to generate models using a computer language called CGA (Computer Generated Architecture), and CGA programs is written in the rule file of CE. The CGA program can be reused in modelling different objects, and its models can be automatically adjusted and adapted to terrain and shape as long as the requirements are defined. Thus, the 3D city models can be constrained and unified or standardized by CGA, reducing the cumbersome process of model generation. The larger the city area and the more regular the city appearance is, the greater the advantage of CE modelling will have [5].

2.3 Thermal environment simulation

This study conducted the thermal simulation using a thermal simulation tool called ThermoRender (TR). Because the 3D models made by CE could not be directly input to TR, a 3D-CAD software called VectorWorks (VW) was used to build simulation models by referencing the

CE models. TR is an integrated simulation program in VW and can evaluate the impact of analyzed buildings or urban blocks on the outdoor thermal environment by two indices based on urban surface temperatures [7]. One index is the mean radiant temperature (MRT) for evaluating the thermal radiant effect, and the other is the heat island potential (HIP), which indicates the total sensible heat from all surfaces of the urban block being analyzed.

Because this study aims to discuss the relationship between design elements and overall thermal environment, HIP is more suitable to be the evaluation index of the thermal environment. HIP is expressed as the measure of a temperature, and is calculated by:

$$HIP = \frac{\int_{all_surfaces} (T_s - T_a) dS}{A}$$

where HIP is heat island potential (°C), T_s is surface temperature of each mesh (°C), T_a is air temperature (given from weather data) (°C), A is plane area of the urban block (m^2), and dS is area of each mesh (m^2). When HIP is positive, it means that the urban air is heated by the urban surface to form a heat island effect; when HIP is negative, it means that the urban air releases heat to the urban surface. Many studies have shown that during daytime in summer, HIP reached 25°C in the areas with concrete-built coverage of 70%. HIP was below 15°C for the areas where vegetation coverage is 50% [7].

3. CASE STUDY

Water Street is a historical district located in the downtown of Nanning, south China (Fig.2). Nanning is in the hot-summer and warm-winter region and its climate can be characterized by strong solar radiation and long hours of sunshine in summer. Water Street is the birthplace of Nanning City. However, with the rapid development of the city, Water Street has been gradually demolished and forgotten by the residents. The preserved buildings still have strong local features and need to be protected (Fig.2). Because of hot weather and

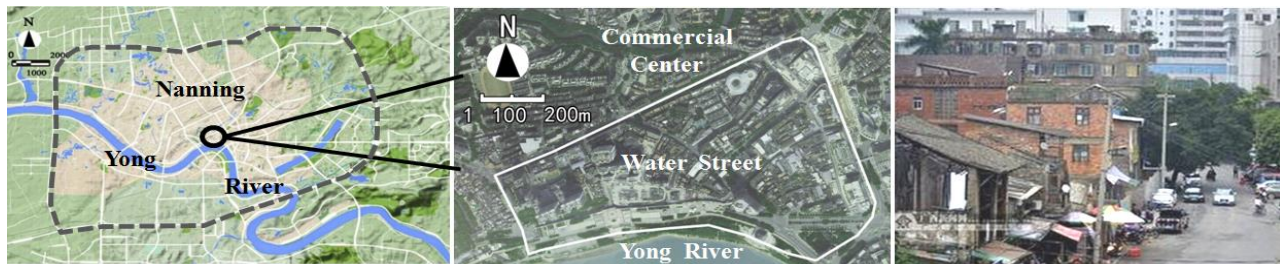


Figure 2: The location and the remaining buildings of Water Street

PLEA 2018 HONG KONG

Smart and Healthy within the 2-degree Limit

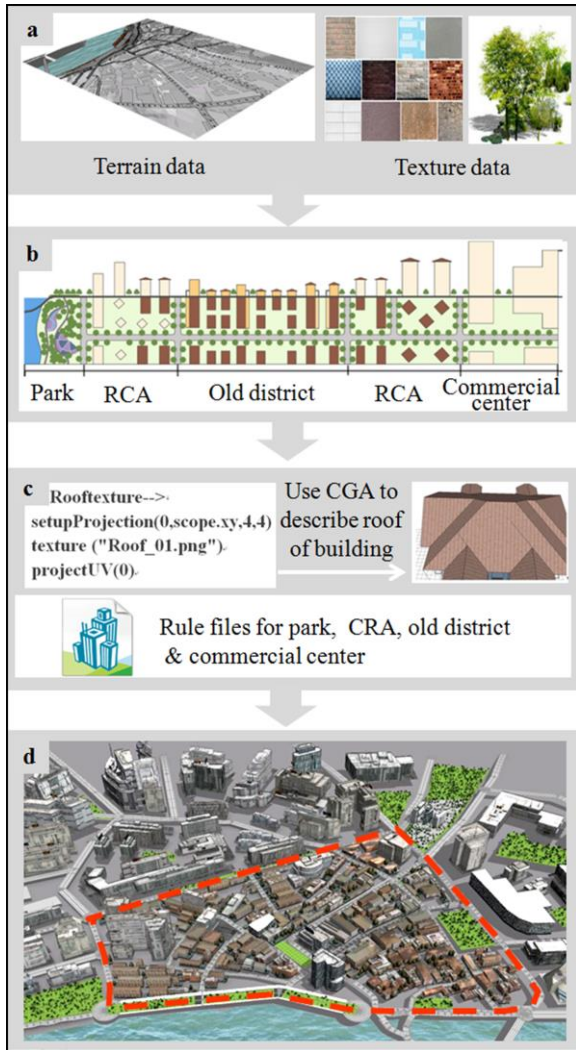


Figure 3: Modeling processes of Water Street on CE

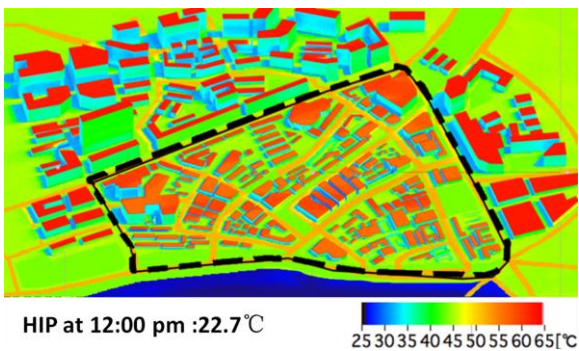


Figure 4: Simulated surface temperature distribution for the present Water Street at noon on a typical summer day.

unreasonable construction, the thermal environment in Water Street was quite uncomfortable, which worsened the living quality and environment. The traditional habits of locals like drinking tea, chatting and playing cards under the shade of trees are gradually disappearing due to the bad outdoor thermal environment.

In order to improve the living environment in Water Street, it is urgent to make optimal design to improve its

thermal environment. Besides, 3D city models should be used to assist the designers to make a better balance between landscape, thermal environment and cost, as well as to improve public participation.

3.2 3D models and present thermal environment in Water Street

The 3D city models for Water Street were built by the rule-based modelling software CE. The modelled areas includes Water Street (0.41km²) and surrounding areas (0.22km²). There were four modelling processes (Fig.3). (More details of modelling steps can be seen in Luo' study [5].)

Data preparation and processing are indicated in Fig.3a. There were two types of data: one was terrain data for the city surface and the other was texture data for enriching 3D models. In this case, the dxf-formatted CAD data contained information of terrain. Texture data was collected from screen capture pictures on the Baidu panoramic map.

Classification of city images is shown in Fig.3b. This step was used to define the different types of city images, providing the reference to describe the rule and enabling one rule applied to several objects as long as these objects had similar images. The city images for Water Street and its surrounding areas were divided into four types: old district, residential and commercial mixed areas (CRA), commercial center and park.

Rule writing and rule assignment are shown in Fig.3c. According to the above classification of city images, four rule files were created to represent the four images. The rule file for the old district was edited in more detail to generate vivid 3D models. The rule files for other areas were relative simple. Fig.3c also presents how to use CGA to describe and define a building roof.

Model generation and modification are illustrated in Fig.3d. The 3D models for trees, buildings, roads and other structures were generated by applying the four rules files for the old district, RCA, commercial centre and park to the corresponding surfaces and choosing the corresponding rule descriptions for different buildings.

Referring to the 3D model information made on CE, a numerical simulation model was built on VW, and numerical simulation of the thermal environment was carried out on TR. The weather condition on a Nanning's typical summer sunny day was chosen for simulation and analysis. Daily variation of meteorological parameters for a typical summer sunny day in Nanning can be summarized as follows: the average daytime temperature is above 30°C, and the average nighttime temperature is around 26°C. The amount of total solar radiation on the horizontal plane is large, and its maximum value is 900W/m² at 12:00. The mean wind speed is about 1m/s, and the peak value is 3m/s at 18:00. The numerical simulation of the present situation in Water Street (Fig.4) shown that the HIP value at 12:00pm

PLEA 2018 HONG KONG

Smart and Healthy within the 2-degree Limit

was 22.7°C, which means that the thermal environment was extremely bad. Most of the buildings in Water Street are made of wood, so the surface temperature of the roof and facade was generally lower than that of the surrounding high-rise buildings. But the surface temperature of the ground reached about 40°C. This result reveals that the outdoor environment would be uncomfortable.

3.3 Optimal design

From the analysis of thermal simulation results for the present environment in Water Street, there are three main problems resulting in the poor thermal environment, as summarized below. Firstly, due to unplanned land exploitation, many high-rise buildings were built outside and inside Water Street and blocked ventilation, resulting in difficulty in heat dissipation. Secondly, almost all outdoor ground was paved with impermeable materials, which resulted in that the ground could not store water to cool down in summer. Thirdly, there was a serious lack of green areas and the greening rate is only 7%. Therefore, the optimal design of the thermal environment in Water Street was conducted under consideration of above issues.

(1) Many studies have shown that high-rise buildings create shadows during summer daytime, having a reducing effect on the ambient air temperature. However, Water Street is completely surrounded by high-rise buildings, which block air circulation and also reduce the cooling effect of nocturnal radiation. Therefore, it is worth conducting thermal simulation to verify whether lowering the building height is positive or negative for the thermal environment. Besides consideration of the thermal environment, the traditional features of Water Street need to be displayed, so it is necessary to control the building height.

In order to discuss how to control the building height to improve the thermal environment better, the following three scenarios were designed. The first was to control the height of buildings outside Water Street, ensuring building height gradually decreases from the outside to Water Street. The second was only to control the height of buildings inside Water Street: ensuring high-rise buildings were restored to the same height as the historical building, which is less than 4 floors. The third was to control all the high-rise buildings. A height map was used to control the building height. The height map is a map to indicate variation of building height in color, e.g., red and black color presented high and low buildings respectively, and diffuse color presented the buildings between high and low buildings. Then a CGA program was written to make a link between the height map and the surface. In this way the building height in the surrounding area could be effectively controlled.

(2) Permeable paving bricks have strong water absorption and storage capacity for rainwater, which

promotes water evaporation and heat dissipation in the ground surface. Sidewalks, parking lots and squares in Water Street are the outdoor places where the residents most frequently used. Therefore, the ground pavement in these three spaces was designed to change from concrete pavement to water permeable bricks.

To discuss how to increase permeable bricks to get a better thermal environment, three scenarios were designed in this study. The first was to design permeable bricks on the sidewalks, with an area of approximately 4.78hm². The second was for parking lots, public squares and other outdoor space, with an area about 8.14hm². The third was for all the outdoor space, with an area about 9.22hm². Through changing the CGA to link the different texture data, the 3D models were easily transformed from the concrete-paved ground to permeable brick pavement.

(3) Green space not only increases evaporative cooling and provides a comfortable cool space, but also has a positive effect on beautifying landscape. As Water Street is seriously lack of green space, new green areas are required to be increased in optimized design. Land use for increasing vegetation includes the empty areas, waste land, and sites for demolition of destroyed temporary buildings.

To discuss the impact of green space on the thermal environment, the increased greening rate was assumed at the following three values: 10%, 20% and 30%, with areas of 4.15hm², 8.21hm² and 12.3 hm² respectively. The new 3D models of green space were generated by modifying the corresponding CGA language on the present 3D models.

Each design element has three design conditions. If they are combined with each other, there will be 27 design schemes. Due to the limited space, this paper only described corresponding combination of design conditions and finally obtained three optimized design plans, namely design A, B and C, as shown in Table 1. Thermal simulation for each design was conducted using TR. Fig.6 shows the simulated results.

4. RESULT

4.1 Support Optimization Design

The vivid 3D city models, HIP values and indicators of design elements could support the planners and designers to conveniently analyze the thermal environment. Through the 3D landscape models and thermal environment simulation for each optimal design, reduction of building height around Water Street is not effective in improving the thermal environment in Water Street, but it would aggravate the discomfort of the

PLEA 2018 HONG KONG

Smart and Healthy within the 2-degree Limit

Table 1: the condition setting of design elements and the three design schemes

Design Elements	Controlling Building Height	Permeable Pavement (area and area ratio)	Green Space (area and area ratio)
Optimal Design A	Building height outside Water Street gradually decreases to Water Street	Sidewalks: 4.78hm ² , 11.7%	4.15hm ² , 10%
Optimal Design B	Building height inside Water Street was restored to the same height as the historical building	parking lots, square and other outdoor space squares: 8.14 hm ² , 19.9%	8.21hm ² , 20%
Optimal Design C	Control the height of buildings both outside and inside Water Street	All the outdoor space: 9.22 hm ² , 22.5%	12.3hm ² , 30%

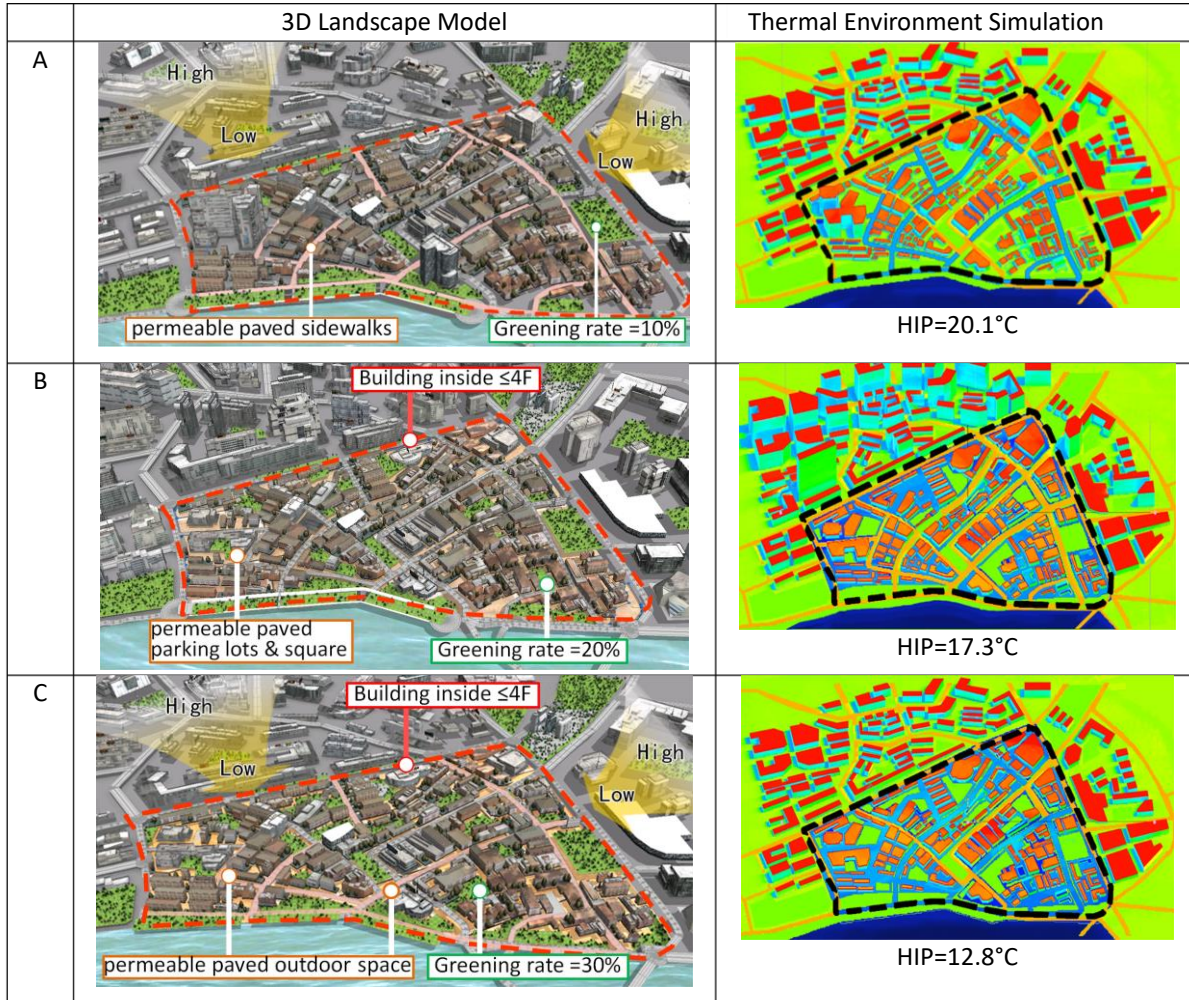


Figure 6: 3D models and thermal simulation results for design A, B and C

thermal environment in the surrounding areas. However, landscape becomes better after adjusting building height. Increase of green space and permeable pavement is quite significant for the improvement of the thermal environment. Where the greening rate is 30% and the ratio of permeable pavement is 20%, the HIP value dropped quickly (down to 12.8°C) and the thermal environment was more comfortable. According to Reference [錯誤! 尚未定義書籤。], when HIP is less than 15°C, the thermal environment will be thermally comfortable in the city. Therefore, considering the

economic cost, 30% and 60% can be used as the maximum design value of greening rate and permeable pavement rate in Water Street.

A radar chart was made to indicate a trade-offs among landscape, cost and thermal environment (Fig.7). The basis of evaluation for landscape, thermal environment and cost is as follows. The economic cost of three optimization schemes is calculated according to the local average cost of green space and permeable pavement (green space: \$310/m², permeable pavement: \$6.3/m²). According to References [8-9], the following six factors:

PLEA 2018 HONG KONG

Smart and Healthy within the 2-degree Limit

location condition, historical value, green landscape, building craftsmanship, public sentiment, and social

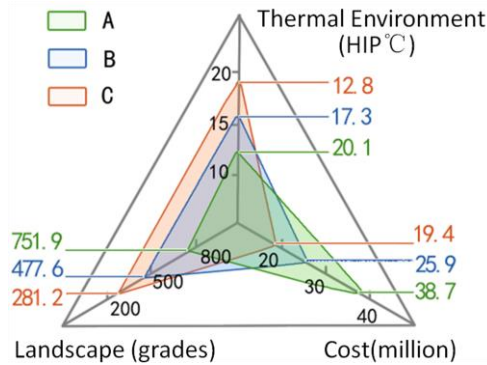


Figure 7: Radar chart for indicating relationship of landscape, thermal environment and cost.

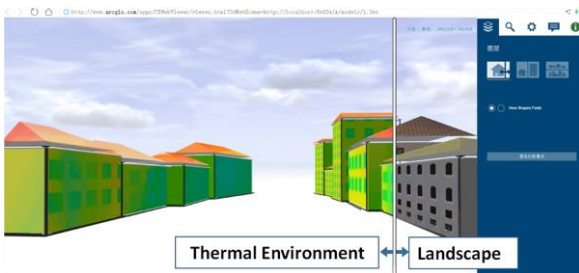


Figure 8: 3D models of Water Street on the web scene.

influence were given with different weights to calculate the scores for the landscape of three optimal designs. The evaluation of the thermal environment is based on the HIP value.

Fig.7 shows that the enclosed areas of the three factors is directly proportional to the thermal environment and cost, and is inversely proportional to the landscape. That is, the larger the surrounding area, the worse the design is, and the smaller the surrounding area is, the better the design is. Therefore, the excellent degree of these three schemes is: $A < B < C$, the area ratio is: $A : B : C = 7.2 : 6.7 : 4.6$, and the comprehensive benefit of the scheme C is the highest. Therefore, although the economic cost is high in the reconstruction of historic blocks, the comprehensive effect of the thermal environment and landscape should be priority considered.

4.2 Promote public participation

To improve public understanding of thermal environment design, simulation results of the thermal environment were visualized as textures to the 3D buildings of Water Street on CE. Then the 3D models were uploaded onto the web scene for web browsing. Fig.8 shows the 3D models of Water Street on the web scene. The public could view the 3D scene of landscape and thermal environment before and after the optimized design in Water Street through the browser. This method does not need to install CE software, providing a convenient approach to promote the public participation.

5. CONCLUSIONS

The following findings were obtained in this study:

- (1) Combination of the rule based rapid modelling method and thermal environment simulation could effectively support visualization analysis of trade-offs between different factors.
- (2) In the reconstruction design for historic districts, green space and permeable pavement play the most important role in improving the thermal environment.
- (3) It should pay more attention to the improvement of landscape and thermal environment in comparison with economic cost.

ACKNOWLEDGEMENTS

We acknowledge the financial support from Innovation Project of the Guangxi Graduate Education (No.T3030098010), the Study Abroad Program for Excellent Ph.D. Students of Guangxi University (No.T2040098001) and the Guangxi Science and Technology Project (No.AB16380193).

REFERENCES

1. Chatzidimitriou, A. and Yannas, S., (2017). Street canyon design and improvement potential for urban open spaces: the influence of canyon aspect ratio and orientation on microclimate and outdoor comfort. *Sustainable Cities and Society*, 33, 85-101.
2. Zhao, Y. and Liu, P., (2017) Design strategies and numerical simulation of thermal environment of street valley. *The Journal of Architecture*, 3: 37-39.
3. Grêt-Regamey A, Celio E, Klein T M, et al., (2013) Understanding ecosystem services trade-offs with interactive procedural modeling for sustainable urban planning. *Landscape and Urban Planning*, 109(1): 107-116.
4. Asawa, T., Hoyano, A. and Nakaohkubo, K., (2008). Thermal design tool for outdoor spaces based on heat balance simulation using a 3D-CAD system. *Building and Environment*, 43: 2112-2123.
5. Luo, Y., He, J. and He, Y., (2017). A rule-based city modeling method for supporting district protective planning. *Sustainable Cities and Society*, 28: 277-286.
6. Rodríguez Algeciras, A., Gómez Consuegra, L. and Matzarakis, A., (2016). Spatial-temporal study on the effects of urban street configurations on human thermal comfort in the world heritage city of Camagüey-Cuba. *Building and Environment*, 101: 85-101.
7. Wei J, He J., (2013) Numerical simulation for analyzing the thermal improving effect of evaporative cooling urban surfaces on the urban built environment. *Applied Thermal Engineering*, 51 (1-2) :144-154.
8. Yang Danfeng., (2017) Landscape planning of historical area based on evaluation of human landscape. Southeast University.
9. Jim, C. Y., (2004). Spatial differentiation and landscape-ecological assessment of heritage trees in urban Guangzhou. (china). *Landscape & Urban Planning*, 69(1), 51-68.

Summertime thermal comfort and adaptive behaviours in mixed-mode office buildings in Harbin, China

RAN ZHANG^{1,2}, CHENG SUN^{1,2}, STEVE SHARPLES³, YUNSONG HAN^{1,2}, HONGRUI ZHANG^{1,2}

¹ School of Architecture, Harbin Institute of Technology, Harbin, China

² Heilongjiang Cold Region Architectural Science Key Laboratory, Harbin, China

³ School of Architecture, The University of Liverpool, Liverpool, United Kingdom

ABSTRACT: This paper presents findings about interactions of occupants' thermal feelings and adaptive actions within office buildings from a two-week longitudinal survey in Harbin, a north-east city in China with hot summers and severely cold winters. Measurements of the indoor and outdoor environmental changes and occupants' window opening behaviours were conducted in six mixed-mode office rooms with fans or air conditioning cooling facilities. Thermal feelings and personal characteristics were gained via a panel questionnaire with 67 subjects from these offices to relate the thermal feeling with adaptations and physical conditions. The results showed the common use of the cooling device simultaneously with window opening behaviour, and an extremely high probability of window opening in office rooms with fans during the summer. Common patterns of the predictors for summer period in the severe cold area are identified in the analysis, while only gender for offices with fans and outdoor temperature, indoor and outdoor relative humidity for offices with air-conditioning were important variables in determining the state of the window opening. By comparing of the window opening changes with environmental factors for different thermal feelings, the mechanism of the interaction of occupant and offices building in summer season was further clarified.

KEYWORDS: Energy, Comfort, Behaviour, Offices

1. INTRODUCTION

Occupants' behaviours have a strong impact on the energy performance and indoor thermal environment of office buildings, and thus warrant research significant attention in the building design and operation process. It has been evaluated in many studies that behaviour including windows, blinds, and heating or cooling switch points provoke the range of energy consumption change up to 50% [1-3]. Many efforts have been made to the influencing elements and prediction mechanism of behaviour study in office and residential buildings [4-7] for different types of occupants, for example elders [7]. In our previous work, the basic characteristics of window opening behaviour were discussed [8], and research also conducted on the interaction between human and building environment via a survey with more samples [9]. Some works on occupancy behaviour reviewed the current results of the influencing factors and predictive methods [9-12], while these reviews also pointed out that the role of the occupants still needed further discussion.

Research has indicated that people are not passive recipients of their environment but interact with it to optimise their comfort via various means, including adaptive control of the environment [13]. These adaptive behaviours are strongly tied to the heating and cooling energy loads, making up 37% and 54% respectively of total energy consume in residential and commercial buildings in the United States [14]. The impact of different actions on energy use can be ranked from the

most to the least as: window, blinds, fans and heaters [15, 16]. Existing studies have also established the significant impacts of the occupant behaviours on the indoor environment and users' feelings by mean of surveying or simulation [6].

Nevertheless, mechanisms behind the interaction are still being explored and further studies are necessary on behaviour characteristics and human-building interaction in more types of buildings of various regions with different climates. This paper presents findings about the interaction of occupants' thermal feelings and adaptive actions in office buildings based on a two-week longitudinal survey in the north-east China city of Harbin, which experiences hot summers and very cold winters. The behavioural categories of the study are mainly about opening and closing windows along with fan use. It is because the window is an important and sensible factor among others affecting the environment, leading the occupant taking a more active role of operating it. Through the acquisition and analysis of the surveyed data, this study examined:

Characteristics of window opening behaviours in mixed-mode offices of severe cold area, Harbin.

Influencing variable and regression models of thermal sensation and window opening behaviour in office with different types of cooling facilities.

Interaction with thermal experience with behavioural control in a common mixed-mode office context.

PLEA 2018 HONG KONG

Smart and Healthy within the 2-degree Limit

2. METHODOLOGY

A longitudinal survey was conducted in six mixed-mode office rooms of different sizes. Long-term data were collected via an online daily survey and data logger measurements of the local thermal environment and adaptive behaviours. Before the longitudinal survey, a pre-investigation of the office buildings in Harbin was conducted for the background information. The thermal experience results and adaption outcomes were tested by both environmental and personal parameters, and the correlation between thermal feeling and behaviours analysed.

2.1 Field measurements

Continuous measurements were made of weather changes, indoor environmental variables, behaviour actions and geometric design parameters in the surveyed offices across the longitudinal survey period. Indoor ambient temperature and relative humidity were logged at 15-minute intervals for six office rooms using HOBO12 sensors. Window opening behaviour was measured by HOBO UX90-001 status loggers and the use of fans and air conditioning (AC) via the questionnaire record.

2.2 Questionnaire survey

References Over two weeks, the questionnaires were distributed by Wenjuan Xing software via the most commonly used communication software, Wechat, twice a day for a continuous ten work days during the hot summer season. Fig. 1 gives an overview of the collection and integration of the data streams which was the same as another study [9]. The survey included four stages, test questionnaires, start questionnaires, daily questionnaires and final questionnaires. Test questionnaires were trialled for a one-week period among ten persons who were not occupants of the surveyed offices before the formal investigation (to prevent the fatigue of the questionnaire test). This pilot study helped the formal survey streamlining. The longitudinal survey began with the start survey which included questions about basic personal information, seating plan, thermal feelings of occupant office rooms' environment to get a general knowledge of these subjects and then would be made comparison with the daily questionnaires and the final one. There are only thirteen questions in the daily survey which is short and pith, including the questions of thermal comfort, behaviour state and remaining related items such as clothing. The answers of subjects who were not stay in the office for more than 20 minutes were excluded to avoid possible effects of exercise on thermal sensation. Once the daily surveys had been completed for the full two-week course, each user answered a final questionnaire about their overall experience. Among the questions of these two-week feelings, the final one included items of accessibility, general clarity of the daily

survey along with the time expense of one time questionnaire and the entire survey period. The final questionnaire also provided a blank space for the subjects to fill in their feelings on anything not included in the three stages survey at the end of the survey.

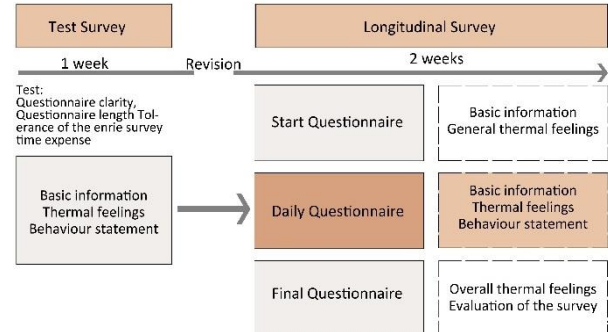


Figure 1: Stream and content of the panel questionnaire [9].

2.3 Sample selection

Harbin has long, cold winters that reduce occupants' tolerance of hot summer temperatures. Based on the cross-sectional pilot investigation, the use of fans and air conditioners was often accompanied by window opening behaviour, which is unlike other places with hot summers. Six mixed-mode office rooms of different sizes and occupant numbers in three buildings of Harbin were selected for the study. Fig.2 shows the location and sites of the surveyed office buildings. Table 1 shows the offices and occupant details. Some samples were the same as those of previous studies [8,9]. All the occupants of the surveyed offices in building A, B and over 42% of C were invited to join the survey for two weeks panel survey and were sent the daily questionnaire in the morning time and afternoon time.

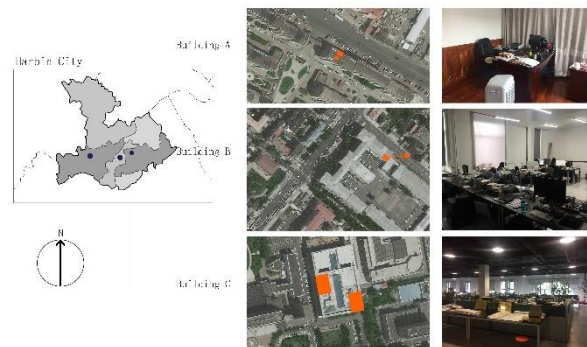


Figure 2: Building types and surroundings of the investigated office building [8].

Table 1 Basic information of the subjects, the surveyed offices and the cooling options

Building Office No.	Office type (no. of people, no. of males)	Room size (m ²)	Cooling options
A1	Private (1,0)	25.62	Fan

PLEA 2018 HONG KONG

Smart and Healthy within the 2-degree Limit

A2	Shared-private (2,0)	15.47	Fan
B1	Open (15,6)	66.2	Fan
B2	Open (6,6)	37.66	Fan
C1	Open (22,15)	380	AC + fan
C2	Open (21,9)	380	AC + fan

2.4 Data analysis

This study firstly examined the distribution of the environmental variables and window open behaviours changing during the summer season in Harbin. The influencing variables and mechanisms of thermal sensation were analysed by linear regression, comparing indoor and outdoor temperatures of both mixed-mode offices with fan and AC. Three methods were adopted for examining the related parameters of window opening behaviours: the binomial logistic regression, Point Biserial Correlation and Guttman's coefficient of predictability, where logistic regression was used to detect whether parameters could be used as a predictor; Point Biserial Correlation was used to examine the relevance of continuous variables and binary variables (a scale with only two values) and Guttman's coefficient of predictability was suitable for analysing the correlation between two non-continuous variables (either a symmetrical or a non-symmetrical relationship). The control mechanisms of window open are analysed by means of binomial logistic regression. The relationship between the probabilities of window opening and the influencing variables can be expressed as in Equation (1):

$$\text{Logit}(P) = \ln \frac{P}{1-P} \quad (1)$$

where P is the probability of window opening ;

$P/(1-P)$ is the odds ratio.

The odds ratio, which was gained via the binomial logistic regression, was used for describing the probability ratio of occurrence of two variables.

3. RESULTS

3.1 Environmental variables characteristics

The measurements from the loggers and the weather station revealed indoor and outdoor environment variables during the two-week run (Fig. 3). The survey period was the same as another study [9]. The outdoor temperature in the first week was obviously higher than for second week, with the mean daily value of 28.2°C and the maximum one reaching to 32.6°C during the first week, while the mean temperature was 26.7°C during the second week.

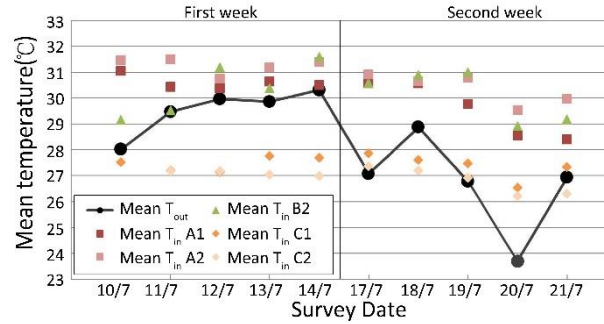


Figure 3: The distribution of indoor and outdoor environmental parameters during the survey period [9].

3.2 Behavioural changes

In each surveyed office, the state of the most frequently used window was recorded by data logger and the window open frequency of other openings was obtained via daily questionnaire feedback. In the summer, fans were used alongside window opening behaviour in buildings A and B and were also utilized in building C with central AC, indicating the common characteristics of mixed use of cooling equipment and natural ventilation. From the field measurements of behaviour state data loggers shown in Fig. 4, all the recorded windows in all the offices kept a high rate of opening, of which room A1 and B1 had the highest proportion of 100% opening. Influenced by the continuous high temperatures in summer, the window state changes were not affected by the arrival and departure of occupants, suggesting that cooling via ventilation at night happened in almost all investigated office buildings. The two rooms of the AC offices, C1 and C2, showed a significant difference in the use of the window opening, the former with more probability to open windows, which may be because of the personal differences between thermal sensation and the habit of window opening by the people closest to the window.

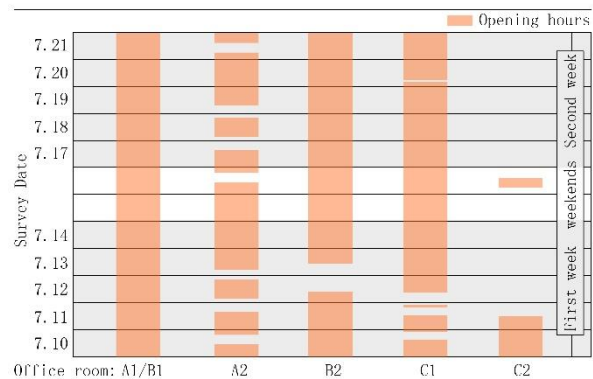


Figure 4: The distribution of changes in window states from data loggers during the surveyed period.

The behaviour states at 10.00am 3.00 pm were also recorded via the panel questionnaire. For the smallest offices in building A from the daily record, and the proportion of window opening reached 100% during the two weeks run. The multi-person offices with three to

PLEA 2018 HONG KONG

Smart and Healthy within the 2-degree Limit

twenty users kept natural ventilation at a probability of over 80% in most cases. Window open probability of the two rooms in the AC building, C1 and C2, maintained a high consistency with the date distribution in the scale being below 40%. For the entire length of the survey, the window opening proportion of offices with fans was greater than 90%, whilst the ones with AC were around 20%. It is noteworthy that, in the second week, with the decrease of outdoor temperature, the F building window ratio increased due to the statistics from the questionnaire results. Fig. 5 summarizes the statistical results from the behavioural data.

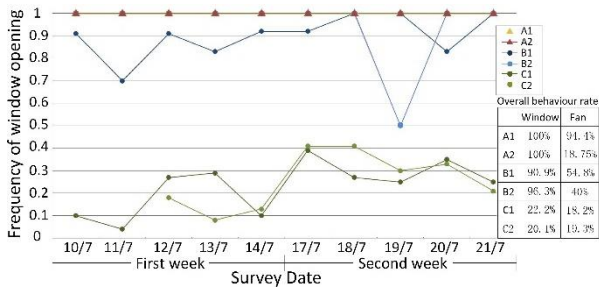


Figure 5: The distribution of changes in window states from questionnaire surveys during the survey period.

3.3 Influencing variables and regression of thermal feelings - rooms with fans

The extremely high window opening probabilities shown in Figs. 4 and 5 indicate a high degree of interaction between the interior space and the outdoor environment in the offices with fan use.

Therefore, the higher correlation coefficient of the outdoor temperature and the thermal sensation were more closely linked than the indoor temperature, which has been recognized as the predictive variable of the thermal sensation vote. The higher R^2 level of the outdoor temperature also presents a better linear regression than the indoor temperature (Table 2). The indoor humidity and overall satisfaction experienced a similar situation because the large percentage of the openings lead to the close relationship of the occupants' feelings and outdoor physical parameters. The outdoor environment variables, relative humidity and temperature, were not only more closely related parameters, but also had better fitness for predicting the mean thermal feelings reflected by the R and R^2 value. Scatter diagrams were plotted and linear regression equations were established, as shown in Fig. 6.

Table 2: Influencing variables on mean value of thermal feelings in mixed-mode offices with fans.

Variables	Correlation R	R^2	Asymp. Sig ^a
T_{in}	0.53*	0.28	0.323

Mean thermal sensation	T_{out}	<u>0.617*</u>	0.38	0.916
Mean humidity feeling	RH_{in}	0.281*	0.08	0.89
	RH_{out}	<u>0.406*</u>	0.17	0.397
Mean overall satisfaction	T_{in}	-0.34*	0.12	0.885
	T_{out}	<u>0.418*</u>	0.17	0.916

* $p < 0.05$.

^a when the value is > 0.05 , residuals are independent, indicating the data gained from the questionnaire were independent. Best regression results are in bold and underlined.

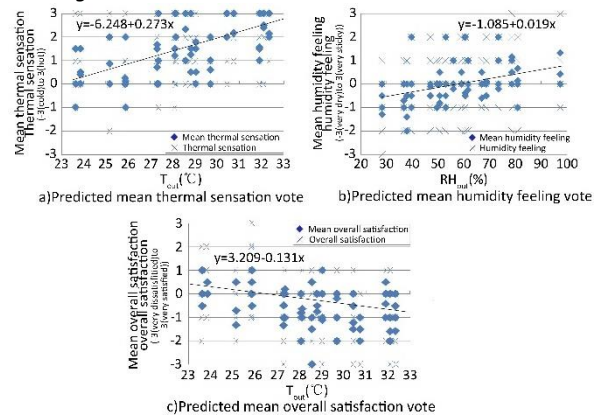


Figure 6: Regression results of mean thermal sensation, humidity feeling and overall satisfaction vote.

3.4 Influencing variables and regression of thermal feelings - rooms with AC

For mixed-mode offices with AC, none of the indoor and outdoor physical parameters were associated with occupants' thermal sensations, humidity feelings and overall satisfaction, and could not be linearly regressed.

3.5 Influencing variables and regression of adaptive behaviour - rooms with fans

Using the logistic regression, the expected probabilities of window opening behaviour may be modelled in terms of the local thermal environment of the occupants, the time of day and personal characteristics. Table 3 presents an initial understanding of the relationship between behaviour probabilities and influencing factors for the mixed-mode Harbin offices. Figs 4 and 5 reveal an important phenomenon of a large proportion of the windows being open day and night in most of the mixed-mode office, and not changing with the indoor and outdoor environmental variables. This is consistent with the correlation analysis and logistic regression analysis results presented in Table 3 that physical parameters and the arrival and departure of occupants are not independent of the summer window probability in Harbin. Table 3 also suggests that the perceived outdoor noise feelings and the width of the

PLEA 2018 HONG KONG

Smart and Healthy within the 2-degree Limit

room have certain connection with the behavioural state, but the only predictor of these three variables was just gender.

Table 3: Correlation analysis and Nagelkerke R^2 for logistic regression model of window opening behaviour in mixed-mode offices.

Variable	Logistic regression				Point biserial correlation coefficient	
	Levels	Odds Ratio OR	p	Ng R^2	r_{pq}	p
Outdoor noise (quiet)	Neutral	0.23	0.03	-	-0.26	<0.01
	Noisy	-	NS	-		
Room width	-	-	NS	-	-0.15	0.043
Gender (Female)	Male	4.36	0.03	0.075		Guttman's coefficient of predictability λ 0.03 p 0.02

3.6 Influencing variables and regression of adaptive behaviour - rooms with AC

Quantitative results of the correlation analysis and logistic regression on window opening behaviour are presented in Tables 4 and 5 for the mixed-mode offices with AC. For the correlation analysis, the outdoor temperature, indoor and outdoor relative humidity shows significantly impact on the window open probability and can be predictor for modelling the window open prediction (Table 4).

Further analysis of the logistic regression on behavioural data found the regression coefficients for each predictor variable together with their standard errors and statistical significance levels, and the predictive power of the various models compared using Nagelkerke R^2 . Models using indoor relative humidity as inputs had a higher predictive power (higher Ngk R^2) than models using either outdoor temperature or outdoor humidity. The fitting degree of these three models is close but low.

3.7 Correlation of thermal feelings and behaviours

Table 4 reveals the impact degree of thermal satisfaction on the probabilities of opening windows. The correlations of the indoor humidity and windows compared with different thermal satisfaction level were modelled and Table.6 presents the results of the modelling. The interaction between the

Table 4: Correlation analysis and logistic regression analysis of window open behaviour in mixed-mode offices with AC.

Variables	Logistic regression			Point biserial correlation coefficient	
	levels	OR	p^a	r_{pq}	p
Outdoor temp.	°C	0.83	< 0.0001	0.138	0.1
Indoor humidity	%	1.11	< 0.001	-0.15	0.005
Outdoor humidity	%	1.03	< 0.001	-0.16	0.003
Thermal satisfaction (satisfied)	neutral	3.16	0.002		
	satisfied	4.31	< 0.0001	0.122	0.02

The thermal satisfaction votes were cast on 7-point interval scale. Due to the distribution, the variable was transformed. Dissatisfaction refers to votes between -3 and -0.1, neutral refers to -0.1 to 0.1, and satisfaction refers to 0.1 to 3.

Table 5: Parameter coefficients, Nagelkerke R^2 for three logistic regression models (M1 to M3) for window open behaviour in mixed-mode offices with AC.

	M1	M2	M3
Intercept	3.997	-6.18	-2.88
Outdoor temperature	-0.187		
	0.051		
Indoor relative humidity		0.103	
		0.026	
Outdoor relative humidity			0.027
			0.008
Ngk R^2	0.061	0.072	0.057

Table shows regression coefficient estimates with standard errors and statistical significance levels indicated below each estimate.

respondent's overall satisfaction and the indoor relative humidity had a significant impact on the window opening actions. These results agreed with the previous study [9]. When the relative humidity was below 45%, the occupants with the moderate thermal satisfaction had the highest window opening rate, whilst when the value rose over 45% the dissatisfied users tended more to open the windows. With the increase of relative humidity, the possibility of window opening increases dramatically for the uncomfortable occupants. For the users around the neutral overall satisfaction level, the probability of opening windows also showed a slowly rising trend with an increase of relative humidity (Table. 6).

PLEA 2018 HONG KONG

Smart and Healthy within the 2-degree Limit

Table 6: Association between the probability of window opening and indoor humidity in different thermal satisfaction scale.

Thermal Satisfaction scale	Indoor relative humidity				
	40%	45%	50%	55%	59%
Satisfied	2.22%	5.4%	12.52%	26.42%	42.85%
Neutral	18.29%	22.85%	28.15%	34.14%	39.34%
Dissatisfied	11.55%	22.86%	40.23%	60.44%	74.65%

4. CONCLUSION

Subjective thermal experiences and objective physical measurements of the indoor environment were taken in six mixed-mode office rooms from a summer longitudinal survey in Harbin. The conclusions drawn from detailed analyses and discussions are as follows:

The windows were kept open day and night for natural ventilation cooling at night and were not affected by the arrival and departure of occupants. Window opening probability of the offices rooms with fans was maintained at an extremely high level.

The interior spaces of the office buildings that had fans had a strong interaction with the outdoor environment, which suggests physical variables of the outdoor environment are better predictors for indoor feelings.

The only (but weak) predictor for evaluating window opening probabilities for offices with fans was gender (97.2% of the females with the state of an open window, compared with 89% for males); the predictive factors (but weak) for AC offices were outdoor temperature, indoor and outdoor relative humidity. This indicates that summertime window opening behaviour in the north-east China may not be well predicted via environmental parameters which is different from many previous studies conclusion [12].

The interaction between the respondent's overall satisfaction and the indoor relative humidity had a significant impact on the window opening actions.

ACKNOWLEDGEMENTS

The authors would like to acknowledge that this paper is financially supported by National Natural Science Foundation of China (Grant No. 51578172), China Postdoctoral Science Foundation funded project (Grant No. 2017M621276) and the Research and Development Projects in Science and Technology Projects of the Ministry of Housing (2016-K1-001).

REFERENCES

1. Al-Mumin, A., O. Khattab and G. Sridhar, (2003). Occupants' behavior and activity patterns influencing the energy consumption in the Kuwaiti residences, *Energy and Buildings*, 35: p. 549-559.

2. Tzempelikos, A., (2010). The impact of manual light switching on lighting energy consumption for a typical office building. In *International High Performance Buildings Conference*. Purdue University, USA, July 12-15

3. Wang, L. and S. Greenberg, (2015). Window operation and impacts on building energy consumption. *Energy and Buildings*, 92: p. 313-21.

4. Hunt, D., (1979). The use of artificial lighting in relation to daylight levels and occupancy. *Building and Environment*, 14(1): p.21-33.

5. Humphreys, M., F. Nicol, (1998). Understanding the adaptive approach to thermal comfort. *ASHRAE Transactions*, 104 (1): p.991-1004.

6. Haldi, F. and D. Robinson, (2008). On the behaviour and adaptation of office occupants. *Building and Environment*, 43: p. 588-600.

7. Jiao, Y., H. Yu, T. Wang, Y. An and Y. Yu, (2017). Thermal comfort and adaptation of the elderly in free-running environments in Shanghai, China. *Building and Environment*, 118: p. 259-272.

8. R. Zhang, C. Sun, S. Sharples, H.R. Zhang. Thermal Comfort and Behaviour Control in Mixed-mode Office Buildings in Harbin, China. International Conference for Sustainable design of the Built Environment, 318-330, 2017.

9. C. Sun, R. Zhang, S. Sharples, Y.S. Han, H.R. Zhang. A longitudinal study of summertime occupant behaviour and thermal comfort in office buildings in northern China. *Building and Environment*, 404-420, 2018.

10. Burak Gunay, H., W. O'Brien and I. Beausoleil-Morrison, (2013). A critical review of observation studies, modeling, and simulation of adaptive occupant behaviors in offices. *Building and Environment*, 70: p. 31-47.

10. Stazi, F., F. Naspi and M. D'Orazio, (2017). A literature review on driving factors and contextual events influencing occupants' behaviours in buildings. *Building and Environment*, 118: p. 40-66.

11. Hong, T., D. Yan, S. D'Oca and C. Chen, (2017). Ten questions concerning occupant behavior in buildings: The big picture. *Building and Environment*, 114: p. 518-530.

12. Nicol, F., M. Humphreys (2004). Stochastic approach to thermal comfort-occupant behaviour and energy use in buildings. *ASHRAE Transactions*, 110(2): p. 554-68.

13. U.S Department of Energy, Buildings Energy Data Book. [Online]. Available:

<http://web.archive.org/web/20130214012609/http://buildings.databook.eren.doe.gov/default.aspx>

[31 March 31, 2014]

14. Lee, Y. S. and A. M. Malkawi, (2012). Simulation multiple occupant behaviors in buildings: an agent-based modelling approach. *Energy and Buildings*, 49: p. 367-79.

15. Bonte, M., F. Thellier and B. Lartigue, (2014). Impact of occupant's actions on energy building performance and thermal sensation. *Energy and Buildings*, 76: p. 219-27.

16. Andersen R., J. Toftum, K. Andersen K and B. Olesen (2009). Survey of occupant behaviour and control of indoor environment in Danish dwellings. *Energy and Buildings*, 41: p. 11-16.

Passive Downdraft Cooling Towers Performance Evaluation: Results of data collected from built prototypes

OMAR DHIA SADULAH AL-HASSAWI^{1,2}

¹Washington State University, Pullman, Washington, United States of America

²Arizona State University, Tempe, Arizona, United States of America

ABSTRACT: This research aims to advance performance of the single stage passive downdraft evaporative cooling tower (PDECT) and expand its applicability beyond the hot dry conditions where it is typically used by developing and testing a design of a multi-stage passive and hybrid downdraft cooling tower (PHDCT). Experimental evaluation on half-scale prototypes of these towers was conducted in Tempe, Arizona, during Summer, 2017. Cooling systems in both towers were operated simultaneously to evaluate performance under identical conditions. Results indicated that the hybrid tower provides significant advantages over the single stage tower as the former outperformed the latter under all ambient conditions.

KEYWORDS: Passive Cooling, Passive Downdraft cooling, Passive Downdraft Evaporative Cooling Tower, Passive and Hybrid Downdraft Cooling Tower, Experimental Evaluation

1. INTRODUCTION

Passive cooling techniques, specifically passive downdraft cooling (PDC), have proven to be a solution that can address issues associated with air conditioning (AC). Globally, over 100 buildings have integrated PDC in its different forms, most of which use direct evaporative cooling. Even though all surveyed buildings were energy efficient and cost-effective, and most surveyed buildings were thermally comfortable, application of PDC remains limited [1].

This can be attributed to three main reasons. The first is the perception that PDC consumes more water on site when compared to water consumed by electric powered AC. Since the former typically utilizes direct evaporative cooling as its main cooling mechanism, it makes it challenging to consider, especially in hot dry regions where water supplies are limited. However, when accounting for the total water consumed to provide cooling, both on site and that used to produce electricity at the power plant, PDC could be a competitive solution [2].

The second is the notion that PDC is incapable of maintaining desired human thermal comfort levels for the entire cooling period, making it more convenient to solely rely on AC. Performance of PDC towers was demonstrated by building a full-scale prototype attached to the 1000 ft² test house located at the University of Arizona Environmental Research Laboratory's (ERL) Passive Solar Village, and significant temperature drops, up to 30°F, were witnessed over a two-day long test between August 22 and 23, 1985 [3].

The third is that examples were rarely found in the literature that advanced PDC by introducing other stages of cooling with direct evaporative cooling to reach outlet conditions like that usually achieved by AC systems. The

PDC hybrid system in the atrium space at the Malta Stock Exchange achieved 60 percent savings in energy consumption when compared to its predicted consumption if large fan coil units were used to solely cool the space [4].

This research aims to advance performance of PDC, specifically the single stage passive downdraft evaporative cooling tower (PDECT) and expand its applicability beyond the hot dry conditions where it is typically used, by designing and testing a multi-stage passive and hybrid downdraft cooling tower (PHDCT). This paper describes the process followed to develop the experiment setup and the results obtained from the data collection campaign conducted in Tempe, Arizona, during summer of 2017.

2. EXPERIMENT DESIGN

To understand the extent that a multi-stage tower can advance performance of a single stage tower, it was critical to define what design represents a traditional single stage tower and use that design as a basis to develop the hybrid tower prior to building the experimental setup.

2.1 Single stage tower prototype design

The single stage tower design was developed after analysing seven studies found in the literature that collected data from PDECT using an experimental setup [3], [5-11]. The 4 tower elements which impact conditions of the air exiting the system that were analysed in these experiment setups were the tower shaft, the tower inlet, the tower outlet, and the tower direct evaporative cooling system.

Based on the analysis of the major components of the 7 towers used in these studies, the characteristics of the

PLEA 2018 HONG KONG

Smart and Healthy within the 2-degree Limit

single stage tower built for this research are listed in Table 1 below. This tower is approximately a half-scale reduction of the ERL tower. Figure 1 below is a section cut through the proposed design.

Table 1: Characteristics of single stage tower.

Tower element	Description
Cross-section area (ft ²)	9
Cross-section shape	Square
Shaft total height (ft)	10
Inlet vertical surface area (ft ²)	36
Inlet type	Cube + diagonal baffles
Outlet area (ft ²)	8
Outlet discharge direction	Side
Evaporative cooling system	Misting nozzles

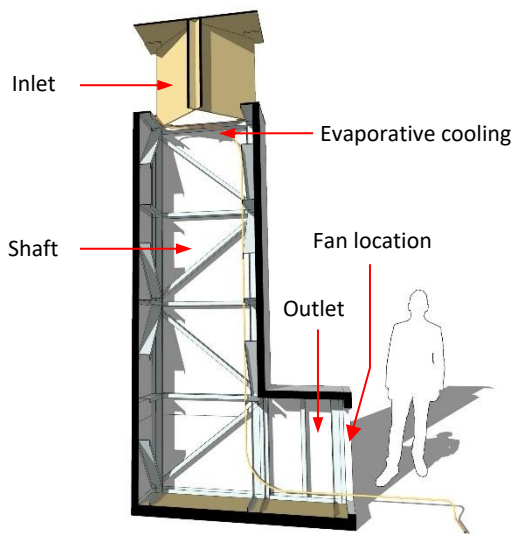


Figure 1: Section cut through single stage tower design.

2.2 Hybrid tower prototype design

Several design iterations were explored for a hybrid tower with minimum alterations on the design developed for the single stage tower. The main intent was to precool the air entering the tower through a sensible cooling system (stage 1) prior to it being cooled by the direct evaporative cooling system (stage 2).

Some of the explored iterations involved major changes to the design proposed for the single stage tower with modifications to the tower shaft physical dimensions. Other iterations involved minor changes solely related to the tower inlet. The iteration built for this study, shown in Figure 2 below, met the requirement of incorporating the sensible cooling prior to the evaporative cooling, while using the exact enclosure dimensions and construction method of the single stage tower. This resulted in a minimum impact on the construction timeline.

To achieve this, a rectangular heat exchanger available in the local market was placed at the top of the tower and parallel to the ground plane. It was topped with a shading device to protect it from direct solar radiation. Unlike the

PDECT, there is no clear inlet vertical surface area. As chilled water flows through the exchanger, the air surrounding it drops in temperature, infiltrates through the openings between the exchanger fins, and down the tower shaft. This downdraft would further increase by evaporative cooling and/or electric fan assistance.

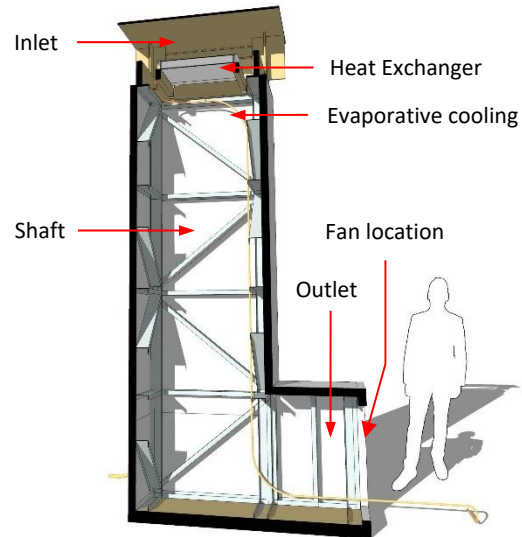


Figure 2: Section cut through hybrid tower design.

3. EXPERIMENT CONSTRUCTION

Construction of the towers took place at Arizona State University (ASU) in Tempe, Arizona, during Spring, 2017. Tempe was the city selected for this study because it provides the opportunity to understand performance of PDC under hot dry as well as hot humid conditions. The selected site was ASU Design School Solar Lab, which is located on the fourth floor of the School's north building with access to the roof where several experimental evaluations have been conducted in the past. The towers were built out of materials readily available in the local market in case repairs were required.

The shaft and outlet for each tower were built as one piece from identical materials. The structural frame was made from 25-gauge steel track typically used for drywall construction. The outer layer was made from 2-inch-thick polyisocyanurate rigid insulation panels with reinforced aluminium foil facers on two sides that has a total resistance value of 13 ft²Fh/Btu. The towers were mounted onto a structural insulated base made from 2-inch-thick polyisocyanurate rigid insulation sandwiched between two layers of 1/2-inch-thick plywood. Each enclosure was mounted onto the metal grating that covers the roof floor using four 3/32-inch wire ropes that span from the tower top corners down to the floor. The structural base was covered on the inside with PVC liner up to 1 ft high.

The inlet for the PDECT was made from 1/2-inch-thick plywood. The inlet for the PHDCT had two main components which were the heat exchanger and its

PLEA 2018 HONG KONG

Smart and Healthy within the 2-degree Limit

shading device. To place the heat exchanger on top of the shaft, it was first mounted onto framing lumber which had a 2-inch by 3-inch cross section, and then placed into joist hangers attached to a wood frame mounted on top of the shaft made from framing lumber with a 2-inch by 8-inch cross section. The frame had a perimeter dimension identical to the perimeter of the tower shaft. The shading element protecting the exchanger was made from 1/2-inch-thick plywood.

The direct evaporative cooling system installed in each tower was identical and was supplied from Arctic Cove. This system uses brass misting nozzles with a water flow rate of 0.5 gal/h per nozzle as per manufacturer's specifications. Four mister openings were provided at the top of each tower directly below the tower inlet. A water filter was placed at the main water supply valve to prevent solid sediments from clogging the system. The heat exchanger used in the PHDCT was donated to this project by Emmegi Heat Exchangers Inc. located in Phoenix, Arizona. The exchanger has an all-aluminium bar and plate construction, which makes it highly robust and resistant to external damage [12]. Its inlet was connected to the chilled water supply available on site using an open loop system.

The towers were positioned along the northern end of the roof with their outlets facing south. The towers were placed side by side and spaced 6 ft apart so that conditions surrounding one inlet would not affect the other. To block wind from entering the towers at the outlet and creating a stack effect, a 6 ft high enclosure was built around the towers along the south, east, and west. In addition, the enclosure was placed 7 ft away from the towers along the south and 2 ft away from the towers along the east and west to prevent it from causing any back flow of cool air exiting the towers. Another wind block was placed in the gap between the two towers along the north.

4. DATA ACQUISITION

Three sets of measurements were required to evaluate tower performance which were measurements of ambient conditions, measurements inside tower, and measurements at tower outlet. Ambient conditions are considered identical for both towers, but conditions inside tower and at tower outlet are different. For this reason, two sets of data acquisition systems were used, one to measure + record ambient conditions and another to measure + record conditions inside tower and at tower outlet.

To measure and record ambient conditions, a weather station completely supplied from Onset Computer Corporation was used. The data logger was the HOBO U30 USB with one temperature/RH smart sensor, one wind direction smart sensor, one wind speed smart sensor, one barometric pressure smart sensor, and one silicon pyranometer smart sensor.

To measure and record conditions inside tower and at tower outlet, a customized system completely supplied from Onset Computer Corporation was assembled. The HOBO H22 Energy Data Logger was used with four temperature/RH smart sensors, one temperature smart sensor rated for immersion in water, two air velocity analog sensors, and one pulse output water flowmeter.

To evaluate the two towers under identical ambient conditions, it was necessary to be able to record data while operating their cooling systems simultaneously. Thus, each tower was equipped with two temperature/RH smart sensors, one inside the tower and one at the tower outlet, as well as one air velocity analog sensor at tower outlet. The PHDCT was equipped with the other two sensors. The pulse output water flowmeter was placed along the heat exchanger water supply line to measure water flow through the exchanger. The temperature smart sensor was submerged in the heat exchanger water return line to record chilled water temperature exiting the tower.

Data was recorded in 30 second logging intervals. This was preferred over longer logging intervals as it provided a better understanding of the cooling processes taking place. With longer intervals, readings that might be considered an anomaly to what preceded and followed it tend to occur more often. For the data analysis, the average of every ten recordings was then calculated to obtain measurements at five-minute intervals. All data processing and analysis was performed using Microsoft Excel.

Preliminary data acquisition was conducted during the hot and dry days between Friday, May 26, 2017, and Wednesday, June 7, 2017. This data set was used to evaluate preliminary sensor locations and to identify the combinations of operation modes to test for the formal data collection. In addition, actual water flow through misters was measured using an acrylic rotameter supplied from Omega. This test indicated that the average water flow rate was 0.7 gal/h per mister rather than 0.5 gal/h stated by the manufacturer.

Formal data acquisition spanned for 42 days between Thursday, June 8, 2017, and Thursday, July 20, 2017. The conditions in the PDECT and PHDCT were measured using different operational modes by changing the water flow rates through the misting system (0.7 gal/h, 1.4 gal/h, 2.1 gal/h) and the heat exchanger (1.0 gal/min, 3.0 gal/min, and 5.0 gal/min). Whenever a fan was used in these tests, it remained at a constant speed of approximately 60 fpm. Figure 3 illustrates final sensor locations inside towers and at towers outlets and Figure 4 is a photo of the final experiment setup.

PLEA 2018 HONG KONG

Smart and Healthy within the 2-degree Limit

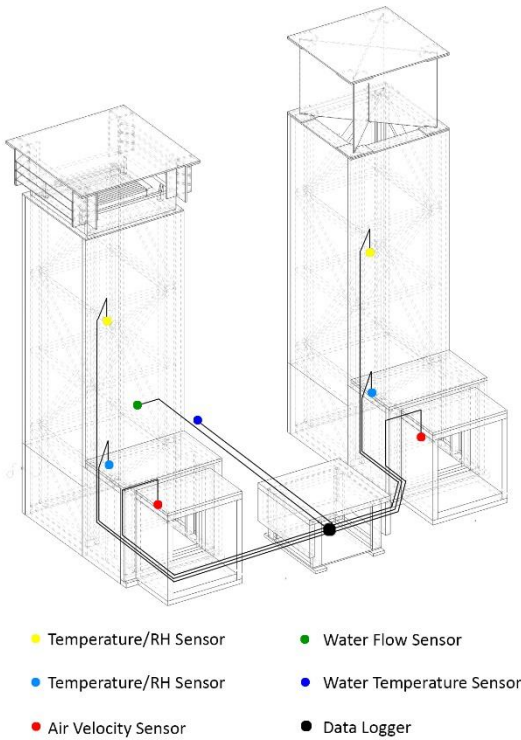


Figure 3: Towers sensors and data logger locations



Figure 4: Photo of final experiment setup from southeast corner. Left: hybrid tower, right: single stage tower.

Tests under hot dry conditions were conducted during the daytime with cooling systems operating mainly between 11:00 am and 7:30 pm. Each operation mode was repeated at least once on a different day to better understand its impact on outlet conditions.

Tests under hot humid conditions were conducted during the monsoon season. The objective of these tests was to understand the potential of cooling from the heat exchanger only as it was illogical to add more moisture to already humid air. Cooling systems were working during the evenings and overnight due to higher levels of humidity in the ambient air. Operating times were mainly between 8:00 pm and 9:00 am the following day. Instead of repeating each operation mode at least once, these tests were performed over a longer period of time. This decision was made due to the fewer hot humid days that occurred compared to the number of hot dry days. However, total running hours for identical operation modes were nearly the same in both climate conditions.

5. DATA ANALYSIS AND RESULTS

Performance obtained from each tower was evaluated based on results from the following sets of calculations on the data collected from all operational modes after processing it to the five-minute recording interval: Comfort levels. As per ASHRAE Standard 55-2013, tower outlet conditions were considered comfortable when dry-bulb temperatures were between 68°F and 80°F, humidity ratios were below 0.013, and air velocities were below 300 fpm.

Evaporative efficiency.

$$E_{evap} = (T_{DB,in} - T_{DB,out}) / (T_{DB,in} - T_{WB,in}) \quad (1)$$

where E_{evap} - evaporative efficiency (%);

$T_{DB,out}$ - exiting air dry-bulb temperature (°F);

$T_{DB,in}$ - entering air dry-bulb temperature (°F);

$T_{WB,in}$ - entering air wet-bulb temperature (°F).

Cooling capacity.

$$Q = \sum (V_{out} \times \rho \times C_p \times A \times \Delta T \times 5) / H \quad (2)$$

where Q - cooling capacity (Btu/h);

V_{out} - measured air velocity at tower outlet (ft/min);

ρ - 0.067 lb/ft³, air density;

C_p - 0.24 Btu/lb°F, air specific heat;

A - 7.28 ft², tower cross-section area, taken to the centerline of the structural framing;

ΔT - Measured air dry-bulb temperature at tower inlet (°F) subtracted from measured air dry-bulb temperature at tower outlet (°F);

H - hours of operation.

Total source water consumption if electric powered AC was used to provide the same amount of cooling provided by the towers.

$$t_{source} = (\sum Q / (COP_{AC} \times 3412 \text{ Btu/kWh})) \times t_w \quad (3)$$

where t_{source} - total source water consumption (gal);

$\sum Q$ - Total cooling (Btu)

COP_{AC} - 4.0 which is the coefficient of performance for residential scale AC [13].

t_w - 2.0 gal/kWh, which is the U.S. weighted total of evaporated water at source per kWh of electricity consumed at the end-use [14].

PLEA 2018 HONG KONG

Smart and Healthy within the 2-degree Limit

Total evaporative cooling site water consumption was calculated by multiplying 0.7 gal/h, which is the water consumption per mister, to the number of misters and the total hours of operation. No source water consumption was assumed in this case as no electricity was required to supply water to the top of the tower.

5.1 Results from hot dry days

This set of data was collected between June 8, and July 5, 2017, where ambient air dry-bulb temperatures during hours of operation ranged between a low of 86.8°F (30.4°C) with 11.0 percent coincident relative humidity and a high of 123.4°F (50.7°C) with 7.8 percent coincident relative humidity. This was the highest temperature recorded throughout the entire data collection process. When evaporative cooling was the only system operating in both towers and ambient temperatures were below 115°F (46.1°C), the single stage tower outperformed the hybrid tower. The single stage tower consistently generated 4.0 tons of cooling when 3 misters were operating with no fan and 100 percent of the conditions at tower outlet within comfort limits. The hybrid tower only achieved 2.3 tons of cooling with approximately 25 percent of the measurements within comfort limits, mainly due to temperatures falling below comfort zone lower limits. When ambient air temperatures rose above 115°F (46.1°C), PDECT continued to outperform PHDCT in terms of cooling capacity but was inconsistent in achieving comfortable conditions.

When the second stage of sensible cooling and fan were concurrently operating with evaporative cooling, the hybrid tower outperformed the single stage tower. The hybrid tower reached approximately 4.2 tons of cooling in this mode, with more than 85 percent of the conditions at outlet within comfort limits. The heat exchanger and fan helped advance performance of PHDCT by approximately 2 tons. The single stage tower with evaporative cooling and fan still achieved 4.3 tons of cooling, but with only 20 percent of the conditions within comfort limits. Figure 5 below is of outlet conditions obtained from both towers on June 24 and 25, 2017, when towers were operated in this mode.

In all operation modes, site water consumption by both towers was at least 2 time lower than source water required by residential scale AC unit to provide same amount of cooling provided by the towers. This is with the assumption that the hybrid tower uses a closed loop system for the heat exchanger and only consumes water through evaporative cooling. The calculation of water consumed by the towers includes the unevaporated water that was accumulating at the base of both towers. When operating evaporative cooling at three misters, approximately one third of the misting water that was injected into each tower shaft did not evaporate and was collecting at the base. This can be recirculated back into the cooling system or reused for other purposes.

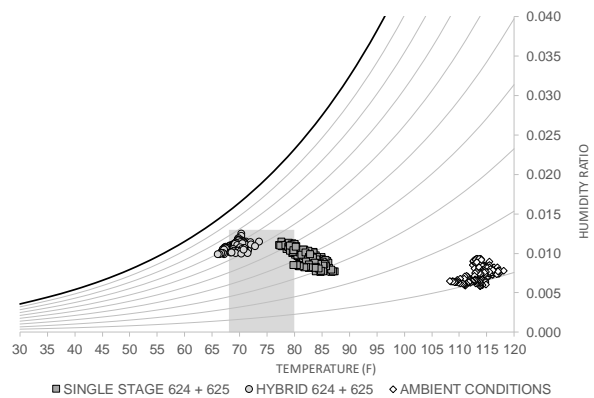


Figure 5: Towers outlet conditions from June 24 and 25, 2017, plotted on the psychrometric chart.

5.2 Results from hot humid days

This set of data was collected between July 12, and July 21, 2017, where ambient air dry-bulb temperatures during hours of operation ranged between a low of 73.0°F (22.7°C) with 82.9 percent coincident relative humidity and a high of 97.8°F (36.5°C) with 43.8 percent coincident relative humidity. The highest relative humidity percentages from the entire data collection process were recorded during these days and reached 90 percent. Wind speeds reached a high of 2359.5 fpm (12 m/s), also the highest speed recorded throughout the entire data collection process.

PDECT performance decreased in comparison with its own performance under hot dry conditions as cooling capacity when water flow was set at three misters only reached 1.6 tons, compared to the average 4.0 tons reached when operating under hot dry conditions. Average temperature drops at this water flow rate were only 17.1°F (9.5°C) in hot humid conditions vs. 36.4°F (20.2°C) in hot dry conditions. This is because temperatures at tower outlet would not drop below ambient air wet-bulb temperatures which is common in the evaporative cooling process as evaporative efficiencies reached 100 percent.

PHDCT performance remained nearly identical in comparison with its own performance under hot dry conditions when only the heat exchanger and fan were operating (no evaporative cooling). Maximum cooling capacity reached was approximately 1.1 tons during hot humid days vs. 1.0 ton during hot dry days. Even though tower inlet temperatures under hot humid conditions were lower than those recorded under hot dry conditions, average temperature drops were nearly identical at 12°F (6.6°C). This is due to tower outlet temperatures continuing to drop beyond ambient air wet-bulb temperatures which is common in the sensible cooling process.

Comfort requirements were not met by the hybrid tower in these operation modes, mainly due to increased levels of humidity inside the tower shaft caused by ambient air

PLEA 2018 HONG KONG

Smart and Healthy within the 2-degree Limit

moisture content condensing on the heat exchanger, dropping down the tower shaft, and collecting at the base. This can be solved by immediately removing water accumulating at the base and circulating it back into the system or using it for other purposes.

6. CONCLUSIONS AND LIMITATIONS

Results indicated that the hybrid tower outperformed the single stage tower under all ambient conditions and that towers site water consumption was at least 2 times lower than source water required by residential scale AC to achieve the same amount of cooling achieved by the towers.

Under the hot dry conditions of June, and when the single stage tower operated in its best mode (three misters with no fan), it produced average temperature drops of 35°F (19.4°C) (5°F higher than what was reported in the literature), average air velocities of 200 fpm (1 m/s), and average cooling capacities of 4 tons. Furthermore, when the hybrid tower operated in its best mode (three misters with sensible cooling and fan), it produced average temperature drops of 45°F (25°C) (50°F with three misters, sensible cooling, and no fan), average air velocities of 160 fpm (0.8 m/s), and average cooling capacities exceeding 4 tons. Under the hot humid conditions of July, temperature drops from the single stage tower were limited to the ambient air wet-bulb temperatures whereas drops continued beyond the wet-bulb in the hybrid tower, resulting in 60 percent decline in the former's cooling capacity while maintaining the capacity of the latter.

This study demonstrated the tremendous potential of downdraft cooling in general and hybrid downdraft cooling in specific for cooling indoor and outdoor spaces. Studies at full-scale are required to ensure that the average temperature drops recorded in this study can be maintained, while concurrently supplying larger volumes of air. The author expects that the outcomes from this study will act as an incentive for designers to incorporate PDC into their designs as a viable replacement/supplement to AC; thus, reducing the impact of the built environment on the natural environment.

ACKNOWLEDGEMENTS

The author would like to thank the Herberger Institute Research Council and Arizona Public Service (APS) for awarding him the APS Endowment for Sustainable Design Research Grant which helped fund the experimental component of this study.

REFERENCES

1. Ford, B., Schiano-Phan, R., & Francis, E. (2010). *The architecture & engineering of downdraught cooling: a design sourcebook*. PHDC Press.
2. Bryan, H. (2004). Water Consumption of Passive and Hybrid Cooling Strategies in Hot Dry Climates. In *Proceedings of 33rd*

- American Solar Energy Society (ASES) and the 29th National Passive Solar Annual Conference*. Portland, Oregon.
3. Givoni, B. (1994). *Passive and low energy cooling of buildings*. New York: Van Nostrand Reinhold.
4. Ford, B. (2002). *Passive Downdraught Evaporative Cooling (PDEC) applied to the central atrium space within the New Stock Exchange in Malta*. Retrieved from <https://web.archive.org/web/20131102061631/http://www.managenergy.net/download/nr35.pdf>
5. Cunningham, W. A., & Thompson, T. L. (1986). Passive cooling with natural draft cooling towers in combination with solar chimneys. In *Proceedings of PLEA' 86, Passive and Low Energy Architecture* (pp. 23–34). Pecs, Hungary.
6. Institute of Energy and Sustainable Development. (2004). Application of Passive Downdraught Evaporative Cooling (PDEC) to Non-Domestic Buildings. Retrieved from http://www.iesd.dmu.ac.uk/contract_research/projects/pdec.htm
7. Al-Hemiddi, N. A. M. (1995). *Passive cooling systems applicable for buildings in the hot-dry climate of Saudi Arabia*. University of California Los Angeles.
8. Yajima, S., & Givoni, B. (1997). Experimental performance of the shower cooling tower in Japan. *Renewable Energy*, 10(2–3), 179–183. [https://doi.org/10.1016/0960-1481\(96\)00060-2](https://doi.org/10.1016/0960-1481(96)00060-2)
9. Givoni, B. (1997). Performance of the “shower” cooling tower in different climates. *Renewable Energy*, 10(2–3), 173–178. [https://doi.org/10.1016/0960-1481\(96\)00059-6](https://doi.org/10.1016/0960-1481(96)00059-6)
10. Chiesa, G., & Grosso, M. (2015). Direct evaporative passive cooling of building. A comparison amid simplified simulation models based on experimental data. *Building and Environment*, 94, 263–272. <https://doi.org/10.1016/j.buildenv.2015.08.014>
11. Chakraborty, J., & Fonseca, E. (2005). Analysis and Evaluation of a Passive Evaporative Cool Tower in conjunction with a Solar Chimney. In *Proceedings of 22nd International PLEA Conference*. Beirut, Lebanon.
12. Emmegi Heat-Exchangers. (2017). *Emmegi Heat-Exchangers Mobile Oil Coolers Elements*. Retrieved from <http://emmegiinc.com/wp-content/uploads/2014/06/2000K-E-Series-Coolers-R1.pdf>
13. U.S. Department of Energy. (2015). *Central Air Conditioner Standards Brochure*. Retrieved from https://www.energy.gov/sites/prod/files/2015/11/f27/CAC_Brochure.pdf
14. Torcellini, P. A., Long, N., & Judkoff, R. D. (2004). Consumptive Water Use for U.S. Power Production. *ASHRAE Transactions*, 110, 96–100.

Neutral global warming potential target of electricity storage as threshold for greenhouse gas emission mitigation in buildings

DIDIER VUARNOZ¹, THOMAS JUSSELME¹

¹Building 2050 Research Group, Ecole Polytechnique Fédérale de Lausanne (EPFL), Fribourg, Switzerland

ABSTRACT: Coupling photovoltaic (PV) systems with energy storage (ES) in buildings, enables to increase the building's energy autonomy and the self-consumption of onsite renewables. ES increases nonetheless the life cycle environmental impact of the stored energy. As such, there exists a threshold where the GHG emission benefits of using ES start to compensate its own embedded and operational impact. In this study, a methodology to assess this neutral global warming potential target of ES is proposed, and is extended to the primary energy and its non-renewable part. The methodology is tested on a case study consisting of a feasibility project of a building located in Switzerland. When the surplus of renewable energy that cannot be used or stored directly is exportable to the grid, the operational benefits of the ES cannot balance anymore its embedded impact. In regards to market products, these neutral targets are tighter for GHG emissions than energy. Neutral targets are greatly affected by the characteristics of the grid mix supplying the building so the use of energy storage for the mitigation of GHG emissions in buildings may be efficient in Germany, but might be technologically more challenging with low-carbon French electricity.

KEYWORDS: Energy storage; GHG emissions; Primary Energy; LCA; Global warming

NOMENCLATURE

CED	Cumulative energy demand (MJ _{eq} /kWh)
CED _{nr}	Non-renewable CED (MJ _{eq} /kWh)
C _{ES}	Storage capacity (kWh)
E	Final energy (kWh)
E ₀	Building electricity demand (kWh)
E _T	Transit (kWh)
Exp	Export
ES	Energy storage
f _{ES}	Fading capacity factor (% kWh ⁻¹)
GWP	Global warming potential (kgCO _{2eq} /kWh)
GHG	Greenhouse gas (kgCO _{2eq})
PV	Photovoltaic
RE	Renewable energy
η	Efficiency (%)

1. INTRODUCTION

The energy transition towards a low-carbon society is a driver for the implementation of renewable energy (RE) systems in the building sector. Many countries have imposed targets concerning the amount of onsite RE production (e.g. [1]). One main problem with intermittent renewable sources (e.g. wind, solar) lies in the temporal mismatch between their availability and the energy demand. In buildings, energy storage (ES) coupled with photovoltaic (PV) systems are a promising solution to increase the self-consumption of onsite RE, the building's energy autonomy, and to reduce the stress on the grid. When embedded into buildings' energy systems, the consequences of ES on GHG emissions, as measured by its CO_{2-eq} emissions at the building level, have not been yet explored. Anyhow, ES increases the life cycle environmental impacts of the energy which is

stored because extra elements are added to the building energy system (BES), each one with its own embodied energy and losses. Nowadays, the challenge is not only the financial and energy viability of an energy storage coupled to a PV system, but also to provide an electricity that has accumulated less life cycle GHG emissions than grid electricity.

The functional unit to express the footprint of an electric energy storage varies in the literature: one unit of mass of storage in kg (e.g. [2]), one unit of storage capacity in kWh (e.g. [3]), or one unit of energy (kWh) at the output of the battery (e.g. [4]). In this study, we adopt the last one in order to make comparison between the global warming potential (GWP) of the three different sources of supply. This quantity is also known as the carbon footprint of electricity [5], CO_{2-eq} footprint [6], conversion factor for the GHG emissions [4], or emission factor [7], and is expressed in kg CO_{2-eq} per kWh of electricity (final energy).

GWP_{ES} has therefore a maximum allowable value beyond which the energy storage will not mitigate the life cycle GHG emissions of the energy system at the building level. In this paper, this threshold is hereafter called the energy storage GWP neutral target (GWP_{ES,max}) and a methodology is developed to assess it. Two schemes of the renewable surplus power management are addressed: i.e. when electricity exports to the grid are possible or not. The methodology is tested on a building case study and the obtained results are discussed. The same methodology is applied for assessing the neutral target for the primary energy and its non-renewable part. Obtained results are compared with LCA data related to

real storage systems. The paper ends up with a discussion on the limits of the study.

2. METHODOLOGY

2.1 GHG emissions mechanism

To illustrate the GHG mechanism in which the operational benefit of using an ES is combined with its own embedded impact, let us consider a baseline consisting of a building with an energy system that does not comprise an energy storage. The resulting GHG emissions at the building level is taken as a baseline (Case 0 in the right part of Fig. 1).

Then we consider the implementation of an ES, which has a low GWP (GWP_{ES1}). According to that, the GHG emissions of the system is lower than the one considered in the initial case (as seen in the case I. in the right part of Fig. 1)

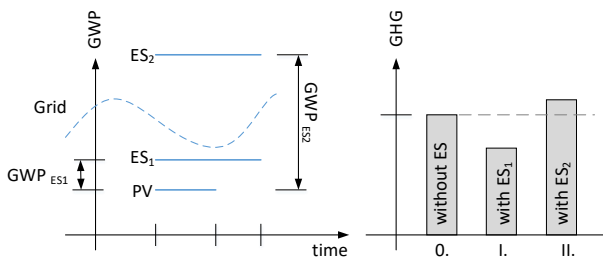


Figure 1: The GWP of the different sources of electricity supply (Left) combined with operational benefits of an energy storage govern the mechanism of the lifecycle GHG emission at the building level (Right).

A second case (case 2 in Fig 1) is considered to illustrate the GHG mechanisms, and depicts another storage with its GWP much higher than case 1 (GWP_{ES2}). This is the case when a large storage capacity is at disposal, but seldom used. As a consequence, associated GHG emissions assessed at the building level would be so high that they cannot be balanced during the lifetime of the energy storage.

2.2 Carbon footprint of energy sources

In a national electricity grid, the share of each electricity generation technology (e.g. coal, hydro, etc.) varies continuously over time according to the fuel characteristics (availability and possibility to modulate the power production) in order to adapt the supply to an ever-changing demand. The same applies to domestic export and import of electricity. Therefore, each kWh at the consumer's disposal does not have the same carbon footprint GWP_G over time (see Fig.1, left part). Despite this situation, it is still common to use yearly averaged GWP_G when considering an electricity mix for performing GHG emissions assessments. This usual practice could be soon revised due to the potential large inaccuracies in carbon emission assessment [7-9] and the late emergence of hourly GWP for different countries (see e.g.

[7;10-11]). In this study, hourly GWP values of a grid mix are compulsory.

For PV-based electricity, we assess its GWP as the ratio of the cradle-to-grave embodied GHG emissions of the PV system [12-13], over its predictable energy generation during its entire lifetime. The value of GWP_{PV} is time-independent when E_{PV} is available i.e. during the sunshine duration (see Fig.1).

The carbon footprint of the electricity delivered by an ES is composed of the initial footprint of the electricity feeding its inlet (usually provided by PV) and the footprint of the storage itself GWP_{ES} (see Fig. 1). The assessment of GWP_{ES} is performed on the basis of an inventory of the material resources and the total energy processed during the storage system lifetime.

2.3 GHG emissions balance at the building level

Now consider a building, a PV system, an energy storage, and a connection with an electric grid. These elements and the different energy fluxes between them are presented in Fig. 2. The possibility to export the surplus of onsite RE generated is shown by the horizontal red dashed line that vanishes when exports are not possible.

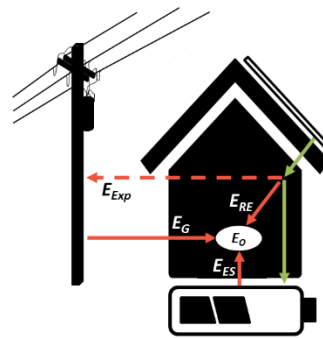


Figure 2: The possible energy fluxes occurring between the main components of a BES considered in this study.

The GHG emissions of the operational phase of the building GHG_O are assessed on the base of a cradle-to-grave LCA, following Equation (1):

$$GHG_O = (E_{RE} \times GWP_{RE}) + (E_G \times GWP_G) + (E_{ES} \times (GWP_{RE} + GWP_{ES})) - E_{EXP} \times (GWP_G - GWP_{RE}) \quad (1)$$

where E denotes the energy flux and GWP the global warming potential. Indices O, RE, G and ES stand respectively for operative, RE, grid and energy storage fluxes supplying the building energy final electricity consumption. Within a balancing period of one year, all energy fluxes within the BES (Fig. 2) and their associated GHG emissions are assessed at the hourly time step. The energy fluxes that are important to solve Eq. (1) are colored in red.

2.4 Neutral GWP target assessment

PLEA 2018 HONG KONG

Smart and Healthy within the 2-degree Limit

To determine the energy storage GWP neutral target, we propose the following four-step methodology. Step (1): the final energy consumption of the considered building, its RE production, and the grid's GWP need to be collected. These data should be evaluated at the hourly time step during one year. Step (2): The annual GHG emissions of the building operational phase without ES are assessed. Step (3): We then consider the implementation of an ES of a given size. We process to another assessment of the GHG emissions with the considered storage, but with its GWP_{ES} set to zero. Step (4): The two assessments performed during the steps (2) and (3) are compared. The GHG benefits obtained by the ES implementation are divided by the amount of energy transited in the ES during the evaluation period. This value is the energy storage GWP neutral target ($GWP_{ES,max}$) that the energy storage should exhibit for having a positive impact on the CO_{2-eq} balance at the building level.

2.5 Modeling framework

A versatile modeling framework previously developed [14] is used to simulate the running conditions of the BES at the hourly time step, and to assess its annual performances according to the Swiss standard SIA 2040 [15]. The energy storage is modeled with the following parameters: An initial storage capacity C_{ES} in kWh, a fading capacity factor f_{ES} in $\% \cdot kWh^{-1}$, and a roundtrip efficiency η in $\%$.

3. ENERGY-MANAGEMENT PROCEDURE

An energy-management procedure (EMP) consists in a set of rules governing the energy fluxes between the components of the BES. A lot of different EMP schemes are possible (see e.g. [16]) and affect the operation system so that the performance depends strongly on the chosen EMP. Different optimization can be prioritized, such as the price of energy [17], the solar forecast coupled with energy price [18], or the GWP of the energy source [14]. In this study, as in most of simple commercialized EMP, the following general rules apply: For the supply of E_0 , the merit-order of energy sources is: 1) from RE; 2) from ES; 3) from Grid. If one source is not available or not sufficient, then the next one is considered.

For the management of the onsite renewable production, energy goes: (1) to supply E_0 ; if a surplus of RE occurs, (2) to ES. In the case ES would be full, the remaining energy excess could be either exported to the surrounding electric grid (3), or thrown away (4) if export is not possible.

4. CASE STUDY

An appropriate case study consists in a building for which the energy demand, RE production, and carbon footprint of the electricity supply mix are all assessed hourly during

one year long. This is why the project of the building for the smart living lab, whose construction is planned for 2022 in Fribourg, Switzerland, makes a perfect case study. An architectural feasibility study considering an energy reference area of 4000m² serves as a basis for the assessment of the building energy demand (more details can be found in [14]). The needs of the building users are assimilated to an office building according to SIA 2024 [19]. The planned technical installations include solar thermal panels for covering 60 % of the domestic hot water energy demand. All other thermal needs are provided by a heat-pump. Electricity originates either by PV panels or by the Swiss grid mix.

Cadmium telluride PV panels ($\eta=15.1\%$) are considered to partly cover the building according to Table 1. In order to assess the GWP of the electricity provided by PV (GWP_{PV}), embedded emissions and energies have been taken from [9], and the amount of RE harvested by BIPV has been evaluated with the help of crmsolar software [20] with hourly weather data files from Meteo Suisse at Station Fribourg - Posieux. The lifetime of a photovoltaic system is assumed to be 30 years [9].

Table 1: Characteristics of the PV system

Orientation	GWP (kg CO_{2-eq} /kWh)	Area (m ²)
East (75°)	0.094	343
West (255°)	0.067	343
Roof (165°)	0.041	343

Due to the location of the case study, the Swiss grid is considered. Hourly GWP data of the grid have been evaluated on the base of an attributional cradle-to-grave LCA in [4]. From this study which considers a one-year period of 2015-2016, the values of GWP_G range from 0.029 to 0.414 kg CO_{2-eq} /kWh, with a mean annual GWP of 0.203 kg CO_{2-eq} /kWh and a relative standard deviation of 41%.

A lithium-Ion electrochemical battery is considered in the study. The values of the storage roundtrip efficiency (0.9) and a capacity fading factor ($-6E-04$ %/kWh) have been evaluated on the base of measurements performed by the product manufacturer [14].

5. RESULTS

First, we look at the annual amount of energy E_T transited in the storage. This amount is independent of the scheme of export management (see Fig. 3) and evolves similarly to a $E_T = a \cdot (1 - \exp(-b C_{ES}))$ function. This function, also known as EaseOut curve, is centred at the origin, with a horizontal asymptote when increasing C_{ES} . This feature is explained by the finite amount of solar irradiance, independently of the size of the storage.

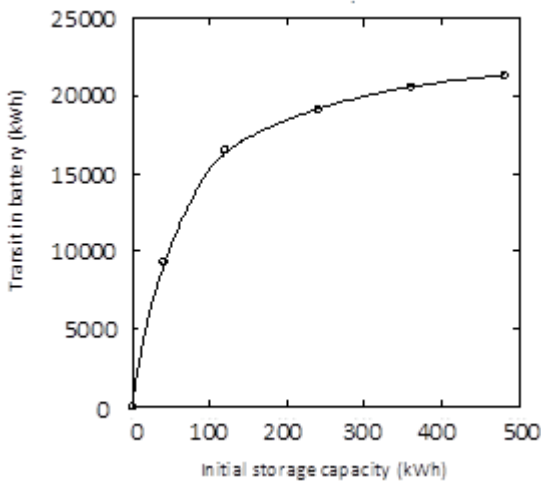


Figure 3: Amount of energy transited in the energy storage during a one-year period. Same results are obtained with or without export to the grid of the surplus RE generation.

The CO_{2-eq} results obtained when applying the methodology explained in Section 2 to the considered case study (section 3) and for two schemes of renewable excess power management are presented in Fig. 4 as a function of the size of storage capacity. When the export of excess PV electricity is impossible (or not allowed), when increasing from zero to the ES capacity the GHG emissions appear to first decrease and then converge (top of Fig. 4). When implementing an ES, the excess of PV electricity that is not used instantaneously for the building can be stored for a later use, instead of being fully thrown away. This reduces the amount of electricity imports and increases the share of RE in the building's energy consumption. As a result, compared to a system without ES ($C_{ES}=0$), a reduction of the GHG emissions is now obtained. The gap δ which is indicated in the top of Fig. 4 corresponds to the operational benefits of using an ES. This gap corresponds to the maximum embodied carbon that an ES should exhibit in order to lead to emission neutrality. On the bottom of Fig. 4, the energy storage GWP neutral target ($GWP_{ES,max}$) is presented as a function of the ES capacity size and shows a converging value of 0.122 (kgCO_{2-eq}/kWh).

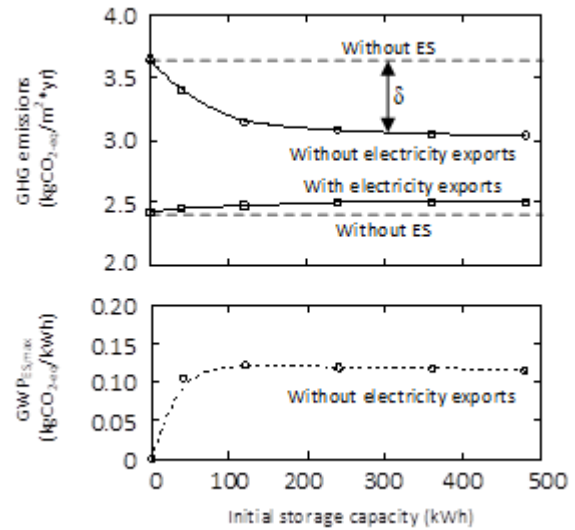


Figure 4: Top figure: GHG emissions at the building's level. Bottom figure: $GWP_{ES,max}$ to ensure GHG emission mitigation at the building level.

In the case of possible exports of surplus PV electricity, a direct valuation of this RE excess is possible through the grid, even if no ES is part in the BES. The valuation of export to the grid is possible without extra embedded impacts and energy losses of local ES. Although the GHG emissions stagnate when increasing the ES capacity size, higher GHG emissions are always obtained in comparison with the initial case without ES (top of Fig. 4). Consequently, the proposed method exposed in section 2 provides negative values for $GWP_{ES,max}$ that are – mathematically correct – but a physical nonsense. This is further addressed in the discussion

6. EXTENSION OF THE METHOD TO ENERGY TARGETS

The same method explained in section 2 may be easily extended to other life cycle indicators. We propose in this section to treat the cumulative energy demand (CED) and its non-renewable part (CED_{nr}). The energy footprints of the electricity generated by the PV panels considered in the case study are presented in Table 2 and come from [14].

The hourly energy footprints of the Swiss grid used in this study come from [4]. The mean annual values for the Swiss mix are 11.86 (MJ_{eq}/kWh) for the CED and of 10.46 (MJ_{eq}/kWh) for CED_{nr} with a relative standard deviation of respectively 10.9 and 18.1%.

Table 2: Energy footprints of the PVs considered in Table 1

Orientation	CED (MJ _{eq} /kWh)	CED _{nr} (MJ _{eq} /kWh)
East	1.52	1.41
West	1.09	1.00
Roof	0.66	0.61

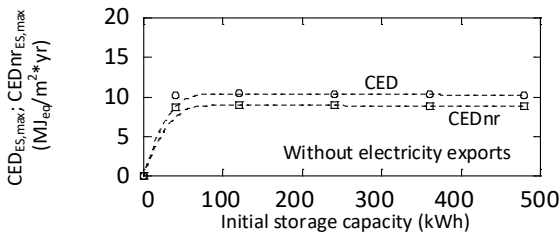


Figure 5: $CED_{ES,max}$ and $CEDnr_{ES,max}$ to ensure a mitigation of respectively the primary energy and its non-renewable part at the building level when implementing an energy storage

For the same reasons of the neutral GWP assessment, only the scheme that does not consider exports possible is presented in Fig. 5. The obtained tendencies of both functions $CED_{ES,max}=f(C_{ES})$ and $CEDnr_{ES,max}=f(C_{ES})$ are similar to the one obtained for the GWP (see bottom part of Fig. 4). The convergence values for the primary energy neutral target ($CED_{ES,max}$) is 10.2 (MJ_{eq}/kWh) and 8.8 (MJ_{eq}/kWh) for its non-renewable part.

7. CONTEXTUALISATION

The investigated range of the storage capacity has been chosen in order to understand the evolution and tendency of given indicators. To illustrate possible battery sizes within the frame of the case study, a full day of autonomy during mid-season (spring and autumn) corresponds to 350 kWh (3070 kg with an energy density of 114 Wh/kg). During the same period of the year, storing the daily excess PV production would require a storage capacity of 120 kWh (which represents 1050 kg). Considering Li-Ion technology, these two possible capacity sizes (350 and 120 kWh) and their associated embodied CO_{2-eq} correspond to respectively to 33 and 11 % of the GHG emission targets proposed by the Swiss standard SIA2040 [15] for the construction and exploitation of a new building.

To put in regards the results obtained with products from the market, we have assessed the embedded GHG emissions and primary energy of commercial batteries with an inventory analysis performed with the ecoinvent database [21] and the deterioration measurement performed by the manufacturer [14]. Obtained results are presented in Table 3. These values are far below the neutral targets evaluated specifically for our case study. The extra margin is larger for the energy than for carbon footprint.

Table 3: Energy and carbon footprints of commercialized Li-ion battery found in the literature.

Li-Ion Technology	GWP ($kgCO_{2-eq}/kWh$)	CED (MJ_{eq}/kWh)	CEDnr (MJ_{eq}/kWh)
Graphite-based [14]	0.021	0.351	0.319
Titanate-based [14]	0.007	0.117	0.106
Neutral targets	0.122	10.226	8.794

The characteristics of the electricity provided by the grid mix which supplies the building are of prior importance when assessing the neutral targets of the storage. Let's consider the same case study, with the same energy demand but with the grid electricity supplied by another national grid than the Swiss mix. According to [4], the mean annual carbon footprint of the French and German grid assessed on the base of hourly time steps exhibit a carbon footprint of respectively 0.080 and 0.860 ($kgCO_{2-eq}/kWh$). Looking back at Fig. 1, it is clear that a carbon-intensive grid mix would generate a larger GWP neutral target for the storage. This is the case when placing our case study in Germany, with a resulting target $GWP_{ES,max}$ of 0.785 ($kgCO_{2-eq}/kWh$). Opposite to that, the very low carbon footprint of the French electricity allows a value of only $GWP_{ES,max}=0.002$ ($kgCO_{2-eq}/kWh$), which is at the current time, very challenging to respect with commercialized energy storage.

8. CONCLUSION

This study aims at investigating the impacts of an energy storage on a building's GHG emissions. We propose a methodology to determine the energy storage GWP neutral target as a threshold for GHG emission mitigation at the building level. This is particularly relevant when selecting an appropriate storage technology and its capacity size. This methodology requires hourly data of both the grid carbon footprint and the building final energy consumption, and is easily applicable by engineers and building designers to ensure environmental prerequisite of energy storage at the building level already during the design stage. The methodology could be used for any kind of ES technology, and for any kind of environmental indicators used in LCA. But one must be aware that the obtained results are dependent of the investigated case study, i.e. how and in which environment the building is designed.

The limit of the study and the robustness of the obtained results are the same than the usual ones that engineers and LCA practitioners face when dealing with environmental impacts in buildings. In particular, if LCA studies are known to be appropriate for performing comparative studies, at the same time they have severe drawback for generating robust absolute values. This is particularly true when dealing with construction materials and energy medium uncertainties [22-23]. Nevertheless, "estimation for life cycle environmental emissions cannot be avoided because of the uncertainty involved" [24].

The methodology has been tested on a case study consisting of a feasibility project of a high-performance building located in Fribourg, Switzerland. The results obtained by simulations show the importance of the scheme for the surplus RE management. GHG emissions mitigation by ES implementation is achievable only without electricity exports to the grid. In such a case, the

PLEA 2018 HONG KONG

Smart and Healthy within the 2-degree Limit

numerical example performed on the base of the case study indicates that the targets are easily satisfied with commercial products. Following the same calculation procedure, the neutral target for the primary energy and its non-renewable part have also been worked out. The numerical results have also confirmed the possibility to stay below these sustainability thresholds with commercial energy storage. On the other hand, we found that the characteristics of the grid where the building is planned are of prior importance when assessing the neutral target of an energy storage. If it is very easy to mitigate the GHG emissions in buildings by the use of an energy storage in Germany, this might be technologically very challenging with low-carbon electricity such as the one delivered by the French grid.

ACKNOWLEDGEMENTS

The work presented in this paper has been funded by the State of Fribourg and the EPFL. We thank Margaux Peltier for valuable discussions and Thibault Schafer with Labview programming support.

REFERENCES

1. Parlement Européen, (2010). Directive 2010/31/UE, Directive sur la performance énergétique des bâtiments, 1-23.
2. European Commission, (2010). ILCD International Reference Life Cycle Data System (ILCD) Handbook; European Commission, Joint Research Centre, Institute for Environment and Sustainability: Luxembourg, 1-417.
3. Messagie, M., et al. (2014). The hourly life cycle carbon footprint of electricity generation in Belgium, bringing a temporal resolution in life cycle assessment. *Applied Energy*, 134, 469-476.
4. Vuarnoz et al., (2018). Temporal variation in the energy use and greenhouse gas emissions of the electricity provided by the Swiss grid. *Energy* 161, 573-582.
5. Kopsakangas-Savolainen, M., et al. Hourly-based greenhouse gas emissions of electricity—cases demonstrating possibilities for households and companies to decrease their emissions. *Journal of Cleaner Production* 153 (2017): 384-396.
6. Roux, C, et al. (2016) Accounting for temporal variation of electricity production and consumption in the LCA of an energy-efficient house. *Journal of Cleaner Production* 113 (2016): 532-540.
7. Milovanoff, A. (2016) *Optimisation environnementale de la gestion des consommations électriques en temps réel*. Diss. Ecole Polytechnique, Montréal, Canada.
8. Spork, C.C., et al. (2015) Increasing Precision in Greenhouse Gas Accounting Using Real-Time Emission Factors. *Journal of Industrial Ecology* 19.3: 380-390.
9. Frischknecht, R., et al. (2015) Life cycle inventories and life cycle assessment of photovoltaic systems. *International Energy Agency (IEA) Report IEA-PVPS 12-04:2015* (2015).
10. Vuarnoz et al., (2016). Studying the dynamic relationship between energy supply carbon content and building energy demand. *PLEA 2016 Los Angeles - 36th Int. Conf. on Passive and Low Energy Architecture*.
11. Nealer, R., Hendrickson, T.P. (2015) Review of recent lifecycle assessments of energy and greenhouse gas emissions for electric vehicles. *Current Sustainable/Renewable Energy Reports* 2.3: 66-73.
12. McManus, M.C. (2015) Environmental consequences of the use of batteries in low carbon systems: The impact of battery production. *Applied Energy* 93: 288-295.
13. Peterson, S. B., et al. (2010). Lithium-ion battery cell degradation resulting from realistic vehicle and vehicle-to-grid utilization. *Journal of Power Sources*, 195 (8), 2385-2392.
14. Vuarnoz et al., (2018). Integrating hourly life-cycle energy and carbon emissions of energy supply in buildings. (Submit.)
15. SIA 2040, 2017. Efficiency path for energy, 1-27.
16. Zhou, B., et al. (2016). Smart home energy management systems: Concept, configurations, and scheduling strategies. *Renewable and Sustainable Energy Reviews* 61: 30-40.
17. Gridsense product. Retrieved (March 12, 2018), <https://www.gridsense.ch/en/home.html>
18. Hoan-Anh, D., et al. (2013) Toward autonomous photovoltaic building energy management: modeling and control of electrochemical batteries. *Proc. of 13th Conf. of IBPSA, Chambéry, France*.
19. SIA 2024, 2015. Données d'utilisation des locaux pour l'énergie et les installations du bâtiment, 1-152.
20. Smarsys (2017) Retrieved (March 12, 2018), <http://www.smarsys.com/services/gestion-de-parc-photovoltaique/>
21. Frischknecht, R et al. (2005). The ecoinvent database: Overview and methodological framework (7 pp). *The International Journal of Life Cycle Assessment*, 10(1), 3-9.
22. Reap, J., et al. (2008). A survey of unresolved problems in life cycle assessment. *The International Journal of Life Cycle Assessment*, 13(5), 374-388.
23. Hoxha, E et al. (2017). Influence of construction material uncertainties on residential building LCA reliability. *Journal of Cleaner Production*, 144, 33-47.
24. Weber, CL et al. (2010) Life cycle assessment and grid electricity: what do we know and what can we know? *Environ. Sci. Technol.* 44, 1895-1901.

Assessing the Adaptability of the Saudi Residential Building's Energy Code for Future Climate Change Scenarios

MOHAMMED AWAD ABUHUSSAIN¹, DAVID HOU CHI CHOW¹, STEVE SHARPLES¹

¹School of Architecture, University of Liverpool, Liverpool, United Kingdom

ABSTRACT: Due to the expectation of climate change and increasing global temperature, new building rates will face challenges. Nearly 40% of world-wide carbon emissions can be linked to building's energy consumption. Therefore, it is significant to understand how a building's energy consumption will behave under future climate change in order to reduce carbon emissions. The residential sector's demand for energy in the KSA is massive at 50%. Based on recent government initiatives of KSA, mandatory new residential buildings must meet stringent energy codes. This study investigates the effects of applying the new Saudi residential building energy codes for a detached single-family house (villa) located in Jeddah, KSA. This study aims to see how the code might perform under current and future climate change scenarios. Although the current code already shows a significant improvement in combating future climate change, a total reduction of 38% in the annual cooling demands of existing villas in Jeddah after applying the new standards will be illustrated. However, increases in cooling energy demand due to climate change still exist. Applying more passives strategies that are not included in the code would assist the researcher in knowing if there are other means to achieve significant decreases in cooling demand.

KEYWORDS: Climate Change, Energy Consumption, Residential Villas, Energy Code, Hot Climate

1.1 INTRODUCTION

Saudi Arabia mainly depends on oil and natural gas as sources of energy. More than half a million barrels of oil is being used daily in the country in order to generate electricity[1]. The per capita CO₂ emissions that results from the energy consumption in the KSA in 2012 increased and is ranked the highest in comparison with many developed countries in the world[2]. The building sector is a major contributor to energy demand in the Kingdom of Saudi Arabia (KSA) due to the reliance on air conditioning for cooling. Buildings (residential, governmental, and commercial) consume around 75% of the total electricity generated in KSA with an annual growth rate of 7%[3]. Among different types of buildings, the residential building sector represents more than 50% of the total electricity consumed in the country figure 1.[4] This is due to the fact that currently most of the residential buildings are not insulated. In addition to this, the hot climate of KSA causes high demands for air conditioning particularly during the summer season. Furthermore, the building sector is considered to be in a need for building 2.32 million new houses by 2020 in order to meet the requirements of population growth, as at present only 24% of the Saudi citizens have their own home[5].

In view of this issue, many researchers have indicated that setting out energy standard and code can play an important role to enhance the buildings energy efficiency[1]. Based on the recent initiative provided by the government of KSA, a mandatory new build residential buildings' energy code has been established to reduce energy consumption. According to the Saudi

Energy Efficiency Centre(SEEC), this code is expected to achieve 30-40% energy reduction in the residential sector[3]. However, the issue of energy consumption of the existing and new build residential buildings will be exacerbated because of climate change. Based on the study conducted by Almazroui et al.2012[6], it was found that the temperature in KSA will increase at a rate of 0.72°C mean temperature each decade. Furthermore, by 2050 the temperature will see an increase in a rate between 2.0–2.75°C. Therefore, the building capability to tackle future climate change is critical [7]. Based on reviewing the residential buildings' energy code, it was found that predicted future climate change was not given any consideration. Therefore, this study focuses on examining the capacity of the Saudi residential building's energy code to cope with future climate change.

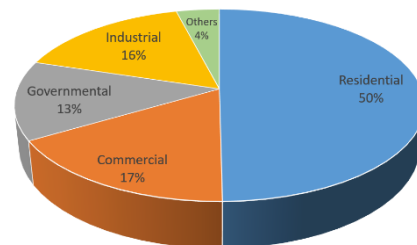


Figure 1: Energy consumption by building sectors in Saudi Arabia.

1.2 LITERATURE AND BACKGROUND

Due to advanced building technologies, the lifespans of buildings are increasing, so the demolition rate of buildings will fall in the future. Another important consideration is that worldwide building energy

PLEA 2018 HONG KONG

Smart and Healthy within the 2-degree Limit

consumption contributes around 40% of global total carbon emissions. Therefore, to achieve rational use of energy in the context of future climate change, it is crucial to understand the potential impact of global warming on the thermal performance of a building and to take appropriate measures to prevent unnecessary energy waste, through both energy-saving designs and operational management.[8] The influences of global warming on building energy performance and the corresponding adaptive strategies have gained much attention worldwide.

A recent research was conducted by Radhi to assess the potential impact of climate change on residential buildings in the United Arab Emirates. The study found that the energy demand for cooling buildings would increase at a rate of 23.5% when the temperature increased in Al-Ain city by 5.9°C.[9] Wong et al. investigated future trends of cooling load in the residential sector in subtropical Hong Kong under dynamic weather scenarios in the 21st century. The results of the study show that the percentage increase for the last 30 years of the 21st century is predicted to be 21.6%.[10] Another study in Australia was conducted to evaluate the climate change impact on residential building's heating and cooling energy requirements. It was found that the predicted increase in the total heating and cooling energy consumption was up to 120% and 530% if the global temperature increases 2°C to 5°C respectively.[11]

Although the Gulf region has its fair share of academic research on this subject, the topic of global warming and its effects on building energy performance is surprisingly scant. The bulk of research on construction energy performance has been conducted on buildings assumed to be constructed in limited weather conditions.[9] The aim of this study is to shed light on the effects of climate change on the energy usage of newly-built and existing air-conditioned living residences in The Kingdom of Saudi Arabia.

1.3 DESCRIPTION OF THE CODE

In response to the crisis of high energy consumption that results from massive growth of building sector, in 2012 the government of Saudi Arabia introduced a royal Decree No.6927 by applying the thermal insulation for all building sector and this was aimed at improving the energy efficiency in buildings mainly by requiring the use of thermal insulation. In 2013, the standard No.2856/2014 Thermal Transmittance Values for Residential Buildings was issued by the Saudi Standards Metrology and Quality Organization. This standard is derived from Saudi Building Code Chapter 601(Energy Conservation).The standard particularly regulates maximum thermal transmittance U-values for residential buildings envelope such as Walls, roofs and window glazing. These U-values were applied and become a

mandatory for all residential buildings in two stages as code 1 and code 2. Code 1 was implemented for all the residential buildings that were built after 2013. Then, code 2 was applied to be required for all residential buildings that were built after January 2017.

1.4 BACKGROUND AND CLIMATE OF JEDDAH CITY

This research selected Jeddah city as a case study to investigate. This city faces the western coast of Saudi Arabia and it has tropical arid climate base on Koppen's climate classification. Jeddah is also one of the fastest growing city into a future buildings construction in the region .Jeddah city is a vital city in Saudi Arabia with a population more than 4 million which accounts for almost 15% of the total population of Saudi Arabia.[12] Furthermore, the severity of Jeddah's weather necessitates the investigation of energy consumption in this city as it is considered one of the greatest challenges in the country.

Jeddah city has a hot climate with high humidity most of the year especially in the summer season which extends from May till October. The monthly average temperature range is between 30°C to 33°C and the maximum temperature reaches 40°C in July. The Winter season is from November to April with monthly average temperature from 23 °C to 27°C. Figure 2 shows the maximum, minimum and monthly average dry-bulb temperature for Jeddah city.

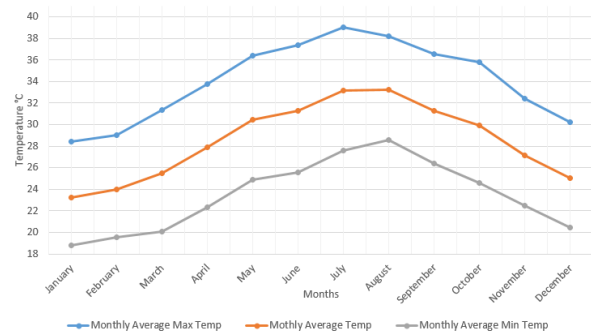


Figure 2: The monthly maximum, minimum and average outdoor temperature for Jeddah, Saudi Arabia.

2.1 METHODOLOGY

In order to evaluate the performance of the residential buildings' energy code in KSA, a detached single-family house (villa) located in Jeddah city has been selected for this study. This villa was built in 2008 before applying the Saudi residential building's energy code. This is becoming a typical villa and represents the dominant type of residential buildings in Jeddah city. This housing type represents 20% of the total housing number in KSA.[13] A three-dimensional model for this typical villa that was built based on the architectural drawings using DesignBuilder software (version 5.0.1) as shown in figure 3.

PLEA 2018 HONG KONG

Smart and Healthy within the 2-degree Limit



Figure 3: villa under study.

The use of this simulation tool as investigatory method is to principally assess the performance of the residential buildings' energy code under future climate change. The building characteristics including construction materials, cooling system types, lights and equipments of the physical villa were applied and modelled in DesignBuilder with occupancy and activity profile as shown in table 1. Current and future weather data files for the periods (2010, 2050 and 2080) also greenhouse gas emission scenarios the A2, A1B, and B1 for Jeddah city were obtained from the climate generator software Meteonorm 7. This software is a climate generator tool that provides users with weather data files for most locations world-wide. [14]

2.2 MODEL VALIDATION

Hourly temperature calibrations between the DesignBuilder model and the actual interior temperature were conducted by recording the indoor and outdoor temperature at hourly intervals. Ibutton dataloggers (DS1921H-F5 Thermochron) were placed in each single room in the house in a constant position to be away from any heat source and to record the indoor temperature. Also, Ibutton dataloggers (DS1923-F5# Hygrochron) were sheltered from direct sunlight and rainfalls and fixed on the top of the villa's roof to record the outdoor temperature Figure 4 shows the equipment that were used for on-site measurements. The process of field measurements began in June 2017 and ended in August 2017. The study intends this period of time because this three months during summer represents the hottest weather in the year where the use of the air conditioner peaks. Monitoring process were also attempted to monitor and extract the occupancy and the schedule of the house for those three months.

Table 1: characteristics of the villa and simulation options.

Parameters	Villa
No. of floor	2 floors+ annex
Total area	439.25 m ²
Building Height	9.6 m
Orientation	North
External/ Internal walls	20 mm mortar (outer surface)
	200 mm Hollow red-clay brick
	20 mm mortar (inner surface)
Internal floors	10 mm ceramic tiles (outer surface)
	25 mm mortar
	150 mm Reinforced Concrete
Roof	20 mm mortar (inner surface)
	25 mm Terrazzo Tiles (outer surface)
	25 mm mortar
	4 mm Bitumen layer
	150 mm Reinforced Concrete
WWR	14.5 %
Window glazing	6 mm Single clear glazing
Infiltration rate	0.7 ac/h (estimated)
HVAC system	Constant volume DX with no heating
Occupancy	0.0136 person/m ²
Thermal zones	Multi zones
Cooling set point temperature	25.5 °C (stated in the code)



Figure 4: Equipment used for on-site measurements.

Figure 5 displays hourly comparison between the actual measured data and DesignBuilder results for the living room in the villa for five days while the building was a free-running. The calibration results show that there is no more than $\pm 4\%$ difference between the measured and simulated temperature. According to Taleb [15] the researcher can consider the model to be valid as long as the difference between simulated and measured results is less than 5%. In addition, billed monthly consumptions of electricity for the villa were obtained from the Saudi Electricity Company to compare with those calculated for the base case villa. Figure 6 draws a comparison between utility bills consumption and DesignBuilder results during three months. The calibration processes were employed to principally validate the calculations of the DesignBuilder model and supporting the state of being

PLEA 2018 HONG KONG

Smart and Healthy within the 2-degree Limit

confident and certain about the simulations in order to conduct a study under the impact of climate change.

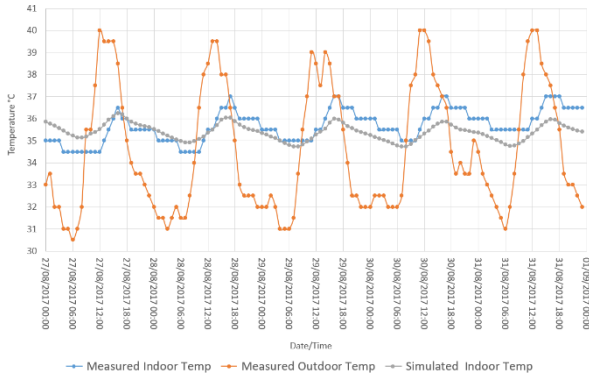


Figure 5: Hourly calibration between on-site measured data and calculated consumption for living room in the villa.

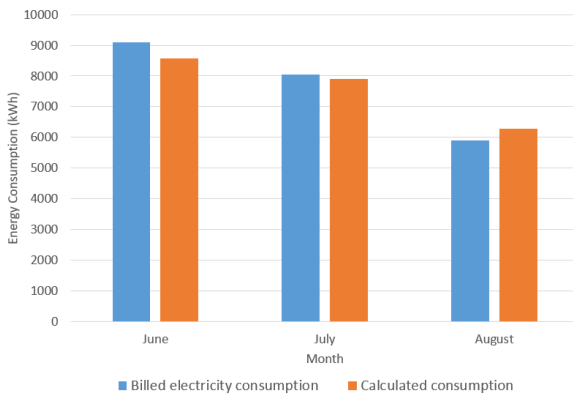


Figure 6: comparison between utility bills consumption and DesignBuilder results for the three months.

2.3 SIMULATION PROCESS

In order to ensure the constancy of the annual simulations analysis results, the typical Saudi daily schedules pattern for lighting, equipment and occupancy were specified from previous study of energy conservation in the existing residential buildings in Saudi Arabia.[16] The monthly energy DesignBuilder simulation results for the base case villa under the current climate is acquired and shown in figure 7. As expected, figure 7 shows that the space cooling represents 83% of the total annual electricity energy consumption for the villa. The next stage was to apply code 1 and code 2 to the base case villa in order to evaluate the performance of the base case villa against code 1 and against code 2 under the current climate. Table 2 draws a comparison between U-values of the typical villa and the current codes which have been studied in this research. In order to achieve the thermal transmittance U-values that are listed in the code for walls and roofs, practical construction materials and methods that are commonly used in Saudi Arabia were selected. Table 3 summarized the specifications of construction methods and materials for walls and roofs that are currently used in KSA. Finally, extensive

simulations by engaging climate change scenarios were conducted to examine the requirements of the Saudi residential building's energy codes for external walls, roofs and openings specifications.

Table 2: U-values (W/m²K) for existing typical villa and the Saudi residential building's energy codes (code1 and 2).

U-Value (W / m ² K)	Existing Building	Code1	Code 2
Roofs	3.40	0.31	0.20
Ext. Walls	1.82	0.53	0.34
Windows	5.71 SHGC - 0.81	2.67 SHGC - 0.25	2.67 SHGC - 0.25

Table 3: Construction characteristics for walls and roofs.

Parameter	Code 1	Code 2
Wall	20 mm mortar (outer surface) 100 mm Hollow red-clay brick 50 mm expanded polystyrene 150 mm Hollow red-clay brick 20 mm mortar (inner surface)	20 mm mortar (outer surface) 100 mm Hollow red-clay brick 80 mm expanded polystyrene 150 mm Hollow red-clay brick 20 mm mortar (inner surface)
Roof	25 mm Terrazzo Tiles (outer surface) 25 mm mortar 4 mm Bitumen layer 100 mm expanded polystyrene 150 mm Reinforced Concrete 20 mm mortar (inner surface)	25 mm Terrazzo Tiles (outer surface) 25 mm mortar 4 mm Bitumen layer 160 mm expanded polystyrene 150 mm Reinforced Concrete 20 mm mortar (inner surface)

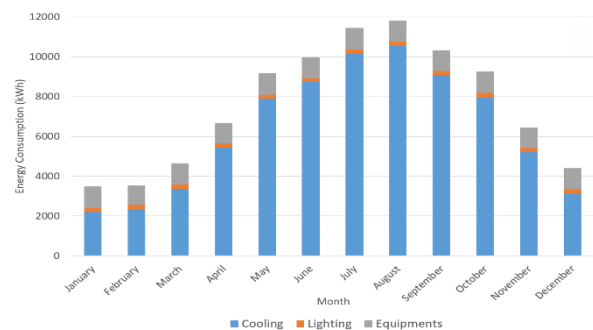


Figure 7: Monthly electricity consumption for the base case villa.

3. RESULTS AND DISCUSSION

Figure 8a shows the monthly cooling energy consumption for the existing villa under the current climate and the A2 future climate scenarios. It can be

PLEA 2018 HONG KONG

Smart and Healthy within the 2-degree Limit

clearly seen that the yearly cooling loads with the existing villa under the current climate extend from 2000 kWh in January to a peak cooling load of 10000 kWh in July but with the future climate A2 scenario in 2080, the cooling load increases from 6000 kWh in January to 14000 kWh in July. Figure 8b shows the same 12-month time frame of cooling energy consumption for the retrofitted villa to code 1 under the current climate and the A2 future climate scenarios. The graph shows the result that the yearly cooling load with the retrofitted code 1 under the current climate range from 1200 kWh in January to a high cooling load of 6800 kWh in August but with the future climate A2 scenario in 2080, the apex cooling load of 8400 kWh is achieved in August and a trough of 2000 kWh is attained in February.

Figure 9 shows the total annual cooling energy consumption in the current and future climate periods under different climate change scenarios for the base case villa (in blue), retrofitted villa to code 1 (in orange) and retrofitted villa to the standard of the code 2 (in grey). It is shown that applying code 1 to the existing villa has achieved a high reduction in the total annual cooling demands with a rate of 38% calculated. The saving rate in the total annual cooling requirements by applying code 2 to the base case villa is approximately the same level as applying code 2 as it achieved 40 %. As it can be seen, the 2% difference in cooling energy savings from code 2 and code 1 is negligible. As mentioned previously by Saudi Energy Efficiency Centre (SEEC), this code is expected to achieve 30-40% energy reduction in the residential sector. This prediction meets the results of this study that shows 40 % reduction in the total annual cooling loads for the base case villa by applying code 2. Therefore, applying code 2 to this housing type (villa) which represent one fifth of the overall total number of the residential buildings in KSA can improve the energy performance and reduce the consumption of energy in the building sector in Saudi Arabia. As figure 7 shows, A2 is the worst scenario. However, this is due to abnormally high temperatures. Based on the climate condition from the current climate to 2050 (A2 scenario), the most consumed energy of annual cooling for the retrofitted villa to code 1 is being increased at a rate of 23 %. While over the climate change from the current to 2080, this increase will reach at a rate of 38%.



Figure 8: the changes in monthly cooling energy consumption for the base case villa (a), code 1 villa (b) and code 2 villa (c) under the current climate and future climate change (A2 scenario).

In general, the results indicate that the global warming will negatively cause an impact on the demand of the total electricity. This is based on the changing the climate producing a rise in the cooling energy demand. As a result, applying code 1 can nullify the effects of the future climate changes in the 2080s. This is so due to the total annual cooling energy consumption for the code 1 retrofitted house not being as high as the cooling energy use for the base case villa under the current climate. The outcome of applying code 1 for the base case villa is considered as a major contribution by reducing the cooling energy consumption and combating the effects climate change.

PLEA 2018 HONG KONG

Smart and Healthy within the 2-degree Limit

4. CONCLUSION

This study investigated the effects of applying the Saudi residential building's energy code for a detached single-family house (villa) located in Jeddah, Saudi Arabia. Also, this study aimed to see how the code would perform under the current climate and future climate change scenarios. The software DesignBuilder was used for this study as a simulation and investigatory tool to principally assess the performance of the residential building's energy code under future climate change scenarios. It is clear that the base case existing villa specification will not be able to tackle the effects of future global warming as cooling is the main worry due to the harsh weather conditions in Saudi Arabia. Administering the Saudi Residential buildings energy standards to the existing villa attained a high reduction in the total annual cooling demands equalling to 38%. Applying code 1 can minimize the effects of future climate changes. However, there is still an increase in cooling energy demand due to climate change.

Further studies are required to improve the current code by using the code 1 and code 2 as a base case. Also, more investigative and passive strategies that are not included in the Saudi Residential buildings energy code for different climate zones in Saudi Arabia in order to neutralize the effects of future climate change should be considered in future analyses.

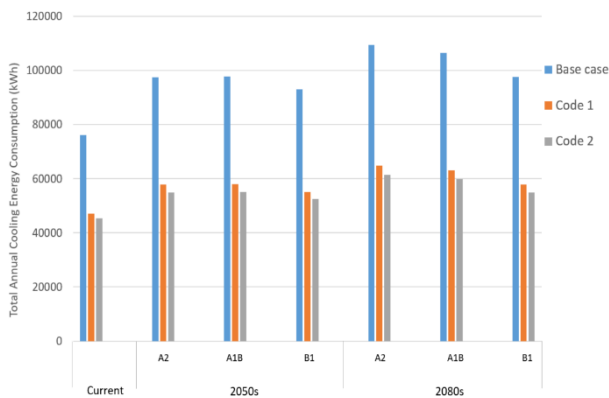


Figure 9: the total annual cooling energy consumption in the current and future climate periods under different climate change scenarios for the base case villa, retrofitted villa to code 1 and code 2.

REFERENCES

M. Abdul and O. S. Alshamrani, "Prospects of energy conservation and management in buildings – The Saudi Arabian scenario versus global trends," vol. 58, pp. 1647–1663, 2016.

N. Al-Tamimi, "A state-of-the-art review of the sustainability and energy efficiency of buildings in Saudi Arabia," *Energy Effic.*, 2017.

Saudi Energy and Efficiency Center, "Building energy sector." [Online]. Available: <http://www.seec.gov.sa/en/buildings-en>. [Accessed: 19-Nov-2017].

"Electricity Cogeneration Regulatory Authority, KSA ,Annual statistical booklet for electricity & seawater desalination industries," 2016.

F. Alrashed and M. Asif, "Analysis of critical climate related factors for the application of zero-energy homes in Saudi Arabia," *Renew. Sustain. Energy Rev.*, vol. 41, pp. 1395–1403, 2015.

M. Almazroui, M. Nazrul Islam, H. Athar, P. D. Jones, and M. A. Rahman, "Recent climate change in the Arabian Peninsula: Annual rainfall and temperature analysis of Saudi Arabia for 1978-2009," *Int. J. Climatol.*, vol. 32, no. 6, pp. 953–966, 2012.

N. A. Aldossary, Y. Rezgui, and A. Kwan, "Domestic energy consumption patterns in a hot and humid climate: A multiple-case study analysis," *Appl. Energy*, vol. 114, pp. 353–365, 2014.

K. T. Huang and R. L. Hwang, "Future trends of residential building cooling energy and passive adaptation measures to counteract climate change: The case of Taiwan," *Appl. Energy*, vol. 184, pp. 1230–1240, 2016.

H. Radhi, "Evaluating the potential impact of global warming on the UAE residential buildings - A contribution to reduce the CO2 emissions," *Build. Environ.*, vol. 44, no. 12, pp. 2451–2462, 2009.

S. L. Wong, K. K. W. Wan, D. H. W. Li, and J. C. Lam, "Impact of climate change on residential building envelope cooling loads in subtropical climates," *Energy Build.*, vol. 42, no. 11, pp. 2098–2103, 2010.

X. Wang, D. Chen, and Z. Ren, "Assessment of climate change impact on residential building heating and cooling energy requirement in Australia," *Build. Environ.*, vol. 45, no. 7, pp. 1663–1682, 2010.

"The General Population and Housing Census | General Authority for Statistics KSA." [Online]. Available: <https://www.stats.gov.sa/en/13>. [Accessed: 18-Oct-2017].

M. Alhashmi *et al.*, "Energy Efficiency and Global Warming Potential in the Residential Sector : Comparative Evaluation of Canada and Saudi Arabia," vol. 23, no. 3, pp. 1–12, 2017.

"Meteonorm," 2017. [Online]. Available: <http://www.meteonorm.com/>. [Accessed: 11-May-2017].

H. M. Taleb, "Using passive cooling strategies to improve thermal performance and reduce energy consumption of residential buildings in U . A . E . buildings," *Front. Archit. Res.*, vol. 3, no. 2, pp. 154–165, 2014.

A. H. Monawar, "A Study of Energy Conservation in the Existing Apartment Buildings in Makkah Region , Saudi Arabia," *PhD Thesis, Sch. Archit. Plan. Landscape, Univ. Newcastle upon Tyne, United Kingdom.*, 2001.

Green Roofs for Cooling: Tests in a Hot and Dry Climate

LAURA RODRIGUEZ¹, PABLO LA ROCHE²

¹Architecture and Design Department, University of Zulia, Maracaibo, Venezuela

²Lyle Center for Regenerative Studies & Architecture Department, California State Polytechnic University, Pomona, USA

ABSTRACT: This paper discusses the cooling potential of three types of green roofs, insulated, uninsulated, radiant- evaporative, evaluated with test cells. Different rules and schedules were tested for irrigation, water movement through the radiant pipes, plenum fan operation, and cooling with outside air. Results indicate that on warm days with maximum outdoor temperatures below 32 °C the uninsulated green roof will perform better and on drier days up to 44 °C and a Wet Bulb Temperature below 24 °C, the green roof with a radiant system and evaporative cooling performs better. On very warm days with high maximum temperatures above 33 °C the insulated green roof and the insulated roof (non-green) perform better. Optimum zones for the green roofs are plotted on the Building Bioclimatic Chart.

KEYWORDS: Green Roofs, Passive Cooling, Radiant- Evaporative Passive Cooling.

1. INTRODUCTION

Green roofs, also called “eco-roofs”, “living roofs” or “roof gardens”, are roofs substantially covered with vegetation. They have many benefits over conventional roofs, reducing storm water runoff, the heat island effect in cities, and energy requirements for cooling; all of this while sequestering CO₂ from the atmosphere [1]. However, because of their expense, the building industry has yet to fully embrace them.

Green roofs shade the rooftop layer, reducing the direct influence of solar radiation [2] [3]. Green roofs have also been proposed as a summer energy conservation strategy that reduces heat flow from the exterior to the interior. In a typical non-vegetated roof with some thermal mass, accumulated daytime heat continues its transfer to the interior during the night. The vegetation of a green roof reduces solar gains so that there is less heat flowing to the interior at night [4].

This paper discusses the cooling potential of several green roofs developed by the authors including one based on a previous prototype [5] and tested from September to December of 2017. More tests are being done in 2018 and will be included in future papers.

2. EXPERIMENTAL SET UP

The cooling potential is evaluated using test cells with different roof configurations. The performance of the proposed green roof is compared with other green roofs and a control cell with a well-insulated, non-vegetated roof. The test modules are located at the Lyle Center for Regenerative Studies at Cal Poly Pomona University, 30 km east of Los Angeles, in California. The climate is hot and dry with an average high temperature of 31.5 °C in August and an average low of 5.3 °C in January.



Figure 1: View of the Test Cells with Shade

All modules are 1.35 m. × 1.35 m. × 1.35 m. The walls of the test cells are 178 mm thick, with drywall on the inside, 50.8 mm × 101.6 mm studs with glass wool insulation, OSB board, XPS insulation board, and plywood on the outside. The floor of the cell is OSB board and XPS insulation board. The U-value of the wall is 0.308 W/m² K and the U-value of the floor is 0.299 W/m² K. The walls are painted white to reduce the heat gains. A double glazed window 610 mm wide × 610 mm high was installed in the south wall, and was tested with and without shade. A 101.6 mm (Diameter) exhaust fan and intake flap were installed to provide ventilation with different schedules. Plastic wheels (89 mm diameter) were installed under the cell to adjust orientation and location of the cells.

The design of the roof is the only difference between the cells: an insulated green roof, an uninsulated green roof, a green roof with a radiant system and misting irrigation, and a non-green insulated roof as a control were compared over several series with and without night ventilation and shade (Fig 1).

Every roof assembly except the cell with the non-insulated green roof had 140 mm glass wool insulation. Cells with green roofs had climate appropriate succulents with a Leaf Area Index (LAI) of 4.

3. GREEN ROOF SYSTEMS

3.1. Insulated green roof

This green roof had insulation underneath the planting material (Fig. 2). The U value of the insulated green roof including the wood structure was 0.282 W/m² K (See Fig: 3). The conditions inside the insulated green roof are affected by the thermal mass inside the space, the ventilation rates, and the amount of shade in the window.

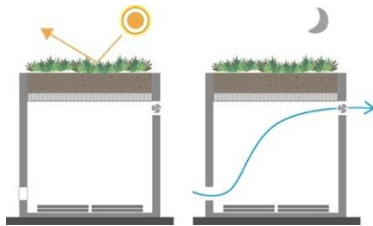
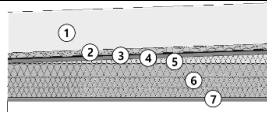


Figure 2: Insulated Green Roof



#	Material	mm	W/mK	U-Value (W/m ² K)
1	Soil	130	0.610	0.282
2	Gravel	20	2.000	
3	Water Proofing Liner	1	0.210	
4	Metal Pan	2	44.000	
5	OSB	11	0.130	
6	Glass Wool	21	0.044	
7	XPS	127	0.043	
8	Dry Wall	11	0.180	

Figure 3: Insulated Green Roof U- Value

Many tests with different combinations of these variables were done. Best results were achieved with night ventilation, more window shade and more thermal mass. Because the green roof's thermal mass is not coupled to the interior of the space it requires additional thermal mass inside the space to perform better. This thermal mass acts as a heat sink during the daytime reducing maximum temperature and daily swing. In this type of green roof, the insulation reduces solar gains during the day and increases the applicability of the green roof under very hot conditions. However, the building should be shaded, night ventilated, and with thermal mass, providing some thermal comfort (28°C) with outdoor temperatures up to 43 °C.

3.2. Uninsulated Green Roof

In the uninsulated green roof, the planting material is thermally coupled with the interior of the space via a

metal plate under the green roof. There is no insulation between the green roof and the space below. The U value of the uninsulated green roof including the wood structure was 2.534 W/m² K (See Fig: 5). An uninsulated green roof combined with night ventilation cools a space in two ways: during the daytime, the vegetated canopy layer reduces solar gains through shade while the growth medium acts as a heat sink. During the night, the cell is night ventilated and the growth medium cooled with outside air (Fig 4).

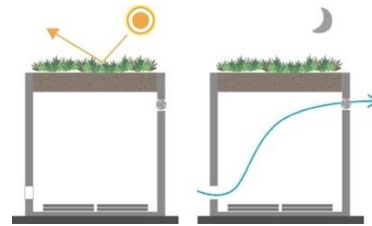


Figure 4: Uninsulated Green Roof



#	Material	mm	W/mK	U-Value (W/m ² K)
1	Soil	130	0.610	2.534
2	Gravel	20	2.000	
3	Water Proofing Liner	1	0.210	
4	Metal Pan	1	44.000	

Figure 5: Uninsulated Green Roof U- Value

Night ventilation is provided with a fan and all the cells are equipped with dimmers and timers to adjust the ventilation rate and start/end times. The climatic parameters that determine the cooling effectiveness of night ventilation are the minimum air temperature, which determines the lowest temperature achievable inside the building; the daily temperature swing, which determines the potential for lowering the indoor maximum below the outdoor maximum; and the water vapor pressure level, which determines the upper temperature limit of indoor comfort with still air or with air movement. The main building parameters that affect the effectiveness of cooling with night ventilation are the insulation level, the amount of thermal mass and the amount of glazing [6]. Different ventilation cooling strategies were tested using temperature-based rules or schedules.

3.3. Radiant-Evaporative cooled green roof

The radiant-evaporative cooled green roof consisted of a radiant water pipe, water pump, and sprinkler (mist type) on the green roof. The water flow in the pipe and the sprinklers can operate on different schedules, based on their different functions. The sprinkler was typically scheduled to operate during the daytime and reduced the soil temperature with the evaporatively cooled water.

PLEA 2018 HONG KONG

Smart and Healthy within the 2-degree Limit

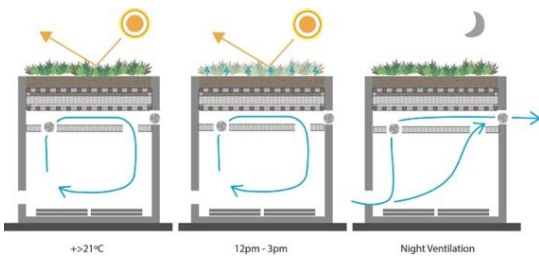
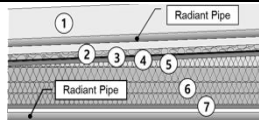


Figure 6: Radiant- Evaporative Green Roof



#	Material	mm	W/mK	U-Value (W/m ² K)
1	Soil	130	0.610	0.282
2	Gravel	20	2.000	
3	Water Proofing Liner	1	0.210	
4	Metal Pan	2	44.000	
5	OSB	11	0.130	
6	Glass Wool	21	0.044	
7	XPS	127	0.043	
8	Dry Wall	11	0.180	

Figure 7: Radiant- Evaporative Green Roof U-Value

The radiant system consists of a closed-loop pipe with a total length of 33 m. embedded in the soil of the green roof and which continued inside the test cell. A pump circulates the water inside the pipe and was operated by a digital timer, which turned on or off according to different schedules. The pipes are separated from the space by a plenum and an insulated ceiling (Fig 6), also with a sensor operated fan that provides cool air when needed below. The radiator absorbs heat from the interior of the cells which is dissipated through the green roof and the evaporation. The U value of the radiant-evaporative green roof was also 0.282 W/m² K. (See Fig: 7). The activation temperature of the fan is set a 21 °C, transferring air from the plenum, cooled by the radiant system, to the interior of the space, thus cooling it.

4. MONITORING SYSTEM AND SCHEDULE

HOBO type data loggers by Onset computer were used for data collection (Model: U12-012, UX 120-006 M, TMC6-HD). These data loggers and sensors were installed in multiple locations inside and outside of the test cells to monitor dry bulb temperature and relative humidity (Fig. 8). Every sensor was connected to the data logger, and the sensors were installed according to DIN EN 60751 regulations. A wire type temperature sensor with metal sensing tip was used to measure outdoor temperature, which is connected to the HOBO device. The sensor that measured outdoor dry bulb temperature was inside a solar radiation shield designed to block solar

radiation with multiple louvers while providing maximum air flow. [5]

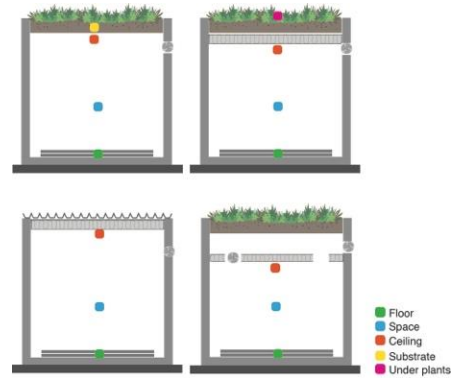


Figure 8: Sensor location

The data loggers were set up to collect information every 5 minutes. Fans provided night ventilation and were tested with different operating schedules, for example programmed to turn on at 8pm and turn off at 8am. The exhaust fans in the ceiling of the green roof with radiant cooling and the green roof with air space were programmed to turn on if the interior space temperature increased above 21 °C.

For these series, the water in the radiant cooling pipes is programmed to flow all day. Sprinklers operate during the warmest/ driest time of the day, turning on for five minutes every half hour, from 12:15 pm to 3pm, a total of 45 minutes of irrigation every day. (Fig.9)

A total of nine monitoring series were conducted between September and December of 2017. Different rules and schedules were tested for irrigation, water movement through the radiant pipes, plenum fan operation, and cooling with outside air.

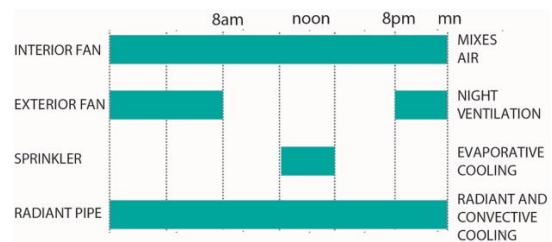


Figure 9: Operation Schedule

5. RESULTS AND DISCUSSION

Results indicate that all cells with green roofs have lower indoor maximum temperatures than outdoor maximums. Under certain conditions, both the test cell with the radiant/evaporative cooling system and the uninsulated green roof perform better than the test cells with the insulated green roof and the conventional insulated roof (Fig 10).

The indoor temperature swing is a variable that helps to understand the thermal performance of the system. A smaller swing close to the comfort zone indicates more

PLEA 2018 HONG KONG

Smart and Healthy within the 2-degree Limit

thermal stability and probably better performance. In general, the additional thermal capacity of the green roof improves performance of the uninsulated green roof as does the green roof with a radiant system. An exception is with very high daytime temperatures when the uninsulated green roof does not have enough thermal capacity to store more solar gains and the green roof overheats, later transferring this heat to the interior.

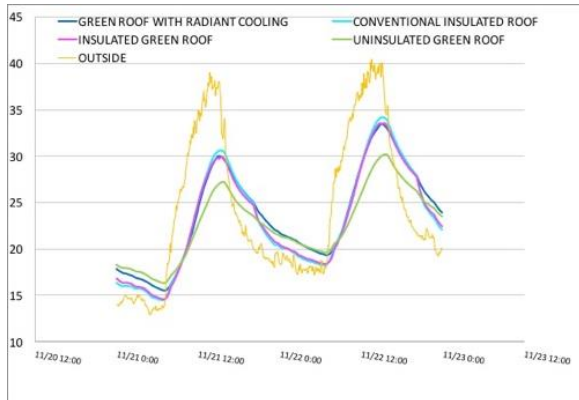


Figure 10: Series Nov 22-23: Night ventilated and shade.

Comparing the average maximum temperature inside the cells with the average maximum exterior temperature also helps to determine thermal performance. A higher temperature difference indicates more cooling, because the indoor maximum is much lower than the outdoor maximum. Figure 11 compares the average reduction of the maximum temperature in the green roof cell with radiant/ evaporative cooling compared with the conventional insulated roof, with and without shade. In both cases the cell with the radiant/evaporative system performs better than the insulated roof, with a larger reduction of the outdoor maximum temperature. The difference between the two types of roofs is 0.4 °C for the shaded series and 0.7 °C for the non-shade series. Even though the value is relatively small it is consistent over different conditions.

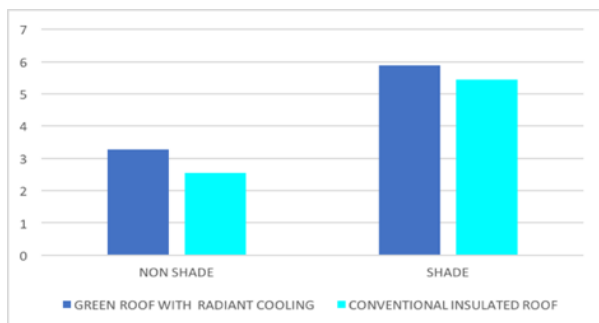


Figure 11: Average Maximum Temperature Reduction of Green Roof with Radiant/ Evaporative Cooling and Conventional Roof. Shaded and Non-Shaded Series

6. APPLICABILITY OF GREEN ROOF SYSTEMS UNDER DIFFERENT CONDITIONS

Plotting and comparing daily recorded indoor and outdoor maximum temperature and minimum relative humidity on the Building Bioclimatic Chart on the psychrometric diagram helps to understand the performance of the system.

A lower indoor maximum temperature indicates a better cooling performance. The limits of outdoor optimum performance for each system are determined by the relationship between the indoor temperature and the comfort zone for a given exterior maximum temperature. If the indoor conditions are inside the comfort zone, the strategy is assumed as effective for those exterior temperature and relative humidity conditions.

Data for the maximum temperature and minimum relative humidity outside and inside were plotted on the psychrometric chart. A total of 26 usable data points were plotted for 26 selected days tested under different conditions with and without shade.

The goal of this analysis was to determine the applicability of the different green roof strategies under varying outdoor conditions. Colors were used to represent each option, blue for the green roof with radiant/ evaporative system, purple for insulated green roof and green for a non-insulated green roof (Fig. 15). If the indoor temperature was inside the comfort zone (up to 27 °C) when the outdoor temperature was above the comfort zone, the strategy was assumed to be effective to achieve indoor thermal comfort during this period. If indoor comfort was not completely achieved, but the temperature inside the cell was between 27°C and 31 °C, we described the area with this condition as having medium effectiveness to achieve comfort.

The comfort zone used for this analysis was generated by combining the winter and summer zones proposed by ASHRAE Standard 55. The comfort zone is between 20 °C and 27 °C DBT, Absolute Humidity below 12 g / Kg and a Relative Humidity above 10%.

6.1 Green roof with evaporative cooling

Fig. 12 shows the psychrometric Chart with the data for the cell with the green roof with evaporative cooling and the lines that define this design strategy in blue. The area in which the evaporative cooling strategy is effective to achieve indoor thermal comfort is between 20°C and 33°C Dry Bulb Temperature; 10 °C and 21 °C Wet Bulb Temperature; and below the 60% Relative Humidity curved line.

PLEA 2018 HONG KONG

Smart and Healthy within the 2-degree Limit

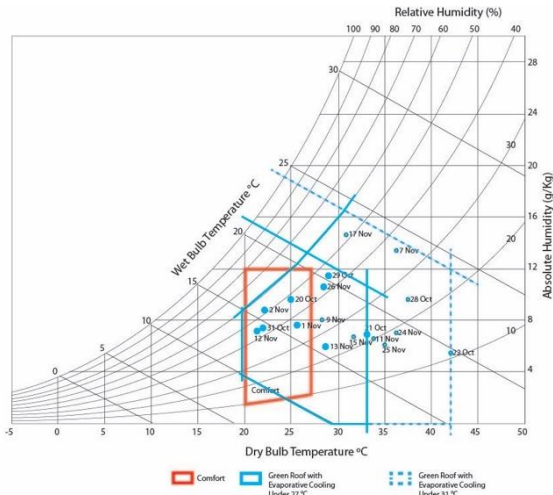


Figure 12: Building Bioclimatic Chart with Evaporative Cooling

The medium effectiveness area for evaporative cooling is indicated with a dotted blue line between 33°C and 42°C Dry Bulb Temperature and 21 °C to 24 °C Wet Bulb Temperature.

6.2. Uninsulated green roof

The area in which the uninsulated green roof strategy is effective to achieve indoor thermal comfort is between 20°C and 29°C Dry Bulb Temperature; up to 21 °C Wet Bulb Temperature; and below the 70% Relative Humidity curved line (Fig. 13). The medium effectiveness area is marked with a green dotted line between 29°C and 39°C Dry Bulb Temperature and below 23 °C Wet Bulb Temperature; and the 70% Relative Humidity curved line.

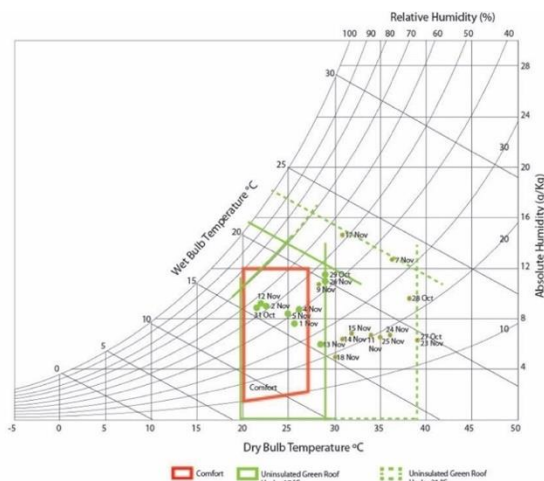


Figure 13: Building Bioclimatic Chart with Uninsulated Green Roof

6.3. Insulated green roof

The area in which the insulated green roof is effective to achieve thermal comfort is indicated by a purple line in Fig. 14; between 20 °C and 33°C Dry Bulb Temperature, and 12 g/ Kg of Absolute Humidity. The medium effectiveness area is indicated with a purple dotted line

between 33°C and 43°C Dry Bulb Temperature, and 12 g / Kg of Absolute Humidity.

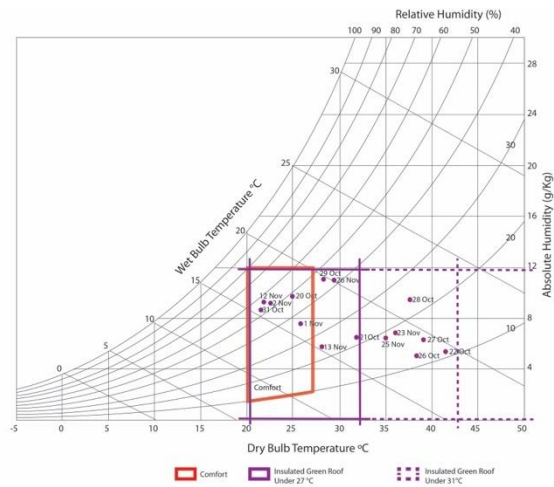


Figure 14: Building Bioclimatic Chart with Insulated Green Roof

7. CONCLUSION

Results indicate that on warm days with maximum outdoor temperatures below 32 °C the uninsulated roof will perform best and on drier days up to 44 °C with a Wet Bulb Temperature below 24 °C, the radiant system with evaporative cooling performs better. On very warm days with high maximum temperatures above 33 °C the insulated green roof and the insulated roof (non-green) perform better than the uninsulated green roof.

The daily temperature swing is also an important factor that affects performance, especially when night ventilation is implemented and daily temperature swings are above 10 °C and minimum outdoor temperatures are below 18 °C.

On cooler days, with maximum temperatures below 31°C the uninsulated green roof performs better than the insulated green roof, as is the case on November 14 and 17, where the maximum temperature recorded outside was 31 °C, producing an interior temperature of 29 °C and 28 °C respectively. In these two days, the thermal swing outside was 20 °C.

Analysis indicates that in locations with a daily swing greater than 25 °C, an insulated green roof with thermal mass works better, and in places where the amplitude does not exceed 20 °C it is acceptable to use an uninsulated green roof. However, both work better with a higher daily temperature swing.

On drier days with maximum outdoor temperatures below 40 °C and very low outdoor relative humidity, the green roof with radiant and evaporative cooling performs better than the control roof. An example is November 23, when the maximum exterior temperature reached 39 °C, with 15% Relative Humidity, in these conditions the radiant/ evaporative system performed best.

PLEA 2018 HONG KONG

Smart and Healthy within the 2-degree Limit

The conditions under which these green roofs are most effective are defined on the psychrometric chart (See Fig. 15). This is a first approximation of what could be a useful design guide to select the most effective green roof for cooling in each climate.

The "green roof with evaporative cooling" (See Fig. 12) works best between 20°C and 33 °C DBT and 10 °C to 21 °C WBT. The medium effectiveness area is between 33 °C and 42 °C DBT and below 24 °C WBT, and below 60% RH. The "uninsulated green roof" (See Fig. 13) works best between 20°C and 29 °C DBT and a WBT up to 21 °C. The medium effectiveness area is between 29 °C and 39 °C for DBT and below 23°C WBT, and between 0 g / Kg of Absolute Humidity and 70% RH.

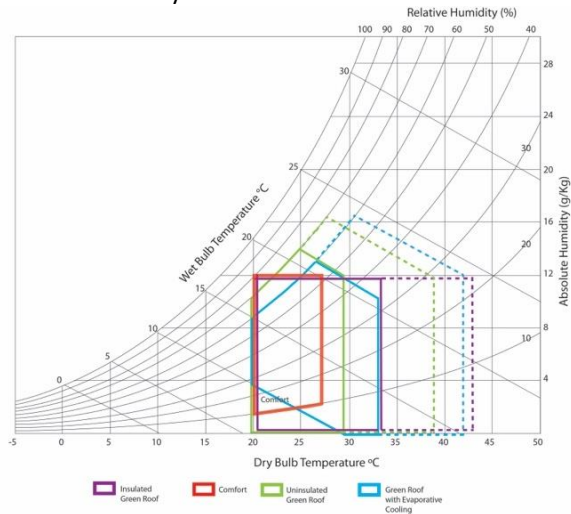


Figure15: Building Bioclimatic Chart with the strategies

The "insulated green roof" (See Fig. 14) works best between 20 °C and 33°C DBT, and below 12 g/ Kg of Absolute Humidity. The medium effectiveness area is from 33 °C to 43 °C DBT, and from 0g / Kg to 10g/ Kg of Absolute Humidity.

ACKNOWLEDGEMENTS

The authors want to express their gratitude to the Lyle Center of Regenerative Studies for its continuous support of this research.

REFERENCES

1. U. Berardi, A. Ghaffarian Hoseini, (2014). A critical analysis of the environmental benefits of green roofs, *Applied Energy*. Volume 115, Pages 411–428.
2. H. Niu, C. Clark, J. Zhou, P. Adriaens, (2010) Scaling of economic benefits from green roof implementation in Washington, DC, *Environmental Science and Technology*. Volume 44, No. 11, Pages 4302–4308.
3. S.E. Ouldboukhitine, R. Belarbi, I. Jaffal, A. Trabelsi, (2011) Assessment of green roof thermal behavior: a coupled heat and mass transfer model, *Building and Environment*. Volume 46, Pages 2624–2631.
4. Castleton, H.F. Stovin, V. Beck, S.B.M. Davison, J.B. (2010) *Green roofs; building energy saving and the potential for*

retrofit. Energy and Buildings. Volume 42, Issue 10, October, Pages 1582-1591.

5. D. Yeom, P. La Roche, (2017). Investigation on the cooling performance of a green roof with a radiant cooling system. *Energy and Buildings*. Volume 149, Pages 26–37.

6. Geros V., Santamouris M., Tsangasoulis A., Guarrancino G., (1999). Experimental evaluation of night ventilation phenomena. *Energy and Buildings*. Volume 29, Pages 141- 154.

Potential Wind Power Utilization in Diverging Passages Between Two High-Rise Buildings Using “Venturi effect” on the windward side

YU-HSUAN JUAN¹, CHIH-YUNG WEN¹, AN-SHIK YANG², HAMID MONTAZERI^{3,4}, BERT BLOCKEN^{3,4}

¹The Hong Kong Polytechnic University, Hong Kong

²National Taipei University of Technology, Taiwan

³Eindhoven University of Technology, Netherlands

⁴KU Leuven, Leuven, Belgium

ABSTRACT: The objective of this study is to investigate the urban wind power potential from the proper arrangement of high-rise buildings in a complex and dense urban environment. There is great prospective in the formulation of the building design at early stages to maximize wind power production in dense urban areas. We employed the 3D steady Reynolds-averaged Navier-Stokes computational fluid dynamics (CFD) simulations to investigate the impact of the arrangement of high-rise buildings on the wind energy potential. Two arrays of high-rise buildings with height = 90 m and aspect ratio (height/width) of 4.5 is studied, which focuses on different distances between the side façades of the upstream buildings, ranging from 3 to 21 m. The findings of the study support the high-rise buildings design with respect to integrated urban wind energy harvesting and the concept of sustainable urban development.

KEYWORDS: Urban Wind Energy, High-rise Building, Wall Effect, Urban Design

1. INTRODUCTION

Recently, the wind power has become one of the most accessible resources among renewable energy alternatives in high-rise and high-density urban areas. Because of the disturbed flows around buildings, the structures can accelerate wind speeds to increase the wind power density as compared to the case for the airflow over open areas. Incorporating wind turbines into the building design are stepping into our lives. Nonetheless, the high-rise buildings are subject to the significant interaction with the wind power resource. The urban wind environment is substantially affected by the presence of buildings with the wind velocities increased especially on the roof, edges and vertical windward walls of buildings [1]. Lu and Ip explored the feasibility and enhancement methods of wind power utilization around high-rise buildings of Hong Kong [2]. Khayrullina et al. conducted CFD simulations to examine the wind conditions in passages between parallel buildings for assessing wind energy potential [3]. Chaudhry et al. studied the influence of building morphology, including triangular, square and circular cross-sections, on the efficiency of building-integrated wind turbines (BIWT) [4]. Balduzzi et al. evaluated a wind turbine for installation on the roof of a selected building with certain roof geometric features [5]. However, the above research lacked to consider the wind flows behind high-rise buildings.

In high-density urban areas, the high-rise buildings may result in an insufficiency of air ventilation, since the airflow is blocked by structures along the coastal line.

The number of high-rise buildings has continually increased in recent years. Those buildings can impede the flowing of fresh air, which is vital for ventilation and pollutant dispersal in street canyons [6]. Clusters of buildings can obstruct air flow into the street pass ways and thereby reduce air flow velocity.

We devise two different scenarios. Scenario A consists of a 1×2 array of high-rise buildings, while Scenario B a 2×2 array of buildings. Essentially, we investigate the building orientations of $\theta = 0$ and 45° in the passages, which varied the distance between upstream buildings. Recent studies showed that the “Venturi effect” arrangement coupled with the building diverging passages can be a better choice to promote ventilation at the pedestrian level [1, 6-10]. While several studies have been performed to investigate the urban wind energy potential, the impact of the arrangement of high-rise buildings has not yet investigated in detail. In this paper, therefore, the impact of the arrangement of high-rise buildings on the wind energy potential is investigated. The findings of the study support the design of high-rise buildings with respect to integrated wind energy harvesting especially. In addition, the studied results can be of interest to urban planners, designers and builders. The building dimensions, and the vertical inlet profiles of velocity is based on a dense urban area in the central region of Hong Kong, to address the schemes on the development of wind power in local urban areas for maximizing wind energy utilization.

PLEA 2018 HONG KONG

Smart and Healthy within the 2-degree Limit

2. METHODS

2.1 Building geometries for different scenarios

This study investigates the urban wind power potential using the concentration effect between an arrangement of a representative parallel high-rise building array (90 m × 20 m × 20 m with a distance of 3 m) as Scenario A, simplified from a realistic urban pattern of Central, Hong Kong, as displayed in Fig. 1.

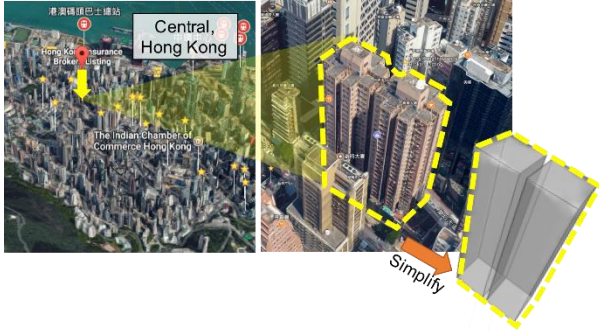


Figure 1: Two parallel building blocks simplified from two high-rise buildings in Central, Hong Kong

Two scenarios are considered to investigate the wind flows over high-rise buildings, with varied geometrical situations in terms of building layouts and distances, as listed in Table 1. To study the concentration effect of two parallel high-rise buildings without placing the barrier of buildings on the windward side in Scenario A, Case 0 was simulated with the distance of 3 m, as depicted in Fig. 2. In contrast, Scenario B considered varied canyon layouts at the distances from upstream buildings of $D=3\text{ m}, 6\text{ m}, 9\text{ m}, 12\text{ m}, 15\text{ m}, 18\text{ m}$ and 21 m . Besides, the building orientation was turned 135° of the diverging passage on the windward side (detailed in Ref. 8) to compare the wind flow field with that of Scenario A, which is expected to be an appropriate arrangement for forming the “Venturi effect” shape, as depicted in Fig. 2. From the predictions, this study then inspects the effectiveness of the concentration effect of high-rise buildings to fully utilize urban wind energy.

Table 1. Geometries of Scenario A and B

Scenario	Case	Upstream buildings distance
A	0	-
	1	3 m
	2	6 m
B	3	9 m
	4	12 m
	5	15 m
	6	18 m
	7	21 m

2.2 CFD validation study

The simulations are based on validation with the wind tunnel experiment by Stathopoulos and Storms [11] for a scale of 1/400 in the boundary layer wind tunnel of the Centre for Building Studies (CBS). Two buildings with dimensions of $20\text{ m} \times 20\text{ m} \times 40\text{ m}$ ($H \times D \times L$ in a full scale) with a 6-m passage distance in the wind-tunnel experiments are considered, while the wind flow direction was parallel to the passage center line. In this section, we first reproduced the geometric details of the wind tunnel to the simulation model, implementing a high grid resolution near the ground of the computational domain to comply with the requirements of near-ground flows.

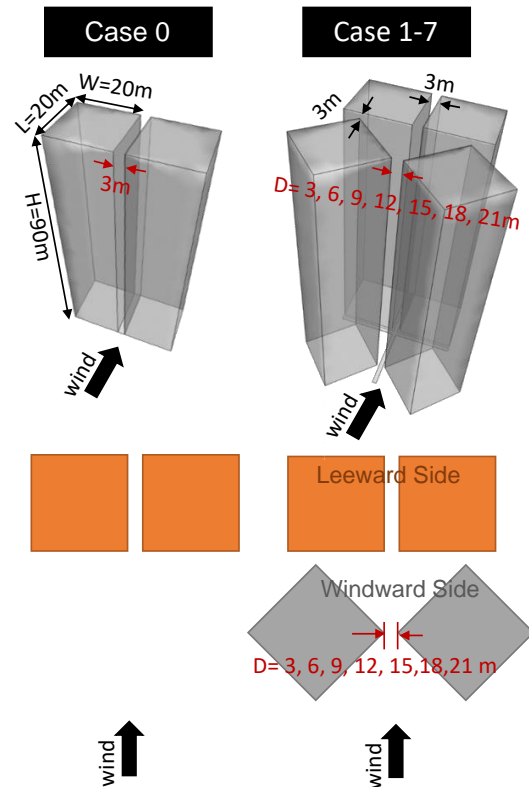


Figure 2. Geometries of Scenario A and B

The neutral atmospheric boundary layer (ABL) was described using a power-law form with exponent 0.15. The reference wind speed U_{ref} was 5.9 m/s at 2m height of the pedestrian level (in full scale), and the turbulence intensity of the incident flow ranged from 20% at 2m height to 5% at a gradient height of 360 m. The profiles of the mean wind speed and turbulence intensity at the inlet were prescribed employing the incident profiles from the wind-tunnel measurements. The computational domain and grids are based on the CFD guidelines [12, 13]. The distances from the buildings to the top, inlet,

PLEA 2018 HONG KONG

Smart and Healthy within the 2-degree Limit

outlet and lateral boundaries are 5H, 5H, 15H and 5H (with the term H representing the building height), respectively. The wall roughness was expressed by an equivalent sand-grain roughness K_s in the wall functions, setting as 30 times of z_0 [14]. We only used the hexahedral grids with a grid expansion ratio of 1.1 and the least grid size of 0.005 m. The total number of cells was 2,246,100. The grid is generated based on a grid-sensitivity analysis, where coarsening and refining is performed with an overall linear factor 2. The commercial CFD software ANSYS/Fluent® 18.0 is used to solve the three-dimensional Reynolds-averaged Navier–Stokes (RANS) equations in combination with the realizable $k-\varepsilon$ model [15]. The SIMPLE algorithm is used to couple the velocity and pressure [16-17]. Second-order discretization schemes are used for both the convection terms and the viscous diffusion terms. The validation results reveal that the calculated streamwise velocity and turbulent kinetic energy profiles from the standard and realizable $k-\varepsilon$ models are relatively more accurate than those from the RNG and SST $k-\omega$ models. Moreover, the predictions of the Z velocity profiles by the standard and RNG $k-\varepsilon$ models agreed reasonably well with the measurement data. The prediction capability of the standard $k-\varepsilon$ turbulence model shows the best agreement between the CFD calculations and the wind tunnel measurements.

2.3 Computational approach

At the inlet of the domain neutral ABL inflow profiles of mean velocity (U_{ABL}), turbulent kinetic energy (k), and turbulence dissipation rate profiles (ε) are imposed [14].

$$U_{ABL} = \frac{u_{ABL}^*}{K} \ln\left(\frac{z + z_0}{z_0}\right) \quad (1)$$

$$k = \frac{(u_{ABL}^*)^2}{\sqrt{C_u}} \quad (2)$$

$$\varepsilon = \frac{(u_{ABL}^*)^3}{K(z + z_0)} \quad (3)$$

$$u_{ABL}^* = \frac{KU_h}{\ln\left(\frac{h + z_0}{z_0}\right)} \quad (4)$$

where z_0 and κ are the aerodynamic roughness and the von Karman's constant (≈ 0.4), respectively. The ABL

friction velocity u_{ABL}^* is computed from a specified velocity U_h at a reference height h . The mean inlet velocity at the height of z (U_{ABL}), was obtained via Eq. (1) to generate a velocity profile in the ABL with the turbulence kinetic energy k and dissipation rate ε computed by Eqs (2) and (3), respectively. From the data of a local meteorological station, the annual mean speed of 4.4 m/s at 10 m was used to calculate the ABL velocity. In essence, roughness will increase the drag for the cross-flow over the surface, causing the case that the logarithmic law for velocity profile, being the basis of the standard wall function, is not valid in the roughness case. This study modeled the real obstruction effect on the wind flow in terms of equivalent roughness by the roughness wall functions to replace the obstacles applied to the bottom plane of the domain [6,14].

This case specified the aerodynamic roughness z_0 as 0.7 m to replicate the terrain of high-rise buildings in accordance with the updated Davenport roughness classification. In addition, we set the constant static pressure boundary condition at the outlet. The symmetric conditions were implemented by prescribing the zero normal component of velocity and zero normal derivatives for all flow variables at the top and lateral boundaries. Zero-gauge static pressure was set at the outlet. Convergence is assumed to obtain when all the scaled residuals levelled off and reached a minimum of 10^{-5} for continuity and turbulence dissipation rate, 10^{-6} for velocities and turbulent kinetic energy.

Table 2. Boundary conditions of CFD simulations

Boundary	Type
Inlet	Velocity-inlet
Outlet	Pressure-outlet
Top	Symmetry
Lateral	Symmetry
Building	Wall
Ground	Wall

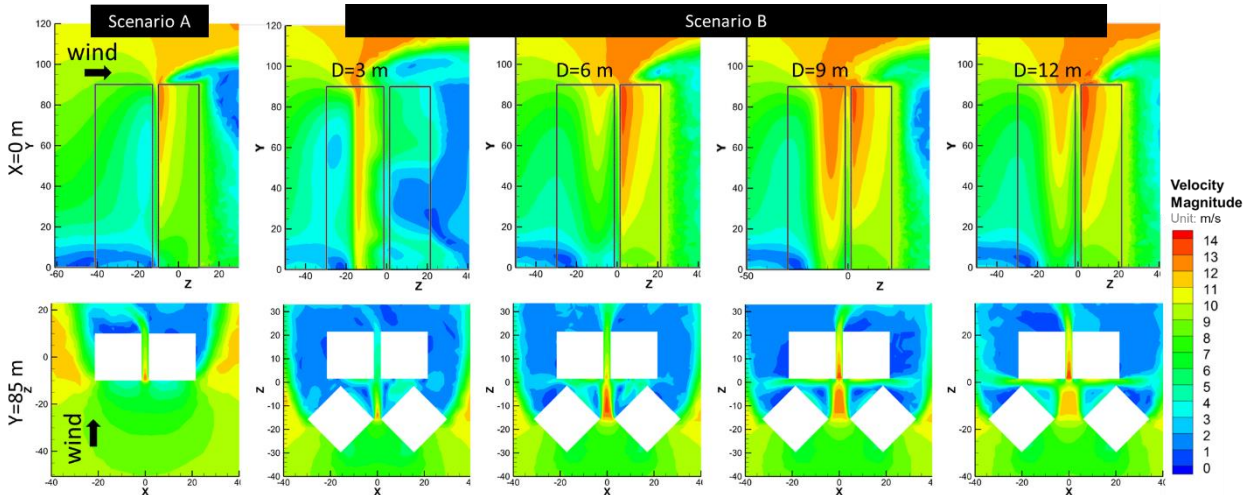


Figure 3: Predicted velocity magnitude contours in vertical sections at $x=0m$ and $y=85m$

3. RESULTS

3.1 Scenario A

CFD simulations considered Case 0 as the baseline case with no obstacle of upstream high-rise buildings on the windward side in a high-rise building 1x2 array. We analysed the conditions at a building distance of 3 m, as displayed in Figs. 3 and 4. Figure 3 illustrates the wind speed distributions in vertical sections at $x=0m$ and $y=85m$ for Scenario A and B. It can be observed that the wind speed in the vertical channel of two buildings augmented sharply from the inlet boundary, arrived at the greatest value at the narrowest point of two buildings and then decreases. For Scenario A in Fig. 3, the maximum wind velocity reaches approximately 12.3 m/s near the leading edge between buildings. In this study, the wind power density is used to evaluate the wind power potential, as the following Equation (5):

$$P = 0.593 \rho v^3, \quad (5)$$

where P - power density (W/m^3);
 ρ - air density (kg/m^3);
 v - air speed (m/s).

Figure 4 shows the predicted power density contours in three different sections at $x=0m$, $y=85m$ and $y=93m$ for Scenario A. As a result, the associated power density can be up to $1200 W/m^2$. In Scenario B, the wind energy over the roof generally grows with the increasing distance between upstream buildings because of the concentration effect of downstream buildings.

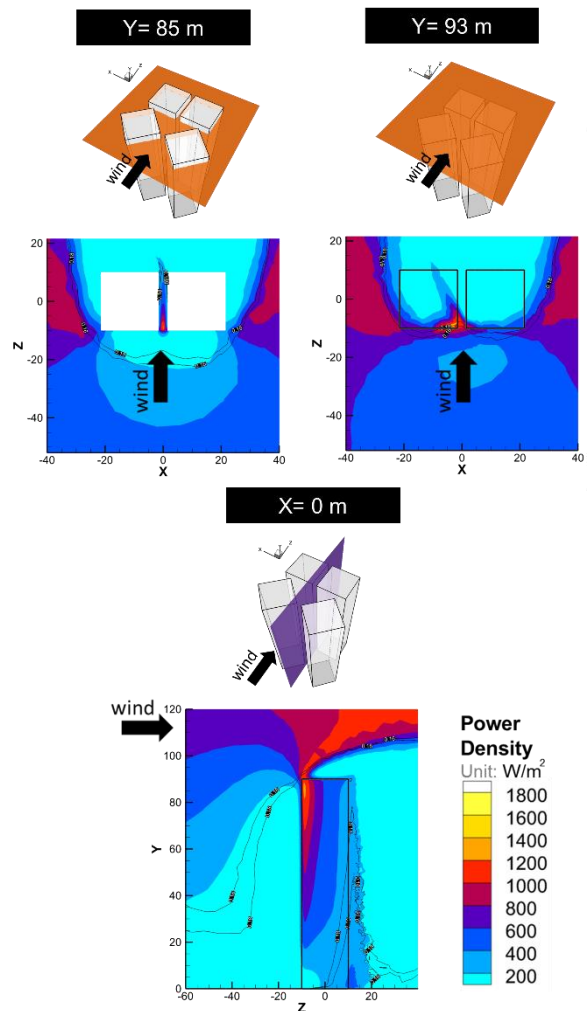


Figure 4: Predicted power density contours in three different sections at $x=0m$, $y=85m$ and $y=93m$ for Scenario A

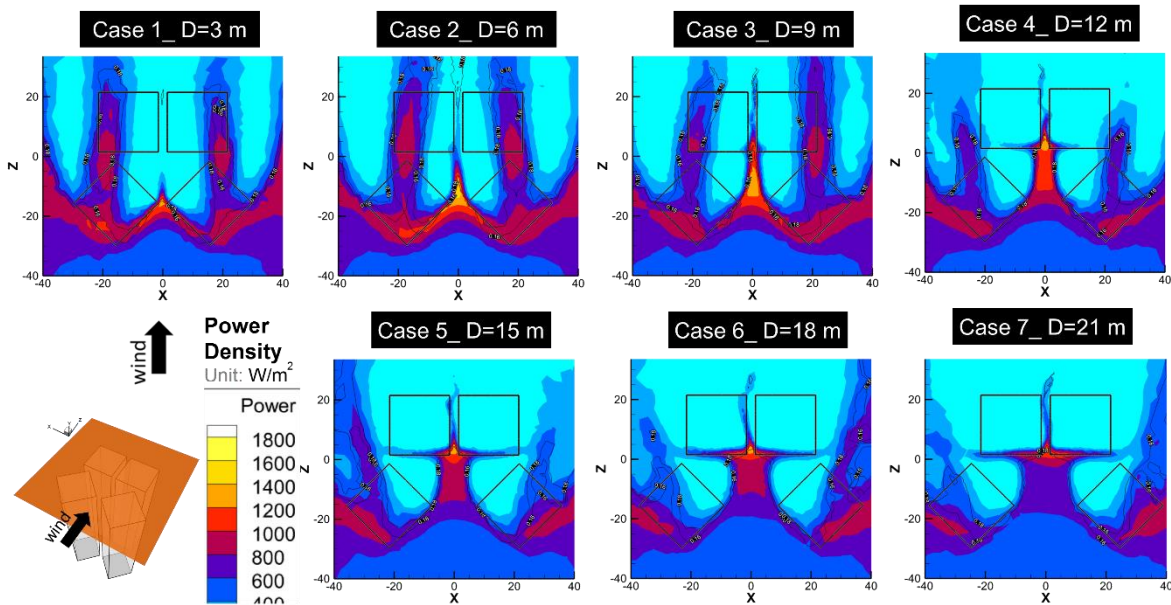


Figure 5: Predicted power density contours in horizontal sections of $Y=93$ m above the roof

3.2 Scenario B

Reducing the obstacle behind high-rise buildings, Scenario B further incorporated the Venturi effect in the passages configuration into upstream buildings with the building orientation arranged 45° of passage. To examine the influences of upstream buildings on the urban wind power production, different distances are considered $D=3\text{m}, 6\text{m}, 9\text{m}, 12\text{m}, 15\text{m}, 18\text{m}$ and 21m (i.e. Case 1-7) to make a comparison of the energy yields from the above cases with that from Case 0 in Scenario A without upstream high-rise buildings. The CFD results in Fig. 3 reveal higher wind speeds at the widest distance between upstream high-rise buildings. Thus, the predictions indicates that the wind speeds of $D=9\text{m}$ and 12m over the upstream buildings are higher than those of $D=3\text{m}$ and 6m . The situation without blocking of upstream buildings observed smooth flow of the approaching wind through the street canyon, leading to higher velocities in the downstream area. Figure 5 shows the predicted power density distributions above the roof in horizontal sections of $Y=93$ m. It can be seen that wind energy harvesting over the roof generally raises by the increase of the distance between upstream high-rise buildings due to the concentration effect of downstream high-rise buildings. The results in Figs. 3 and 5 indicated that the “Venturi effect” configuration on the windward side can significantly increase the wind velocity and power generation.

Figure 6 illustrates the predicted power density profiles against height at the point $(X, Z) = (0\text{m}, 2.8\text{m})$ between the leading edge of downstream buildings for all cases in Scenario A and B. We notice that the wind power densities in Scenario A were greater than those for the

cases at $D=3\text{m}$ and 6m . Moreover, the power densities for the incidents at $D=9\text{m}, 12\text{m}, 15\text{m}, 18\text{m}$ and 21m appear to be productive in Scenario B. We identified the site between downstream buildings passage under the top roof as the most appropriate location to install micro wind turbines for operation and maintenance of wind power management. More precisely, a further increase in width for the best case at $D=12\text{m}$ provided less than 1% variation in the wind velocity and power generation.

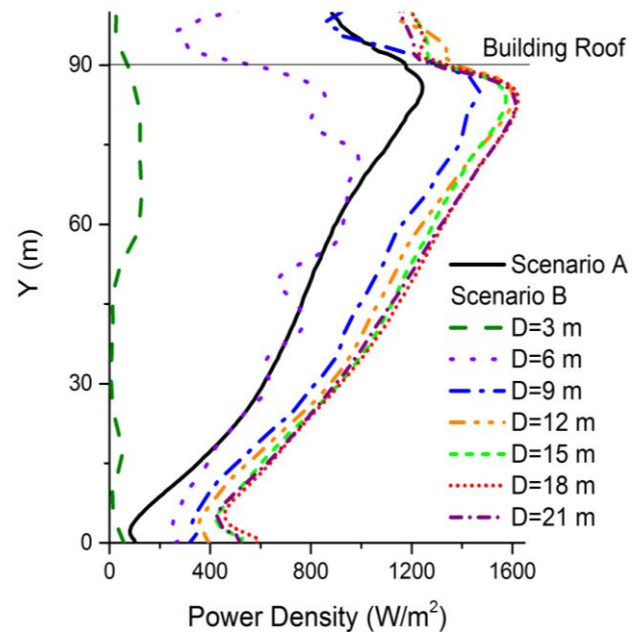


Figure 6: Predicted power density profiles against height at varied distances from upstream buildings in Scenario A and B

PLEA 2018 HONG KONG

Smart and Healthy within the 2-degree Limit

4. DISCUSSION

The limitations of this study are listed as follows and will be addressed in future work.

This study is conducted based on one wind direction of wind velocity.

The focus in this paper is on wind speed and power density for assessing the potential wind power utilization. Future work should apply and compare different indices like turbulence intensity, to assess urban wind power utilization.

In spite of these limitations, the issue of concern here is on the appropriateness of using the variations upstream building layout to check the effectiveness of the concentration effect of high-rise buildings for fully utilization of the urban wind energy. It provides practical implications for urban planners, designers and policymakers to adopt the upstream buildings configurations with the optimization of the street geometry and urban morphology for enhancing city breathability and increasing urban wind power usage.

5. CONCLUSION

From the aforementioned studies examining the influences of upstream and downstream buildings on urban wind power exploitation, the results led to the following conclusions.

The 'Venturi effect' on the windward side can noticeably increase the wind velocity and power generation with respect to the increasing distance between upstream buildings.

The diverging inlet in Scenario B produced greater concentration outcome of the wind at a height under the roof than that above the roof.

The best case for the model with $D=12$ m showed that a further increase in width provided less than 1% discrepancy in the wind velocity and power generation.

ACKNOWLEDGEMENTS

This study represents part of the results obtained under the support of Environment and Conservation Fund, Hong Kong, ECF 51/2016 and Ministry of Science and Technology, Taiwan, ROC (Contract No. MOST105-2221-E-027-098 and 107-2917-I-027 -001).

REFERENCES

1. Yang, A.S., Su, Y.M., Wen, C.Y., Juan, Y.H., Wang, W.S. and Cheng, C.H., (2016). Estimation of wind power generation in dense urban area. *Applied Energy*, 171:p. 213-30.
2. Lu, L., & Ip, K. Y. (2009). Investigation on the feasibility and enhancement methods of wind power utilization in high-rise buildings of Hong kong. *Renewable and Sustainable Energy Reviews*, 13(2), 450-461.
3. Khayrullina, A., van Hooff, T. v., & Blocken, B. (2013). A study on the wind energy potential in passages between parallel buildings. Paper presented at the Proceedings of the 6th European-African Conference on Wind Engineering (EACWE), Cambridge, UK.
4. Chaudhry, H. N., Calautit, J. K., & Hughes, B. R. (2014). The influence of structural morphology on the efficiency of building integrated wind turbines (biwt). *AIMS Energy*, 2(3), 219-236
5. Balduzzi, F., Bianchini, A., & Ferrari, L. (2012). Microeolic turbines in the built environment: Influence of the installation site on the potential energy yield. *Renewable Energy*, 45, 163-174.
6. Juan, Y.H., Yang, A.S., Wen, C.Y., Lee, Y.T., Wang, P.C. (2017). Optimization procedures for enhancement of city breathability using arcade design in a realistic high-rise urban area. *BUILD ENVIRON*, 121, p.247-261.
7. Blocken, B., Moonen, P., F.ASCE, T. S., and Carmeliet, J., (2008). Numerical study on the existence of the venturi effect in passages between perpendicular buildings. *Journal of Engineering Mechanics*, 134(12):p. 1021-1028.
8. Li, B., Luo, Z., Sandberg, M., and Liu, J., (2015), Revisiting the 'venturi effect' in passage ventilation between two non-parallel buildings. *Building and Environment*, 94, p. 714-722.
9. Montazeri, H., Blocken, B. (2013). CFD simulation of wind-induced pressure coefficients on buildings with and without balconies: Validation and sensitivity analysis. *Building and Environment*, 60, p.137-149.
10. Rezaeiha, A., Montazeri, H., Blocken, B. (2018). Towards accurate CFD simulations of vertical axis wind turbines at different tip speed ratios and solidities: Guidelines for azimuthal increment, domain size and convergence. *Energy Conversion and Management*, 156, p.301-316.
11. Stathopoulos, T., Storms, R. (1986). Wind environmental conditions in passages between buildings. *Journal of Wind Engineering and Industrial Aerodynamics*, 24, p.19-31.
12. Franke, J., Baklanov, A. (2007). Best practice guideline for the CFD simulation of flows in the urban environment COST action 732 Quality assurance and improvement of microscale meteorological models. Hamburg: Meteorological Inst.
13. Casey, M., Wintergerste, T. (2000). ERCOFTAC best practice guidelines : ERCOFTAC special interest group on "quality and trust in industrial CFD". London: ERCOFTAC.
14. Blocken, B., Stathopoulos, T., Carmeliet, J. (2007). CFD simulation of the atmospheric boundary layer: wall function problems. *Atmospheric Environment*, 41, p.238-52.
15. Hang, J., Sandberg, M., Li, Y. (2009). Effect of urban morphology on wind condition in idealized city models. *Atmospheric Environment*, 43,p.869-78.
16. Hang, J., Luo, Z., Sandberg, M., Gong, J. (2013). Natural ventilation assessment in typical open and semi-open urban environments under various wind directions. *Building and Environment*, 70,p.318-33.
17. ANSYS Inc. (2013). A. ANSYS Fluent Theory Guide for Release 15.0. U.S.A.

3DFOGTECH©

Portable Fog Water Station for Water-stressed Environments

CRISTIAN SUAU^{1,2}

¹EU H2020 Marie Skłodowska-Curie

²ACCIO TecnioSpring Plus

ABSTRACT: 3DFOGTECH© is a water enhancement technology applied in fog collection. This study is focus on geo-climatic data collection in selected fog sites, including design and structural test. 3DFOGTECH© is a portable, lightweight and modular polyhedral space-frame with light-coloured and water-repellent textile screens that collects condensed water drops in 360° from fog promoted by physical surface effects such as cooling, coalescence and condensation following the multi-directionality of winds, without any active energy demand. It offers autonomous water management in water-stressed areas with frequent dense fog events. Previous experiments made by author and collaborators (2010-16) were focused in obtaining efficient forms and designs through lighter space-frames and affordable hydrophobic meshes to secure clean water for drinking and irrigation. 3DFOGTECH© can harvest at least six times more water than planar fog collectors. Tubular frames are made with aluminium, which is a light, strong, durable and recycling material, whilst modular meshes are made with textiles treated with water-repellent coating solutions, light coloured surfaces and natural, synthetic or remanufactured polymers. Advanced design, connectors and structural prototypes are tested digitally and physically. 3DFOGTECH© is an applied research project co-financed by EU H2020 Marie Skłodowska-Curie and ACCIO TecnioSpring Plus programmes.

KEYWORDS: Design science, Water technology enhancement, 3D fog collection, Portable water station, Space-frames

1. THE FUTURE OF WATER IS IN THE AIR

Fog is a result of a complex earth system embodying a delicate balance between ocean, atmosphere, and land processes that shape and alter fog and its liquid water content (LWC) over time. Among alternative water supplies, the potential to collect water from air is by far the most underexplored resource. Only a thousandth of 1% of the water on Earth is in the atmosphere as water vapour. As part of the natural global water cycle, at any given time, the amount of water in the atmosphere is 12,900 km³, which represents 0.001% of total water and 0.04% of freshwater existing in the planet [1]. Fog originates from the accumulation of water aerosols suspended in the air, which create masses of humid air over land or sea. At low levels, air may contain fog or suspended liquid water droplets with diameters typically from 1 to 50 µm.

In airflow crossing natural formations like cliffs, mountains or ridges, orographic clouds might occur below, at or above the top of the obstacle, i.e. Fohn effect. Orographic influence on wind leads to the development or enhancement of clouds on the exposed side, which generally dissipates on the protected side due to downward motion. A cross-barrier flow might produce waves on the sheltered side, depending on atmospheric conditions and the topographic features. Sometimes, the oscillations of air on the sheltered side form lenticular clouds on the crests of such waves, which is airflow alteration due to relief. The most common orographic clouds belong to the genera Altopcumulus,

Stratocumulus and Cumulus. It is critical to observe cloud formations in highlands because they may provide an indication of weather changes that could have implications on fog collection [2].

Fog collection can contribute to alleviate water scarcity in water-stressed regions harvesting fog water to supply clean water for drinking and irrigation during hot seasons in arid lands like coastal deserts being viable solutions in remote locations with high fog occurrence. As potential source of water in coastal arid environments, fog collection is achievable by the collision of fog on a vertical mesh, where they coalesce, after which water runs down into a collecting drainage system and harvesting tank.

2. NEW CHALLENGES AND POTENTIAL USES OF FOG COLLECTION IN THE MEDITERRANEAN REGION

Nowadays water provision is a fundamental challenge in many water-stressed environments, natural, rural or urban. Risks associated with water shortage increase as the limited surface freshwater resources gradually diminish as result of rapid transformations and ineffective water grid distribution in the built environment. By 2050 2.3 billion more people than today (in total over 40% of the global population) will live in water-stressed regions [3]. Circa 14 million people in Europe do not have access to basic drinking-water source, in 2015 more than 62 million lack access to an adequate sanitation facility and 14 million do not use a basic drinking-water source Seven out of ten people without

PLEA 2018 HONG KONG

Smart and Healthy within the 2-degree Limit

access to basic drinking water sources live in fragile rural areas [4].

Fog collection is a simple, affordable and sustainable technology to obtain fresh water for irrigation and drinking in remote arid areas -nearby the coast- where surface water is limited [5]. Usually, users of fog collection are low-income farmers or rural villagers. In doing so, author has established a viable terrace-down model for fog water distribution, which follows natural slopes and water cycles. This scheme is well-adapted to both local water management and traditional agricultural techniques applied in dry and arid coastal zones in Mediterranean regions, including the Western Mediterranean reliefs of the Iberian Peninsula [6]. The harvested water is stored in tanks and then filtered and distributed via gravity through two separate pipelines: One branch supplies settlement with drinking water and the other extension is for irrigation of ecological restoration (native flora) and farms to prevent and mitigate the ongoing effect of desertification [7].

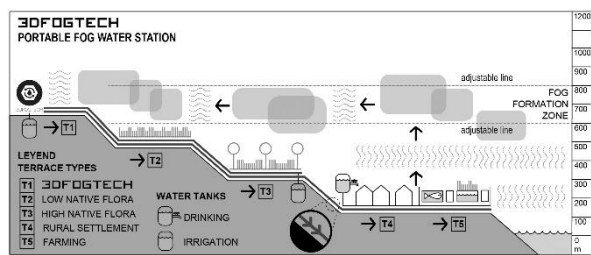


Figure 1. 3DFOGTECH® passive water distribution using gravity and slope to supply water for agricultural irrigation, ecological restoration and drinking. Source: author (2018).

3. RESEARCH, WORK PLAN AND OBJECTIVES

The duration of the overall project is two years. It is divided in three working packages (WPs) with distinctive tasks, milestones and deliverables. WP1 (ongoing stage; 8-month duration) is about climatic analysis, selection of fog sites and structural frame development. The next WP2 (10-month duration) will explore advanced textile development. WP3 (6-month duration) will test water capacities, yield and quality by monitoring, evaluating and disseminating technology.

The initial phase of this project (ongoing working package) is to (a) collect and map relevant geo-climatic data (selection of fog sites in Catalonia) and (b) develop a 3D fog collector, which is both adaptive and modular. Form follows climate. Climatic and geographic parameters are used to develop the design of portable fog water station (hexagonal array), which is made of lightweight metal structures that support strong winds and, through condensation, collect atmospheric water in water-repellent meshes facing multidirectional upwinds.

The objectives are to (a) explore innovative eco-design solutions (C2C) applied in advanced frames and screens with remanufactured materials like recycled and reused metal structures, remanufactured polymers, etc.; (b)

develop modular, portable and lightweight frames and hydrophobic screens through digital and manual simulations, mock-ups, and proof of concepts; and (c) Integrate systemic design with high structural, textile and water yield performances during experimentation.

4. METHODS

The overall research encompasses six disciplines: eco-design, climatology, geography, structural engineering, materials science and textile chemistry.

The applied methodology in WP1 is research-by-design using theoretical, empirical and design-based tools. It is supported by literature review; precedent studies; fieldwork and site visits; digital design simulations; physical mock-ups; and workshop, lab and onsite tests of pilot project developed in labs and selected climatic stations and disseminated in relevant scientific media:

a. Literature review on precedent studies (study of planar vs. 3D fog collectors in Spain and worldwide).

b. Geo-climate data collection and analysis taken from the automatic/manual stations of AEMET (Spain) <http://www.aemet.es>; SMC (Catalonia) <http://www.meteo.cat>; and Wunderground <https://www.wunderground.com>. Real-time satellite maps from EUMESAT are used. Refer to EUMESAT-view, fog; <https://www.eumetsat.int>

Fog and low clouds are based upon infrared channel data from the Meteosat Second Generation satellite. It is composed from data from a combination of the SEVIRI IR3.9, IR10.8 and IR12.0 channels. It is designed and tuned to monitor the evolution of night-time fog and low stratus. Individual survey includes fieldwork and site visits to all selected fog sites to measure, document visibility, wind, RH and temperature and climate parameters through photography and portable weather station. Psychrometric charts, spreadsheets and tables were used.

c. 3D Structural design and tests using AutoCAD & Sketch Up Pro to model space-frames; details and views. Design includes manual and digital representation in sketches, diagrams, CAD technical drawings and components; physical models. Each screen size is 1M². They are elevated 2-3 metres above ground. Final prototype will be built in 1:1 scale and monitor by a Davis Pro 2 portable weather station with wireless integrated sensor, console and Weatherlink software.

d. 3D-printing. Connectors (joints) were modelled scales 1:5 and 1:1 using Flashforge 3D printer

e. Structural and CFD (Computational Fluid Dynamics) simulations using model making. Two structures were chosen and build in physical wiring models 1:5 scale (timber and aluminium bars). COMSOL Multiphysics 5.3 tools is used in both structural mechanics to measure axial, moment, shear and torsion and fluid flows to map lift and drag forces hexagonal prisms.

PLEA 2018 HONG KONG

Smart and Healthy within the 2-degree Limit

- f. Open demos and citizen science talk in Barcelona Science Festival (June 2018).
- g. Textile tests: Demonstration not achieved yet (WP2). Experiments will analyse wettability, surface area and adsorption parameters of selected textiles in a fog chamber at lab and then in-situ.
- h. Water yield and quality test: Demonstration not achieved yet (WP3). Chemical and microbiological analysis of water samples.

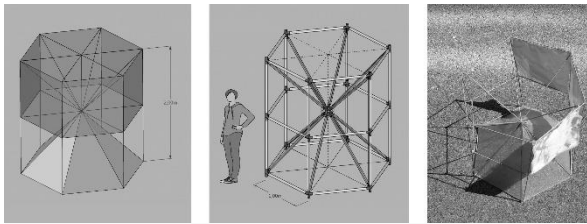


Figure 1. 3DFOGTECH@ snowflake type: a. Concept; b. Frame and c. 1:5 Model. Source: Source: author, 2018

5. FOG ANALYSIS, MAPPING & SITE SELECTION

The Mediterranean Region (Cfb) is experiencing a significant shortage of rainfall, with severe impacts on rainfall-dependent settlements, farms and natural parks. In Spain, fog formations with high LWC are mainly located in Canary Islands and the Western Mediterranean Basin of the Iberian Peninsula, with annual rates of fog water yield between 3-10 l/m²/day average. Water needs will double by 2021 in Catalonia (Agència Catalana de l'Aigua, 2015). In Catalonia, frequent fog formations occur between 10km and 50km distance far from the Mediterranean coastline.

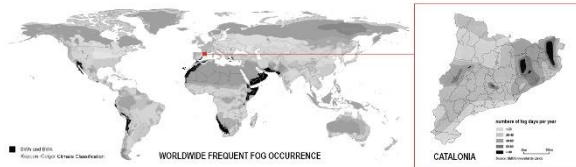


Figure 2. Map of frequent fog occurrence in Catalonia and worldwide (fog in black / dark grey). Sources: author (2018).

In Catalonia, advection fog (from sea to land) is mainly a phenomenon of cyclone episodes that occur in the Mediterranean littoral and pre-littoral zones, especially during cold seasons, between October and January. Prevailing wind direction is N and NE with wind speed between 2 and 5m/s. RH is higher (>80%) and temperatures are lower (<12°C). The average dew point temperature is between 7.1°C and 7,8°C [6]. Between 2006 and 2017, Montserrat Observatory (MO) recorded 96.1 foggy days per year, reaching 162 foggy days in 2001, and 2,7 m/s wind speed average.

The optimal places to catch advection fog are situated in Barcelona, Girona and Lleida provinces, mainly in high formations such as national parks and the Mediterranean Pyrenees. The best massifs or are Montserrat, Montseny and Albera [7]. However, the period for harvesting fog

varies from site to site not offering a consistent pattern but rather randomized. The best fog harvesting point is Puig Neulós in Albera massif with 27.2 l × m² × day of fog water in cold seasons, including Springtime, whilst in Montseny massif roses 11.6 l × m² × day during Autumn [8].

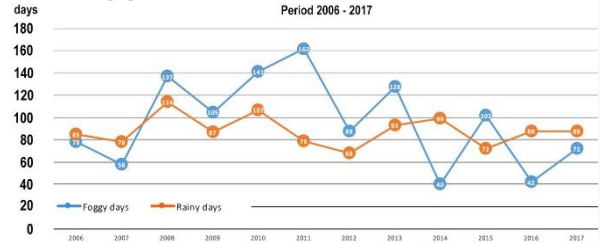
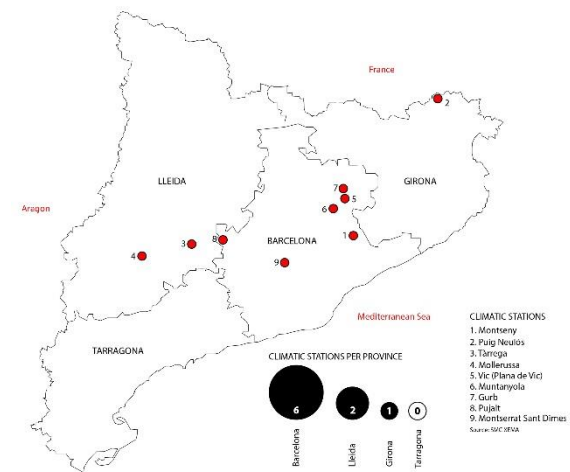


Table 1. Comparative table between foggy and rainy days in Montserrat abbey, 2006-2017. Source: MO (2018)

For instance, Puig Neulós offers the best conditions for setting experiment. It is a remote climatic station at 1256m a.s.l. (42° 28' 51" N; 2° 56' 47" E) with 7.1°C dew point; over 75% RH; and 3.9 m/s wind speed. Fog water is 22.3 l × m² × day, annual average [9]. The other suitable locations to set onsite experiments are Observatory and Sant Dimes stations (740m a.s.l. and 916m a.s.l. respectively) in Montserrat massif and also Turó d'Home (1712m a.s.l.) in Montseny massif. There is great potential in the rural landscapes of Gurb, Muntanyola, Vic (Plana de Vic), Pujalt, Mollerussa and Tàrraga.



Location	Dry bulb (°C)	RH (%)	Dew point (°C)	Abs. Humidity (g/m ³)	Enthalpy (kJ/kg)	Sp. Vol (l/kg)	Atmospheric pressure (hPa)	Wind speed (m/s)	Altitude (meters)	Köppen (classification)
Puig Neulós Montseny	7.1	75.5	7.1	0.007	31.7	0.98	1027	4.96	1660	EFs
Puig Neulós	13.5	86.8	7.8	0.008	36.2	0.88	1113	3.89	1256	EFs
Tàrraga	14.1	72.9	7.8	0.008	35.8	0.87	1020	3.89	422	Cfa
Mollerussa	14.7	74.4	7.8	0.008	34.3	0.85	1030	3.84	247	Cfa
Vic (Plana de Vic)	13.4	79	7.8	0.008	33.7	0.87	1072	3.43	492	Cfa
Montseny	12	81	7.8	0.008	32.2	0.8	1024	3.50	816	Cfa
Gurb	13.5	86.8	7.8	0.008	36.2	0.88	1070	3.54	562	EFs
Pujalt	17.2	79	7.8	0.008	34.6	0.9	1045	3.52	266	EFs
Montserrat - Sant Dimes	13.2	85.4	7.8	0.008	34.8	0.91	1070	2.68	916	EFs
TOTAL (average)	12.522	80.822	7.722	0.008	32.756	0.893	1028.356	3.273	794.667	n/n

Table 2. Comparative table of selected fog sites in Catalonia using psychrometric and climatic data calculations. Source: SMC XEMA & author (2018).

The potential beneficiary population represents circa 900,000 inhabitants, which means up to 12% of the

PLEA 2018 HONG KONG

Smart and Healthy within the 2-degree Limit

population in Catalonia (IDESCAT, 2016). The Catalan Weather Service (SMC) employs different terminologies and methods to define and measure fog occurrence. Regarding weather data constrains, fog episodes are not recorded by automatic stations in Catalonia. Fog occurrence is measured in terms of visibility. In Catalan, Boira means dense fog (less than 1km of visibility); boirina is fog (visibility between 1-10km); and calitja means mist (visibility between 1-10km). The regional weather observation network (XEMEC) was founded in 2009, so it cannot offer retrospective data. Records of period 2010-18 have helped to identify trends in areas with frequent fog. As the fog observation points (i.e. airports) did not coincide with the location of the automatic stations, author has interpreted the general climatic data available in Osona, Urgell, Pla d'Urgell, Bages and Vallès Oriental regions. This study unfolds an updated climatic map of best sites for fog harvesting in Catalonia. Based on findings and permissions, two trials will be tested in the next research stages.

6. DESIGN & STRUCTURE ADVANCEMENTS

Problem: Planar fog collectors are structurally fragile tensile structures. They frequently fail under the heavy load of strong wind events. Meshes keep using polyolefin sun-shading nets with poor mechanical and spanning properties. Nets tear, gutters and pipes leak, and wind blow the whole structure over. Steel frames and tensile cables normally rust, and birds wreck textiles spoiling the process of fog water harvesting [10]. If wind changes its perpendicular direction, yield of fog harvesting decreases. This inefficiency is mainly due to the lack of fog-responsive design integration between dynamic weather factors; forms and geometries; and new materials and textiles advancements.



3DFOGTECH

FOG COLLECTOR		CONVENTIONAL	3DFOGTECH
Structure	Form	2D planar	3D polyhedron
	Frame	tensile canvas type	modular space-frame, air-frame
	Connectors	tensors only	timber noods gutter clips column clips
	Foundation	permanent concrete pad	portable metal pad
	Manufacture	in-situ construction	off-site prefabricated construction
	Materiality	timber or metal posts	metal, Plastic, Timber, Paper
	Weight	heavyweight	lightweight
	Permanence	fixed	demountable
Mesh	Screen Ratio	1:2 / 1:3 / 1:4	1:1 / 1:2
	Fibre Texture	higher porosity	lower porosity
	Fog Collection	unidirectional (prevailing wind only)	multidirectional (windrose based)

Table 3. Comparative scheme of planar vs. 3D frames on textile and structural capacities. Source: author (2018).

Form follows multidirectional winds: The more wind, the more harvested fog water. In order to develop a high fog-responsive design, should integrate these multiple parameters: (a) Climate: Relative humidity, liquid water content (LWC), wind speed and direction, air temperature (wet bulb, dry bulb and dew point), visibility

and atmospheric pressure; (b) Topography: Altitude, wind orientation, slope clearance (physical obstacles), soil mechanics and accessibility; (c) Shape: Screen ratio (height/length); height from ground, volume geometry, and structure types; and (d) Textiles advancement: Mesh pattern, textural porosity (spacing), colouring, polymer types, hydrophobic features and coating solutions.

In this early phase, throughout CFD simulations (computational fluid dynamics), model making and structural design, author is testing several experiments with light space-frames by eliminating tensors; reducing the amount of embracing elements; and creating a catalogue of connector including anchorage solutions following presumptive bearing capacity values for three different types of soils.

Design experiments: FOGHIVE© [11] is a 6-side fog collector that was tested in Atacama (Peña Blanca, Chile) in August 2014. Three mesh experiments were carried out: T1 (day 1) with 6-side insect nets (HDPE); T2 (day 2) with 6-side 3D mesh nets of polyester (PES); and T3 (day 3) with 5-side insect nets and one-side 3D mesh. Experiments examined (a) affordable insect net with lower porosity (white) and (b) 3D specialised fabric with higher porosity (black). Six PVC U-shape gutters and 10l tanks were installed, one gutter and one tank per 1m x 1m screen ratio. All fog collecting screens harvested equal fog water volume per screen regardless uniform and mixed meshes (T1, $4,1 \text{ l} \times \text{m}^2 \times \text{day}$ per mesh; T2, $3,8 \text{ l} \times \text{m}^2 \times \text{day}$ per mesh; and T3, $5,7 \text{ l} \times \text{m}^2 \times \text{day}$ per mesh). Due to geometry and form of the selected volume and its wind multi-directionality, FOGHIVE© harvested six times more water content than planar devices.



Figure 3. FOGHIVE© test in Atacama Desert, Chile (2014). Source: author, 2018

3DFOGTECH© is an upgraded portable, lightweight and modular polyhedral space-frame with light-coloured and water-repellent textile space screens that collects condensed water drops in 360° from fog promoted by physical surface effects such as cooling, coalescence and condensation following the multi-directionality of winds, without any active energy demand. This hexagonal cylinder consists of six screens (ratio 1:1 or 1:2). It can

PLEA 2018 HONG KONG

Smart and Healthy within the 2-degree Limit

easily be installed on flatten or uneven grounds. It uses advanced polyhedral frames (towers), advanced textile materials and surfaces formed by coating processes, and remote wireless weather monitoring.

Shape and fluid dynamics: Relevant literature review on wind effect on solids with hexagonal cross section and computational fluid dynamics tests conducted by mechanical and wind engineers denotes that the pressure coefficients are calculated from the measured values of the surface static pressure distributions on the cylinder. Both drag and lift coefficients are obtained from the pressure coefficients by numerical integration methods [12].

As result, the hexagonal cylinder shows that there is significant drop in the drag coefficient values for the single hexagonal cylinder in comparison to that of the single square cylinder and the values approaches to that of the circular cylinder [13]. In addition, the drag coefficient for a single hexagonal cylinder at zero angle of attack is about 0.95 in contrast to that of 2.0 for a single square cylinder at the same angle of attack. The variation of the lift coefficient on the single hexagonal cylinder is not appreciable and they are close to zero value except at angles of attack of 100 and 500, where some insignificant values are observed. Drag coefficients become remarkably smaller compared with sharp-edge square cylinder. The hexagonal cylinder offers a variation of lift and drag coefficients (c_d) facing airflows at various rotational angles respectively.

Structural types: Doing the most with the least. Mimicking scaffolding modules, author simplified structural elements of previous hexagonal cylinders eliminating tensile wires and screen cross-bracing; reducing the number of connectors and bars; and allowing stacking and honey-comb expansions. The experiments are tested in 1:5 models made of timber rods and aluminium tubes prior 1:1 fabrication.

As result, there are two distinctive modules made with aluminium tubes (33mm outer diameter; 2-4mm thickness; and 1000-1600mm length).

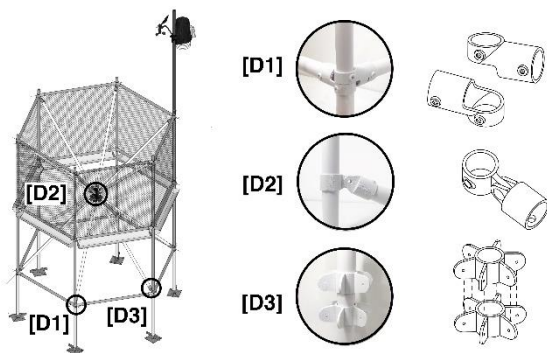


Figure 4. 3DFOGTECH® snowflake type: Details of rigid connector digitally designed and then made in 3D-printing. Source: author (2018).

(a) *Snowflake type:* It is a hexagonal prism with a core node of inner 12-way hub connector branching out and embracing the structure through the repetition of six large triangles spinning 60° around central axis. It is a double height volume with adjustable anchorage.

(b) *Tower type:* It is a hexagonal with an inner triangulated tower, which provides self-embracing to six perimeter screens. It is a double or triple height volume with adjustable anchorage.

Both types are horizontally embraced with triangular rings at bottom and top positions to avoid torsion and secured 100% stiffness.

Connectors, tubes, gutters and anchorage: Prior the fabrication of the 1:1 prototype, author is designing optimal joints. All connectors are rigid. They are made with plastic using 3D-printing. Being accurate and affordable, 3D-printing is quite slow. Plastic joints do not resist high heat. They have poor mechanical properties. Then chosen connectors are made in galvanized steel, which is also cheap but good with UV and oxidation. In addition, gutters are made of copper (high antibacterial qualities). Based on presumptive bearing capacity values for different types of soils, aluminium posts will rest on six adjustable jack screws (500mm) or shallow pad foundations. The four types of soils are: (a) soft rock and coarse sand (4.4 kg/cm²); (b) medium sand (2.2 kg/cm²); (c) stiff/soft clay (1 kg/cm²); or (d) rocks (>32.40 kg/cm²) where they are replaced by climbing anchors [14].

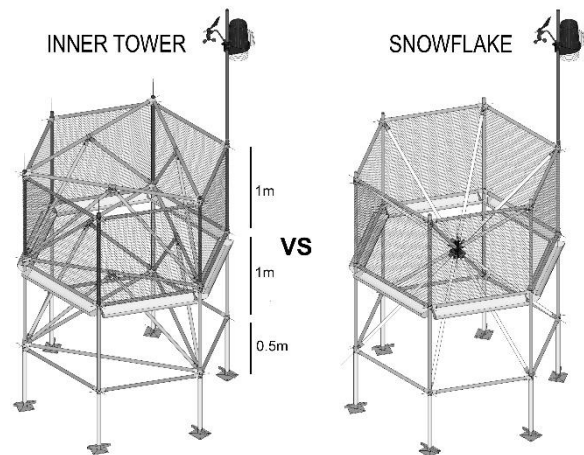


Figure 5. Comparative study between snowflake and tower structures. Source: author (2018)

6. CONCLUSION

Nowadays water management remains heavily dominated by conventional mechanised and human-built infrastructures. 3D fog collection is an adaptive water enhancement technology that uses horizontal precipitation to mitigate the effects of climate change on remote water-stress environments, particularly Mediterranean natural parks and rural settlements. Its synergy is aligned with the shifting towards sustainable development in rural areas in Catalonia and the Mediterranean Region allowing the preservation and

PLEA 2018 HONG KONG

Smart and Healthy within the 2-degree Limit

promotion of biodiversity whilst fostering the creation of liveable, diverse and balanced ecosystems for the primary and tourist sectors.

The main achieved tasks of WP1: (a) process geo-climatic data collection in nine fog sites chosen for advanced experimentation; (b) obtain design efficiency through (i) finding optimal forms, geometries and structural frames with high portability, lightness and modularity and (ii) developing building components and connectors with great mechanical strength and air permeability. This study bridges design, climate, and structural by (i) Integrating site-specific climatic conditions in various simulations; (ii) augmenting mechanical properties of space-frames using lightweight metal bearing and spanning elements; (iii) simplifying connectors, including modularity, portability and montage; and (iv) minimizing visual and ground impact of immediate surroundings, mainly using reflective surfaces and adjustable anchorage.

3DFOGTECH© is the first 3D portable fog water station in the world (EUIPO community design registered). It is an autonomous water management solution for water-stressed areas with frequent dense fog events. New structures provide greater stability and stiffness against strong winds and rocky soils.

ACKNOWLEDGEMENT

In memory of Edison Suau (RIP), an inspiring father and visionary designer.

Many thanks to the EU H2020 Marie Skłodowska-Curie and ACCIO TecnioSpring Plus programmes for supporting the development of this technology. Author is the principal investigator and scientist in charge.

Leitat is my host technology center. Special thanks to Dr Llorenç Bautista, research supervisor; Carolina Carbó, project manager; and Mercè de la Fuente, lead of advanced material division at Leitat; Prof. Javier Martin Vide (IdRA); and Jéssica Amaro (Servei Meteorològic de Catalunya) for their generous support in various research aspects. Author is visiting researcher in the Water Research Institute (IdRA) at University of Barcelona and member of the International Fog and Dew Association (IFDA), COST Action RESTORE CA16114 and the Marie Skłodowska Curie Alumni Association (MCAA).

The development of 3DFOGTECH© began with the experimentation of FOGHIVE©, ART ART© and AIRDRIP© at ECOFABRICA and associated (2010-2015) followed by the preliminary idea of 3DFOGTECH© project developed in Studio Pop (2016). Author expresses his special gratitude to Laura Petruskeviciute and collaborators.

REFERENCES

- Gleick, P. H., 1996: Water Resources. In *Encyclopedia of Climate and Weather*, S. H. Schneider (ed.), Oxford University Press, New York, vol. 2, p. 817-823.
- Taalas, P. ed. (2017) *International Cloud Atlas. Manual on the Observation of Clouds and Other Meteors* (WMO-No. 407). World Meteorological Organization, Hong Kong. [Online] available: <https://cloudatlas.wmo.int>
- UN World Water Development Report (2018). United Nations: Educational, Scientific and Cultural Organization, France: p. 1-139. [Online] available: <http://www.unwater.org/publications/world-water-development-report-2018/>
- WHO Regional Office for Europe (2017) Fact Sheet 7 - Water, Sanitation and Hygiene. Transforming the Regional Agenda towards Equitable Access to Safe and Sustainable Services. [Online] available: <http://www.euro.who.int>
- Gischler, C. (1991) *The Missing Link in a Production Chain: Vertical Obstacles to Catch Camanchaca*. Montevideo, UNESCO: p. 1-191.
- Laureano, P. (2001). *Atlas del Agua*. Barcelona, UNESCO Laia editorial: p. 112-338, 662-710.
- San Juan, M., del Barrio, G., Ruiz, A., Rojo, L., Puigdefabregas, J. & Martinez, A. (2014) *Evaluación de la Desertificación en España: Mapa de la Condición de la Tierra 2000-2010*. Ministry of Agriculture, Food and Environment, Madrid, Spain: p. 1-80.
- Corell, D. (2014) *Estudio Estadístico de la Potenciación de Uso del Agua de Niebla como Recurso Hídrico en el Litoral Mediterráneo de la Península Ibérica*. Universitat Politècnica de Valencia, Spain: p. 87.
- 9a. Idem: p. 79-81.
- 9b. Data of selected stations (2007-16). [Online] available: <http://www.meteo.cat/wpweb/climatologia/serveis-i-dades-climatiques/normals-climatiques-recents/>
- Schemenauer, R. S., & Cereceda, P. (1994) *A Proposed Standard Fog Collector for Use in High-elevation Regions*. Journal of Applied Meteorology (33): p. 1313-1322.
- 11a. Suau, C. (2012) *FOGHIVE©: 3D Fog Collection in the Coastal Atacama Desert*. PLEA 2012 Conference, Lima, Peru [Online] available: <http://www.plea2012.pe>
- 11b. Suau, C. (2010). *Fog Collection and Sustainable Architecture in the Atacama Coast*. 5th International Conference on Fog, Fog Collection and Dew, Münster. pp. 179-188. [Online] available: <http://www.fogconference.org>
- Kaledi, H. & Andersson, H. (2011) *On Vortex Shedding from a Hexagonal Cylinder*. Elsevier, New York, Physics Letter A, vol. 375 (45): p. 4007-4021. DOI: <https://doi.org/10.1016/j.physleta.2011.09.046>
- Sultana, K.; Mandal, A. and Hai, B. (2014) *An Experimental Investigation of Wind Load on Buildings with Hexagonal Cross-Section*. Procedia Engineering 90. p. 314-319. DOI: 10.1016/j.proeng.2014.11.855
- Bond, A. J., and Harris, A. J. (2008). *Decoding Eurocode 7*. London UK: Taylor & Francis: p. 1-618. [Online] available: http://eurocodes.jrc.ec.europa.eu/doc/2013_06_WS_GEO/report/2013_06_WS_GEO.pdf

An Analysis of a Handful of Solar Decathlon Europe 2014 Prototypes

Thermal and comfort performances in local context

DENIS BRUNEAU¹, MARCO DELUCIA², PHILIPPE LAGIÈRE², MARIE PAULY³,
PASCALE BRASSIER³, BRUNO MESUREUR⁴

¹ENSAPBX (Ecole Nationale Supérieure d'Architecture et de Paysage de Bordeaux), France;

²Université de Bordeaux, France;

³Nobatek-INEF4, France;

⁴CSTB (Centre Scientifique et Technique du Bâtiment), France

ABSTRACT: Solar Decathlon Europe 2014 (SDE2014) was an international competition organized to promote experimentation and research in the field of zero-energy buildings. Thanks to the monitoring and observation work carried out during the competition, a large database on actual performances and behaviours of different types of sustainable house prototypes was created. In this work, five participating prototypes were selected (houses designed for different climates, architectural characteristics, passive systems and strategies) and their thermal models were developed. A BPS of each prototype was carried out with the Pleaides+COMFIE software, adopting a multi-zone approach. Qualification of the thermal modelling was achieved due to the good match between simulated interior temperatures and real interior temperatures monitored in Versailles (France) during the competition. A specific method was also created to overcome uncertainty and lack of knowledge regarding some competition usage scenarios. A BPS of the qualified models was subsequently carried out within the related local context, optimizing usage scenarios with the purpose of obtaining low energy consumption and excellent interior comfort at the same time. This gives an appreciation of the energy performances of the five selected prototypes.

KEYWORDS: Solar Decathlon, Energy models, Thermal, Comfort, Simulation

1. INTRODUCTION

In 2014, Versailles hosted the third edition of Solar Decathlon Europe (SDE). This is a sustainable solar house competition, in which universities, organized in teams, design, build and operate zero-energy prototype houses. Houses are equipped with all the technologies needed to exploit environmental energy, especially solar, with the goal of reducing the consumption of energy from non-renewable sources. The project manuals of all the houses are available in [1], with full details on building innovative technologies and construction systems, such as building envelope characteristics, passive or active energy systems, water treatment and re-use systems, uses and appliances, etc. [1].

Each house is designed to fit within the environmental context and specificities of its home country. Teams built their prototypes in Versailles (France), at the competition site called "La Cité du Soleil", to test them in identical weather conditions. The challenge is divided into 10 contests, making this event a Decathlon.

Contests can be grouped into two evaluation types: evaluations by a multidisciplinary jury and evaluations by means of measurements.

During the competition days in Versailles, the performance of the houses was constantly monitored, mainly for the purpose of scoring the prototypes.

The efficacy of passive strategies and design solutions while the houses were in the "Cité du Soleil" was estimated through the monitoring system.

Thanks to the monitoring system, each prototype was evaluated on its performances regarding comfort and accommodation (temperature, air humidity and CO₂ concentration), house functioning (home appliances and multimedia) and the global electrical energy balance. Many different sensors were installed in each area of the houses, in order to monitor the competing prototypes in real time. In each house, there were three sensors for dry bulb temperature monitoring, placed on poles at 150 cm from the finished floor level. The SDE2014 organizers chose the position of the sensors. Usually, one was placed at the center of the living room, one in the bedroom and the last one in a room or space selected for its specific qualities. Humidity sensors were placed close to the temperature sensors.

The SDE2014 rules included a Passive Evaluation Period of 56 hours, the aim being to evaluate the effectiveness of passive systems or adopted strategies. During this passive period, according to the competition rules, "...the participating houses will be allowed to use only "passive" cooling or heating. "Passive", for the purposes of the Competition, means any form of strategy that is not relying on a "thermodynamic cycle" or internal heat or cool production devices. During this Period, the use of

PLEA 2018 HONG KONG

Smart and Healthy within the 2-degree Limit

pumps and fans, for a total electric power less than 100W, is permitted. Teams thus have to plan passive strategies to maintain the internal comfort conditions, and electrical production and consumptions are still monitored.”

In the field of sustainable solar houses, the design phase assumes a central role in predicting house thermal behavior. Building energy simulation programs are capable of simulating energy consumptions, according to the purpose of these consumptions. They also provide knowledge and understanding of the effectiveness of the adopted passive systems during the design process, and can thus lead to change or improvements in the corresponding architectural choices.

Simulation results can be very different from the real behavior of the buildings. This depends on many factors (software, users, modelling, etc.). Building thermal modelling can be validated by matching the results of the simulation with the real measured data (e.g. for house interior temperatures). Events like the Solar European Decathlon give us a better understanding of the thermal behavior of different experimental solar buildings with high energy efficiency (and thus of the architectural choices made by SDE2014 teams during the early design phases), thanks to the incredible database both of passive solutions analysis and of measurement values built during the competition.

The aim of this paper is to exploit the monitored data acquired during SDE2014. The work consists in qualifying the thermal models of five selected projects. This is achieved by comparing the results of the Building Performance Simulation (BPS) of the thermal modelling with the measurements taken during the competition phase (internal air temperature data). Subsequently, the BPS of the qualified thermal model was carried out within the related local context, optimizing the usage scenarios in order to obtain good values both for annual energy consumption and thermal comfort, using calculations of the PMV and PPD indices and local thermal comfort criteria.

The work is focused on how passive design strategies may increase interior comfort and contribute to the reduction in energy consumption in buildings, and does not include the study of the houses' energy production systems. It is organized as follows: Section 2 presents the general approach and methodology adopted to obtain the thermal modelling qualification. In Section 3, the result of each qualification is shown and explained. The BPS of the selected prototypes within the related local contests is presented in Section 4. Conclusions are expounded in section 5.

2. GENERAL APPROACH AND METHODOLOGY

SDE2014 was a challenge between twenty high energy efficient houses, but it also produced an extraordinary resource of data in the field of new zero-energy housing

solutions. For twelve days, all the prototypes were continuously monitored. This large amount of data can be exploited to understand and simulate the annual behaviour of different passive houses within the related local context. From the twenty competing prototypes at SDE 2014, five houses were selected, each with particular and different architectural characteristics and passive systems.

To qualify a thermal model, it is fundamental to have all the necessary data required to simulate the behaviour of the prototypes. If any data is missing (mainly values for air infiltration and some usage scenarios) then we must devise a method to obtain these data, in order to achieve the most objective BPS and modelling qualification.

A multi-zone modelling approach is used in order to simulate the behaviour of the prototypes as realistically as possible. A modified Météo-France weather file from the Trappes Weather Station (near Paris, France), was used to simulate the selected prototypes in identical weather conditions, as in the competition period.

Once thermal modelling has been qualified (by comparing simulations and experimental results in Versailles), this thermal model is used to carry out the annual BPS of the 5 prototypes within their local meteorological context. Values that concern usual scenarios (e.g. window coverings and opening), and local uses (e.g. dish and clothes washing, cooking periods), were then chosen, taking into account suggestions from the competitive teams concerned. Lastly, the usual scenario values were changed with the aim of optimizing both energy consumption and comfort conditions, always taking into account a realistic utilization of the houses.

2.1 Architectural characteristics and passive systems of the selected projects



Figure 1: from left to right, top to bottom: Rhome For Dencity, OnTop, Casa Fenix, Home with a skin, Maison Reciprocity.

The selected prototypes are: Rhome for Dencity, ROME, ONTOP, FRANKFURT, Casa Fenix, CHILE/FRANCE, Home with a skin, DELFT, Maison Reciprocity, USA/FRANCE (Fig. 1).

PLEA 2018 HONG KONG

Smart and Healthy within the 2-degree Limit

Each project is different both in typology and in climate family, in order to include a diversity of passive design approaches (Table 1).

The **“RhOME for denCITY”** project, winner of the Solar Decathlon Europe 2014 competition, is part of an urban regeneration program for the *Tor Fiscale* district of Rome that aims to replace illegally inhabited buildings with high-performance and efficient houses. The prototype is an apartment designed to be sustainable, modular and prefabricated. The wood envelope is composed of balconies, loggias, fixed and movable screens, in order to exploit solar gains and natural ventilation.

Thanks to its thermal inertia properties and the stratigraphy of the large wall, inside air temperature and external temperature fluctuations have been optimized. Materials and technologies have been handpicked with the aim of reducing the building’s impact on the environment. To achieve this, a dry and lightweight prefabricated structure has been used.

Adjustable photovoltaic shading screens give flexibility and originality to the facade.

The goal of the **“OnTop”** project is the densification of German inner cities. This is made possible by building additional housing on top of existing buildings

In fact, building at ground level is no longer feasible, due to the great density of city centres.

In addition, the elevated position ensures a great production of solar energy, thanks to the integrated solar energy systems. The new building is able to produce solar energy both for itself and partly for the old building.

The project also includes the renovation of the existing building facade by enlarging openings and improving insulation.

Walls are composed of prefabricated wood panels, with an external insulation made of two layers of wood fibre panels. A phase change material compensates the lack of thermal mass of the wood panels. PCM is more ecological, sustainable and lighter than bricks or concrete. The position of the windows promotes a good natural cross ventilation.

Chile is affected by devastating earthquakes and flooding. The **“Casa Fenix”** project aims to solve the issue of Chile’s emergency housing, thanks to prefabricated, flexible and modular houses, designed with a wood frame in order to be easily assembled and built by volunteers and victims during these difficult situations.

The prototype structure is made by alternating posts and an envelope of light elements, which can be rapidly assembled.

An ecological thermal wall, made from bottles filled with water, accumulates heat from solar energy during winter days, in order to discharge this accumulated heat during the night.

An innovative passive system (VMI-Solèhom system) allows the exploitation of external environment energies, in order to improve interior comfort, thanks to an air

blowing system associated with an air collector (which preheats the air during winter), with a PCM storage to store and destore thermal energy when it is useful, and with an optional mechanical over-ventilation if natural ventilation is not sufficient.

Typical Dutch row houses are usually poorly insulated.

The **“Home with a skin”** project aims to improve their energy efficiency, by adding a second skin, more precisely a solar greenhouse, on one facade of existing houses. More than half of Netherlands’ houses are row houses with gardens. By adding an adaptable glasshouse over the envelope, it is possible to use the garden also in winter, and thus create a new and useful extra space.

Thanks to the new skin, the garden space can be used all year round and for different seasonal activities. Without greenhouses, the current gardens can only be used 50% of the time in the Dutch weather conditions.

The project attempts to maximize both energy consumption and food production. The prototype built in Versailles was a replica, on a small scale, of an example of the typical Dutch houses to be renovated.

It was built with wood panels making it easier to assemble than the original brick structure. A glasshouse, on the principal facade, completed the prototype.

“Maison Reciprocity” is a Franco-American collaboration project that aims to revisit the established townhouse on both sides of the Atlantic, notably those of the French and American traditional habitats.

The goal of the Franco-American team was to design a modular housing unit, adapted to the urban context, for use as a single-dwelling home with the potential to assemble into a collective housing building. The three principal components of the house are the “Urban Shell”, an envelope with standard thermal insulation, “the Chord”, the area relative to the kitchen and bathroom, and the “Living Brise-Soleil”, which concerns all the components of the facade and roof designed to produce energy and to ensure climate protection. The Maison Reciprocity prototype exploits solar energy through a 4.9 kW monocrystalline photovoltaic array, an evacuated tube drain back solar thermal collection system, and ISAAC, a building facade integrated solar air-to-air collector coupled with AAPS, a bio-phase change storage material

2.2 Weather conditions in Versailles

During the competition, real-time weather data were measured in Versailles. This gave us the environmental conditions in which the prototypes were competing. In addition, these data are useful to recreate the same weather conditions for a thermal model of the prototypes in Versailles.

PLEA 2018 HONG KONG

Smart and Healthy within the 2-degree Limit

2.3 Usage scenarios of the selected prototypes during the SDE 2014 competition

Some of the prototypes' usage scenarios are uncertain (temperature set points for heating and cooling, occupancy, windows covering and shading, mechanical and natural ventilation). A method has been considered to choose values for the usage scenarios. In the selected prototypes, the window covering in the Rhome prototype during the competition was known thanks to observations (95% obscured during most of the day). This allowed us to eliminate any uncertainty from a very influential parameter in BPS. A careful analysis of measurements taken and the competition rules (consumption data for household appliances, minute by minute, and prototype occupancy rules) reduced the uncertainty related to usage scenarios. For set-point temperature values and operation of the VMC (controlled mechanical ventilation) the values declared by the Rhome team relative to the project in the local context were used. For natural ventilation values, the diagram of interior temperatures for the first 7 days of the competition was "fitted". For the last week (including 56 passive hours), a steady and very low natural ventilation was assumed (assumptions based on a cold outside temperature).

The table summarizes the typology of usage scenario data (actual data, team's hypothesis, personal hypothesis, fitting work) used to make the BPS of the Rhome prototype (Table 1).

Table 1: Usage scenario data used for the Rhome model.

SCENARIOS	PROTOTYPE
	Rhome
Temperature set points	Team's hypothesis
Occupancy	Actual data (rules and calendar of the competition)
Internal heat gains	Actual data (measured during the competition)
Covering	Actual data (observations)
Mechanical ventilation	Team's hypothesis
Natural ventilation 1 st week	Fitting
Natural ventilation 2 nd week	Hypothesized steady and very low (very low external temperature)

Similar work was carried out for the other four selected prototypes. In this case, to overcome the obstacle of the lack of information about covering scenarios, the same natural ventilation was used as for the last week, hypothesized for the Rhome prototype (steady and very low natural ventilation). Based on these settings, the diagram of interior temperatures was "fitted" for each prototype, using plausible shading scenario values (Table 2).

2.4 Multi-zone thermal modelling

A multi-zone approach was used during thermal modelling, for all the selected prototypes, with the exception of the Reciprocity prototype. In this way, it was possible to analyse, simulate and qualify prototypes

SCENARIOS	PROTOTYPES				
	Rhome	OnTop	Fenix	Home-Skin	Reciprocity
Temperature set points	Team's hypothesis				
Occupancy	Actual data (rules and calendar of the competition)				
Internal heat gains	Actual data (measured during the competition)				
Covering	Actual data (observations)	Fitting			
Mechanical ventilation	Team's hypothesis				
Natural ventilation 1 st week	Fitting				
Natural ventilation 2 nd week	The same for all the prototypes Rhome natural ventilation, hypothesized steady and very low (very low external temperature)				

Table 2: Usage scenario data used for the five selected prototypes.

more precisely, mainly thanks to the different usage scenarios selected for each room.

For example, for thermal modelling, the OnTop prototype was divided into 4 thermal zones (living room/office, bedroom, bathroom and kitchen) (Fig. 2).

For each zone, the relative usage scenarios were applied, with particular attention to the location of

PLEA 2018 HONG KONG

Smart and Healthy within the 2-degree Limit

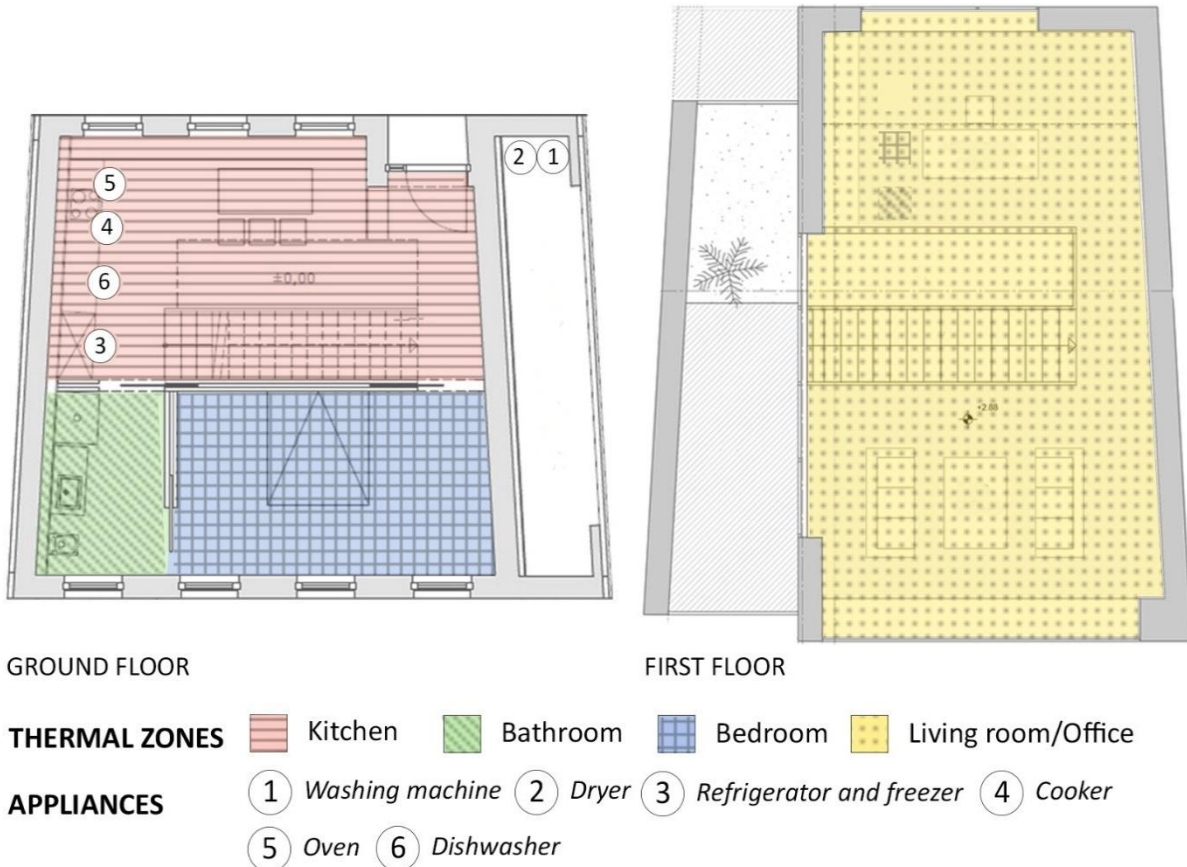


Figure 2: Thermal zones and position of the appliances for the OnTop model.

appliances, mechanical ventilation ducts and internal ventilation (by opening doors) between the different areas.

By using a multi-zone approach, it was therefore possible to make a BPS that was closer to the real thermal behaviour of the prototypes.

3. THERMAL MODELLING QUALIFICATION

The internal temperature values of each prototype BPS were compared with the internal temperature measurements taken during the competition. The thermal modelling qualification of the 5 prototypes was

achieved thanks to the excellent agreement between the BPS internal temperatures and real temperatures (Fig. 3). The internal temperatures of three zones (living room, bedroom and kitchen) were compared with the respective temperatures taken during the twelve days of the competition.

4. BPS OF THE PROTOTYPES WITHIN THE RELATED LOCAL CONTEXT

A BPS of the qualified thermal models, in their local contexts, was carried out. The related local context METEONORM was used to simulate the weather conditions of each model.

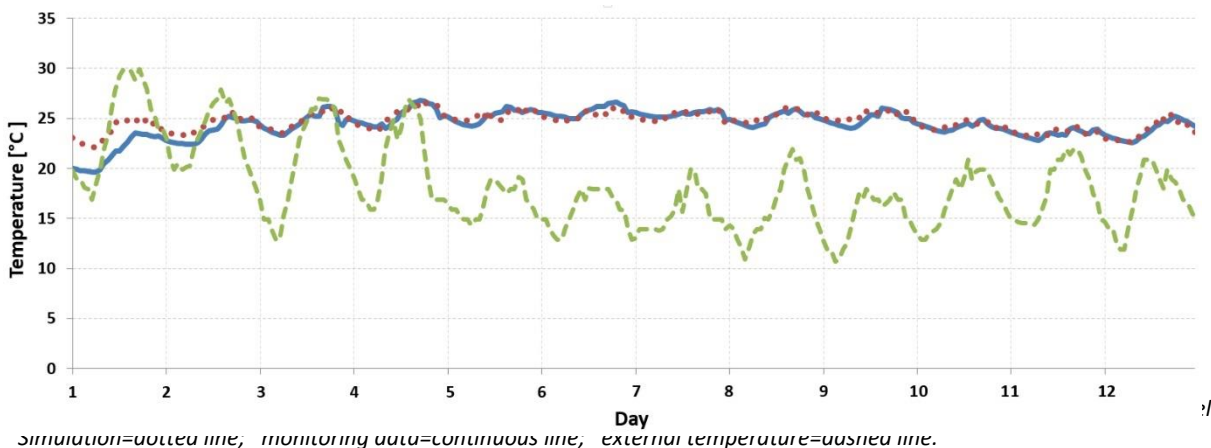


Table 4 shows the results of the OTP

PLEA 2018 HONG KONG

Smart and Healthy within the 2-degree Limit

prototype simulated in Frankfurt. Usage scenario values were chosen according to both real usages (data about usage scenarios of appliances from the first week of the competition were used for internal heat gain scenarios) and a good usage of the prototypes, in order to optimize both energy consumption and interior comfort.

Values for the scenarios of temperature set points, shading and natural ventilation were chosen for a good exploitation of external environment energy, thus minimizing energy consumption and increasing interior comfort, always taking into account the importance of exploiting natural light for indoor lighting

Table 4: Energy consumptions for the OTP prototype in Frankfurt, compliant with ISO 7730 "comfortable" comfort criteria in 98.5% of occupation time or more.

Zone	Surface area (m ²)	Heating needs (kWh/(m ² .year))	Cooling needs (kWh/(m ² .year))
Living room/Office	40	19	0
Bedroom	18	43	1
Kitchen	28	5	0
Bathroom	7	0	0
TOTAL	93	18	0

Comfort analysis was carried out in accordance with European Norms EN-15251 and UNI EN ISO 7730 [2, 3]. Comfort indices were calculated using a specific feature in Pleiades. For each zone, some parameters were set: ambience class (housing), air speed (a 0.1 m/s steady value for all the prototypes), type of activities and clothes worn. With the goal of having comfortable thermal conditions, ISO 7730 Predicted Mean Vote range value is [+0.5; -0.5] and the corresponding Predicted Percentage of Dissatisfied value is lower than 10%.

Table 5 presents the annual heating and cooling needs of the 5 prototypes, complying with "comfortable" comfort conditions almost all the time. These predicted needs suggest that these prototypes are able to respect current French thermal regulations.

Table 5: Energy consumptions for the 5 selected prototypes in their local context, compliant with ISO 7730 "comfortable" comfort criteria in 98.5% of occupation time or more.

Prototype	Surface area (m ²)	Heating needs (kWh/(m ² .year))	Cooling needs (kWh/(m ² .year))
Rhome	62	7	4
OnTop	93	18	0
Fenix	52	24	3
Home-Skin	100	22	0
Reciprocity	107	11	5

4. CONCLUSIONS

Data and measurements collected for the competing prototypes at the SDE 2014 in Versailles have been exploited in this work, in order to obtain important information about the behaviour of prototype experimental solar buildings with high energy efficiency, designed for different climatic conditions and usages. An empirical method was created in order to overcome the lack of data about usage scenarios for five selected prototypes, during the twelve days of the competition. Once qualified, the thermal models of the prototypes selected for their different technological systems and architectural envelopes, were simulated in their local contexts.

Thanks to empirical optimization work, BPS results for the qualified thermal models, are very good, with regard to both annual energy consumption and comfort conditions.

All the work was carried out without taking active systems into account, in order to consider only passive systems and strategies.

ACKNOWLEDGEMENTS

We thank the CSTB (French Scientific and Technological Buildings Center) and its partners in the organisation of SDE2014 in France (Solar Decathlon Europe 2014), namely ENSAG, ENSAM, INES, Nobatek-INEF4, for giving us access to the SDE2014 Monitoring Database.

REFERENCES

1. Project manual and project drawings with details for each project available <http://www.solardecathlon2014.fr/documentation>
2. NF EN 15251 (2007): Critères d'ambiance intérieure pour la conception et évaluation de la performance énergétique des bâtiments couvrant la qualité de l'air intérieur, la thermique, l'éclairage et l'acoustique.
3. UNI EN ISO 7730 (2005): Ergonomie des ambiances thermiques – Détermination analytique et interprétation du confort thermique par le calcul des indices PMV et PPD et par des critères de confort thermique local.

Building Energy Models in the Operational Phase: Automation of the Model Calibration Process

CATHERINE CONAGHAN¹, STEPHEN EARLE¹, ROHAN RAWTE¹, VEDA BALIGA²

¹Integrated Environmental Solutions Limited (IES), Glasgow, UK

²BPMG, UK

ABSTRACT: Building Energy Models, which consider all energetic aspects of a building's performance, are a beneficial tool for use in a building's design and operational stage to optimise the design or performance of a building, aid in decision making, and carry out code compliance. Model calibration is a term which refers to the improvement in the performance of a BEM simulation to better match the actual building in design or operation, which will in turn improve the results in using the BEMs in their various applications. Model calibration is particularly relevant in a building's operational stage considering that, as well as the number of dynamic elements involved in a building's performance on a day-to-day basis, buildings quite often perform differently to the initial design intent. Despite the benefits, model calibration is a time-consuming process which typically requires expert user knowledge. This paper details a methodology focused on improving and automating elements of the calibration process to address these current known limitations.

KEYWORDS: Energy, Calibration, Building Energy Models, Buildings, Comfort

1. INTRODUCTION

Building Energy Models (BEMs) are often employed to predict and assess a building's performance, to carry out code compliance or voluntary environmental rating systems, and to aid in decision making on system configurations or building performance choices at the building design stage. In a building's operational stage, creation of BEMs representative of the building's actual operating conditions can be useful in identifying sub-optimal performance, system faults and can better determine the implications of proposed energy conservation measures (ECMs) and retrofit options to the building in terms of consumption, cost and comfort.

BEMs consider all energetic and thermo-dynamic aspects of the buildings they represent and the software typically requires hundreds of model inputs, many of which have associated levels of uncertainty because they rely on software default assumptions and/or imperfect field-data collection procedures. While this approach can be highly effective at the design stage for analysing design approaches based on the same operating assumptions for determination of optimal design configurations, the use of BEMs in a building's operational stage presents different challenges. This is mainly due to the range of dynamic and difficult to measure parameters involved in an operational environment which are challenging to accurately account for in models, resulting in a gap between the simulated model results and the actual building performance, often referred to as the "performance gap".

Research has shown that significant differences between the predicted BEMs and actual building performance are often detected even in energy-efficient buildings [1]

which can hinder the implementation of optimised building energy management strategies and decision making which incorporate BEMs. According to a study of 121 buildings, significant discrepancies between the simulation results and actual measured consumption of real buildings were observed, with the predicted performances in the range of 0.25 to 2.5 times the actual performance of the building [2].

These differences observed typically arise from inaccurate information in the three-way interaction between the building, people and climate [3]. At building level, this can often be due to a lack of relevant building audit information, inadequate Building Management Systems (BMSs) in place, or insufficient knowledge on the "as-designed" building control. People, or user behaviour, has a significant influence on the building performance due to their control actions within a building, which usually relates to improving the indoor environmental conditions and needs to be addressed in more detail on a specific building model level [4]. Climate information is also an important aspect, as the surrounding climatic conditions affect both the building performance and user behaviour.

The process of improving and tuning the building energy model inputs to close the performance gap between simulated and measured building performance is referred to as Calibration. Calibration is widely acknowledged as a complex task; it is over-specified (in that simulation programs require hundreds of model inputs) and under-determined (where the number of output parameters for comparing actual versus simulated performance are relatively few). Most current calibration approaches require significant expert

PLEA 2018 HONG KONG

Smart and Healthy within the 2-degree Limit

knowledge and numerous manual interventions using different tools/methods to achieve high levels of accuracy. Considering the benefits of using BEMs in the operational stages of a building's life-cycle, in order to make the calibration of models a viable and less costly undertaking, a calibration approach was investigated with the objectives of:

Accelerating the end-to-end calibration process

Reducing the manual intervention and expert knowledge required, and

Consistently improving the results of the calibrated model when compared with the actual building performance beyond current best practice model performance evaluation targets (Measurement & Verification).

2. METHODOLOGY

This paper details a methodology aimed at delivering an improved and more robust calibration process when compared to traditional practice. The methodology involves a four-step process:

Operational Models are created by feeding metered building data into a BEM

Sensitivity Analysis is conducted to identify the most relevant parameters for optimisation

Final Optimisation (either consultancy based or using an automated optimisation program called 'Optimise') is performed to determine the appropriate values for the remaining uncertain and influential parameters in the models

A final calibration Measurement and Verification (M&V) exercise is undertaken to measure the performance of the calibrated simulation models.

This methodology was tested and validated by creating calibrated building models using IES<VE> building simulation software for four demonstration sites in a range of building types across Europe:

Airport in Portugal

Office Building in Finland

Office Building in Romania

Hotel in Northern Finland

The Airport is the main use case selected to describe the steps and results of the methodology developed.

2.1 Operational Models

Typically, an operational model will be developed either from an existing BEM design model, or from a new model created based on design details provided. An operational model refers to a building energy model in which the dynamic parameters (initially based on design assumptions) are updated with actual metered data streams typically obtained from a building's Building Management System (BMS) or Automated Meter Readings (AMR). Dynamic parameters are for instance

occupancy or equipment energy consumption profiles, HVAC control schedules and weather data.

This is an important step in the calibration process, as the measured data provides much more accurate inputs to the model which will result in improvement in the M&V of the BEM compared to actual building performance. Figure 1 shows the comparison of the energy consumed by the Airport design model (red line) compared to the actual performance (blue line), where a significant difference.

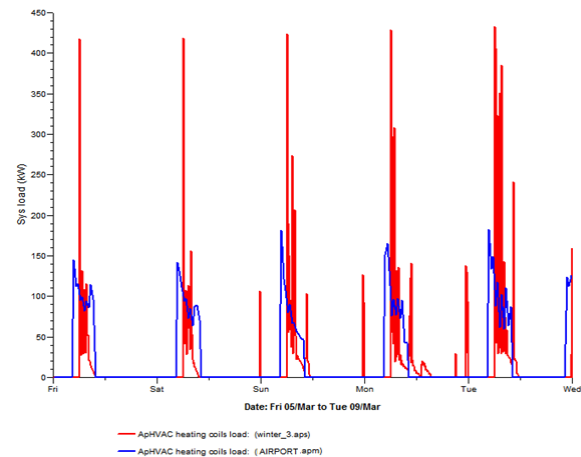


Figure 12: Design model vs actual performance

Figures 2 and 3 illustrate examples of measured model data inputs (red) which replaced the assumed profiles (blue) in the design model to create the operational model.

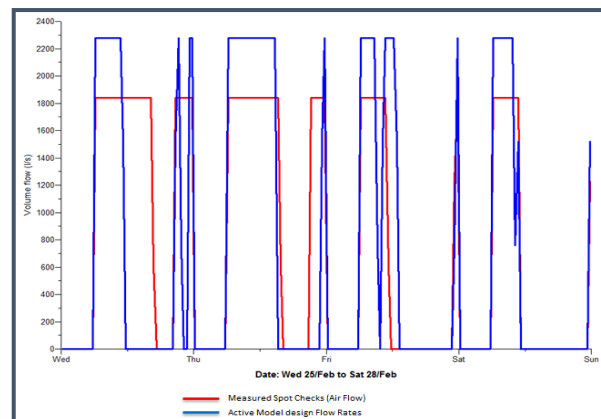


Figure 13: Assumed vs actual data (airflow)

Once all of the measured inputs were added to the model, along with accurate local weather data for the corresponding period, a significant improvement can be seen in Figure 4 between the BEM simulated energy (blue) from the operational model, and the measured energy consumption (red) of the building over a period one week.

PLEA 2018 HONG KONG

Smart and Healthy within the 2-degree Limit

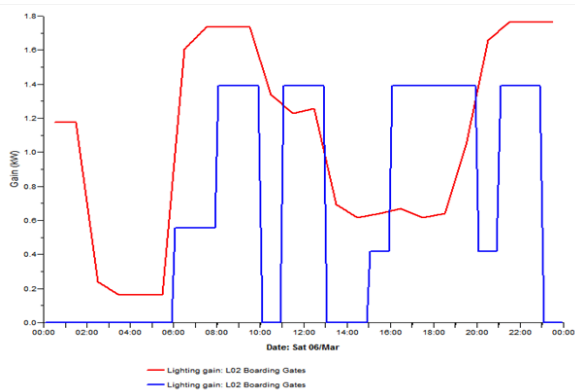


Figure 3: Assumed vs actual data (lighting gains)

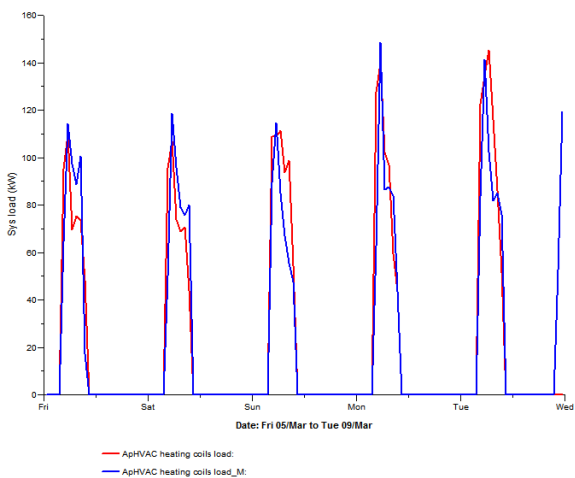


Figure 4: Improved operational model vs actual performance

All four tested BEMs resulted in visible improvements in M&V after this first step of the methodology to varying degrees; the remaining calibration process steps aimed to further close the performance gap.

2.2 Sensitivity Analysis

Sensitivity analysis is a process used to determine the parameters of greatest influence on the model outputs, and thus the overall calibration performance. It is a key step in determining which parameters should be focussed on for calibration, as well as reducing the overall calibration effort through identifying parameters with very little influence on the model/building's energetic performance. Traditionally this process is based on expert user experience or manual analysis of the effect of changes to model parameters on the results of building model simulation. To advance beyond this and create a faster, structured and robust approach using the IES <VE> simulation software for each of the four test models, a semi-automated Sensitivity Analysis procedure was developed and implemented. Although the detail and developments required are specific to the IES <VE>, the methodology described can be replicated and applied to any simulation modelling software to achieve the same the goal.

A relevant range of parameters of interest for each of the demo sites were selected, across the following primary categories:

- Weather
- Building Fabric
- Constructions
- HVAC Central Plant
- HVAC terminal Units

The individual variables and their variance investigated for each pilot site are summarised in 錯誤! 找不到參照來源。 , 2 and 3 below.

Table 1: Sensitivity Analysis Parameters – HVAC Units

Component/Variable	Reference	Variance	
HVAC Terminal Units	Fresh Air Volume	Minimum Flow (l/s)	+/- 20%
	Heating/Cooling Flowrate	Flow rate (l/s) at Max sensed DB temp (°C)	+/- 50%
		Flow rate (l/s) at Min sensed DB temp (°C)	+/- 50%
		Deadband	+/- 20%
	Cooling/Heating Supply Air Temp	Proportional Bandwidth (k)	+/- 20%
		Dry bulb Temp at Max sensed DB temp (°C)	+/- 50%
		Dry bulb Temp at min sensed DB temp (°C)	+/- 50%
	Heat Exchanger	Max change per time step	+/- 20%
		Deadband	+/- 20%
		Sensible Effectiveness	+/- 30%
Humidifier	Latent Effectiveness	+/- 30%	
	Total Efficiency %	+/- 20%	
	Ductwork Heat Pick-up	Ductwork Heat Pick-up	+/- 20%
Radiator	Weight (kg)	+/- 50%	
	Water Capacity (l)	+/- 50%	
	Radiant Fraction	+/- 50%	
	Orientation	n/a	
	Max change per time step	+/- 20%	
Underfloor Heating Zone	Flow at min sensed signal DB Temp	+/- 20%	
	Water Temperature to Underfloor	+/- 20%	
	Internal Ceiling: Concrete Screed Conductivity	+/- 50%	
	Internal Ceiling: Conductivity for insulation between floors	+/- 50%	
	External Wall: Conductivity	+/- 50%	
	Slab Zone: Inner Volumes on	n/a	
	Slab Zone: Inner Volumes off	n/a	

Table 2: Sensitivity Analysis Parameters – HVAC Control

Component/Variable	Reference	Variance	
HVAC Central Plant	Chilled Water Loop Supply Temp (primary circuit)	+/- 50%	
	Chilled Water Temp Difference (primary circuit)	+/- 10%	
	Chilled Water Loop	Chiller Supply Temp	+/- 50%
		Chilled water flow rate	+/- 50%
		Minimum chilled-water flow fraction	+/- 30%
	Ice Thermal Storage	Minimum part-load ratio for continuous operation	+/- 30%
		Condenser fan electric input ratio	+/- 20%
		Condenser heat gain to condenser water loop (fraction)	+/- 20%
		Chiller Part Load Range and Sequence	+/- 30%
		Distribution Losses	+/- 20%
	Hot water loop	CHWL Heat Exchanger Approach	+/- 20%
		Loop Fluid (Ethylene glycol water) mix %	+/- 50%
		Discharge Supply Temp	+/- 50%
Design Delta T		+/- 50%	
Chiller Charging Supply water temp		Cooling Supply Temperature (Secondary Circuit)	+/- 50%
		Chiller Charging Supply water temp	+/- 50%
		Tank Capacity Losses %/h	+/- 50%
		Discharge Design Flow (l/s)	+/- 50%
		Charge Design Flow (l/s)	+/- 50%
Hot water loop		Charge Design Temperature	+/- 50%
	Minimum Discharge Capacity	+/- 100%	
	Hot water Supply temp (primary circuit)	+/- 50%	
	Hot water temp diff (primary circuit)	+/- 20%	
Boiler Part Load Range and Sequence	Distribution Losses	+/- 20%	
	Boiler Part Load Range and Sequence	+/- 30%	

Table 3: Sensitivity Analysis Parameters – Building Level

Component/Variable	Reference	Variance	
Constructions	Glazing/Roof lights	Conductivity	+/- 50%
		Transmittance	+/- 50%
	Ground/Exposed Floor	Conductivity	+/- 50%
	Internal Ceiling/Concrete	Conductivity	+/- 50%
	Roof	Conductivity	+/- 50%
Room Variables	External Wall	Conductivity	+/- 50%
	Infiltration (Fabric)	Air Leakage	+/- 100%
	Lighting	Fluorescent Lighting Gain	+/- 50%
Weather	Equipment	Equipment Gain	+/- 50%
	Occupancy	People Gain	+/- 100%
Weather	Weather Files Actual Vs Average	n/a	

Figure 5 below shows an example of the results of the Sensitivity Analysis carried out for the Airport BEM. As discussed, the process automates the identification of the key parameters to focus on for calibration, as the

PLEA 2018 HONG KONG

Smart and Healthy within the 2-degree Limit

ranked parameters nearer the top of the graph have a greater effect on the BEM energy consumption and should therefore be the highest priority for improving input data to the model for calibration. Parameters lower down the list require less focus or can even be ignored when calibrating, as they have a lesser impact on the overall energy consumption. This step automates a part of the calibration process that would typically be carried out manually or based on expert knowledge gained over years of experience.

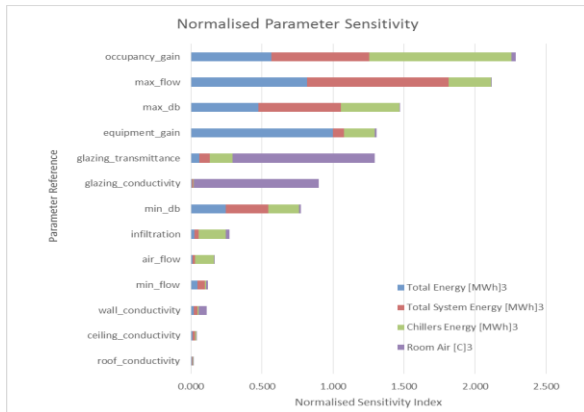


Figure 5: Sensitivity Analysis results – Airport

2.3 Final Optimisation

Once Steps 1 and 2 are accomplished the initial operational models are set-up, key parameters for further calibration have been identified, and final optimization of remaining model parameters is undertaken. This step can be described as semi-automated and is achieved through a combination of two approaches:

Consultancy Based Desktop Calibration – where consultants (building and energy simulation expert users) undertake a series of defined checks on the current version of the operational model, carry out analysis on the required parameters and apply reasonable updates to the model where operational data may be missing, to ensure that the simulated building and systems are performing as expected and to further progress the calibration.

Optimise Tool – where an automated optimisation program ‘Optimise’ has been enhanced and employed in the automated calibration process to determine the appropriate values for the remaining uncertain and influential parameters in the models. Optimise is a proprietary tool initially developed through a European Commission 7th Framework Programme (FP7) project, ‘Umbrella’ [6]

The Optimise tool is based on genetic algorithms, where each parameter for calibration is given a reasonable

upper and lower limit. The calibration objective function is set in the tool (M&V metrics), and Optimise automatically runs thousands of batch simulations within a number of hours and with no manual intervention to determine the best fit for the selected parameters to meet the set objective functions.

Figure 6 shows the best-fit occupancy profile for the Airport model generated using the Optimise tool which, as shown from the sensitivity analysis results, is the key parameter that influences the performance of the model.

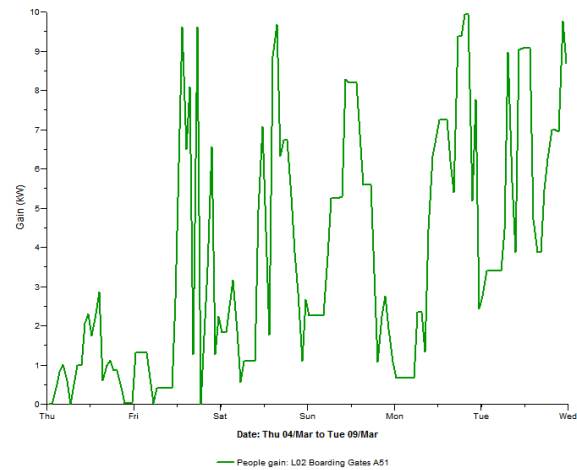


Figure 6: Best-fit occupancy profile generated using the Optimise tool – Airport

Depending on the level of uncertainty in the parameters remaining, the calibration levels achieved in the previous steps and remaining available information or expert knowledge that can be applied, either/or both of the approaches described may be applied for this step of the calibration procedure.

2.4 Measurement and Verification

Measurement and Verification (M&V) is the final and a key step in the calibration process, where calibration metrics are used to evaluate the accuracy of the simulation models through comparison of the simulation outputs with the measured building data. In order to measure the performance of the calibrated simulation models, the following standard statistical indices were used. [7, 8]

Mean Bias Error (MBE) (%): This is a non-dimensional bias measure (i.e. sum of errors), between measured and simulated data for each hour.

$$MBE(\%) = \frac{\sum_{i=1}^{N_p} (m_i - s_i)}{\sum_{i=1}^{N_p} (m_i)}$$

Where; m_i and s_i are the respective measured and simulated data points for each model instance ‘i’ and N_p is the number of data points at interval ‘p’ (i.e. Nmonthly=12, Nhourly=8760).

PLEA 2018 HONG KONG

Smart and Healthy within the 2-degree Limit

Root Mean Square Error (RMSE) (%): The root mean square error is a measure of the variability of the data. For every hour, the error, or difference in paired data points is calculated and squared. The sum of squares errors (SSE) are then added for each month and for the total periods and divided by their respective number of points yielding the mean squared error (MSE); whether for each month or the total period. A square root of the result is then reported as the root mean squared error (RMSE).

Coefficient of Variation of Root Mean Square Error CV(RMSE) (%): This is essentially the root mean squared error divided by the measured mean of the data. CV(RMSE) allows one to determine how well a model fits the data; the lower the CV(RMSE), the better the calibration.

$$CV\ RMSE(\%) = \frac{\sqrt{\frac{\sum_{i=1}^{N_p} (m_i - s_i)^2}{N_p}}}{\bar{m}}$$

Where; m_i and s_i are the respective measured and simulated data points for each model instance 'i'; N_p is the number of data points at interval 'p' (i.e. Nmonthly=12, Nhourly=8760) and \bar{m} is the average of the measured data points.

Currently the *International Performance Measurement and Verification Protocol (IPMVP), Option D: Calibrated Simulation* [7] is considered the best practice standard for assessing building model calibration levels using M&V. The guidance targets for IPMVP Option D metrics are based on reducing Mean Bias Error (MBE) and Coefficient of Variation of the Root Mean Squared Deviations (CV).

For monthly based calibrations the targets are:

CV = 15%
MBE = ±5%

For hourly based calibrations the targets are:

CV = 30%
MBE = ±10%

3. FINDINGS/RESULTS

Using the methodology outlined all four of the calibrated test models achieved M&V exceeding the targets set out by IPMVP. The Airport model, which is described in more detail, through this process achieved a CV of 21% and an NMBE 1.74% for hourly calibration, which is well beyond the best practice targets.

Figure 7 graphically illustrates the M&V results for the Airport BEM, comparing measured energy performance to simulated energy performance on an hourly basis over the course of a week.

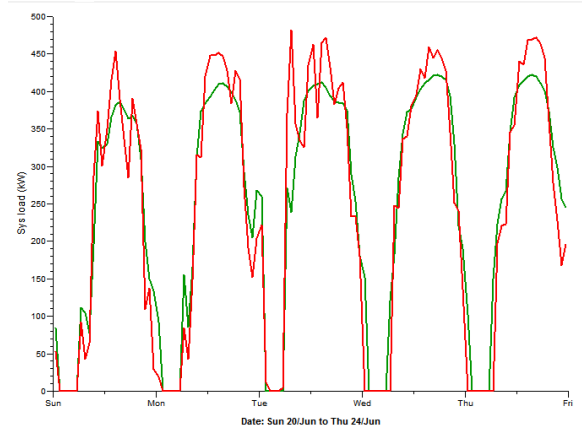


Figure 5: Airport – simulated (green) and measured (red) cooling loads for a calibration period in the summer

4. CONCLUSION

Even where high levels of metered data were not available, accurate calibrations beyond the current best practice levels of IPMVP were achieved using the methodology developed. Across the four test buildings, the Normalised Mean Bias Error (NMBE) for each model ranged between -0.301% and 3.2% for hourly calibration, meaning all models adhered well within the required ±10%.

The calibration results achieved for each model for the selected calibration periods exceeds current best practice M&V targets for the model's simulated energy performance matching the building pilot areas actual performance (NMBE of <10%). The approach developed also greatly improves the speed of the calibration process through the introduction of the automated and semi-automated processes, and reduced the amount of user intervention and expertise requirement, making the approach replicable across a range of building model types.

Further work will focus on testing of the methodology on building types in different climates, and better measurement of the time and effort associated with traditional calibration compared to the methodology presented.

ACKNOWLEDGEMENTS

This work was carried out as part of the European Commission 7th Framework Programme (FP7) funded project "Energy in Time."

REFERENCES

- H Bell, R Milagre, C Sanchez, (2013). "Achieving the Green Dream: Predicted vs. Actual - Greenhouse Gas Performance in Green Star-certified office buildings", Green Building Council of Australia.
- G.R. Newsham, S. Mancini, B.J. Birt, (2009). "Do LEED-certified buildings save energy? Yes, but...", Energy and Buildings 41, 897–905.

PLEA 2018 HONG KONG

Smart and Healthy within the 2-degree Limit

A Widjaya, (2013). *"Predicted VS Actual Energy Performance of Building Information Modelling in New Building Constructions"*, Building Performance Modelling - Summary 2, 48-722.

Hoes, P, Hensen, J.L.M., Loomans, M.G.L.C., Vries, B. de and Bourgeois, D, (2009). *"User behavior in whole building simulation"*, Energy and Buildings, 41(3), 295-302.

International Performance Measurement & Verification Protocol Committee, (2002). *"International Performance Measurement & Verification Protocol Concepts and Options for Determining Energy and Water Savings Volume I"*, United States

Umbrella Project, European Commission 7th Framework Programme, accessed 12th December 2017 <<http://www.e-umbrella.eu>>

Coakley, D., (2014). *"Calibration of Detailed Building Energy Simulation Models to Measured Data using Uncertainty Analysis"*. National University of Ireland, Galway.

Coakley, D., Raftery, P. & Keane, M., (2014). A review of methods to match building energy simulation models to measured data. Renewable and Sustainable Energy Reviews, 37(September), pp.123–141.

Building-integrated carbon capturing 2.0: Moving a concept from R&D to a prototype

HARVEY BRYAN¹, FAHAD BEN SALAMAH¹

Herberger Institute for Design and the Arts, Arizona State University, Tempe, Arizona, USA

ABSTRACT: Building-integrated carbon capturing is a system that provides carbon dioxide (CO₂) capture and regeneration within buildings using a moisture-swing air capture technology developed by Dr. Klaus Lackner at Arizona State University's Centre for Negative Carbon Emissions. This paper serves as a continual ideation towards moving a concept from the research and development phase into prototype development to perform experimental evaluation of how such a project would perform in real-life scenarios. We intend to build on strengths and overcome past design weaknesses through cross-industry innovation to create a more robust mechanism that is capable of carbon capture and regeneration.

KEYWORDS: Carbon, Capture, Building-integrated, CO₂, Shade.

1. INTRODUCTION

Atmospheric carbon dioxide (CO₂) concentrations have been on the rise since the beginning of the Industrial Revolution due to various human activities involving the burning of oil, coal and gas, as well as deforestation. According to NASA, humans have increased CO₂ by a third since the Industrial Revolution, and CO₂, the heat-trapping greenhouse gas, is the long-living/key factor of climate change [1]. The United States of America is the second largest emitter, as it is responsible for almost 15% of global CO₂ emissions, and stabilizing the atmospheric CO₂ concentrations is becoming less and less possible, specifically after the current administration's intentions to withdraw from the Paris Climate Agreement [2] and its termination of the Clean Power Plan that the previous administration issued [3]. The central aim of the Paris Climate Agreement is to keep global temperature change below 2 degrees Celsius for this century [4]. Achieving this goal will require considerable effort toward a host of aggressive and innovative strategies to meet that challenge. To date, most strategies to combat climate change have focused on CO₂ mitigation. While this task is critically important, it is equally important to combat this challenge through the capture and reuse of CO₂.

2. BUILDING-INTEGRATED CARBON CAPTURING

This paper serves as a continuation of the paper we presented at PLEA 2017 titled "Building-Integrated Carbon Capturing," wherein we envisioned a form of biomimicry that models the natural process of photosynthesis, in which plants capture CO₂ and turn it into carbohydrates and oxygen. To summarize the last paper's goal, we proposed a building-integrated carbon capturing (BICC) device that treats building facades as giant artificial leaves, creating facades that are capable of self-shading and absorbing CO₂ from the air and turning it into useful carbon-based materials without harming

the environment. BICC will capture CO₂ by adapting a carbon-capture technology called moisture swing air capture technology, which has been developed by Dr. Klaus Lackner at Arizona State University's Centre for Negative Carbon Emissions [5]. This technology uses thin fibres of sorbent material that can capture carbon dioxide when in a dry state and then release it when moisture is applied. Dr. Lackner and his team were able to translate their lab experiments into the design of a "Carbon Carousel" machine that could be packaged in a single cargo shipping container for ease of transportation and would be capable of capturing one ton of CO₂ per day.



Figure 1: Carbon Carousel (Source: Kevin Hand, Courtesy of Columbia University, 2010).

The air filters embodied in the sorbent resin are placed on a moving conveyor for natural air exposure. Once the air filters are saturated with CO₂, an automated mechanism will remove the air filter and place it in a regeneration chamber, where the CO₂ will be extracted. BICC will mimic the properties of the air filters used in the carbon carousel machine but differ in the operating mechanism of the cleaning chamber. BICC filters will be attached to building façades and will not move through a conveyor into the cleaning chamber; instead, once the air

PLEA 2018 HONG KONG

Smart and Healthy within the 2-degree Limit

filters are loaded with CO₂, they will enter a moveable cleaning chamber that has been designed as a replacement for the large stationary cleaning chamber in the carbon carousel machine for CO₂ extraction.



Figure 2: Representation of BICC moveable cleaning chambers

Extensive description and detailed graphical representations of the Carbon Carousel and BICC can be found in our paper presented in the PLEA 2017 proceedings.

3. AIM

The aim of this paper is a continual ideation toward an appropriate and applicable building-integrated shade and CO₂ capture system that will build upon the previous BICC design while taking into consideration feedback received during the few past months from colleagues and professionals in the field to create a robust and mechanically feasible option. Our intention is to build on the previous design's strengths and minimize any weaknesses. The paper will showcase developments in filter design, size, CO₂ regeneration chamber design modifications, and alterations to the regeneration process mechanism, and it will finally present the newer version of BICC that will overcome the past design weaknesses.

4. DISCUSSION OF THE PREVIOUS BICC DESIGN

BICC's strength is that it serves a dual function. It replaces an existing, integrated building element—a shading device that blocks the sun for cooling purposes—and captures CO₂ for utilization. In addition, shading devices have an advantage over other building-envelope elements because they protrude beyond the building envelope, which allows for wind flow across the air filters' exterior surface, thereby assisting the moisture swing technology, which was developed to capture CO₂ at natural low air speeds. The following subsections discuss in detail the areas that require further development to overcome the previous design weaknesses.

4.1 Shade and carbon capture

The current BICC device was designed so that its air filters were fixed on a building façade, but shading devices are only useful during the day and when the sun is out. To improve the design, air filters can be rolled up during the

day to provide shade and capture CO₂ and then rolled down during the night, when there is no need for shade, to regenerate the captured CO₂.

4.2 Carbon capture capacity and utilization

Knowing that today's infrastructure is not ready for the capture and transport of CO₂, as it would require substantial investment in piping networks for carbon transportation, the CO₂ captured by BICC would have to be utilized within the city. Utilizing carbon instead of transporting it to remote locations for storage would require reducing the amount of carbon that BICC captures, leading to alterations in the air filters' size and thickness. The developed BICC would have thinner air filters than the current version has, which could facilitate the rolling aspect mentioned above. This alteration would entail transforming the air filters from the bulky shape typically used to collect particles from airflow in ducts into lighter forms (similar to sails) that can be rolled up and down.

4.3 Cleaning chamber

The cleaning chamber's mobility was also a concern. Although the regeneration process is effective, the machine's design and its moving mechanism must be reformulated. The cleaning chamber was designed with the idea that it would move along tracks installed on the building's façade, where it would attach to each filter in turn, vacuum the filters, apply moisture to them, evacuate the CO₂ from the chamber, and finally send the captured CO₂ through hoses to the storage area located on the building's roof. We thought this design involved "lots of moving parts," indicating that it would be expensive to have part of the BICC continuously moving along the tracks; this continuous movement may also lead to long-term operation and maintenance costs for the building's owner. This discussion led to reversing the process of CO₂ regeneration so that the BICC's cheaper element (the air filter) becomes the moving part and the more expensive element (the cleaning chamber) becomes stationary. This alteration could minimize the cost of building the device and lower the system's long-term operation and maintenance costs. In addition, this change is also in harmony with the other ideas mentioned above: thinning the air filters to reduce capturing capacity and rolling the air filters for shading and regeneration.

4.4 Form

In addition to the BICC's motion, the cleaning chamber's shape must be revisited. The current process requires vacuuming and involves voiding the air from the enclosed space to regenerate the CO₂ efficiently. Displacements, strains, and stresses occur during the vacuum process, so the vacuum chamber's shape must be carefully designed to respond to such factors. According to Hauviller's

PLEA 2018 HONG KONG

Smart and Healthy within the 2-degree Limit

“Design Rules for Vacuum Chambers,” a vacuum chamber can take any shape during the initial design phase, but its shape must be carefully studied and analysed during a detailed design phase to ensure that it can respond to stressing and buckling forces. Hauviller [6] concludes that curved surfaces are preferable to flat panels when in response to the forces mentioned above. In the current BICC design, the cleaning chamber is rectangular, the least favourable shape for a vacuum. Additionally, the current device is composed of two parts that embrace the air filter during the regeneration process, which may lead to further complications during the vacuum process, including air leaks.

The idea of rolling the air filters into a stationary unit guides the new cleaning chamber’s design, as a curvilinear form is best suited to housing rolling air filters. According to Hauviller [6], tubular shapes are the most common for vacuum chambers. Therefore, the developed BICC should have a tubular cleaning chamber that can house rolled air filters and withstand the vacuum process during the CO₂ regeneration process.

4.5 Modularity

Another concern is modularity, which is the use of various modules to create a system by combination [7]. The current design is limited by the filters’ and cleaning chamber’s sizes, as the air filters were designed to be 1.6 m high, 0.6 m wide, and 0.1 m thick. This essential element’s fixed size may become an obstacle in the system’s implementation on buildings that differ in height or shading requirements, which could require modifications to the air filters’ height, width, and thickness, resulting in substantial investment for the manufacturing of such a system. Therefore, the ability to roll the filters into the stationary cleaning chamber provides the advantage that the system could work on various building heights simply by changing the air filter height.

5. DEVELOPED DESIGN FOR THE BICC

To summarize the ideas mentioned above, we envision the developed BICC as a modular system that is made of thin, sail-like air filters, which are attached to building facades and are capable of rolling in and out of a tubular stationary cleaning chamber, thus meeting the BICC’s original goals: self-shading to lower buildings’ solar-heat gain for energy conservation while capturing and regenerating carbon for use within the city. To visualize the above-mentioned features in a product design, we used cross-industry innovation. This method involves taking existing, proven solutions from other industries and creatively imitating or transforming them to meet our concept’s needs [8]. We chose this method so we could use another industry’s working, problem-free mechanism to take advantage of existing know-how and overcome past design difficulties related to cost, time,

and probable malfunctions. Many examples show successful cross-industry innovations, including BMW’s iDrive system (a transfer from the gaming industry) and Nike’s shoe shock absorbers (adapted from Formula One racing technology) [8]. Therefore, we designed two versions of the developed BICC, which we call CarbonSail and CarbonCabinet. Both include the functions and features mentioned earlier in the paper, but they differ in terms of their mechanisms.

5.1 CarbonSail

The CarbonSail is the first version of the developed BICC in our attempt to overcome the concerns raised with the previous version of the system. The name is derived from the sails used in sailboats, in which a piece of fabric is sewn together and stretched across a mast to catch wind and convert it into force to drive a vessel. Our version of sails will resemble a boat sail’s shape (i.e., they will extend over the building’s façade as a sail does across a boat mast) but will capture carbon from the air instead of catching wind for propulsion. Our sails will be made from a combination of materials, including resin-embodied polypropylene sheets for carbon capture and synthetic fibres such as Dacron (which is known for its durability). Boat sails are typically coated with resin to ensure stiffness and airtightness [9], but in our case, air catching is not needed, so our sails will be coated with a strong-base ion-exchange resin to best capture carbon. The concept of cross-industry innovation shines in our sails’ rolling aspect. Sailboats use various methods for storing sails when not in use; the one that we are interested in is a sail furling system. Ted Hood introduced the idea of furling a sail into a boat’s mast or boom in the 1970s, and this idea was largely responsible for the growth of sailing in the following decades [9]. A furling system can be fully automated so that an electric motor rolls the sail up or down at the touch of a button.

The system that we are most interested in is the in-boom furling system, in which a shaft running along the length of the boom (the horizontal piece that extends from the bottom of the mast and attaches to the bottom of the sail) is used for raising the sail and lowering it for stowing purposes.

PLEA 2018 HONG KONG

Smart and Healthy within the 2-degree Limit



Figure 3. In-boom furling system (source: Hancock, 2003).

This system has all the properties needed to perform the BICC's desired functions. First, the sail can be rolled up and down based on need. Second, the furling unit (boom) is stationary and can be attached to a building's surfaces. Third, the boom is tubular, which is the most suitable shape for vacuum purposes. Finally, in-boom furling units are already modular, as many sailboat manufacturers have produced such systems in large quantities. This sail-furling unit has been around for almost 50 years, and the knowledge required to manufacture and maintain such a system is available in the market. We intend to imitate this sail system and transform it to match the needs of the building industry, where it will not only store sails (in this case, CarbonSails) but also provide a newer function of regenerating captured CO₂ within the tubular boom.

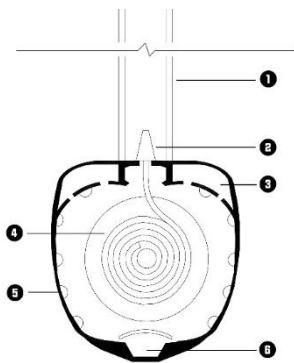


Figure 4. A preliminary section drawing of the CarbonSail cleaning chamber unit, with additions. 1) Tracks. 2) Top of the sail seal. 3) Air Vacuum. 4) Rolled CarbonSail. 5) Moisture sprays. 6) Water gutter.

A series of modifications needs to be added to the older furling system for it to work in the new system. The rolling mechanism will stay the same, as the sail will still be rolled up and down based on the desired function (e.g., shade or carbon capture). The very top of the sail would, however, have to be equipped with a sealing element to ensure that when the sail is rolled down, the unit can act as a vacuum chamber. The unit will also be equipped with hoses to feed the chamber with water for CO₂ regeneration and to exhaust the CO₂-enriched air.

Water sprayers will also be distributed along the inner shell, and a gutter system will be added to remove excess water.

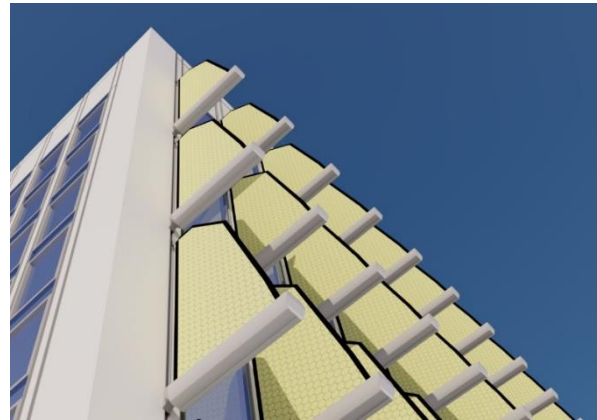


Figure 5. Illustration of CarbonSail on buildings

During the day, the CarbonSail will be unrolled along the building's façade, forming columns of sails that run from the bottom of the building to the top, arranged so that they fit between the window bays. The sails will treat the building façade as a mast; they will be attached to tracks through hocks similar to those used in sailboats. In this phase, the sails will provide shade for the building and capture CO₂. Unlike the old version of the BICC, the cleaning chamber will not move to the filters to regenerate CO₂; rather, the regeneration process will occur in the newly designed stationary chamber. Once the sun sets, the sails will automatically roll down into the cleaning chamber. Once the cleaning chamber is completely sealed, water will be applied to moisten the sails and dissolve the bicarbonate on the fibres, thereby producing carbonate and CO₂. The CO₂ is then evacuated and compressed into liquid to be locally stored for use in the building or city.

The envisioned CarbonSail will have the following properties: a tubular cleaning chamber with a diameter of 0.3 m and a depth of 0.9 m, allowing it to be modular and to be sold in a box that contains all the required hardware. Each unit will be responsible for serving a column of windows where the sail's height is modifiable, as it can be extended to serve more than one floor.

5.2 CarbonCabinet

The CarbonCabinet is another version of the developed BICC and is a similar attempt to overcome the concerns about the system's previous version. Similar to the CarbonSail, the CarbonCabinet system will have the properties needed to perform the desired BICC functions: self-shading and carbon capturing and regeneration. The air filter will roll in and out based on shading and carbon-capturing needs, and the cleaning chamber will be stationary and have a tubular form for vacuum purposes. This system is designed to be modular for applicability and manufacturing purposes.

PLEA 2018 HONG KONG

Smart and Healthy within the 2-degree Limit

The rolling fabric for this system will mimic the CarbonSail’s properties, as it will be made of resin-embodied polypropylene sheets (for carbon capture) and Dacron (which is known for its resiliency). The cross-industry concept also plays a role in this system’s rolling aspect, as it was inspired by an existing rolling method that the Darman Manufacturing Company invented for use with one of its products, called a cloth-roll towel cabinet. The company was founded in 1936, and it is the sole American maker of cloth hand-towel dispensers, manufacturing around 13,000 units per year. The towel cabinet consists of two chambers—a clean chamber and a soiled chamber—that are completely separated. Within the cabinet case, a rolled towel is fed from the clean chamber and then, once used, is rolled into the soiled chamber. The rolling force is driven by the user’s hands, as the user grasps the edges of the towel and pulls down to dispense an unused portion [10].

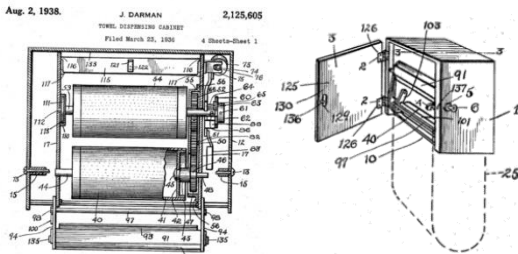


Figure 6. Darman’s cloth-roll towel cabinet illustrations. Left: The two separate chambers within the cabinet case. Right: The cabinet, with a dotted line representing the cloth towel (source: Darman Manufacturing Company).

Similar to the furling system used in the CarbonSail version, the Darman system has the features required to serve as a starting mechanism that performs the desired BICC functions. It makes perfect sense to roll a dangling fabric (in our case, one used for shade and carbon capture) in and out of a stationary chamber (in our case, used for carbon regeneration), as this system can be built in a modular fashion with existing industry knowledge. We are interested in the rolling mechanism and the separation of cabinets, two aspects that work in harmony with our goals. However, for this system to work for BICC, modifications and additions are required.

First, the envisioned device will follow the same operation mechanism (rolling), but in our version, it will be positioned in an alternate way—rotated 90 degrees—so that it can cast shade, capture carbon capture, and allow for visibility. Second, the system’s size needs to be scaled up so that it is applicable for building integration. Unlike the first version of BICC, this device would be placed on top of window bays, where the fabric would form a loop around the window bays to provide shading and capture carbon.

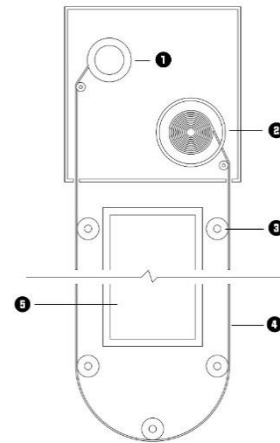


Figure 7. Preliminary section drawing of the Carbon Cabinet. 1) Motor 1. 2) Cleaning chamber and motor 3. 3) Rollers. 4) Carbon Capture fabric. 5) Window Bay.

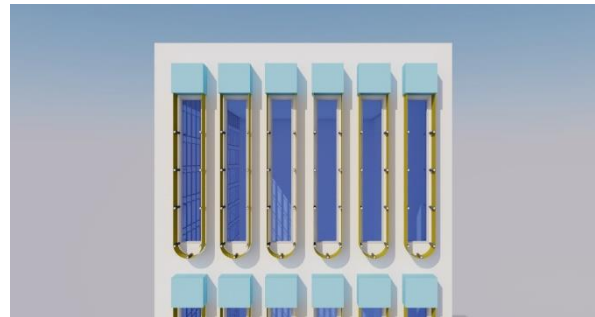


Figure 8. Front view of Carbon Cabinet on buildings

A series of rollers would be placed along the window bays, allowing the fabric to roll and keeping it in shape for shade purposes. Third, one of the two inner chambers needs to be tubular and completely sealed (for vacuum purposes). This tubular, sealed chamber must be equipped with water sprayers and air vacuum channels for CO₂ regeneration. The second (unsealed) chamber will control the other end of the fabric, where cables will be attached to control the mechanism’s roll. Additionally, the device’s operation needs to be automated, and it will be equipped with rolling motors for this function. Finally, the fabric should be of the desired length for building integration and should be customizable to the end users’ needs. This requirement wouldn’t incur a large cost, as the fabric would be manufactured in large rolls to meet such needs.

In the CarbonCabinet’s operation, the rolling operation will be controlled by two motors in the chamber, one operating during the first phase (rolling down the fabric to provide shade and capture carbon) and one serving to roll the fabric into the chamber during the second phase, in which carbon is regenerated. At first, the fabric will roll out of the main cabinet to form a continuous loop around the building’s window bays. During the first phase, the motor will pull cables connected to the fabric, assisted by the rollers attached to the building surface, thus forming

PLEA 2018 HONG KONG

Smart and Healthy within the 2-degree Limit

a loop. Once the fabric is saturated with CO₂ and shade is no longer needed (i.e., at night), the second motor will pull the fabric back into the sealed chamber in the cabin in order for the carbon regeneration to occur. The two motors will not operate instantaneously; when one motor operates, the other one will be idle. Once the fabric is in the sealed chamber, the CO₂ regeneration process will begin (similar to the CarbonSail process discussed earlier).

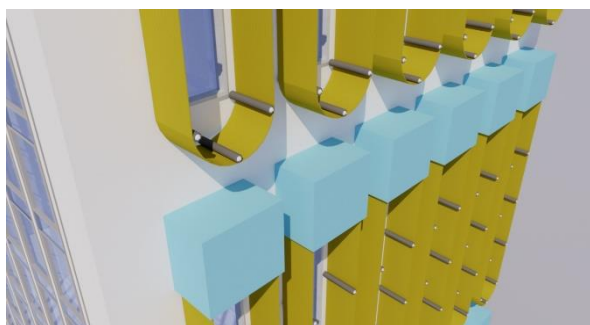


Figure 9. Alternate view of Carbon Cabinet

The dimensions for the presented CarbonCabinet are as follows: both housing chambers are 1.2 m in width, 1.2 m in height, and 1 m in depth. This cabinet would be placed on top of the window bay, allowing for the carbon capturing fabric to form a semi-loop around the window bays, thereby providing shade and capturing carbon. Like in the CarbonSail, the fabric's length is modifiable based on the number of floors it is intended to cover.

6. DISCUSSION AND PROPOSED TRAJECTORY

This paper produced a number of designs applicable to the development of an appropriate building-integrated shade and CO₂ capture system that overcome the weaknesses of previous designs. The ultimate goal of our research is to build a prototype with which to perform experimental evaluation studies and investigate BICC's ability to achieve the original goals: self-shading, and carbon capture and regeneration. We intend to produce inexpensive, scaled-down versions of the envisioned devices to investigate solutions to the problems generated in the previous stage. This work will form the project's experimental phase; the solutions will be investigated and either accepted, improved, re-examined, or rejected based on the data generated. Further alterations and refinements may occur to rule out as many malfunctions as possible and produce the best possible device.

On the other hand, our continual ideation of BICC determined that although passive carbon capturing (taking advantage of natural air flow) through implementation on the building envelope seems interesting, it may be unlikely to happen at this time, as it is considered a costly building element and its performance may not be as good as we would like. Therefore, we are thinking about shifting to active

(forced air using fan power) carbon capturing systems for better performance. Yet, due to the energy required to operate fans, we cannot dedicate this energy solely for carbon capturing, it must be hybridized to be used for other purposes in addition to carbon capturing. Therefore, we are currently considering implementing such technology within buildings' heating, ventilation, and air conditioning (HVAC) systems to take advantage of the fan used for air circulation in addition to the higher concentration of CO₂ in buildings. Building-integrated carbon capturing systems would be the next piece of the puzzle in our attempt to combat climate change through building-integrated carbon capturing, and it would be a suitable option for current implementation in buildings, as it would serve as an addition (filter-like mechanism) to a building's existing HVAC system for the purposes of carbon capturing and regeneration, in addition to indoor air quality control.

ACKNOWLEDGEMENTS

We would like to thank Dr. Klaus Lackner and his colleagues at Arizona State University's Centre for Negative Carbon Emissions for all their help in developing this paper.

REFERENCES

1. Climate Change: Vital Signs of the Planet. (2018). Climate change causes: A blanket around the Earth. [online] Available at: <https://climate.nasa.gov/causes/> [Accessed 10 May 2018].
2. New York Times, (2017) Our Disgraceful Exit From the Paris Pact. June 2, p.A24.
3. Davenport, C. & A. Rubin, (2017) Trump Signs Executive Order Unwinding Obama Climate Policies. New York Times. March 28, p.A1.
4. FCCC, (2015) Adoption of the Paris Agreement. Framework Convention on Climate Change (FCCC), United Nations, Paris.
5. Lackner, K.S., (2010) Washing carbon out of the air. In Scientific American, 302(6), p.66-71.
6. Hauviller, C., (2007). Design rules for vacuum chambers.
7. Miller, T. D., & Elgard, P. (1998). Defining modules, modularity and modularization. In Proceedings of the 13th IPS research seminar, Fuglsoe.
8. Enkel, E., & Gassmann, O., (2010). Creative imitation: exploring the case of cross-industry innovation. R&D Management, 40(3), 256-270.
9. Hancock, B., (2003). Maximum sail power: the complete guide to sails, sail technology and performance. Norwich, VT: Nomad Press.
10. Darman, P., (2003). U.S. Patent No. US 6578936 B1. Washington, DC: U.S. Patent and Trademark Office.

Statistical Analysis of Architectural Features Effects on Indoor Environmental Conditions in A Plus Energy House Prototype

MIGUEL ALEJANDRO CHEN AUSTIN^{1,3}, DENIS BRUNEAU^{1,2}, ALAIN SEMPEY¹, LAURENT MORA¹

¹CNRS, I2M (UMR 5295), 33400 TALENCE, France;

²GRECCAU, EA MCC 7482, 33405 TALENCE, France;

³Universidad Tecnológica de Panamá, Ciudad de Panamá, Panamá

ABSTRACT: Data from an experimental investigation, carried out during the summertime (from the end of July to mid-September, 2016), have been statistically analyzed, with the purpose of proposing a post-installment-evaluation technique by assessing the effects that some architectural features have on the indoor environmental conditions in a prototype of Plus Energy House in southwest France. The proposed correlation analysis is tested first, to evaluate its reliability for distinguishing strong from weak correlations. Since the proposed analysis appears to be acceptable, it was used then for studying the relationship between outdoor and indoor environments. Results from the correlation analysis strongly suggest that the impact of direct solar radiation on the indoor environment is well attenuated by the double-glazed windows with blinds implemented in the house.

KEYWORDS: Statistical correlation analysis, assessment of architectural features, post-installment-evaluation.

1. INTRODUCTION

The cravings of bioclimatic architecture for the sustainable design of buildings focuses mainly on indoor environment quality under any climatic conditions, by encouraging the endeavor of improvement in buildings' upstream dynamic simulation and downstream empirical observations. Such empirical observations assess the post-installment-evaluation of the effects that architectural features have on indoor environmental conditions.

In this context, data from an experimental investigation dedicated to studying the interaction between the natural ventilation and thermal behavior of a Plus Energy House (PEH) prototype, are analyzed, using a correlation analysis approach, to highlight the effects that its architectural features have on the indoor environment thermal behavior. Such features are mainly: double-glazed windows, window blinds, natural ventilation openings, and envelope.

Since such an approach is not conventional for the assessment of architectural features; no similar investigations reported in the literature have been encountered. However, there are other methods of evaluation [1-2]. In the end, it is intended to characterize the architectural features designed for this PEH prototype, mainly regarding: (a) the reduction of indoor radiative heat gains from external sources, (b) the influence of wind effects in the indoor air movement.

2. EXPERIMENTAL PLATFORM AND METHODOLOGY

After participating in the Solar Decathlon Europe 2012 competition, the PEH prototype used in this experimental study had, afterward, became an

experimental platform for research purposes located in Bordeaux, southwest France.

The building's envelope, enclosing a 211 m³ air volume and a 46 m² floor surface area, can be briefly described as an external structure of maritime pine, with 32 cm of thermal insulation and outdoor cabinets at the east and west facades (1.4 W.m⁻².K⁻¹ each), and 32 cm of thermal insulation at the North façade (1.2 W.m⁻².K⁻¹), ceiling, and floor. South and north façades include natural ventilation openings (bottom hung window type) representing the 9.58% and 7.51% of each façade, respectively; apart from this, the south façade is fully glazed corresponding to the 90.42% of the total surface (with a total heat transfer coefficient of 1.6 W.m⁻².K⁻¹).

Moreover, this platform was designed to promote a charge-discharge sensible energy strategy to control the indoor air temperature rising and reduce artificial acclimatization usage, in the summertime.

2.1 Experimental protocol

The experimental approach adopted was to instrument the indoor space of the platform, consisting mainly of the following measurements: (i) air and surface temperatures (T), (ii) airspeed (V), and (iii) convection (φ_C) and radiation (φ_R) heat fluxes. These parameters were measured at the ceiling and floor surfaces (Fig. 1 and 2). The indoor air temperature (T_{in}) was measured at 1.70 m height; the outdoor air temperature was also measured by our means (T_{out}); their locations are shown in figure 1 and 2. Other outdoor environmental conditions (direct solar radiation and wind speed) were

acquired from a meteorological station at 10 m height and a distance of 1.5 km from the platform's location.

observations per day will be used for the indoor environment data.

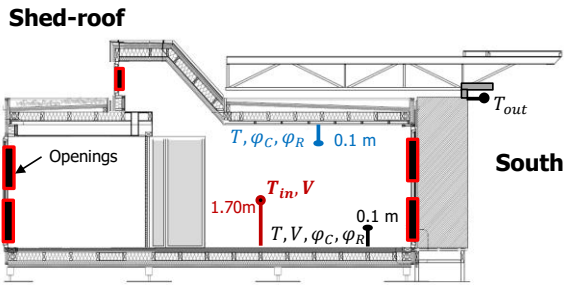


Figure 1: West-side view of the experimental platform with sensors distribution.

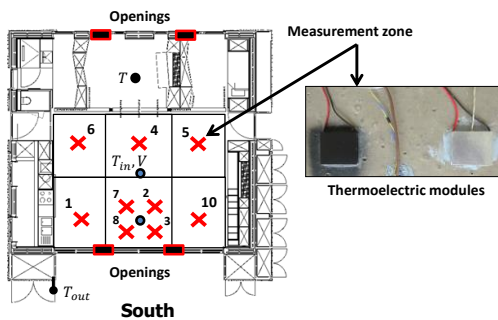


Figure 2: Top view of the experimental platform and sensors distribution.

A measurement campaign was carried out from July 27th to September 12th, 2016 (except from July 30th to August 11th). During this campaign, the natural ventilation openings were configured as to promote a night stack ventilation strategy; programmed to open only when the outdoor air temperature falls lower than the indoor air temperature, which happened mostly at night. The platform was unoccupied, and the window blinds were kept down during the entire campaign.

Three physical variables implemented later in this study are: (i) the mean radiant temperature, (ii) the total incident radiation heat flux, and (iii) the convective heat flux on the floor surface. These variables were obtained by data processing, implementing analytical models developed in previous studies [3-4].

2.2 Statistical approach

2.2.1 Data collection and sample rate

During the measurement campaign (34 days in the summertime), data were collected from the indoor environment (including the outdoor temperature) at a sample rate of an observation every minute, equivalent to 1440 observations per day. From the outdoor environment, data were collected at a sample rate of an observation every ten minutes, equivalent to 144 observations per day. Here, a reduction for the indoor environment data was performed to be consistent with the outdoor environment sample rate: only 144

2.2.2 Correlation analysis

A correlation analysis based on the Pearson correlation coefficient R was implemented to evaluate how strong the relationship between indoor and outdoor measurements is and to better understand the coupling between the heat transfer and airflow effects in the platform. The value of R indicates a perfect linear relationship between two concerned physical quantities when R is equal to one ($R = 1$), a no linear relationship when R is equal to zero ($R = 0$), which might mean a curvilinear relationship, which is not detected by R , and a perfect but inverse linear relationship when R is equal to negative one ($R = -1$) [5].

As the implementation of a correlation analysis of such physical problem via only the correlation coefficient R may lead to subjective conclusions, the significance of R is further analyzed using other approaches concerning its interpretation. To do this, we have implemented the following three approaches as presented in [5]:

The verification of the null and alternative hypothesis state via the p-value (we will assume 0.95 as confidence level).

The explained variability of the data via the squared value of R .

The visual trend that verifies the linear or curvilinear relationship via scatter plots.

Regarding the first approach, the null hypothesis states, as default, that there is no significant correlation between the two variables studied (a p-value greater than or equal to 0.05). Once the p-value of the supposed correlated data is determined, if its value lays under 0.05, it is said that the null hypothesis is rejected and the alternative hypothesis holds: there is a significant correlation in between the two variables studied.

Regarding the second approach, as stated in [5], the squared value of R indicates the percentage of the variability that can be explained by the knowledge of the correlated variables. Regarding the third approach, the visualization of the two correlated variables will verify their relationship subjected by R . In the case where R values near zero are encountered (indicating no linear relationship exists), the visual trend can help us to determine whether to accept the “no correlation” implied by the value of R or to consider the determination of another correlation coefficient that allows evaluating the strengths in the trend encountered. Finally, regarding the last part of the previous paragraph, the Spearman's coefficient (or Spearman rank-order correlation coefficient) will be determined, since it allows evaluating monotonic relationships. In such relationships,

PLEA 2018 HONG KONG

Smart and Healthy within the 2-degree Limit

the variables tend to change together, but not necessarily at a constant rate.

It is worth mentioning that it is possible to meet a situation where Pearson’s coefficient is negative while Spearman’s coefficient is positive or vice versa, which might lead to infer that this is an inconsistency. However, with a logical understanding of the difference between these two coefficients, such “inconsistencies” are justified [6].

In addition to correlation plots, to present the results with Spearman’s coefficient, we use correlation matrices using the software **R**, as they allow us to group the three approaches mentioned earlier.

2.2.3 Distinguishing strong from weak correlations

Here, we establish a threshold for the value of R that could help us to distinguish, as unbiased as possible, strong from weak correlations. This threshold is chosen based on the statistical interpretation of R^2 , described in §2.2.2.

As a value of R^2 greater than 0.51 indicates that the 51% of the variability of variable A is explained by a variable B, we extend this to the following: the variable B can explain the variability of variable A at least 51% of the times, which represents the majority. Thus, the threshold value for R results in 0.71 (the squared root of 0.51).

Then, a correlation will be classified as strong if the R value is greater than 0.71 and as weak if the R value is lower or equal to 0.71. Similar threshold or critical values were proposed by Cohen in 1988, as encountered in [7].

2.2.4 Day/night-time criteria for data sorting

As the aspects we wish to analyze here are the impacts of external sources on the indoor environment and the impact of the night natural ventilation strategy implemented, the experimental data collected will be analyzed separately in the daytime and the night-time. To do this, we have sorted the data using the following criteria:

Night-time: Solar radiation = 0 & indoor-outdoor temperature difference > 0.

Daytime: Solar radiation ≠ 0 & indoor-outdoor temperature difference < 0.

Here, we have included the condition of the temperature difference, because of the configuration proposed for the natural ventilation openings (§2.1).

3. RESULTS AND DISCUSSION

3.1 Classification of the correlations as strong or weak

The results from the meteorological station have shown that the majority of days presented cloudy and windy daytime and clear and no-windy night-time. Nevertheless, first, we decided to apply the statistical approach to days with similar meteorological conditions: sunny and windy daytime and no-windy night-time

(August 15th, 16th, 22nd, and 23rd); the corresponding total sample size is 576: four days with 144 observations.

The correlation analysis results, based on the Pearson’s coefficient, are presented in figures 3 and 4, for no-windy night-time (sample size of 196), and sunny and windy daytime (sample size of 271), respectively, using the criteria presented in §2.2.4. The missing 109 observations laid outside the day/night-time criteria established.

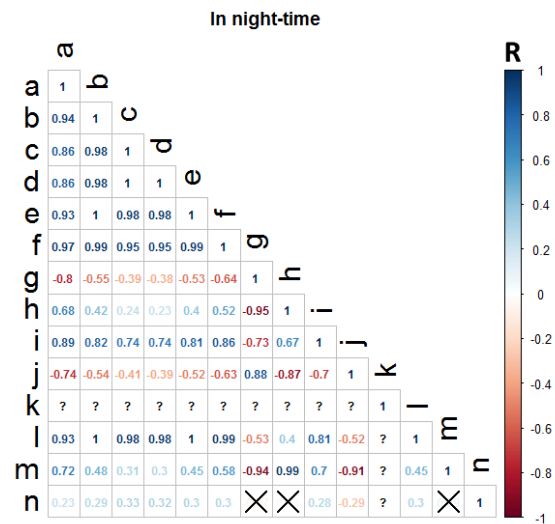


Figure 3: Correlation plot based on the Pearson coefficient for experimental results from no-windy night-time: the sample size resulted in 196.

The variables presented in figure 3 and 4 are: temperature of the (a) outdoor air, (b) indoor air, (c) floor surface, (d) ceiling surface, (e) averaged of surrounding surfaces and (f) air near floor surface. Also, the temperature difference between (g) the indoor and outdoor air, and (h) the air near the floor and the floor surface. The airspeed at (i) the location where the indoor air temperature was measured and (j) near the floor. Additionally, the following heat fluxes: (k) outdoor, direct solar radiation, (l) incident radiation on the floor surface, and (m) convection. And finally, (n) the external wind speed.

To read these graphs, we can assign to each segment (frames containing numbers) a pair of variables: (vertical-axis variable, “stairs”-axis variable). For example, in figure 4, the Pearson’s coefficient between indoor and outdoor air temperatures is the cross value between letter “b” in the vertical axis the letter “a” in the “stairs” axis, namely $R = 0.64$. Additionally, segments presenting an “X” indicates no significant statistical correlation, since the computed p-values resulted in being greater than 0.05.

PLEA 2018 HONG KONG

Smart and Healthy within the 2-degree Limit

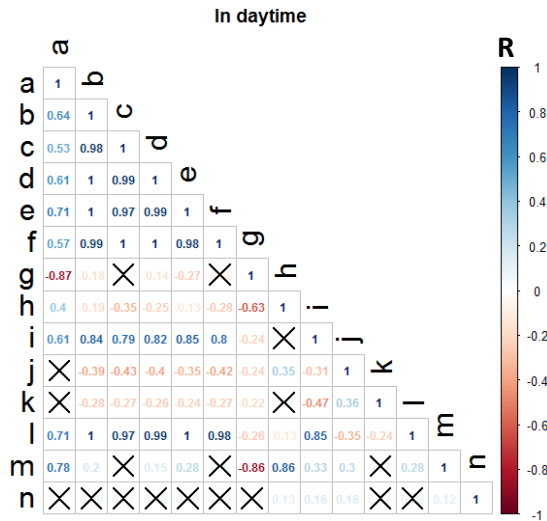


Figure 4: Correlation plot based on the Pearson coefficient for experimental results from windy and sunny daytime: the sample size resulted in 271.

Before going further, in order to evaluate if the proposed correlation analysis can be considered as acceptable or not, it is applied to correlate variables that normally, in agreement with the physical laws, should present strong correlations coefficients. For instance, consider the convective heat flux (m) and the temperature difference between the air near the floor surface and the floor surface (h). Since these variables are known to be directly related, as stated by Fourier’s law of convection, a strong R value should be expected; this can be observed in segment (m,h) in figures 3 and 4, which R values are 0.99 and 0.86. These values indicate that the correlation between m and h are both strong ($R > 0.71$) and positively correlated, as expected.

The difference in the previous R values for each period (daytime and night-time), can be explained by the fact that convective heat flux values are stronger when the openings are opened than when they are closed. Another fair and obvious example can be the solar radiation heat flux (k) during night-time. Since this variable is normally zero during this period, no correlation whatsoever should be encountered between this and other variables; this can be observed in figure 3, of which every R value related to the variable k resulted in a question mark (?) (in other words: “NA”).

Moreover, another fair example, not as obvious as those presented before, is that all the temperatures from the indoor environment (b,c,d,e,f) should present strong correlations between one-another all the time. This can be observed in both figures 3 and 4, as expected. From the aforementioned, the statistical method proposed here, *a priori*, seems to be a reliable method to evaluate the strengths of correlated variables.

3.2 Correlation between the outdoor and indoor environments

The variables from the outdoor environment selected for the correlation analysis are: the air temperature (a), the direct solar radiation (k), and the wind speed (n). To evaluate the influence that these three variables have on the indoor environment, we choose the following variables for the indoor environment: the air temperature (b), the floor surface temperature (c), the total incident radiation on the floor surface (l), and the airspeed (i) and (j). In this way, we can evaluate, specifically, the contribution of the direct solar radiation to the thermal behavior of the floor surface temperature, and also the contribution of the wind speed to the air movement inside the platform.

First, from the variables mentioned here before we depurate by focusing on the R values greater than 0.71, and the “X” presented in both figures 3 and 4. Every segment is presenting an R value lower or equal to 0.71 and an “X,” is eliminated from the analysis. This allows us to obtain the relevant variables and to consider the third approach mentioned in §2.2.2, using correlation matrices with the Spearman’s coefficient (refer to Figs. 5 and 6).

The correlation matrices include the following: The graphs of each pair of correlated variables, as well as their magnitudes (visual trends). The distribution of each corresponding sample (represented by histograms).

The statistical significance due to the p-value with red asterisks; where three asterisks (***) indicate that the p-value is very close to zero, two asterisks (**) that are very close to 0.001, and one asterisk (*) that is very close to 0.01. A point (·) indicates that the p-value is very close to 0.1, and nothing () indicates that is very close to 1.

The interest in using Spearman’s coefficient is for comparison purposes as the Pearson’s coefficient are already presented before. This type of graph (refer to Figs. 5 and 6) can be read in the same way as figures 3 and 4, but here the correlation coefficients of two correlated variables are presented above the diagonal with histograms; under this diagonal are the scatter plots of those variables showing their trend.

3.2.1 Wind speed and indoor air movements

In figures 5 and 6, for the wind speed (variable n), it is clear that there is no strong correlation presented between variable n and those representing the air movement in the indoor environment (i and j). This is fairly expected for the night-time periods (refer to Fig. 5) since they presented no-windy conditions. In daytime (refer to Fig. 6), the weak correlations encountered between variables n, i and j, might be explained by the fact that the openings remained closed; as a consequence, the air infiltrations are minimal.

PLEA 2018 HONG KONG

Smart and Healthy within the 2-degree Limit

It is worth mentioning that in cases of no-windy night-time periods, thermal buoyancy dominates the ventilation airflow in the platform.

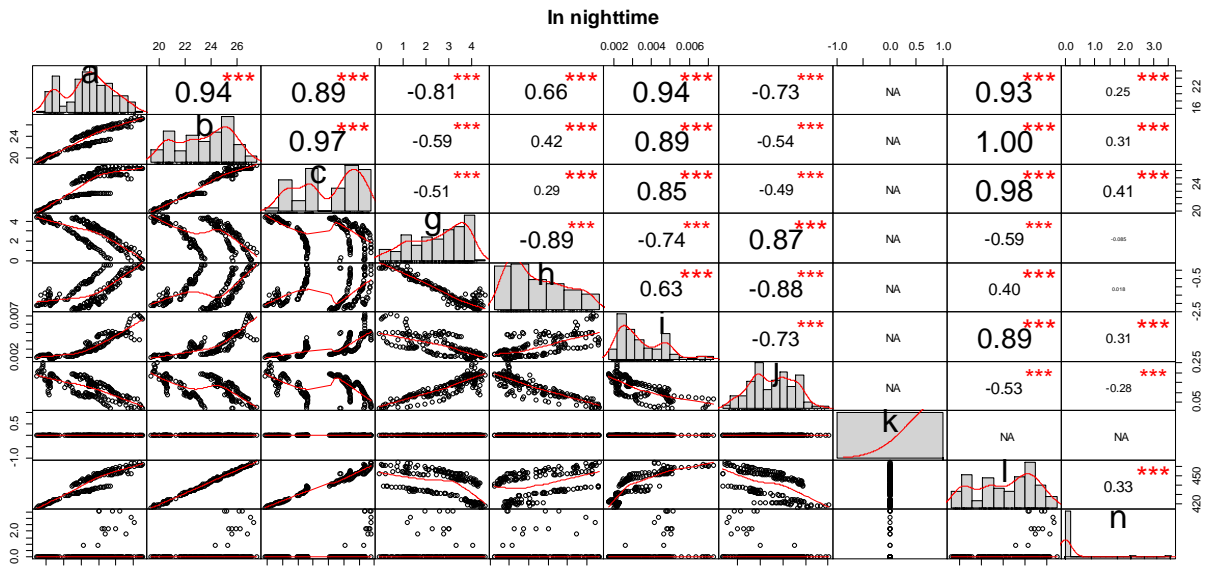


Figure 5: Correlation results for no-windy night-time with Spearman's coefficient: sample size of 196.

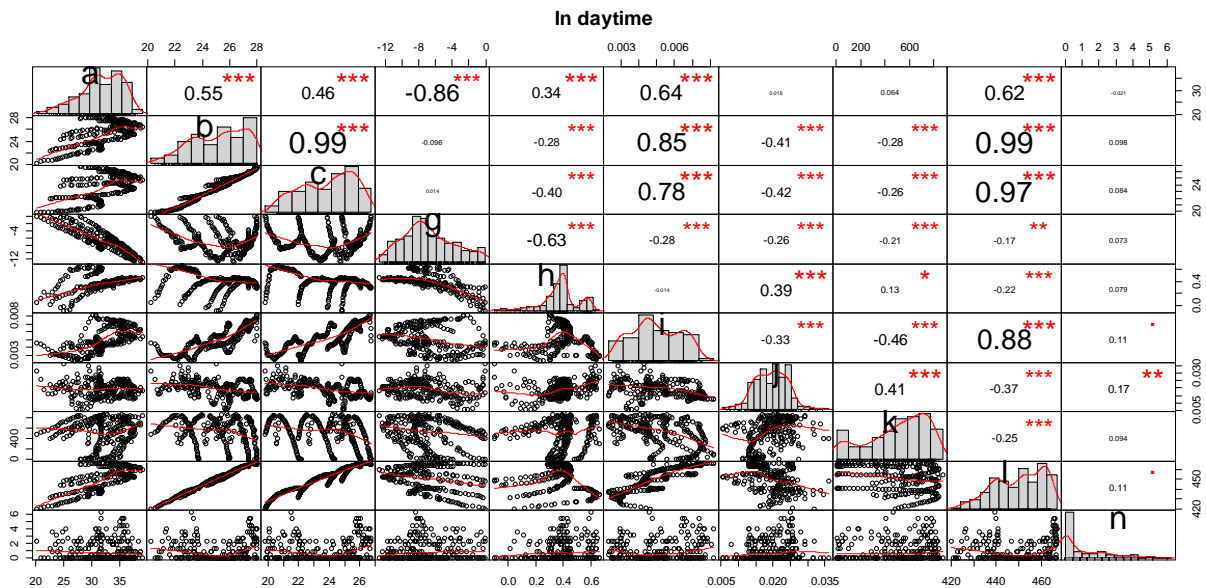


Figure 6: Correlation results for sunny and windy daytime with Spearman's coefficient: sample size of 271.

Therefore, it can be inferred that the air movements in the indoor environment may be strongly correlated with a specific temperature difference. In this matter, figure 5 shows that there are strong correlations between the air movements (i and j), and the temperature differences: g and h. Between the segments (g,i), (g,j) and (h,j), which are the strongest ones, higher R values were encountered when using Spearman's coefficient (refer to Fig. 5), than when using Pearson's (refer to Fig. 3). This indicates that the relationship between these correlated

variables is rather curvilinear than linear. In fact, based on the physical laws of natural convection and thermal buoyancy, relating the temperature difference and the resulting airspeed, a 1/2 power law trend is expected to be encountered. This trend can be observed in figure 5 segments (h,j), (g,i), and (g,j). Moreover, similar correlation coefficient values and trends were encountered when using data from periods of windy nighttime (sample size of 187 observations). This indicates that wind effects do not play an essential role

PLEA 2018 HONG KONG

Smart and Healthy within the 2-degree Limit

in the air movement near the concrete slab surface nor near the center of the platform.

3.2.2 Outdoor solar radiation and the indoor radiative environment

Results from correlation analysis showed that the direct solar radiation heat flux does not play an essential role in the indoor radiative environment, whether using the Pearson's coefficient (refer to Fig. 4, segment (l,k): $R = 0.24$) or Spearman's (refer to Fig. 6, segment (l,k): $R = -0.25$). In fact, the solar radiation heat flux (k) is not strongly correlated with any other variable, when considering the R threshold criterion proposed. This *a priori* means that the implemented double-glazed windows with blinds, reduce the incoming solar radiation heat flux, which lead to suspect that the indoor radiative environment is driven by internal long wavelength (LWL) radiation. This implies that the floor surface is heated by the surrounding surfaces, i.e., the glazed-façade, ceiling, and other vertical walls.

However, the fact that no strong correlations have been encountered for the variable k can also be explained by the position of the Sun in the summertime and the solar eave facing south, on the ceiling. Since the Sun position is higher, the solar eave prevents the sunrays from reaching the glazed-façade, and thus, the indoor floor surface. Also, a consequence of the orientation of the platform, the windows at the north façade won't be heated by direct solar radiation.

It is worth mentioning that this analysis was first applied to data from only one day (sample size of 144), and greater correlation coefficient values have been encountered when a larger sample size was used.

3.3 Correlation analysis when using data with mixed meteorological conditions

So far, we have analyzed data from days with similar meteorological conditions. In addition to this, we decided to apply the correlation analysis to days with mixed meteorological conditions, to observe if the correlation results hold: July 28th and 29th, and August 15th, 16th, 19th, 20th, 22nd, and 23rd.

In general, all the R values were encountered to be lower than those found in the analysis presented before. This lead to conclude that if the variability of a variable A wants to be statistically studied regarding a variable B, data from experiments with similar meteorological conditions should be used, rather than mixing data from experiments under different conditions together, as expected.

5. CONCLUSION AND PERSPECTIVES

Results from an experimental research project dedicated to studying the interaction between natural ventilation and thermal behavior in buildings have been analyzed by a statistical approach, reporting the effects of some

architectural features on the indoor environmental conditions.

The correlation analysis, using experimental data, strongly suggests that direct solar radiation is well attenuated by the solar protections (doubled glazed with blinds and solar eaves). Thus, the LWL radiation dominates the indoor radiative heat exchanges. Also, the correlation analysis strongly indicates that buoyancy forces (and not winds effects) dominate the indoor air movement, whether the openings are kept open or not, whether the night-time is windy or not.

This kind of correlation analysis might emerge as a suitable post-installment-aid tool (after *in situ* implementation) to evaluate the effectiveness of architectural features on indoor environmental conditions.

ACKNOWLEDGEMENTS

We would like to acknowledge the support given by the Institute de Mécanique et d'Ingénierie de Bordeaux (I2M), and the IUT of Université de Bordeaux. We also like to and extend our gratitude to IFARHU Panamá and Universidad Tecnológica de Panamá, for their financial support.

REFERENCES

1. Cammarano, S., Pellegrino, A., Maria Lo Verso, V. R. and Aghemo, C., (2014). Assessment of daylight in rooms with different architectural features. *Building Research & Information*, doi: 10.1080/09613218.2014.922359.
2. Bkowski, J., (2017). Analytical tools for functional assessment of architectural layouts. In *IOP Conference Series: Materials Science and Engineering*, 245 042044, doi:10.1088/1757-899X/245/4/042044.
3. Chen Austin, M., Sempey, A., Bruneau, D., Mora, L., Sommier, A. and Vogt-Wu, T. (2016). Stockage/déstockage d'énergie sensible et ventilation naturelle en bâtiment : une approche expérimentale à l'échelle 1. In *SFT Conference*. Toulouse, France, May 29th to June 1st.
4. Chen Austin, M., Sempey, A., Bruneau, D., Mora, L., (2018). Evaluation expérimentale d'une stratégie domotique de pilotage des éléments mobiles : vers un contrôle semi-passif simple du confort d'été en BEPos. In *SFT Conference*. Pau, France, May 29th to June 1st.
5. Schumacker, R. and Tomek, S., (2013). Understanding Statistics Using R. *Springer New York Heidelberg Dordrecht London*. ISBN 978-1-4614-6226-2.
6. Hauke, J. and Kossowski, T., (2011). Comparison of values of Pearson's and Spearman's correlation coefficients on the same sets of data. *Quaestiones geographicae*, 30(2): p. 87-93, doi: 10.1.1.466.4196.
7. Randolph, K. A. and Myers, L. L., (2013). Basic Statistics in Multivariate Analysis. *Oxford University Press New York*. ISBN 978-0-19-976404-4.

Reducing Thermal Stress in Philippine Classrooms: Review and Application of Passive Design Approaches

JUAN PAOLO FLORES¹, SIMOS YANNAS¹

¹Architectural Association, London, United Kingdom

ABSTRACT: School buildings in Manila are ill equipped to deal with the high demand for student places. This has manifested in overly dense classrooms, which in combination with standardised geometries has led to poor thermal and daylighting conditions. This research contextualises passive design strategies from literature and built precedents then applies these approaches to a theoretical classroom. The result is a design proposal that improves indoor comfort through simple interventions in geometry, ventilation, and materiality.

KEYWORDS: Tropical, Classroom, Thermal, Daylight, Comfort

1. INTRODUCTION AND METHODOLOGY

In 2017, Metropolitan Manila has a shortage of some 18,000 classrooms [1]. Consequently, public school classrooms in the region suffer from overpopulation, with upwards of 50 pupils per classroom in some districts [2]. There is an urgent need to apply measurable sustainable design strategies on typical school buildings – with special attention given to the thermal and visual comfort of classrooms.

The end goal is a classroom design appropriate to Manila's climate. To determine a framework for the design proposal, existing literature on school environments are first contextualised within Manila's climate in Section 2. An examination of both historical and contemporary precedents to derive architectonic applications of environmental theories in existing literature is in Section 3. These applications are then validated and optimised with simulations using Ladybug Tools and EnergyPlus in Section 4 before being synthesised in a design proposal in Section 5 [3].

2. CLIMATE AND THEORETICAL FRAMEWORK

To determine an adaptive thermal comfort band for free-running applications, Meteonorm 7.0 weather data for Manila was processed using Equation (1) to obtain an exponentially weighted running mean of outdoor temperatures [4].

$$T_{rm(n)} = (1 - \alpha_{rm})T_{e(d-1)} + \alpha_{rm}T_{rm(n-1)} \quad (1)$$

where $T_{rm(n)}$ - running mean temperature for day n (°C);
 α_{rm} - running mean constant;
 $T_{e(d-1)}$ - daily mean outdoor temperature for previous day (°C).

Then, Equations (2) and (3) were applied to the running mean outdoor temperature to set the upper and lower margins of the adaptive thermal comfort band for a new-build [4].

$$T_{imax} = 0.33T_{rm} + 21.8 \quad (2)$$

$$T_{imin} = 0.33T_{rm} + 15.8 \quad (3)$$

where T_{imax} - indoor upper margin (°C);
 T_{imin} - indoor lower margin (°C);
 T_{rm} - outdoor running mean temperature (°C)

The 1-2K differentials between the peaks of the average hourly temperatures and the upper margin of the comfort band in Figure 1 imply that indoor temperatures can easily go above the upper margin once internal heat gains are factored in.

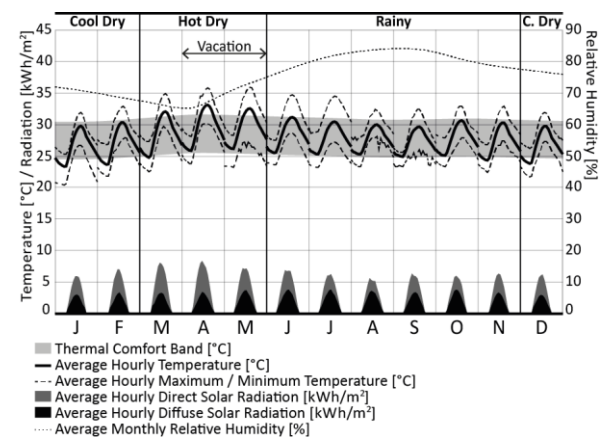


Figure 14: Climate summary for Metropolitan Manila showing comfort band, temperature, relative humidity, and solar radiation sourced from Meteonorm 7.0

The conditions shown above are an opportunity to reassess the Department of Education (DepEd) Facilities Manual occupancy load targets of 1.40 m² per student in 63 m² classrooms [5]. Research shows that 12-16 students in primary school and 16-20 students in secondary schools are best for learning performance and student-teacher relations [6]. Socio-economic forces not covered in this research make these generous targets

PLEA 2018 HONG KONG

Smart and Healthy within the 2-degree Limit

impractical but there is an impetus to go lower than the 45-student target.

Regarding potential plan typologies for a school, a courtyard plan or linear plan are desirable in the climate as these have more exposed surface area for heat loss that would allow for the use of wind as a cooling device [7]. Initial computations using Equation (4) show that that heat loss arising from infiltration and fresh air requirements will not be enough to bring indoor temperatures to comfort [3] thereby signifying that the built form must provide more surface area for heat losses and substantial inlets for passive cooling.

$$T_i = T_o + HG_{SI} / (\Sigma(AU) + 0.33 \times V \times ACH) \quad (4)$$

where T_i - indoor temperature (°C);
 T_o - outdoor temperature (°C);
 HG_{SI} - solar and occupancy heat gains (W);
 A - building element surface area (m²);
 U - thermal transmittance (W/m²K);
 V - building volume (m³)
 ACH - air exchanges per hour (ac/h)

Radiation domes for Manila show that direct solar radiation will mostly come from overhead. Early-stage thermal simulations with just physiological heat and solar gains as inputs confirm that diffuse radiation will account for nearly half the heat gains. Physiological heat accounts for a third while direct solar radiation accounts for the remaining 16.67% [3]. This means that shaving off direct radiation by shading over openings will yield shallower benefits than by reducing opening areas where diffuse radiation can enter.

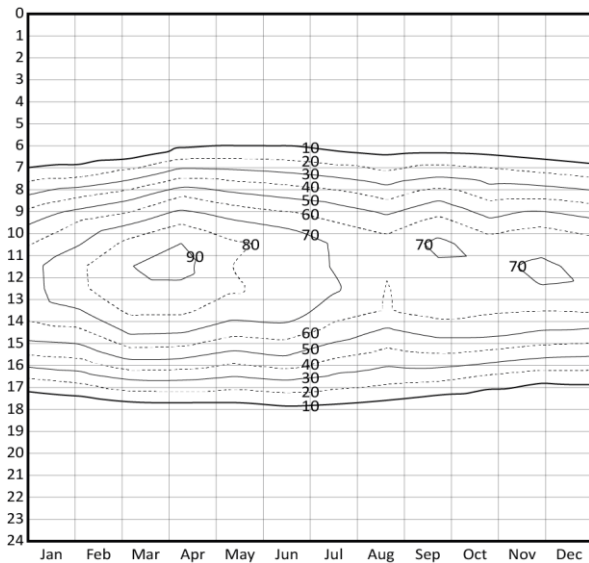


Figure 15: Monthly average global horizontal illuminance levels for Manila in klx sourced from *Meteonorm 7.0*

Scaling back on solar radiation gains with smaller fenestration areas may reflect poorly on daylight

conditions – undesirable in a school where visual acuity is important. However, the substantial amounts of available daylight illustrated in Figure 2 would allow lower initial daylight factor targets than those based on a CIE sky as seen in Table 1.

Table 4: Daylight factor equivalents for Manila [3]

Space	Illum. (lx)	CIE Sky _a %	Manila _b %
Auditorium	100	1.00	0.05
Classroom	300	2.50	1.50
Office	500	4.19	2.50

^aBased on overcast CIE sky (11,921 lux)

^bBased on average at 08:00 of Figure 2 (20,000 lux)

3. REVIEW OF BUILT PRECEDENTS

The theoretical framework established the need to design surfaces that support heat loss, fenestrations that protect against diffuse solar radiation while accommodating daylight, and substantial inlets for passive cooling. Two typologies with differing approaches to the needs above were examined.

3.1 Historical precedent: the Gabaldon Schoolhouse

The Gabaldon Schoolhouses are precedents built from 1911 to 1916 based on prototypes by William Parsons. These were praised by the American Governor General for openness, high wind exposure, and lightweight construction in response to the climate [8].

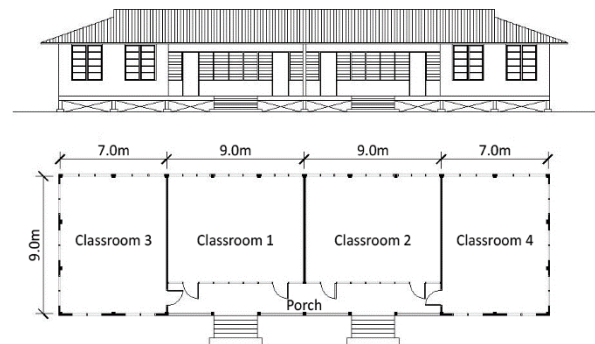


Figure 16: Typical floorplan and elevation of a Gabaldon Schoolhouse based on surviving drawings

The typical Gabaldon, seen above in Figure 3, is a one-storey structure on stilts designed to experience surface heat loss through wind exposure on its tongue-in-groove slatted floor in addition to its walls and roof. The wind exposure increases the rate of heat loss by reducing the thermal resistance of external building elements [9]. In addition, all four classrooms have 2 to 3 fenestrated walls and emphasise opportunities for natural ventilation in its simple linear plan.

While the window-to-wall ratios (WWR) are substantial and typically range from 52% to 70%, the sashes are translucent rather than transparent thereby reducing transmitted solar radiation and daylight. These sashes, shown in Figure 4, are a traditional building element

PLEA 2018 HONG KONG

Smart and Healthy within the 2-degree Limit

constructed by trimming windowpane oyster (*Placuna placenta*) shells into squares and inlaying these within a timber lattice grid. Rather than reduce the number and area of windows to counteract diffuse radiation, the vernacular solution is to maximise wall areas occupied by operable windows but use a translucent glazing material to cut back on transmitted radiation.

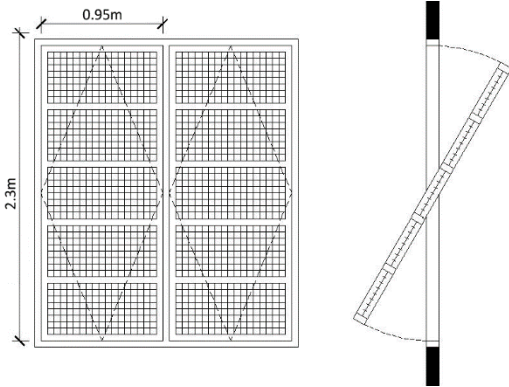


Figure 17: Elevation and section of typical capiz window found in Gabaldon Schoolhouses

3.2 Current paradigm: the government standard

In contrast to the lightweight construction and high wind-exposure of the Gabaldon Schoolhouses, contemporary facilities built to DepEd specifications are often dense, multi-storey, and exclusively built with concrete save for the steel roof structure [5].

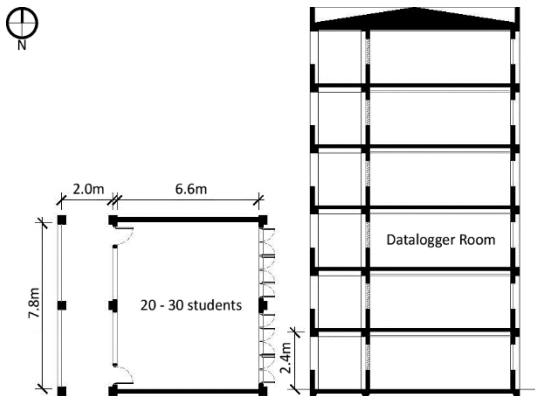


Figure 18: Plan of observed classroom and position in section of Rizal High School: Science Building, a typical DepEd structure

The indoor temperature and relative humidity of the classroom depicted above in Figure 5 was observed for a week from the 2nd to 8th of August. The datalogging results illustrated in Figure 6 show internal temperatures cooler than the outdoor conditions during the warmest hours around noon from the 2nd to 6th of August. During the weekend of the 7th and 8th, the internal temperature drops from 31°C and plateaus at 29°C, in direct contrast to the fluctuations of the exterior.

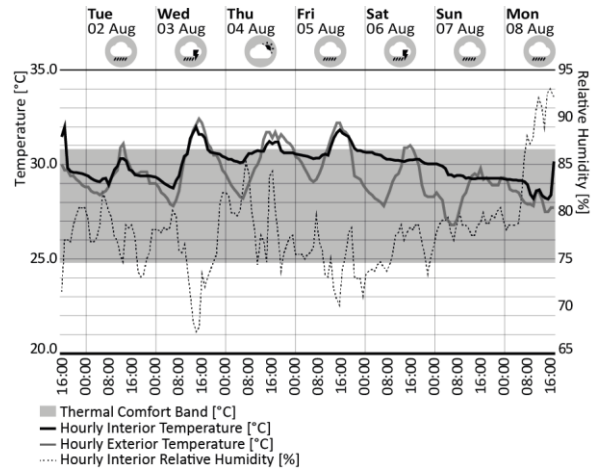


Figure 19: Interior Temperature, Exterior Temperature, and Interior Relative Humidity of a typical classroom measured from 01 August to 08 August

The cooler interior temperatures relative to the exterior conditions at noon in Figure 6 is an effect of the east-west orientation reducing direct solar radiation entering the room. However, this orientation allows the preheating of the interior before occupant ingress at 7:00.

Spot measurements performed from 13:16 to 14:20 on every floor on 15 August also revealed poor daylight performance due to the orientation. The recorded illuminance at the centres of the classrooms range from 80 to 323 lux despite the exterior corridor recording illuminance from 287 to 97550 lux [3].

Figure 6 also shows the heavyweight material smoothing the temperature fluctuations and delaying the effects of the warm exterior conditions on the interior. Thermal mass is especially apparent in the contrast of rising exterior temperatures and falling interior temperatures from 8:00 to 16:00 of 7 August. This behaviour is corroborated by the 2K difference between surface temperatures and air temperatures recorded in the spot measurements on 15 August [3].

4. VALIDATION THROUGH SIMULATION

The Gabaldon review raised the possibility of using the floor as an additional surface for heat loss through wind exposure and a vernacular solution to diffuse radiation protection while providing as many inlets for natural ventilation. The DepEd case study revealed the utility of heavyweight thermal mass while emphasising undesired preheating and poor daylight performance due to wrong orientation. Simple reinterpretations of beneficial approaches were tested on a reference.

4.1 Definition of reference case

While past studies on class density and learning quality recommend ideal quantities, the range of 20-25 children per class is stated as the point beyond which the impact of density on learning diminishes [6]. To account for Manila's classroom shortage and socioeconomic context,

PLEA 2018 HONG KONG

Smart and Healthy within the 2-degree Limit

the occupancy is set at 30, a 20% increase from the 25-student threshold.

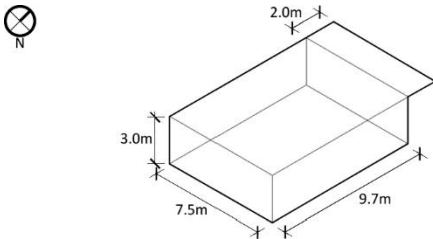


Figure 20: Isometric line diagram of reference case showing interior dimensions and 2.0m overhang to simulate corridor

Figure 7 is the resulting reference volume for study after drawing furniture and clearances for 30 students. It is 15% larger than the DepEd standard and deeper along the window axis in anticipation of substantial available ambient illuminance.

4.2 Solar control: fenestrations for daylight

Manila's east-west prevailing winds conflict with the north-south orientation for solar control. The solar path is prioritised as wind does not necessarily follow prevailing directions.

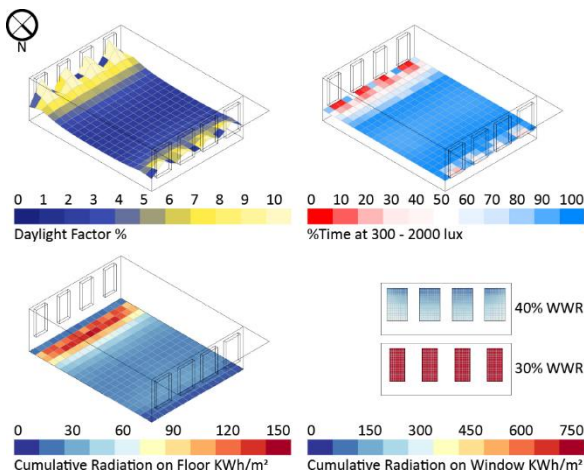


Figure 21: Daylight and Radiation simulation results for window-to-wall ratios of 40% at North and 30% at South

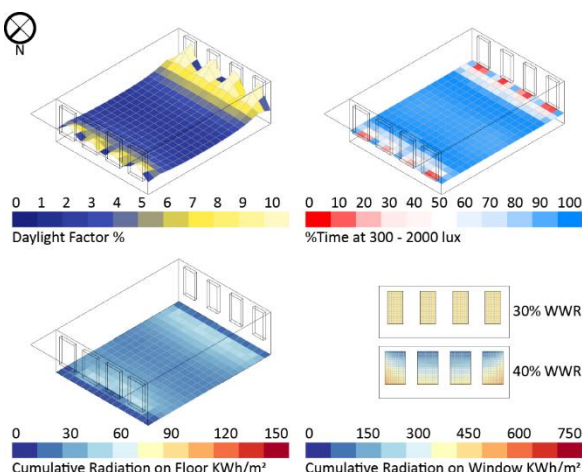


Figure 22: Daylight and Radiation simulation results for window-to-wall ratios of 30% at North and 40% at South

The translucent fenestrations of the Gabaldon are reinterpreted as a smaller WWR, with the 1.50% daylight factor for 300 lux in Table 1 of Section 2 as a target for the room centre. The windows are defined with a 2.4m high soffit to maximise daylight penetration depth with a 0.6m clearance above the soffit to anticipate structural members.

Figures 8 and 9 are the performance of the volume with the smallest window-to-wall ratios that achieve the target daylight factor at the room centre.

In both cases, the ratio of average daylight factors between the brightest third and the darker middle third is 3.3 [3] – a figure close to the recommended ratio of 3 [10]. While the ratio between the second brightest third and darker middle third is 2.1 [3], this bodes well for avoiding a flat distribution of daylight.

The Useful Daylight Illumination metric was modified to range from 300 – 2000 lux then simulated. The results show that the middle portion will be within the desired range of illuminance for 80 to 90% of time occupied while the sides will require shading to avoid visual discomfort. Figure 8 shows that an unprotected south-facing window will experience upwards of 750 kWh/m² of radiation cumulatively in a year. Figure 9 shows that despite a 2.0m deep overhang, lower portions of south-facing windows will experience up to 525 kWh/m² of radiation cumulatively in year. These results emphasise why minimising window area as the first level of solar protection is essential in the Philippine context.

4.3 Solar control: shade depth

Under the pretence of an optimal shading depth balancing a reduction of cooling loads and good daylight performance, shade-benefit calculations using the Ladybug Tools implementation of the SHADERADE method [11] were performed.

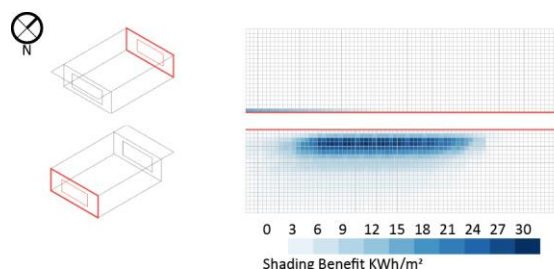


Figure 23: Shade benefit in KWh/m² for every additional 100mm depth of shading over windows

Figure 10 is a map of points representing cooling load reduction as a function of shading depth that is generated by the correlation of required cooling loads with back-traced sun vectors from grid points on the window and their corresponding transmitted direct solar radiation values.

PLEA 2018 HONG KONG

Smart and Healthy within the 2-degree Limit

The results show that North-facing windows won't require a substantial overhang. Recessing the window by 0.1m will reduce cooling loads by 12kWh/m². In the Southern case, the mapping gives a range of 0.2m to 1.0m for shading with corresponding shade benefits.

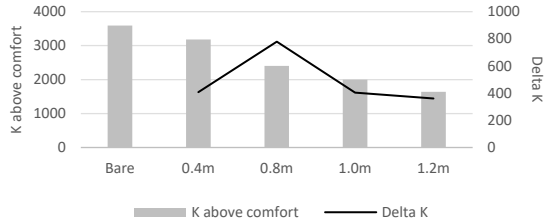


Figure 24: Annual cumulative Kelvin above comfort per shade depth

Figure 11 is an annual summary of total degrees K that each case is above the comfort band and by how much each case improves upon the last. A 0.8m depth shows the most dramatic reduction in relation to other depths and was implemented. The 0.1m and 0.8m depths are optimisations on the conventionally traced 0.3m and 1.53m depths for the June and December solstices respectively [3].

4.4 Passive cooling: ventilation

The effects of natural ventilation depending on availability were simulated using a fixed air change rate of 4.67 - derived from the fresh air requirement of 30m³/person/hour.

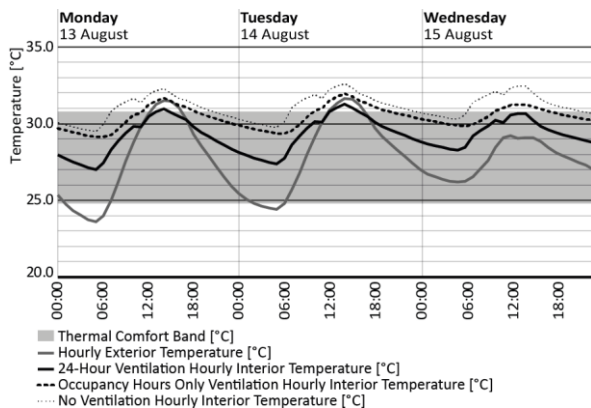


Figure 25: Effect of ventilation availability on operative temperature

The three cases tested are "No Ventilation" as a control, "Occupancy Hours Only Ventilation" that approximates closing windows during unoccupied hours for security, and "24-Hour Ventilation." The results of "24-Hour Ventilation" express the benefits of passively cooling the interior at night. Without solar and interior gains, cooling is maximised and the severity of tip-over into discomfort at mid-day is reduced. The "24-Hour Ventilation" case also demonstrated 68% in contrast to the 22% of "Occupancy Hours Only Ventilation" [3]. This result

states a need to provide ventilation openings separate from windows for daylight.

4.5 Choosing an appropriate material

The effects of timber and concrete construction on the thermal environment was simulated in EnergyPlus to determine the merits of the lightweight Gabaldon and the heavyweight DepEd standard.

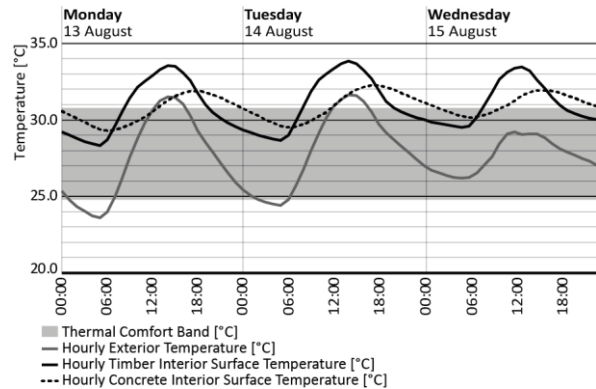


Figure 26: Interior surface temperatures of timber vs. concrete; both with 800mm overhang at Southern exterior

As EnergyPlus gives temperatures at the volume centroid, the difference between exterior air and interior surface temperatures was focused on.

The results show a 4-hour delay and 3K difference between the peaks of the interior surface temperature of concrete and the exterior air temperature. This contrasts with the near-synchronous rise and fall, 4K difference, and higher peak and valley deltas of timber construction. Since both behaviours have merit, both materials may be expressed in different contexts. That is, to use lightweight construction when the adjacent exterior condition is supported by a microclimate and to use heavyweight construction when the adjacent exterior is less malleable.

5. CLASSROOM DESIGN PROPOSAL

The proposal illustrated in Figures 14 and 15 applies preceding learnings on the reference volume.

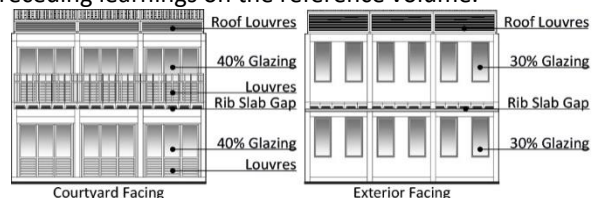


Figure 27: Elevations of classroom design proposal

The WWR of 30% and 40% reduce diffuse radiation while admitting enough daylight.

Louved timber walls on corridor-facing sides allow passive ventilation and coupling with a designed microclimate.

PLEA 2018 HONG KONG

Smart and Healthy within the 2-degree Limit

Shaded concrete walls on exterior-facing sides are protected from direct solar radiation and delay effects of uncontrollable exterior conditions.

A ribbed floor-slab reinterprets the vernacular use of a raised floor as a heat loss surface and creates additional inlets for ventilation without security drawbacks.

A louvred roof air cavity over a concrete slab both protects the first floor from solar radiation conducted through the ceiling and delays the effect of heat gains.

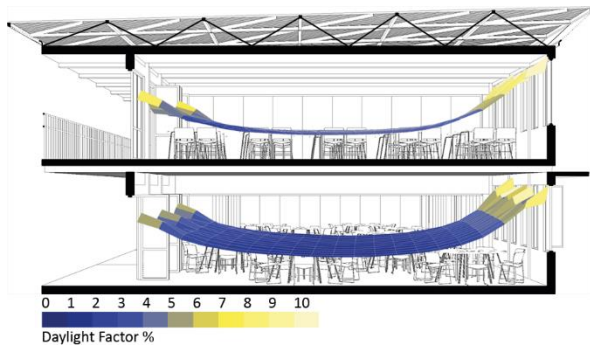


Figure 28: Daylight Factor simulation overlaid on section perspective of proposal

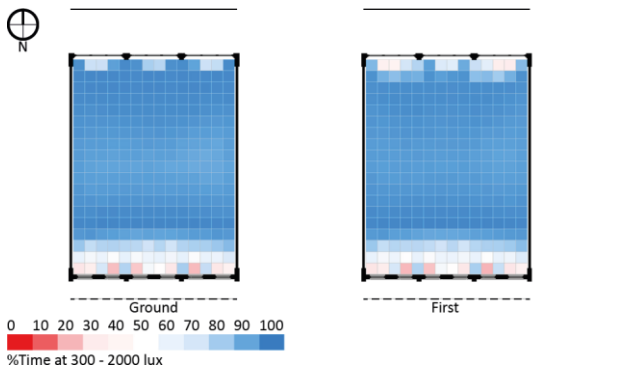


Figure 29: %Time daylight is between 300 - 2000 lux for ground and first floor of proposal

The daylight factor simulations in Figure 15 have a slightly steeper curvature than the data in Section 4, indicating lower daylight factors at the centre of the room. This is not necessarily a loss, as simulations in Figure 16 show a higher percentage time within the desired lux range and a shallower problem area at the Southern façade than the results in Section 4.

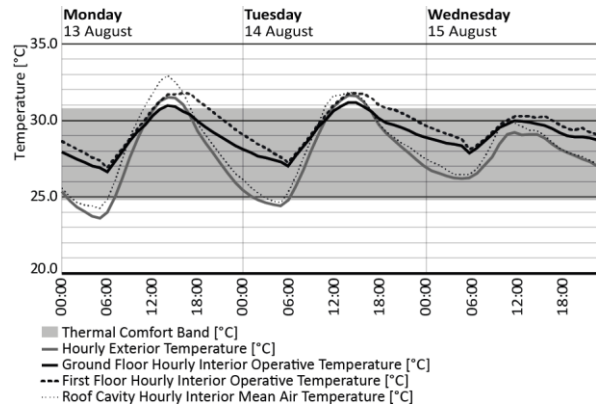


Figure 30: Excerpt of thermal simulations for final classroom design proposal representative of average days

Thermal simulation results in Figure 17, corroborate Section 4 and show the impact of ventilation and wind-exposure in bringing operative temperatures to comfortable levels. Materiality plays a role in the slower rise and fall of temperatures by delaying radiation through conduction.

By combining these effects with smaller apertures on shading devices on both exterior faces, the indoor operative temperatures can, at times, become lower than the exterior temperature as seen in the 0.5-1K cooler temperatures from 12:00 to 16:00 in the ground floor simulation results for 13 and 14 August. Simulated over a year, this results in 82% and 76% [3] of occupied hours being in comfort for the ground floor and first floor, respectively.

6. CONCLUSION AND RECOMMENDATION

Thermal performance is improved by reducing WWR, separating daylight openings from ventilation inlets, and selectively using thermal mass. Daylighting is balanced with thermal performance by optimising shading depths. The preceding research framework for new-build classrooms can be applied to refurbishment cases to further alleviate Manila's classroom shortage.

REFERENCES

1. Geronimo, G., (2017). *How DepEd plans to address PH classroom shortage*. [Online] Available: <https://www.rappler.com/nation/172372-deped-address-ph-classroom-shortage> [27 November 2017].
2. Philippines Department of Education, (2015). *Public Schools Enrolment SY 2015-2016*. [Online] Available: <http://www.deped.gov.ph/sites/default/files/datasets/2015/SY%202015-2016%20Public%20Schools%20Enrolment.xlsx> [14 May 2016].
3. Flores, J. (2017). *Design of an Educational Complex in Metro Manila* (Graduate dissertation). London: Architectural Association School of Architecture Graduate School Environment & Energy Studies Programme.
4. CIBSE. (2006). *CIBSE Guide A* (7th ed.). Norwich: Page Brothers.
5. Philippines Department of Education, (2011). *Guidelines for the Implementation of the 2011 Basic Educational Facilities Funds*. Pasig: Philippine Department of Education.

PLEA 2018 HONG KONG

Smart and Healthy within the 2-degree Limit

6. Walden, R., (2002). *Schools for the Future*. Washington: Hogrefe & Huber.
7. Koch-Nielsen, H. (2002). *Stay cool: a design guide for the built environment in hot climates*. New York: Earthscan
8. Lico, G., (2010). *Arkitekturang Filipino: A History of Architecture and Urbanism in the Philippines*. Quezon: University of the Philippines Press.
9. Yannas, S., (1994). *Design of Educational Buildings: Primer*. London: Architectural Association School of Architecture Graduate School Environment & Energy Studies Programme.
10. Baker, N. & Steemers, K., (2014). *Daylight Design of Buildings: A Handbook for Architects and Engineers*. Hoboken: Routledge.
11. Sargent, J., Niemasz, J. & Reinhart, C., (2011). *SHADERADE: Combining Rhinoceros and Energyplus for the Design of Static Exterior Shading Devices*. Sydney, s.n.

Physical Monitoring of Replacement Infill Panels for Historic Timber-Framed Buildings in the UK: Comparing hygrothermal simulations and dual climate chamber testing

CHRISTOPHER J. WHITMAN¹, ORIEL PRIZEMAN¹, JULIE GWILLIAM¹, ANDY SHEA², PETE WALKER²

¹Welsh School of Architecture, Cardiff University, Cardiff, UK

²Department of Architecture and Civil Engineering, University of Bath, Bath, UK

ABSTRACT: *With the aim of reducing carbon emissions and increasing hygrothermal comfort, buildings across the UK are undergoing energy retrofits. With historic buildings, it is important that retrofit actions have a limited negative impact on the building's fabric and cultural significance. Work to date in the UK has focused on the retrofit of historic solid masonry construction, with little research into the retrofit of historic timber-framed buildings. Changes to these buildings must be managed through the use of established conservation principles. However, where infill panels are beyond repair or have previously been substituted with inappropriate materials, there exists the potential to retrofit a material with a higher thermal performance. Nonetheless, it must be ensured that this retrofit does not create interstitial hygrothermal conditions that could threaten the survival of surrounding historic fabric. In this paper the authors present the hygrothermal simulation and physical monitoring of three different potential replacement infill panels. Results from Glaser calculations, WUFI® Pro and WUFI® 2D are compared to measured results of physical test panels mounted between two climate-controlled chambers. Whilst all three prediction methods successfully identified interstitial condensation where it was measured to occur, major discrepancies existed both between simulated and measured results, and between different simulation methods.*

KEYWORDS: *Timber-Framed, Hygrothermal simulation, Hygrothermal monitoring, Interstitial condensation, Retrofit*

1. INTRODUCTION

As we seek to improve the energy efficiency of our built heritage it is important that care is taken to minimise negative impacts and avoid damage to the building's significance, character and fabric [1]. A key consideration is the influence of thermal insulation on the hygrothermal performance of the external envelope, where increases in moisture content arising from interstitial condensation could adversely affect the pre-existing historic materials. Research in the UK has so far focused on the impact of insulation on solid masonry construction [2-4] with little investigation into the retrofit of the 68,000 historic timber-framed buildings which form an important part of Britain's cultural identity.

2. RETROFITTING HISTORIC TIMBER-FRAMED BUILDINGS IN THE UK

Historic timber-framed buildings in the UK consist of a structural timber frame with a solid infill. This is traditionally wattle-and-daub, a framework of thin timber members (wattlework) covered by an earthen render (daub). Other historic infills include lath and plaster and brick nogging [5]. Whilst some of these buildings are over clad with tiles, weatherboarding or continuous plaster, in many cases the timber frame is exposed both internally and externally (Fig.1&2).



Figure 1: Externally exposed timber frame. (Whitman, 2015)



Figure 2: Internally exposed timber frame. Whitman, 2015)

When retrofitting these buildings, in order to retain the aesthetics and character of the building, the exposed framing often precludes the use of internal or external wall insulation. This leads to problems created by the thermal bridging of the frame, potentially focusing interstitial condensation at the junction between the infill panel and the timber-frame. In addition, achieving a seal at this junction is often problematic, leading to issues with moisture ingress and poor airtightness. Work to any historic building in the UK should follow a set of ethical principles as set out by each of the four national governmental bodies related to heritage, Historic England [6], Cadw [7], Historic Environment Scotland [8] and the Northern Ireland Department for Communities, Historic Environment Division [9]. In general, it is expected that where possible, every effort will be made to retain existing historic fabric, and where replacement is required that this normally takes place on a "like-for-like" basis [ibid]. It is, however accepted that

PLEA 2018 HONG KONG

Smart and Healthy within the 2-degree Limit

this is not always possible or the best option. For example, where historic infill is beyond repair, has been replaced with inappropriate modern materials, or its removal is required to facilitate the repair of adjacent timbers, there exists the opportunity to retrofit an infill material with a higher thermal resistance [10]. Due to the need to maintain the vapour permeability of the panel, potential alternative infill materials include wood fibre, expanded cork, sheep's wool and hemp-lime. For this experiment the performance of traditional wattle-and-daub, expanded cork and a detail using wood fibre and wood wool as suggested by Historic England [11] were compared (Fig.3).

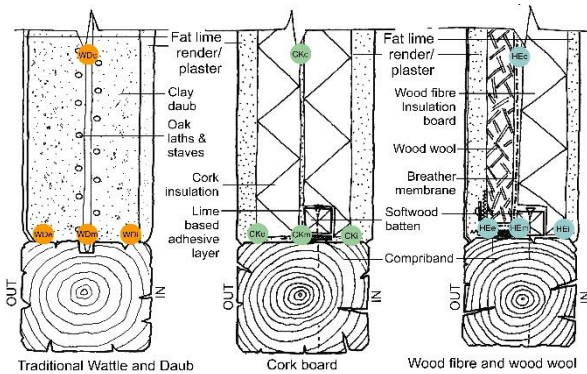


Figure 3. Detailed sections of three panel infill build-ups showing monitoring positions

3. METHODOLOGY

In order to physically measure the hygrothermal performance of these three details, three test infill panels 820mm x 820mm x 100mm (L x W x D) were constructed within oak frames constructed from reclaimed oak. The dimensions of the panels were dictated by the test facility, however a review of a representative sample of 100 surviving UK timber-framed buildings was undertaken to establish the average infill panel size for comparison (Fig.4).

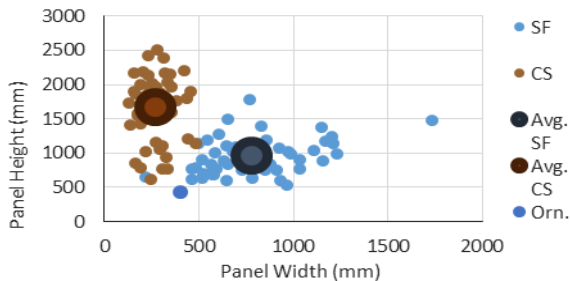


Figure 4. Dimensions of 100 representative sample infill panels. Square Framed (SF), Close Studded (CS), Ornamental (Orn).

This indicates that 53% were “square framed”, 46% “close studded” (tall rectangular panels) and 1% “ornamental”. The average dimensions of the square framed panels were 785mm x 950mm with a standard

deviation of ± 260 mm. As such, the test panels can be said to be typical in size.

The use of reclaimed oak was chosen for the frames following dynamic vapour sorption (DVS) testing of three oak samples felled during the 17th, 19th and 21st centuries. The results, measuring the vapour sorption profiles for each sample, showed that the older the timber the less moisture it absorbs (Fig.5).

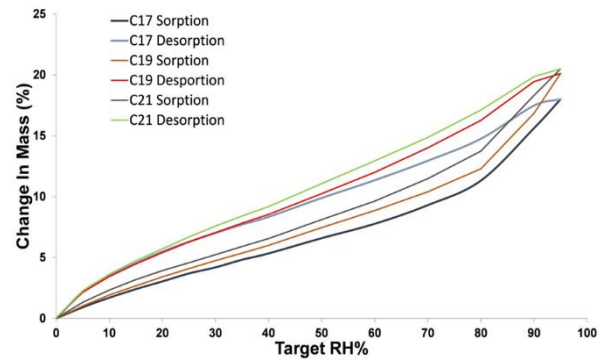


Figure 5. Sorption profiles for 3 samples of oak felled in different centuries.

Experimental testing took place at the University of Bath's Building Research Park using their Large Environmental Chambers. The three panels were mounted as part of a dividing wall between the two climate-controlled chambers (Figs.6&7).

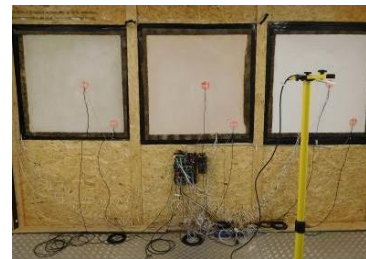


Figure 6. Panels in climate chamber. View from “internal” chamber.



Figure 7. Dual climate chamber

Temperature ($^{\circ}\text{C}$) and moisture content (%) were monitored in four positions within each panel, one in the centre of the panel at a depth of 50mm and three in the centre of the lower timber frame at a depth of 10mm, 50mm and 90mm (Fig.3). The temperature was measured using type-T thermocouples (range -75°C to $+250^{\circ}\text{C}$, accuracy $\pm 0.5^{\circ}\text{C}$) connected to a Campbell Scientific CR1000 data logger. The moisture content was measured using electrical resistance. For each monitoring position, copper wires were attached to two stainless steel screws, inserted in the oak frame, placed 20mm apart, parallel to the wood grain. The copper wires were connected back to a Campbell Scientific CR1000 data logger measuring resistance, wired and programmed according to advice provided by Historic England [12], originally developed by Dr Paul Baker of

PLEA 2018 HONG KONG

Smart and Healthy within the 2-degree Limit

Glasgow Caledonian University. This method was selected due to the potential for continuous measurements and the small size of the wire/screw arrangement, thereby limiting the influence of the sensor on the wall's performance. The wiring for both electrical resistance and temperature measurements was also routed to minimise the creation of any direct paths for hygrothermal movement.

In addition, the dry-bulb air temperature (°C) and relative humidity (%) of each climate chamber were monitored with Campbell Scientific CS215 RHT probes (range- 0 to 100% RH, -40°C to +70°C, accuracy ±2% RH, ±0.4°C). Concurrently, in situ U-value measurements were undertaken in accordance with BS ISO 9869-1 [13]. These measurements were taken in two monitoring positions per panel, one close to the centre (offset from the interstitial monitoring position to avoid interference) and 100mm from a corner to assess the edge effect from the timber frame. Measurements were made using Hukseflux HFP01 heat flux plates and type-T thermocouples connected to a Campbell Scientific CR1000 data logger with readings taken at 5-minute intervals.

To determine the set temperature and relative humidity of the test chamber, Glaser calculations were undertaken in accordance with BS EN ISO 13788:2012 [14]. These calculations plot the vapour pressure against the saturation vapour pressure, across the thickness of the panel build-up under steady-state conditions and constant heat transfer. Where the vapour pressure touches or crosses the saturation vapour pressure, interstitial condensation is deemed to occur. The results of these calculations showed that with internal conditions of 21°C/70% RH and external of 5°C/80% RH, interstitial condensation would occur within the wood fibre panel, and the wattle-and-daub would see an increase in moisture towards its inner face. Conditions would have to be increased to 90% RH, internally and externally, to produce any increase in moisture content within the cork panel. Although subsequently modified, at the time of testing prolonged operation of the climate chamber at 90% RH was not possible due to technical constraints. Therefore, the set points of 21°C/70% RH for the internal chamber and 5°C/80% RH for the external chamber were used for the experiment.

Following 3 weeks of monitoring, the datasets were downloaded and analysed. The measured hygrothermal conditions within the two climate chambers were then used to simulate the interstitial hygrothermal performance of the panels using WUFI® Pro 5.3 (one dimensional hygrothermal movement) and WUFI® 2D (two dimensional). All material data used in the simulations was taken from the Fraunhofer materials database provided with the software. There is therefore a degree of error with the use of this material data, as it is data measured on German materials which may differ

from the UK materials used in the construction of the test panels. This constraint is however unavoidable due to the lack of adequate data for UK building materials, especially those in historic buildings.

3. RESULTS

3.1 Thermal Performance

Table 1: Measured and calculated U-values

Panel type	Centre (W/m ² K)	Corner (W/m ² K)	Calculated (W/m ² K)
Wattle-and-daub	2.72	2.10	2.85
Cork	0.49	0.47	0.45
Wood fibre	0.59	0.60	0.63

The results of the in situ U-value monitoring are presented in Table 1 along with the values calculated according to BS EN ISO 6946:2007 [15]. A positive edge effect is seen for the wattle-and-daub due to the thermal conductivity of the oak frame being lower than the panel. A negative edge effect is seen for the wood fibre as the infill has a lower thermal conductivity than the frame. The positive edge effect for the cork was not expected, however thermography showed this was due to a horizontal central joint in the cork panel reducing the thermal performance at the central measuring location. Overall the cork had the best thermal performance.

3.2 Interstitial Moisture Content

The results of the Glaser calculation, the WUFI® Pro 5.3 and WUFI® 2D simulations and the interstitial moisture content measured in the test panels were compared and are presented in Table 2.

Table 2: Moisture content as measured and simulated. Increase (↑), slight increase (↗), decrease (↓), slight decrease (↘) and steady (→). Key findings highlighted in red.

Infill	Loc.	Glaser	WUFI® Pro5.3	WUFI® 2D 3.3	Measured	Agreement
Wattle and Daub	Ext.	→	↓	↓	↑	✗
	Cen.	→	↗	↗	→	✓
	Int.	↑	↑	↑	↗	✓
Cork	Ext.	→	↗	↓	↑	✗
	Cen.	→	→	→	→	✓
	Int.	→	↘	↑	→	✗
Wood fibre	Ext.	→	↗	↓	↑	✗
	Cen.	↑	↑	↑	↑	✓
	Int.	→	↓	↑	↓	✗

Table 2 indicates if the moisture content increased, decreased or remained steady throughout the duration of the test/simulation period for each of the prediction methods, compared to the measured results. The final column of the table indicates if there was found to be agreement between the simulated and measured results

PLEA 2018 HONG KONG

Smart and Healthy within the 2-degree Limit

for each monitoring location. The results demonstrate that there was agreement between simulations and measurements for four of the nine monitoring positions (44%). Most importantly, the measured rise in moisture content in the centre of the wood fibre panel, arising from interstitial condensation, was successfully identified by all three prediction techniques. However these failed to foresee the measured rise in moisture content in each of three external lime renders. Equally there can be seen to be contradictions between results generated by the two versions of WUFI®. Further research is required to investigate the reason for these discrepancies.

None of the simulation techniques nor the measured data showed any suggestion of interstitial condensation within the cork infill panel. Coupled with the superior thermal performance of this detail, these results would suggest that this potentially could be a good retrofit solution.

4. CONCLUSION

The results show that for steady state conditions the simulations successfully anticipated interstitial condensation where it occurred, however increases in moisture content towards the external face of all three panels were not predicted.

Overall the cork infill detail performed the best, with the greatest thermal performance and no interstitial condensation being identified. It should however be noted that these results are all for forced steady-state conditions that are unlikely to exist in real life. Dynamic cyclic testing on the same panels has since been undertaken and funding for a longer term monitoring programme with real climatic conditions is currently being sought.

ACKNOWLEDGEMENTS

The work presented in this paper has been made possible by the Association for Preservation Technology's Martin Weaver Scholarship, in addition to the help of Royston Davies Conservation Builders and Ty Mawr Lime Ltd.

REFERENCES

Historic England. (2012). *Energy Efficiency and Historic Buildings: Application of Part L to historic and traditionally constructed buildings* (Revised 2012). p.4.

Gandhi, K. Jiang, S. & Tweed, C (2012). *Field Testing of Existing Stone Wall in North Wales Climate. SusRef: Sustainable Refurbishment of Building Facades and External Walls*. Cardiff University.

Rye, C., Scott, C. & Hubbard, D. (2012). *The SPAB Research Report 1. U-Value Report*. Revision 2 ed.: Society for the Protection of Ancient Buildings.

Baker, P. (2015). *Hygrothermal Modelling of Ditherington Flax Mill*. Research Report Series. Historic England.

Harris, R. (2010). *Discovering Timber-Framed Buildings*, Oxford, UK, Shire Publications. p.20

Historic England (2008). *Conservation Principles: Policies and Guidance for the Sustainable Management of the Historic Environment*. Historic England. p.52

Cadw (2011). *Conservation Principles for the Sustainable Management of the Historic Environment in Wales*. Cadw. p.24

Historic Environment Scotland (2016). *Historic Environment Scotland Policy Statement*. Historic Environment Scotland. p.9

Historic Environment Division (2017). *Historic Environment Fund Repair Stream*. Northern Ireland Department for Communities. p.15

Ogley, P. (2010). *Insulating timber-framed walls*, London, English Heritage.

McCaig, I. & Ridout, B. (2012). *English Heritage practical building conservation- Timber*, London; Farnham, Surrey; Burlington, VT, English Heritage; Ashgate.

McCaig, I. (2016). *RE: CR1000 Data logger programme*. Personal email to Whitman, C.

British Standards Institution (2014). *BS ISO 9869-1:2014 Thermal insulation- Building elements- in situ measurement of thermal resistance and thermal transmittance Part 1: Heat flow meter method*. London: BSI.

British Standards Institution (2012). *BS EN ISO 13788:2012 Hygrothermal performance of building components and building elements - Internal surface temperature to avoid critical surface humidity and interstitial condensation - Calculation methods*. London: BSI.

British Standards Institution (2007). *BS EN ISO 6946:2007 Building components and building elements — Thermal resistance and thermal transmittance — Calculation method*. London: BSI.

Embodied Carbon Benefits of Reusing Structural Components in the Built Environment: A Medium-rise Office Building Case Study

CATHERINE DE WOLF¹, JAN BRÜTTING¹, CORENTIN FIVET¹

¹Structural Xploration Lab, Swiss Federal Institute of Technology (EPFL), Lausanne

ABSTRACT: This paper provides parametric estimates of embodied carbon reductions when structural components are reused in a typical office building. First, a lower bound of structural material quantities is estimated for a typical steel frame structure in a low-rise office building. The embodied carbon of this conventional design is then compared with values collected from a series of similar existing steel buildings (deQo database) as benchmark. Various scenarios regarding the impact of selective deconstruction, transportation, and cross-section oversizing are modelled and parameterized. The study eventually computes carbon savings over one life cycle of the building project. Results show that reuse remains beneficial for long transport and high oversizing. The discussion calls for more comprehensive studies and refined metrics for quantifying selective deconstruction.

KEYWORDS: Embodied carbon, Reuse, Circular Economy, Office Building, Steel

INTRODUCTION

Embodied carbon and waste

The Intergovernmental Panel on Climate Change recommends that the building sector becomes zero carbon by 2050 in order to meet the Paris Climate Agreement [0,0] and to avoid extreme climate catastrophes. The whole life greenhouse gas (GHG) emissions expressed in carbon dioxide equivalent (CO₂e) and shortened as “carbon” in this paper, include both, operational and embodied carbon of buildings.

Operational carbon relates to GHG emissions during the use phase of the building, which includes heating, cooling, ventilation, lighting, and equipment.

Embodied carbon refers to GHG emissions during all other life cycle phases: material extraction, component production, transport, construction, maintenance, and demolition.

Recent technical standards and political initiatives have successfully reduced the operational carbon of buildings. However, significant improvements are still required to lower the embodied carbon of new buildings.

Besides, up to 50 % of material use in Europe is related to the built environment [0, 0], which generally constitutes the most resource intensive sector in many industrialized countries [0]. In addition, more than 30 % of the waste generated in Europe originates from the construction sector [0-0]. From these observations, it follows that the design and construction of buildings and infrastructures could be improved by making a more efficient use of materials.

Load bearing systems, because of their high material mass and energy intensive production, are currently responsible for the biggest portion of embodied carbon emissions and waste production in buildings [0]. Structural engineers have therefore a responsibility to reduce the environmental impact of buildings.

Circular economy and reuse

A potential path to increased sustainability of building structures is the integration of circular economy principles in the structural design. Circular economy, a concept originally introduced by architect and economist Walter Stahel [0], advocates a closed loop flow of materials and components in order to extend their service life [0]. The European Commission considers that circular economy would boost competitiveness, innovation, local employment, business opportunities, and social integration and cohesion while protecting against shortage of resources, volatile prices, and air, soil and water pollution [0]. Circular economy involves five strategies: reduce, repair, reuse, recycle, and recover energy. Most sources, including the European Union [0], prioritize them in the same sequence, i.e. reduce must take precedence over repair, repair over reuse, reuse over recycling, and recycling over energy recovering. Although academic literature evolves to bring circular economy into the building sector, its application in building practice remains difficult due to a number of economic, cultural and technological reasons, the description of which is out of scope for this paper. In light of the urgent need to reduce material waste and embodied carbon in the construction sector, this project explores the opportunities of redefining materials value chains through circular economy.

In particular, the reuse of structural elements is a promising strategy that is still scarcely studied. Contrary to recycling which requires energy to process material, e.g. to remelt steel, reuse extends the service life of components while limiting their physical transformation and changing their location and/or function. Reusable structural components may consequently have a longer service life than the systems to which they initially belong. Disassembled buildings become a mine for new constructions, and functional obsolescence is not a reason for waste production anymore.

Problem statement

The industry is currently lacking benchmarks to assess the beneficial impact of structural reuse. This paper therefore provides a first answer to the following question. How would

PLEA 2018 HONG KONG

Smart and Healthy within the 2-degree Limit

the reuse of structural components be beneficial for reducing the environmental impact of office buildings and to what extents? In particular how impactful are design parameters that typically arise when considering reuse strategies, e.g. material transportation, cross-section oversizing, and selective deconstruction?

METHODOLOGY

The load bearing system of a steel frame five-story high office building is used as a case study. This building typology is commonly found in urban areas where land pressures and therefore demolition and transformation rates are high. The chosen building typology also fits within the available benchmarks (see section 2.1) for medium-rise steel office buildings. First, buildings of similar construction type, i.e. steel constructions with four to six stories, are selected from an industry-collected database. The embodied carbon of those buildings is analysed and defines the *benchmark*. This benchmark is then used to relate the case study to the existing practice. Second, the design of the case study is analysed and serves as the *baseline* of minimally required material quantities and embodied carbon related to its conventional construction. Third, embodied savings due to the reuse of steel structural components in the studied design are assessed. For various assumptions of cross-section oversizing, the savings are parametrically studied as a function of the impact related to selective deconstruction and transportation.

In total three scenarios are compared:

Benchmark of existing buildings: the lower bound of the industry-collected office buildings;

Baseline for a conventional office building: the new construction of a typical steel-framed office;

Reuse design cases: parametric analyses of buildings reusing steel components from other, obsolete buildings. This original methodology can be used to explore and compare more complex reuse scenarios or other case studies.

Benchmark of existing buildings

Benchmarking embodied carbon in structural systems of buildings has been historically challenging due to uncertainty and unavailability of data and due to the difficult comparability of buildings as complex entities [0]. Leading structural engineering firms have developed in-house databases to start benchmarking their own projects [0-0]. The Waste & Resources Action Programme (WRAP) initiated the collection of whole building life cycle assessment (LCA) results from industry, but only the end results of embodied carbon calculations were collected, leading to a lack of transparency [0]. In comparison, the *database of embodied Quantity outputs* (deQo, available at <http://deqo.mit.edu>) collects both embodied carbon coefficients (ECCs) and structural material quantities (SMQs) in recent constructions, which offers a greater degree of transparency to the users [0]. The process starts by extracting mass and volume of used materials from the bill of quantities or from building information models (BIM), shared by global structural design firms [0,0]. The Carbon Leadership Forum used the deQo data and other industry-collected databases and case studies to create the first benchmarks for embodied carbon in buildings [0-0].

The ECCs (expressed in $\text{kg}_{\text{CO}_2\text{e}}/\text{kg}$) of the considered materials are then used to calculate the total embodied carbon of existing buildings, as shown in the following equation:

$$\text{Embodied Carbon}_{\text{building}} = \sum_{m=1}^M \sum_{l=1}^L \text{SMQ}_i \times \text{ECC}_i$$

where:

m is a particular material or component in the building $m = 1, 2, 3, \dots, M$;

l is the number of replacements within the lifespan of the building for each material

$l = 1, 2, 3, \dots, L$;

SMQ are Structural Material Quantities (kg);

ECC are the corresponding Embodied Carbon Coefficients ($\text{kg}_{\text{CO}_2\text{e}}/\text{kg}$)

Results from this data collection are evaluated and presented in boxplots. Figure 1 summarizes structural material quantities for all stored buildings with four to six stories and with steel as the main structural material. The SMQs are normalized by gross floor area. The diagram is divided into buildings with small gross floor area (up to $10'000 \text{ m}^2$) and big gross floor area (more than $10'000 \text{ m}^2$). The thick line inside the grey box of the boxplot reports the median value, whereas the boundary of the box indicates the inner quartiles. Whiskers represent the minimum and maximum values.

Figure 2 similarly indicates the corresponding embodied carbon, normalized per gross floor area. What is considered in the material quantities and embodied carbon results shown in Figures 1 and 2 are the impacts related to the manufacturing and construction of the structural steel system, but also to slabs, connections, load-bearing walls included in the basement, a base plate, and foundations.

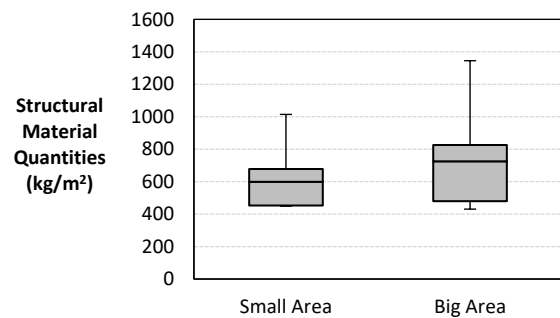


Figure 1: Structural material quantities of 23 existing steel buildings with four to six stories.

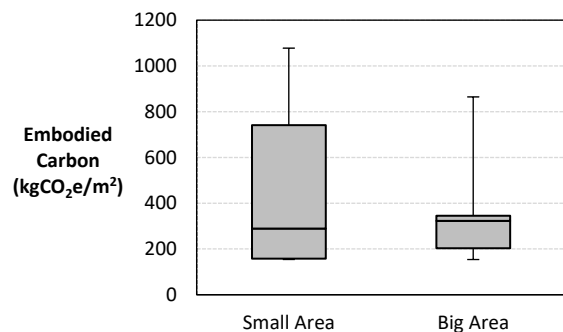


Figure 2: Embodied carbon of 23 existing steel structures with four to six stories.

PLEA 2018 HONG KONG

Smart and Healthy within the 2-degree Limit

To be comparable with the case study building introduced in the next sub-section, this subset of all deQo projects results from a query of similar structural systems, materials, and number of floors. From the hundreds of buildings in deQo, 23 entries currently correspond to the criteria aligned with these constraints.

Baseline building

To evaluate the environmental benefits of reusing structural components, the main structure of a baseline building is designed as a case study. The building is composed of a steel frame with steel columns and a grid of primary and secondary steel beams supporting prefabricated concrete slab elements. The conventional construction of this structural system is compared parametrically with scenarios where steel elements are reused from one or more dismantled buildings (see next subsection). The baseline building has a width of 32 m, a length of 60 m and a height of 17.5 m. The building has five stories, a story height of 3.50 m, ten bays in the length direction with a column spacing of 6.00 m, and four bays in the width direction with a column spacing of 8.00 m. A schematic view of the structural skeleton is shown on Figure 3.

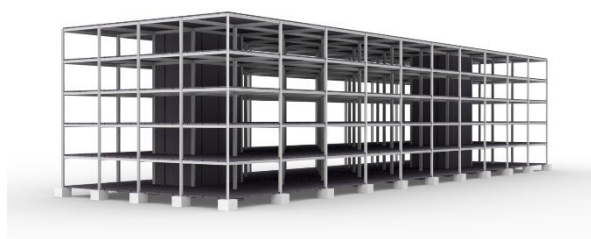


Figure 3: Schematic view of the case study structural system.

Dead load of the slab elements as well as a superimposed dead load of 2.0 kN/m² and a (conservative) life load of 5.0 kN/m² are considered. These assumptions are used to size the baseline structure from standard I-sections at ultimate limit state including standard safety factors. The general strategy for sizing is to utilize cross section capacities in the best way possible.

A life cycle assessment is performed to quantify the corresponding embodied carbon of the main structural elements. For the purpose of this study, an ECC for the production of new steel, including a typical recycled content, equal to 1.10 kg_{CO_{2e}}/kg and an ECC of reinforced concrete equal to 0.15 kg_{CO_{2e}}/kg are used. These values are averages derived from the Inventory of Carbon and Energy [0], GaBi [24], Athena [25], and EcoInvent [26], evaluated in [0]. In addition to production, impacts related to the transport of elements over 110 km to the building site are considered. The transport emissions of 0.36 kg_{CO_{2e}}/(t·km) are obtained from [27] for typical road freights. The overall embodied carbon for a conventional construction of the baseline building (including the new production of steel elements) is 140 kg_{CO_{2e}}/m² of which 39 kg_{CO_{2e}}/m² are due to the steel elements, while 72 kg_{CO_{2e}}/m² are caused by the slabs and base plate. The embodied carbon of the foundations, here assumed as 22.5 kg_{CO_{2e}}/m², varies however greatly in practice depending on soil properties [0].

Reuse design cases

On the one hand, reuse avoids sourcing raw materials and requires little energy for reprocessing. On the other hand, reuse requires energy during the selective deconstruction of obsolete

buildings as well as for transport, refurbishment and storage. In the studies of this paper, we only consider the reuse of load-bearing components.

To design a structure based on an available stock of reclaimed elements means that a-priori given geometric and mechanical properties of components might lead to a non-optimal capacity utilization of available elements that counteracts the potential savings through reuse [0-0]. Reused structural elements are ultimately oversized. Few quantifications of finally achieved benefits exist. Through a parametric case study, this research evaluates how much embodied carbon can be saved through the reuse of structural elements compared to a conventional construction.

Embodied carbon comparison

The embodied carbon of the conventional baseline structure is compared to the case where the same structure is made from reused steel elements. A parametric study analyses the sensitivity of environmental savings through reuse for two key parameters: selective deconstruction and transport related carbon emissions.

The total building material quantities of the case study building include the steel frame, the reinforced concrete slab elements, a base plate, elevation cores and foundations. The material quantities and embodied carbon associated with all non-steel elements are kept constant in the parametric study and are equal for both conventional baseline and reuse scenarios. The parametric study only focuses on the reuse of the structural steel elements. The quantities of all concrete elements are here included in order to allow a comparison of the baseline and reuse design cases to the buildings extracted from the deQo database. Connections, bracing systems, and secondary structure were not considered in this preliminary design, such that the resulting material quantities and embodied carbon will be on the lower bound of the case studies reported in deQo.

Figure 4 summarizes the steps considered for the LCA of the different reuse scenarios. It is assumed that the steel elements are reclaimed from obsolete buildings through selective deconstruction. This process includes the opening of connections as well as the hoisting of elements with a crane. A corresponding impact of 0.267 kg_{CO_{2e}}/kg is reported in [0], which is based on a review of data provided by Athena in [30]. In the parametric study, this value is varied between 0.0 kg_{CO_{2e}}/kg and 1.0 kg_{CO_{2e}}/kg to account for the uncertainty of this data.

The transport distances are the second parameter analysed in the parametric study. Transport distances between 0 and 500 km from the deconstruction site over the fabrication site to the building site are considered.

The last parameter that is analysed is the cross-section oversizing of the structural steel elements. Indeed, when structural elements from an obsolete building are reused in a new configuration, not all elements can be used at a utilization level as high as in the original configuration. Among other reasons, this is due to the unavailability of desired cross sections [0]. It is therefore assumed that material quantities in reuse scenarios are 'oversized' compared to the conventional case where cross sections are selected with optimal size. The extra steel mass is parametrically varied between additional 0 to 50 % of the material quantities used in the baseline building.

PLEA 2018 HONG KONG

Smart and Healthy within the 2-degree Limit

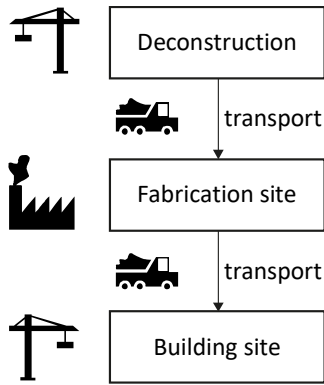


Figure 4: Diagram representing the impacts of reuse

RESULTS

Influence of transport

Figure 5 illustrates the influence of transportation distances on the embodied carbon of the reuse design cases. The considered oversizing of steel element mass is expressed in 10 % steps by the corresponding grey lines. In addition, Figure 5 shows the lower bound benchmark, i.e. the first quartile (Q1) of collected low area steel buildings (section 3) as well as the embodied carbon of the conventional baseline building. It is visible that even with 50 % oversized steel element sections and a transport distance of 500 km, the embodied carbon of the reuse design case does not exceed that of the conventional load bearing system. These results indicate that longer transport distances are acceptable in order to facilitate the supply of reclaimed steel elements. Only when considering transport distances over 2000 km and an oversize ratio of 25 % the embodied carbon of the reuse case would exceed that of the baseline case.

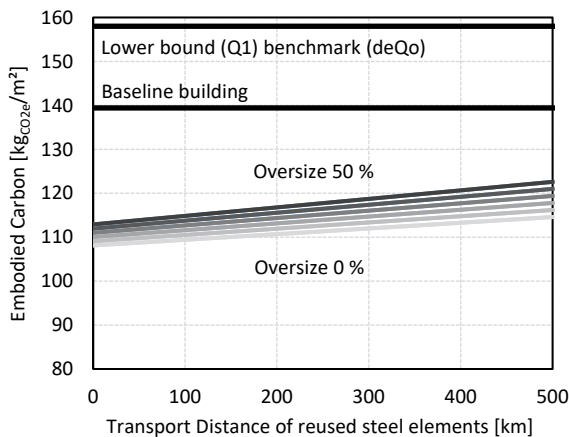


Figure 5: Embodied carbon of benchmark lower bound, baseline and reuse design cases for varying transport distances and oversize percentages.

Influence of selective deconstruction

Figure 6 shows the influence of selective deconstruction related carbon emissions on the total embodied carbon of the load bearing system made from reused elements. Again, grey lines indicate the considered percentage of element oversizing. The reference ECC of 0.267 kgCO_{2e}/kg for selective deconstruction obtained from [0] is also indicated. The results show that embodied carbon of reuse design cases only exceed the

embodied carbon of the baseline building when elements are oversized and impacts of the selective deconstruction are unexpectedly high. As introduced before, the reference impact of new steel production is 1.1 kgCO_{2e}/kg.

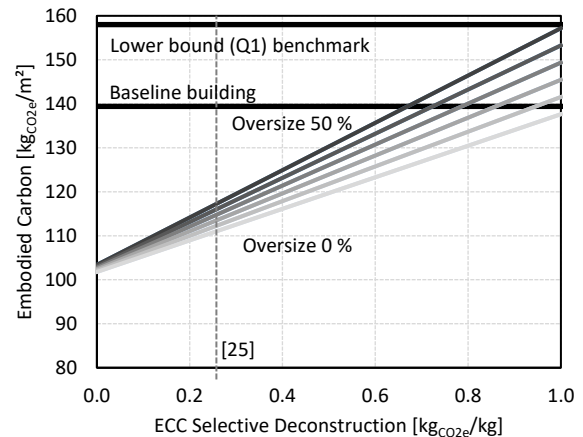


Figure 6: Embodied carbon of benchmarked lower bound, baseline and reuse design cases for varying selective deconstruction values and oversize percentages.

In general, the obtained results show that when oversizing and emissions spent for transport and selective deconstruction are low, the benefits of structural reuse are significant. The potential savings in greenhouse gas emissions through reuse relatively to the baseline conventional building can be up to 20 % when considering the reference impacts for selective deconstruction, a transport distance of 300 km and only 25 % oversizing.

DISCUSSION AND CONCLUSION

This paper presents the study of a structural system for an office building realised with new steel elements and with reused structural elements. The embodied impact of the building is computed parametrically and compared to data collected industry-wide.

Results show that for this case study embodied carbon savings of 20 % can be obtained by designing with reused structural elements. It should be noted that the parametric study is only applied to the steel structural skeleton. The foundation, core and slabs are kept at a constant amount of materials. It is assumed that the same concrete quality was used in all concrete elements and the same steel quality in all steel elements for simplicity of the modelling. In addition, impacts of new connections, bracing system and secondary structure are not taken into account. Further research should give separate coefficients for slabs, foundations, cores, connections, and bracing elements. However, as these values are kept constant in this case study, they do not influence the relative comparison of results.

The embodied carbon savings would be even higher if the prefabricated concrete slabs could be equally reused. Indeed, the slabs contributed about half of the total embodied carbon in the baseline building. This confirms previous findings [0] that slabs are the structural elements with the highest environmental impacts in typical building structures.

Results show that reuse remains beneficial even when transport distances, selective deconstruction related

PLEA 2018 HONG KONG

Smart and Healthy within the 2-degree Limit

impacts, and oversizing are relatively high. Only when selective deconstruction and oversizing are both much higher than expected, the impacts exceed those of a conventional new construction. Impacts due to selective deconstruction are currently computed as ratios of structural mass, it therefore depends on the oversizing. In practice, however, it may be assumed that selective deconstruction is much more related to the complexity of the disassembly process than the weight of the system. Future studies should therefore include ECCs for selective deconstruction that are not directly dependent on mass.

In future research, different scenarios will also include the impacts calculated over multiple life spans, with the functional unit being one service life. Such scenarios would account for material degradation more precisely. The parametric study should also be extended to concrete elements and should address serviceability constraints. Further, an optimization of the utilization of available stock elements would allow the reduction of oversizing and allow an informed design processes. In this paper, refurbishment, storage, new connections, and remaining structural capacity are neglected. Future work can expand on including the impacts related to these aspects.

ACKNOWLEDGEMENTS

This project has received funding from the European Union's Horizon 2020 research and innovation programme under the Marie Skłodowska-Curie grant agreement No. 665667 and from the Swiss Government Excellence Scholarship.

REFERENCES

IPCC (2014) "Climate Change 2014: Synthesis Report. Contribution of Working Groups I, II and III to the Fifth Assessment Report of the Intergovernmental Panel on Climate Change." Synthesis Report, Geneva, Switzerland: Intergovernmental Panel on Climate Change.

UNFCCC (2015) "Adoption of the Paris agreement. Proposal by the President. Draft decision -/CP.21" United Nations Framework Convention on Climate Change, December 2015.

Herczeg, M. et al. (2014) "Resource efficiency in the building sector." Final Report, Rotterdam: European Commission, DG Environment.

BIO Intelligence Service (2013) "Sectoral Resource Maps." Prepared in response to an Information Hub request, European Commission, DG Environment.

EEA (2010) "Material Resources and Waste - The European environment State and outlook." Luxembourg: Publications Office of the European Union.

Eurostat (2018) Waste statistics, 2018-2-15, from: http://ec.europa.eu/eurostat/statistics-explained/index.php/Waste_statistics

Pérez-Lombard, L., Ortiz, J., and Pout, C. (2008) A review on buildings energy consumption information, *Energy and buildings*, 40(3), 394-398.

Allwood, J. M. and Cullen, J. M. (2012) *Sustainable materials - with both eyes open*, Cambridge: UIT Cambridge.

De Wolf, C. (2017) "Low Carbon Pathways for Structural Design. Embodied Life Cycle Impacts of Building Structures." PhD thesis MIT.

Stahel, W. R. and Reday-Mulvey, G. (1981) *Jobs for tomorrow: the potential for substituting manpower for energy*. University of California: Vantage Press.

McDonough, W. and Braungart, M. (2010) *Cradle to cradle: Remaking the way we make things*. New York: North Point Press.

European Commission (2015) "Closing the loop - An EU action plan for the Circular Economy." Report, Brussels.

European Union (2008) Directive 2008/98EC - Waste Framework Directive.

De Wolf, C., Droguett, B.R., and Simonen, K. (2017) "Counting Carbon: What We Know and How We Know It," from King, B. (ed.), *The New Carbon Architecture*, New Society Publishers.

Kaethner, S. and Burridge, J. (2012) Embodied CO2 of structural frames, *The Structural Engineer*, 90(5), 33-40.

Project Embodied Carbon and Energy (PECD), led by Arup in 2012.

Thornton Tomasetti (2018) Embodied Carbon and Energy Efficiency Tool, from: core.thorntontomasetti.com/embodied-carbon-efficiency-tool/

WRAP (2017) Embodied Carbon Database (ECDB), Waste & Resources Action Programme, from: ecdb.wrap.org.uk

Database of embodied Quantity outputs (deQo) (2018) from: deqo.mit.edu

Simonen, K., Rodriguez, B.X., McDade, E., and Strain, L. (2017a) Embodied Carbon Benchmark Study: LCA for Low Carbon Construction, from: <http://hdl.handle.net/1773/38017>.

Simonen, K., Rodriguez, B.X., Barrera, S., and Huang, M., (2017b) CLF Embodied Carbon Benchmark Database, from: <http://hdl.handle.net/1773/38017>.

Simonen, K., Rodriguez, B.X., and Li, S. (2017c) CLF Embodied Carbon Benchmark Data Visualization, website, from: www.carbonleadershipforum.org/data-visualization/

Hammond, G., and Jones, C. (2011) Inventory of Carbon and Energy (ICE), Version 1.6a. Sustainable Energy Research Team (SERT), Department of Mechanical Engineering. Bath, UK: University of Bath.

GaBi PE International (2018) GaBi 4 extension database III: steel module and GaBi 4 extension database XIV: construction materials module, from: www.gabi-software.com

Athena Sustainable Materials Institute (2009) Impact Estimator for Buildings, from www.athenasmi.org.

EcoInvent (2018) Swiss Centre for Life Cycle Inventories, from: <http://www.ecoinvent.ch>

Department for Environment Food & Rural Affairs (DEFRA) (2018) Government conversion factors for company reporting, from www.ukconversionfactorscarbonsmart.co.uk

Pratt, Q. (2016) Material quantities of foundation systems in building structures, Master thesis, MIT.

Brütting, J., Senatore, G., and Fivet, C. (2018) Optimization Formulations for the Design of Low Embodied Energy Structures Made from Reused Elements, *Advanced Computing Strategies for Engineering*, under review.

Brütting, J.; Desruelle, J.; Senatore, G., and Fivet C. (2018) Optimum Truss Design with Reused Stock Elements, *Proceedings of the IASS Symposium 2018*, MIT, Boston, Massachusetts, USA, July 16-20, 2018.

PLEA 2018 HONG KONG

Smart and Healthy within the 2-degree Limit

Athena Institute (1997) Demolition energy analysis of office building structural systems. The Athena Sustainable Materials Institute, Ottawa.

De Wolf, C., Ramage, M., and Ochsendorf, J. (2016) Low carbon vaulted masonry structures, *Journal of the International Association for Shell and Spatial Structures*, 57(4), December n. 190, 275-284.

Findings from a Survey on the Current Use of Life-Cycle Assessment in Building Design

THOMAS JUSSSELME^{1,3}, EMMANUEL REY², MARILYNE ANDERSEN^{1,3}

¹Building 2050 Research Group, Ecole Polytechnique Fédérale de Lausanne (EPFL), Fribourg, Switzerland

²Laboratory of Architecture and Sustainable Technologies (LAST), School of Architecture, Civil and Environmental Engineering (ENAC), Ecole Polytechnique Fédérale de Lausanne (EPFL), Lausanne, Switzerland

³Laboratory of Integrated Performance In Design (LIPID), School of Architecture, Civil and Environmental Engineering (ENAC), Ecole Polytechnique Fédérale de Lausanne (EPFL), Lausanne, Switzerland

ABSTRACT: The built environment is facing environmental regulations more ambitious than ever before. In Europe, a law will lead all new buildings to the Nearly Zero-Energy performance level. However, even if a building does not have any energy consumption for its operation phase, it still has embodied impacts. To that end, Life-Cycle Assessment (LCA) methods have been developed and improved since the 1960s. However, LCAs are still not used as a standard practice among the architecture, engineering and construction industry. This study aims to discover the reasons for the low use of life-cycle performance approaches thanks to a web survey targeting practitioners, and to formulate key recommendations to improve their usability. This research reveals the low penetration rate of LCA software among building designers due to their limited efficiency within the design context. The main reasons for this situation are the cost of use, too heavy for the early design stage constraints, and the functionality, which is limited to the environmental assessment. Indeed, practitioners expect much more design support functionalities (multi-criteria approach, exploration mode, etc.). The survey findings aim to support the usability improvement of new LCA-based methods and the research and development of new tools at early design stages.

KEYWORDS: Life-cycle performance assessment, Survey, Practitioners, Software, Europe

INTRODUCTION

The built environment is one of the major contributors to climate change. Since the 1970s and its energy crises, countries have set up regulations to decrease the operative energy consumption of buildings. Their performance targets have been strengthened over the years, and the next generation of regulations will lead to generalizing Nearly Zero-Energy Buildings (NZEB) in 2020 within the European Union [1]. Still, the NZEB performance level will not be sufficient to reach the objectives in terms of climate change mitigation at the international level. Indeed, the building itself has embodied impacts that need to be considered when assessing its environmental performance. This is specifically the purpose of life-cycle assessments (LCA) that will be mandatory in future regulations (e.g. in France), and which are promoted by green building certification systems (e.g. LEED, BREEAM, HQE...).

The LCA methodology has been continuously improved since the 1960s, leading to the development of several tools and software. However, LCA tools are still not widely used by engineers and architects in the building industry. Therefore, the aim of this study is to better understand the practitioners' needs in terms of Life-Cycle Performance (LCP) design support methods. By using LCP, the authors would like to voluntarily embrace a wider range of practices that help designers integrate life-cycle targets into the design process, and not limit the scope of the study to the current LCA users in the sense of the

ISO 14040 [2]. To that end, the present paper summarizes the first results of a survey on the current use of LCP tools and methods targeting architects, engineers, and real estate developers on the European scale.

REVIEW OF PREVIOUS SURVEYS

To the best knowledge of the authors, there are very few surveys targeting the usability of LCP tools so far. Some of the previous studies highlighted theoretical knowledge and practical experiences of the users about LCA [3–8]. From these previous works, it is already known that building LCA is time consuming, expensive, and problematic in the early design stages [8]. Also, the complexity of the method is identified as one of the main barriers for practitioners [6]. Finally, in North America, a contradiction has been noticed between a large awareness of building LCA and its low usage by practitioners, mainly due to a lack of market demand [4]. However, prior researches are limited when it comes to understanding the LCA practitioner context and requirements. In addition, none of them targeted the European geographical scope, as they were mainly focused on the US.

METHODOLOGY

According to Maguire [9], among several context-of-use methods (e.g. user observation, diary keeping, etc.), the survey of existing users is the one that best fits the aim

PLEA 2018 HONG KONG

Smart and Healthy within the 2-degree Limit

of our study. It allows us to collect quantitative data and to target a diverse and difficult-to-reach population at the European scale, whereas other approaches describe the context of use by direct observation, making them unsuitable considering the geographical scope of our study. Thus, an online questionnaire was set up thanks to the web-based instrument, Survey Monkey [10]. It was spread via emails to 33'000 European professionals from the Architecture, Engineering and Construction community through the author's network and commercial mailing lists. The professional network LinkedIn was also used to share the survey among green building communities of practitioners using LCA tools, or interested by sustainable construction and green label discussions. The survey has been inspired by usability context analysis guidelines [11] and adapted to this study.

represents 17 questions out of 40. The survey was answered by 495 participants, which is a high population compared to the previous studies [3–8] in which the average number of respondents was below 200. After cleaning the data, 414 of them matched the target population of the survey, i.e. working in geographical Europe, and practicing as engineers, architects or real estate developers. According to their answers, participants were directed differently to other questions, which explains why all questions do not have the same number of answers. Also, some participants quit the survey before the end, but their answers have still been taken into account. Around 400 participants answered specifically the questions addressed in this paper. For more details, each graph interpreting the answers to a specific question will specify its number of respondents.

SURVEY FINDINGS

The survey results have been interpreted across the following three subjects.

About the practitioners in this survey

The survey reaches its ambition in terms of geographical scope: the participants that answered are working in 26 different countries within Europe. However, more than 80% of them are located in the UK, France, Switzerland, Germany, Italy, Spain and the Netherlands - that is to say the Western part of Europe. This might be induced by two factors. First, the author's network is more connected to this part of Europe. Second, participants' feedback in open questions point out that in some countries, economic and social issues have priority over environmental questions. Regarding the profession, 82% of the participants are working as architects, 13% as practicing engineers, and 5% as real estate developers. This fits well with the goal of this survey to target the practitioners working at early design stages.

Within the survey population, it is worth mentioning that most of the practitioners (60%) claimed that they often or very often consider LCP during the building design. Only 3.7% (i.e. 15 people) never consider it but agree that they will have to in the future. Looking at the seven countries that represent 80% of the answers, we noticed that the distribution of respondent interest to LCP per country was quite stable, varying from 72% in Spain to 51% in Germany. The robustness of these results must be considered in light of the number of respondent per country, highlighted by the black line in Figure 2 (e.g. only 4.3% of them were coming from Spain). Still, one can deduce that a large majority of the respondents are concerned by the life-cycle performance, which is now of major importance for practitioners. However, the question was very open on purpose, embracing every method that permits a consideration of the LCP. Then, if there is no doubt about the awareness of life-cycle performance, the practice behind this notion embraces a

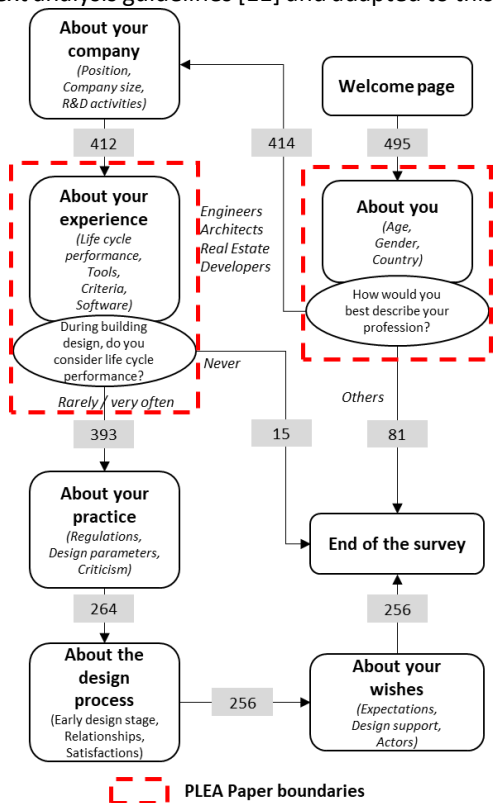


Figure 1: Presentation of the Overall Survey. The parts interpreted in this paper are those within the dashed perimeters. The numbers in the rectangular grey boxes correspond to the number of participants that reached a particular point in the survey.

The overall questionnaire included 40 questions that address two specific topics. The first one is the use and requirements of design practitioners regarding current LCA software. It is the purpose of this paper to explore and interpret the results related to this topic. The rest of the survey is concentrated on the context of use of LCA, in order to better understand the social environment in which the methodology is used. This part is the purpose of another journal article [12]. Figure 1 highlights the survey perimeter discussed in this paper, which

PLEA 2018 HONG KONG

Smart and Healthy within the 2-degree Limit

large diversity of methods and tools (cf. section 4.2), and probably of *LCP* definitions.

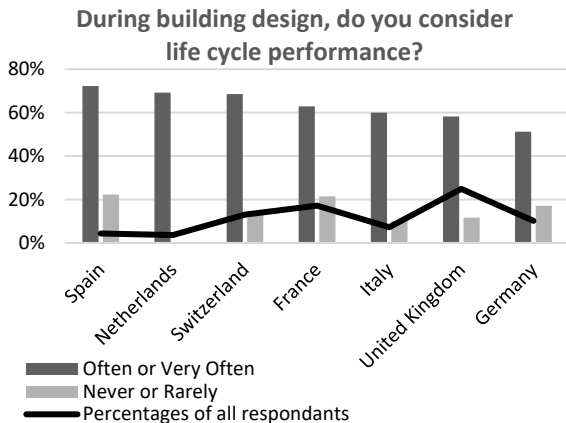


Figure 2: Life-cycle performance considerations, out of 408 answers. Bars represent the respondents of each country that considers *LCP*, and the line represents the country distribution of 80% of the respondents.

Practitioners and *LCA* software

The participants mostly work in small architecture companies (<10 employees for 70% of the participants). If this ratio is very low, it is still higher than what is observed in a country like France, where 94% of the architecture offices have less than 10 employees [11]. This segmentation has a direct impact on the skills and tools that are able to handle designers. It has already been noticed in the UK, for instance, that the companies having more than 100 employees used Building Information Modelling on half of their projects while it represents only 17% of the projects for small companies with less than 10 people [13]. Following the same trend, Figure 3 illustrates the very low penetration rate of computer software dedicated to *LCA* among the professionals (27%).

The same phenomenon is observed when looking deeper into the answers, with an equipment rate slightly higher in large companies than small ones. In addition, only 6% of the architects use a *LCA* software, compared to 42% of the engineers. As a comparison, the participants are more likely to use rules of thumb (33%) or guidelines (43%) for instance.

Using what kind of tool or method do you assess the life cycle performance at the conceptual design stage?

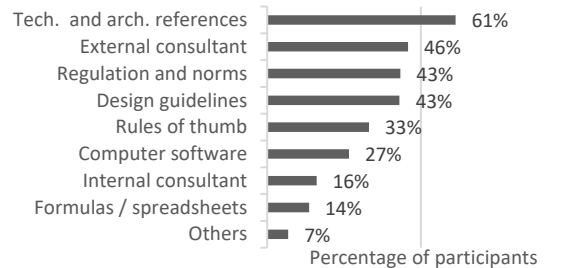


Figure 3: Answers about the tools and methods used to assess life-cycle performance at the conceptual design stage, out of 323 answers.

The most popular approach is the use of technical and architectural references (61%). Indeed, according to Jusselme et al. [14], they are commonly used by designers to feed the iterative design process between problems and solutions. However, considering the still small corpus of reference buildings in terms of *LCP*, the complexity, and the context-dependant specificity of an *LCP* approach, one can wonder about the efficiency of such methods. The complexity of life-cycle thinking is underlined by the fact that 46% of the respondents are working with an external consultant, demonstrating the difficulty of internalizing this competence.

In Figure 4, 38 respondents specified the software they use. It is interesting to note that they use more than 14 different types of software, and the most used (Elodie) concerned no more than 26% of them. This statement has to be moderated according to the country distribution of the survey participants. However, this means that there is no clear leadership of one of the tools, probably induced by country-specific Environmental Product Declaration (*EPD*) databases used to perform the *LCA*. Elodie software, for instance, is dedicated to the French building context, using a French *EPD* database (INIES) and is used in the frame of this survey at 90% by France-located practitioners. Among those who answered "Other," Brightway, Smeo and a homemade Excel file were mainly cited.

The importance of several criteria according to *LCA* software users have been characterized and illustrated in Figure 5. Among the three first-ranked criteria, the time spent conducting a *LCA* and the interoperability with *CAD* tools are both related to a willingness to reduce and lighten the time consumption of filling in input data or more generally using the software. Indeed, architects and engineers spend most of their time managing existing information [15], rather than creating new information.

PLEA 2018 HONG KONG

Smart and Healthy within the 2-degree Limit

Which of the following Life Cycle Assessment (LCA) software do you use?

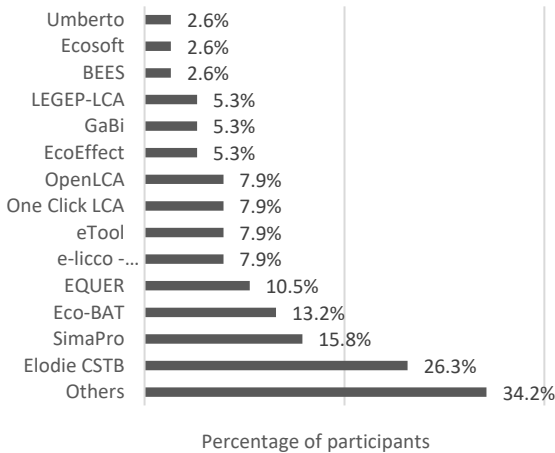


Figure 4: LCA Software distribution, out of 38 answers.

How would you rank the importance of these criteria for you when using LCA tools?

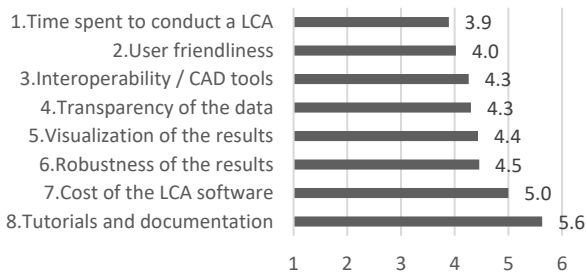


Figure 5: Average ranking of several criteria when using a LCA software, out of 46 answers (1=highest importance; 8=lowest).

The user friendliness is also a major concern, which might be related to the desire for an easier interpretation process. This could be improved with the use of data-visualization techniques of the results as suggested by Jusselme et al. [16].

These criteria have also been rated in terms of satisfaction levels thanks to a Likert scale with five levels from “not at all satisfied” (1st level) to “completely satisfied” (5th level). The weighted average of the answers highlight that users are satisfied with criteria two and four to eight in Figure 5 with an average score of between 3 and 3.11 on the Likert scale. However, criteria one and three, namely the time spent and the interoperability have a lower satisfaction with a score of 2.84 and 2.49, respectively.

Overall, a major issue regarding the use of life-cycle tools is their cost of use, which is too high for practitioners. This is also clearly reported in several open answers. This survey also found out the LCP is a voluntary approach for 71% of the practitioners, while it is a client’s requirement for only 41%. In this context, and especially with the early

designs, the engineering fees might fail to make up for the time consumption of current software.

Figure 5 also highlights a lower emphasis on the importance of tutorials and documentation. This is paradoxical, as the survey shows on another note that they are used by 82% of the respondents, while 44% are helped by colleagues, and 38% have internal or external training courses. Thus, tutorials are highly popular, but are probably considered a basic feature of the software compared to the other criteria.

Practitioners’ wishes

Regarding the services expected by the participants, more than 50% of the practitioners are willing to perform the following: (a) to check the compliance of the project with the objectives; (b) to assess the performance of the building project; (c) to evaluate the sensitivity of the design parameters; (d) to know what would be the optimum in terms of sustainability; (e) to explore which design alternatives fulfil the objectives; and (f) to compare the performances of different building design alternatives. While current software is able to meet requirements (a) and (b), this is commonly not the case for the others, which highlights a major gap with practitioner’s needs that expect much more than a simple life-cycle performance assessment. Indeed, if the compliancy of a project with a specific environmental target is a fundamental need, it does not efficiently support the design process and its iterations. On the other hand, the sensitivity analyses of design parameters and design alternative explorations, for instance, are much more powerful [14,17]. When focusing specifically on early design stages, 59% of the respondents agreed to use simplified performance assessment to handle the low resolution of details of these stages (Figure 6). However, the exploration of a gallery of possible design options is acclaimed by 48% of them, with a higher rate among the engineer’s sub-population (62%).

The survey also reveals a strong willingness to perform multi-criteria assessments as most of the respondents also take care of acoustics, lighting, thermal comfort and energy consumption. This finding is in line with the need for interoperability compliancy of LCA software, and it demonstrates the will to have more holistic tools to integrate the complexity of multiple performance targets into the design process.

Regarding the design parameters, Figure 7 highlights that more than 80% of the practitioners consider the building shape and the building orientation at the conceptual design stage. If the building shape has a direct incidence on the embodied impacts of a building, this is not the case for the building orientation, which affects exclusively its operational impacts. This strengthens the need to develop LCA tools that also evaluate the energy consumption and then the life-cycle efficiency ratio as

PLEA 2018 HONG KONG

Smart and Healthy within the 2-degree Limit

developed by Brambilla et. al [18], in order to balance the operational and embodied impact of a design parameter.

At conceptual design stages, where your project usually has a poor resolution of details, what kind of decision support would you prefer to be provided with?

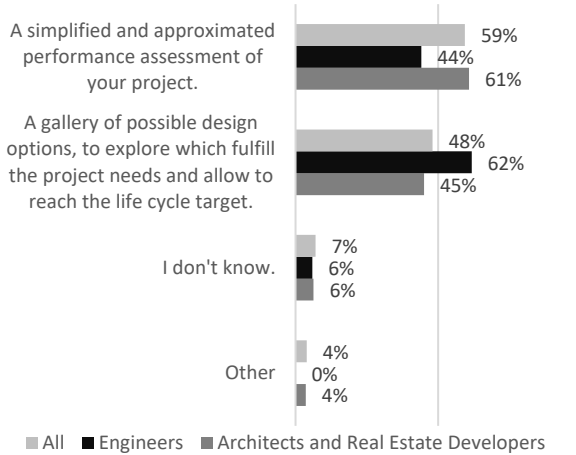


Figure 6 Comparison of exploration and assessment approaches, out of 256 answers.

Which parameters do you take into account during conceptual design stages?

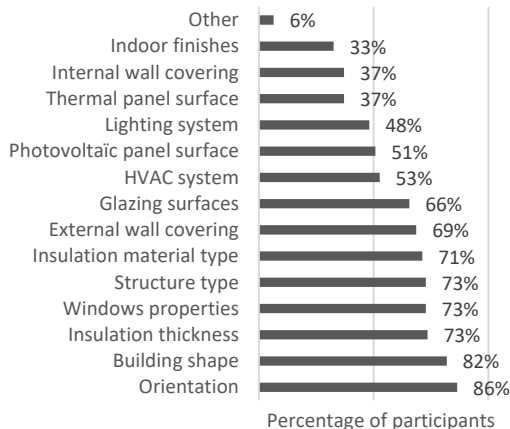


Figure 7: Consideration of design parameters at conceptual design stages, out of 263 answers.

As seen in Figure 7, there is a decreasing interest of the design parameters from macro (building shape and orientation) to micro (indoor finishes and internal coverings). However, all proposed parameters are considered by more than 30% of the participants, which is counter-intuitive at the early design phase. In fact, life-cycle performance assessments consider all the building components in their calculations. This means that using a low performing structure will perhaps lead to a decrease in design options by choosing only the best products in terms of indoor finishes. Vice-versa, if the client's brief specifies low performing indoor finishes, this may have an impact on the building shape or structure possibilities. In that sense, it is interesting to

note that designers want to understand the consequences of design choices commonly made at early stages, on details with high environmental impacts that will be fixed in later phases.

OUTCOMES AND DISCUSSION

The major finding of this survey is the important gap between the *LCP* issue awareness among practitioners, and the low equipment rate of these professionals with a dedicated *LCA* software. On the one hand, the present survey clearly confirms that life-cycle performance is a question placed high on the agenda of practitioners. There is no doubt there is an awareness of the topic, even if there might be a bias inherent to the survey, as those that answered were plausibly already interested in the survey subject. On the other hand, only 27% use computer software, which is a very low rate considering the difficulty of reaching meaningful and robust conclusions with any other approach.

This underutilization of *LCA* software is explained by their low efficiency, i.e. a high time investment for a low satisfaction. Software mismatches the design process and its context. Indeed, current tools are mainly limited to the assessment functionality, and should propose many other benefits such as sensitivity assessment, exploration mode, etc., to fit better with the design iterations. These iterations are currently fed by the use of architectural references, which are highly popular among architects and engineers during the iterative design process, but are very limited from the author's point of view when it comes to the *LCP* issue.

LCA software should also be more interoperable with CAD tools in order to decrease their cost of use, i.e. the time for processing the input parameters and interpreting output data. Indeed, the time spent in conducting a *LCA* is judged too high while in most of the cases, the clients do not require them, with probably no engineering fees for these specific assessments. This compatibility with the BIM environment might extend the boundaries of current *LCA* software with more functionalities. Indeed, the increasing performance-oriented trend of design briefs calls for designers to adopt a multi-criteria approach, assessing other metrics such as energy, lighting, acoustics, etc. In addition, the life-cycle approach should include all building components in its perimeter, leading designers to an anachronistic situation where design parameters usually discussed at detailed phases, which have heavy environmental impacts, can actually influence the early stage design options.

CONCLUSION

Thanks to 414 valid responses from 26 different European countries, this survey aims to accurately depict the situation of practitioners regarding their use and understanding of life-cycle performance (*LCP*). Given the

PLEA 2018 HONG KONG

Smart and Healthy within the 2-degree Limit

current lack of knowledge regarding this field, particularly in Europe where the regulation context is ambitious, the idea was to target the design community at large. Indeed, by focusing on practitioners who are already LCA software users, the consequence would have been to exclude from the survey those interested in LCP, but not equipped yet.

In a few words, it is suggested that LCA software developers should focus their future work on the following contradiction. First, to decrease the cost of use of the software with more interoperability and user friendliness. Second, to increase the design support added-value by coupling more interpretation techniques of the assessments, extending the scope of analysis to other metrics, and including all building components starting from the early design phases.

This challenge might feed further research as the resulting answer would be to increase the complexity of LCA assessments and associated analysis, and in the meantime to spread the methodology among a wider community, that have probably fewer skills than the early adopters, who were mostly specialist consultants. These objectives might be achievable with the coupling and implementation of the latest findings in research. The data-collection should be easier with the increasing BIM industry. LCA should also better use data-science techniques to increase its usability thanks not only to higher computational power (e.g. cloud computing), statistical analysis (e.g. sensitivity analysis), but also data-visualization techniques that interpret multidimensional and heterogeneous LCA inputs and outputs.

The highlight of current LCA software weaknesses along with the practitioner's wishes and situation might be useful to further work led by developers and researchers towards new tools with higher usability.

ACKNOWLEDGEMENTS

The work presented in this paper has been funded by the State of Fribourg (message du Conseil d'Etat au Grand Conseil 2014-DEE-22).

REFERENCES

1. EU - EPBD (2010) Directive 2010/31/EU of the European Parliament and of the Council of 19 May 2010 on the energy performance of buildings (recast). *Off. J. Eur. Union*, 18 (06), 2010.
2. ISO 14040 (2006) ISO 14040:2006 - Environmental management -- Life cycle assessment -- Principles and framework. 20.
3. Sibiude, G., Lasvaux, S., Lebert, A., Nibel, S., Peuportier, B., and Bonnet, R. Survey on LCA results analysis, interpretation and reporting in the construction sector.
4. Olinzock, M.A., Landis, A.E., Saunders, C.L., Collinge, W.O., Jones, A.K., Schaefer, L.A., and Bilec, M.M. (2015) Life cycle assessment use in the North American building community: summary of findings from a 2011/2012 survey. *Int. J. Life Cycle Assess.*, 20 (3), 318-331.
5. Hofstetter, P., and Mettler, T.M. (2003) What Users Want and May Need. *J. Ind. Ecol.*, 7 (2), 79-101.
6. Cooper, J.S., et Fava, J.A. (2006) Life-Cycle Assessment Practitioner Survey: Summary of Results. *J. Ind. Ecol.*, 10 (4), 12-14.
7. Saunders, C.L., Landis, A.E., Mecca, L.P., Jones, A.K., Schaefer, L.A., and Bilec, M.M. (2013) Analyzing the Practice of Life Cycle Assessment. *J. Ind. Ecol.*, 17 (5), 777-788.
8. Schlanbusch, R.D., Fufa, S.M., Häkkinen, T., Vares, S., Birgisdottir, H., and Ylmén, P. (2016) Experiences with LCA in the Nordic Building Industry – Challenges, Needs and Solutions. *Energy Procedia*, 96, 82-93.
9. Maguire, M. (2001) Methods to support human-centred design. *Int. J. Hum.-Comput. Stud.*, 55 (4), 587-634.
10. Finley, R. (1999) SurveyMonkey. *Portland OR*, 97209.
11. Thomas, C., and Bevan, N. (1996) Usability context analysis: a practical guide.
12. Jusselme, T., Rey, E., and Andersen, M. (2018) Social context-of-use for environmental performance assessments: application to building life-cycle at early design stages. *Be Submitt.*
13. RIBA (2017) RIBA Business Benchmarking 2017.
14. Jusselme, T., Cozza, S., Hoxha, E., Brambilla, A., Evequoz, F., Lalanne, D., Rey, E., and Andersen, M. (2016) Towards a pre-design method for low carbon architectural strategies. *PLEA2016*.
15. Flager, F., Welle, B., Bansal, P., Soremekun, G., and Haymaker, J. (2009) Multidisciplinary process integration and design optimization of a classroom building. *J. Inf. Technol. Constr.*, 14, 595-612.
16. Jusselme, T., Tuor, R., Lalanne, D., Rey, E., and Andersen, M. (2017) Visualization techniques for heterogeneous and multidimensional simulated building performance data sets. *Proc. Int. Conf. Sustain. Des. Built Environ.*, 971-982.
17. Jusselme, T., Rey, E., and Andersen, M. (2018) An integrative approach for embodied energy: Towards an LCA-based data-driven design method. *Renew. Sustain. Energy Rev.*, 88, 123-132.
18. Brambilla, A., Bonvin, J., Flourentzou, F., and Jusselme, T. (2018) Life cycle efficiency ratio: A new performance indicator for a life cycle driven approach to evaluate the potential of ventilative cooling and thermal inertia. *Energy Build.*, 163, 22-33.

Passive Cooling with Phase Change Materials: Integrative Method for Design of Dendritic Encapsulation Prototype

IVA REŠETAR¹, NORBERT PALZ¹

¹Institute for Architecture and Urban Planning, Berlin University of the Arts, Berlin, Germany

ABSTRACT: New methods for designing with phase change materials (PCM) could widen the range of applications of passive systems for indoor cooling in architecture. This paper investigates material and formal strategies for generative architectural design that support the thermal performance of PCM. Dendritic geometry of PCM encapsulation with a large surface area per unit volume is proposed for enhancement of the heat transfer between PCM and surroundings. The prototype of the PCM ceiling component is digitally designed, manufactured in glass and tested in an experimental set-up for thermal cycling. Correlations are made between geometric configurations and cooling performance of dendritic and spherical PCM containments. The presented methodology integrates tools and techniques from digital design and energy technology, with an aim to contribute to novel PCM-based concepts for local thermal regulation in architecture.

KEYWORDS: Phase change materials, passive cooling, encapsulation geometry, digital design, thermal cycling

1. INTRODUCTION

Novel phase change materials (PCM) differ fundamentally from conventional building materials for their inherent thermodynamic behaviour, suitable for management of thermal environments in architecture [1]. For PCM to gain more significance in the realm of architectural design, integrated environmental design strategies are needed that evolve from their phase-change behaviour. Coupling digital design with advanced thermal energy storage systems (TES) can renew technological aspects of architectural design important for improving buildings' energy performance and occupants' comfort.

PCM are substances capable to absorb, store and release energy in the form of latent heat during melting and solidification at a certain, predictable temperature. PCM are a suitable medium for TES due to their large phase change enthalpy – the large amount of heat that needs to be added or released during the phase transition that occurs at almost constant temperature [1, 2] (Fig. 1).

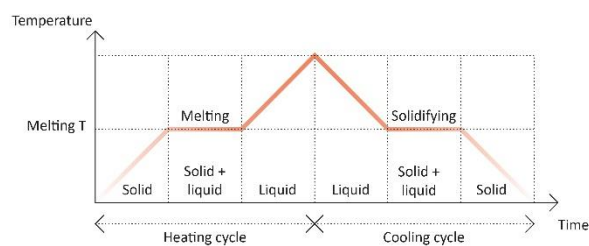


Figure 1: An ideal melting and solidification cycle showing temperature plateau of PCM during the phase change

Having the melting point within a desired temperature range, PCM take advantage of surrounding

temperature fluctuations to store the latent heat: when the ambient temperature rises above the comfort zone, the material melts and absorbs the excess heat; after the temperature has dropped, the material solidifies and releases the stored heat. In this manner, PCM can undergo reversible melting and solidification cycles without degradation.

1.1 Overview of building applications of PCM

An integration of PCM into building materials and components is widely researched in the domain of energy technology and suggests a promising method for decreasing the dependency on high energy consuming mechanical systems, reduction and shifting of thermal loads and improving overall thermal stability of buildings [3,4].

Numerous studies provided an overview of building applications of PCM [3-6], spanning from micro-encapsulated elements commonly incorporated into walls and ceilings, to macro-encapsulated that take form of poaches, tubes or panels placed into building cavities, (e.g. above the suspended ceiling). However, PCM have been often regarded as additives that improve the thermal performance of conventional materials such as gypsum or concrete, and, with rare exceptions [7], have remained marginal for architectural design.

By contrast, this study extends the architectural design agenda with PCM towards visible, transparent ceiling elements for passive indoor cooling. A design method is presented that correlates geometric configuration of the PCM containment and its cooling performance, with an aim to extend the range of PCM elements for local thermal regulation in architecture.

2. ROLE OF THE ENCAPSULATION GEOMETRY FOR PASSIVE COOLING WITH PCM

In passive cooling applications for buildings, PCM respond to diurnal temperature differences without requiring additional mechanical equipment to influence the heat absorption or release [2]. The operating principle of passive cooling is to release the coolness stored at night during the day when the temperature rises above the comfort zone. Certain factors, such as sufficient diurnal temperature difference (15°C) and the operating temperature of PCM within that range (21-25°C), are preconditions for such applications [8,9].

Heat transfer mechanisms that govern the phase transitions of PCM are conduction and natural convection (Fig. 2). During melting, the conduction is responsible for transferring the excess heat from surrounding air to the material. At later stages of phase transition, when the fraction of the melted material increases, natural convection within the container affects the PCM melting rate [10].



Figure 2: Solidification of bio-based PCM during 10h; crystallization by conduction in contact with containment cooled by the surrounding air

When designing PCM elements, the geometry of the encapsulation plays an important role for increasing the contact surface between PCM and the surrounding heat transfer medium, and thus the ability of the material to undergo the phase change. The major drawback of PCM is their low thermal conductivity that limits the conduction and the heat absorption during the high demand cooling time. Therefore, both geometrical configuration and the conductivity of the encapsulation are crucial parameters for the design of PCM containment that need to be considered to overcome these limitations. The geometry and orientation of containment as well as the expansion of surface area by adding fins have been widely investigated strategies for improving the heat transfer and conductivity [10,11]. This paper addresses the heat transfer enhancement by proposing dendritic geometry with 3D fins in the combination with glass as a containment material.

2.2 Dendritic typologies – literature overview and advantages for thermal performance

The term dendrite (from Greek *déndron*, tree) refers to structures undergoing branching during the growth process. Although the term is associated with

branching process of the tree-like neural cell extensions, dendritic typologies are found in other growth-related phenomena in nature, such as crystal solidification of metals, alloys and water, or the coral and bacterial growth. Common for these formations are their efficient energy or nutrient transportation paths [12]. Having the large surface around the small volume, these spatial organizations offer a principle for enhancing the heat transfer between PCM containment and surroundings. Current advancements in the field of digital design and fabrication make such complex geometries feasible in architecture.

Early mathematical models that described dendritic geometries were introduced in ground-breaking concepts of fractals, L-systems and diffusion-limited growth processes [13-15]. In fields of physics and mechanical engineering, the constructal theory investigated occurrence of dendritic form in nature and proved its efficiency in various engineered systems involving convection and conduction flows [12,16,17]. Here, increasing the degrees of freedom of a constrained system optimized towards a certain objective results in more “natural” dendritic flow structures.

The evolution of computational fluid dynamics and topology optimization methods in thermal sciences saw proliferation of dendritic typologies for solving various problems of thermal control, e.g. conductive heat transfer for electronics cooling [18].

More recently, shape and topology optimizations were proposed for the heat transfer enhancement in PCM containments with dendritic fin geometries [19-21]. A novel approach for the maximization of performance of a PCM storage unit involving time evolution was presented for the optimization of Y-shaped fins. Parameters such as bifurcations and fin angle were adjusted for different operating scenarios [19]. More organic dendritic configurations arose in topology optimization of highly conductive fins, when they freely evolved through optimization process. The study led to different fin layouts optimized for melting and solidification and reported the reduction in PCM charging and recharging time [20]. Same authors arrived at a 3D coral-like fin design in a PCM storage system optimized to steadily absorb heat over time and decrease the discharge time of PCM [21].

3. METHODOLOGY

The proposed methodological framework for the design and the analyses of the thermal performance of the dendritic glass prototype couples digital modelling and fabrication techniques with the experimental set-up for thermal cycling (Fig. 3).

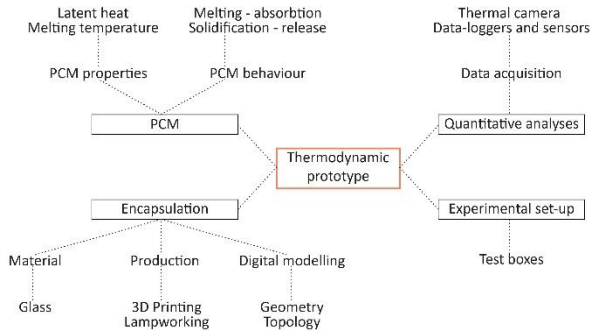


Figure 3: Method for design and evaluation of thermodynamic performance of dendritic prototype

3.1 Digital design and manufacturing of the dendritic prototype

A spherical containment was adopted as a reference PCM encapsulation geometry in this study, since the sphere represents the minimal surface enclosing a certain volume. A standard labware borosilicate glass flask of 500ml volume, 10.5cm diameter and surface area 376cm² was chosen as a reference containment. The design goal was to generate a structure of the same volume, but with a contrasted, large surface to experimentally investigate the effect of an increased surface area on the heat transfer between the PCM containment and surroundings. After considering different growth algorithms that result in surface differentiations, the digital design strategy for maximizing the surface was to transform the compact spherical containment into dendritic using the network of minimal paths (Fig. 4).

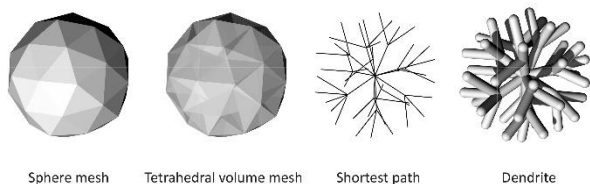


Figure 4: From tetrahedral mesh to dendritic topology

Design criteria for the digital model was (a) the feasibility of the structure in the borosilicate glass of the same thickness as the glass flask (b) structural stability and robustness (c) radial geometry and relatively uniform material distribution in all directions from centre to periphery of the containment (d) good exposure to surrounding air of all parts, without pockets or creases that would block melting or solidification.

3D and algorithmic modelling software Rhinoceros and Grasshopper were used to generate the geometry of the dendritic containment. The starting point was an icosahedron surface mesh, smoothed and approximated to a sphere by Loop subdivision, resulting in series of evenly distributed mesh vertices

on the outer surface. The surface domain was discretised into volume cells using a TetGen mesh tetrahedralization component.

The aim was to explore a variety of connections between centre and the periphery of the domain, using intermediate points of tetrahedral cells as branching nodes. Provided with all connections of the given points, Shortest Walk algorithm calculated minimal paths, outputting the topology of the minimal containment volume. Since the complexity of the dendritic configuration was limited by the glass production, the size of the tetrahedral cell was chosen to yield two bifurcations (two generations of branches) and one layer of intermediate points on the equidistance from the centre.

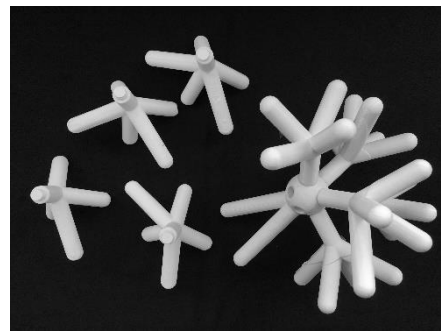


Figure 5: 3D printed model with removable branches

Once the branching topology was set, the thickness of tubes and the overall size of the structure were adjusted to fit the 500ml volume, resulting in a structure of the double diameter (ca. 21cm) and the triple surface of the initial flask (ca. 1369cm²). The digital model was 3D printed with removable branches attached to the perforated round core (Fig. 5). With the help of the 3D printed model that served as a mock-up, a full-scale glass prototype was manufactured using the lampworking technique.



Figure 6: Empty dendritic glass containment after annealing

Glass tubes of an inside diameter 16mm were first connected into branches, then attached to the round glass core and finally left for annealing in the oven over 24h (Fig. 6). Due to the nature of lampworking technique that caused smoothing of connections between glass branches, the core and branching nodes

expanded in size, leaving the upper branches of the volume empty during the experiment. However, this space was partially filled during the heating cycle, when the convective forces and the buoyancy pushed the liquid portions of the material up.

3.2 Experimental set-up for thermal cycling



Figure 7: Experimental set-up for thermal cycling

Spherical and dendritic encapsulations were filled with bio-based PCM with melting temperature 21°C for their thermal performance to be compared in an experimental set-up of test boxes.

Table 1. Physical properties of the bio-based PCM from the data sheet of the producer.

Property	Values
Melting temperature	21°C
Crystallization temperature	19°C
Latent heat	190 KJ/kg
Specific heat capacity solid	2.1 kJ/(kg·°C)
Specific heat capacity liquid	2.3 kJ/(kg·°C)
Thermal conductivity solid	0.18 W/(m·°C)
Thermal conductivity liquid	0.15 W/(m·°C)
Density solid / liquid	891 / 850 kg/m ³

Following previous reports on comparative analyses of the thermal performance of PCM using test boxes [22], an experimental set-up was developed that consisted of two identical boxes - the first one containing the PCM sample and the second being an empty reference box. Boxes were placed in a steady climate environment and simultaneously exposed to thermal excitation with the temperature range 17-30°C, set to enable the phase change. Boxes of an inside dimension 50x50x50cm were made of 18mm birch plywood and covered by 30mm thick insulation panels. The front face was glazed by 4mm thick glass to allow thermal excitation by halogen lamps of 750W placed in the front (Fig.7).

Indoor, material and ambient room temperatures were continuously measured in one-minute interval during two subsequent heating (3h) and cooling (6h) cycles of the total duration of 18h. The resulting

heating rate of 4°C/h was slightly above the average in the buildings exposed to direct solar radiation in the summer. The measuring equipment comprised dataloggers with 4 PT-100 probes and the thermal camera attached to the bottom of the test box. Two probes measuring indoor box temperature were placed behind reflective radiation shields.

Before commencing tests with PCM, multiple calibration cycles with empty boxes exhibited temperature differences within tolerance values (0.1°C) and no temperature gradients in boxes. Two tests of each containment were carried out: the first without the ventilation during the recharging time and the second with natural ventilation of the box.

4. RESULTS

The proposed dendritic prototype acts like a heat absorber. The large surface of 3D fins maximizes the contact between PCM and surroundings and accelerates the first stage of melting of PCM dominated by conduction. At later stages of the phase change, governed by both conduction and natural convection, this encapsulation typology allows for multiple melting fronts within thin interconnected elements and enables relatively fast recharging by solidification.

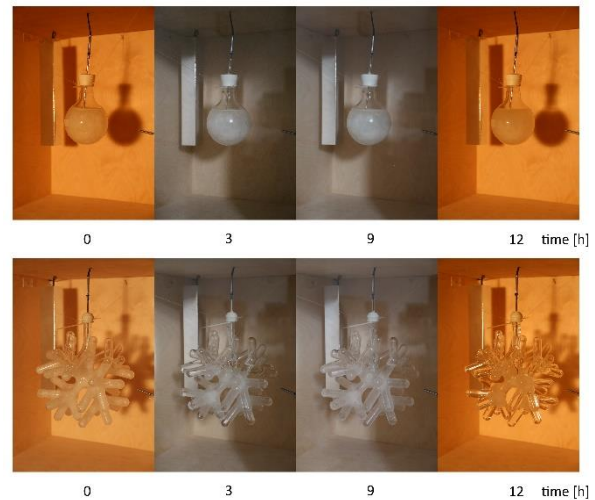


Figure 8: Spherical and dendritic encapsulations with material undergoing the phase change. Images show the minimum and maximum melting portions at the beginning and the end of two heating cycles

Whereas the spherical containment enabled only a small portion of the material to melt, the dendritic prototype allowed full melting of PCM (Fig. 8). However, PCM did not entirely regenerate during 6h of cooling in ventilated box and regenerated poorly in test without ventilation. The results point to the importance of the sufficient length of cooling by ventilation and dimensioning of elements with less than 20mm thickness for faster recharging, as recommended in [2].

PLEA 2018 HONG KONG

Smart and Healthy within the 2-degree Limit

Table 2. Summary of peak temperature differences at the end of heating cycles.

Containment geometry	ΔT [$^{\circ}\text{C}$] 1 st Cycle	ΔT [$^{\circ}\text{C}$] 2 nd Cycle
Test without ventilation (Fig. 10)		
Sphere	0.96	1.2
Dendrite	2.25	1.7
Test with ventilation (Fig. 11)		
Sphere	1.15	1.13
Dendrite	2.55	2.05

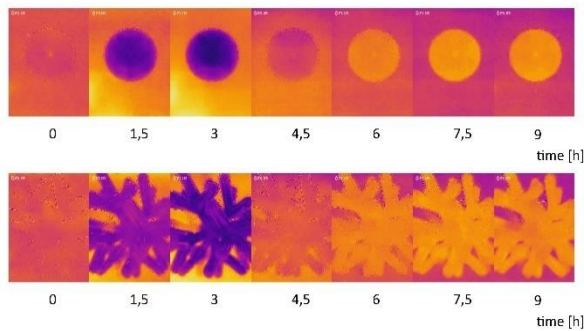


Figure 9: Thermographic images of heating and cooling cycle of spherical and dendritic containments

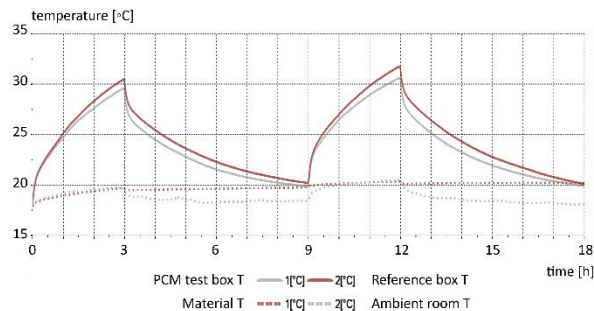


Figure 10a: Impact of phase change on temperature reduction – spherical containment tested without box ventilation

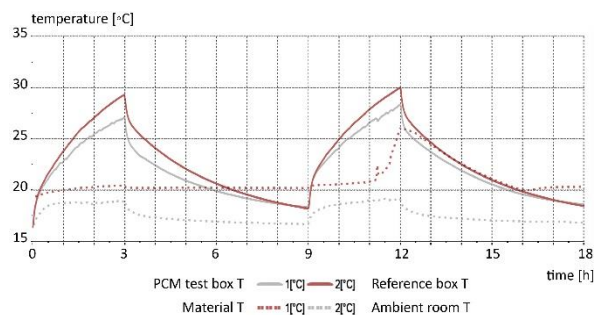


Figure 10b: Impact of phase change on temperature reduction – dendritic containment tested without box ventilation

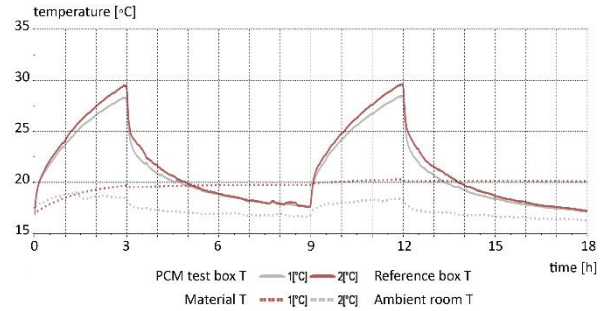


Figure 11a: Impact of phase change on temperature reduction – spherical containment tested with box ventilation

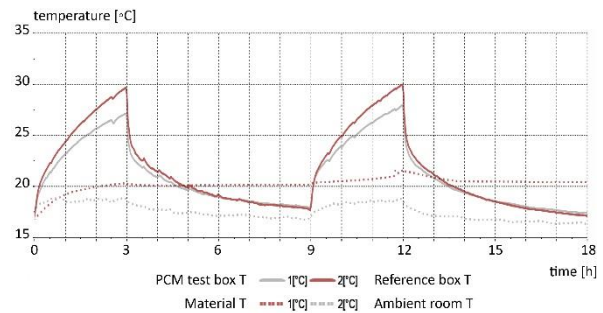


Figure 11b: Impact of phase change on temperature reduction – dendritic containment tested with box ventilation

Later stages of melting showed a significant influence of natural convection and buoyancy on the material movement in dendritic containment. Further optimization of containment geometry by limiting the branching to the domain of lower hemisphere could improve this behaviour.

5. CONCLUSION

An integrative methodological framework was presented for the design of the transparent, macro-encapsulated PCM ceiling element for indoor passive cooling. Three-dimensional dendritic structure was proposed as a design strategy for improving the heat transfer between PCM and surroundings. The digital model, constructed with minimal branching paths, increased the heat exchange area of the spherical containment more than three-fold.

An experimental-set-up of test boxes was used for thermal cycling and comparative analyses of spherical and dendritic encapsulations with contrasted surface areas – minimal to large – to determine their cooling effect.

In comparison to spherical containment, dendritic geometry more than doubled the cooling performance of PCM and caused the temperature reduction in the test box of max. 2.55°C. Experimental results showed benefits of digital design strategies for increasing the surface area of PCM containment and proved the three-dimensional dendritic geometry as a suitable concept for passive cooling with PCM, open for further full-scale investigations. Further improvements in

PLEA 2018 HONG KONG

Smart and Healthy within the 2-degree Limit

optimization of dendritic configurations and manufacturing process are needed. Future scaling of the current prototype into a larger material system should consider (a) preserving the thickness of dendrites (b) optimizing the branching domain to account for natural convection (c) improving manufacturing process by further application of additive manufacturing (d) sufficient regeneration of the material by night ventilation.

ACKNOWLEDGEMENTS

We would like to thank developers of open access software: TetGen - Hang Si from Weierstrass Institute for Applied Analysis and Stochastics, Grasshopper Plug-ins, Shortest Walk and Weaver Bird - Giulio Piacentino and TetGen component for Grasshopper - Nik Willmore.

This project has received funding from the European Union's Horizon 2020 research and innovation programme under the Marie Skłodowska-Curie grant agreement No. 642328.

REFERENCES

1. Addington, M. and Schodek, D. (2005). *Smart Materials and New Technologies: For the architecture and design professions*. Amsterdam : Boston: Elsevier, Architectural Press.
2. VDI. (2016). VDI Standard 2164, *PCM energy storage systems in building services*. Düsseldorf: Verein Deutscher Ingenieure.
3. Zalba, B., Marin, J.M., Cabeza F.L., Mehling, H. (2003). Review on thermal energy storage with phase change materials, heat transfer analysis and applications. *Applied Thermal Engineering*, 23, p. 251–283. [https://doi.org/10.1016/S1359-4311\(02\)00192-8](https://doi.org/10.1016/S1359-4311(02)00192-8)
4. Kośny, J. (2015). *PCM-Enhanced Building Components: An Application of Phase Change Materials in Building Envelopes and Internal Structures*. Cham: Springer.
5. Navarro, L., de Gracia, A., Niall, D., Castell, A., Browne, M., McCormack, S. J., Griffiths, P., Cabeza, L. F. (2016). Thermal energy storage in building integrated thermal systems: A review. Part 2. Integration as passive system. *Renewable Energy*, 85, p. 1334–1356. <https://doi.org/10.1016/j.renene.2015.06.064>
6. Mavriaggiannaki, A., and Ampatzi, E. (2016). Latent heat storage in building elements: A systematic review on properties and contextual performance factors. *Renewable and Sustainable Energy Reviews*, 60, p. 852–866. <https://doi.org/10.1016/j.rser.2016.01.115>
7. Available: <http://glassx.ch/index.php> [15 August 2018]
8. Raj, V.A.A. and Velraj, R. (2010). Review on free cooling of buildings using phase change materials. *Renewable and Sustainable Energy Reviews*, 14, p. 2819–2829. <https://doi.org/10.1016/j.rser.2010.07.004>
9. Iten, M., Liu, S., Shukla, A. (2016). A review on the air-PCM-TES application for free cooling and heating in the buildings. *Renewable and Sustainable Energy Reviews*, 61, p. 175–186. <http://dx.doi.org/10.1016/j.rser.2016.03.007>
10. Khan Z., Khan Z., Ghafoor A. (2016). A review of performance enhancement of PCM based latent heat storage system within the context of materials, thermal stability and compatibility, *Energy Conversion and Management*, 115, p. 132–158. <https://doi.org/10.1016/j.enconman.2016.02.045>
11. Ibrahim, N. I., Al-Sulaiman, F. A., Rahman, S.; Yilbas, B. S., Sahin, A. Z. (2017). Heat transfer enhancement of phase change materials for thermal energy storage applications: A critical review. *Renewable and Sustainable Energy Reviews*, 74, p. 26–50. <https://doi.org/10.1016/j.rser.2017.01.169>
12. Bejan, A. (2000). *Shape and Structure, from Engineering to Nature*. Cambridge: Cambridge University Press. <https://doi.org/10.1016/j.ijheatmasstransfer.2009.03.003>
13. Mandelbrot, B. B. (1982). *The fractal geometry of nature*. San Francisco: W.H. Freeman.
14. Lindenmayer, A. (1968). Mathematical models for cellular interactions in development I. Filaments with one-sided inputs. *Journal of Theoretical Biology*, 18(3), p. 280–299. [https://doi.org/10.1016/0022-5193\(68\)90079-9](https://doi.org/10.1016/0022-5193(68)90079-9)
15. Witten, T. A., and Sander, L. M. (1981). Diffusion-Limited Aggregation, a Kinetic Critical Phenomenon. *Physical Review Letters*, 47(19), p. 1400–1403. <https://doi.org/10.1103/PhysRevLett.47.1400>
16. Bejan, A. (1997). Constructal-theory network of conducting paths for cooling a heat generating volume. *International Journal of Heat and Mass Transfer*, 40(4), p. 799–816. [https://doi.org/10.1016/0017-9310\(96\)00175-5](https://doi.org/10.1016/0017-9310(96)00175-5)
17. Lorente, S., Wechsato, W., Bejan, A. (2002). Tree-shaped flow structures designed by minimizing path lengths. *International Journal of Heat and Mass Transfer*, 45(16), p. 3299–3312. [https://doi.org/10.1016/S0017-9310\(02\)00051-0](https://doi.org/10.1016/S0017-9310(02)00051-0)
18. Dbouk, T. (2017). A review about the engineering design of optimal heat transfer systems using topology optimization. *Applied Thermal Engineering*, 112, p. 841–854. <https://doi.org/10.1016/j.applthermaleng.2016.10.134>
19. Sciacovelli, A., Gagliardi, F., Verda, V. (2015). Maximization of performance of a PCM latent heat storage system with innovative fins. *Applied Energy*, 137, p. 707–715. <https://doi.org/10.1016/j.apenergy.2014.07.015>
20. Pizzolato, A., Sharma, A., Maute, K., Sciacovelli, A., Verda, V. (2017). Design of effective fins for fast PCM melting and solidification in shell-and-tube latent heat thermal energy storage through topology optimization. *Applied Energy*, 208, p. 210–227. <https://doi.org/10.1016/j.apenergy.2017.10.050>
21. Pizzolato, A., Sharma, A., Maute, K., Sciacovelli, A., Verda, V. (2017). Topology optimization for heat transfer enhancement in Latent Heat Thermal Energy Storage. *International Journal of Heat and Mass Transfer*, p. 113, 875–888. <https://doi.org/10.1016/j.ijheatmasstransfer.2017.05.098>
22. F. Kuznik and J. Virgone. Experimental Investigation of Wallboard Containing Phase Change Material: Data for Validation of Numerical Modelling. *Energy and Buildings*, 2009, 41 (5), p.561-570. <https://doi.org/10.1016/j.enbuild.2008.11.022>

Optimization of Intensive Daylight Simulations: A Cloud-based Methodology using HPC (High Performance Computing)

MILI KYROPOULOU¹, PAUL FERRER¹, SARITH SUBRAMANIAM²

¹HKS Architects, USA

²Department of Civil Engineering, TU Kaiserslautern, Germany

ABSTRACT: Large scale daylight simulations and representations on one single analysis grid are currently impossible with the use of conventional software and computers. Computational limitations that relate to the capacity of computer machines as well as analysis restrictions that relate to the allowable grid node count imposed by daylight simulation software prohibit daylight-coefficient based calculations on large scale analysis grids. The present paper utilizes a real aviation project and presents the development of a workflow that provides the ability to perform very demanding processes in acceptable time. Radiance related ray-tracing processes and matrix multiplications occur on the cloud using High Performance Computing and custom scripts that facilitate and accelerate the progression. The analysis grid count is decomposed into manageable fragments and after the calculation is performed, the fragmented values are recomposed in one single list of results that are utilized for colouring the analysis grid mesh. Processes are sped up by approximately 32 times. Customized tools can be adaptive and reused in other applications with minimum modifications. The methodology can also be adopted for performing other annual climate-based simulations or for glare studies.

KEYWORDS: Daylight simulations, cloud-based High-Performance Computing, Ray-tracing, Large Scale Applications

1. INTRODUCTION

The calculation of annual climate-based daylighting metrics is an integral part of whole building performance simulations [1,2,3]. Due to the computational footprint and magnitude of data such calculations entail, there is usually an upper threshold of analysis points for grid-based simulations that a software can handle within a reasonable amount of time. This limitation often forces users to develop alternative ways of compartmentalizing the initial model into smaller, manageable, segments. The manual processing of segments can become time consuming and difficult to validate with results lacking accuracy, integrity and continuity from one area to another.

Industry standard daylighting tools usually employ the Radiance-based Daysim engine for performing annual simulations. Daysim was introduced as a research tool nearly two decades ago and has been primarily tested in small-scale models [4]. On Windows operating systems (OS), both Radiance and Daysim are not designed to leverage multi-threading with modern processors like Intel i7® and Xeon®. Due to these shortcomings, grid-based daylight simulations of large floor areas with complex geometry are difficult to perform and must be prepared to specifically address these computational limitations.

In this paper, a large-scale airport terminal project is used as an example to initially evaluate existing methods, and further suggest a multi-stage, cross-platform workflow that overcomes current limitations. Honeybee for Grasshopper in Rhino [5] is used as the main interface to translate the CAD model to a

simulation-specific RAD format and visualize the results in the end. Radiance is used as the raytracing engine to run annual daylight simulations. Ray-tracing and matrix multiplications, the computationally intensive part of daylighting simulations, are performed on a cloud-based Microsoft Azure® High Performance Computing (HPC) system, the specifications of which can be seen in Figure (1). HPC systems are typically scalable and can be tailored specifically to particular tasks [6,7,8,9]. For large-scale simulations like the one described herein, the on-demand cost structure of HPC systems is also more economical in the long term than investing in high-end desktop computers.

```
CPU(s): 16
On-line CPU(s) list: 0-15
Thread(s) per core: 1
Core(s) per socket: 8
Socket(s): 2
NUMA node(s): 2
Vendor ID: GenuineIntel
CPU family: 6
Model: 63
Model name: Intel(R) Xeon(R) CPU E5-2667 v3 @ 3.20GHz
Stepping: 2
CPU MHz: 3192.527
BogoMIPS: 6385.05
Hypervisor vendor: Microsoft
Virtualization type: full
L1d cache: 32K
L1i cache: 32K
L2 cache: 256K
L3 cache: 20480K
```

Figure 1: Specifications of the computing machine used to perform multi-stage, cross-platform calculations

2. CLIMATE BASED ANNUAL METRICS

Spatial Daylight Autonomy (sDA) and Annual Sunlight Exposure (ASE), the annual daylight metrics proposed by the IES LM-83-12 [10], and since adopted by LEEDv4

PLEA 2018 HONG KONG

Smart and Healthy within the 2-degree Limit

[1], require the calculation of annual time series of illuminance values in a space.

2.1 The Daylight Coefficient Method

Annual climate-based daylighting simulations have their basis in the Daylight Coefficient (DC) Method [11]. The DC method employs a form of Finite Element analysis for optimizing the amount of time taken for performing 8,760 (one for each hour of the year) calculations of illuminance in the space. These calculations rest on two validated assumptions: 1) The nature and shape of building surfaces and contextual geometry remains the same, and 2) The celestial hemisphere can be approximated as a hemisphere consisting of luminous patches. As per the Perez Sky Model considered for climate-based daylight modelling, the luminosity of the patches are a function of the time of day, geographical location, direct-normal radiation and diffuse-horizontal radiation [12]. ASE is derived through a DC calculation with sun as the only illuminant. It considers only direct solar illuminance and ignores any reflections from sunlight. sDA requires a conventional DC simulation that incorporates diffuse sky calculations, indirect sun calculations and direct sun calculations. The computational effort required for any DC calculation is directly proportional to the amount of illuminance sensors in a room [11]. For reasons attributed to simulation runtime at the time of its development, Daysim, the most popular DC-based software, approximates and interpolates the position of the suns that derive from the 3,760 sun positions of a Typical Meteorological Year (TMY) weather file, to less than 63 annual positions in the celestial hemisphere [4,13] (Figure 2). The total number of hours in an annual simulation is 8,760 (based on 24 hours x 365 days). The value of 3,760 is specific to the TMY data considered for this research and accounts for only those hours of the year when the sun is visible in the celestial hemisphere.

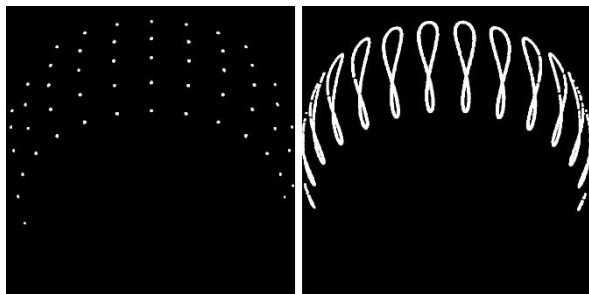


Figure 2: Improvements in accuracy: 63 independent sun positions considered by Daysim vs. the 3,760 sun positions derived through the (TMY) weather data.

2.2 The grid size parameter

Typically, the density of the illuminance analysis grid is set based on the LEED minimum requirement of a 2' or

0.6m spacing [1]. The test geometry subdivision results in DC simulations with up to a few hundred illuminance sensors, and, depending on the complexity of geometry involved, the computation time can range from a few minutes to several hours on a desktop computer.

3. SAN FRANCISCO INTERNATIONAL AIRPORT (SFO) AS BASE LINE EXAMPLE

The SFO extension project covers an area of approximately 300,000 square feet (27,870m²). Unlike other large-scale projects, every space in this area is unique as far as its design parameters are concerned. No floor area can be described as repetitive or with semi-similar daylight performance related design factors as is common in multi-story buildings with typical floors. The subdivision per Regularly Occupied Spaces [1] is also impossible because most of the main floorplate is one single space with no physical partitions. It is therefore hard to perform any calculation in fragments unless the model is subdivided exclusively for the purposes of the daylight calculation. The entire model involves an initial analysis grid with over 109,000 illuminance sensors.

3.1 Challenges of attempting such a simulation

Radiance uses a hybrid approach of stochastic and deterministic ray tracing to achieve a reasonably accurate result in a reasonable time [14]. For DC calculations with Radiance, matrix-based data-structures with 8-bit floating point values are used to store intermediate data files and results [15,16,17]. In the case of diffused sky illuminance calculation, the size of the sky matrix will be close to 48 Million floating point numbers (109,453 sensors x 146 sky segments x 3 RGB values). For the direct sun coefficient calculation, the size of the matrix will be over 1.2 Billion numbers (109,453 sensors x 3,760 sun locations x 3 RGB values). The file size of the two matrices is in the order of over 20GB.

Table 1: Coefficient Matrices for ASE and sDA calculations

	Sun (ASE) and Sky (sDA) Patches	Grid Points	Float Point Values
ASE Calc	3760	109,453	1,234,629,840
sDA Calc	146	109,453	47,940,414

Coefficient matrices (Table 1) are converted into illuminance values after multiplying them with sky matrices that contain luminance values for sky patches.

PLEA 2018 HONG KONG

Smart and Healthy within the 2-degree Limit

In the case of ASE, this translates to parsing and loading 1.2 Billion floating point values in RAM and then multiplying them with a matrix containing over 98 Million numbers (3,760 sun patches x 8,760 h x 3 RGB values) as Table 2 denotes.

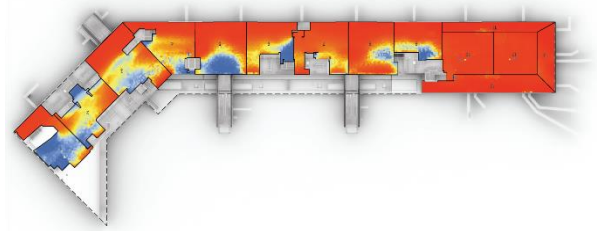
Table 2: Sky and Sun Matrices for ASE and sDA calculations

	Sun (ASE) and Sky (sDA) Patches	Vectors in Sky Matrix	Numbers to be held in memory (during multiplication)
ASE Calc	3,760	8,760	121,997,231,453,952,000
sDA Calc	146	8,760	183,941,615,668,320

The magnitude of these operations is not compatible with the configurations of even the most high-end desktop computers. Most industry standard 3D modelling environments such as Revit, Rhino etc are only compatible with Windows OS. As discussed previously, both Daysim and Radiance do not support multi-threading on Windows. Therefore, even where the hardware resources exist, it is currently impractical to perform such simulations on Windows-based systems.

3.1 Attempt 01: Floor plate subdivision

To overcome the challenges of such a simulation, the initial building geometry and analysis surface are geometrically subdivided into 14 smaller floor plates. Illuminance calculations are performed individually for those segments using only DIVA for Grasshopper in Rhino [18]. Each simulation is limited to a fixed number of analysis points, and the number of necessary simulations is determined by dividing the floor area into zones containing roughly equal numbers of sensors at the required 2' (0.6m) spacing. As each simulation will engage only one CPU core, this process can be slightly accelerated by running multiple instances of the host program and launching simulations for different grids on each open instance. In this case, the test machine can run 8 concurrent simulations within 8 separate sessions of DIVA for Rhino. The results are then weighted per the area they represent to estimate one single sDA and one single ASE value for the entire analysis surface. For graphical representation, the resultant mesh faces of each simulation are compiled into a single image (Figure 3). Attempt 01 lacked integrity between simulated zones, was time consuming, and, was prone to errors introduced while manually performing post processing operations. Additionally, as explained in chapter 2.1 through Figure (2), this approach is potentially less accurate than a simulation involving accurate sun positions. However, it provided a relatively effective



answer to the limitations of the case and created the foundation for further optimizing the workflow.

Figure 3: Attempt 01 floor plan. Note the dividing markers between each simulated section. The results from each section are combined into one value.

3.2 Attempt 02: Cloud-based calculation

The second attempt involved performing the entire simulation of the complete analysis grid in one single, multi-threaded instance. This was made possible by running the simulations on a cloud-based HPC with a Linux 16.04 OS. Potential RAM-related issues associated with attempting such an intensive simulation were addressed through the development of custom scripts built to manage memory usage.

3.2.1 Methodology

A conventional annual daylight simulation using the DC method can be seen in Equation (1).

$$E = \sum_{i=1}^p \left(\sum_{j=1}^{146} DC_{xS} - \sum_{j=1}^{146} DC_D \times S_D + \sum_{k=1}^{3760} DC_{sun} \times S_{sun} \right) \quad (1)$$

where p the number of illuminance sensors
 j the number of sky patches, and
 k the number of direct-sun patches used in the ray-tracing simulation.

The above equation can be expressed in matrix format as shown in Equation (2).

$$E = E_{sky} - E_{sky_{direct}} + E_{sun} \quad (2)$$

Initial attempts at performing the simulation as per the conventional method were unsuccessful as the number of points resulted in memory overflows despite the availability of nearly 230GB of RAM. Similar issues pertaining to both memory and processing time have been acknowledged by Zuo et al [19]. The solution suggested by them involves the use of proprietary GPU-based calculations that are not applicable to all types of HPC systems. Lack of sufficient memory became more apparent in the case of the direct-sun simulation that involved a sun-coefficient matrix of the dimensions 109,453 x 3,760 and a sun-matrix of the dimensions 3,760 x 8,760.

PLEA 2018 HONG KONG

Smart and Healthy within the 2-degree Limit

Several customized scripts written in Python allowed for the direct sun parameter E_{sun} to be calculated in 100-node segments after Equation (3). Although this step is not required on all simulations of this kind, the ability to identify breakpoints in matrices and parse them sequentially is key to scaling this process to analyze extremely large building footprints.

$$E_{sun_{1-100}} = \sum_{i=1}^{100} \sum_{k=1}^{3760} DC_{sun} \times S_{sun}$$

$$E_{sun_{101-200}} = \sum_{i=101}^{200} \sum_{k=1}^{3760} DC_{sun} \times S_{sun}$$

until

$$E_{sun_{109401-109453}} = \sum_{i=109401}^{109453} \sum_{k=1}^{3760} DC_{sun} \times S_{sun}$$

(3)

The grid-based figures were then associated with the Rhino model and by using native Honeybee components, the analysis surfaces were colored based on the measured results of the calculation (Figure 4).

3.2.2 Workflow and custom components

The workflow for the cloud-based calculation method progressed through a series of software tools depending upon the specific task at hand (Figure 5). Building geometry was exported from the construction documentation model residing in Revit and organized by material type within Rhinoceros 3d/Grasshopper. Utilizing the Honeybee analysis plugin within Grasshopper, the analysis grid was generated for all evaluation spaces per LM83 requirements. As this evaluation area was comprised of multiple non-repeating floor areas, to ensure correct graphical visualization of the results, the lists of mesh-faces and analysis points were organized in matching data structures prior to being exported into a Radiance compatible RAD format. Various scripts written in Python were developed to automate the processing of Radiance commands on the HPC system to calculate both ASE and sDA metrics.

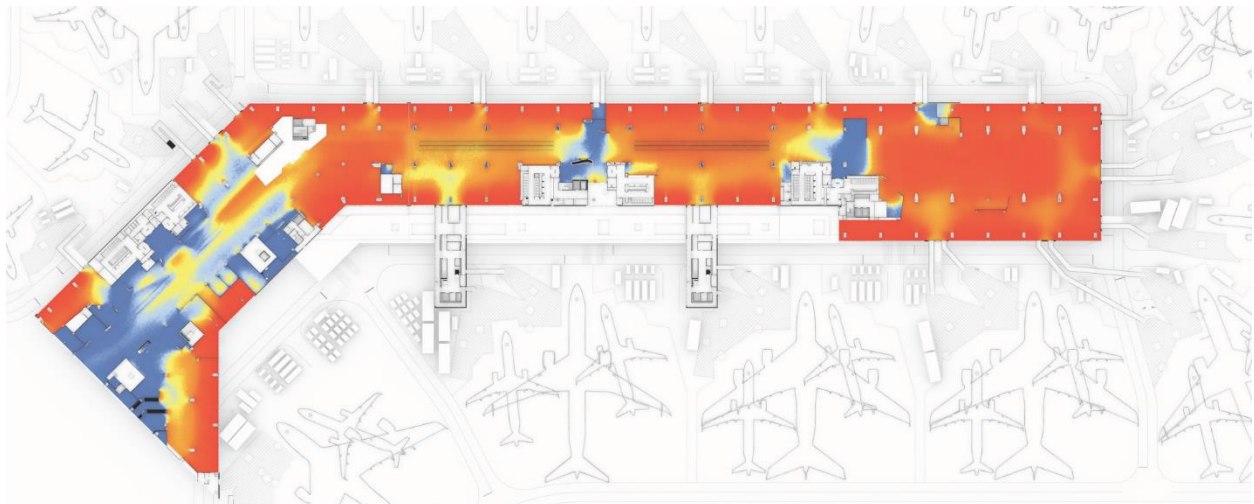


Figure 4: Attempt 02 floor plan (not directly comparable to Figure 3, due to changes in design. This image is meant to compare quality and integrity of result)

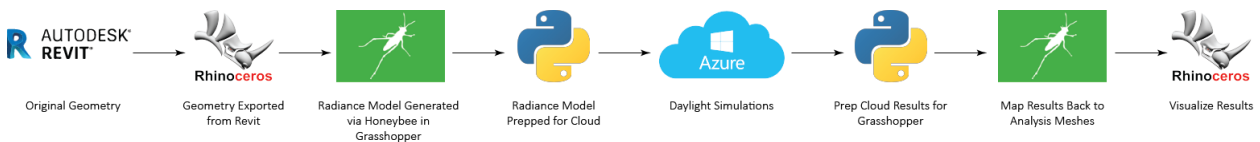


Figure 5: Tool progression for cloud-based simulation workflow

Finally, the individual results were combined to create one single matrix as Equation (4) denotes.

$$E_{sun} = E_{1-100} + E_{101-200} + E_{201-300} + \dots + E_{109401-109453} \quad (4)$$

4. Potential repurposing of the methodology for other daylight studies

This methodology is not limited to horizontal grids. Vertical grids are equally possible using the same workflow as is.

PLEA 2018 HONG KONG

Smart and Healthy within the 2-degree Limit

The same methodology can also be used for any illuminance based annual metrics, such as Useful Daylight Illuminance (UDI), Daylight Autonomy (DA), continues Daylight Autonomy (cDA) etc. The population of the matrices and the illuminance calculations, the intensive part of the overall process, remains the same. The script needs to only be expanded at its further end, when the results are already extracted from Radiance and are being post-processed, to calculate the percentage of space or the percentage of time that qualifies with the set threshold for every dynamic daylight metric.

Furthermore, the same methodology can be used for glare studies [20]. Instead of specifying grid points, it will require the generation of input rays for individual pixels. The raw output will then have to be redirected to a tri-channel RGB format file to generate HDR files instead of illuminance files. Based on the results presented in [21], such an approach can curtail the simulation time by nearly 60%.

One more application that could benefit from that methodology is the evaluation of active shading systems [22]. Active shading systems require the modification of the nature or shape of the building (i.e. glazing properties) or the obstruction elements (i.e. shading geometry), which is one of the two constants the DC method is assuming (as discussed in chapter 2.1 of the present). The calculation needs to be performed separately for the multiple iterations with the shading system as the independent variable. The results need then to be reconstructed based on shading controls or after a predefined schedule. The benefit of this methodology lies on the significantly reduced time required to run the multiple iterations before recomposing them.

5. CONCLUSION

The use of dedicated Unix HPC systems allowed the simulations to be hyper-threaded with almost 99% utilization. In contrast, a Windows-based system running Daysim allows for only 26-50% utilization on a single thread. The actual ray-tracing processes were sped up by nearly 32 times (on a 16-core processor). Utilizing a better processor and running the simulation on the cloud was proven insufficient to perform a calculation of that magnitude. The calculation became possible only with the scripted subdivision and re-composition of the grid (sensors).

Compared to the existing method utilized in Attempt 01, the introduction of the proposed workflow allows one single simulation to be performed on the whole analysis grid, which provides an immediate benefit to the design team. In addition, utilizing this workflow results in significantly reduced time required to calculate annual daylight metrics, it eliminates possible errors that often derive from manual post-processing and provides a more uniform and reliable

result that can be successfully represented on a colored grid plane. For large-scale applications that involve non-repeating floor areas, this method is a viable alternative to currently available workflows.

Outsourcing intensive calculations to the HPC servers allows project work to continue unimpeded on local machines as simulations are processed remotely. Software and hardware costs are also minimized as all machines ran open-source software on an adaptive infrastructure that can scale to accommodate the project at hand with little to no modification.

Although this methodology has proven especially useful for the simulation of large scale spaces commonly encountered in architectural practice, the knowledge necessary for implementation spans several disciplines and introduces a high barrier to entry for a typical office studio environment. As such, in its current format, this method is best utilized as a supplement when encountering projects that surpass the technical limitations of existing workflows.

ACKNOWLEDGEMENTS

The authors would like to thank Yeng Vue for assisting them to successfully operate Azure.

REFERENCES

- US Green Building Council, (2013). LEED V4 for Building Design and Construction. Washington, DC, USA.
- DiLaura D.L., Mistrick R.G., Houser K.H., Steffy G., (2011). The Lighting Handbook: Reference & Applications. New York, USA.
- Hensen J.L., (2011). Building Performance Simulation for Design and Operation. Oxford, USA. Routledge. p. 235-276.
- Reinhart C.F., Walkenhorst O., (2001). Validation of Dynamic RADIANCE-based Daylight Simulations for a Test Office with External Blinds. *Energy & Buildings*. 33(7):683-697. Available: www.sciencedirect.com/science/article/pii/S0378778801000585
- Roudsari M., Pak M. (2014). Ladybug: A Parametric Environmental Plugin for Grasshopper to Help Designers Create an Environmentally-Conscious Design. *13th Conference of International Building Performance Simulation Association*. Chambéry, France. Available: http://www.ibpsa.org/proceedings/BS2013/p_2499.pdf
- Microsoft Corporation. Microsoft Azure, [Online], Available: <https://azure.microsoft.com>
- Digital Ocean LLC. Digital Ocean Droplets [Online], Available: <https://www.digitalocean.com/products/droplets/>
- Amazon Web Services Inc. High Performance Computing on the cloud, [Online], Available: <https://aws.amazon.com/hpc/>
- Google Inc. Architecture: High Performance Computing, [Online], Available: <https://cloud.google.com/solutions/architecture/highperformancecomputing>

PLEA 2018 HONG KONG

Smart and Healthy within the 2-degree Limit

Illuminating Engineering Society, (2012). LM-83-12 IES Spatial Daylight Autonomy (sDA) and Annual Sunlight Exposure (ASE). New York, USA.

Tregenza P.R., Waters I.M., (1983). Daylight coefficients. *Lighting Research and Technology* 15(2):65-71. Available: <http://journals.sagepub.com/doi/pdf/10.1177/096032718301500201>

Perez R, Seals R, Michalsky J., (1993). All-weather model for sky luminance distribution—preliminary configuration and validation. *Solar Energy*. 51(5):423.

Brembilla E., (2016), Survey on Climate-Based Daylight Modelling workflows. *15th International Radiance Workshop*; Padova, Italy. Available: <https://www.radiance-online.org/community/workshops/2016-padua/presentations/204-Brembilla-CBDMsurvey.pdf>

Ward G., Shakespeare R., Ehrlich C., Mardaljevic J., Phillips E., Apian-Bennewitz P., (1998). *Rendering with Radiance: the Art and Science of Lighting Visualization*. San Francisco, CA, USA, Morgan Kaufmann.

Subramaniam S., (2017). Daylighting Simulations with Radiance using Matrix-based Methods. Available: <https://radiance-online.org/learning/tutorials/matrix-based-methods>

LBNL, Rcontrib, (2005), [Online]. Accessed: 08/14/2018. Available:

<https://www.radiance-online.org/learning/documentation/manual-pages/pdfs/rcontrib.pdf>

LBNL, Gendaymtx, (2013) [Online]. Accessed: 08/14/2018. Available:

<https://www.radiance-online.org/learning/documentation/manual-pages/pdfs/gendaymtx.pdf>

Alstan J.J., Reinhart C.F., (2011). DIVA 2.0: Integrating Daylight and Thermal Simulations using Rhinoceros 3d, Daysim and Energyplus. *Proceedings of Building Simulation 2011: 12th Conference of International Building Performance Simulation Association*, Sydney, Available: http://ibpsa.org/proceedings/BS2011/P_1701.pdf

Zuo W., McNeil, A., Wetter M., Lee E., (2011). Acceleration of Radiance for Lighting Simulation by Using Parallel Computing with OPENCL., *Proceedings of Building Simulation: 12th Conference of International Building Performance Simulation Association*, Sydney.

Geisler-Moroder D., Lee E.S., Ward G., (2017). Year Validation of the Five-Phase Method for Simulating Complex Fenestration Systems with Radiance against Field Measurements. *15th International Conference of the International Building Performance Simulation Association*. California, USA. Available:

<https://escholarship.org/uc/item/24h966pp>

Subramaniam S., (2018). Parametric Modeling Strategies for Efficient Annual Analysis of Daylight in Buildings (Doctoral Dissertation). The Pennsylvania State University, The Graduate School Department of Architectural Engineering. Available:

https://www.researchgate.net/publication/325248582_Parametric_modeling_strategies_for_efficient_annual_analysis_of_daylight_in_buildings

Jakubiec J.A., Neimasz J., Modeling Dynamic Shading Devices with the DIVA Advanced Shading Module, 2012, [Online], Available:

https://www.solemma.com/img/Events/2012/DD2012_Jakubiec-

[Neimasz_ModelingDynamicShadingDeviceswiththeDIVAAdvancedShadingModule.pdf](https://www.solemma.com/img/Events/2012/DD2012_Jakubiec-Neimasz_ModelingDynamicShadingDeviceswiththeDIVAAdvancedShadingModule.pdf)

Dynamic Microclimate Modelling for Urban China: Assessing pedestrian comfort, air quality and building ventilation potential

VEDA BALIGA¹, MARK DEKAY², RUGGIERO GUIDA³, SITAN ZHU⁴

¹BPMG, Glasgow, UK, ²University of Tennessee, Knoxville, USA, ³BPMG, Glasgow, UK, ⁴Hubei University of Technology, Wuhan, China

ABSTRACT: It is common practice to use hourly dynamic thermal modelling for building design, yet climate responsive urban design, is often based on predominant wind directions analysed for particular 'typical' days or times. Such a snapshot view does not reflect how often these conditions occur and whether design changes based on single instances are warranted. This paper explores the efficacy of using an annual dynamic approach, by extending and comparing results from a previous study of district massing on local microclimate. These dynamic annual analyses were undertaken using a new cloud-based microclimate analysis tool that employs open source software for Computational Fluid Dynamics (CFD) and post-processing of results. This tool allows for complex hourly analyses of solar radiation, wind and comfort distribution to be conducted within a commonly used 3-D modelling software environment. Following the previous study, this paper compares the resulting urban form across three major issues: pedestrian comfort, air quality and building cross-ventilation potential. Pedestrian comfort assessment includes thermal comfort, using the Universal Thermal Climate Index (UTCI) and wind comfort, using the Dutch standard NEN 8100. Air quality is approximated by air age distribution. Building ventilation potential is assessed by mapping pressure differentials at points on opposing building faces.

KEYWORDS: Pedestrian comfort maps, CFD-based microclimate, Air quality, Natural ventilation potential, Urban physics

INTRODUCTION

Buildings are commonly modelled using dynamic hourly thermal software, yet a more limited approach is used in climate evaluation for urban design. The computational intensity required often results in a simplification of the wind regime; limiting analysis to particular dates and times, e.g. summer or winter solstices, at mid-day. This "snapshot view," helps designers generalize about design improvements in response to wind or solar access, but does not reflect the frequency with which these conditions occur or whether decisions based on these instances achieve the desired improvement at other times of the year.

This paper explores the efficacy of using an annual dynamic simulation approach, by extending and comparing results from a previous study of urban district massing based on local microclimate [1,2]. The first phase of the study assessed five "super-block" housing developments in Wuhan, China for pedestrian comfort, air quality and building ventilation potential. The second phase redesigned the neighborhood using Transit-Oriented Design (TOD) guidelines for China [3] and compared it to an existing, comparable density super-block scheme, Fudidonghu (Fudi). In this study, we compare the resulting TOD scheme and the original Fudi design across three major issues: pedestrian comfort, air quality, and building cross-ventilation potential. Pedestrian comfort assessment includes

thermal comfort, using the Universal Thermal Climate Index (UTCI) [4] and wind comfort, using the Dutch standard NEN 8100 [5]. Air quality is approximated by age of air distribution and building ventilation potential is assessed by measuring pressure differentials at points on opposing building faces.

These analyses use a new, original, cloud-based microclimate analysis tool that employs open source software OpenFOAM [6] for the Computational Fluid Dynamics (CFD) and ParaView [7] for data analysis and visualization. This tool allows for complex hourly dynamic analyses of solar radiation, wind, and comfort distribution to be conducted within SketchUp [8]. Analyses can be undertaken for as many or as few hours of the day and days of the year as required and results can be mapped back onto the 3-D model. This approach allows one to probe microclimate behavior at specific times of year as well as explore varying seasonal patterns, all within the context of the 3-D geometry.

Typical Chinese super-block development has poor walkability, transit support and street life, along with high energy use and auto dependence. TOD guidelines address these issues, but may reduce building ventilation potential at lower levels due to greater site coverage and block perimeter buildings.

The project's hypotheses are 1) On an annual basis, TOD development can be designed to equal super-block wind performance; 2) Dynamic annual wind and

PLEA 2018 HONG KONG

Smart and Healthy within the 2-degree Limit

comfort modeling improves performance feedback time and quality for urban design, as compared to simpler CFD methods.

METHODOLOGY

We assessed Super-block and TOD schemes of equivalent density on an annual basis. Figure 31 shows overview of the massing layout.

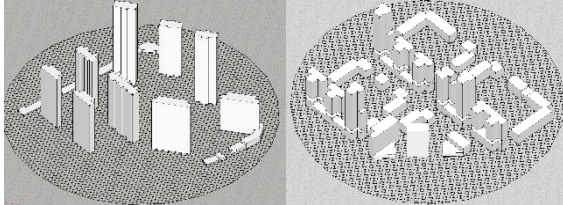


Figure 31: Superblock Massing (L) and TOD Massing (R)

All analyses share a common analysis grid on which the final results are mapped. For this study, the grid used was 400m in diameter and comprised of 5000 individual points. To encourage walkability, the analyses used times of day that spaces are most likely to be occupied; nominally between 8 AM to 10 PM.

The annual radiation analysis looks at distribution of radiation on site, accounting for direct and diffuse shortwave radiation, longwave radiation and overshadowing from buildings.

The CFD analysis used OpenFOAM. The wind inlet boundary condition used was the default Atmospheric Boundary Layer condition in OpenFOAM (D.M. Hargreaves and N.G. Wright). The solver used for simulation was SimpleFoam with a k-epsilon turbulence model. The domain size was generated automatically based on standard practice; with domain width 10 times the height of the tallest building, and domain height 5 times the height of the tallest building. The domain was octagonal to account for the eight wind directions. This approach has the advantage of having to mesh the domain only once for all wind directions at the cost of slightly larger meshes, resulting in a total of up to 20 million cells - predominantly hexahedral - for both cases in this study, with a ground boundary layer refinement. Annual hourly weather data used was obtained from the EnergyPlus website as an EPW file [9].

We then combined the results of these analyses to generate comfort indicators for each point in the mesh for each annual hour occupied. The overall methodology for this study was:

Run dynamic microclimate analysis and extract age of air and comfort maps for particular dates to compare with previous “snapshot” studies

For each scheme, generate seasonal statistics and graphical maps for pedestrian comfort, age of air, and façade ventilation potential

For one of the TOD massing 'courtyards,' quantify the impact of typical passive design measures on occupant comfort

Analyze results to find strategic ways to improve the TOD design for wind performance

Evaluate the results to test the hypotheses in a subsequent paper

RESULTS AND DISCUSSION

The results for occupant comfort, air quality and natural ventilation potential, along with comparative review with the previous results, are discussed in sub-sections 3.1 to 3.6.

3.1 Comparison with previous results

The initial study undertook age of air and comfort analyses for specific dates and times. The key differences between the parameters for the previous study and the current analysis are shown in Table 5

Table 5: Difference between standard and dynamic analysis

STANDARD ANALYSIS	DYNAMIC ANALYSIS
NE & SE directions only, fixed initial wind speed 2.6 m/s	All wind directions & speeds in hourly weather file
Typical summer day (June 22) and winter day (Jan 20), Single hour, 12 noon	365 days a year Hours, 8 AM to 10 PM
PMV comfort for Summer, 30°C (86°F) Winter, 5°C (41°F)	UTCI comfort for local wind speeds from CFD and hourly weather file

The comparison between age of air results from the previous and current study are shown in Figure 32 to Figure 35.

The age air results are not a like for like comparison as the initial study combined a wind speed and direction and date that didn't necessarily occur concurrently in the weather data set used. However, both sets of analyses indicate that the Fudi superblock massing tends to have a greater rate of air change (lower air age) than the TOD massing.

PLEA 2018 HONG KONG

Smart and Healthy within the 2-degree Limit

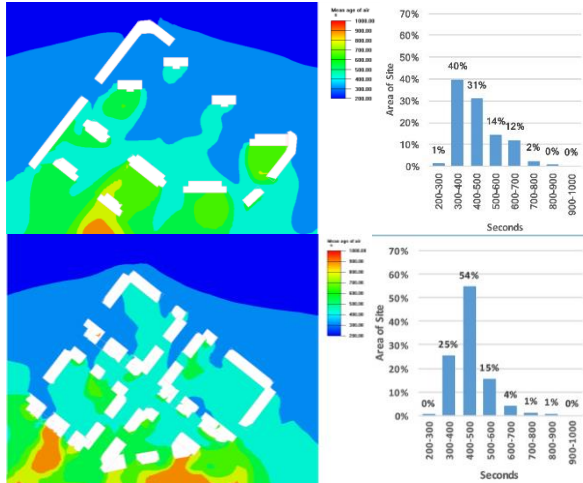


Figure 32: NNE Age of Air Snapshot (original study)

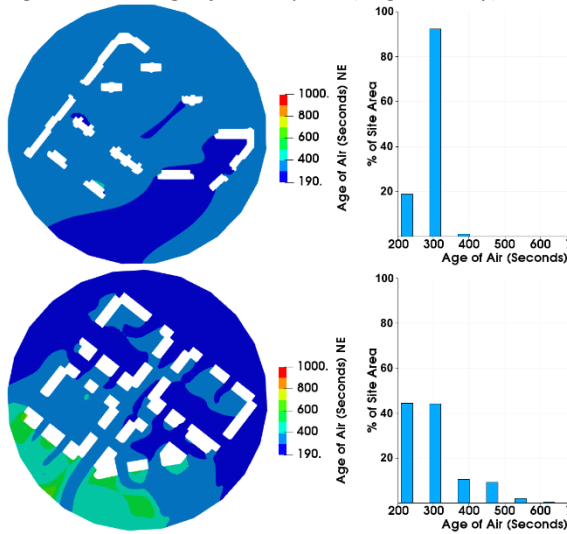


Figure 33: NNE Age of Air Snapshot (extract)

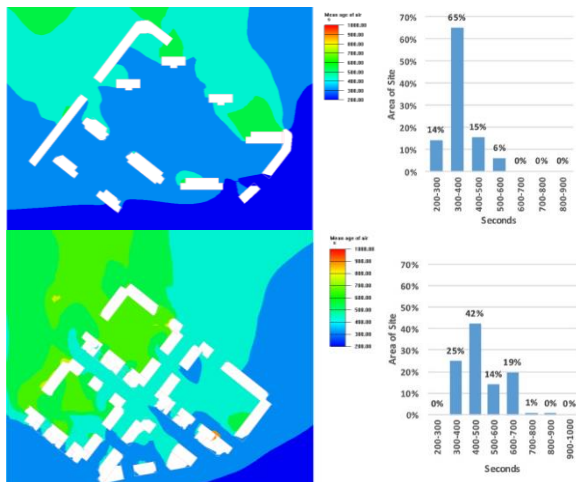


Figure 34: SE Age of Air Snapshot (original study)

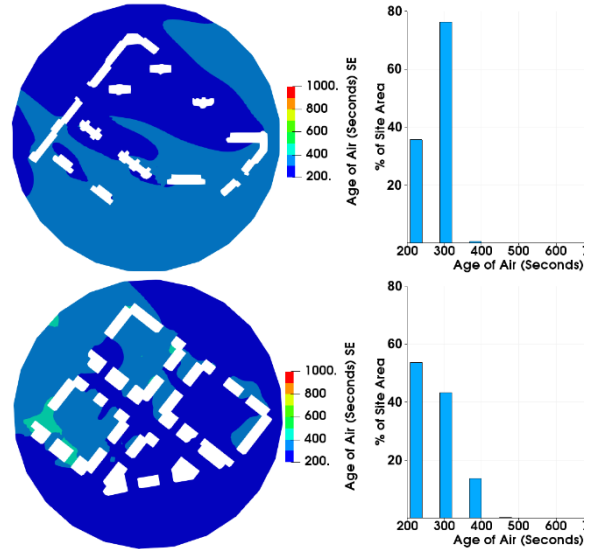


Figure 35: SE Age of Air Snapshot Comparison

The comfort results also do not directly correlate with each other because, in addition to the issues described above, they use different metrics (PMV in the previous study vs UTCI in this simulation). Both sets of results concur on the fact that a majority of the site experiences discomfort on both dates; cold discomfort on Jan 20th and warm discomfort on June 22nd.

3.2 Wind comfort distribution

The wind comfort calculation references the Dutch standard NEN-8100, which evaluates how often the wind speed exceeds 5m/s throughout the year and its impact on different activity levels in external spaces. An overview of the standard is shown in Figure 36.

% Hours/Year Wind Speed > 5m/s	Sitting	Standing	Strolling	Grade
<2.5%	Good	Good	Good	A
2.5% - 5%	Moderate	Good	Good	B
5% - 10%	Poor	Moderate	Good	C
10% - 20%	Poor	Poor	Moderate	D
>20%	Poor	Poor	Poor	E

Figure 36: NEN8100 Wind Comfort Criteria

Overall, the wind speeds on site are quite low and the results outlined in Figure 37 indicate that wind speeds greater than 5 m/s occur for less than 2.5% of the year, rendering all areas of the site suitable for all levels of activity.

PLEA 2018 HONG KONG

Smart and Healthy within the 2-degree Limit

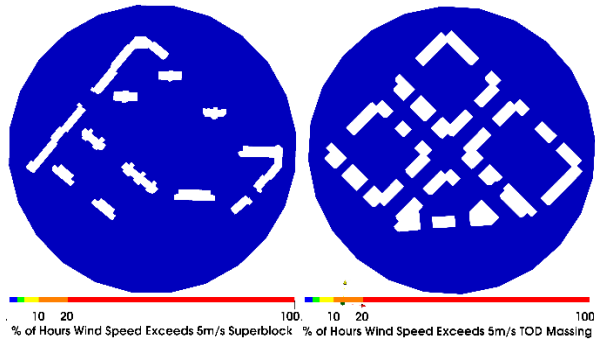


Figure 37: Annual Wind Comfort Comparison

3.3 Thermal comfort distribution

UTCI is a comfort index that models in detail, the thermal exchange between the human body and its environment through combining environmental variables (local air speed, temperature, relative humidity, radiant gain/loss) and physiological variables (clothing and activity levels) to provide an indication of the perception of the thermal environment by occupants. The standard comfort range for UTCI is from 9 to 26.

A value below 9 indicates cold discomfort and above 26 indicates warm discomfort.

The results in Figure 38 and Figure 39 provide an overview of how often the UTCI occurs within the comfort range (9-26) in each season. Overall, the TOD massing experiences marginally higher comfort levels (see legend). However, both massing types show a similar pattern of distribution annually, where Spring is the most comfortable season and Winter is the least.

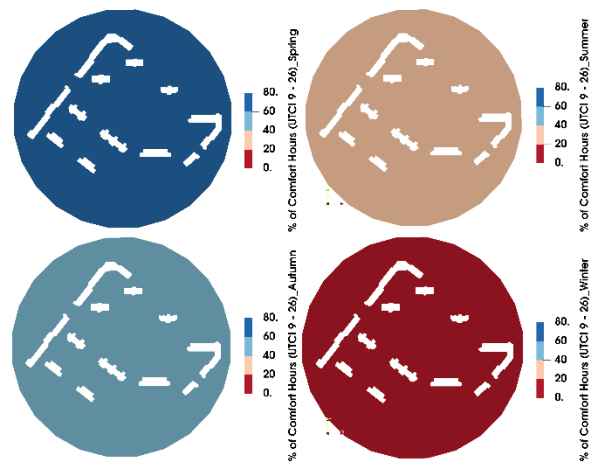


Figure 38: Fudi Superblock Seasonal Comfort Comparison

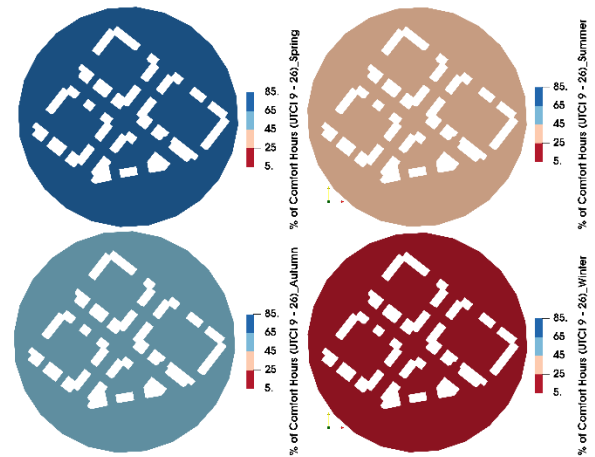


Figure 39: TOD Seasonal Comfort Comparison

Since the results in Figure 38 and Figure 39 don't show the distribution and variation in comfort levels within the site, Figure 40 shows the difference in results for both schemes in Spring. The histogram for the Fudi massing is stacked towards the left of the chart; i.e. majority of the site area experiences relatively fewer hours with UTCI in the comfort range (9-26). The marginally improved comfort observed for the TOD massing likely relates to greater overshadowing from surrounding buildings.

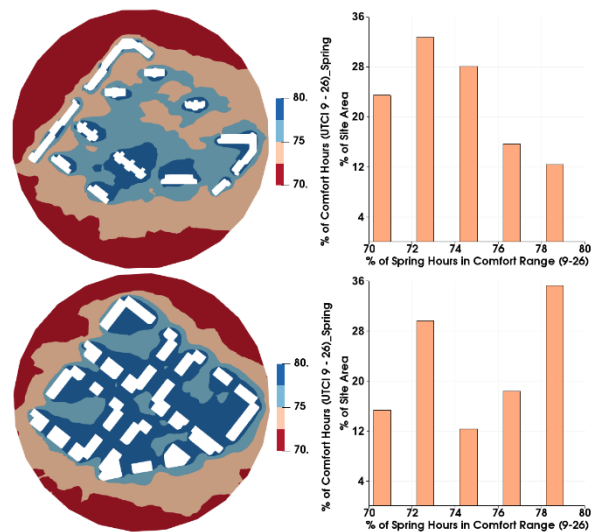


Figure 40: Spring Comfort Comparison

3.4 Age of air distribution

Typically, age of air is a metric used for indoor spaces to indicate air quality; i.e. how often air is replaced with fresh air from outside. The upper limit is 5 minutes or 300 seconds. This approach does not directly translate to outdoor spaces and at best, serves as a comparison of how long it takes air at any point to be displaced from the time it enters the domain.

PLEA 2018 HONG KONG

Smart and Healthy within the 2-degree Limit

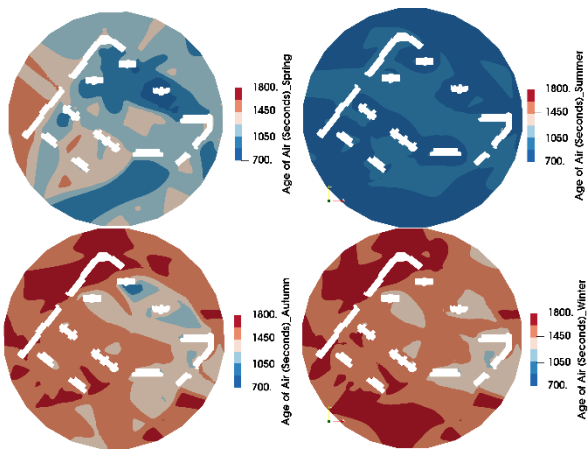


Figure 41: Fudi Superblock Median Age of Air by Season

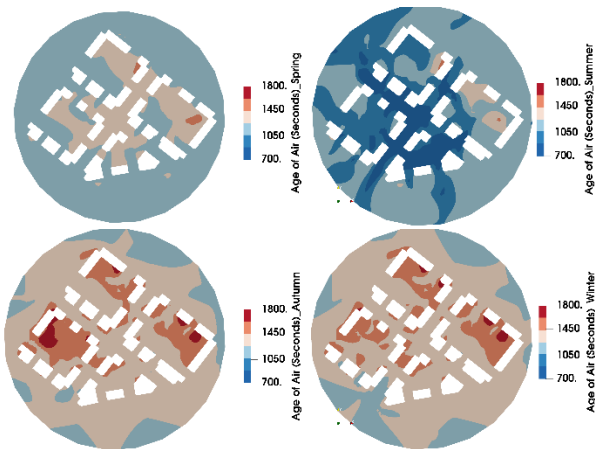


Figure 42: TOD Median Age of Air by Season

This study looks at wind speed and direction for each occupied hour of the year, making the age of air indicative of local wind patterns.

Overall, the results in Figure 41 and Figure 42 indicate that age of air is lowest in summer and highest in autumn and winter. This has positive implications for thermal comfort as this is closely correlated with air speed. Spring shows the greatest variation within the site, but overall the superblock massing has lower age of air; i.e. better air circulation, for at least part of the site, as compared to TOD, which includes a few 'dead' spots in all seasons, including summer.

Figure 43 shows the comparative age of air results for both massing types in Spring. The Fudi superblock experiences a wider range of age of air with roughly 5% of the western part of the site showing very low air change. While the overall age of air in the TOD massing is higher, on average the air change rate is in the range of 18-20 minutes.

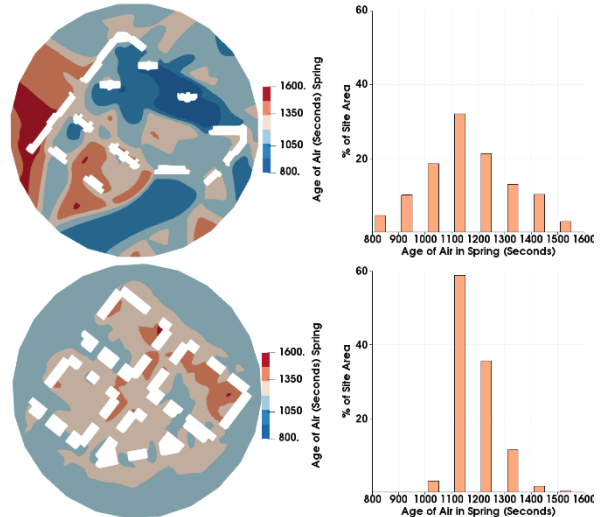


Figure 43: Spring Age of Air Comparison

3.5 Natural ventilation potential

Chinese ventilation standards for double-sided through ventilation of housing call for a minimum pressure difference between opposite openings of 1.5 pa [10]. The pressure differential was mapped at a distance of 0.5m from the wall surface across 24 hours to include night cooling. Mapped results in Figure 44 show the percentage of hours that the pressure differential exceeds the 1.5 pa minimum threshold for ventilation potential. The TOD massing shows greater variation in ventilation potential but also improved performance relative to the Fudi superblock massing, at least in the taller buildings. The low rise buildings within the TOD massing tend to show an equivalent or worse performance compared to the Fudi superblock. Figure 45 shows a histogram that plots the proportion of surface area that exceeds the 1.5pa differential against the proportion of hours.

PLEA 2018 HONG KONG

Smart and Healthy within the 2-degree Limit

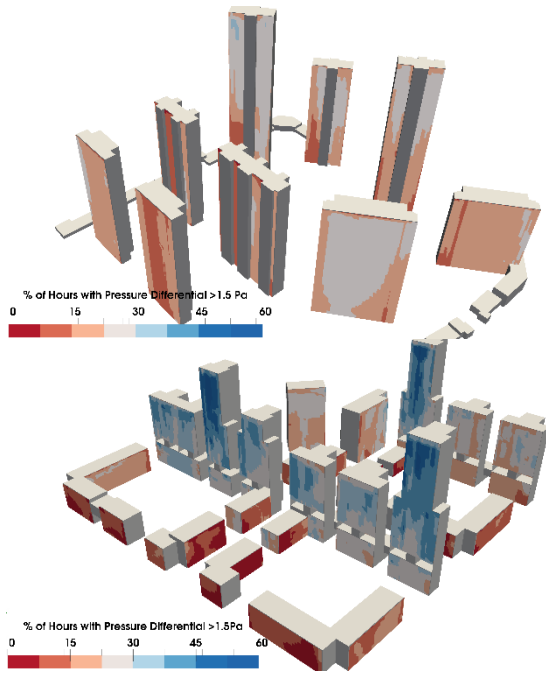


Figure 44: Natural Ventilation Potential Comparison

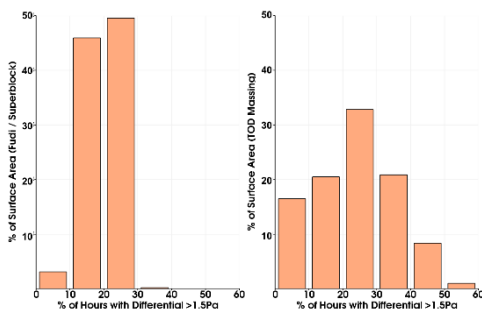


Figure 45: Natural Ventilation Potential Histogram

3.6 Impact of passive design measures

Results for the TOD massing indicated that a majority of the site experienced warm discomfort for >50% of hours in summer. One of the benefits of undertaking an annual assessment is that it allows us to quantify the impact of design interventions.

A point in one of the courtyards in the TOD massing was evaluated for comfort without any interventions and then, including design interventions, such as adding vegetation and physical shading, as shown in Figure 46.

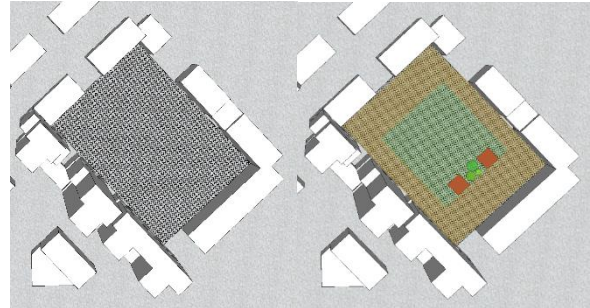


Figure 46: Unshaded Baseline (L) and Shading Inclusion (R)

The maps resulting from of this evaluation are shown in Figure 47 and point A within this map was further analyzed to determine the change in distribution of comfort occurrence at this point throughout summer.

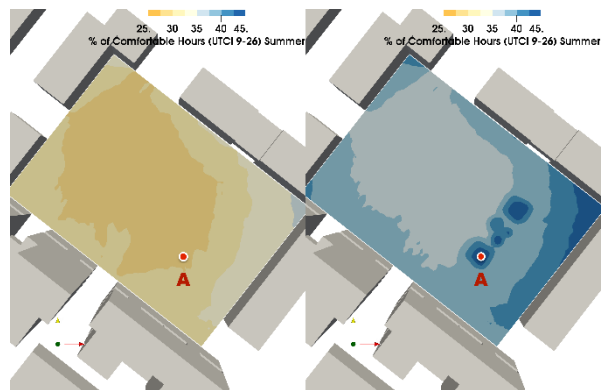


Figure 47: TOD Massing – Impact of Design Measures

Figure 48 shows the comfort distribution at point A across the summer months as a heat map; with the x-axis showing the time of year and the y-axis, the time of day. The areas that show up in dark orange are $UTCI > 26$ and as a result, are outside of the comfort range. The most noticeable improvements in comfort occur in early June and late August and September.

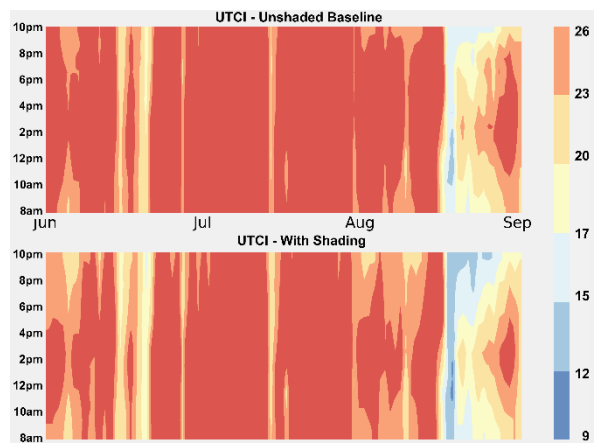


Figure 48: Heat Map of Summer UTCI for Point A

Overall, there are 179 more hours that fall within the comfort range, an improvement of 14% or the equivalent of 11 additional days where it's comfortable for every hour of the day.

PLEA 2018 HONG KONG

Smart and Healthy within the 2-degree Limit

4. CONCLUSION

The methods used so far mostly look statistically at the site as a whole. The final example in 3.6 is an exception, aimed at clarifying the level of granularity this approach affords. Further developments of the methodology can extend this approach to improve comfort in primary pedestrian areas, such as sidewalks and building entrances, in addition to gathering places and seasonal activity areas.

The results in 3.6 indicate that even basic passive design measures can noticeably improve comfort levels in Wuhan during the warmer months. Covered outdoor circulation, such as arcades along the streets, plus street trees for shading would improve pedestrian comfort locally where people walk most. Locating summer public outdoor spaces in breezeways under buildings or on the north side of tall buildings offers further refinement for warmer months.

Winter is almost always uncomfortable in this climate and the passive measures available include local wind blockage and increased exposure to radiation. The latter suggest a tension between solar access for buildings and outdoor sun for open spaces. Solar exposure for buildings, as required by Chinese codes, is expressed in the TOD guidelines by locating tall buildings to the southern edge of blocks; overshadowing much of the open space in winter. This indicates that there is a need to include specific winter outdoor spaces with access to sunlight. These might also benefit from deciduous trees to provide some shade in summer.

One way to improve air circulation might be to stagger the heights of the buildings even more, to create a greater variation in pressure distribution and as a result, increase air movement.

REFERENCES

1. Mark DeKay, et al (2017). Urban Wind Patterns in High-Rise Residential Super-Blocks: assessing pedestrian comfort, air quality and building ventilation potential. *Proceedings, PLEA*
2. Mark DeKay, et al (2018). Urban Wind Field Patterns in Transit-Oriented Development for China: Assessing pedestrian comfort, air quality and building ventilation potential. *Unpublished*
3. Calthorpe Associates, China Sustainable Cities Program, and FEHR & PEERS (2012). *Design Manual for Low Carbon Development*. The Energy Foundation
4. Bröde, P., et al (2010). The Universal Thermal Climate Index UTCI in Operational Use, [Online], Available: <https://dspace.lboro.ac.uk/2134/6086>
5. NEN-8100 (2006). Wind comfort wind danger in the built environment, [Online], Available: <https://www.nen.nl/NEN-Shop-2/Standard/NEN-81002006-nl.htm>
6. OpenFOAM CFD software, [Online], Available: <https://openfoam.org/>
7. ParaView data analysis and visualization software, [Online], Available: <https://www.paraview.org/>
8. SketchUp 3D Modeling software, [Online], Available: <https://www.sketchup.com/>
9. Weather Data for Wuhan 574940, [Online], Available: https://energyplus.net/weather-region/asia_wmo_region_2/CHN%20%20
10. MOHURD (2013). *Design standard for thermal environment of urban residential areas, JGJ 286-2013*, Ministry of Housing and Urban Development of the PRC

Artificial Neural Network Based Smart Forecast Models: High-performance close-control and monitoring in art gallery buildings

SHASHWAT GANGULY¹, FAN WANG¹, NICK TAYLOR¹, MICHAEL BROWNE²

¹Heriot-Watt University, Riccarton, Edinburgh, UK

²The National Galleries of Scotland, Edinburgh, UK

ABSTRACT: This paper presents the application of Artificial Neural Network (ANN) algorithms to develop forecast models to predict future energy consumption, outdoor weather and indoor microclimatic conditions in a historical art gallery. Each of these prediction models were implemented on two separate cases of sampling frequencies – daily and hourly sampling; providing a case of day-ahead and a case of hour-ahead predictions, respectively. The ANN models were trained with historical real-data obtained from the various sources, such as building sensors, building management information, and MetOffice. Excellent accuracy in the prediction results were observed through the statistical platform of coefficient of correlation (R) between the real-data and the ANN-predicted counterpart. It was observed that the prediction models for hour-ahead forecasting performed stronger compared to the same for day-ahead forecasting for all the cases of outdoor weather parameters, indoor microclimatic parameters, and NGS energy consumption parameters. The study further reinstates that the ANN-based forecast models can prove to be an ideal platform to investigate various optimisation strategies of the building operation in future, especially in the case of restrictive traditional building types where any retrofit solution needs a strong scientific backing before practical implementation.

KEYWORDS: Artificial Neural Networks, Forecasting, Optimisation, Condition Monitoring, Conservation

1. INTRODUCTION

Historic Art Gallery buildings require a tight indoor temperature and moisture controls, which in turn demands significant energy from air handling units [1,2]. Complex dynamic building systems, stringent conservation restrictions, and lack of detailed monitoring make diagnosing and optimising their energy use difficult.

It is known that the first step for optimising energy use in buildings is to have a mean for adequate energy usage prediction [86], not only for the building owners but also for urban planners and energy suppliers. With the potential of buildings to contribute towards the reduction in CO₂ emissions well recognised [87], urban planners seek to the prediction of building energy systems to assess the impact of energy conservation measures [88]. It is also known that the building energy and indoor environmental predict model forms the core of a building's energy control and operation strategy design to induce energy savings including peak demand shaving [89], [90].

Building simulation software programmes have proven to be effective but have tended to rely on data generated by simulation model itself. These approaches bear the drawback of requiring detailed information and parameters of the buildings, energy systems, and outside weather conditions which are difficult to obtain or even unavailable [3]. Also, creating these models demand a lot of calculation time investment and expertise [4].

Alternate to using simulation software for modelling the building system, methods involving Black-Box models or purely data-driven models carry the benefit of easy to build and being computationally efficient [5–8], especially when a large amount of historical data is available to train the models. Many artificial-intelligence-based prediction models have been developed in the recent past. To predict the monthly energy consumption in buildings, a combination of multiple linear regression and self-regression techniques were employed in [9]. Fuzzy inferences system is also extensively used [10,11]. Building loads are predicted using an autoregressive with exogenous (ARX) model in [12]. An optimal trade-off between comfort and energy using a meta-model based on regression techniques was developed in [13]. The application of ANN models in building modelling sector has mostly been towards prediction and optimisation of building energy consumption [14–16], cooling loads [15,17–19], and temperature [16,20,21]. It was found that this development was not extended to the special case of moisture critical buildings such as museums and art galleries.

On discussions with the building management team and building services contractors associated with these types of buildings, it was found that there is a great need for forecasting of indoor environmental conditions and building's energy use in a complex case of a historical building type which functions as an art gallery. This will have the following benefits:

PLEA 2018 HONG KONG

Smart and Healthy within the 2-degree Limit

The ANN-predicted dataset will help the building management to test various building performance optimisation options. These options can either be management changes, such as building opening hours or limit on occupancy, or system performance changes, such as air handling unit control strategy, changing of system components, etc.

The ANN-based predicted database can be used as a comparative tool to check against live data (condition monitoring). This enables the building management to take immediate action instead of periodic maintenance works, saving maintenance resources and time.

For special purpose buildings such as museums and art galleries, applying an energy saving solution may prove to be detrimental for artwork conservation. ANN-based system model, trained with the indoor specifications for artwork conservation mimics the actual building system and aids in providing the management team freedom to try various optimisation strategies.

The application of ANN-based forecast models promises better management and operation of such special-purpose buildings, ensuring a good balance between energy optimisation and adequate indoor environmental conditions for conservation of delicate artefacts and collections housed in the building.

In this paper, the feasibility of using ANN to predict the indoor environmental conditions and energy consumption inside an art gallery housed in a historic building is demonstrated by means of prediction models developed for individual cases of indoor microclimate and building energy consumption. Outdoor weather conditions are also forecasted to further test the prediction accuracy and versatility of the same algorithm and platform.

This paper is arranged as follows. Section 2 describes the research methods applied in developing the ANN-based forecast model, individually for each forecast target areas – outdoor weather, indoor microclimatic conditions and building energy consumption. The section also follows up with details of the ANN algorithm used, the structure, training method convergence criterion and performance evaluation metrics used for the study. Section 3 presents the set of results obtained on application of the methods for all the three cases. Finally, Section 4 concludes the key findings from the study.

2. RESEARCH METHODS

2.1 Outdoor Weather Forecast Models

For weather forecasting, the only data available for the study pertained to timestamp, outdoor temperature and outdoor relative humidity. While the factors influencing outdoor temperature and humidity can be plentiful (solar activity, wind speed, precipitation, etc), this study attempts to forecast the two outdoor

weather parameters using only timestamp (which involves day, month, year and hour). These inputs were applied to the ANN algorithm to train to obtain the corresponding outdoor weather parameters.

Present and previous instances of outdoor temperature and relative humidity were also fed as inputs into the model. For instance, $T_{out}(n)$ pertains to the outdoor temperature at the present time instant, n . Hence, $T_{out}(n-1)$, $T_{out}(n-2)$, and $T_{out}(n-3)$ pertains to outdoor temperature values at $(n-1)^{th}$, $(n-2)^{th}$, and $(n-3)^{th}$ hours (for hour-ahead forecasting) or days (for day-ahead forecasting), respectively.

The ANN model training targets were chosen as the future instances of outdoor temperature and humidity. For instance, $T_{out}(n+1)$ pertained to the outdoor temperature at the next time instance (next hour, for hour-ahead forecasting; next day, for day-ahead forecasting).

It is also worth noting that the ANN model for outdoor weather forecasting involved a combined input of temperature and humidity, unlike the case of individual forecast models for room temperature and humidity forecasting, as described in the next section. This is mainly due to the fact that the amount of data available pertaining to outdoor weather was very limited for the study. Individual models would lead weaker model performance in terms of forecasting estimation inaccuracies.

2.2 Indoor Conservation Parameters Forecast Models

Individual ANN models were developed for forecasting future room temperature and humidity. In addition to time parameters, a vast pool of data was available from the NGS BMS servers, pertaining to *supply* and *return* temperatures and humidity of the air handling units. The occupancy was assumed to be constant throughout the year with 280 occupants per hour in the building during the opening hours, resulting to a range of 1960 to 2520 occupants in a day (To account for extended opening hours of the NGS building during Thursdays).

2.3 Building Energy Consumption Forecast Models

Similar to the case of forecasting indoor microclimatic conditions, individual ANN models were developed for forecasting future gas and electricity consumption in the NGS for the next day and next hour.

ANN model training involved employing *supply* and *return* temperatures and humidity of the air handling units, occupancy, building opening hours, room conditions, outdoor weather and time-based parameters, as inputs, in each individual model. In addition to these parameters, corresponding gas and electricity consumption records for the previous three hours (or days) were included as inputs for the ANN model development and the future records of energy consumption were set as the training targets.

2.4 Data Normalisation, Randomisation and Fragmentation

The ANN algorithm chosen for this study is *Levenberg-Marquardt* algorithm. The entire database (458 daily-samples, 10768 hourly-samples) was first normalised. Following this, the entire database was randomised using Latin Hypercube Sampling (LHS) method. This method has proven to be more effective owing to the extra precision offered by the Monte Carlo sampling method [22]. Then this randomised database was divided into two parts i.e. 80 % (366 daily, 8615 hourly samples) for Training database (TDb) and 20% (92 daily, 2153 hourly samples) for Prediction database (PDb), to select the optimum ANN model on PDb results rather than TDb.

During the ANN model development in MATLAB environment, the TDb was further split into three subsets, in the ratio of 60:20:20 for training, validating and testing, for cross-validation – a standard step for any ANN model development.

2.5. ANN Model Architecture

During the development of ANN, the learning cycle is iterated for all the different sets of input and target samples until one of the following convergence criterions is reached.

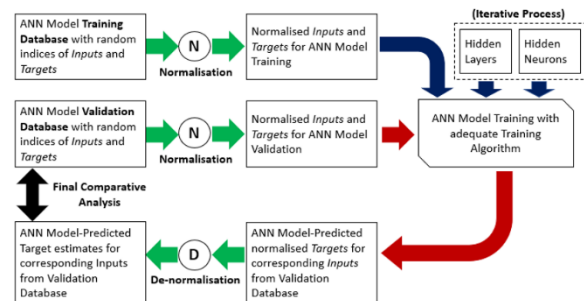


Figure 1: Process diagram for ANN model training and validation

Figure 1 illustrates a process diagram highlighting the steps involved in the ANN model development process for this study. Training of an ANN model was performed using the training database and choosing an arbitrary combination of hidden layer(s) and hidden neurons in each hidden layer. The ANN model then generated estimates of Targets for corresponding Inputs in each randomised sample (index) belonging to the training database. This step is followed by the validation process in which the Input values of the validation database is passed to the trained ANN model to generate corresponding predicted Target values for each randomised index. Finally, a comparative analysis is performed between the Target estimates of ANN predictions and the ones present

(but kept separate from ANN model) in the validation database.

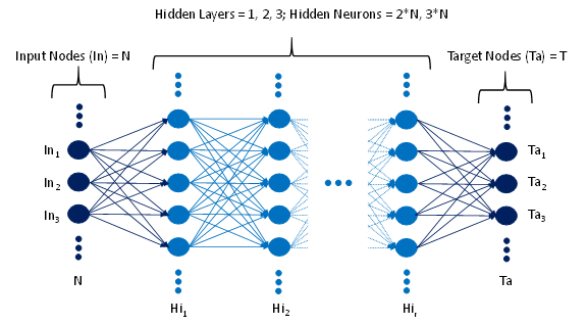


Figure 2: Topology of the ANN models developed in this study

The effectiveness of the ANN model in making accurate predictions is based on the statistical platform of coefficient of correlation (R-value). It presents the mathematical expression of the coefficient of correlation (R) between the ANN model-predicted estimates of Target values against their counterpart from the validation database (Equation 1).

$$R = \frac{\sum_{i=1}^N (X_{predicted,i} - \bar{X}_{predicted,i})(X_{record,i} - \bar{X}_{record,i})}{\sqrt{\sum_{i=1}^N (X_{predicted,i} - \bar{X}_{predicted,i})^2 \sum_{i=1}^N (X_{record,i} - \bar{X}_{record,i})^2}}$$

Where, X corresponds to the forecast parameter.

3. RESULTS AND DISCUSSIONS

3.1. Outdoor Weather Forecasting

Figure 3 show the comparison of ANN-predicted outdoor air RH and temperature.

It is to be noted that these graphs are different from conventional *variable-time* graphs. The comparison (between ANN-predicted estimates and actual recorded data of the same) in these graphs were performed over random *daily instances*. Hence, the horizontal axis in these comparison graphs comprise of several '*Daily indices*' instead of a conventional chronological sequence. These daily instances were randomly selected *time instances* from the downloaded data and were separated from the initial ANN model training. This practice is common in ANN model training and validation – randomisation allowing thorough validation of ANN predictions. Hence, all the comparison graphs between ANN-predicted estimates and actual recorded data of the same follow this format throughout this paper.

PLEA 2018 HONG KONG

Smart and Healthy within the 2-degree Limit

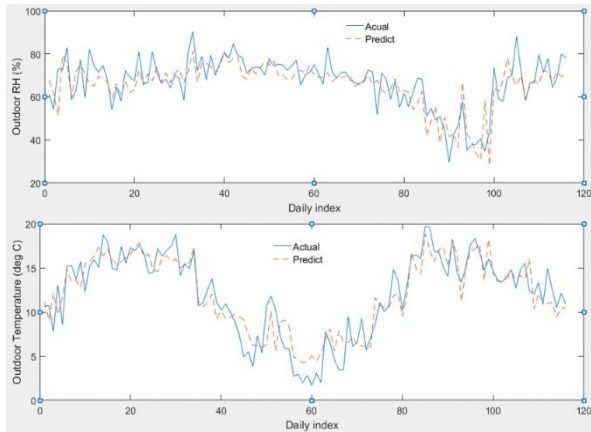


Figure 3: Comparison of future predicted and actual records of outdoor air RH (top) and temperature (bottom) for day-ahead forecasting.

It is observably clear that ANN predicted model accurately predicts outdoor T and RH for the majority of the daily instances.

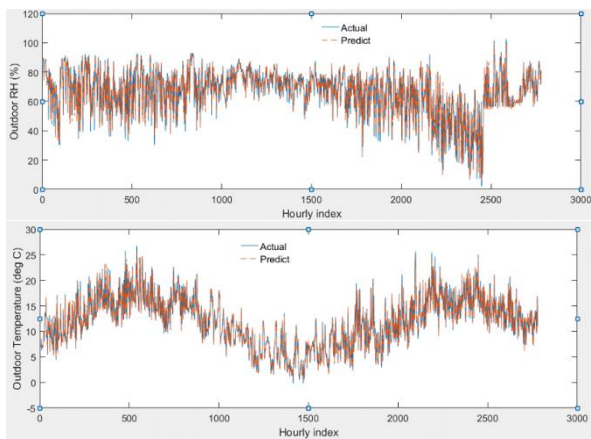


Figure 4: Comparison of future predicted and actual records of outdoor air RH (top) and temperature (bottom) for hour-ahead forecasting.

Similar to the day-ahead forecasting case, Figure 4 presents the results of comparative analysis of the ANN-predicted estimates (hour-ahead) of outdoor T and RH with the same coming from already obtained recorded data, over randomly selected hourly samples of future data. These future data were saved and kept separate from the initial ANN model development and were to be used only for validation purpose.

It can be seen that the hour-ahead forecast model accurately predicts outdoor weather T and RH over the entire spread of hourly instances considered in this study. This marks the excellent potential of ANN-based prediction models to predict for both cases of day-ahead and hour-ahead with excellent accuracy.

The R for combined T and RH model was 0.89 for day-ahead forecasting, and 0.98 for hour-ahead forecasting. The better performance of the hour-ahead forecasting models is owing to the significantly

greater number of data samples for the ANN model training for the hourly cases.

3.2. Room Conditions Forecasting

Figure 5 captures the excellent capability of the prediction model to forecast day-ahead instances of future room RH and temperature. The horizontal axis is randomly selected time instances and the vertical axis is the comparison of corresponding ANN-predicted estimates and actual observation data recorded by sensors. The performance is marginally weaker in the case of RH predictions, in comparison to temperature but still with high R-value score of more than 0.9.

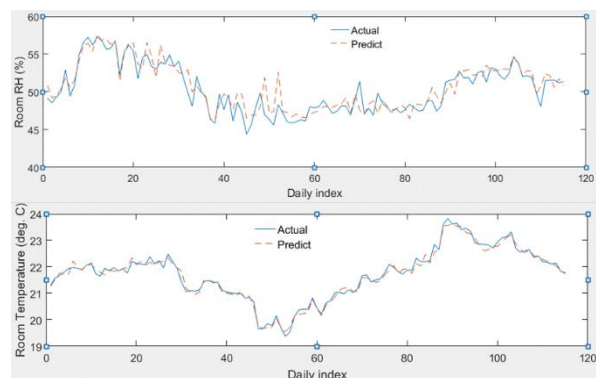


Figure 5: Comparison of future predicted and actual records of NGS room air RH (top) and temperature (bottom) for day-ahead forecasting.

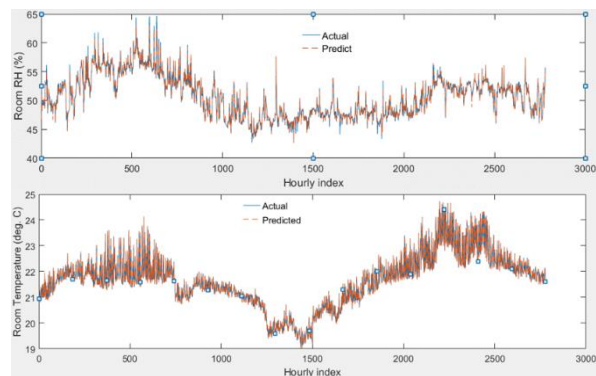


Figure 6: Comparison of future predicted and actual records of NGS room air RH (top) and temperature (bottom) for hour-ahead forecasting.

Figure 6 show the results of the comparative analysis of ANN-predicted estimates (hour-ahead) of room T and RH over randomly selected hourly samples of future data. These future data were saved and kept separate from the initial ANN model development.

The R for separate ANN models for NGS room T and RH forecast was 0.99 and 0.93, respectively, in the case of day-ahead forecasting. Similarly, for hour-ahead forecasting, the R for separate ANN models for NGS room T and RH was the same, being 0.99.

PLEA 2018 HONG KONG

Smart and Healthy within the 2-degree Limit

3.3. Energy Consumption Forecasting

Figure 7 captures the excellent capability of the prediction model to forecast day-ahead instances of future NGS gas consumption. These future day-instances were kept separately from the initial ANN model training and development.

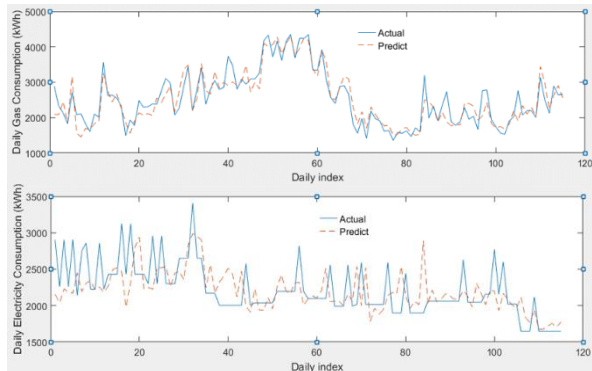


Figure 7: Comparison of future predicted and actual records of NGS building gas consumption (top) and electricity consumption (bottom) for day-ahead forecasting.

Figure 7 also highlights the weak performance of ANN-based prediction model of electricity consumption with the predicted estimates of day-ahead electricity consumption failing to capture the peaks and troughs marked by actual estimates of consumption figures obtained from the electricity supplier. This is owing to two reasons – firstly, the amount of data available to train the ANN model for day-ahead forecasting is lesser than the case in hour-ahead forecasting. Secondly, the number of approximations involved in splitting the monthly electricity energy consumption to daily estimates affected the performance of ANN model. This can be improved by obtaining a detailed breakdown of electricity consumption on daily and hourly basis from the electricity supplier.

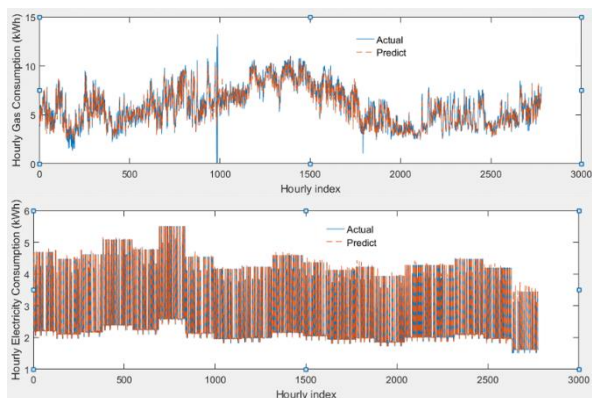


Figure 8: Comparison of future predicted and actual records of NGS building gas consumption (top) and electricity consumption (bottom) for day-ahead forecasting.

Figure 8 shows the results of comparative analysis of ANN-predicted estimates (hour-ahead) of gas and electricity energy consumption at the NGS over randomly selected hourly samples of future data.

These future data were saved and kept separate from the initial ANN model development.

The R for separate ANN forecast models for NGS building's electricity usage and gas usage was 0.92 and 0.73, respectively, in the case of day-ahead forecasting. Similarly, for hour-ahead forecasting, the R for separate ANN models for NGS room T and RH was 0.97 and 0.99, respectively.

4. CONCLUSION

It was observed that the prediction models for hour-ahead forecasting performed stronger compared to the same for day-ahead forecasting for all the cases of outdoor weather parameters, indoor microclimatic parameters, and NGS energy consumption parameters. This can be justified to the fact that the ANN models trained for hour-ahead forecasting had a significantly greater number of data samples available for training, due to higher sampling frequency and hence more data samples over the same period of study.

The outdoor weather forecast models performed satisfactorily with R-value in the range of 0.85-0.9. This can be improved by including more influencer data such as wind speed, wind direction, rainfall, solar activity, and cloud cover. These data were not available at the time of this study and it only involved time-based parameters (day, month, year, and hour) as inputs for model training.

The room parameters (air temperature and RH inside NGS) exhibited the best performance, with significantly high R-value of about 0.99, consistently over the period of study. This is due to the availability of a lot of data samples for various influencers affecting room temperature and RH.

The NGS energy consumption results experienced the poorest of all the cases as far as performance is concerned. This is due to the fact that the energy information available for the study was on monthly scale for electricity and daily case for gas consumption. These estimates were split into hourly and daily cases with the help of several assumptions. These assumptions affected the ANN performance. In future, this can be improved by making detailed information available from the energy suppliers for both gas and electricity consumption.

ACKNOWLEDGEMENTS

The authors thank Energy Technology Partnership Scotland, Craig James, John Armstrong and Alan Cree from CraigAlan Controls Ltd., and Michael Browne and Charles Sclater from the National Galleries of Scotland, for their constant support in this study.

REFERENCES

F. Wang, K. Pichetwattana, R. Hendry, R. Galbraith, Thermal performance of a gallery and refurbishment solutions, Energy Build. 71 (2014) 38–52.

PLEA 2018 HONG KONG

Smart and Healthy within the 2-degree Limit

- L. Bellia, A. Capozzoli, P. Mazzei, F. Minichiello, A comparison of HVAC systems for artwork conservation, *Int. J. Refrig.* 30 (2007) 1439–1451. doi:10.1016/j.ijrefrig.2007.03.005.
- X. Li, J. Wen, Review of building energy modeling for control and operation, *Renew. Energy Rev.* 37 (2014) 517–537. doi:10.1016/j.rser.2014.05.056.
- H. Huang, L. Chen, M. Mohammadzakeri, E. Hu, M. Chen, Multi-zone temperature prediction in a commercial building using artificial neural network model, 2013 10th IEEE Int. Conf. Control Autom. (2013) 1896–1901. doi:10.1109/ICCA.2013.6565010.
- X. Li, J. Wen, Building energy consumption on-line forecasting using physics based system identification, *Energy Build.* 82 (2014) 1–12. doi:10.1016/j.enbuild.2014.07.021.
- M.S. Kiran, E. Özceylan, M. Gündüz, T. Paksoy, Swarm intelligence approaches to estimate electricity energy demand in Turkey, *Knowledge-Based Syst.* 36 (2012) 93–103. doi:10.1016/j.knsys.2012.06.009.
- Y.S. Lee, L.I. Tong, Forecasting time series using a methodology based on autoregressive integrated moving average and genetic programming, *Knowledge-Based Syst.* 24 (2011) 66–72. doi:10.1016/j.knsys.2010.07.006.
- H. Ltifi, E. Benmohamed, C. Kolski, M. Ben Ayed, Enhanced visual data mining process for dynamic decision-making, *Knowledge-Based Syst.* 112 (2016) 166–181. doi:10.1016/j.knsys.2016.09.009.
- J. Ma, J. Qin, T. Salisbury, P. Xu, Demand reduction in building energy systems based on economic model predictive control, *Chem. Eng. Sci.* 67 (2012) 92–100. doi:10.1016/j.ces.2011.07.052.
- J. Xu, Y. Wang, Z. Tao, Rough approximation based strategy model between a green building developer and a contractor under a fuzzy environment, *Knowledge-Based Syst.* 46 (2013) 54–68. doi:10.1016/j.knsys.2013.03.002.
- M. Nilashi, R. Zakaria, O. Ibrahim, M.Z.A. Majid, R. Mohamad Zin, M.W. Chughtai, N.I. Zainal Abidin, S.R. Sahamir, D. Aminu Yakubu, A knowledge-based expert system for assessing the performance level of green buildings, *Knowledge-Based Syst.* 86 (2015) 194–209. doi:10.1016/j.knsys.2015.06.009.
- K. Yun, R. Luck, P.J. Mago, H. Cho, Building hourly thermal load prediction using an indexed ARX model, *Energy Build.* 54 (2012) 225–233. doi:10.1016/j.enbuild.2012.08.007.
- B. Eisenhower, Z. O'Neill, S. Narayanan, V. a. Fonoberov, I. Mezić, A methodology for meta-model based optimization in building energy models, *Energy Build.* 47 (2012) 292–301. doi:10.1016/j.enbuild.2011.12.001.
- N. Nassif, S. Moujaes, M. Zaheeruddin, Self-tuning dynamic models of HVAC system components, *Energy Build.* 40 (2008) 1709–1720. doi:10.1016/j.enbuild.2008.02.026.
- M. Shin, S.L. Do, Prediction of cooling energy use in buildings using an enthalpy-based cooling degree days method in a hot and humid climate, *Energy Build.* 110 (2016). doi:10.1016/j.enbuild.2015.10.035.
- J. Zhu, Q. Yang, J. Lu, B. Zheng, C. Yan, An adaptive artificial neural network-based supply air temperature controller for air handling unit, *Trans. Inst. Meas. Control.* 37 (2015) 1118–1126. doi:10.1177/0142331214557171.
- B. Yuce, H. Li, Y. Rezgui, I. Petri, B. Jayan, C. Yang, Utilizing artificial neural network to predict energy consumption and thermal comfort level: An indoor swimming pool case study, *Energy Build.* 80 (2014) 45–56. doi:10.1016/j.enbuild.2014.04.052.
- M.J. Sanjari, H. Karami, H.B. Gooi, Micro-generation dispatch in a smart residential multi-carrier energy system considering demand forecast error, *Energy Convers. Manag.* 120 (2016) 90–99. doi:10.1016/j.enconman.2016.04.092.
- S.S.K. Kwok, A study of the importance of occupancy to building cooling load in prediction by intelligent approach, *Energy Convers. Manag.* 52 (2011) 2555–2564. doi:10.1016/j.enconman.2011.02.002.
- A.E. Ben-Nakhi, M. a. Mahmoud, Cooling load prediction for buildings using general regression neural networks, *Energy Convers. Manag.* 45 (2004) 2127–2141. doi:10.1016/j.enconman.2003.10.009.
- Q. Li, Q. Meng, J. Cai, H. Yoshino, A. Mochida, Predicting hourly cooling load in the building: A comparison of support vector machine and different artificial neural networks, *Energy Convers. Manag.* 50 (2009) 90–96. doi:10.1016/j.enconman.2008.08.033.
- S. Pandey, D.A. Hindoliya, R. Mod, Artificial neural networks for predicting indoor temperature using roof passive cooling techniques in buildings in different climatic conditions, *Appl. Soft Comput. J.* 12 (2012) 1214–1226. doi:10.1016/j.asoc.2011.10.011.

Experimental Study on an Air-Phase-Change-Material Unit for Summer Thermal Comfort in a Naturally Ventilated Building

Maria De Los Angeles Ortega Del Rosario^{1,4}, Miguel Chen Austin¹, Denis Bruneau²,
Jean-Pierre Nadeau¹, Patrick Sébastien¹, Dimitri Jaupard³

¹2M Bordeaux, France;

²GRECCAU, EA MCC 7482, F-33405 Talence, France;

³Arts et Métiers Campus de Bordeaux - TALENCE F33405 TALENCE Cedex;

⁴Universidad Tecnológica de Panamá, Ciudad de Panamá, Panamá

ABSTRACT: The concern about the increasing consumption and the greenhouse gases emissions associated with heating, ventilation and air-conditioning applications in the residential sector has led to the search for solutions that can mitigate these adverse effects. Thermal energy storage with phase change materials is presented as an attractive solution because it allows storing large amounts of energy in small volumes and it can be adapted to meet the cooling and heating needs of a building. In this work, we detail the design, manufacture, and experimental tests of a prototype of an air-PCM unit with a tube bundle geometry. These tests were carried out on a plus energy house prototype located in the South of France, during the summertime of 2017. The thermal performance of this air-PCM unit was evaluated through indicators such as the indoor air temperature and the operating time of the unit. The results suggest that the air-PCM unit limits the indoor temperature rise during the unit operating time, keeping a temperature value around the upper thermal comfort limit.

KEYWORDS: Phase change material, energy storage, summer thermal comfort, natural ventilation, buildings.

1. INTRODUCTION

The increase of the world energy consumption represents a significant concern nowadays, considering that still in 2015, 82% of the energy production was based on fossil fuels. Additionally, the residential sector represented around 22% of the total energy consumption, which was associated with 17% of CO₂ emissions [1]. Most of the energy demand for this sector comes from heating, ventilation and air-conditioning applications (HVAC), making them a major contributor to global greenhouse gas emissions. The balance of the current situation increases the pressure to adopt actions, such as those established recently at the Paris Agreement (COP21), that limits the increase of the greenhouse emissions to avoid climate change, by holding the increase in the global average temperature to well below 2°C [2].

Therefore, the reduction of energy consumption related to HVAC, and the improvement of the efficiency of technologies used in these applications is a current trend. One example of these technologies is the use of thermal energy storage systems as a source of cooling and heating in the buildings.

The inclusion of phase change materials (PCM), as part of thermal energy storage systems, has increased during the last years, because they allow storing large amounts of energy in reduced volumes. PCM can be included as part of the building's envelope, working as a passive system that could increase the thermal inertia of the building reducing the energy consumption. Its operation can also be found as part

of an active cooling system. The main advantage of these active systems with PCM is that they can be controlled to match their use with the peak load periods, contributing to the reduction of the primary energy consumption in cooling applications. Also, these active systems can be well adapted to already existing buildings, where the cooling needs can be met by taking advantage of the large thermal energy storage in the PCM, without the need of refurbishing the structure of the building. This presents a major advantage regarding the passive systems where the PCM is included in the main structure of the building. Furthermore, active systems usually dispose of macroencapsulation for storing the PCM, allowing large amount of PCM in small volumes, and thus to proper efficiency-compacity rate if we compared with such rates for passive uses of PCM. In the present work, our focus is on active systems.

The melting temperature of the selected PCM must match the environmental conditions: it must be lower than the diurnal outdoor temperature, to be able to store the surplus heat from the air.

Active PCM systems present three operation modes during the day. First, during the daytime when the indoor temperature rises above the comfort limit, the system is activated. This activation allows the hot indoor air to pass through the air-PCM unit. While this happens, the PCM absorbs the surplus heat from the air. When the PCM reaches the phase change temperature, the PCM begin to melt. Since the air loses heat to the PCM the air will present a lower

PLEA 2018 HONG KONG

Smart and Healthy within the 2-degree Limit

temperature at the outlet of the air-PCM system, cooling down the place to the comfort temperature. This operation mode of the air-PCM unit corresponds to the cooling of the air or cooling cycle.

After a cooling cycle, the PCM are in a liquid state and they need to be regenerated in order to be available for next use. Then, the second operation mode, the regeneration of the PCM, occurs during the nighttime. When the outdoor air is lower than the phase change temperature, the system is activated, forcing this colder air to pass through the air-PCM unit. This air takes away the surplus heat stored in the PCM. When the phase change temperature is reached, the material begins to solidify. Finally, the last operation mode consists of the standby periods of the system, which occurs in between the active periods, when the system is not under operation. Indeed, the least amount of losses to the surroundings is desired during this operation mode.

In the present study, an air-PCM unit prototype was designed and built. It was tested as a cooling unit in a plus energy house (PEH) prototype, called Symbiosi. This study aims to characterize the system behavior during a typical summer day in Bordeaux, France. The performance of this air-PCM unit will be evaluated through thermal performance indicators such as the operation time and the indoor air temperature of the place.

2. AIR-PCM HEAT EXCHANGER UNIT

2.1 Design of the unit:

The main design parameter of an air-PCM heat exchanger is the selection of the PCM itself. It plays a vital role because, if it is not selected correctly, the unit will not work under the building conditions as a latent heat storage system.

There is a large variety of commercial and non-commercial materials that are considered as PCM. For building applications, as cooling and heating, these materials should meet specific criteria that make them suitable. For instance, for cooling applications, the range of melting temperature of those materials should match the range of human comfort which is quite limited and within 23°C and 27°C during summertime [3]. Besides, it is also desired that this phase change occur isothermally to guarantee temperature stability at the outlet of the unit. Further, the melting point selection depends mainly on the amplitude of the ambient air temperature oscillation of the diurnal temperature [4], rather than the average ambient temperature of the region where the system is installed [5].

Since the choices of PCM that match the criteria for achieving a good performance as storage material are limited, usually the shape of the container and the geometry distribution are chosen as the design criteria for enhancing the thermal performance. A suitable

design choice of the air-PCM unit that fits the needs of the building can ensure the supply of the cooling demand during a day in the summertime. Therefore, the choice of containers and quantity, in relation with the local climate, is the key to success for the air-PCM unit to cover between 80 and 90 % of summer cooling needs [6].

The air-PCM unit used in here has been designed and built at the *Institute de Mécanique et d'Ingénierie de Bordeaux* (I2M). We went through a design process that aimed to enhance the thermal performance of the unit regarding the selection of the container and geometrical distribution, resulting on a tube bundle geometry with the possibility of an in-line or staggered arrangement of such tubes [7].

2.2 Air-PCM unit description:

Once the design was complete, we proceeded to establish the requirements and specifications for the construction of a prototype adapted to perform tests under in-situ conditions, where the following are the most important of them:

The dimensions and weight of the unit must allow manual transport so that one person can push it with the help of wheels.

Aluminum as envelope material for the unit, due to the simplicity of fabrication and weight, accompanied by polystyrene insulation to minimize the heat losses.

Use of commercial paraffin.

Electricity consumption as low as possible consisting of four fans that ensure the passage of hot air through the unit.

A staggered distribution of 288 tubes (6 plates x 48 tubes) that maximizes the thermal performance and limits the weight of the unit.

PET tubes with a diameter of 2cm as PCM containers.

The proposed design is presented in figure 1, where sub-figure a and b presents the 2D and 3D plans of the air-PCM unit design, respectively. These plans were made in Catia®, which eased the fabrication process since it could be associated with the machinery by directly loading the plans and then facilitating the production of each piece. The trimming of the structure, the assembly and the filling of tubes with PCM was performed in the laboratory. Figure 2 presents the trimming process (a), a piece of the structure (b), the PCM containers (c), and the final air-PCM unit (d). Note here that the constructed air-PCM energy storage unit is a demonstrative one. Its external dimensions (0,7m x 0,36m x 0,4m) are directly linked with the height of the PCM container (0,27m), and with the amount of PCM (less than 30kg) according with the target energy storage capacity. These containers were especially developed for these thermal applications are very low costs, air-tight and provide architects with free choice of integration in any reservation in buildings internal volume. For

PLEA 2018 HONG KONG

Smart and Healthy within the 2-degree Limit

instance, Rouault et al. [6] integrate its PCM unit in the ground and a sitting of the living room of a positive energy family house.

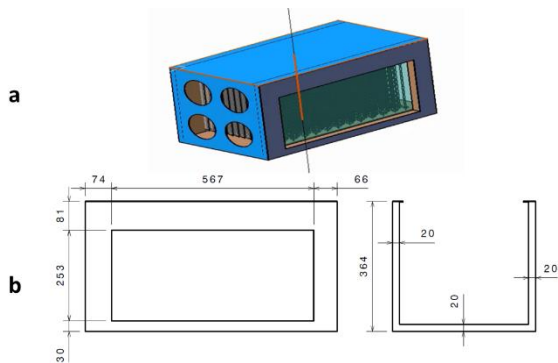


Figure 1: (a) Mobile System 3D Plans in Catia®, (b) 2D main structure of the air-PCM unit in Catia®.

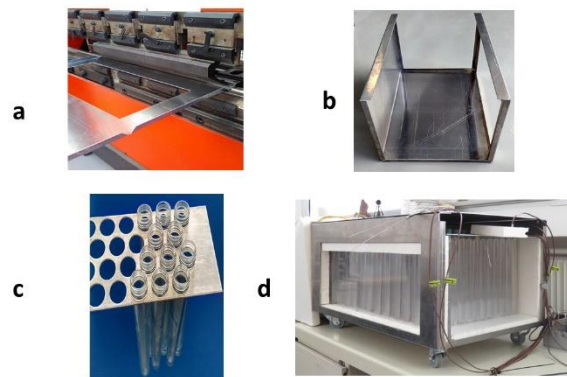


Figure 2: Fabrication of the air-PCM unit: a) folding of the metallic structure, b) base piece of the structure, c) placement of the PET tubes during assembly, and d) final air-PCM unit.

One side of the unit consists of a plexiglass plate, allowing a visual track of the melting inside the unit since the tubes are also transparent. The indoor airflow across the PCM unit is ensured by four DP200A Sunon fans (22W, 44 dB, 95 CFM).

The selected PCM is an organic-inorganic mixture fabricated by Rubitherm® under the commercial name SP25E. This material could be corrosive, making PET a suitable material for PCM containers. Regarding the thermal properties, this PCM presents a melting range of 24°C to 26°C, an estimated density of 1500 kg·m⁻³ for both phases, a heat storage capacity of 190 kJ·kg⁻¹ and a specific heat capacity of 2 kJ·kg⁻¹·K⁻¹ [8]. The unit was filled up with 28kg of this PCM.

3. PLATFORM DESCRIPTION AND METHODOLOGY

3.1 Experimental platform

The PEH prototype located in Gradignan, Bordeaux, at the southwest of France, was used as an experimental platform for the present study during the summer of 2017. This house was designed and constructed for the Europe Solar Decathlon 2012 competition [9], later

becoming an experimental platform for research purposes. A schematic of this PEH experimental platform is presented in figure 3.

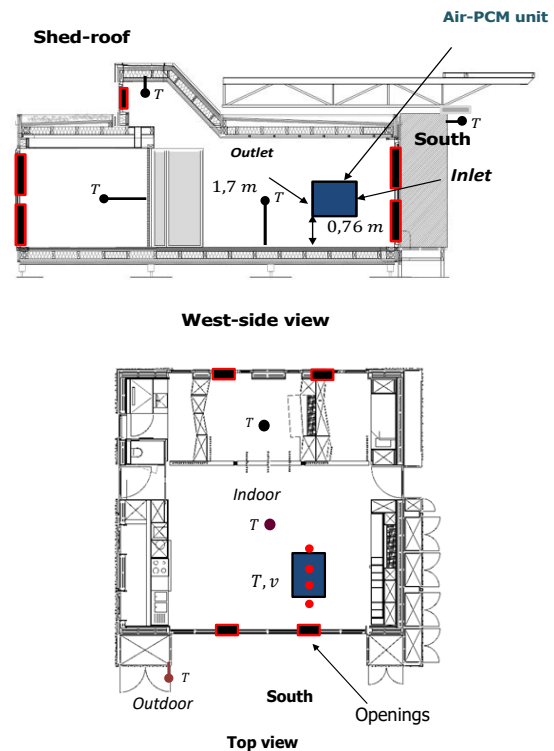


Figure 3: Experimental platform schematic. a) West-side view of the house showing the location of the unit inside the house and sensors distribution. b) Top view of the house; the colored dots symbolize the position of the temperature and velocity sensors.

The house envelope consists of a wooden façade, made out of maritime pine, with thermal insulation of 32 cm at the floor, ceiling and North façade, and between the living places and to the outdoor cabinets at the East and West façades. These outdoor cabinets act as thermal buffer spaces between outdoor thermal conditions and indoor thermal comfort conditions, especially in summer when these buffer spaces quite fully nearly avoid any thermal overheating during afternoons (and in early mornings). The South façade contains large double-glazed windows. The thermally heavier-weighted of the house envelope is located on the floor due to the presence of a concrete slab within it.

Moreover, the house has ten bottom-hung openings to promote the establishment of different natural ventilation strategies by choosing suitable opening-closing configurations. These openings are distributed as follows: four on the South façade, four on the North façade and two at the shed-roof. Each window disposes of blinds to limit the entry of solar radiation to the indoor environment of the house.

PLEA 2018 HONG KONG

Smart and Healthy within the 2-degree Limit

3.2 Metrology

To describe the physical phenomena and the thermal behavior of both systems (the house and the air-PCM heat exchanger), temperature, velocity and heat flux sensors were placed in different locations within the house. The unit was placed near the openings located at the South facade, at the height of 0,76 m. The indoor temperature was measured at the height of 1,70 m, as shown in sub-figures a and b of figure 3.

Figure 4 shows, the position of the air-PCM unit within the house along with the following elements: (a) the natural ventilation openings; (b) the rheostat, to control the airflow rate in the air-PCM unit, which is connected to four fans at the inlet of the unit (c); (d) one of the locations of a couple of black and shiny heat flux meters to measure the heat losses; (e) the air temperature measurement point at the unit outlet, and (f) the airspeed measurements. During the standby periods, an insulating polystyrene plate is placed at the outlet to avoid losses through it.

Type T thermocouples were installed to measure the outdoor (T_{outdoor}) and indoor air (T_{indoor}) temperatures, as well as, the inlet (T_{in}) and outlet (T_{out}) temperatures in the air-PCM unit (see figure 4). In order to know the PCM's state during the cycle, two thermocouples were placed inside two tubes: one tube (T_{pcm1}), was located in the second-third of the heat exchanger (in the middle of the 17th row) and the other one (T_{pcm2}), on the last row of the exchanger. Finally, the air temperature within the air-PCM unit was measured in two locations. The first measurement point was located between 8th and 9th rows, and the second between 16th and 17th rows (T_{air1} and T_{air2} , respectively).

Figure 4: Air-PCM unit near the South façade at 0,7 m high from the floor: a) the natural ventilation openings, b) power source, c) inlet, d) heat flux meters at the plexiglass side, e) outlet temperature measurement and f) airspeed measurement at the outlet.

3.3 Testing protocol

The empirical performance of the unit was evaluated through thermal indicators. The indoor temperature (T_{indoor}) achieved during the operation time of the unit (Δt_{op}) is a good indicator of thermal comfort [9], and therefore, it was selected for the evaluation. From the

operating time, we can also determine the electrical consumption of the unit and the energy savings.

The thermal comfort was defined by a temperature range, being 27°C at the upper limit. For this reason, this temperature value was selected as a set-point value to begin the PCM unit operation. This choice agrees with the Art. R. 131-29 of the French Construction and Housing Code, which states that - "In rooms in which a cooling system is installed, it must only be put into operation or kept in operation when the internal temperature of the rooms exceeds 26 °C" [10].

The PCM regeneration is activated when the inlet temperature of the unit is lower than the solidification temperature of the selected PCM (24°C). Hence, to promote this PCM regeneration, a night natural ventilation strategy is launched, which consists of opening the bottom-hung openings, and the east and west, large double-glazed windows at the south façade, to take advantage of the cold outdoor air.

4. EXPERIMENTAL RESULTS AND ANALYSIS

In order to ensure suitable conditions for the operation of the air-PCM unit, the weather forecast was used to evaluate in which days the predicted outdoor air temperature was sufficiently low to guarantee the solidification of the PCM and also the system operation during the next selected day. Figure 5 shows the weather forecast for August 14th and the next 13 days, for Gradignan in France. It can be highlighted in this figure that for August 22nd, the predicted outdoor air temperature was above 30°C. Besides, during the nighttime of the previous days, the temperatures were expected to be low enough which could ensure a total solidification of the PCM.

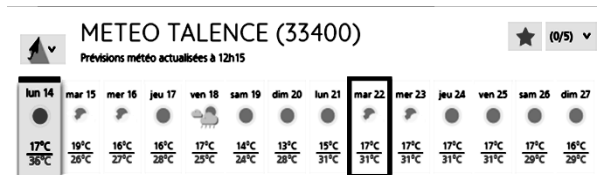


Figure 5: Weather forecast for Gradignan, France (consulted on August 14th, 2017).

Figure 6 shows the outdoor and indoor air temperature measurements obtained from August 22nd to August 24th, 2017.

PLEA 2018 HONG KONG

Smart and Healthy within the 2-degree Limit

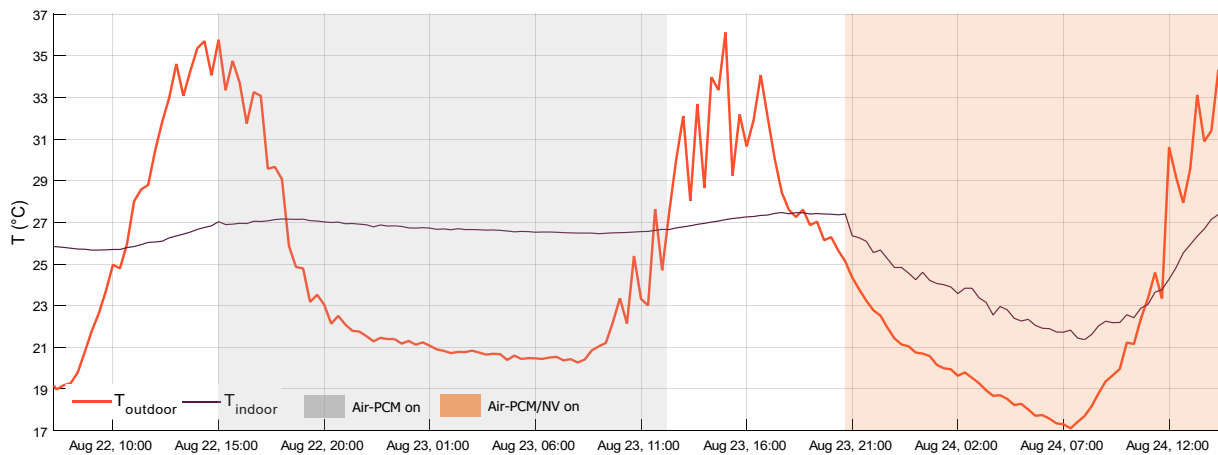


Figure 6: Indoor and outdoor air temperatures profiles, from August 22nd to August 24th, 2017. Temperature color code: orange: outdoor air temperature, purple: indoor air temperature. Gray zone: air-PCM unit is active; orange zone: natural ventilation (NV) is coupled with active air-PCM unit.

It can be observed in figure 6 that even if the outdoor air temperature (T_{outdoor}) reached high values (36°C), the indoor air (T_{indoor}) remained within the thermal comfort range established. Around 3:00 p.m. August 22nd, the air-PCM system was activated, once T_{indoor} reached 27°C, the openings and doors remaining closed. At this time, the outdoor air temperature reached its maximum value for the day. The use of this air-PCM unit helped to maintain the indoor air temperature (from 3:00 p.m. to 6:00 p.m., when $T_{\text{outdoor}} > T_{\text{indoor}}$), or act to diminish this indoor air temperature (from 6:00 p.m. to 11:00 a.m. the day after when $T_{\text{outdoor}} < T_{\text{indoor}}$).

Note that the maximum value of the outdoor air temperature predicted by the weather forecast during August 22nd day (31°C in fig. 5) was smaller than the temperature recorded (36°C in fig. 6); for that reason, we did not initially plan a PCM regeneration operation during the night between August 22nd and August 23rd. Since we did not regenerate the PCM after using the air-PCM unit during the daytime of August 22nd, thus the unit was not able to maintain the indoor air temperature during August 23rd day, and this indoor air temperature value overpassed the 27°C temperature set value. Then, during the night between August 23rd and August 24th, in order to refresh the experimental house platform and regenerate the PCM, a nocturnal natural ventilation strategy was carried out; the indoor air was able to regenerate the PCM about 2:00 a.m. on August 24th, when indoor air temperature value passed under 24°C. In figure 7 is shown the air-PCM unit temperatures. In here, we can observe that the indoor air temperature decreased after the activation of the unit during more than half an hour and then increased again, but slower, if it is compared to the slope before the air-PCM unit activation. The temperature increasing slope changed

from a 0,005°C·min⁻¹ before 3:00 p.m. to an average value of 0,001°C·min⁻¹ value after 3:30 p.m. This thermal behavior (regarding the indoor air temperature) suggests that, even if the PCM unit is a small one, compared to the house volume (136 m²), presents a positive effect on the indoor thermal comfort.

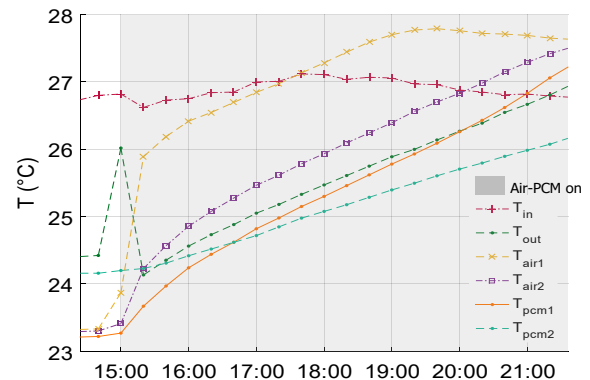


Figure 7: Temperature profiles for the air-PCM unit during August 22nd, 2017. Temperature color codes: magenta: inlet of the unit, green: outlet, yellow and purple: the air temperature at one third and two-thirds of the unit, orange, and cyan: PCM of a tube located in the middle of the 17th row and on the last row, respectively. The gray zone: the air-PCM unit was active.

Furthermore, the isolation at the outlet allowed maintaining an almost constant value in the temperatures of the PCM before the activation of the unit, which was also reflected in the outlet temperature. This is convenient regarding heat losses during periods of standby of the unit.

Regarding the PCM behavior, it can also be observed that the unit outlet air temperature, T_{out} , is governed by the PCM temperature (T_{pcm1} and T_{pcm2}), showing a difference between them of about 0,5 °C. Besides according to the PCM temperature measurements, a

PLEA 2018 HONG KONG

Smart and Healthy within the 2-degree Limit

sensible storage component is shown for this material, which is in agreement with the data provided by the PCM manufacturer. Moreover, the operating time of the unit, Δt_{op} , is approximately 8 hours (from 3:00 p.m. to 11:00 p.m.), observed in the figure within the grey zone.

Furthermore, a temperature stratification within the house was observed: when the unit was not in service, the air temperature value at 0,7 m from the floor was smaller than the one at 1,7 m ($T_{in} < T_{indoor}$). This air stratification of around $0,8 \text{ }^\circ\text{C}\cdot\text{m}^{-1}$, may suggest that placing the unit in a higher position, improve airflow distribution. During the unit operation time, the air-PCM unit ensured satisfactory thermal conditions; this means, indoor air temperature around or less the temperature comfort condition established at the beginning of the experiment. Although considering the thermal inertia of the building, this unit should have been activated before the indoor air temperature value reached the $27 \text{ }^\circ\text{C}$ set value.

Figure 8 shows the temperature profiles during the PCM regeneration process. Once the night natural ventilation strategy was activated (around 9:00 p.m.), the temperature within the unit began to decrease. We can observe that the outlet air and the PCM temperatures decrease until about 4:00 a.m. when the PCM reached a temperature of $23 \text{ }^\circ\text{C}$. This behavior is also in agreement with the data provided by the manufacturer.

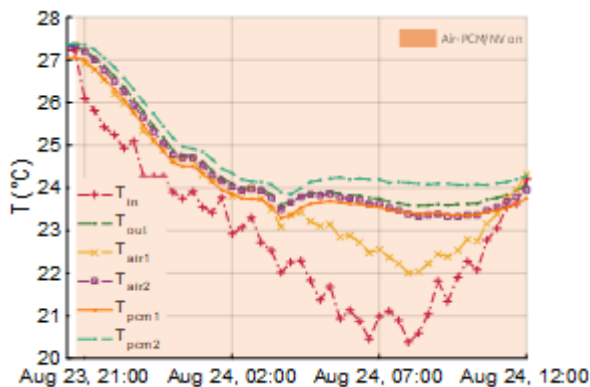


Figure 8: Temperature profiles for the air-PCM unit between August 23rd and August 24th, 2017 Temperature color codes: magenta: inlet, green: outlet, yellow and purple: the air temperature at one third and two thirds of the unit, orange and cyan: PCM of a tube located in the middle of the 17th row and on the last row, respectively. The orange zone: the air-PCM unit and the natural ventilation were actives.

5. CONCLUSION AND PERSPECTIVES

This study was carried out with the aim of achieving an understanding of a PCM unit behavior under real condition inside a house. The results suggest that the air-PCM unit limits the indoor temperature rise during the unit operating time, keeping a temperature value around the upper thermal comfort limit. The operating time of the unit was greater than the minimum

required to maintain the thermal comfort conditions in the house. It also points out that the vertical position of this unit may influence minimizing the temperature stratification.

As future work it must be considered a higher placement of the unit to get a better distribution of air in the room. Also, include tests during different seasons of the year to observe other operations of this kind of systems. Besides, the starting setpoint of the tests could be changed to a lower temperature in order to observe the operation of the unit for a longer time.

ACKNOWLEDGEMENTS

The authors acknowledge the financial support provided by IFARHU Panamá and Universidad Tecnológica de Panamá. Additionally, we want to recognize the active participation of Mr. Ignacio Hernanz during the manufacturing of the prototype.

REFERENCES

1. IEA Key World Energy Statistics 2017 (2017) [Online], Available: <https://webstore.iea.org/key-world-energy-statistics-2017> [27 May 2018].
2. Burluson, E. (2016) Paris Agreement and Consensus to Address Climate Challenge. *ASIL INSIGHT*, forthcoming.
3. ASHRAE (2001). Handbook of fundamentals American Society of Heating, Refrigeration and Air Conditioning Engineers Inc., Atlanta, GA.
4. Medved, S, Arkar, C. (2008). Correlation between the local climate and the free-cooling potential of latent heat storage. *Energy and Buildings*, 40: p. 429-437.
5. Takeda, S, Naganao, K, Mochida, (2004). T. Development of a ventilation system utilizing thermal energy storage for granules containing phase change material. *Solar Energy*, 77: p. 329-338.
6. Rouault, F., Bruneau, D., Sébastien, P., Nadeau, J-P. (2016). Use of a Latent Heat Thermal Energy Storage System for Cooling a Light-Weight Building: Experimentation and Co-simulation. *Energy and Buildings*, 127: p. 479-487.
6. Ortega, M.D.L.A., Nadeau, J.-P., Bruneau, D., Sébastien, P., Sommier, A., Lopez, J., (2016). Design and optimization of PCM-air heat exchangers. In Proceedings of Virtual Concept Workshop on Major Trends in Product Design, Bordeaux, March 17-18.
7. PCM mit hoher Dichte, [Online], Available: <https://www.rubitherm.eu/index.php/produktkategorie/an-organische-pcm-sp> [29 November 2017].
8. SOLAR HOUSES 2012, [Online], Available: <http://www.sdeurope.org/> [9 December 2017].
9. Lázaro, A., Dolado, P., Marín, J. and Zalba, B., (2009). PCM-air heat exchangers for free-cooling applications in buildings: Empirical model and application to design, *Energy Conversion and Management*, 50: p. 444-449.
10. Code de la construction et l'habitation, [Online], Available: <https://www.legifrance.gouv.fr/affichTexteArticle.do?cidTexte=JORFTEXT000000645843&idArticle=LEGIARTI000006261359> [27 May 2018].

Investigation of the Implications of Future Bioclimatic Potential on Annual Heating And Cooling Energy Load In Residential Buildings In India

NAVEEN KISHORE KHAMBADKONE¹

¹Department of Architecture and Planning, Maulana Azad National Institute of Technology (MANIT), Bhopal, India

ABSTRACT: This paper aims to investigate the implications of present and future bioclimatic potential of passive heating and cooling design strategies for future climate change scenarios for a location within a composite climate zone of India. Weather data for the future climate scenarios were developed for A2 (medium-high) scenario of the Intergovernmental Panel on Climate Change (IPCC) for four scenarios, namely TMY (Typical Meteorological Year), 2020, 2050 and 2080. The impact of the changing bioclimatic potential on annual heating and cooling energy load was quantitatively evaluated at the building level. A case study residential building was used for calibration and validation of the bioclimatic potential using building simulation technique. Results show a strong correlation between the annual passive heating and cooling potential and the corresponding annual heating and cooling energy load for the changing climate scenarios. A decrease in passive heating potential from 948 hrs. to 232 hrs. and an increase in passive cooling potential from 3477 hrs. to 4165 hrs. was observed. An overall 150% increase in annual cooling energy load and a 100% decrease in annual heating energy load (in Kwh/m²) was observed if residential buildings continue to be operated in the same manner as it is done today.

Keywords: Bioclimatic potential, climate change, passive heating and cooling, Composite climate, India.

1. INTRODUCTION

Climate is a major determinant for designing energy-efficient buildings. The recent Assessment Report (AR5) [1], by Intergovernmental Panel on Climate Change (IPCC) for mitigation of climate change, identifies *maximization of passive features* such as day-lighting, *passive heating, cooling strategies* as an essential step towards the design of low energy buildings. Passive heating and cooling design strategies must be developed considering the local climate. The importance of bioclimatic potential in relation to climate change and building energy performance has been well highlighted in some recent studies [2-4]. For example, in the study by Pajek and Kosir [2], the authors highlight the importance of re-evaluating the bioclimatic potential of any location in relation to climate change as it can have a major impact on indoor thermal conditions in buildings. Buildings need to be designed to adapt themselves to the future climate change phenomena and for this purpose bioclimatic passive heating and cooling design strategies will have to be re-evaluated for the future climate change scenarios.

This paper aims to investigate the impact of changing climate scenarios on the bioclimatic potential of passive heating and cooling design strategies. Further, their subsequent implications on indoor thermal comfort and annual heating and cooling load for a case study residential building located in Bhopal within a composite climate zone of India is also investigated. The A2 (medium-high) scenario of the

Intergovernmental Panel on Climate Change (IPCC) is used in this study to generate the climate change scenarios for future time slices namely, 2020, 2050 and 2080.

2. METHODOLOGY OF STUDY

The methodology of the conducted study is given below.

2.1 Climatic data and Climate change scenarios

The climatic data for this study is taken from the recently developed Typical Meteorological Year (TMY) hourly weather data files, by the Indian Society of Heating Refrigeration and Air Conditioning Engineers (ISHRAE). The Climate change world weather file generator (CCWorldWeatherGen) utility tool [5] is used to generate the future climate change scenarios, namely 2020, 2050 and 2080, for the climate of Bhopal, India using the base TMY hourly weather data file.

2.2 Bioclimatic potential for present and future scenarios

Bioclimatic potential is defined as the effectiveness of a passive strategy to extend or provide additional comfort conditions in a typical year over and above the existing base comfort conditions in a particular location. The bioclimatic potential was evaluated as a function of the effectiveness of passive heating and cooling design strategies in hours, namely Passive solar heating potential (PSHP hrs.) for passive heating and Natural ventilation potential (NVP hrs.), Direct evaporative cooling potential (DECP hrs.) for passive

PLEA 2018 HONG KONG

Smart and Healthy within the 2-degree Limit

cooling. This was done at the climate level as well as the building level using a bioclimatic analysis tool (Figure 1) developed by the author in a recent study [6].

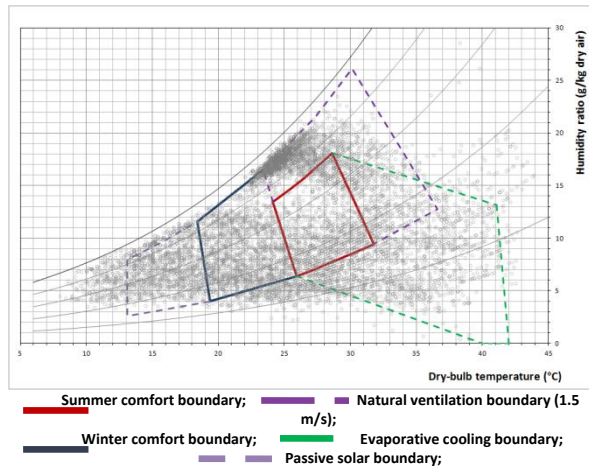


Figure 1: Bioclimatic chart showing outdoor conditions for TMY base scenario-Bhopal, Composite climate-India.

The bioclimatic tool is essentially a bioclimatic chart consisting of the base comfort zone and the passive design zones namely, *passive solar heating*, *direct evaporative cooling* and *natural ventilation*. This tool has been developed in MS-Excel. Each climatic data point is plotted on the Cartesian coordinate system with dry bulb temperature on X-axis and Humidity ratio on Y-axis. The base comfort and passive heating and cooling potential is assessed by calculating the total number of hourly climatic data points identified within a given boundary or envelope of that strategy. The annual bioclimatic potential is calculated using the equation (1) given below:

$$C_y = \left(\frac{P_y}{8760} \right) \times 100 \quad (1)$$

where C_y is comfort potential (in %) for a year and P_y is the number of climatic data points identified within a given boundary (for either base comfort or passive heating or cooling zones). The acceptable temperature ranges for the passive heating and cooling boundaries were calculated using the IMAC (Indian Model of Adaptive Comfort) model for adaptive comfort [7]. This adaptive model of thermal comfort has been incorporated in the recently revised National Building Code (NBC-2016) of India. The adaptive comfort equation for the IMAC [7] for naturally ventilated buildings is given below in equation (2).

$$T_c = 0.54 T_o + 12.83 \quad (2)$$

where T_c is the Neutral or comfort temperature in °C and T_o is the 30-day outdoor running mean air temperature ranging from 12.5 to 31 °C.

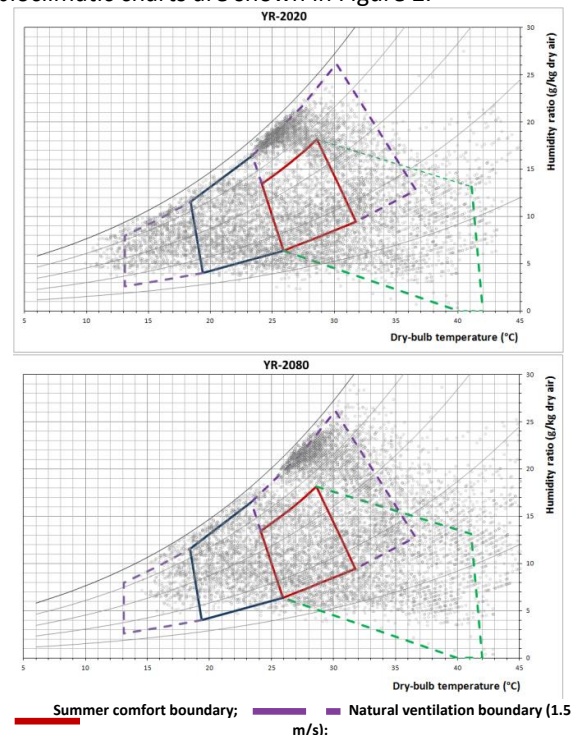
The calculated adaptive comfort temperatures for the hottest and coldest month for the city of Bhopal are given in Table 1 below:

Table 1: Indoor adaptive comfort temperatures (in °C) in hottest and coldest months for Bhopal, India.

For 90% Acceptability Range	Dec	Jan	May	Jun
Max (in °C)	26.2	25.1	32.6	33.2
Min (in °C)	21.5	20.4	27.8	28.4

The adaptive comfort temperatures given above in Table 1 indicate the temperatures at which occupants living in naturally ventilated buildings make themselves comfortable after having applied their adaptive actions like opening of windows, switching on ceiling fans, closing curtains or blinds, etc as per seasonal requirements. The lowest temperature occurs in January (winter) and the highest temperature occurs in the month of June (Summer). The lowest adaptive temperature is used to define the lower limit of the passive solar heating boundary and the highest adaptive temperature is used to define the upper limit of the natural ventilation zone. This highest adaptive temperature is below the skin temperature and hence is the maximum limit beyond which occupants would feel discomfort due to hot blowing winds in summer. A detailed discussion on the development of the tool can be found in the previous study by the author [6].

The hourly climatic data for the future climate change scenarios, namely 2020 and 2080 was plotted on the bioclimatic tool using the above method to generate the bioclimatic charts for the future scenarios. These bioclimatic charts are shown in Figure 2.



PLEA 2018 HONG KONG

Smart and Healthy within the 2-degree Limit

Winter comfort boundary; Evaporative cooling boundary;
Passive solar boundary;

Figure 2: Bioclimatic charts showing outdoor conditions for 2020 and 2080 scenarios-Bhopal, Composite climate-India.

2.3 Building calibration

An unoccupied conventional duplex residential building (Figure 3) is considered as case study for the purpose of calibration.



Figure 3: Case study house monitored for calibration.

Hourly indoor and outdoor temperatures were measured simultaneously for the period of 2 months on the first floor bedroom facing the balcony. The same building was modelled in Designbuilder and the surveyed building envelope characteristics like wall, roof, glazing thermal properties and thicknesses, were specified in the simulation model. The thermal properties and specifications of the building envelope components are given in Table 2. The building represents a typical conventional house typology without any passive features applied to it.

A TMY data file, incorporating the in-situ hourly measured outdoor dry bulb temperature data for the monitored period, was created and used as the weather data file for simulating the model. Test simulations were run on an iterative basis and the results of the measured and simulated temperatures were compared. Statistical compliance (Table 3) was derived using two indicators, namely MBE (Mean Bias Error %) and CVRMSE (Coefficient of Variance of root mean square error %) as per the ASHRAE Std 14-2002 guideline [8], which is currently the standard criteria for validating building energy simulation models [9]. The values from Table 3 indicate that if hourly temperatures are used for calibration then the permissible error range would be $\pm 10\%$ for MBE and 30% for CVRMSE. In this study, the simulation model was calibrated using hourly air temperature.

Table 2: Thermal properties of building envelope for case study residential building. (Source: Author)

Building element	Outside to inside	Construction details	U-value (W/m ² -K)
------------------	-------------------	----------------------	-------------------------------

Main Wall (190 mm Thk)	LAYER 1	20 mm thk cement plaster	2.26
	LAYER 2	190 mm thk Brick	
	LAYER 3	12 mm thk cement plaster	
Partition Wall (90 mm Thk)	LAYER 1	20 mm thk cement plaster	3.13
	LAYER 2	90 mm thk Brick	
	LAYER 3	12 mm thk cement plaster	
Roof (130 mm thk)	LAYER 1	20 mm thk cement plaster	3.67
	LAYER 2	100mm thk RCC slab	
	LAYER 3	12 mm thk cement plaster	
Floor	LAYER 1	15 mm Ceramic Tiles	3.80
	LAYER 2	100 mm thk PCC SLAB	
	LAYER 3	12 mm thk cement plaster	
Window (SHGC=0.82, VLT=0.8)	LAYER 1	6 mm clear glass	5.5

Note: RCC- Reinforced Cement Concrete; SHGC- Solar Heat Gain Coefficient; VLT- Visible Light Transmission

Table 3: Threshold limits of statistical criteria for calibration in compliance with ASHRAE Guideline 14. (ASHRAE Std 14-2002)

Statistical indices	Monthly calibration	Hourly calibration
MBE (in %)	± 5	± 10
CV-RMSE (in %)	15	30

2.4 Annual heating and cooling energy load simulation

The hourly weather data files for the above 4 scenarios were used for simulating the building model in 2 stages. In the first stage the building model was simulated in naturally ventilated (NV) mode. The simulated indoor operative temperatures and relative humidity values, representing the indoor conditions of the case study building were then plotted on the bioclimatic chart for all 4 scenarios. In the second stage the simulation was carried out in the AC mode with defined occupancy and AC operational schedules to simulate the annual

PLEA 2018 HONG KONG

Smart and Healthy within the 2-degree Limit

heating and cooling energy load. The input data for annual energy load simulation is given in Table 4.

Table 4: Input settings for annual energy load simulation of case study building.

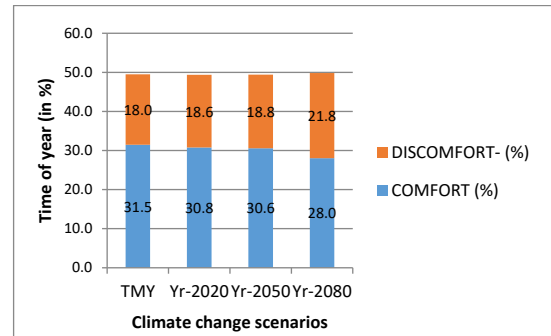
Room	Parameter		Details/ Specifications	
Bedroom 02 (First floor-Case study building)	i) Average occupation		2 persons	
	ii) Internal thermal load	Lighting	6 W/m ²	
		People	70 W/m ² (Sedentary activity)	
	iii) Ventilation mode		Air Conditioning (AC)	
	iv) AC settings	HVAC system (type)		Fan coil unit (4-pipe), Air cooled chiller
		Setpoint temperatures		Heating setpoint- 22 °C Cooling setpoint- 24°C
		Efficiency	Heating system seasonal COP	0.85
	Cooling system seasonal COP		1.80	
	Usage (operational) hours	Heating season (winter)	Weekdays 21.00 – 5.00 hrs. Weekends 21.00 – 5.00 hrs.	
		Cooling season (summer)	Weekdays 16.00 – 24.00 hrs. Weekends 12.00 – 24.00 hrs.	

3. RESULTS

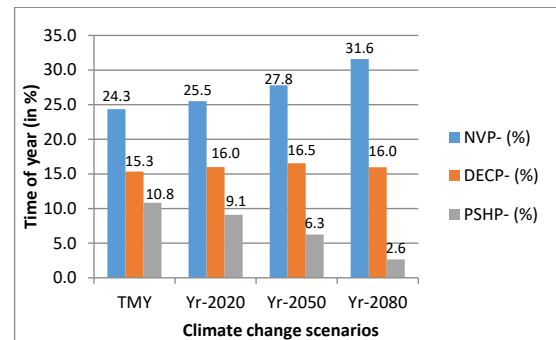
3.1 Climate level assessment

Based on the outdoor conditions as shown in Figure 2, the bioclimatic potential was calculated for the 4 scenarios. The results are shown in Figure 4. The annual discomfort hours (Fig 4 a) in terms of % was found increasing for the future scenarios. Similarly the annual bioclimatic potential also varied with the changing scenarios. It was found that the passive solar heating potential (in %) (Fig 4 b) was steadily decreasing whereas the passive cooling potential (NVP+DECP in %) was steadily increasing for the future

scenarios. This indicates that passive heating will have less applicability and buildings will be more cooling dominated in the future.



a) Comfort-Discomfort Hrs. (in % of time in a year)



b) Bioclimatic potential Hrs. (in % of time in a year)

Figure 4: Bioclimatic potential for present and future scenarios (in %)-Bhopal, Composite climate-India.

3.2 Building model calibration

The results of the performed hourly building calibration are given below in Table 5. MBE (in %) measures the bias between measured and simulated temperatures for each hour. Therefore it indicates the overall bias in the model across all data (measured and simulated). But since it uses the actual values and not the absolute values, it suffers from the cancellation effect because positive bias compensates negative bias. Hence CVRMSE is an additional measure of model error which overcomes the limitations of MBE. It measures the variability of the data and allows one to determine how well the model fits the data by capturing offsetting errors between measured and simulated temperatures. It

does not suffer from the cancellation effect. The comparison between the measured and simulated hourly DBT (in °C) is shown in Figure 5. The values of MBE and CVRMSE for the simulated model are well within the standard criteria as defined in ASHRAE Std 14 -2002 (Table 3).

PLEA 2018 HONG KONG

Smart and Healthy within the 2-degree Limit

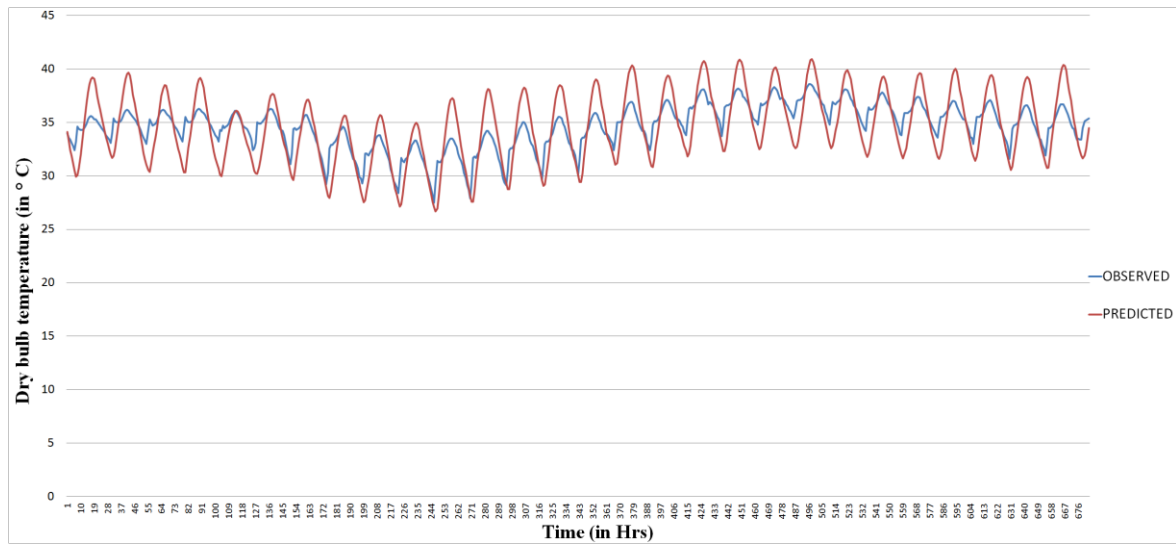


Figure 5: Comparison of measured and simulated indoor DBT(in °C) of the monitored bedroom for simulation model.

Table 5: Hourly calibration results for monitored period.

Period of monitoring	MBE (in %)	CVRMSE (in %)
1 st March to 29 th April 2017	-0.56	7.25

3.3 Building level assessment

3.3.1 NV- mode simulation: A further assessment was carried out at the building level to ascertain the indoor thermal conditions for the case study building for the 4 scenarios. The indoor conditions are represented as the plot of hourly indoor operative temperatures (in °C) and humidity ratio (in g/Kg), as shown in Figure 7, obtained from the annual simulation in the NV mode. The indoor comfort and discomfort hours were calculated based on adaptive comfort criteria using the bioclimatic tool and is shown in Figure 6. The general observation shows that the indoor conditions follow the outdoor climatic conditions for all 4 scenarios due to the poorly insulated building envelope leading to inefficient thermal performance. Another important observation shows that the buildings would be more cooling dominated in the future as was corroborated in section 3.1 in the climate level assessment. Architects and building designers will have to design new buildings or retrofit existing buildings considering passive cooling as the main paradigm of design for climate responsive buildings in India.

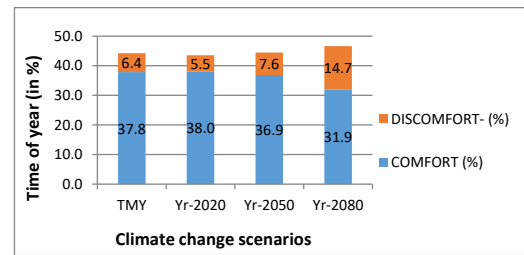


Figure 6: Comfort-discomfort hrs (in%) for case study building

3.3.2 AC-mode simulation: In order to assess the impact of the bioclimatic potential on the annual energy consumption, an annual energy load simulation was run for calculating the annual heating and cooling energy load (in Kwh/m²). The simulated annual heating and cooling energy load (in Kwh/m²) and the corresponding annual Passive heating potential hours (PSHP in Hrs.) and Annual passive cooling potential hours (NVP+DECP in Hrs.) is shown in Table 6. The changing trend in the annual heating and cooling energy load (in %) is shown for the 3 changing scenarios in Figure 8. Observations from Table 6 and Figure 8 confirms the fact that if the case study building continues to be operated in the same way as it is done today, then it will lead to an increase in annual cooling energy load by almost 150% and a decrease in annual heating load by almost 100%.

PLEA 2018 HONG KONG

Smart and Healthy within the 2-degree Limit

Table 6: Simulated bioclimatic potential and annual heating and cooling load for Case study building

Climate scenarios	TMY	2020	2050	2080
Annual Passive heating potential (PSHP in Hrs.)	646	320	130	6
Annual Heating energy load (in KWh/m ²)	5.1	2.31	0.61	0.02
Annual Passive cooling potential (NV+DEC in Hrs.)	4236	4628	4734	4669
Annual Cooling energy load (in KWh/m ²)	262.3	282.74	324.6	394.51

Another important observation from Table 6 shows the relationship between the annual bioclimatic potential (in hrs.) and the annual energy load (in Kwh/m²). A decreasing passive heating potential (in Hrs.) shows a corresponding decrease in annual heating load (in Kwh/m²) if the case study building is operated only in the AC mode without applying any passive heating strategies (like direct heat gain systems). Similarly an increasing passive cooling potential (in Hrs.) shows a corresponding increase in annual cooling load (in Kwh/m²) if the building is operated only in AC mode without applying any passive cooling strategies (like natural ventilation and evaporative cooling systems) to the building. It is important to recall here that the selected conventional case study building has no passive strategies applied to it and is simulated as the base case.

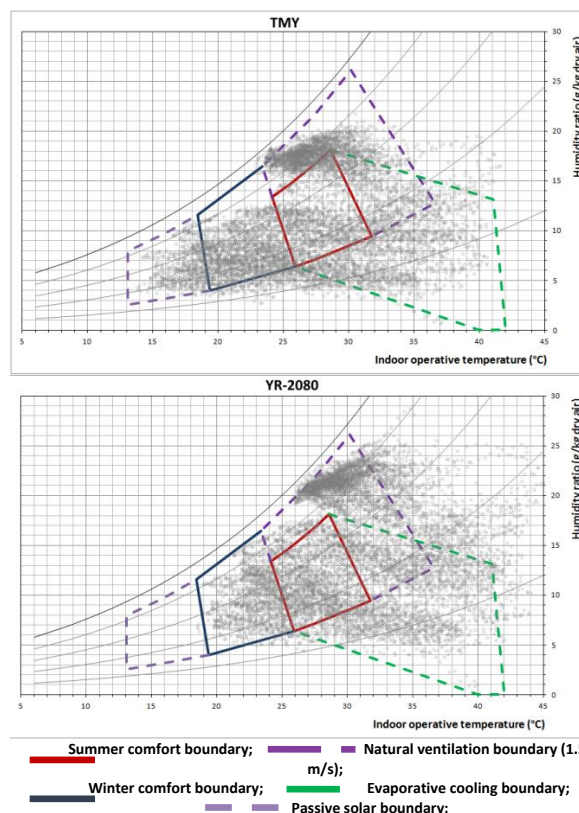


Figure 7: Simulated indoor conditions (in NV-mode) for case study residential building for TMY & 2080 scenarios

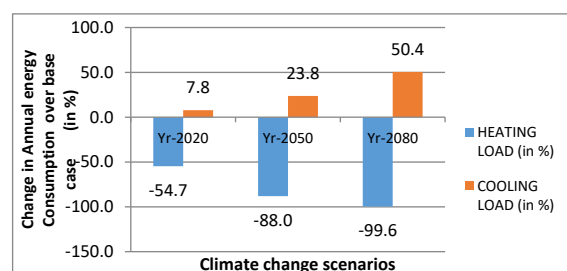


Figure 8: Changing trend of annual heating and cooling energy load (in % over base case) for different climate scenarios.

4. CONCLUSION

This paper demonstrated a simple yet robust method to assess the bioclimatic potential and its implications on building energy consumption for present and future scenarios for a location within a composite zone in India. With the changing climate becoming warmer, buildings will have to be designed to be adaptable to future climate change in terms of passive cooling rather than passive heating. More such studies covering locations under different climate zones need to be conducted in order to assess their implications for climate responsive building design for a sustainable future and energy security in India.

REFERENCES

Urge-Vorsatz, Cabeza, L.F. & Jiang, Y., 2014. Ch-9-Buildings, pp.671- 738., *Climate Change 2014 Mitigation of Climate Change Working Group III Contribution to the Fifth*

PLEA 2018 HONG KONG

Smart and Healthy within the 2-degree Limit

Assessment Report of the Intergovernmental Panel on Climate Change (AR 5- IPCC 2014).

Pajek, Luka, and Mitja Košir. 2018. Implications of present and upcoming changes in bioclimatic potential for energy performance of Residential Buildings." *Building and Environment* 127:157–72.
doi:10.1016/j.buildenv.2017.10.040

Invidiata, Andrea, and Enedir Ghisi. 2016. "Impact of Climate Change on Heating and Cooling Energy Demand in Houses in Brazil." *Energy and Buildings* 130: 20–32.

Miró, Juan Javier, María José Estrela, Vicente Caselles, and Jorge Olcina-Cantos. 2016. "Fine-Scale Estimations of Bioclimatic change in the Valencia Region, Spain." *Atmospheric Research* 180:150–64.

University of Southampton. CCWorldWeatherGen, <http://www.energy.soton.ac.uk/ccworldweathergen>, 2009.

Khambadkone, Naveen Kishore, and Rekha Jain. 2017. "A Bioclimatic Analysis Tool for Investigation of the Potential of Passive Cooling and Heating Strategies in a Composite Indian Climate." *Building and Environment* 123: 469–93.

Manu, Sanyogita, Yash Shukla, Rajan Rawal, Leena E Thomas, and Richard De Dear. 2016. "Field Studies of Thermal Comfort across Multiple Climate Zones for the Subcontinent : India Model for Adaptive Comfort (IMAC)." *Building and Environment* 98. Elsevier Ltd: 55–70.

ASHRAE. Guideline 14-2002: Measurement of energy and demand savings. Atlanta, GA 30329: American Society of Heating, Refrigerating and Air Conditioning Engineers; 2002.

Coakley, Daniel, Paul Raftery, and Marcus Keane. 2014. "A Review of Methods to Match Building Energy Simulation Models to Measured Data." *Renewable and Sustainable Energy Reviews*.

doi:10.1016/j.rser.2014.05.007.

Evaluation of soil-cement blocks: Response to water tightness factor, heat-shock action

Giane de Campos Grigoletti¹, Rogério Antochaves de Lima¹, Luciani Somensi², Priscila Giorgi³

¹Laboratório de Materiais e Construção Civil, Universidade Federal de Santa Maria, Santa Maria, Brazil

²Laboratório de Ensaios e Modelos Estruturais, Universidade Federal do Rio Grande do Sul, Porto Alegre, Brazil

³Universidade Regional Integrada do Alto Uruguai, Santo Ângelo, Brazil

ABSTRACT: The building sector is responsible for a significant consumption of natural resources. Sustainable buildings decrease environmental impact, such as energy consumption, soil, water, and air pollution. Raw soil may be an alternative for the sustainable development of the construction sector. Raw soil is cured without burning, mixed with Portland cement, pressed and stabilized to produce soil-cement blocks, which are regulated by the Brazilian Association for Standardization. In order to increase its acceptance and verify its efficiency as a building material for social housing, it is necessary to investigate its properties and performance. The present study aimed to evaluate the performance of an external vertical sealing system composed of hollow blocks of soil-cement without structural function following determinations of the Brazilian standards and focusing on habitability and sustainability requirements. Tightness against rainwater, water permeability, and durability through heat action and thermal shock tests were analyzed. The system met limits set by standards for tightness against rainwater, heat action, and thermal shock, but not for water permeability. The vertical sealing system composed of hollow blocks of soil-cement has potential to be employed in construction, although there is still much to be improved.

KEYWORDS: Soil-cement, Performance evaluation, Habitability, Sustainability

1. INTRODUCTION

The building sector is responsible for a significant consumption of natural resources around the world. Sustainable buildings contribute to reducing environmental impact, such as energy consumption, soil, water, and air pollution. In this scenario, raw soil as a building material has become an alternative for the development of sustainable buildings. Raw soil is cured without burning and, when mixed with Portland cement, pressed and stabilized, produces soil-cement blocks that are an alternative for the development of sustainable buildings. The benefits of soil-cement blocks range from the manufacturing to the construction site, reducing embodied energy consumption. Soil can be obtained from construction sites, which reduces the need for transportation and is more easily incorporated into natural environments at the end of its life cycle. In addition, the equipment used to produce soil-cement blocks has low-cost as they do not require skilled labor, which is important aspect for developing countries, such as Brazil. Torgal and Jalali [1] reported that almost 50% of the population in the world lives in houses made of earth, most of which can be found in Brazil. Numerous studies have been carried out around the world aiming to evaluate and develop soil-cement as a building material. In this context, soil-cement is widely accepted as a suitable and reliable material, although due to specific features, its characterization is necessary, according to the local context.

Soil-cement blocks are a standardized material by the Brazilian Association for Standardization (ABNT) [2].

Despite soil-cement quality, it is necessary to demonstrate its performance such as durability and structural stability, among others, as a result of a large variability of soil used in its composition, since soil varies extensively from site to site. The ABNT guideline [2] evaluates housing performance dealing with safety, habitability (e.g. water tightness factor), and sustainability (thermal behavior). In addition, the standards present the minimum requirements and criteria for external wall system (EWS) and laboratory tests for habitability and sustainability. Therefore, the present study aimed to evaluate the performance of an EWS composed of hollow soil-cement blocks without structural function. Additionally, it also focused on building one-floor single-family social housing while following Brazilian standards and focusing on habitability and sustainability requirements.

2. FUNDAMENTALS

Adequate soil-cement techniques depend on soil composition and properties, including granulometry, plasticity, shrinkage, humidity, and compaction. For this purpose, various tests have already been consolidated and can be divided into two groups: field and laboratory tests. According to ABNT [2], soil-cement is a homogeneous mixture composed of soil, Portland cement, and water in proportions established by standard, which is compressed by a press and hardened without burning in order to create blocks. The brick manufacturing process consists primarily of preparing the soil and mixture, molding, curing, and

PLEA 2018 HONG KONG

Smart and Healthy within the 2-degree Limit

storing. To estimate the components of the mixture, Brazilian standards [3] recommend the preparation of three different traits of soil-cement as well as 20 massive blocks molded or leaked for each of them. The curing of the elements takes a minimum of 14 days, being that the first 7 days they have to be maintained wet. After that, the elements should be submitted to laboratory analysis to determine compressive strength and water absorption. The preparation of the mixture can be accomplished either manually or mechanically and can incorporate other materials, such as industrial waste.

Brazilian standards [2] evaluate the housing performance by approaching: i) safety, ii) habitability, which evaluates tightness against water, thermal performance, acoustic and light performance, health, hygiene and air quality, functionality and accessibility, tactile and anthropodynamic comfort, and iii) sustainability, which analyzes durability, maintainability, and environmental impact. In addition, the standards present the minimum requirements and criteria for EWS and laboratory tests for habitability and sustainability. The tests concerning EWS are presented in Table 1.

Table 1. Occupants' requirements and laboratory tests for evaluation of habitability and sustainability

Occupants' requirements	Laboratory test according to Brazilian standards
habitability/water infiltration and humidity	rainwater tightness and permeability tests
sustainability/durability and maintainability	heat-shock test

In Brazil, there are few studies addressing soil-cement performance and applying the standards to evaluate EWS, since building standardization has been recently introduced.

Hattge [4] carried out a comparative study of the permeability of walls in ceramic blocks and in concrete blocks in order to analyze their performance in terms of moisture penetration. First, walls without coating and after coating with 1:1:6 mortar (cement, lime, and sand) of 1.5 cm in thickness on the outer face (submitted to water) and of 1.0 cm on the inner face were evaluated. The test to determine the rainwater tightness consisted of subjecting the specimens to a water film with pneumatic pressure on the surface through an airtight chamber of prismatic shape in the dimensions of 90 cm x 110 cm. The test was divided into two stages: the first test consisted of applying the water film without pressure, and the second one consisted of applying pressure of 260 Pa. The specimens were evaluated visually in both steps by marking the humidity stains on the opposite side of the water spray at the times of 5, 15, 30, 60, 90, 120, and 150 min for the first step, and 5, 15, 30, 60, 90, and

120, for the second one. This procedure was different from the present study, which subjected the walls to 7 h of water spray with a pressure of 50 Pa, as established in NBR 15575. Hattge [4] observed that the performance against rainwater tightness was satisfactory in neither ceramic nor concrete block walls without coating, since the area with moisture spots on the specimens at the end of the tests covered 1/3 of the area (33.3%). The specimens of both coating systems showed no damp staining.

Rodrigues [5] also analyzed the performance regarding water permeability, following the specifications of NBR 15575 [2]. In the same wall of ceramic blocks, different types of coating were tested (uncoated, acrylic sealer, acrylic sealer plus PVA paint, acrylic sealer plus acrylic sealer, acrylic sealer plus acrylic sealer and PVA ink and with acrylic sealer plus acrylic texture and acrylic paint) and coating mortar (ratio 1:1:6, industrialized and ratio of 1:2:9). From 0 to 60 min, none of the specimens complied with the limit of the standard. Oliveira; Fontenelle; Mitidieri Filho [6] presented the results of the thermal and thermal shock tests according to the Brazilian standards in two cold-formed and cold-formed steel profile walls fixed to the profiles with screws. The standard determines that horizontal cracks and shifts in the specimen that may hinder the performance of the external sealing system should not appear. Two conformations of the same wall were tested; however, the treatment of the joints between the sealing plates, dimensions of the test piece, and external bond (restriction of lateral movement of the wall) varied. The walls differed in the length of the section tested (1.20 m and 2.40 m with restriction in lateral movement), maintaining the same height (2.60 m). The results indicated that wall 1 (1.20 m length without restriction) met the criteria of the standard, whereas wall 2 (2.40 m length with restriction) did not respond, indicating that the test recommended as standard may not represent the actual performance of the wall. Varisco [7] evaluated an EWS formed by blocks of autoclaved cellular concrete with no structural function according to heat-shock standardized tests. The dimensions of the test piece were 1.80 m x 2.75 m x 0.10 m. The test resulted in 0.1 mm cracks on both sides of the specimen in the third heating and cooling cycle and the horizontal displacement was lower than the minimum criterion established in the standard. Varisco [7] also performed the rainwater tightness test for the same wall before and after the heat-shock test. The author verified that there were no spots on the opposite side of the EWS, reaching the level of intermediate or superior performance, which is in accordance with Brazilian standard.

PLEA 2018 HONG KONG

Smart and Healthy within the 2-degree Limit

3. METHOD

The evaluated EWS consisted of hollow blocks of soil-cement with dimensions of 25 cm × 7 cm × 12.5 cm (Fig. 1).

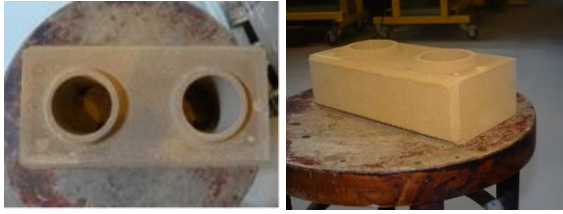


Figure 1: Soil-cement blocks.

The soil was characterized based on Atterberg limits, soil plasticity, and sieving analysis, according to standards [8], [9], [10]. The characterization of the soil used in the bricks is presented in Table 2.

Table 2. Soil characterization according to Brazilian standards

BRAZILIAN STANDARD	REQUIREMENT	CRITERIA	RESULTS
6.459	Atteberg limit	≤ 45	23.8
7.180	Soil plasticity	≤ 18	18,0
7.181	Sieve analysis - sieve No. 4 (4.75mm) (%)	100%	100%
7.181	Sieve analysis – sieve No. 200 (0.075mm) (%)	10% a 50%	1.5%

The proportion of mortar and soil was 87% of soil and 13% of mortar. The water was dosed according to soil humidity.

Two specimens with 1.25 m × 2.38 m were built and submitted to tests of habitability and sustainability. For the purposes of this study, the walls were named wall A and wall B. The constructive system of the specimens consisted of embedded soil-cement blocks seated with polymer mass, grafted at the lateral ends and at the vertical center axis. This formed columns with 0.98 m at the lower base and upper end, forming beams, with 8 mm iron reinforcement and filled with grout. After 24 h, the outside joint walls were grouted with mortar (Figure 2).

The external surface was covered with three layers of waterproofing acrylic resin after the cement had been cured for 28 days. The grouting and waterproofing was only on the external face of the element. The drying period of resin was 120 days.



Figure 2: Soil-cement specimens.

In relation to habitability requirements, the water tightness factor was analyzed through rainwater tightness and water permeability tests. In terms of sustainability requirements, the durability factor was analyzed through the heat shock test [2].

The rainwater tightness test consisted of subjecting the external surface of the wall to a continuous water flow rate of 3 liters per minute per square meter for 7 h. This created a homogeneous and continuous film with the simultaneous application of a pneumatic pressure of 50 Pa on the exposed face. The test time was recorded visually with the use of a stopwatch for each test piece once the first moisture spot appeared on the face opposite to the water spray. The percentage of the moisture spot area at the end of the test in relation to the total area of the face that was not exposed to water spray was recorded.

The maximum area of the moisture spot at the end of the test in relation to the total wall area was calculated and based on [2]. According to [2], moisture spots with an area below or equal to 10 % of the total area of non-structural walls are acceptable after seven hours of exposure.

The water permeability test consisted of submitting a wall section to the presence of water with constant pressure by means of a box-shaped chamber coupled to the wall, with internal dimensions of 34 cm x 16 cm x height (Figure 3).



Figure 3: Permeability test apparatus.

To maintain constant pressure inside the chamber and measure the volume of water infiltrated in the

PLEA 2018 HONG KONG

Smart and Healthy within the 2-degree Limit

specimen (only wall B was submitted to the experiment), a burette graduated in cubic centimeters was used. This burette was embedded in the chamber in order for its mouth to tangle the water level inside. Then, when the water infiltrated the sample, the same volume of infiltrated water was replaced by the water contained in the burette. This process maintained the water level inside the chamber constant and allowed the quantification of the infiltrated water. Water levels were recorded at 30, 60, 120, 240, 360, and 1,440 min of assay [2].

The heat-shock test consisted of submitting each specimen to 10 successive cycles of heating and cooling through radiant source and cold-water jets at 20 ± 5 °C. This was done in order to simulate the conditions of exposure of the façades during its lifespan (i.e. variations in temperature and humidity). Five thermocouples connected to a fieldlogger were installed over the surface exposed to the action of heat and thermal shock in order to record temperature variations. On the opposite side of the heating and cooling, an electronic deflectometer was installed in the center of the specimen in order to measure the instantaneous horizontal displacements (Figure 4).

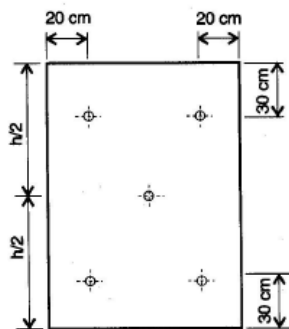


Figure 4: Apparatus for heat and shock test and position of thermocouples.

Brazilian standards [2] recommend that the EWS does not present instantaneous horizontal displacement above $H/300$ after 45 min of temperature stabilization in a plane perpendicular to wall, where H is the height of specimen. Additionally, fissures, detachments, blisters, and discolorations must not appear during the test.

4. FINDINGS

Considering the area of the specimens, the criteria for maximum area of moisture spots on the face opposite to the incidence of water, after the rainwater tightness test, is 0.2975 m^2 [2]. As both specimens were subjected to the rainwater tightness test before (T1) and after thermal shock test (T2), for nomenclature

purposes, wall A was subdivided into Wall-A Test 1 (WAT1) and Wall-A Test 2 (WAT2). The results for wall B was subdivided into Test 1 of Wall B (WBT1) and Test 2 (WBT2) in the same way. Results obtained in this test are shown in Table 3.

Table 3: Findings for rainwater tightness after seven hours

Test/specimen	wet area/indoor	criteria $\leq 0.295 \text{ m}^2$?
WAT1	0.11 m^2	Yes
WAT2	0.23 m^2	Yes
WBT1	0.12 m^2	Yes
WBT2	0.14 m^2	Yes

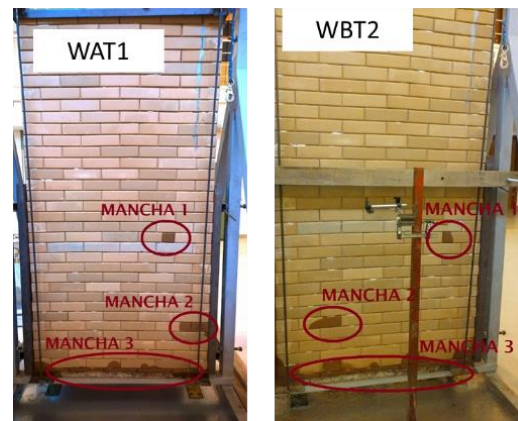


Figure 5: Moisture spots observed.

A continuous moisture spot was observed at the base of specimen due to lack of sealing in its borderline. This result indicates that, without the acrylic resin, the wall was not water tight (Figure 5). Nevertheless, the specimens satisfied established criteria both before and after the thermal shock.

Comparing this result with Hattge [4], who evaluated brick and concrete blocks, the performance was better than soil-cement blocks. This difference can be associated to the use of outside and inside surfacing mortar.

According to [2], the amount of water that can penetrate the EWS should not exceed 3 cm^3 for a period of 24 h. Wall B did not meet the criteria for the water permeability test, as shown in Table 2.

Table 2: Findings for water permeability

time (min)	0	30	60	120	240	360	1,440
seep of hum. (cm^3)	0	36	11.6	17.8	18	16.5	54
amount	153.9 cm^3						

Comparing this result with the findings obtained for ceramic blocks [4] with mortar coating, the infiltration reached $2,925.00 \text{ cm}^3$, and in concrete blocks with mortar coating, the infiltration reached $3,435.00 \text{ cm}^3$,

PLEA 2018 HONG KONG

Smart and Healthy within the 2-degree Limit

higher values when compared to the system studied. The same was verified for ceramic blocks without mortar coating, but with different finishing layers, such as acrylic and PVA paint [7]. All specimens tested also failed to achieve the criteria specified by the standards.

For the heat shock-test, the maximum instantaneous horizontal displacement allowed is 8.0 mm. Results for wall A and wall B are presented in Table 3.

Table 3: Results for displacements for wall A and wall B

Wall A			Wall B				
cycles	Dhi (mm)	Dhr (mm)	Dh (mm)	cycles	Dhi (mm)	Dhr (mm)	Dh (mm)
1	0.85	0.21	0.64	1	0.95	0.43	0.52
2	0.60	0.18	0.63	2	0.23	0.16	0.39
3	0.51	0.03	0.66	3	0.34	0.16	0.50
4	0.64	0.03	0.64	4	0.66	0.10	0.56
5	0.73	0.03	0.73	5	0.52	0.04	0.48
6	1.03	0.11	0.95	6	1.02	0.51	0.51

The displacements of walls A and B are expressed, per cycle, in terms of Dhi, instantaneous horizontal displacement measured after 45 min of the temperature stabilized at 80 ± 3 °C; Dhr, residual horizontal displacement measured after the wall reached 20 ± 5 °C; and Dh, total horizontal displacement (Table 3).

The maximum instantaneous displacement (Dhi) for wall A was 1.03 mm and wall B was 1.02 mm, both meeting the criteria. It was observed that, in all cycles, wall A practically returned to its initial position after cooling to 20 ± 5 °C, which reveals that this specimen did not suffer significant Dhr. Similar behavior was observed in wall B, except in cycles 1 and 6, where there was pronounced Dhr (0.46 mm and 0.51 mm). After the test, a visual analysis identified that there were no occurrences of cracking, blisters, detachment, discolorations or any other damages that could compromise the performance of EWS, which is in accordance with the criteria by [2].

5. CONCLUSION

The results indicate that the EWS evaluated met habitability requirements, water tightness factor, including after the heat-shock action test. This demonstrates that the system should remain sealed against rainwater with the time action. However, the criterion for water permeability was not met. The EWS also met sustainability and durability requirements as indicated in the heat-shock test, since the parameters indicated by [2] were met in all cycles. It was found that, in almost all cycles, the specimens practically returned to their initial position after cooling to 20 ± 5 °C, demonstrating that the EWS tested did not suffer

significant horizontal displacement when exposed to the action of the heat. These results allow us to conclude that the constructive system evaluated has significant potential to be used as EWS, especially for low-income housing because it has lower costs than conventional systems. However, it needs to be improved, since one of the evaluated factors was not met. In addition, according to Brazilian standards, the EWS must satisfy structural safety, fire security, and others not mentioned in this study.

An improvement of the system, considering water permeability, may be to stabilize the soil with more adequate proportions of cement [11]; more adequate compaction method [12]; the use of different stabilizer [13]; and the use of an external cement plaster layer, which increases the consumption of cement, making the EWS less sustainable.

REFERENCES

1. Torgal, F. P. and Jalali, S. (2012). Earth construction: lessons from the past for futures eco-efficient construction. *Construction and Building Materials*, 29: p. 512-519.
2. ABNT (2013). *NBR 15575: Edificações habitacionais – Desempenho*, Rio de Janeiro.
3. ABNT (2013). *NBR 10833: Fabricação de tijolo e bloco de solo-cimento com utilização de prensa manual ou hidráulica – Procedimento*, Rio de Janeiro.
4. Hattge, A.F., (2004). *Estudo comparativo sobre a permeabilidade das alvenarias em blocos cerâmicos e alvenarias em blocos de concreto*. Dissertação MSc. Porto Alegre, Brasil, UFRGS.
5. Rodrigues, A.H., (2010). *Estanqueidade de alvenaria revestida com diferentes argamassas e acabamentos: aplicação da NBR 15575-4/2008*. Monografia Eng Civil. Porto Alegre, Brasil, UFRGS.
6. Oliveira, L. A.; Fontenelle, J. H.; Mitidieri Filho, C. V. (2014). Durabilidade de fachadas: método de ensaio para verificação da resistência à ação de calor e choque térmico. *Ambiente Construído*, 14: p. 53-67.
7. Varisco, M. (2014). *Análise do desempenho de blocos de concreto celular autoclavado em um sistema de vedação externa*. Dissertação M. Sc. Curitiba, Brasil, Instituto de Engenharia Civil.
8. ABNT (2016). *NBR 6459: Solo – Determinação do limite de liquidez*, Rio de Janeiro.
9. ABNT (2016). *NBR 7181: Solo – Determinação do limite de plasticidade*, Rio de Janeiro.
10. ABNT (1988). *NBR 7180: Solo – Análise granulométrica*, Rio de Janeiro.
11. Bahar, R.; Benazzoug, M.; Kenai, S. (2004). Performance of compacted cement-stabilised soil. *Cement & Concrete Composites*, 26: p. 811-820.
12. Kenai, S.; Bahar, R.; Benazzoug, M. (2006). Experimental analysis of the effect of some compactation methods on mechanical properties and durability of cement stabilized soil. *Journal of Materials Science*, 41: p. 6956-6964.
13. Eires, R.; Camões, A.; Jalali, S. (2017). Enhancing water resistance of earthen buildings with quicklime and oil. *Journal of Cleaner Production*, 142: p. 3281-3292.

Development of an Energetic Profile of Buildings: From Current Status to Achievable Improvement

GAL RINGEL¹, ISAAC GUEDI CAPELUTO¹

¹Faculty of Architecture and Town Planning, Technion – Israel Institute of Technology, Haifa, Israel

ABSTRACT: The term "Profile" is often used in different disciplines to identify fundamental properties of an object, while analyzing future steps to use them. In this research, the concept of Energetic Profile for Existing Office Buildings and its features are presented. The Energetic Profile consists of seven architectural parameters ranging from macro to micro, taking into consideration its surrounding environment, the building's morphological characteristics up to the typical floor plan design. The Energetic Profile enables the identification of energy saving opportunities and enables distinction between energetic-architectural typologies of office buildings which are not commonly discussed in environmental conscious standards. For each of the parameters a methodology was developed to investigate its total energy impact (divided into cooling, heating and lighting) in a theoretical office building located in a hot and humid climate. Performed case studies demonstrate the effectiveness of the tool to identify potential action directions for energy savings, compare design alternatives, and examine the influence of various construction phases of the building. The case studies proved up to 50% in savings potential compared to current condition, when implementing the conclusions of the profile. Future contribution is expected as an auxiliary tool for designing also new office buildings.

KEYWORDS: Energy, Lighting, Profile, Office, Design

1. INTRODUCTION

In many disciplines The term "Profile" is used to define and characterise an object or an idea, describing its main features: companies and corporations use Business Profile for firms or products to assess their assimilation into the market, employment agencies use Personality Profile -MMPI [1], to identify the suitability of a candidate for a job, and a Constructive Profile is used for testing a structure's resistance to earthquakes [2].

In this research an Energetic Profile for existing office buildings was developed. It is based on a doctoral dissertation conducted at the Technion-Israel Institute of Technology [3]. Seven parameters comprise the proposed Energetic Profile: (1) Building's environment, (2) Building's envelope, (3) Compactness, (4) Form factor, (5) Flexibility, (6) Floor efficiency and (7) Space type division. The parameters are geometric and fundamental in nature, simulating the building in its construction stage, before finishing materials and building systems were added. The Energetic Profile enables the analysis of energy saving opportunities for different office buildings, identifying their unique characteristics.

The study focuses on office buildings, which constitute a large and significant sector in the overall energy consumption of buildings [4] in the US, Israel and other countries [5], and can be extended to additional building types.

A series of studies conducted by the New Buildings Institute indicate that lighting is a significant and potentially main factor for energy savings in office and

commercial buildings [6]. Therefore efforts are being made to reduce the use of electric lighting by end users in office and exploit even a small part of the potential inherent in these savings. Energy consumption for heating and cooling are the other two major groups with a great potential for energy savings in office and commercial buildings [4]. This research focuses on reducing energy consumption in the areas of lighting, cooling and heating.

The increasing environmental awareness in Israel and around the world led to the development of rating systems and standards according to green principles such as LEED and Israeli standards 5281 [7], 5282 [8]. In the United States, more than 32,500 commercial buildings were certified by LEED [9].

In a research conducted by Shaviv & Capeluto [10] it was concluded that climate conscious design already in the initial design stages, using passive and active means, form a better basis for achieving optimal energy saving and comfort conditions. In a new building, this basis can be created under appropriate environmental conditions, and in the absence of other functional constraints. In the case of an existing building, several parameters cannot be changed and other historical, constructive, architectural, psychological and functional considerations may influence the building's potential energetic savings. Nevertheless, there are major opportunities for energy savings when the building is facing a change due to different reasons such as compliance with new standards, replacement of roof or part of façade, added wing, renovation and so on [11]. It is agreed

PLEA 2018 HONG KONG

Smart and Healthy within the 2-degree Limit

that in both cases the main energy savings lie in the early design stage or -in a given existing building- in its basic and fundamental architectural properties. Morphological design variables such as the building's shape, size and proportion have a great influence on the building's life cycle and especially on the efficiency and flexibility of the building over time.

1.1 Background: Office building design and energy consumption

The office building is one of the most prominent icons of the 21st century. It is the most visible product in the city reflecting economic activity, technological progress, financial and social progress.

The office building is an immediate consequence of employment patterns. Over the past four decades, the typology of the office building has changed along with the development of work patterns.

The morphological differences between buildings and space types affect their energy consumption [3]. A skyscraper building with a typical open floor plan that serves high-tech companies is morphologically different from a three-story bank building with a closed plan in its design, function, daily use, type of envelope, size, shape, systems and other attributes. However, green building standards generally classify them under the same category and apply to them the same criteria for an energetic score. This has led to the need of creating an applicable energetic profile for office buildings

2. RESEARCH GOALS

The aim of this study is to create an Energetic Profile to help identifying opportunities for potential energy savings in existing office buildings. The main objectives are:

1. Identifying the "DNA" of the building in accordance with its energetic, geometric and functional characteristics.
2. Evaluating the hidden potential for energy efficiency in office buildings while using a fast, non-simulation based method, which is appropriate for use in many existing buildings.
3. Creating a scale of values pointing on failures and opportunities for energy savings in the building.
4. Developing a tool that can be implemented on any office building while keeping its unique characteristics and typology.

3. METHODOLOGY

A comprehensive literature review allocated different parameters influencing the energy consumption of an office building to groups such as geometric-non geometric, schematic-detailed, large scale-small scale, functional-architectural and long term-short term effect on the building's life cycle. From these groups

seven key parameters were identified. Each of these parameters was tested independently. As part of the methodology, new indicators were developed in place where the ones found in the literature were not sufficient. The analysis of each parameter was done performing a set of tests using ENERGYui [13], comparing the different cases in each parameter against the energy consumption in a theoretical building considering cooling, heating, lighting and total energy consumption. Each parameter was analyzed by a wide range of buildings scenarios. These parameters are:

1. Building's Environment (measured by SSA- Sky solid angle [12]). A detailed description of the analysis of this parameter is presented in Section 3.1.
2. Envelope (WWR- window wall ratio and WFR- window to floor ratio). The combination of these two variables allows the analysis of buildings with various depths and floors' height. WWR varied from 0-90%, while office depth changed from 3 to 16m. As part of this study, we developed a combination formula between WWR and WFR which connects the qualities of these two indicators together.
3. Compactness (RC- relative compactness). This parameter refers the area of the envelope relative to the size of the building, through which one can learn about the meaning of the building's form. We tested cases from low and wide buildings (30 office modules by 3 floors), to high rise and narrow buildings (3 office modules by 30 floors, office module defined by 8.20m/8.20m/2.80m).
4. Shape Factor (a specific indicator created for this purpose representing the relation between N-S to W-E facades in different aspects). We analyzed from rectangular, cube or L shape buildings to amorphous buildings and their relation to orientation.
5. Flexibility (Perimeter area/total floor area). Focuses on the analysis of a typical floor. The concept of Perimeter Area is used - a perimeter strip adjacent to an external wall that expresses the potential of the building to exploit its potential for natural ventilation and daylighting. We consider three depths: until 5m, between 5 and 8.2 m and beyond 8.2m.
6. Floor Efficiency (Main area/total area). This parameter considers the ratio between main and service areas and its impact on building design and the total building's energy consumption. The considered range varied from a ratio between main and service areas of 100% to 0, until 50% to 50% respectively.
7. Space Type Division (XS,S,M,L,XL according to types of spaces- from single offices division up to complete open space). This parameter goes down to the highest resolution and looks at the interior division of the floor and its effect on daylight penetration and energy consumption. The reference building was divided into units which represent modules of different sizes, location of the floor plan (corner: 2 windows directions,

PLEA 2018 HONG KONG

Smart and Healthy within the 2-degree Limit

external: 1 window direction, internal: no windows), location in building section (ground floor, middle floor and roof) and orientation.

These analyses created the basis for the construction of the building profile. A full description of the method for analysing the remaining parameters and their integration into the EP will be presented in a following journal article.

The theoretical building used in this work is a model of a common-practice 5 story office building, 1210 m² per floor, length to width ratio 2:1 tested North- South orientation and East-West orientation, in Tel- Aviv city's climate (Fig. 1). The building was modeled using ENERGYui interface which serves the Israeli Standard 5282 for Energy rating of buildings and is based on Energy plus engine. The theoretical building was designed according to Israel's planning laws and standards, and is considered a medium height building. Tests were conducted for ground level, typical middle floor and roof level. The basic office module is 8.20m depth by 8.20m width which is compatible with 5282 standard. The office space was defined as an open space allowing the transition of air and light between the modules. In the middle of each office module we defined a lighting control point, 4 m from the facade. The internal space of the building (depth above 8.20m from the façade) was defined as an internal office space (artificially lighted and acclimatized with no passive means) in order to distinguish between energy consumption in peripheral areas and internal spaces.

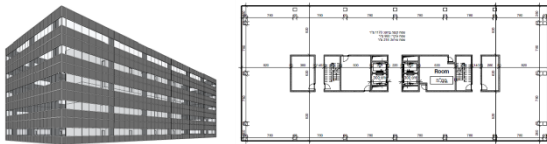


Figure 1: Typical floor plan and 3D model of base case office building

According to the range of values tested for each variable, the delta between maximum and minimum energy consumption was calculated in each case and a graph of change in energy consumption for each parameter was created and analyzed. The results were incorporated into the Energetic Profile for assessing the building's potential savings by giving each parameter its relative importance measured by the delta between maximum and minimum energy consumption found.

3.1 Parameter #1: Building's Environment

The starting point of any design process depends on receiving a plot or an existing building in a given urban situation. Even before the design begins, the architect has constraints and limitations, from the shape of the plot, its area and dimensions, orientation and the buildings surrounding it, their distance, height and

shape in relation to the planned building. Depending on the height of the building, its distance to adjacent buildings, the shape and height of the buildings surrounding it and the topography, it is possible to determine the Visible Sky seen from the building's facade as a result of obstructions [12]. The solid angle subtended by a surface is defined as the surface area of a unit sphere covered by the surface's projection onto the sphere. Since a vertical window can potentially reflect only half of the hemisphere, the maximum possible value of the SSA for a completely unobstructed window, measured in the external wall layer is π steradians. It has been shown by Capeluto [12] and in a similar way by Compagnon [14] that there is a clear correlation between the SSA subtended from the center of the window and the DF_{ave} as defined by CIBSE, 1987 [15] that can be expected over the workplane in the building. Reinhart & LoVerso [16] also pointed on the connection between DF_{ave} and sky angle. Yet, they all relate to a single point of view on the façade.

In this research we expanded the use of SSA in order to find the mean SSA not only for a single window but for the whole façade and eventually for the whole building as a way of understanding its overall potential for daylighting use. Furthermore we examined the influence of the building's mean SSA on energy consumption for lighting, cooling, heating and overall energy consumption in various urban situations.

Two geometric correlations were studied (Table 1):

$H_i / W / H_n$ - The ratio of the height of the tested building (H_i), the width of the road (W) and the height of the neighbouring building (H_n).

W / W_n - The ratio between the width of the road (W) and the width of the neighbouring building (W_n).

Table 1: Combinations of geometric relationships between $H_i/W/H_n$ tested (*1= 5 floors 2=10 floors 4= 20 floors $W=0.5$ (9.25 m= 2.5 floors) $W=1$ (18.5m=5 floors) $W=2$ (37m=10 floors) $W=4$ (74m=20 floors))

W	H _n	H _i	W	H _n	H _i	W	H _n	H _i	W	H _n
0.5	1	1	1	1	1	2	1	1	4	1
0.5	2	1	1	2	1	2	2	1	4	2
0.5	4	1	1	4	1	2	4	1	4	4
0.5	1	2	1	1	2	2	1	2	4	1
0.5	2	2	1	2	2	2	2	2	4	2
0.5	4	2	1	4	2	2	4	2	4	4
0.5	1	4	1	1	4	2	1	4	4	1
0.5	2	4	1	2	4	2	2	4	4	2
0.5	4	4	1	4	4	2	4	4	4	4

When these two set of tests are combined together, they can reflect a wide range of urban situations, from uniform low urban tissue to dense, high urban tissue, and even a combination of vertical and horizontal randomness in the building environment. The purpose of the test was to create a set of geometric relationships (Table 2), which enables the immediate

PLEA 2018 HONG KONG

Smart and Healthy within the 2-degree Limit

identification of the average visible sky (SSA) of the building without the need for simulation. The SSA was tested in each floor of the building between 0 to 20 floors while using Sketch-Up [17] and SunTools for SSA calculations [18].

Table 2: Average SSA test results for façade in 36 cases representing different urban situations

Hi	W	Hn	W/Wn	Average SSA (sr) for façade	Average SSA (%) for façade	DF
1	1	1	0.36	2.59	83	5.43
1	1	2	0.36	1.96	62	4.48
1	1	4	0.36	1.51	48	3.52
2	1	1	0.36	2.86	91	5.68
2	1	2	0.36	2.23	71	4.96
2	1	4	0.36	1.57	50	3.66
4	1	1	0.36	3.00	96	5.78
4	1	2	0.36	2.67	85	5.52
4	1	4	0.36	1.83	58	4.23
1	2	1	0.71	2.93	93	5.73
1	2	2	0.71	2.64	84	5.48
1	2	4	0.71	2.33	74	5.10
2	2	1	0.71	3.03	97	5.79
2	2	2	0.71	2.76	88	5.60
2	2	4	0.71	2.37	75	5.16
4	2	1	0.71	3.09	98	5.82
4	2	2	0.71	2.94	94	5.74
4	2	4	0.71	2.52	80	5.34
1	4	1	1.42	3.08	98	5.82
1	4	2	1.42	2.97	95	5.76
1	4	4	1.42	2.82	90	5.65
2	4	1	1.42	3.10	99	5.83
2	4	2	1.42	3.01	96	5.78
2	4	4	1.42	2.84	91	5.67
4	4	1	1.42	3.12	99	5.84
4	4	2	1.42	3.06	98	5.81
4	4	4	1.42	2.89	92	5.71
1	0.5	1	0.18	2.11	67	4.77
1	0.5	2	0.18	1.26	40	2.86
1	0.5	4	0.18	0.87	28	1.70
2	0.5	1	0.18	2.62	84	5.46
2	0.5	2	0.18	1.64	52	3.82
2	0.5	4	0.18	0.91	29	1.84
4	0.5	1	0.18	2.88	92	5.70
4	0.5	2	0.18	2.38	76	5.17
4	0.5	4	0.18	1.20	38	2.71

For every geometric configuration SSA was determined (% and steradians) and DF(%) was found according to the conversion formula [12]. The minimum SSA tested was 28% and the maximum was 99% which is equivalent to DF 1.70-5.84% (acceptable effective average daylight factor range is between 2-5%). An average SSA for each façade in each analyzed urban situation was found. The range between SSA 30%-100% was later tested in ENERGYui every 10% to examine the influence of average SSA on energy consumptions for cooling, heating and lighting. We show that when average SSA was lower than 45%, the energy consumption remains high and almost constant, meaning that natural lighting doesn't penetrate sufficiently to the building and therefore electric lighting is on most of the time (Fig. 2). When looking at each façade separately the most dramatic

change was observed in the north façade, where SSA below 70% does not supply enough lighting (Fig. 3 upper-left).

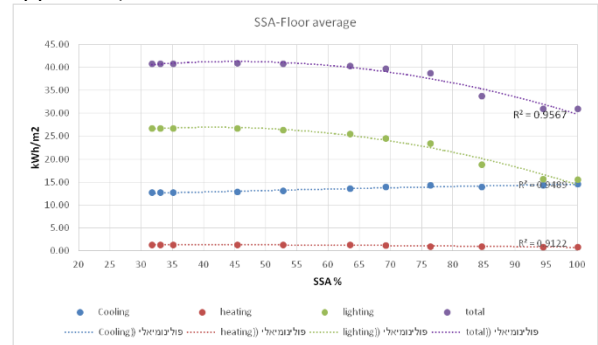


Figure 2: Average energy consumption in middle floor in accordance with SSA

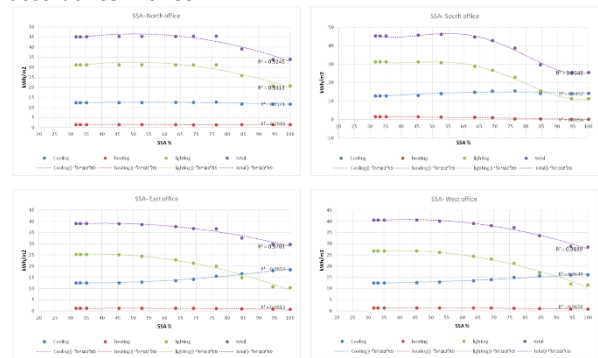


Figure 3: Energy consumption in a middle office (3rd floor, non corner office) in accordance with SSA

3.2 Application in the Energetic Profile:

The total energy consumption of the building depending on the change in SSA% is presented on the left graph in Fig 4. The right graph shows the feasible expected improvement of the parameter when 0% represents no possible improvement (the best SSA% case registered) and 100% represents the worst SSA% case and maximum improvement need.

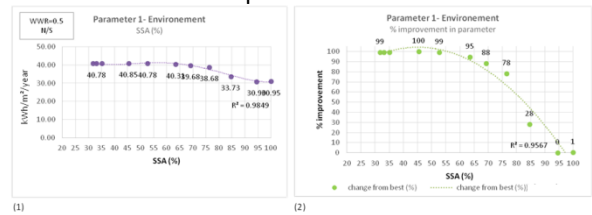


Figure 4: Total energy consumption (kWh / m2) and percentage of improvement – SSA

Fig. 5 shows the representation of these results in the profile scale:

Below SSA=30% means DF(ave) lower than 2% and therefore is marked in red. Between SSA 30-60% there is limited contribution for natural lighting and therefore this area is marked orange-yellow. Above 70% SSA there is a significant decrease in energy consumption mostly above 80% SSA and that is why this area is marked green (recommended) in the scale. In the same way all other profile's parameters are

PLEA 2018 HONG KONG

Smart and Healthy within the 2-degree Limit

represented by a colored scale from red (bad) to green (good), when the color changing of the scale follows the internal improvement graph of each parameter.

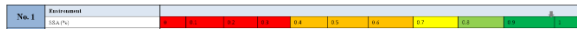


Figure 5: the colored scale of parameter #1: Environment according to graph of change in energy consumption depending on SSA percentage.

4. DISCUSSION

The results of each parameter were integrated into the Energetic Profile, creating a scale of values in each one of them. The Energetic Profile was then defined in two ways (Fig. 6):

- (1) Design Energetic Potential of the building representing the savings potential of the building compared to the maximum energetic potential line of the profile, representing the minimum energetic consumption found in each parameter.
- (2) Actual Achievable Energetic Potential of the building which is derived from the building's "AS IS" function, and considering constraints which may avoid changes in the building.

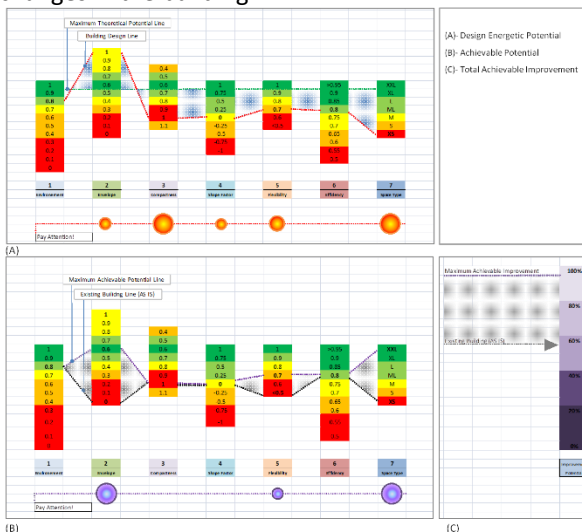


Figure 6: Energetic Profile for Existing Office Building: (A) Designed Energetic Potential (above) (B) Achievable Energetic Potential (below) (C) Total Achievable Improvement

4.1 The Energetic Profile- Part A:

The first part (Fig. 6 up) allows comparison of the designed building to other buildings, as they all measured against the minimum consumption line of the profile- and identifying the opportunities for energy savings. The top green line represents the maximum theoretical performance line for any office building. It is composed of the minimum values of energy consumption found in each parameter. The red line represents the building as it is planned in its geometric components. The polygons created between the theoretical green line and the buildings red line are the theoretical opportunities areas for

energy savings. This allows comparing different design alternatives, as they are all compared to the same theoretical line. It also allows comparing different buildings and examining their morphological aspects. As the polygon grows that means more potential for improvement. When the red line is close to the green line the meaning is that the building is well planned according to the parameters of the Profile.

4.2 The Energetic Profile- Part B:

The second part (Fig. 6 down) enables determination of the actual achievable savings in the building based on its own geometric, constructive and functional constraints.

The upper purple line represents the building's maximum potential line when applying the maximal changes possible in each parameter up to constructive limitations. The black line represents the building's actual function mode ("AS IS" line), the polygons between these two lines represent the actual possible improvement in energy savings for the building. For example a change of the typical plan from single office to open space or semi open space can improve its expose to daylight and therefore improve its values in parameters 5 and 7. In a similar way a building in which WWR is below recommendation can easily reach its goals by enlarging the windows actual glassed area (parameter no.2). Along with this chart there is a summary scale which sums the improvement percentage when X improvement percentage means X improvement percentages left for realization.

It is important to read the two parts of the Profile together in order to understand the problematic parameters and their solutions. As a value reaches the red area of a parameter a warning point will show up. One parameter can also affect values of other parameters therefore when a warning point is showing up it can also point at other parameters that should be closely tested.

4.3 Validation

The credibility of this system was tested in two different office buildings: Ayalon Tower and CU office buildings in Tel Aviv.

In Ayalon Tower we investigated the use of the Profile versus a simulation model built in ENERGYui. At the first stage the model was simulated according to its real conditions at all aspects concerning the plan, section, envelope, type of glass, systems and daily use as it was verified with the buildings operation manager. In the second stage the building was modelled while using its potential saving opportunities according to the profile. In each case the energy consumption for heating, lighting and cooling was calculated in kWh/m²/year. It was found that 40% improvement in energy consumption is achievable using the conclusions of the profile while the profile itself (with

PLEA 2018 HONG KONG

Smart and Healthy within the 2-degree Limit

no simulation) showed a 47% improvement and pointing on the range between 40-60% improvements. The second case study tested include 4 buildings 5-6 floor height, and one building which is planned to be 15 story height in a future second stage. The buildings were analyzed using the Profile in both conditions: present and future. Using the new parameters we demonstrated that the added height actually benefits its condition over the current status, while reducing the potential for daylight for other buildings around it. In this case study the results of the simulation were also very similar to the results of the profile and demonstrated how the profile can be used as a tool to analyze different design stages of a project.

5. CONCLUSION

The Energetic Profile for Existing Office Buildings proposed in this study enables the easy identification of strengths and weaknesses of energetic potential in different office buildings according to their location design and function.

The profile is a tool to compare buildings not only to other similar buildings, but also to themselves: from their current status to their achievable improvement. The profile is suitable for use in a primary stage of investigation pre-intervention in existing buildings. The case studies presented in this work proved up to 50% in savings potential compared to current condition, when implementing the conclusions of the profile.

Though the profile was developed for existing buildings, it can also add a significant value at the different design stages of new building by utilizing the results regarding energy savings in each parameter.

Furthermore, although the focus of the profile was to reduce the total level of energy consumption of the building, much emphasis was placed on the subject of natural daylight. Natural light does not only serve as a major contributor for energy savings, but it also holds benefits for the quality of the building's interiors and human activity.

A further research could extend the conclusions found in this work to other climate zones and building types, as well as developing the Profile as a design tool for new construction.

This work focuses on the possible lines between a restricting building design and a flexible building design. It invites the user to be familiar with morphological differentiations in buildings. These features are not solely limited to office buildings but can expand the discussion to any other building types. It is important to emphasize that the profile examines the energetic potential savings assuming the use of appropriate detailed design. The profile does not contradict energy savings by technologies.

Beyond the general conclusions of the profile, detailed inference were included in each parameter regarding

parts of the building, the envelope, different types of geometric relations in the building that can be relevant and useful for specific interventions or retrofit processes.

REFERENCES

1. McKinley, J. C. & Hathaway, S. R. (1944). A multiphasic personality schedule (Minnesota) *Journal of Applied Psychology*, 28, p. 153-174.
2. Guendelman, B.T., Guendelman, M., Lindenberg, J. (2010). Instrumento de Calificación Sísmica: Perfil Bio-Sísmico de Edificios, Terremoto Chile.
3. Ringel, G. (2017), An Energetic Profile for Existing Office Buildings. PhD Research Thesis, Technion – Israel Institute of Technology, 2017
4. D&R International, Ltd. (2012). 2011 *Building Energy Data Book*, U.S Department of Energy, Pacific Northwest National Laboratory, p.114.
5. IEC- Israel Electricity Company (2011). *Statistic report* p.21.
6. NBI- New Building Institute (2011). A search for deep energy savings, *Meta report*, NEEA- Northwest Energy Efficiency Alliance
7. Israel Standard 5281 (2011). Sustainable buildings, The Standards Institution of Israel.
8. Israel Standard 5282 – part 2 (2011) Energy rating of buildings: office buildings. The Standards Institution of Israel.
9. Shutters C., Tufts R. (2016). LEED by numbers, USGBC statistics.
10. Shaviv, E., Capeluto, I.G (1992). Relative importance of various geometrical design parameters in a hot, humid climate, *ASHRAE Transactions* 98:589-605.
11. Pacific Northwest National Laboratory & PECL (2011). Advanced Energy Retrofit Guide: Office Buildings, U.S Department of Energy.
12. Capeluto, I. G. (2003). The influence of the urban environment on the availability of daylighting in office buildings in Israel, *Building and Environment* 38 (2003) 745-752.
13. EnergyUI website, Available:: <http://EnergyUI.com>
14. Compagnon, R. (2000). PRECis: Assessing the Potential of Renewable Energy in Cities- Solar and Daylight Availability in Urban Areas- *Final Technical Report*, The European Commission, Ecole d'ingénieurs et d'architectes de Fribourg.
15. CIBSE, (1987). Chartered institution of building services engineers, *applications manual: window design*. London: CIBSE.
16. Reinhart, CF., LoVerso, V.R.M. (2010). A rules of thumb- based design sequence for diffuse daylight, *Lighting Research and Technology* 2010; 42: 7-31.
17. SketchUp 3D modelling software website, <https://www.sketchup.com>

PLEA 2018 HONG KONG

Smart and Healthy within the 2-degree Limit

18. Capeluto G. (2011). The meaning and Value of Information for Energy Conscious Architectural Design, *Proceedings of Building Simulation 2011 Simulation, Sidney, Australia.*

Shadowing windows with BIPV blinds: Delicate balance for office buildings in low latitudes.

JOÁRA CRONEMBERGER¹, ESTEFANÍA CAAMAÑO-MARTÍN²

¹Faculdade de Arquitetura e Urbanismo, Universidade de Brasília, Campus Universitário Darcy Ribeiro, 70910-90 Brasília, Brazil

²Instituto de Energía Solar, Universidad Politécnica de Madrid, Av. Complutense 30, E-28040 Madrid, Spain

ABSTRACT: An office building offers several opportunities to integrate Building integrated Photovoltaics (BIPV) elements. Shading blinds form combines perfectly two functions: preventing part of the irradiation from reaching a glazed surface controlling the inner comfort conditions, as well as producing solar electricity. In regions where high irradiation is available and less demanding climates from the point of view of heating loads, this application is particularly advantageous for this kind of building. Nevertheless, at low latitudes locations, due to relative position of sun rays, the increasing effect of self-shading must be carefully analyzed - there is a delicate balance between optimal tilt angle and latitude to achieve a surface suited to integrate BIPV shadowing components. A methodology and practical results have been presented, easily possible to be used to design such devices in office buildings in Brazil, and, to a certain extent, in other countries at similar latitudes. Also, contribute to the further development of knowledge in this so far unexplored producing and saving energy saving strategy.

KEYWORDS: BIPV, shading devices, low latitudes, energy

1. INTRODUCTION

An office building offers several opportunities to integrate Building integrated Photovoltaics (BIPV) elements. The shading blinds form combines perfectly two functions: preventing part of the irradiation from reaching a glazed surface controlling the inner comfort conditions, as well as producing solar electricity [1]. In regions where high irradiation is available and less demanding climates from the point of view of heating loads, this application is particularly advantageous for this kind of building .

Several studies state that fixed shading components protecting windows South oriented (Northern Latitudes) cause significant reductions in cooling loads in summer, and help control glare [2-3], although they could increase the demand for energy in winters in colder climates, possibly also due to the need for more artificial lighting [5].

Horizontal shading devices in office buildings are normally preferred because allows unobstructed outdoor visual contact, which is usually favorable to users [6,7,8,9] providing at the same time more surface less susceptible to auto shading for integration of photovoltaic modules, and therefore potentially more efficient from the point of power generation [10]. Nevertheless, at low latitudes locations, due to relative position of sun rays, the increasing effect of self-shading must be carefully analyzed [11]. It is what we have done and are presenting in this research paper.

2. METHODOLOGY

The methodology used was based on calculations and simulations. Starting from a common case of an office building, a Reference Case (no shadings) and a Case Study (with PV Blinds) and their parameters were defined. Afterwards they were calculated, simulated and analyzed for seven different cities located from latitudes -1.4° to -30° in Brazil (Fig. 1). Results of more than 500 simulations are presented and discussed.

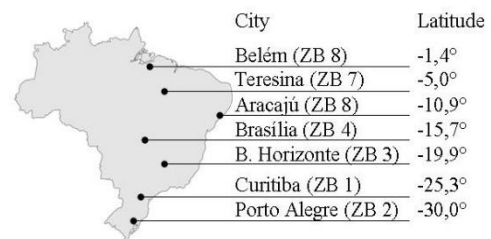


Figure 1: Latitudes and cities analyzed. Source: Authors.

The seven cities represent most of the Brazilian climates distributed in its extensive territory. They are separated from each other by approximately 5 degrees of latitude were chosen. The main design strategy of BIPV blinds was to reduce cooling loads. Regarding availability of the solar resource and optimal tilt surfaces, methodology and data indicated by Cronemberger et al [12] and Caamaño [13] were used.

2.1 Reference office building and case study

Office buildings in Brazil, despite the variability of climates and microclimates, frequently present an

almost uniform typology, often not adapted to the climatology of the area where they are built. Prototype building is then a 15 stores rectangular shaped, 46% WWR (window to wall rate). Glazing is a float 6mm grey glass, completely unshaded (Fig.2 left).

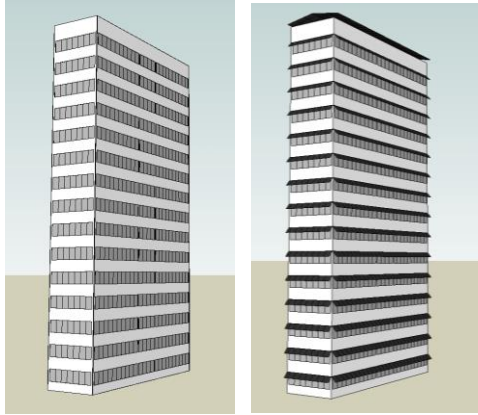


Figure 2: Reference Case (left) and Case Study (right). Source: Authors.

As the basic prototype is rectangular with an elongated floor plan (7,80 x 27,0 m), different WWT for each orientation influences the building's thermal behavior and PV energy production. For that reason, two orientation options have been investigated: North-South (NS) and East-West (EO) (Fig. 3). Case Study was defined applying BIPV blinds all along the windows as horizontal shading devices, considering the back sheet opaque and light colored (Fig. 2, right).

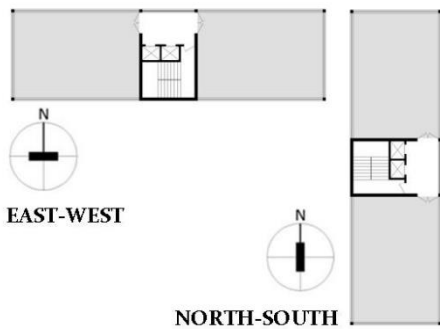


Fig. 3. Building orientation alternatives. Source: Authors.

2.2 Definition of shading geometry optimized for climate conditions and solar photovoltaic energy production

The goal was making the shading surface effective as a solar protection for the window, with a reasonable electrical productivity to the PV technology incorporated to them. An important consequence of this decision is that the dimensions of the PV shading module vary according to the latitude, making the comparison among them complex. An angle to solar mask was defined upon the latitude and orientation of window (α =Vertical Shading Angles). Tilt (β) and length

of horizontal BIPV blinds were then defined (Fig.4), aiming to protect windows oriented to North, South, East and West. Climate conditions of each for each one of seven locations were taken into account [14]. Solar charts were used, both analogical and with specific solar analysis software's, such as Ecotec Solar Analysis and Analysis Sol-Ar [15].

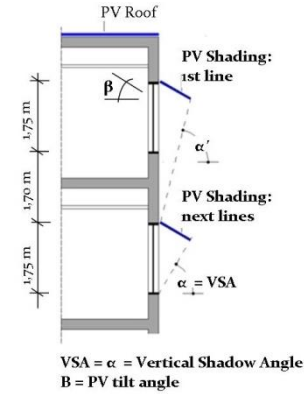


Figure 4: Measurements and angles to a BIPV horizontal blind. Source: Authors.

2.3 Quantifying annual solar irradiation losses - Shading Factors (SF)

The IES/UPM Methodology [13] was used to calculate Shadowing Factor (SF). This methodology is a version adapted for negative latitudes of a 1998 proposal, which has been adopted by the Building Technical Code of Spain since 2006 [16]. It allows estimating the irradiation losses based on the representation of obstacles interposed between a surface and the solar path, using a simplified solar path diagram.

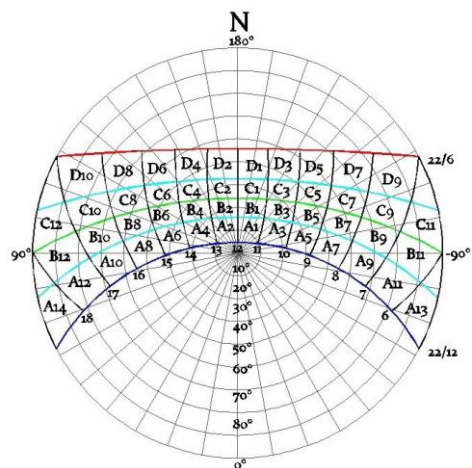


Fig. 5. Stereographic solar diagram for Porto Alegre (Latitude -30°). Adapted from IES-UPM Method. Source: Authors.

Solar diagrams of stereographic projection were used (Fig. 5). The total area of the sun's path has been divided into zones identified by letters and numbers. To each zone a "weight" is attributed to the annual global irradiation expected to affect a surface. Thus,

PLEA 2018 HONG KONG

Smart and Healthy within the 2-degree Limit

the obstacle profile determined by the PV blinds analyzed incurs a loss of the direct and diffuse circumsolar components, according to the Pérez and Seal model [17-17]. Shading Factor (SF) was obtained by adding the contributions of each zone of the diagram affected by the obstacles, calculated in the most unfavorable point. Results were transferred to tables resulting in a percentage of the expected annual global irradiation for each analyzed surface, for a certain latitude and azimuth.

2.4 Estimating potential impact on cooling loads and cooling energy demand

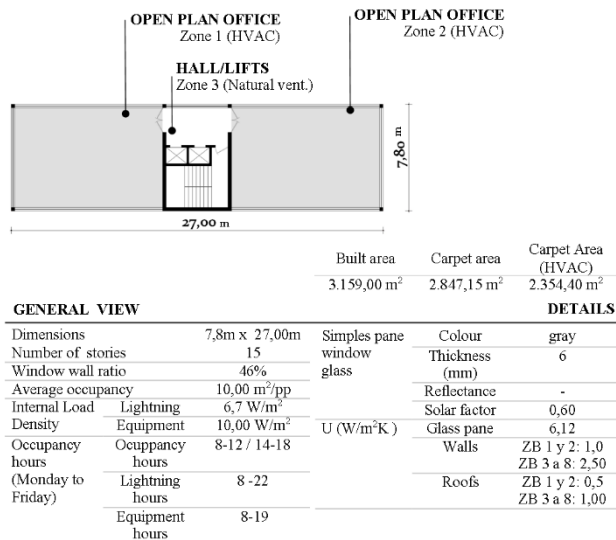


Figure 6: Office building model for energy simulation. Source: Authors.

To assess potential impact on cooling loads and cooling energy demand, annual electricity energy demand for HVAC, lightning and office equipment were estimated for each one of the case studies in the different locations and orientations. Furthermore, heat transfer through walls and glazing, cooling and heating loads have been identified in order to analyze building thermal behavior with and without sunshades. Figure 6 presents the basic features of an office building in Brazil, used as a reference model for the energy simulations performed in this research. DesignBuilder was employed, a well-known software for dynamic simulations with EnergyPlus calculation engine. It allows modeling the energy behavior of buildings based on a three-dimensional model perfectly characterized in terms of its physical construction, material properties, conditions of use, HVAC equipment and hourly weather data. All simulations used the same climatic EPW data files based on hourly data from INMET, revised in 2012 [14-15].

3. RESULTS AND DISCUSSION

3.1 Shading geometry optimized for climate conditions and solar photovoltaic energy production

High WWF (46%) and glazing thermal characteristics ($U=6,12 \text{ w/m}^2\text{K}$), posed a great challenge defining adequate AVS of shading devices for the specific climatic conditions and latitudes. In Porto Alegre (Lat. -30.0°) and Curitiba (Lat. -25.7°) it is sufficient to protect glazing in Summer and Spring, whilst in Belo Horizonte (Lat. -19.9°) and Brasília (Lat. -15.7°) it should be extended till the first month of Autumn, due to the high air temperatures. Closer to Equator, Aracajú (Lat. -10.9°), Teresina (Lat. -5.0°) and Belém (Lat. -1.4°), shading geometry must be sized for the whole year.

Table 1: Measurements to BIPV horizontal blinds: L = length; α =AVS=Vertical Shading Angles, α' =shading angles between blinds; β = PV tilt. Source: Authors.

LAT.	FAÇ	L (cm)	AVS = α	α' (°)	β (°)
$-30,0^\circ$	N	85	59,9	76,3	30
	E/W	85	40	75,8	10
	S	60	69,5	80	10
$-25,3^\circ$	N	75	64,5	77,8	25
	E/W	85	60	76	25
	S	60	69,6	80	10
$-19,9^\circ$	N	90	58,3	76,3	25
	E/W	90	63	75	25
	S	60	69,5	80	15
$-15,7^\circ$	N	90	62,4	77,2	24
	E/W	80	33	76	10
	S	60	71	80	10
$-10,9^\circ$	N	105	55,6	72	14
	E/W	80	24	76	10
	S	60	71	80	10
$-5,0^\circ$	N	85	61,5	76	12
	E/W	85	27	76	12
	S	85	61,5	76	12
$-1,4^\circ$	N	75	61,5	78	7
	E/W	85	17	78	10
	S	75	61,5	78	7

Ideally, North façades would have to be protected by shading devices with horizontal and vertical combined components, although the horizontal element is more relevant. The presence of the vertical component increases, however, with latitude. This is also true for South façades, though in this orientation the vertical component is more important when more distant to Equator. To block properly East and West glazing from sunshades would require mobile horizontal devices. Contrary to the usual practice, fixed vertical devices are not very effective for the orientations and latitudes analyzed. In fact, for hot weather regions, it would be appropriate to reduce the WWR proportion. Although the ideal shading would require horizontal and vertical combined elements, this arrangement would provoke self shading for PV shading devices. When North

PLEA 2018 HONG KONG

Smart and Healthy within the 2-degree Limit

oriented (Southern latitudes) they should be tilted considering the Optimal Angle (β) for PV production.

3.2 Annual solar irradiation losses - Shading Factors (SF)

The higher lines of BIPV blinds (15th store) are affected by the shadows thrown by the building itself, being positioned at a certain distance from the crowning. As expected, the next lower lines are self shaded, presenting higher annual irradiation losses. However, surprisingly, all the cities analyzed presented suitable surface to receive BIPV blinds, except for the South orientation in the cities located between latitudes -30° and -15.7° .

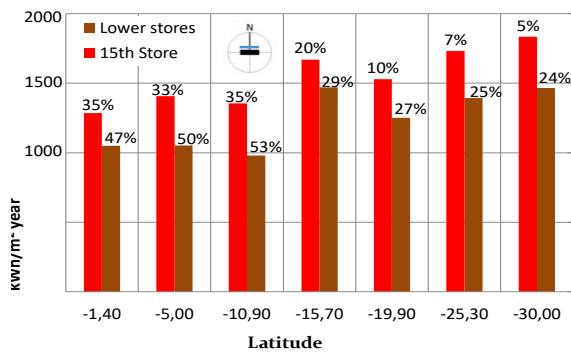


Figure 7: Shading Factor (SF) and Annual Global Irradiation (kWh/m^2) in BIPV Blinds for several latitudes when North oriented. Source: Authors.

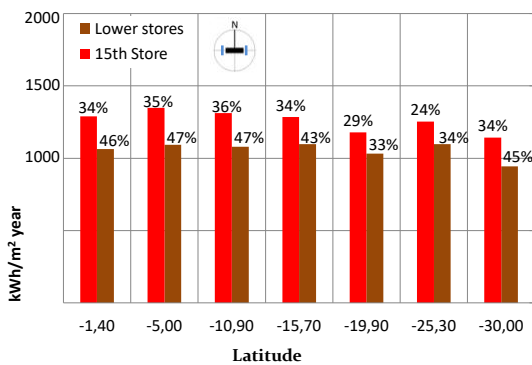


Figure 8: Shading Factor (SF) and Annual Global Irradiation (kWh/m^2) in BIPV Blinds for several latitudes when East/West oriented. Source: Authors.

North orientation presented as expected best results. Higher shading factors (SF) percentages, and therefore less available solar direct irradiation would happen in lower latitudes. Nevertheless, PV sun shadings may potentially receive from $979-1.833 kWh/m^2$ annually (Fig. 8). East/West oriented PV blinds would have SF's from 24-47%, but might yield from $944-1.348 kWh/m^2y$. Due to solar altitudes, losses would be higher for Latitudes over -15° (Fig. 9). South oriented blinds would only be suitable for PV integration though in low latitudes - even with high shading factors (42-

66%) surfaces could harvest from $701-1.177 kWh/m^2y$ (Fig. 10).

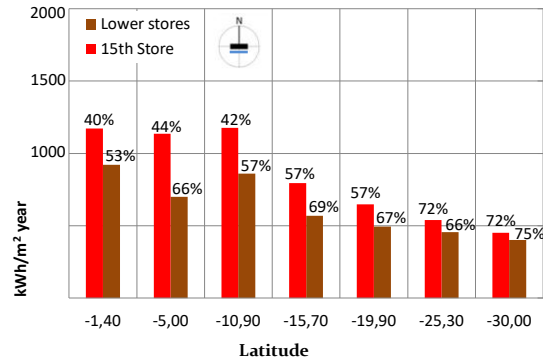


Figure 9: Shading Factor (SF) and Annual Global Irradiation (kWh/m^2) in BIPV Blinds for several latitudes when South oriented. Source: Authors.

3.3 Potential impact on cooling loads and cooling energy demand

The complete absence of solar shading in the reference case, and glazing high thermal transmittance ($U=6,12 w/m^2K$) resulted in high thermal gains by direct solar irradiation. As expected, cities getting closer to Equator have higher cooling loads (figures 7 and 8), from $74kWh/m^2$ in Curitiba (Lat. $-25,3^\circ$) to $226 kWh/m^2$ in Belém (Lat. $-1,4^\circ$). Simulations showed also that, compared to reference case, applying PV Blinds may provoke reductions in cooling loads from 19.4% to 42.8% for NS oriented buildings. For the other building orientation (EO) reductions are slightly lower, but also expressive, from 16,1% to 39,3%.

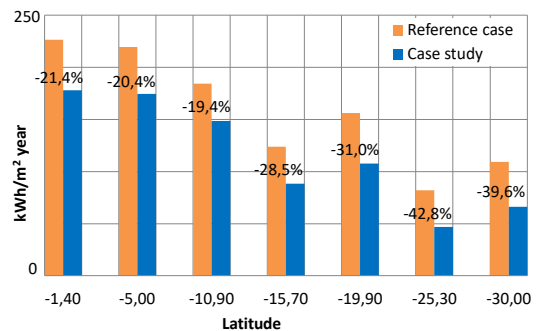


Figure 10: Cooling loads comparison for building NS orientation. Source: Authors.

Due to rectangular proportion of the floor plan, those buildings NS oriented are more exposed to direct solar irradiation, resulting in until 45% more cooling loads than EO orientations. Interesting to note that heating loads were not found - even in those cities with winter lower temperatures (Curitiba and Porto Alegre), the internal thermal loads due to occupancy and office equipment are sufficient to keep inner temperature above the set point temperature ($22^\circ C$) in office hours.

PLEA 2018 HONG KONG

Smart and Healthy within the 2-degree Limit

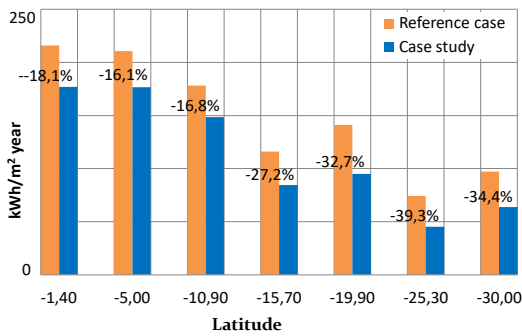


Figure 11: Cooling loads comparison for building EO orientation. Source: Authors.

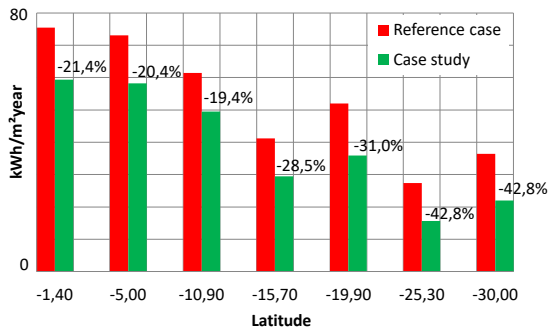


Figure 12: Cooling electricity energy demand comparison for building NS orientation. Source: Authors.

Figures 9 and 10 expose energy demand for cooling only - requirements for lighting and office equipment was considered uniform for all cases, estimated in 92 kWh/m² yearly. Cutting cooling loads lead to considerable electricity energy demand reductions, very much depending on the latitude and their specific climate conditions.

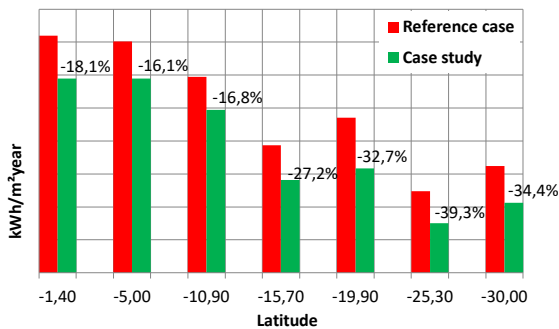


Figure 13: Cooling electricity energy demand comparison for building EO orientation. Source: Authors.

When $-1,4^{\circ} \leq \text{Latitude} \leq -10,9^{\circ}$ were observed savings from 16% to 21% and when $-15,7^{\circ} \leq \text{Latitude} \leq -30,0^{\circ}$ this percentage increased to 29% to 43%. It can be better understandable looking the results for Belém (Lat. $-1,4^{\circ}$) and Curitiba (Lat. $-25,3^{\circ}$) - in the first city, there is not significant variation in external temperature throughout the year, energy demand cooling can be reduced from 75 kWh/m²y to 59 kWh/m²y, savings of 21%. On the contrary, Curitiba is

located in the coldest region of Brazil - blocking radiation with horizontal blinds resulted in savings of 43%, from 27 kWh/m²y to 16 kWh/m²y.

4. CONCLUSION

This study suggests that applying PV Blinds in office buildings located in low latitudes may provoke reductions in cooling loads from 16% to 42.8%. Despite the high Shading Factors percentages (24-47%) PV sun shadings may potentially receive from 944-1.833 kWh/m² annually, indicating potentially high solar resources available to generate electricity energy.

When integrating PV systems in buildings in those regions, the reduction of cooling loads must be prioritized. West-facing façades, difficult to be shaded in the latitudes under study, are eligible for reduction of the glazed surfaces or even for completely opaque walls: this would, at the same time, increase the PV generating surface and reduce solar heating. Using BIPV louvers may help to recover the Brazilian tradition of “brise-soleils”, architectural shading elements that have been progressively abandoned since the 80s: their effectiveness as a means of blocking irradiation on the surfaces, and therefore reducing solar heating of the building, has been demonstrated, and the ways to calculate their optimal inclination (β_{opt} angle) have been shown. Given that the load profiles are similar, it is possible to consider extrapolating the results of this study to other building typologies of the tertiary sector, i.e. small business buildings in industrial areas, less subject to shading from neighboring buildings. In countries like Brazil, where electricity is the main buildings energy source, a solution to in-site productions might also help to achieve zero energy buildings (ZEB) solutions. Using sunshades also affect internal lightning conditions, and deserve specific analysis.

The adoption of PV modules as a shading element for opaque and translucent parts in the investigated office building prototype has proved effective as a strategy for thermal improvements and reduction of energy demand. The concomitant adoption of other proven strategies [19-21], such as reducing the ratio of glazing to the façade and the use of thermally more efficient glass, not only it is compatible, but it is also recommended.

This research pointed out the delicate balance between optimal tilt angle and latitude to achieve a surface suited to integrate BIPV shadowing components. Office buildings normally have floor areas of small dimensions compared to the total built area, posing the challenge of the limited surface available to integrate photovoltaic components on the roof, where energy yield is more favorable. A methodology and practical results have been presented, easily possible to be used to design such devices in office buildings in Brazil, and, to a certain

PLEA 2018 HONG KONG

Smart and Healthy within the 2-degree Limit

extent, in other countries at similar latitudes. Also, contribute to the further development of knowledge in this so far unexplored producing and saving energy saving strategy.

ACKNOWLEDGEMENTS

This work is supported by the TISE Research Group and the UPM - Technical University of Madrid, through a research grant to carry out Ph.D. studies on the subject Design and Testing of Innovative Technical Solutions (Ref. CH/019/2008) in E.T.S. of Architecture, Department of Construction and Building Technology.

REFERENCES

1. Mandalaki, M. et al. (2014). Integrated PV shading systems for Mediterranean countries: Balance between energy production and visual comfort. *Energy and Buildings*, 77: p. 445-456.
2. Yoo, S. and Manz, H. (2011). Available remodelling simulation for a BIPV as a shading device. *Solar Energy Materials and Solar Cells*, 95: p. 394–397.
2. Kiritmat, A. et al. (2016). Review of simulation modelling for shading devices in buildings. *Renewable and Sustainable Energy Reviews*, 53: p. 23-49.
5. Khezri, N. A. (2012). Comparative Analysis of PV Shading Devices for Energy [Master Thesis] Supervisor: Prof. Haase, M. s.l.: Norwegian University of Science and Technology.
6. Kim, J., et al. (2009). Comfort-Driven Optimization of PV Integrated Shading Devices. Korea: SHB2009-2nd International Conference for Healthy Buildings.
7. Ossen, D.R., Ahmad, M.H. and Madros, N.H. (2005). Optimum overhang for building energy saving in tropical climates. *JAABE*: 4, p. 2.
8. Voss, K. et al. (2007). Energy efficient office buildings with passive cooling – Results and experiences from a research and demonstration programme. *Solar Energy*, 81: p. 424-434.
9. Aries, M.B.C., Veitch, J. A. y Newsham, G. R. (2010). Windows, view, and office characteristics predict physical and psychological discomfort. *Journal of Environmental Psychology*, V.30: 4. p. 533-541
10. Yun, G., Yoon, K. P. and Kim, K. S. (2014). The influence of shading control strategies on the visual comfort and energy demand of office buildings. *Energy and Buildings*, 84: p.70-85.
11. Mehrotra, M. (2005). Solar control devices: balance between thermal performance and daylight. Santorini, Greece: International Conference Passive and Low energy cooling for the built environment.
12. Cronemberger, J. et al. (2012). Assessing The Solar Irradiation Potential For Solar Photovoltaic Applications In Buildings At Low Latitudes - Making the Case for Brazil. *Energy and Buildings*, 55: 264–272.
13. Caamaño-Martin, E. (2014). Análisis de Pérdidas de Captación Solar: Método IES-UPM. Madrid, Spain.
14. Roriz, M. (2012). Correções nas Irradiâncias e Iluminâncias dos arquivos EPW da Base ANTAC. São Carlos, SP: ANTAC – Associação Nacional de Tecnologia do Ambiente Construído.
http://www.labeee.ufsc.br/sites/default/files/correcao_epw_antac.pdf . Available: [Online].
15. <http://www.labeee.ufsc.br/downloads/softwares/analysis-sol-ar> . Available: [Online]
16. Spain Government (2009). Código Técnico de la Edificación - HE5 Ahorro de Energía - Contribución Fotovoltaica Mínima de Energía Eléctrica. <https://www.codigotecnico.org>. Available: [Online].
17. Pérez, R. y Seals, R. (1987). A new simplified version of the Perez diffuse irradiance model for tilted surfaces. *Solar Energy*, 39: p. 221-231.
18. Pérez, R., et al. (1990). Modelling Daylight Availability and Irradiance Component from Direct and Global Irradiance. *Solar Energy*, 44:p.271-289.
19. Carvalho, M.M.Q., La Rovere, E.L. and Gonçalves, A.C.M. (2010). Analysis of variables that influence electric energy consumption in commercial buildings in Brazil. *Renewable and Sustainable Energy Reviews*, 14: p. 3199-3205.
20. Signor, R. (1999). Análise de regressão do consumo de energia elétrica frente a variáveis arquitetônicas para edifícios comerciais climatizados em 14 capitais brasileiras. [Master Thesis]. Brazil, Florianópolis: Santa Catarina Federal University (UFSC).
21. Correna Carlo, J. (2008). Desenvolvimento de Metodologia de Avaliação da Eficiência Energética do Envoltório de Edificações Não-residenciais. [PHD Thesis]. Brazil, Florianópolis: Santa Catarina Federal University (UFSC).

Downscaling Climate Models: Running Nested Simulations In The Microclimate Model ENVI-met A Case Study Using WUDAPT2ENVI-met Simulation Data

HELGE SIMON¹, TIM KROPP¹, FRANCESCA SOHNI¹, MICHAEL BRUSE¹

¹Department of Geography, Johannes Gutenberg University Mainz, Mainz, Germany

ABSTRACT: Due to their high resolutions, microclimate models have high computational demand causing rather long simulation times and limiting the size of model areas. As such limited model areas only cover a small part of the atmosphere, the boundary conditions driving the microclimate simulation play a crucial role in determining the quality of the simulation. In order to incorporate larger scale processes and to ensure the boundary conditions represent the actual conditions at a model's border, a nesting module was implemented into ENVI-met. Using the new module, coupled simulations can be run where a (smaller) model area is nested into a larger model domain that provides horizontally and vertically dynamic boundary conditions. Since the surrounding larger model domain is typically simulated at a coarser spatial resolution, downscaling methods need to be applied. In the present study the nesting algorithms that manage the extraction of model outputs and the downscaling onto the nested model area's resolution are presented. Furthermore, a nested model run using a large WUDAPT obtained host model domain is compared against a standard model run using simple forcing boundary conditions. The results showed that nesting provides a reliable way to provide boundary conditions to high resolution, microscale climate simulations.

KEYWORDS: Urban Climate Modelling, Boundary Conditions, Downscaling, ENVI-met, High Resolution Climate Modelling, WUDAPT, Nesting

1. INTRODUCTION

Microclimate models like ENVI-met have the advantage that, thanks to their high resolutions, very little parameterization is needed to represent objects of the urban environment [1]: Trees, building materials and complex structures can be directly reproduced within the model. However, this high resolution comes at a disadvantage as well: With increasing spatial resolutions, the differential equations guiding the model have to be solved with smaller time steps (Courant-Friedrichs-Lewy Condition). This drastically increases the time needed to run the simulations and limits the size of the model area that can be simulated within a reasonable frame of time. Even with the advancements of 64bit compatibility and heavy parallel processing, high horizontal and vertical resolutions of around 2 meters only allow the simulation of model areas of around 1000 meters x 1000 meters x 60 meters on personal computers. With these rather small model areas, the boundary conditions driving the microclimate simulation play a crucial role in determining the outcome and quality of the simulation.

This contribution presents a new method to obtain realistic boundary conditions that include the surrounding meteorology and introduces the nesting algorithms that manage the extraction of model outputs and the downscaling of the meteorological parameters onto the nested model area's resolution. Furthermore, a nested model run using the

downscaled data from a larger model domain is compared against a "traditional" model run using simple forcing.

2. METHOD

To include realistic boundary conditions, ENVI-met already offers the so-called "simple forcing" method which allows the definition of diurnal variations of various meteorological parameters as boundary conditions for the microclimate model [2].

The simple forcing method, however, only provides the possibility to define horizontally homogenous, one-dimensional profiles at all inflow boundaries of the model area. Using this method the same vertical profiles are attached to the entire inflow border, denying horizontal alterations. However, in heterogeneous environments such as cities, where the meteorological parameters can vary greatly along the borders of the model domain, being limited to horizontally one-dimensional profiles may yield unrealistic results. To include heterogeneous distributions of meteorological parameters at the model borders, the simulations need to be provided with horizontally and vertically dynamic boundary conditions.

To obtain such dynamic, more-dimensional boundary conditions, a nesting module was implemented into ENVI-met. With the new module, coupled simulations can be run in which the small model area is nested into a larger model domain that provides horizontally and

PLEA 2018 HONG KONG

Smart and Healthy within the 2-degree Limit

vertically dynamic boundary conditions for the nested model area. When nested model runs are used, the high resolution boundary conditions are driven by previously run ENVI-met model results of a larger model domain that surrounds the smaller high resolution model area. This offline coupling method offers the possibility to first simulate a large, so called “host” model domain in a coarse resolution. The three-dimensional model results are then being used to drive the high resolution model with three-dimensional, dynamical boundary conditions. That way, larger scale processes provided by the host model can be incorporated in the nested simulation (see Fig. 1).

In the current version, the following parameters can be forced upon the nested model area:

- wind speed and direction^a
- air temperature^a
- specific air humidity^a
- turbulent kinetic energy & dissipation^a
- horizontal and vertical exchange coefficient impulse / heat^b
- direct shortwave radiation^c
- diffuse shortwave radiation^c
- longwave radiation^c

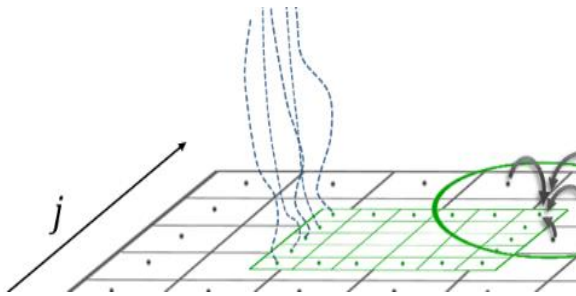


Figure 1: Schematic of the interpolation of host cells (black) within a search radius (green circle) to provide heterogeneous inflow profiles (blue) to the nested model area (green).

Since the larger scale host simulations are typically run at a coarser resolution than the nested simulations, the simulation outputs of the host simulation have to be interpolated to provide boundary conditions for the nested model area. The interpolation is carried out using a three-dimensional inverse distance weighting (IDW) algorithm, taking into account all cells of the larger scale model area within a predefined search radius of the nested boundary cells (see Fig. 1):

$$\bar{R}_{int} = \sum_{n=1}^m w_n R_n \quad (1)$$

with \bar{R}_{int} as the interpolated value, R_n as the larger scale cell’s output value and w_n as the weight corresponding to the grid cell. The summation runs over all host cells within the search radius of the nested cell. The calculation of the weighting factor is carried out as:

$$w_n = \frac{d_n^{-1}}{\sum_{n=1}^m d_n^{-1}} \quad (2)$$

with d_n as the Euclidean distance calculated using the 3D Pythagorean Theorem between the boundary position in the nested model area and the position of the output cell of the host model. Summing up all individual weights, the result must be equal to 1.

In case the boundary cells for the nested model run are occupied by obstructions in the host simulation (e.g. buildings), the algorithm searches for free adjacent atmospheric cells in the host model domain to extract the boundary conditions. Since this data might not be located along the lateral boundary of the nested model area, the atmospheric data is interpolated again using the three-dimensional inverse distance weighting (IDW) algorithm (see Equations 1 & 2).

Since larger differences in spatial resolutions between the host and the nested model area result in a greater loss of information due to the spatial downscaling, the downscaling ratio is often limited to about 3:1 [5,6]. In case a higher downscaling is needed, the nesting can be run in a cascade of nestings, where intermediary simulations gradually downscale the resolution.

To extract data from an ENVI-met simulation, the host model writes three-dimensional outputs of all data needed to perform a nested simulation within its limits. Using a small tool, the boundary conditions of the nested area are then extracted from the datasets of the host simulation and a nesting file is being created.

3. PROOF-OF-CONCEPT-SCENARIO

In a proof-of-concept-scenario model runs using nested boundary conditions are compared against model runs using simple forcing boundary conditions.

For the nested simulation boundary conditions were obtained from a previously run WUDAPT2ENVI-met simulation (=host simulation). For the simple forced simulation, boundary conditions were obtained from weather data.

While simple forced simulations use user-provided meteorological conditions to create horizontally homogenous boundary conditions, the nested

^a 3D-profile

^b 1D-profile

^c Top of model domain

PLEA 2018 HONG KONG

Smart and Healthy within the 2-degree Limit

simulation incorporates local variations obtained from the larger host simulation.

In addition, the boundary conditions for the simple forcing are typically derived from reference weather data measured outside the city. These reference weather data often differ quite substantially from actual conditions within the city, leading to further inaccuracies for simple forced simulations. In contrast, in nested simulations the inflow conditions are altered and thus “urbanized” by the larger scale model domain. It is therefore to be expected that nested simulations represent the local conditions better than simple forced simulations.

In order to quantify the variations in the inflow conditions of the nested versus the simple forced reference simulation, both the reference as well as the WUDAPT2ENVI-met model are run using the same hourly weather data to create the boundary conditions. That way the alterations in the boundary conditions of the nested model run can be directly attributed directly to the influences of the larger model domain.

3.1 Model area

The proof-of-concept-scenario has been performed for an area within the city of Vienna, Austria. The urban architecture consists mostly of compact midrise structures with smaller parks, grassy areas, and wide streets with scattered trees [3].

In order to compare the model results of the nested simulation against the simulation running with simple forcing boundary conditions, two model areas had to be digitized: one high resolution model area used for the reference as well as for the nested simulation and one larger area for the WUDAPT2ENVI-met simulation to extract boundary conditions for the nested simulation.

To create the large model domain, a local climate zone classification using the WUDAPT-scheme (World Urban Database and Access Portal Tools) was obtained for Vienna [7]. Based on the gridded information of WUDAPT, the city was classified into distinct local climate zones (LCZ – by Stewart & Oke 2012 [3]).

While the WUDAPT2ENVI-met simulation is run using a coarse resolution and idealized structure types (Local Climate Zone Classification by Stewart and Oke [3]), the model area of the reference and nested simulation is digitized using the actual geometry of the urban structures (see Fig. 2 and 3).



Figure 2: Aerial photo of the high resolution model area used in the nested and simple forced model run.

To stay within the downscaling limits, the larger WUDAPT2ENVI-met model domain was digitized in a horizontal resolution of 7.5 meters and 2.5 meters vertically. Consisting of $240 \times 240 \times 30$ grids, the total domain extends to 1.8 km x 1.8 km horizontally and 75 meters vertically.

The smaller model area used for the nesting as well as for the reference model run is located in the center of the larger model domain. It is located in the inner city of Vienna, close to the Hofburg. The spatial resolution was set to 2.5 meters horizontally and 2 meters vertically. This results in a horizontal downscaling factor of 3:1 (see Figure 3). The model area consists of 240 grids in the horizontal directions and 40 grids in the vertical direction. The extent of the model area is thus 600 meters x 600 meters x 76 m meters.

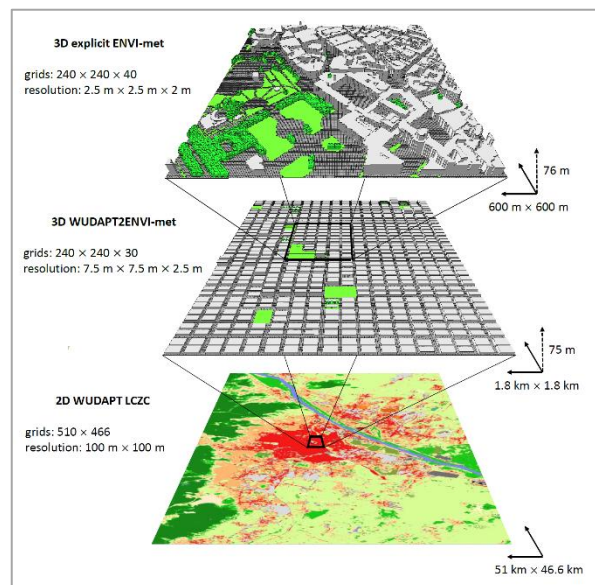


Figure 3: Downscaling schematic using the classified WUDAPT data and 3D WUDAPT2ENVI-met model.

PLEA 2018 HONG KONG

Smart and Healthy within the 2-degree Limit

3.2 Boundary conditions

When running in simple forcing mode, ENVI-met only allows to manually define diurnal variations of air temperature and relative humidity. Based on these user-defined data, ENVI-met creates one-dimensional profiles that are subsequently used as lateral boundary conditions for the model.

To simulate a typical summer day in Vienna, hourly values of air temperature and relative humidity from the dataset Vienna Schwechat 110360 - ASHRAE International Weather for Energy Calculation (IWEC) were used [4]. The day chosen from the dataset was August 12th 1988. Table 1 and Figure 3 display the initial conditions and the boundary conditions for air temperature and humidity.

Table 1: Initial conditions and meteorological parameters of the simulation runs.

Parameter	Value
simulation start date	August 12th 1988
simulation start time	06:00:00
total simulation time	24 h
wind speed in 10 m height	3.3 m/s
wind direction	170°

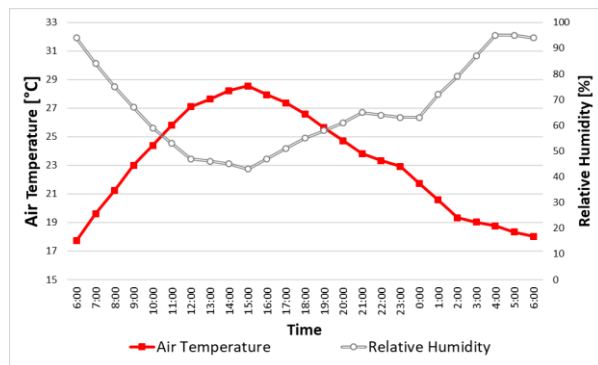


Figure 3: Diurnal cycle of air temperature and humidity used as boundary conditions for the simple forced and the host model run.

Both the high resolution model area of the reference simulation and the larger scale WUDAPT2ENVI-met model domain were simulated using these boundary conditions in a simple forced setting.

The nested model run featuring the same model area as the reference model run was then simulated using the boundary conditions extracted from the WUDAPT2ENVI-met simulation results.

4. RESULTS

The comparison between the reference and the nested simulation is carried out in two steps. In a first step, the diurnal inflow conditions between the two simulations are compared to visualize the “urbanization” of the boundary conditions due to the larger scale model domain. In a second step, differences in the three-dimensional model areas as

well as in the distribution patterns of microclimatic parameters caused by the differences in the boundary conditions are examined.

Since the inflow conditions of the nested simulation differ for every boundary cell, a direct comparison with the homogenous inflow in the reference simple forced model is not possible. Therefore the average, minimum and maximum values of the upwind borders were calculated for different meteorological parameters of the nested simulation.

Table 2 shows the comparison of the diurnal cycle of air temperature and wind speed in a height of 1.8 meters of the nested and the forced simulation at the inflow border.

As measures of fit, root-mean-square error (RMSE) and R^2 have been calculated. Since values of RMSE depend on the absolute values and can thus not be compared across meteorological parameters, RMSE values are normalized by dividing by the range in the simple forced run (nRMSE).

Both observed parameters show large absolute differences (RMSE 4.102 K and 0.946 m/s) between the nested and the simple forced run. This indicates that the reference weather data measured outside the city used in the simple forced model run does not fit the local conditions at the model border within the city sufficiently well. The urban structures of the larger scale WUDAPT model domain modify the inflow conditions for the nested model substantially. This is especially the case for the wind speed as the comparison of the nRMSE values of air temperature and wind speed shows (nRMSE wind speed = 0.379 vs. nRMSE air temperature = 3.232). The quite low R^2 values (air temperature 0.602, wind speed 0.533) also corroborate the large discrepancies between the inflow conditions.

Table 2: Root Mean Square Error and R-Squared values comparing the nested and simple forcing boundary conditions.

RMSE	air temperature [K]	4.102
	wind speed [ms^{-1}]	0.946
nRMSE	air temperature	0.379
	wind speed	3.232
R^2	air temperature [K]	0.602
	wind speed [ms^{-1}]	0.533

Figure 4 plots the diurnal cycles of air temperature and wind speed of the nested and the simple forced model run against each other. The diagram visualizes the large discrepancy: It shows that the maximum air temperature is one, considerably higher (around 4.5 K) in the nested model run and two, occurs much later – around 18:00h – than in the simple forcing data (around 15:00h). Furthermore, the air temperature is not cooling down as sharply as in the weather data outside the city used in the simple forced run. The time

PLEA 2018 HONG KONG

Smart and Healthy within the 2-degree Limit

lag as well as the lower cooling rates further indicate that by “urbanizing” the raw meteorological data – using nesting –, effects like the nocturnal urban heat island and its heat storage can be captured much more accurately.

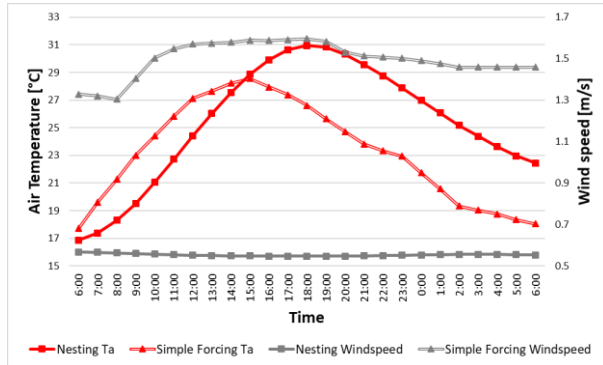


Figure 4: Comparison of the diurnal cycle of air temperature and wind speed in 1.8 m height between the average boundary conditions for the nested and the simple forced model run.

The comparison of the wind speed shows even larger discrepancies: $\sim 1.5 \text{ m s}^{-1}$ vs. $\sim 0.6 \text{ m s}^{-1}$. When using the simple forcing, the measured data from the reference weather station outside the city is used to create boundary conditions. These do not take into account the actual conditions surrounding the model area and thus lead to unrealistic results. This further indicates the need to “urbanize” meteorological data.

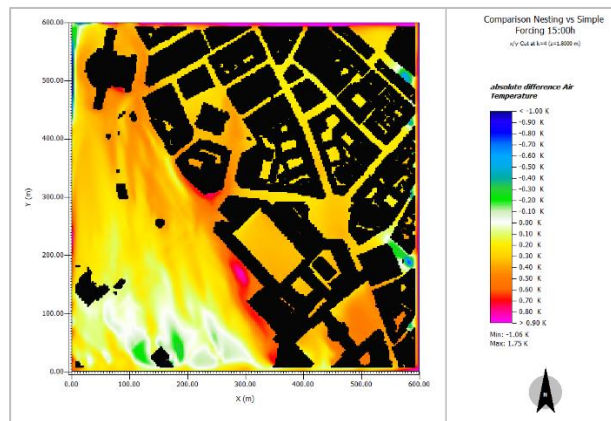


Figure 5: Difference map of air temperature between the nesting and simple forced model run for 15:00h.

To examine spatial differences in the three-dimensional model areas, so-called “difference maps” were created. In these difference maps, model results of atmospheric parameters of the nested simulation are subtracted from the simulation results of the forced simulation run. Figure 5 and 6 show spatial differences of air temperature at 15:00h and 05:00h. As expected the differences in air temperature at 15h are very small due to the small differences in the boundary conditions at that time (see Figure 4). The

differences in wind speed however can be seen clearly in the flow structures parallel to the wind direction of 170° .

The greater differences in the boundary conditions of the air temperature in the early morning hours (see Fig. 4) also lead to greater differences in the spatial distribution (see Fig. 6). Here the whole model area shows positive values indicating higher air temperatures in the nested model run. This is especially the case for the open areas such as the park in the west.

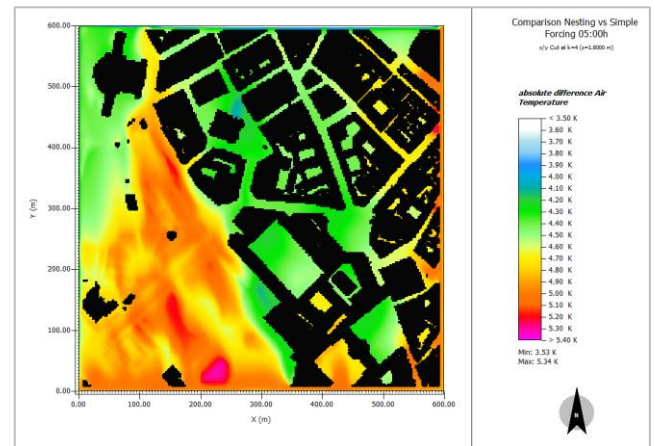


Figure 6: Difference map of air temperature between the nesting and simple forced model run for 05:00h.

5. CONCLUSION

The comparison between the nested and the simple forced model run showed large differences in the inflow conditions and consequently the three-dimensional model results. By nesting the high resolution model area into a larger scale model domain, the reference weather data measured outside the city was urbanized, i.e. adjusted to provide inhomogeneous, spatially diverse boundary conditions matching the local conditions at the high resolution model borders.

This is especially remarkable since the larger model domain was not explicitly digitized using the actual building structures but “only” abstract WUDAPT2ENVI-met tiles.

Even though the proof-of-concept simulation only covered 24 hours and one high resolution model area the combination of low resolution, large scale simulations with high resolution nested simulations showed very promising results. In longer simulation periods, the effects of heat storage might be very interesting to examine the diverging trend in the inflow conditions over the simulation time between the weather data measured outside the city and the inner city “urbanized” meteorology.

Downscaling coarse models into high resolutions allows to further examine areas that show local hotspots in the coarser simulations and to examine

PLEA 2018 HONG KONG

Smart and Healthy within the 2-degree Limit

adaptation strategies like façade greening or increasing the number of trees under different larger scale meteorologies.

Summing up, the new tool provides a reliable way to incorporate larger scale processes on a high resolution, microscale climate simulation. Using three-dimensional boundary conditions opens up a wide range of possibilities to analyze high resolution microclimate models with different larger scale meteorologies.

REFERENCES

Bruse, M. and H. Fler, (1998). Simulating surface-plant-air interactions inside urban environments with a three dimensional numerical model. *Environment Modelling & Software*, 13(3-4): p. 373-384.

Huttner, S., (2012) Further development and application of the 3D microclimate simulation ENVI-met. Dissertation, Johannes Gutenberg University Mainz.

Stewart, I. D., and T. R. Oke, (2012). Local climate zones for urban temperature studies. *Bulletin of the American Meteorological Society*, 93(12): p. 1879-1900.

ASHRAE, (2001). International Weather for Energy Calculations (IWEC Weather Files), [Online], Available: <https://www.ashrae.org/technical-resources/bookstore/ashrae-international-weather-files-for-energy-calculations-2-0-iwec2> [30 May 2018].

Christensen, O., J. Christensen, B. Machenhauer and M. Botzet, (1998). Very High-Resolution Regional Climate Simulations over Scandinavia - Present Climate. *Journal of Climate*, 11(12): p. 3204-3229.

Giorgi, F. and L. O. Mearns (1999). Introduction to special section: Regional Climate Modeling Revisited. *Journal of Geophysical Research* 104(D6): p. 6335-6352,

Mills, G., J. Ching, L. See, B. Bechtel, and M. Foley, (2015). An Introduction to the WUDAPT project. In 9th International Conference on Urban Climate, Toulouse.

Variations of Microclimatic Conditions in Residential Neighbourhoods in Ho Chi Minh City

HUNG THANH DANG¹, ADRIAN PITTS¹

¹Department of Architecture and 3D Design; School of Art, Design and Architecture;
University of Huddersfield, Huddersfield, UK

ABSTRACT: The 5-year cycle of residential planning in Ho Chi Minh City (HCMC) has underestimated population growth since 1991. This has resulted in the disruptive and uncontrolled expansion of settlement across the city. The outcome is a complicated mix of new spontaneous dwelling areas in the city featuring a number of distinct urban morphologies. Some previous studies have shown impacts of such urban morphologies on the comfort levels in outdoor environments. The paper examines the correlation of microclimatic conditions and constituents that create the urban spatial form of residential neighbourhoods in HCMC. A total of seven dwelling urban patterns were studied. Field measurements of physical variables were conducted in summer 2017 whilst the meteorological data were recorded. Furthermore, in studies of two urban types, the microclimatic characteristics were found to vary under different urban contexts. During warm months, the outdoor thermal conditions for pedestrians were found to have average air temperatures between 32-34°C; a range of wind flow at the occupied level from 0.1-0.9m/s, and average humidity level of 57-60% over all types surveyed. The occupants' delight in outdoor comfort was found in formally planned dwelling blocks; meanwhile, the compact neighbourhoods were characterised by cooler temperatures but poor airflows and daylighting.

KEYWORDS: Urban structure, microclimate, comfort, residential buildings, Ho Chi Minh City

1. INTRODUCTION

Since the initiation of the 'Doi Moi' economic renovation in 1986, many reforms have occurred across Vietnam, in which HCMC has played the leading role [1]. The economic changes are linked to an explosion of population and urbanisation. The census 2015 concluded the total population of HCMC to be nearly 9m people; this figure is almost 1.8 times higher than in 1999. Over 90% of citizens live in urban areas [2,3]. The population growth is linked to a massive urban expansion and increase of housing demand from both local people and immigrants. The city area covered by hard construction surfaces increased by 20% between 1989 and 2006 and is associated with an increase in average surface temperature of 4°C in urban areas [4].

The exacerbation of urbanisation and population results in chaotic urban development without clear management of long-term planning and priorities in HCMC. The increasing urban heat island (UHI) impact caused by land use and city configuration along with climate change have negative influences on comfort conditions, health, and energy use of buildings [5]. Variations of urban geometries contribute to the differences of microclimate and outdoor comfort for occupants which can be beneficial. Many authors pointed out this relationship at different urban scales: building-to-building, urban blocks, and city scale [6,7]. Using a database for systematical classification of urban structure types in HCMC [8], this paper analyses the variations of urban patterns related to residential

buildings through their urban constituents. It then identifies the variation in environmental performance according to the different urban types. Finally, the effects of urban morphology on microclimate are determined by application of a combination of three methods (consisting of mapping, field measurements, and simulation).

The study goes on to propose appropriate recommendations for the urban design of residences to improve outdoor thermal comfort that can lead to greater satisfaction with indoor ambient conditions and consequent reductions in energy demand.

2. AREA OF STUDY

HCMC is the second largest city in Vietnam and is located in the South-Central part of the country. The city experiences a climate of high air temperature, high humidity, and heavy rainfall throughout the year. The mean annual temperature is 28°C; however, over summer the extreme temperature peaks at 40°C. The average monthly relative humidity ranges from 70% to 85% [9]. Two prevailing winds through the city are west and southwest monsoon winds in the rainy season and the north and northeast monsoon winds in the sunny season. Furthermore, the trade wind from south and southeast also operates from March to May. The total of city area of 2093 km² is occupied by four regions: core-centre, former inner, new inner, and suburban. The city projections to 2025 expect a rise in population to 13.9m, an expansion to 750km² of built-up area, urbanisation of new inner and suburban

PLEA 2018 HONG KONG

Smart and Healthy within the 2-degree Limit

districts and a decline in population in the centre [10]. Since 2015, over 300 residential projects have been developed across the city; mainly in new districts and peripheral areas. Impacts from expanding residential neighbourhoods as well as global warming have accelerated the urban environment's vulnerability. The microclimate has changed with greater variability between neighbourhoods and increasing risks for comfort and air quality experienced by occupants in HCMC. The city's mean temperature has risen by 0.9-1.2°C since 1958 [11]. The climate changes and man-made modification result in the unsatisfactory microclimatic conditions in and around buildings, and trends for increased energy use by households.

3. STUDY ON URBAN STRUCTURE TYPES

Between 2010 and 2014, a research group from the University of Cottbus, Germany carried out a project on the adaptation of HCMC to climate change. One valuable outcome was the categorisation of the urban structures related to building types, urban elements, and their constitution for both fully planned and informally designed areas. By using a tool of Land-use Map 2010 at a scale of 1:25,000 combined with fieldwork, a total of 82 city structure typologies were identified covering 16,292 blocks. In this, a subset of 5 major types was classified: residential, public & special use, industrial & commercial, green spaces, and traffic system & water networks.

Table 1: Summary of urban structure types of 'shophouses' (source: Downes & Storch, 2014)

Type	'Shophouse' category	No of blocks	Build. ratio	Surface area (ha)
1	Regular new community	62	60	392
2	Regular new	100	70	450
3	Regular + narrow street	592	75	2,063
4	Irregular high density	425	78	1,602
5	Irregular + yards	794	57	4,444
6	Shophouse irregular & regular	23	69	350
7	Regular + yards	153	44	2,020
8	Irregular clustered	741	30	5,490
9	Irregular scattered	815	28	6,990
10	Irregular +large gardens	2,342	5	17,133
11	Irregular temporary			85
12	Shophouse + industry	222	74	1,292

Settlement structures were assigned to 6717 blocks including 12 patterns and with 6436 blocks categorised as urban low-rise dwellings, which occupied 20.5% of the total HCMC surface area (Table 1) [8]. The density of all dwelling urban structures differs over the city. The morphologies of residential blocks are determined by land use, coverage ratio, road patterns, housing archetypes, building stories, green areas, spatial planning, and population density. For this paper, seven urban geometries highlighted in Table 1 were studied considering physical characteristics, climate, and impacts of urban components on the environment.

4. RESEARCH METHODS

4.1 Collection of residential urban types for analysis

All seven categories which provide a good selection of commonly dwelling urban structures were visited and outdoor environmental parameters were measured. The proportions of the investigated urban types are shown in Figure 1, in which, Type 3 & 4 are the most dominant. Each type is characterised by a distinct spatial morphology; however, because of some similar constituents of some urban typologies, four groups of urban types were identified: Group 1 (Type 01 & 02), Group 2 (Type 3), Group 3 (Type 04, 05 & 06), and finally, Group 4 (Type 7) (Figure 2).

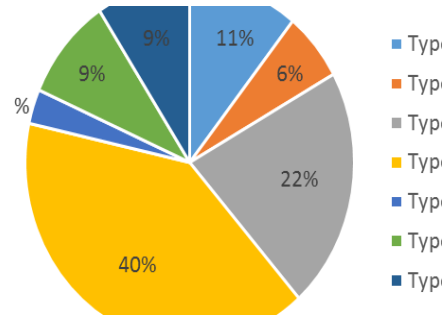


Figure 49: Sector of urban housing types in the research

Group 1 was characterised by terraced housing archetypes located perpendicular to main streets in a back-to-back pattern, and with communal spaces within each residential block. The distribution of Group 1 is high in new and peripheral districts of HCMC. Group 2 has a high density of occupancy found in the 2060ha of the inner-core and new inner areas of the city. The spatial structure of Group 2 has the regular development of low and high shophouses facing to narrow streets/alleys. The spaces within buildings are usually narrow and open to the main streets. Group 3 includes three urban types; the major feature of this group is an irregular and non-homogeneous high-density pattern of dwellings with narrow streets or alleys. The buildings are located along the outer edges of the main streets. The houses' architecture varies with no single archetype. Group 4 is generally found in the new inner and suburban neighbourhoods of HCMC. This group's morphology is characterised by a less dense structure and regular arrangement of houses. The housing types found in this group include new and rudimentary houses of one to three stories along main streets. Within buildings, many unplanned green spaces can be found.



PLEA 2018 HONG KONG

Smart and Healthy within the 2-degree Limit



Figure 50: Five urban structure types for studying (1: Type 1, 2: Type 2, 3: Type 3, 4: Type 4+5+6, and 7: Type 7)

4.2 Research techniques

Three techniques of analysis were used: mapping, field measurements and simulation. Mapping is a tool to understand the urban form and building footprints of the urban blocks through satellite photos and negative drawings. The microclimate of the urban blocks was estimated from simulation software. For the field study, 59 locations covering seven urban typologies of terraced houses around HCMC were visited in April and May 2017. The climate in these two months is the most rigorous because of heat and lower precipitation. For each dwelling block, a house was selected with measurement of indoor and outdoor air temperature, relative humidity (RH), and airspeed. Date and time of measurement, as well as, sky condition were also recorded. The measurements were carried out from 9:00 am until 17:00 pm over two months. The outdoor environmental parameters were collected from manual instruments at the level of pedestrians and were read after 3 minutes of calibration. Air velocity was averaged by a number of measurements over 3 minutes. Along with the field measurements, the meteorological data of city weather station were also recorded.

For simulation, the software of ENVI-Met was used to estimate the thermal conditions in terms of air temperature and air movement for the months of March, June, September and December; and from 9:00 am to 15:00 pm. The simulation was processed for sample areas defined by zones of 100mx100m (Figure 7).

5. RESULTS AND DISCUSSION

5.1 Outdoor climate

The meteorological data of HCMC from Tan Son Hoa weather station published by the Ministry of Construction in 2009 show that the maximum, minimum, and average temperature was 34.6°C, 26°C, and 29.2°C respectively over both April and May. Furthermore, the RH values ranged from 72% to 79%, and the average airspeed varied from 2.5 to 3.3m/s [9]; however, it was also noted that the city macroclimate was changing so more recent years were examined. World Weather Online (WVO) predictions for HCMC in 2017 indicated changes with mean values of temperature, RH, and airspeed in those months being 34°C, 67%, and 3.8m/s respectively. Additionally, the air temperature peaked at 38°C in April. The total summer sun hours also increased to more than 300. The HCMC WVO climate predictions are relatively similar to the on-site measurements in terms of

temperature and RH, but there is a significant divergence for air velocity measured in the field study and the recorded meteorological data. Although values of air velocity at a height of 10m are closer and more closely matched to the weather station, this is not the case for lower levels within urban areas.

Summarising data from 59 environmental measuring points around the city at levels under 10m shows that the average temperature was 32.6°C (SD 1.63); mean RH was 61% (SD 8.06) and air velocity was 0.32m/s (SD 0.19) (Table 2). Over summer, the outdoor temperature and airspeed reached a peak at nearly 38°C and 0.9m/s respectively. Furthermore, when comparing to official Ministry data for microclimates, the environmental values of actual measurements were higher than the threshold of the acceptable thermal zone in hot months (29.5°C) [12]. In short, the microclimatic conditions surrounding the dwellings of HCMC in summer are more likely to provide urban discomfort for residents because of hot air and still winds.

Table 2: The outdoor environment in summer over 59 cases

	N	Min.	Max.	Mean	Std. Dev.
Air temperature °C	59	29.5	37.8	32.6	1.63
Relative humidity RH	59	41	79	61	8.06
Air velocity m/s	59	0.07	0.9	0.32	0.19

5.2 Summer microclimatic conditions

The on-site measurements of the physical variables at 59 different locations across the city in summer 2017 show the variations of the urban environment at micro-scale of the residential blocks. The environment surrounding dwellings classified according to four groups of urban structures was evaluated using boxplot analysis of air temperature, RH, and air movement.

Air temperature

Figure 3 shows the hottest thermal condition in Type 3 dwellings, which was characterised by the highest median and maximum air temperature over summer. The hot environment around the buildings in this urban type may be the result of solar radiation being reflected by buildings and absorbed by asphalt roads. Due to the paucity of tree shading, the uncomfortable air temperature at the level of pedestrians is usually added to by the radiant and convective heat from high surface temperatures of unshaded roads. Reflected glare from the streets is also a problem for visual comfort.

PLEA 2018 HONG KONG

Smart and Healthy within the 2-degree Limit

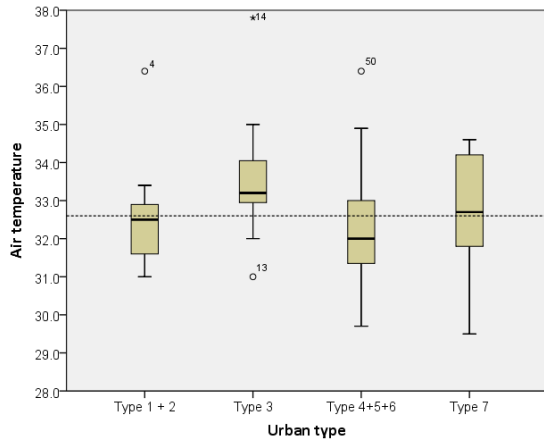


Figure 51: Distribution of air temperature

The average air temperature in Type 1&2 and Type 7 areas was similar and close to the average of 32.6°C. However, the variability of the thermal conditions during the day and between different locations in Type 1&2 was narrower at 2.5°C (31-33.5°C) compared to the variation of 5°C (29.5-34.5°C) in Type 7. In Type 4, 5 & 6, the mean of air temperature outdoors was the lowest of all seven urban patterns. Under the urban form depicted by the irregularity and high dwelling density in Group 3, overshadowing between buildings reduces the impact of solar heat, producing a cooler thermal condition in these types. However, the compact urban pattern may provide an obstruction for airflow and comfort convective cooling. In addition, the observations indicate a minimum temperature in Group 3 & 4 was the coolest at 29.5°C. The unplanned large green areas in Group 4 probably play a significant role in moderating the microclimatic conditions around residential neighbourhoods. Thus, the thermal environments here are more pleasant for the occupants.

Relative humidity

Relative humidity varied quite widely between 48% and 80% across the urban types during summer. Some details are shown in Figure 4. The hot air temperature caused the dry environment over summer in Group 2, while the air condition was more moisture in Group 1, 3, & 4. However, acceptable relative humidities as defined by TCVN 7438:2004, show that almost 100% and 75% of RH conditions surrounding Group 2 and Group 1,3,&4 respectively comply with the standard from 30% to 70%.

Data collated for the lowest density neighbourhoods (Type 1+2) and the highest density blocks (Type 4+5+6), the climate can be more humid; therefore the supplement of breezes is significance in improving the thermal comfort by dissipating moisture in the hot condition. In summer, the relative humidity in Group 1 and 3 peaked at 80% and 77% respectively.

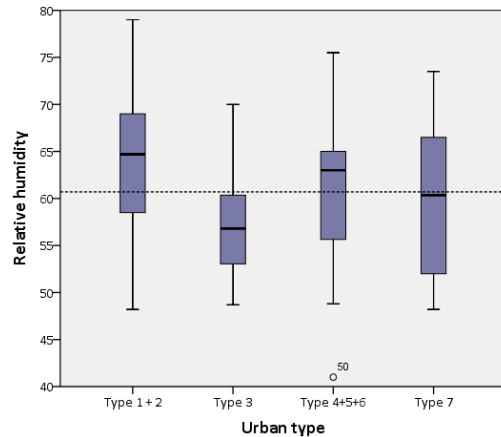


Figure 52: Distribution of relative humidity

Natural wind environment

Unlike the meteorological data, the observations of the wind environment at the lower level within urban dwelling blocks show the majority of air velocities were weak, typically less than 0.3m/s over the summer period. The difference found between climatic data and actual measurements is significant for planning and design of dwellings.

From previous studies, the acceptability of natural wind range for occupants in the tropics was predicted as either 0.3-0.9m/s (i) [14] or 0.5-1m/s (ii) [15]. The histogram analysis of air movement in hot months concluded that the cooling effect provided by natural wind was not beneficial and insufficient over 53% or 75% of residential neighbourhoods surveyed in total corresponding to findings (i) or (ii).

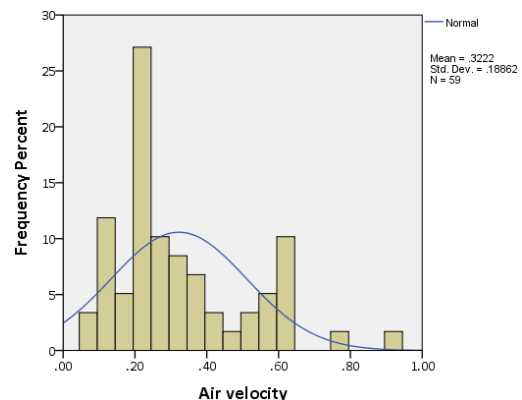


Figure 53: Distribution of air velocity measured in summer 2017

Airflow in the city ranged from 0.1-0.9m/s in summer months (Figure 5). However, the spatial structure of different urban types causes variations in the air movement environment. In observations of seven urban types, the condition of air flow in Type 1, 2, & 7 was the most comfortable because of certain beneficial urban characteristics, for example, the low population density, green sidewalks, regular road pattern, simple road system, and large open spaces around. Approximately 70% of airspeed values

PLEA 2018 HONG KONG

Smart and Healthy within the 2-degree Limit

observed fell into the acceptable zone of 0.3-1m/s in these urban patterns. The maximum air velocity in Type 7 was recorded at 0.9m/s (Figure 6). High-density construction and the irregular urban morphology may well explain the poor performance of wind flows in Types 4+5+6. 75% of airspeeds were lower than 0.3m/s, causing summer thermal discomfort in these types. In Type 3, the variability of wind speed was wide from 0.1 to 0.8m/s, and half the values were above 0.3m/s in the hot months.

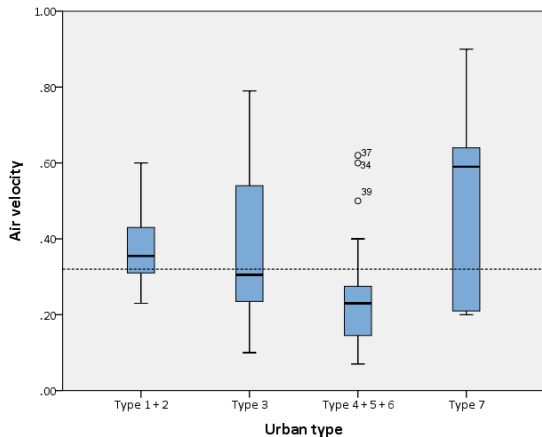


Figure 54: Distribution of air movement by urban types in 2017

5.3 Investigating the thermal environment of two samples of residential neighbourhoods

This section studies the microclimate of two dwelling blocks: Type 2 (sample 1) and Type 3 (sample 2) by using computational analysis. The urban morphology of the two samples is described in Figure 7 and there are variations of urban parameters between both samples. Firstly, for building form and coverage, in sample 1, the housing design complies with some archetypes; the building height is 4 stories, and the building density is medium. In sample 2, the design of 4-story houses is non-homogeneous and the construction coverage is much denser. Secondly, despite the same regular road pattern in both samples; the pattern is more compact in sample 2 of Type 3. In sample 1, more open spaces and green sidewalks/driveways are observed; while the narrow/medium streets without trees/pavements are the only empty spaces within the block.



Figure 55: Urban pattern of two samples: Type 2 (1), Type 3 (2)

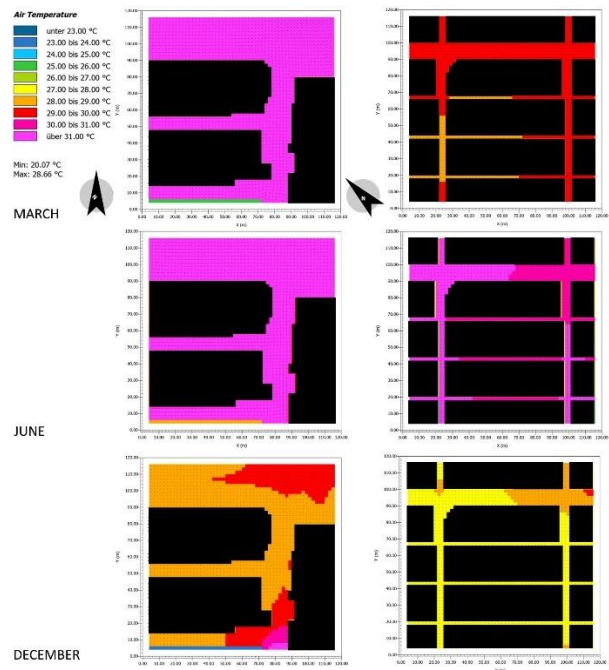


Figure 56: Distribution of air temperature of two studied urban types at 15:00 pm, on the 21st date (Vi Ho, 2017)

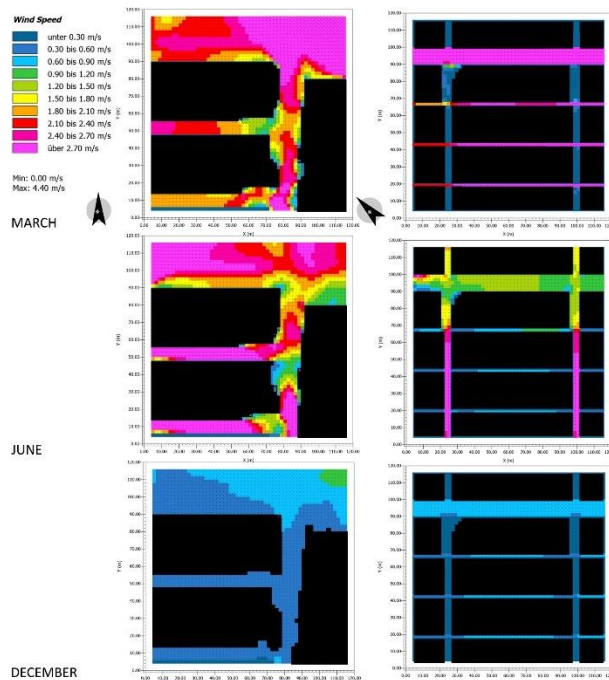


Figure 57: Air pattern of two studied urban types (Vi Ho, 2017)

Figure 8 shows the outdoor thermal performance of two samples at 15:00 pm, on the 21st date of March, June, and December. Despite the more green areas in sample 1, the wide asphalt roads contribute to an increase in temperature in the air around the dwellings. The thermal condition outdoors in this urban type is hotter than in sample 2 of Type 3 which gets the benefit of overshadowing between buildings. In December, the cooler climate of the city has caused

PLEA 2018 HONG KONG

Smart and Healthy within the 2-degree Limit

the temperature to drop by 2-4°C in both samples compared to the hot ambient temperatures in summer. The hot condition in sample 1 can provide discomfort not only for the passengers outdoors but also for the occupants in naturally ventilated houses due to thermal exchange between internal and external climates. Moreover, in sample 2, the compact building pattern is effective in protection from solar heat and retaining coolness, but that is also a problem of weak air flows and poor daylighting.

Building density and narrow common spaces in sample 2 give a rise to the poor quality of wind flow through urban canyons within building groups over three studied months (Figure 9). In sample 2, the monthly change of wind direction has an impact on the variation of air flows. During March, wind typically flows horizontally in front of the building; however, vertical wind patterns along to building side is observed in June. Figure 9 shows the simulated results of air pattern are comfortable for the occupants in March and June in sample 1 of Type 2. The free open spaces combining vegetation can accommodate the air flows around the block with a wide air movement range of 0.6-2.7m/s. However, in December, the wind condition is still with an air velocity of under 0.3m/s in both samples, which may impact on occupants' thermal satisfaction.

6. CONCLUSION

The study confirms thermal discomfort in exterior climates in cities of the tropics such as HCMC. This arises from urban development and human activities and likely subsequent to affect indoor comfort and lead to higher levels of energy use.

The field measurements show the existence of heat islands in macro-neighbourhoods across the city. The unplanned and planned development of compact urban areas may result in warmer conditions and reduced natural wind flows. The outdoor environments were thermally uncomfortable due to observations of hot air temperature and the still air velocity across the majority of the city.

At the micro-scale of housing urban blocks, spatial planning factors have significant impacts on the environmental conditions around buildings. Variations in microclimate were found in the field studies and simulation under different urban morphologies. The deviation of physical values between urban types includes 0.5-1°C of air temperature, 3-7% of humidity, and 0.2-0.4m/s of wind speed in summer. The more comfortable environment was found in Type 1,2 & 7. The results of the study encourage practitioners to consider urban microclimate and to find the correlation between changes of outdoor climate and interior environment at the beginning of the design process. Further measurements carried out simultaneously in more and different urban areas of

the city would facilitate even better analysis. In addition, comfort surveys for pedestrians would offer potential to correlate between climate and human sensations.

ACKNOWLEDGEMENTS

The authors would like to acknowledge the financial support of the Vietnamese Government, and the Newton Fund and the British Council

REFERENCES

- Tran, G. V., & Tran, D. B. (1998). *Cultural monography of Ho Chi Minh City - Volume 1: History*. Ho Chi Minh City: The Ho Chi Minh City Publishing House.
- CPHSC. (2010). *The 2009 Vietnamese population and housing census: Major findings*. Hanoi: Central population and housing census steering committee.
- Statistics Office. (2015). *Population and labour*. Ho Chi Minh City: Statistics Office of Ho Chi Minh City.
- Tran, V. T., & Ha, B. D. (2010). Study of the impact of urban development on surface temperature using remote sensing in Ho Chi Minh City, Southern Vietnam. *Geo. Research*, 86-96.
- Allegrini, J., Dorer, V., & Carmeliet, J. (2015). Influence of morphologies on the microclimate in urban neighbourhoods. *Journal of Wind Engineering*, 108-117.
- Asfour, O. S. (2010). Prediction of wind environment in grouping patterns of housing blocks. *Energy and Buildings*, 2061-2069.
- Rajagopalan, P., Lim, K. C., & Jamei, E. (2014). Urban heat island and wind flow characteristics of a tropical city. *Solar Energy*, 159-170.
- Downes, N. K., & Storch, H. (2014). *The urban structure types of Ho Chi Minh City, Vietnam*. Brandenburg: Cottbus, Brandenburgische Technische Universität, IKMZ.
- IBST. (2009). *Vietnam Building Code: Natural physical & Climatic data for construction*. Hanoi: Ministry of Construction.
- Storch, H., & Downes, N. (2011). The dynamics of urban change in times of climate change – The case of Ho Chi Minh. *REAL CORP 2011: CHANGE FOR STABILITY: Lifecycles of Cities and Regions* (pp. 977-984). Essen: CORP.
- Thuc, T., Nguyen, T. V., Huynh, H. T., Mai, K. V., Nguyen, H. X., & Doan, P. H. (2016). *Climate change and sea level rise scenarios for Vietnam*. Hanoi: MoNRE.
- MOC, M. (2004). *TCXDVN 306:2004 - Dwelling and public buildings - Parameters for microclimates in the room*. Hanoi: Ministry of Construction.
- VSQI, (. (2005). *TCVN 7438:2004 - Ergonomics. moderate thermal environments. determination of the PMV and PPD indices and specification of the conditions for thermal comfort*. Hanoi: Ministry of Science and Technology.
- Gong, N., Tham, K., Melikov, A., Wyon, D., Sekhar, S., & Cheong, K. (06 de 06 de 2006). The acceptable air velocity range for local air movement in the tropics. *HVAC&R Research*, pp. 1065-1074.
- Szokolay, S. V. (1997). Thermal comfort in the warm-humid tropics. *ANZASCA'97 - Principles and Practice* (pp. 7-12). Brisbane: ANZASCA.

Predicting Changes in Spatial Planning Using Artificial Neural Networks on the Basis of Satellite Images: Examples of selected cities in Lodz agglomeration (Poland)

TOMASZ JASINSKI¹, ANNA BOCHENEK²

¹ Faculty of Management and Production Engineering, Lodz University of Technology, Lodz, Poland

² Faculty of Civil Engineering, Architecture and Environmental Engineering, Lodz University of Technology, Lodz, Poland

ABSTRACT: The study addresses issues of the detection of built-up areas based on satellite images and prediction of changes in spatial planning using artificial neural networks. Using satellite images from the Landsat satellite, the authors have developed a built-up areas detection model using a combination of indexes such as NDBI, NDVI and MNDWI. The quality of classification was empirically verified on the basis of a set of randomly selected image points. Forecasts of changes in spatial planning were carried out with the use of two types of neural networks: MLP and RBF. For MLPs, the activation functions, such as logistic, hyperbolic tangent, Gaussian and sine, were tested. In total, more than 5.000 different models of artificial neural network have been built and verified. The simulations covered two areas diversified in terms of building density – fragments of the cities of Lodz and Zgierz located in central Poland in central Europe. Developed model provided changes in built-up areas between 1998 and 2006. In order to confirm the quality of model’s operation, the authors calculated percentage correctness of the area classification, which was 94.06% for the area with a higher degree of urbanization and 91.86% for the less urbanized area.

KEYWORDS: Satellite Images, Spatial Changes, Urbanization, Artificial Neural Networks

1. INTRODUCTION

Changes in spatial planning have an undoubtedly significant impact on both the local and consequently global climate. This clearly translates into the quality of people’s life. Progressive urbanization can partly be controlled on a legislative basis, but in the long term it is highly dependent on economic issues related to the degree of “attractiveness” of the particular area. The possibility to predict the direction of future changes in spatial planning is an important element from the point of view of persons, who have a key role in development of urban areas, as well as for individual investors. Thanks to the knowledge of estimated future demand for the particular type of property, it is possible already a few years earlier to implement appropriate legal regulations and thus to ensure appropriate, sustainable, infrastructure development. It should be noted that such elements of technical infrastructure as e.g. electricity system require relatively large-scale investment and time to build them.

An aim of the study was to build a universal model forecasting the development of urban structures in two selected areas of central Poland – the Lodz agglomeration (fragments of Lodz and Zgierz cities) with different levels of development intensity. A tool from the field of artificial intelligence, i.e. artificial neural networks (ANNs) was used in this study to

predict changes of urban development based on images from the Landsat satellite.

2. ARTIFICIAL NEURAL NETWORKS

Artificial neural networks (ANNs) date back to the 1940s of the 20th century. McCulloch and Pitts [1] are commonly considered to be the creator of artificial neurons used today.

2.1 Construction of the artificial neuron

The diagram of nerve cell is shown in Fig. 1. Signals are introduced into the cell via inputs (x_n), which are equivalent to biological dendrites. With each of described inputs a certain number of real is coupled – so-called weight (w_i). The values entered into the cell are multiplied by these weights, and resulting products are added up. This results in so-called total stimulation of the neuron. This value is then transformed by means of so-called activation function (f).

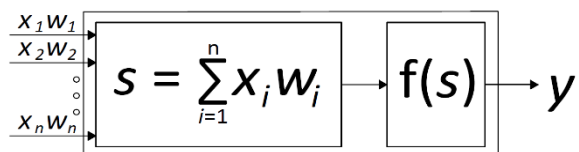


Figure 1: Diagram of an artificial neuron.

The most popular functions are: logistic, hyperbolic tangent, modified sine, Gaussian and identity (Fig. 2 shows graphs of selected activation functions). The

resulting value is then derived from the cell by means of output (y), which is the equivalent of biological structure called axon.

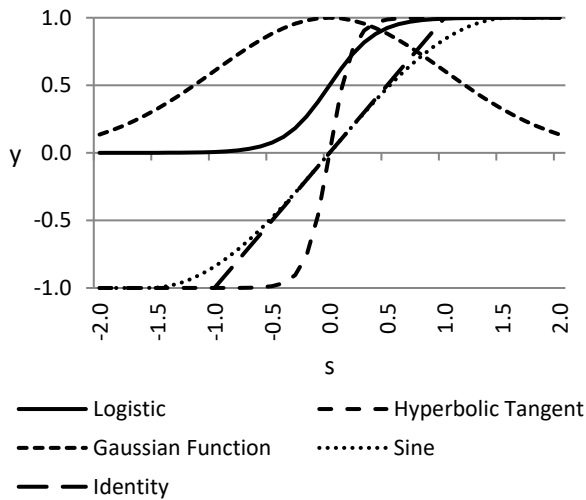


Figure 2: Graph of selected activation functions.

2.2 Types of ANNs

The individual nerve cells are combined with one another to form a network of cells called ANNs. There are many types of ANNs that differ in a number of cells, their interconnectivity and way they are trained. In view of the last of mentioned elements, a distinction is made between supervised and unsupervised networks. In the first, there is a subprogram indicating ANN with appropriate algorithms (usually gradient), which neuron contributed to the extent to which model error occurred and how to modify weights in all neurons in order to make ANN responses more precise. This method requires knowledge of the output patterns.

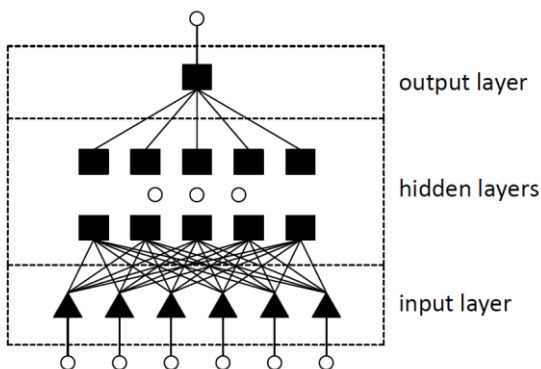


Figure 3: Diagram of MLP.

Knowledge of output patterns is not required when using unsupervised teaching method. Only the network input data is needed. In the process of training the network, it is possible to notice a tendency to increase the value of weights on entries of neurons. This implies some kind of feedback. Increasing weight causes greater activity of nerve cells. Some neurons (or

their entire groups in which cells cooperate) are activated when the given model is stimulated. In self-organizing networks, there is both the effect of competition within and between neurons, as well as cooperation between neurons. ANN training would not be possible without the redundancy of teaching data. Repeated presentation of the ANN of similar data enables the network to draw conclusions allowing it to gain knowledge [2].

Networks based on the first of these methods – supervised teaching – were used in the research. Models of feedforward multi-layered networks with the architecture of multi-layered perceptron (MLP) and radial base functions (RBF) have been used. In feedforward network, the signals flow from the ANN input to its output. There is no feedback (as in case of recurrent networks). The nerve cells are grouped in ANNs into so-called layers. In case of multi-layered networks, the ANN shall have at least one so-called hidden layer, in addition to input and output layers. Diagram of MLP construction was presented in Fig. 3. The RBF networks are a modification of MLP. There is always a single hidden layer in them, which neurons use bell-shaped activation functions, i.e. symmetrical in relation to x-axis (e.g. Gaussian function). The neurons of output layer are built on the basis of linear activation functions, and they aggregate the values of output signals of the hidden layer neurons by calculating their weighted sum. The diagram of RBF network construction was presented in Fig. 4.

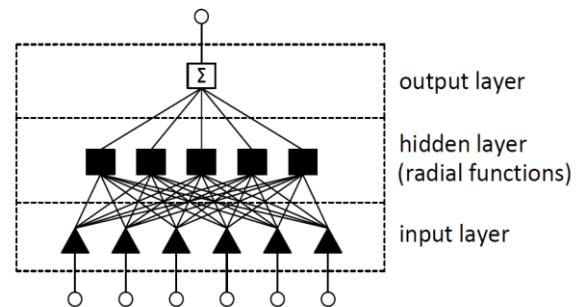


Figure 4: Diagram of RBF.

2.3 Training the neural network – the MLP example

In the process of supervised ANN teaching, the training data are repeatedly presented. The reaction of network to their presentation is compared to reference signals in each case. Any deviations result in activation of training algorithms (usually gradient) resulting in the modification of weights in neurons so that subsequent ANN responses were less error-prone. The described method requires separation of its part called the teaching set from the data set. Each time all data from the set is entered into the ANN, it is called an epoch. Along with continue the training process, the error generated by networks decreases

PLEA 2018 HONG KONG

Smart and Healthy within the 2-degree Limit

asymptotically to zero. However, it turns out that only until a certain point ANN learns in an “intelligent” way, gaining the ability to generalize knowledge, and then comes so-called effect of overtraining. As a result, the ANN’s response to the training set data is improving, but the ANN’s errors are increasing dramatically when entering data from outside the training set into the network. In order to prevent the occurrence of overtraining effect, it is necessary to isolate another set of data – validation one. Its task is to control the calculation of ANN error in the training process, but without running the weights modification mechanisms. At a time when the operation error of ANN for the validation set increases, this means that the training process has to end as its continuation will lead to this overtraining effect. The error course for data from both sets is presented in Fig. 5. Only this way the ANN taught can be subjected to final testing with data from the third set – the test – which has never been shown to the networks before. The used approach guarantees a high reliability of results.

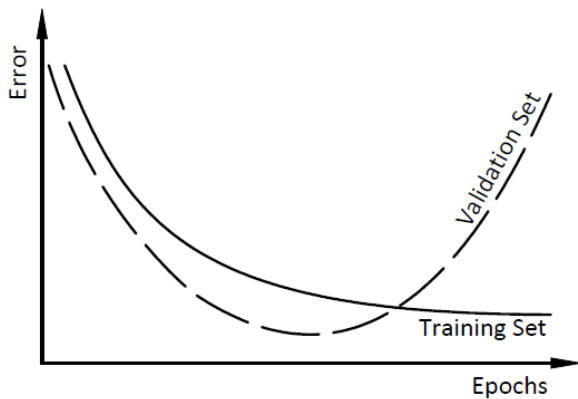


Figure 5: Error course during ANN training.

RBF networks use different training algorithms than MLP. More about training the RBF network can be found in [3].

Regardless of the type of used ANN, it is necessary to select the appropriate input and output variables. This process is most often of an experimental nature. Applied variables are usually similar to those used in models not based on ANN.

3. RECOGNITION OF LAND COVER TYPES

Satellite images have now become widely available and their quality grows (among others by increased resolution). One of the most popular sources of satellite images is the Landsat program, which has been collecting earth images since 1972. In 1984 and 2013, in the orbit the Landsat 5 satellite was in operation, officially setting a new Guinness World Record for “longest-operating Earth observation satellite”. Due to the availability of satellite images over many years, data from this satellite have been

used for empirical studies. Table 1 contains a list of available bands along with lengths of received waves. [4]

One of the popular recognition methods of spatial planning types based on satellite images is the use of such indexes as: Normalized Difference Vegetation Index (NDVI), Normalized Difference Built-up Index (NDBI), Index-based Built-up Index (IBI), Enhanced Built-Up and Bareness Index (EBBI) and Modified Normalized Difference Water Index (MNDWI).

Table 1: Satellite bands of Landsat 5.

Bands	Wavelength (micrometers)
Band 1 – BLUE	0.45 – 0.52
Band 2 – GREEN	0.52 – 0.60
Band 3 – RED	0.63 – 0.69
Band 4 – Near Infrared (NIR)	0.76 – 0.90
Band 5 – Shortwave Infrared (SWIR) 1	1.55 – 1.75
Band 6 – Thermal Infrared (TIR)	10.40 – 12.50
Band 7 – Shortwave Infrared (SWIR) 2	2.08 – 2.35

Among the most commonly used are Normalized Difference Vegetation Index (NDVI) [5] presented on Equation (1).

$$NDVI = (NIR - RED) / (NIR + RED) \quad (1)$$

The construction of NDVI predisposes it as a tool to identify the types of green areas. [6] It does not work well enough as a classifier of other spatial planning types of the area. In the subject literature, indexes derived from NDVI are used to define them. One is the Normalized Difference Built-up Index (NDBI). Its construction is shown on Equation (2).

$$NDBI = (SWIR - NIR) / (SWIR + NIR) \quad (2)$$

The application of NDBI alone often turns out to be insufficient due to the fact that some green areas have been incorrectly classified as built-up areas. The aim of their elimination is to use the NDVI, which enables identification of green areas and their final removal from the set. This approach was applied by He et al. [7] and confirmed by Bhatti and Tripathi [8].

Other indexes used for detection of built-up areas are the Index-based Built-up Index (IBI) [9] and the Enhanced Built-Up and Bareness Index (EBBI) calculated according to Equations (3) and (4). [10]

$$IBI = [2 \times SWIR / (SWIR + NIR) - ((NIR / (NIR + RED)) + (GREEN / (GREEN + SWIR)))] / [2 \times SWIR / (SWIR + NIR) + ((NIR / (NIR + RED)) + (GREEN / (GREEN + SWIR)))] \quad (3)$$

$$EBBI = (SWIR - NIR) / 10V(SWIR + TIR) \quad (4)$$

The Water Ratio Index (WRI), the Normalized Difference Water Index (NDWI) and the Modified Normalized Difference Water Index (MNDWI) are

PLEA 2018 HONG KONG

Smart and Healthy within the 2-degree Limit

commonly used to detect water areas. [11] The last was described below – Equation (5) – due to its use in empirical studies.

$$\text{MNDWI} = (\text{GREEN} - \text{SWIR}) / (\text{GREEN} + \text{SWIR}) \quad (5)$$

The possibility of predicting changes in land cover with the use of ANNs was confirmed in research conducted by among others: Jiang et al., Qiang and Lam, Mishra and Rai [12-14].

4. METHODOLOGY

The process of predicting changes in spatial planning was divided into the following stages:

Selection of areas and acquisition of images from Landsat satellite for 1988, 1998 and 2006;

Calculation of selected remote sensed indexes and classification of the area into one or a few classes;

Construction of ANN model (based on data from 1988 and 1998), as well as prediction of changes in spatial planning and their verification with data for 2006.

Fragments of the largest cities in Lodz agglomeration – Lodz and Zgierz were selected to this study. Poland is a country located in the Eastern Europe. Lodz is the third largest population and fourth largest city of the country. The first of selected areas (in Lodz) covered the urban tissue with high intensity of building development. The second covered the city of Zgierz along with suburban areas. The described choice of areas has been made due to different type of spatial planning and different dynamics of its changes.

At the first stage, images were acquired from the Landsat satellite for 1988, 1998 and 2006. It should be noted that the ideal solution would be to use images between which is exactly the same time interval. Unfortunately, due to poor quality of images taken in 2008, it was necessary to use material from 2006. On acquired images, one pixel corresponded to the area of 30 m x 30 m.

The second stage included calculation of selected indexes of remotely sensed analysis in order to determine the type of spatial planning of the represented area as a single pixel on acquired satellite imagery.

In case of analyzed area, a usage of NDVI turned out to be impossible due to low precision of obtained results – classifying the single-family building development as agricultural lands. In view of above, for determining the urbanized area were used indexes: NDBI, IBI and EBBI. The obtained classification was characterized by a higher precision of results; however to built-up areas were included water reservoirs and vegetation. It was necessary to eliminate them by distinguishing in the raster image of green areas with NDVI (value>0.2) and water areas based on MNDWI (value>0.15). The given threshold values were experimentally estimated. Finally, the urban lands in central part of Lodz and Zgierz were outlined. Fig. 6 shows the areas of studied

fragment of the city of Lodz for 1998 classified as built-up by NDBI (left) and after correction taking into account NDVI and MNDWI (right). An analogous classification for Zgierz is presented in Fig. 7.

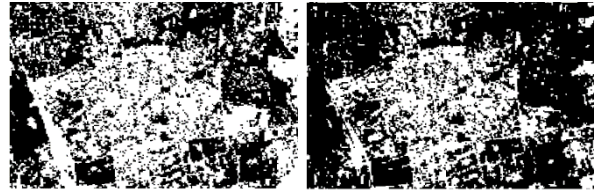


Figure 6: Built-up areas of Lodz (in 1998) determined using the NDBI (left) and using the method presented by the authors of this study (right).

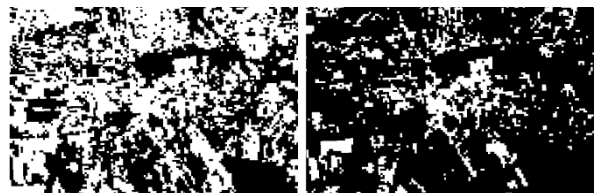


Figure 7: Built-up areas of Zgierz (in 1998) determined using the NDBI (left) and using the method presented by the authors of this study (right).

Results obtained for 2006 (Fig. 8) were randomly verified in the empirical way by comparing them with the actual state both on available maps and direct observation. For selected randomly 100 points, 93.00% of the classification level has been reached. This result should be considered to be highly satisfactory. Similar classification quality (92.65%) using similar methods obtained by Zha et al. [15].

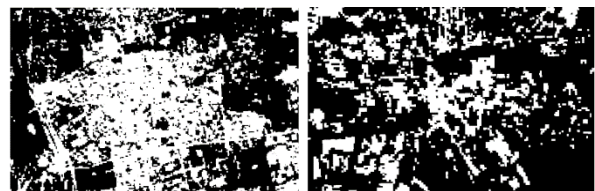


Figure 8: Built-up areas of Lodz (left) and Zgierz (right) in 2006.

The above division was tantamount to distinguish between built-up and undeveloped areas. In this case, green areas were only a subset of unbuilt areas. NDVI as previously was used in order to detect them.

The third stage of study consisted on building and testing about 5000 different models of artificial neural networks. Among them were both MLP and RBF network. The set of activation functions included: logistic, hyperbolic tangent, Gaussian and sine. The input variables were coordinates of the pixel's position in the image, information on the number of built-up areas and green areas in the neighborhood of 4 (Fig. 9a) and 8 pixels (Fig. 9b). The former variables were used to determine to what extent the analyzed area (pixel) is surrounded by built-up areas and green areas.

PLEA 2018 HONG KONG

Smart and Healthy within the 2-degree Limit

The year of the forecast was not directly used in the model because the test set contained the value of the dependent variable only for 2006. The use of an additional, in this case unnecessary variable due to the construction of a neuron (Fig. 1) might only lead to adding up the additional signals burdened with forecast error in the nerve cells' subsequent layers. The number of pixels, from which each of analyzed images was built, took out 480940 (865 pixels x 556 pixels).

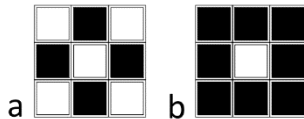


Figure 9: Types of pixels' neighborhood: a) 4-elements, b) 8-elements.

5. RESULTS

The best of built models was MLP of 8-11-1 architecture (Fig. 10), which neurons in hidden layer had activation function in the form of hyperbolic tangent, and in the output layer a logistical function.

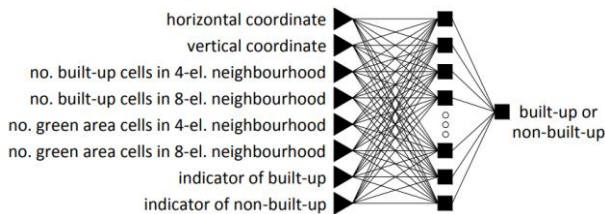


Figure 10: Scheme of the best MLP.

The network was taught using the conjugate gradient algorithm. Table 2 includes statement of the prediction accuracy. The correctness of forecasts concerning the built-up areas (2006) was over 90% for both Lodz and Zgierz. It should be noted that in both cases most of the areas did not lose their function, i.e. undeveloped areas remained undeveloped, and developed areas did not undergo the process of de-urbanization. Therefore, it is justified to verify the correctness of forecasts only in case of those areas which were subject to urbanization in the analyzed period. The correctness of forecasts for the areas covered by urbanization process was noticeably lower. For Zgierz area it was 70.48%. For a highly urbanized area, i.e. the city of Lodz, the correctness of forecasts reached 78.02%, which should be considered as a highly satisfactory result. None of the RBF networks has reached the acceptable precision of the forecasts. All of them generated less than 65% of correct answers.

Table 2: Statement of the percentage of built-up areas prediction correctness.

Area	Correctness of forecasts (%)
------	------------------------------

	built-up areas in 2006	changes of areas from unbuilt areas in 1998 to built-up areas in 2006
Lodz	94.06 %	78.02 %
Zgierz	91.86 %	70.48 %

6. CONCLUSION

Results of conducted empirical studies confirm the possibility and validity of predicting changes in spatial planning using ANN. The best of tested models turned out to be MLP. It was characterized by a high precision of obtained results. Special emphasis should be put on the degree of prediction correctness on the level of 94.06 % in case of the city of Lodz. Developed model achieved noticeably better results in an area having higher level of urbanization. Further research to improve the quality of projections should be carried out in the field of optimizing the set of explanatory variables. For example, it would be recommended to enrich the information on distance of each area represented by a single pixel of the image from selected technical infrastructure components. However, this is related to technical problems consisting in identification of the type of infrastructure based on satellite imagery. Therefore, it is necessary to carry out further studies, including data available from other sources.

The disadvantage of applied research method is necessity of experimental selection of threshold values of NDVI and MNDWI in order to correctly identify green areas and water areas. Threshold values can vary considerably, not only depending on the time of year for which they are calculated, but also on the area covered by the analysis. Therefore, it would make sense in the future to use the ANN also for the purpose of automating the identification process of spatial planning. The literature analysis confirms this possibility [16-18]. In combination with the model described in this work, it would enable the creation of a comprehensive analytical and forecasting system for the assessment of progressing urbanization process. Moreover, such a system could be the starting point for planning works to design urban areas in accordance with the sustainable development principle. The usage of these models may contribute to the economic optimization of investments in future built-up areas, as well as give a potential opportunity to stem the often undesirable phenomenon of a suburbanisation on the legislative ground.

ACKNOWLEDGEMENTS

This research has been supported by funds of the Laboratory of Artificial Neural Networks in the Innovative Economy at Faculty of Management and Production Engineering, Lodz University of Technology and by the Young Scientists' Funds at the Faculty of

PLEA 2018 HONG KONG

Smart and Healthy within the 2-degree Limit

Civil Engineering, Architecture and Environmental Engineering, Lodz University of Technology, Lodz.

REFERENCES

1. McCulloch, S. and W. Pitts, (1943). A logical calculus of the ideas immanent in nervous activity. *Bulletin of Mathematical Biophysics*, 5: p. 115-133.
2. Osowski, S., (1996). *Neural networks in algorithmic depiction* (in Polish), Warsaw, Poland.
3. Eickhoff, R. and U. Ruckert, (2007). Robustness of radial basis functions. *Neurocomputing*, 70: p.2758–2767.
4. Landsat Missions, [Online], Available: <https://landsat.usgs.gov/> [10 May 2018].
5. Jeevalakshmi, D., Narayana Reddy, S. and B. Manikiam, (2016). Land cover classification based on NDVI using LANDSAT8 time series: A case study Tirupati region. In *2016 International Conference on Communication and Signal Processing*, April 6-8, India, IEEE, p. 1332-1335.
6. Zheng, Y. and G. Yu, (2017). Spatio-temporal distribution of vegetation index and its influencing factors - a case study of the Jiaozhou Bay, China. *Chinese Journal of Oceanology and Limnology*, 35(6): p. 1398-1408.
7. He, C., Shi, P., Xie, D. and Y. Zhao, (2010). Improving the normalized difference built-up index to map urban built-up areas using a semiautomatic segmentation approach. *Remote Sensing Letters*, 1(4): p. 213-221.
8. Bhatti, S.S. and N.K. Tripathi, (2014). Built-up area extraction using Landsat 8 OLI imagery. *GIScience & Remote Sensing*, 51(4): p. 445-467.
9. Huong, D.T.V., Linh, N.H.K. and T.D.M. Phuong, (2016). Usage of indices for mapping built-up and open space areas from Landsat 8 OLI imagery: A case study of Da Nang city, Vietnam. In *International Conference on Geoinformatics for Spatial-Infrastructure Development in Earth & Allied Sciences (GIS-IDEAS)*, Ha Noi, Viet Nam.
10. As-syakur, A.R., Adnyana, I.W.S., Arthana, I.W. and I.W. Nuarsa, (2012). Enhanced Built-Up and Bareness Index (EBBI) for Mapping Built-Up and Bare Land in an Urban Area. *Remote Sensing*, 4(10): p.2957-2970.
11. Gautam, V.K., Gaurav, P.K., Murugan, P. and M. Annadurai, (2015). Assessment of Surface Water Dynamics in Bangalore using WRI, NDWI, MNDWI, Supervised Classification and K-T Transformation. *Aquatic Procedia*, 4: p. 739-746.
12. Jiang, J., Zhou, J., Wu, H., Ai, L., Zhang, H., Zhang, L. and J. Xu, (2005). Land cover changes in the rural-urban interaction of Xi'an region using Landsat TM/ETM data. *Journal of Geographical Sciences*, 15(4): p. 423-430.
13. Qiang, Y. and N.S.N. Lam, (2015). Modeling land use and land cover changes in a vulnerable coastal region using artificial neural networks and cellular automata. *Environmental Monitoring and Assessment*, 187(57).
14. Mishra, V.N. and P.K. Rai, (2016). A remote sensing aided multi-layer perceptron-Markov chain analysis for land use and land cover change prediction in Patna district (Bihar), India. *Arabian Journal of Geosciences*, 9(249).
15. Zha, Y., Gao, J. and S. Ni, (2003). Use of normalized difference built-up index in automatically mapping urban areas from TM imagery. *International Journal of Remote Sensing*, 24(3): p. 583-594.
16. Weng, Q. and X. Hu, (2008). Medium Spatial Resolution Satellite Imagery for Estimating and Mapping Urban Impervious Surfaces Using LSMA and ANN. *IEEE Transactions on Geoscience and Remote Sensing*, 46(8): p. 2397-2406.
17. Mackin, K.J., Nunohiro, E., Ohshiro, M. and K. Yamasaki, (2006). Land Cover Classification from MODIS Satellite Data Using Probabilistically Optimal Ensemble of Artificial Neural Networks. In *10th International Conference, KES 2006*, Bournemouth, UK, October 9-11, p. 820-826.
18. Yamaguchi, T., Mackin, K.J., Nunohiro, E., Park, J.G., Hara, K., Matsushita, K., Ohshiro, M. and K. Yamasaki, (2009). Artificial neural network ensemble-based land-cover classifiers using MODIS data. *Artificial Life and Robotics*, 13: p. 570–574.

Sizing Natural Ventilation Systems for Cooling:

The potential of NV systems to deliver thermal comfort while reducing energy demands of multi-storey residential buildings in India.

LUCIANO DE FARIA¹, MALCOLM J COOK¹, DENNIS LOVEDAY¹, CHARALAMPOS ANGELOPOULOS¹, SANYOGITA MANU², YASH SHUKLA²

¹Loughborough University, United Kingdom

²CEPT University, Ahmedabad, India

ABSTRACT: This paper aims to identify the potential of natural ventilation for cooling a representative two-bedroom residential apartment layout in India. India faces an unprecedented demand for residences and must reduce energy consumption associated with air-conditioning. Three significant climates and cities in India are investigated in this paper. The potential to extend the hours of the year for which thermal comfort is achievable using natural ventilation strategies is tested. This potential is identified by employing analytical methods to design and size ventilation capacity. Five natural ventilation design strategies are used over several scenarios varying window free area and ceiling fan speed. Indoor temperature setpoints are based on the India Model for Adaptive Comfort. Results are given as percentage of hours of the year for which natural ventilation is capable to remove calculated heat gains. Percentages of hours are divided into day-time and night-time. Findings show that the combination of large windows or balcony doors with additional ventilation openings and ceiling fan increases the total percentages of hours of the year for which natural ventilation is effective impacting on substantial energy consumption reduction with air-conditioning. Conversely, this potential varies with climate, and hence location.

KEYWORDS: Natural ventilation, Residential buildings, IMAC, Ceiling fan, Tropical climate

1. INTRODUCTION

The demand for residences in India will result in an increase of 400% in built area over the next three decades [1]. This demand will be fulfilled mostly with high-rise apartment blocks. Rise on income, growing expectation of thermal comfort and falling cost of air-conditioning (AC) systems will result in a record amount of AC being installed in residences in India: from 25 million now to 380 million in 2050 [2]. Energy consumption with AC will represent 45% of the total demand with buildings [3]. The development of high-rise residential buildings that are suitable for Indian climates and able to curb the energy consumption with AC has been considered of high priority for the Indian Government to tackle a future energy crisis. This is aligned with international efforts such as the Mission Innovation Project and the Advanced Cooling Challenge launched by the Clean Energy Ministerial. Natural ventilation (NV) has the potential to improve thermal comfort while reducing energy consumption due to AC. This potential can be increased when NV is applied in conjunction with ceiling fans. Based on international collaborative research, this paper identifies the potential to expand the effectiveness of NV operating concurrently with ceiling fans for providing thermal comfort in residences in the challenging climates encountered in India. Three representative cities and climates in India are investigated. The potential of five NV design systems is identified using analytical methods [4,5]. Indoor

temperatures are based on the India Model for Adaptive Comfort (IMAC) [6].

2. METHODOLOGY

The following steps were employed in this work: define climate thresholds and temperature set points for each climate investigated; identify the percentage of hours of the year suitable for NV in each location; define size of windows and ventilation openings in a two-bedroom apartment layout; assess the impact of ceiling fans on the thermal comfort sensation; calculate the required airflow rates to remove heat gains; and calculate to what extent five NV design strategies can supply the required airflow rates.

2.1 Climate thresholds and internal temperature

Weather data from the Indian Society of Heating Refrigeration and Air-conditioning Engineers (ISHRAE) [7] were used for the three cities and climates in India investigated: Ahmedabad (hot-dry), New-Delhi (composite), and Mumbai (warm-humid). The internal temperature (T_i) is defined using the IMAC for mixed-mode (MM) buildings, which operate as NV when temperatures allow and are assisted with mechanical devices when thermal comfort is not reached with NV alone. The IMAC-MM adaptive thermal comfort approach uses 30-day running mean outdoor temperatures ranging from 13°C to 38.5°C to calculate the neutral temperature ranging from 21.5°C to 28.7°C for these limits [6]. The algorithms calculate the

PLEA 2018 HONG KONG

Smart and Healthy within the 2-degree Limit

neutral temperature considering a ceiling fan to be operating at variable speed concurrently to NV. Here the IMAC-MM neutral temperature is considered as the initial T_i .

2.2 Hours of the year suitable for NV

The percentages of hours of the year for which climatic conditions allow NV for cooling to occur in each city is identified based on thresholds of relative humidity (RH) and air temperature. Firstly, weather data related to hours of the year were sorted for RH between 30% and 70%. Secondly, hours for which the inside to outside temperature difference results in negative values (outdoor > indoor temperature) were rejected, indicating that NV for cooling is not feasible. The remaining hours of the year were considered feasible to apply NV for cooling. The percentages calculated were then compared to percentages of hours for which NV is feasible from three adaptive thermal comfort models: IMAC-MM and IMAC-NV [6] and ASHRAE-55 [8] (Table 1).

Table 1: Percentages of hours for which NV is feasible as presented here and compared with reference models.

MODEL	Ahmedabad			New Delhi			Mumbai		
	day	night	total	day	night	total	day	night	total
IMAC MM	10%	21%	31%	12%	13%	25%	7%	9%	16%
IMAC NV			34%			29%			27%
ASHRAE 55			21%			20%			27%
			20%			20%			16%

2.3 Apartment layout and openings for ventilation

A two-bedroom residential apartment layout is used as case study (Fig. 1), as described in the GBPN Technical Report [1], which is based on a residential building design survey. Residential blocks with this layout will be widely built to meet the increasing demand for residences in India. These new buildings must be suitable for, and allow adaptations driven by the different Indian climates, as well as being environmentally and economically viable.

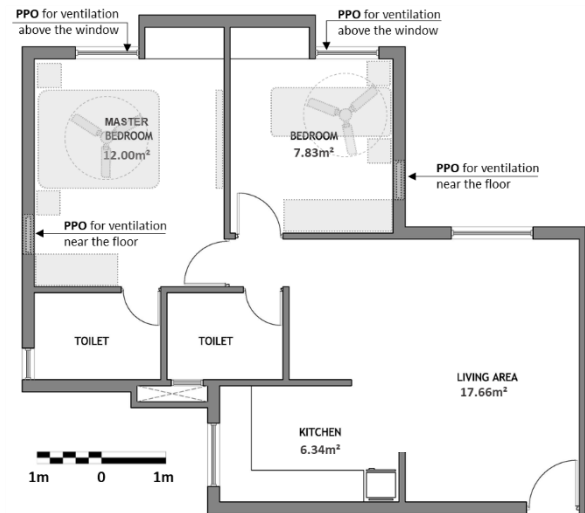


Figure 1: Apartment floorplan and cross-section [3].

The efficacy of two windows and a balcony door (Fig. 2) to provide ventilation for this apartment layout is tested. The width of these openings is kept as designed for the apartment: 1.0m. The horizontal sliding window type 'A' is commonly employed in recent buildings across India, but it provides a small opening free area (A_f). The double side-hung window type 'B' is an alternative to increase A_f by two times with the same frame size as 'A'. The type 'C' consists of a balcony door increasing A_f by three times. A pair of purpose provided openings (PPOs) [9] for ventilation was inserted in each bedroom (type 'D', also in fig. 2): one near the floor and the other near the ceiling to improve buoyancy. These PPOs should be placed in opposite or adjacent walls to allow wind-driven cross-ventilation. These PPOs are aimed to operate together with each of the three other types (A, B and C). Their efficacy was tested for some of the NV design scenarios (see section 2.6).

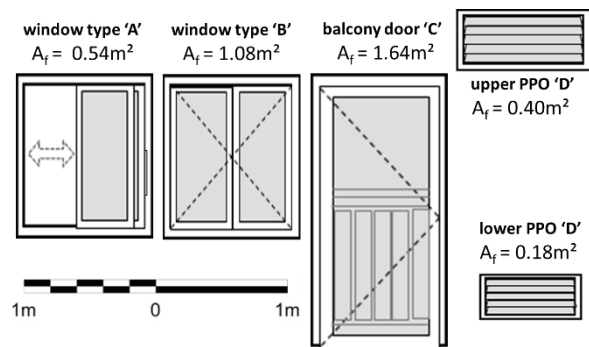


Figure 2: Schematic view of the openings for ventilation.

2.4 The impact of air velocity on the calculated T_i

Ceiling fans operating concurrently with NV have the capacity to keep thermal comfort sensations at increased temperature setpoints, thus reducing the overall time for which AC must operate. The increase

PLEA 2018 HONG KONG

Smart and Healthy within the 2-degree Limit

in the air velocity allows a proportional rise in the T_i whilst maintaining thermal comfort [10,11,12]. This proportionality is calculated as an exponential trendline based on values from ASHRAE-55 [8] (Fig. 3). Based on Fig. 3 the T_i calculated via IMAC-MM is adjusted considering a ceiling fan operating at three speeds: 0.6m/s, 1.2m/s and 1.8m/s. While ASHRAE-55 indicates 1.5m/s as the limit for comfort in offices other authors report air velocities up to 2.0m/s as comfortable for residential environment [13,14,15].

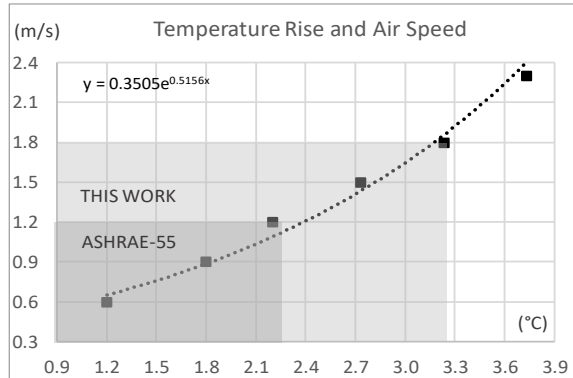


Figure 3: Relationship between temperature and air speed.

2.5 Required airflow rates to remove heat gains

Information about equipment density and occupant numbers [1] and metabolic rates [5] were used to calculate internal heat gains. Heat change with outside was obtained using Energy Plus dynamic thermal modelling software for a simplified construction modelled in Design Builder. After calculating the total heat balance, then airflow rates necessary for cooling were calculated [16,17].

2.6 Achievable airflow rates with five NV systems

The metric adopted to define the extent to which NV can be effective is the percentage of hours of the year for which the maximum achievable airflow rate with a given NV design system is either equal to or higher than the required airflow rate to remove the total heat gains. These NV systems are based on the guides CIBSE AM-10 [4] and CIBSE Guide A [5]. The NV design systems employed in this work are:

- Single-sided ventilation, one opening (window or balcony door) buoyancy-driven
- Cross ventilation, two or more openings (window or balcony door and PPOs) buoyancy-driven
- Single-sided ventilation, one opening (window or balcony door) wind-driven
- Cross-ventilation, two or more openings (window or balcony door and PPOs) wind-driven
- Cross-ventilation, two or more openings (window or balcony door and PPOs) combined buoyancy and wind-driven

The capacity of each of these five NV design systems to provide the required airflow rates is tested based on

the presented metric and applied for the two-bedroom apartment layout. The openings type A, B and C are assumed to be fully open. The PPOs type D are added in the NV design systems that make use of two or more openings for ventilation (the second, the fourth and the fifth NV design systems), and are also assumed to be fully open, while in operation. Discharge coefficients (C_d) adopted for each of these openings are: for single-sided ventilation $C_d = 0.25$, for cross-ventilation $C_d = 0.60$, and for the PPOs with external louvres at 45° $C_d = 0.32$ [4,5,18,19,20].

3. RESULTS AND ANALYSIS

The results are displayed in this section in several charts. Percentages of hours are given for five NV scenarios separated for day-time, night-time and total time for the three cities and for openings type 'A', 'B' and 'C'. Figures 4, 5 and 6 show results for a ceiling fan operating at 0.6m/s; Figures 7, 8 and 9 for a ceiling fan at 1.2m/s; and Figures 10, 11 and 12 for a ceiling fan at 1.8m/s. All percentages hours are compared with benchmark percentage values obtained from reference methods: IMAC-NV, IMAC-MM and ASHRAE-55 (as previously shown in Table 1).

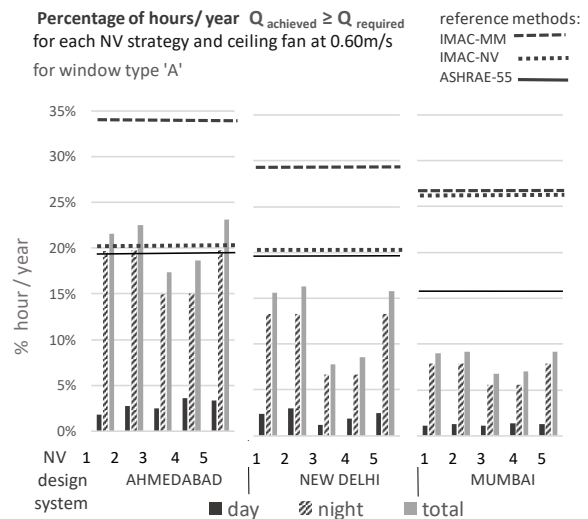


Figure 4: Results for scenario with window type 'A' and ceiling fan at 0.60m/s (initial scenario).

PLEA 2018 HONG KONG

Smart and Healthy within the 2-degree Limit

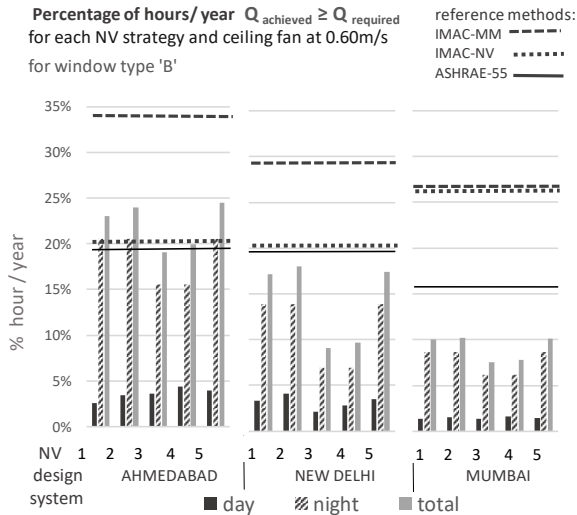


Figure 5: Results for scenario with window type 'B' and ceiling fan at 0.60m/s.

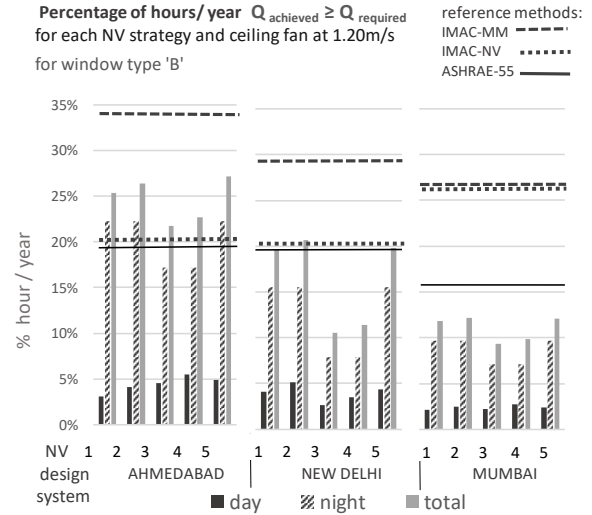


Figure 8: Results for scenario with window type 'B' and ceiling fan at 1.20m/s.

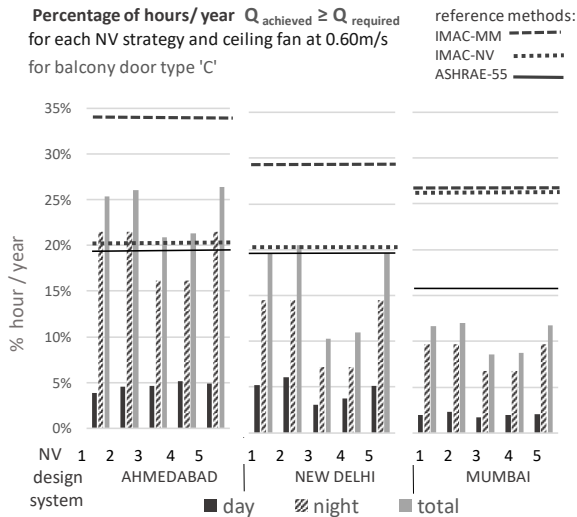


Figure 6: Results for scenario with balcony door type 'C' and ceiling fan at 0.60m/s.

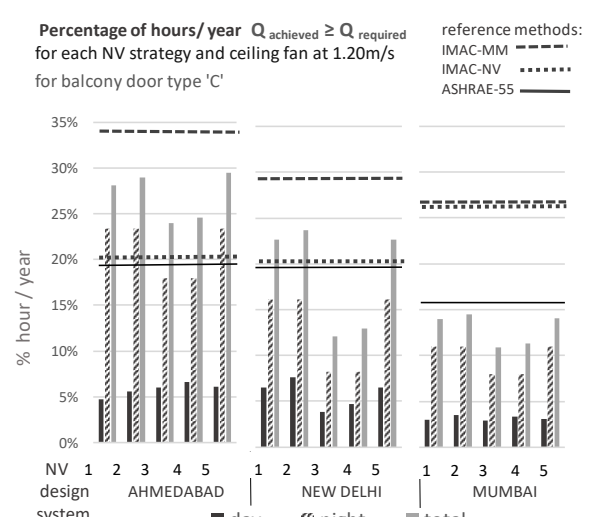


Figure 9: Results for scenario with balcony door type 'C' and ceiling fan at 1.20m/s.

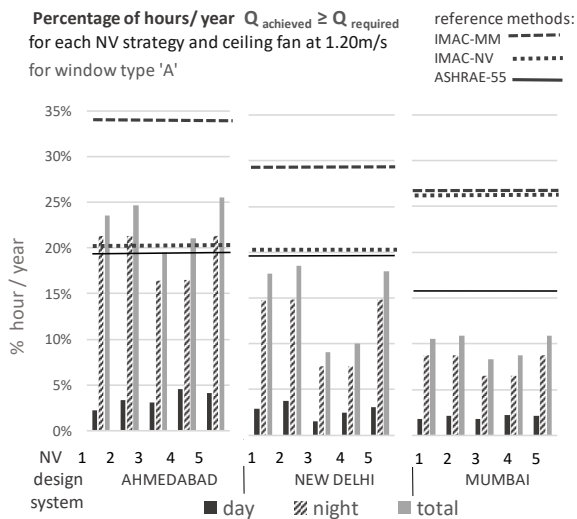


Figure 7: Results for scenario with window type 'A' and ceiling fan at 1.20m/s.

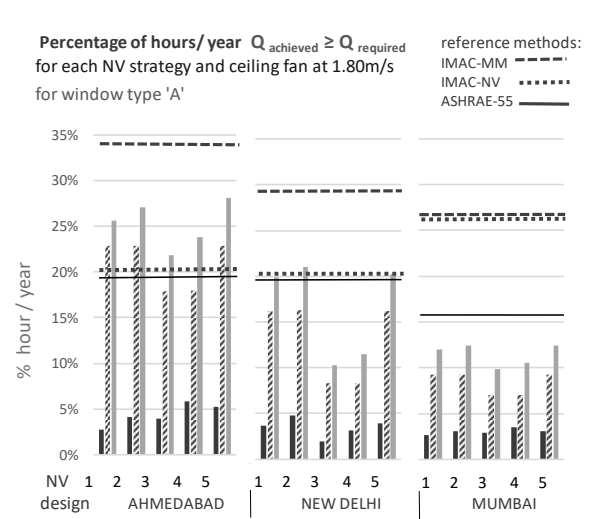


Figure 10: Results for scenario with window type 'A' and ceiling fan at 1.80m/s.

PLEA 2018 HONG KONG

Smart and Healthy within the 2-degree Limit

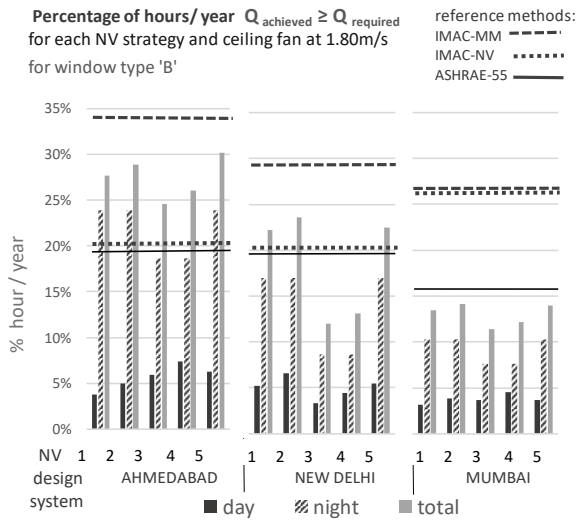


Figure 11: Results for scenario with window type 'B' and ceiling fan at 1.80m/s.

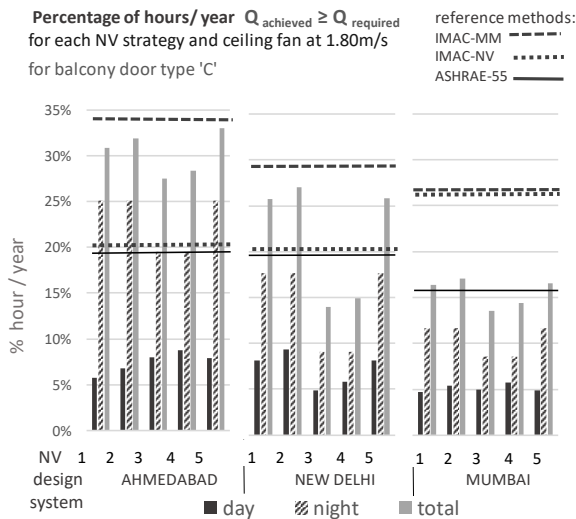


Figure 12: Results for scenario with balcony door type 'C' and ceiling fan at 1.80m/s.

3.1 Analysis of the potential for NV based on the climate of each city

The maximum percentages of hours of the year for which NV can provide thermal comfort range depending on the climate and location (see Table 1): Ahmedabad (hot-dry climate), with 31%, shows more potential for NV than New Delhi (composite), with 25%, which performs better than Mumbai (warm-humid), with 16%. Furthermore, NV occurs two times more during night-time than day-time in Ahmedabad (21% in contrast to 10%) and is more evenly distributed in New Delhi (13% in contrast to 12%) and Mumbai (9% in contrast to 7%). Reach or not these maximum percentages of hours for the two-bedroom apartment layout investigated will vary according to the NV system adopted, and it is not possible to declare a

single strategy that meets all criteria for the three cities and climates analysed.

3.2 Analysis of the potential for NV based on the design system adopted for each city

For the five NV design systems employed, results from Fig. 4 to 12 show that, for the three climates and locations investigated, single-sided single-opening ventilation systems are less efficient than multiple openings which allow cross ventilation. This can be noticed comparing the results for the first and the second NV design systems or the third and the fourth NV design systems. Cross-ventilation is achieved using the windows or the balcony door and the PPOs for ventilation in the bedrooms. Furthermore, for the three cities, buoyancy-driven ventilation is more efficient than wind-driven ventilation. This can be noticed comparing the results for the second and the fourth NV design systems. The fifth NV design system, which combines buoyancy and wind-driven ventilation, showed the best performance among the five options in all scenarios for Ahmedabad. Conversely, for New Delhi and Mumbai, results from the second and the fifth NV design systems are either practically the same or alternate the lead by a small difference according to the combination of the size of the openings and the ceiling fan speed.

Table 2: Percentages of hours for which NV is efficient considering buoyancy and wind-driven ventilation combined (fifth NV design system) and varying the opening type (A,B,C) and the ceiling fan speed (0.6, 1.2, 1.8m/s).

	AHMEDABAD			NEW DELHI			MUMBAI		
	0.6m/s	1.2m/s	1.8m/s	0.6m/s	1.2m/s	1.8m/s	0.6m/s	1.2m/s	1.8m/s
A	23.1%	25.5%	28.1%	15.8%	17.9%	20.2%	9.2%	10.9%	12.4%
B	24.5%	27.1%	30.1%	17.4%	19.8%	22.5%	10.1%	12.1%	14.0%
C	26.4%	29.5%	33.0%	19.6%	22.6%	25.8%	11.7%	14.1%	16.5%

Results of the total percentages of hours of the year for which NV for cooling can be employed for each of the cities varying the opening type/area (types A, B and C) and the ceiling fan speed (0.6, 1.2, 1.8m/s) are shown in Table 2. These results were obtained applying the fifth NV design system (buoyancy and wind-driven combined).

Increasing the free area of the opening type A by two times (type B) and then by three times (type C) allows a respective rise in the percentages of hours of 1.4% and 1.9% in Ahmedabad (total increase from using the opening type A to the opening type C of 3.3%), 1.6% and 2.2% in New Delhi (total of 3.8%), and 0.9% and 1.6% in Mumbai (total of 2.7%), when ceiling fans operates at low speed (0.6m/s). The same increase of the free area for ceiling fans operating at 1.8m/s causes the following rise in the percentages of hours: 2.0% and 2.9% in Ahmedabad, 2.3% and 3.3% in New Delhi, and 1.6% and 2.5% in Mumbai.

PLEA 2018 HONG KONG

Smart and Healthy within the 2-degree Limit

Conversely, larger glazed areas bring the disadvantage of increasing the heat gains during the hours of the year for which NV is not an option and, therefore, glass panels are closed. This situation is worsened for the façade receiving direct solar radiation. In this case, adopting windows with external louvered shutters could be an option to provide protection for glazed surfaces. Louvered shutters also allow NV to happen on rainy days when external temperature is within comfortable limits. A balcony or terrace (as in the solution presented as opening type C) also provides shading with the additional benefits of increased occupants' privacy, attenuate urban noise and create a buffer-zone between inside and outside.

Furthermore, the rise in air velocity from 0.6m/s to 1.2m/s and then from 1.2m/s to 1.8m/s increases respectively the percentages of hours for which NV can operate by 2.4% and 2.6% in Ahmedabad (total rise in the air velocity from 0.6m/s to 1.8m/s of 5.0%), 2.1% and 2.3% in New Delhi (total of 4.4%) and 1.7% and 1.5% in Mumbai (total of 3.2%) for openings type A. The same rise in air velocity will increase respectively the percentages of hours by 3.1% and 3.5% in Ahmedabad (6.6% in total), 3.0% and 3.2% in New Delhi (6.2% in total) and 2.4% and 2.5% in Mumbai (4.9% in total) with openings type C.

Finally, based on the results from Table 2, the greatest impact on the percentages of hours is observed when the increase on the free area of the openings are combined with rising fan speed. For example, comparing the results for the scenario with the opening size as designed for the apartment (type A: horizontal sliding window) and ceiling fan at 0.6m/s with a scenario combining the opening type B (double side-hung window) and ceiling fan at 1.2m/s and then with a scenario combining the opening type C (balcony door) and ceiling fan at 1.8m/s, the respective rise in the percentages of hours are: 4.0% and 5.9% in Ahmedabad (total impact on the percentages of hours of 9.9%), 4.0% and 6.0% in New Delhi (total of 10.0%), and 2.9% and 4.4% (total of 7.3%) in Mumbai.

4. CONCLUSIONS

This paper applies current engineering-based design methodologies to the case of a two-bedroom residential apartment of a design that will become widespread in India in coming years. The aim is to establish and increase the extent to which NV systems operating concurrently with ceiling fans can deliver thermally acceptable indoor conditions, thereby eliminating unnecessary use of air-conditioning at certain times. Five NV design systems in three representative climates and cities in India were investigated. The main findings are as follows:

Windows sizes as currently designed for this apartment layout have limited capacity to deliver required airflow rates for cooling. Increasing typical

sizes of windows free area by a factor of 3, combined the use of PPOs for ventilation and with ceiling fan usage, can rise the total number of hours in the year that NV can remove total heat gains by 9.9%, in Ahmedabad, 10.0% in New Delhi and 7.3% in Mumbai. Corresponding reductions in AC usage are: 36 days in Ahmedabad and New Delhi and 26 days in Mumbai, implying in substantial energy savings.

Whilst results are climate (location) dependent, they show the potential for improvement that can be achieved, even in some of the most challenging climates encountered across India.

The design changes envisaged for this apartment layout are considered both practical and feasible, and the analytical results reported here are due to be further analysed via dynamic thermal comfort model coupled with computational fluid dynamics and validated using a specially-constructed test facility at CEPT University, Ahmedabad, India.

ACKNOWLEDGEMENTS

This research is part of an International research collaboration involving Loughborough University, UK, CEPT University, India, SE Controls UK and India, and supported by an advisory panel. The project is entitled: 'Low Energy Cooling and Ventilation for Indian Residences (LECaVIR)' and is financially supported by the UK Engineering and Physical Sciences Research Council (EPSRC) under grant reference: EP/P029450/1. The authors express their gratitude for all support received.

REFERENCES

- Rawal, R., & Shukla, Y. (2014). Residential Buildings in India: Energy Use Projections and Saving Potentials. *Global Buildings Performance Network (GBPN). Building Policies for a Better World*, [September].
- The Future of Cooling. Opportunities for energy-efficient air conditioning. OECD/IEA, 2018. International Energy Agency. Available at: http://www.iea.org/publications/free_publications/publication/The_Future_of_Cooling.pdf [22 May 2018].
- Shah, N, Wei, M, Letschert, V, Phadke, A. (2015). Benefits of Leapfrogging to Superefficiency and Low Global Warming Potential Refrigerants in Room Air Conditioning. LBNL Report. Energy Technologies Area. [October].
- CIBSE AM 10. (2005). APPLICATIONS MANUAL 10: NATURAL VENTILATION, *The Chartered Institution of Building Services Engineers*, London.
- CIBSE Guide A. (2010). Environmental design. The Chartered Institution of Building Services Engineers, London. ISBN: 1-903287-66-9.
- Manu, S., Shukla, Y., Rawal, R., Thomas, L. E., & de Dear, R. (2016). Field studies of thermal comfort across multiple climate zones for the subcontinent: India Model for Adaptive Comfort (IMAC). *Building and Environment*, 98, 55–70. <http://doi.org/10.1016/j.buildenv.2015.12.019>
- Huang, J. (2015). New typical year weather data for 62 Indian locations now available on the Web.

PLEA 2018 HONG KONG

Smart and Healthy within the 2-degree Limit

- Manu, S., Yash S., Rajan R., Thomas, E., de Dear, R. (2014). Assessment of Air Velocity Preferences and Satisfaction for Naturally Ventilated Office Buildings in India. *PLEA 2014 - 30th INTERNATIONAL PLEA CONFERENCE* (December): 1–8. http://www.plea2014.in/wp-content/uploads/2014/12/Paper_7C_2720_PR.pdf.
- Jones, B. M., Cook, M. J., Fitzgerald, S. D., Iddon, C. R. (2016). A review of ventilation opening area terminology. *Energy and Buildings*, 118. pp. 249-258. ISSN 1872-6178.
- Vyas, D., & Apte, Effectiveness of Ventilation Cooling Strategies in Hot and Dry and Temperate Climate of India. In *38th AIVC - 6th TightVent & 4th Venticool Conference*.
- Callahan, M., and Gum, H. (2000). Development of a High Efficiency Ceiling Fan. In *Proceedings of the Twelfth Symposium on Improving Building Systems in Hot and Humid Climates*, San Antonio, TX, 270–77.
- Babich, F., Cook, M., Loveday, D., and Cropper, P. (2016). Numerical Modelling of Thermal Comfort in Non-Uniform Environments Using Real-Time Coupled Simulation Models. *Proceedings of Building Simulation and Optimisation 2016: 3rd IBPSA-UK Conference*: 4-11.
- ASHRAE. (2013). ANSI/ASHRAE Standard 55-2013 Thermal Environmental Conditions for Human Occupancy. Atlanta: *American Society of Heating and Air-Conditioning Engineers*.
- CIBSE KS 17. (2011). Knowledge Series 17: Indoor Air Quality & Ventilation. *The Chartered Institution of Building Services Engineers*, London. ISBN: 9781906846190.
- Parker, J. and Teekaram A. (2005). Wind-driven Natural Ventilation Systems. BG2/2005. Bracknell, *BSRIA*. ISBN: 0 86022 647 6.
- Indraganti, M., Ooka, R., Rijal, H. (2012). Significance of air movement for thermal comfort in warm climates: A discussion in Indian context. *Proceedings of 7th Windsor Conference*. UK, 12-15.
- Yingxin, Z., Maohui L., Quyang Q., Huang L., Cao B. (2015). Dynamic characteristics and comfort assessment of airflows in indoor environments: a review. *Building and Environment*, 91, pp 5-14.
- CIBSE Guide Volume C. (1986). Reference data. *The Chartered Institution of Building Services Engineers*, London.
- Awbi, H. (2003). *Ventilation of Buildings*. 2 ed. London: *Spon Press*.
- Heiselberg, P. and Sandberg, M. (2006). Evaluation of Discharge Coefficients for Window Openings in Wind driven Natural Ventilation. *International Journal of Ventilation* 5(1), pp. 43-52.

Vehicular Anthropogenic Heat in the Physical Parameters of An Urban Canyon for Warm Humid Climate

RUTH M.GRAJEDA ROSADO¹, ELIA M.ALONSO GUZMAN², CARLOS J. ESPARZA LÓPEZ³

¹ Interinstitutional Program of Doctorate in Architecture and School of Architecture, Veracruzana University, Mexico

² School of Civil Engineering, Michoacán University of San Nicolás de Hidalgo, Morelia, Mexico

³ School of Architecture and University Design of Colima, Colima, Mexico

ABSTRACT: Field measurements were made in an urban canyon, located in the center of the City and Port of Veracruz, Mexico, where higher temperatures are compared to its surrounding areas. Research focused on better understanding the behavior of the microclimates of a city and its impact on thermal comfort. Temperature (T) and Relative Humidity (RH), are the variables considered to be measured by an autonomous flight system (MeVA), for the determination of the behavior of the street's thermal profile and its fluctuations due to the vehicular park that it transits. It is determined that the increase in temperature as a result of the cars increases from 3.50 to 1.50 °C, and this effect is dissipated at a height of 3 meters. The investigation allows establishing parameters of adequate control of the vehicular tributary and a better planning in the aspect ratios of an urban canyon so as not to increase the temperature and achieve hygrothermal comfort values for the pedestrian

KEYWORDS: Canyon, Vehicular, Anthropogenic heat, Parameters.

1. INTRODUCTION

The phenomenon of the Island of Urban Heat, which alludes to the rise of temperature in the internal zones, of the cities in comparison to their suburban and adjacent zones, allows the justification of the present investigation [1].

Faced with this, there is a reflection on the research that determines its causes, its measurement method, the effects of these events on the quality of human life, its mitigation strategies and its legislation, as an indicator of the sustainability of cities.

It was discovered that the factors that generate the Urban Heat Island (UHI) are the properties of the construction surfaces, the geometry and urban density, the configuration of the land use of the city, the decrease of evapotranspiration, and the heat itself generated by man, called anthropogenic heat Q_F [2].

The anthropogenic heat is divided: metabolism, industry, buildings and vehicular. The least studied is vehicular anthropogenic heat (Q_{FV}). Currently, experts such as Chow [3] and Sailor [4], seek to estimate these values in more detail for several regions and generate a database in sustainable urban planning.

In most of the investigations, the magnitude of Q_F is quantified by means of a statistical methodology, considering it as an energy consumption and dividing it in the spatial extent of the analysis area, the literature reflects data considering the four types of anthropogenic heat, so the values of the results can be very varied, the only constant is that its magnitude is inversely proportional to its scale of study. For example, at a microscale like a canyon, values of 1,590

Wm^{-2} were recorded during the winter of central Tokyo [5] and on a macroscale of 10 to 100 Wm^{-2} in Lodz, Poland [4].

By simplifying the study of the Q_{FV} variable in a microclimate, the basic urban unit "canyon" is used; According to Stromann-Andersen and Sattrup [6] we can find repetitive patterns in the measurements, which can be extrapolated to a whole.

By understanding the influence of the parameters (H= height, W= width and L= length) that make up the canyons of a city and its relationship with Q_{FV} , simultaneous planning is required, from large areas (outdoor areas, parks, squares) to smaller scale (buildings) to obtain the thermal comfort of the users, located in the canopy scale.

Using the MeVA method (Meteorological Measurement in Autonomous Flight) it was possible to obtain data in correlation to the thermal variant with the heat expelled by the cars. The reason for MeVA is to regulate the vehicular flow, as a mitigation technique to reduce heat degrees, taking into account its socioeconomic cost.

2. METHOD MeVA

The research proves the scope that can be achieved with the displacement of UAVs (Unmanned Aerial Vehicles) called "drones", in urban areas used in the collection of environmental variables. The measurements allowed to collect data in a transectional way in a "photography" type, to correlate the variables of Temperature (T) and Relative

PLEA 2018 HONG KONG

Smart and Healthy within the 2-degree Limit

Humidity (RH) with the vehicular flow that transited at the time.

Several measurements will be made in different types of canyons, to future work, in order to perform simulation scenarios with different vehicular tributaries and to compare the results obtained with MeVA, modifying the dimensions of the streets and vehicle load, being able to calculate the contributions of QFV to the microclimatic conditions of the environment.

3. BACKGROUND

The dry bulb temperature, surface temperature, relative humidity, wind speed and direction, are constants that are based on a reference frame of different climatic studies, in several cities.

In Adelaine, Australia thermal profiles were generated, by comparing an official meteorological station nearby and the streets under study [7]. Curitiba, Brazil, to evaluate the impact of street geometry with the Sky View Factor [8].

And in Serres and Athens, Greece, microclimatic conditions were analyzed in different canyons and their relationship with wind speed and direction [9].

Drone measurements have been generalized in three studies, the evaluation of air quality in pollution, the monitoring of emissions related to climate change and atmospheric measurements at the level of the stratosphere [10].

4. MeVA DESIGN

For the manufacture and systematization of the MeVA, the Arduino software was used, open source platform based on flexible hardware and software, achieving its programming through a microcontroller.

4.1 Measuring equipment

The drone used was the Phantom 3, with operating parameters of -10 to 50°C , maximum load of 500gr, maximum speed of ascent and descent of 6m/s, maximum flight speed of 10m/s and flight time of 19 minutes.

The SHT75 sensor was selected to measure the temperature and relative humidity, with an accuracy of $T=\pm 0.3^{\circ}\text{C}$ and $HR=\pm 1.8\%$, resolution of $T=0.01^{\circ}\text{C}$ and $HR=0.05\%$, response time $T=5-30\text{sec}$ and $HR=8\text{sec}$, and operating temperature from -40°C to 123.8°C [12] (Fig. 1). A serial GPS module NEO-6M was also introduced (Fig. 1), to give the information of the exact position of the measurement points to locate the data mesh.



Figure 1: Temperature and Relative Humidity Sensor (SHT75) and GPS Module (Serial NEO-6M, GY-GPS6MV2).

For the data collection, without being modified by the turbulence of the support system and rotary wing flight of the drone, a support was built in the upper part for the SHT75 sensor (Fig. 2).



Figure 2: Drone and its superior sensor support system.

4.2 Measurement protocol

With the analysis of the investigations, it was determined the measurement of T and HR in three positions, X, Y, and Z achieving a hexagonal mesh to be compared in the future with the results of a simulation. The protocol for the location of the drone was: on the X axis, three measurements, one position at 0.50 m from the west façade, one at the center and one at 0.50 m from the east façade. In Z, parallel to the pavement, three data: 1.50, 3.00 and 4.50 m, and on the Y axis, a measurement every 5m of the total length of the street (Fig. 3).

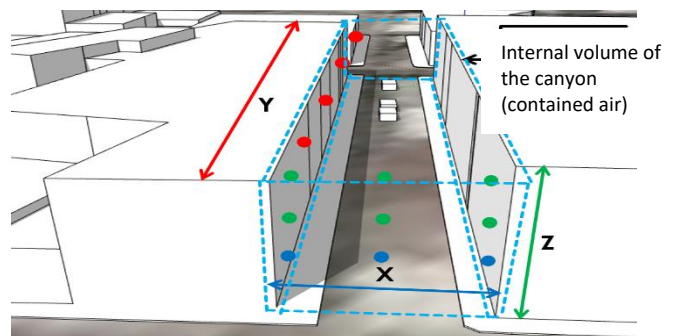


Figure 3: Three-dimensional drone position of the barrel, X (Width = W), Y (Length = L) and Z (Height = H).

It is crucial to clarify that the measurement taken at 1.5m height was made with Hobo Data Logger sensors, by means of a walking and vehicle route.

The study period was during the month of May, at the beginning of high temperatures and with less eventualities of rain and strong winds, you qualify colloquially as the "veranito".

At the proposal of Sailor [12], there must be detailed information on the number of vehicles, their typology and the estimate of the hourly speed. The vehicular tributary that the study canyon presented during the field measurement was monitored at fixed control points.

PLEA 2018 HONG KONG

Smart and Healthy within the 2-degree Limit

5. CASE STUDY

The investigation is carried out in the city and port of Veracruz (Latitude: 19°10'51"N, Longitude: 96°08'34"W and Altitude above sea level of 15m) located in the Gulf of Mexico, with a tropical climate type Aw2 (warm humid greater than 55.3% RH) by the Köppen-Geiger and average annual precipitation of 1516mm focused in summer.

Its weight of study is due to the rise in temperature of 0.59°C per decade (Fig. 4) presented by the city, according to the analysis of the data obtained from the Regional Hydrometeorological Center above the statistical trend of the large settlements in Mexico [13].

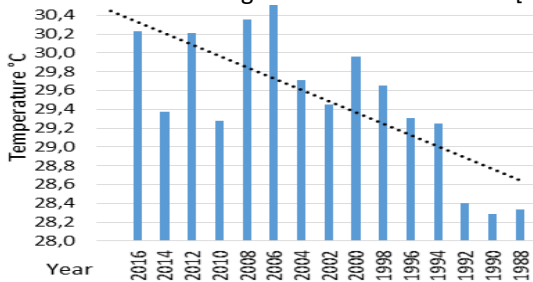


Figure 4: Tendencies of average annual temperature from 1986 to 2016, data provided by the Regional Meteorological Center.

The population statistics data, according to the ONU [14], is 552,156 inhabitants with an urbanization index of 94.76%, a total area of 245.90 km², with a population density of 2,379 inhabitants/km² and a housing density of 1,098 per km². The city has several urban sectors, originated by its economic development (industrial, port and tourist) and social typology (regular and irregular settlements). Figure 5 allows to clarify the type of city where the study area is immersed.

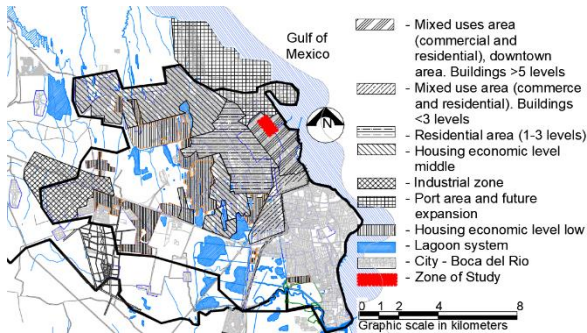


Fig. 5. City map of the urban typology. Modified from the official map of the municipality of Veracruz

The study microscale was Avenue Independencia (Fig.6 and 7), located in the center of the city.



Figure 6: Photograph of Avenue Independencia

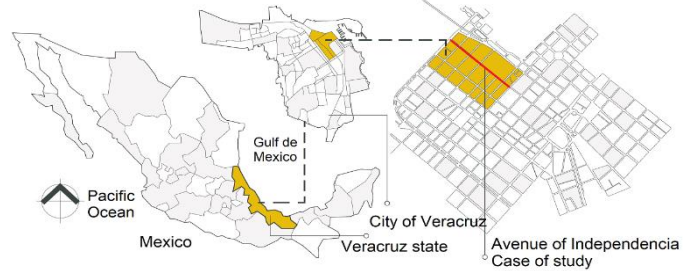


Figure 7: Location map of the avenue, Veracruz, Veracruz, Mexico.

Avenue selected according to:

Preliminary study carried out in the city [15], indicating the presence of a high isotherm during the UHI phenomenon at 1:00 pm in May; construction materials used in façade and floor coverings: waterproof and with a high radiation absorption capacity (concrete and masonry); city traffic analysis [16]; and study of the aspect relationships of the streets that make up the avenue.

The study canyon has a length (L) of 750m distributed in 12 blocks (Fig. 8) and 11m wide (W). The sidewalks are 1.25m; the road is distributed in three lanes of 3.8m each; two for movement and one destined for parking. The canyon has an N-S orientation, therefore, the façades of the buildings are oriented towards the E and W.

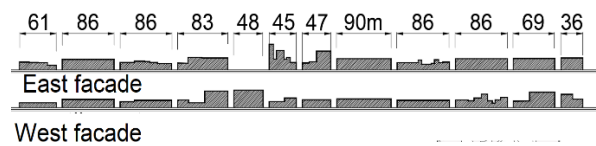


Figure 8: Profiles of Independencia Avenue in meters

Analyzing the measurements, the aspect ratios are obtained, according to the classification of Vardoulakis et al. [17], where a deep canyon equals $H/W \Rightarrow 2$ and long $L/H \Rightarrow 7$ (Table 1).

Table 1: Aspect Relations and general observations

Street	H/W	L/W	Observation
1	Semi-Deep	Medium	Asymmetric
2	Uniform	Long	Asymmetric
3	Uniform	Long	Symmetric
4	Uniform	Long	Symmetric
5	Deep	Medium	Asymmetric and green area
6	Deep	Medium	Asymmetric

PLEA 2018 HONG KONG

Smart and Healthy within the 2-degree Limit

7	Uniform	Medium	Asymmetric
8	Uniform	Long	Asymmetric
9	Uniform	Long	Symmetric
10	Uniform	Long	Symmetric
11	Deep	Medium	Asymmetric
12	Uniform	Short	Symmetric

6. DATA COLLECTED

The data reached for the investigation were on days 19 and 20 (Saturday and Sunday) of May 2018. On the 19th, a vehicular tributary of 12 cars per minute is presented at a speed of 40 km/hr (average) and on the 20th a traffic of 6 cars per minute at 40 km/hr at a time of 13:30 to 14:30 hours.

The general temperatures registered in the city during the days were of 32°C of temperature with 70% RH, reached a thermal sensation of 36°C. The collection started at 13:30 hours, however, during the process, the west facade had shade and the east facade a 30-minute solar exposure. The wind speed was 1.5m/s with an S-N direction, at the end of the streets there was an incoming wind turbulence movement with an E-W orientation and a velocity of 2.0m/s.

The results of both variables are exemplified in the 3D surface graphs at a height of 1.5m and 3.0m. On the Z axis, the T and HR is plotted, on the X axis it represents the length in meters of the entire avenue and the Y is the width of the street, locating the three measurements. From the results with the thermal data, the following relationships were interpreted:

At the height of 1.50 m with a traffic of 12cars/min, the highest point of temperature is in the eastern facade, due to the solar radiation of the afternoon, however, there is a peak in the center of the canyon. In this case, the temperatures showed a greater oscillation, between 32 and 36.5°C on the sides of the sidewalks (Fig. 9).

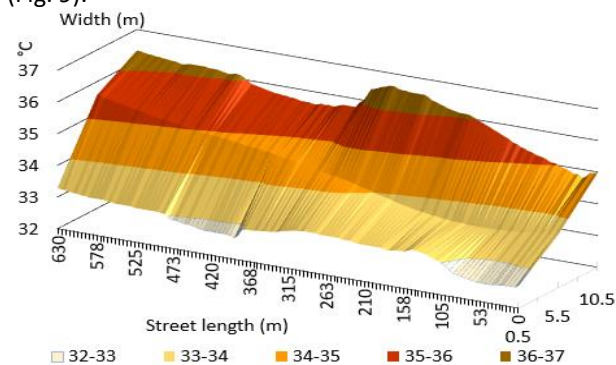


Figure 9: Thermal profile at 1.50 m and traffic of 12 cars / min

At the height of 1.50 m with a traffic of 6 cars/min, the highest point in temperature is in the center of the street; with variations of 1.5°C with respect to the western facade and 1°C to the east, determining that the increase in temperature in the center is a

consequence of the pavement (concrete), increased to 3°C the microclimate of the canyon (Fig. 10).

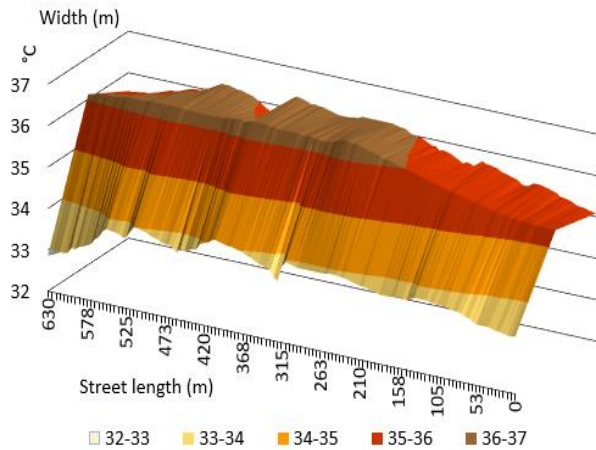


Figure 10: Thermal profile at 1.50 m and traffic of 6 cars / min

At 3.00 m high, with traffic of 12 cars/min, the temperature is lower at the midpoint, and its difference with the temperature of the extremes is from 1.50 to 2.5°C; possible caused by the wind current generated by the cars with a direction towards the ends of the barrel (Fig. 11).

At 3.00 m high, with traffic of 6 cars/min, the high temperature points were found in the eastern facade, however their difference is not so pronounced, and becomes almost stable. In this case, the difference between the rise is almost 1.5°C (Fig. 12).

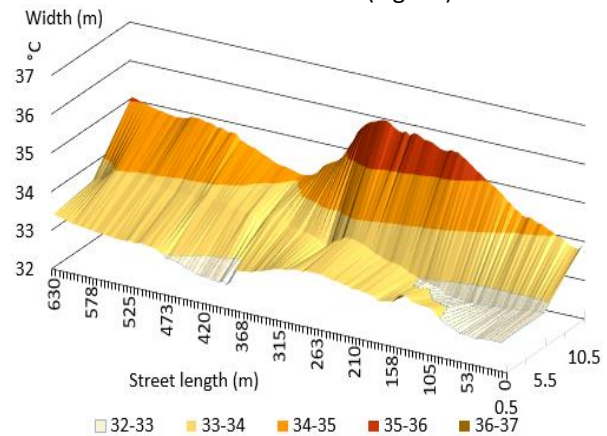


Figure 11: Thermal profile at 3.00 m and traffic of 12 cars / min

PLEA 2018 HONG KONG

Smart and Healthy within the 2-degree Limit

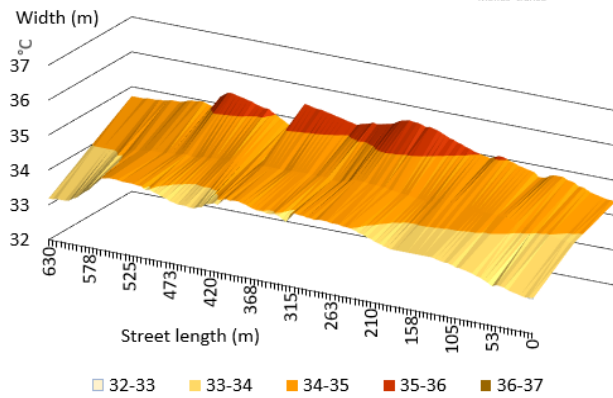


Figure 12: Thermal profile at 3.00 m and traffic of 6 cars/min

From the results with the data, the following relationship of the variables was interpreted: relative humidity and vehicular traffic:

With a traffic of 6 cars/min, the lowest HR measurement is located in the center of the street, at a height of 1.5m, HR = 58% and 3.0m, HR = 64%. On the sides, higher HR is present, at 1.5m the value is 66% and at 3.0m it is equal to 68% (Fig. 13 and 14). With a traffic of 12 cars / min, the HR charts are more stable, especially at a height of 3.0m with almost no difference (Fig. 15 and 16).

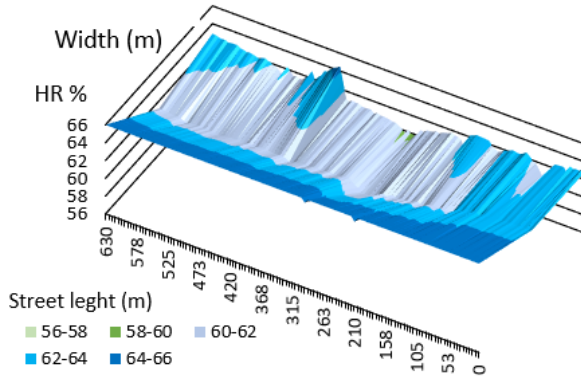


Figure 13: Profile of HR at 1.50 m and traffic of 6 cars/min

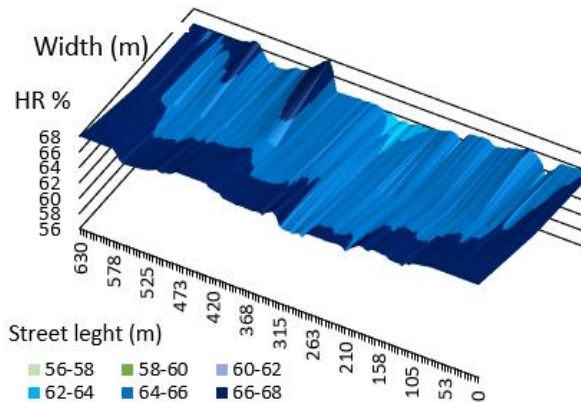


Figure 14: Profile of HR at 3.0 m and traffic of 6 cars/min

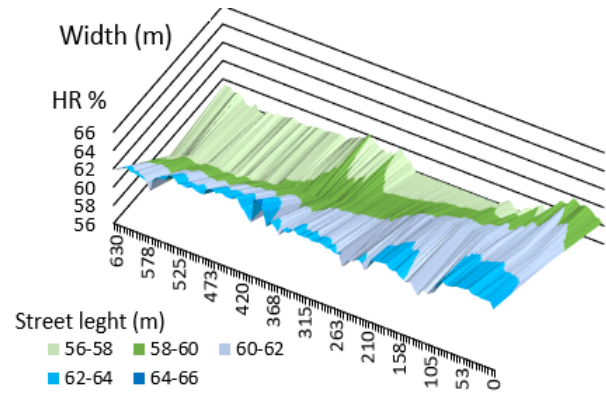


Figure 15: Profile of the HR at 1.50 m and traffic of 12 cars/min

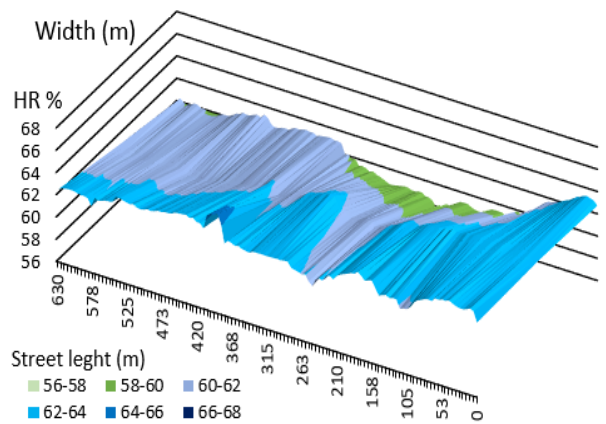


Figure 16. Profile of HR at 3.00 m and traffic of 12 cars/min

7. CONCLUSION

The coastal human settlements have an intensity of Urban Heat Island weaker in relation to cities far from the sea, due to the sea breeze, which cools the environment [18].

Such characteristic "marine breeze" forces the investigation, to determine the affectation of the vehicular flow with the variables T and HR, presented in the guns, whose effects are perceived by the population in its thermal comfort.

The results determine that the temperature in the center of the canyon is higher, when there is less automobile movement per minute. From this statement it can be added that vehicles at speeds under 40km/h or stationary traffic creates a halo of heat around cars that expands as sensible heat.

With a traffic of 12 vehicles per minute in constant motion, the highest temperatures recorded in the field investigation, occurs on the sidewalks, because the vehicular tributary in its transfer, creates air currents dissipating it and therefore directly affecting to passers-by.

There is the possibility that parked vehicles generate more heat than those that are in motion, because their sheeting tends to reflect and increase more heat.

PLEA 2018 HONG KONG

Smart and Healthy within the 2-degree Limit

In relation to the validity of the temperature results, from Stefan Boltzman's radiation formula, considering an emittance of 0.58 (average of the surfaces of the car) [19], a surface temperature of 95°C (internal combustion engines) [20] and the ambient temperature of the present study (32°C), a value of 318 Wm⁻² is obtained, close to the vehicular anthropogenic heat flow of 301 Wm⁻² achieved through the investigation of Sailor and Lu [12] for the city of Houston, Texas in summer.

The results show the impact of the need to plan the geometry of the streets in the future; and in cases where it is no longer feasible, the authority must adapt urban mobility to regulate the vehicular fluidity that affects the hygrostatic comfort of the transient.

The investigation opens the subsequent analysis of mitigation techniques such as the temporary closure of streets or the design of passive devices. If the horizontal elements are designed for shading, it is important to consider that in addition to mitigating the radiation in bystanders, it must allow the expulsion of heat and humidity generated by the combustion of the engines.

ACKNOWLEDGEMENTS

Interinstitutional Program of Doctorate in Architecture, Institute of Engineering of the Universidad Veracruzana, Institute of Micro and Nanotechnology of the Universidad Veracruzana, Regional Hydrometeorological Center and the Municipality of Veracruz.

REFERENCES

1. Santamouris, M., Synnefa, A., & Karlessi, T. (2011). Using advanced cool materials in the urban built environment to mitigate heat islands and improve thermal comfort conditions. *Solar Energy*, 85(12): p. 3085-3102.
2. Gartland, L. (2008). *Heat Islands, Understanding and mitigation heat in urban areas*. New York: Earthscan from Routledge.
3. Chow, W., Salamanca, F., Georgescu, M., Mahalov, A., Milne, J., & Ruddell, B. (2014). A multi-method and multi-scale approach for estimating city-wide anthropogenic heat fluxes. *Atmospheric Environment*, 99: p. 64-76.
4. Sailor, J., Georgescu, M., Milne, J., & Hart, M. (2015). Development of a national anthropogenic heating database with an extrapolation for international cities. *Atmospheric Environment*, 118: p. 7-18.
5. Ichinose, T., Shimodozono, K., & Hanaki, K. (1999). Impact of anthropogenic heat on urban climate in Tokyo. *Atmosphere Environment*, 33, 3897-3909.
6. Stromann-Andersen, J., & Sattrup, P. (2011). The urban canyon and building energy use: Urban density versus daylight and passive solar gains. *Energy and Buildings*, 43(8): p. 2011-2020.
7. Errell, E., & Williamson, T. (2006). Simulating air temperature in an urban street canyon in all weather conditions using measured data at a reference meteorological station. *International Journal of Climatology*, 26, 1671-1694.
8. Krüger, E., Minella, F., & Rasia, F. (2011). Impact of urban geometry on outdoor thermal comfort and air quality from field measurements in Curitiba, Brazil. *Building and Environment*, 46(3), 621-634.
9. Dimoudia, A., A., K., Z. S., Pallas, C., & Kosmopoulos, P. (2013). Investigation of urban microclimate parameters in an urban center. *Energy and Buildings*, 64, 1-9.
10. Villa, T., Gonzalez, F., Miljevic, B., Ristovski, Z., & Morawska, L. (2016). An Overview of Small Unmanned Aerial Vehicles for Air Quality Measurements: Present Applications and Future Prospective. *MDPI Journal: Sensors*, 16(7). Doi: 10.3390/s16071072.
11. Newark. (2018). On line: www.newark.com/sensirion. <http://mexico.newark.com/sensirion/sht75/humidity-temperature-sensor/dp/18M2988?CMP=KNC-GUSA-GEN-KWL->
12. Sailor, D., & Lu, L. (2004). A top-down methodology for developing diurnal and seasonal anthropogenic heating profiles for urban areas. *Atmospheric Environment*, 38: p. 2737-2748.
13. Jáuregui, E. (2005). Possible impact of urbanization on the thermal climate of some large cities of Mexico. *Atmosphere*, 18(4), 249-252.
14. ONU Hábitat. (2016). Índice básico de las Ciudades Prósperas City Prosperity Index, CPI, Informe Final Municipal. Veracruz: ONU Hábitat.
15. Baca, C. A. (2011). Identificación y Comportamiento de la Isla de Calor en la zona conurbada de Veracruz - Boca del Río en el año 2011. Universidad Veracruzana.
16. INECC, I., DGICUR, D. U., & DICA, D. I. (2012). Estudio de emisiones y actividad vehicular en el puerto de Veracruz Ver. Reporte Final. Ciudad de México: SEMARNAT Secretaría de Medio Ambiente y Recursos Naturales.
17. Vardoulakis, S., Fisher, B., Pericleous, K., & Gonzalez-Flesca, N. (2003). Modelling air quality in street canyons: a review. *Atmospheric Environment*, 37: p. 155-182.
18. Y. Sakakibara, K. Owa (2005). Urban-rural temperature differences in coastal cities: influence of rural sites, *Int. J. Climatology*, 25 (6): p. 811-820.
19. Levinson, R., Pan, H., Ban-Weiss, B., Rosado, P., Paolini, R., Akbari, H., (2011). Potential benefits of solar reflective car shells: Cooler cabins, fuel savings and emission reductions. *Applied Energy*, 88: p. 4343-4357
20. Volkswagen do Brasil (2012) Manual de Instruções

Smart and Healthy Buildings Factor of Reality: A Comparative Analysis of Green Buildings Performance between Design Predictions and Actual Performance

IHAB M.K. ELZEYADI¹

¹High Performance Environments Lab, University of Oregon, Eugene, USA

ABSTRACT: The US Green Buildings Council (USGBC) has created a market transformation program led by a certification process to promote, build, and renovate buildings into LEED™ rated green facilities. One of the goals of the LEED rating system is to reduce carbon and energy expenditure in buildings while improving occupant's health and wellbeing. Due to a lack of systemic evaluation of buildings undergoing this certification process, however, the effects of this program on building resource utilization, indoor comfort, and occupant's well-being remain contested. This paper reports on a cross-sectional survey study that investigates discrepancies between LEED certified buildings credits achieved as well as predicted and actual performance. The survey assessed 14 buildings, matched in pairs of two, of LEED and non-LEED buildings. Resource consumption and indoor environmental quality were assessed between both building pairs and their relationship to the LEED certification credits achieved. Results show that while LEED buildings outperformed their non-LEED comparatives, their resource consumption, however, exceeded their predicted expectations in most categories. In addition, the amount of credits achieved were not directly related to better performance. The paper concludes with a framework to integrate occupant feedback and building performance into the way we design, deliver, and operate buildings.
KEYWORDS: LEED™ Buildings, Certification Credits, Simulations, Performance Evaluation, Occupant's Comfort

THE GREEN BUILDINGS GAP

Between the idea... and the reality
Between the motion... and the act
Falls the Shadow
T.S. Elliot, 1925

The demands placed on green buildings, such as Leadership in Energy and Environmental Design (LEED™) certified buildings are significant. Using less energy and resources, they are expected to provide superior indoor environmental quality (IEQ) for occupants that meets or exceeds industry-standard for thermal, lighting, ventilation, acoustics, and indoor air quality. Despite the favorability of these objectives, most recent studies have failed to prove these linkages leading to a non-conclusive evidence of green building performance and its positive triple bottom-line impact on the environment. Among the problems reported in green buildings performance are discrepancies between predicted design simulation and actual building performance (1,2,3). Bordass et al. (12) suggest that "credibility gaps" are not necessarily due to mistakes but rather assumptions made at the design stage.

Previous limitations point to methodological deficiencies in quantifying occupant's experience, as well as a lack of studies to compare simulated energy and resource consumption to actual measured performance (6, 12, 13). The problem is magnified as

many of the LEED™ buildings aren't evaluated systematically in longitudinal studies that go beyond a point-in-time measurement. Akerstream et al. (14) points out that most green building rating systems such as LEED™ have focused on predicted performance at the design stage. Delivered performance is rarely voluntarily verified by building owners. The specific question of this paper is whether a well-planned evaluation study comparing LEED™ certified buildings design simulation data to post-occupancy actual performance would reveal gaps in knowledge about how we can design, operate, and behave in green buildings to achieve a smarter and healthier planet. Of equal interest is to investigate whether earning certain LEED™ certification credit related to energy performance, water consumption, and sustainable site credits would predict actual energy, water, and carbon expenditures and emissions of the final building as compared to the predicted scores or the LEED™ credits achieved.



PLEA 2018 HONG KONG

Smart and Healthy within the 2-degree Limit

Figure 1: comparative research settings of LEED™ certified buildings evaluated for the study

This paper reports on a state-of-the-art cross-sectional survey study quantifying resource consumption and building performance impacts of LEED credits achieved, simulated and actual energy performance, as well as IEQ occupant's experience inside 14 high performance buildings, 50% of which are LEED™ Gold or Platinum certified buildings (fig. 1). The study attempts to quantify an important yet not scientifically proven assumption concerning the relationship between green building certification and actual building performance and its impacts on the triple bottom line of people, planet, and profit. The specific hypothesis tested is whether LEED credits related to energy and water consumption as well as indoor environmental quality could have a relationship to designers predicted performance. A related question is what can we learn from the gaps between predicted and actual performance that would guide us into designing smarter buildings with better design expectations in the future? This is an objective to answer and quantify a long debated hypothesis regarding the importance of green buildings and LEED credits earned on the triple bottom line impacts for people, planet, and profit.

2. GREEN BUILDINGS PERFORMANCE EVALUATION

This project conceptualized green certified buildings from a place-based experience perspective. This conceptualization (Figure 2) relies on the general assumption that any environment is composed of "people" and "buildings" on the macro-scale as well as "buildings" and the overall "environment" on the mega-scale (Elzeyadi, 2003). This framework grows out of a perspective that treats occupants and their environments as interdependent elements of a system. This systems epistemology rests on the idea that the environment is an organic structure; it has parts that are connected to each other by complex interactions in a way that smaller parts of the system can be identified. In this regard, a comprehensive Building Performance Evaluation (BPE) would evaluate a building through its life cycle from design stages to certification and post-occupancy evaluation (POE). It also assess multi-dimensions of a building performance including; energy consumption, water usage, sustainable sites performance, transportation energy expenditures, indoor environmental quality, occupant's multi-comfort, and Green House Gas (GHG) emissions.

Comprehensive BPE

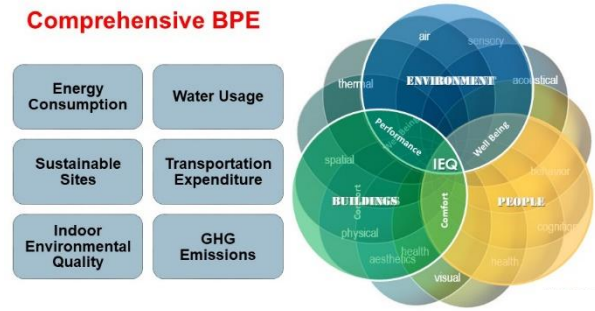


Figure 2: Comprehensive BPE framework for the study

3. A CROSS-SECTIONAL COMPARATIVE STUDY

A market transformation program led by the US Green Buildings Council (USGBC) has been influential in setting certification process to promote, build, and renovate schools into LEED™ rated green facilities. One of the goals of the LEED rating program is to improve carbon and energy expenditure in buildings while improving occupant's health and wellbeing. Due to a lack of evaluation and assessment of this certification program, however, the effects of these guidelines on building resource utilization, and occupant's health and behavior remain contested. This gap in knowledge related to green buildings performance studies could result in a low market penetration of these strategies in new building construction, in general, as well as LEED and green buildings in particular.

This paper reports on a comprehensive multi-year comparative study evaluating the performance of 14 LEED and non-LEED buildings in the USA Pacific Northwest region and its sub-climate zones. For the first systematic study of this scale, we assessed LEED credits earned, land use, sustainable site variables, and indoor environmental quality together with their impact on simulated and measured resource consumption and operations data, carbon expenditure and occupant's energy behaviors and performance. To control for organizational and economic variables, the comparative study explored educational and non-profit building types within the same sub-climates to control for climatic, organizational, as well as socio-economic disparities between buildings. Comparative buildings were matched for their size, location, organizational culture, building type, geographic location and Full-time occupancy equivalent (FTE).

The study used a comparative survey research design using the buildings' physical assessments, LEED submittal documentation, simulated energy and water consumption calculations, energy and water metered consumption surveys from the buildings, utility bills, mapping and Geographic Information Systems (GIS) analysis, transportation energy intensity metrics, and

PLEA 2018 HONG KONG

Smart and Healthy within the 2-degree Limit

occupant's surveys of the indoor environmental quality (IEQ) perceptions of their buildings to gather actual performance data and multi-comfort perceptions of their performance. In addition, on-site observations and tallying of transportation behavior was also conducted and compiled. The diverse methods enhanced the research's external and internal reliability and provided rich data that could cover the phenomena under study from different perspectives and viewpoints. The implemented methods aim to exemplify a model and state of the art for building performance evaluation studies. The multi-phase research design facilitated a grounded theory approach where the results of each phase informed and focused the direction of investigation and provided action items and design patterns for the development of the evidence-based design guidelines (Figure 3).

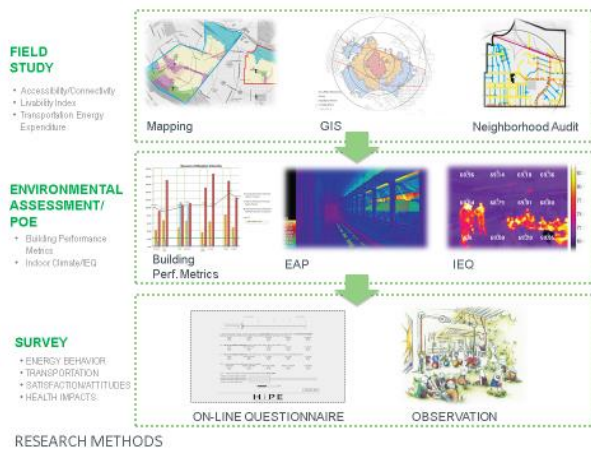


Figure 3: Multi-Methods approach and instruments employed

The research setting consisted of 14 buildings, 50% of which were LEED certified gold or platinum, in a 2x2 comparative analysis. Each LEED certified building was matched to another non-LEED building within the same context and typology with careful attention to maintaining similar numbers of occupants, organizational factors, cultural use of space, socio-economic variables, and hours of operations between each member of the pair. The buildings studied were carefully matched to control for variables related to their social, organizational, and economic environments, leaving the physical characteristics of the environment to vary between and within LEED and non-LEED certified buildings.

4. RESULTS: GREEN BUILDINGS IN THE BALANCE

Univariate statistical analysis was performed on the data to uncover actual performance trends of LEED buildings compared to simulated consumption predictions, comparative non-LEED buildings, LEED credits achieved in comparative categories, and reference standards.

4.1 Energy Utilization Index (EUI) with Energy & Atmosphere credits

Net-metered site EUI metric in KBTU/Sq. ft./year was calculated for each building based on yearly metered total energy consumption from multiple fuel types (electricity, gas, chilled water, steam, etc.). Energy produced on site integrated to the building, such as energy produced from building integrated photo voltaic cells were subtracted from the consumption as a credit (net-metered). In addition, comparative base line from the Commercial Buildings Energy Consumption Survey (CBECS) data base was computed as a median building and based on this an Arch 2030 target was computed (70% reduction from baseline). Results differed markedly, between predicted simulations EUI and other comparatives to the actual building performance (Figure 4). In general LEED certified buildings out performed comparative non-LEED buildings and consumed 20-50% less energy, with the exception of one case LEED #4 consuming 40% more energy over the comparative non-LEED school. Similarly all LEED buildings, except LEED #4, outperformed the median comparative building from the CBECS data base (red dots, Fig. 4). Most LEED buildings surveyed, however, did not meet their predicted simulated goals not the Arch 2030 target (orange dots, Fig. 4).

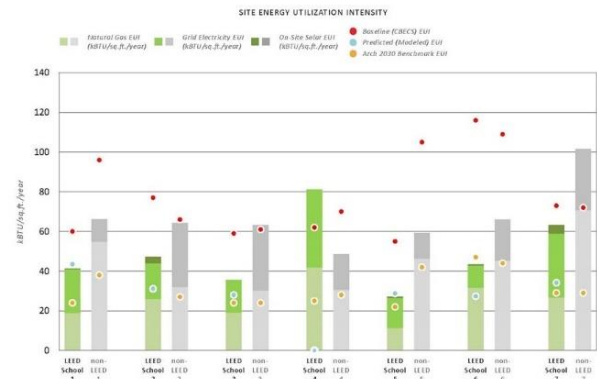


Figure 4: Site Energy Utilization Intensity (EUI) across the 14 buildings surveyed (Green: LEED, Gray Non-LEED actual performance compared to simulated values in blue dots)

In most cases this gap in performance shown LEED buildings surveyed consuming 10-35% more than their simulation predictions and 20-60% more over their Arch 2030 targets, with the exception of one building LEED #5 that met its simulation predictions and is also close to the Arch 2030 target. Achieving more LEED credits in the Energy and Atmosphere was in agreement with better energy performance in buildings achieving 90-100% of the credits. Similarly, achieving very few LEED credits in this category reflected poorly in energy performance, e.g. LEED #4 (Figure 5).

PLEA 2018 HONG KONG

Smart and Healthy within the 2-degree Limit

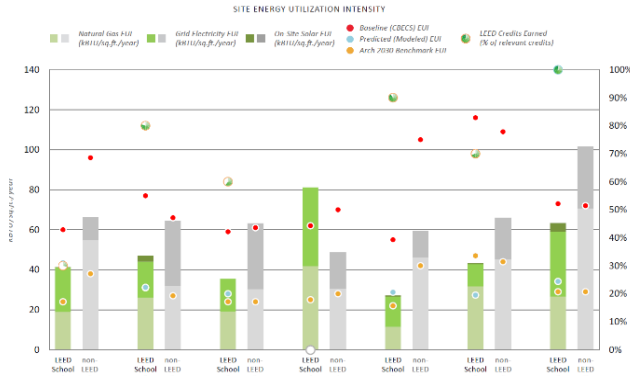


Figure 5: Site Energy Utilization Intensity (EUI) across the 14 buildings surveyed in relation to LEED credits achieved for Energy and Atmosphere category

4.2 Water Use Index (WUI) with Water & Waste Credits

Metered water consumption from utility bills of the buildings surveyed was compared to estimated water budgets from LEED documentation submissions as well as national averages of facility types based on the US Federal Energy Management Program (FEMP) data base and FEMP benchmark of 20% reduction in use.

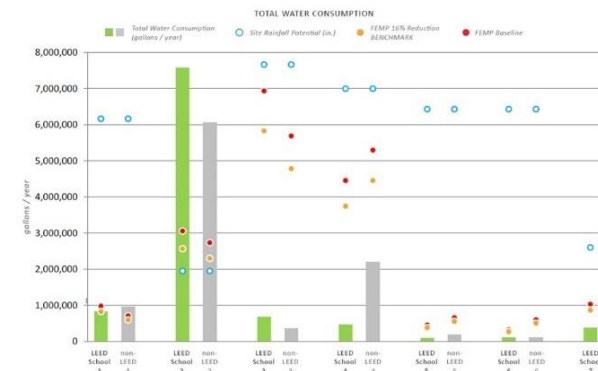


Figure 6: Water Use Intensity (WUI) across the 14 buildings surveyed in relation to simulated performance and LEED credits achieved for Water and Waste categories

In general most LEED buildings performed well and consumed less water than their estimated budgets, with the exception of LEED #2 building due to excessive landscaping dishwashing as this building eliminated all disposable cups and plates from use in their cafeteria. (Figure 6). With regard to comparing their performance against non-LEED buildings, the differences in WUI of LEED and non-LEED buildings is trivial, with some non-LEED buildings even outperforming LEED ones. This might be due to the fact that federal regulations and innovation in water conserving fixtures have become mainstream practice and accessible technology across all building types.

4.3 Land Use, Transportation expenditures, and Sustainable Sites Credits

Sustainable site amenities were collected using GIS mapping data and site surveys. The study investigated the impact of the physical environment of LEED building sites and their surrounding neighborhoods by relating their degree of availability and the number of sustainable site LEED credits earned to commuting behavior, energy and carbon expenditures of the buildings sites. Following a triangulation of research methods and an extensive data collection and analysis procedures, the study's results positively supported a relationship between livability changes in the built environment and their influence on active travel patterns. Even though there was no clear pattern of difference in activities between the groups of LEED and non-LEED buildings, there were numerous associations of activity with other LEED credits earned that are specific to sustainable sites (Figure 7).

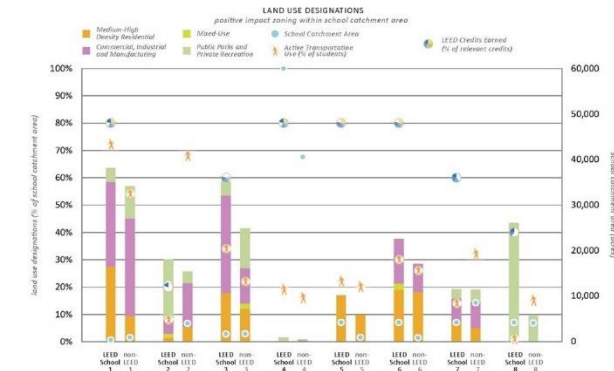


Figure 7: Land use and sustainable sites amenities across the 14 buildings surveyed, active modes of transportation, engineering interventions, and LEED credits

The differences are not trivial, especially with respect to the site boundary areas, suggesting that smaller boundary areas--of building types such as schools--within the 0.5 mile radius are attributed to increased active transportation. As would be expected, most of the measures related to the walkability of surrounding streets were associated with the percentage of travel that was active. Active travel was more common in sites with transportation engineering interventions in the form of easier to navigate intersections for street widths between 20'-28', more medians, roundabouts, islands, and pinch-points and curb extensions. Dead-ends streets show lower connectivity rates of the neighborhoods and reduced walkability and bicycling behavior. It is interesting to note that these sites have earned higher walkscores and were associated with better performing LEED buildings. Active travel was also more common in sites that include more amenities and support for pedestrians including more marked crosswalks at 0.5 miles, bike/pedestrian signals, bike racks, bus shelters, and bus stops that were all associated with more active travel. It is interesting to note that the study also confirmed previous findings regarding the positive relationship

PLEA 2018 HONG KONG

Smart and Healthy within the 2-degree Limit

between active transportation and certain land use zoning. Active travel was less in neighborhoods with low density residential, light industrial, agricultural or un-zoned areas. Active transportation benefited from livability metrics on the neighborhood scale such as more planters, attractive architecture, art and activities, fewer fire and hospital facilities, more benches for sitting, and more animals. The better performing buildings sites in terms of active transportation patterns show strong relationship to the presence of physical indices related to street connectivity and livability metrics in addition to LEED Sustainable Sites credits earned. This could suggest the possibility of additional inputs to the Sustainable Sites credits of the LEED certification (Figure 8).

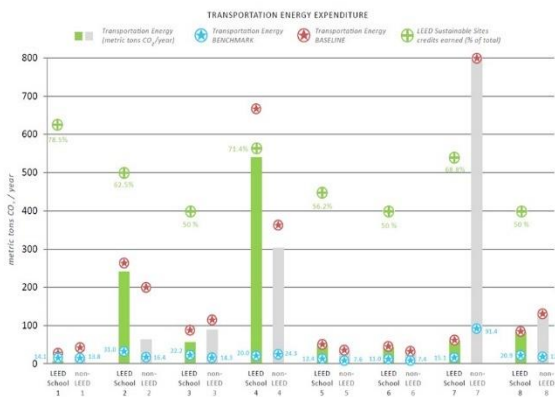


Figure 8: Transportation Energy Expenditures (TEE) across the 14 buildings surveyed in relation to LEED credits achieved for Sustainable Sites category

4.4 Indoor Environmental Quality (IEQ) Perceptions and Achieved Credits

IEQ perceptions—of visual, thermal, acoustical, indoor air, ergonomics, views, spatial, security, privacy, and way finding across the surveyed buildings were compiled and represented by a single metric representing occupant’s complains towards the building multi-comfort sub-systems on a scale of 0-100, with zero representing total IEQ satisfaction and zero complaints and a score of 100 representing occupants complains across all sub-systems of IEQ. While in general LEED buildings were perceived to have a better IEQ over non-LEED buildings, there was no significant relationship between the numbers of IEQ credits achieved and better perception of IEQ parameters (Figure 9).

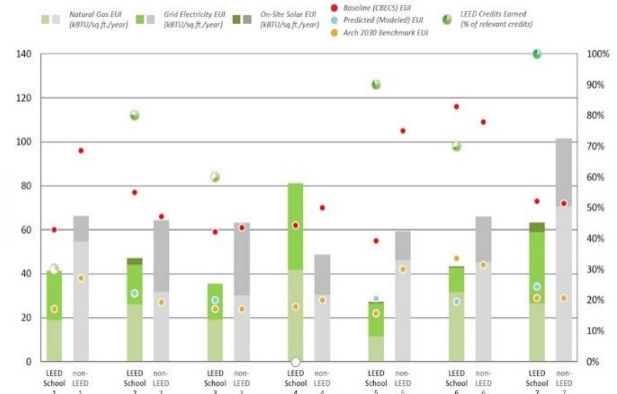


Figure 9: Indoor Environmental Quality Perceptions as compared to IEQ LEED credits achieved

4.5 Carbon Emissions Comparatives

Energy, water, and transportation energy expenditures of the sampled buildings surveyed were converted to tons of CO2 emissions equivalency to evaluate the impacts of LEED and non-LEED buildings on the environment and climate change. Results show that although LEED certified buildings might consume less energy and water, their locations in areas that are typically new and less developed might lead to high transportation energy expenditures. Similarly, the building’s foot print and parking availability affected transportation patterns with smaller footprint, built up and paved areas showing positive relationships with lower levels of CO2 emissions. This impacted overall positive performance of green buildings and resulted in less favorable performance of LEED certified buildings sampled on overall carbon emissions (Figure 10).

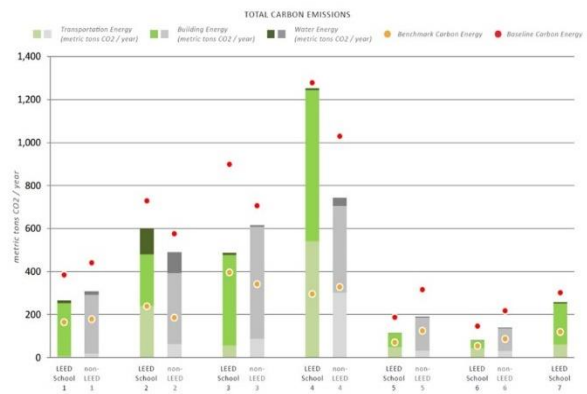


Figure 10: Total carbon emissions across the 14 buildings surveyed in relation to Arch 2030 projections

5. CONCLUSIONS: Green Buildings Factor of Reality (FR)

The paper reports on the findings from a comparative case study analysis of building performance data across the 14 LEED certified and non-LEED buildings. The aim is to provide a realistic picture of the impact

PLEA 2018 HONG KONG

Smart and Healthy within the 2-degree Limit

of green building certification on the triple bottom line approach of people, planet, and profit. A building performance evaluation is not complete without a look at objective and subjective measures of performance for both buildings and their occupants. By comparing results with original design goals, the paper shed light on the importance of collecting occupant data and thoughts on ways to integrate occupant feedback and building performance into the way we design, deliver, and operate buildings.

Resource consumption in terms of energy, water, transportation expenditures, as well as indoor environmental quality was assessed between both building pairs and their relationship to the LEED certification credits achieved. Results show that while LEED buildings, in general, outperformed their non-LEED comparatives, their resource consumption, however, exceeded their predicted expectations in most categories. In addition, the amount of credits achieved were not directly related to better performance unless the building achieved most credits in the respective category. It should be noted that achieving some minor credits in each category might also result in lower performance buildings than traditional comparative non-LEED buildings (such as case study #4). This information will be invaluable to green buildings designers and planning professionals in designing future buildings that aim to balance high performance with occupant's satisfaction and environmental stewardess.

ACKNOWLEDGEMENTS

The author would like to thank former graduate students and HiPE lab research assistants; Caitlin Milton, Shane, O'Neil, and Hadis Hadipour involved in the data collection of this study. Special thanks are also due to the facility managers in the LEED and non-LEED buildings surveyed for supporting this study's tasks.

REFERENCES

Cao, B., Ouyang, Q., Zhu, Y., Huang, L., Hu, H., & Deng, G. (2012). Development of a multivariate regression model for overall satisfaction in public buildings based on field studies in Beijing and Shanghai. *Building and Environment*, 47(1), 394–399.

Chiang, C. M., & Lai, C. M. (2002). A study on the comprehensive indicator of indoor environment assessment for occupants' health in Taiwan. *Building and Environment*, 37(4), 387–392.

Chinazzo, Giorgia; Wienold, Jan; Andersen, M. (2016). A preliminary study on the sensitivity of people to visual and thermal parameters in office environments. In *Proceedings of 9th Windsor Conference: Making Comfort Relevant*. Windsor, UK.

Elzeyadi, I. (2012). Post-occupancy evaluation: A design, operations and performance assessment of a LEED Platinum building." *World Health Design Journal*. January 2012, pp. 60–69.

Elzeyadi, I. (2015). A Tribute to Performance Arrows: Designing for Better Indoor Environmental Quality. In: *Thought and Leadership in Green Buildings Research*. Greenbuild 2015: Monumental Green. Washington, DC: USGBC Press.

Elzeyadi, I. (2017). A Comparative Analysis of Predictive and Actual Performance of High Performance LEED Buildings. In W. Prieser, U. Schramm & A. Hardy (eds.), *Building Performance Evaluation: From Delivery Process to Life Cycle Phases* (Second Edition). NY: Springer.

Frontczak, M., Schiavon, S., Goins, J., Arens, E., Zhang, H., & Wargocki, P. (2012). Quantitative relationships between occupant satisfaction and satisfaction aspects of indoor environmental quality and building design. *Indoor Air*, 22(2), 119–131.

Gou, Z., Lau, S. S.-Y., & Shen, J. (2012). Indoor Environmental Satisfaction in Two LEED Offices and its Implications in Green Interior Design. *Indoor and Built Environment*, 21(4), 503–514.

Heinzerling, D., Schiavon, S., Webster, T., & Arens, E. (2013). Indoor environmental quality assessment models: A literature review and a proposed weighting and classification scheme. *Building and Environment*, 70, 210–222.

Humphreys, M. A. (2005). Quantifying occupant comfort: Are combined indices of the indoor environment practicable? *Building Research and Information*, 33(4), 317–325.

Kim, J., & Dear, R. De. (2012). How does occupant perception on specific IEQ factors affect overall satisfaction? In *7th Windsor Conference: The changing context of comfort in an unpredictable world* (pp. 12–15). Windsor, UK.

Lai, J. H. K., & Yik, F. W. H. (2007). Perceived Importance of the Quality of the Indoor Environment in Commercial Buildings. *Indoor and Built Environment*, 16(4), 311–321.

Leder, S., Newsham, G. R., Veitch, J. A., Mancini, S., & Charles, K. E. (2016). Effects of office environment on employee satisfaction: A new analysis. *Building Research and Information*, 44(1), 34–50.

Marino, C., Nucara, A., & Pietrafesa, M. (2012). Proposal of comfort classification indexes suitable for both single environments and whole buildings. *Building and Environment*, 57(December 2002), 58–67.

Wong, L. T., Mui, K. W., & Hui, P. S. (2008). A multivariate-logistic model for acceptance of indoor environmental quality (IEQ) in offices. *Building and Environment*, 43(1), 1–6.

Effects of Urban Space Opening Layouts on Pedestrian-level Wind Conditions

WEI YOU¹, LIAN TANG¹, WOWO DING¹

¹ School of Architecture and Urban Planning, Nanjing University, Nanjing, China

ABSTRACT: This research aims to provide some knowledge for architects and urban designers on urban public space form optimization in terms of wind environment during initial design stage. In this paper, different vertical opening layouts were investigated on the influence of different region's spatial ventilation by CFD numerical modelling. Spatial mean velocity magnitude at pedestrian-level and air flow rate at space vertical opening and top boundaries were calculated to evaluate spatial ventilation. Simulation results show that appropriate vertical opening layouts could improve velocity magnitude of space's recirculation area. When the inlet opening is approaching the opposite side of the outlet opening, spatial mean velocity of some recirculation regions could be increased by more than 60%. In terms of the inlet opening position, when the opening is located at the side of south space boundary (windward direction), more airflow could be induced into space.

KEYWORDS: Urban public space, Opening layout design, Spatial ventilation performance, CFD simulation.

1. INTRODUCTION

As better air quality is essential for urban public space, improving urban spatial ventilation through the optimization of space configurations is more considered by architects in urban design process. But how to design spaces through appropriate building arrangement is a challenge for architects. Although many qualitative studies had revealed relationships between design variations and wind environments [1], the trial-and-error method is still adopted in the microscale urban design process, as the relationships are not clear to be used as guidelines to control the space configuration in the design process. Thus, more detailed effects of design variations on spatial ventilation are needed on an operational level. This study focus on the influence of urban public space opening layouts on pedestrian-level wind conditions, as the openings are the space boundaries at which air flow are exchanged.

For describing of the public space forms, Krier and Rowe [2] classified the spatial types according to the types of street intersection laid out and put forward four intersections at four possible points of entry. They also sketched a series of spatial forms according to the geometrical characteristics (Figure 1). Recently, several studies had discussed influence of building layouts on spatial ventilation, but very few studies had investigated the wind conditions of urban public spaces in term of the considerations of space boundary opening layouts (street intersections). For example, Asfour [3] investigated the effect of housing blocks layouts on ventilation potentials by numerical modelling. Six hypothetical arrangements of dwelling buildings were assessed by calculating wind pressure difference of building facades. Hong and Lin further assessed the effect of the six residential building

layout patterns on outdoor thermal environment [4] and air quality [5]. Tree arrangements were also considered in their studies. Yin et al. [6] analysed the different regions of wind environment around a building group consisting of six square high-rise buildings for six types of building layouts. Similar studies were carried out by Arkon and Özkol [7], Iqbal and Chan [8], You et al. [9] and Shui et al [10]. The wind ventilation conditions of real urban spaces had also been investigated by Antoniou et al [11] and Shen et al [12]. But these studies mainly focus on simulation and/or ventilation performance method rather than passive design strategies. In addition, Givoni [13] had carried out systematic experiment studies on the effect of space opening layouts on spatial ventilation, a 65×65×50 (cm) cubic room with openings located at different positions was build and the wind velocity ratio were investigated for different regions. However, these performances were carried out for interior spaces, without considering air exchange at top boundary.

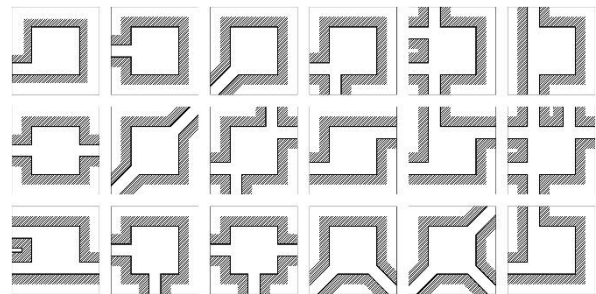


Figure 1: Sketches of a series of urban spatial forms [2]

This paper tried to obtain the principle of opening setting for optimizing the ventilation performance in urban space. Several ideal square spaces were built to

discuss the influence of different lateral opening layouts on spatial ventilation. To consider the effect of surrounding buildings, building blocks were built around the square space. Within the space, several typical spaces were evaluated under the south wind direction. This could analyse the typical wind condition to buildings in the east China monsoon region. To calculate the airflow patterns within the studied spaces, computational fluid dynamics (CFD) method was adopted in this study. The calculation tool used was ANSYS-Fluent. Spatial mean velocity magnitude and air flow rate were selected as the indices for spatial ventilation performance.

2. Method

2.1 Urban space configurations

To discuss the influence of urban space lateral openings layouts on spatial ventilation of different regions, several 3x3 square spaces with different lateral opening layouts were built for investigation. Two types of spaces were set according to the inlet opening locations, as shown in Figure 2. Type A represented the space with one inlet opening located in the middle of south space boundary, while Type B represented the space with one inlet opening located in the side of south space boundary. Cases A0 and B0 were the spaces with only one inlet opening (opening1), while the other cases were the spaces with one inlet opening and one outlet opening (opening2). The effects of surrounding buildings were also considered by setting building blocks around the studied cases.

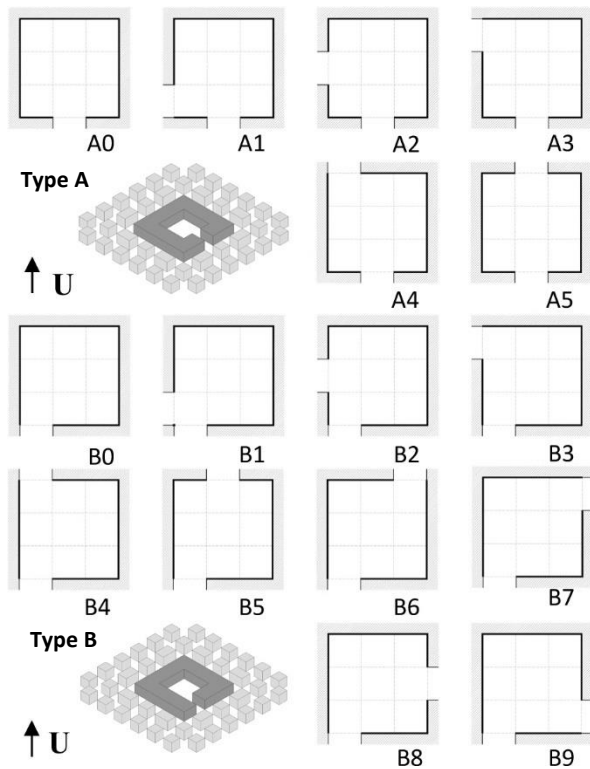


Figure 2: Study cases

In this study, the location combination of the inlet and outlet opening were investigated and the opening size were kept constant. The studied spaces were built by one or two surrounding buildings. The depths of the buildings were set as 24m and the building height H were 12m.

The studied space was divide into 9 different regions for ventilation evaluation (Figure 3). They represent different space feature, i.e. corner space surrounded by two walls, side space adjacent to one wall and central space far away from walls. According to the characteristics of the flow field, the regions were classified into two areas, naming jet area (J) and recirculation area (R). And according to the air flow route, the two areas were further divided into up-wind (J_u, R_u), middle-wind (J_m, R_m) and down-wind (J_d, R_d) areas. As the recirculation area in type B is deeper than type A, the areas adjacent to jet area were named as R_{d1}, R_{m1} and R_{u1} , while the far away areas were named as R_{d2}, R_{m2} and R_{u2} .

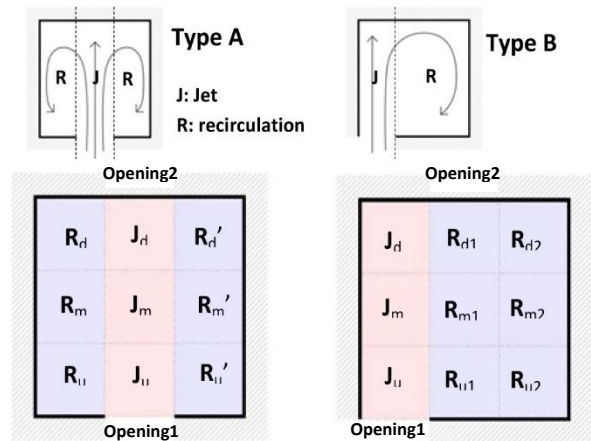


Figure 3: Regional spaces for ventilation performance

2.2 CFD simulations

For wind flow predicting using CFD simulation, it is generally acknowledged that large eddy simulation (LES) can provide more accurate results than steady Reynolds-Averaged Navier Stokes (RANS). However, LES consumes much more computational time than the RANS approach, and the turbulent model setup is also more complex [14]. In addition, if the urban wind prediction focused on the mean wind speed rather than on an effective wind speed, RANS approach could provide sufficient results. Considering that RANS turbulence models are less time-consumption and this study mainly focuses on mean wind velocity, the steady RANS approach with standard $k-\epsilon$ turbulence model is adopted in this study.

The accuracy of predicting outdoor wind velocity using RANS approach had been verified by many studies [4,12,15]. Some guidelines, such as AIJ (Architectural Institute of Japan) guideline [16], had provided important recommendations of using the CFD

technique for appropriate prediction of pedestrian wind environments. This study referred to the simulation method which had been validated by wind tunnel tests [15]. Calculation domain and boundary conditions are shown in Figure 4. Hexahedral elements were built in the computational domain. Minimum grid control is 0.022H in direction z and 0.044H in direction x-y. Maximum expansion factor between grids is 1.25. The inlet vertical wind velocity profile (U), turbulent kinetic energy profile (k) and turbulent dissipation rate profile (ε) were calculated as the following Equation (1) - (3):

$$U_{(z)} = \frac{u_{ABL}^*}{\kappa} \ln\left(\frac{z + z_0}{z_0}\right) \quad (1)$$

$$k_{(z)} = \frac{u_{ABL}^{*2}}{\sqrt{C_\mu}} \quad (2)$$

$$\varepsilon_{(z)} = \frac{C_\mu^{3/4} k_{(z)}^{3/2}}{\kappa z} \quad (3)$$

Where z_0 - the aerodynamic roughness length (m), and z is the height coordinate (m);

H - the building height (m);

$U_{(H)}$ - the reference wind speed is 4 m/s at the reference building height H.

C_μ - constant 0.09 (-);

u_{ABL}^* - the friction velocity 0.33 (m/s);

κ - Karman constant 0.4 (-).

Symmetry boundary conditions were imposed on the top and lateral sides of the domain. At the outlet boundary of the domain, a pressure-outlet condition was used. No-slip wall boundary conditions were used for all solid surfaces. The SIMPLE algorithm was utilised for pressure-velocity coupling. Pressure interpolation was in second-order accuracy. For both the convection terms and the viscous terms of the governing equations, second-order discretisation schemes were used.

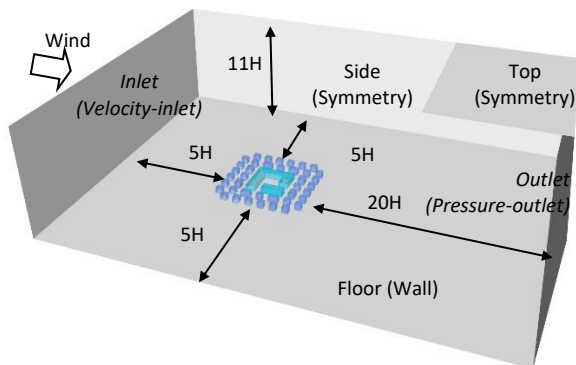


Figure 4: Computational domain and boundary conditions (Building height H = 12 m)

2.3 Ventilation performance of regional space

To assess the space ventilation of different regions, spatial mean velocity and air flow rate were adopted in this study. They can reflect the air flow patterns

within different regions and the air exchange characteristic at opening boundaries, respectively.

The normalized spatial mean velocity ($\langle V^* \rangle$) in each specified region (Vol) was calculated as Equation (4):

$$\langle V^* \rangle = \frac{1}{V_{ref}} \frac{1}{Vol} \iiint_{Vol} V(x, y, z) dx dy dz \quad (4)$$

Where V_{ref} - the reference velocity (m/s);

Vol- a specified volume which height H is from ground to 1.8 m above the ground (m^3);

V - the velocity magnitude (m/s).

Air flow rate means the frequency for certain area where air is replaced by outside "fresh" air. Air flow rates through space openings and the roof were calculated using Equation (5-6) [15]:

$$Q = \int_A \vec{v} \cdot \vec{n} dA \quad (5)$$

$$Q_{turb\pm} = \pm \int_A 0.5 \times \sigma_w dA \quad (6)$$

Where \vec{v} - wind speed vector (m/s);

n - the normal direction of street openings or the street roof (-);

A - In Equation (5), the area of opening1, opening2 and Top at space boundary (m^2); In Equation (6), the area of Top (m^2);

σ_w - the vertical velocity fluctuation across the street roof based on the approximation of isotropic turbulence (m/s).

As the inflow flux in the space is affected mostly with the value of the mean part of the flux [17], so only the mean part of the flux was calculated in this study.

3. SIMULATION RESULTS AND ANALYSIS

3.1 Type A - space with middle inlet opening

Figure 5 shows the distribution of wind velocity at pedestrian level (1.8m above floor) with openings of Type A. From the figure it can be found that the combination of opening1 (inlet) and opening2 (outlet) positions could affect wind field patterns. When the opening2 is not at the opposite of the opening1 (A1-A3), wind flow pattern is similar with that of case A0.

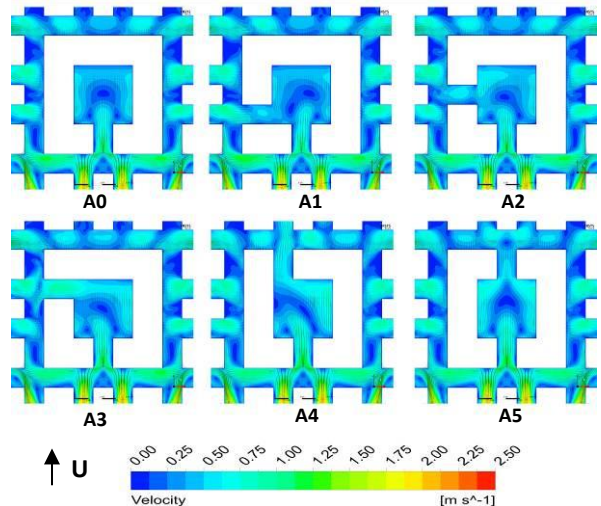


Figure 5: Wind flow pattern of type A cases (0.15H)

When opening2 is at the adjoining side (A1-A3) or opening2 is not opened (A0), recirculation flow appears at the central region (J_m) and two sides of the recirculation space (R_u and R_u'). And when opening2 is at the opposite side of opening1, more flow wind could be induced out form opening2. This wind characteristic can also be found by analysing air flow rate through each opening (Figure 6). When opening2 varies from the adjoining side to the opposite side of the opening1. The outlet airflow form opening2 increases gradually. Take A2 and A5 as an example, airflow rate increases by 7 times. Corresponding, the outlet airflow from top boundary decrease and the inlet airflow form top boundary increases. This reflect the variation of airflow characteristics within the spaces. In Case A1 and A2, the wind mainly entered the space form opening1, and get out form top by turbulence. The influence of opening2 position can be neglect. When opening2 approaches the opposite side of opening1, more wind could get out form opening2. The percentage of outlet flow from opening2 is only 48% for Case A3, while 79% for Case A5. Meantime, more wind flow could enter into the space from top boundary. This is because the vertical flow exchange at the top boundary is less influenced by the air flow entering form the opening1.

Form Figure 6, It can also be found that as opening2 approaches the opposite side of opening1, the total Air flow rate increases, although more wind exchanges occur at the jet areas.

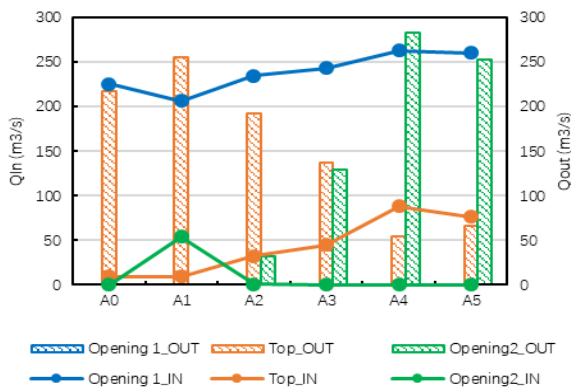


Figure 6: Air flow rate at opening1, opening2 and top boundary for different type A design cases

Figure 7 shows the spatial mean velocity of the nine regions within jet and recirculation areas under different combinations of opening1 and opening2. In subplot (a), when outlet opening changes from A0 to A5, the $\langle V^* \rangle$ of jet area's three spaces (J_d , J_m , J_u) increase slightly. For example, the $\langle V^* \rangle$ of J_u space increases by 35%. The $\langle V^* \rangle$ of recirculation areas are also improved as opening2 move towards the opposite side of opening1 (Figure 7b-c). Take Case A1 and A5 as an example, the $\langle V^* \rangle$ variation of R_d and R_d' spaces

increase by 67% and 52%, respectively. It is due to the strengthen of wind flow form opening1.

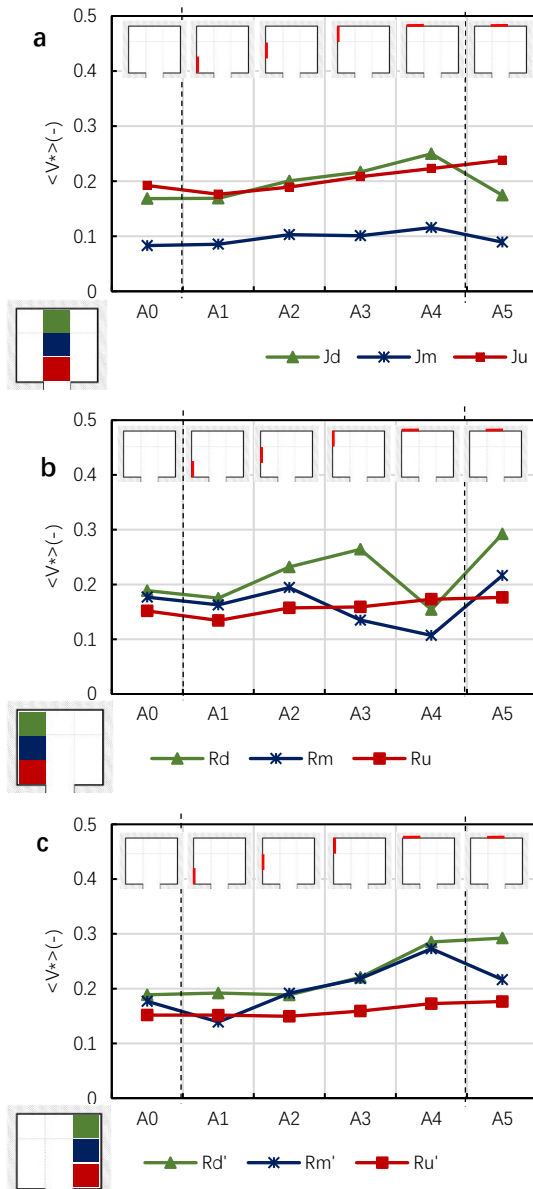


Figure 7: Spatial mean velocity of different regions within jet and recirculation areas for different opening2 layout design cases.

3.2 Type B - space with side inlet opening

Figure 8 shows the distribution of wind velocity at pedestrian level (1.8m above floor) with openings of Type B. Similar to Type A, when the opening2 is approaching the opposite of the opening1 (B2-B5), the wind flow pattern differs greatly with others. Recirculation flow phenomenon occurs at R_{d1} , R_{m1} and R_{u1} regions. When pening2 is approaching opening1 (Case B1), or at the R_2 region (B6-B9), the wind flow patterns are similar with that of case B0. It might be due to the airflow entering form opening1, strike on the wall of R_{d1} spaces and is induced to recirculation areas. The flow patterns are more reflected by the analysis of airflow rate, as shown in

PLEA 2018 HONG KONG

Smart and Healthy within the 2-degree Limit

Figure 9. In Case B1 and B9, airflow entering into the studied spaces not only form opening1 but also from opening2, and get out form top boundary. Opening1 and opening2 are all inlet openings, when opening2 is adjoining to opening1. But in other cases (except Case B0), opening2 serve as outlet opening. Airflow enters from opening1 and get out form top and opening 2. It is especially true when opening2 is opposite opening1 (B4 and B5). At this time, the percentage of outlet flow from opening2 could reach more than 79% and 74%. In case B6 – B9, the pedestrian level wind velocity patterns are similar. In these design cases, airflow mainly enters form opening1 and get out form opening2 and top boundary. When opening2 move away from the opposite of opening1, airflow rate from opening2 decrease evidently.

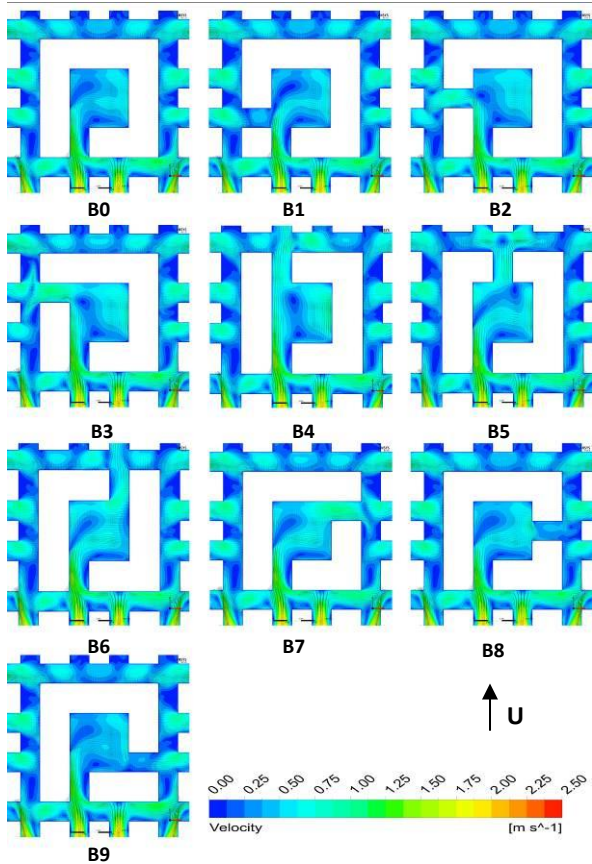


Figure 8: Wind flow pattern of type B cases (0.15H)



Figure 9: Air flow rate at opening1, opening2 and top boundary for different type B design cases.

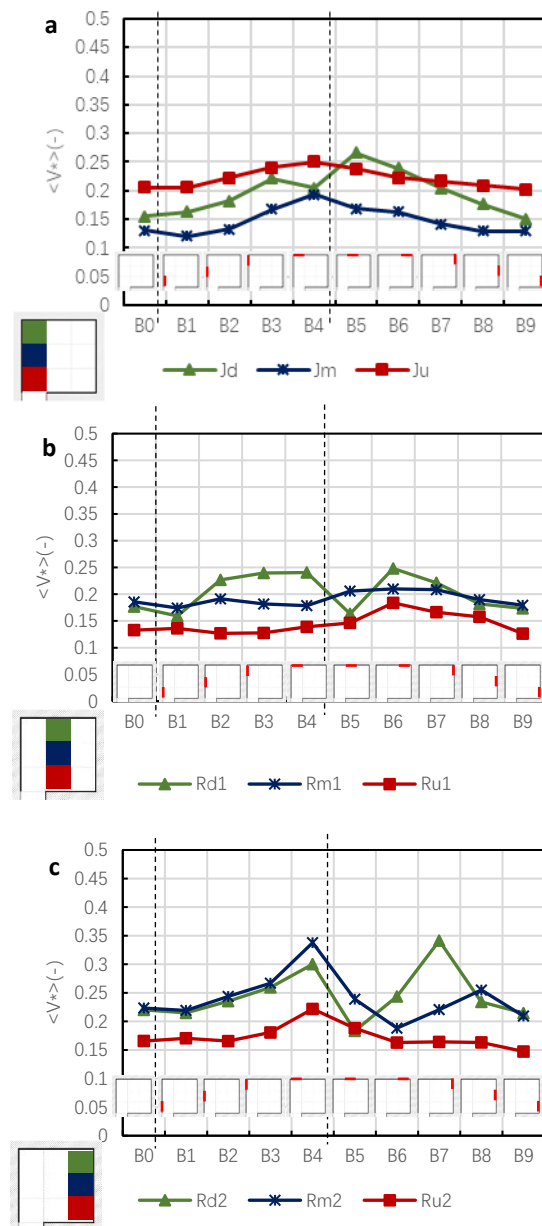


Figure 10: Spatial mean velocity of different regions within jet and recirculation areas for different opening2 layout design cases

PLEA 2018 HONG KONG

Smart and Healthy within the 2-degree Limit

Similar to Type A, the mean wind velocities $\langle V^* \rangle$ of different regions are also improved as opening2 move towards the opposite side of opening1 (Case B4). In Figure 10, it can be found that the $\langle V^* \rangle$ of B4 and B5 cases are generally higher than that of other cases, and it is especially evident for jet (Figure 10a) and far away recirculation area (Figure 10c). For example, in jet area, the mean wind velocities of J_u , J_m and J_d regions increase by 22%, 61% and 25%, when design cases change from B1 to B4. It is mainly due to the airflow improvement, when opening2 moves to the opposite side of opening1 (Figure 9).

Due to the recirculation flow, which occurs at certain region, there are some exception. For the B5 case (Figure 10b), which the opening2 is located at the opposite side of opening1, the $\langle V^* \rangle$ of certain recirculation region (R_{d1}) could be even worse than other cases. Take B5 and B6 as an example, the $\langle V^* \rangle$ of R_{d1} decreases by 52%. And in other cases, which opening2 are not the opposite side of opening1, the $\langle V^* \rangle$ of certain recirculation region (R_{d2} of case B7) could be improved, as shown in Figure 10c. This recirculation flows can be clearly seen in Figure 8.

4. CONCLUSION

This paper preliminary discussed the influence of space lateral opening layouts on spatial ventilation of different regions. Simulation results show that the variations of opening1 and opening2 locations could influence the airflow exchange at space boundaries, and ultimately affect the wind velocity distribution of the urban ground spaces.

The spatial ventilation of different regions could be improved by designing the outlet opening at the opposite side of the inlet opening. When the outlet opening is approaching the opposite of the inlet opening. The airflow rate entering from inlet opening could increase by 26% and 16% for type A and type B. It could generally improve the spatial ventilation of different regions. However, exceptions also exist for this improvement due to the recirculation flow phenomenon.

When the outlet opening (opening 2) is laid at the boundary of recirculation area, the pedestrian-level wind velocity pattern is generally less affected by the outlet opening layouts.

In terms of the inlet opening position, Type B is better than Type A, as more airflow could be induced into space when opening is located in the side of south space boundary.

This research preliminary analyses the influence of space opening layouts on the spatial ventilation. Due to complexity of urban forms, the conclusions are confined to these studied cases. More studies are needed to further investigate opening size changes under different wind directions.

ACKNOWLEDGEMENTS

This study was financially supported by the National Natural Science Foundation of China (No. 51538005 and 51708274). The authors would like to acknowledge the valuable comments provided by Dr. Zhi Gao and Dr. Riccardo Buccolieri on the simulation technique and wind ventilation performance.

REFERENCES

1. Erell, E., D. Pearlmutter and T. Williamson, (2011). *Urban Microclimate: Designing the Spaces Between Buildings*. Earthsan: Oxon, OX14 UK & New York, NY, USA.
2. Krier, R. and C. Rowe, (1979). *Urban space*. London: Academy editions.
3. Asfour, O.S., (2013). Prediction of wind environment in different grouping patterns of housing blocks. *Energy and Buildings*, 42: p. 2061-2069.
4. Hong, B. and B.R. Lin, (2015). Numerical studies of the outdoor wind environment and thermal comfort at pedestrian level in housing blocks with different building layout patterns and trees arrangement. *Renewable Energy*, 73:18-27
5. Hong, B., H.Q. Qin and B.R. Lin, (2017). Prediction of Wind Environment and Indoor/Outdoor Relationships for PM2.5 in Different Building-Tree Grouping Patterns, *Atmosphere*, 9: 39.
6. Ying, X.Y., W. Zhu, K. Hokao and J. Ge, (2013). Numerical research of layout effect on wind environment around high-rise buildings. *Architectural Science Review*, 56: p. 272-278.
7. Arkon, C.A. and Ü. Özkol, (2014). Effect of urban geometry on pedestrian-level wind velocity. *Architectural Science Review*, 57:1 p. 4-19.
8. Iqbal, Q.M.Z. and A.L.S. Chan, (2016). Pedestrian level wind environment assessment around group of highrise cross-shaped buildings: Effect of building shape, separation and orientation. *Building and Environment*, 101: p. 45-63.
9. You, W., Z. Gao, Z. Chen and W.W. Ding, (2017). Improving residential wind environments by understanding the relationship between building arrangements and outdoor regional ventilation. *Atmosphere*, 8: 102.
10. Shui, T.T, J. Liu, Q. Yuan, Y. Qu, H. Jin, J.L. Cao, L. Liu and X. Chen, (2018). Assessment of pedestrian-level wind conditions in severe cold regions of China. *Building and Environment*, 135: p. 53-67.
11. Antoniou, N., H. Montazeri, H. Wigo, M. K-A. Neophytou, B. Blocken and M. Sandberg, (2017). CFD and wind-tunnel analysis of outdoor ventilation in a real compact heterogeneous urban area: Evaluation using "air delay". *Building and Environment*, 26: p. 355-372.
12. Shen J.L., Z. Gao, W.W. Ding and Y. Yu. 2017. An investigation on the effect of street morphology to ambient air quality using six real-world cases. *Atmospheric Environment*, 164: p. 85-101.
13. Givoni, B., (1965). Laboratory study of the effect of window size and location on indoor air motion. *Architectural Science Review*, 8:2, p. 42-45.
14. Tominag, Y. and T. Stathopoulos, (2010). Numerical simulation of dispersion around an isolated cubic building: Model evaluation of RANS and LES. *Building and Environment*, 45: p. 2231-2239.

PLEA 2018 HONG KONG

Smart and Healthy within the 2-degree Limit

15 Hang, J., M. Sandberg and Y.G. Li, 2009. Effect of urban morphology on wind condition in idealized city models. *Atmospheric Environment*, 43: p. 869-878

16 Tominaga, Y., A. Mochida, R. Yoshie, H. Kataoka, H. Nozue, M. Yoshikawa and T. Shirasawa, (2008). AIJ guidelines for practical applications of CFD to pedestrian wind environment around buildings. *Journal of Wind Engineering and Industrial Aerodynamics*, 96: p. 1749-1761.

17 Bady, M., K. Katob and H. Huang, (2008). Towards the application of indoor ventilation efficiency indices to evaluate the air quality of urban areas. *Building and Environment*, 43: p. 1991–2004.

Reducing Building Waste through Light Timber Frame Design: Geometric, Assembly and Material Optimisations

GERARD FINCH¹, GUY MARRIAGE¹

¹School of Architecture, Victoria University of Wellington, Wellington, New Zealand

ABSTRACT: There is an urgent need for construction systems that enable the recovery of materials at the end of a building's life. The current widespread use of adhesive-based fixings and single-life materials formed from petrochemical derivatives has led to the unprecedented generation of toxic material waste. Consequently, up to 40% of global waste is estimated to come from the construction sector. This design-led research study examines the potential of new light timber frame designs to facilitate material recovery. The research focuses the geometric and jointing properties of the components within the light timber frame and their potential for reuse. To validate the success of the proposed design ideas, a lifecycle assessment of the product was undertaken. This has been supported by a detailed discussion of the durability performance of the system. The study finds that the geometric and assembly conditions of the frame significantly increase long-term sustainable measures. The proposed design is estimated to represent a 70% reduction in embodied energy over an extended product's lifetime versus conventional light timber platform framing.

KEYWORDS: Closed Loop Design, Circular Economy, Material Reuse, LCA.

1. INTRODUCTION

This design-led research project aimed to develop a prefabricated and modular timber frame construction solution that promoted material reuse to effectively eliminate the production of waste in a building's life cycle. This paper documents key design details of the proposed construction approach that enables each independent building element, material and material fastener to be easily separated and reused or up-cycled without complication.

1.1 The Waste Problem

The building and construction industry generates more than 40% of global waste [1]. This is a direct consequence of the widespread specification of single use and non-reversible fixings, a result of the prioritisation of assembly speed (driven by monetary factors), which leads to the contamination and irreversible damage of materials [2]. Today the reuse of building materials is highly unattractive from an economic standpoint as materials often need significant reprocessing or regrading to be used again effectively [2].

1.2 Theoretical Framework

Design with the intention to reuse materials at the end of the building's life fits into a range of sustainable design frameworks. These include Design for Deconstruction (DfD), Design for Disassembly, Cradle to Cradle Design (C2C), Circular Economy Design (CE) and Closed Loop Design [3, 4]. As noted, the intention of these agendas is largely the same: prevent end-of-life waste by ensuring reuse potential and end-of-life recovery is 'designed-in' from the beginning. This

research takes a holistic view of these frameworks and uses key design principles from all to ensure a fit-for-purpose design outcome.

1.3 Success Criteria

Following these 'design for reuse' frameworks, a construction system designed for reuse must ensure minimal reprocessing (minimal damage or contamination to the main material) between use cycles and rapid deconstruction times to guarantee economically viable reuse. As such, design optimisations must ensure that jointing systems are durable and reusable without complication. This should include the specification of timber products that are not easily damaged when being assembled and/or disassembled. Similarly, the dimensional properties of the structure must be attractive for a diverse range of building applications if the dismantled product is to retain significant value through reuse cycles [3].

2. KEY DESIGN DEVELOPMENTS

These ideas were applied to the design of an alternative modular timber frame [4]. The final research outcome was a prefabricated modular and reciprocal structure named 'X-Frame' (Fig. 1). Key features of the X-Frame system are covered in the following section.

PLEA 2018 HONG KONG

Smart and Healthy within the 2-degree Limit



Figure 1: A full-scale prototype test of the modular and reusable X-Frame structural system.

2.1 Assembly Optimised Structure

To enable rapid assembly and disassembly, X-Frame was designed to require minimal supplementary fixings. Timber components were fabricated in such a way that enabled them to interlock and create a rigid structural grid inherently capable of resisting lateral loads (Fig. 2). This is significant as the amount of time required to separate fixings is reduced. The need for structural sheet material to be fixed to the face of the frame for lateral load resisting bracing is also removed [4]. The structural frame is therefore free of contaminants (such as adhesives and parts of damaged plasterboard) and panelised linings can be reversibly fixed without the need to provide lateral bracing.



Figure 2: Interlocking reusable and scalable structural grid with non-damaging fixings.

The triple-layer intersection detail is optimised to facilitate assembly and lifecycle performance (see right side of Fig. 2). The central component (X-Slot) acts to align disparate components during assembly quickly and prevent out-of-plane separation while in use. The two identical outer layers then act to lock the spanning members in place across their span. These 'X-Lock' components also help to self-correct the frame during assembly. If the central 'X-Slot' component is not correctly aligned these locking plates will pull the spanning elements into plumb. Furthermore, the triple

layer intersection detail allows insulation to sit in a separate cavity to the building services. This ensures that insulation materials do not have to be shaped around services and that both service and insulation materials can be recovered quickly without potential for cross-contamination. Collectively these integrated self-correcting assembly parameters are advantageous to encourage material reuse. They significantly speed up the construction process and ensure that integrated fixing points are always in the correct position.

2.2 Geometrically Optimised Modules

The resulting frame is an expandable matrix based on a 900mm module (Fig. 3). This allows maximum use of available sheet material at the time of fabrication (with two 1180mm long members at 45-degree angles forming the 900mm module – Fig. 2) and fits within functional architectural geometries [5]. The module is designed to work for all building elements (floor, walls and roofs – free spanning horizontally up to 5.4m) (Fig. 4 and 5). This leads to the need for fewer discrete components and aids in increasing the attractive reuse value of this alternative structural frame.

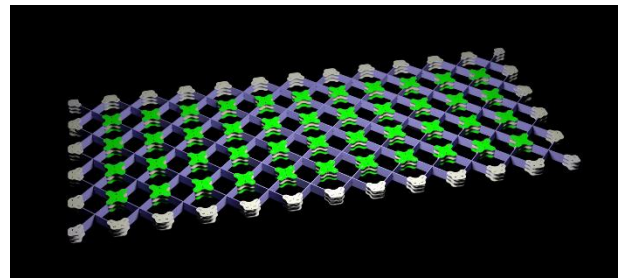


Figure 3: Grid structure formed from five primary components.

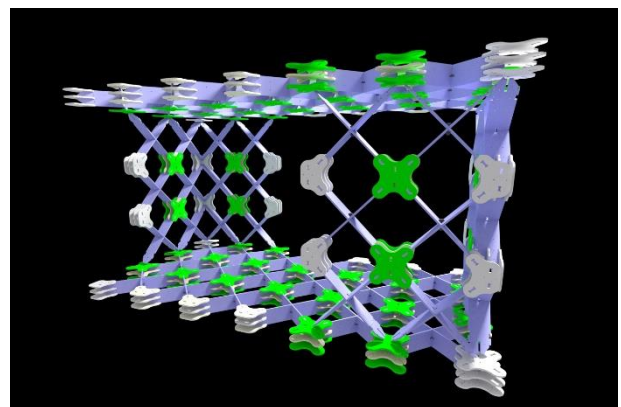


Figure 4: Grid structure operating effectively in all building elements and configurations.

2.3 Detailing and Offset Management

To further simplify the module-based structure each principle spanning element (Fig. 2) has been bevelled at both ends to remove the need for any offset or additional components when two (or more) vertical

PLEA 2018 HONG KONG

Smart and Healthy within the 2-degree Limit

elements intersect (Fig. 5). Rather than introducing more components, each span now has the inherent capacity to be placed at a point of intersection. This development simplifies construction processes as builders do not need to locate a specific prefabricated component to complete an intersection at the time of initial construction. Likewise, at the time of renovation or structural modification, changes are made easier by the existing structure's ability to accept new elements.

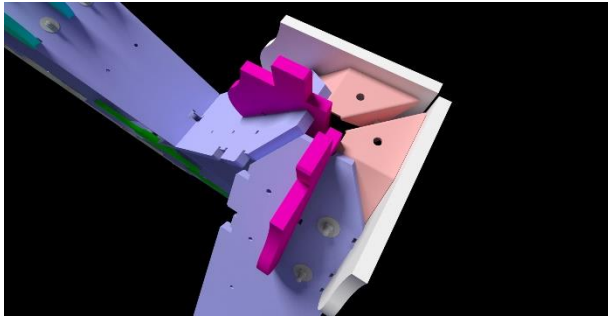


Figure 5: Chamfering of primary geometry to remove offsets when the grid intersects itself.

3. PERFORMANCE ASSESMENT

The following discussion critiques the performance of this design proposal against conventional light timber platform framing.

3.1 Life Cycle Assessment

There are a range of established methods to quantify the performance of products that aim to reduce waste or perform an existing function in a more sustainable way. For the purposes of comparison this study uses a streamlined Life Cycle Assessment (sLCA) and compares an X-Frame wall assembly with a 'conventional' light timber frame (LTF). This analysis results in comparative values that assist in determining the effective benefits of X-Frame.

Additional calculations were required to accurately represent the reusability opportunities of X-Frame in the sLCA. Based on prototype deconstruction tests within this research it was established that the X-Frame system had a material recovery rate of approximately 97.5%. Meaning that through one complete use cycle approximately 2.5% of the total materials (by weight) were irreversibly damaged. We know from literature and testing that conventional platform buildings enable the recovery of between 50% and 70% of all materials [6]. These 'recovery rates' were then used to predict the effective lifespan of material in each system. A conservative lifecycle period of 20 years was assumed to somewhat allow for incremental changes and renovation. An effective reuse limit was also established to more accurately reflect practical reuse limitations such as external environmental influences. This reuse limit dictated that when less than 10% of the original structure

remained no further reuse cycles were calculated. These assumptions allowed the estimation of the effective embodied energy consumption for one square meter of X-Frame or LTF structure over its entire practical lifespan.

The sLCA is based on New Zealand information for key construction materials and is limited to the material themselves. The sLCA is for one square metre X-Frame/LTF and includes an interior lining, structure, insulation and external waterproof system. Fixings have not been calculated due to an unavailability of relevant information.

Platform Light Timber Frame specification: 90x45mm dressed and H1.2 boron treated New Zealand *Pinus radiata* frame with studs at 400mm spacings. Lined with 10mm of standard plasterboard. Framing cavity filled with 90mm-thick R2.2 glass fibre insulation batts. Enclosed with a polyethylene waterproofing membrane and a 12mm-thick untreated New Zealand *Pinus radiata* plywood cladding product.

X-Frame specification: 17mm-thick untreated New Zealand *Pinus radiata* plywood CNC-routed and assembled as per X-Frame design (10.2kg). Lined internally with a 7mm New Zealand *Pinus radiata* plywood. Framing cavity filled with 90mm-thick R2.2 glass fibre insulation batts. Enclosed with a polyethylene waterproofing membrane and a 12mm-thick untreated New Zealand *Pinus radiata* plywood cladding product.

Table 1: Table of streamlined Life Cycle Assessment (sLCA) results for one square metre of Platform LTF and X-Frame systems with LCA data from SCION [7].

	Platform LTF	X-Frame
Total lifetime energy (MJ):	329	379
Number of use cycles (until less than 10% of the original material remains):	5	22
Time of 1 use cycle (years):	20	20
Estimated lifespan (years):	100	440
Energy (MJ) /year/square meter:	3.29	0.86

Table 2: Table of streamlined Life Cycle Assessment (sLCA) results for one square meter of Platform LTF and X-Frame systems (for a single use – one cycle) [7].

	Platform LTF	X-Frame
Global Warming Potential (kg-CO ₂ -equiv.):	-11.46	-19.62
Acidification (kg-SO ₂ -equiv.):	0.053	0.056
Eutrophication (kg-PO ₄ ³⁻ equiv.):	0.0065	0.0072
Photochemical Oxidation (kg-C ₂ H ₂ -equiv.):	0.0072	0.0075

This design-led research project set out to reduce the quantity of waste produced at the end of a building's

PLEA 2018 HONG KONG

Smart and Healthy within the 2-degree Limit

lifetime. The calculated 70% reduction in lifetime embodied energy of construction materials, facilitated by building systems designed specifically to enable material reuse, suggests far wider positive environmental implications than mere waste reductions (Table 1) [8]. A reduction on this scale has direct implications for material manufacturing, energy production and the construction industry's potential to mitigate global warming [8]. It is, however, important to note the limitations of this sLCA. Real world constraints, such as the cost (time) of extracting the materials from the existing building, could notably reduce the likelihood of material reuse. Adverse environmental conditions are also very likely to impact the lifespan of reusable materials. New Zealand's high susceptibility to earthquakes is likely to reduce the estimated lifespan of the X-Frame system and reduce the product's energy advantage.

3.2 Alternative Measures

To generate an alternative performance comparison between X-Frame and conventional framing techniques all measurable construction information were recorded. This included raw material cost, manufacturing costs, assembly and disassembly time, the number of varying components and the quantity of directly reusable materials. These figures, again, represent the materials in one square metre of wall.

Table 3: Table of comparable quantitative performance measures for the construction of a square metre of insulated and clad wall for Platform LTF and X-Frame.

	Platform LTF	X-Frame
Timber structure weight (kg)	7.02	15.48
Time to assemble (minutes)	20	15
Waste in fabrication (kg)	1.90	1.57
Number of components (no.)	3	3
Disassembly time (minutes)	47	27
Time to prepare components for reuse (minutes)	18	0
Recovery rate (percentage)	58%	97.5%
Lifecycle waste (kg)	14.9	1.96

Records of assembly and disassembly tests indicated that X-Frame had significantly accelerated disassembly times which could help to make material recovery more economically viable (Table 3). A 30% reduction in disassembly time, and the total elimination of time needed to prepare the materials for reuse, results in a decrease of more than 55% in effective reuse cost (Table 3). Given that it is estimated to cost twice as much to deconstruct a conventional LTF building than it does to demolish it, deconstruction of X-Frame would be economically preferable [9]. Furthermore,

these savings do not include the potential resale value of the recovered materials which could further elevate the economic advantages of disassembly. Over the estimated 400-year lifespan of the product such resale earnings would be substantial.

4. DURABILITY EVALUATIONS

4.1 Cyclic Durability

The economic advantages of material reuse and X-Frame depend on the durability of structural connections and components throughout multiple life-cycles. However, measuring the durability performance of a circular economy product like X-Frame is difficult due to the multiple aspects that must be considered. To understand the range of durability factors that needed to be considered, performance was broken down into three phases: Phase One included the durability of the product in transportation, handling and assembly; Phase Two covered the durability of the product while it is in service (use); and Phase Three's durability covered the ability for the product to be disassembled and reused directly.

X-Frame performed highly in all phases and coupled with the appropriate cladding and lining systems, achieved 97.5% material recovery through a single-use cycle. Of the twelve different components that made up X-Frame, only two failed. The first of these failed members was the X-Span component which is categorised as the largest spanning component of the system – the element that when two intersect, creates the 'X' geometry. When the X-Span failed it did so consistently at its centre, where a 17mm-wide slot extended 108.5mm through the 200mm-deep section. This failure happened in four span elements (out of a total of 108) in Durability Phase One and Three. It was identified that unexpectedly large forces occurred in the transverse direction while assembling and separating the structural frame. Further design improvements (X-Frame 9 over X-Frame 7) have worked to change the way in which the structure is assembled and by doing so eliminated strain on this part of the X-Span (Fig. 6).

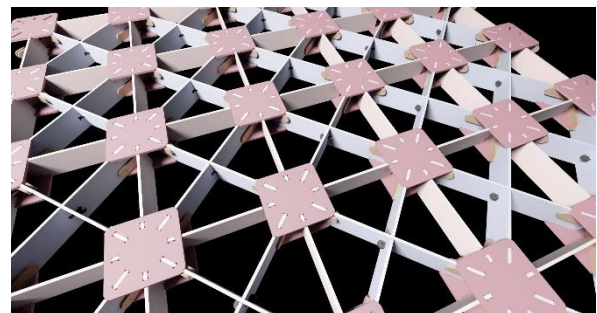


Figure 6: X-Frame 9 – a further developed version of X-Frame that is more cost effective reduces the opportunity for damaged components during assembly/disassembly.

PLEA 2018 HONG KONG

Smart and Healthy within the 2-degree Limit

Full-bend and stress testing is yet to be carried out for both X-Frame 7 and 9. This is required to validate the structural benefits of each iteration. It is also important to note that geometric variations between versions make the two systems unable to work together. This could become an issue if multiple X-Frame versions are circulating at the same time as interoperability in reuse would be extensively compromised. The second and final component that failed completely was a perimeter span element. One of these members (out of 48) failed at its end while being removed. This failure was a result of repetitive mallet impact on the end tab due to high levels of stiffness between the slotted span member and the lock it was intersecting (Fig. 7). A redesign of the edge condition in X-Frame 9 has eliminated this perimeter span component entirely.



Figure 7: Failure of a perimeter span element of the X-Frame system due to variations in material thickness.

A portion of X-Frame was assembled and disassembled (one use 'cycle') four times in different conditions. While there was no critical damage to any other members during these cycles, some of the plywood pieces began to show signs of wear and tear. A key concern here is the veneers of plywood beginning to separate where tenons are inserted into mortise slots (Fig. 8). Separating plywood layers suggest a significant weakening of the connection which could lead to joint failure. This issue was relatively rare, occurring in six out of 248 connections, and occurred both during assembly and disassembly. Splitting layers only occurred on the X-Lock component where four or more mortise and tenon joints were occurring.

4.2 Material Environmental Durability

Plywood is subject to expansion and contraction due to environmental moisture. An excessively dry environment may cause shrinkage of connection elements to a point that results in structural failure. This shrinkage is not uniform however as plywood has very low rates of longitudinal and tangential shrinkage (approximately half that of conventional timber). Yet

plywood is subject to the same radial shrinkage rate as solid timber [10]. The result of these dimensional variances is that joint stiffness can change over time. To reduce the impact of this variation all structural load bearing plywood connections adhere in more than one timber orientation. This ensures that if there is shrinkage across the thickness of the material the joint remains in contact due to the comparatively low shrinkage across the length of the material.



Figure 8: Plywood veneer layers separating on the 'X-Lock' component at a mortise connection.

To achieve the necessary durability rating in respect to structural timber components' resistance to moisture, the members must be treated. In New Zealand the treatment level mandated is H1.2. In conventional timber this is achieved by soaking the material in a bath of boron. The resulting product has a pink dye added to it to identify it as H1.2 treated timber. *Pinus radiata* structural plywood is available off-the-shelf in untreated or H3.2 CCA (copper, chrome, arsenic) or H3.1 LOSP (Light Organic Solvent Preservative) treated varieties with H1.2 treated product available on bulk order. In an ideal circular economy process, any treatment would be a natural derivative or process (such as Accoya™) and applied only after the components have been manufactured. This ensures that the sawdust waste produced during manufacture remains uncontaminated and can be effectively contained within a biological resource cycle. If X-Frame was to adopt materials other than engineered timber (plywood and oriented strand board), treatment requirements and dimensional variations would likely change.

5. WASTE IN FABRICATION

X-Frame is fabricated from manufactured plywood sheets using an industrial computer numerically controlled (CNC) router. This type of 'reductive manufacturing technology' is notorious for producing large quantities of waste. This is a direct result of pre-sized sheet materials (1.2m by 2.4m sheet plywood) conflicting with the desired forms being cut. To counteract this concern X-Frame was designed to

PLEA 2018 HONG KONG

Smart and Healthy within the 2-degree Limit

maximise effective use of the available material. Even with this intent however X-Frame 7 (Fig. 1) only used 81% of the available sheet material. Although this wood waste can be collected and used to produce Orientated Strand Board (OSB) or similar reconstituted wood products, this loss of efficiency is not ideal. X-Frame 9 therefore aimed to improve material usage and consequently achieved a 91% usage rate of the available material.

Achieving higher rates of material use efficiency is highly unlikely with this manufacturing technology due to the way material is formed. For example, the width of the router cutting piece is required to be of a minimum thickness to achieve economically cutting speeds. For X-Frame 9, cut with a 9.5mm-wide router piece, 8.2% of the entire sheet area becomes sawdust. This means that less than 1% of the plywood sheet remains as solid waste. Thus, a significant change in geometry would be the only viable solution to further improve material use efficiencies when CNC router fabrication is used. The authors of this study are actively perusing alternative fabrication methods in the hope of eliminating disused materials at the time of manufacture.

6.0 FIRE RESISTANCE

This study is yet to quantify X-Frame's performance in the event of a fire. However, based on the similarities between X-Frame and existing plywood structural systems achieving sufficient fire performance is expected to be straightforward. An example of a closely aligned product with many completed designs and an excellent fire record is the FACIT Homes' system [11]. The FACIT system uses an orthogonal structural frame with a perpendicular plywood sheet fixed to the face to create a panelised wall component. To protect the slender structural timber members from fire, FACIT "use non-combustible insulation and fireproof linings" [11]. Typically, this is in the form of Gypsum plasterboard screwed and glued to the plywood structure. This level of fire resistance is adequate in New Zealand for detached and semi-detached residential buildings. If there is a significant concern regarding fire resistance it would also be possible to treat the shaped plywood using fire retardant chemicals. These chemicals could be applied to the components once shaped. The inherent reuse potential of X-Frame would ensure these chemicals do not enter waste streams. However, chemical treatment is undesirable as it does ultimately compromise the cradle-to-cradle potential of untreated plywood.

7. CONCLUSION

The building and construction industry faces major waste management challenges. Current building practices that depend on single-use materials and

adhesive based connections must be eradicated to eliminate the production of downcycled or waste materials. This research demonstrates that alternative timber structures can be shaped and detailed to enable direct and economically efficient reuse of deployed materials. The proposal is a digitally fabricated light structural frame that integrates all connection and assembly functions. Streamlined life cycle analysis and durability studies suggest that a reusable structural frame is a feasible low waste building proposition.

ACKNOWLEDGEMENTS

The authors would like to acknowledge the generous support of The New Zealand Institute of Buildings' Charitable Trust, Makers of Architecture, the Building Research Levy, Victoria University of Wellington and Carter Holt Harvey Limited.

REFERENCES

1. Inglis, M. (2007). Construction and Demolition Waste – Best Practice and Cost Saving. Ministry for the Environment. New Zealand Government. p. 1.
2. Storey, J. B., Gjerde, M., Charleson, A., & Pedersen, M. (2005). The state of deconstruction in New Zealand. Centre for Building Performance research, Victoria University, New Zealand. p. 17-18. 60-61.
3. Braungart, M. and McDonough, W. (2014). The Upcycle. 1st ed. New York: Farrar, Straus and Giroux, pp.87-91.
4. Circular economy for the built environment: a research framework. Francesco Pomponi^{1*} and Alice Moncaster¹ 1 University of Cambridge, Department of Engineering - Centre for Sustainable Development
5. Finch, G., Marriage, G. and Forbes, N. (2018). Timber Frame Construction for a Circular Materials Economy; Alternative Framing Methods and Post-Use Certification. In: 51st International Conference of the Architectural Science Association. Wellington: p. 480.
6. Chini, A, (2003). Deconstruction and materials reuse in the United States. Special Issue article in: The Future of Sustainable Construction – 2003. p. 10.
7. Nebel, B., Alcorn, A. and Wittstock, B, (2011). Life Cycle Assessment: Adopting and adapting overseas LCA data and methodologies for building materials in New Zealand. Ministry of Agriculture and Forestry. SCION. p. ii.
8. Building Research New Zealand, (2014). *Level: Material Use: Embodied Energy*. Building Research New Zealand (BRANZ), [Online], Available: <http://www.level.org.nz/material-use/embodied-energy/> [18 May 2018].
9. Endicott, B., Fiato, A., Foster, S., Huang, T. and Toyey, P (2005). *Research on Building Deconstruction: Final Project Report*. University of California, Berkeley. p. 2.
10. The Wood Database, (2014). The Wood Database: Dimensional Shrinkage. The Wood Database. [Online], Available <http://www.wood-database.com/wood-articles/dimensional-shrinkage/> [23 May 2018].
11. Facit, (2014). Facit Homes: Precision Built Modern Homes, Informed By The Way You Want To Live. Facit UK Limited t/a Facit Homes, [Online], Available: http://facit-homes.com/wp-content/uploads/2014/08/Facit_Brochure.pdf. [06 May 2018].

Unmanned Aerial System (UAS) Applications in Energy Audits: Towards Standardizing Automated Building Inspections using Drones

TAREK RAKHA¹, ALICE GORODETSKY¹

¹School of Architecture, Syracuse University, Syracuse, NY, United States

ABSTRACT: Unmanned Aerial Systems (UAS) have evolved over the past decade as both advanced military technology and off-the-shelf consumer devices. There is a gradual shift towards public use of drones, which presents opportunities for effective remote procedures that can disrupt a variety of built environment disciplines. UAS equipment with remote sensing gear present an opportunity for analysis and inspection of existing building stocks, where architects, engineers, building energy auditors as well as owners can document building performance, visualize heat transfer using infrared imaging and create digital models using 3D photogrammetry. This paper presents a comprehensive review of various literature that addresses this topic, followed by the identification of a standard procedures for operating a UAS for energy audit missions. The presented framework is then tested on a university campus site based on the literature review to showcase: 1) pre-flight inspection procedure parameters and methodologies; 2) during-flight visually identified areas of thermal anomalies using a UAS equipped with Infrared (IR) cameras and; 3) 3D CAD modelling developed through data gathered using UAS. A discussion of the findings suggests refining procedure accuracy through further empirical experimentation, as well as study replication, as a step towards standardizing the automation of building envelope inspection.

KEYWORDS: Unmanned Aerial System (UAS) Building inspection, Retrofitting, Energy audit, Thermography

1. INTRODUCTION

Humans live in aging built environments. Maintaining the energy efficiency of such infrastructure and building stock is integral in moving towards an environmentally sensitive and sustainable future in the age of climate change. 40% of U.S. homes were built before 1970 [1] and the buildings sector accounts for 40% of CO₂ emissions in the United States [2]. Therefore, to address the inefficiency of older infrastructure, building energy retrofitting practices typically identify, diagnose, and design solutions that address issues of building usage, systems and envelope [3].

To identify problematic issues specific to the building envelope, energy auditors typically use tools such as blower door tests to detect infiltration/exfiltration regions, as well as thermal bridges [3]. Technologically advanced tools such as infrared cameras and Unmanned Aerial Systems/Vehicles (UAS/UAV) enable professionals to analyse such issues rapidly and accurately while reducing operational costs and minimizing safety risks, and when paired with video recording, photography, or multi spectral imaging, drones can safely, economically, and efficiently carry out a broad variety of surveying services [4]. UAS provide experts across industries with a unique aerial perspective. This viewpoint allows easy access to remote or inaccessible areas without compromising the safety of the pilot [5], and this combination of technology has and will continue to permeate a wide range of varying fields as its applications, innovations, and capabilities are discovered and improved upon [6].

The primary barrier to energy efficient retrofitting is the uncertainty over return on investment, an uncertainty that can be addressed when focusing on the building envelope with relatively quick and cheap visualization of thermal anomalies [7]. Thermal patterns gathered with infrared cameras attached to drones can be converted into automatically generated 3D CAD models using 3D photogrammetry software. This paper's goal is it to report on a comprehensive review of contemporary developments in UAS technologies specific to such building performance inspection applications, and presents a novel proof-of-concept study for thermography-based building auditing using UAS. The manuscript, therefore, addresses this aim through the following objectives: 1) reviewing literature focusing on site investigations, 2) examining building analysis techniques using UAS and 3) investigating drone flight planning procedures for building performance inspection. The results specifically focus on applications of thermography and 3D CAD model generation, and a case study is presented for the methods on a university campus in the United States. The paper concludes with a discussion that contextualizes past investigation directions, current research challenges, and a framework for future developments.

2. RESEARCH METHODOLOGY

The review initiated with a literature survey via multiple online scholarly sources. The sources were selected based on their ability to detail the applications and current abilities of UAS and thermal

infrared technology in improving existing building audit practices. This necessitated scholarly foundations that detail the design of flight paths in relation to buildings, large expanses of landscape, and/or geoclusters.

As the review specifically focuses on stages of an energy audit using UAS equipped with thermal cameras, an experimental setup is proposed as part of the work in each of the reviewed topics and is presented in the discussion section. For pre, during, and post flight analyses, investigation methods are developed, calibrated, and tested on a university campus as part of the findings for the literature review.

3. RESULTS

The workflow is divided into three main categories; site acquisition, flight path planning, and post-analysis (Fig. 1). Results are split into three steps; pre-flight drone path planning, in-flight infrared thermography, and post-flight image processing, segmentation, and 3D model generation.

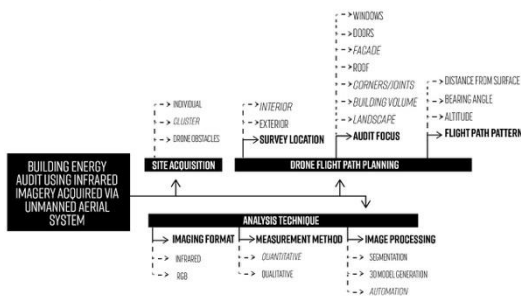


Figure 1: Categorical decision tree for the workflow of UAS literature investigations.

3.1 Pre-flight Path Planning

Planning a drone flight demands an awareness of multiple factors such as distance from target, altitude, speed, overlap, and pattern [8]. The accuracy of the drone flight as well as avoidance of obstacles is heavily reliant on the accuracy of the Global Positioning System (GPS) and Inertial Navigation System (INS) [9]. The most common path has been to fly the drone in either vertical or horizontal strips in a zig-zag pattern across the area of interest. This method is frequently referred to as the strip method [9,10]. Eschmann & Wundsam elaborate further on the strip method by testing the differences between utilizing vertical strips or horizontal strips. Their study finds that vertical strips result in unfavourable movement of the lens which decreases the clarity and quality of data gathered. Horizontal strips are proven to be more reliable especially when paired with a low flight speed [11]. In addition to being a proponent of the strip method, Steffen & Forstner present research which advocates for the use of archimedic spirals to optimize flight plans [9]. Multiple researchers plan their flights according to a grid overlaid on the pre-determined site

boundaries, so that the drone flies to gather data of each grid unit [12,13].

The strip method frequently involves specified overlaps to ensure not only a robust and thorough collection of data, but also to ensure an easy transition into photogrammetry, 3D model generation, and/or analysis. To survey archaeological ruins, Stek recommends a >35% overlap [14]. However, there is a great range found that includes 60% [15], >70% [16], 60–80% [17], 70% lateral and 80% forward [18] and 90–95% [19] For surveys of large or urban areas, a height of 100–200 m allows for high (unspecified) overlap and high-resolution data capturing [17].

3.2 Infrared Thermography

Building thermography for the purpose of anomaly detection can be carried out in a range of methods that include but are not limited to: aerial surveys, automated fly-past surveys, street pass-by surveys, perimeter walk around surveys, walk through surveys, repeat surveys, and time-lapse surveys [20]. Innovative approaches have been detailed for many of these methods and include use of various combinations of vehicles (whether unpiloted or robotic) paired with cameras of various capabilities, including research on building energy audits conducted by a terrestrial robot laden with infrared, photo and Light Detection and Ranging (LiDAR) technology [21].

The use of infrared thermography in buildings is especially useful for visualizing the thermal patterns within the building envelope as well as the movement through and across various building materials [22]. The non-contact nature of infrared visualization is less likely to be inaccurate than any contact measurement method readily available due to the fact that it does not affect thermal equilibrium. By using airborne infrared cameras, auditors are able to capture a large surface with minimal effort. This is thought to be the only way to achieve a correct mean value and measure local anomalies [6]. To ensure accurate results, Borrmann et al. recommend a temperature difference of about 10 degrees Kelvin between the interior of the building and the exterior ambient air temperature. The ideal conditions for infrared auditing require stable weather conditions over a long period of time [23]. In addition, extensive exposure to solar radiation is not ideal as it may oversaturate and obscure smaller instances of leaks. For this reason, ideal weather conditions are partly cloudy morning hours during the winter months [21]. To insure an easy transition to the next step, photogrammetry and 3D model generation, Ham & Golparvar-Fard reinforce the necessity for captured thermal imager to be ordered, calibrated, and geo-tagged [24].

3.3 Post Processing (Photogrammetry & Modelling)

PLEA 2018 HONG KONG

Smart and Healthy within the 2-degree Limit

Post processing begins with the awareness of five different conditions; altitude, quality, timing, spectrum, and overlap [25]. Photogrammetry techniques can either utilize direct geo-referencing, ground control points, manual tie-in points, or a combination thereof [26]. Geo-referencing is most easily achieved with time-stamped GPS data recorded during flight [27]. It is typical to use photogrammetry techniques to create a large and complete image of a singular façade [28]. Specifically, in regards to building energy inspection, the most common methodology for post processing uses threshold techniques and software to segment or enhance image saturation to further emphasize the region of interest [4, 29].

3D modelling techniques can be organized into two sets of goals; groups of buildings (geoclusters), or singular buildings [30]. Although extensive research has been conducted, Borrmann et al. bring attention to the fact that, to the best of their knowledge at the time of publication, no truly autonomous system for 3D model generation of building geometry using thermal imaging has been recorded in a scholarly article [21]. LiDAR is argued to be superior for this task [31]. Most literature focusing on photogrammetry experimented with point clouds and have yielded commendable results though none with as much fine detail as with LiDAR technology. Lizarazo et al. use RGB photos to create 3D geometry first because the spatial resolution tends to be more optimized than the infrared photos. In addition, they developed algorithms and applied Wallis filters to successfully improve the accuracy of the final product [10]. Multiple researchers tested a methodology where RGB photos were used to create an initial 3D model where the infrared images would later be overlaid as they found that 3D model generation software tends to be more successful with RGB photos [32,33].

4. DISCUSSION

Reviewed literature varies and sometimes overlaps in recommended inspection methodologies. A case study was therefore developed as an application that combines and tests reviewed literature outcomes. The case study is investigated through the paper's objectives, by detailing pre-flight path design, during-flight data gathering and post-flight analysis. The inspected building was chosen as a generic residential structure on a university campus. All flight parameters were varied, including flight path design, image capturing density, overlap and distances from buildings and external environmental conditions for surveys. The aim was to develop empirical setups for building inspection using UAS equipped with thermal cameras.

Field tests were conducted with a DJI Inspire 1 drone, paired with a FLIR Zenmuse XT thermal camera. The accompanying DJI app was used during flight to

monitor the thermal data. The flight path was pre-determined and automated using the Litchi and DroneDeploy app for roof images. The images were processed and analysed using the FLIR Tools program. We empirically found that using both the strip pattern and the archimedic spiral, as detailed earlier, have proven to be effective methods. The strip pattern with at least a 70% overlap is suitable for gathering data to audit or visualize energy use in buildings. An elliptical flight path with as much as 95% overlap is appropriate for photogrammetry and 3D model generation. A distance of 12 m away from the target surface with changing bay widths of 2–3m is fitting for capturing images every one and a half meters along the path. For the generation of 3D models, flying multiple elliptical flights at varying altitudes can be ideal. The most effective altitudes have been found to be 18, 22, and 27 m, or twice the height of the building and twice the size of the building footprint. The flights should increase in altitude and size by roughly 1.25X per flight. Although this seems redundant, current 3D model generation software, like Pix4D, works best with a repetitive surplus of images. Fig. 2 represents the empirical parameters of flight path planning.

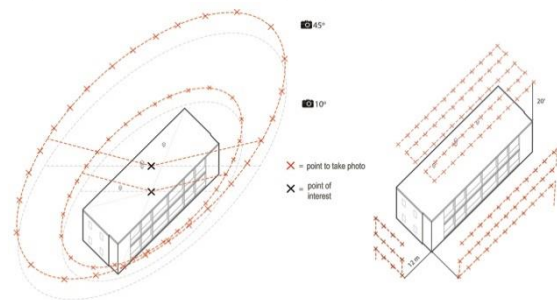


Figure 2: Flight path parameters for building inspection.

For thermography purposes using UAS, our experimentation confirms that better conditions for thermal imaging are cloudy morning or evening hours with stable temperatures and no precipitation. At the time of writing this paper, a difference between indoor and outdoor temperature of at least 10 degrees Kelvin is recommended when a FLIR camera is being used [34]. This may not be necessarily the case for more sensitive state-of-the-art IR cameras, and also may not be feasible in regards to commercial year-round UAS applications. INS and GPS systems should be correctly calibrated to accurately geo-tag the images. Fig. 3 demonstrates examples of compromises of an example building envelope, identified with thermal imaging.

PLEA 2018 HONG KONG

Smart and Healthy within the 2-degree Limit

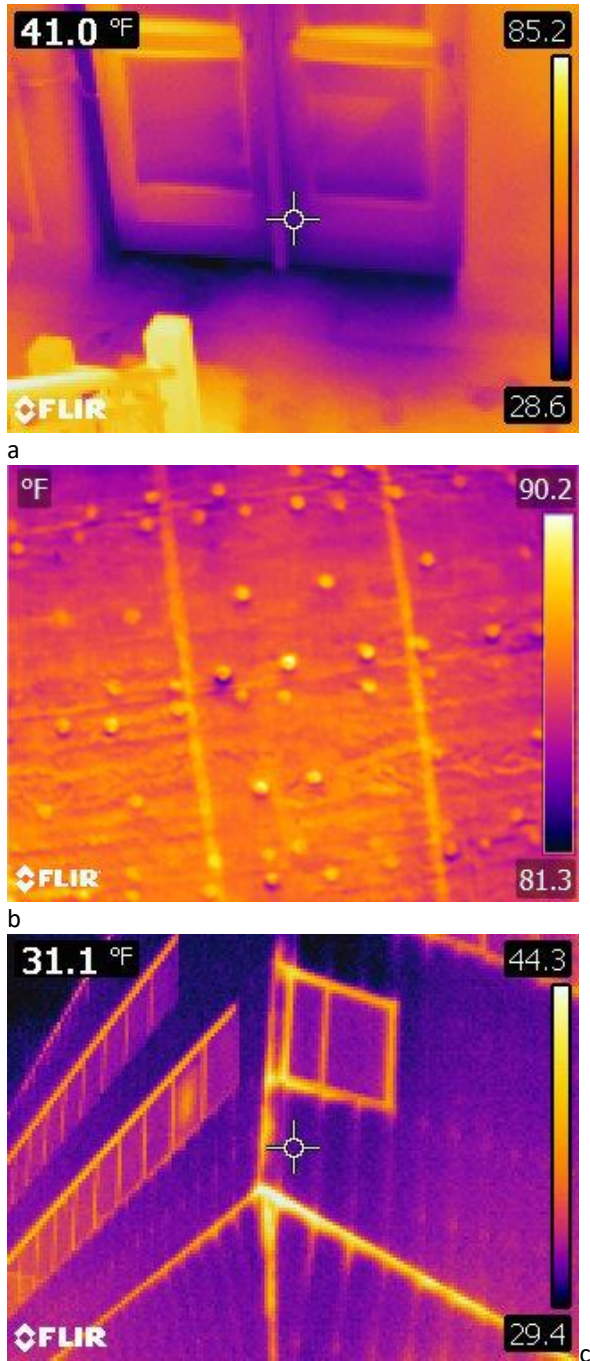


Figure 3: Envelope issues identified using an IR camera.
a. Door infiltration, with change in floor temperature.
b. Possible thermal bridging by nails that effect the roof.
c. Leakage as a result of envelope installation malfunction.

Photos taken during our test drone flight were used in the program Pix4D to generate a 3D point cloud from the 2D images. Multiple models may be recommended based on the number of photos taken. Based on empirical trials and observations, approximately 1000–1300 photos are recommended as a suitable number of photos for one simulation, due to current software limitations that may be resolved in the future. Multiple models may be merged upon completion, and this allows the operator to eliminate photos that

may not calibrate properly. The program extracts pixels from 2D images by triangulation and locates individual pixels from photos within a 3D point cloud model. During this process, images of inferior quality and images that did not capture the subject will be rejected by the program. Upon generation of the model, we observed that the façade that produced the most detailed model is consistently located on the southern face of the inspected building due to solar radiation exposure. Using Pix4D modeler, the program runs a 15-point process that results in a report output noting the efficiency of the photos used in generating the model, image overlap, location, among other variables. This output notes weaknesses of the image retrieval process and should influence future flights. The model can be processed in other 3D modelling and CAD software such as Rhino3D. When opened in a .FBX file format, the 3D model will maintain render and texture capabilities. The model is compatible and is able to be used in rendering and 3D printing (Fig. 4).

5. CONCLUSION

This review detailed current procedures and methodologies of UAS-based thermal imaging practices. An experiment was conducted to empirically assess reviewed work, and a UAS-based building inspection method was presented, tested, and results were stated. Currently aging infrastructure and building stock necessitate energy retrofitting action and advancements in the methods with which thermal issues are identified will enable more action. In the age of climate change, the use of UASs and infrared imaging has proven to be a significant improvement on traditional auditing methods and techniques [6]. The increased accessibility, efficiency, and safety present a unique opportunity to expedite the improvement and retrofitting of aging and energy in-efficient building stock and infrastructure. Existing software and mathematical concepts present a variety of options for post processing, analysis, and visual representation with reduced manual workflow, as a step closer towards fully automated building performance inspections using drones. Future research should build on the presented workflows to develop a standardized approach for building energy audits. This should include references to existing technological capabilities and further parameterization of the process to become more global through replicated experiments that validate the presented work.

PLEA 2018 HONG KONG

Smart and Healthy within the 2-degree Limit

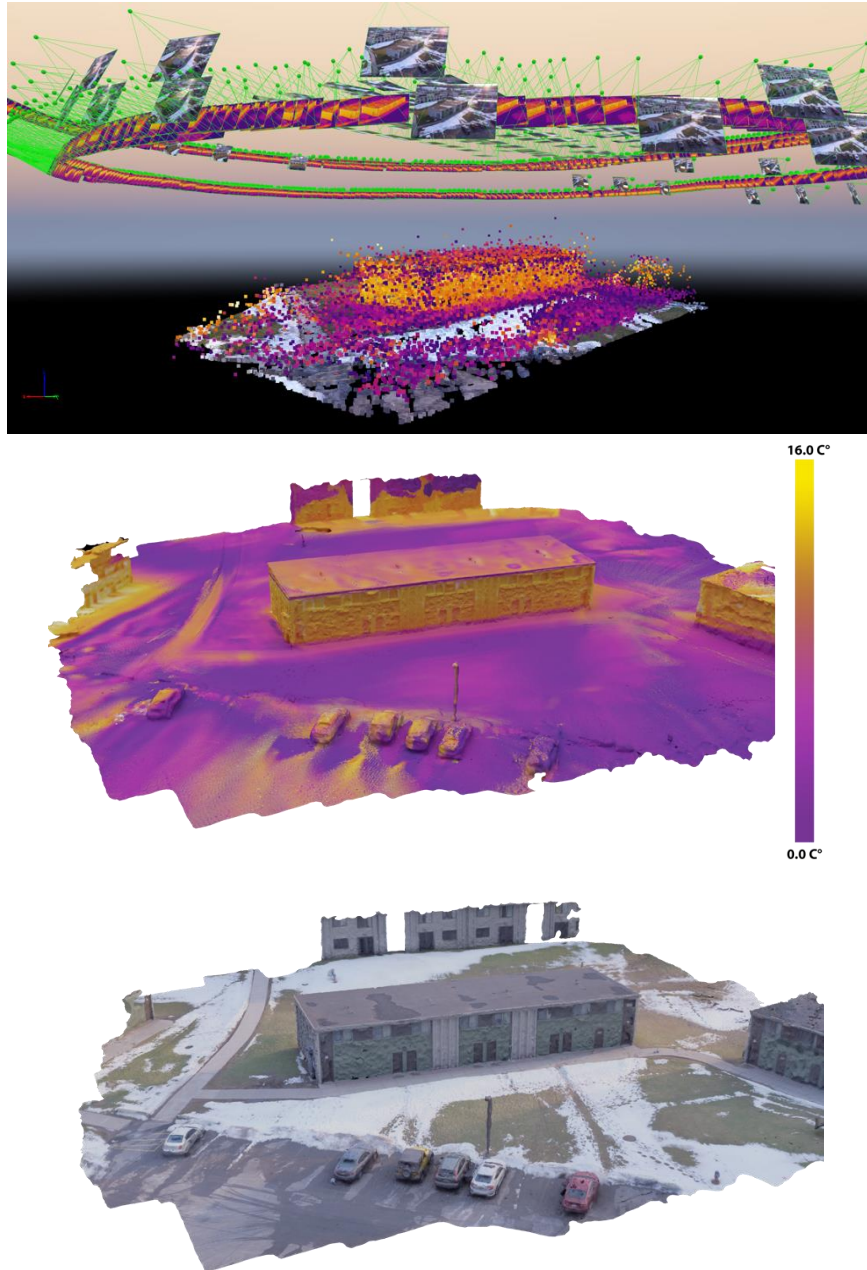


Figure 4: Infrared and RGB models generated using 3D photogrammetry using Pix4D and Rhino3D CAD modelling software

ACKNOWLEDGEMENTS

This publication is based on work funded in part by Gryphon Sensors, Syracuse University's Office of Research (Grant #SP-29403-2) and the Campus as a Lab for Sustainability program at Syracuse University. The authors would like to thank Mr. Ian Joyce, the Center for Advanced Systems Engineering (CASE) and the Syracuse Center of Excellence at Syracuse University for drone flight, data gathering and faculty development support. The authors are also grateful for the student work Amanda Liberty and Rasan Taher provided to support this manuscript.

REFERENCES

1. U.S. Census Bureau, [Online]. Retrieved from: [https://www.census.gov/programs-](https://www.census.gov/programs-surveys/ahs/data/interactive/ahstablecreator.html?s_area=s-a00000&s_year=n2015&s_tableName=Table1&s_byGroup1=a1&s_byGroup2=a1&s_filterGroup1=t1&s_filterGroup2=g1&s_show=S)

[surveys/ahs/data/interactive/ahstablecreator.html?s_area=s-a00000&s_year=n2015&s_tableName=Table1&s_byGroup1=a1&s_byGroup2=a1&s_filterGroup1=t1&s_filterGroup2=g1&s_show=S](https://www.census.gov/programs-surveys/ahs/data/interactive/ahstablecreator.html?s_area=s-a00000&s_year=n2015&s_tableName=Table1&s_byGroup1=a1&s_byGroup2=a1&s_filterGroup1=t1&s_filterGroup2=g1&s_show=S), (2015), Accessed date: 6 February 2017.

2. U.S. Energy Information Administration, How much energy is consumed in U.S. residential and commercial buildings? [Online]. Retrieved from: <https://www.eia.gov/tools/faqs/faq.php?id=86&t=1>, (2017), Accessed date: 14 May 2017.

3. U.S. Department of Energy, Thermographic inspections, [Online]. Retrieved from: <https://energy.gov/energysaver/thermographic-inspections>, (2012), Accessed date: 18 May 2017.

4. A. Kylili, P.A. Fokaides, P. Christou, S.A. Kalogirou, Infrared thermography (IRT) applications for building diagnostics: a review, Applied Energy, 134 (2014) 531–549.

PLEA 2018 HONG KONG

Smart and Healthy within the 2-degree Limit

5. L.E. Mavromatidis, D.J. L. R. Saleri, J.C. Batsale, First experiments for the diagnosis and thermophysical sampling using impulse IR thermography from unmanned aerial vehicle (UAV), Quantitative InfraRed Thermography Conference, Bordeaux, 2014.
6. C. Corsi, History highlights and future trends of infrared sensors, *Journal of Modern Optics*, 57 (18) (2010) pp. 1663–1686.
7. S. Schuffert, T. Voegtle, N. Tate, A. Ramirez, Quality assessment of roof planes extracted from height data for solar energy systems by the EAGLE platform, *Remote Sensing*, 7 (12) (2015) 17016–17034.
8. K. Kakaes, F. Greenwood, M. Lippincott, S. Dosemagen, P. Meier, S. Wich, Drones and aerial observation: new technologies for property rights, human rights, and global development, New America, <https://www.newamerica.org/international-security/events/drones-and-aerial-observation/>, (2015), Accessed date: 7 September 2017.
9. R. Steffen, W. Forstner, On visual real time mapping for unmanned aerial vehicles, the International Archives of the Photogrammetry, Remote Sensing, and Spatial Information Sciences. XXXVII (B3a) (2011) 57–62.
10. I. Lizarazo, V. Angulo, J. Rodriguez, Automatic mapping of land surface elevation changes from UAV-based imagery, *International Journal of Remote Sensing*, 38 (8–10) (2017) pp. 2603–2622.
11. C. Eschmann, T. Wundsam, Web-based georeferenced 3D inspection and monitoring of bridges with unmanned aircraft systems, *Journal of Surveying Engineering*, 143 (3) (2017), pp. 04017003-1–04017003-10.
12. A. Choi-Fitzpatrick, T. Juskauskas, Up in the air: applying the Jacobs Crowd formula to drone imagery, *Procedia Engineering*, 107 (2015), pp. 273–281.
13. F. Tauro, M. Porfiri, S. Grimaldi, Surface flow measurements from drones, *Journal of Hydrology*, 540 (2016), pp. 240–245.
14. T.D. Stek, Drones over Mediterranean landscapes. The potential of small UAV's (drones) for site detection and heritage management in archaeological survey projects: a case study from le Pianelle in the Tappino Valley, Molise (Italy), *Journal of Cultural Heritage*, 22 (2016), pp. 1066–1071.
15. K.N. Tahar, Aerial terrain mapping using unmanned aerial vehicle approach, the International Archives of the Photogrammetry, Remote Sensing and Spatial Information Sciences. XXXIX (B7) (2012), pp. 493–498.
16. D. Gonzalez-Aguilera, S. Laguela, P. Rodriguez-Gonzalvez, D. Hernandez-Lopez, Image-based thermographic modeling for assessing energy efficiency of building facades, *Energy in Buildings*, 65 (2013) pp. 29–36.
17. F. Nex, F. Remondino, UAV for 3D mapping applications: a review, *Applied Geomatics*, 6 (1) (2014), pp. 1–15.
18. W. Volkmann, G. Barnes, Virtual surveying: mapping and modeling cadastral boundaries using Unmanned Aerial Systems (UAS), Proceedings of the Federation Internationale des Geometres (FIG) Congress: Engaging the Challenges—Enhancing the Relevance, Kuala Lumpur, 2014.
19. D. Roca, S. Laguela, L. Diaz-Vilarino, J. Armesto, P. Arias, Low-cost aerial unit for outdoor inspection of building facades, *Automation in Construction*, 36 (2013) pp. 128–135.
20. M. Fox, D. Coley, S. Goodhew, P. de Wilde, Thermography methodologies for detecting energy related building defects, *Renewable and Sustainable Energy Reviews*, 40 (2014), pp. 296–310.
21. D. Borrmann, A. Nuchter, M. Dakulovic, I. Maurovic, I. Petrovic, D. Osmankovic, J. Velagic, A mobile robot based system for fully automated thermal 3D mapping, *Advanced Engineering Informatics*, 28 (4) (2014), pp. 425–440.
22. E. Grinzato, IR thermography applied to the cultural heritage conservation, 18th World Conference on Nondestructive Testing, Durban, 2012.
23. N.D. Opfer, D.R. Shields, Unmanned aerial vehicle applications and issues for construction, 121st American Society of Engineering Education (ASEE) Annual Conference & Exposition, Indianapolis, 2014.
24. Y. Ham, M. Golparvar-Fard, An automated vision-based method for rapid 3D energy performance modeling of existing buildings using thermal and digital imagery, *Advanced Engineering Informatics*, 27 (3) (2013) pp. 395–409.
25. S. Yahyanejad, B. Rinner, A fast and mobile system for registration of low-altitude visual and thermal aerial images using multiple small-scale UAVs, *ISPRS Journal of Photogrammetry Remote Sensing*, 104 (2014), pp. 189–202.
26. M. Hollaus, High resolution aerial images from UAV for forest applications, <http://www.newfor.net/wp-content/uploads/2015/02/DL14-Newfor-SoA-UAV.pdf>, (2014), Accessed date: 29 June 2017.
27. P. Rodriguez-Gonzalvez, D. Gonzalez-Aguilera, G. Lopez-Jimenez, I. Picon-Cabrera, Image-based modeling of built environment from an Unmanned Aerial System, *Automation in Construction*, 48 (2014) pp. 44–52.
28. O. Kung, C. Strecha, A. Beyeler, J.C. Zufferey, D. Floreano, P. Fua, F. Gervais, The accuracy of automatic photogrammetry techniques on ultra-light UAV imagery, *Unmanned Aerial Vehicle in Geomatics*, Zurich, 2011.
29. J.R. Martinez-de Dios, A. Ollero, J. Ferruz, Infrared inspection of buildings using autonomous helicopters, 4th International Federation of Automatic Control (IFAC) Symposium on Mechatronic Systems, Loughborough, 2006.
30. X. Feifei, L. Zongjian, G. Dezhu, L. Hua, Study on construction of 3D building based on UAV images, the International Archives of the Photogrammetry, Remote Sensing and Spatial Information Sciences, Volume XXXIX (B1) (2012), pp. 469–473.
31. S. Emelianov, A. Bulgakow, D. Sayfeddine, Aerial laser inspection of buildings facades using quadrotor, *Procedia Engineering*, 85 (2014), pp. 140–146. Part of special issue: selected papers from Creative Construction Conference, Prague, 2014.
32. M.N. Zulfafli, K.N. Tahar, Three dimensional curve hall reconstruction using semi-automatic UAV, *ARPN Journal of Engineering and Applied Sciences*, 12 (10) (2017), pp. 3228–3232.
33. L. Lopez-Fernandez, S. Lagüela, I. Picon, D. Gonzalez-Aguilera, Large scale automatic analysis and classification of roof surfaces for the installation of solar panels using a multi-sensor aerial platform, *Remote Sensing*, 7 (9) (2015), pp. 11226–11248.
34. FLIR Systems, Thermal Imaging Guidebook for Building and Renewable Energy Applications, http://www.flirmedia.com/MMC/THG/Brochures/T820325/T820325_EN.pdf. (2013)

Enhancement of the WUDAPT Portal Tool WUDAPT2ENVI-met: Introducing Site-Specific Local Climate Zones to WUDAPT2ENVI-met

TIM KROPP¹, HELGE SIMON¹, PAULA SHINZATO², LUCIANA SCHWANDNER FERREIRA², CAROLINA DOS SANTOS GUSSON², DENISE DUARTE², MICHAEL BRUSE¹

¹Department of Geography, Johannes Gutenberg University Mainz, Mainz, Germany

²Faculty of Architecture and Urbanism, University of Sao Paulo, Sao Paulo, Brazil

ABSTRACT: The new WUDAPT portal tool 'WUDAPT2ENVI-met' supplies a fast and easy way to generate large urban areas for ENVI-met simulations in a worldwide consistent manner. WUDAPT's Local Climate Zone Classifications provide spatial information based on satellite imagery, which is translated into large ENVI-met model areas by templates of ENVI-met objects called Standard LCZ tiles. While 17 Local Climate Zone classes seem to be sufficient to describe the inhomogeneity of urban morphologies within one urban area, the inhomogeneity of urban morphologies across different urban areas worldwide might call for more, site-specific morphology classes. Based on this requirement WUDAPT2ENVI-met was enhanced allowing the import of user-generated, site-specific LCZ tiles for the translation. In order to examine whether the Standard LCZ tiles are versatile enough to dissect urban areas worldwide, a classification using the Standard LCZ tiles and specific, user-generated morphologies is compared in a case study of Sao Paulo. Furthermore, the results are compared against a simulation of the same area consisting of the actual building morphology. The comparison showed that the use of site-specific morphologies, materials and plants improved the results, better fitting the results of the actual morphology simulation, which states an important enhancement of the tool.

KEYWORDS: WUDAPT, ENVI-met, Modelling Urban Climate, Urban structure types, city morphology analysis

1. INTRODUCTION

Urban climate models require coherent and high-resolution input data to account for the spatial inhomogeneity of urban areas. The availability of such data varies greatly depending on the area. To provide coherent high-resolution data for the entire globe, an international collaborative project for climate-relevant physical geography data for the world's cities has been called into existence: the World Urban Database and Access Portal Tools (WUDAPT) [1]. Its main goals are described in two objectives: One, to acquire high-resolution, consistent, climate-relevant information on urban morphological structures on a worldwide basis. This objective is carried out by using globally available satellite data, based on which gridded morphology data is created that classifies cities into Stewart & Oke's 17 distinct local climate zones (LCZ) [2]. Two, to create tools, which will make use of this classification. Here, the urban parameters and properties of the LCZs shall be used as input data for various applications such as climate simulations or urban planning purposes [3].

In this contribution, applications of the WUDAPT Portal Tool "WUDAPT2ENVI-met", linking the widely used microclimate model ENVI-met with WUDAPT, are presented. The WUDAPT2ENVI-met tool uses the WUDAPT output, a LCZ classification based on satellite imagery, to generate ENVI-met model areas.

With ENVI-met's high-resolution model, where the urban environment is modelled with little to no

parametrization, distinct information about each LCZ's design is needed. Therefore, the guidelines of Stewart and Oke were translated into explicitly digitized 100 m x 100 m large areas called "Standard LCZ tiles". These templates were digitized as vector graphics and contain information about morphology, distribution, and parameter assignment for every ENVI-met object type (buildings, surface/soil materials, simple vegetation, 3D vegetation).

ENVI-met's newly developed vector editor Monde is able to import shapefiles and export them to ENVI-met model areas by gridding the objects in user-defined resolutions [4]. Within this editor, WUDAPT2ENVI-met loads the LCZ tiles as templates and arranges them according to the spatial distribution information provided by WUDAPT's LCZs, thus offering the possibility to quickly create city-scale model areas. However, the use of only the Standard LCZ tiles might come at a disadvantage: While 17 classes seem to be sufficient to describe the inhomogeneity of urban morphologies within one urban area, the inhomogeneity of urban morphologies across different urban areas worldwide might call for more, site-specific morphology classes.

In order to examine whether the Standard LCZ tiles are versatile enough to dissect urban areas worldwide, a classification using the Standard LCZ tiles and user-generated, site-specific morphologies is compared against a model area with actual building morphologies in a case study in Sao Paulo.

PLEA 2018 HONG KONG

Smart and Healthy within the 2-degree Limit

2. METHODOLOGY

In order to understand the differences between Standard and site-specific LCZ tiles, their basic layouts and properties are presented: First, the general digitization process is introduced. Then, the digitized representations of the supposedly worldwide applicable Standard LCZ tiles and the presumably better fitting site-specific LCZ tiles for Sao Paulo are presented.

2.1 General properties

All LCZ tiles were digitized as shapefiles according to the guidelines of Stewart & Oke, which define certain properties for every LCZ. Each LCZ tile covers an area of 100 m x 100 m, which represents a typical building block size of urban morphology types in cities worldwide. To ensure that all LCZ tiles fit together seamlessly when they are assembled into an array creating a 3D city-mosaic, all LCZs are digitized having an open, non-built-up area at the borders. Furthermore, all LCZ tiles are mirrored at their primary and secondary axis in order to give them regularity in themselves, aiming for a high self-similarity (Fig. 1).

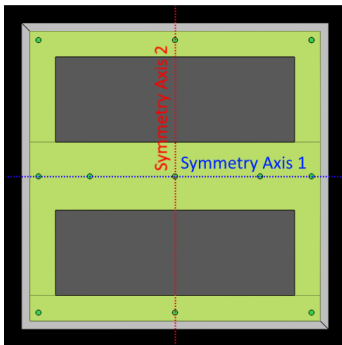


Figure 58: Schematic representation of the self-similarity objective for the digitization process

In order to achieve high accuracy in digitization, the LCZ tile layout was arranged by aligning the objects at a vector grid of 2.5 m resolution. Most objects or gaps, however, feature a multiple of this resolution, e.g. 5 m, 7.5 m, or 10 m, which allows to create coarser, and thereby larger, model areas without distortion, when the vector objects are exported to raster voxels with a distinct resolution.

All LCZ tiles are covered by objects or surfaces according to the LCZ properties defined by Stewart & Oke 2012 [2]. The layout of each LCZ tile is primarily determined by the surface fraction range of buildings and impervious/pervious areas as well as a high level of self-similarity. The height of buildings and trees is modeled according to the defined average height of roughness elements.

2.2 Standard LCZ tiles

All Standard LCZ tiles use homogenous standard IDs of the ENVI-met database. Open soil of pervious areas is defined as Loamy Soil [LO]. Impervious areas are mostly covered with Pavement [PP], whereas LCZ tile borders are often digitized as Asphalt Road [ST]. Water surfaces are defined as Deep Water [WW]. The materials of walls and roofs of single buildings are not specified. Default values for all buildings can be set within the model area file. Simple plants are always defined as grass of 50 cm height with average density [XX]. 3D vegetation of urban LCZs is split into three groups: small, medium, and large trees. All used trees and their dimensions are shown in Table 1.

Table 1: IDs and dimensions of 3D plants used in Standard LCZ tiles

Plant name	ID	Height [m]	Crone width [m]	LCZ
White Poplar	PA	7.0	5.0	urban
Black Locust	03	12.0	7.0	urban
Tilia	PR	18.0	13.0	urban
Ash	B5	20.0	11.0	A
Norway Maple	07	18.0	7.0	B
Field Maple	A9	12.0	9.0	B
Pine Trees	PI	4.0	5.0	C

All these ENVI-met IDs, as well as the building heights for building polygons, are determined in specific attribute columns called 'ENVIID' or 'height', respectively. All shapefiles of the Standard LCZ tiles must be named uniformly in order to be automatically identified by the tool. The first two characters of the shapefile name define the LCZ numbered from 01 to 17. After the separation using an underscore, the object type is declared as 'areas', 'buildings', 'simpleplants', or '3Dplants'. All 17 Standard LCZ tiles are displayed in Fig. 2.

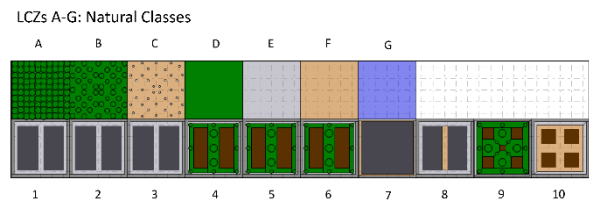


Figure 59: Representation of all Standard LCZ tiles in vector editor Monde

Standard LCZ tiles 1-3 and Standard LCZ tiles 4-6 are digitized with the same respective surface fraction properties, showing the only difference in building heights (Fig. 3). By choosing those similar appearances for the three main inner city and three main outer city urban morphology types, respectively, high homogeneity is achieved.

In order to generate large model areas, WUDAPT model areas will often be simulated in coarse resolution. Thus, highly detailed building morphologies, for example for the midrise or low-rise LCZs, are not necessary. Moreover, those details could

PLEA 2018 HONG KONG

Smart and Healthy within the 2-degree Limit

cause complications since building gaps with a size below gridding resolution may distort the model area when gridded.

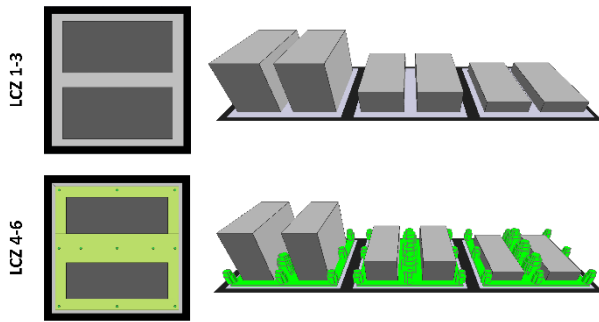


Figure 60: Representation of the Standard LCZ tiles 1-3 and 4-6 gridded in 1 m resolution (they differ in building height only)

As Standard LCZ tiles, their appearance is rather monotonous, mainly varying in building height and amount of vegetation. These tiles, however, only represent the standard topology, which enables a uniform translation of LCZ classes into ENVI-met model areas applicable for most regions of the world. Additionally, the user can still manually edit model areas. Single objects, like trees or buildings, can be modified, added, or deleted to approximate the real urban environment.

2.3 Site-Specific LCZ tiles

In order to compare whether the 17 Standard LCZ tiles are sufficient to represent urban morphologies worldwide, the portal tool was enhanced to allow the replacement of Standard LCZ tiles by site-specific, user-generated LCZ tiles. Specific building shapes or heights, different materials, soils, or trees, which might fit the conditions of the project area better, can be provided for all LCZs.

The collaborating working group at the Faculty of Architecture and Urbanism at the University of Sao Paulo acted as local expert delivering additional information like local building morphologies or materials for the site-specific LCZ tiles.

As of yet, the first 6 LCZs have been built by the local experts. The site-specific LCZ tiles consist of specific vegetation, building materials, and soils. The specific Brazilian tree [M9] is medium sized with a height of 10 m and a width of 7 m. Simple Plants are characterized as standard grass [XX]. Building walls are defined as a newly designed brick wall [B4]. 3 cm of the inner and outer side of the wall consist of plaster [P1]. The wall's core is built up of a 20 cm thick brick layer [BB]. The roof's inside is also specified as a 3 cm thick layer of plaster [P1], the outer 3 cm layer as a specific roof plaster [PR]. Its core consists of reinforced concrete [CR] with a thickness of 12 cm (Tab. 2).

Besides the standard soil profile of pavement [PP] for general impervious areas, two new profiles were created. Asphalt roads are digitized with [AK], consisting of the specific asphalt [KB] in the layer of the top 40 cm, which features a volumetric heat capacity of $2.62 \cdot 10^6 \text{ J/m}^3\text{K}$ and a heat conductivity of 1.26 W/mK. Deeper layer are filled with the standard soil material clay [TO]. The whole soil profile [AK] has a roughness length of 0.01, an albedo of 0.2 and an emissivity factor of 0.95. Pervious areas are characterized as Brazilian soil [OS], which is entirely composed of the standard soil Sandy Clay Loam [TS], thus having a roughness length of 0.015, an albedo of 0.33, and an emissivity factor of 0.9.

Table 2: Physical properties of the materials used in site-specific LCZ tiles

	Plaster [P1]	brick wall [BB]	roof plaster [PR]	roof concrete [CR]
Thickness [m]	0.025	0.2	0.025	0.1
Absorption	0.5	0.65	0.65	0.8
Transmission	0	0	0	0
Reflection	0.5	0.35	0.35	0.2
Emissivity	0.85	0.9	0.9	0.9
Specific Heat Capacity $\left[\frac{\text{J}}{\text{m}^3 \cdot \text{K}} \right]$	754	1005	650	1005
Thermal Conductivity $\left[\frac{\text{W}}{\text{m} \cdot \text{K}} \right]$	0.85	0.91	0.5	1.75
Density $\left[\frac{\text{kg}}{\text{m}^3} \right]$	1800	1700	1500	2400

The most striking difference exists in the design of the LCZ morphologies (Fig. 4). In contrast to the uniform layout of the Standard LCZ tiles, the Sao Paulo specific LCZs feature several instead of two single buildings and are digitized with increased heights. They also depict the high amount of impervious areas for the LCZ tiles 1-3 and increased vegetation in LCZ tiles 4-6. The tree distribution is quite heterogeneous, thus leading to slightly lower self-similarity.

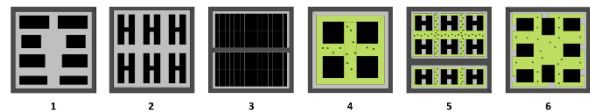


Figure 4: Representation of the site-specific LCZ tiles 1-6

All 6 user-defined morphologies correspond to real urban blocks, which were digitized using aerial photography. Thereby, the building shapes became very complex and detailed. Complex structures may negate one of the main advantages of WUDAPT2ENVI-met: gridding in coarse resolutions with little distortion. However, the site-specific LCZ tiles need specifications to set themselves apart from the standard ones. Thus, a tradeoff should be achieved between the homogenous Standard LCZ tiles and the heterogeneous and complex site-specific LCZ tiles.

PLEA 2018 HONG KONG

Smart and Healthy within the 2-degree Limit

3. PROPERTIES OF THE CASE STUDY

To examine, whether the Standard LCZ tiles are sufficient to represent the urban morphologies in a specific metropolitan region, the case study area Sao Paulo was digitized in three versions. The first and second model area derive from the WUDAPT2ENVI-met tool using the Standard and site-specific LCZ tiles, respectively. The third model area consists of the actual city morphology originating from OpenStreetMap data.

3.1 Case study area

Because the metropolitan region of Sao Paulo covers around 8000 km² [5], only a small part can be extracted and simulated. Since the subset represents an application example of WUDAPT data, the subset should show as many different LCZs in a recognizable morphology as possible.



Figure 5: Presentation of the LCZC subset with the corresponding color code [6]

The chosen subset area is located in the city's west in a district called 'Pinheiros'. The UTM coordinates of the top left corner are X: 325853, Y: 7393472, UTM zone 23K (Fig. 5).

The horizontal dimensions are 2220 m in X direction and 1420 m in Y direction. The subset area is gridded in 5 m horizontal resolution resulting in a model area of 444 x 284 grids. This size and resolution offers a good tradeoff between short simulation durations and relatively high resolutions with little to no gridding distortion (Fig. 6).

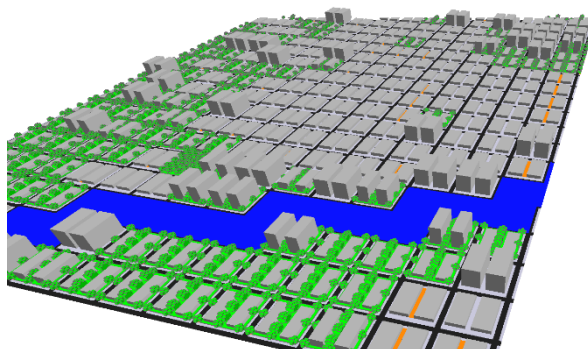


Figure 6: 3D view of the exported model area in ENVI-met's raster editor Spaces; translated with Standard LCZ tiles, gridded in 5 m horizontal resolution, view direction 230°

Buildings of the site-specific LCZ tiles consist of the Sao Paulo specific brick wall [B4] and the roof [CS]. The first 6 urban LCZ classes are replaced by the site-specific LCZ tiles, the other classes are still represented by Standard LCZ tiles, although they also feature newly created specific building materials. Soil profiles and trees of the residual Standard LCZ tiles still contain their standard definitions.

The model area's appearance changed considerably with the utilization of site-specific LCZ tiles because of the more complex building morphologies. The *Open* LCZ tiles consist of several single buildings instead of one or two large ones. LCZ 3, which covers most of the subset center, is digitized with no or only small building gaps resulting in compact building morphologies when gridded in coarse resolution.

Due to the adapted morphologies and materials in the site-specific LCZ tiles, it is to be expected that the results of both WUDAPT-based simulations vary. Furthermore, the contrast between different LCZ classes might be more pronounced in the site-specific than in the standard versions of the case study area due to their comparatively more heterogeneous appearance.

In order to evaluate the quality which can be achieved by replacing the Standard LCZ tiles with site-specific LCZ tiles, the same area was again digitized, this time using the actual city morphology including vegetation, building structures and surfaces. It is to be expected that the simulation results using the actual city morphology represent the microclimatic conditions of the case study area with the highest accuracy. Since the site-specific LCZ tiles match the actual city more precisely, it can be assumed that these results are at least more accurate, i.e. closer to the actual scenario, than the Standard LCZ tiles.

In order to test this hypothesis, the differences in the model outputs between Standard LCZ tiles and actual morphology are compared against the differences between site-specific LCZ tiles and actual building morphology. A lower difference between site-specific LCZ tile and actual morphology simulation results than between Standard LCZ tile and actual morphology simulation results should then indicate the quality of improvement caused by the usage of the site-specific LCZ tiles.

3.2 General simulation properties

General properties and meteorological conditions are set equally for all simulations to ensure that discrepancies are caused by the morphology of the model area. The simulation time covers 24 hours, starting at 07:00 on December 10th 2017 in order to simulate a warm summer day. The meteorological boundary conditions of wind speed, wind direction,

PLEA 2018 HONG KONG

Smart and Healthy within the 2-degree Limit

temperature, and humidity derive from climatic average values for Sao Paulo in December [7]. Wind speed is specified as 1.5 m/s in 10 m height coming from 135°. Diurnal cycles of air temperature and relative humidity are provided as boundary conditions using Simple Forcing (Fig. 7). Additionally, constant parameters are set for temperature and relative humidity in every soil layer: 293 K and 85 %.

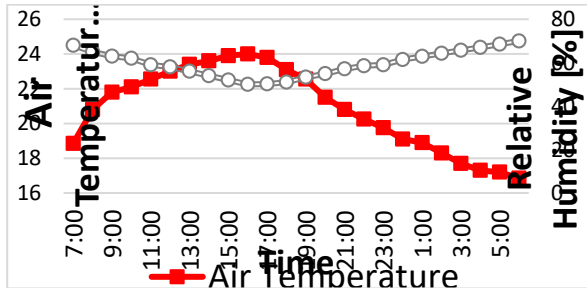


Figure 7: Linear interpolation of the Simple Forcing values used in the case study

4. RESULTS

At first, simulation results using the standard translation method are compared against the simulation, which uses the site-specific LCZ tiles for the WUDAPT2ENVI-met translation. Those site-specific LCZ tile simulation results are then compared against the run with actual morphologies, which is assumed to fit the microclimate best. In a last step, air temperature values of all three simulations, averaged over the whole model area, are compared in order to evaluate the quality of improvement achieved by the use of site-specific LCZ tiles.

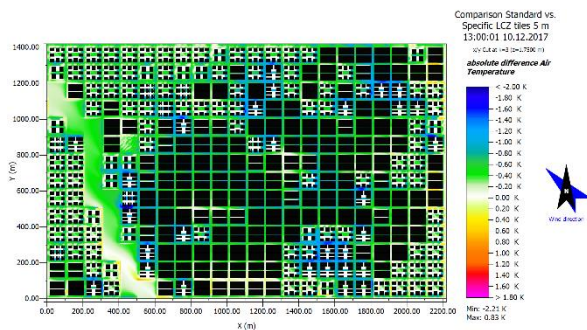


Figure 8: XY Cut in 1.75 m height of the comparison between the Sao Paulo subset simulations using Standard LCZ tiles and the simulation using site-specific LCZ tiles at 13:00

Fig. 8 shows a difference map of Standard and site-specific LCZ tile simulation including the site-specific building morphologies in 1.75 m height. The x/y cut in 1.75 m height is chosen because of its relevance for human beings as it represents the air temperature at face level. Colors indicate the absolute air temperature difference in 1.75 m height between Standard and site-specific LCZ tile simulation. Due to the varying building distribution and appearance depending on

the LCZ origin, the result map contains several white areas. These are areas, where Standard LCZ tile buildings are located and thus cannot be accounted for air temperature comparison. The utilization of site-specific LCZ tiles led to an air temperature decrease of up to 2.2 K near the compact subset center (Fig. 8), which is caused by shading of the generally higher building morphologies.

The difference map in Fig. 9 features the actual building morphology. Colors indicate the absolute air temperature difference in 1.75 m height between the results of the site-specific run and the actual morphology simulation. Again, the white rectangular areas, which show no difference in air temperature, are caused by buildings being placed in the site-specific simulation, thus neglecting a direct comparison in these places. Large asphalt streets of the actual morphology simulation feature around 3 K hotter air temperatures compared with the riverside or shaded areas of the site-specific LCZ tile simulation. In general, however, the model area of actual morphologies shows cooler temperatures due to a higher amount of shading caused by more and higher buildings as well as narrower streets.

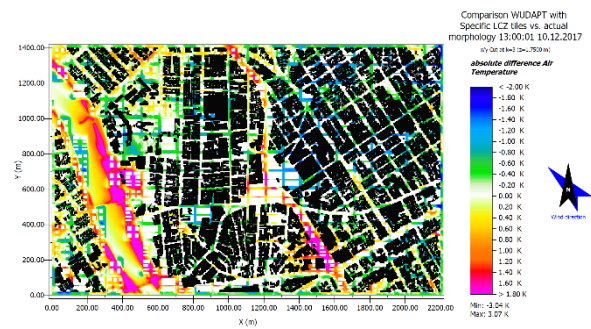


Figure 9: XY Cut in 1.75 m height of the comparison between the Sao Paulo subset simulations using site-specific LCZ tiles and the simulation using actual morphologies at 13:00

In order to evaluate the increase in accuracy due to the introduction of site-specific LCZ tiles, the air temperature values of all atmosphere cells in 1.75 m height were averaged for every timestep.



Figure 10: Root Mean Square Error values comparing the simulations using Standard/site-specific LCZ tiles and actual morphologies

Using the Root Mean Square Error (RMSE) of these averaged air temperature values, the effect of site-specific LCZ tiles is evaluated by examining the difference between the simulations. The RMSE value between Standard and Actual (less than 0.7 K) shows a low difference of absolute values in general. The relatively small discrepancies might be caused by the

PLEA 2018 HONG KONG

Smart and Healthy within the 2-degree Limit

exchange of only 6 site-specific LCZ tiles. The largest difference occurs between the simulation with Standard LCZ tiles and actual morphologies (0.641), while smaller variation occur between Standard and site-specific LCZ tiles (0.342) as well as between site-specific LCZ tiles and actual morphologies (0.406) (Fig. 10).

Since RSME is based on squared values, the deviation can be both, positive or negative. In order to point out the deviation, averaged air temperature values are displayed in a diagram (Fig. 11). The curves' progression is quite similar, which is validated by R-squared values of more than 0.99 between the averaged values. Mainly during daytime, the site-specific LCZ tiles fit the air temperature values of the actual morphologies better than the Standard LCZ tile simulation. Thus, the results of the site-specific simulation do not only feature a lower RMSE with the actual morphology simulation but also approach the results more precisely with cooler temperatures in general. During nighttime, however, both WUDAPT based simulations are much warmer than the actual morphology simulation.

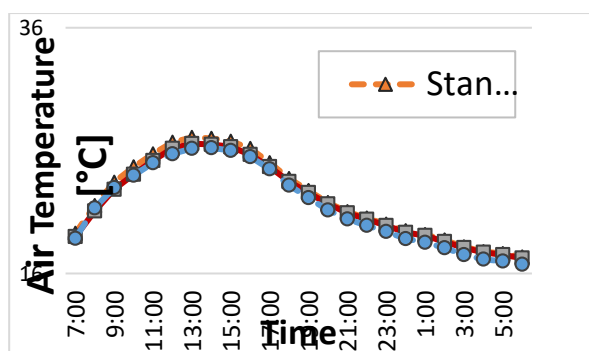


Figure 11: Linear interpolation of the averaged air temperature values of all atmosphere cells in 1.75 m height per timestep for every simulation

5. DISCUSSION & OUTLOOK

By introducing user-generated, site-specific LCZ tiles into WUDAPT2ENVI-met, the inevitable error of a wrong translation of recognized urban morphology types into predefined Standard LCZ tiles can be reduced. As shown in this small case study, the lower RSME value of the averaged air temperatures between site-specific LCZ tile and actual morphology simulation and the approach in curves' progression, corroborate the importance of using site-specific instead of Standard LCZ tiles.

The comparison of the simulation results shows that specific adaptations concerning appearance and composition of LCZ tiles influence the simulation results. However, the quality of improvement, which is gained by using site-specific instead of Standard LCZ tiles, is smaller than expected, thus requiring a thorough estimation of effort and benefit. Hence,

more case studies comparing the three model area topologies are needed in order to examine the possible benefits of using site-specific versus Standard LCZ tiles.

In addition, modifying and exchanging LCZ tiles allows to manually add specific structures, elements, and materials to intentionally alter the microclimatic effects of the LCZ tile and the surrounding area. A use case might be façade greening or increased tree numbers to mitigate local hotspots of large area simulation results. Thus, the effect of mitigating strategies tackling the challenges of the Urban Heat Island Effect can be analyzed on city-scale level. Range and strength of vegetation's cooling effect can be examined by incorporating more vegetation or other mitigation strategies into Standard LCZ tiles.

In a further step, the resulting city-scale simulation data might also be used to examine local hotspots by providing boundary conditions for ENVI-met's newly developed nesting module. In these nested simulations, the model area can be analyzed in even higher resolutions, where the actual building and vegetation structure is used instead of the generalized LCZ tiles.

REFERENCES

1. Mills, G., Ching, J., See, L., Bechtel, B. and Foley, M. (2015). An Introduction to the WUDAPT project. In 9th International Conference on Urban Climate. Toulouse, FR, July.
2. Stewart, I. D., and Oke, T. R. (2012). Local climate zones for urban temperature studies. *Bulletin of the American Meteorological Society*, 93(12): p. 1879-1900.
3. Ching, J., Mills, G., See, L., Bechtel, B., Feddema, J., Adel, H., Milcinski, G., Masson, V., Neophytou, M., Martilli, A., Brousse, O., Chen, F., Grimmond, S. (2015). The portal component, strategic perspectives and review of tactical plans for full implementation of WUDAPT. In 9th International Conference on Urban Climate. Toulouse, FR, July.
4. ENVI-met Homepage (2018). Tech News. <https://www.envi-met.com/news/>
5. Prefeitura de Sao Paulo (2018). Dados Demográficos Dos Distritos Pertencentes Às Subprefeituras. <http://www.prefeitura.sp.gov.br>.
6. Ferreira, L.S., Shimomura, A.P., Ferreira, A.T. & Duarte, D.H.S. (2017). Mapping Local Climate Zones for Sao Paulo Metropolitan Region. A Comparison between the Local Climate Zone Map and Two Other Local Maps. In: 33th PLEA Conference 2017, Edinburgh.
7. KNMI Climate Explorer (2018a). Monthly Historical Climate Data of Sao Paulo in December. <https://climexp.knmi.nl>

A Parametric Study to Optimize the Thermal Performance of Mongolian Self-built Houses in Terms of Energy Efficiency: Towards a cleaner environment for Ulaanbaatar

TAMER GADO¹, TERESA SARAH GAMES²

¹Architecture and Urban Planning, University of Dundee, Dundee, United Kingdom

²Mongol Vision Non-Government Organisation, Ulaanbaatar, Mongolia

ABSTRACT: This research focuses on the thermal performance of Mongolian self-built houses within the capital city; Ulaanbaatar. The main aim was to optimize the thermal performance in terms of energy efficiency. Fieldwork in Mongolia and computer-based analyses were undertaken. The intention of the fieldwork was to a) visit a range of self-built houses and create a design interpretation of the typical Mongolian self-built house, and b) monitor the internal and external temperatures of one house for validating the computer model. The computer based study used Autodesk Ecotect software to model both the monitored and the typical design. Monitored data was statistically compared to simulated temperatures and mean internal temperatures inside the typical house were simulated. A parametric study was carried out to optimise the walls, floor and ceiling insulation to reduce the annual heating loads. The optimum insulation level for the external walls was found to be 300mm of expanded polystyrene on the outside of the walls. Infiltration rate was found to significantly affect the heating loads. The effect of several construction combinations were simulated and the best case scenario was found to reduce the total annual heating loads from 37,990 kW to 12,692 kW.

KEYWORDS: Self-built houses, Energy, Heating loads, Monitoring, Computer simulation

1. INTRODUCTION

This paper presents a research project focusing on thermal performance of the Mongolian self-built houses within the capital city, Ulaanbaatar. In wintertime Ulaanbaatar has a severe pollution problem caused by smoke emitted from stoves used by around 216,000 households. Stoves use wood and coal due to the lack of other affordable cleaner options. Stove heated self-built houses using wood and coal [1] are usually detached houses that are poorly constructed [2]. Previous research into the energy efficiency of this type of houses in this part of the world is very limited. It is believed from the initial survey that the poor construction of these houses could be one of the main contributing factors to their poor thermal performance and thus the severe pollution problem in Ulaanbaatar. This work tried to investigate the opportunities of improving the situation using parametric analysis.

Located between Russia and China, Mongolia has an extreme continental climate, with long cold winters and short hot summers. The average winter temperature in Ulaanbaatar is -20°C which makes it the coldest capital city in the world and heating is needed for eight months of the year [3].

Rapid migration across the country to urban areas, such as Ulaanbaatar, has significantly increased since the forming of the independent Mongolian state in the early 1990's [4]. In 2016, Ulaanbaatar was home to

44% of the country's population [8]. Such a high density further contributes to the pollution of the city. The centre of Ulaanbaatar is surrounded by unplanned settlements known as 'ger districts' which contain both what are known as gers (yurts) and self-built houses. These areas, connected to the electricity grid but not to a gas grid, lack basic water and sanitation infrastructure and are connected by just dirt roads [5]. So the occupants of the 216,000 households [6] in the ger districts are forced to burn coal and wood for cooking and heating [1] despite the high cost and in doing so they hugely pollute the air of the city. It is not uncommon for people to struggle to heat their homes sufficiently in winter, spending up to a staggering 40% of their income on fuel for heating [4]. A recent study by the World Bank found that the calculated exposure of Ulaanbaatar's ger districts population of PM2.5 was "on average throughout the year, 10 times higher than the Mongolian Air Quality Standards and 6-7 times higher than the most lenient World Health Organization targets" [7].

Poor or lack of maintenance of existing buildings in the ger districts and low level of awareness mean thermal performance and energy efficiency of those buildings are extremely poor [8]. A previous study into the heat loss of Mongolian houses [2] investigated the building material and construction methods of 101 dwellings, and measured the infiltration rates inside 90 of those cases. It was found that most of the houses were not built to any basic building standards and as a

PLEA 2018 HONG KONG

Smart and Healthy within the 2-degree Limit

consequence they suffer from a very high level of heat loss and high rate of energy consumption. Air change per hour of 22ACH was found to be the most common among all the houses, and was said to account for 27% of the overall heat loss of the case studies. The average values for thermal resistance of the walls, floors and ceilings were 2-3 times lower than the Mongolian building standards at the time. It was clear from this study that the houses overall heat loss need to be reduced.

2. RESEARCH AIMS AND METHODOLOGY

The main aim of this research is to optimise the performance of the typical self-built Mongolian house in Ulaanbaatar in terms of energy efficiency. This was ascertained by four studies: a) preliminary study using a typo-morphological technique to establish the typical design of the Mongolian self-built house and the common materials used, b) field survey to further establish the typical house design, gain understanding of the case studies and collect data for the computer simulations, c) monitoring of the case study to collect data for modelling the thermal behaviour of one of the case studies for the purpose of model validation, and d) computer-based study that aims to model the monitored case study and the typical house to conduct a thermal simulation for model validation, and to perform a parametric analysis to optimise the performance of the typical house design in terms of energy efficiency.

2.1 Preliminary study

Thirty three photographs provided by two local online housing advertisement websites were examined. Houses were randomly chosen from the data bases of the agents: (www.ezar.mn) and (zarmedee.mn). Housing design and building materials were classified and recorded from the photos. Limitations of this study include inability to identify certain details such as the composition of the walls, presence of insulation, type of floor and number of rooms.

2.2 Field survey

Two representative ger district areas were chosen for the study, an inner area, and an area on the outskirts of the city. The first area was the closest ger district to the city centre and is known as 'Gandan'. The second area was the 'Chingeltei' area which is a ger district area approximately 7km to the north of the city centre. In total 16 houses were entered and surveyed. Data about each case were collected through a combination of conversations with the occupants, observation, inspection and measurement. The exterior and the interiors of the houses were methodologically photographed and the surrounding landscape or structures photographed where necessary.

By collecting and analysing the field data, the typical design of the self-built house was established. To estimate the typical house design in the wider context of Ulaanbaatar, walking surveys of the two study areas were undertaken and aerial photos were used to compare buildings. Using this method, the number and type of houses in the study areas were determined. The typical house design details were established by measuring the frequency of each building element in the case study houses, and by using average values.

2.3 Monitoring of a case study

One house in the Chingeltei area (fig. 1) was chosen for thermal monitoring in order to understand the thermal behaviour of a representative case study over an extended period of time. Collection of the monitored data was also necessary for use in the computer based study undertaken later. Both indoor and outdoor temperatures were collected for a period of 24 days, from the 20th June to 14th July 2012; the hottest period of the year.



Figure 61: The monitored case study house.

Aiming to get a good representation of the overall internal temperature four temperature and humidity HOBO data loggers were used, each with additional sensors. The data loggers were placed in two main locations inside the case study; two in the living room and two in the kitchen (fig. 2). The data loggers were installed at the seated head height, and the sensors were installed at the feet height to gain a better understanding about the thermal comfort inside the spaces. The occupants were asked to press a button on the data logger if a fire was lit to mark the incident.

PLEA 2018 HONG KONG

Smart and Healthy within the 2-degree Limit

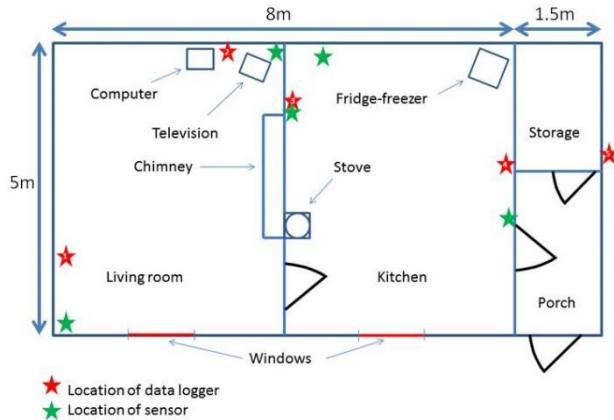


Figure 62: Plan of the monitored case study with location of data loggers and sensors. (Note: Not to scale)

2.4 Computer based study

The computer based study consisted of two main parts. The first involved building a model of the monitored case study, running a thermal simulation and validating the results with the monitored indoor data. The second part of the study was to create a model of the typical house, as established by the field survey, and use the model to undertake a parametric analysis to optimise the design of the house in terms of energy efficiency.

Part one: Each building element is added individually to the Ecotect model to the desired dimensions, and the material composition specified. After building a computer model of the monitored case study a thermal analysis was carried out. The recorded outdoor temperatures, from the monitored house, were used to create a weather file used in the model to simulate the internal temperatures over the entire year. In order to validate the model, the simulated results were statistically compared to the monitored data. A two-sample t-test was used to compare the simulated and monitored data, using a significance level of 0.01. In addition to the model validation, a sensitivity test was undertaken on the model to understand the limitations of the model. This involved changing several parameters one at a time by a small increment. Variables changed were occupancy level, activity level, sensible gains, air infiltration rate, clothing level, wind sensitivity, lighting level, humidity and air speed.

Part two: This included a parametric analysis to find the optimum combination of passive measures that would lead to the lowest heating load. This involved improving the thermal properties of the walls, floor and ceiling. Using the information collected from the field survey, an interpretation of the typical house was assumed and a representative model was constructed in Ecotect using the construction details of the houses as built. Using a TMY weather file for Ulaanbaatar, heating loads of the base case were simulated for the

whole year. The thermostat upper limit was set to 26°C and the lower limit was set to 18°C. Variable parameters were changed and the resulting simulated heating loads were recorded. Internal and external wall insulation, insulation above and below the floor, and roof insulation were changed at 10mm intervals. Thermal lag of internal and external walls was changed in one hour increments. The simulated heating loads were recorded after each change of variable.

3. RESULTS AND DISCUSSION

3.1 Preliminary study

Results from the preliminary study showed the common materials and the common building types used in Ulaanbaatar. Four main house types were established as follows: Type 1: Single storey, Type 2: Single storey house with an attic room, Type 3: Basic two storey, and Type 4: Elaborate two storey house. Examples of each house type can be seen in figure 3. The most common house type was found to be type 1; the single storey house.



Figure 63: The four main house types.

Roofing materials identified were corrugated metal sheets, flat metal sheets, black tar paper and fibre cement roofing. External wall materials identified were clay render, with or without a lime finish, cement render, brick, stacked wood logs and weatherboard. The stacked wood appeared in two forms, cut square or left as round logs. Several houses had adjoining structures, identified as a garage, porch, shed or extension.

3.2 Field survey

Corroborating the results of the preliminary study, the fieldwork indicated that house type one was the most common type. The walking survey of the two study areas, examining the aerial pictures, also confirmed this. In the two study areas a house of each of the four types identified by the preliminary study were selected for a visit. In addition, as Type one was established as the most common type, it was decided another eight single storey houses should be visited to ensure sufficient data was available for the typology.

PLEA 2018 HONG KONG

Smart and Healthy within the 2-degree Limit

morphological analysis. Out of the 16 houses visited, seven were in the Gandan area, and nine were in the Chingeltei area. The shed category identified in the preliminary study was dismissed, as no structure with this function was found.

In all houses the internal space was split into rooms or defined spaces. Almost all houses followed the same basic planning, with the chimney in the centre. The exceptions to this were the two elaborate two storey buildings (type 4), as these were both heated by radiators. The form and internal layout of the houses is therefore influenced by the type of heating, with a central heating system giving more freedom to use complex internal planning. The central heating is either powered by a coal fired boiler or electricity. In some cases, houses that meet the current building regulations in the central parts of the city are connected to a district heating network [9].

81% of the houses use some kind of material as roof insulation. Older houses used stove ash, sawdust or earth. Only two types of materials intended for use as insulation were found, expanded polystyrene and glass wool, and these were mainly used in newer houses. The most frequently used roof insulation was ash, followed by expanded polystyrene and glass wool. 44% of the houses visited were built of timber and clay plaster. The most frequent number of rooms was two. The most frequent house area found was between 50 and 54m², with dimensions of the three houses being 10x5m, 10x5m and 9x6m. Consequently it was decided to use the dimensions 10x5m to represent the typical house.

By far the most common roofing material was metal. The majority of both the entrance doors and inside doors were timber. Although timber framed windows were common, especially in older houses, the most frequently used type of windows were uPVC double glazed windows with a vacuum between the glass panes. The dimensions of the windows of the typical house, 0.8m x 1.2m, were taken as an average of all the case study window dimensions. It was found that the self-built house typically has three south facing windows and one east facing window and no north or west facing window.

Around 63% of the houses had the entrance doors facing south, and 88% of the houses had an entrance porch. An equal number of houses faced both south and south-east and for this reason the typical house orientation was chosen to be in the middle as a compromise, south-south east. The two main kinds of floor were a suspended wooden floor and concrete slab.

81% of the houses used a wood burning stove and chimney as the main source of heating. Table 1 gives the specifications of the typical house as determined from the analysis of the field survey data.

Table 1: The specifications of the typical house elements.

House element	Specification
House type	Type 1: Single storey house
Main wall material	Wooden planks and clay plaster
Number of rooms	2 rooms
Ground floor dimensions	10m x5m
Floor	Suspended wooden floor
Ceiling	Suspended ash insulated
Roof	Metal sheet roofing
Entrance doors	Wooden framed doors
Internal door	Wooden
Heating type	Stove and masonry chimney
Orientation	S-SE (10m side)
Window dimension	800mm x1200mm
Entrance porch	South side entrance porch
Number and orientation of windows	4 windows; 3 south facing and 1 east facing
Type of windows	uPVC double glazed

3.3 Case study monitoring

Indoor and outdoor temperatures were monitored for 24 days (fig. 4). The results from the data loggers did not log any incident of fire use, therefore it was assumed that no fire was lit.

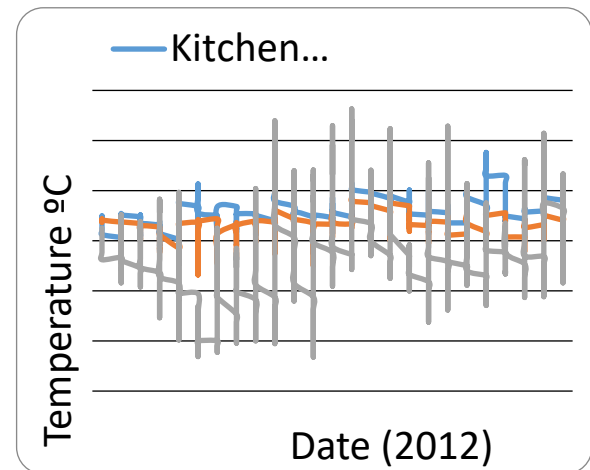


Figure 64: Monitored indoor and outdoor data as collected from the case study.

3.4 Computer-based study

The computer-based study was conducted in two parts. In part one the geometry of the case study model (fig. 5) was created using the fieldwork data collected. The house was split into five thermal zones; living room, kitchen, porch, storage and roof zone.

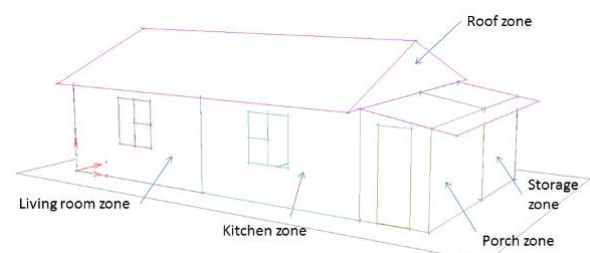


Figure 5: The Ecotect model of the monitored case study.

PLEA 2018 HONG KONG

Smart and Healthy within the 2-degree Limit

New materials for Ecotect were created for this work as there were no pre-programmed materials that fitted the Mongolian materials in the software material database. The new u-values, admittance and other properties were automatically updated, with the exception of thermal lag which was changed manually. The walls of the case study house were constructed from timber with diagonally latticed laths covered in a layer of clay. In the model, this was created as a layer of timber between two layers of alluvial clay. The case study house had stove ash as insulation above the ceiling. Earth was used in the model as a replacement. No topography, surrounding structures or trees were simulated so the house was assumed to have no overshadowing. An occupancy schedule was created for the case study and applied to the kitchen and living room zones. For the storage and porch zones the occupancy was set to zero. Table 2 shows the building elements of the case study house.

Table 2: Case study elements and their properties.

House Element	Description
Walls	100mm wood + 50mm clay plaster on both sides
Living room floor	Carpeted suspended timber floor with a 200mm air gap
Ceilings	Framed fibreboard, wood and 50mm earth layer on top
Kitchen, porch, and storage floors	Suspended timber floor with a 200mm air gap, covered with linoleum
Doors	40mm solid pine
Windows	Single glazed, timber frame
Roof	Wood and tar paper
Porch/storage walls	Timber with fibreboard panels on the inside
Porch/storage roof	Tar paper with fibreboard panels on the inside
Internal wall	Framed fibreboard partition
Chimney	Brick plaster partition
Other	2 lights: incandescent bulbs, 140L fridge-freezer, computer and TV

An Ecotect weather file was created using the monitored outdoor data. As the outside data was only recorded for 24 days, when the weather file for the whole year was created the remaining days of the year were filled with the monthly means to give better accuracy. Monthly means were obtained from the Ulaanbaatar airport weather station. This data included temperatures, wind speed and precipitation. After the initial thermal analysis of the case study model, the simulated data was significantly different to the monitored data. To address this problem, some aspects of the model were modified and the analysis was repeated. Despite changing the u-values of the walls, floor, windows and roof, the data remained significantly different. Only when the fridge was

turned off and the sensible gains were set to 1, was the simulated data not significantly different from the monitored data.

A sensitivity test was conducted. The most notable issue from this test was the effect of air infiltration. The standard deviation of the data increased significantly after reaching 4 ACH, indicating possible error in the results.

In part two of this study, the typical house model was constructed in Ecotect (fig. 6). Many of the materials created for the case study were also used for the typical house. The typical house had four zones; Living room, kitchen, porch and roof zone.

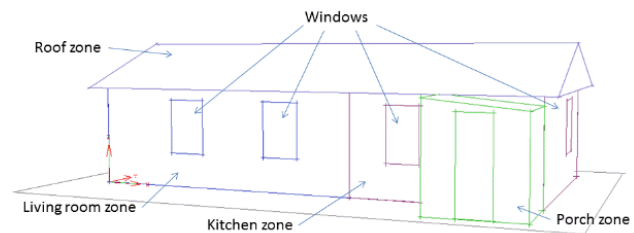


Figure 6: The typical house Ecotect model.

The TMY weather file for Ulaanbaatar used for the analysis of the typical house was obtained from the U.S department of energy. "Heating only" was the chosen heating mode. The maximum and minimum temperature of each zone was set. In the model, the kitchen and living room zones were set to heating only. It was decided not to use any appliances in the typical house, because the validation of the previous model had highlighted some problems with the heat from appliances when applied to the model. This requires further investigation by future research. The only two types of insulation used in reality are expanded polystyrene and glass wool. As Ecotect did not have a specific glass wool material, expanded polystyrene was used. It was thought best to initially keep the thermal lag constant to avoid another variable affect the results. Three hours was chosen as the value to represent the thermal lag while the other variables were incrementally changed.

Simulations expectedly showed that change in the thickness of insulation in the walls, ceiling and floor, reduces the annual heating loads. However, the decrease in heating loads for the first 10mm of insulation was most pronounced for the walls and ceiling insulation and less so for the floor insulation. The effect of the position of insulation in the walls and floors was tested. The effect of wall insulation position, inside or outside the walls was examined, and the insulation above and below the floor was tested. There was little difference in heating loads for the different location of insulation in the floor. However, there was a greater reduction in heating loads due to wall insulation being on the outside of the walls. For 10mm

PLEA 2018 HONG KONG

Smart and Healthy within the 2-degree Limit

of insulation on the outside of the walls the heating loads were reduced by 12,6734W when compared to insulation on the inside. For 300mm of outside insulation, when compared to the same insulation inside, the difference was reduced to 594W. The effect of thermal lag was tested by calculating the heating loads for different thicknesses of insulation with a 0 and 12 hour lag. The difference in annual heating loads between the material with 0 lag and a 12 hour lag was 168kW. The cut-off for the effectiveness of additional insulation was approximately 300mm for the walls, 190mm for the ceiling and 200mm for the floor. When these values were chosen for the best case house in addition to a 12 hour thermal lag, it was possible to reduce annual heating loads from 37,990kW to 28,021kW, a reduction of 9,969kW.

The air infiltration rate of the typical house was assumed to be leaky. By reducing the air infiltration from 2 ACH to 0.5 ACH, the annual heating load was reduced again by 15,106kW. This suggested that the air infiltration is as important as insulation, if not more important, to reducing heat loss.

The best case scenario used 300mm of expanded polystyrene insulation for the walls, 200mm for the floor and 190mm for the ceiling, in addition to a 12 hour thermal lag and an air infiltration rate of 0.5ACH. This best case found a reduction in total annual heating loads from 37,990kW to 12,692 kW.

4. CONCLUSION

This research was concerned with enhancing the energy efficiency of the self-built houses of the Mongolian capital; Ulaanbaatar. It was found that all the self-built houses from the two ger districts included in this study were poorly constructed and this expectedly negatively affects their energy efficiency. It also means that large quantities of wood and coal - the two most widely used fuels there - are burned in large quantities every winter for heating, increasing the levels of air pollution to world record levels.

A parametric study was carried out to optimise a number of passive measures to reduce energy consumption. Overall, the optimisation as detailed in the results successfully reduced the annual heating loads by 25,298kW. If these findings were applied to the real situation in Mongolia there would be many benefits in terms of the energy efficiency of the houses, the economy of the struggling families and air quality of the city.

REFERENCES

1. Allen, W., GombojavBaldorj E., Barkhasragchaa, B., Byambaa, T., Lkhasuren, O., Amram, O., Takaro, and T., Janes, C., (2013). An assessment of air pollution and its attributable mortality in Ulaanbaatar, Mongolia. *Journal of Air quality, Atmosphere & Health*. 6(1): p. 137-150.

2. Namkhainyam, B. and Tserendolgor, D. (2007). Study results of heat loss for private houses. 2007 International forum on strategic technology (IFOST): p. 440-443.

3. Asia Development Bank, (2008). Energy Conservation and Emissions Reduction from Poor Households: Mongolia. ADB project number 42059-012. Asia Development Bank.

4. Lawrence, D. *Mongolia's growing shantytowns: the cold and toxic ger districts*. World Bank. 2009. [Online] Available from: <http://blogs.worldbank.org/eastasiapacific/mongolias-growing-shantytowns-the-cold-and-toxic-ger-districts> [Accessed 1 June 2012]

5. Leblanc, M., Reed, A., Kingdom, W., Gambrell, P., Rodriguez, J., (2017). Challenges and Opportunities for Improving Household Sanitation in the Ger Areas of Ulaanbaatar. World Bank.

6. National Statistic Office of Mongolia. 2018. [Online] Available: <http://www.nso.mn> [Accessed 26 May 2018].

7. The World Bank. *Curbing Air Pollution in Mongolia's Capital*. The World Bank. 2012. [Online] Available from: <http://www.worldbank.org/en/news/feature/2012/04/25/curbing-air-pollution-in-mongolia-capital> [Accessed 05 June 2018].

8. European Bank for Reconstruction and Development, (2013). Strategy for Mongolia. EBRD.

9. Mongolian Ministry of Construction, (2005). Нэг Айлын Сүүц БНБД 31-05-05 (Single Family Houses). State Construction Regulations, Ulaanbaatar.

Sensitivity of Passive Design Strategies to Climate Change: Thermal comfort performance of natural ventilation in the future

ARFA N. AIJAZI¹, GAIL S. BRAGER¹

¹Center for the Built Environment, University of California, Berkeley, CA, USA

ABSTRACT: Observed global warming trends undermine the conventional practice of using historic weather files, such as Typical Meteorological Year (TMY), to predict building performance during the design process. In order to limit adverse impacts such as improperly sized mechanical equipment or thermal discomfort, it is important to consider how the building will perform in the future. Like all passive design strategies, natural ventilation, relies on local climate to be effective in improving building performance. This paper combines future weather files with whole building energy simulations to assess the sensitivity and feasibility of natural ventilation in providing thermal comfort in three locations, representing different climate types. The results show how building performance, as measured by thermal comfort metrics, changes over time. Natural ventilation can provide a buffer against warming climate, but only to a certain extent. Future weather files are useful for identifying where and when there is a risk that an exclusively passive design is no longer possible.

KEYWORDS: Natural Ventilation, Climate Change, Thermal Comfort, Simulation

1. INTRODUCTION

Weather is a significant predictor of building thermal performance as it relates directly to heating and cooling loads. Since weather for a given location can vary significantly from year-to-year, designers commonly use synthetic weather files, such as Typical Meteorological Year (TMY), to predict building performance. These files aggregate historic values for key weather parameters such as temperature, so that the model prediction reflects long-term performance. However, observed global warming trends undermine the validity of this practice.

The ASHRAE Handbook of Fundamentals 2013 reports increases in design day temperatures and cooling degree-days and decreases in heating degree-days over 30 years of historical weather data over all ASHRAE locations [1]. Weather files based solely on aggregating historic weather data do not capture these long-term trends, which can have significant design implications.

Future weather files can equip designers to consider the impact of climate change on building performance. These files transform existing weather files to reflect the changes predicted by global or regional climate models. Inserting the new future weather files into building performance simulations can show changes in predicted heating and cooling loads, energy consumption, thermal comfort, and other performance metrics used to quantitatively compare design options.

Passive design strategies, by definition, take advantage of the local climate to reduce or eliminate the need for auxiliary heating and/or cooling in a building. Climatic changes over the lifetime of the building can thereby influence the efficacy of passive

design strategies and result in improperly sized ancillary mechanical equipment and, if unresolved, large numbers of discomfort hours.

This paper focuses on natural ventilation, which relies on pressure differences to move fresh air through openings, such as windows, through the building. Pressure differences can arise from wind or the difference between interior and exterior temperature and relative humidity. This paper uses building energy simulation to assess natural ventilation effectiveness in a specific building.

While natural ventilation offers a number of benefits, we concentrate on its potential as a passive cooling strategy in lieu of any mechanical cooling. We evaluate occupant comfort metrics with and without natural ventilation using present and future weather files. The goal is inform designers of where and when this strategy will remain effective over the lifetime of the building, even as the climate changes.

2. METHODOLOGY

We set up a parametric study to consider the impact of natural ventilation, climate change scenario, and future year on building performance for three locations in the continental United States, represented by Miami, FL, Boston, MA, and San Francisco, CA. The Köppen–Geiger system classifies these cities as tropical, continental, and temperate and the International Energy Conservation Code (IECC) classifies them as climate zones 1A, 5A, and 3C respectively [2-3].

We chose to model a residential building because passive design strategies are generally most effective for buildings with low internal heat gains. The Pacific Northwest National Laboratory's (PNNL) residential

PLEA 2018 HONG KONG

Smart and Healthy within the 2-degree Limit

single-family EnergyPlus prototype model with a slab foundation and gas furnace heating serves as the base building for each climate [4]. Table 1 summarizes the prescriptive code requirements from Table R402.1.3 in IECC 2012 and represents physical characteristics of

which are the minimum and maximum warming percentile available from WeatherShift. The combination of RCP 4.5 and 10th percentile warming forms a lower bound and RCP 8.5 and 95th percentile warming forms an upper bound for future weather due to climate change. The most recent generation of TMY weather files, TMY3, uses historical data from 1991-2005, and represents the present. We evaluate the results for three future time-periods terminating in 2045, 2075, and 2099.

Table 1: IECC 2012 prescriptive code requirements for building envelope by location

Location	Fenestration SHGC	U-Factor (Btu/hr-sf-°F)			
		Fenestration	Ceiling	Frame Wall	Floor
Miami	0.25	NR ¹	0.035	0.082	0.064
Boston	NR ²	0.32	0.026	0.026	0.033
San Francisco	0.25	0.35	0.030	0.057	0.047

NR: No requirement per IECC 2012 prescriptive code

¹ Miami fenestration U-Factor modelled as 0.50

² Boston fenestration SHGC modelled as 0.39

the PNNL model in each climate [4]. The PNNL model contains two thermal zones: 1) a living unit that spans two-stories and is 223 m² and 2) an unconditioned attic that is 111 m². The living unit contains a single window per floor and per elevation. On the north and south elevations, the window-to-wall ratio is 13% while that on the east and west elevations is 15%.

We modified the PNNL energy models to add natural ventilation, turn off mechanical cooling, and adjust the heating set point to 18°C in accordance with the lower limit of the adaptive thermal comfort model. For each iteration, we ran an annual simulation in EnergyPlus v. 8.9.0 to calculate the living unit's hourly mean air temperature (MAT), mean radiant temperature (MRT), and ventilation air change rate [5]. From the simulation outputs and weather file, we calculated thermal comfort performance.

The subsequent sections detail how we modelled future weather, natural ventilation, and thermal comfort for this study.

2.1 Future Weather

For a given location, we compared the results using the TMY3 weather file and a future weather file from WeatherShift™ v. 2.0 [6]. We bookended our analysis with an upper and lower bound for the emission scenario and the warming percentile.

Representative Concentration Pathways (RCP) is a framework adapted by the IPCC to express four trajectories of future GHG emissions, each with different socio-economic assumptions. The RCP number refers to radiative forcing in W/m² in the year 2100, with lower numbers representing a smaller increase in greenhouse gas emissions. This research considers RCP 4.5 as a lower bound and RCP 8.5 as an upper bound for greenhouse gas emissions, which are the two options available from WeatherShift. Warming percentile captures uncertainty in how GHG emissions affect meteorological systems and the resulting weather parameter prediction. This study considers the 10th and 95th percentiles as a lower and upper bound respectively for the warming percentile,

2.2 Natural Ventilation

We modelled natural ventilation using simplified ventilation calculations in EnergyPlus's Wind and Stack Open Area model, in which we only considered wind-driven natural ventilation. EnergyPlus calculates the ventilation rate according to Equation (1).

$$Q_w = C_w A_{opening} F_{schedule} V \quad (1)$$

Where Q_w is the volumetric air flow rate driven by wind (m³/s); C_w is the opening effectiveness calculated from the window orientation and wind direction and defined as 0.3 for diagonal winds and 0.55 for perpendicular winds (EnergyPlus interpolates values for angles in between); $A_{opening}$ is the opening area (m²); and $F_{schedule}$ is the opening area fraction, which is set by the occupancy schedule and temperature controls; V is local wind speed (m/s).

$A_{opening}$ is 50% of the total window area for the case with natural ventilation, and 0% for the case without natural ventilation. $F_{schedule}$ is set from occupancy and temperature controls, both of which must be satisfied for the window to open. The PNNL base energy model defines hourly fractional occupancy per day. We considered hours with at least one person in the thermal zone as occupied.

For temperature controls related to window opening, we set the minimum interior and exterior temperature to 18°C based on the minimum comfortable temperature in the adaptive comfort model. We set the minimum temperature difference between interior and exterior temperature as 3°C based on CIBSE AM 10 Natural Ventilation in Non-Domestic Buildings, which states that the cooling effect is very small for interior-exterior temperature differences less than 3 K (i.e. 3°C) even for high ventilation rates [7]. Since there is no mechanical cooling available, we set the maximum interior and exterior temperature to the EnergyPlus maximum for this parameter. To summarize, $F_{schedule}$ is 1 as long as the zone is occupied, the interior and exterior temperatures are both greater than 18°C, and the interior temperature

PLEA 2018 HONG KONG

Smart and Healthy within the 2-degree Limit

is at least 3°C warmer than the exterior temperature. Otherwise $F_{schedule}$ is 0. Our assumptions for $F_{schedule}$ are appropriate for daytime comfort cooling.

2.3 Thermal Comfort

Since there is no energy use related to mechanical cooling, we evaluated building performance based on design objectives related to thermal comfort: hours with 80% acceptability and exceedance metrics.

Section 5.4 of ASHRAE Standard 55-2017 Thermal Environmental Conditions for Human Occupancy defines criteria for 80% acceptability [8]. We calculated the prevailing mean outdoor air temperature, T_{pmo} , as the 30-day running average of the exterior dry bulb temperature (DBT) from the weather file. We calculated operative temperature, T_o , as the mean of the MAT and MRT, which is valid for air velocities less than 0.2 m/s [8]. We used Equation (2) to define temperature thresholds for 80% acceptability [9].

$$T_{comfort} = 18.9 + 0.255 \times T_{pmo} \quad (2)$$

Where $T_{comfort}$ is the optimum comfort temperature (°C) and T_{pmo} is the prevailing mean outdoor temperature (°C). The design criteria for 80% acceptability is T_o within $\pm 3.5^\circ\text{C}$ of $T_{comfort}$.

We also calculated exceedance, but considered only warm discomfort since we are assessing the effects of natural ventilation as a cooling strategy. In this regard, exceedance represents the percent of occupied hours when the operative temperature is warmer than the 80% acceptability threshold (i.e. 20% discomfort). Equation (3) describes exceedance, E , mathematically [10].

$$E = \frac{\sum_{i=0}^{\text{all hours}} n_i \text{ if discomfort} > 20\%}{\sum_{i=0}^{\text{all hours}} n_i} \quad (3)$$

Where n_i is the number of occupants in hour i , and discomfort is the percent of people who are dissatisfied and is set to 20%, which complements the definition of 80% acceptability. European standard EN15251 recommends that no more than 5% of occupied hours fall outside of acceptable values for indoor environmental conditions, which serves as a rule of thumb for assessing exceedance [11].

3. RESULTS AND DISCUSSION

The following subsections describe results from the parametric study.

3.1 Future Weather

Before analysing changes in building performance, we compared weather parameters pertinent to natural ventilation in the present for each location, as well as

how those weather parameters changed in the future based on WeatherShift's morphing methodology. The climatic variables most relevant to natural ventilation performance are the exterior dry bulb temperature (DBT), relative humidity (RH), wind speed, and wind direction.

Figure 1 shows the daily average exterior DBT in the present and the monthly change in exterior DBT relative to the present in 2099 for each study location. Looking first at present conditions, unsurprisingly from the Köppen–Geiger system classification, Miami is overall the warmest, Boston has extremely cold winters and hot summers, and San Francisco has mild temperatures year round.

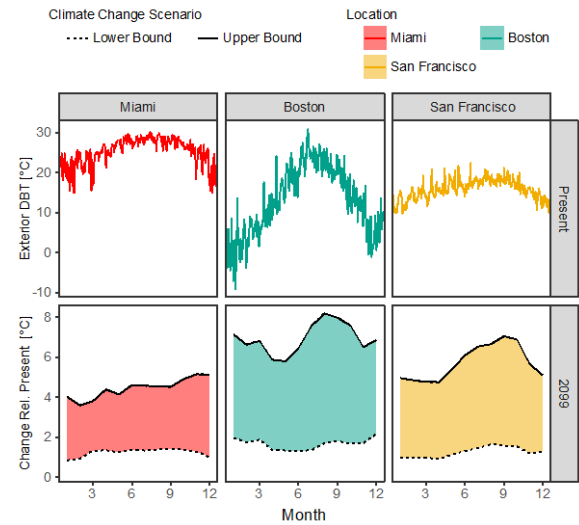


Figure 1: present day exterior drybulb temperature (DBT) and change in exterior DBT relative to the present in 2099 for each location.

Predictions for the future suggest that all study locations experience a net warming, even for the lower bound climate change scenario. In Miami, the temperature increase is relatively constant throughout the year. In Boston and San Francisco, the temperature increase in the upper bound climate change scenario varies seasonally, with the largest increases occurring in the late summer and early fall. It is interesting to note that even though San Francisco is a relatively mild climate in comparison to Boston, the ΔDBT increases predicted for the future are somewhat comparable for the summer, while Boston will experience more warming in the winter. We found that monthly average RH and wind speed did not change significantly and wind direction did not change under WeatherShift's morphing methodology. Therefore, changes in exterior DBT drive the changes in building performance observed in subsequent sections.

3.2 Natural Ventilation

With regard to window opening, temperatures acts as both a driving force and a response variable. Changes

PLEA 2018 HONG KONG

Smart and Healthy within the 2-degree Limit

in exterior temperature affect when windows can open, but the act of opening a window also changes the interior temperature, which in turn affects the interior-exterior temperature difference, and may eventually lead to windows closing.

In Figure 2, the upper graphs show the total number of hours windows were open per month in the present, and the lower graphs show the change in the number of “open” hours relative to the present in 2099 for each study location. The ventilation air change rate serves as a proxy simulation output to measure the window controls described in Section 2.2. We considered windows open when the living unit ventilation air change rate was greater than 0.25 air changes per hour, which is the baseline infiltration rate.

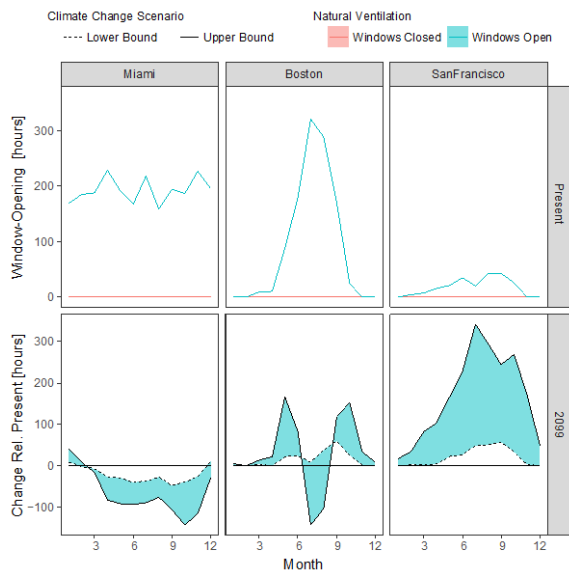


Figure 2: Monthly present day window-opening hours and change in window-opening hours relative to the present in 2099 for each location.

In the present, windows open for about 200 hours per month year-round in Miami. In Boston, windows open for as much as 300 hours in the summer months, but substantially less at other times in the year. In San Francisco, windows open less than that in the other two locations, only a maximum of 50 hours per month, due to this location’s limited need for cooling.

In the future, in Miami, windows open for less time throughout the year than in the present under both climate scenarios. A notable exception is January, where window-opening hours increase. In Boston, in the spring and fall, window-opening hours increase relative to the present under both climate change scenarios. The increase in exterior DBT in the spring and fall results in more hours where the exterior DBT is greater 18°C, the minimum exterior temperature for windows to open in our controls. In the summer, window-opening hours increase in the lower bound climate change scenario, but decrease under the upper bound climate change scenario. Large increases

in exterior DBT as predicted by the upper bound climate change scenario for the summer, make it harder to satisfy the condition of a minimum interior-exterior temperature difference of 3°C. In San Francisco, window-opening hours increase relative to the present throughout the year under both climate change scenarios. In terms of magnitude, the largest change in window-opening hours occurs in San Francisco and the least in Miami.

3.3 Thermal Comfort

Figure 3 shows the number of hours per year within 80% acceptability in all three locations with and without natural ventilation, with the x-axis representing time between the present and 2099.

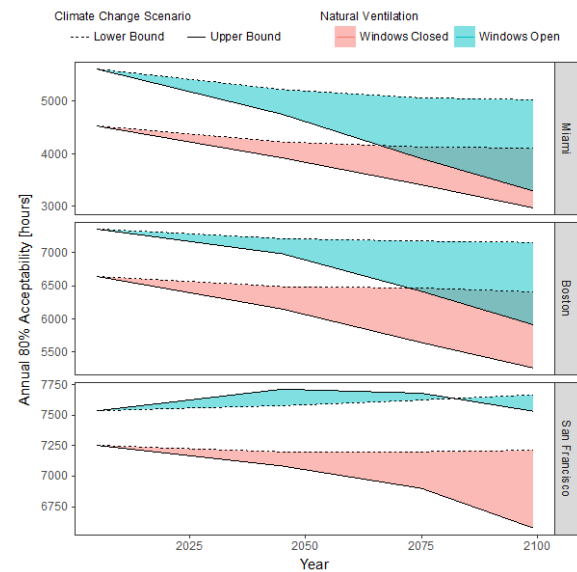


Figure 3: Annual 80% acceptability hours over time for the case with and without natural ventilation in each location.

In all three locations, natural ventilation increases the number of hours within 80% acceptability relative to the case without natural ventilation (and no mechanical cooling), regardless of year. In the future, without natural ventilation, the number of thermally comfortable hours decreases over time in all three locations. With natural ventilation, the number of thermally comfortable hours decreases over time in Miami and Boston, where the outdoor climate is getting much warmer than the upper limit of the adaptive comfort zone, but stays relatively constant in temperate San Francisco.

While Figure 3 shows the total number of thermally acceptable hours, it does not tell us anything about the magnitude of the deviations from comfort. Figure 4 uses a density plot to show the distribution of the difference between T_o and $T_{comfort}$ for the present and 2099 under the lower and upper bound climate change scenario. A temperature difference of 0 on the x-axis means that T_o is the ideal comfort temperature from Equation (2). The design criteria for 80%

PLEA 2018 HONG KONG

Smart and Healthy within the 2-degree Limit

acceptability allows T_o to be $\pm 3.5^\circ\text{C}$ of $T_{comfort}$, marked as dashed lines in Figure 4. Therefore, the part of the curve falling within the dashed lines represents conditions of 80% acceptability.

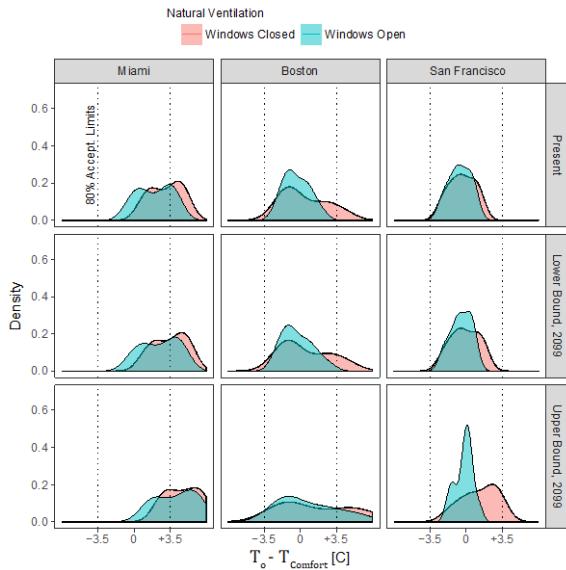


Figure 4: Distribution of $T_o - T_{comfort}$, in each location for present and lower and upper bound climate change scenarios in 2099. Limits for 80% acceptability included for reference.

Looking first at the upper graphs for the present, in Miami, the distribution's median is greater than 0 for both the case with and without natural ventilation, meaning that T_o tends to be warmer than $T_{comfort}$ most of the time, but in Boston and San Francisco, the distribution is centred closer to 0. In the present in San Francisco the case with and without natural ventilation is nearly identical because as we saw in Figure 2, windows are open for relatively few hours in comparison to Miami and Boston. For all locations, in the case without natural ventilation T_o is warmer, i.e. higher values for $T_o - T_{comfort}$.

In all three locations, the distribution in 2099 under the lower bound climate change scenario is similar to that of the present. From Figure 1, in the lower bound climate change scenario, the monthly average temperature increase is 1-2°C. The adaptive comfort model, $T_{comfort}$ is a function of the prevailing outdoor mean temperature to account for behaviour adjustments by occupants, such as changing expectation. The distribution being similar in the present and in 2099 under the lower bound climate change scenario suggests that occupants can adjust to this level of warming, allowing the building to maintain a similar level of thermal comfort in the future. The ability to apply an adaptive comfort model can therefore contribute to the design's overall resiliency. In 2099 at the upper bound climate change scenario, the distribution's median for Miami increases relative to the present, i.e. the peaks shift to the right. In addition, there is less of a distinction between the case

with and without natural ventilation. From Figure 2, we see that in Miami windows are open for fewer hours in the upper bound climate change scenario, so it follows that the two cases will have similar operative temperatures.

In 2099 in Boston, the median of the distribution is similar to that in the present, but the variance increases, i.e. the peaks flatten. This is likely because, from Figure 2, in Boston windows are open more in the spring and fall, but less in the summer. Additionally from Figure 1, we see that in the upper bound climate change scenario, the temperature increase is greatest in the summer, which results in a large increase in the number of overheated hours, or when $T_o - T_{comfort}$ is greater than $+3.5^\circ\text{C}$.

In San Francisco in the future, the case with natural ventilation has a lower variance than that of the present, i.e. the peak is taller and the spread is narrower. In the case without natural ventilation, the distribution biases towards higher temperature differences, but is still mostly within 80% acceptability. We can quantify the percentage of time that temperatures fall on the warm side of the 80% acceptability zone shown in Figure 4 by using the exceedance metric. Figure 5 shows the exceedance per year over time in all three locations with and without natural ventilation. We include the 5% threshold from EN15251 as a dashed line for reference.

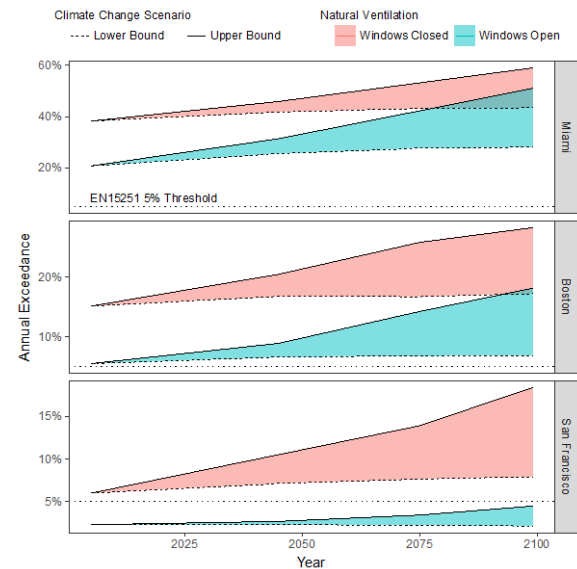


Figure 5: Annual exceedance over time for the case with and without natural ventilation in each location. Exceedance threshold of 5% from EN15251 included for reference.

In all three locations, exceedance increases over time, and is lower for the case with natural ventilation. As observed with 80% acceptability in Miami and Boston, the difference between the case with and without natural ventilation shrinks over time. Larger increases in exterior DBT, particularly in the summer, result in fewer hours that windows can open, and so the case

PLEA 2018 HONG KONG

Smart and Healthy within the 2-degree Limit

with and without natural ventilation approach each other. In San Francisco, natural ventilation can keep exceedance below the 5% threshold through 2099, even for the upper bound climate change scenario. In Boston, the lower bound climate change scenario has an annual exceedance of 5-7%, which is close to but does not satisfy EN15251.

4. CONCLUSIONS

In this paper, we used future weather files to compare thermal comfort performance over time with and without natural ventilation in three locations representing different climates. The results inform where and when natural ventilation will continue to be a viable strategy for passive cooling as the climate warms.

For a tropical climate, like Miami, for the simplified building used in these simulations, natural ventilation cannot exclusively provide thermal comfort either in the present or in the future. While performance does improve with natural ventilation, this benefit shrinks as the climate warms and there are fewer hours when opening windows provides a cooling advantage. Even with a more climatic responsive building than the PNNL model, this future trend is likely to still be relevant.

In a continental climate, like Boston, using natural ventilation exclusively for cooling is nearly possible in the lower bound climate change scenario, and maybe entirely possible in combination with other passive design strategies. However, in the upper bound climate change scenario, natural ventilation alone cannot achieve thermal comfort due to summertime overheating. In this scenario, while windows can open more frequently in the spring and fall, reduced opening hours in the summer offsets the overall passive cooling benefit.

In a temperate climate, like San Francisco, it is possible to cool exclusively with natural ventilation. As the climate warms in the future, increased window-opening hours provides sufficient cooling to maintain and even improve thermal comfort relative to the present.

From this analysis, we find that using future rather than historical weather files may be less informative for natural ventilation design in a tropical climate like Miami, where it's already a challenge to rely entirely on this passive strategy (again noting that this simulation was based on a fairly generic model and these results might change when simulating a more sophisticated design) present. However, future weather files are still important to ensure adequately sized mechanical cooling systems, given that the thermal comfort metrics clearly changed moving forward.

In a continental climate like Boston, natural ventilation design is very effective both in the present and in the

lower bound climate change scenario. However, in the upper bound climate change scenario, entirely natural ventilation design is no longer sufficient for maintaining comfort. Further refinement of boundary conditions for future weather scenarios can help manage risk in terms of thermal comfort performance. In a temperate climate like San Francisco, future weather files are informative in showing that natural ventilation can still achieve thermal comfort through 2099 even under the upper bound climate change scenario.

Finally, even if natural ventilation is not exclusively sufficient now or in the future for a particular climate, it still contributes towards improving thermal comfort, and thereby offsets the mechanical cooling load needed for acceptable building performance. Another interesting takeaway from this work is that due to adaptive comfort, occupants can adjust to limited temperature increases, such as those predicted by the lower bound climate change scenario, which contributes towards the building's overall resiliency. Further work will expand to more climates, building types, and passive strategies and evaluate the sensitivity of these results to different window opening controls algorithms. In addition, we will consider weighting exceedance not only by occupancy, but also by the magnitude of overheating.

5. REFERENCES

1. ASHRAE, *Handbook of Fundamentals (IP-ed)*. Atlanta, GA: ASHRAE, 2013.
2. M. C. Peel, B. L. Finlayson, and T. A. McMahon, "Updated world map of the Köppen-Geiger climate classification," *Hydrol. Earth Syst. Sci. Discuss.*, vol. 4, no. 2, pp. 439–473, 2007.
3. International Code Council, *2012 International Energy Conservation Code*. 2011.
4. PNNL, "Residential Prototype Building Models | Building Energy Codes Program," 2013. [Online]. Available: https://www.energycodes.gov/development/residential/iecc_models. [Accessed: 06-Jun-2018].
5. U.S. Department of Energy, *EnergyPlus*. 2018.
6. Arup and Argos Analytics, "WeatherShift," 2018. [Online]. Available: <http://weathershift.com/>. [Accessed: 23-Feb-2018].
7. CIBSE, *AM10 Natural ventilation in non-domestic buildings*. London: CIBSE, 2011.
8. ASHRAE, *Standard 55-2017 Thermal Environmental Conditions for Human Occupancy*. ASHRAE, 2017.
9. R. de Dear and G. S. Brager, "Developing an adaptive model of thermal comfort and preference," *ASHRAE Trans.*, vol. 104, p. 145, Jan. 1998.
10. S. Borgeson and G. Brager, "Comfort standards and variation in exceedance for mixed-mode buildings.," *Build. Res. Inf.*, vol. 39, no. 2, pp. 118–133, 2011.
11. CEN, *EN15251 Indoor environmental input parameters for design and assessment of energy performance of buildings addressing indoor air quality, thermal environment, lighting and acoustics*. 2006.

Heat Stress Pattern of Air-Conditioned Buildings with Shallow Plan Forms and Single Skin Facades: Colombo as a case study

UPENDRA RAJAPAKSHA¹

¹Department of Architecture, University of Moratuwa, Sri Lanka

ABSTRACT: The paper explores the effects of building morphology characteristics on thermal performance, and thus indoor climate and Building Energy Index (BEI) of air-conditioned office buildings in warm humid climates. 86 multilevel office buildings were investigated and two critical cases that were both in shallow plan form and similar in terms of other morphological characteristics such as orientation, occupant and equipment density and façade architecture were identified for a field investigation of heat stress patterns on their facades and thus indoor environment. Measuring indoor air temperature during office hours in 3mX3m multi zones across the depths and lengths of these two buildings using Hobo metres revealed air temperature deviations up to 10.5^o from the set point temperature (24^o C). The work highlights the severity of heat stress on air conditioned indoor environments and thus an energy sustainability issue related to shallow plan form typology.

KEYWORDS: Energy, Shallow plan forms, Air-conditioned buildings, Warm humid tropics

1. INTRODUCTION

Studies that have quantified the effects of global warming and projections of ambient temperature increases [1] indicate that more warm days are expected in most parts of sub-tropics and tropics. Warming climates increase internal temperatures of buildings and studies have shown that this relationship is linear [2]. Increase of extreme air temperatures may considerably impact on the electricity demand [3] and thus emissions. With the projected increase in energy use and the demand for more comfortable indoor environments in office buildings, there is a growing concern about high energy consumption and its likely adverse impacts on the environment [4].

A linear correlation between the increase of average external air temperature and the increase of building cooling load and total energy use is established for air-conditioned buildings [5]. Further, urbanization inflates building population in cities and enhances the formation of urban heat islands (UHI). Colombo, the Capital of Sri Lanka is no exception for the existence of warming climates due to global warming and Surface Urban Heat Island (SUHI) effects due to increase of building density, population and anthropogenic heat from traffic, etc. Colombo is known as a typical warm humid city in Asia.

Morphological characteristics of existing building population in terms of plan form, sectional form, envelope, orientation and fenestration details and their effects on energy consumption are known [6]. Of them, plan form is a major contributor that controls the level of building – climate interplay [7] and thus the indoor air temperature levels in free running buildings. Comparative studies on air conditioned buildings are

less known due to set point temperatures of conditioned environments.

Patterns of environmental heat gain from outside, better termed “heat stress” due to direct radiation on different types of plan forms are known. Shallow and linear plan forms with narrower facades facing east-west axis may promote least direct exposure to direct solar heat gain. However, heat stress due to diffused or reflected radiation and conduction of heat through facades is least investigated for air-conditioned buildings of any form, whether shallow or deep. A recent study on office building stock in Colombo reveals that nearly 85% of the buildings demonstrate a combination of linear and deep plan forms with conditioned indoor environments [8]. Facades are predominately composed of single skin glass and aluminium cladding with varied proportions of solid to void ratios facing five primary orientations (Table 3). Study concluded that buildings with East West oriented glazed facades demonstrate higher annual mean Building Energy Indices (BEI) around 220- 400 kWhm²a. The work explicitly demonstrated that air-conditioned multi-level office buildings with shallow plan forms and longer facades facing east and west are subjected to higher BEIs due to increased energy consumption for cooling.

Few studies on building heat stress in warm humid Sri Lanka that does exist are focussed on energy efficiency measures of orientation, building envelope and lighting on free running indoors. Reducing the risk of excessive heat gain into air conditioned buildings is also an essential phenomenon to study. When a building is air-conditioned, the risks of getting excessive heat indoors through facades may not be

PLEA 2018 HONG KONG

Smart and Healthy within the 2-degree Limit

visible and sensible to the occupants due to the conditioned environment inside, but contribute to increase the energy use in air conditioning, thus exacerbating the emissions and global warming problem [9]. An in-depth understanding of performance improvement of building design for air conditioned indoors in tropics is yet to be achieved.

This paper explores a preliminary investigation on air-conditioned shallow plan form building population to assess the heat stress on the indoor climate through facades. The work is limited to multi-level office buildings with longer facades appropriately orientated to north and south so that the impact of orientation on heat stress can be least considered.

1.1 Climate in Colombo

Warm humid tropical climates are found in the region extending 15° North and South of the equator (Figure 1). Sri Lanka (latitude 5°55' to 9°49'N and longitude 79°51' and 81°51'E) is an example of this climate and has lack of seasonal variations in temperature. The mean monthly temperatures range from 27°C in November to 30°C in April, relative humidity varies from 70 to 80% during a typical year. The daily maximum temperatures are high as 25° to 38°C and the daily pattern in the dry season (September to November and March to May) has diurnal temperature range of 7 to 8°C.

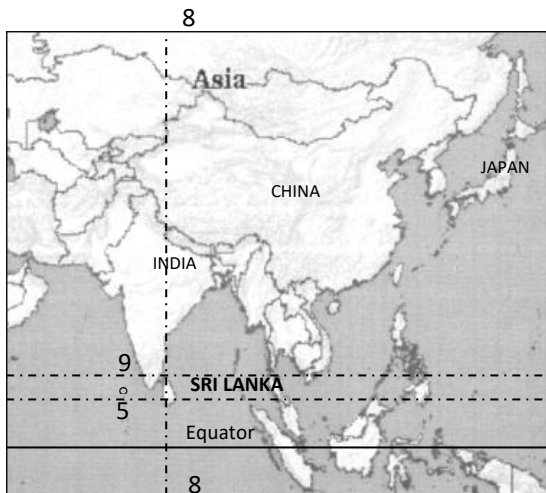


Figure 1: Sri Lanka in the world map

Köppen Geiger climate classification demonstrates that nearly 60% of the geographical area of Sri Lanka represents the type “Af”, an equatorial fully humid climate. Of the 8760 hourly data points of dry bulb temperature in psychrometric chart, developed from Climate Consultant 5.5 software, nearly 60% and 40 % of data points represent air temperatures in the range of 27-38°C and 21-27°C respectively (Figure 2). Annual monthly mean, maximum temperature and relative humidity in Colombo varies within the range of 26.2 to

28.8°C, 29.2 to 31.4°C and 73.8 to 83.6, 90.2 to 97.9% respectively.

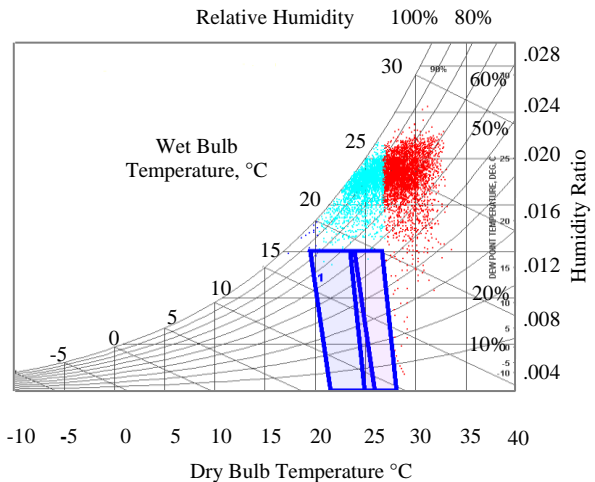


Figure 2: Psychrometric chart for Colombo developed from Climate Consultant 5.5

The main characteristic of warm humid climate in Colombo, from the human comfort and building design viewpoint, is the combination of high temperature and high humidity which in turn reduces the dissipation of body’s surplus heat. Irradiation in Colombo is ranging from 400-6000W/m² throughout the year. Therefore, shading plays [10] a major role in order to minimise inward heat transfer and thus reduce mean radiant temperature.

2. METHOD OF STUDY

Methodology involved a walk through survey of 65 air-conditioned buildings with shallow plan forms, which identified two critical cases for experimental investigation of indoor air temperature variations across their shallow plan depths. The two critical cases are oriented with the longer facades facing north and south, due to which it can be assumed that heat stress due to orientation is minimal.

PLEA 2018 HONG KONG

Smart and Healthy within the 2-degree Limit

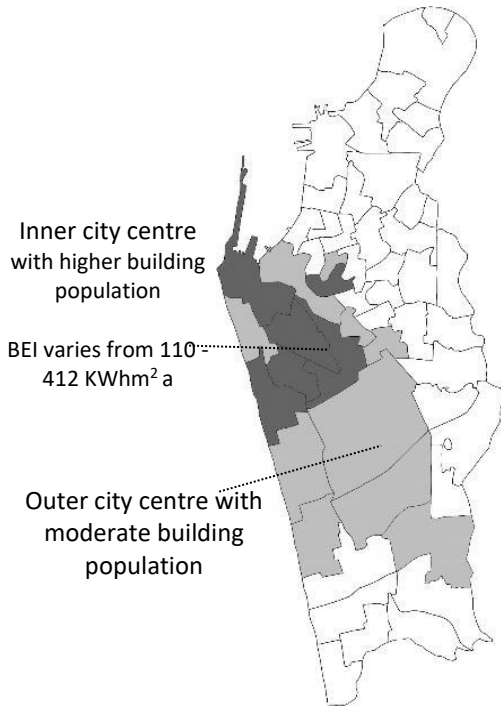


Figure 3: A map Colombo City showing distribution of Building Energy Index with building population

Office building stock in Colombo is predominately centrally air-conditioned and average Building Energy Index of such buildings in the populated city centre is 212 kWhm² per annum. BEI of office building population in the less dense city centre is approximately 110 kWhm² per annum. In both situations, the range of building height varies between 6-10 floors. This paper is more focussed on the shallow plan form buildings with single skin facades. The selected buildings are used exclusively for administrative activities of both private and public organizations such as banks and other typical high end offices. Data on building morphology includes architectural design strategies such as plan form, depths, orientation, façade characteristics, solid to void ratio, construction materials and fenestration details. In addition, technical and operational characteristics recorded were work hours, office equipment density, occupant density, space conditioning systems. Indoor environment in respect to air temperature, surface temperature and humidity was assessed during the daytime from 8 am to 6 pm over a week during April 2018, a typically hot month.

2.1 Sampling of the building stock

Figure 01 shows the distribution of building stock in Colombo city. Inner city centre occupies the majority of modern office building as compared to the outer city centre. Annual BEI of 86 office buildings totalling an approximate floor area of 73,000 m² were assessed. In general, BEI of office building stock falls between 91 and 412 kWhm² annum and of them nearly 95% of the

building stock has BEIs higher than 110 kWhm²a, an accepted standard for energy efficient building codes [11]. Findings highlight the need to investigate morphology of air-conditioned building stock.

Table 1: Morphology of a recent building population in Colombo

	Shallow	Deep	Composite
Population	62%	26%	12%
Orientation	Varied	Varied	Varied
Fenestration Solid/void ratio	Nearly 50% glass	Nearly 50% glass	Nearly 50% glass
Façade	Single skin glass & brick - concrete	Single skin glass & brick	Single skin glass, brick & concrete

Plan forms of 86 buildings falls into three broader categories namely shallow, deep and composite which consists of both shallow and deep (Table1). Major facades of these buildings are orientated to different directions (Tables 2 and 3) but in nearly 80% of shallow plan forms, linear building mass is orientated along the east-west axis. Most of these buildings are facing major traffic arteries that run from north to south or east to west of Colombo.

The BEI survey of 86 office buildings revealed that the BEI of 56% of buildings with a BEI of above 110 kWhm²annum moves above 200 kWhm²a and of them nearly 30% are above 250 kWhm²a.

From this survey of 86 buildings, 14 buildings of shallow plan forms were shortlisted and a pilot thermal performance investigation was conducted. This pilot study derived 2 sample buildings for further studies.

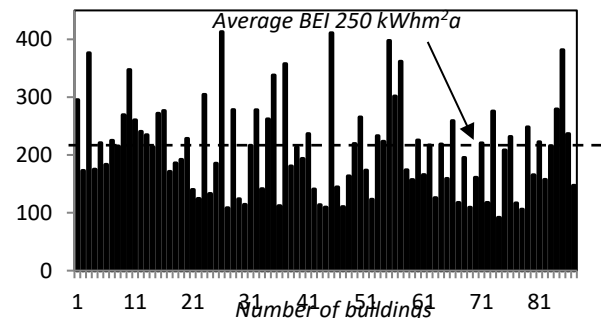


Figure 4: Building Energy Index of 86 buildings

2.2 Façade, orientation and location in the context

Large facades of buildings along major traffic arteries such as Galle Road, High Level Road, D.R Wijewardene Mawatha, Sir James Peiris Mawatha and Dharmapala Mawatha, are facing diverse orientations as shown in Table 2. Both shallow and deep plan forms have similar envelope properties of high mass concrete and brick and nearly 50-60 per cent glass in the total outer facades. Floor to floor height varies between 3-3.5 m in all buildings.

PLEA 2018 HONG KONG

Smart and Healthy within the 2-degree Limit

Table 2: Plan form typology and Building Energy Index (EUI)KWhm²a of selected investigated building stock

Shallow	Deep	B E I
317	226	
120		
102	98	

Table 3: Orientation of main façades, plan depth and Building Energy Index of a building population of 86

Orientation	Shallow or Deep	Mean BEI kWhm ² a
East-West	Shallow	246
East-West	Deep	200
North-South	Shallow	200.2
NE-SW	Shallow	200
NW-SE	Shallow	205

Buildings attached or close to another structure were eliminated from the study. Only free standing buildings were considered so that impact of urban climate on all façades of any particular chosen building can be assessed. The two samples (“A” and “B”) derived from the pilot investigation consisting of 14 free standing buildings with shallow and linear plan forms (the majority of the stock) consisted of similar building morphologies (rectangular linear) and orientation with longer façades facing the north and south (hence, direct radiation due to orientation can be disregarded in the investigation). The objective of the field investigation was to assess the distribution pattern of heat stress on indoor environment with the plan depth.

Office building “A” and “B” are in the same morphological character, orientation, operational profile, occupant and equipment density but different from the BEI point of view. Both buildings are occupied from 8 am to 6 pm on weekdays and located with the longer axis positioned along east-west axis in similar urban contexts just a kilometre apart.

Table 4: Plan form and physical characteristics of investigated buildings

Building “B”

Shallow plan form







North facade

Shallow Plan form – size 12 m X 56 m

COMMON CHARACTERISTICS

Orientation – longer axis along east – west

Set point temperature – 24 C degrees

Occupant population 6 persons/20m²

Wall and slab construction – brick and concrete

U-Value of external envelope – 0.22 W/m² K

Front façade is facing east

Solid to void ratio is nearly 50:50

Occupied hours – 8 am to 6 pm on weekdays

Building “A”







North facade

Shallow Plan form – size 16 m X 38 m

Elevation from the main road

PLEA 2018 HONG KONG

Smart and Healthy within the 2-degree Limit

Building “A” has BEI as high as 340kWhm²a whereas the Building “B” has a moderate level of 120 kWhm²a, which is close to acceptable level. Front narrower façade with the main entrance is positioned facing east orientation in both cases. Table 4 explains similarity of the operational and physical characteristics of the two buildings. The only difference between the two building forms is the floor area where a typical floor plate of Building “B” is relatively larger than the same of Building “A”.

Multi-zone indoor air temperature reading at 3 m intervals across the plan depth (and along the building length) were taken using HOBO data loggers during three working days in the month of April 2018 (23rd - 27th of April 2018) at 10 minute intervals and then averaged to hourly values. The measurement rationale was to ascertain a number of comparisons that are as follows,

Dynamics of air temperature distribution in peripheral and middle zones on a typical floor plate to assess to collective heat stress effect of façade and plan depth

Dynamics of air temperature deviation against set point temperature to assess stress on air-conditioning system

The study acknowledges that any dynamics in the indoor air temperature demonstrates an effect of environmental loads on air-conditioning and the indoor thermal behaviour. Microclimatic data just outside the building were recorded onsite. Central air-conditioning system of both cases is similar in specifications (15tons per 1 AHU). However, Building “A” has a higher number of diffusers (1 for each 13 m²) than in Building “B” (1 for each 36 m²) per floor. Readings were taken in three typical floors above 6th level in both buildings. Temperature fluctuations during the day that the study was conducted without equipment running, demonstrates the effect of environmental load on indoor thermal behaviour.

3. RESULTS AND DISCUSSION

Set point temperature of all office and useable floors of both buildings is 24 C degrees. Despite set point temperature at 24 degrees C, dynamics of indoor air temperature in varied levels was seen during daytime in both buildings.

Results show that an increase of indoor air temperature up to 31- 32 degrees C across all zones along sections A-A, B-B and C-C, in Building “B” while temperature readings in the internal zone close to west façade and east facades along D-D remained at 34 and 31 respectively during the midday (Figure 5). During this time the sun was just above the building and no direct radiation could penetrate through fenestration. Solar axis to buildings in Colombo during 23rd – 27th April is closely over the latitudes of Sri Lanka. This thermal behaviour explicitly suggests the

presence of heat stress on the air-conditioning system from the outside. Office equipment inside the three floors remained switched off from the morning to assist the research, so that indoor heat generation was limited to a minimum. As mentioned in a previous section, the BEI of this building was approximately 120 kWhm² a, but heat stress of 10.7 degrees C indoor air temperature above the set point is an issue to be addressed.

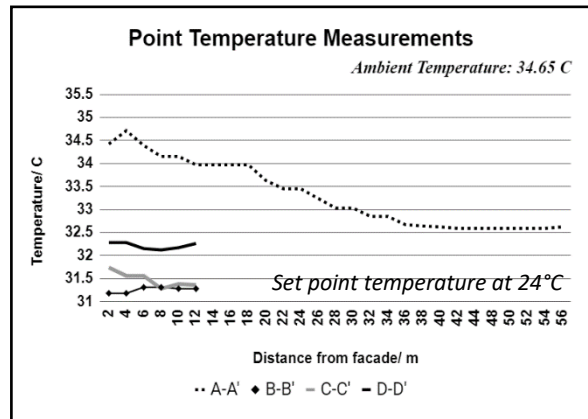


Figure 5: Multi zone air temperature behaviour in this air-conditioned Building “B”- move between 31.5 – 34.7° C despite set point temperature at 24° C – BEI is around 120 kWhm²a but high risks of heat gain is visible

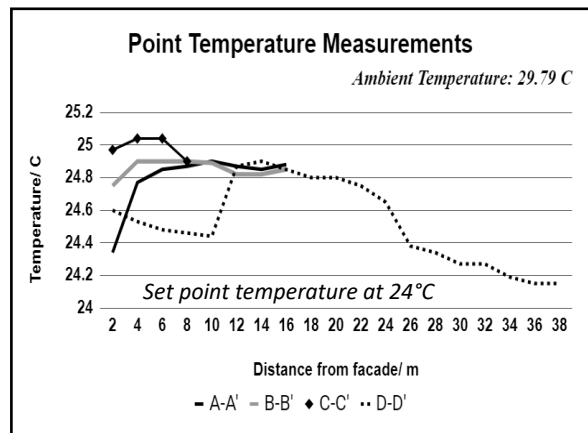


Figure 6: Multi zone air temperature behaviour of this air-conditioned Building “A” moves just 1.1°C above set point temperature of 24°C but at a very high energy cost of nearly 340 kWhm²a.

Set point temperature of both buildings was at 24 degrees C. Despite this similarity, Building “A” was assessed as having a very high BEI of 340kWhm²a and a smaller elevation of indoor air temperature range between 24. 4 - 25.1 degrees C. Building “A” has a highly dense AC diffuser points than Building “B” and results show that air conditioner system in Building “A” is capable of maintaining indoor air temperature closer to set point temperature but at a very high cost of energy foot print of 340 kWhm²a.

PLEA 2018 HONG KONG

Smart and Healthy within the 2-degree Limit

Both buildings, “A and B” are having the same orientation and shallow linear plan forms and similar occupant and equipment density. However, Building “A”’s higher BEI informs its criticality in respect of energy consumption. Results suggest the criticality of shallow plan forms on end user energy demand of the office building stock.

Shallow plan depths of Building “A” and “B” are 16m and 12m respectively. Length of the floor plates of Building “A” and “B” are 38m and 56m respectively. Multi zone air temperature distribution across the depth and length of floor plates are shown in the two graphs above (Figures 5 and 6). Considerable dynamics of air temperatures well above set point temperature in all zones across the depth and length of floor plates demonstrate increased demand on cooling energy due to high levels of external gains through facades.

4. CONCLUSION - Generalising findings

Results suggest a problem associated with shallow plan form buildings. Although the work is mainly focused on two specific buildings, they represent most of the thermo-physical characteristics of the larger building population in Colombo. Inward heat transfer across the plan depth up to 16 m in Building “A” and 12 meters in Building “B” from the façade is a critical problem that may be addressed through proper façade design. Findings suggest that presence of heat stress in terms of higher air temperature in air-conditioned indoors along the length of the plan form is visible.

Elevation of indoor air temperature in air conditioned environments by 10.5 degrees C above the set point temperature is considered critical in respect to energy demand. The two buildings investigated fall within the following two extremes of thermal performance scenarios:

Air-conditioned buildings with shallow plan forms may be able to maintain indoor air temperatures close to set point temperatures at 24 degrees C but at a very high energy cost.

On the other extreme, air-conditioned buildings with shallow plan forms can maintain building energy index around 120 kWhm²a but maintaining indoor air temperature close to set point temperature becomes problematic and sometime an elevation of indoor air temperature by even 10.5 degrees C could be visible. More research is underway to further strengthen these findings for a wider section of buildings in warm humid climates.

ACKNOWLEDGEMENTS

Author acknowledges Grant No 118-13 of National Research Council of Sri Lanka for funding of equipment, Ms Waruni Jayasinghe and Ms. Ruksala Ishani for collecting data on building population and performance.

REFERENCES

- Garnaut. R, 2008, The Garnaut Climate Change Review, Final Report, The Cambridge University Press, <http://www.garnautreview.org.au> viewed on Nov12 2017
- Coley D and Kershaw T, 2010, Changes in internal temperatures within the built environment as a response to a climate change, Building and Environment, Elsevier Science, Volume 45, pp; 89-93
- Howden. SM, and Crimp. S, 2001, Effect of climate and climate change on electricity demand in Australia, In: Ghassemi F, Whetton P, Little R, Littleboy M, editors, Integrating models for natural resources management across discipline, Issue and scales, Canberra, Australia MSSANZ Inc p 655-660
- Pieter de Wilde and David Coley, 2012, The implications of a changing climate for buildings, *Building and Environment* 55 (2012) 1–7, Elsevier
- Guan. L, 2009, Implication of global warming on Air-Conditioned office buildings in Australia, Build Research Information, 37(1), 43-54
- Dascalaki, E.G., Droutsa,K., Gaglia, A.G., Kontoyiannidis, S., Balaras, C.A., 2010, Data collection and analysis of the building stock and its energy consumption, Energy and Building, 42(8), pp.1231-7
- Hyde, R. 2000 Climate responsive design: a study of buildings in moderate and hot humid climates, London: E and FN Spon
- Rajapaksha. I and Rajapaksha. U, 2017, Criticality of Building Morphology on End Use Energy Demand: Evidence based assessment of urban office stock in Colombo Metropolitan Region, Proceedings of the Symposium of Sri Lanka Sustainable Energy Authority, December 2017, Colombo
- Yau YH and S.Hasbi, 2013, A review of climate change impacts on commercial buildings and their technical services in the tropics, Renewable and Sustainable Energy Reviews, 18 (2013) 430–441
- Baker, N.V. 1987 Passive and low energy building design for tropical island climates, Commonwealth Secretariat, London
- ECD19, 2003, Energy Consumption Guide: Energy use in offices, <http://www.cibse.org>

Simplified Sensing and In-situ Measuring Approach for Building Window Properties

YANXIAO FENG¹, JULIAN WANG^{1,2}

¹Department of Civil and Architectural Engineering and Construction Management, University of Cincinnati, Cincinnati, USA

²School of Architecture and Interior Design, University of Cincinnati, Cincinnati, USA

ABSTRACT: Windows and glazing systems play an important role in making an energy-efficient home. A portable easy-to-use in-situ measuring system of the window properties using low-cost Arduino platforms and compatible sensors is developed, 3D-printed, and fabricated in this project and used to measure the parameters including U-factor, Solar Heat Gain Coefficient (SHGC), and Visible Light Transmittance (VT). Comparing resultant output from the Arduino sensing and measurements to professional in-situ instruments, we demonstrate that this simple and compact Arduino-based instrument can obtain major window properties with reasonable accuracy. This simple but scalable sensing and measuring approach and Do-It-Yourself (DIY) fabrication workflow could be performed by creative people and even home owners without needing complex trainings and building physics knowledge.

KEYWORDS: Window properties; Arduino; digital light sensor; temperature sensor; 3D printing.

1. INTRODUCTION

Completing a home energy evaluation, also known as an energy audit or assessment, usually requires assessing building enclosures, appliances, and ways in which the home consumes energy. Windows have large impacts on the performance of building's lighting, heating, and ventilation, thus influencing building energy consumption and indoor occupant's health and well-being. Indeed, the U.S. Department of Energy reports that windows account for up to 25 percent of the utility bill of an American household [1].

Therefore, retrofitting home windows to achieve energy savings and indoor comfort is an effective way for households to reduce utility bills. However, it is difficult for occupants, especially for the households living in older houses, to make decisions of window retrofitting or replacements without knowing the properties of the existing windows. The conventional method to attain window properties relies on professional instruments and procedures of home energy-related companies or consultants. Currently, there are several professional in-situ instruments (e.g., Hukseflux Model-TRSYS01, Fluxteq - Model PHFS, MAE - Model TLOGWLS) available in the market that can measure thermal insulation of building envelopes, which could be used for window insulation measurements. These instruments are not applicable, affordable, and easy-to-use for home owners. Furthermore, to the best of our knowledge, no field instruments exist in the market for the field measurement of all window properties including U-factor, Solar Heat Gain Coefficient (SHGC), and Visible Light Transmittance (VT). Such measurement must be performed in laboratory with controlled ambient environment.

On the other side, some efforts have been made with regard to incorporating diverse sensors in an Arduino-based control system for buildings to better analyze and control energy consumption by appliances [2]. The application of the Arduino board as a microcontroller enables the integration of various sensors to detect the signals and interact with building indoor and outdoor environment. Notably, a ubiquitous healthcare monitoring system was developed by [3] to integrate ubiquitous sensors into the monitoring application in hospitals. The data were collected from the patients and sent to the web server through the Arduino thus they can be viewed and analyzed. A small smart home system based on Arduino board was designed by authors in [4] to provide a more comfortable and energy efficient home. The microcontroller of this system can monitor the data from the connected sensor that can detect the signals from people's motion, lights, room temperature and other appliances. A more comprehensive automated control system using Arduino board, Bluetooth and smartphone was proposed in the paper [5]. The smartphone can communicate with the actuators via Bluetooth and send the control signals to wireless network. The Arduino board was used for controlling and integrating different sensors in this system and enabling the information sharing among the smart phone, sensors and actuators.

The wide adoption of this hardware platform is attributed to its advantage of interactive control, open source programming and easily environmental adaptation [6], which enables the possibility of using Arduino-based platforms and compatible sensors for building window property measurements. In this paper, we present a simplified but scalable in-situ

measurement system using the Arduino Uno board and low-cost sensors for window properties. The primary contribution of this paper is the DIY fabrication approach for prototyping this in-situ measurement device that integrate components for physical environmental/surface sensing, processing, and displaying.

2. METHODOLOGY

The Arduino-based module is developed as a prototype of the window measuring tool with low-cost and small size electronic elements, mainly including luminosity sensor, phototransistor, temperature sensor, surface temperature sensor, and display screen. These low-cost electronic components have been widely used and verified in various applications, such as indoor air quality monitoring, smart parking kit, virtual reality station, disaster alarm systems, etc.[7-9]. The finished module will have a user-friendly interface using a display screen to show the measured real-time data.

2.1 Module design

The National Fenestration Rating Council (NFRC), a non-profit organisation in the U.S., has established a reliable energy performance rating system for building windows in terms of five major window properties: U-factor, Solar Heat Gain Coefficient (SHGC), Visible Transmittance (VT), Air Leakage (AL) and Condensation Resistance (CR) [10]. The properties of U-factor, SHGC, and VT are focused on in this paper as they have major influence on energy use and indoor environmental performance. Also, the air leakage is much more to do with window frames and sashes rather than glazing. Two sets of data are employed to calculate the property values, each of which representing a ratio that compares the number of outdoor parameters to indoor parameters. The correlated parameters which are required to be measured or accessed including: air temperatures of building's indoor and outdoor, surface temperatures of window's internal layer and external layer, incident solar irradiance, transmitted solar irradiance, incident visible light, and transmitted visible light. The major equations used for this sensing and measuring system are the following:

$$Q = A \cdot \Delta T \cdot U \quad (1)$$

where Q - rate of heat flow through a building assembly (in Btu/h);

A - area of the assembly (in ft²);

ΔT - temperature difference between the outdoor and indoor temperature (in F°);

U - U-factor (in Btu/ft²·hr·F°).

$$SHGC = T_s + N_i A_s \quad (2)$$

where T_s - Direct solar transmittance;

N_i - inward flowing fraction of absorbed radiation;

A_s -solar absorptance.

$$VT = \frac{L}{L_T} \quad (3)$$

where L - daylighting passing through glazing;
 L_T - total daylight landing on glazing.

2.2 Arduino board and the selection of sensors

In this model, Arduino Uno is used as the microcontroller board and to serve as a programming platform to integrate the above sensors and electronic units (see Table 1). The analog and digital input function enable us to convert signals/raw data output by the sensors to readable numbers. The Arduino Uno module built in this experiment is shown in Fig.1.

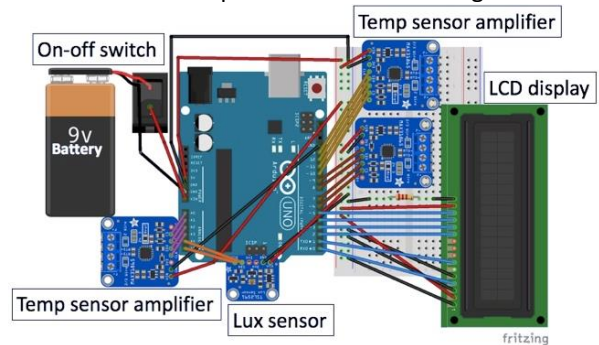


Figure 1: Arduino board module

Table 1: Key electronic sensors used in this system

Sensor Specification	
Luminosity sensor	Adafruit TSL2591
Surface temperature sensor	RTD PT100

1) Luminosity sensor

The TSL2591 luminosity sensor is an advanced digital light sensor and can be used in a wide range of light conditions. It is more accurate compared with other CdS cells and enables exact lux calculations. The more convenient part of this sensor is that it contains both infrared and full spectrum diodes [11]. This means the infrared and visible light can be separately measured. The ADC design makes it can be used in almost any microcontroller. The lux range that it measures is from 188 μ Lux sensitivity up to 120,000 lux.

The visible light measured via TSL2591 in the unit of lux is used to calculate a window's property of VT. The full spectrum light source signal measured is used to calculate the incident solar irradiance on the glass and through the glass. The heat gain through window may come from directly transmitted solar radiation and the subsequently released heat by window shown in the Equation 2 [12]. For simplicity, it is assumed that the fraction of the directly solar transmitted (T_s) is much larger than the fraction of absorbed and reemitted solar irradiation. From the solar irradiation measured inside of a window and the outside of the same window in a very small interval, the SHGC can be approximately calculated from equation 4:

PLEA 2018 HONG KONG

Smart and Healthy within the 2-degree Limit

$$SHGC = \frac{E}{E_T} \quad (4)$$

where E-solar irradiance passing through glazing;

E_T - total solar irradiance landing on glazing.

The lux sensor was connected to four wires which were wrapped by extended insulation plastic (Shown in Figure 2). The other ends of wires were connected to Arduino board.



Figure 2: Lux sensor processing

2) RTD PT100 temperature sensor

Resistance temperature detectors (RTDs) are temperature sensors that contain a resistor that changes resistance value as its temperature changes [13]. Compared with other NTC/PTC thermistors, the RTD is more stable and accurate. It has been used in laboratory and industrial processes for many years. Different construction techniques of RTDs have been developed to provide a reliable solution for surface contact temperature measurement [14]. The RTD PT100 temperature sensor is selected to measure the surface contact temperature. The Platinum RTD PT100 has a resistance of 100 ohms at 0 °C so it is named PT100 [15].

Three RTD sensors are used to design and construct a component with two 3D printed cuboid parts with acrylonitrile butadiene styrene (ABS) plastic. The sectional view of the interior of two cuboids are shown in Figure 3 and the 3D printed cuboids are shown in Figure 4. The heat transmission resistance of this component can be calculated with known thermal resistance of the ABS plastic and the air gap. The thick cuboid with two embedded RTD probes is used outside of the window and the thin cuboid with one embedded RTD probe is used inside of a window at the same time. In order to measure the heat flux through the glass, the temperatures of the different surface of thick cuboid and the temperature of the thin cuboid surface need to be measured. When the width and height of an insulation are far greater than its thickness, it can be assumed that the heat flux intensity is equal through the insulation. Thus it can be concluded that the heat flux intensity through the cuboid is equal to the that through the glass. Through mathematical calculation, the heat flux Q in equation 1 can be calculated and then U-factor of the window can be solved.

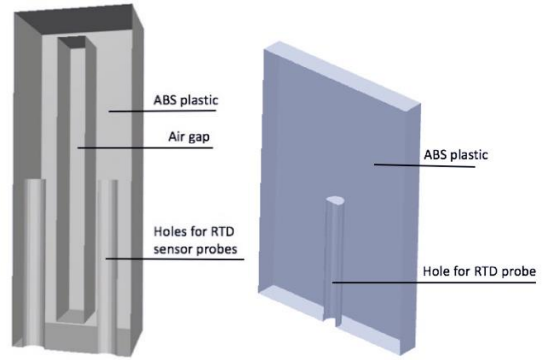


Figure 3: Section view of cuboid parts

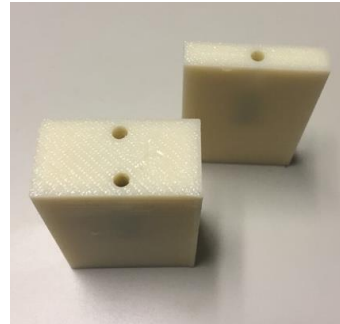


Figure 4: 3D printed cuboids

3) LCD display screen

A standard LCD screen is selected to display the real-time data collected using the Arduino module. The LCD screen has 16 characters wide and 2 rows. The LED backlight can be dimmed with a resistor. The display will alternately display the information of lux and solar irradiance, and three surface temperature from the RTD sensors.

2.3 Data calibration

Although the sensors have been calibrated individually when they come out of factories, the output values may still need comprehensive calibrations. Hence, in this study, a few professional instruments are used to generate reference values for calibrating these simplified sensing module outputs. These instruments are listed in the following table 2. The lux sensor is used to measure two wavelength ranges of solar radiation: visible light range and full spectrum light range. It is calibrated correspondingly by two professional lux measure tools. In the process of collecting solar radiation data, the lux sensor was placed at the angle and height from the light source as same with the measurement tools as possible to reduce and eliminate the errors.

Table 2: Professional instruments used for calibrating the simplified sensing module outputs

Sensor	Output (unit)	Professional Instrument
Adafruit	Spectral irradiance (w/m ²)	ASEQ LR1-T v.2
TSL2591	Visible light illuminance (lux)	KM T-10MA

PLEA 2018 HONG KONG

Smart and Healthy within the 2-degree Limit

1) Spectral irradiance calibration

The spectrometer ASEQ LR1-T v.2 is a mini irradiation measurement tool that has the custom design. It enables the users to select the spectral range and resolution to satisfy their needs. LR1 can be recognized by Windows operational system [16]. The graph data obtained with LR1 software is possible to see a spectrum with a black line corresponding to the irradiance energy at single wavelength. The tool has self-calibration design and has three configurations. One of them has the spectral range from 200 nm to 1200 nm which is used for the sensor calibration.

For the full spectrum of solar irradiance, a power relationship between the source signal for the full spectrum from the TSL2591 light sensor and the energy measured in LR1-T is found (See Figure 5). The source signal for full spectrum can be as high as 50,000 which approximately indicates the solar irradiation on a sunshine day at 2:00 PM on June in Cincinnati, Ohio. The power function can be put in the Arduino code and the irradiation can directly be read in the LCD display.

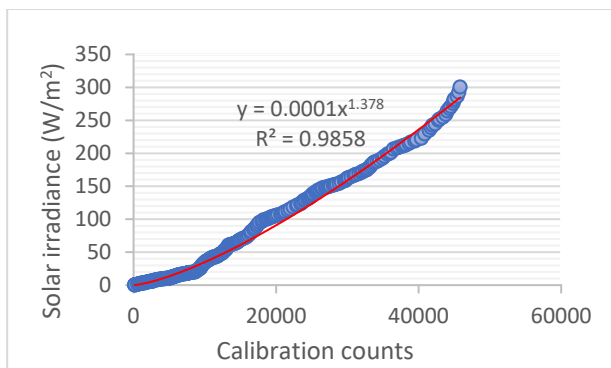


Figure 5: Relationship between the measured data of TSL2591 sensor and ASEQ LR1-T v.2

3) Illuminance calibration

This illuminance meter has one sensor with a connected long wire and adaptor connected with the main body. This instrument can measure a light source with fluctuations in a low-frequency accurately [17]. The receptor is very sensitive to the light and it must be placed stably in the process of measurement.

For the visible light, the TSL2591 measuring range is from 0 to 120,000 lux. There are totally 300 set of lux data gathered to compare the accuracy of the TSL2591 sensor to the KM T-10MA. The regression line for the wide lux wavelength ranges is shown in Figure 6.

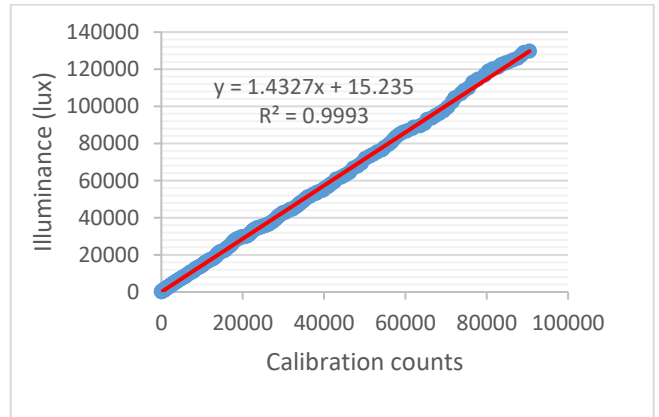


Figure 6: Relationship between the measured data of lux sensor and Illuminance meter T-10MA

3. OUTPUT TESTING AND RESULTS

All the electric parts are placed in an Arduino enclosure including the LCD display, battery, holes for USB connection and the on-off button. The finished look of the final fabricated instrument is shown in Figure 7.

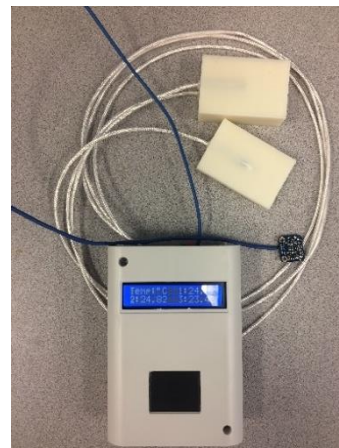


Figure 7: Fabricated instrument

The usage of this Arduino measurement system is exhibited in Figures 8 and 9, which was to measure an office building's window on the University of Cincinnati campus.

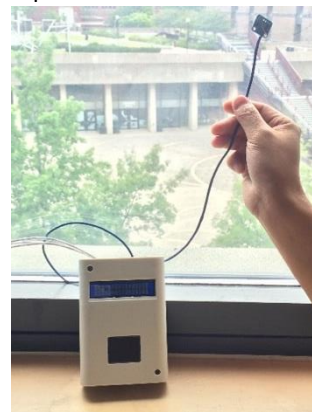


Figure 8: Measuring the lux

PLEA 2018 HONG KONG

Smart and Healthy within the 2-degree Limit

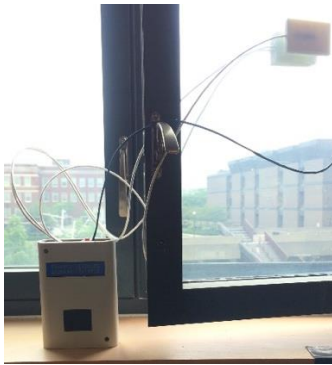


Figure 9: Measuring heat lux

It showed that the Arduino measuring system can obtain the parameters in terms of major window properties including U-factor, SHGC, and VT, with reasonable accuracy.

3.1 VT and SHGC measurement

The two calibration equations for the TSL2591 light sensor to measure solar irradiance and illuminance were write into the Arduino code. The measurements for the two parameters outside and inside window are correspondingly compared with the measurement results from the tools of ASEQ LR1-T v.2 and KM T-10MA. And it showed the maximum difference between these two sets of data is less than 5% (see Table 3).

Table 3: Illuminance and irradiance measurement

	Arduino	KM T-10MA	Difference
Illuminance (Lux)	1160	1201	3.40%
	5105	5280	3.30%
	28985	29770	3.60%
	Arduino	ASEQ LR1-T v.2	Difference
Irradiance (W/m ²)	27.53	28.96	4.9%
	138.76	142.48	2.5%
	216.38	220.26	1.8%

3.2 U-factor measurement

The equation for the glass U-factor can be described as:

$$U = \left| \frac{T_2 - T_3}{(T_3 - T_1) * R * 5.67} \right| \quad (5)$$

where, U—the U-factor of the glass (Btu/hr-ft²·°F);
 T₂—the temperature of block surface exposed to air inside of the glass (in °C);
 T₃—the temperature of the interface between the block and the glass (in °C);
 T₁—the outside glass surface temperature (in °C);
 R—the thermal resistance of the 3D printed block (in W·m⁻¹·K⁻¹);

The three temperature T₀, T_S, T_I were recorded in a one-hour test for a double pane clear glass sample. The graphs including the three temperatures, the temperature difference and U-value for three measurements are shown in the following Figure 10. The graph of U-factor indicates that a stable state is reached in a measurement time of around 35 minutes.

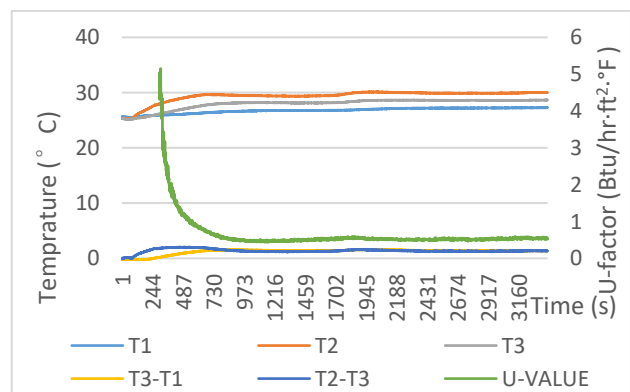
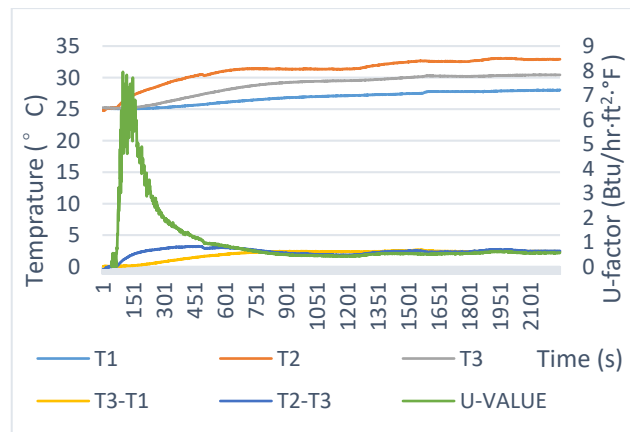
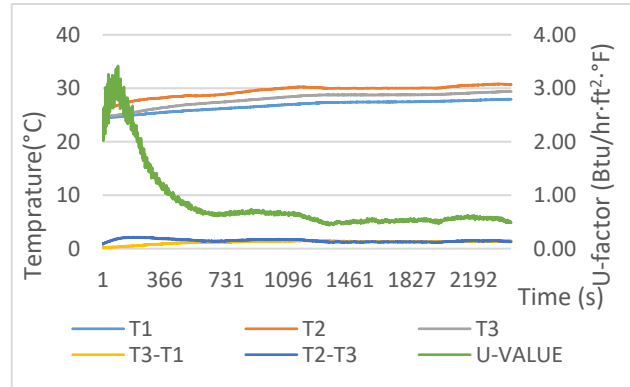


Figure 10: Double pane clear glass measurement results

The analysis of three measurement results are shown in Table 4. The maximum difference of the three results are 9.4%. The maximum difference of the test is larger than the criteria stated in ISO 9869, of which is 5% with minimum periods of 7 hours [18]. However, the criteria are obtained under the strict test environment. To approximately evaluate the window's energy performance by home owners, this

PLEA 2018 HONG KONG

Smart and Healthy within the 2-degree Limit

easy-to-operate and overall instrument trade-offs a fast-delivered result against accuracy.

Table 4: Three measurements analysis

	U-factor	Std. Dev
1 st measurement	0.56	3.0 %
1 nd measurement	0.58	2.5 %
3 rd measurement	0.53	2%
Average	0.56	2.5%

4. DISCUSSION

The total cost for all this measuring system including various sensors, enclosure, LCD display, Arduino board, battery and connection wires and ABS is approximately \$60-100 depending on the selection of electronic element types and brands. The cost for the tools such as Hukseflux Model-TRSYS01, Fluxteq - Model PHFS, MAE - Model TLOGWLS for in-situ measurement ranges from \$1,200 to \$2,000. However, compared with these professional instruments, to achieve the best result, the designed instrument should be used within certain environmental conditions.

In principle, the U-factor can be obtained by measuring heat-flow using heat flux meter and recording the temperature on both sides of windows under steady state conditions. A new design to measure the heat flow is proposed in this paper. Since steady-state conditions are never achieved on site in practice, we have to assume that mean values of heat flow rate and temperatures over a long period of time give an estimate of the steady-state condition. That means the measuring environment should be relatively stable and also with apparent temperature difference between interior and exterior.

The primary sensor for solar irradiance and visible lighting illuminance in this design is the TSL2591 light sensor. The sensor will be saturated under environmental conditions with direct and strong sunshine. Despite the constraint, this lux sensor is able to measure irradiance closely similar to that measured by the illuminance meter T-10MA after calibration. The other sensor in this proposed system is PT100 RTD temperature sensor with $\pm 0.5^{\circ}\text{C}$ accuracy from -10°C to $+85^{\circ}\text{C}$. RTD sensors with different configurations can be tested to improve its accuracy and stability.

5. CONCLUSIONS

In this paper we have proposed a design and implementation of a low-cost and easy-to-use measuring approach and instrument to the home window's measurements. Test of the functionality and accuracy of this measure module showed that this simple and compact Arduino-based module can obtain major window properties including U-factor, SHGC, and VT, with reasonable accuracy. This study is the

initial step of developing decision-making support tools for home energy efficiency upgrades.

Future work for this measuring system comprehend a more accurate and smaller surface temperature sensor to allow a more accurate easurement of the heat transferred through the glass. In addition, within the scope of Smart Cincy initiatives (a regional program in Ohio, U.S.) and the U.S. Environmental Protection Agency Sensible Home project, we have established local community and high school outreach programs for disseminating home energy saving knowledge and information, promoting energy saving behaviors and environmental sustainability awareness, and sharing useful low-cost toolkits and fabrication approaches. Engaging into these programs and projects, we will develop a series of DIY tools for in-situ building performance measurement associated with descriptive information and energy efficient retrofit strategies.

REFERENCES

1. Energy Advice for Owners of Older and Historic Homes (2017). <https://archive.epa.gov/region5/sustainable/web/html/energyadvice.html>.
2. Han, D.-M., and Lim, J.-H. (2010). Smart home energy management system using IEEE 802.15.4 and ZigBee. *IEEE Transactions on Consumer Electronics*, 56(3), 1403–1410.
3. Kemis, H. et al. (2012). Healthcare Monitoring Application in Ubiquitous Sensor Network: Design and Implementation Based on Pulse Sensor with Arduino. *Information Science and Service Science and Data Mining (ISSDM)*, 2012 6th International Conference on New Trends In. 34–38.
4. Adriansyah, A. and A. W. Dani. (2014). Design of Small Smart Home System Based on Arduino. *Electrical Power, Electronics, Communications, Controls and Informatics Seminar (EECCIS)*, 2014 121–25.
5. Ramli, K N, a Joret, and N H Saad. (2014). Development of Home Energy Management System Using Arduino: 12–15.
6. <https://www.arduino.cc/en/Guide/Introduction>
7. Abraham, S., & Li, X. (2014). A cost-effective wireless sensor network system for indoor air quality monitoring applications. *Procedia Computer Science*, 34, 165-171.
8. Urdiain, L. O., Romero, C. P., Doggen, J., Dams, T., & Van Houtven, P. (2012, September). Wireless sensor network protocol for smart parking application experimental study on the arduino platform. In 2nd International Conference on Ambient Computing, Applications, Services and Technologies.
9. Yawut, C., & Kilaso, S. (2011, May). A wireless sensor network for weather and disaster alarm systems. In *International Conference on Information and Electronics Engineering, IPCSIT* (Vol. 6, pp. 155-159).
10. Measuring Performance: National Fenestration Rating Council, <http://www.efficientwindows.org/nfrc.php>
11. <https://www.adafruit.com/product/1980>
12. <http://www.efficientwindows.org/shgc.php>
13. <https://www.omega.com/prodinfo/rtd.html>
14. <http://www.aseq-instruments.com/LR1.html>
15. <https://www.adafruit.com/product/3290>
16. <https://sensing.konicaminolta.us/products/t-10a-t-10ma-illuminance-meters/>

PLEA 2018 HONG KONG

Smart and Healthy within the 2-degree Limit

17. <https://www.defelsko.com/positector-dpm>

18. International Organization for Standardization (ISO), Thermal Insulation —Building Elements —In-Situ Measurement of Thermal Resistance and Thermal Transmittance —Part 1: Heat Flow Meter Method, ISO Standard, 2014 9869-1.

Experimental Biases in Discomfort Glare Evaluations

MICHAEL G. KENT¹, STEVE FOTIOS², SERGIO ALTOMONTE³

¹ Department of Architecture and Built Environment, University of Nottingham, Nottingham, United Kingdom

² School of Architecture, University of Sheffield, Sheffield, United Kingdom

³ Architecture et Climat, Université catholique de Louvain, Louvain-la-Neuve, Belgium

ABSTRACT: The multiple criterion scale developed by Hopkinson is extensively utilised to analyse the subjective degree of discomfort due to glare. Using a luminance adjustment procedure, the brightness of a glare source is adjusted to reveal four levels of discomfort, typically: just imperceptible, just acceptable, just uncomfortable, and just intolerable. In many experimental studies, observers are requested to attend to each level of discomfort in ascending order, from the lowest to the highest criterion. There are, however, reasons to believe that assessments made using adjustments might be affected by the initial anchor, i.e. the setting of the variable stimulus before an adjustment is made, and by order effects, this influencing the reported thresholds of discomfort. To investigate anchor bias and order effects, two Hopkinson-like multiple criterion adjustment experiments were performed, respectively with three different initial anchors and three order sequences (ascending, descending, and randomised). The results revealed substantive bias due to anchor and order effects, primarily at lower glare criteria. This demonstrates the need for caution when interpreting subjective evaluations of discomfort due to glare and estimating the robustness of glare indices derived from studies that used models fitted to data obtained with Hopkinson's multiple criterion scale and luminance adjustment procedure.

KEYWORDS: Discomfort Glare, Experimental Bias, Luminance Adjustment, Anchor Bias, Order Effects

1. INTRODUCTION

This paper critically synthesises research studies by the authors focusing on the design of experiments carried out to explore the evaluation of discomfort due to glare [1, 2]. Discomfort glare is a psychological sensation causing distraction or annoyance, which is associated with a luminance, or luminance contrast, within the visual field of an observer that is sufficiently greater than that to which the eyes can adapt [3]. Many studies have sought to characterise this discomfort, leading to the proposal of several glare models and indices. Among these, there are three fundamental studies. Hopkinson [4] used an experimental procedure whereby the brightness of a light source was incrementally adjusted to the points at which observers suggested that a visual scene represented four specific thresholds of discomfort glare, the multiple criterion scale (MCS). In its most typical form, the MCS features the following criteria: Just Imperceptible (JImp), Just Acceptable (JA), Just Uncomfortable (JU), and Just Intolerable (JInt). Luckiesh and Guth [5] also used an adjustment procedure to determine one threshold, the Borderline between Comfort and Discomfort (BCD). Petherbridge and Hopkinson [6] later established an empirical relationship between the discomfort reported by observers and lighting parameters: the Glare Constant. Various glare indices have been developed from these fundamental studies, such as the Illuminating Engineering Society Glare Index (IES-GI) [7] and the Unified Glare Rating (UGR), which is currently recommended by the Society of Light and Lighting [8],

the Illuminating Engineering Society of North America [9] and the International Commission on Illumination [10]. The Daylight Glare Index (DGI) [11] was also developed using a procedure similar to [4]. The purpose of glare indices is to provide robust predictions of the discomfort reported by an observer in a luminous environment. However, since the studies on which glare indices are based have mostly used fixed-order luminance adjustment, in this paper we discuss the potential influence of two sources of experimental bias on errors between predicted and actual discomfort: 1) anchor; and, 2) order effects.

2. ANCHOR BIAS

2.1 Adjustments and heuristic anchoring

When observers use an adjustment procedure to make judgements of a variable stimulus, it has been proposed that the final setting might be influenced by the initial stimulus; this phenomenon is known as anchoring [12]. Anchors can affect a large range of assessments, such as responses to general knowledge questions, economic evaluations, etc. When making a subjective judgement, different starting points lead to different values, which tend to be biased towards the initial settings. Anchoring has been demonstrated also in lighting studies [13], providing reasons to believe that the adjustment procedure traditionally used in glare experiments might be biased towards the initial luminance setting. If this proves correct, the results from the fundamental studies mentioned above – and, hence, the subsequent glare indices – might provide an incorrect estimate of the relationship between

PLEA 2018 HONG KONG

Smart and Healthy within the 2-degree Limit

background and target luminance associated with each glare criterion. To test this hypothesis, an experiment was designed to confirm whether the initial luminance setting of a variable stimulus (anchor) influences the luminance associated with a given discomfort glare sensation.

2.1 Experimental design and procedure

Discomfort from artificial lighting was investigated in a laboratory test, using a procedure designed to explore whether an anchor bias could be detected. The setup of the testing apparatus (Figure 1) was informed by previous studies by the authors [14].

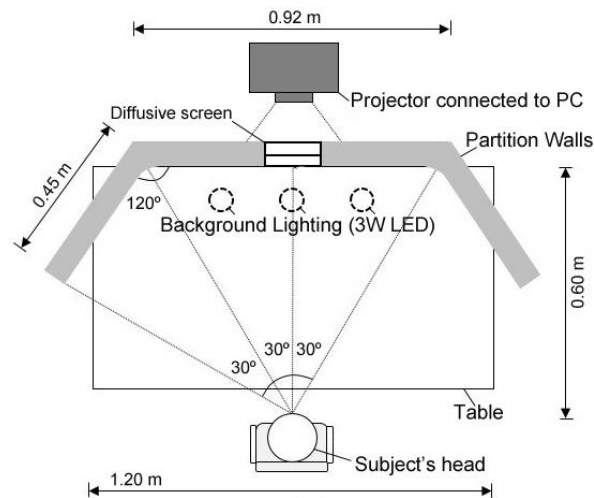


Figure 1. Plan of the testing apparatus

The testing apparatus was semi-hexagonal in plan. The interior surfaces (2.7 m in height) were painted matte white, and three 3W LED lamps produced a background lighting with a constant luminance distribution of 65 cd/m². A desk with a diffusive white surface was mounted within the wooden partitions. The subject's head position was set at a height of 1.2 m, facing a diffusive screen (0.08 m x 0.04 m) made from three sheets of translucent paper and mounted in front of a projector connected to a computer. The diffusive screen subtended an angle at the eye of 0.009 steradians and provided a variable luminance in the range between 200 and 32,000 cd/m². The source luminance could be progressively increased using the relative brightness function of an image editing software. To test the hypothesis that different initial source luminances lead to different adjustment settings for the same level of glare sensation, test subjects were asked to provide judgements under three initial settings corresponding to a low, medium, and high anchor. Since no established luminance value could be applied to specify these anchors, the luminance associated to each of the following IES-GI discomfort glare criteria were used [15], respectively: Just Imperceptible (Low anchor); Borderline between Comfort and Discomfort, or BCD (Medium anchor);

and Just Uncomfortable (High anchor). The Just Uncomfortable criterion was used for the high anchor to avoid any potential harm to participants (Table 1).

Table 1. Definition of the three initial anchors

Anchor	Luminance [cd/m ²]	IES-GI	Glare Criterion
Low (L)	1,627	10	Just Imperceptible
Medium (M)	5,414	18.5	BCD
High (H)	8,999	22	Just Uncomfortable

During the experiment, participants were asked to make judgements of visual discomfort using the IES-GI glare criteria [15]. Since it was considered that each criterion could be open to self-interpretation due to the abstraction caused by the assessment, to aid subjects giving more meaningful judgements the criteria were linked to time-span descriptors [16].

At the start of the experiment, the brightness of the diffusive screen was set to one of the initial luminance anchors chosen at random. Participants directed their gaze towards the centre of the diffusive screen and were asked whether they would like the experimenter to increase, decrease, or keep constant its brightness to reach a glare sensation of Just Imperceptible (JImp). Once the lowest of the four criteria was set, the luminance of the screen was increased at a controlled pace and subjects were asked to indicate when the other criteria – Just Acceptable (JA), Just Uncomfortable (JU), and Just Intolerable (JInt) – were reached. The IES-GI was calculated from the recorded luminances. After making the initial four evaluations, participants were given a short relaxation period (two minutes) before continuing the experiment starting with a different luminance anchor. The test procedure was again repeated until the subject had provided all four levels of glare sensation under each of the three different luminance anchors. Twenty-two subjects participated to this experiment, recruited via an online advertisement. The sample comprised 8 males and 14 females, with a mean age of 29.6 years (SD=3.75).

2.2 Results

Table 2 presents the mean source luminance and standard deviation of the diffusive screen for each glare criterion under the three anchors (L, M, H). Initial inspection of the data shows that mean values increase when considering a higher anchor for each glare criterion, suggesting that adjustments were made closer to the luminance of the initial setting.

Table 2. Mean source luminance (and standard deviation)

Anc	Mean source luminance (SD) [cd/m ²]			
	JImp	JA	JU	JInt
L	1,784 (1,031)	3,043 (1,534)	4,517 (2,027)	8,238 (4,135)
M	3,192 (1,341)	4,350 (1,982)	5,858 (1,982)	10,130 (3,388)
H	5,663 (2,923)	7,224 (3,037)	9,031 (3,232)	13,548 (4,858)

PLEA 2018 HONG KONG

Smart and Healthy within the 2-degree Limit

Figure 2 presents the mean IES-GI values calculated for the four glare criteria provided by test subjects under the three anchors. According to Hopkins [15], IES-GI benchmarks for each glare criterion are, respectively: No glare \leq 10; 10 \leq JImp \leq 16; 16 \leq JA \leq 18.5; 18.5 \leq BCD \leq 22; 22 \leq JU \leq 28; JInt \geq 28.

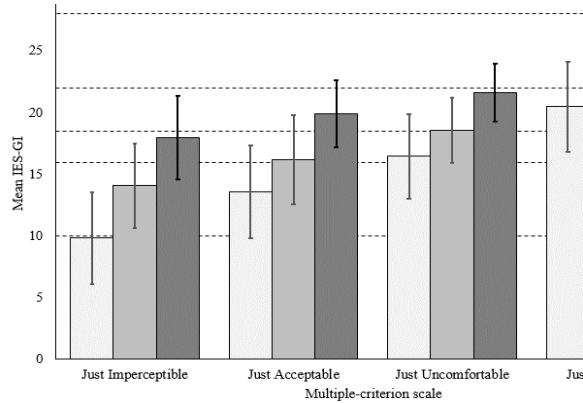


Figure 2. Mean IES-GI for the luminance anchors and the four glare criteria (error bars show standard deviations)

Figure 2 confirms the tendency for the IES-GI to be consistently influenced by the luminance anchors for all glare criteria. Differences in mean IES-GI across the three anchors also appear to decrease at higher levels of discomfort glare. Null hypothesis significance testing (NHST) was performed to determine if differences between groups were statistically significant. However, since NHST is dependent on both the size of the sample and on the magnitude of the influence under testing, emphasis of the analysis was placed on the effect size (i.e., a standardised measure of the difference across the independent variable) and not only on the statistical significance [17]. Since data were not normally distributed and differences in variance were not significant, a parametric repeated-measures Analysis of Variance (RM-ANOVA) was run to compare glare indices across the three anchors. The RM-ANOVA demonstrated that the differences in mean values of IES-GI across the three anchors for all glare criteria were all highly significant and with substantive effect sizes, ranging between large ($\eta^2 \geq 0.71$ for Just Imperceptible) and moderate ($0.25 \leq \eta^2 < 0.64$ for all other glare criteria).

Post-hoc testing was then performed, comparing against each other all combinations between anchors. Statistical significance of differences was calculated using one-tailed paired t-tests to identify the variations detected in the RM-ANOVA. Bonferroni corrections were applied in consideration of the experiment-wise error rate caused by the alpha level inflating across multiple pairwise comparisons. The interpretation of the outcome was derived from the benchmarks given by Ferguson [18] for small, moderate, and large effect sizes ($d \geq 0.41$, 1.15 and 2.70,

respectively). Table 3 reports the results of the post-hoc t-tests providing, for each MCS glare criterion, the comparison between initial anchors, the mean and standard deviations for the IES-GI, the mean differences (ΔM) and their statistical significance (NHST), and the effect size (Cohen's d).

Table 3. Paired comparison t-tests and effect sizes

MCS	Comparison	M(SD)	M(SD)	ΔM ^{NHST}	d
JImp	Low v. Medium	9.81 (3.74)	14.07 (3.43)	-4.26***	-1.18
	Medium v. High	14.07 (3.43)	17.97 (3.40)	-3.90***	-1.14
JA	Low v. Medium	13.57 (3.78)	16.17 (3.58)	-2.60**	-0.71
	Medium v. High	16.17 (3.58)	19.92 (2.73)	-3.75***	-1.18
JU	Low v. Medium	16.45 (3.44)	18.55 (2.66)	-2.10*	-0.68
	Medium v. High	18.55 (2.66)	21.61 (2.36)	-3.06***	-1.22
JInt	Low v. Medium	20.47 (3.67)	22.47 (2.13)	-2.00**	-0.67
	Medium v. High	22.47 (2.13)	24.42 (2.40)	-1.94***	-0.86

Bonferroni corrections: *weakly significant **significant;

***highly significant; n.s. = not significant

$d < 0.41$ = negligible; $0.41 \leq d < 1.15$ = small; $1.15 \leq d < 2.70$ =

moderate; $d \geq 2.70$ = large

The inferential data show that the sign of the mean differences and the effect sizes are consistently negative, therefore signalling higher values of IES-GI when participants adjusted the luminance of the glare source starting from a higher anchor. All differences were statistically significant and with a substantive effect size, hence confirming that, when the initial anchor was higher, test subjects made adjustments to higher luminance settings for the same level of reported glare sensation. The effect of the anchor on the glare settings also appear to be stronger when considering a larger difference in the luminance of the initial anchor. In fact, comparisons between the 'low' and 'high' anchors produced the largest differences in mean IES-GI and effect size for every glare criterion. The findings also show that, when considering higher levels of visual discomfort, the differences in mean and the effect sizes reduce across comparisons, suggesting that the influence of the initial anchor decreases at higher glare sensation. However, this might have occurred since participants were instructed to make adjustments using only a sequence of increasing glare stimulus. Conversely, the experimental procedure did not consider how adjustments could have influenced the outcome of the study if other order sequences had been used.

3. ORDER EFFECTS

3.1 Experimental design and procedure

PLEA 2018 HONG KONG

Smart and Healthy within the 2-degree Limit

Based on these results, a further experiment was designed to explore whether order effects in a luminance adjustment procedure could be detected under controlled laboratory conditions. The same testing apparatus described above was used (Fig. 1).

During the experiment, participants were asked to make judgements of discomfort glare using the same MCS criteria utilised by Petherbridge and Hopkinson [4] with the ascending-only order sequence from where the Glare Constant formula was derived. Three different order sequences were used:

- Ascending: JImp, JA, JA, JInt
- Descending: JInt, JU, JA, JImp
- Randomised: the order of criteria was shuffled.

Comparing the luminances set for each criterion in the three sequences would demonstrate whether or not order had any significant effect. A repeated-measures design was used. At the outset of the experiment, the diffusive screen was set to an initial luminance corresponding to an IES-GI of 10 (Just Imperceptible). This anchor was used only for the first trial, and then the luminances set by test participants became the anchor for the subsequent setting. For each trial, the experimenter adjusted the luminance of the glare source at a controlled pace according to the participant's instruction (increased, decreased, or kept at its current brightness) to reach a glare sensation corresponding to each of the four predefined criteria, in the order described in one of the three sequences. The test procedure was repeated until the participant had provided all four criteria of glare sensation under each of the three sequences, these being presented in a random order. Twenty participants (different from the previous experiment) volunteered to this test, recruited via an online advertisement. The sample included 7 males and 13 females, with a mean age of 24.2 (SD= 5.76).

3.2 Results

Figure 3 shows the mean source luminance and standard deviation of the glare source at the point in which participants reported each criterion of glare sensation under the three order sequences.

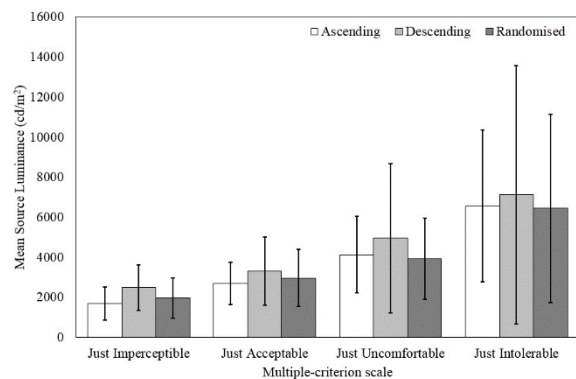


Figure 3. Mean source luminances and standard deviations for the four discomfort glare criteria under the three orders

Visual inspection of the plots suggests that mean source luminances were higher when adjustment settings were made using a descending sequence for each glare criterion. The standard deviations become consistently larger when assessments were made at higher levels of discomfort across all three sequences. Null Hypothesis Significance Testing (NHST) was used to determine if the differences in source luminance were statistically significant. Emphasis of the analysis was again placed on the effect size and not only on the *p*-value. A repeated-measures Analysis of Variance (RM-ANOVA) was performed to compare against each other the source luminance settings for each criterion of reported glare sensation across the three order sequences. The results of the RM-ANOVA showed that the differences across the independent variable (order sequence) were highly significant for the Just Imperceptible criterion, weakly significant for Just Acceptable and not significant for the other two glare criteria. The differences detected had a substantive effect size ranging from moderate ($0.25 \leq \eta^2 < 0.64$ for JImp) to small ($0.04 \leq \eta^2 < 0.25$ for JA and JU). Not substantive differences were found for the Just Intolerable criterion ($\eta^2 < 0.04$). In the data, the magnitude of the effect decreased at higher levels of discomfort. Hence, the effect of order on the luminance settings made by test participants appeared to be weaker for higher glare criteria, confirming the observations from Figure 2. Post-hoc testing was performed to compare all combinations of order sequences for each glare criterion. Statistical significance of the differences was calculated using two-tailed paired t-tests to determine the locations of the differences detected in the RM-ANOVA. The effect size was estimated by the Pearson's *r* (Table 4).

Table 4. Paired t-test comparisons across order sequences

MCS Comparison	M(SD) ₁	M(SD) ₂	ΔM^{NHST}	<i>r</i>
JImp Asc. vs. Des.	1,676 (829)	2,484 (1123)	-807***	-0.69
JImp Asc. vs. Ran.	1,676 (829)	1,972 (1005)	-296*	-0.36
JImp Des. vs. Ran.	2,484 (1123)	1,972 (1005)	511**	0.44
JA Asc. vs. Des.	2,686 (1065)	3,317 (1707)	-631**	-0.54
JA Asc. vs. Ran.	2,686 (1065)	2,962 (1419)	-276*	-0.27
JA Des. vs. Ran.	3,317 (1707)	2,962 (1419)	354*	0.29
JU Asc. vs. Des.	4,130 (1905)	4,044 (3718)	-815**	-0.27
JU Asc. vs. Ran.	4,130 (1905)	3,922 (2034)	207 n.s.	0.18
JU Des. vs. Ran.	4,044 (3718)	3,922 (2034)	1,022**	0.38
JInt Asc. vs. Des.	6,562 (3783)	7,116 (6459)	-554 n.s.	-0.16
JInt Asc. vs. Ran.	6,562 (3783)	6,443 (4702)	120 n.s.	0.03
JInt Des. vs. Ran.	7,116 (6459)	6,443 (4702)	674 n.s.	0.21

Asc.= Ascending, Des.= Descending, Ran.= Randomised
Bonferroni corrections: ***highly significant; **significant;

PLEA 2018 HONG KONG

Smart and Healthy within the 2-degree Limit

*weakly significant; n.s.= not significant; $r < 0.20$ = negligible; $0.20 \leq r < 0.50$ = small; $0.50 \leq r < 0.80$ = moderate; $r \geq 0.80$ = strong

Table 4 reports the results of the t-tests, providing, for each glare criterion, the comparison between order sequences under examination, the mean (M) and standard deviations (SD) of the glare source luminance for each sequence, the differences between means (ΔM), their statistical significance (NHST), and the effect size (Pearson's r).

Inspection of descriptive and inferential statistics shows no consistent directionality of the sign for the mean differences and the effect sizes across all comparisons, this being consistent with the adoption of a two-tailed hypothesis. Out of the twelve comparisons, the differences between mean values of source luminance are highly significant in one case, significant in four cases, weakly significant in three cases, and not significant in four cases. For all settings made to the highest criterion of discomfort (Just Intolerable), the effect of order sequence was not statistically significant. The differences detected were mostly of substantive magnitude, with effect sizes ranging from moderate ($0.50 \leq r < 0.80$ in two cases) to small ($0.20 \leq r < 0.50$ in seven cases). Negligible effects were detected for three comparisons ($r < 0.20$).

4. DISCUSSION AND LIMITATIONS

Two experiments were designed to study the potential influence of sources of experimental bias on errors between predicted and actual discomfort due to glare: 1) anchor; and, 2) order effects.

From the anchor effects experimental data, Table 5 displays, for each MCS level of glare sensation, the anchor used, the mean IES-GI, and the corresponding glare criterion based on Hopkinson's scale [15].

Table 5. Initial anchor and corresponding glare criteria

MCS	Anchor	Mean IES-GI
JImp	Low	9.81 (No Glare)
	Medium	14.07 (Just Imperceptible)
	High	17.97 (Just Acceptable)
JA	Low	13.57 (Just Imperceptible)
	Medium	16.17 (Just Acceptable)
	High	19.92 (BCD)
JU	Low	16.45 (Just Acceptable)
	Medium	18.55 (BCD)
	High	21.61 (BCD)
JI	Low	20.47 (BCD)
	Medium	22.47 (Just Uncomfortable)
	High	24.42 (Just Uncomfortable)

The results of the anchor effects experiment show that, for the same level of glare sensation across the three anchors, the mean values of IES-GI correspond to different discomfort glare criteria (on Hopkinson's

scale). This demonstrates that, when luminance adjustment are performed from different anchors, the final settings can vary considerably. This finding questions the alleged precision of glare index values from artificial light sources calculated to estimate the levels of visual discomfort perceived by an observer.

Inferential analysis of the data from the order effects experiment confirmed that the sequence of tests had substantive influence on the final settings made by participants for the same level of discomfort glare. The order effect on glare settings appeared to be larger at lower levels of glare sensation.

Before drawing conclusions on the theoretical and design implications of these results, some methodological limitations need to be acknowledged. Among these, it should be noted that in the anchor effects experiment the mean IES-GI values presented in Table 5 are all lower than the corresponding discomfort criterion for the same reported level of glare sensation, regardless of the anchor used. Although it is difficult to determine the reasons for this, it is likely that glare evaluations were influenced by the available range of the variable stimulus. In fact, in the experimental procedure, the maximum luminance was set at $32,000 \text{ cd/m}^2$. If a lower or higher maximum luminance had been used, the results could have been different. The study of range bias needs to be the object of further work.

For the order effect experiment, it must be considered that the ascending sequence was used to replicate the test methodology used in the mentioned fundamental glare studies [4, 5, 6], the descending sequence was adopted as its reverse procedure, and the randomised sequence was used as a potential good practice to overcome order effects [19]. The Ascending vs. Randomised comparison, therefore, should reveal the differences in results between a study that uses Hopkinson's approach in terms of scale and procedure and one that follows good experimental practice. This comparison suggests that the magnitude of the order effect was significant and substantive (non-negligible effect size, $r > 0.20$) for Just Imperceptible and Just Acceptable, but not for the other two glare criteria.

One might question whether combining the data obtained under an ascending and a descending order, and using the mean as best estimate, might lead to results that are in accordance with those achieved under a randomised sequence. Randomised orders are, in fact, generally considered the most robust experimental approach. Where this is not possible, taking the mean of results gained using lower and upper anchors may provide the best estimates [20].

To offer an initial exploration of such hypothesis, the mean source luminances of the glare source corresponding to the adjustment settings made for the four discomfort glare criteria under the ascending and descending orders were combined and then compared

PLEA 2018 HONG KONG

Smart and Healthy within the 2-degree Limit

to the mean source luminance settings made by test subjects under the randomised sequence. Figure 4 illustrates the results of the comparison in terms of mean source luminances, standard deviations, and mean differences. At the lowest two criteria of discomfort glare, the plots show a relatively small difference in mean source luminance between the combined and the randomised sequences (respectively, $\Delta M = 68.11$ and 38.93 cd/m^2). At higher glare criteria, the mean luminance values obtained from the combined data are larger than the adjustment settings made under the randomised sequence (with differences, respectively, of $\Delta M = 615.08$ and 436.24 cd/m^2).

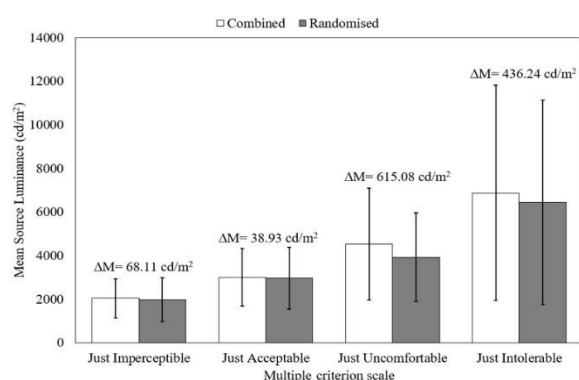


Figure 4. Mean source luminances for the four glare criteria under the combined and the randomised test sequences.

This was to be anticipated considering that, as shown in Figure 3, at lower levels of visual discomfort, the mean source luminance values under the randomised sequence fell between the mean values recorded for the ascending and descending orders. Conversely, at higher discomfort glare criteria, the adjustment settings made under the ascending and descending orders were both performed at higher luminances than the randomised sequence.

Further testing could not be performed to analyse the statistical and practical significance of the differences detected since, due to the methods used for the collection of our data, the assumption of independence could not be met. In fact, the statistical significance of the differences cannot be calculated when the luminance settings given by the same test participant in separate conditions (e.g., ascending and descending orders) are combined. However, these initial observations can be useful for future experimental designs, particularly in the presence of constraints in terms of time and resources.

4. CONCLUSION

While it is not common in discomfort glare research to question the procedures used to derive experimental data in fundamental studies, there is a need to identify

key sources of methodological bias to address current limitations of glare models [21].

In this context, the results of two experiments, conducted under artificial lighting controlled laboratory conditions, provided statistically significant and practically relevant evidence that: 1) luminance adjustments used to test the level of discomfort due to glare from a bright light source are biased by the initial luminance setting (anchor); (2) a luminance adjustment experimental procedure is influenced by order effects, particularly at lower glare criteria.

These results suggest the need to critically review the test methodology used in glare studies that have used luminance adjustments from only a low initial glare source setting (anchor bias) and uniquely under an ascending sequence of glare stimulus (order effect). Conversely, this study demonstrates the importance of providing strong reasoning when specifying experimental design and procedures for glare evaluations, and suggests a need to question the robustness of current indices for discomfort glare.

ACKNOWLEDGEMENTS

This work was funded by the UK's Engineering and Physical Sciences Research Council [EP/N50970X/1]. This paper presents a critical synthesis and review of previously published articles listed in references [1,2].

REFERENCES

1. Kent MG, Fotios S, Altomonte S (2017). Discomfort glare evaluation: The influence of anchor bias in luminance adjustments. *LR&T*, doi.org/10.1177/1477153517734280.
2. Kent MG, Fotios S, Altomonte S (2018). Order effects when using Hopkinson's multiple criterion scale of discomfort due to glare. *Build Env*, 136: 54-61.
3. CIE (2011). *CIE S 017/E:2011 ILV: International Lighting Vocabulary*. CIE: International Commission on Illumination.
4. Hopkinson RG (1940). Discomfort glare in lighted streets. *Trans Illum Eng Soc*, 5(1-9): 1-32.
5. Luckiesh M, Guth SK (1949). Brightnesses in Visual Field at BCD. *Illum Eng*, 44: 650-670.
6. Petherbridge P, Hopkinson RG (1950). Discomfort glare and the lighting of buildings. *Trans Illum Eng Soc*, XV: 39-79.
7. Robinson W, et al. (1962). The development of the IES Glare Index System. *Trans Illum Eng Soc*, 27(1): 9-26.
8. SLL (2012). *Code for lighting: Society of light and lighting*.
9. IESNA (2010). *Lighting Handbook*. New York: IESNA.
10. CIE 177-1995. *Discomfort glare in interior lighting*. CIE.
11. Hopkinson RG, Bradley RC (1960). A study of glare from very large sources. *Illum Eng*, 55(5): 288-294.
12. Chapman GB, Johnson EJ (1999). Anchoring and values construction. *Org Beh & Hum Dec Proc*, 79 (2): 115-153.
13. Logadottir A, Christoffersen J, Fotios S (2011). Investigating the use of an adjustment task to set the preferred illuminance. *LR&T*, 43: 403-422.
14. Kent MG, Altomonte S, Tregenza PR, Wilson R (2015). Discomfort glare and time of day. *LR&T*, 47: 641-657.
15. Hopkinson RG (1960). Note on use of indices of glare for a code of lighting. *Trans Illum Eng Soc*, 25(3): 135-138.

PLEA 2018 HONG KONG

Smart and Healthy within the 2-degree Limit

16. Velds M (2002) User acceptance studies to evaluate discomfort glare in daylight rooms. *Sol Ener*, 73(2): 95-103.
17. Altomonte S, Schiavon S (2013). Occupant satisfaction in LEED and non-LEED buildings. *Build Env*, 68: 66-76.
18. Ferguson CJ (2009). An effect size primer: a guide for clinicians and researchers. *Prof Psych*, 40(5): 532-538.
19. Field A, Hole G (2013) *How to design and report experiments*. London: Sage.
20. Gescheider GA (1997). *Psychophysics: The fundamentals*. New Jersey: Lawrence Erlbaum Associates.
21. Fotios S (2018). Correspondence: New methods for the evaluation of discomfort glare. *LR&T* 50: 489-491.

Investigating the Impact of Architectural Form and Wind Direction on the Performance of a Passive Downdraught Evaporative Cooling Tower in Saudi Arabia

MOHAMMAD A. ALSHENAIFI¹, STEVE SHARPLES¹

¹University of Liverpool, Liverpool, UK

ABSTRACT: Buildings in Saudi Arabia consumes approximately 80% of the electricity generated in the country. Saudi Arabia's hot, arid climate, with summer temperatures frequently exceeding 45°C, means that air conditioning uses nearly 50% of the country's electricity, and virtually all the electricity is generated from fossil fuels. Passive cooling techniques could be a sustainable alternative to conventional air-conditioning systems when integrated properly within a building. A Passive Downdraught Evaporative Cooling (PDEC) tower is considered as one of the most efficient passive systems and was investigated in this study. A single storey open plan room with a PDEC tower was digitally modelled and then changes in wind direction and architectural form were simulated to see the effect on the PDEC performance. IES VE software was selected for the simulations as it can conduct a dynamic thermal simulation for PDEC systems. A weather file for Riyadh was obtained from the software Meteonorm. The study demonstrated that significant cooling can be achieved by PDEC towers, but that their effectiveness was greatly reduced by changes in wind direction linked to opening distributions in the room attached to the PDEC tower.

KEYWORDS: Passive Cooling, Passive Downdraught Evaporative Cooling, Cool Towers, Buffer Zone

1. INTRODUCTION

In 2016 Saudi Arabia was the largest oil consuming nation in the Middle East, and 10th in the world, with a total consumption of approximately 3.9 million barrels per day (b/d). The average direct burn of crude oil for power generation is more than 700,000 b/d during the summer months [1]. Buildings consume approximately 80% of the total electricity generated, and air conditioning represent most of that consumption [1]. It is obvious that buildings play a substantial role in Saudi Arabia's energy consumption. Passive cooling systems can significantly reduce cooling demand for buildings. This study investigated one such cooling system – the Passive Downdraught Evaporative Cooling (PDEC) tower – and assessed how architectural form and wind direction affect the performance of a PDEC system in a Saudi summer.

2. LITERATURE AND BACKGROUND

The term 'passive cooling' describes a process that relies on a natural environmental heat sink to achieve cooling. Passive cooling strategies can be classified to four major types based on the natural heat sinks: (i) Natural ventilation (night ventilation), (ii) night sky radiation, (iii) ground cooling, (iv) evaporative cooling [2]. Passive Downdraught Evaporative Cooling (PDEC) towers are categorized as a direct evaporative cooling technique. When hot dry air passes through a water medium, the evaporation of the water occurs as sensible heat is converted into latent heat, and the air temperature decreases as the relative humidity level

increases. A PDEC tower consists of a wind catcher at the top of a tower, an evaporative/water medium, and a shaft to deliver the caught, cooled air to an occupied space via openings at the bottom of the tower. Hot and arid climatic regions provide an ideal environment for PDEC systems, and an up to 80% reduction of wet bulb depression (WBD) can be produced, which would ultimately lead to a significant reduction in cooling energy consumption [3]. Contemporary applications of PDEC towers can be classified as four different types based on the evaporation method [3]:

- Cool towers (wetted pads).
- Shower towers (large droplets of spray)
- PDEC with wetted porous ceramic
- Misting towers (misting nozzles)

In this study, the PDEC with misting approach was used. The flexibility to control water pressure and droplet size in this technique makes it the most efficient among the various options [3]. A smaller droplet size increases the evaporation rate, which leads to a higher amount of cooling.

Due to the climatic dependency of the PDEC system, several factors can affect PDEC performance. These factors include climate, the tower geometry, the tower height, water droplet size, water flow rate and the evaporation technique. Several recent studies have investigated, analytically and experimentally, some of these factors [4,5]. However, most studies have treated the PDEC tower as a standalone structure. In

PLEA 2018 HONG KONG

Smart and Healthy within the 2-degree Limit

this study the tower was coupled to a large room and openings in the room were altered to see the influence of the attached building's architectural form on PDEC performance.

2.1 PDEC case study with misting nozzles

The Torrent Research Centre in Ahmadabad, India involved the first large application of misting nozzles spraying in to the top of a tower inlet. The Centre had incorporated the PDEC system in to four buildings. In each building the PDEC system was located above a central atrium separating offices from laboratories. When the outside temperature reached its maximum, the PDEC could reduce the interior temperature by between 10 to 15°C. The system has achieved a 64% energy savings in cooling demand when compared to a conventional air conditioning system [6].

2.2 Climate of Riyadh, Saudi Arabia

Riyadh, latitude 24.65°N, in the central region of Saudi Arabia, was the chosen site for this study. Its climate is characterized as hot and arid, with external dry bulb temperatures (DBT) in summer reaching 45°C (Fig. 1). The average DBT and wet bulb temperatures (WBT) are 36.5°C and 18.8°C, respectively. The daytime relative humidity is below 20% during the same period. The prevailing wind directions during the summer season are north and north-west (Fig. 2). The high potential for PDEC systems in Riyadh is because of the significant difference between dry-bulb and wet-bulb temperature (WBD).

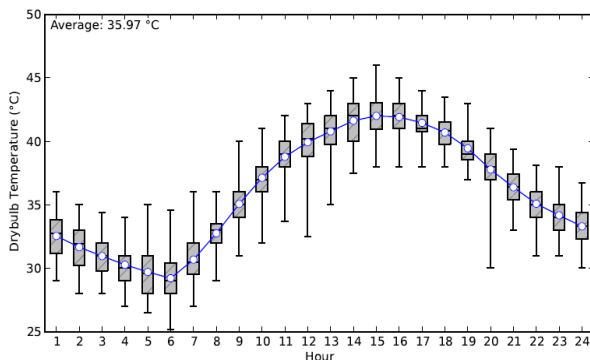


Figure 65: Range of mean hourly summer dry bulb temperatures, Riyadh. Source: epw.klimaat.ca

3. RESEARCH METHODOLOGY

This study aimed to evaluate the effect of the architectural design of a space linked to a PDEC tower. The purpose of the research was to maximize the performance of the PDEC tower in Saudi Arabia by improving the architectural design of the coupled building to act as one integrated design.

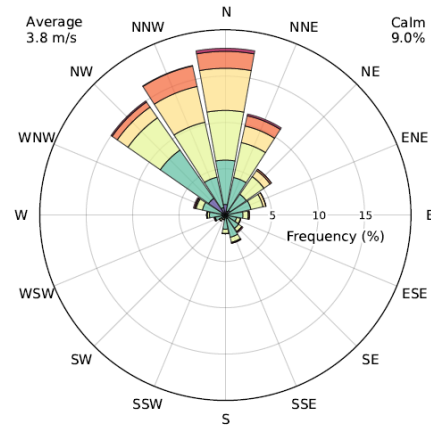


Figure 66: Frequency of wind direction and speed in summer, Riyadh. Source: epw.klimaat.ca

This study evaluated how wind direction and the addition of a buffer space to a room impacted on PDEC performance. A PDEC tower was located centrally and internally against the rear north wall of a single storey room connected to the tower (Fig. 3). The developed computer model applied the typical construction/material details of Saudi Arabia. The model construction specification is described in Table 1, and the tower specifications in Table 2. Most of the literature considers either 4:3 or 3:2 as a suitable aspect ratio for a rectangular tower. The dimensions of this study's tower cross-section were 1.6m x 2.5m, following the 3:2 aspect ratio. The width of the tower was parallel to the direction of the prevailing wind direction.

A previous study recommended a tower height of double to triple the width of the tower [5]. As a result, a tower height of 5m was initially set for this study. At the base of the tower three openings faced the room and had a total opening area of 3.43 m². A horizontal clerestory window was placed in the room's south façade with an opening area of 3.55m² (i.e. slightly larger than the tower's supply openings). This model was used as the base case design for the computer study (Fig. 3). Other opening configurations were also tested (shown in Fig. 13).

IES VE software was selected for the study as it can simulate PDEC systems that use misting nozzles and changeable cooling efficiency rates [7]. A current epw weather file for Riyadh was produced from Meteonorm, which is a commercial weather reference software tool [8]. Two different weather scenarios were tested in the simulations – (i) a very hot July day with northerly winds and (ii) a slightly cooler August days with some southerly winds.

PLEA 2018 HONG KONG

Smart and Healthy within the 2-degree Limit

Table 1: Construction specifications for the building

Table 2: PDEC tower parameters and specifications

Construction Specifications	
Building Height	3.5m
Floor dimensions	7.5m x 9m
Floor area	63.75 m ²
External walls	25mm external cement plaster + 100mm hollow concrete block + 50mm expanded polystyrene + 150mm hollow concrete block + 25mm internal cement plaster
Roof	gravel + 100mm expanded polystyrene + membrane+ 200mm concrete slab
Glazing	6mm outer pane + 12mm cavity + 6mm inner pane
South opening area	3.55 m ²

PDEC tower specifications	
Assumed cooling efficiency	80%
Tower Height	5m
Tower cross-section Dimensions	1.5m x 2.5m
Wind Catcher	Four sides louvres with 80% openable area (total area: 5.76 m ²)
Supply openings	Three openings facing the room (total area: 3.43 m ²)

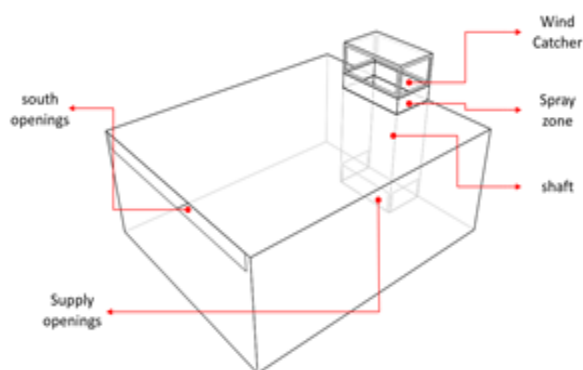


Figure 3: Base case building model and PDEC tower geometry

3.1 Model Validation

To check that the IES model had been configured correctly, the model was tested against experimental data derived from a European Union (EU) PDEC project [9]. The experimental building, shown in Fig. 4, was built in Catania, Italy, and consisted of a tower with two rooms attached to the north and south sides of the tower [9]. The PDEC tower dimensions were 4.1m x 4.4m x 10.7m. The wind catcher had two openings, each measuring 1.7m x 3.7m, and facing the east and west, which represented the prevailing wind direction. Data loggers were placed outside and within the building. The outdoor data recorded included solar radiation, air temperature, relative humidity, wind direction, and wind speed. Air temperatures and relative humidities were measured at different locations within the tower and the room.

A model of the Catania tower was created in IES VE. All the building details and opening profiles were considered when running the simulation. The simulation was run for 24 hours for the 30th July at a two minute time step.

The IES results for the north-coupled room were compared with average measured data. Figs. 5 and 6 show the good agreement between the measured and predicted data for the internal DBT and relative humidity, which gave confidence to develop an IES model for the Riyadh tower and room.



Figure 4: Experimental PDEC tower built in Catania [9].

4. RESULTS AND DISCUSSION

For the Riyadh tower the efficiency of the PDEC system was set in the IES model to be approximately 80% of the dry bulb to wet bulb temperature (wet bulb depression). Two days (scenarios) were considered. For scenario (i) on July 29th the maximum external air temperature peaked around 46°C mid-afternoon while the maximum external wet bulb temperature was around 21.5°C. The average external relative humidity was 14%.

Fig. 7 shows the wind speed and wind direction for July 29th generated from the weather file using IES software. The right vertical line represents the wind speed. The left vertical line refers to the wind direction, with the convention that a wind direction from the North is 0°, East 90°, South 180° and West 270°.

PLEA 2018 HONG KONG

Smart and Healthy within the 2-degree Limit

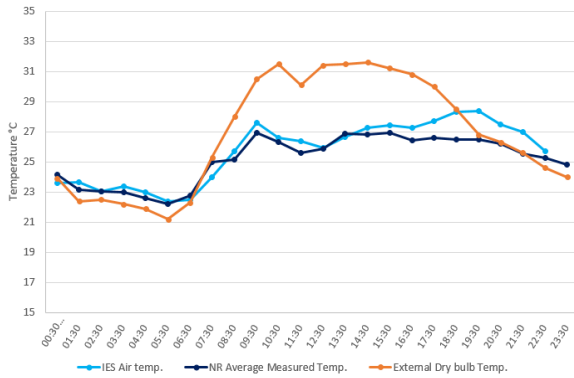


Figure 5: Comparison between measured and predicted internal air temperatures in room in Catania PDEC tower

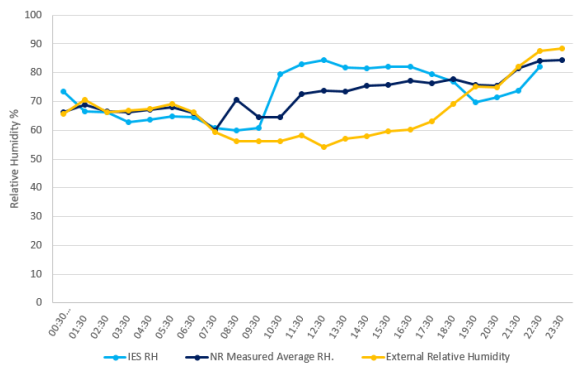


Figure 6: Comparison between measured and predicted internal relative humidities in room in Catania PDEC tower

The sharp fluctuation in the wind direction line does not necessarily mean a big change in the wind direction. For instance, in Fig. 7, the wind direction was approximately between 250° and 325° (WNW) for most of the day, and then suddenly swung around to 15° (NNE) at 14:00. This means the wind direction has only moved from WNW to NNE although the change looks more dramatic on the graph. Thus, for scenario (i), the winds were mostly from the north (i.e. directly on to the tower) with a maximum wind speed of 4.6m/s (Fig. 7). Fig. 8 shows the hourly external dry bulb and wet bulb air temperatures and the PDEC-generated internal air temperatures in the room. Fig. 8 shows how effective the PDEC system was, with a peak internal temperature around 27.2°C compared to an outdoor peak around 46°C. The internal relative humidity dramatically increased to around 60% during the day (Fig. 9). This is attributed to the stable weather conditions and lower humidity levels during the day (Figs. 7 and 9).

For scenario (ii) on August 2nd the day was slightly cooler, with a maximum external DBT and WBT of around 40°C and 18.7°C respectively, and a mean relative humidity around 15%. The wind direction was mostly from the north west but changed to the south and south east from 14.30 to 16.30 and 20.00 to 21.00 and so struck the building before reaching the tower

(Fig. 10). The wind speed was higher compared to scenario (i), increasing through the day and reaching 9.2m/s around 16.00 (Fig. 10).

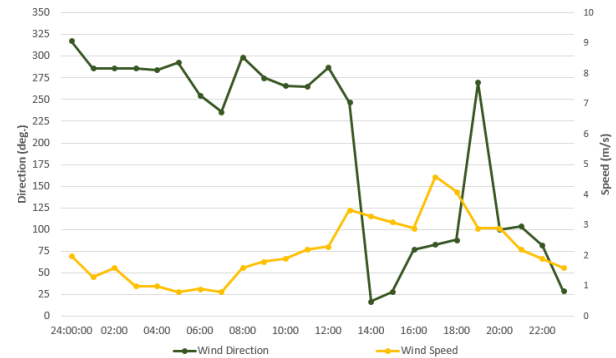


Figure 7: Wind speed and wind direction, July 29th.

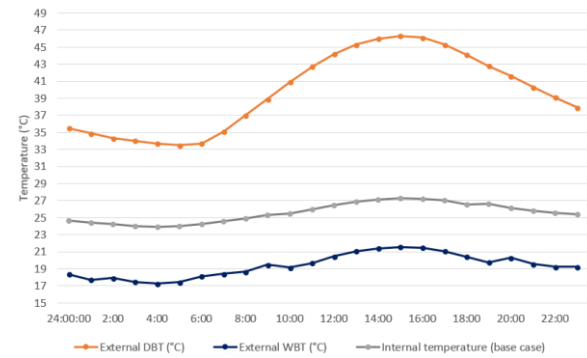


Figure 8: External and internal air temperatures, July 29th.

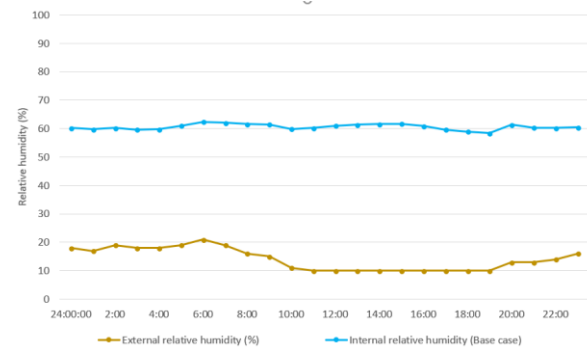


Figure 9: External and internal relative humidity, July 29th.

The results for scenario (ii) were not as expected when compared to those from scenario (i), with a reduction in the PDEC effectiveness being observed that was related to the unstable weather conditions. Figs. 10 and 11 show how the change in wind direction greatly reduced the effectiveness of the PDEC tower between 14.30 and 16.30 and between 20.00 and 21.00, when the wind direction became southerly. Internal temperatures peaked around 35.5°C and stayed higher than in the July scenario. The internal relative humidity had dramatically decreased when the winds were southerly (Fig. 12). This suggests that the clerestory window opening in the south façade was allowing a

PLEA 2018 HONG KONG

Smart and Healthy within the 2-degree Limit

positive pressure to be generated in the room that acted against the ingress of cool air from the tower.

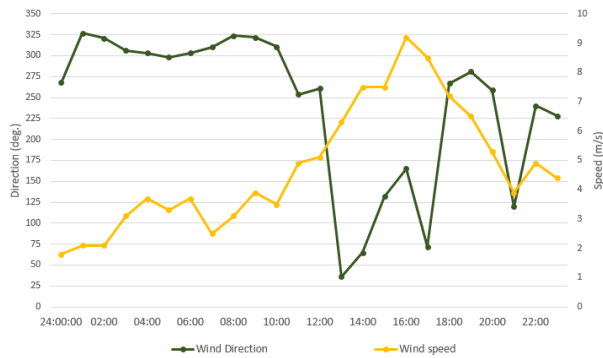


Figure 10: Wind speed and wind direction, Aug 2nd.

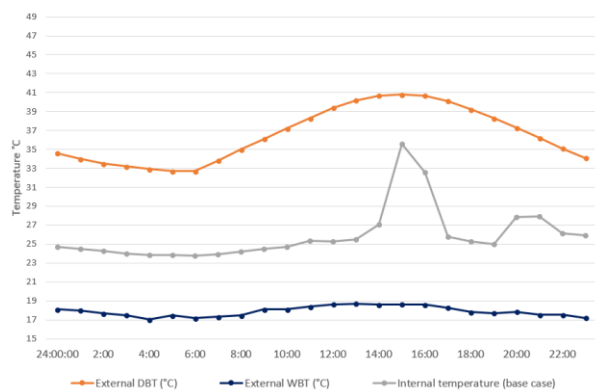


Figure 11: External and internal air temperatures, Aug 2nd.

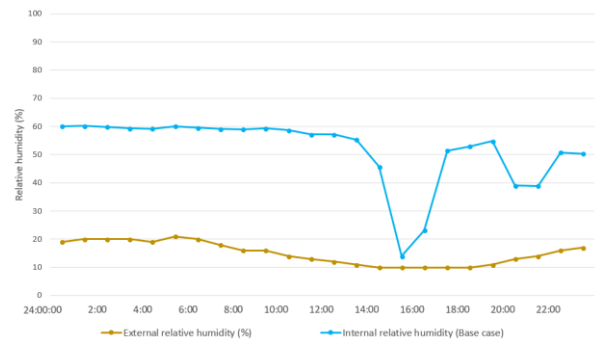


Figure 12: External and internal relative humidity, Aug 2nd.

Since wind direction played an important role in the performance of the PDEC tower, a double-skin type buffer zone corridor was then created on the south façade to test if the window could be protected and the tower performance improved for southerly winds. The buffer zone and the further improvements were developed based on recommendations from the literature [10]. The parameters that have been considered included buffer depth, buffer height, opening sizes, and opening placement. The investigation included many different configurations to improve the air movement of the PDEC within the space. Several cavity depths were tested, and it was found out that this parameter had no large influence on the overall performance of the PDEC tower. So, a

cavity depth of 0.4m was chosen for this study. Three configurations were chosen for this study in addition to the base case (Fig. 13). These three configurations represented the major changes that has been discovered during the research modelling process. The first configuration had two openings located at the floor and ceiling of the buffer zone. The second configuration had two openings at the top north and south side of the buffer zone in addition to the floor opening. The floor opening was removed for the third configuration.

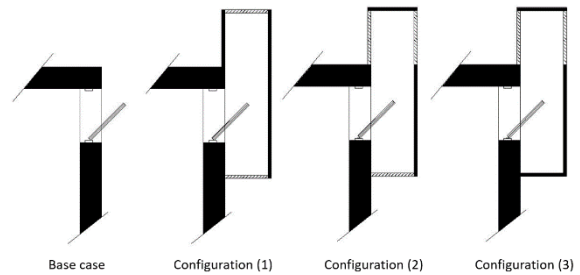


Figure 13: Base case and the three different configurations

Fig. 14 shows the internal air temperatures for the July 29th (northerly wind) conditions for the base case without the buffer zone and the three different zoned configurations. The addition of the buffer zone had little impact on the July tower performance, which might be expected for northerly low speed winds. However, Fig. 15 shows the positive impact of the buffer zones on the August tower performance during southerly wind conditions between 14.30 and 16.30 and between 20.00 and 21.00, but there was a negative impact after the wind changed direction. An interesting finding was that the internal temperature went up between 12.00 and 14.00, and between 16.30 and 18.30 when winds were blowing from north. The only logical explanation for this change was the higher wind speed as this scenario was working properly during steady wind conditions. The pressure increases on the buffer openings due to higher wind speeds has affected the performance negatively. So, the first configuration would provide better results only for southerly winds and lower wind speed conditions, otherwise, the base case performed better most of the time as the prevailing wind direction was northerly. For the second configuration, the top opening was replaced with two openings at the top north and south side of the buffer zone. This was developed to minimize the positive pressure of the wind speed, so the leeward side opening could negatively pressurize the buffer zone. Although the results showed that the situation had improved, the negative effect of the wind speed still had an impact on this configuration (Fig. 15).

The bottom opening was then eliminated for the third configuration. The purpose behind this was to create a stack effect within the buffer zone. The results showed

PLEA 2018 HONG KONG

Smart and Healthy within the 2-degree Limit

that significant improvement was achieved during this scenario (Fig. 15). This configuration gave the best results compared with the other scenarios for most of the time and during different weather conditions. The two upper openings had decreased the pressure within the buffer zone cavity while the elimination of the bottom opening helped to create a stack effect.

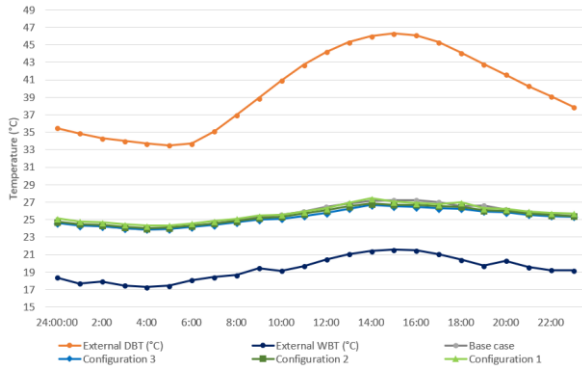


Figure 14: Comparison between results of the base case and the three buffer zone configurations, July 29th

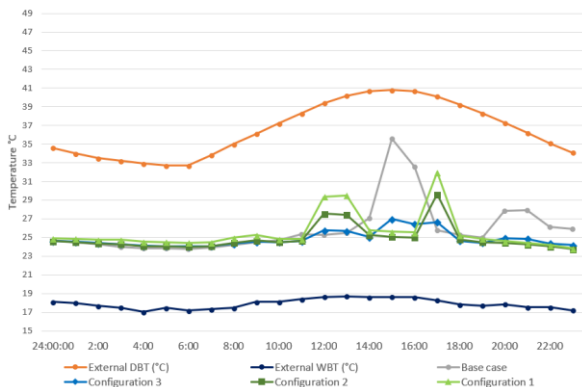


Figure 15: Comparison between results of the base case and the three buffer zone configurations, Aug 2nd

Although many summertime simulations have been made, the two scenarios presented here give a good representation of how the PDEC system performed for a range of summer wind speeds and wind directions. Due to a limitation on number of pages, it was not possible to represent more analyses here for the whole summer. However, it should be mentioned that the findings that were observed in the second scenario (Aug 2nd) occurred during many other days (e.g. Jun 4th, Jun 6th, Jul 2nd, Aug 8th etc.), and under similar weather conditions. Overall, the PDEC tower performed well as Riyadh has a climate that is generally dry and hot throughout the summer. Full season analysis and representation in the future is highly recommended to better understand the overall performance of the PDEC system and will be presented in future work.

4. CONCLUSION

This paper has investigated the impact of architectural form on the performance of a PDEC tower. The tower was virtually created and linked to a room. The software IES VE was used to conduct the simulation of the PDEC system, and the tower's predicted performance was impressive in Saudi Arabian climatic conditions. However, the performance was affected by changes in wind direction and wind speed. A buffer zone was added to the south side of the coupled space to minimize the negative effect of the winds. By assessing many configurations of the suggested solution, the performance was improved significantly. Further analysis, involving modelling and monitoring, will be conducted to better understand the relationships between the tower and room factors. Other architectural elements, such as roof openings might improve the performance of the PDEC system and provide more architectural design options. Detailed analysis including CFD would also provide a deeper understanding of the findings.

REFERENCES

1. Electricity & Cogeneration Regulatory Authority (ECRA Statistical Booklets 2016, [Online], Available at: <http://www.ecra.gov.sa/> [10 Nov 2017].
2. Lechner, N., (2014) *Heating, Cooling, Lighting: Sustainable Design Methods for Architects*. 4th ed., John Wiley & Sons.
3. Ford, B. and R. Schiano-Phan, (2010). *The Architecture and Engineering of Downdraught Cooling*. PHDC Press, Bologna, Italy.
4. Belarbi, R., Ghiaus, C. and F. Allard, (2006). Modeling of water spray evaporation: application to passive cooling of buildings. *Solar Energy*, 80: p. 1540–1552.
5. Kang, D. and R. K. Strand, (2016). Significance of parameters affecting the performance of a passive downdraught evaporative cooling (PDEC) tower with a spray system. *Applied Energy*, 178: p. 269-280.
6. Ford, B., Patel, N., Zaveri, P. and Hewitt, M., (1998). Cooling without air conditioning: The Torrent Research Centre, Ahmedabad, India. *Renewable Energy*, 15: p. 177-182.7.
7. Buckley, L., (2014) Simulating a Passive Downdraft Evaporative Cool Tower. In *Proceedings eSim 2014*. Ottawa, Canada, May 8-9
8. Meteonorm: [Online]. Available at: <http://www.meteonorm.com/> [29 Nov 2017].
9. Galatà, A and S. Sciuto, (1997). Passive Evaporative Cooling : the PDEC project. In *International Thermal Energy and Environment Congress*. Marrakesh, Morocco, June.
10. Gratia, E. and A. de Herde, (2007). Guidelines for improving natural daytime ventilation in an office building with a double-skin façade. *Solar Energy*, 81: p. 435-448.

Improving Louvers With Indirect Evaporative Cooling As Heat Exchanger: Hot sub-humid climate

CARLOS JAVIER ESPARZA LÓPEZ¹, SERGIO RAFAEL AGUILAR LUCAR¹, CARLOS ESCOBAR DEL POZO², MARCOS EDUARDO GONZALEZ TREVIZO³

¹Faculty of Architecture and Design, University of Colima, Colima, Mexico

²Faculty of Electrical and Mechanical Engineering, University of Colima, Colima, Mexico

³Faculty of Engineering, Architecture and Design, Autonomous University of Baja California, Ensenada, Mexico

ABSTRACT: Evaporative cooling has been proved as one of the most efficiency strategies to cool down air temperature. In this paper, the performance of a device that combines the sun protection with fresh ventilation using evaporative cooling is presented. This strategy has been used as heat exchanger in vertical set up, but this configuration precludes the solar protection. The experimental trial was taken in Colima, Mexico, where the climate is classified as hot sub-humid Aw0, according to Köppen. In the experimental stage, two equal devices were compared. One of the remained as control and the other one using water to apply the indirect evaporative cooling as a case. The maximum difference of temperature between the entrance air and the exit was of 8 K° in the experimental cell versus 5.5 K° of the reference cell. Indirect evaporative cooling strategy improves the reduction of heat exchange around the device. This allows to used louvers to block solar radiation and to pre-cold the air before introducing it to the space.

KEYWORDS: Indirect evaporative cooling, Solar shading devices, Convective cooling

1. INTRODUCTION

In hot humid climates inside the tropics, the best passive strategies to apply are the sun protection and ventilation [1, 2, 3]. There are many shading configurations for the devices to protect or allow some amount of solar radiation for the inner space. One of the best solar protection devices are the louvers. Almost any material can be used to build louvers, but the most commons are woods, plastics, and metals.

Usually, shading and ventilation are opposite when the louvers are used. When the louver is working correctly, the surface temperature of each louver receives solar radiation avoiding it to get inside the space but raising up the surface temperature and the air temperature above each louver. If the window is open to let the air pass through, the pre-heated air is the one that passes over it. So, the inhabitant decides if keeps the windows closed avoiding hot air but having shaded his inner space or open it raising up the temperature.

The evaporative cooling (EC) consists in the transfer of heat between air and water. When this occurs, both air and water present a decrease of the temperature due to the transfer of latent heat to sensible heat thanks to the evaporation of water. This is how dry air sets the temperature as its humidity increases, until it reaches the point where it will not be possible to evaporate more water (saturation).

Indirect evaporative cooling presents the same principle, but in this there are at least two separate air flows, the first is cooled by IEC, while the second is

cooled by heat conduction between these air flows, without being combined [4]

In this paper, the performance of a device that combines the solar protection with fresh ventilation using evaporative cooling is presented. Evaporative cooling has been proved as one of the most efficiency strategies to cool down air temperature [5, 6, 7, 8]. This strategy has been used as heat exchanger in vertical set up [9], but this configuration precludes the solar protection.

The experimental trial was taken in Colima, Mexico. According to Köppen [10] the climate is classified as Aw0 hot sub-humid.

In the experimental stage, two equal devices were compared. One of the remained as control and the other one using water to apply the indirect evaporative cooling as a case. The maximum difference of temperature between the entrance air and the exit was of 8 K in the case versus de 5.5 K of the reference.

PLEA 2018 HONG KONG

Smart and Healthy within the 2-degree Limit

2. METHOD

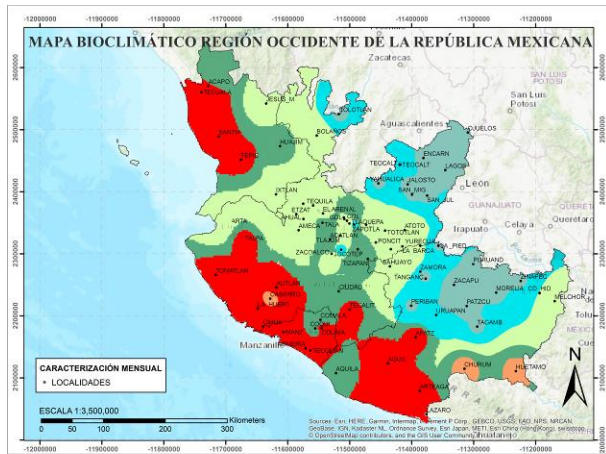


Figure 1. Map of southwest México.

The experimental trial was carried out in the city of Villa de Álvarez, Colima, Mexico (Figure 1) which is located between latitude 19 ° 16 '53 "North and longitude 103 ° 44' 18" West. The climate according to Köppen is warm sub-humid (Aw0) (Figure 2). The annual mean temperature is 28.0 °C and RH is 49%. The maximum temperature occurs in April with 40.8 °C and the minimum in February and March with 12.5 °C. For humidity, the maximum occurs in September with 82.7% and the minimum in March with 19%. Three seasons can be identified; warm sub-humid (in colour gray) in the months of January, February and March with a mean temperature of 23.3 °C and mean RH of 43%. Hot sub-humid (in colour orange) from April to June and December with a mean temperature of 25.2 °C and mean RH of 45%. Finally, the hot humid season (in colour blue), from July to November, has a mean temperature of 25.3 °C and mean RH of 55%.

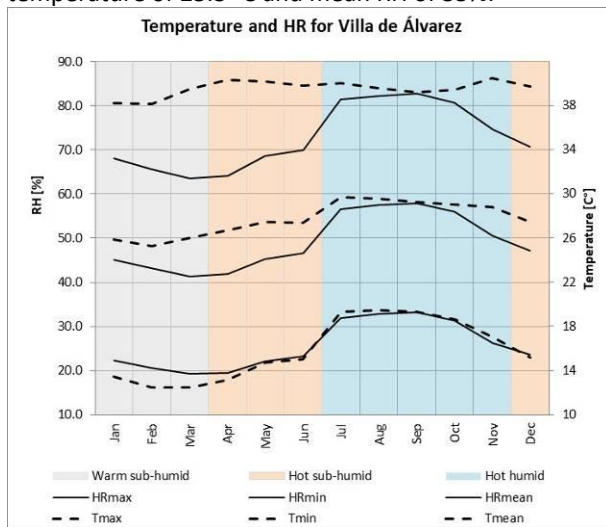


Figure 1. DBT and RH of Villa de Álvarez, México.

The main purpose of the device (Fig. 4) is to apply the indirect evaporative cooling of the water inside of it to reduce the temperature of the water, the device and

the air above and below it. It allows to be used as shading and ventilation device.

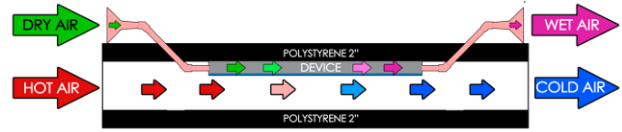


Figure 3. Operation of the cooling system.

A comparative analysis was performance with two cells (Fig. 2). To compare the efficiency of the evaporative cooling, two devices were built but only one was tried with 80 ml of water (experimental cell), and another one without water (reference cell). To distribute and to improve evaporation rate inside the device, a porous media was placed inside of it [4, 11].

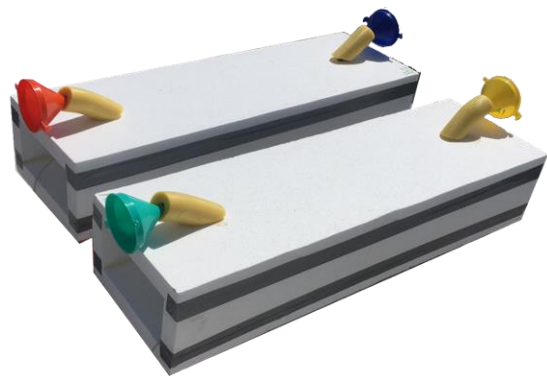


Figure 4. Experimental and reference cells.

The experimental cells worked as wind tunnels where the air could circulate inside them. The inside dimensions are 0.24 m high, 1.22 m large and 0.38 m wide. The material was polystyrene of 0.05 m width used as insulation to avoid heat from solar radiation. long, 0.28 wide and 0.04 m high.

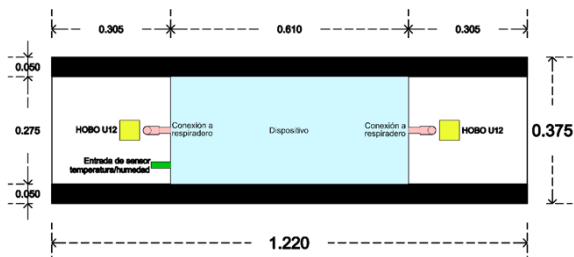


Figure 5. Top view of experimental cell.

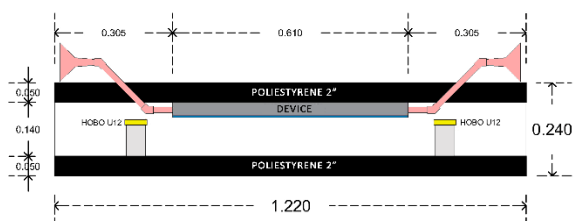


Figure 6. Side view of experimental cell.

PLEA 2018 HONG KONG

Smart and Healthy within the 2-degree Limit

Each cell is composed of four pieces of polystyrene, which were joined with industrial tape of 5.08 cm of thickness. This provided the necessary structural solidity and in turn managed to seal the joints between the pieces, thus avoiding air filtrations.

Each experimental cell has a device inside of it (Fig. 6 and 7), which aims to be a cooling system by indirectly evaporating a liquid. The dimensions of the devices were 0.61 m the dimensions of the devices were 0.61 m long, 0.28 m wide and 0.04 m high.

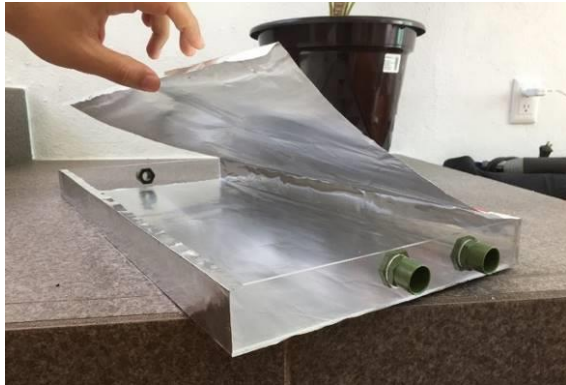


Figure 6. Cooling device before being sealed.

A high conductivity material was used for the surface of the device to improve the exchange of energy between the inside and the outside of the device. The material used was aluminum, where they were placed sheets in all contact areas (Figure 6).

The lateral sides were made of transparent plastic of 3mm of thickness, to maintain the visibility of the device, allowing to log the humidity and observe the progress in water evaporation.

To remove the saturated air, the addition of water and the monitoring of the device, two openings were placed opposites to introduce low RH air and take out high RH air from inside the device. The perforations (0.0125 cm of diameter), were made on both acrylic plates of each device. In each opening, funnels were placed to improve the quantity of introduced air. The material used was PVC of 0.0125 m wide. A material of low conductivity to avoid energy exchanges through it.



Figure 7. Cotton blanket inside the device

In order to spread the water added into the device over the entire contact surface, a cotton blanket was used inside the device (Figure 7), which allowed

absorbing and preventing water from accumulating at a single point [4, 11]

Finally, the rest of the device was sealed to avoid relative humidity (RH) air infiltration into the wind tunnel.



Figure 8. Funnel to maximize ventilation

A 0.15m diameter funnel was attached to the end of each tube (Figure 8). The function of these was to maximize the amount of air that entered the device, avoiding saturation and allowing an optimal indirect evaporative cooling.

The external pipe that connects the device with the funnels was covered with expanded polyurethane foam, to avoid solar energy gains, in this way the entire experimental cell was completely insulated from external factors, allowing to obtain more accurate data in the measurements.

2.1 Equipment

In order to analyze the dry bulb temperature and the external relative humidity, two HOBO U12-012 - data loggers were used inside each experimental cell. They were placed in the opposite sides of each cell (located at 0.20 m) to log the air temperature at the entrance and the exit of the device, on bases of 0.08 m of height of expanded polyurethane (Figure 9 and 10).

The specifications of the HOBO U12-012 – Data logger are measurement range: Temperature: -20° to 70°C (-4° to 158°F), RH: 5% to 95% RH. Accuracy: temperature: ± 0.35°C from 0° to 50°C (± 0.63°F from 32° to 122°F), RH: ± 2.5% from 10% to 90% RH typical, to a maximum of ±3.5%.

The dry bulb temperature and the relative humidity inside the device were analyzed, in order to identify the level of saturation, and thus to know if the ventilation inside the device is adequate or insufficient. To carry out this measurement, a Micro-station Data Logger H21-002 was used, in conjunction with 12-bit external temperature / humidity sensors, which were located inside each device, in the previously designed duct.

PLEA 2018 HONG KONG

Smart and Healthy within the 2-degree Limit

The specifications of the HOBO Micro Station Data Logger H21-002 are operating range: -20° to 50°C (-4° to 122°F) with alkaline batteries, -40° to 70°C (-40° to 158°F) with lithium batteries. 12-bit external temperature / humidity sensor measurement range: temperature: -40° to 50°C (-40° to 122°F) in water; -40° to 100°C (-40° to 212°F) in air. RH: 0-100% RH at -40 ° to 75 ° C (-40 ° to 167 ° F); exposure to conditions below -20 ° C (-4 ° F) or above 95% RH may temporarily increase the maximum error of the HR sensor by an additional 1%. Accuracy: temp de precision: w/U12: ±0.25°C from 0° to 50°C (±0.45°F from 32° to 122°F) RH: +/- 2.5% from 10% to 90% RH (typical), up to +/- 3.5% including hysteresis at 25 ° C (77 ° F); below 10% and above 90% ± 5% typical.

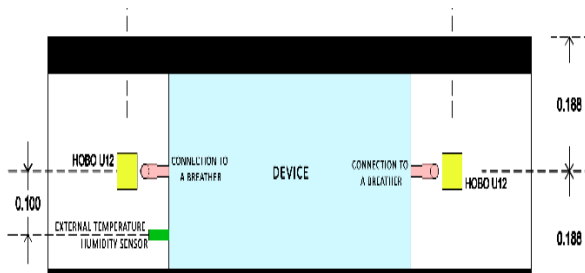


Figure 9. Top view of data loggers in experimental module

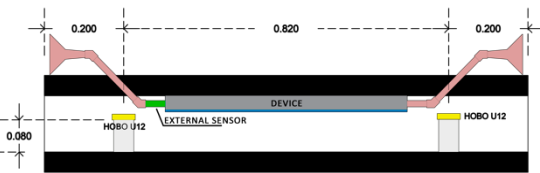


Figure 10. Side view of data loggers in experimental module

2.2 Experimental cases

The experimental cells were arranged parallel to 20cm each other, pretending that the same amount of air was admitted to both devices. These were oriented to the southwest, to make the most of the dominant diurnal winds.

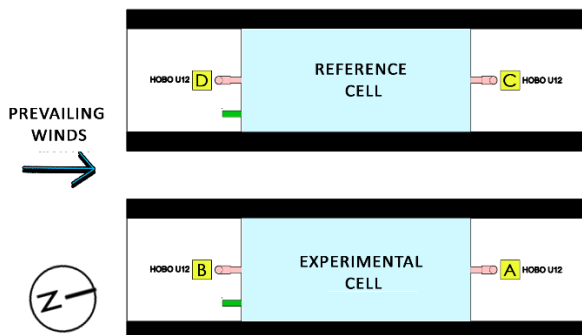


Figure 11. Selection of cases for experimentation

Experimental cell (Device with water)
Polystyrene cell, with the evaporative cooling device, with 80ml of water inside.

Data logger "B" was located in the air inlet, and data logger "A" in air outlet

Reference cell (Device without water)

Polystyrene cell, with evaporative cooling device, without water inside.

The data logger "D" was located in the air inlet, and the data logger "C" in the air outlet

2.3 Calibration

Before carrying out the measurement, a calibration of the data loggers was carried out for a week, in order to compensate for the differences in measurement between the same equipment.

For this, the data logger "A" was chosen as a reference, and by means of a correlation of the obtained values a linear correlation equation was obtained between each device, with which the measurement difference could be compensated.

Table 1. Inter-Device correlation table

	Reference/ Device B	Reference/ Device C	Reference/ Device D
r	R ² = 0.9993	R ² = 0.9991	R ² = 0.9951
Equation	y = 1.0078x - 0.2616	y = 1.0016x - 0.0653	y = 0.9634x + 1.0589



Figure 12. Calibration of data loggers.

2.4 Periodicity

The experiment was performance for 48 hours (13th and 14th) of November 2017. The water (80 ml) was placed inside the device (experimental cell) at 11:00 o'clock civil hour. Two hours before local zenith. Dry bulb temperature was logged each five minutes.

3. RESULTS

After the experimentation stage, the data obtained was analyzed and graphed, some of which are shown in the following graph (Figure 13). It can be appreciated the temperature difference between the air intake and data logger, and the air output data logger.

PLEA 2018 HONG KONG

Smart and Healthy within the 2-degree Limit

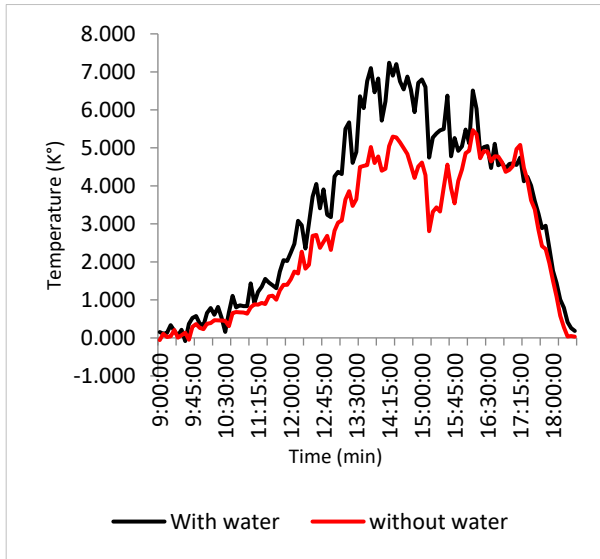


Figure 13. Graph of difference K between the experimental cell and reference cell (November 13th).

In the hours of higher temperature (Fig. 17) a better cooling performance of case 1 can appreciate, with a difference of up to 2.5 K° at some moments, and up to an average of 0.8 K° during the hours when solar radiation affects with greater intensity.

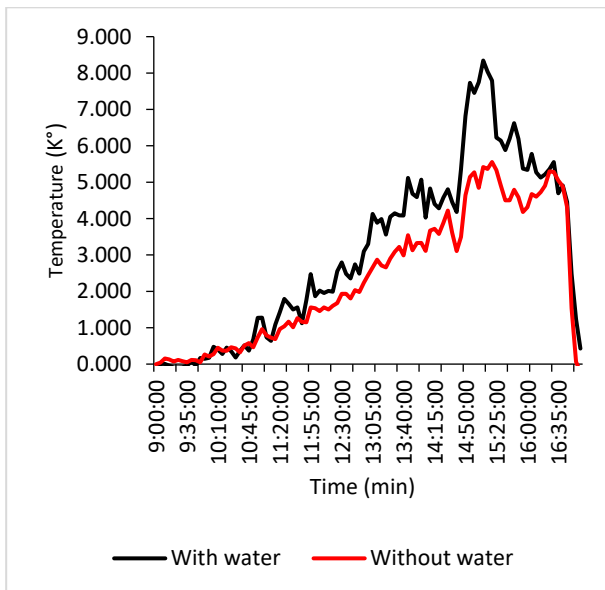


Figure 14. Graph of difference K between experimental cell and reference cell (November 14th).

Afterward, we continued to analyze the data obtained inside the evaporative cooling device, through the Micro-station data logger, in conjunction with external sensors for relative humidity. It can be appreciated in the graph of November 13th (Fig. 18), where it is observed that in the hours when solar radiation does not affect, the relative humidity levels are similar in both cases, but just when the sun begins to warm the outside air, the relative humidity of reference cell drops considerably, while the experimental cell

remains constant, reaching to such an extent that it reaches a point close to saturation.

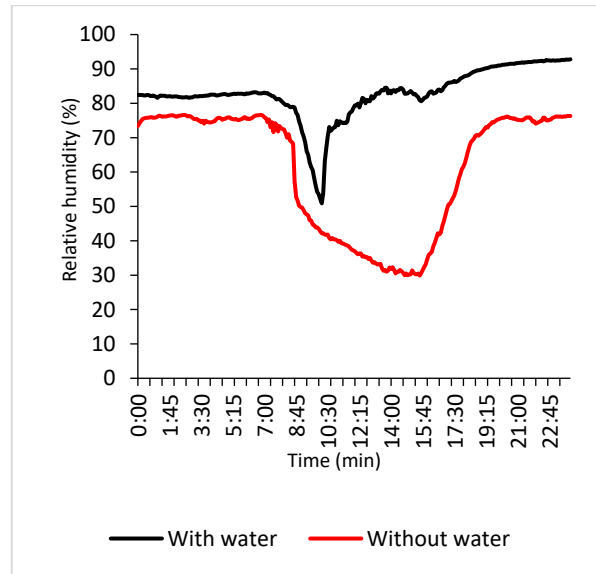


Figure 15. Graph of relative humidity within the cells (November 13th).

The measurement made on November 14 (Fig. 19) shows results similar to those represented on November 13, where it is appreciated that the relative humidity of both cases is similar until the heat begins to affect the outside air. This shows that the ventilation inside the device was insufficient when extracting the saturated air inside.

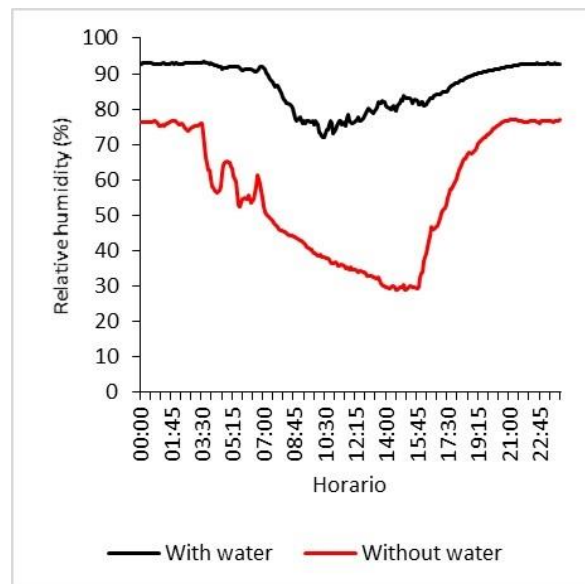


Figure 16. Graph of relative humidity within the cells (November 14th).

4. CONCLUSION

A single louvers trial was presented as experimental device. Indirect evaporative cooling improves the reduction of heat exchange below the device. The

PLEA 2018 HONG KONG

Smart and Healthy within the 2-degree Limit

average reduction of the air against the cell without evaporative cooling goes around 2.2 K. An important reduction if it is considered that just natural ventilation is used combined with solar shading devices.

These results are presented in the humid season. Better results are expected for the dry season where the evaporation rate is higher than present.

The final configuration of the device assumes the repetition serial of the experimented device one over other to complete a shading device for a vertical opening. This allows to used louvers to block solar radiation and to pre-cold the air before introducing it to the space.

The thermal performance of the indirect evaporative cooling device could increase if it manages to maximize the inflow of air, which would allow to decrease the relative humidity inside it. It is important to bring back that these high humidity air will not be in touch with the cooled air that is introduced into the space.

Is considered convenient for future investigations to carry out the experiment under controlled conditions, where the main intervening variables can be modified, such as solar radiation and ventilation, in order to obtain data with greater precision.

As limits or inconveniences could be mention the requirements to introduce water into each louver and to evacuate the humidified air from the louvers into the exterior ambient avoiding to mixed with the inlet flow into the space.

ACKNOWLEDGEMENTS

The first author thanks the University of Colima for the financial supports to attend the congress.

REFERENCES

1. Givoni, B. (2011). Indoor temperature reduction by passive cooling systems. *Solar Energy*, 85(8), 1692–1726.
2. Givoni, B. (1994). Building design principles for hot humid regions. *Renewable Energy*, 5(5–8), 908–916.
3. Koenigsberger, O. H., Ingersoll, T. G., Mayhew, A., & Szokolay, S. V. (1977). *Viviendas y edificios en zonas cálidas y tropicales* (1er ed.). Madrid: Paraninfo.
4. Esparza L. Carlos J., Escobar del Pozo, Carlos, Gómez A. Adolfo, Gómez A. Gabriel, Gonzalez C. Eduardo (2018) Potential of a wet fabric device as a roof evaporative cooling solution: Mathematical and experimental analysis. *Journal of Building Engineering*. <https://doi.org/10.1016/j.jobee.2018.05.021>.
5. El-Refaie, M.F. & Kaseb, S., 2009. Speculation in the feasibility of evaporative cooling. *Building and Environment*, 44(4), pp.826–838.
6. Fernandez-Gonzalez, A. & Hossain, A., 2010. Cooling performance and energy savings produced by a roofpond in the United States Southwest. In *American Solar Energy Society*. p. 8.
7. Spanaki, A. (2007). Comparative studies on different type of roof ponds for cooling purposes: literature review. In *2dn PALENC Conference and 28th AIVC Conference on Building*

Low Energy Cooling and Advanced Ventilation Technologies in the 21 st Century (Vol. 2, pp. 1009–1015). Crete Island, Greece.

8. Porumb, B., Ungureşan, P., Tutunaru, L. F., Şerban, A., & BĂlan, M. (2016). A Review of Indirect Evaporative Cooling Operating Conditions and Performances. *Energy Procedia*, 85(November 2015), 452–460.

<https://doi.org/10.1016/j.egypro.2015.12.226>

9. Finocchiaro, P., Beccali, M., & Nocke, B. (2012). Advanced solar assisted desiccant and evaporative cooling system equipped with wet heat exchangers. *Solar Energy*, 86(1), 608–618. 5.

10. Köppen, W., & Geiger, R. (1936). *Handbuch der Klimatologie. Das geographische System der Klimate*. Berlin.

11. Esparza-López, C. J., Gómez-Amador, A., Escobar del Pozo, C., Elizondo Mata, M. F., & Gómez-Azpeitia, G. (2016). Experimental analysis of a humid fiber as an indirect evaporative cooling device against roofpond and gunny bags in a hot sub-humid climate. In P. LaRoche & M. Schiler (Eds.), *PLEA 2016: 32nd International Conference on Passive and Low Energy Architecture* (pp. 1368–1374). Los Angeles: Cal Poly Pomona.

The Partial replacement of Ordinary Portland Cement with Rice Husk Ash to Stabilize Compressed Earth Blocks for Affordable Building Materials

ADEDAMOLA MOBOLANLE OJERINDE¹, ADEKUNLE M AJAO², BABATUNDE F OGUNBAYO², VICKI STEVENSON¹, ESHRAR LATIF¹

¹Cardiff university, United Kingdom

²Covenant university, Nigeria

ABSTRACT: The study investigated potentials of rice husk ash as a replacement for Ordinary Portland Cement in the production of Compressed Earth Block (CEB) with a view to reducing building construction cost and the embodied energy of the blocks in the context of Nigeria. Graded levels (i.e. 10, 20, 30 and 40%) of RHA replaced cement in the mix for CEB moulding. The results of X-ray diffraction showed that RHA contained 80% SiO₂. Also, the results of the compressive strength, water absorption capacity, and bulk density testing indicated that low compressive strength, high water absorption capacity, and low bulk density exhibited by RHA-CEB make doubtful the suitability of RHA as a partial replacement for Ordinary Portland cement in the building construction in the wet regions. However, RHA could find useful application as a stabilizing agent in CEB rather than as a partial replacement of cement.

KEYWORDS: Ordinary Portland cement, Rice Husk Ash, Compressed Earth Block, Low-Cost Housing.

1. INTRODUCTION

The rate of urbanization in Nigeria has increased significantly in the last decade. These episode has led to rise in population in the cities which has caused shortage of dwelling units. These shortage has led to overcrowding, high rent, poor living condition and poor infrastructure [1]. The need to provide low cost houses in Nigeria cannot be over emphasized. Indeed, Nigeria is estimated to have 17-million-unit housing shortfall, and unfortunately about 62% of Nigerians live below the international poverty line [1], which makes it difficult for them to afford modern day building. Over 90% of low-income earners cannot afford decent accommodation even if they saved 100% of their income for 10 years [2]. Government's efforts at solving the problem of housing shortage proved futile because it ended in providing costly and unaffordable houses.

It is noticed that construction materials accounts for 60-70% of the total cost of building construction [3], hence the use of cheaper, available and suitable alternative materials could contribute to housing sustainability in future. In this regard, use of earth material in building construction may find useful application. While the use of earth material is not new in Nigeria, it is necessary to improve the strength and durability of such construction materials if intended for the construction of multi dwelling unit.

Compressed earth block (CEB) is earth material that needs stabilization to improve on its mechanical properties [4, 5]. The use of several agricultural waste products has been used as stabilizer in other building

materials other than CEB, example of such agricultural waste includes rice husk ash [5, 6], waste sugarcane bagasse [6, 7], palm oil fuel ash [8], sawdust or wood ash [6], etc. RHA is preferred because the government has invested heavily in rice production to shift the economy from being crude oil-dependent to agriculture. By this the agricultural sector would increase and waste will be generated. Such agricultural wastes should therefore be reused to avoid the pollution which will be at the result of disposal.

Cost of cement has been of concern in the provision of sustainable housing. The production of cement leads to 7-8% global CO₂ emission[9]. The material functions as a binding agent in compressed earth block moulding. Sourcing acceptable alternative low-cost binding agent will significantly reduce cost of providing housing. Rice husk ash, like other sustainable pozzolans will serve useful application here [5, 6]. Kazmi [10] suggested that addition of RHA in brick manufacturing could lead towards sustainable and economical construction.

Apart from reducing cost, RHA's utilization in construction will displace the use of cement in the construction industry thereby reducing pollution as result of production and utilization of OPC. In 2010, construction industry utilized 32% global energy consumption. 19% of the total consumption was as a result of total energy was as a result of greenhouse gases [11]. Rice husk ash can be used to produce alternative binder(pozzolan), a geopolymer or an alkali-activated binders, these binders can be used to

PLEA 2018 HONG KONG

Smart and Healthy within the 2-degree Limit

produce 73% lower greenhouse gas emission, 43% less energy consumption, 25% less water when used in the production of conventional concrete [9]. Also, RHA requires lower embodied energy compared to cement hence its use will save energy cost [12]. Rice husk ash being a product of agricultural production will raise the farmers' income. It will be worthwhile to see the possibility of replacing cement with rice husk ash in compressed earth block.

The present study is aimed at investigating the potentials of RHA as a partial replacement for Ordinary Portland Cement in the production of CEB for the construction of residential houses.

2. MATERIALS

The materials to use for CEBs are; laterite soil, Ordinary Portland Cement (OPC) and RHA.

2.1 Lateritic soil

It has been described as highly weathered tropic or sub-tropical residual soil varying in size from clay size to gravel [13]. Features characterizing of strong weathering of silicates, the release of Iron oxides and prevalence of kaolin. They are formed from different geologies of silicate rocks and limestone [14]. Laterite remains one of the best natural material to be used in CEB because its well graded soil that combines both cohesive (silt and clay) and non-cohesive soil (sand and gravel) part of soil which have natural binding property as well as present of most chemical binders. The colour varies from light brown to rusted red, when drainage is poor in laterite soil, black cotton soil is formed. [13].

2.2 Ordinary Portland cement

Cement is manufactured from calcium carbonate in the form of crushed limestone or chalk and argillaceous material such as clay, marl or shale. The process involves decarbonisation of calcium carbonate (chalk or limestone) by expulsion of carbon dioxide and sintering [15]. During the production of OPC, the kiln is fired at temperature as high as 1480oC [16].

The production of cement emits pollutants including carbon dioxide, sulphur dioxide and at extremely high temperature the material can emit heavy metals. Dust is another pollutant in the environment that can cause skin allergies[17].

2.3 Rice Husk Ash

The Chemical composition of RHA is largely dependent on the type of paddy, soil type and condition, geographical conditions, combustion temperature, and cooling method. RHA pozzolan is prepared by burning RH at a controlled temperature ranging from 600-800°C and cooled uniformly to maintain amorphous silica content of 77-95% [8, 18-20]. The X-

ray Diffraction (XRD) device can be used to identify the different phases within RHA:

- Cristobalite (Crystalline phase)
- Glass phase – SiO₂ (amorphous phase)

The required phase for RHA in pozzolans is the amorphous state.

3. PRODUCTION OF RICE HUSK ASH

Method 1

The rice husk ash used for the test was gotten from Abeokuta, Ogun state in Nigeria. The rice husk was first charred to remove the moisture and organisms from the waste using a local burning method in a local mud pot. The colour of the husk changed from cream to black and the husk reduced to about half its size in mass. The charred husk was then combusted in a furnace for about 2-3 hrs at temperature ranging from 550-780°C. The furnace was left to cool for about 24 hrs before the RHA was brought out of the furnace. The colour of the resulting rice husk ash was whitish grey colour.

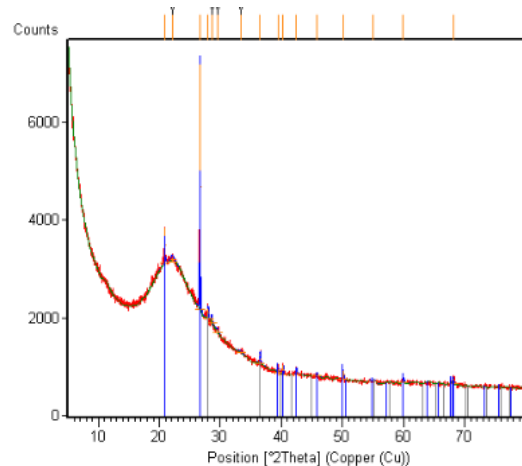


Figure 1. 80% SiO₂ (xrd analysis software)

Method 2

The rice husk was combusted directly in the furnace for 2½ hrs- 3hrs. The colour of the rice husk changed from cream to whitish grey. The furnace was fed with the same quantity of husk used in 'method 1', the burning of the hush took a long time and cost more because the mass of the husk has not been reduced from the charring step which removes moisture and organisms. The second method was introduced to reduce the time of production process.

A representative sample was analysed using XRD to establish that the RHA had a suitable proportion of amorphous material, which was confirmed (see Figure 2).

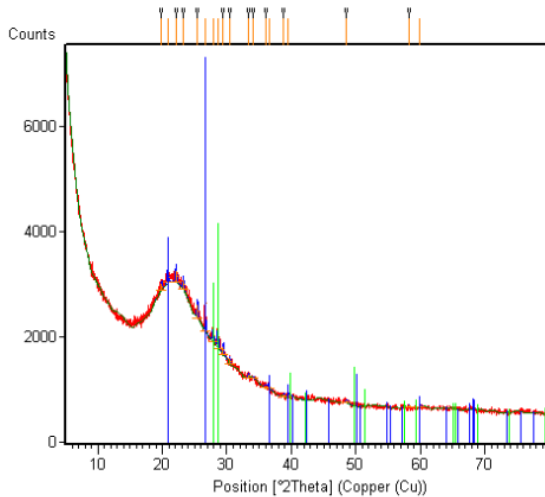


Fig 2 Method 2- 96% SiO₂ xrd analysis software

Pozzolan has been defined as siliceous or siliceous and aluminous material, which when in a finely divided form and in the presence of moisture chemically react with calcium hydroxide at ordinary temperatures to form compounds possessing cementitious properties [10]. The RHA used in this study contained amorphous SiO₂ of 80% (Figure 1) and 96% (Figure 2) that suggest it could have pozzolanic properties in the presence of moisture and cement. Also, that it could be used as stabilizing agent in CEB or as partial replacement for Ordinary Portland cement.

4. EXPERIMENTAL PROCEDURE

The mix ratio 1:10 of OPC and laterite was used for the moulding of the control CEB. Then, the cement portion was replaced with graded levels of RHA at 10, 20, 30 and 40% to give five experimental treatments. The resulting mixes were fed into the CEB Pressing machine to produced CEB with and without RHA inclusion. All the CEB were then allowed to cure for 14, 21 and 28 days. The blocks were placed on a platform outside in the open, covered with nylon, and then wet with water daily to achieve curing for the respective periods. The wetting prevented the blocks from drying fast and cracking during curing.

4.1 Laboratory Tests

Duplicate samples of blocks were removed randomly from the control and RHA-CEB treatment groups for laboratory tests. Compressive strength and water absorption capacity are tested as described in BS EN 771-1. Bulk density is described as the mass per unit volume each block.

4.2 Results

Results of compressive strength of experimental CEB cured for 14, 21, and 28 days are shown in Figure 3. The results show that compressive strength of the blocks varied with varying levels of RHA inclusion in the

mix. The highest values were recorded in the control group (0% RHA) thus suggesting that inclusion of RHA in the mix resulted in the lowering of compressive strength.

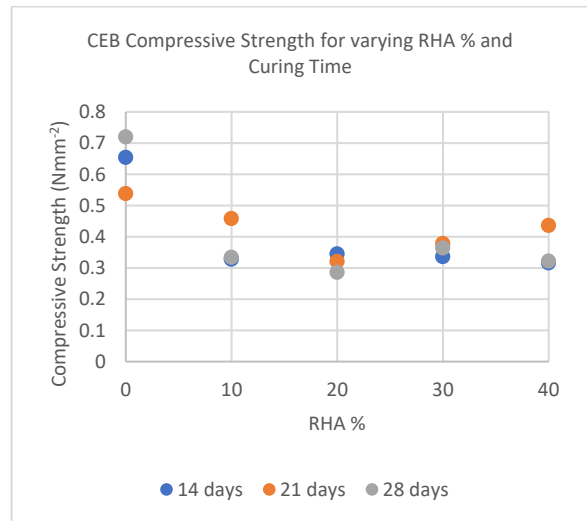


Figure 3. Compressive Strength of CEBs with varying RHA levels cured for 14, 21 and 28 days: (3 samples per data point given)

The trend in the compressive strength of the CEB as affected by the RHA inclusion is depicted in Figure 3. Indeed, the results seemed to suggest that inclusion of RHA in the mix caused the reduction of strength by almost half.

The mean water absorption capacity of the test block samples is presented in Figure 4. The results show that RHA inclusion typically raised the water absorption compared to the control; however, the variation is not consistent. Among the samples with RHA inclusion, the least water absorption capacity value occurs for 20% RHA after 28 days curing.

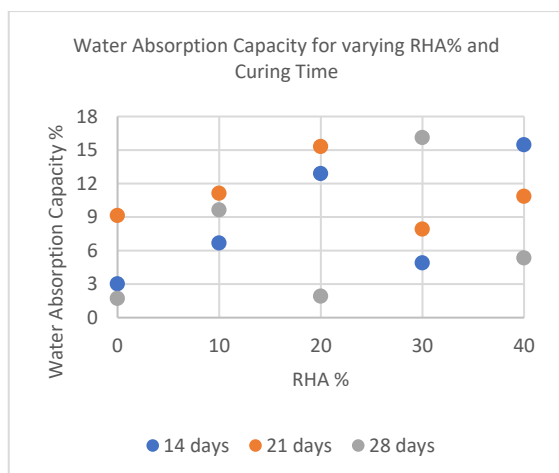


Figure 4. Water Absorption Capacity of CEBs with varying RHA levels cured for 14, 21 and 28 days: (3 samples per data point given)

The results of the bulk density of the experimental CEB as affected by RHA inclusion is shown in Figure 5. That is, the bulk density values decreased with increasing duration of curing.

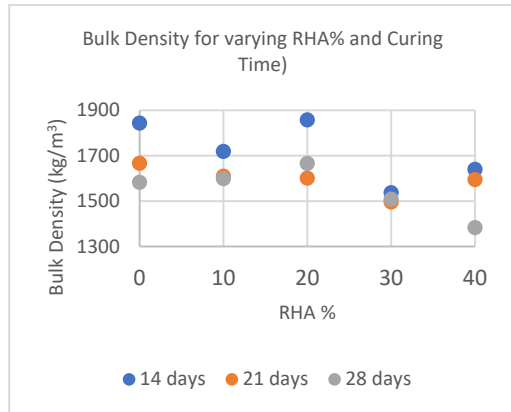


Figure 5. Bulk Density of CEBs with varying RHA levels cured for 14, 21 and 28 days: (3 samples per data point given)

5. DISCUSSION

Compressive strength, along with other parameters is an important parameter used in ascertaining the quality of materials for building construction. Consequently, compressive strength value as high as $3\text{-}4\text{Nmm}^{-2}$ and as low as 0.35Nmm^{-2} depending on the bulk density of stabilized CEB had been reported [21, 22]. In the present study, compressive strength for CEB with and without RHA inclusion ranged from $0.317\text{-}0.637\text{Nmm}^{-2}$ (Fig. 3).

Furthermore, the authors noted that the variation in the compressive strength values reported for the CEB were due to the differences in the bulk densities ($1800\text{-}2100\text{kg/m}^3$) of the blocks [22]. Bulk density obtained in the present study ($1513\text{-}1708\text{kg/m}^3$) for the CEB with and without RHA inclusion (Fig. 3) is lower than the range reported by Mansour [22]. The difference might be attributed to the differences in mixes used for the various CEB.

Bulk density, a function of the weight of material in a unit volume of space, depends on the extent to which the material is compressed per unit of space during block moulding. Conversely, water absorption capacity is a function of voids in the block. Therefore, an inverse relationship is expected to exist between bulk density and water absorption capacity. The results seemed to suggest that more earth material (laterite) should be used incorporated in the mix for CEB. Additionally, greater force should be applied in the block-pressing machine to increase the bulk density and compressive strength of the CEB.

In the present study, gradual replacements of cement with 0% to 40%RHA in the mix for CEB were tested. The results appeared to suggest that compressive strength and water absorption capacity tends to be stable at between 20 and 40%RHA inclusion, and that

beyond 20% RHA inclusion, there was a remarkable decrease in the bulk density of the test block (Figures 5). Furthermore, RHA-CEB required 21 days of curing to raise its compressive strength, whereas it needed 28 days for keeping water absorption capacity at the barest minimum. Bulk density of RHA-CEB decreased with increasing duration of curing. A minimum of 21 days of curing appeared sufficient to stabilize the bulk density of the blocks (apart from with 40% RHA).

The suitability of RHA-CEB in the provision of low-cost housing for low-income earners needs to be addressed. It's generally low compressive strength, high water absorption capacity, and low bulk density make its suitability doubtful particularly in Nigeria where rainfall is heavy and persists for longer period of the year. However, its use in building construction might necessitate provision for protection from water in the architectural design of the building. That is, making provision for roof overhangs, elevated level of the foundation from the ground level, and using a damp proof course.

Furthermore, the results tended to suggest that RHA could not entirely replace cement in the CEB mix. As a pozzolan, RHA cannot show cementitious properties without the presence of calcium hydroxide (Ca(OH)_2) and water [10]. Indeed, it needs cement to produce Ca(OH)_2 for the reaction with its silica to form calcium-silicate hydrate gel, the cementitious compound. Therefore, the use and application of RHA could probably be limited to a stabilizing agent rather than a replacement for cement.

6. CONCLUSION

The provision of a standard wall material for residential building need to meet some standard requirement in terms of mechanical, durability properties. The testing of compressive strength, bulk density and water absorption test was the first step taken to ensure adequate requirement was achieved. From the foregoing, it may be concluded that low compressive strength, high water absorption capacity, and low bulk density exhibited by RHA-CEB make doubtful the suitability of RHA as a replacement for Ordinary Portland cement in the building construction in the wet regions.

However, the use of RHA in the CEB could be confined to serving as a stabilizing agent.

The result of the blocks (CEBS) did not meet the required standard which would need to be improved in further test carried out in the future.

- This can be achieved by exploring the inclusion of sharp sand to the mix proportion, increasing the bulk density of each unit of CEBs.
- Explore design modifications which could compensate for weakness of RHA stabilised blocks

PLEA 2018 HONG KONG

Smart and Healthy within the 2-degree Limit

- Explore passive design options appropriate to climate for small residential buildings to maximise comfort while respecting societal requirements.

ACKNOWLEDGEMENTS

I would also like to appreciate Covenant University, Nigeria for provision of facility to carry out necessary test.

REFERENCES

1. Ugochukwu, I.B. and M.I.B. Chioma, Local Building Materials: Affordable Strategy for Housing the Urban Poor in Nigeria. *Procedia Engineering*, 2015. 118: p. 42-49.
2. Awofeso, P. (2010). One Out of Two Nigerians now Lives in a City: There are Many Problems but One Solution. *World Policy Journal* 27:67
3. Khyomesh V.P and Chetna M.V., National Conference on Recent Trends in Engineering and Technology. Construction materials management on project sites, 2011.
4. Cid-Falceto, J., F.R. Mazarrón, and I. Cañas, Assessment of compressed earth blocks made in Spain: International durability tests. *Construction and Building Materials*, 2012. 37: p. 738-745.
5. Heung Fai, L.A.M., et al., The Proceedings of the Twelfth East Asia-Pacific Conference on Structural Engineering and Construction Study on Strength Characteristics of High Strength Rice Husk Ash Concrete. *Procedia Engineering*, 2011. 14: p. 2666-2672.
6. Prusty, J.K., S.K. Patro, and S.S. Basarkar, Concrete using agro-waste as fine aggregate for sustainable built environment – A review. *International Journal of Sustainable Built Environment*, 2016. 5(2): p. 312-333
7. Domone, P.L.J. and J.M. Illston, Construction materials : their nature and behaviour. 4th ed. / edited by Peter Domone and John Illston. ed. *Construction materials : their nature and behaviour*, ed. P.L.J. Domone, J.M. Illston, and B. Dawson. 2010: London : Spon.
8. Alsubari, B., P. Shafiq, and M.Z. Jumaat, Utilization of high-volume treated palm oil fuel ash to produce sustainable self-compacting concrete. *Journal of Cleaner Production*, 2016. 137: p. 982-996.
9. Tong, K.T., R. Vinai, and M.N. Soutsos, Use of Vietnamese rice husk ash for the production of sodium silicate as the activator for alkali-activated binders. *Journal of Cleaner Production*, 2018. 201: p. 272-286.
10. Kazmi, S.M.S., et al., Manufacturing of sustainable clay bricks: Utilization of waste sugarcane bagasse and rice husk ashes. *Construction and Building Materials*, 2016. 120: p. 29-41.
11. Darko, A., et al., Driving forces for green building technologies adoption in the construction industry: Ghanaian perspective. *Building and Environment*, 2017. 125(Supplement C): p. 206-215.
12. Prasara-A, J. and S.H. Gheewala, Sustainable utilization of rice husk ash from power plants: A review. *Journal of Cleaner Production*, 2017. 167: p. 1020-1028.
13. Oyelami, C.A. and J.L. Van Rooy, A review of the use of lateritic soils in the construction/development of sustainable housing in Africa: A geological perspective. *Journal of African Earth Sciences*, 2016. 119: p. 226-237
14. Preetz, H., et al., Relationship between magnetic properties and reddening of tropical soils as indicators of weathering. *Geoderma*, 2017. 303(Supplement C): p. 143-149.
15. Lyons, A., *Materials for architects and builders*. Fifth edition. ed. 2014: London : Routledge.
16. Horsley, C., M.H. Emmert, and A. Sakulich, Influence of alternative fuels on trace element content of ordinary portland cement. *Fuel*, 2016. 184: p. 481-489.
17. Richardson, B.A., *Defects and deterioration in buildings*. 2nd ed. ed. 2001, London: London : Spon.
18. Chiang, K.-Y., et al., Lightweight bricks manufactured from water treatment sludge and rice husks. *Journal of Hazardous Materials*, 2009. 171(1-3): p. 76-82.
19. Ganesan, K., K. Rajagopal, and K. Thangavel, Rice husk ash blended cement: Assessment of optimal level of replacement for strength and permeability properties of concrete. *Construction and Building Materials*, 2008. 22(8): p. 1675-1683.
20. Sore, S.O., et al., Synthesis and characterization of geopolymer binders based on local materials from Burkina Faso – Metakaolin and rice husk ash. *Construction and Building Materials*, 2016. 124: p. 301-311.
21. Mostafa, M. and N. Uddin, Experimental analysis of Compressed Earth Block (CEB) with banana fibers resisting flexural and compression forces. *Case Studies in Construction Materials*, 2016. 5: p. 53-63.
22. Mansour, M. B. et al. 2016. Optimizing thermal and mechanical performance of compressed earth blocks (CEB). *Construction and Building Materials* 104, pp. 44-51. doi: <http://dx.doi.org/10.1016/j.conbuildmat.2015.12.024>

Summertime Overheating and Heat Stress in Multi-Family Colonial Revival Style Timber-Frame Buildings

TIMOTHY O. ADEKUNLE¹

¹Department of Architecture, College of Engineering, Technology, and Architecture (CETA), University of Hartford, West Hartford, Connecticut, USA

ABSTRACT: This paper discusses thermal comfort of occupants, summertime overheating and heat stress in multi-family Colonial Revival style timber-frame buildings located in the Hartford region of Connecticut, United States. The study considered a thermal comfort survey of occupants using subjective questionnaire and on-site measurements of environmental parameters (such as temperature, relative humidity, and dew-point temperature) as the research methods. The Wet-Bulb Globe Temperature (WBGT) heat index and the Universal Thermal Climate Index (UTCI) heat index are also calculated using the variables measured during the field investigation. Across the buildings, the results show a mean temperature of 25.3°C, a mean relative humidity (RH) of 61.2%, and an average dew-point of 17.2°C. The occupants feel warm as over 67% responses are on the warm part of the thermal sensation scale while 74% prefer to be much cooler and 83% of the revealed the occupants are thermally satisfied with the thermal environment. The study shows the average number of hours of temperature rise above the 28.0°C threshold for 11.4% of the time. The study reveals the occupants of the buildings are prone to summertime overheating. Applying the WBGT heat index and the UTCI mathematical model to find the temperatures at which the vulnerable occupants are susceptible to the thermal environment, the study recommends the WBGT of 21.7°C and the UTCI of 25.8°C as possible heat stress thresholds in the buildings. Also, the study found out the basement areas provide the most comfortable thermal environment for the occupants. The results show a higher heat stress index is reported in this study than the existing research on heat stress in buildings.

KEYWORDS: Summertime Overheating, Heat Stress, Thermal Comfort, Colonial Revival Style, Timber-Frame Buildings

1. INTRODUCTION

Summertime overheating in buildings has been investigated in existing research [1-4]. Summertime temperatures were evaluated in different homes [2]. The study concluded summertime overheating occurs in homes even in the occupied period when occupants are expected to explore various adaptive measures to regulate the thermal environment [2]. Thermal comfort of occupants, summertime temperatures and overheating were evaluated in residential buildings built with prefabricated structural timber products such as cross-laminated timber and structural insulated panels [4]. The study highlighted that thermal mass is a crucial issue to consider towards improving the performance of timber buildings [4]. Summertime temperatures in multiple timber-frame homes [2] and structural timber buildings have also been studied [4-6]. Different studies have examined summertime overheating in various buildings using on-site measurements [2,4-5] and building simulation [1,4-5]. The impacts of summertime overheating have also been evaluated [3], and some adaptation strategies were recommended [3,7]. However, none of the existing studies have examined summertime overheating, occupants' comfort and heat stress in multi-family Colonial Revival style timber-frame buildings.

Multi-family Colonial Revival style timber-frame buildings are common in New England (Northeast) region of the United States. The construction of various buildings with Colonial architecture started in the geographical location around the 1600s. Figure 1 below shows an exterior view of a typical Colonial Revival style timber-frame building illustrating some of the significant characteristics of the building. Figure 2 shows the architectural patterns of a classic Colonial Revival style building. According to a recent report on the building stock in Hartford region, over 40% of the current buildings in the study location are built before 1950 [8]; and the majority of the pre-1950 buildings are multi-family Colonial Revival style buildings. The data provided by CERC [8] showed the importance of multi-family Colonial Revival style buildings to the study location. Timber-frame buildings are considered in this study as more than 90% of residential buildings in the US are constructed with timber-frames [5,9]. Based on existing studies on summertime temperatures in timber buildings [2,4-5], the current building stock in the study location suggests many people may be susceptible to summertime temperatures in multi-family Colonial Revival style timber-frames buildings. Therefore, it is important to investigate the thermal comfort of occupants in the buildings.

PLEA 2018 HONG KONG

Smart and Healthy within the 2-degree Limit

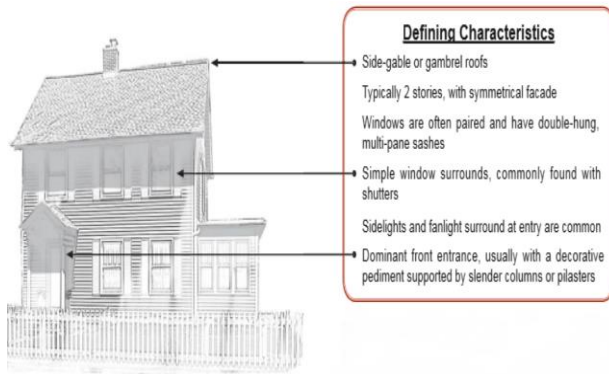


Figure 1: An external view of a typical Colonial Revival style timber-frame building [10].

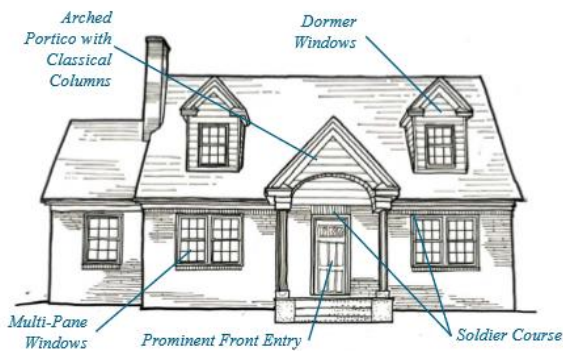


Figure 2: Architectural patterns of a classic Colonial Revival style building [11].

Heat stress has been discussed in existing studies [12-13]. The WBGT heat index defined as the combination of natural wet bulb temperature (T_{nwb} °C) and black globe temperature (T_g °C) has been used in existing research using the Equation 1 [11]. While the Universal Thermal Climate Index (UTCI) has been described as a function of air temperature determined by the actual values of air and mean radiant temperature (T_{mrt}), wind velocity (V_a) and humidity also regarded as water vapour pressure (V_p) or relative humidity (RH) [13]. The UTCI is computed using the Equation 2 to determine the temperature at which the vulnerable occupants are prone to summertime overheating.

$$WBGT_{ind} = 0.7T_{nwb} + 0.3T_g \quad \text{Equation 1}$$

$$UTCI = T_a + \text{Offset} (T_a; T_{mrt}; V_a; V_p) \quad \text{Equation 2}$$

Also, indoor temperatures above the 28°C threshold are considered critical to occupants' comfort [14] of different age groups and gender [5-6]; and indoor temperatures above the threshold for more than 1% of the time can lead to summertime overheating within the thermal environment [15]. Since none of the existing studies in the field have considered summertime overheating and heat stress in one study, this paper intends to address this gap. Moreover, due

to the importance of multi-family Colonial Revival style timber-frame buildings in the study location, this study intends to investigate summertime overheating, occupants' comfort and heat stress in the buildings.

2. RESEARCH METHODOLOGY

The study considered a field investigation to collect data for analysis. As a result, the research employed on-site measurements of environmental parameters (such as temperature, relative humidity, and dew-point temperature) and thermal comfort survey of occupants as the research methods. The research methods have been used in existing research [1-2,4-5]. The environmental parameters were measured at every 1 hour using data loggers placed on the wall at the height of 1.7m above the floor level. The height is considered an average height of a man in non-sitting position [14]. The field investigation was conducted from July-September 2017. The external weather data recorded at a nearby airport were used for analysis. The indoor data measured in the buildings were used to compute the wet-bulb globe temperature to determine the heat stress index for the vulnerable occupants. The number of hours of temperatures (that is, 1%) above the critical threshold (28°C) is used to assess summertime overheating in the case study buildings. Also, the study considered the number of hours of temperatures above 30°C (1%>30°C) to evaluate the elevated summertime temperatures in the buildings.

The subjective questionnaire was administered to the residents of the buildings. The residents were instructed to fill out the questionnaire three times per day. The questionnaire considered questions on thermal sensation, thermal acceptability, thermal satisfaction, lighting level, preference for fresh air movement into the buildings, sound level, control level and others. Over 110 questionnaires were completed and returned. The data were analysed using the statistical software to plot charts and find the relationship between the various variables. For this study, the findings on thermal sensation, thermal satisfaction, and thermal preference are briefly discussed.

The environmental variables measured during the field investigation were used to calculate the WBGT heat index using the Equation 1 while the UTCI was computed using the Equation 2 highlighted in the literature. The average values for the parameters are used to assess the temperatures at which the vulnerable occupants will be susceptible to summertime overheating in the buildings.

3. CASE STUDY

The case study buildings are multi-family Colonial Revival style timber-frame buildings. The buildings are sited in the Hartford region of Connecticut, United

PLEA 2018 HONG KONG

Smart and Healthy within the 2-degree Limit

States. The case study buildings are built before 1950 and occupied a significant percentage of the current building stock in the region. Most of the buildings have two household units each, and they are sited on an average plot of 689m². The buildings have an average floor area of 144m². Each household of the multi-family buildings has a living room, dining/kitchen area, a bath on the ground floor (level 1), and two bedrooms and a large bath on the upper level while the basement area is used for laundry and other purposes like playing area for children during the winter months. The measurements were taken in the living areas, bedrooms, and the basement area. On average, three to four people are living in each of the households. Based on the information collected on the buildings during the survey, the mean U-values of the external walls varied from 0.30-0.50W/m²K while mean value of about 0.35W/m²K is estimated for windows and doors. This paper discussed the field investigation carried out in four of the case study buildings. Figure 3 shows the front view of one of the case study buildings.



Figure 3: A front view of one of the case study buildings (MLTFR).

4. DATA ANALYSIS

The thermal comfort surveys were carried out concurrently in all the buildings. In all, more than 70% of the questionnaires were completed by female respondents while male respondents completed only 30%. All the respondents are above the age of 18, and over 85% of the respondents are between 30 and 45 years. The analysis reveals the respondents are adults and can vote on the thermal environment of the buildings. The respondents spent between 12-21 hours within the buildings per day.

For the external conditions, the mean external temperature for the period of the field investigation was 21.7°C. A maximum temperature of 34.0°C and a minimum temperature of 8.0°C were recorded during the period. The mean maximum temperature was 32.7°C while the average minimum temperature of 10.7°C was reported for the external conditions. The mean dew-point temperature of 15.7°C was observed

at the study location. The average RH was 68.7%. For the period of the field study, the mean WBGT of 19.1°C and the mean UTCI of 22.2°C were calculated for the location. The months considered for the monitoring (July-September) are the hottest months of the year (Figure 4). Table 1 provides the summary of the external data for the period of the survey. The analysis also showed a mean of 7 cooling degree days per month for the period of the investigation.

Table 1: Summary of the external data for the study location.

Month	July	August	September
Mean temp (°C)	23.0	22.0	20.0
Max. temp (°C)	34.0	32.0	32.0
Min. temp (°C)	12.0	12.0	8.0
Mean RH (%)	68.9	68.8	68.4
Mean Dew-point (°C)	17.0	16.0	14.0
Cooling degree days	9	7	5

Comparing the external temperatures of the summer months (May-September) between 2016 and 2017, the study found out average values for the period of the monitoring in 2017 was slightly lower than the average values in 2016 (Figure 5). The analysis suggests extreme summertime overheating may occur within the buildings when the heat waves occur for consecutive days. Also, the cooling degree days are reported during the field investigation with the highest cooling days observed in July. Likewise, the external temperatures rise above 30°C for several hours for a few days in each of the summer months during the field survey.

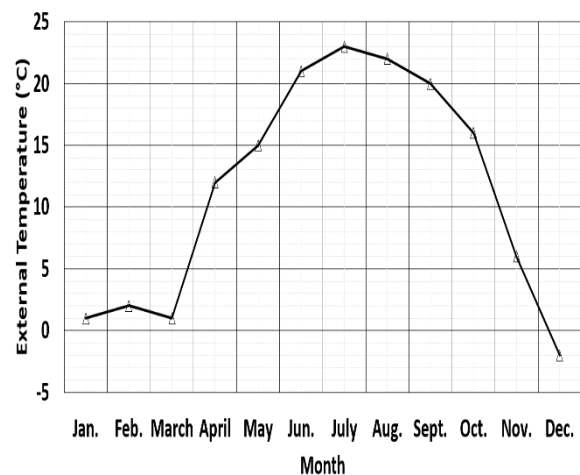


Figure 4: Average mean temperatures from Jan-Dec. 2017.

PLEA 2018 HONG KONG

Smart and Healthy within the 2-degree Limit

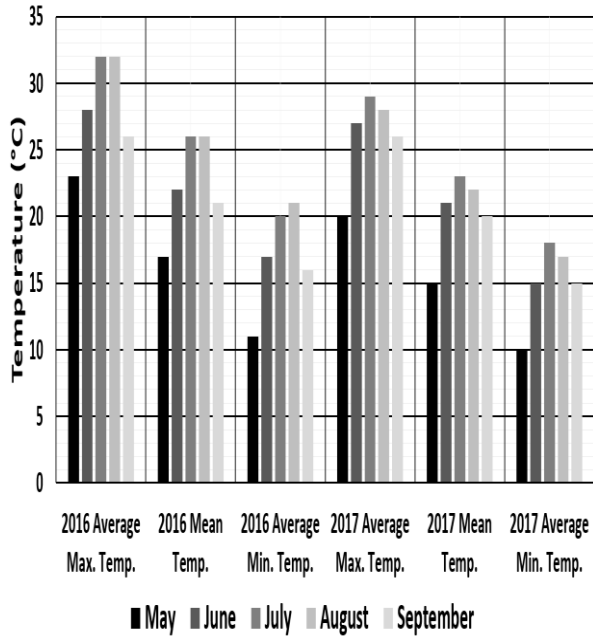


Figure 5: Average maximum, minimum and mean temperatures for the external conditions during the summer

5. RESULTS AND DISCUSSION

The finding on the maximum number of hours spent within the buildings per day (approximately 88%) agrees with the outcome from existing research that people in the advanced countries especially in the United States (the study location) spent up to 90% of their time indoors per day [16]. The result of thermal sensation votes on a 7-point scale (ASHRAE) showed the occupants feel warm in the building with a mean value of 6.1 where 1 represents cold, and 7 represents hot. More than 67% of the occupants' responses also showed they feel warm within the buildings. Regarding the question on the thermal preference of occupants, about 74% of occupants prefer to be cooler within the thermal environment. Also, approximately 83% of the respondents are comfortable in the thermal environment of the buildings.

The mean temperatures in the case study buildings range from 24.2°C to 26.1°C. The average RH varied from 58.9% to 65.2% while the mean dew-point temperatures range from 16.9°C to 17.5°C. The results showed the mean temperatures are below the critical threshold of 28.0°C. Across the buildings, higher temperatures are reported in the buildings during the field investigation. Also, the responses on thermal sensation showed higher votes on the warm part of the scale during the two warmest months (July and August).

The results of the analysis to find the relationship between the internal temperatures and the external temperatures showed the internal temperatures are strongly influenced by the external temperatures (Figure 6). Higher temperatures are also observed in the buildings. The low thermal mass of timber-frame

buildings may be a contributing factor to the elevated temperatures measured in the buildings as highlighted in existing research that thermal mass is a vital parameter influencing the thermal behaviour of timber buildings [4]. The outcomes showed the indoor temperatures are within a range of about 2.2°C to 6.5°C. MLTFR appears to be the warmest building (the approach view has a southeast orientation). On the contrary, the lowest temperatures are recorded in MLTBS. The larger part of the MLTBS building appears to be below the ground level which may be a contributing factor to the lower temperatures observed in the building. The results suggest the ground cooling strategy which involves integrating a basement may be a reliable approach to reducing the elevated temperatures in timber-frame buildings as well as other types of buildings. However, this approach needs to be thoroughly evaluated in terms of the cost and maintenance before it is considered.

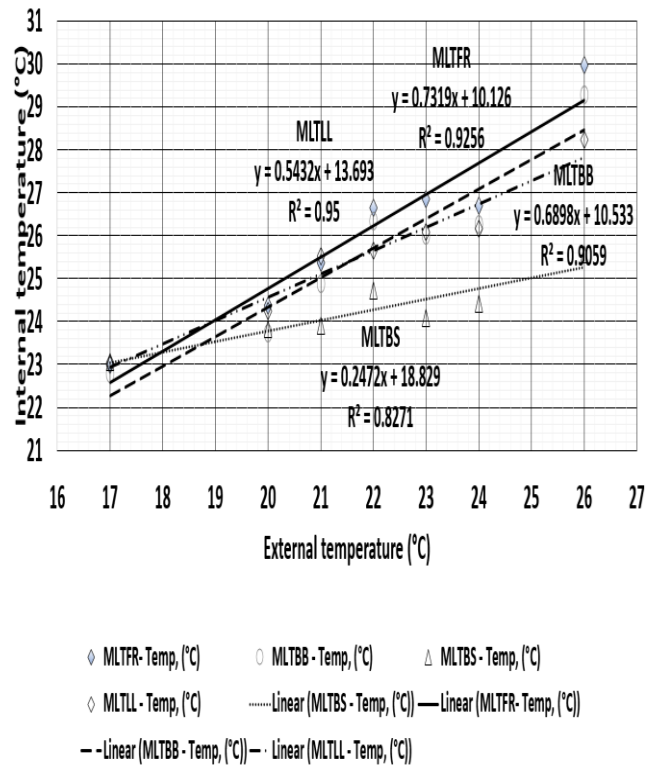


Figure 6: Relationship between the internal temperatures and the external temperatures in the summer.

The results regarding the number of hours of temperatures above the critical thresholds revealed the internal temperatures rise above the 28°C threshold for more 1% of the time across the buildings excluding the MLTBS building as shown in Figure 7. Also, the temperatures also rise above 30°C for more than 1% of the time in all the buildings except in MLTBS. The results showed summertime overheating occurs in the buildings which may affect the thermal comfort of occupants in the buildings.

PLEA 2018 HONG KONG

Smart and Healthy within the 2-degree Limit

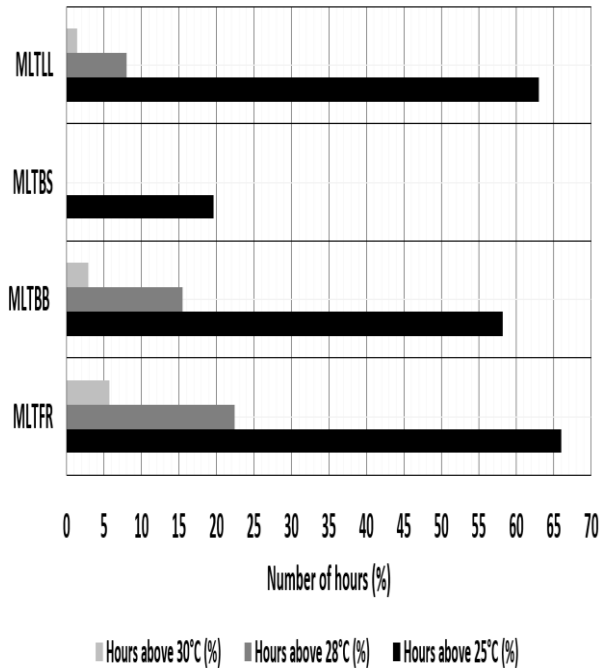


Figure 7: Number of hours of temperatures above the threshold in the buildings during the summer.

Equation 1 and Equation 2 are applied to calculate the WBGT heat index and the UTCI threshold as discussed in the literature. The results showed the WBGT index varied from 21.1°C to 22.2°C in the buildings. The UTCI heat index ranges from 24.8°C to 26.5°C. The study showed a higher WBGT and UTCI heat indexes are calculated in MLTFR than other buildings considered in this study. The mean WBGT for all the buildings showed the heat index of 21.7°C. For the mean UTCI, the heat index of 25.8°C is calculated for all the buildings. The study showed the possible heat indexes at which the vulnerable occupants will be prone to the risk of heat stress within the buildings.

Table 2: Summary of the mean temperatures, average WBGT, and UTCI heat indexes.

Variables	MLTFR	MLTBB	MLTBS	MLTLL
Mean temp (°C)	26.1	25.6	24.2	25.6
WBGT (°C)	22.2	22.0	21.1	21.8
UTCI (°C)	26.5	26.1	24.8	25.9

Concerning the relationship between the WBGT and the UTCI, the study found out a relationship exists between the variables in all the buildings considered in this study (Figures 8-9). The study showed more than 99% of the data collected revealed an increase in the value of the WBGT leads to an increase in the value of the UTCI (Table 3). The results also showed that higher heat stress indexes are reported in this study than the existing research [11,17].

Table 3: Summary of the relationship between the WBGT and UTCI heat indexes.

Variables	MLTFR	MLTBB	MLTBS	MLTLL
WBGT versus UTCI (R ²)	0.9962	0.9956	0.9964	0.9970

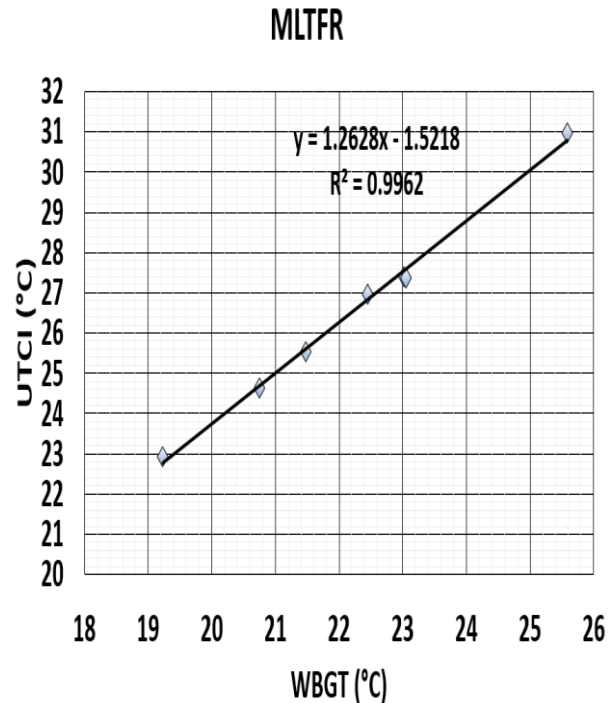


Figure 8: Relationship between the WBGT and the UTCI heat indexes in the MLTFR building.

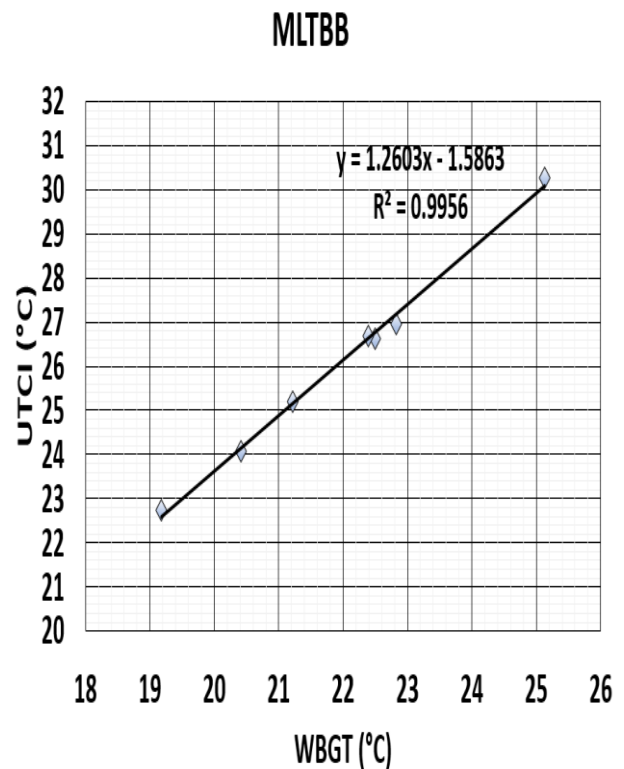


Figure 9: Relationship between the WBGT and the UTCI heat indexes in the MLTBB building.

PLEA 2018 HONG KONG

Smart and Healthy within the 2-degree Limit

6. CONCLUSION

This paper considered summertime overheating, occupants comfort and heat stress in multi-family Colonial Revival style timber-frame buildings. The field study was conducted in the summer of 2017. The study considered on-site measurements and thermal comfort surveys to collect data for analysis. The data were analysed using the relevant statistical software. The results showed an average temperature of 25.3°C, a mean RH of 61.2% and a mean dew-point of 17.2°C. The votes on thermal sensation revealed over 67% of the respondents feel warm in the summer. Also, about 74% of the respondents prefer to be cooler, and 83% of the participants highlighted they are thermally satisfied within the thermal environment of the buildings during the survey. The result showed the average number of hours of temperatures rise above the threshold (28°C) for 11.4% of the time. Also, the average number of hours of temperatures rise above the 30.0°C for 2.5% of the time. The study revealed the residents of the multi-family building are susceptible to overheating in the summertime. The outcomes of the research aligned with the findings presented in the existing study [4], that the lack of thermal mass in timber is a contributing factor to the elevated temperatures reported in timber buildings. The outcomes showed that prolonged elevated temperatures recorded in the buildings contribute to the thermal discomfort of occupants in the summer. The paper explained the buildings with substantial parts below the ground level tend to be cooler than those with larger parts above the ground level during the summertime. The research highlights ground cooling strategy may be a reliable approach to reducing elevated summertime temperatures in timber-frame buildings. The strategy needs to integrate the basement areas of buildings, and it must be evaluated regarding the cost as well as maintenance before the approach is considered. Applying the WBGT heat index and the UTCI mathematical model to find the average heat indexes within the thermal environment, the mean WBGT of 21.7°C and the mean UTCI of 25.8°C are calculated as possible heat stress thresholds in the buildings. The results showed a higher heat stress index is reported in this study than the existing research on heat stress in buildings.

ACKNOWLEDGEMENTS

The author would like to thank the survey participants for their participation and support throughout the field investigation.

REFERENCES

1. Gupta, R., & Gregg, M., (2012). Using UK climate change projections to adapt existing English homes for a warming

- climate. *Building and Environment*, 55: p. 20–42. doi: 10.1016/j.buildenv.2012.01.014
2. Morgan, C., Foster, J.A., Poston, A., Sharpe, T.R., (2017). Overheating in Scotland: contributing factors in occupied homes. *Building Research & Information*, 45(1-2): p. 143–156. <https://doi.org/10.1080/09613218.2017.1241472>
3. Tillson, A-A., Oreszczyn, T., & Palmer, J., (2013). Assessing impacts of summertime overheating: some adaptation strategies. *Building Research & Information*, 41(6): p. 652–661. <https://doi.org/10.1080/09613218.2013.808864>
4. Adekunle, T.O., Nikolopoulou, M., (2016). Thermal comfort, summertime temperatures and overheating in prefabricated timber housing. *Building and Environment*, 103: p. 21-35.
5. Adekunle, T.O., (2014). Thermal performance of low-carbon prefabricated timber housing. PhD Thesis, *University of Kent*, Canterbury, UK.
6. Adekunle, T.O., Nikolopoulou, M. (2018). Post-occupancy evaluation on people's perception of comfort, adaptation and seasonal performance of sustainable housing: a case study of three prefabricated structural timber housing developments. *Intelligent Buildings International*. 10.1080/17508975.2018.1493677
7. Porritt, S., Shao, S., Cropper, P., & Goodier, C., (2011). Adapting dwellings for heat waves. *Sustainable Cities and Society*, 1(2): p. 81–90. doi: 10.1016/j.scs.2011.02.004
8. CERC (2017). CERC Town Profile for West Hartford. Connecticut Economic Resource Center. <https://www.westhartfordct.gov/civicax/filebank/blobdload.aspx?BlobID=32923>
9. CEI-Bois. 2010. Tackle Climate Change: Use Wood. Available at: www.cei-bois.org/files/b03500-p01-84-ENG.pdf
10. City of Independence. Historic Preservation Design Guidelines. Residential Architectural Styles. CH. 6-63. [Online], <http://www.ci.independence.mo.us/userdocs/comdev/historicpreservation/06%20Architectural%20Styles%20-%20Residential.pdf> [13, April 2018].
11. Colonial Revival (1880-1950). <https://www.roanokeva.gov/DocumentCenter/View/1472/Architectural-Patterns---Colonial-Revival-PDF>. [22, May 2018]
12. Lemke, B., Kjellstrom, T., (2012). Calculating workplace WBGT from meteorological data: A tool for climate change assessment. *Industrial Health*, 50: p. 267-278.
13. Blazejczyk, K., Jendritzky, G., Brode, P., Fiala, D., Havenith, G., Epstein, Y., Psikuta, A., Kampmann, B., (2013). An introduction to the Universal Thermal Climate Index (UTCI). *Geographia Polonica*, 86(1): p. 5-10
14. ANSI/ASHRAE Standard 55, (2013). Thermal environmental conditions for human occupancy. *American Society of Heating, Refrigerating and Air-conditioning Eng.*, Atlanta, USA.
15. CIBSE, (2015). CIBSE Guide A: Environmental design. *Chartered Institute of Building Service Engineers*, UK.
16. EPA (2017). Indoor Air Quality. US Environmental Protection Agency, [Online], Available: <https://cfpub.epa.gov/roe/chapter/air/indoorair.cfm> [29, Jan 2018]
17. Adekunle, T.O., (2018). Thermal comfort and heat stress in CLT school buildings during occupied and unoccupied

PLEA 2018 HONG KONG

Smart and Healthy within the 2-degree Limit

periods in summer. In proceedings of the Windsor
Conference, London, UK, April 12-15

Retrofitting Strategies for Social Housing Buildings in Different Climate Conditions.

The CORVI 1010-1020 Block Type in Three Chilean Cities

WALDO BUSTAMANTE^{1,2}, CRISTIAN SCHMITT¹, VICTOR BUNSTER^{1,2}, PAULA MARTINEZ¹, FRANCISCO CHATEAU¹

¹School of Architecture, Pontificia Universidad Católica de Chile, Santiago, Chile

²Center for Sustainable Urban Development (CEDEUS) Pontificia Universidad Católica de Chile

ABSTRACT: Currently, less than 2% of the residential building stock in Chile meets minimum of thermal performance conditions while the current approach to social housing development has proved incapable of ensuring appropriate living standards. Demolishing housing blocks to replace them with new buildings is economically inefficient, environmentally damaging and socially unacceptable, as these structures represent an opportunity to renovate and upgrade existing buildings without disrupting consolidated communities. This ongoing research focuses on renovating the CORVI 1010-1020 housing blocks, a building type that was massively built across the country between 1968 and 1978. Today it is possible to find more than 2,000 units of this type of building—with no significant design variations—throughout Chile, hence between latitudes 18°S and 53°S of extremely diverse climates.

This paper analyses the impact of different energy retrofitting strategies in the thermal performance of these emblematic housing estates. Accordingly, building energy simulation is used to evaluate three scenarios, i.e., the original design without changes, a retrofitting proposal focused on meeting current thermal code requirements, and an expansion proposal aimed at increasing both thermal performance and life quality conditions. In order to assess the performance of these scenarios, the simulations focused on three cities with contrasting climatic conditions, i.e., hot-arid (Arica, 18°27'S), Mediterranean (Santiago, 33°27'S) and tundra (Punta Arenas, 53°08'S). Operational energy demand, accumulated hours of thermal discomfort, and payback time periods are considered for comparative analysis.

Whereas the results evidence that the cost-effectiveness of the proposed alternatives increases in colder climatic conditions dependant on space heating; overall, this study demonstrates that the retrofitting of these social housing buildings can help achieving significant heating and cooling energy savings as well as improving indoor thermal comfort conditions.

KEYWORDS: Energy Retrofitting, Social Housing, Heating Demands, Cooling Demands, Sunspace

1. INTRODUCTION

By the year 2050, in Chile, 18 million (90%) of inhabitants will live cities [1] and it will be necessary to provide one million new urban dwellings, mostly for low-income families. The existing growing model is oriented to the peripheral sprawl of cities and the demolition of obsolete homes and later reconstruction of buildings. This practice turns out to be inefficient, economically and environmentally unsustainable and socially unacceptable. Chilean residential buildings are responsible for 24% of Greenhouse Gas (GHG) emissions while less than 2% of the existing homes meet minimum standards of thermal comfort with energy efficiency [2]. The current social housing developments have proved incapable of achieving appropriate living standards. In fact, 65% of people living in these buildings would move out of their apartments immediately if they could and 90% feel ashamed of the place where they live [3].

The rehabilitation of existing collective housing has been developed as a sustainable alternative for the

growth and densification of cities [4]. According to IPCC [5], retrofitting of existing structures has been fundamental in mitigating GHG emissions from the building sector. Most social housing buildings will remain operational until 2050 and their upgrade represents great potential for the mitigation of these emissions through improving their thermal performance and avoiding demolition. These structures represent an opportunity to upgrade existing buildings in consolidated communities as they have functioning infrastructure and utilities. This paper is part of an ongoing initiative that, in collaboration with government agencies, aims to rehabilitate these buildings and public areas, to expand apartment units, and to improve their energy performance.

1.1. Case study: CORVI 1010 & 1020 social housing blocks

Since the late 60s, the Chilean government has focused on erecting thousands of mid-rise buildings

PLEA 2018 HONG KONG

Smart and Healthy within the 2-degree Limit

throughout the country to respond to the social housing deficit. The CORVI 1010-1020 housing block was originally conceived for the city of Santiago but, due to the efficiency of its design and construction process, it was massively replicated throughout Chile between 1968 and 1978. Today it is possible to find more than 2,000 units of this type of building -with no significant design variations- throughout the country, hence between latitudes 18° S and 53°S and a context of extremely diverse climatic conditions (Fig. 1).



Figure 1: CORVI 1010 social housing block

This four-story building is 20.07m wide and 11.10m deep and has a symmetrical plan layout with 4 two-bedroom units per floor organized symmetrically. Each apartment has an area of 48m². However, the units do not consider balconies nor exterior spaces and it is common to see qualitative deficiencies related to the built area of the apartment units. Apartments do not meet current living standards from the residents. The building does not have elevators as the Chilean Building Code [6] allows the use of stairs when main accesses to units are located up to the 5th floor.

The envelope is mainly composed of 17 cm. thick reinforced concrete walls with no insulation, masonry infills, and steel framed single glazed windows. All reinforced concrete slabs are 14 cm thick, including the roof slab, a rare feature in social housing blocks. The roof structure considers a minimum insulation of 50mm.

1.2. Case study location, thermal performance codes, and standards

When CORVI 1010-1020 blocks were built, Chile had no thermal performance regulations for residential buildings. These buildings considered minimum thermal insulation according to local customs without considering climate differences throughout the country. However, the building's structure presents higher standards than later social housing projects and could hold improvements to update their performance to meet the current code requirements.



Figure 2: Arica, Santiago and Punta Arenas in Chile

In Chile, thermal performance standards are regulated by the Chilean Building Code [6] in the Article 4.1.10 first issued on the year 2000. The first version only defines maximum U-values for roof assemblies of houses while the 2007 updated version specifies maximum U-values for roofs, walls and external floor assemblies, as well as maximum allowed area for windows according to their U-value. However, current requirements for residential buildings have low standards as the code establishes requirements only for heating periods and no regulation for cooling periods. The current code does not consider specifications for air infiltrations, thermal bridges or room ventilation requirements.

In 2016, the Ministry of Housing (MINVU) issued a publication on sustainable housing construction standards with recommendations to increase the thermal performance standards of residential buildings [7]. This proposal specified new construction standards for the building envelope (wall, floor, windows and roof) and includes considerations to reduce infiltration rates of the building. However, the application of these guidelines is non-mandatory [8].

This research focuses on three locations as representative cases of the country's climatic diversity to evaluate the thermal performance of the buildings (Fig.2). The code defines maximum thermal transmittance values for different envelope building components according to the geographical location of the building according to Table 1.

Table 1: Location and climatic conditions of the buildings under analysis

	Arica	Santiago (Pudahuel)	Punta Arenas
Latitude	18°27' S	33°27' S	53°08' S
Climate	Bwh Hot-arid	Csb Mediterranean	ET Tundra
Mean T°	18.7 C°	13.6 C°	5.9 C°
Min T°	16.1 C°	6.7 C°	2.8 C°
Max T°	22.4 C°	22.4 C°	9.7 C°
Mean Humidity	74%	72%	76%
No of Buildings	13	52	6

PLEA 2018 HONG KONG

Smart and Healthy within the 2-degree Limit

Although each location has unique climates and different thermal performance requirements, existing CORVI 1010-1020 buildings have the same constructive solution for the envelope. Thermal transmittance (U-value) maximum required for residential buildings according to the current code are shown in Table 2.

Table 2: Maximum U-value (W/m²K) allowed by the current regulation for the locations of the buildings under analysis

	Arica	Santiago	Punta Arenas
Walls	4.0	1.9	0.6
Roofs	0.84	0.47	0.25
Windows	Single Glazing	Single Glazing	Single Glazing

Local code standards allow the use of single glazed windows even in southern cities of the country with cold weather such as Punta Arenas. However, recent trends have encouraged the use of double glazing that allows increasing the window to wall ratio (WWR). E.g. in Punta Arenas the window/facade ratio is 12% for single glazed window and 28% for double glazed units

2. METHODS

To assess the impacts of the different retrofitting approaches to be applied in different climates of Chile, the thermal performance of the residential blocks was using the building energy simulation software DesignBuilder Engineering Pro v.5 [9].

The simulations consider all four apartment units of a typical third floor of the building. Heating and cooling demands were estimated for target indoor temperatures between 20.0°C (heating setpoint) and 26.0°C (cooling and natural ventilation setpoint). Infiltration rates were set to 3.0 ACH for the baseline and current code scenarios, and 1.0 ACH for the extension. For all cases, a 4-people nuclear household was considered according to the national average (126W/p metabolic rate). In parallel, the thermal comfort of the apartments was estimated using the CEN 15251 Adaptive Comfort Model, Category III (i.e., moderate expectations, intended for existing buildings) [10].

Table 3: Thermal conductivity and material properties of envelope walls for the three scenarios under evaluation

Scenario	City	Concrete [m]	EPS [m]	Gypsum [m]	U-value [W/m ² K]
Baseline	Arica				
	Santiago	0.170	n/a	n/a	3.121
	P. Arenas				
Current Code	Arica		n/a		3.121
	Santiago	0.170	0.015	n/a	1.438
	P. Arenas		0.055		0.590
Extended	Arica		0.010		1.638
	Santiago	0.170	0.055	0.010	0.576
	P. Arenas		0.090		0.383

Table 4: Thermal conductivity and material properties of envelope windows for the three scenarios under evaluation

Scenario	City	Window Type	U-value [W/m ² K]
Baseline	Arica		
	Santiago	Single Glazed	5.894
	P. Arenas		
Current Code	Arica	Single Glazed	5.894
	Santiago	Double Glazed	3.159
	P. Arenas		
Extended	Arica		
	Santiago	Double Glazed	3.159
	P. Arenas		

The analysis considers three scenarios applied to each city (Arica, Santiago and Punta Arenas) (Tables 3 and 4):

Scenario 1. The 4 apartments of a standard second floor according to their original 65m² layout per unit (apart from Unit 4 with 71m²), original envelope materials, and finishes.

Scenario 2. The 4 apartments of a standard second floor after retrofitting of envelope materials towards meeting current Chilean thermal regulation requirements. In this scenario, only upgrading of building components and reduction of infiltrations were considered.

Scenario 3. The 4 apartments of a standard second floor including a retrofitting proposal consisting of an extension attached to the existing building without compromising its original structure. The resulting 110m²-unit layout (with the exception of Unit 4 with 116m²) responds to current user requirements and a new thermal regulation standard currently under evaluation. A sunspace on the facade is also considered towards increasing heat gains in the cold season (Fig. 3). This proposal considers the non-mandatory standards suggested by MINVU for windows, wall and roof assemblies (Table 2).

PLEA 2018 HONG KONG

Smart and Healthy within the 2-degree Limit

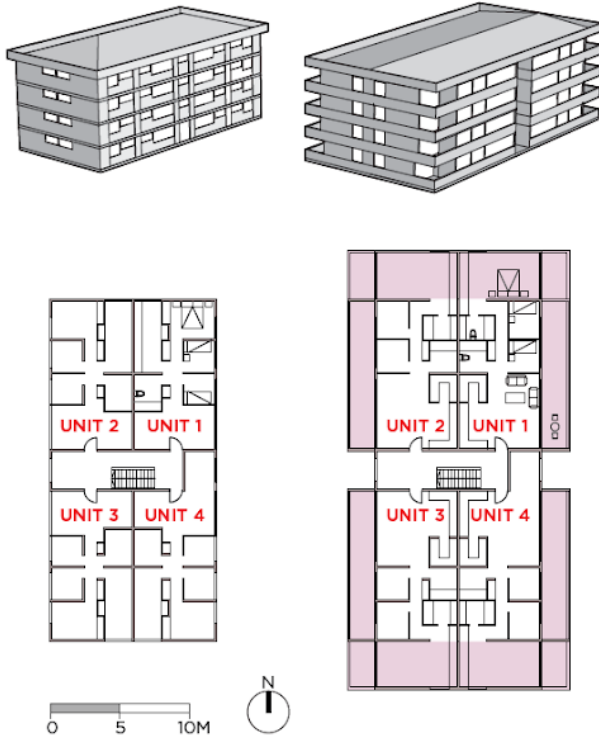


Figure 3: CORVI 1020 isometric view and typical floor plan of the original design (left) and the modified layout and expansion proposal (right, highlighted)

Given the non-normal distribution of the results, Kruskal-Wallis H test was used to assess the statistical significance of the changes in performance after implementation of different retrofitting alternatives and the Dunn-Bonferroni approach for pairwise comparisons was used as post-hoc test.

Although the construction and retrofitting costs are assumed to be covered by public subsidies or governmental programs rather than by the owners of the units, a payback period was calculated to provide a cost-benefit overview of the different alternatives. Accordingly, an estimate of 857.65 USD per m² and of 694.28 USD per m² were used to estimate construction and retrofitting costs respectively. The energy costs were estimated using LPG heaters, one of the most commonly used space-heating artefacts in this building type. The mean costs of this fuel were estimated as 2.565 USD and 1.624 USD per Kg for Santiago and Punta Arenas respectively [11], where 1 lt. was assumed to be equivalent to 0.51 Kg of fuel. The calorific value of LPG was estimated as 50,628 KJ/Kg and the performance of the heaters as 95% [12]. Arica was not included in the payback time estimations for not being in a heating-dependant climatic zone.

3. RESULTS

Table 5 summarises annual heating demand results for the three different scenarios for each city under

evaluation. No cooling demands were found with the building energy simulations.

Table 5: Annual heating demand for baseline (1), current code (2) and extended (3) scenarios in the tree cities under analysis

City	Scen	Unit 1	Unit 2	Unit 3	Unit 4	
Arica	(1)	16.06	16.27	17.10	17.44	kWh/m ²
		1,044	1,058	1,112	1,238	kWh
	(2)	16.06	16.27	17.10	17.44	kWh/m ²
		1,044	1,058	1,112	1,238	kWh
	(3)	13.20	11.61	13.01	14.46	kWh/m ²
		1,452	1,277	1,431	1,677	kWh
Stgo.	(1)	133.93	136.84	143.79	145.23	kWh/m ²
		8,705	8,895	9,346	10,312	kWh
	(2)	116.09	119.12	124.19	124.05	kWh/m ²
		7,546	7,743	8,072	8,808	kWh
	(3)	99.45	98.94	101.89	102.64	kWh/m ²
		10,939	10,884	11,208	11,907	kWh
Punta Arenas	(1)	404.08	415.23	425.23	432.60	kWh/m ²
		26,265	26,990	27,640	30,714	kWh
	(2)	306.87	314.52	319.14	324.22	kWh/m ²
		19,947	20,444	20,744	23,019	kWh
	(3)	270.78	270.74	275.22	293.43	kWh/m ²
		29,786	29,782	30,274	32,277	kWh

Total kWh results provide an overview of the operational energy demand for HVAC of the different apartments however, as one of the retrofitting alternatives includes changes to the layout and an increase in their total surfaces, kWh/m² is a better metric for comparisons. In this sense, adjusting the envelope of the baseline apartments to current thermal codes results in an average improvement of 13.62% in Santiago and 24.58% in Punta Arenas (no changes in Arica, as the baseline complies with the current code). While the greatest improvement in this scenario was found in Unit 3 with 24.95% in Punta Arenas, the lowest improvement was 12.95% in Arica. The improvements of the extended retrofitting alternative when compared to the baseline building were greater, with an average of 21.85% in Arica, 27.98% in Santiago and 33.81% in Punta Arenas. While the lowest improvement for this retrofitting scenario was in Arica for Unit 4 with 17.07%, in Punta Arenas the greatest improvement reached 35.28%.

Table 6 summarises the accumulated hours of thermal discomfort results for the three different scenarios for each city under evaluation. All the hours of discomfort found were below the comfort zone defined by the CEN 15251 adaptive model (Category III) (Table 7). While improving the thermal performance capabilities of the building envelopes until meeting current codes resulted in an average reduction of accumulated hours of thermal discomfort of 23.59% in Santiago and 46.93% in Punta Arenas, the improvements found after simulation of the proposed retrofitting extension were substantially higher with an average of 64.27% for Arica, 55.57% for Santiago and 80.59% for Punta Arenas. The lowest improvement found for this

PLEA 2018 HONG KONG

Smart and Healthy within the 2-degree Limit

retrofitting alternative was 49.51% for Unit 2 in Santiago, and the greatest was 83.94% for Unit 1 in the case of Punta Arenas.

Table 6: Total annual accumulation of thermal discomfort hours for the multiple zones of the 4 units under different scenarios according to CEN 15251 Adaptive Comfort Model

City	Unit	Baseline [hrs.]	Curr. Code [hrs.]	Extended [hrs.]
Arica	Unit 1	5,509	5,509	2,027
	Unit 2	3,172	3,172	783
	Unit 3	4,644	4,644	1,898
	Unit 4	7,035	7,035	2,856
Santiago	Unit 1	5,014	3,626	1,880
	Unit 2	4,070	3,132	2,055
	Unit 3	4,988	4,058	2,503
	Unit 4	6,139	4,606	2,429
Punta Arenas	Unit 1	2,921	1,379	469
	Unit 2	2,356	1,261	432
	Unit 3	2,395	1,429	559
	Unit 4	2,980	1,546	594

Table 7: Mean thermal comfort range according to CEN 15251 Adaptive Model (III) for the cities under analysis

	[°C]	Arica	Santiago	Punta Arenas
Summer	Max	30.14	29.52	26.15
	Min	22.14	21.52	18.15
Autumn	Max	29.40	27.59	24.97
	Min	21.40	19.58	20.00
Winter	Max	28.23	25.67	23.48
	Min	20.23	18.00	18.00
Spring	Max	28.69	27.49	24.91
	Min	20.69	19.49	18.00

A Kruskal-Wallis H test confirmed these observations by evidencing statistically significant differences between retrofitting alternatives for accumulated hours of discomfort, total heating demand and heating demand per m² in Arica, Santiago and Punta Arenas (Table 8). A disaggregation of these results using the Dunn-Bonferroni post-hoc test is shown in Table 9. While the performance of the extended scenario evidenced significant improvements when contrasted the baseline scenario for the three test variables in the three cities under analysis, the performance improvement when contrasting the current code and the extended scenario was significant only for Arica. All other differences were not statistically significant.

Table 8: Result of Kruskal-Wallis H test where $p < .05$ is considered significant

		H	Sig.
Arica	Discomfort		
	Heating (total)	7.489	.024
	Heating (m2)		
Santiago	Discomfort		
	Heating (total)	9.269	.010

Heating (m2)			
Punta Arenas	Discomfort		
	Heating (total)	9.846	.007
	Heating (m2)		

Table 9: Result of Dunn-Bonferroni post-hoc test where $p < .05$ is considered significant

City		Baseline vs Current	Current vs Extended	Baseline vs Extended
Arica	Discomfort			
	Heating (total)	1	.018	.018
	Heating (m2)			
Santiago	Discomfort			
	Heating (total)	.170	.096	.002
	Heating (m2)			
Punta Arenas	Discomfort			
	Heating (total)	.350	.117	.005
	Heating (m2)			

The estimated payback periods for the different retrofitting alternatives are summarised in Table 10. While retrofitting the original units to meet current thermal codes resulted in a payback period of 26.41 years and 18.07 years in average for Santiago and Punta Arenas respectively, the investment of building the proposed extensions resulted in a payback period of 45.29 years and 25.77 years in average for the cities under analysis.

Table 10: Payback period in years for the different scenarios under analysis in heating-dependant cities

City	Unit	Current Code [years]	Extended [years]
Santiago	Unit 1	27.57	45.86
	Unit 2	26.98	46.09
	Unit 3	25.68	44.76
	Unit 4	25.42	44.43
Punta Arenas	Unit 1	18.61	26.05
	Unit 2	18.15	26.05
	Unit 3	17.89	25.63
	Unit 4	17.61	25.35

Overall, the simulation results and analyses demonstrate that the proposed retrofitting extension is capable to significantly improve the performance of the original apartments in terms of reduction of energy demand for space heating and accumulated hours of thermal discomfort. Although adjusting the thermal transmittance of envelope components to meet current regulatory standards can result in important improvements, these are negligible when contrasted to the ones achieved with the proposed transformations to the building configuration and tighter thermal performance standards. The results also show that the payback times increase significantly in warmer climatic zones that do not depend on space heating. Nonetheless, any reduction in operational energy costs can have a strong impact

PLEA 2018 HONG KONG

Smart and Healthy within the 2-degree Limit

on low-income households such as the ones living in the apartment blocks analysed in this study [12]. Hence, the need for public initiatives to support the materialisation of energy retrofiting. Significantly, scope of this payback evaluation is at the household level, thus disregards any benefits they may have on energy consumption, CO₂ and particulate matter emissions. This is the focus of related research on the area [13].

4. CONCLUSIONS AND FURTHER RESEARCH

This research evaluates heating and cooling demands as well as the thermal comfort of an existing social housing building type that have been built in different climates of the country without significant differences in their architectural design and building components. In order to improve the thermal performance of these buildings, both an upgraded envelope and an expansion proposal were evaluated as energy retrofiting alternatives. The results demonstrate that simple retrofiting of social housing can help to achieve significant heating and cooling energy savings that may also help to improve indoor thermal comfort conditions for the occupants of the dwellings. In parallel, the differences in the payback periods for different retrofiting alternatives in the cities under analysis demonstrates that introducing this type of intervention is more cost-effective in colder areas with higher energy demand for space heating. Nonetheless, reduction of operational energy consumption can have strong impacts both for the budget of low-income dwellers and in minimising energy demand as well as CO₂ and particulate matter emissions at a country level.

Further work to extend this research will consider strategies such as natural diurnal or nocturnal ventilation for decreasing cooling demand. In parallel, the architectural design of the building extension will be refined to meet the different climatic conditions of the cities under analysis. Finally, future thermal comfort analysis will assess the conditions of different internal spaces of each apartment block in order to minimise risks of overcooling or overheating.

ACKNOWLEDGEMENTS

This work was partially funded by the Pontificia Universidad Católica de Chile and the VRI Research Fund for Interdisciplinary Studies in Sustainability Issues 170411006 and the National Commission for Science and Technological Research (CONICYT) of Chile under the FONDECYT N°3171502 Postdoctoral Fellowship.

The authors also gratefully acknowledge the research support provided by the Centre for Sustainable Urban Development (CEDEUS) and the research grant CONICYT/FONDAP 15110020.

REFERENCES

1. United Nations, Department of Economic and Social Affairs, Population Division, (2015). World Population Prospects: The 2015 Revision, World Population 2015 Wallchart. ST/ESA/SER.A/378.
2. OECD, (2014). LEED Programme (Local Economic and Employment Development).
3. Rodríguez, A. and A. Sugranyes, (2005). Los con techo. Un desafío para la política de vivienda social. Ediciones SUR, Santiago.
4. Druot, F., Lacaton, A. and J.P. Vassal, (2007). PLUS - Les Grands Ensembles de Logements, Territoires d'Exception", Gustavo Gili, Barcelona
5. IPCC, (2007). Climate Change: Synthesis Report. Contribution of Working Groups I, II and III to the Fourth Assessment Report of the Intergovernmental Panel on Climate Change. IPCC, Geneva, Switzerland.
6. Ministerio de Vivienda y Urbanismo (MINVU), (1992). Ordenanza General de Urbanismo y Construcciones. Ministerio de Vivienda y Urbanismo, Santiago, Chile.
7. Ministerio de Vivienda y Urbanismo (MINVU), (2016). Estándares de Construcción Sustentable para Viviendas, Tomo II: Energía. División Técnica de Estudio y Fomento Habitacional - Ditec, Minvu.
8. Bustamante, W., (2013). Propuesta de actualización de la reglamentación térmica, Art. 4.1.10 de la OGUC. Ministerio de Vivienda y Urbanismo. Chile.
9. Tindale, A., (2005). DesignBuilder software. Stroud, Gloucestershire, Design-Builder Software Ltd.
10. European Committee for Standardization, (2007). CEN 15251, Indoor environmental input parameters for design and assessment of energy performance of buildings addressing indoor air quality, thermal environment, lighting and acoustics., Brussels, Belgium.
11. Gobierno de Chile, (2018). Gas en línea [Online] <http://www.gasenlinea.gob.cl/> [14 August 2018].
12. L.A. Cifuentes, Cabrera, C. and P. Busch, (2016). Manual para Desarrollo de Inventarios; Informe solicitado por Subsecretaría del Medio Ambiente Licitación ID 608897-500-SE16, Santiago, DICTUC.
13. Bunster, V. and M. Noguchi, (2015). Profiling space heating behavior in Chilean social housing: Towards personalization of energy efficiency measures. *Sustainability*, 7: p. 7973-7996.
14. Bustamante, W., Jorquera, H., Brahm, M., Bunster, V., Encinas, F. and S. Vera, (2017). A Methodology to Assess Environmental Impacts of Thermal Performance Improvements in Chilean Residential Buildings. Proceedings of SEEP 2017. June 27-30, Bled, Slovenia, University of the West of Scotland & University of Maribor.

Vegetation as a Potential Tool for Improving Thermal Comfort and Exposure to Solar Radiation in the Streets of Quito

Comparative analysis of two streets in the center of the city

SANTIAGO POZO¹, GRACE YEPEZ^{1,2}, NICOLAS SALMON^{1,2}

¹Pontificia Universidad Católica del Ecuador, Quito, Ecuador

²YES Innovation, Quito, Ecuador

ABSTRACT: Generating walkable cities is a major stake for urban areas and the transformation of public open spaces, as streets, is a key process for it. Solar radiation exposure may be an important parameter for comfort of public spaces users. In the case of Quito, radiation levels are so high all years long this parameter is a strong health issue. While street refurbishment based on pedestrians and bikers' requirements is still not a common practice in Ecuador, the present work proposes an approach of doing so based on simulating with ENVIMET two similar streets of Quito's centre against thermal comfort and hence indirectly radiation exposure, one being highly vegetated and the other not. Simulations evaluate the energy exchange between street components considering their thermal characteristics, indicating the potential satisfaction level of pedestrians. The influence of street vegetation, especially the presence of large covering trees, is demonstrated as being strong. It allowed to propose an improvement process for the comfort deficient street, thus offering a potential larger solution for Quito's streets configuration.

KEYWORDS: Street, Comfort, Heat island, Solar radiation, Vegetation

1. INTRODUCTION

Transportation in Quito is insured at 70% by public transport and the first metro line of the city is currently in construction. Its opening in late 2019 should further increase the level of public transport in the mobility panel of the city, also increasing the number of pedestrians in the streets reaching the bus, trolley or metro stations.

Quito is facing a strong sunny period each day, almost all year long, with one of the highest UV radiation level for a city in the world [1] due to its altitude (2800m a.s.l.) and localization on the Equator. The World Health Organization indicates an ultraviolet index of 11 as maximum tolerable limit for human beings [2]. A study [3] realized between 2009 and 2011 in Quito by the Secretaria de Territorio, Habitat y Vivienda showed this level is reached in the city more than 45% of the year, especially at mid-day. Such phenomenon should be further increased by climate change in coming years [4].

Quality of life and health are affected, and this situation can also represent a strong barrier to the development in the city of alternative open street mobility solutions like biking or walking where the exposition to climatic conditions is higher. Against this strong climate, the city did not develop any protection strategy and most of the streets lacks shading devices. As measured within the Treepedia Initiative carried out by the MIT Senseable LAB in 2015 [5,6] the city of Quito has an average green cover of 10,8% which is

among the lowest of the 27 other international cities evaluated in this work.

Urban heat island effect has already been measured in Quito [7], and although it is not traduced by extreme temperatures for residents, it often means uncomfortable conditions at certain time of the day and dangerous exposure to extreme UV levels.

Natural conditions in Quito could afford much better vegetative coverage as the local permanently temperate climate is particularly propitious to plants development. Street tree planting and gardening buildings front spaces might be an interesting technique to be applied in Quito to generate comfortable public space conditions. Few streets in Quito already have an interesting highly vegetated configuration, most of them corresponding to the period of the beginning of the expansion of city outside the historical center (first half of the 20th century) and in areas greatly influenced by European architecture like the La Mariscal district [8].

Hence the present research is focused on assessing in this district the potential of vegetation as a tool to prevent outside comfort issues and radiation exposure.

2. EXPERIMENTATION

The La Mariscal district is a central area of Quito for its location and for its importance in terms of touristic and economic activities. It is also a key transport hub and hence a strategic place to improve smooth mobility patterns in the city.

PLEA 2018 HONG KONG

Smart and Healthy within the 2-degree Limit

Land use in the district is diverse as it includes public equipments, residences, commercial areas, hotels, health establishments and schools. As shown in Figure 1, construction profile is also quite diverse with highest buildings reaching 20 floors (80m high), buildings in the main streets being 16 floors high as an average and buildings in secondary streets, representing 82% of the constructed lots, being 3 to 6 floors high. For its representativeness of the district, but also of the whole city, the present study focuses on this last typology.

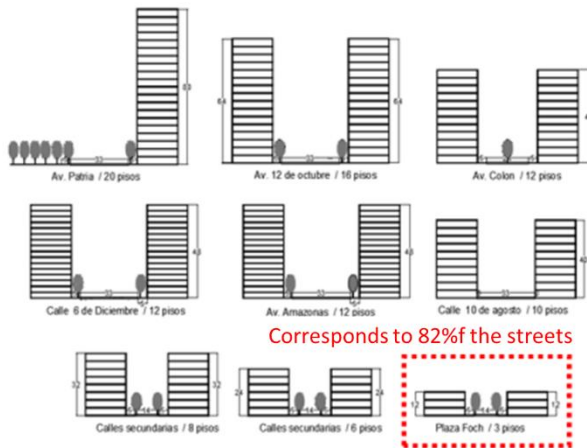


Figure 1: Building height and streets' profiles in the La Mariscal district in Quito

Further to an extended street configuration analysis in the district, comparing streets in terms of architectural configuration and presence of vegetation, the present study focused on analyzing two parallel streets of this same district showing similar characteristics in terms of buildings and size but having a different vegetal configuration. This district has a lot typology repeated in multiple areas, and this lot is very characteristics of the neighborhood.



Figure 2: Pictures of Lizardo Garcia Street (left) and Juan Rodriguez Street (right) in the district of La Mariscal in Quito

The first street is Calle Juan Rodriguez, where a regular tree coverage (sycamore tree - *Platanus acerifolia*) on the public sidewalk produces large areas of shade throughout the day and increases the relative humidity of the environment preventing excessive evaporation. Although it is considered as an exotic species in Quito, this type of tree can grow up to 20 m high and live 300 years in the city. The second street is Calle Lizardo Garcia, just next to Calle Juan Rodriguez and with a similar size, proportion, orientation,

buildings' scale and street width. This second street has however suffered from important modifications on the type of buildings (flat roof modern buildings have replaced half of the existing large houses), the use of vegetation for the front garden often replaced by asphalted parking lots, the street pavement was modified and above all the tree covering has diminished to almost zero has shown in Figure 2.

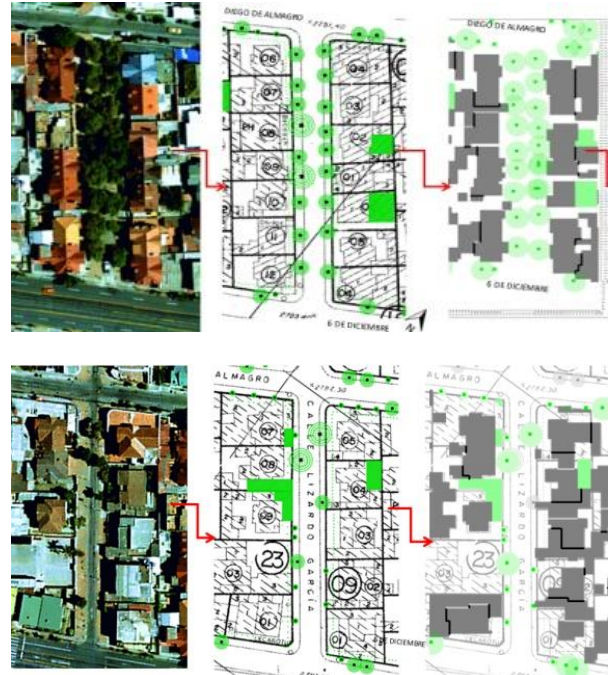


Figure 3: ENVI_met modelling of Juan Rodriguez (a) and Lizardo Garcia (b) including streets, buildings, vegetation covers pavement surface and roads. From aerial photo to 3D model process

As shown in Figure 3, we used the ENVI-met 4.2 simulation software, which is a tool that allows to model the urban structure and to analyse the microclimates and their physical foundations in a holistic way. ENVI-met was used to simulate the two streets in similar conditions, both in winter and summer seasons, with the objective to obtain the comfort potential and the useful hours of the streets in comfortable conditions, through Predicted Mean Vote (PMV) and Predicted Percentage of Dissatisfied (PPD) indexes, as defined in ISO 7730 [9]. The modeling is based on a 40m x 100m x 35m high 3D net applied on each street with a 1,2m resolution. It composes a complete lot integrating constructions from both sides of each street and going from the Avenida 6 de Diciembre to the Calle Diego de Almagro. Although the climatic conditions are stable along the year in Quito there are some differences between the northern hemisphere summer period and the rest of the year. We focus in this paper on the results obtained for the warmer season – from June to august

PLEA 2018 HONG KONG

Smart and Healthy within the 2-degree Limit

- at the warmest hours of the day – between 11AM and 2PM.

3. RESULTS

Figure 4 presents the simulations results obtained for the Lizardo Garcia Street in the warm season at the warmest moment of the day. Overall temperatures are not reaching extreme values but go beyond comfortable conditions. The whole street is exposed to the same level of heat and the few trees planted in the northern part of the street are not enough to balance this situation.

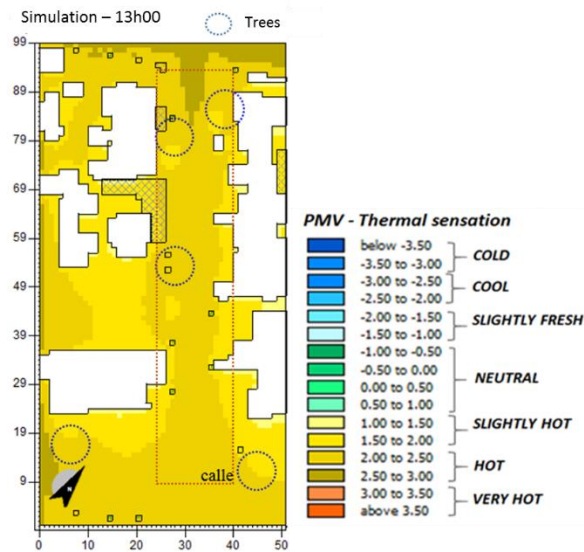


Figure 4: PMV thermal sensation simulated with ENVI-met in the Lizardo Garcia Street (Quito) during the warm period (August 2016)

A graphical representation of the average comfort values in the street among the day is presented in Figure 5. It appears clearly that the heat peak at mid-day generates an important discomfort with up to 93% in the PPV evaluation. This peak, beyond “neutral” thermal conditions as shown in Figure 5 b, last 6h20 in the case of the Lizardo Garcia street. It gets more severe from 12AM to 2PM where it reaches the level “hot” during 2h03. Hence the street cannot be a comfortable place for pedestrians or cyclist for most of the useful time of the day. The comfortable “neutral” period lasts 3h50 in this case, representing only 24% of the useful day (i.e. as night starts at 6h30 PM every day in Quito).

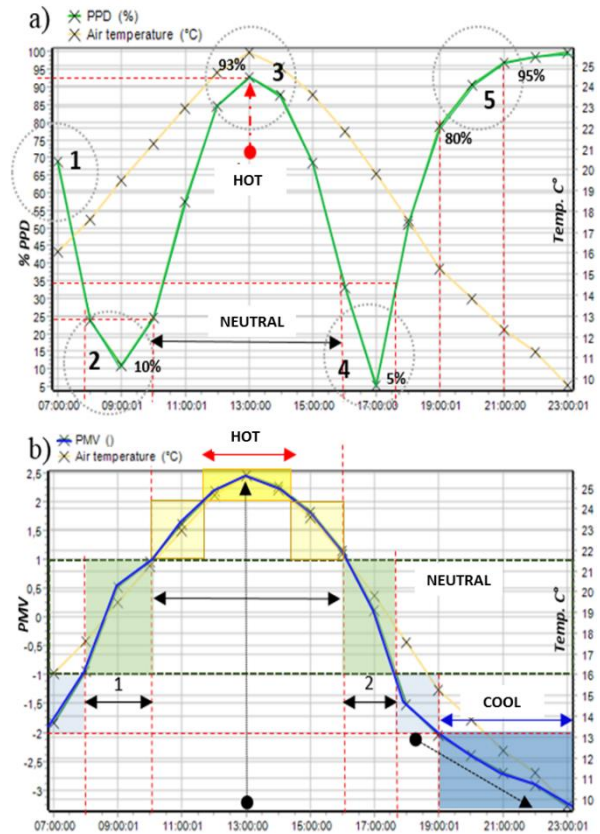


Figure 5: Thermal comfort conditions among the day evaluated from the ENVI-met simulation of Lizardo Garcia Street during the warm period (August 2016)

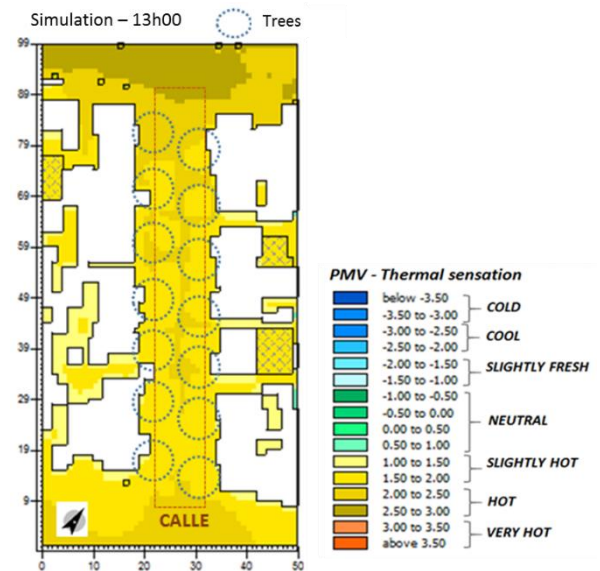


Figure 6: PMV thermal sensation simulated with ENVI-met in the Juan Rodriguez Street during the warm period (August 2016)

Similar analysis was realized for the same conditions of the same day in the case of the Juan Rodriguez street, as shown in Figure 6. At the warmest time of the day, the thermal sensation is “slightly hot” in most parts of the street. Simulation shows that in the center of the

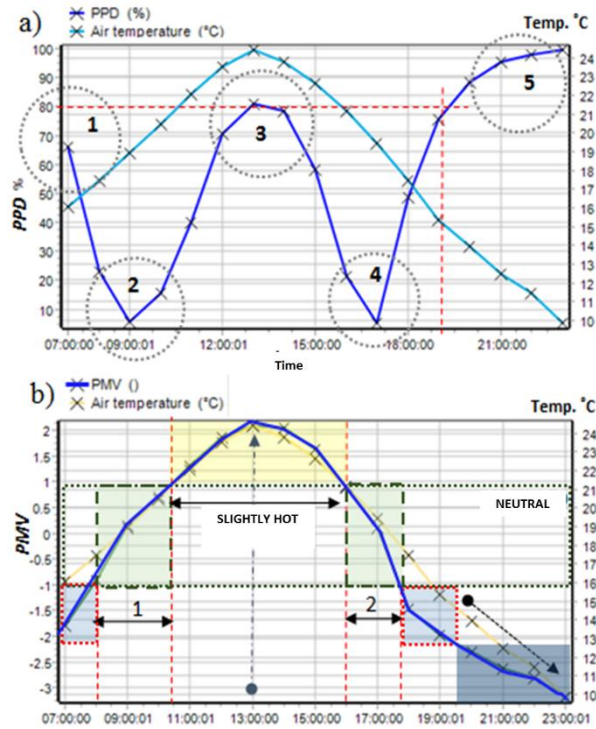
PLEA 2018 HONG KONG

Smart and Healthy within the 2-degree Limit

street, where the crown and foliage of the trees do not generate optimum shade coverage, they produce changes in thermal sensation indexes compare to the public sidewalk where the shadow zone generates greater coverage and trees prevent the pavement to be hot. Although this is not a crucial issue as the central axe of the street is not often used by pedestrians and cyclists.

Figure 7: Thermal comfort conditions among the day evaluated from the ENVI-met simulation of Juan Rodriguez Street during the warm period (August 2016)

We can observe on the graph in Figure 7 that the level of dissatisfaction potential (PPD) rises at mid-day but does not reach so high level as it does in Lizardo Garcia Street. PMV evaluation over the day does not reach the “hot” level in this case. The thermal condition is “neutral” during most of the day (30,4% of the useful day, i.e. 4h51min), except in the early morning where it is “slightly cold” and between 11 AM and 4 PM where it is “slightly hot” (i.e. lower than 26°C).



4. DISCUSSION

These values demonstrate a clear difference as for thermal conditions for the two neighbor streets during the same day. Vegetation, being the principal difference factor between them, allows an opportune and efficient protection against solar radiation and local overheating. The use of trees with a high covering potential like sycamore trees proved to be an efficient tool for insuring pedestrian comfort and supporting soft mobility in Quito. Other species may insure similar effect while being more representative of the local flora. Native trees like the “algarrobo” (*Mimosa Quitensis*) or the “arrayan de Quito” (*Myrcianthes Hallii*), both declared as “emblematic specie of the city of Quito” could also insure similar effect while preserving and showing the genuine local nature within the urban area.

Based on these results an improvement strategy was defined for a potential refurbishment plan of the Lizardo Garcia Street (Table 1).

Table 1: Street improvement measures evaluated against feasibility and impact factors

FACTORS	Viability Yes = 2 Limited = 1 No = 0	Cost Low = 3 Medium = 2 High = 1	Implementation time 6 - 12 months = 3 1 - 2 years = 2 3 - 5 years = 1 5 - 10 years = 0	Impact on urban space quality From 1 to 5	Impact on thermal comfort From 1 to 5	Global evaluation
Change of pavement material	1	1	1	1	3	7
Tree planting (covering trees)	2	3	3	3	4	15
Street pedestrianisation (limited access to autos)	2	1	2	4	1	10
Introducing vegetation bands in the street and in private front gardens	2	3	2	4	3	14
Introducing water based components (rain water retention basins for example)	2	2	2	3	3	12
Generating more compact urban tissue	0	1	0	2	3	6
Eliminating massive and closed private-public separations	2	3	2	2	3	12

PLEA 2018 HONG KONG

Smart and Healthy within the 2-degree Limit

Considering factors of viability, cost, implementation time and impact potential, a set of measures was analyzed for improving thermal comfort and generating further impact on urban space quality. Assessment was realized with a group of expert using qualitative values for each measure/factor. As shown in Table 1 tree planting comes as one of the most pertinent option for street improvement in the present context. It can be combined with the other solutions judged as the most pertinent, i.e. introducing low vegetation in public and private areas, introducing water based elements and eliminating/reducing separation between private and public areas. Such pool of simple nature-based solutions would give a complete added value on urban quality and comfort in street of Quito.

5. CONCLUSION

The present study focused on the impact generated by two different street configurations in the case of Quito, the main difference being in the level of vegetation covering. For this purpose, two neighbor and similar streets, one vegetated and the other almost not, were analyzed using the ENVI-met simulation tool aiming at evaluating the outdoor comfort indexes in both cases. It demonstrated the strong impact of vegetation with 20% comfort in the case of the vegetated street. As mentioned earlier the natural context in Quito would allow quite easily to implement much more vegetation in the streets than what they have today, allowing a higher quality of life and insuring better protection for pedestrians.

Climatic data used in the present study are statistical data from past years measures realized in the available meteorological stations located in the city and solar radiation levels were calculated by the ENVI-met solution. Simulation data would gain in value if it could be compared to real measures. Hence a future study will complete the presented results with on-site measurements in both streets, on a representative time frame.

REFERENCES

Blumthaler, M., W. Ambach, and R. Ellinger (1997). Increase in solar UV radiation with altitude. *Journal of Photochemistry and Photobiology (B: Biology)* 39:130–134.

Lucas R., McMichael T., Smith W., Armstrong B., (2006). Solar Ultraviolet Radiation. Global burden of disease from solar ultraviolet radiation. *Environmental burden of disease series*, No 13, WHO

Cuidado con el sol fuerte, causa cancer de piel (25 de Agosto de 2016). *La Hora*

Ando, M., Carcavallo, R., Epstein, P.R., Haines, A., Jendritzky, G., Kalstein, L.S., McMichael, A.J., Odongo, R.A., Patz, J., Piver, W.T., Sloof, R. (1996). *Climate change and human health*, WHO

Li, X., Zhang, C., Li, W., Ricard, R., Meng, Q., Zhang, W. (2015). Assessing street-level urban greenery using Google

Street View and a modified green view index. *Urban Forestry & Urban Greening* 14 (3), 675-685

Seiferling, I., Naik, N., Ratti, C., Proulx, R. (2017). Green streets – Quantifying and mapping urban trees with street-level imagery and computer vision. *Landscape and Urban Planning* 165: 93–101

Proaño, R., & Pozo, S. (2016). DOCUMENTOS DE RESPALDO, INVESTIGACION HABITAT III. Quito, Pichincha, Ecuador.

Ponce, A. (2011). La Mariscal history of a modern neighborhood in Quito S. XX. Quito: Municipality of the Metropolitan District of Quito.

ISO 7730:2005, Ergonomics of the thermal environment – Analytical determination and interpretation of thermal comfort using calculation of the PMV and PPD indices and local thermal comfort criteria

Two-Phases Evaporative Cooling for Better Outdoor Thermal Comfort in High-Density Tropical Cities

A computational parametric study

YUAN, CHAO¹; ZHENG, KAI²; AYU, SUKMA ADELIA¹; TAN, CHUN LIANG²; WONG, NYUK HIEN²

¹Department of Architecture, National University of Singapore, Singapore

²Department of Building, National University of Singapore, Singapore

ABSTRACT: Evaporative cooling technology, specifically the use of misting fans, have been adopted in many temperate countries to attain thermal comfort among occupants. Yet, many of these studies are conducted in small scale scenarios like Wind Tunnels, and no research has been done to study the synergy between the urban canyon and these systems. This paper seeks to address the above knowledge gap using CFD simulations with input data typical of a tropical country like Singapore. Existing misting systems can be broadly categorized into non-atomizing and atomizing sprays, and this paper seeks to study the impact on cooling for both systems in terms of reduction in air temperature. The results show that the urban canyon aspect ratio plays a significant role in determining the degree of cooling and area of coverage from misting systems, where even with significantly lower water mass flow rates, an aspect ratio of 2.5 can attain the same thermal comfort as that of aspect ratio 0.4. Also, high density areas with low wind flow tend to dampen the evaporative cooling impacts.

KEYWORDS: Evaporative cooling, CFD, Parametric study

1. INTRODUCTION

Outdoor thermal discomfort is one of the key environmental issues in high density sub/tropical cities, due to local hot and humid climates and urban heat island (UHI). Taking Singapore as example, the annually-averaged daily maximum air temperature and relative humidity are 31.5 °C and 95.6% respectively in Singapore [1]. Meanwhile, the intensity of UHI (ΔT) is about 2-5 °C [2, 3]. Due to this weather conditions, Singapore has known to have a high dependency of mechanical cooling systems to enhance thermal comfort, in which the cooling is achieved by a refrigeration cycle that depends on chemical refrigerants such as Freon [4].

Compared to conventional air conditioning, evaporative equipment (e.g., misting fan) is a more environmental-friendly alternative, since only water droplet is sprayed to cool down the surrounding air through the latent heat of vaporization, rather than refrigerants. As a result, evaporative equipment would be ideal for the urban areas to improve the thermal comfort in outdoor and semi-outdoor environments. Evaporative cooling system has been applied in many cities, especially in hot and arid regions, since it can benefit the thermal comfort by both decreasing the air temperature and increasing the humidity [5, 6]. However, a successful evaporative cooling system applied in one particular location might not give the same performance within different local micro climatic conditions, which have the impact on water evaporation [7]. Therefore, it is necessary to assess the

feasibility of evaporative cooling based on the environment and climatic condition.

The investigation of two-phase flow in water spray system is challenging due to the complexity of the evaporation process involved. Three methods that researchers mostly conducted on this field are: full-scale measurement, wind-tunnel measurement, and numerical simulation. Field measurements have been broadly applied to test various physical parameters such as air temperature, humidity, solar radiation, elapsed time of spray, and nozzle characteristics [8, 9]. Field measurement includes all the complexity of the real situation, but at the same time, it also causes the difficulty to control the input boundary conditions, which are crucial in the simulation and result assessment [5, 8]. On the other hand, wind tunnel experiment offers a good control of boundary conditions, but it is considerably expensive and the number of data-collecting points is also limited. CFD simulation is a tool that has grown rapidly in the last five decades for its wide range applications in assessing urban climate and microclimate. It has also been used to evaluate water spray performance both in building and urban scale [5, 8].

From those number of studies that have been conducted to evaluate the performance of evaporative cooling, very few of them are conducted in hot and humid regions because evaporative cooling will increase the humidity ratio of the immediate environment. It is possible that the increase in humidity in such high humidity environment may offset the reduction in dry-bulb temperature thus

decrease the efficiency of evaporative cooling [4, 10]. On the other hand, there is few studies have been conducted to clarify the surrounding microclimate, which depends immediate urban context, on the efficiency of evaporative cooling. Therefore, further studies need to be done to assess the viability of the misting system for application in outdoor or semi-outdoor tropical areas.

Compared with conventional study, this study aims to clarify the coupling effects of tropical climate and high density urban context on the performance of evaporative cooling effect. The computational parametric study is the main research method in this study. First, a validation study was conducted by cross-comparing the wind tunnel experiment data and CFD simulation. Second, a parametric study was conducted to investigate the sensitivity of cooling effect to the change of several parameters, i.e. location of injections, building-height-to-street-width (H/W) ratio, relative humidity (RH), and nozzle size. The simulation results were discussed, and based on the scientific understandings from parametric study, corresponding design strategies were developed to integrate the misting spray into urban design for efficiently improve outdoor thermal comfort at high density tropical cities.

2. METHODOLOGIES

We modelled the evaporation of water droplet in a turbulent two-phase flow using commercial CFD simulation software (ANSYS Fluent) in this study. A Lagrangian-Eulerian approach was used, in which water droplets were represented in the Lagrangian frame, while the continuous airflow is represented in the Eulerian frame. These two frames are solved via two-way coupling, where each frame is solved alternately until convergence is achieved. The misting spray is modelled by Discrete Phase Model (DPM) in Fluent.

2.1 Validation

A validation study was conducted by cross comparing CFD simulation results and wind tunnel experimental data published by Sureshkumar, et al. [11]. To facilitate the cross-comparison, CFD simulation settings are the same as the ones from wind tunnel experiment, in which a hollow cone spray was used with the domain size 585 x 585 mm of cross section and 1.9 m long. It should be noted that the spray angle is not reported in the wind tunnel study, therefore we used the same spray angle in Montazeri, et al [8], in which they also used Sureshkumar wind tunnel experiment data to validate their numerical simulation. The droplet size distribution measured a mean diameter of 369 μm , where the smallest is 74 μm , largest is 518 μm . In terms of particle numbers, Montazeri, et al. [12] conducted a sensitivity analysis and confirmed that there is no further significant improvement in the

accuracy of results with more than 300 particle streams, thus this value is used in this study.

In the validation study, we tested the performance of standard K-Epsilon and Transition SST model to identify the optimal turbulence model to reproduce water evaporation. The performance of Transition SST could be better than standard K-Epsilon to reproduce a wall-bounded flow, since Transition SST combines k- ω transport equations with two other equations to deal with intermittency and transition onset criteria. Air temperature data were collected at 9 (3x3) different locations on the outlet plane as wind tunnel experiment did. The Dry Ball Temperature (DBT) from experiment data, K-Epsilon, and Transition SST (SST) results are cross-compared in Figure 1 by the deviation analysis conducted via the SPSS statistical software, where the dotted lines are representative of 5% deviation from exact fit. As shown, the k-e model tends to overestimate the outlet DBT, whereas the SST model shows a more balanced result, with points spreading out equally among the y=x line of fit. Consequently, while we can generally conclude that both the CFD results are in good agreement with experimental results, the Transition SST model has proven to be more accurate and is thus used for further studies in this paper. CFD simulation result was shown in Figure 2, which is the dispersion and size of water droplets in the computational domain.

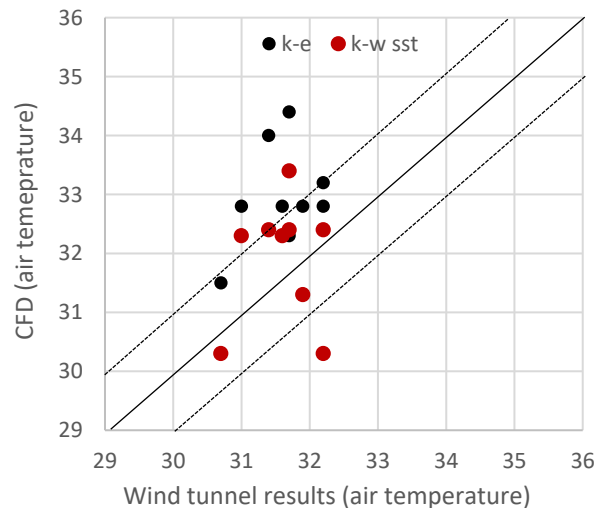


Fig 1: Cross-comparison between CFD simulation and wind tunnel experiment.

2.2 Parametric Study

A parametric study (Figure 3) was conducted to investigate the sensitivity of misting cooling effect on change of spray and microclimate characteristics, i.e. air flow and relative humidity (RH) in the urban canopy layer. Parameters include the canyon aspect ratio, RH, misting spray nozzle size. The canyon aspect ratio (H/W) is the building's height (H) to the street's width

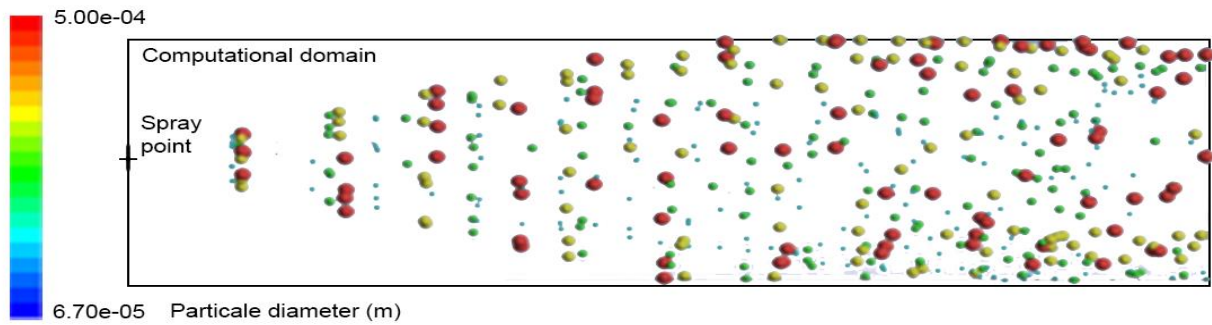


Fig. 2. Temperature contour along flow field.

(W) ratio and has been found to strongly correlate with air flow in the urban canopy layer (references). Therefore, we investigated the sensitivity of evaporative cooling on changing air flow at surrounding microclimate, by changing values of H/W. In the parametric study, the misting sources are located at the street canyons with different H/W ratios, i.e. 0.4, 1.0, 2.5 and 5.0.

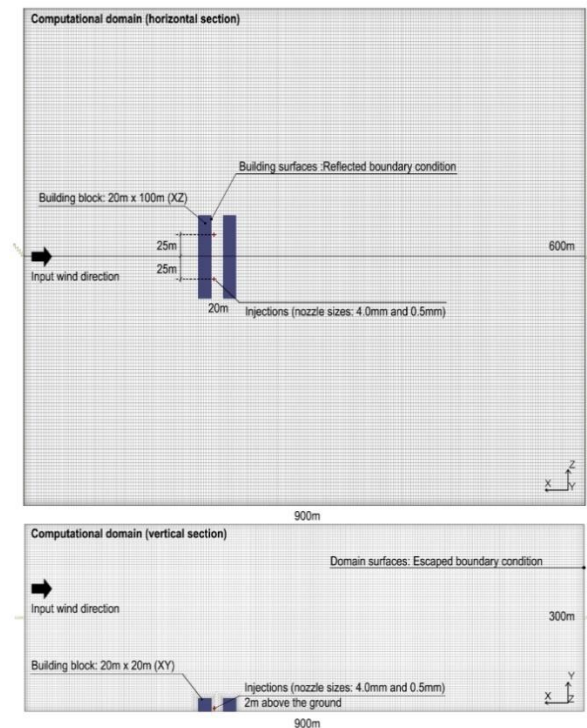


Fig 3: Modelling configurations in parametric study.

In terms of misting sprays, two main types of sprays are tested – 4.0mm nozzle and 0.5mm nozzle. Like described above, the 4mm nozzle specifications are adopted based on the previous Wind Tunnel study [6], whereas the 0.5mm nozzle is modelled based on assumed values for the droplet distribution and supplemented by data from different manufacturers. The purpose of using the smaller nozzle size is to represent a spray with much finer water droplets, that do not cause ‘wetting’ of human skin upon contact,

thus improving thermal comfort among pedestrians. The mass flow rate for the 0.5mm nozzle has been reduced significantly by 60 times magnitude than the 4mm nozzle since the mass flow rate for 4mm nozzle does not work to 0.5mm nozzle.

The relative humidity is an indicator of how much water vapor is present in the air and is thus an important consideration in employing misting systems. Theoretically, in an ideal scenario, the wet bulb depression is the limit of maximum cooling from evaporative cooling systems. This is defined as the difference between the dry-bulb and wet-bulb temperature. When the RH is 100%, the wet bulb depression is zero, and thus the potential for evaporative cooling also diminishes. The RH conditions in the previous Wind Tunnel study [6] is significantly smaller than that of a tropical country like Singapore, and thus this study used values that are more representative to tropical climate. Two main values are thus chosen – 60% and 90% RH, which fall within the range of a typical day in Singapore. The cooling potential in the 60% RH case will be more significant, but regardless, this study seeks to investigate the potential even in the more extreme case of 90% RH. The inlet air temperature remains constant through all the cases at 31°C. This translates to a Wet Bulb Depression of 6.32°C in the 60% RH case, and 1.44°C in the 90% RH case. All the parametric cases and CFD simulation settings in the parametric study are summarized in Tables 1 and 2 respectively.

Table 1 Summary of parametric cases.

Canopy Aspect Ratio*	Relative Humidity (%)		Nozzle Size (mm)		Cases	
	I	II	1	2		
A	0.4	60	1	0.5	Case A-I-1	
			2	4	Case A-I-2	
	90	1	0.5	Case A-II-1		
		2	4	Case A-II-2		
B	1.0	60	1	0.5	Case B-I-1	
			2	4	Case B-I-2	
	90	1	0.5	Case B-II-1		
		2	4	Case B-II-2		
C	2.5	I	60	1	0.5	Case C-I-1

PLEA 2018 HONG KONG

Smart and Healthy within the 2-degree Limit

				2	4	Case C-I-2
		II	90	1	0.5	Case C-II-1
				2	4	Case C-II-2
D	5.0	I	60	1	0.5	Case D-I-1
				2	4	Case D-I-2
		II	90	1	0.5	Case D-II-1
				2	4	Case D-II-2

*: Street width is 20m at all parametric cases.

Table 2 Summary of settings of evaporation modelling.

Discrete Phase Model (DPM) Iteration Interval	5
Particle time step (s)	0.01
Number of time steps	1
DPM Condition	Escape (Ground); Reflect (Buildings)
Tracking max number of steps	5000
Injection type	Hollow cone
Number of streams	300
Material	Water-liquid
Evaporating Species	H2O
Diameter Distribution	Rosin-Rammler
Water temperature (oC)	25
Velocity Magnitude (m/s)	23.24
Cone angle	20°
Outer Radius (m)	0.5 mm nozzle size: 0.00025; 4.0 mm nozzle size: 0.002
Total flow rate (kg/s)	0.5 mm nozzle size: 0.00347; 4.0 mm nozzle size: 0.2083
Min, Max, Mean Diameter (µm)	0.5mm nozzle size: 9.5, 49.9, 15.2 4.0 mm nozzle size: 74, 518, 369
Spread parameter	0.5 mm nozzle size: 1.4 4.0 mm nozzle size: 3.67
Number of diameters	20
Drag law	Spherical
Breakup model	Taylor Analogy Breakup model
Stochastic Tracking	Discrete random walk model, Random eddy lifetime
Vaporization model	Convection/Diffusion-controlled
Inlet air temperature (oC)	31

3. RESULT AND DISCUSSION

3.1 Locations of Injections

The contour of air temperature is partly presented in the Figure 4 to analyze the impact of different injection point locations (either windward or leeward face) on air temperature: Case 1 (H/W ratio= 0.4). It can be observed that the distribution of cooled air is influenced by the airflow near the injection points. Due to sharp edges and close spacing between two buildings, the airflows starts to skim over the top of the buildings and creates a lee vortex on the cavity (street)

when the wind is perpendicular to the long axis of the street [13]. The downwind, which is deflected downwards by the windward wall of the succeeding building, carries the cooled air from the water spray down near the ground and pushes it upwards when the flow reaches the leeward face on the other side. As a result, the cooled air is distributed horizontally and cover almost the entire pedestrian level. On the other hand, leeward injections create a vertical distribution of cooled air along the leeward wall surface while horizontal dispersion is quite limited. This might not be significant and helpful to the pedestrian level cooling.

3.2 Urban Density (H/W)

Figure 5 shows the impact of different urban densities, i.e. H/W, on the cooling effect. Street width (20 m), nozzle size (4 mm), injection points (leeward face) and RH (60%) were constant for all the selected cases. When the injections were located on the leeward position in Case 1 and 2 that represent low-mid density, the cooled air were indeed moving upwards influenced by the upstream near leeward surface (Figure 4, left) however in Case 3 and 4 that represent mid-high density the cooling effect was dispersed in horizontal manner instead (Figure 5). Lower temperature were found near the ground surface and distributed uniformly due to the decrease of vertical streams, increase of horizontal airflows and the buoyancy within the street canyon. It shows that in high dense areas, injection points can be on either side of the street, i.e. the discrepancies between injections from windward or leeward face becomes less significant.

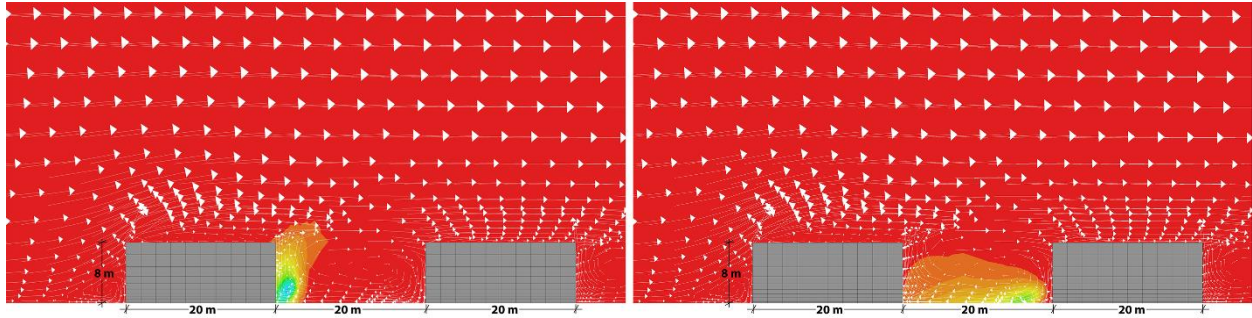


Fig. 4. Contour of air temperature on leeward and windward injections in Cases 1 with the same nozzle size (4mm) and RH (60%).

In high dense area, as represented by Case 3 and 4 (Figure 5), the effect of vertical airflows deflected from the top of the buildings becomes very weak, due to the larger frontal area density. In this condition, the wind deflected from the side of the building can still penetrate from the both edges of the street canyon on

condition, the temperature reduction can only reach about 1°C. The area of coverage in low humidity condition is also significantly larger than in high humidity condition.

This result indicates that in high humidity condition, there is less evaporation process happening due to the

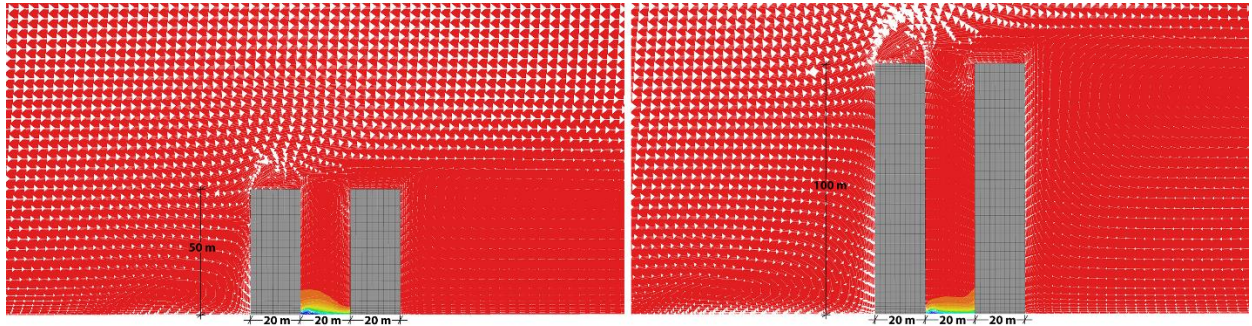


Fig. 5. Contour of air temperature on leeward injections in Cases 3 and 4 with the same nozzle size (4mm) and RH (60%).

the pedestrian level and influence the cooling effect. This result is consistent with Yuan et al. [14], where the mean building height determines the z_0+z_d value in high-density urban areas, while urban ventilation performance from the pedestrian perspective mostly depends on the pedestrian-level building porosity.

high concentration of water vapor in the air. When the water sprayed out from the nozzle, the heat in the air get absorbed by the water in order to transform from water droplets into vapor and thus reduce the air temperature of the surrounding area. The more and faster the water evaporates, the more heat taken away from the surrounding air and the more the temperature drops.

3.3 Inlet air humidity ratio (ω) (Relative humidity)

The impact of humidity level on evaporative cooling in Case 1 (windward injection and 4 mm nozzle size) on air temperature is shown as Figure 6 (left RH: 60%; right RH: 90%). When the humidity is lower (60%), air temperature reduction can reach up to 2°C, ranging between 29°C and 31°C. Whereas in high humidity

4. IMPLEMENTATION

Based on the above discussion, the dispersion of evaporative cooling effect is significantly affected by airflows near the injection points. Therefore, the distribution of evaporative cooling could be different

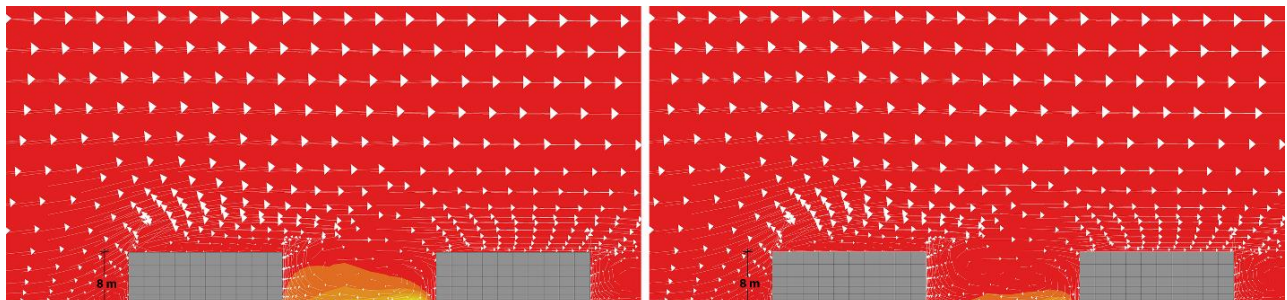


Fig. 6. Contour of air temperature on Case 1 (windward injections) with different relative humidity values.

PLEA 2018 HONG KONG

Smart and Healthy within the 2-degree Limit

at high, medium and low density urban areas. Location of injections then can be determined by the H/W ratio, windward wall is the suggested location in low density areas, meanwhile in high density areas injection can be located on either windward or leeward wall. The magnitude, however, would depend on other factors, such as nozzle size and relative humidity, which has been discussed in the full journal version. Leeward injection on low density areas is might be less impactful in reducing the air temperature in the street canyon, but it can be considered to be implemented in some building typologies, such as housing estates with porous corridors and tertiary schools with open-air classrooms, that can be explored further in future study. Based on the above discussion, the design strategies are summarized in Figure 7.

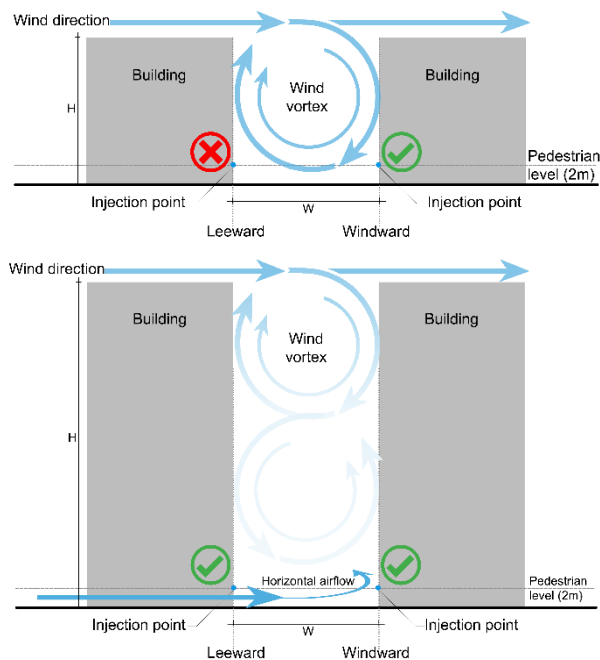


Fig. 7: Vertical section shows suggested injection point location, low-dense buildings (above) and high-dense buildings (below).

ACKNOWLEDGEMENT

This research is supported by Ministry of Education, Singapore, ACADEMIC RESEARCH FUND TIER 1 (grant no. R-295-000-140-114).

REFERENCES

Climate of Singapore. Meteorological Service Singapore. Retrieved from <http://www.weather.gov.sg/climate-climate-of-singapore/>, 2010.

Roth, M., & Chow, T. L., A historical review and assessment of urban heat island research in Singapore, Singapore Journal of Tropical Geography 2012, 33: 381-397.

Wong, N. H. , Urban heat island research: challenges and potential, Frontiers of Architectural Research 2016, 5:276-278.

Wong, N. H., & Chong, A. Z. M., Performance evaluation of misting fans in hot and humid climate. Building and Environment 2010, 45(12): 2666-2678.

Montazeri, H., Blocken, B., & Hensen, J. L. M., CFD analysis of the impact of physical parameters on evaporative cooling by a mist spray system. Applied Thermal Engineering 2015, 75(1): 608-622.

Sureshkumar, R., Kale, S. R., & Dhar, P. L., Heat and mass transfer processes between a water spray and ambient air - I. Experimental Data. Applied Thermal Engineering 2008, 28: 349-360.

El-Refaie, M. F., & Kaseb, S., Speculation in the feasibility of evaporative cooling. Building and Environment 2009, 44(4): 826-838.

Montazeri, H., Toparlar, Y., Blocken, B., & Hensen, J. L. M., Simulating the cooling effects of water spray systems in urban landscapes: A computational fluid dynamics study in Rotterdam, The Netherlands. Landscape and Urban Planning 2017, 159: 85-100.

Wong, N. H., & Chong, A., Z. M., Performance evaluation of misting fans in hot and humid climate. Building and Environment 2010, 45: 2666-2678.

Yu, F. W., & Chan, K. T., Application of direct evaporative coolers for improving the energy efficiency of air-cooled chillers. Solar Energy Engineering 2005, 127: 430-433.

Sureshkumar, R., Kale, S. R., & Dhar, P. L., Heat and mass transfer processes between a water spray and ambient air - II. Simulations. Applied thermal engineering 2008, 28:361-371.

Montazeri, H. H., Blocken, B. J. E. B., & Hensen, J. L. M. J., Evaporative cooling by water spray systems : CFD simulation, experimental validation and sensitivity analysis. Building and Environment 2015, 83: 129-141.

Oke, T. R., Boundary layer climates (²nd ed.). London: Methuen & Co, 1987.

Yuan, C., & Ng, E., Building porosity for better urban ventilation in high-density cities - A computational parametric study. Building and Environment 2012, 50: 176-189.

CFD Analysis on Irregular Breezeway Patterns in High-Density Asian Urban Areas

YUEYANG HE¹, ABEL TABLADA¹, NYUK HIEN WONG²

¹Department of Architecture, National University of Singapore, Singapore, Singapore

²Department of Building, National University of Singapore, Singapore, Singapore

ABSTRACT: In high-density urban areas in Asia, pedestrian-level wind environment is highly-related to human health and thermal comfort. However, it is still uncertain how irregular breezeways should be connected and oriented for optimizing the pedestrian-level wind velocity ratio (VR_w). This paper used computational fluid dynamics (CFD) simulations to compare VR_w in regular and irregular breezeway patterns in four actual high-density urban areas of Hong Kong, Singapore and Tokyo. Sixteen wind directions were considered for each urban area. The simulation method was validated by the wind tunnel experimental data of an actual urban area in Japan. Three indices, road density (RD), irregularity ratio (IR) and open space ratio (OSR), were proposed to estimate VR_w by applying regression analysis. The paper suggests the following results: 1) urban patterns with lower RD and higher OSR have better ventilation regardless of wind directions; 2) urban patterns with higher IR tends to benefit the airflow penetration in the deep urban area; 3) OSR ($R^2 = 0.64$), as a single index, can most effectively estimate VR_w ; 4) IR together with OSR or RD ($R^2 > 0.85$) can more effectively estimate VR_w . The proposed indices, especially IR and RD, may help planners to improve road pattern design for obtaining better ventilation.

KEYWORDS: Irregular breezeway pattern, Pedestrian-level ventilation, Asian cities, Urban planning

1. INTRODUCTION

In high-density urban areas in Asia, pedestrian-level wind environment is highly-related to human health and thermal comfort, while it is prone to impermeable urban arrangements. The porosity of an area can be increased by simply introducing more open-space for breezeways, such as streets and linked plazas [1]. However, it is still necessary to investigate how these breezeways, especially the irregular ones, should be allocated and oriented for optimizing the overall outdoor ventilation. Compared with regular breezeway patterns, where breezeways are orthogonal, irregular breezeway patterns are also commonly seen in actual Asian urban areas while they obtain much less studies [2-3]. In addition, there are insufficient effective descriptors to account for the impact of irregular urban morphological features on outdoor ventilation.

Therefore, to extend the existing knowledge, this paper focuses on two objectives:

To compare pedestrian-level wind conditions between irregular and regular breezeway patterns

To propose practical indices for assessing the impact of irregular breezeway patterns on wind velocity ratio at the pedestrian level

This research is expected to be significant and practical for urban planning and design in high-density urban areas considering that the ground open space in these areas is usually very limited and has to be efficiently used.

2. METHODOLOGY

This study was conducted by computational fluid dynamics (CFD) simulations. The computational settings followed the recommendations given by AIJ guidelines [4] and validated by wind tunnel experimental data.

2.1 Urban patterns and indices calculation

Four actual high-density urban areas were selected from the downtown in Hong Kong, Singapore and Tokyo. As shown in Figure 1, the cases in Hong Kong represent an old-style urban pattern, which has been developed since the early twentieth century. This urban pattern consists of a fine road network and small-sized plots with mixed-functional buildings; the cases in Singapore and Tokyo represent a contemporary urban pattern in central business districts. This urban pattern is formed by a coarser road network and larger plots with bulky commercial buildings. To define the road density, or in other words, the degree of urban fragmentation, the following equation is used:

$$\text{Road density (RD)} = L_T / A_T \quad (1)$$

where L_T - total length of road centerlines;

A_T - total area of the site.

Besides, in each abovementioned urban pattern, the cases are further categorized into regular and irregular patterns. In this study, the regular pattern refers to the pattern mainly formed by orthogonal roads, while the irregular pattern has a larger portion of non-

PLEA 2018 HONG KONG

Smart and Healthy within the 2-degree Limit

orthogonal roads with oblique intersection angle(s) (i.e. the angles between the road centerlines at the intersection point).

To define the degree of urban irregularity, the following equation is used:

$$\text{Irregularity ratio (IR)} = N_i / N_t \quad (2)$$

where N_i - number of irregular road intersections;
 N_t - total number of road intersections.

Finally, in addition to the descriptors of breezeway patterns, we also indicate the pedestrian-level urban permeability by the open space ratio, which has been reported to have fairly good correlation with the wind velocity ratio [5]. The equation is as follow:

$$\text{Open space ratio (OSR)} = A_o / A_T \quad (3)$$

where A_o - total area without building coverage.

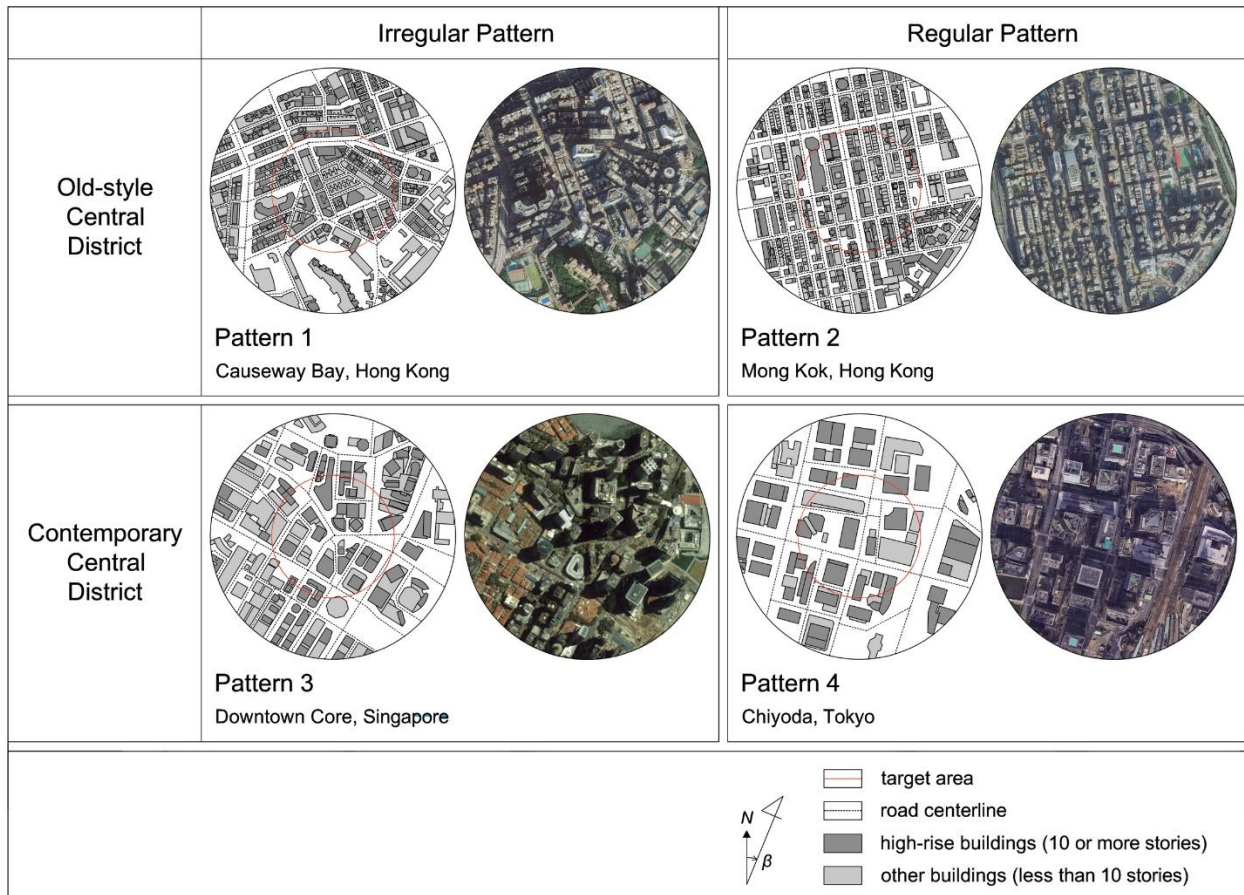


Figure 1: Model and actual morphologies of the selected urban areas (source: google earth).

PLEA 2018 HONG KONG

Smart and Healthy within the 2-degree Limit

The three indices were calculated at the target area (radius = 200m), which is at the center of the whole urban area (radius = 400m), as shown in Figure 1. The calculation results of the indices are summarized in Table 1.

2.2 Computational settings and validation

The CFD simulations were conducted by scSTREAM (version 13). The same inlet wind profiles were set to every case for cross-comparison.

Table 1: Calculation results of the three indices (RD: road density; IR: irregularity ratio; and OSR: open space ratio)

	RD (km/km ²)	IR (%)	OSR (%)
Pattern 1	26.8	37.5	47.9
Pattern 2	24.0	0	52.3
Pattern 3	19.1	50.0	58.3
Pattern 4	13.7	11.1	58.5

These wind profiles were estimated by logarithmic equations with Singapore's long-term average wind speed (2.65m/s) at Changi climate station [6] and the average terrain roughness (1m) of Singapore's urban areas.

To comprehensively study the urban morphologies, sixteen inlet wind directions were considered for each case in CFD simulations. Amongst these wind directions, two representative wind directions were highlighted as following:

In Hong Kong, 225° and 67.5° were used to represent prevailing wind direction in summer and winter, referring to the annual statistics of Waglan Island weather station [7];

In Singapore, 180° and 22.5° were used to represent prevailing wind direction in southwest and northeast monsoon, referring to the annual statistics of Changi climate station [6];

In Tokyo, 180° and 0° were used to represent prevailing wind direction in summer and winter, referring to the annual statistics of Tokyo international airport [8].

Since the above stations are surrounded by flat terrains, the obtained wind directions can be assumed to be the wind directions at the gradient height of the city center during the same seasons.

Besides, two overlay mesh blocks were applied for the target area and the whole computational domain, respectively. Finer meshes were arranged in the inner block to ensure at least ten cells covering each major breezeway at the target area. Standard k-ε and QUICK were used as the turbulence model and advection scheme.

The simulation method was validated by the wind tunnel experimental data of an actual urban area in Japan [9]. As shown in Figure 2(a), this area has lower building heights than those in the four cases in this study. However, considering that the area's pedestrian-level building coverage is as similar as

those in the studied cases, we decided to use its experimental data for CFD validation.

3. RESULTS AND DISCUSSION

Wind velocities at 2m's height above the ground were obtained in the CFD simulations. The measuring positions are along the road centerlines at the target area with an interval of around 20m. For CFD validation, wind velocities were directly used for comparison. For the rest of the cases, wind velocity ratio was used as the indicator of pedestrian-level ventilation. The equation is as follow:

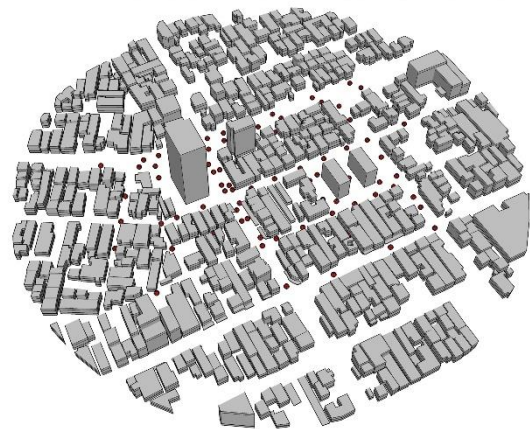
$$\text{Wind Velocity Ratio (VR}_w\text{)} = U_p / U_\infty \quad (4)$$

where U_p - wind velocity at pedestrian-level;

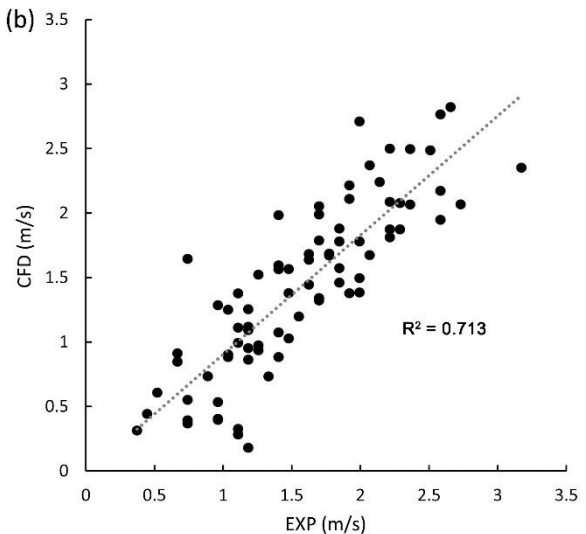
U_∞ - wind velocity at gradient height.

In this study, U_∞ is constantly set to 6 m/s, which is the wind velocity at 550m of the urban canopy layer height. Since U_∞ is not affected by the ground roughness, we may assume that VR_w is not affected by the surrounding of the target area and only represents the ventilation condition of the local area [1].

(a)



(b)



PLEA 2018 HONG KONG

Smart and Healthy within the 2-degree Limit

Figure 2: (a) The urban model and measuring points for CFD validation; and (b) correlation between simulation (CFD) and experimental (EXP) results at all measuring points.

3.1 Validation result

The experimental result from the north wind direction was used for validating the simulation result. Data from eighty measuring points at pedestrian level, as shown in Figure 2(a), were compared with the simulation result of the same urban model.

As presented in Figure 2(b), a good correlation is observed, although this correlation is worse than the one obtained in the validation with a single building [2]. Given the complicated morphologies in an actual and high-density urban area, the CFD simulation approach proposed in this study can be considered as reliable for wind velocity estimation. Therefore, this method will be used for the rest of simulation jobs in the study.

3.2 CFD results

The pedestrian-level VR_W of four urban areas in sixteen wind directions are shown in Figure 3. Overall, compared with the old-style central districts, higher VR_W is observed in the contemporary central districts, where open space coverages are higher and road networks are coarser. It can be also seen that VR_W in the irregular patterns are larger than the regular patterns. This phenomenon is more obviously seen in the old-style central districts. We may also point out

that wind direction has evident impacts on the airflow patterns. This phenomenon is out of the study scope of the current paper, since the proposed indices are non-directional. However, the impact of wind direction will be addressed in subsequent studies.

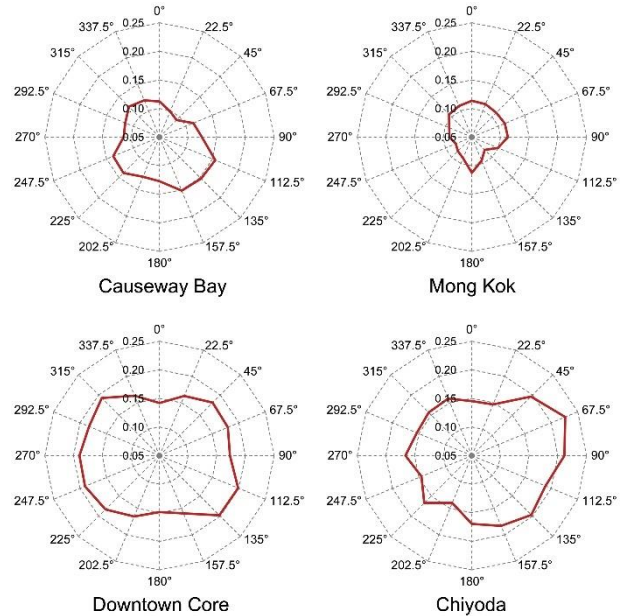


Figure 3: VR_W of 16 wind directions (north: 0°) at the pedestrian-level (2m above the ground).

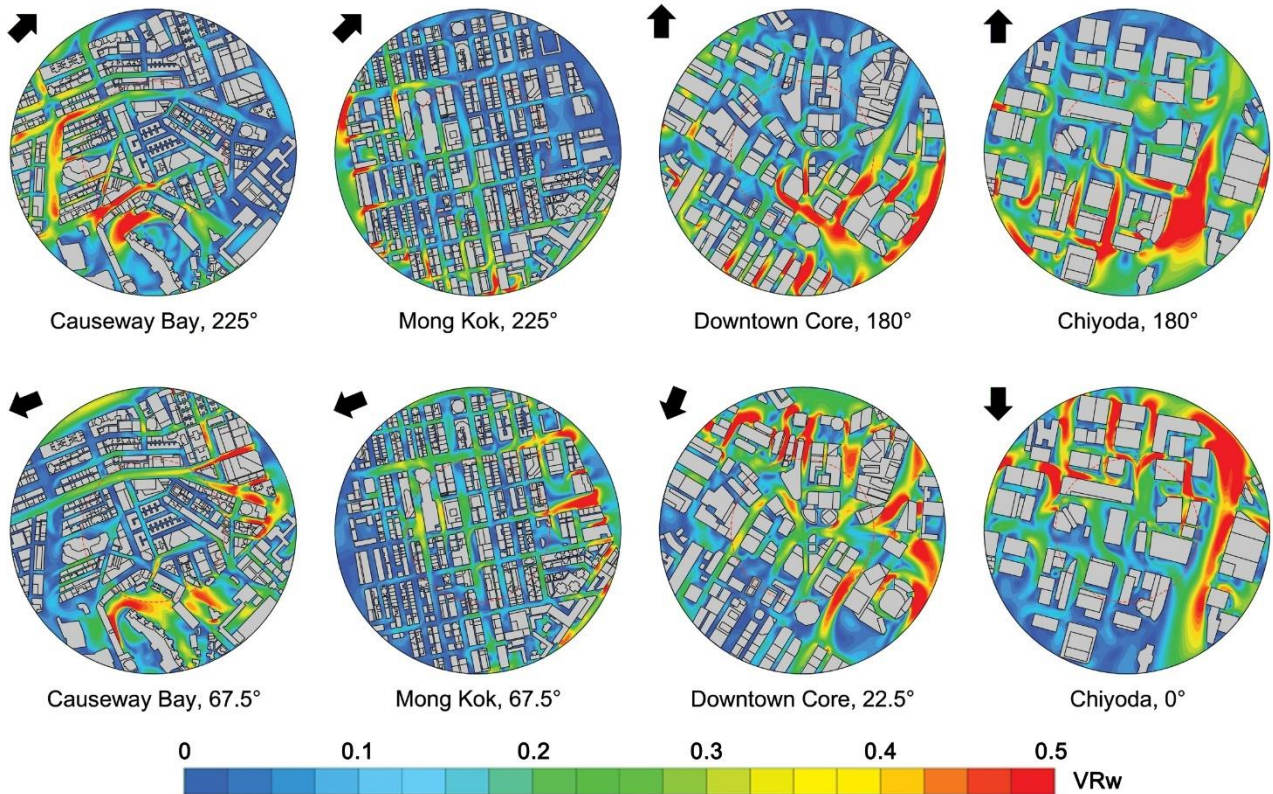


Figure 4: Contours of VR_W at the pedestrian-level (2m above the ground).

PLEA 2018 HONG KONG

Smart and Healthy within the 2-degree Limit

Numerical contours of VR_W in two prevailing wind directions are compared across four urban areas in Figure 4. As can be seen in the CFD results, urban patterns with higher RD and lower OSR obviously have worse ventilation regardless of wind directions. This phenomenon is more evident in regular patterns (i.e. pattern 2 versus pattern 4). There are two reasons. Firstly, compared with pattern 4, pattern 2 has a larger number of straight streets with smaller widths. This means that the incoming airflow in these streets encountered more viscous force of the building walls, hence dropping to a lower velocity in the deep urban area. Secondly, compared with pattern 4, the major streets in pattern 2 are oriented to the prevailing wind directions with larger angles. As a result, the incoming airflow encountered larger form drag of the longer building cross-sections.

Besides, urban patterns with higher IR tends to benefit the airflow penetration in the deep urban area. For example, compared with pattern 4 in 0° , pattern 3 in 22.5° generated significantly higher VR_W at the target area. This result is consistent with the finding of a previous study [10], where the authors explained that wind can easily flow into irregular street patterns because of the horizontal momentum.

3.3 Regression results of indices

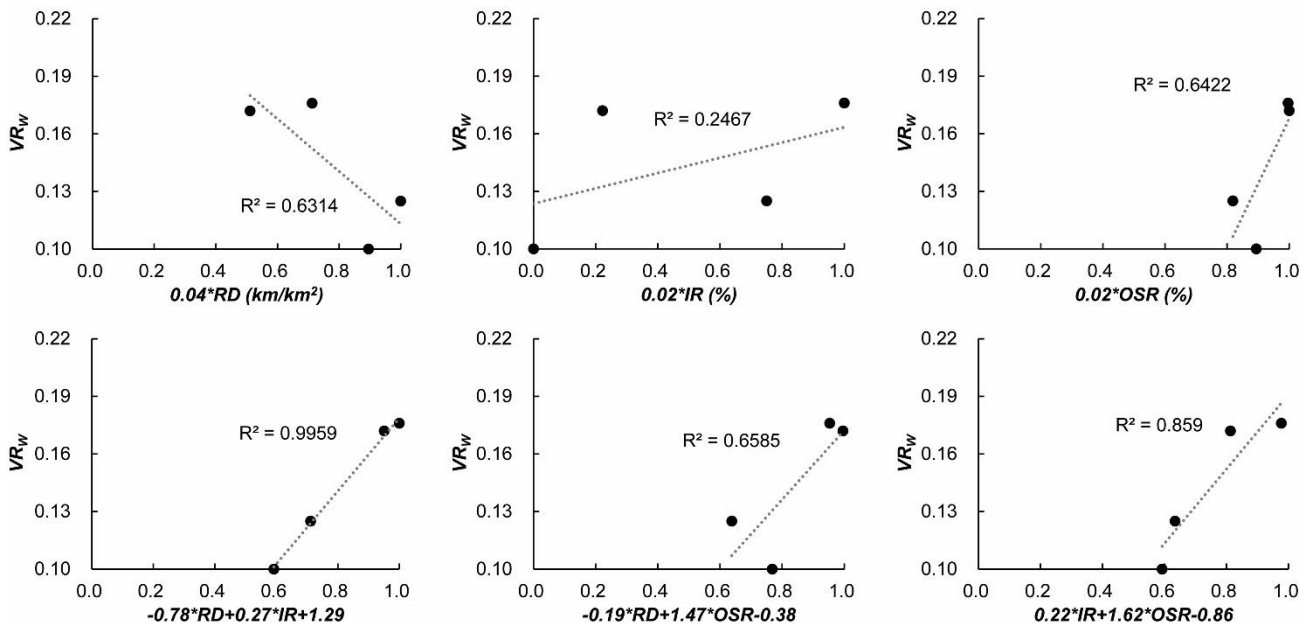


Figure 5: Regression results between wind velocity ratio (VR_W) and the three indices (RD , IR , and OSR).

To improve the regression result, we further conduct a regression analysis with two indices. The normalized result is shown in the second row of Figure 4. It can be seen that by including IR in the regression model, substantial improvement is obtained in the estimation of both OSR and RD ($R^2 > 0.85$). This result suggests

A regression analysis was conducted between the simulation results of VR_W , and the three proposed indices. Since the proposed indices are non-directional, we represent the ventilation conditions for each urban area by averaging VR_W of sixteen wind directions, which is a comprehensive index to estimate the ventilation condition of a site, as suggested by previous studies [11-12].

The normalized regression result with each single index is shown in the first row of Figure 5. As to be seen, OSR has the highest correlation ($R^2 = 0.6422$) with VR_W amongst the three indices. This result is consistent with the previous finding [5], where the author further suggests that OSR has even higher correlation with the pedestrian wind velocity, if the calculated open space excludes roads and areas around buildings. This result suggests that OSR , as a single index, can most effectively estimate the pedestrian-level ventilation. Besides, RD can also estimate VR_W at a good agreement ($R^2 = 0.6314$). This is because in high-density urban development, the road density is usually negatively correlated to the open space ratio due to the similar road widths. Therefore, RD can be roughly used to indicate the urban permeability. However, OSR and RD cannot reveal the impact of urban irregularity, which, as shown in the simulation results, has considerable impact.

that IR is an effective complement in pedestrian-level wind prediction. Although IR itself has weak correlation with VR_W because of the strong interference of urban permeability, it can help the index, such as RD , to better describe the urban morphologies. More importantly, IR can give

PLEA 2018 HONG KONG

Smart and Healthy within the 2-degree Limit

additional information for supporting urban design and planning. The current result further indicates that the pedestrian-level ventilation can be improved by introducing more oblique road intersections even though the building density is controlled.

4. CONCLUSION

This paper used CFD simulations to compare the pedestrian-level wind velocity ratio (VR_w) in regular and irregular breezeway patterns in four actual high-density urban areas of Hong Kong, Singapore and Tokyo. The simulation method was validated by wind tunnel experimental data of an actual urban area in Japan. Three indices, road density (RD), irregularity ratio (IR) and open space ratio (OSR) were proposed to estimate VR_w in the regression analysis. The major findings are summarized as follow:

Urban patterns with lower RD and higher OSR have better ventilation regardless of wind directions.

Urban patterns with higher IR tend to benefit the airflow penetration in the deep urban area.

OSR ($R^2 = 0.64$), as a single index, can most effectively estimate VR_w .

IR together with OSR or RD ($R^2 > 0.85$) can more effectively estimate VR_w .

The final results of this study indicate to what extent the irregular breezeway patterns influence the outdoor ventilation conditions in high-density urban areas. These results are particularly important for suggesting proper strategies related to the linkages and orientation of street canyons and open-spaces in new urban developments. They are also useful for renewing the outdoor wind environments in old high-density urban areas, where street patterns are usually irregular. We also try to explore practical and simple indices to help planners assess their designs. We believe that, urban streets and open-space should be designed and planed by striking a balance between traditional demands (i.e. traffic, human activity and landscape) and advanced demands (i.e. environment and human health). To achieve this goal, the relations between pedestrian-level wind velocity and the design parameters of breezeways should be better understood.

REFERENCES

1. Ng, E., 2009. Policies and technical guidelines for urban planning of high-density cities – air ventilation assessment (AVA) of Hong Kong. *Build. Environ.* 44 (7), 1478–1488.
2. He, Y., Tablada, A., & Wong, N. H., 2018. Effects of non-uniform and orthogonal breezeway networks on pedestrian ventilation in Singapore's high-density urban environments. *Urban Climate.* 24, 460-484.
3. He, Y., Tablada, A., & Wong, N. H., 2017. The influence of angular road orientations on high-density urban ventilation at pedestrian level. The 33rd International Conference on Passive and Low Energy Architecture, Edinburgh, UK.
4. Tominaga, Y., Mochida, A., Yoshie, R., Kataoka, H., Nozu, T., Yoshikawa, M., Shirasawa, T., 2008. AIJ guidelines for practical applications of CFD to pedestrian wind environment around buildings. *J. Wind Eng. Ind. Aerodyn.* 96 (10), 1749–1761.
5. Takebayashi H., 2015. Evaluation of wind environment in street canyon for use in urban climate map. *J. Environ. Eng.* 80, 795-801.
6. Meteorological Service Singapore, Singapore government, 2017. Climate of Singapore. Retrieved from <http://www.weather.gov.sg/climate-climate-of-singapore/>.
7. Hong Kong Observatory, 2016. Summary of meteorological and tidal observations in Hong Kong 2016. Retrieved from <http://www.weather.gov.hk/publica/smo/smo2016.pdf>.
8. Japan Meteorological Agency, 2015. Aerodrome climatological tables (2015 edition). Retrieved from http://www.data.jma.go.jp/obd/stats/koku/kikohyo/rjtt_e.pdf.
9. Tominaga, Y., Yoshie, R., Mochida, A., Kataoka, H., Harimoto, K., Nozu, T., 2005. Cross Comparisons of CFD Prediction for Wind Environment at Pedestrian Level around Buildings. Comparison of Results for Flowfield around Building Complex in Actual Urban Area. The Sixth Asia-Pacific Conference on Wind Engineering, Seoul, Korea, September 12-14, 2005.
10. Yuan, C., Norford, L., Britter, R., Ng, E., 2016. A modelling-mapping approach for fine-scale assessment of pedestrian-level wind in high-density cities. *Build. Environ.* 97, 152-165.
11. Kubota, T., Miura, M., Tominaga, Y., Mochida, A., 2008. Wind tunnel tests on the relationship between building density and pedestrian-level wind velocity: development of guidelines for realizing acceptable wind environment in residential neighborhoods. *Build. Environ.* 43 (10), 1699–1708.
12. Ng, E., Yuan, C., Chen, L., Ren, C., Fung, J.C., 2011. Improving the wind environment in high-density cities by understanding urban morphology and surface roughness: a study in Hong Kong. *Landsc. Urban Plan.* 101 (1), 59–74.

Integration of LCA tools in BIM toward a regenerative design.

TIZIANO DALLA MORA¹, ERIKA BOLZONELLO¹, FABIO PERON¹, ANTONIO CARBONARI¹

¹University Iuav of Venice, Italy

ABSTRACT: In the case of regenerative processes, design can receive significant benefits from information that can be obtained by applying the life cycle assessment methodology. The LCA (life cycle assessment) approach can be implemented both for a single building material and for the whole building. An effective and efficient real application of this methodology requires the integration of LCA databases and analysis routines to the simulation tools (Building Energy Simulation, Building Information Modelling). The integration of LCA tool significantly impacts the design efficacy especially in reducing environmental impact of the construction industry. This paper reviews the integrated LCA tools in simulation software currently available for BIM platforms and will explore the possibilities given to restorative design informed by LCA analysis, through a test on two construction typologies for a case study.

KEYWORD: LCA, regenerative, BIM

1. INTRODUCTION

This paper presents a preliminary overview of interoperability and application of LCA and BIM software within the activities of the EU-funded RESTORE (REthinking Sustainability TOwards a Regenerative Economy) COST Action [1]: this project aims to affect a paradigm shift towards restorative sustainability for new and existing buildings across Europe.

The literature on regenerative design defines 'sustainability' as a transitional stage between 'green design' on the one hand, and 'regenerative design' on the other [2,3]. The paradigm shift envisioned by the RESTORE project is aimed to move from the 'green design', which is essentially focused on doing 'less bad', and the 'sustainability', which implicates a 'neutral' state where the ideal performance is 'zero' (meaning nearly zero energy and low emissions building), towards an approach that permits regenerative capabilities to evolve, a net-positive restorative sustainability to incrementally do 'more good' [4,5].

The main challenges for implementing regenerative development are focused on the current lack of an integrated approach and on the scarcity of comprehensive examples providing quantifiable evidence of the benefits of regenerative built environments. In the long term, a regenerative approach to the built environment that integrates with ecosystems will increase the chances of a continuous suitable environment for humans. Although this may be difficult to test currently, development that aims to repair and integrate with ecosystems is more conducive to positive healthy outcomes than that which only slows the rate of degradation [6].

Although, the real strategies and design tools for evaluating the environmental impacts are not yet standardized for the regenerative design and

developed for Regenerative design. The growing sensibility to the ecological aspects and the emergency due to the economic crisis pushed the architectural, engineering and construction communities to realize a negative environmental impact of the built environment. Buildings are responsible for 40% of carbon emission, 14% of water consumption and 60% of waste production worldwide [7]. According to the European Union Directive, land is the scarcest resource on earth, making land development one of the fundamental components in effective sustainable building practice [8,9]. Over 50% of the world's population live in cities. Environmental damage caused by urban sprawl and building construction is severe and we are developing building construction and human facilities at a speed that the earth cannot compensate [10]. Buildings affect ecosystems in different ways and their extension increasingly overtake agricultural lands and wetlands or bodies of water compromising existing wildlife. Energy is the building resource that has gained the most attention within the built environment research community. Moreover, building materials are another limited resource within a building's life cycle [6].

Regenerative design could be one of the most important strategies in reducing the environmental impacts of the building sector. There are several tools and methods to help the implementation of sustainable development into the built environment. Life Cycle Assessment (LCA) is considered as a complete method to assess the sustainability of a building over its life cycle; and has growing importance in the scientific community. Several studies highlight the importance of improving and simplifying LCA application to buildings. Thus, it is recognized that the integration of BIM (Building Information Modeling) with LCA can reduce and optimize LCA application [11].

PLEA 2018 HONG KONG

Smart and Healthy within the 2-degree Limit

Regenerative theories propose to examine the historical, cultural and technological nuances, beside the elaboration of identification signs, focusing on design strategies linked to the place, the context and communities [12].

Since the design stage does not allow to make predictions on future regenerative performances of the building, the regenerative design involves the stakeholders of the project since from the very beginning. The proper way to implement a regenerative intervention suggests an alternative to change the present model of intervention on the context, advancing connections among constituent elements, coevolution of man and nature and the needs for adaptation and flexibility more than the economic income.

The Regenerative design process can also receive significant benefits from information and data given by the application of the LCA methodology toward the construction process [13]. LCA is a tool already used to analyse the environmental impacts of a product, an activity or a process along all the phases of the life cycle, through the quantification of the use of resources ("inputs" such as energy, raw materials, water) and emissions into the environment ("emissions" into the air, in water and soil), proposing also the best solution to be adopted in terms of environmental impacts.

In this context, the role of BIM appears as a building tool that facilitates the application of LCA in the construction sector: the use of BIM at the early stage of designing construction projects empowers the decision-making process in the construction sector [14]. BIM provides designers, architects, and engineers with data required to evaluate energy consumption and environmental impacts in the construction sector throughout the entire lifecycle of building materials. It can be really considered that BIM harmonizes both the information of building materials and the evaluation of their environmental impacts [15].

2. METHODOLOGY

This paper analyses how could be integrated BIM and LCA processes in a practical way for evaluating the environmental impacts of building materials in the construction sector.

The first step of the research is focused on the investigation of the state-of-the-art about the more used available LCA software: the analysis was developed according to the typology of tools (stand alone, plugin, suite tool) and their main characteristic in terms of database, products, data availability, obtaining the selection of: Caala [16], One click LCA [17], Primus LCA [18], SIMAPRO [19], Open LCA [20], Tally [21], Impact Compliant [22], Umberto Lca Soft [23], Gabi Soft [24].

The second step is to select the tools that could be implemented on BIM software: in this specific case Autodesk® Revit® [25] is analysed to conduct the 3D modelling and to apply the inventory database of building materials, in relation to the characteristic of the local climate, the building site and the local material production and supply.

After the quantification of building materials in the construction components, the environmental impacts are evaluated and discussed by a comparison of database and solutions.

Among the listed tools, this study focuses on the evaluation on those with a direct connection or plugin for BIM models: Tally and One click LCA.

Tally is a plugin application for Autodesk® Revit® software, developed by Kieran Timberlake and PE International, that allows users to quantify the environmental impact of building materials for whole building analysis as well as comparative analyses of design options.

This study adopted the educational licence, Version 2017.06.15.01 (6/18/2017): Tally analysis accounts for the full cradle-to-grave life cycle according to the EN 15978 and utilizes a custom-designed LCA database developed in GaBi 6 and using GaBi databases, consistent with LCA standards ISO 14040-14044.

One click LCA, developed by Bionova®, is a Life-Cycle Assessment and Life-Cycle Costing (LCC) software that allows to design greener building, to create Environmental Product Declarations (EPD) for building materials and to earn valuable certification credits, including LEED v4's MRc1 Building Life-Cycle Impact Reduction, BREEAM Mat 01 Life cycle impacts.

The tool works as a plugin by importing data from Revit or BIM model, gbXML Energy model, Excel, or use the manual import within the cloud software itself and obtain a ready-made report.

This study adopted the educational licence, Version 1.0.2 (13/10/2017): the tool is also third-party verified for EN 15978, ISO 21931-1, ISO 21929-1 and for input data for ISO 14040/44 and EN 15804 standards; One click LCA disposes of an own database for generic construction materials and a wide list of available databases, among the most used in the world (such as Environdec and other national version of EPD system). Other software have been tested and evaluated, but their application is not proposed in this study because the absence of a direct link or plugin with BIM model: so data, values and geometry need to be implemented as spreadsheet and then inserted into the LCA tools.

3. APPLICATION - CASE STUDY

Further step proposed in this paper is a test on different tools and database using the same case study for comparing the results.

PLEA 2018 HONG KONG

Smart and Healthy within the 2-degree Limit

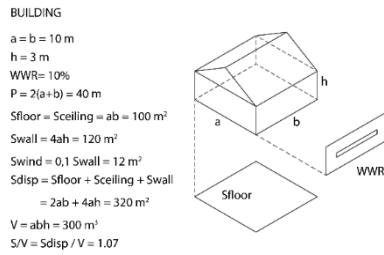


Figure 67: Case study characteristics

The proposed case study (Figure 67) concerns a small residential building, which could be built with two different kind of structure: a masonry envelope and a wooden one. The envelope energy performances were defined in the technological and thermal characteristics according to the Italian law D.M. 26/06/2015 [26]. The building is located in Venice area (Italian Climate Zone E), according to the Italian law (Table 6).

Table 6: Thermal Transmittance for each technological component of the two different structures of case study.

	Thermal Transmittance U [$Wm^{-2}K^{-1}$]	
	Case 1, masonry building	Case 2, wooden building
Basement	0.21	0.21
Wall	0.17	0.21
Flat Floor	0.18	0.19
Roof	0.19	0.18
Window	0.99	0.99

4. SYSTEM BOUNDARIES AND DELIMITATIONS

The analysis accounts for a full Cradle-to-Grave life cycle of the design process, including material manufacturing, maintenance and replacement, eventual end-of-life. The lifespan is considered for 50 years.

The two buildings are described with two different construction typologies, so the environmental assessment recognizes Revit categories, technological components, materials and energy used across all life cycle stages. The Life Cycle Stages are presented and analysed according to EN 15804 and EN 15978, as described in Table 7.

Table 7: Life Cycle Stages according to EN 15804.

Life Cycle Stages	Sections	Data references
Product Stage	A1: Raw material supply	Quantity Take-off by Revit abacus of materials and integration with database, Gabi US (Tally) and Ecoinvent (One click LCA).
	A2: Transport	
	A3: Manufacturing	
	A4: Transport to building site	Stage not evaluated

Life Cycle Stages	Sections	Data references
Construction Process Stage	A5: Installation into building	Data taken by database, Gabi (Tally) and Ecoinvent (One click LCA)
Use Stage	B1: Use / application	Stage not evaluated
	B2: Maintenance	
	B3: Repair	
	B4: Replacement	
End of Life Stage	C1: Deconstruction / demolition	Calculation database, Gabi (Tally) and Ecoinvent (One click LCA)
	C2: Transport	
	C3: Waste processing	
	C4: Disposal	
Benefit and Loads beyond the System Boundary	D: Recycling	

5. ASSESSMENT RESULTS AND DISCUSSION

In order to understand the role of BIM and LCA integration in the evaluation of environmental impacts of building materials, this research a preliminary application of LCA tools on Autodesk Revit that aims to calculate the environmental impacts of the selected building materials.

Both Tally and One click LCA allow to investigate the direct impact of each materials to identify which ones are causing the most environmental impact in any given category.

The identification of materials is the most important stage in the plugin use because it depends on the database quality, the availability, the congruence of information, the presence of specific products. Even if the quantity of available materials is restricted, Tally interface presents an organized structure, an easily research filters and also it presents a very detailed characterization of materials (thermal properties, density, take-off method, service life).

The results of environmental impact given by the analyses are selected and discussed with reference to the Global Warming Potential (GWP) [$kg CO_2 eq$] and the Primary Energy Demand (PED) [MJ]: the choice of these environmental impacts is given according to the development of activities of RESTORE Cost Action and the requirements described in the Materials Petal Handbook [27] for the achievement of the Living Building Challenge certification.

According to the TRACI 2.1 characterization scheme [28], the GWP is a measure of greenhouse gas emissions, such as carbon dioxide and methane. These gases increase the absorption of radiation emitted by the earth. This may in turn have adverse impacts on

PLEA 2018 HONG KONG

Smart and Healthy within the 2-degree Limit

ecosystem, human health, and material welfare. The PED is a measure of the total amount of primary energy extracted from the earth: PED is expressed in energy demand from non-renewable resources (e.g. petroleum, natural gas, etc.) and energy demand from renewable resources (e.g. hydropower, wind energy, solar, etc.). Efficiencies in energy conversion (e.g. power, heat, steam, etc.) are taken into account. The results of both alternatives of case study are presented and discussed (Table 8, Table 9).

Impact results are quite different due to the adoption of databases: in Tally the GaBi data are intended to represent the United States region and the year 2013, while in One click LCA this research adopted Ecoinvent with a selection of France market data, due the not available collection for Italy. In fact, during the workflow of materials analysis, the connection from Revit abacus to LCA database is developed by a selection the available list of materials, by a choice among those with similar characteristics and by the conversion of service life.

Table 8: Environmental impact for masonry building

Stage	GWP [kgCO ₂ eq]		PED [MJ]	
	Tally	One click	Tally	One click
A1-A3	82'280	50'960	1'074'010	966'797
B1-B6	339'268	330'289	5'678'943	5'695'184
C1-C4, D	7'303	6'227	111'898	105'442
Total	428'851	388'676	6'864'851	6'767'423
		-9.4%		-1.4%

Table 9: Environmental impact for wooden building

Stage	GWP [kgCO ₂ eq]		PED [MJ]	
	Tally	One click	Tally	One click
A1-A3	41'928	44'428	913'590	1'142'400
B1-B6	349'223	323'562	5'752'942	5'555'106
C1-C4, D	21'093	953	109'350	16'661
Total	412'244	368'944	6'557'182	6'714'166
		-10.5%		2.4%

Moreover, Tally and One click LCA present different materials selection and calculations; while One click LCA considers all materials separately, in Tally the default procedure gives the possibility to choose how to consider a component: for example, a masonry wall could be treated as a single whole impact, or as sum of different layers, so the mortar and the finishing are considered as distinct materials. This is a positive plus for Tally, but also it needs more attention into the construction of the building model in both tools. The same situation is given for other materials: for example, in case of reinforced concrete component, Tally requires to specify the quantity of concrete and steel in the same label; One click LCA interface need to insert a new layer in BIM model linked to the reinforcement and then to choose the proper code "reinforced steel for concrete structures" in the database. In this case the user had to make more attention and to alter the BIM model in order to

consider all the layers for the LCA; this is the reason why the research has ignored the quantity of mortar in Tally, in such a way that the quantity is conform in One click LCA.

The results of LCA are given as descriptive report, spreadsheet file, or graphical dashboards (Figure 68, Figure 69) that provides a summary of all energy, construction, transportation, and materials inputs in the study.

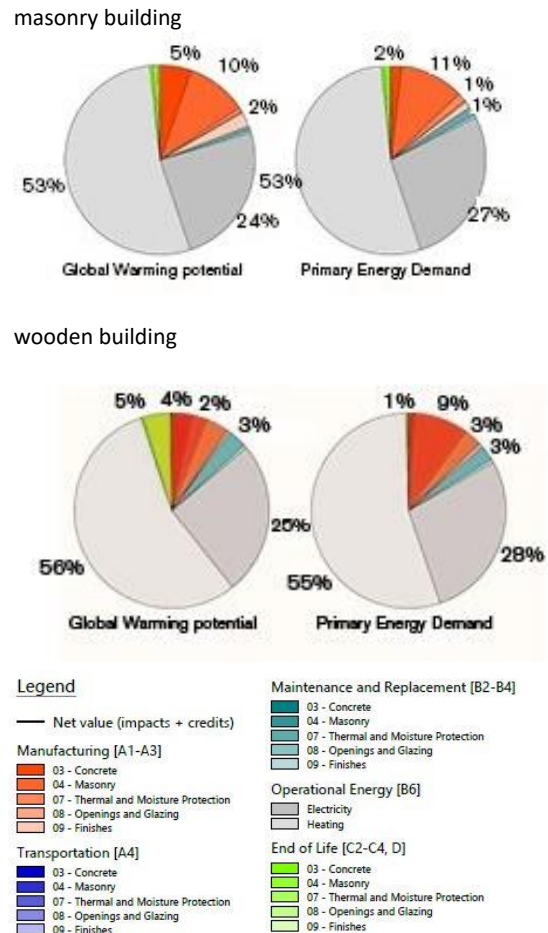
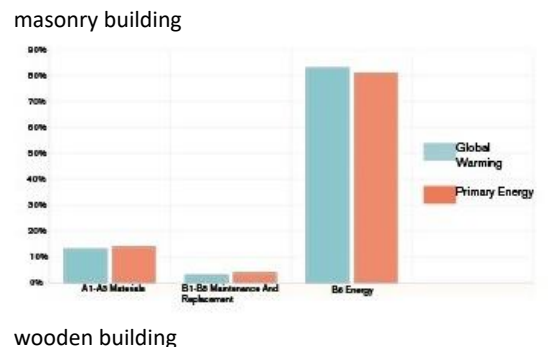
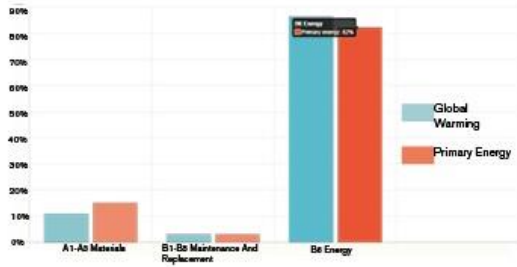


Figure 68: Environmental impact by Tally calculation for masonry and wooden building



PLEA 2018 HONG KONG

Smart and Healthy within the 2-degree Limit



wooden building

Figure 69 - Environmental impact by One click LCA calculation for masonry and wooden building

The chosen of database is more evident in case of comparison of tool, as shown in the results for masonry external wall (Table 10). In Tally, the database doesn't list type of hollow brick, so the analysis was conducted using a generic brick, even if with a higher impact than hollow brick. So, for comparing the outputs, the solid brick was selected in both software, even though the One Click database gives data for hollow brick.

Table 10: Environmental impact for masonry external wall

masonry building				
Materials	GWP [kgCO2eq]		PED [MJ]	
	Tally	One click	Tally	One click
Brick	31'2412	18'708	526'687	426'403
Mortar	7'849	4'253	45'584	108'819
EPS	795	1'045	23'524	17'260
Plaster	323	7'387	7'111	92'801
Total	40'209	31'392	602'906	645'283
		-22%		+7%

The high value of GWP in Tally can be due to the absence of a materials with characteristics comparable to mortar plaster; as consequence cement data was selected, even if the higher impact than a lime mortar usually used as a finish for the walls.

6. CONCLUSIONS

The paper evaluates the interoperability of LCA tools a BIM software in order to evaluate environmental impacts in the construction sector throughout the entire lifecycle of building materials; in particular this study evaluates the available plugins for Autodesk® Revit®: Tally and One click LCA.

In Tally the user could define relationships between BIM elements and construction materials from the database, while working on a Revit model. The result is LCA on demand, and an important layer of decision-

making information within the same time frame, pace, and environment that building designs are generated. One click LCA works with structural and architectural models and is able to adapt to material labelling practices. The cloud service to which the plugin connects detects the materials used in your model and calculates their environmental impacts automatically. Database should be enhanced due to the difficulty in finding related products that the actual building has. Some relevant notes are reported according to the workflow during the application.

The Tally application works directly in Revit, while One click LCA send the analysis in cloud.

The tools present different procedure for materials selection and method of calculation; One click LCA considers materials separately, and the list of products is organized by assessment method and by country source; Tally allows to choose how to consider a component and the layer of inner materials with a strict connection and cohesion to Revit, even if the available list of products is quite delimited.

Both tools allow a comparison of construction technology and choice of materials, giving exhaustive reports, charts for evaluate the impacts of products, materials at each stage of life span, and also spreadsheets for further data elaboration (especially in One click LCA).

The outputs given by a test on the two type of buildings shows how the use of both tools gives similar values only for PED (about 1.5%), not for GWP (about 10%); the differences emerged using different databases, that get available not the same products, so the environmental impact of each material presents very different values (about 22% average). These issues could be solved with a deep knowledge of manufacturing process of materials, but, in relation to the aim of this research, it needs firstly an awareness of database content and the availability to modify and add database values of the tools, still precluded by software houses.

The next step of the research will regard the analysis and the achievement of environmental requirements according to Living Building Challenge, in term of embodied carbon footprint and full LCA calculation.

REFERENCES

- RESTORE COST Action, www.eurestore.eu
- du Plessis C., (2012), Towards a regenerative paradigm for the built environment. *Building Research and Information*. 40(1), 7–22. doi:10.1080/09613218.2012.628548.
- Mang P, Reed B., (2012), Designing from place: a regenerative framework and methodology. *Building Research and Information*. 40(1), 23–38. doi:10.1080/09613218.2012.621341.
- Brown M., (2016). *Futurestorative: Working Towards a New Sustainability*. Riba Publishing, London, UK.

PLEA 2018 HONG KONG

Smart and Healthy within the 2-degree Limit

- Cole R.J., (2012), Regenerative design and development: current theory and practice. *Building Research and Information*. 40(1), 1–6.
- Pedersen Zari M., (2010), Regenerative design for the future. *BUILD 115* December 2009/January 2010, 68-69.
- Petersdorff, C., Boermans, T., & Harnisch, J., (2006). Mitigation of CO2 emissions from the EU-15 building stock. beyond the EU directive on the energy performance of buildings. *Environmental Science and Pollution Research*. 13(5), 350–358.
- EU, (2003). *Towards a Thematic Strategy on the Sustainable Use of Natural Resources*. Brussels, B. Retrieved from <http://eur-lex.europa.eu/legalcontent/EN/TXT/?uri=CELEX:52003DC0572>.
- EEA European Environmental Agency, (2002). *Benchmarking the millennium*, Environmental Signals. Copenhagen, DK.
- Bhatta, B. (2010). *Causes and Consequences of Urban Growth and Sprawl. Analysis of Urban Growth and Sprawl from Remote Sensing Data*, Springer-Verlag Berlin Heidelberg, 17–36. doi:10.1007/978-3-642-05299-6_2
- Soust-Verdaguer B., Llatas C., García-Martínez A., (2016) Simplification in life cycle assessment of single-family houses: a review of recent developments, *Building and Environment*, 103(2016), 215–227. doi:10.1016/j.buildenv.2016.04.014.
- Focà A., Laganà A., (2015). New responsibilities: rethinking regeneration. *TECHNE-Journal of Technology for Architecture and Environment*, 10, 179-185.
- Khasreen M.M., Banfill P.F.G., Menzies G.F., (2009), Life-Cycle Assessment and the Environmental Impact of Buildings: A Review, *Journal Sustainability*. 674–701. doi:10.3390/su1030674.
- Schultz J., Ku K., Gindlesparger M., Doerfler J., (2017), A benchmark study of BIM-based whole-building life-cycle assessment tools and processes, *International Journal of Sustainable Building Technology and Urban Development*. 7(3-4), 219-229.
- Anand C. K., Amor B., (2017). Recent developments, future challenges and new research directions in LCA of buildings: A critical review. *Renewable and Sustainable Energy Reviews*, 67, 408-416.
- www.caala.de/
- www.oneclicklca.com/
- www.acca.it/software-lca-life-cycle-analysis
- www.simapro.com/
- www.openlca.org/
- www.choosetally.com/
- www.iesve.com/software/ve-for-engineers/module/IMPACT-Compliant-Suite/3273
- www.ifu.com/en/umberto/
- www.gabi-software.com/italy/solutions/life-cycle-assessment/
- SmartMarket Report, (2010), *Green Bim. how Building Information Modeling is contributing to green design and construction*. McGraw-Hill Construction. Bedford, UK.
- Decreto del Ministero dello Sviluppo Economico 26 giugno 2015, *Applicazione delle metodologie di calcolo delle prestazioni energetiche e definizione delle prescrizioni e dei requisiti minimi degli edifici*.
- International Living Future Institute, (2017), *Materials Petal Handbook, Living Building Challenge 3.1*, Seattle, US.
- Ryberg M., Vieira M.D.M., Zgola M., Bare J., Rosenbaum R.K., (2016), Updated US and Canadian normalization factors for TRACI 2.1. *Clean Technologies and Environmental Policy*. doi:10.1007/s10098-013-0629-z.:1618-954X.

Assessment of the Building-Integrated Photovoltaic Potential in Urban Renewal Processes in the Swiss Context: Complementarity of urban- and architectural-scale analyses

S. AGUACIL¹, G. PERONATO², S. LUFKIN¹, M. ANDERSEN², E. REY¹

¹Laboratory of Architecture and Sustainable Technologies (LAST) and ²Laboratory of Integrated Performance in Design (LIPIID), School of Architecture, Civil and Environmental Engineering (ENAC), Ecole polytechnique fédérale de Lausanne (EPFL), Switzerland.

ABSTRACT: This paper presents two different approaches to deal with the assessment of the BIPV potential in building renovation projects in urban areas, taking Neuchâtel as a representative middle-size city of the Swiss plateau. 1) A building-scale analysis aiming to show to stakeholders involved in the renovation process that it is important to consider BIPV strategies to achieve the 2050 targets and that it is possible to produce quality architecture using BIPV products already available. For this, five real case studies of residential building archetypes are used. 2) An urban-scale analysis aiming at identifying the priorities of the interventions by comparing the potential of buildings from a large building stock. In each approach, we estimate the total on-site electricity production and the financial incomes provided by the BIPV installation taking into account the electricity self-consumed on-site and the injection of the overproduction into the grid, considering the building energy production and demand at an hourly resolution. Comparing the two approaches allowed us to show that the ranking of the buildings using the two methods remained consistent, despite the – expected – discrepancies in absolute results, and to discuss their complementarity in different stages of the planning and design process.

KEYWORDS: Integrated design, Building renovation, Building-Integrated Photovoltaics

1. INTRODUCTION

In view of the importance of urban renewal processes to reduce the impact on the global warming effect and climate change, building-integrated photovoltaics (BIPV) systems can provide a valid response to the challenges of the energy turnaround and help achieve long-term carbon targets. Functioning as both envelope material and on-site electricity generator, they can reduce the use of both fossil fuels and greenhouse gas (GHG) emissions [1].

This work is part of on-going research focussing on the renovation strategies for the Swiss residential building stock including BIPV to achieve 2050 targets for the energy turnaround fixed by the “2000 Watt Society” concept [2].

The paper presents two different approaches to deal with the assessment of the BIPV potential in renovation projects: 1) a building-scale analysis and renovation of five residential building archetypes (mainly defined by the construction period, from 1909 to 1990), already presented in [1] and illustrated in Figs. 1 through 5; 2) an urban-scale analysis that aims at identifying the priorities for building energy renovation and solar energy installation by comparing the potential of buildings from a large building stock.

show the current status and the characteristics of each residential archetype.

The emphasis of the study is placed on checking whether the ranking of buildings is consistent between the two analysis scales. We also highlight the complementarity of the two analysis scales and discuss their use as subsequent steps in the planning and design process of building energy renovation.



788 m² of floor area, 8 apartments.

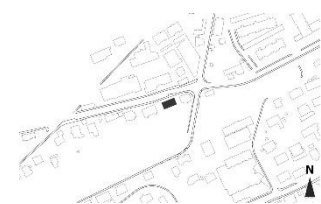


Figure 1: Archetype 1, built in 1909.

The study uses five real residential buildings in Neuchâtel (Switzerland) as case studies; figures 1 to 5

PLEA 2018 HONG KONG

Smart and Healthy within the 2-degree Limit



847 m² of floor area, 10 apartments.

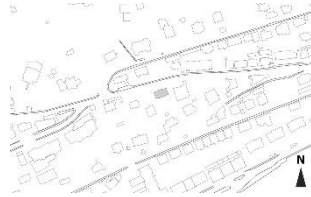


Figure 2: Archetype 2, built in 1938.



4'415 m² of floor area, 48 apartments.

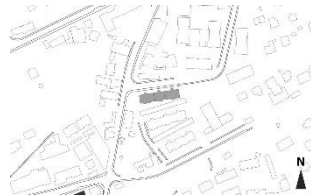


Figure 3: Archetype 3, built in 1968.



5'263 m² of floor area, 52 apartments.

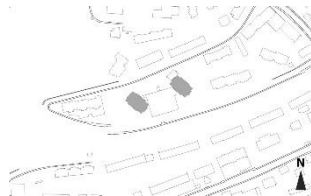


Figure 4: Archetype 4, built in 1972.



4'417 m² of floor area, 30 apartments.

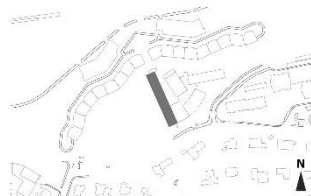


Figure 5: Archetype 5, built in 1990.

2. METHODOLOGY

This work was conducted using a simulation-based approach adapted to each analysis scale. Figure 6 shows an example of the 3D model of the same

building at urban- and building-scales, with different levels of detail (LODs). The level of detail (LoD) of the 3D model is crucial to estimate the accuracy of the assessment. The CityGML standard defines five levels of details from LoD0 to LoD4, depending on the amount of information available about the building [3]. For the needs of PV calculation at the building scale, a LoD3 model is the best option, as it provides all the details about the external aspect of the building. However, at the urban scale, available datasets are often at a lower LoD. In this case, a LoD2 model including dormers and roof overhang is used (Fig 6).

The comparison of the two approaches is based on the same renovation scenario, proposing an envelope transformation that meets the minimum legal requirements according to SIA norm (Swiss Society of Engineers and Architects) 380/1:2016 [4], while maximising the electricity production using both roofs and façades as active surfaces.

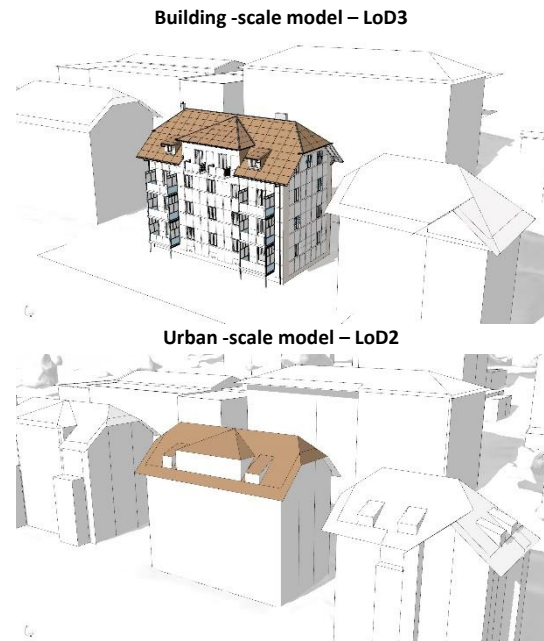


Figure 6: 3D models for the archetype 1, built in 1909.

For both scales, a building energy renovation scenario is proposed, which includes an insulation improvement of the building envelope (insulation of opaque elements and replacement of existing windows) in order to reduce heating energy needs according to the current legal requirements defined by SIA 380/1:2016 [4]. Moreover, in terms of active strategies, we propose an improvement of the heating system through a replacement of the existing oil or gas boiler by an air-water heat pump (AWHP). The latter has a coefficient of performance (COP) of 2.8 and is used for both heating and domestic hot water (DHW) needs.

In order to present the climate conditions of Neuchâtel (Switzerland), Figure 7 shows the monthly diurnal

PLEA 2018 HONG KONG

Smart and Healthy within the 2-degree Limit

average data from the hourly-step weather file used to conduct the calculations.

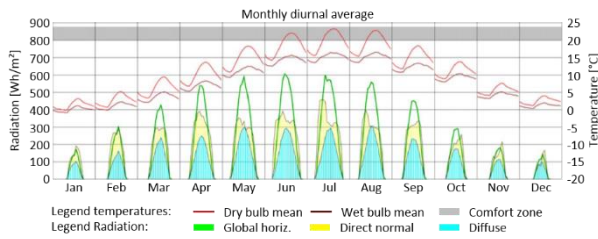


Figure 7: Climate conditions of Neuchâtel, monthly diurnal average

2.1 Building-scale analysis

Thermal simulations are conducted in EnergyPlus (DesignBuilder interface) [5] using a detailed 3D model (LOD3) reconstructed using the original plans of the building for the base-case, and a building-specific design proposal for the renovation scenario. From this simulation phase, hourly-step consumption is obtained for lighting, appliances, heating and domestic hot water (DHW).

We use Daysim [6] to simulate the plane-of-array hourly irradiances, which are then processed in PVLIB [7] to calculate the direct current (DC) power output of the photovoltaic (PV) modules. The arrangement of BIPV modules is defined from an architectural design phase, defining the potential active surfaces by composing the façade and the roof using standardized BIPV elements.

The objective of this design phase consists in identifying the maximum area that could suit PV modules. This approach and the final selection of the active surfaces are described in [8]. In the context of this study, we only consider the approach maximising the number of modules fitting on the building surfaces.

2.2 Urban-scale analysis

Simulations are conducted on a 3D city model, including buildings at LoD2, obtained from a 3D cadastre, and terrain and far-field obstructions obtained from Digital Terrain Models at 1-m and 25-m resolution respectively.

The arrangement of BIPV modules is determined on each surface by an automated algorithm, maximizing the number of modules on each surface. As for the building scale, we use Daysim [6] to simulate plane-of-array hourly irradiances, which are then processed in PVLIB [7] to calculate the DC power of the PV modules. Since the DC production is calculated on the plane of the building surface, we decided to apply a reduction factor of 0.5 for flat roofs (archetype 3 and 4). We assume in fact the use of tilted arrays, which have a lower total production because of the smaller number of modules fitting the roof surface. Similarly, the production for vertical surfaces is corrected by a

reduction factor (= 1-window-to-wall ratio) in order to exclude the installation of BIPV modules on windows. Thermal simulations for the base-case scenario are conducted in CitySim [9], using fixed assumptions for thermal parameters (e.g. U-value, window-to-wall ratio) depending on the year of construction, adapted from [10]. The heating needs for the considered renovation scenario were estimated scaling down the heating energy needs for the base-case scenario so as to reach the current annual requirements defined by SIA 380/1:2016 [4]. The final energy for heating is estimated using a fixed COP of 2.8. The electricity demand for domestic hot water, lighting, appliances and ventilation is estimated using annual values per floor area as calculated in the building-scale simulations, using the reference values and schedules defined by SIA 2024:2015 [11].

2.3 Financial calculations

Considering that both presented methods include on-site electricity production and energy demand estimation on hourly resolution, it is also interesting to compare the self-consumption (SC) and self-sufficiency (SS) potential, as defined in [8]. In particular, the self-consumption ratio represents the quantity of on-site electricity that is consumed directly by the building, i.e. avoiding the necessity of purchasing electricity.

We argue in fact that, in BIPV-driven building energy renovations, the size of the solar installation should be adapted to the real energy demand of the building to avoid too much overproduction and reduce the initial investment costs. In this study, we considered a cost of 0.22 CHF/kWh for purchased electricity and a rate of 0.087 CHF/kWh for injected electricity representing the current prices in the canton of Neuchâtel [12].

Since PV panels produce direct current (DC) electricity, we consider a Performance Ratio of 90% as recommended in [13] to obtain alternating current (AC) that is consumed by the building.

Through the self-consumption ratio, we estimate for each archetype the economic income potential expressed in CHF/m².year obtained after the renovation (building envelope with BIPV installation and HVAC system) [14].

The income is calculated on an hourly resolution using the following equation:

$$\text{Income} = \sum_1^{8760} PV \cdot [PE \cdot SC + IN \cdot (1 - SC)]$$

where PV - AC electricity production from PV (kWh);

PE - purchased electricity cost (CHF/kWh);

IN - injected electricity rate (CHF/kWh);

SC - self-consumption ratio (%).

PLEA 2018 HONG KONG

Smart and Healthy within the 2-degree Limit

3. RESULTS

Table 1 shows the results of the two analyses on the same case studies. It should be noticed that these results are extracted respectively from an urban-scale analysis including thousands of buildings, and a building-scale analysis including other renovation design scenarios. The comparison is here conducted only on the buildings that are comparable across the two analyses.

The total on-site electricity production is a good indicator to prioritise the buildings that could produce the larger amount of electricity per year. Similarly, it is possible to highlight the buildings with worst energy performance to classify them as a priority in urban renovation plans.

The ranking of the absolute production is consistent for both absolute and normalised production, with only a small change in archetype 4 and 5 regarding the absolute production. However, as expected, we can notice large discrepancies in the absolute results, especially for façades.

Table 1: Ranking results for each building archetype using the two analyses scales according to the total on-site DC electricity production.

Archetype	1	2	3	4	5
DC electricity production					
Urban-scale analysis					
Roof [MWh/year]	27	10	60	35	161
Façades [MWh/year]	40	49	119	148	104
Total [MWh/year]	67	59	179	183	265
Ranking [-]	4	5	3	2	1
Total [kWh/m ² year]	91	77	55	42	67
Ranking [-]	1	2	4	5	3
DC electricity production					
Building-scale analysis					
Roof [MWh/year]	29	21	73	23	173
Façades [MWh/year]	47	44	160	107	156
Total [MWh/year]	76	65	233	130	329
Ranking [-]	4	5	2	3	1
Total [kWh/m ² year]	97	77	53	25	74
Ranking [-]	1	2	4	5	3

This is because the urban-scale model considers a fixed window-to-wall ratio to consider the non-available façade surfaces, which cannot represent the variability of the façade configurations, and it does not include balconies. For instance, in terms of absolute results, especially for façade in archetype 4, the values differ mainly because of the characteristics of the façades, presenting a complex geometry typical of concrete prefabricate façade elements from the 70s not represented in the urban-scale model.

Table 2: Ranking results in terms of financial income due to self-consumption ratio for each building archetype using the

two analysis scales and implementing a renovation scenario achieving current regulation defined by SIA 380/1:2016 [4].

Archetype	1	2	3	4	5
Urban-scale analysis					
Total electricity demand [MWh/year]	34	36	172	178	170
Self-sufficiency [%]	36	35	33	26	34
Self-consumption [%]	16	17	22	35	16
Income [CHF/m ² .year]	5.0	3.0	2.4	1.0	5.4
Ranking [-]	1	3	4	5	2
Building-scale analysis					
Total electricity demand [MWh/year]	34	31	178	191	150
Self-sufficiency [%]	30	29	20	22	31
Self-consumption [%]	14	14	29	32	14
Income [CHF/m ² .year]	12.3	9.6	6.0	2.9	9.6
Ranking [-]	1	3	4	5	2

The ranking based on the annual income per m² of floor area is shown in Table 2. We can notice that the ranking remains consistent for both scales. Figure 8 shows that the building energy balance profiles are consistent as well.

These results also highlight the importance of façade – installed systems for archetypes with large and well-exposed façade (archetype 3 and 4) and with more apartments per building (more energy demand intensity), as these have a larger SC ratio (with similar SS) than archetypes 1, 2 and 5. This is because the consumption-production profiles match in a better way for archetypes using more intensively façades.

It is important to note that, in this study, we focussed on the impact of a BIPV installation using all available surfaces (roof and façade) and considering a minimum energy renovation to achieve the legal targets.

However, as recommended in [15], we encourage to implement a deeper energy renovation to achieve the 2050 targets, which include for example carbon reduction too.

PLEA 2018 HONG KONG

Smart and Healthy within the 2-degree Limit

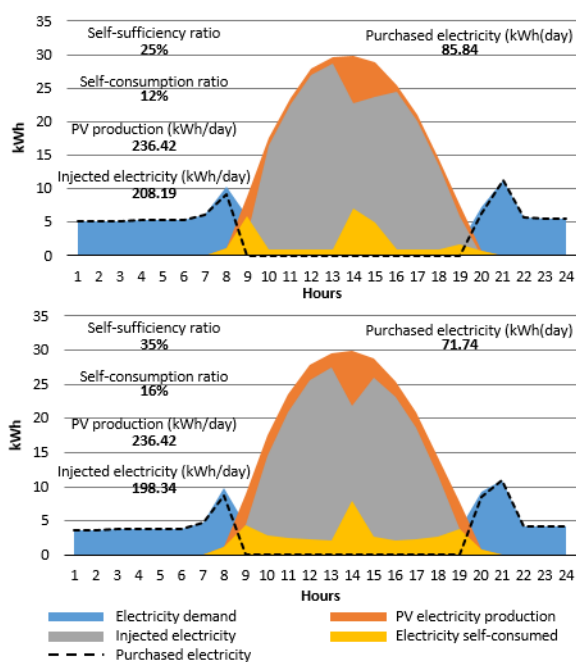


Figure 8: Example of energy balance of 21 march for both, building (top) an urban-scale (down).

4. DISCUSSION

Even if the city-scale 3D model provides a good level of detail, many hypotheses are required to estimate the PV production of façades (e.g. window-to-wall ratio), and of flat roofs (i.e. tilt and spacing), which cannot represent the variability of conditions of the building stock: urban-scale assessments cannot replace detailed assessments of single buildings. Both methods should be also further validated with real measurements. However, we argue that the two methods are rather complementary, as they refer to subsequent stages of the urban renewal process. In this sense, the first phase of this process is to identify the priority intervention areas, for which simplified methods can give enough information. The second phase is to identify possible intervention solutions, with reference to best-case renovation design strategies.

5. CONCLUSION

This article presented two different-scale analysis methods and showed their relevance for assessing the potential for building energy renovation.

We have shown that the ranking of the BIPV potential of the analysed buildings is consistent across the two methods, i.e. we can identify the priority level of the interventions in an urban area, despite the expected discrepancies in absolute results due to different levels of detail, available information, and architectural design specificities.

Urban-scale assessments can help decision-makers identify priority areas/buildings, while architectural-scale analyses offer designers and building owners

valuable benchmarks and guidelines on possible renovation strategies to give a response to different archetypal situation taken into account the soundings of the building.

ACKNOWLEDGEMENTS

This study was conducted at the Ecole polytechnique fédérale de Lausanne (EPFL). The work is part of the Active Interfaces research project www.actievinterfaces.ch funded by the National Research Program "Energy Turnaround" (NRP 70) of the Swiss National Science Foundation (SNSF). Further information on the National Research Program can be found at www.nrp70.ch.

REFERENCES

1. Aguacil, S., Lufkin, S., Rey, E., (2016). Architectural design scenarios with building-integrated photovoltaic solutions in renovation processes: Case study in Neuchâtel (Switzerland). In PLEA 2016 Los Angeles - 36th Int. Conference Passive and Low Energy Architecture, Cities, Buildings, People: Towards Regenerative Environments. Los Angeles, USA, July 11-13.
2. SIA (2011). SIA 2040 - La voie SIA vers l'efficacité énergétique, [Online], Available: <http://www.2000watt.ch/> [16 May 2018].
3. Gröger, G., Kolbe, T.H., Czerwinski, A. (2007). Open Geospatial Consortium Inc. Candidate OpenGIS® CityGML Implementation Specification (City Geography Markup Language), Water, 3: p. 0–119.
4. SIA (2016). SIA 380/1:2016 - Besoin de chaleur pour le chauffage.
5. DesignBuilder (2018). DesignBuilder software v.5, [Online], Available: <http://www.designbuilder.co.uk/> [23 February 2018].
6. Reinhart, C.F., Walkenhorst, O., (2001). Validation of dynamic RADIANCE-based daylight simulations for a test office with external blinds, Energy and Buildings, 33: p. 683–697.
7. Holmgren, W.F., Groenendyk, D.G., (2016). An open source solar power forecasting tool using PVLIB-Python. In Photovoltaic Specialists Conference (PVSC), 2016 IEEE 43rd. Portland, OR, USA, June 5-10.
8. Aguacil, S., Lufkin, S., Rey, E., (2017). Influence of energy-use scenarios in Life-Cycle Analysis of renovation projects with Building-Integrated Photovoltaics – Investigation through two case studies in Neuchâtel (Switzerland). In International Conference for Sustainable Design of the Built Environment. London, UK, December 20-21.
9. Robinson, D. et al. (2009). CITYSIM: Comprehensive Micro-Simulation of Resources Flows for Sustainable Urban Planning. In Eleventh International IBPSA Conference, Glasgow, Scotland, July 27-30.
10. Perez, D., (2014). A framework to model and simulate the disaggregated energy flows supplying buildings in urban areas, PhD Thesis. 6102 (2014) 182. doi:10.5075/EPFL-THESIS-6102.
11. SIA (2015). SIA 2024 :2015 - Données d'utilisation des locaux pour l'énergie et les installations du bâtiment.
12. Vese (2018). Tarif reprise energie PV pvtarif tool, [Online], Available: <http://www.vese.ch/fr/pvtarif-apps/> [29 May 2018].

PLEA 2018 HONG KONG

Smart and Healthy within the 2-degree Limit

13. F. Vignola, F., Mavromatakis, F., Krumsick J., (2008). Performance of PV Inverters. In American Solar Energy Society - SOLAR 2008: Catch the Clean Energy Wave., San Diego, California, US, May 3-8.
14. Cucchiella, F., D'Adamo, I., Gastaldi, M., Koh, S.C.L., (2012). Renewable energy options for buildings: Performance evaluations of integrated photovoltaic systems, *Energy and Buildings*. 55 p. 208–217.
15. Aguacil, S., Lufkin, S., Rey, E., (2016). Towards integrated design strategies for implementing BIPV systems into urban renewal processes: First case study in Neuchâtel (Switzerland). In Sustainable Built Environment (SBE) regional conference, Zurich, Switzerland, June 15-17.

Development of an Adaptive Passive Façade: A replicable approach for managing multiple design solutions

CATERINA PONZIO¹, ADELE RICCI², EMANUELE NABONI³, KRISTIAN FABBRI⁴, JACOPO GASPARI⁴

¹Architect, Vicenza, Italy

²University of Architecture of Bologna, Cesena, Italy

³The Royal Danish Academy of Fine Arts, Copenhagen, Denmark

⁴Department of Architecture – University of Bologna, Cesena, Italy

ABSTRACT: Users' well being and satisfaction are a key priority in the current architectural design trends and represent a relevant issue in a human-centred perspective. Concerning this aim, the application of climate adaptive building shells (CABS) offers relevant opportunities for tackling these challenges. This paper reports the outcomes of a study run on CABS to optimise the indoor comfort while calibrating the configuration of a dynamic facade module. Through the physical measurements of the environment and the integration of these values in the parametric process for integrating daylight and thermal performance into the design phase, a performance-based workflow evaluation supported the design of a Passive Adaptive Façade.

The purpose of this work is to provide a replicable method that is the base of a facade system design. The system, made of simple horizontal louvres, has a controlled movement manoeuvred by an actuator that exploits the expansion of a thermo-active resin. The louvres can rotate and close passively with the increase of the external temperature. Results show the uniformity of distribution of daylight across the entire space and the substantial gain of indoor thermal comfort.

KEYWORDS: Adaptive Façade, Parametric Design, Daylight, Energy Efficiency, Building Shells.

1. INTRODUCTION

Since most of the people spend 90% of their time inside buildings, well-being is an important aspect determining the quality of life of an occupant. Improving this quality and having a “healthy building” that guarantee better levels of indoor comfort (i.e. indoor air quality, thermal comfort, acoustics and lighting quality) are nowadays-key factors in the architectural design [1].

Concerning this aim, the application of climate adaptive building shells (CABS) has recently been of fundamental importance to achieving higher and more consistent levels of indoor environmental quality.

Compared to the “static” facades, the way of operating CABS has important effects on occupants' visual and thermal comfort [2]. An interactive façade should respond intelligently to the changing outdoor conditions and internal performance needs. It should also exploit available natural energies for lighting and heating.

Several studies have investigated the key elements of control in such topic [3,4]. Results from the European HOPE project nevertheless show that “satisfaction with the control of sun shading” was one of the main predictors for comfort about personal control [5].

In spite of its importance is acknowledged in the literature, so far, only limited attention has been paid to human factors research with relation to daylighting, solar control, and the dynamics of adaptable facades [6].

In more recent projects a different approach is rising around the question: “What would be the ideal, dynamic properties of a building shell to get the desired indoor climate at variable outdoors climate conditions? Which would be the parameters to take into account to rise to a higher comfort level?”

Following this perspective, a set of ideal, but realistic building shell parameters is computed for different climate conditions and time scales (seasons, day-night). In this way, the “ideal” adaptive behaviour makes it possible to maximize luminous and thermal comfort.

2. AIMS OF THE STUDIO

The purpose of this work is to provide a replicable method that is the base of a façade system design, passing through the analysis of a concrete example.

This paper outlines the results of a process for testing different strategies for climate adaptive dynamic facades by giving the designer the ability of testing, comparing and selecting the most appropriate solution.

Focusing on CABS that react to micro-mechanism - a material changes its internal energy changing its structure and thermos-physical properties [7] - the paper defines a shell technology by application of an aluminium actuator filled with a density change paraffin.

3. BACKGROUND AND METHODOLOGY

As recent literature shows, successful building performance simulation (BPS) has been taken into account as “the right type of virtual experiment with

PLEA 2018 HONG KONG

Smart and Healthy within the 2-degree Limit

the right model and tool" [8]. For this reason, there is a great demand for tools and instruments that can be used in the design process of kinetic facades [9,10]. In this way, the work of Mahmoud, etc [11] aims to provide a toolkit for daylight control inside buildings, combining different software such as Grasshopper and Diva. Similarly, the study of Loonen, etc [12] explores the potential role that BPS play in designing CABS by taking the window technology Smart Energy Glass as a case study and coupling TRNSTS and DAYSIM to build a model for performance simulations.

From the beginning of the study, the focus was set on the need to keep both luminous and thermal aspects together, to obtain a tool to consider the two major aspects influencing indoor comfort. For this reason, the research targets a series of design problems: design integration through tool development and design process improvement through the incorporation of physics-based modelling and real-world dynamics.

The applied methodology uses parametric design methodologies, dynamics simulation and validation on site measure.

The study is subdivided into three phases:

- on-site physical measurements;
- simulation model and data processing and calibration of a simulation model;
- simulation workflow for designing the façade.

Mean radiant temperature (MRT in °C) and illuminance levels (Lux) were investigated to have a clear picture of the thermal and luminous conditions of the room. Then a simulation model set up on the real environment of measurement was developed. One that would return simulated values of mean radiant temperature and illuminance in two points of the room.

Illuminance values were measured and simulated on two points, one (P1) located at 1.5 m and one (P2) at 5.5 m from the window, to see if the façade could provide adequate shielding near the opening without determining a low-light situation in the bottom of the room.

The luxometer on P1 and P2 was placed at the height of 0.8 m, like the height of a worktop, such as a desk or a small table. The mean radiant temperature was measured and simulated at 1.5 m from the window as main heat dispersion source (on P2) at 1.1 m height, which corresponds to the gravity centre of a man standing.

The software used for the simulation is Honeybee, an environmental design plug-in for Grasshopper that connects Radiance and Energyplus and allows running luminous and thermal simulation together [13]. This model, in which then the facade structure has been inserted, was used for comparing simulated data with

measured data and so for establishing the accuracy of output results.

The simulation model was used to monitor the effects of the facade inside the room and during the technical design phase to evaluate the performance of various intermediate solutions.

3.1 Test environment

Experiments were conducted during November 2017 in a full-scale test room (7.5x5x3m) (Fig.1a-b) designed as daylight laboratory The Royal Institute of Fine Arts in Copenhagen (Denmark). As figure 1 shows, the room has only one opening facing southeast.

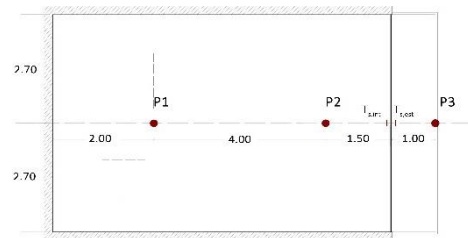


Figure 1a: Floor plan of the room with points of measurements (red dots – P1, P2, P3) and sensors for the surface temperature of the glass (red lines – $T_{s,int}$, $T_{s,ext}$).

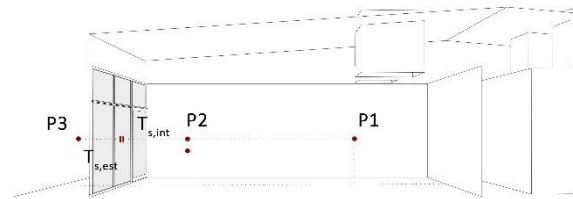


Figure 1b: 3d model of the room with points of measurements (red dots – P1, P2, P3) and sensors for the surface temperature of the glass (red lines on the window).

These parameters were measured - Air temperature, Relative Humidity, Mean Radiant Temperature, Illuminance and Solar Radiation - because they describe thermal and luminous conditions of the room. Those indices are therefore fundamental to be able to compare the output data of the system with the real ones and therefore to be able to understand the veracity of the outputs of the simulation system.

The minimum characteristics of the instruments and the method for measurements were decided following the UNI EN ISO 7726, "Ergonomics of the thermal environment - Instruments for measuring physical quantities" [14].

To collect an adequate number of climatic data, two stations of measurement were placed into the room, and one was placed outside. As explained above, the two indoor points were located at 1.1 m and 0.8 m high above the floor level and 2.7 m from the walls. Furthermore, the two points P1 and P2 were positioned respectively at 5.5 m and 1.5 m from the

PLEA 2018 HONG KONG

Smart and Healthy within the 2-degree Limit

window (Fig.1a-b and Fig.2). The outdoor measurement station (P3) was fixed instead on the railing, 1.1 m above the floor level, on the same virtual line of P1 and P2.



Figure 2: Overview of the stations in the test room (P2 indoor and P3 outdoor) during measurement's phase.

During this first phase, following tools were adopted:
 Hobo U12-012 (Data Logger and Sensors) for Illuminance [lux], Air Temperature [°C] and Relative Humidity [%];
 KIMO Black Ball + Data Logger for Mean Radiant Temperature [°C];
 S-LIB M003 Pyranometer + Data Logger for Solar Radiation [W/m2];
 Onset M-TMB-M006 Temperature Sensor for Air Temperature [°C];
 Rs Pro 1340 Hotwire anemometer [m/s].

3.2 The simulation model: how it works

To return accurate results, the simulation model has to be as similar as possible to the real one, with the same thermal and luminous behaviour. Therefore, the full-scale test room was considered as a thermic zone in the whole building and the specific window area and type of glass was assigned with "Honeybee Glazing based on ratio".

Heat exchanges between thermal zone and environment have been reproduced through the assignment of transmittance of walls with a specific component of Energyplus, so reflectance of revetment has been assigned setting Radiance materials. Moreover, the box was free of cooling or heating systems.

Thanks to previous measurements of the air speed inside the room, the movement of the air was considered irrelevant for simulations and therefore no longer calculated in the simulation model.

Adjacent buildings change the exposure to the winds in the thermic zone, so also the context was added to the thermal simulation (Figure 3).

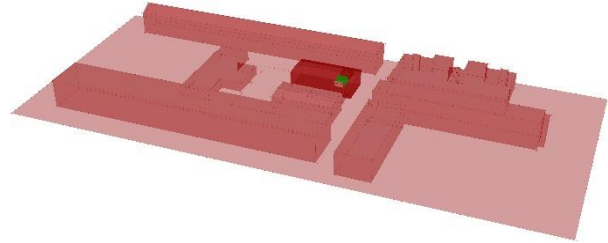


Figure 3: The thermic zone (green) inside the context (red).

A "Climate Based Sky" (Figure 4) - whose radiation values are calculated based on the inserted weather file and are specific for a specific time of the year - was generated. The honeybee grid-based simulation, connected to the command running the Radiance simulation, allowed to calculate illuminance on the two points of the simulated space corresponding to the measurement points in which the Luxometers were placed (P1 and P2).

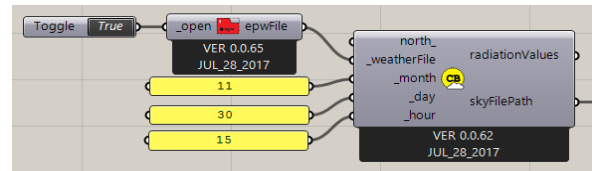


Figure 4: Illustration of parametric logic of the room's model within Grasshopper Algorithm: Honeybee_Climate Based Sky.

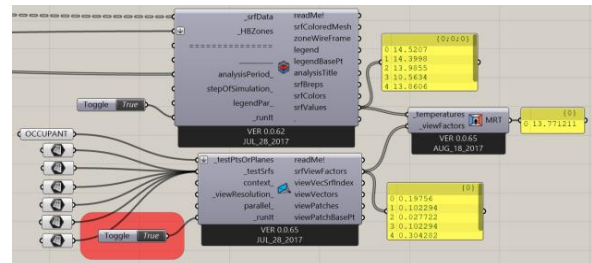


Figure 5: Illustration of the parametric logic of the room's model within Grasshopper Algorithm: MRT workflow calculation.

Thanks to the EnergyPlus simulation is possible to calculate surface temperatures of the test room's walls. The mean radiant temperature calculator has processed these temperatures. The simulation software allowed thus to calculate the mean radiant temperature on P2, where the globe thermometer was placed during the measurement session (Fig. 5). Finally, the façade structure has been inserted in the model, and its effects on indoor comfort monitored through simulated values of illuminance and mean radiant temperature.

3.3 Data processing: from collected data to simulation model

PLEA 2018 HONG KONG

Smart and Healthy within the 2-degree Limit

Data collected during the measurement phase were grouped into Excel files and organised. Then, the indexes that describe the comfort of the room (Air Temperature in °C, Relative Humidity in % and Illuminance in lux) were extracted from this database and included in weather file used in the workflow to calibrate the 3D simulation model.

Among the measurements collected were selected those of two days, which respectively represent the best (sunny day) and the worst (rainy day).

As described above in section 3.2, the simulation model was built as similar as possible to the real room, with the same thermic and luminous characteristics. Thanks to this, the comparison between the measured and simulated data of the mean radiant temperature seems to correspond quite well (Figure 6).

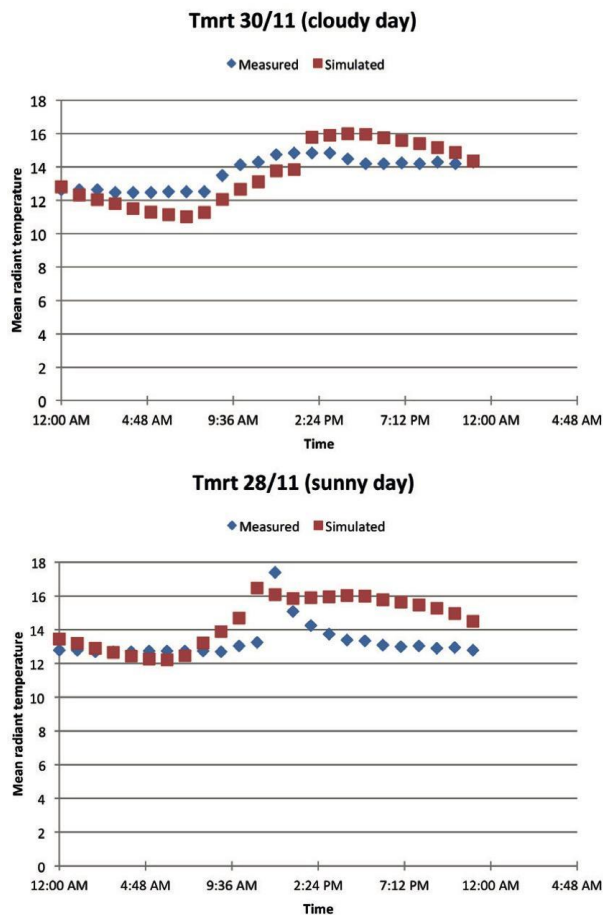


Figure 6: Comparison between measured and simulated data of the Mean Radiant Temperature in the room during cloudy day (upper chart) and sunny day (lower chart).

3.4 New façade design

The façade was designed as a set of horizontal louvres that shield the sun through a downwards-rotary movement. The geometry was shaped by Grasshopper and applied as Honeybee EP context surfaces to the thermal zone.

Several solutions have been explored and compared with the shadow-less scenario (no shells configuration). The best solution, considered as the best performing, is the one that involves the installation of horizontal louvres 500 mm depth, separated from each other by a distance of 500 mm (Figure 7).

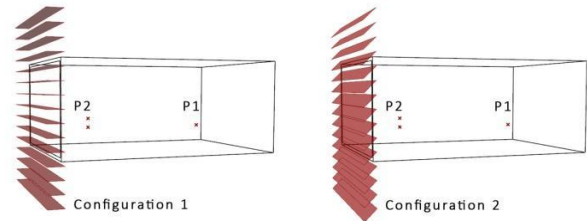


Figure 7: Configurations of the louvres during the day (see results on par.4.1) with two indoor points used to test and verify the results.

The horizontal louvres, fixed to the structural steel bracket with bolts and hooked to a pivot that allows rotation [15], are made of perforated aluminium sheet with dimensions 1200x500mm (Figure 8).

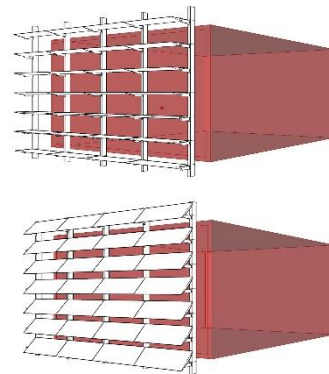


Figure 8: 3D model of the system: horizontal louvres made of perforated aluminium sheet, fixed to the structural steel bracket and hooked to a pivot that allow the rotation.

Facade adaptive systems usually require a large amount of energy to activate sensors and actuators [16]. The energy supplied should ideally be lower than energy savings. Considering the sustainability of the system as a whole, it is necessary to design buildings envelope with high performances of indoor comfort but which are also sustainable from energy supplied for their operation.

Most buildings still have louvres and shutters fixed outside the windows; these devices are low-cost and low-energy if manually activated. These traditional systems provided adaptability in buildings and, if used in innovative ways, they could allow the creation of adaptive environments without complex automatic systems. To increase the sustainability of the system, a facade moved by a passive control system that could increase thermal and lighting comfort without energy

PLEA 2018 HONG KONG

Smart and Healthy within the 2-degree Limit

consumptions has been developed. Thus the geometries of the climate adaptive building shells are moved by a thermal actuator that exploits the expansion of a thermo-active resin during melting by its absorption of thermal energy [17]. This provides a means of operating a mechanism solely from its response to passive energy exchanges given the meteorological conditions.

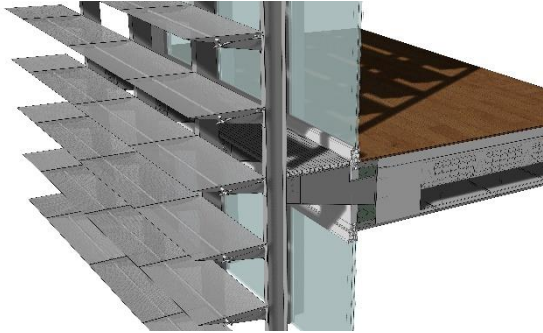


Figure 9: Rendered image in which is showed the actuator technology.

The actuator, designed by an English company, it's usually used for the automatic greenhouse ventilation. It's composed of a hollow aluminium cylinder filled with density-change paraffin. The paraffin increases the volume in relation to the external temperature, allowing the piston to move with a straight movement along its longitudinal axis (Figure 9). Furthermore, the rectilinear movement is transformed into rotational movement by aluminium support and a hinged joint, able to rotate and close louvres [18].

The actuator selected for the façade has an operating temperature range of 8° - from 15 °C (temperature at which the wax starts to melt) to 35 °C (complete melting of the wax), the temperature at which the opening angle reaches 54° of rotation - and is capable of supporting a load of up to 6 kg.

4. RESULTS

This section explains and analyses the outcomes of the experiment in relation to the hypotheses as formulated above. Each scenario is described in the following subsections, with the related results of Mean radiant temperature values (°C) in Table 1 and Illuminance level (lux) in Table 2.

4.1 Simulation scenarios

To verify the effectiveness of the new facade design, three configurations of the shell's positioning were simulated in two days of the year, on June 21st: and December 21st, respectively summer and winter's solstice, supposed to be the worst and best day in terms of air temperature and hour of light:

Configuration 0 : No shells.

Configuration 1: Sun-shutters inclined 0°, horizontal position, when the air temperature is below 16 °C and motion actuators are at rest.

Configuration 2: Sun blinds inclined 45° compared to configuration 1, when the outside air temperature is higher than 24 °C.

4.2 Simulation scenarios' results

Mean radiant temperature [°C]

Day	Hour	Conf.0	Conf.1: 0°	Conf.2: 45°
21 Dec	9:00	11.4	11.8	--
	12:00	13.8	13.8	--
21 Jun	9:00	32.9	27.0	23.1
	12:00	35.1	28.2	24.3

Table 1: Analysis of Mean Radiant Temperature values on P₂ (a globe thermometer was placed during measurements).

In Table 1, the Mean radiant temperature values for the activation of the shell system for each configuration and in the point P₂, are presented. The new facade design point out that:

during winter time, the facade remains in the Configuration 1 and allows to obtain a slight increase in temperature in the morning (about 0.4 °C), compared to the no shells configuration (Configuration 0), while it's null at noon; also, the configuration 2 it isn't obtained because the external temperature of 24°C is not reached.

during summer time, the configuration 2 is obtained. The facade allows decreasing the temperature by 4°C compared to the static configuration (Configuration 1) both at 09.00 AM and at noon.

Illuminance [lux]

Day	Hour	Conf.0	Conf.1: 0°	Conf.2: 45°
21 Dec	9:00	P ₁ =3.51 P ₂ =17.35	P₁ =2.56 P₂ =8.27	-- --
	12:00	P ₁ =330.4 P ₂ =1339.9	P₁ =257.5 P₂ =798.4	-- --
21 Jun	9:00	P ₁ =1744.4 P ₂ =7462.0	P ₁ =1145.9 P ₂ =4044.3	P₁ =320.4 P₂ =1375.5
	12:00	P ₁ =1140.9 P ₂ =5778.8	P ₁ =856.5 P ₂ =2879.9	P₁ =291.8 P₂ =1212.8

PLEA 2018 HONG KONG

Smart and Healthy within the 2-degree Limit

Table 2: Analysis of Illuminance level (lux) on the measuring point P_1 and P_2 .

In *Table 2*, illuminance values for the activation of the shell system for each configuration and in the point P_1 - P_2 are presented. The new facade design point out that:

during winter time (Configuration 1) the facade allows obtaining values always upper than 200 lux. As B. Keller and S. Rutz typify in their guidelines for illuminance according to visual task [17] this threshold is characterised by a "large visual task, large details, strong contrast". Moreover, in Denmark on 21 December at 09.00 AM, very low incoming solar radiation is recorded, Configuration n°1 doesn't preclude the passage of light.

during summer time 45° rotated louvres are necessary to lower the level of illuminance below 1500 lux, threshold characterised by "very difficult visual task, very small details, very low contrast" [17].

Adaptability allows decreasing mean radiant temperature and illuminance values in summer while instead of letting solar radiation come into the room during wintertime.

The optimized solution shows a substantial gain for thermic performance and so environmental sustainability.

5. CONCLUSION

The paper presents a case study about a tool implementation to simulate daylight efficiency for design-centric phases of architecture.

The applied methodology allows monitoring light and temperature inside buildings; these parameters indeed are essential for the control of indoor comfort with a complete passive technologic adaptive system.

The research indicates that through the incorporation of sciences, design computation and an empirical research methodology, design teams can begin to implement the system to manage the simulation and evaluation of daylight and temperature performances during the design process [18].

Some remarks on the results:

Modelling is a useful tool to verify the design choices of the climate adaptive building shells (CABS) if there are accompanied by monitoring and validation of data; CABS are a good solution that also allows improving the control of mean radiant temperature (°C) and the Illuminance level (lux).

Future studies can be built upon the current one and explore an expanded set of optimization criteria, combining energy-related indicator with visual comfort ones, such as glare probability, uniformity of daylight Illuminance and external view factor.

REFERENCES

1. Schumacher M., Schaeffer O, Vogt M., (20). Move: architecture in motion e dynamic components and elements. Basel: Birkhäuser.
2. Cole RJ, Brown Z., (2009). Reconciling human and automated intelligence in the provision of occupant comfort. *Intell Build Int*;1:39-55.
3. Paciuk M., (1989). The role of personal control of the environment in thermal comfort and satisfaction at the workplace. In: *Proc. 21st Environ. Des. Res. Assoc. Meet.*
4. Boerstra A.C., Beuker T., Loomans MGLC, Hensen JLM., (2013). Impact of available and perceived control on comfort and health in European offices.;56:30e41
5. Bluysen P.M., Aries M., Van Dommelen P., (2011). Comfort of workers in office buildings: the European HOPE project. *Build Environ*2011; 46:280e8
6. Galasiu AD, Veitch JA., (2006). Occupant preferences and satisfaction with the luminous environment and control systems in daylight offices: a literature review. *Energy Build* 2006;38:728e42.
7. Loonen R., (20). Climate Adaptive Building Shells. What can we simulate? Master of Science Thesis
8. Godfried A., (2011). The role of simulation in performance based building. *Building Performance Simulation for Design and Operation*. Spon Press.
9. Nielsen M.V., Svendsen S., Bjerreg, L., (2011). Quantifying the potential of automated dynamic solar shading in office buildings through integrated simulations of energy and daylight. *Sol. Energy* 85, 757–768.
10. Shen H., Tzempelikos A., (2012). Daylighting and energy analysis of private offices with automated interior roller shades. *Sol. Energy* 86, 681–704.
11. Ayman H. A. M., Yomna E., (2016), Parametric-based designs for kinetic facades to optimize daylight performance: Comparing rotation and translation kinetic motion for hexagonal facade patterns.
12. R.C.G.M. Loonen, Trčka M., Cóstola D., Hensen J.L.M., (2010). Performance simulation of climate adaptive building shells - Smart Energy Glass as a case study, *Unit Building Physics and Systems, Department of Architecture Building*.
13. Davidson, S., (2013). Grasshopper: Algorithmic Modelling for Rhino, NING/MODE, Brisbane, CA, USA, [Online], Available: <http://www.grasshopper3d.com/>
14. UNI EN ISO 7726, (2002). Ergonomics of the thermal environment - Instruments for measuring physical quantities
15. Leung C., (2014). Passive seasonally responsive thermal actuators for dynamic building envelopes, *The Bartlett School of Architecture, University College London*.
16. <https://www.baylissautovents.co.uk>
17. B. Keller, S. Rutz, (2010). Pinpoint: Key Facts + Figures for Sustainable Buildings, Birkhäuser, Basel.
18. David, M.; Donn, M.; Garde, F.; Lenoir A., (2004). Assessment of the thermal and visual efficiency of solar shades. *Build. Environ.*, 46, 1489–1496.

Influence of Office Building Height in Urban Areas on Surrounding Microclimate and Building Performance

JING LI¹, MICHAEL DONN¹, GEOFF THOMAS¹

¹School of Architecture, Victoria University of Wellington, Wellington, New Zealand

ABSTRACT: This paper presents a methodology intended to integrate building performance modelling and urban microclimate studies and explore their interaction at different heights. In this study, Urban Weather Generator (UWG) is used to evaluate urban microclimates across a 3-dimensional landscape. UWG can calculate the effect of Urban Heat Islands (UHI) on temperature across a 2-dimensional landscape but does not consider wind effects. A new methodology is presented in this paper to model urban microclimates more accurately. Using London as a case study, high-rise office building performance at different heights is examined. The variation of urban microclimate with height and relative to the rural weather data is reported through evaluation of its impact on building performance.

KEYWORDS: Urban microclimate, Building height, Building performance, Simulation, London

1. INTRODUCTION

This paper presents a case study of the application of a methodology to model urban microclimates accurately. It explores to what degree can reliable models be developed of the influence of microclimates of dense urban spaces on building performance.

Building performance simulation in urban areas mostly relies on regional climate data which are typically collected from suburban or rural areas such as nearby airports [1]. This is largely a result of the requirements in climate record standards for a large grass area under the climate measurement station. There have been numerous studies confirming the general suspicion that the modelled performance of buildings is not accurate when it is based on weather data from somewhere else other than their actual dense urban location. [2,3 for example].

Urban Heat Islands (UHI) effect can be modelled. Using data on the density of a city, or empirical data for a specific city, the regional climate data can be modified to be more representative of the temperature ranges experienced in the city. However, this UHI analysis has significant limitations: 1) it does not consider the new building's effects on its surrounding microclimate. 2) to date, UHI effects are modelled in a 2D sense, assuming within the Urban Canopy Layer there is temperature variation from the perimeter to the centre of the city, but not vertically within the city streets.

The influence of the surrounding microclimate caused by building height variation is not clear. Is it significant enough to affect the accuracy of simulation? Is it significant enough to affect its HVAC system or natural ventilation design?

2. OBJECTIVES

This research has as a principal objective the quantification of the magnitude of the difference in building thermal performance simulation when the urban microclimate is modelled as 3-dimensional compared to the conventional 2D model. The common 2D climate model associated with UHI is approximately ground level information. The climate data includes the temperatures, relative humidity and solar radiation measured 1.5m from the ground and wind speed recorded at 10m height every hour in a year. A thermal simulation program like EnergyPlus can adjust the wind speed according to the height of the building thus converting the wind speed from 10m at the airport to an appropriate height at the building. This case study analysis has looked first to establish the effect of having an urban or a regional Turbulent Boundary Layer model of the variation of wind speed with height for this conversion.

In dense urban areas, the maximum temperature difference between the rural temperatures and those in the centre of a UHI could be as much as 6 to 12°C, depending on city size [4]. UHI, is traditionally identified from the height of 2m above the ground surface air temperatures [5]. This case study examines the effect of height on this temperature, and hence on the performance of buildings subjected to this temperature variation. It seeks to answer the question of whether the temperature difference between urban and rural regions at height of 2 meters is the same as at a height of 100 meters? Does the conventional lapse rate [6] of a decrease in temperature of 0.65°C per 100m elevation experienced in the open country apply in the middle of a dense urban environment? Is the temperature at the top of a 100m tall (roughly 30 storey) building actually

PLEA 2018 HONG KONG

Smart and Healthy within the 2-degree Limit

0.65°C higher than at 0m in the middle of urban areas with Urban Heat Islands effect?

Wind speeds increase with height, so the wind speed at the top of a high-rise building is much higher than at the bottom. This rate of increase is much faster in the open country than it is in the city due to drag from taller buildings. In addition, the complex geometry of the interaction of buildings with the wind which leads to downdraughts into the street and channelling between buildings result in the simplistic general equations relating height and wind speed inaccurate. This imprecision in our understanding of the variation of wind speed with height has a direct effect on a) surface heat transfer coefficients; b) air pressures affecting infiltration; c) air pressures affecting the potential for natural ventilation.

3. METHODOLOGY

The vertical variation of temperature in dense urban areas is not well documented. This case study reports the likely effect of accounting for this 3D variation of temperature and wind speed when modelling tall buildings in dense urban areas. In modelling these 3D effects, the case study equally demonstrates significant impact in a high-rise office building is likely to be subjected to a variance in temperatures, humidity and wind speeds both within and above the Urban Heat Island's Urban Canopy Layer.

Table 1: Modelling flow for different height and weather data

		Different Height			Average
		1st Storey	17th Storey	33rd Storey	1&17&33 Stories
1.epw	Thermal Load	Performance of 1st Storey in 1.epw(kWh/m2.yr)	Performance of 17th Storey in 1.epw(kWh/m2.yr)	Performance of 33rd Storey in 1.epw(kWh/m2.yr)	Performance of 3 Stories in 1.epw(kWh/m2.yr)
	Heating				
	Cooling				
2.epw	Repeat calculation for 2.epw				
3.epw	Repeat calculation for 3.epw				
4.epw	Repeat calculation for 4.epw				

4. URBAN MICROCLIMATE

The urban microclimate of London varies from the weather data collected from Gatwick airport. London is one of the cities which is significantly affected by Urban Heat Island effect especially in summer. The first step in this progress, is to therefore obtain the urban microclimate data for London [2].

4.1 Urban Heat Island weather data

Based on GIS information of London, the buildings of the London central area were modelled and the UHI climate data was calculated by Urban Weather Generator (UWG) [8]. The predicted values of Dry Bulb Temperature{°C}, Dew Point Temperature{°C} and Relative Humidity {%} differ from the original Gatwick data (Fig. 1). The difference between original and UHI monthly averaged Dry Bulb Temperature is larger than 10% (The error bars are ±5% to provide scale).

Using London as an example, the case study has been developed of a typical high-rise office building simulation model based on published data on the 32 tallest office buildings in London[5]. The high-rise office building is 72m*50m*154m high and 35 storeys tall (refer to 5.1).

In the first step, the buildings of the London central area are modelled and then the UHI climate data is calculated using Urban Weather Generator (UWG). Then the UHI climate data is calibrated against published empirical data. A comparison is made of the performances of a) this typical high-rise office building based on climate data collected from a weather station in a rural area; and b) the performance of the same building using UHI adjusted climate data calculated by UWG. The second step models the wind environment of the London central area using a wind speed calculator to get an approximately wind speed in city.

The third step models the typical building in a central city area, tests the temperature and wind at different heights and calculates the performance of different floors (refer to Table. 1). Then energy, temperature and air flow at different heights are compared as well as the second step results.

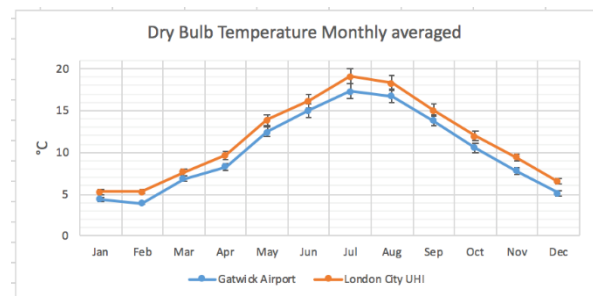


Figure 1: Dry Bulb Temperature Monthly averaged Simulated through Urban Weather Generator (UWG), the maximum of London UHI is 8.3°C and the average of London UHI is 2.32 °C (Fig. 2).

4.2 Urban wind weather data

The EPW (EnergyPlus Weather data file) file of London weather data was collected from Gatwick airport, 47.5km south of Central London. The wind speed collected from airports usually is higher compared to

PLEA 2018 HONG KONG

Smart and Healthy within the 2-degree Limit

the air flow in cities. To ascertain the accuracy of wind speed in urban areas, it is necessary to take terrain into account and calculate relative urban speed.

The Ladybug script, WindSpeedCalculator [9], calculates wind speed at a specific height for a given terrain type (Fig. 3). It is an approximate wind speed and direction of urban area which is used to ascertain whether the air-flow movement has an impact on the building performance.

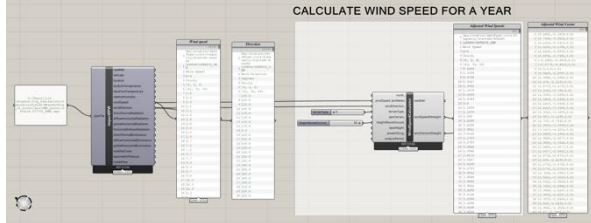


Figure 3: Wind speed and vector of London city calculator

The result for London is that the ratio of the wind Speed of London City to the Wind Speed of Gatwick Airport ≈ 0.4484

4.3 Four kinds of weather data

After taking terrain into calculation, London city weather data with UHI and wind has been predicted.

In addition to the original EPW file of Gatwick Airport, a revised weather file accounting for UHI, a revised weather file accounting for wind and a revised weather combining UHI and wind have been created (Table. 2). These 4 weather data files are used to explore the urban microclimate impacts on simulation of building performance. For example, the influence of UHI on the cooling energy consumption and the influence of air-flow movement on natural ventilation.

Table 2: 4 kinds of weather data of London

No.	Weather data
1.epw	Gatwick airport weather file
2.epw	London city UHI weather file
3.epw	London city wind weather file
4.epw	London city UHI and wind weather file

5. PERFORMANCE OF PROTOTYPICAL OFFICE BUILDING AND ANALYSIS

The building performance at different heights with the different weather data files for a prototypical office building is calculated and compared with each other to explore the influence of height and urban microclimate.

Table 3: Top 32 tallest office building in London [5]

Rank	Name	Height(m)	Floors	Floor to Floor	Floor area(m ²)	Average floor size(m ²)	Year	Primary use	Location
1	22 Bishopsgate	278	62	4.48387097	201863	3255.85	2019	Office	City of London
2	One Canada Square	235	50	4.7	162422	3248.44	1991	Office	Isle of Dogs
3	Heron Tower	230	46	5	43000	934.78	2011	Office	City of London
4	122 Leadenhall Street	225	46	4.89130435	84424	1835.30	2014	Office	City of London
5	8 Canada Square	200	42	4.76190476	164410	3914.52	2002	Office	Isle of Dogs
6	25 Canada Square	200	42	4.76190476	170000	4047.62	2002	Office	Isle of Dogs
7	The Scalpel	192	39	4.92307692	38545	988.33	2018	Office	City of London
8	Tower 42	183	47	3.89361702	30100	640.43	1980	Office	City of London
9	30 St Mary Axe	180	40	4.5	47950	1198.75	2003	Office	City of London
10	100 Bishopsgate	172	40	4.3	73000	1825.00	2018	Office	City of London
11	Broadgate Tower	164	35	4.68571429	37000.3	1057.15	2008	Office	City of London
12	20 Fenchurch Street	160	37	4.32432432	62100	1678.38	2014	Office	City of London
13	One Churchill Place	156	32	4.875	157164	4911.38	2004	Office	Isle of Dogs
14	25 Bank Street	153	33	4.15	97546	2955.94	2003	Office	Isle of Dogs
15	40 Bank Street	153	33	4.63636364	84021	2546.09	2003	Office	Isle of Dogs
16	10 Upper Bank Street	151	32	4.71875	92251	2882.84	2003	Office	Isle of Dogs
17	Heron Quays West 2	147	28	5.25	121789	4349.61	2019	Office	Isle of Dogs
18	25 Churchill Place	130	23	5.65217391	89800	3904.35	2014	Office	Isle of Dogs
19.00	CityPoint	127	36	3.53	110000	3055.56	1967	Office	City of London
20.00	Willis Building	125	26	4.81	50107	1927.19	2007	Office	City of London
21.00	Euston Tower	124	36	3.44	37661	1046.14	1970	Office	Euston
22.00	Millbank Tower	119	33	3.61		0.00	1963	Office	Westminster
23.00	St. Helen's	118	28	4.21	56097	2003.46	1969	Office	City of London
24.00	Centre Point	117	35	3.34	27180	776.57	1967	Office	West End
25.00	Empress State Building	117	31	3.77	43664	1408.52	1961	Office	Earls Court
26.00	1 West India Quay	108	36	3.00			2004	Office	Isle of Dogs
27.00	Shell Centre	107	26	4.12	22761.24	875.43	1961	Office	South Bank
28.00	33 Canada Square	105	18	5.83			1999	Office	Isle of Dogs
29.00	99 Bishopsgate	104	26	4.00	30000	1153.85	1976	Office	City of London
30.00	Portland House	101	29	3.48	29914.78	1031.54	1963	Office	Westminster
31.00	One Angel Court	101	24	4.21	29357.36	1223.22	2017	Office	City of London
32.00	Stock Exchange Tower	100	27	3.70	31000	1148.15	1970	Office	City of London

5.1 Prototypical office building

Under normal circumstances, a real city has a singular urban environment and configuration. The

PLEA 2018 HONG KONG

Smart and Healthy within the 2-degree Limit

prototypical high-rise office building is based on the tallest buildings in London. The average height of the 32 tallest buildings in London is 153m; the average number of floors is 35; and the average floor to floor height is 4.36m (Table. 3). The average floor size of 3592m² is based on the 13rd to 18th tallest buildings as the information on other buildings is not reported. Based on this information, the prototypical high-rise office building for this study is 72m*50m*154m and 35 storeys tall. Three typical floors (defined as top, middle, and bottom) are modelled to represent the performance near the top, near the bottom and around the middle of the building as a whole. A systematic study [10] has shown, these could also be combined to calculate the performance of the whole building. The top floor is the one under the highest floor, and the bottom is floor is the one just above the ground floor (Fig. 4).

Top 33rd floor
 Middle 17th floor
 Bottom 1st floor

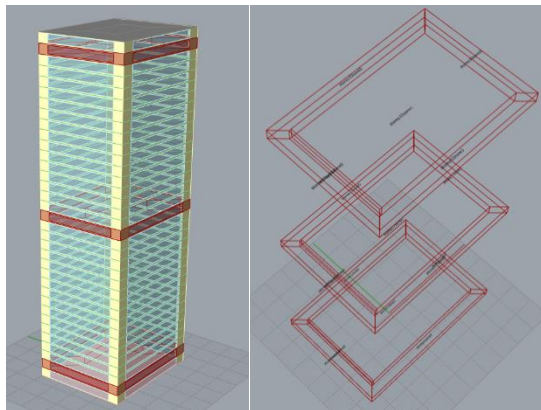


Figure 4: 3 floors of typical high-rise office building

Each floor of the prototypical high-rise office building is split into 6 zones, 4 perimeter zones, 1 core zone and 1 IT room zone (Table. 4). The thermal zones and perimeter zone depth settings are according to PNNL prototype office large [11] and large office studies of Lawrence Berkeley National Laboratory (LBNL 1991) [12].

Table 4: The percentage of each zone

Name	Function	% on floor size
Zone0	IT room	1%
Zone1	Core Zone	67.89%
Zone2-Zone5	Perimeter zone	31.11%

5.2 Urban Microclimate

To explore the influence of UHI and wind in urban areas on the accuracy of modelling, total thermal load, cooling load and heating load of the 3 floors are compared with each other.

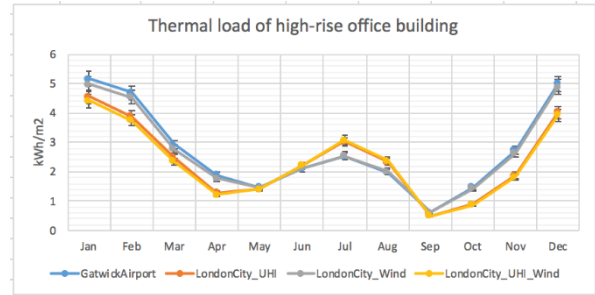


Figure 5: Thermal Load with 4 different weather data

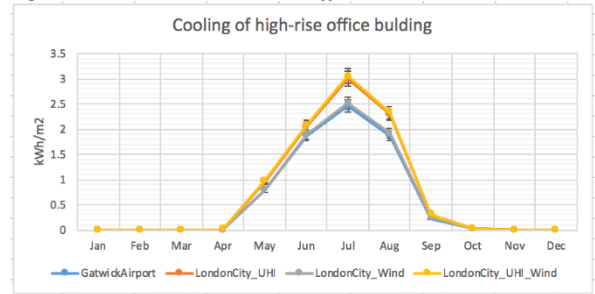


Figure 6: Cooling with 4 different weather data

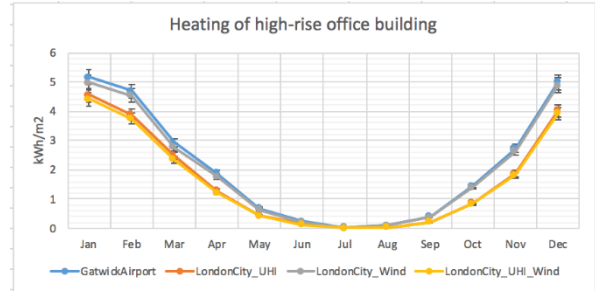


Figure 7: Heating with 4 different weather data

As shown in Figures 5-7, UHI has a significant influence on the building performance simulation. Most of the year, there is a more than 10% difference in energy consumption when UHI effects are taken into account compared with results found using the original weather data. Estimated wind speed in the urban area has a less than 5% effect on the energy performance modelling. It is not clear whether the accurate air-flow movement has more significant influence on the building performance especially on natural ventilation of the building. The additive effect of the wind might be significant for the overall results.

5.3 Height

Three typical floors of the high-rise building have been selected to explore the height influence of building performance.

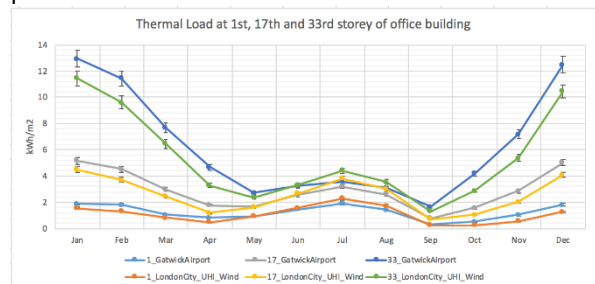


Figure 8: Thermal Load at different floors-UHI and Wind

PLEA 2018 HONG KONG

Smart and Healthy within the 2-degree Limit

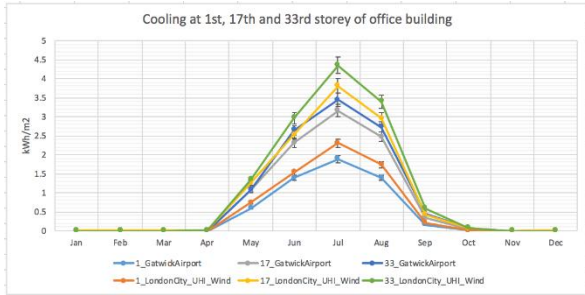


Figure 9: Cooling at different floors-UHI and Wind

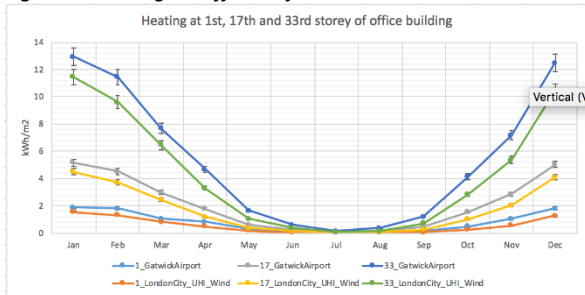


Figure 10: Heating at different floors-UHI and Wind

As shown in Figures 8-10, the higher floor has higher thermal load, higher cooling in summer and higher heating energy consumption in winter. The urban microclimate with UHI and wind has a significant influence on cooling in summer and heating in winter, with more than 10% difference in energy consumption.

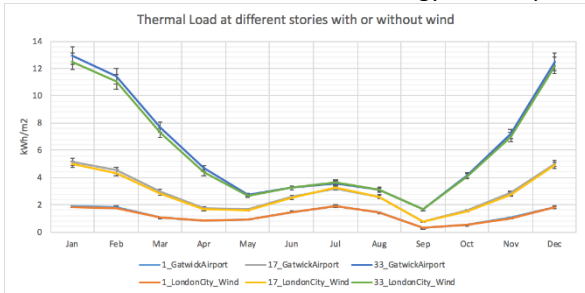


Figure 11: Thermal Load at different floors – wind

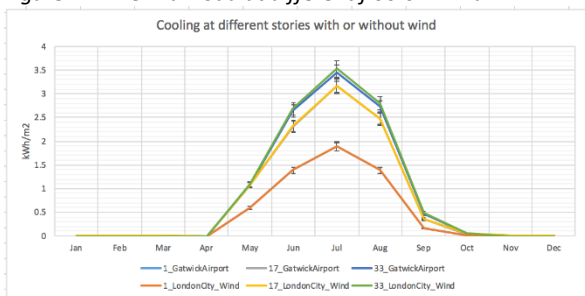


Figure 12: Cooling at different floors – wind

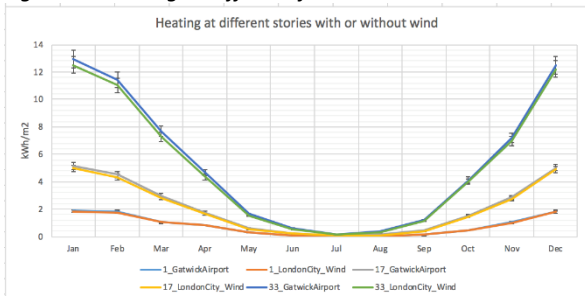


Figure 13: Heating at different floors - wind

As shown in Figures 11-13, wind impacts significantly on the thermal load in winter, cooling in summer and heating in winter at the higher location. Figure 12 shows that the 1st floor cooling with and without wind are almost the same, and the 1st floor heating are quite similar (Fig.13). On the 33rd floor there is a more significant difference. So, as the height increase, the wind has a greater effect.

5.4 Natural Ventilation

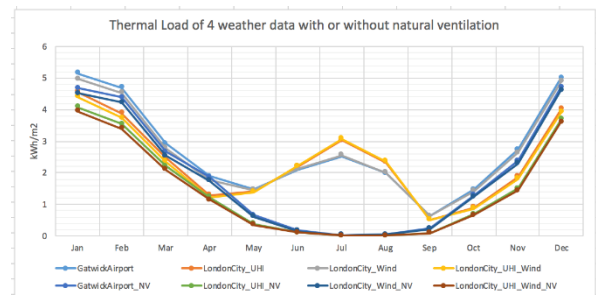


Figure 14: Thermal Load of 4 weather data with or without natural ventilation

Figure 14 shows that, natural ventilation alters the thermal load in summer though reducing the cooling energy consumption, especially when UHI effects are considered.

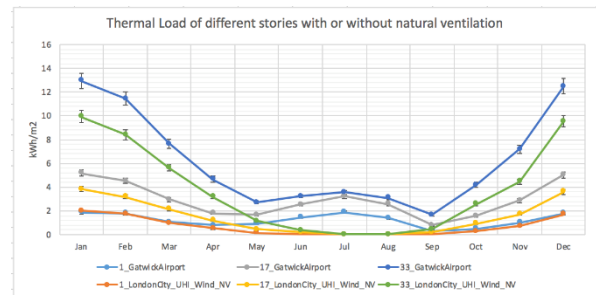


Figure 15: Thermal Load of different stories with or without natural ventilation

Figure 15 shows that as height increase the impacts of urban microclimate and natural ventilation are more pronounced. During winter, the variation of the 33rd floor is more than 20%, but less than 5% at the 1st floor. To determine accurate building performance, it is therefore necessary to take UHI and wind as well as natural ventilation into consideration.

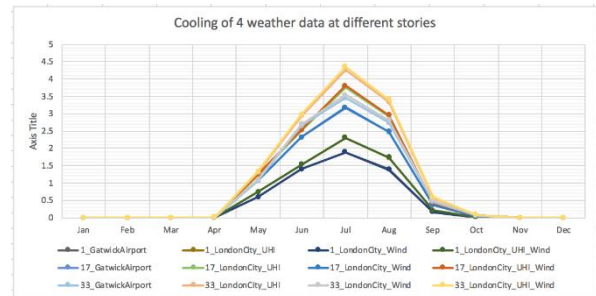


Figure 16: Cooling of 4 weather data at different stories

In this research, the natural ventilation application means the cooling consumption decreases to 0kwh/m². Figure 16 shows that, the higher the floor, the more

PLEA 2018 HONG KONG

Smart and Healthy within the 2-degree Limit

cooling consumption. That means, natural ventilation is much more efficient with increasing height.

5.5 Vertical Variation

The wind speed increases with height, and temperature decreases with height. How these changes impact the simulation results is explored through adding following additional variables into an EnergyPlus model.

HeightVariation:

0.22-Wind Speed Profile Exponent

370-Wind Speed Profile Boundary Layer Thickness {m}

0.0065-Air Temperature Gradient Coefficient {K/m}

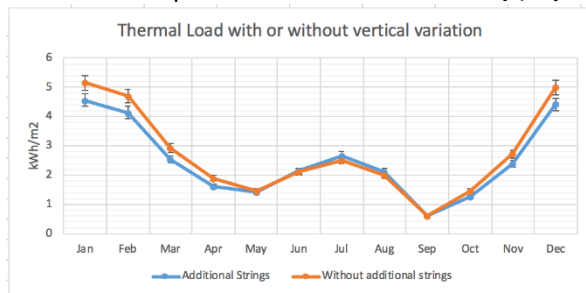


Figure 17: Thermal Load - vertical variation

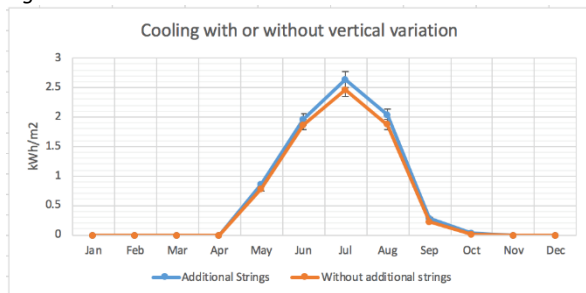


Figure 18: Cooling - vertical variation

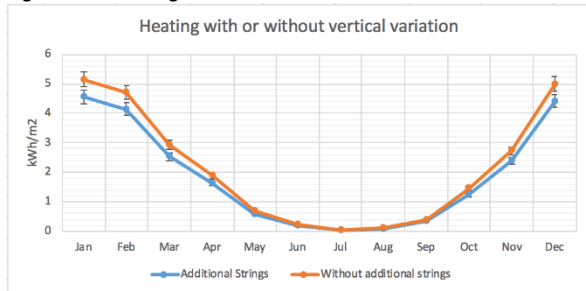


Figure 19: Heating - vertical variation

Figures 17-19 show that, vertical variation has significant impacts in winter and summer which means the vertical wind and temperature variation could not be ignored.

6. CONCLUSION

Accounting for UHI effects results in a more than 10% variation in the performance simulation results.

Accounting for the variation in wind between open field and urban environments results in a less than 5% variation in the performance simulation results, and its influence increases with height.

Natural ventilation efficiency is affected by UHI effects and height.

Vertical variation in weather variables effects has significant impacts on the performance simulation results in winter and summer.

This paper has confirmed that the urban microclimate effects on building performance can be modelled. This generic modelling has also confirmed that the effects are potentially of sufficient size that more detailed modelling is required.

At present, the model of the wind is a generic model recognising that the natural rate of increase of wind speed with height is much slower in the City than it is in the country where weather files for building simulation are typically measured. These generic models are well-validated. This wind model needs to take into account the specific aerodynamics of the real geometry of a city. The next stage of this research will be to evaluate the reliability of a CFD model of these. Similarly, the generic horizontal plane definition of the Urban Heat Island needs to be tested to determine how to make it specific to a particular urban geometry: could isolated tall buildings drag wind down in between lower rise neighbours thus "ventilating" the city?

REFERENCES

1. S., W. & W., M., (2008). Users Manual for TMY3 Data Sets. Available: <http://www.nrel.gov/docs/fy08osti/43156.pdf> [October 26, 2016].
2. Kotthaus, S. and C. S. B. Grimmond (2014). "Energy exchange in a dense urban environment – Part II: Impact of spatial heterogeneity of the surface." *Urban Climate* 10, Part 2: 281-307.
3. Wong, P. P.-Y., et al. (2016). "The impact of environmental and human factors on urban heat and microclimate variability." *Building and Environment* 95: 199-208.
4. Oke, T.R., (1973). City size and the urban heat island. *Atmospheric Environment*, 7(8), pp.769–779.
5. Hafner, J., & Kidder, S. Q. (1999). Urban heat island modelling in conjunction with satellite-derived surface/soil parameters. *Journal of applied meteorology*, 38(4), 448-465.
6. Brunt, D., (1933). The adiabatic lapse-rate for dry and saturated air. *Quarterly Journal of the Royal Meteorological Society*, 59(252), pp.351–360.
7. "List of Tallest Buildings and Structures in London." 2018. Wikipedia. https://en.wikipedia.org/w/index.php?title=List_of_tallest_buildings_and_structures_in_London&oldid=844483518.
8. Software available from <http://urbanmicroclimate.scripts.mit.edu/> (Last accessed, August, 2018)
9. Software available from <https://www.grasshopper3d.com/group/ladybug> (Last accessed, August, 2018)
10. Ellis, P. and Torcellini, P. Simulating Tall Buildings using EnergyPlus. NREL Conference Paper <https://www.nrel.gov/docs/fy05osti/38133.pdf> (Last Accessed, August, 2018)
11. Documents available from https://www.energycodes.gov/development/commercial/p/rototype_models

PLEA 2018 HONG KONG

Smart and Healthy within the 2-degree Limit

12. LBNL (1991). Huang, Joe, Akbari, H., Rainer, L. and Ritschard, R. 481 Prototypical Commercial Buildings for 20 Urban Market Areas, prepared for the Gas Research Institute, Chicago IL, also LBL-29798, Berkeley CA.

Study on Firewood Consumption Patterns in Dhading District of Nepal

POKHAREL TIKA RAM¹, RIJAL HOM BAHADUR¹, MASANORI SHUKUYA¹

¹Tokyo City University, Japan

ABSTRACT: People in rural areas of Nepal have been using firewood for a variety of household purposes. In this paper we analysed the firewood consumption patterns and their relationship with family size and the number of livestock rearing in the study area of Dhading district of Nepal. A survey on periodic household firewood consumption was carried out for 24 hours in 16 households. The per-capita firewood consumption was found 1.75 kg/capita/day and average household firewood consumption was found 12.1 kg/family/day. We found household firewood consumption increases as family size increases but the per-capita firewood consumption decreases with the increase in family size. Firewood consumption also increases with the increase in the number of livestock reared. The rates of firewood combustion of small and big households were 1.28 kg/hour and 1.34 kg/hours respectively. Average period for firewood burning of either small or big households was found from 8.7 to 9.9 hours per day. Based on the information on the firewood consumption patterns of Dhading district obtained from the measurement survey, it is considered that the improvements on traditional cooking stoves together with improvement of indoor environmental condition that influence very much on the health of the rural people is of vital importance.

KEYWORDS: Nepal, Energy, Household firewood combustion rate, Family size, Livestock rearing

1. INTRODUCTION

Firewood is one of the important traditional energy resources for the rural population of developing countries. Like many other developing countries, firewood, crop residues, animal dung, and Liquefied Petroleum Gas (LPG) are the main cooking and lighting fuels in Nepal. Firewood has been used as an energy source since the invention of fire and still used as the major energy source in many developing countries. About 2.6 billion people in developing countries fulfil their basic energy demand for cooking and heating by mostly using fuel wood in a very inefficient, unhealthy and unsustainable way [1] and the trend will persist in the foreseeable future especially in rural areas of those countries [2]. Nepal is one of the least developed and low-energy using country in the world with 83% of the population living in rural area [3]. It has been illustrated that the energy use and energy access situations in Nepal are far below the level of basic human needs, and firewood is expected to remain as the dominant fuel source for the foreseeable future [4, 5]. In Nepal firewood is mainly used for cooking and space heating in winter season.

As of 2010, over 30% of total households lack their access to electricity and 78% of total households rely on traditional biomass for cooking [6]. According to the recent household survey (2015/16) of central bureau of statistics Nepal, firewood is major source of cooking fuel for 60.9% of total household in Nepal. It is used by 76.5% rural and 37.9% urban households. The use of LPG gas is the second most used cooking source in Nepal (26.8%). Electricity has become the prime

source of lighting and used by 76.3% of households. 37.9% of urban household use electricity as cooking fuel. It is also found that 7.5% use cow dung, 2.7% biogas, and 0.3% other source for cooking. In rural Nepal firewood burn in inefficient traditional cook stoves and creates high indoor air temperature and low indoor air quality [7]. Many researches have been done in different parts of country but we found limited studies on firewood consumption pattern in Dhading district. Therefore, this research focused on firewood consumption patterns of the Dhading district.

Households account for nearly 87% of country's total energy uses in Nepal [8, 9]. Choice of household energy depends up on the availability of energy resources for example in the rural area of Nepal there is a less accessibility of commercial fuel resources and people rely on traditional fuels such as firewood and animal dungs where as in the urban households there is less accessibility of firewood and which creates opportunity to use commercial fuels like electricity and LPG.

The use of firewood has led to severe consequences on ecological and environmental degradation. Consumption of dry biomass as fuel in kitchens without proper ventilation has created serious health problems among the rural population.

Expanding economic activity and population growth are the two basic factors behind an increase in energy use. Recent development of modern transportation facility and improvement on the commercial energy availability plays a significant role in the energy use pattern of Nepal.

PLEA 2018 HONG KONG

Smart and Healthy within the 2-degree Limit

In Nepal most of the people directly or indirectly associated with problems caused by firewood burning therefore, the improvements on firewood burning cook stoves play positive impact. Previous studies focused on firewood consumption and its associated environmental and health concern in Nepal reveal that the total firewood consumption 235-1130 kg/capita/year [8]. Fox 1984 [10] conducted a study on firewood consumption in a Nepali village in Bhogateni at Gorkha district. This study shows that the mean firewood consumption was 0.95 m³/person/year. He also concluded that the rate of firewood consumption was influenced by family size, cast and season but not by farm size. Smaller per capita firewood consumption in larger household was found in the study. Bhatta and Sachan [12] suggested that the higher firewood consumption was mainly due to the lack of unconventional energy sources. This study also concluded that the firewood consumption differs according to the family size and smaller families has more per capita firewood consumption than those of medium and large families. They also conducted another research on firewood consumption along an altitudinal gradient in mountain villages of India. They found firewood consumption increases as the altitude is higher [11].

Previous researches on firewood consumption pattern in different parts of the different country has clearly established family size as a key driving force for firewood consumption. However, in Dhading district there has not been sufficient study on firewood consumption pattern and its relationship with family size. Therefore, from this research we compare the existing findings to the present results.

Due to the subsistence farming system in rural area of Nepal, people rear animals for different purpose. For these animals they make feed which require firewood. This amount of firewood also affects the household firewood consumption but there are not sufficient researches which explain whether firewood consumption increases or not with the increase in the number of animal being reared by people. Bewket [12] have investigated the relationship of livestock reared by rural households with the firewood consumption in Ethiopia and found negative correlation between fuelwood use and cattle ownership. In this present research we analyse the effect of smaller animal and bigger animals on firewood consumption.

Many study on firewood consumption focus on the investigation of per capita firewood consumption and household firewood consumption on macro scale time (daily and Yearly basis), However, there has not been any research found on the firewood consumption with respect to micro scale time (hourly basis). Macro scale information alone cannot give clear information on indoor environmental condition of kitchen. Without information of firewood consumption with respect to

micro scale time, it is difficult to find how, when and at what rate indoor air pollutants and heat generate in the firewood burning spaces. Therefore, we concentrate our focus on firewood consumption with respect to time and got rate of firewood combustion and periodic firewood consumption which may give better idea for indoor environmental condition of firewood burning space of rural households

The main objective of this research is to evaluate the rate of firewood combustion of traditional cook stoves of rural households of Nepal. Following are the objectives of this study.

To evaluate the firewood consumption pattern of rural households of Dhading district.

To know relationship between firewood consumption and family size.

To know the relation between firewood consumption and livestock rearing.

To compare firewood combustion rate between small and big family.

2. METHODS AND MATERIALS

2.1 Study area

The research was conducted in Jyamrung village development committee in Dhading district with an altitude of about 1500m. The climate of this region is temperate the average temperature at 22.8 °C, the average minimum temperature at 17.3 °C and the average maximum at 28.4 °C. The annual average rainfall is 2329mm of which 80% is followed in monsoon season [13]. Agriculture and livestock rearing are the main occupations of the households. They use firewood as their primary energy sources for cooking and heating which is available nearby community forest and their own land. The majority of households have traditional cooking stoves made by mud and stones rather than improved cooking stoves. Firewood collection was mainly done by women (figure 1). Men and children also contribute to the firewood collection. Only physical energy was used to collect firewood in studied households. People generally burn firewood inside the enclosure. Most of the houses are facing towards the south and a few of them are facing towards east side.

2.2 Data collection

The field survey was conducted in rural households in Dhading district in winter season. Random sampling method was applied for selection of the sample households. The quantity of firewood consumed was measured over a period of 24 hours using a weight survey method. For this study certain weighted firewood bundle was provided in the beginning of study and remaining amount of firewood was measured every hour for hole day and the same process was followed for one day for every 16 households. The semi structured questionnaires were

PLEA 2018 HONG KONG

Smart and Healthy within the 2-degree Limit

used for the collection of different information during the survey period.



Figure 1: Carrying firewood and preparing animal feed in rural area of Nepal

2.3 Calculation for analysis

Per-capita firewood consumption and average household firewood consumption was calculated by following formula.

Per capita firewood consumption (kg/capita/day) = Total firewood burnt in one day for all households/total number of the family members of all households

Per capita firewood consumption (kg/capita/year) = Total firewood burnt in one day for all households × 365/ total number of the family members of all households

Household firewood consumption (kg/family/day) = Total firewood burnt in one day for all households/ Total households

3. RESULTS

3.1 Firewood consumption

Firewood is the main source of energy for cooking in the study area. All households were using firewood for regular cooking and boiling water. No household in that area used commercial fuel for cooking activities. After cooking a meal fire is often used for boiling water and maintaining thermal environment of the room in the winter season. Some households with aged people maintain fire for the whole day to make hot tea for aged people and to keep their home warmer. The household size was ranged from 2 to 14 members. Average household size was 6.9 persons, which was higher than average household size 4.9 persons of Nepal from the national household survey 2014. In this study we found per capita firewood consumption as 1.75 kg/capita/day and 639kg/capita/year. Likewise, we found average household firewood consumption as 12.1 kg/family/day. This covers firewood for cooking, lighting and heating purpose. Nearby community forest and private land were the source of firewood. All household use traditional cook stoves for firewood burning and cooked meals three times per day.

3.2 Relationship between firewood consumption and household size

Average household size has a significant effect on total firewood consumption. In this research, there was a statistically significant relationship between household size and firewood consumption. Figure 2 showed that the household firewood consumption increases as increase in the family size however the per-capita firewood consumption decreases as increase in the family size. In this study we found comparatively less firewood consumed by small households than big households. In small family, they need more firewood than they actually need. Certain amount of firewood must be burn to heat firewood burning cook stoves, cooking pots and others surroundings in all households which make difference on per capita firewood consumption between small and big family. The sharing of such amount of firewood in big family contribute to make the per capita firewood consumption lower than small family.

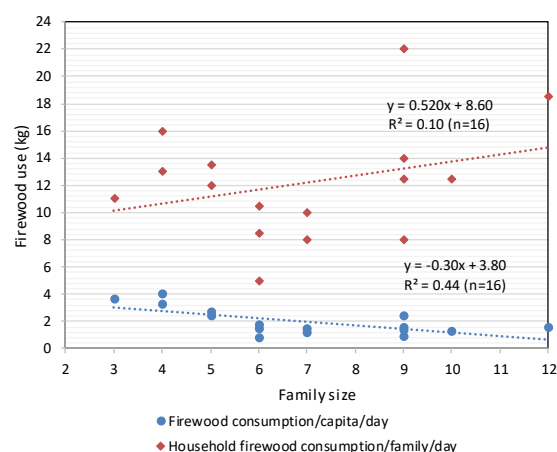


Figure 2. Relationship between firewood consumption and family size

3.3 Relationship between firewood consumption and livestock rearing

From figure 3, we can see the positive correlation between the firewood consumption and livestock rearing. It means that households with more livestock units use more firewood and household having less livestock unit use less amount of firewood. Regression coefficient of big animals was bigger than small animals which is clearly shown in figure 3. This is because of the requirement of more food for bigger animals than smaller animals. Likewise, people give more animal feed for milking animal for better milk production than non-milking animal which also contributes on firewood consumption. In the substantial farming system in Nepal people rear animals for different purposes. In our study people rear buffalo and cow for milk purpose, ox for energy and goat for meat purposes.

PLEA 2018 HONG KONG

Smart and Healthy within the 2-degree Limit

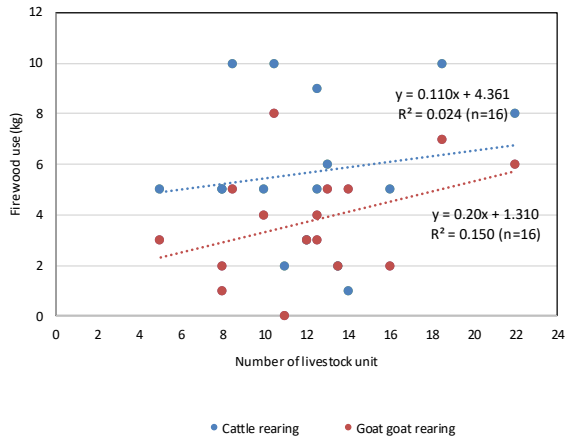


Figure 3. Relationship between firewood consumption and livestock rearing

3.4 Hourly rate of firewood consumption

Hourly household fuelwood consumption was calculated based on hourly data form all studied households in one day. Figure 4 shows the 24-hour firewood consumption pattern. In this figure the horizontal axis indicates the time interval and the vertical axis indicates the cumulative household firewood consumption in 16 households for one day. Figure show that the household firewood consumption was high at the morning time than evening and day time. The maximum firewood consumption in 16 households was 29 kg at 6-7 am, followed by 22kg at 5-6 pm and 16 kg at 3-4 pm.

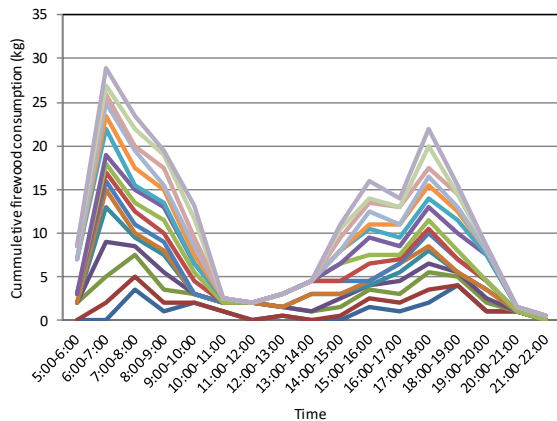


Figure 4. Periodic firewood consumption pattern of 16 households

3.5 Rate of firewood combustion

Rate of firewood combustion is related with the production and distribution of air pollutant around the kitchen, which ultimately affect the health of the people who exposed to the pollutants. The rate of firewood combustion in cook stoves was calculated by dividing total firewood consumed in all households by

total time. For the comparison of the rate of firewood combustion between small and big households, we divided all households in two categories i.e., small households with family member up to 6 persons and big families with family members more than 6 persons. Average family size of small households and big households was found as 5 and 9 persons/family. Average time of firewood combustion was 8.7 hour/day/family and 9.9 hours/day/family for small and big family. The rate of firewood combustion was found as 1.3kg/hours for both small and big family. As shown in figure 5 there was no big difference in the rate of firewood combustion between small and big households. From this information we concluded that the energy requirement of big family was achieved by using firewood for long time instead of burning big amount of firewood in short time therefore the rate of firewood combustion was not markedly differing from each other.

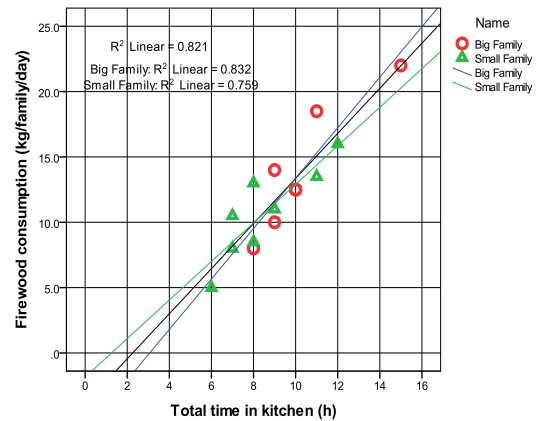


Figure 5. Rate of firewood combustion of small and big households

4. DISCUSSION

A large number of households of the country still depends primarily on firewood for cooking fuels in Nepal. There have been several studies on annual firewood use in the hilly region of Nepal and the annual per capita firewood use very widely: 198kg [14] 464kg [15], 492 [16], 570kg [10], 614 kg [17], 940kg [18], 663kg [19], 511kg [7]. Thus, our estimates of annual per capita firewood use as 639kg/capita/year, which falls in the middle of previous studies on similar research. Several factor could have effect on firewood consumption so that there was big variation on firewood consumption pattern within the similar climatic zones. Other cause may be the difference on the method applied for the research for example some researcher measure firewood use for certain few days but some researcher measure for long time period. That can also differ the amount of firewood consumption.

Per capita firewood consumption, household firewood consumption of this research was found 1.75

PLEA 2018 HONG KONG

Smart and Healthy within the 2-degree Limit

kg/capita/day and 12.1 kg/family/day which is within the range (0.96-1.75 kg/capita/day) of the result obtained from the study on similar climatic region by Fox [10]. Similar study carried out by Rijal et al. [7] found per capita firewood consumption as 1.4 kg/capita/day and household firewood consumption as 8-11 kg/family/day. This result is slightly lower than the result obtained from our present result because our research was conducted only for one day in winter season but the study carried out by Rijal et al. for the whole year. Rijal et al. [7] also investigate the seasonal difference in firewood consumption and found higher firewood consumption in winter season.

Our study showed that there is a significant relation between firewood consumption and household size. Kandel et al. [20] carried out a study on a household firewood composition pattern in Dolakha district and found per capita firewood consumption and average household firewood consumption rate as 1.7 kg/capita/day and 8.4 kg/family/day. Per capita firewood consumption obtained by Kandel is similar to our study but the household firewood consumption is slightly lower than our present study. The cause for the lower household consumption rate might be due to the difference in family size of households. This study also concluded that the total firewood consumption of the household is significantly correlated with household size, ownership of the cultivated irrigated terraces and number of livestock per household. The study also concluded that the firewood consumption shows a typical seasonal pattern.

The household sector accounted for most of the energy consumed in the past and this trend is projected to remain the same in next 30 years [5]. Various factors could have effect on firewood consumption pattern, therefore, the average firewood consumption in different regions of Nepal differs markedly across the country.

Fox, [10] have concluded that the rate of firewood consumption was influenced by family size, cast and season but not by farm size. Smaller per capita firewood consumption in larger household was found in the study. Bhatta and Sachan, 2004 had concluded that the firewood consumption differs according to the family size and smaller families has more per capita firewood consumption than those of medium and large families. Our results on relationship between firewood consumption and family size clearly indicates that the firewood consumption of households increases with increase in the family size however per capita firewood consumption decreases with the increase in the family size (Fig. 2).

Nepal is agriculturally dominant economy where 74% of the households rely on the subsistence-based agricultural sector [21], where people rear many animals in their home for energy, meat and economic purpose which affect the household firewood

consumption pattern. From this research we found the significant positive relationship between firewood consumption and number of livestock rearing. Mahapatra and Mitchell [22], Cooke [23], Baland et al. [24] had found that households with more livestock units consume more firewood, however Bewket [12] found a negative correlation between firewood consumption and animal rearing because animal dung was widely used as a substitute for fuelwood in his study area in Ethiopia. Our finding was similar to the relationship obtained from the research by Mahapatra and Mitchell [22], Cooke [23], Baland et al. [24] and opposite with the finding results of Bewket [12]. In our study area people did not use animal dung as energy source and hence firewood consumption was not decreased with increase in the number of livestock unit. But it increases with the increase in the number of livestock unit.

Firewood burning time has a significant effect on environmental and health condition of the people who exposed to that environment. However, we did not find research on firewood consumption with respect to time. From this research we found average firewood burning time of small and big households as 8.7 hours and 9.9 hours respectively. We also noticed that the maximum firewood was burnt in the morning and evening time (Fig. 4). Therefore, in the rural society the morning and the evening time is more problematic due to the indoor air pollutant. Firewood burning is also related to the indoor thermal environment. People generally burn firewood to make their home warm in winter season. Proper ventilation system and improvements in the firewood burning cook stove helps to improve the indoor air quality and hence can improve the health condition of rural people. Due to the excess burning of firewood, environmental and health problems in the rural households may occur. Installation of the improved cook stoves play significant role for the betterment of indoor air quality and health of the people. An intensive awareness program is suggested for the effective improvements of air quality and health condition. Subsidies for the installation of improved cook stoves may create positive impact.

5. CONCLUSIONS

We collected data of firewood used and investigated the firewood consumption patterns with respect to time in the rural households. All households use traditional firewood burning cook stoves without proper ventilation system which may create health problems to the people who exposed to that environment. The findings are summarized as follows.

The Per capita fuelwood consumption of the study area was found 1.75 kg/capita/day and 639 kg/capita/year. Household firewood consumption was found 12.1 kg/capita/day, which is similar to the other

PLEA 2018 HONG KONG

Smart and Healthy within the 2-degree Limit

studies conducted on similar climatic regions of Nepal. Periodic firewood consumption was found high in the morning and evening time.

Total firewood consumption was affected by family size and units of livestock rearing.

Firewood combustion rate was found 1.28 kg/family/hr. and 1.34 kg/family/hr. for small and big families but big family spend longer time in kitchen for cooking activities.

REFERENCES

Fritsche et al., (2014). Applying resource efficiency principals to the analysis of EU-27 bioenergy options by 2020-findings from a recent study for the European Environment Agency. *Biomass and Bioenergy*, 65: p. 170-182.

Arnold and Persson (2003); Applying resource efficiency principals to the analysis of EU-27 bioenergy options by 2020-findings from a recent study for the European Environment Agency. *Biomass and Bioenergy*, 65: p. 170-182.

CBS (2011), Central Bureau of Statistics Nepal, National Report 2011

Pokharel S. (2007) An econometric analysis of energy consumption in Nepal. *Energy policy*, 35; p 350-361

Malla S., 2013. Household energy consumption patterns and its environmental implications: Assessment of energy access and poverty in Nepal. *Energy Policy*, 61, p.990–1002.

CBS (2011) National Population and Housing Census 2011 National Report, Kathmandu

Rijal and Yoshida (2002). Investigation and evaluation of firewood consumption in traditional houses in Nepal. *Proceeding Indoor Air* p. 1000–1005

CBS (2012). National Population and Housing Census 2011 National Report, Kathmandu).

WECS (2010) Energy Sector Synopsis Report 2010.

Fox J., (1984) Firewood consumption in a Nepali village. *Environ Manage.* 8, p. 243–249.

Bhatta and Schan (2004). Firewood consumption along an altitudinal gradient in mountain villages of India. *Biomass Bioenergy* 27 (1): 55-57

Bewket W. (2005). Biofuel consumption, household level tree planting and its implications for environmental management in north-western highlands of Ethiopia. *EASSRR* 21; p19-38

Climatological records of Nepal from 1995-1996. From the Ministry of science and technology, department of hydrology and metrology Kathmandu Nepal

Adhikari et al. (2004) household characteristics and forest dependency: evidence from common property forest management in Nepal. *Ecol Econ*, 48: 245-247

Shrestha (2005). Fuelwood harvest, management and regeneration of two community forests in central Nepal. *Himal J Sci* 3(5) p: 75-80.

Mahat et al. (1987). Human impact on some forest s of middle hills of Nepal. *Mt Res Dev*, 7: p:111-34

Metz JJ (1994). Forest product use at an upper elevation village in Nepal. *Environ manag* 18 (3); P:371-90.

Bajracharya D. 81983), Fuel, food or forest? Dilemmas in a Nepali village. *World Dev.*,11; P:1057-74

Webb E.L. and Dhakal A., (2011) Patterns and drivers of fuelwood collection and tree planting in a Middle Hill watershed of Nepal. *Biomass and Bioenergy*, 35, p. 121–132

Kandel et al (2016). Consumption pattern of fuelwood in rural households of Dolakha district of Nepal. *Reflections from community forest user group. Small scale forestry* p; 441-495

Joshi et al. (2017). Valuing farm access to irrigation in Nepal. *Water manag*, 181,p;35-46

Mahapatra and Mitchell (1999), Biofuel consumption, degradation and farm level tree growing in rural India. *Biomass Bioenergy* 17(4) p; 291-303

Cooke (2009) Changes in Intrahousehold labor allocation to environmental goods collection: a case study from rural Nepal, 1982 and 1997. *FCND Discussion paper no. 87*

Baland et.al (2012). Fuelwood collection and economic growth in rural Nepal 1995-2010: evidence from a household panel. Department of economics working papers series. University De,Namur, pp;1-51

Pokhrel T.R. 2016. Study on firewood use pattern in different ecological regions of Nepal, Asian science conference 1016, Philippines

Arnold et al. 2006). Wood fuels, livelihoods and policy interventions: changing prospective. *World Dev* 2006; 34(3) 596-611

Passive Down-Draught Evaporative Cooling Applicability and Performance in Single Family Houses

CRISTINA SOTELO-SALAS¹, CARLOS J. ESPARZA L.¹, CARLOS ESCOBAR DEL POZO²

¹Faculty of Architecture and Design, University of Colima, Coquimatlan, Mexico

²Faculty of Electrical and Mechanical Engineering, University of Colima, Coquimatlan, Mexico

ABSTRACT: Elevated energy consumption due to air conditioning dependency in the hot dry climate states of northern Mexico contribute to greenhouse emissions, which in turn is reflected in local and global climate change, higher risk of blackouts, and electric infrastructure viability. This study approaches a passive cooling alternative to air conditioning, through a Passive Downdraught Evaporative Cooling tower, a Computational Fluid Dynamics (CFD) evaluation is realized, to estimate temperature reduction and air flow conditions. Eighteen scenarios were simulated, where the parameters for the assessment were inlet wind velocity, water droplet size, and water flow rate. The best-case scenario is presented, and temperature reduction is sufficient to consider the PDEC tower as a feasible alternative to conventional air conditioning in summer months.

KEYWORDS: Passive Cooling, Passive Downdraught Evaporative Cooling, Evaporative Cooling

1. INTRODUCTION

In 2010 buildings accounted for 32% of total global final energy use. Building energy use will increase due to population growth, migration to cities and lifestyle changes, as well as the effects of climate change on global temperature rise. Developing countries represent a significant opportunity to implement climate change mitigation measures, and as such, buildings are a critical part of sustainable development [1].

Hot dry climate regions of northern Mexico represent an opportunity of mitigation strategy implementation due to elevated energy consumption associated with air-conditioning system dependency to achieve thermal comfort. Therefore, passive cooling measures applicability and performance are addressed in this study, to minimize energy consumption and contribute to climate change mitigation goals.

2. PASSIVE DOWN-DRAUGHT EVAPORATIVE COOLING

Passive downdraught evaporative cooling (PDEC) has been widely studied in the hot dry climates of the Middle East and southwestern United States, and in recent years in more temperate climates of southern Europe, to provide alternatives to mechanical air conditioning to reduce carbon emissions through energy conservation.

The PDEC system, is designed to capture the wind at the top of a tower and cool the outside air using water evaporation before delivering the cooled and humidified outside air to a space [2].

The downdraught may be generated by either: irrigation of a cellulose matrix in the path of the air stream (cool tower), large droplets of water sprayed

into the air stream (shower tower), a mist of water sprayed into the air stream (misting towers) or wetted porous surfaces located within the air stream (porous media in an air shaft) [4]. The smaller the drops the easier water evaporates, due to the increase in the contact surface between water and air [3].

3. METHOD

Case studies were selected to determine PDEC performance. They were evaluated in the climatic conditions of Mexicali, Mexico, a border town with southern California, with extreme hot dry weather. These evaluations were made for the summer period. Evaporative cooling potential was determined through a psychrometric analysis, a Passive Down-draught Evaporative Cooling system is selected accordingly, the system was pre-sized through PHDC Air Flow software developed by the Association of Research and Industrial Cooperation of Andalusia (AICIA) [4] and air flow and performance were obtained through simulation in ANSYS FLUENT® CFD Software.

3.1 Comfort range assessment

Comfort range was determined with the ASHRAE 55-2010 Standard, as 26.8°C-30.4°C in the critical summer month studied.

PLEA 2018 HONG KONG

Smart and Healthy within the 2-degree Limit

3.2 CASE STUDIES

Two case studies were selected, a one-story dwelling of 56 sq. meters, and a two-story dwelling of 72 sq. meters. Together they constitute 75% of the social interest housing segment in Mexico [5], and therefore present a clear picture of housing conditions in the hot dry climate states of northern Mexico.

Misting towers were selected because they do not incorporate additional elements such as wetted pads or ceramics, that may prove costly to the intended market, and unlike shower towers, they do not require a pool to gather excess water and provide significantly less moisture content in the supply air. Perimeter towers were proposed to take advantage of the existing building envelope for cost-efficiency purposes.

3.2.1 SINGLE STORY DWELLING (56 m²)

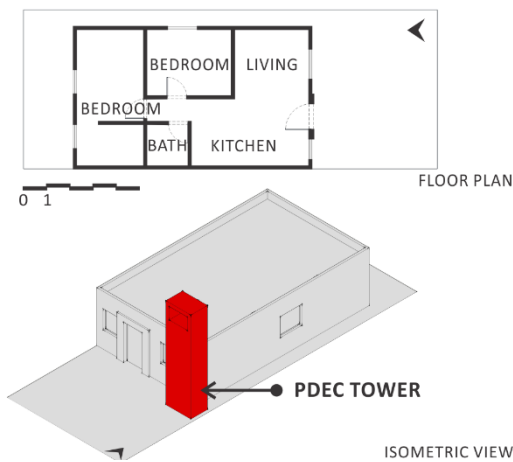


Figure 1: One-story dwelling, architectural plan and isometric.

The single-story dwelling of 56 m², has two bedrooms, one full bathroom and kitchen, dining and living room area. Average indoor height is 2.4 m. Envelope materials are 0.12 m concrete masonry blocks, and a 0.17 m concrete beam and polystyrene vault roof. The proposed location of the PDEC tower is indicated in fig.1, considerations for location selection were air distribution capabilities and architectural integration.

3.2.2 TWO-STORY DWELLING (72 m²)

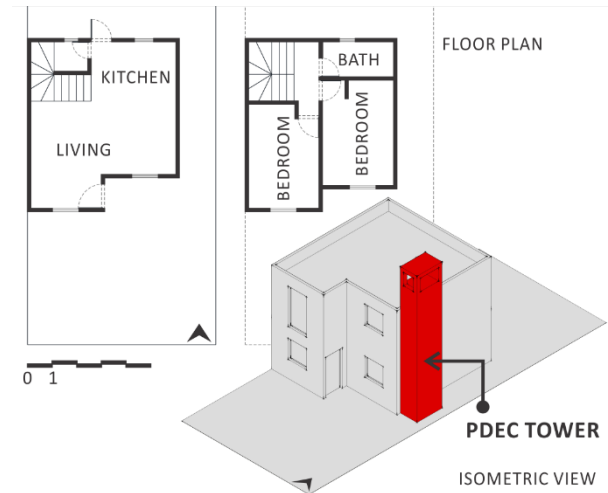


Figure 2: Two-story dwelling, architectural plan and isometric.

The single-story dwelling of 72 m², has two bedrooms, one and a half bathrooms, as well as kitchen, dining and living room areas. Average indoor height is 2.5 m. Envelope materials are 0.12 m concrete masonry blocks, and a 0.17 m concrete beam and polystyrene vault roof. The proposed location of the PDEC tower is indicated in fig.2, considerations for location selection were air distribution capabilities and architectural integration.

3.3 PDEC TOWER DESIGN

3.3.1 Pre-sizing process

The PHDC Air Flow program calculated an air flow of 866.97 m³/h, and temperature at the outlet of 29.4°C for the single-story dwelling (see fig. 3); as for the two-story dwelling, the estimated air flow is 846.34 m³/h, with 543.05 m³/h distributed to the first floor, and 303.29 m³/h for the second floor, finally the temperature at the outlet of the tower is 29.4°C (see fig. 4).

Both case studies show temperature reduction in the pre-sizing phase, and despite the difference in air path due to double outlet in the case of the two-story dwelling, equal air cooling is expected with the same tower configuration, which is shown in the program's interface as an architectural section of the PHDC tower (see fig. 3 and fig. 4), therefore the tower geometry for detailed airflow analysis will consider a cross section of 1.5m² and height of 5m, which is approximately three (3x) times the cross-section area, and is feasible to integrate in both dwelling's building geometry.

PLEA 2018 HONG KONG

Smart and Healthy within the 2-degree Limit

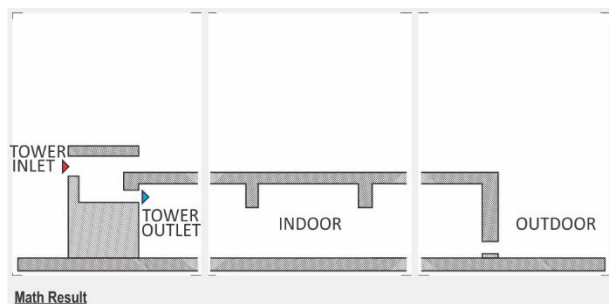


Figure 3: One-story dwelling, pre-design sizing with PHDC Air Flow program.

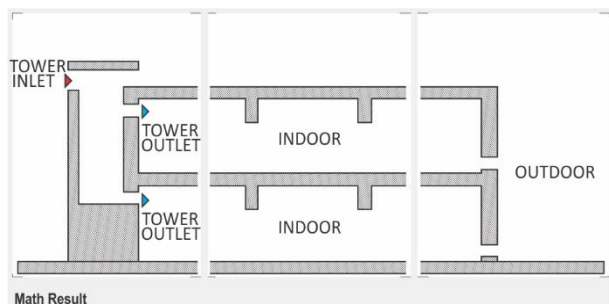


Figure 4: Two-story dwelling, pre-design sizing with PHDC Air Flow program.

The inlet of the tower was selected as a fixed unobstructed profile.

3.3.2 CFD simulation parameters

The parameters selected to estimate the PDEC tower performance were: inlet velocity, water flow rate and water droplet size. The tower cross-section and height are maintained from the pre-sizing phase.

The PDEC tower configuration considers three spray nozzles, located at a height of 4m, a south facing inlet of 0.75m by 1.5m, and an outlet of 0.75m by 1.5m (figure 5). The simulation also considers outdoor Dry Bulb Temperature (DBT) as 42°C, which is the mean maximum temperature for the critical summer month, and water temperature at 25°C for the spray droplets is considered.

Inlet velocity

Wind velocity scenarios were selected as 1.5 m/s and 3 m/s, were the first value is recommended by Kang and Strand [6], and the latter value is obtained from the local available wind resource, according to the Mexicali's International Airport weather file (2010, with weather data from 2000-2009), from an adjustment made for the height of the weather station [7], typically 10m, to the height of the PDEC tower inlet, 5m.

Wind direction was considered perpendicular to the south facing inlet, due to higher wind frequency in the case study location for the summer period.

Water flow rate

Water flow rate scenarios considered were 50 l/h, 125 l/h and 200 l/h.

Water droplet size

Water droplet sizes were considered as 10 µm, 100 µm and 300 µm.

4. RESULTS

The temperature reduction obtained through the PHDC Air Flow software was calculated as a 12.6°C drop, from the 42°C of the outside DBT at a wind speed of 3 m/s (determined by the software). Once the PDEC tower geometry was defined, eighteen CFD simulation scenarios (table 1) generated temperature and velocity profiles for the inside of the tower. Temperature and velocity at the outlet are indicated (table 2), although greater temperature reduction is achieved at the spray nozzle height of 4m, the outlet values considers the air conditions that will be introduced in the living space, and a best-case scenario was selected to further illustrate the wind flow in the interior of the single-story dwelling.

Table 1: Simulation scenario identification criteria.

Case number	Wind velocity [m/s]	Water flow rate [l/h]	Water droplet size [µm]
C1	1.5	50	10
C2	1.5	50	100
C3	1.5	50	300
C4	1.5	125	10
C5	1.5	125	100
C6	1.5	125	300
C7	1.5	200	10
C8	1.5	200	100
C9	1.5	200	300
C10	3	50	10
C11	3	50	100
C12	3	50	300
C13	3	125	10
C14	3	125	100
C15	3	125	300
C16	3	200	10
C17	3	200	100
C18	3	200	300

Table 2: Temperature and wind velocity at tower outlet.

Case number	Temperature [°C]	Wind velocity [m/s]
C1	19.3	1.6
C2	29.5	3
C3	38.6	2.2
C4	26.9	4.4
C5	28.0	1.7
C6	36.9	2.1
C7	21.4	1.6

PLEA 2018 HONG KONG

Smart and Healthy within the 2-degree Limit

C8	26.3	1.5
C9	29.7	2.1
C10	30.8	4.4
C11	36.6	4.5
C12	39.9	4.6
C13	33.2	4.2
C14	35.1	4.4
C15	39.6	4.6
C16	30.4	4
C17	37.4	4.3
C18	38.2	4.5

The best-case scenario is C1, which delivers temperature of 19.3°C, at a wind velocity of 1.6 m/s. The temperature profile of the PDEC tower is shown in figure 5, with the given units from the CFD software, and its wind velocity profile is shown in figure 6.

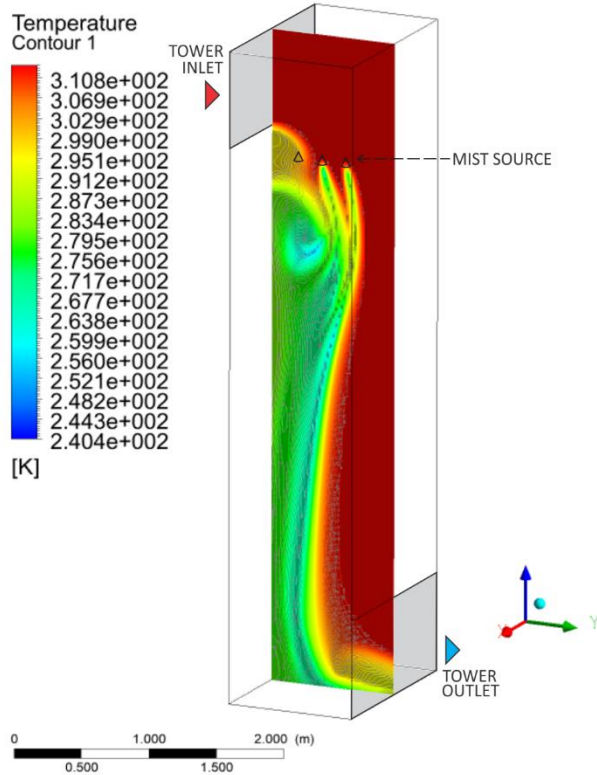


Figure 5: Temperature profile of PDEC tower interior for best case C1.

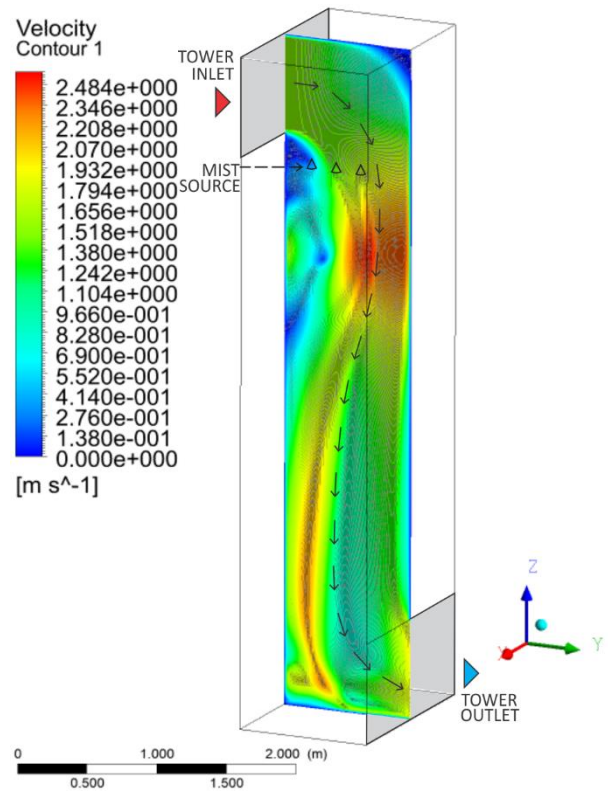


Figure 6: Wind velocity profile of PDEC tower interior for best case C1.

Although C1, was selected as the overall best performance, the case with the most uniform wind pattern (lower turbulence) was C5 (see fig. 7).

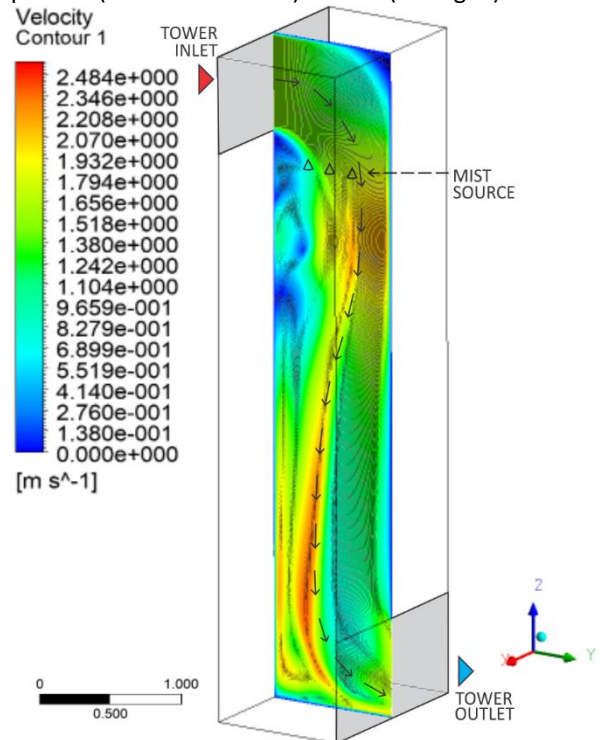


Figure 7: Wind velocity profile of PDEC tower for case C5.

4.1 Air flow in single-story dwelling

PLEA 2018 HONG KONG

Smart and Healthy within the 2-degree Limit

Air flow with the wind velocity and temperature from Case C1 were introduced in the kitchen and living room area of the single-story dwelling and is shown in figure 8.

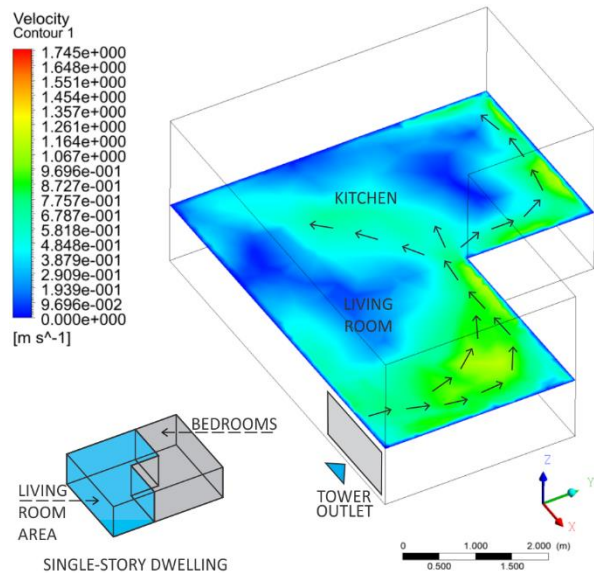


Figure 8: Air pattern from tower outlet in living room and kitchen area.

The living room area shows a greater wind flow and speed because of the proximity to the tower outlet, but as the dwelling inner surfaces move further away from the outlet, there are areas of stagnant air, or considerably low wind velocity.

The PDEC tower provides cool moist air during the day, when the mist source is active, and although the night function of the tower is not studied in this instance, at night the thermal mass of the tower would be able to provide hot air extraction as a stack ventilation shaft, increasing the benefits of the system's implementation.

4.2 PDEC Tower maintenance

Although direct evaporative systems have been associated in the past with legionnaire's disease, in recent years, care has been taken to ensure proper maintenance and cleaning in these systems.

Legionella growth is relative to the temperature of water. The optimum growth occurs at about (37°C-41°C) [8]. The proposed PDEC Tower system operates at approximately 19.3°C, which is well below the ideal growth range for the bacteria.

There are currently checklists available to periodically revise the systems condition, and as such, regular maintenance, involving draining, cleaning and drying out of the system, these measures as well as appropriate water treatment should be enough to reduce the possibility of Legionella originating [9].

5. CONCLUSION

The results show that the scenarios C1 through C9 achieved greater temperature reduction than C10 through C18, this indicates that a wind velocity of 1.5 m/s at the inlet is the recommended value, which may require a wind damper, to slow the available wind resource at approximately 3 m/s, which could be achieved by installing a mesh at the inlet.

Additionally, a smaller droplet size produced greater temperature reduction in every case, and a lower water flow rate was also consistent in providing lower temperatures, which can prove helpful to identify as a water conservation measure.

Although the usually associated disadvantages with PDEC systems are present in this study, i.e. strong dependency on climatic conditions, and inconsistent wind flow distribution, the achieved temperature reduction of 22.7°C shows considerable promise and warrants further research, which could be focused on air distribution management, with the ideal spray nozzle activation schedule, and an exploration of tower construction materials for this region, it is also noted, that the current envelope of the mass-produced housing model, is not climatically adequate, as they do not provide thermal mass or the necessary thermal resistance, therefore it is proposed to couple this system, with a building envelope retrofit to enhance system efficiency.

Architectural integration feasibility is shown in both case studies, although the initial investment to construct the PDEC tower could hinder user interest because of the added expense.

ACKNOWLEDGEMENTS

The authors would like to express their gratitude to the Interinstitutional Doctorate in Architecture Program (PIDA for its acronym in Spanish), the University of Colima for their support, and the National Council for Science and Technology (CONACYT for its acronym in Spanish) for its financial support.

REFERENCES

1. Lucon O., et al (2014). Buildings. In *Climate Change 2014: Mitigation of Climate Change. Contribution of Working Group III to the Fifth Assessment Report of the Intergovernmental Panel on Climate Change* [Edenhofer, O., et al (eds.)]. Cambridge University Press, Cambridge, United Kingdom and New York, NY, USA. P. 675-677.
2. Kang, D. and Strand, R. (2009). *Simulation of Passive Down-draught evaporative cooling (PDEC) systems in EnergyPlus*. Eleventh International IBPSA Conference. P. 369-376.
3. Correia da Silva, J. (2005). *Passive downdraught evaporative cooling applied to an auditorium*. Proceedings, International Conference Passive Low Energy Cooling for the Built Environment. P. 555-560.
4. Ford, B., Schiano-Phan, R., and Francis, E., (2010). *The architecture & engineering of downdraught cooling: a design sourcebook*. Nottingham: PHDC Press.

PLEA 2018 HONG KONG

Smart and Healthy within the 2-degree Limit

5. CONAVI (2017). Housing inventory by value of housing. Available : http://www.conavi.gob.mx:8080/Reports/Inv_Viv_Vig/Inv_x_TipViv.aspx [21 January 2018]
6. Kang, D. and Strand, R. (2016). *Significance of parameters affecting PDEC tower performance*. Applied Energy. (40): p. 269-280. DOI: 10.1016/j.apenergy.2016.06.055
7. Thabaz, M. (2009). *Estimation for the wind speed in urban areas -Height less than 10 meters*. International Journal of Ventilation. 8(1): p. 75-84. DOI: 10.1080/14733315.2006.11683833
8. Puckorius, P.R., P.T. Thomas, and R.L. Augspurger (1995). *Why evaporative coolers have not caused Legionnaires' disease*. ASHRAE Journal, 37(1): p. 29-33.
9. Jaber, S. and Ajib, S. (2011). *Evaporative cooling as an efficient system in Mediterranean region*. Applied thermal engineering. 31 (14-15): p. 2590-2596. DOI: 10.1016/j.applthermaleng.2011.04.026

Daylighting in Sacred Buildings: Application of dynamic brightness balance and contrast in divine luminous environment for energy saving and visual comfort

ANNIE SIM¹, BENSON LAU², WAI YING WONG³

¹Northrop Consulting Engineers, Australia

²University of Westminster, London, UK

³CPG Consultants, Singapore

ABSTRACT: Facing the challenges of global warming, daylighting design optimisation for energy saving and visual comfort has become increasingly important. Across the centuries, architecture precedents have showcased daylighting as one of the key defining elements of spatial quality. While light does not exist in any physical forms, it possesses the superiority to reveal, create and enhance the atmosphere of a physical space, which in-turn impacts the perception and experience of users. How then do we meaningfully make use of this profound natural source to reach our goal in energy savings and visual comfort? This paper investigates different daylighting design strategies in sacred environments, aiming to understand how daylighting strategies using dynamic brightness balance and contrast were applied in two unique sacred structures for enhanced visual perception and energy saving. The research methodology included qualitative field studies by subjective recording of the lit scenes through photographs and hand drawn sketches to assess the visual and biological appreciation of the spaces; and quantitative surveys of brightness contrast in selected visual fields by luminance and illuminance distribution mapping. The research outcomes reveal how visual perception and comfort in sacred environments can be enhanced by appropriate use of daylight, leading to substantial long-term energy saving.

KEYWORDS: Daylighting in Sacred Buildings, Qualitative and Quantitative Evaluation, Visual Performance and Comfort, Dynamic Brightness Balance and Contrast, Energy Savings

1. INTRODUCTION

Across the centuries, architecture precedents have showcased daylighting as one of the key defining elements in sacred architecture for enhancing the divine luminous environment and visual comfort. The combination of the unique architectural forms interplayed with the well-tempered daylight provides the opportunities for creating serene and transcendence experiences. The divine moments of encounter between worshippers, space and light are considered critical as it moulds the perception and determines the impressions left on the worshippers. Indeed, daylight itself can be considered as the most profound source that does not exist in any physical forms, yet possesses the ability to determine, create and enhance the spatial and atmospheric quality of physical spaces. The perceptive and emotional impacts of daylight as such is unquestionable. Nevertheless, it is crucial for designers to seek ways to utilise and skilfully manipulate daylight to achieve the desirable effects in luminous environments and consequently lead to less reliance on artificial light.

Although various standards and codes have been established to assist forming the basis for the human perceived visual comfort, it is rare to come upon case studies that combine both the qualitative (i.e. subjective visual appreciation) and quantitative

studies (luminance and illuminance mappings) of the spiritual luminous environments.

In this study, the Church of the Light, Japan designed by Tadao Ando and the Church of St. Mary of the Angels, Singapore designed by WOHA have been selected as case studies for their unique use of daylighting for task illumination and spiritual ambience effects. The aim is to explore and understand the two distinctive ways of dealing with light in sacred environment.

2. RESEARCH METHODOLOGY

Visual perception is the key in creating a pre-defined cognitive experience in one's mind. Qualitative assessment was carried out through questionnaire and subjective observations made on spatial quality, windows typology, materials and finishes used and the emotive experience as one walks through different spaces or follow a spatial sequence in the sacred structures.

In this study, comprehensive evaluations focused on the investigation of brightness distribution of the focus area within the church – the field of view towards the sanctuary. Subjective observation (qualitative) through hand drawn sketches and photos; and objective analysis (quantitative) through digital High Dynamic Range (HDR) mapping of brightness contrast and brightness distribution help to determine the type

PLEA 2018 HONG KONG

Smart and Healthy within the 2-degree Limit

of daylighting strategy adopted in the two churches i.e. either the dynamic luminance contrast or the dynamic luminance balance lighting strategies.

The HDR luminance mapping will be evaluated with reference to the recommended luminance ratio from the CIBSE (CIBSE, 1994) and Baker (Baker, 1993) guide for visual comfort assessment. The CIBSE recommended contrast ratio between the task luminance (focus), immediate surround and general surround is in the order of 10:3:1 at the conical view angle of 5°, 60° and 130°. Anything that goes beyond the recommended luminance contrast ratio would mean the potential occurrence of glare. Meanwhile, Baker's recommended luminance contrast ratios are as follows:

- i) Task: Immediate Surround = 3:1
- ii) Task: Remote (non-adjacent) Surfaces = 10:1
- iii) Light Source: Surroundings = 20:1
- iv) Light Source: Maximum Contrast = 40:1
- v) Light Source: Highlighted Object for Emphasis = 50:1

3. COMPARISON BETWEEN TWO UNIQUE TYPE OF LUMINOUS ENVIRONMENTS IN SACRED STRUCTURES: The Dynamic Luminance Contrast vs. Dynamic Luminance Balance

With reference to Figure 1, the Church of the Light uses dynamic brightness contrast to define its luminous environment. The direct light and high brightness contrast between the window apertures and the adjacent wall surfaces is deliberately used in the Church of Light, to emphasize the presence of God as light.

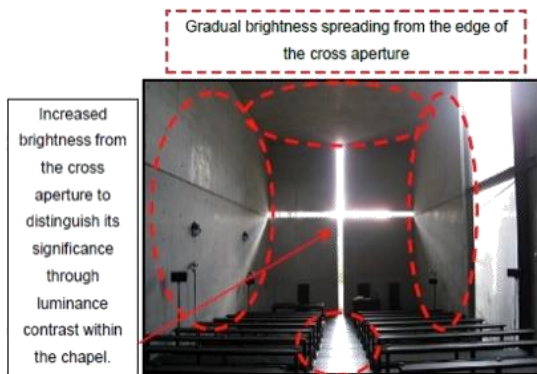


Figure 1a: Church of the Light – Enhancement of Cross and Space Visual Appearance (Image Source: Zoric, 2009)

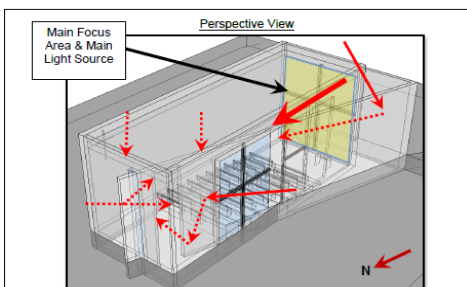


Figure 1b: Church of the Light – Window Aperture Typology Overview (Source: Rendered by A.Sim)

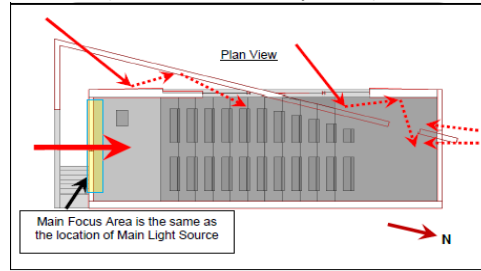


Figure 1c: Church of the Light – High Dynamic Luminance Contrast dramatize the spiritual luminous environment (Source: Rendered by A.Sim)



Figure 1d: Church of the Light – Dynamic lighting events inside the church (Image Source: jowoffinden, 2012; Reksten, 2010; Monte, 2010; Plow, 2012)

The key daylighting strategies are as follows:

Direct light plays the key role within the field of view. Location of the main area of visual focus is the same as the location where the main source of light is coming from. The key focus is the daylit cross with the immediate surround given a relatively low brightness. The visual appearance of the general surround is considered least important.

High brightness contrast within the field of view between the focus (i.e. the Cross) and adjacent surround.

The Cross is back lit to achieve high brightness contrast and heighten the sacredness of the space.

Side and top diffused lighting to control the brightness contrast and to enhance visual appreciation of the spaces.

Dynamic light patterns observed within the field of view are mainly produced by the brightly lit Cross and the side apertures.

In the Church of St. Mary of the Angels, a distinctively different daylighting strategy was adopted. Instead of using high brightness contrast to evoke the sacredness inside the church, here dynamic brightness balance is the key daylighting strategy. Diffused light and controlled brightness contrast is used. This is shown in the images taken on-site in Figure 2a and 2d, and digital model in Figure 2b and 2c.

PLEA 2018 HONG KONG

Smart and Healthy within the 2-degree Limit

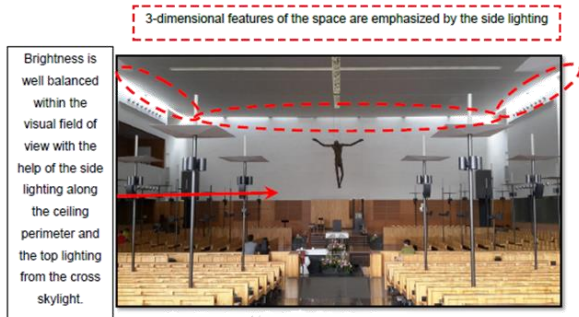


Figure 2a: Church of St. Mary of the Angels – Dynamic luminance balance in the field of view (Source: Image by A.Sim)

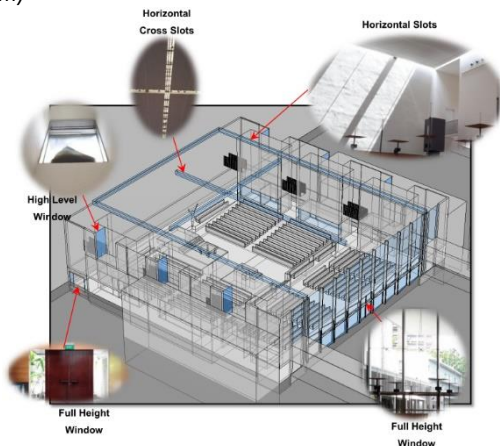


Figure 2b: Church of St. Mary of the Angels – Window Aperture Typology (Source: Rendered by A.Sim)

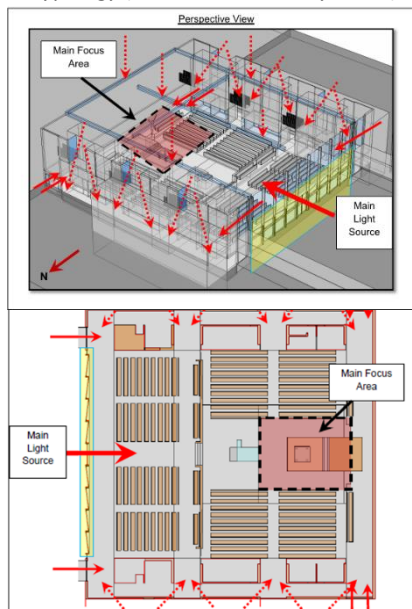


Figure 2c: Church of St. Mary of the Angels – Key Light sources to achieve the desired Dynamic Luminance Balance (Source: Rendered by A.Sim)



Figure 2d: Church of St. Mary of the Angels – Luminous Environment (Source: Image by A.Sim)

The key daylighting strategies are as follows:

Diffused light plays the key role within the field of view. The Christ sculpture as the key focus is illuminated by balanced light from the top and side apertures with the immediate surround given a relatively high degree of importance.

The brightness contrast between the dark Christ sculpture and its surround is well controlled such that the difference is noticeable but not excessive.

Well balanced luminance distribution with low to average luminance contrast within the field of view avoids abrupt change of brightness.

Side and top diffused light to balance and complement the luminance distribution of the interior space.

Dynamic yet balanced light patterns within the field of view is mainly created by the side apertures.

From the above analysis, the unique features that distinguish between the two daylighting strategies are clearly demonstrated. The Church of the Light evokes strong sense of sacredness through the brightly lit glowing cross that result in leaving one in admiration of the contrasting, divine and poetic light dramas within the space. On the other hand, the well balanced luminous environment in Church of St. Mary of the Angels with the hanging Christ sculpture standing out from the homogeneously lit back wall leaves a calming sense of sacredness inside the church. Both lighting strategy relies on daylight as its main source. The next section will use the Church of St. Mary of the Angels to demonstrate the qualitative and quantitative studies that help to distinguish the type of daylighting strategy adopted.

4. CHURCH OF ST MARY OF THE ANGELS: QUALITATIVE AND QUANTITATIVE EVALUATION

Qualitative assessment involved survey questionnaires and subjective appreciation while quantitative assessment was conducted on-site by taking illuminance measurement and HDR luminance mapping following a spatial sequence which is commonly used by the worshipper.

PLEA 2018 HONG KONG

Smart and Healthy within the 2-degree Limit

4.1 Qualitative Evaluation: Dynamic Luminance Balance Lighting Strategies

Qualitative evaluation conducted via survey questionnaires and on-site visual observation indicate positive response in its luminous environment with no indication of excessive visual discomfort caused by excessive brightness contrast. The following table summarised the findings:

Questionnaires	Strongly Disagree	Disagree	Just Right	Agree	Strongly Agree	Biological Factors
Q6: I consider the daylighting of this area to be highly satisfactory for the activities.	0%	0%	0%	45%	55%	Visual Comfort, Sense of Relaxation
Q8: I am able to read my bible or any reading materials.	0%	0%	9%	45%	45%	
Q7: I do not feel confined. The church feels spacious.	0%	0%	0%	45%	55%	Sense of Space
Q6: I feel secure and safe.	0%	0%	0%	55%	45%	Sense of Security
Q5: I like the idea that I have access to outdoor views anytime. It is helpful to give me a sense of the present outdoor and weather condition.	0%	0%	9%	45%	45%	Sense of Orientation, Sense of Time, Sense of Weather Condition
Q4: I can see all that is necessary for safe unobstructed movement.	0%	0%	0%	73%	27%	Sense of Orientation
Q3: I feel the sense of holiness and peace as I enter the place.	0%	0%	9%	45%	45%	Sense of Purpose, Sense of Relaxation

Figure 3: Summary of Survey Results and its Correlation with Biological Factors (Source: Compiled by A.Sim)

In addition to the on-site luminance study, on-site observation through hand drawn sketches were undertaken to record the author's subjective visual perception of the sacred environment. The sketches in Figure 4 capture the atmosphere inside the church.

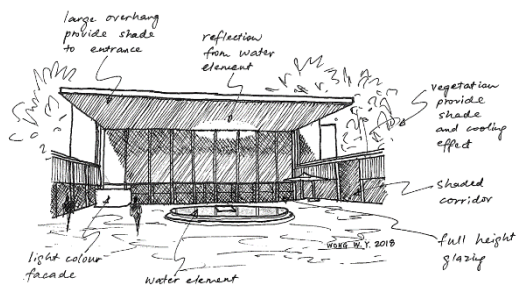


Figure 4a: On-Site Visual Recording – Eastward External View (Source: Sketches by WY.Wong)

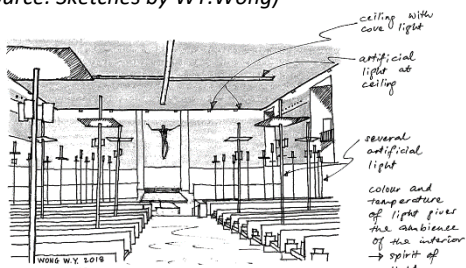


Figure 4b: On-Site Visual Appreciation – Eastward View towards the Main Hall (Source: Sketches by WY.Wong)

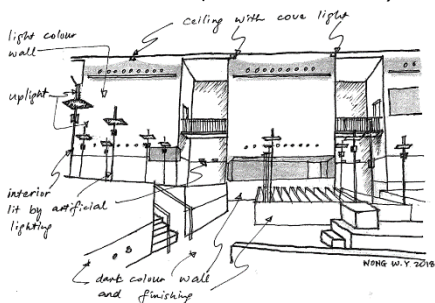


Figure 4c: On-Site Visual Appreciation – Southward View (Source: Sketches by WY.Wong)

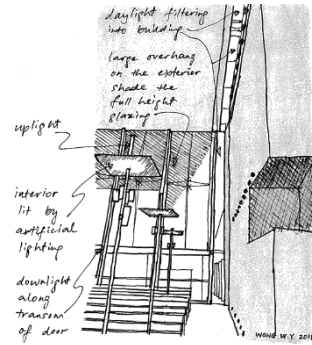


Figure 4d: On-Site Visual Recording – Westward View (Source: Sketches by WY.Wong)

4.2 Quantitative Evaluation: Dynamic Luminance Balance Lighting Strategies

Illuminance spot measurements provides better understanding of the daylit luminous environment.

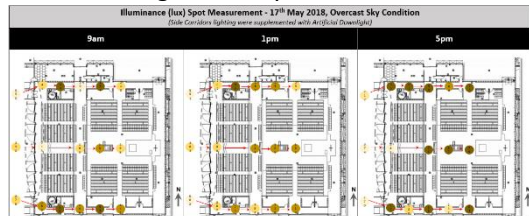


Figure 5: On-site Illuminance (lux) Spot Measurement under an Overcast Sky Condition (Church of St. Mary of the Angels, 2014)

The spot measurement results indicated that the lighting conditions in the main body of the church are well daylit and balanced mostly throughout the day under overcast sky condition. Artificial lighting is only required in the late afternoon when the sun sets. This minimise reliance on artificial lighting during the day which in-turn contributes significantly to energy saving. To assess the brightness contrast within the space, on-site luminance mapping was carried out based on three key spatial sequence routes as indicated in Figure 6.



Figure 6: Luminance Mapping Location and Views Directions (Church of St. Mary of the Angels, 2014)

The on-site luminance mapping was carried out in the morning at 9am, mid-day (1pm – Sun is overhead in Singapore) and late afternoon (5pm). The mapping results obtained (Figure 7) in the morning indicate a well-balanced luminous distribution without excessive brightness contrast that can cause discomfort glare to occupants. The brightness contrast ratio between the focus, immediate surround and far surround within

PLEA 2018 HONG KONG

Smart and Healthy within the 2-degree Limit

the space also falls within the luminance ratio range of both 10:3:1 (CIBSE, 1994) and 20:1 (Baker, 1993) recommendations for visual comfort.

overcast sky condition, variation of the luminance pattern is still noticeable with the movement of clouds and the daylight ingress from the horizontal slots along the perimeter of the main hall. Artificial lighting remains off at the main hall area.

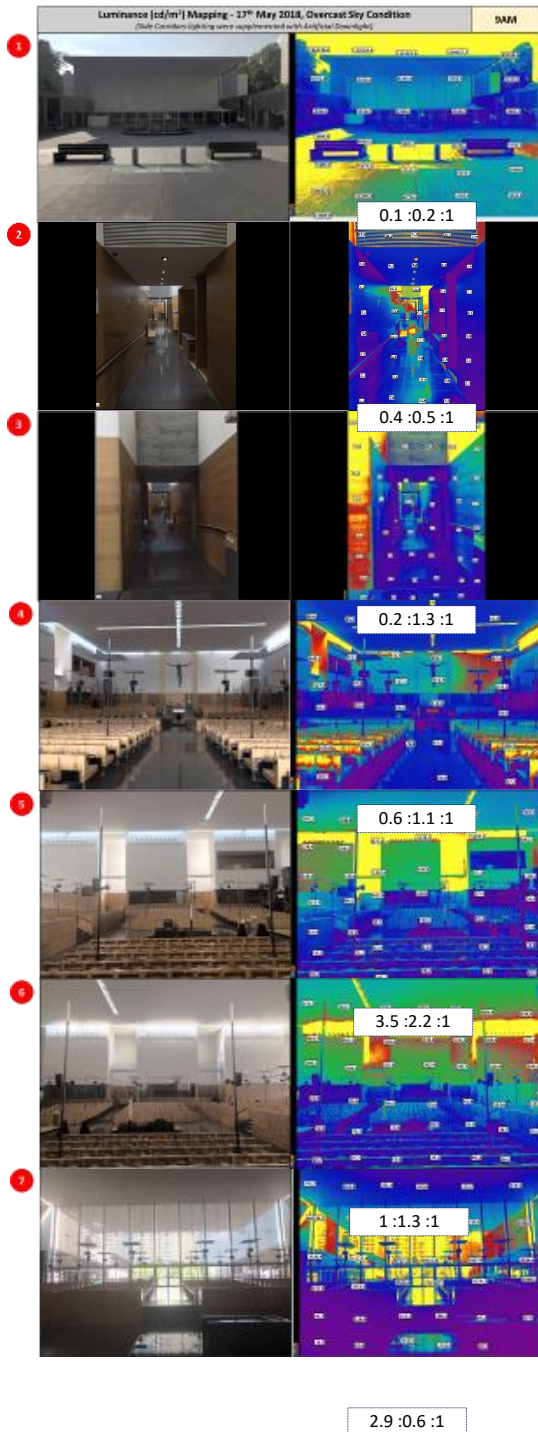


Figure 7: On-Site Luminance Mapping Results in the morning (Source: Rendering by A.Sim)

The brightness contrast ratios derived from the luminance mapping during mid-day (Figure 8) also indicate no risk of visual discomfort caused by excessive brightness contrast. The internal luminous environment remains well balanced and uniform under the overcast sky condition. Although the dynamic daylighting pattern is least visible due to the

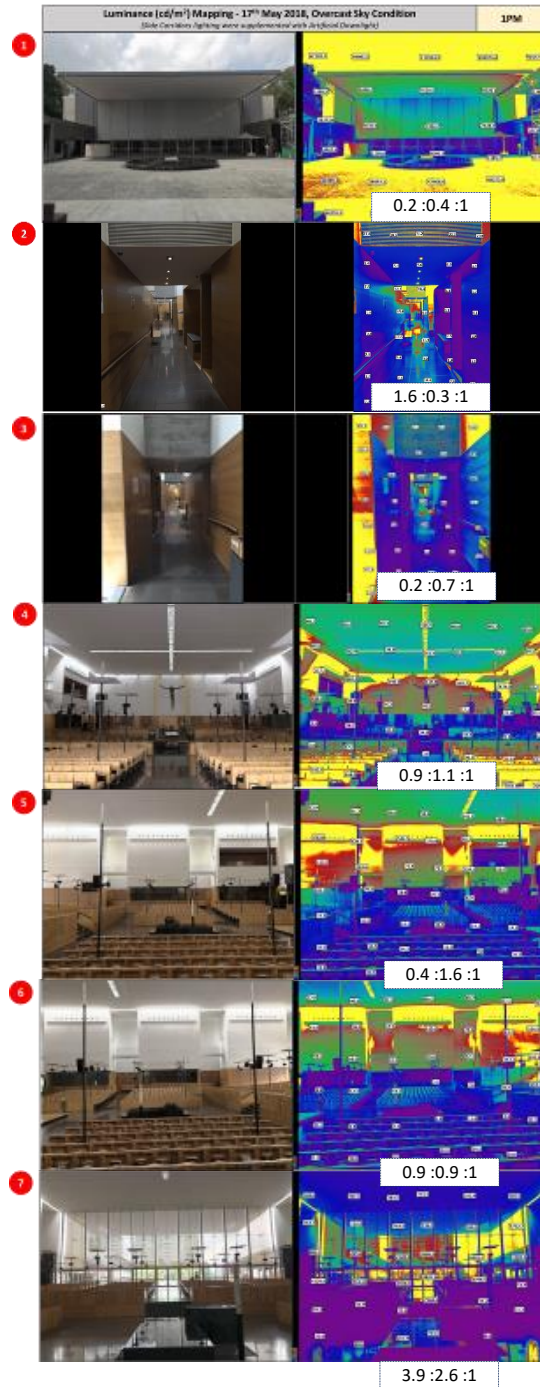


Figure 8: On-Site Luminance contrast Analyses at mid-day (Source: Rendering by A.Sim)

At 5pm when the sun is beginning to set to the West where the main entrance is located, the luminance contrast ratios remain well balanced. View towards the Western main entrance did not indicate any risk of glare from the low angled Western sun (Figure 9).

PLEA 2018 HONG KONG

Smart and Healthy within the 2-degree Limit

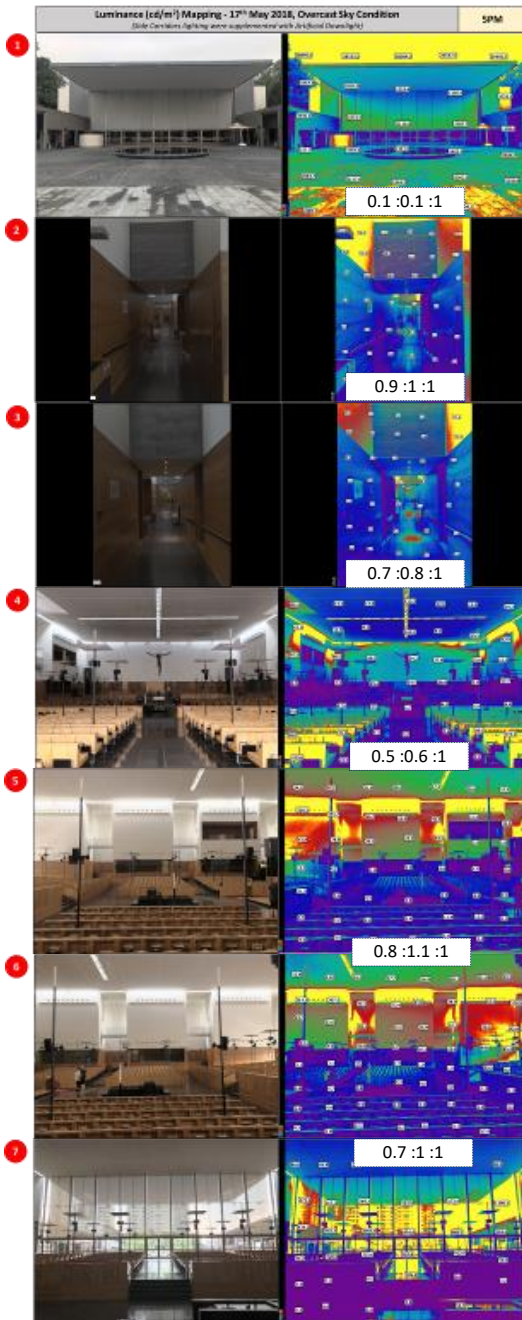


Figure 9: On-Site Luminance Mapping - 17th May 2018, Overcast Sky Condition (Source: Rendering by A.Sim)

5. CONCLUSION

The key defining daylighting strategies employed in the Church of the Light – Dynamic Luminance Contrast and the Church of St. Mary of the Angels – Dynamic Luminance Balance have been qualitatively and quantitatively investigated and analysed. Lessons learnt from this study are useful references for design of energy saving and well-perceived sacred luminous environment.

Overall, this study revealed the high potential, benefits and roles of daylight in creating distinctively different sacred luminous environment from a more holistic perspective; encompassing its role in energy savings

and the physiological and psychological impacts on human responses. In addition, the findings have also highlighted the importance of undertaking both qualitative and quantitative studies in the luminous environment, which involved subjective observation, questionnaire and improved quantitative evaluation via the HDR luminance mapping technique. The research methodology adopted in this study will as well allow a better understanding and appreciation of the human sensory experiences resulted from both the dynamic and static light balance through the skilful manipulation of daylight in the luminous environment.

ACKNOWLEDGEMENTS

This research would not have been possible without the guidance, support and help from several groups of people and individuals; in one way or another contributed and extended their valuable assistance in the preparation and completion of this study. We would like to acknowledge and thank particularly the Church of St. Mary of the Angels, Singapore for their support and generosity in sharing valuable information and allowing access for site validation. We would also like to extend our deepest gratitude to Ms. Chong Sock Meng for her unwavering support in the on-site measurement and validation exercise.

REFERENCES

1. Sinauer Associates, Inc. (2001) *The Anatomy of the Human Eye*, Available at: www.sinauer.com/media/wysiwyg/tocs/HumanEye.pdf
2. Lam, W.M.C. (1977) *Perception and Lighting as Form givers for Architecture*, New York: McGraw-Hill.
3. SPRING Singapore (2006) SS531: 2006 *Code of Practice for Lighting of Work Places*. Singapore: SPRING.
4. Waskett, R.K., Simonella, A., Davies, A., Lau, B., Loe, D., Gosney, J., Littlefair, P., Mardaljevic, J. (2014) *Lighting Guide LG10:2014 - Daylighting: A Guide for Designers*, UK: CIBSE (The Chartered Institution of Building Services Engineers).
5. Baker, N., Steemers, K. (2002) *Daylighting Design of Buildings*, UK: James & James (Science Publishers) Ltd.
6. CIBSE (1994) *Code for Interior Lighting*, UK: The Chartered Institution of Building Service.
7. Church of St Mary of the Angels (2014) *Church of St Mary of the Angels*, Available at: <http://stmary.sg/>
8. Baker, N., Fanchiotti A., Steemers, K. (1993) *Daylighting in Architecture A European*, London, UK: James & James.
9. Robbins, C.L. (1986) *Daylighting: Design and Analysis*, New York: Van Nostrand Reinhold.
10. Igawa, N. and H. Nakamura, (2001). All Sky Model as a standard sky for the simulation of daylight environment. *Building and Environment*, 36: p. 763-770.
11. Kittler, R., (1985). Luminance distribution characteristics of homogeneous skies: a measurement and prediction strategy. *Lighting Research and Technology*, 17(4): p. 183-8.
12. Perraudeau, M., (1988). Luminance models. In *National Lighting Conference*. Cambridge, UK, March 27-30.
13. International Daylight Monitoring Programme, [Online], Available: <http://idmp.entpe.fr/> [16 June 2008].

Urban Microclimate and Energy Performance: An integrated simulation method

DANIELA MAIULLARI¹, MARTIN MOSTEIRO-ROMERO², MARJOLEIN PIJERS-VAN ESCH¹

¹Faculty of Architecture, Delft University of Technology, Delft, The Netherlands

²Architecture and Building Systems, ETH Zurich, Switzerland

ABSTRACT: In the design practice simulation methods are already widely used to support the understanding of energy performance and to help designers in reducing energy demand during the design process. However, energy simulation tools are largely limited to the individual building level, and urban microclimate conditions and variations in local wind, solar radiation, and air temperature patterns in which buildings express their energy performance are largely overlooked. In order to include microclimatic data in the computation of space cooling and heating consumption and enlarge the scale of analysis from single buildings to district scale, a new simulation method has been developed. The proposed coupling procedure links the microclimate software ENVI-met and the City Energy Analyst energy simulation tool and it is employed in the energy assessment of a urban re-development project in the city of Zurich, Switzerland. The results show that, considering microclimatic boundary conditions, the average hourly energy loads vary for daytime and night-time peaks and moreover a variation can be noticed in terms of total space heating and cooling consumption on the hottest and coldest day of a typical year.

KEYWORDS: Energy demand, microclimate, integrated simulation, ENVI-met, CEA.

1. INTRODUCTION

In proceeding through ‘the Grand Transition’, the world energy consumption is predicted to increase by 2060 in all the three main scenarios explored by the World Energy Council [1]. Although new technologies and energy policies will moderate the final energy demand, this is expected to grow between 22% and 46% by 2060 due the global demographic growth.

In European countries, where demographic growth is concentrated in urban areas, urban transformation practices have seen a shift from an expansive development model to a compact and concentrated one, which has implied redevelopment projects in inner city areas. In this phenomenon of ‘Urban re- densification’ one of the main challenges is to understand and control the effects of the designed urban form on the urban microclimate during the design process, which doubly influences the physical well-being of people in the outdoor space and the energy performance of buildings.

Although in the design practice simulation methods are already widely used to support the understanding of energy performance and to help designers reduce energy demand during the design process, energy simulation tools are largely limited to the individual building level. Furthermore, urban microclimate conditions and variations in wind, solar radiation, and air temperature patterns are largely overlooked, as overall climate data are used. The reasons can be found on the restriction of modelling tools for microclimate simulations and on the difficulties in modelling large urban areas.

Therefore, in this paper a method is presented for the integration of urban microclimate and building energy simulations, and it is applied to evaluate the energy performance of a new masterplan for the ‘Hochschulquartier’ in central Zurich, Switzerland.

In Section 2 we present the coupling approach by describing the simulation tools ENVI-met and City Energy Analyst (CEA), and the linking method.

Section 3 presents the case study employed for the testing of the method and the specific setting to perform the analysis. Finally, in Section 4 and 5 the results are presented and discussed.

2. METHODOLOGY

2.1 Simulation tools

In order to understand the impact of urban microclimate on the energy performance two software tools have been used in this study:

ENVI-met [2], an urban microclimate model for outdoor environmental prediction based on spatial configuration;

City Energy Analyst (CEA) [3], an urban simulation engine for the assessment of district energy systems.

ENVI-met is a three-dimensional prognostic microclimate model designed to simulate the interaction between surfaces, plants and air in an urban environment [2]. It is widely used to estimate and assess outdoor thermal comfort [4, 5, 6] and the impact of the urban microclimate on building energy use [7, 8]. The atmospheric model computes mean air

PLEA 2018 HONG KONG

Smart and Healthy within the 2-degree Limit

flow, turbulence, fluxes of direct, diffuse and reflected short-wave and long-wave radiation, and air temperature and humidity. Two groups of inputs are necessary for the computations. A first group of spatial information, such as topography, building geometry and façade/surface materials, is used for the construction of the spatial model. A second group is constituted by meteorological input data such as initial air temperature, humidity and wind speed at 10m height. ENVI-met Version 4.0 Science as used in this study furthermore gives a simple forcing option that allows hourly forcing of air temperature and relative humidity.

The City Energy Analyst (CEA) is a computational framework for the analysis and optimization of energy systems in neighbourhoods and city districts. It consists of a collection of tools for the analysis of urban energy systems [9] based on comprehensive mathematical models using the latest ISO and SIA standards and the state-of-the-art in research. The tool allows users to analyse the energy use, carbon emissions and financial benefits of multiple district-scale design scenarios in conjunction with optimal schemes of distributed generation. In order to run a CEA simulation, two general groups of inputs are necessary. The first are primary inputs to the CEA modelling framework and consist of weather data, spatial information (topography and geometry of the

buildings in the zone of study and in the surrounding buildings in the zone of study and in the surrounding area), as well as general characteristics of the buildings used as secondary, climate conditions for the area of analysis (construction year, renovation dates and functional program of the building). The secondary inputs correspond to additional inputs that are necessary to run simulations but which may be assumed by CEA based on the primary inputs by looking into a database of typical building properties. These include architectural properties (such as building materials, conditioned floor area and window-to-wall ratios), the energy systems used in the buildings (both for supply and distribution throughout the building of heating, cooling and electricity), indoor comfort properties (set point and set back temperatures and ventilation rates), and internal loads (water and electricity demands for various services, and sensible and humidity gains due to occupant presence). Finally, other input information such as system controls and schedules for occupancy, electricity and hot water are selected by default from the CEA database but may again be edited by the user based on a given project's needs.

2.2 Coupling method and procedure

The method to use ENVI-met outputs as boundary conditions for CEA energy simulation consists of three main phases (Fig.1). In the first phase, the spatial model for the selected case study is built in ENVI-met (4.0) and simulations are performed using the simple forcing method by using weather data for the selected days. Secondly, output data for air temperature, wind speed and relative humidity are exported and aggregated in a 3D buffer around single buildings in a GIS platform (ArcGIS, Esri). In the third phase, the aggregated data are imported in the CEA software and

buildings in the zone of study and in the surrounding

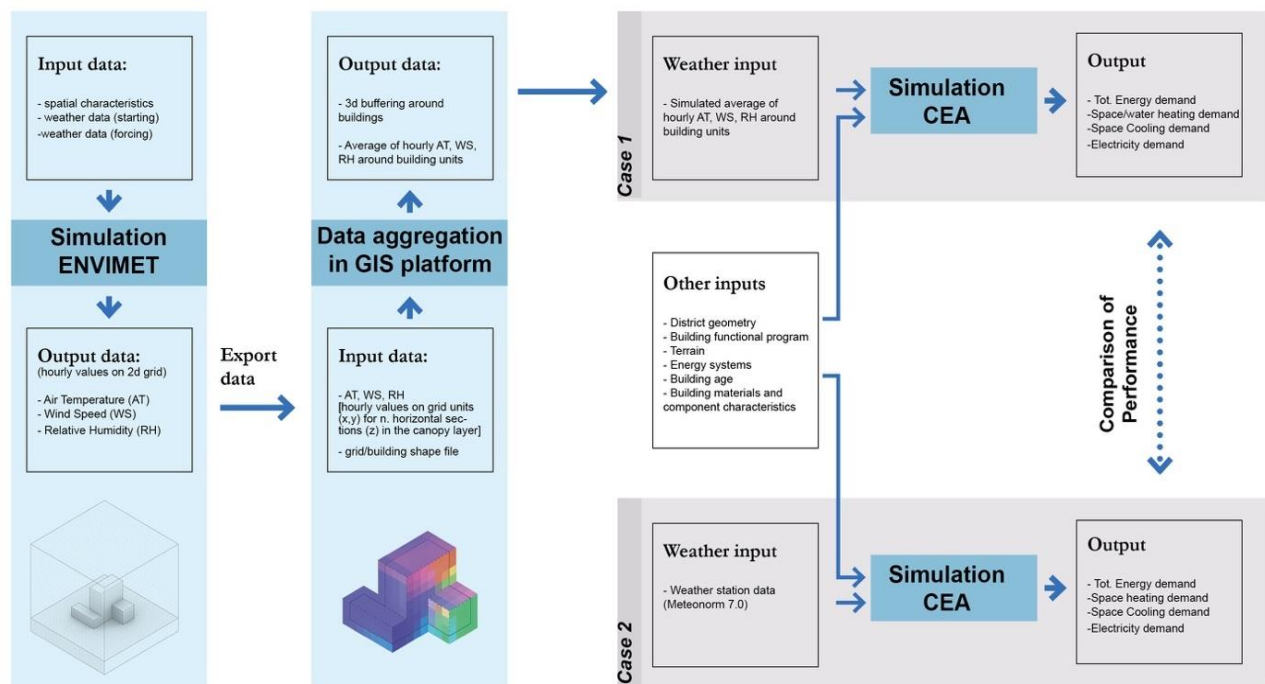


Fig.1. Methodological scheme

area), as well as general characteristics of the buildings used as secondary, climate conditions for the

PLEA 2018 HONG KONG

Smart and Healthy within the 2-degree Limit

calculation of the energy demand for each building in the simulation domain.

The outdoor temperature is used in calculating the thermal loads in the building, which in CEA is done through a resistance-capacitance model based on the methodology described in ISO 13790 [10]. The detailed calculation methods are discussed in Fonseca & Schlueter [9]. The relative humidity, on the other hand, is mainly used in the latent load calculations, which are based on ISO standard 52016-1 [11]. Finally, the wind speed and direction are used for the CEA dynamic infiltration calculation [12]. The CEA demand model produces hourly results on the demands for heating, cooling and electricity for the various services to be provided in each building.

The method described has been used for the assessment of an urban district project. The proposed Masterplan was simulated on an hourly basis for the coldest (CD) and hottest day (HD) in a typical year for two cases:

Case 1: Simulation with CEA using microclimatic simulation results obtained with ENVI-met.

Case 2: Simulation with CEA using atmospheric data input from weather station;

The results for space heating and cooling for each day were then compared to observe the impact of the inclusion of microclimate effects.

3. CASE STUDY DESCRIPTION

The method described in Section 2 has been used for the energy performance assessment of a redevelopment district project in Zurich. This project for a new university campus in the 'Hochschulquartier' (HQ) corresponds to the transformation of a dense and central area which hosts three educational institutions: ETH Zürich, the University of Zurich, and the University Hospital Zurich. The area is currently being redeveloped and densified to create additional floor space for the universities, hospital and complementary services. The spatial interventions are being planned taking into account building energy targets. However, it still appears very difficult to meet the limits imposed by the 2000 Watt Society targets to which the city has been committed since 2008 [13].

This case study is therefore selected as representative of complex district projects that aim for high energy efficiency and for which integrated tools can lead to the selection of spatial-energy sustainable solutions based on local environmental potential. The method presented here is used to investigate to what extent the microclimatic environment, caused by the transformation of urban structure and building geometry, impacts building energy performance. The district configuration analysed in this study is based on the 2014 Masterplan for the area [14].

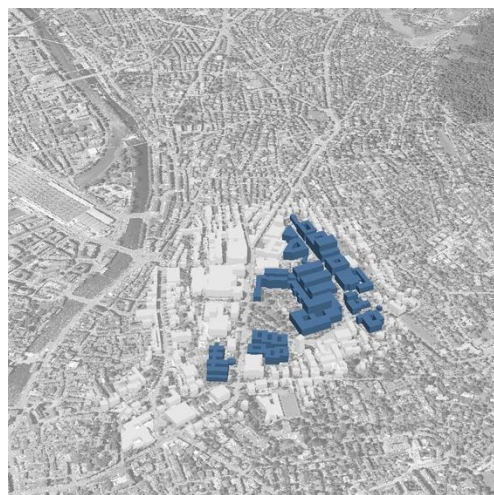


Fig.2. Hochschulquartier Masterplan 2014

3.1 Microclimate simulation and aggregation

In the first phase, the spatial model for the selected case study was built in ENVI-met (4.0). The new buildings were highlighted in the Masterplan and a study area was defined drawing a border that includes the buildings of interest, adjacent street canyons and the first adjacent building façades. From this border an offset area of 100m was taken as area of influence.

The three-dimensional spatial model was built in the ENVI-met simulation tool, including footprint and height of the buildings, topography and ground materials, on a grid unit 10x10x7m for the total selected area.

On this spatial model two simulations were run with ENVI-met for the coldest and hottest day of the typical year by forcing atmospheric boundary conditions on the basis of hourly data taken from a typical year for a nearby weather station from the software Meteonorm 7.0 [15]. Resulting wind speed, air temperature and relative humidity data were selected within a buffer of 10m from the buildings' façades and aggregated in 3D buffers using each building's code for use in CEA as weather input data.

3.2 Energy demand simulation

A model of the HQ case study was created in CEA based on information on building location, construction year and energy supply from local GIS data. The occupancy types for each building were obtained from a combination of GIS data and owner information, while data on energy-relevant retrofits for the main building components was scarce and thus was mostly estimated. Architectural properties and building materials for the existing stock were assigned based on site visits, whereas for new buildings these were assigned based on the CEA archetype database, which includes envelope properties for future constructions [9].

PLEA 2018 HONG KONG

Smart and Healthy within the 2-degree Limit

For the base case, typical year weather data from microclimate simulation, the exterior temperature, relative humidity and wind speed data were replaced for the HD and CD with the results from ENVI-met. Hourly heating and cooling demands for both cases were then calculated using the CEA demand module.

4. RESULTS

4.1. Comparison of microclimatic and meteorological data.

This section analyses the site-specific climate results for the HQ through comparison with the same measured variables derived by the selected weather station.

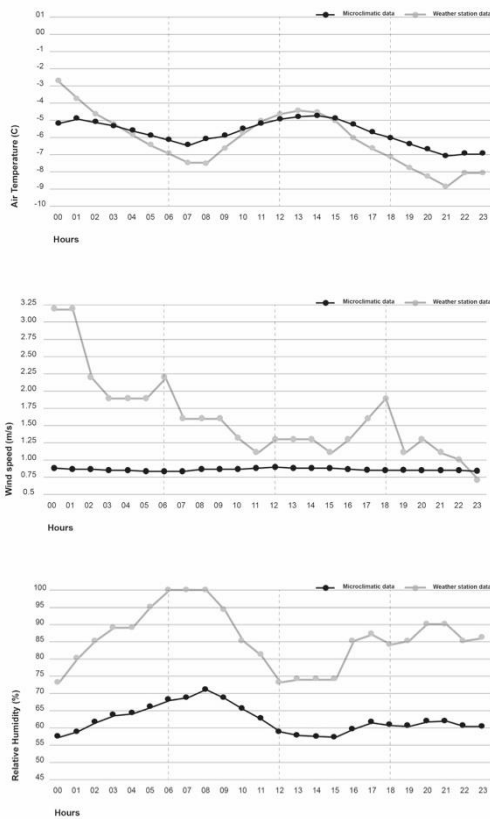


Fig.3. Comparison of the air temperature (top), wind speed (middle) and relative humidity (bottom) from the weather station and average air temperature around the buildings from ENVI-met for the CD.

For the coldest day, Fig.3 shows the comparisons for air temperature, wind speed and relative humidity data. Regarding air temperature, the results show that the urban environment has much smaller diurnal temperature curve compared to the rural environment. Temperature differences between the urban and rural environment are relatively small in the period between sunrise and sunset. During most of the day, the air temperatures in the urban environment are higher, showing a modest heat island effect of max to 2.5°C, which manifests mainly during the night. The

RH curve is rather flattened, with higher humidity levels occurring in the night and early morning, like at the rural site, as a result of the dropping temperatures. In the hottest day, a significant variation between day and night time can be observed regarding average air temperature around the building units. Fig.4 shows that HQ local air temperatures during solar time are significantly lower than the rural ones, with a maximum difference of 3°C at 11 in the morning. In contrast, in the hours before sunrise and after sunset, the curves are inverted, registering lower rural air temperatures. Heat accumulated by urban surfaces and released during night hours contributes to the higher urban air temperatures of 25–26.5°C. In the second comparison it was found that the already low meteorological wind speed, which in the selected day reaches no higher than 0.5 m/s, significantly decreases in the studied area. Finally, data of relative humidity are analysed for the selected summer day. In comparison with the hourly data from the rural weather station, local relative humidity is found to be significantly higher during the daytime. The maximum variation can be observed in the middle of the day when the simulated humidity reaches 57%.

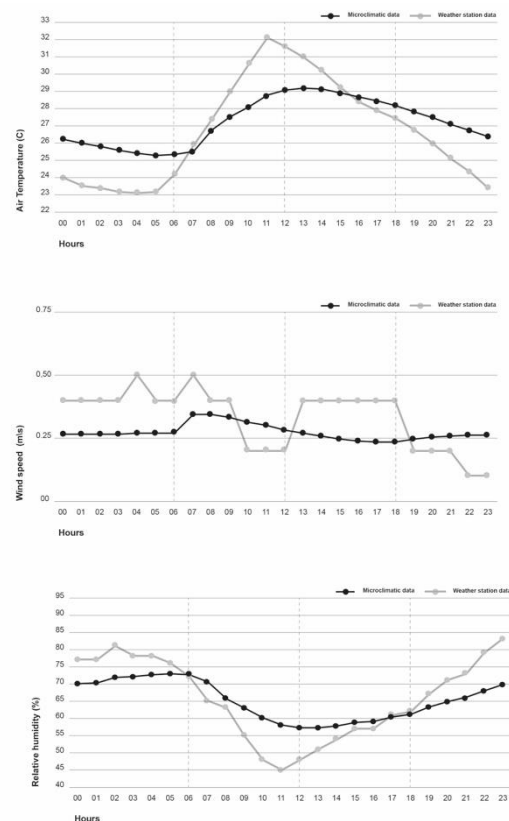


Fig.4. Comparison of the air temperature (top), wind speed (middle) and relative humidity (bottom) from the weather station and average air temperature around the buildings from ENVI-met for the HD.

4.2. Comparison of energy performance

PLEA 2018 HONG KONG

Smart and Healthy within the 2-degree Limit

Since all new buildings were assumed to be built to the Swiss energy efficiency standard Minergie, the space heating demand of the buildings in the area was on average extremely low at 14 kWh/m²-yr for the baseline case without microclimate. As expectable, older buildings had a higher demand, reaching as much as 167 kWh/m²-yr.

On the coldest day of the year, the average space heating demand for Case 2 was 147 Wh/m² for all the buildings in the area. When microclimate effects were taken into consideration, the space heating demand was decreased on average by 2%. Similarly, the peak heating power for the entire district is decreased by 1.8%. The greatest overall decrease in the energy demand was seen in one of the remaining historical hospital buildings, where the space heating demand decreased from 1331 Wh/m² for the baseline case to 1322 Wh/m² for the case accounting for the effects of microclimate. Likewise, the peak heating power for this building on the coldest day of the year decreased from 244 W/m² to 236 W/m².

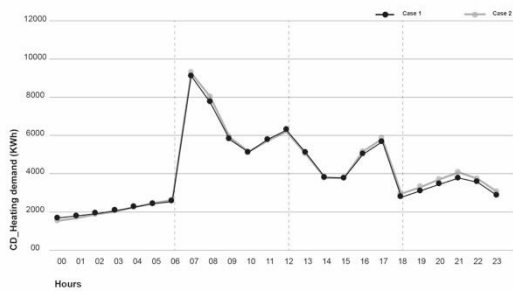


Fig.5. Comparison of hourly heating load in Cases 1 and 2 for the CD in a typical year.

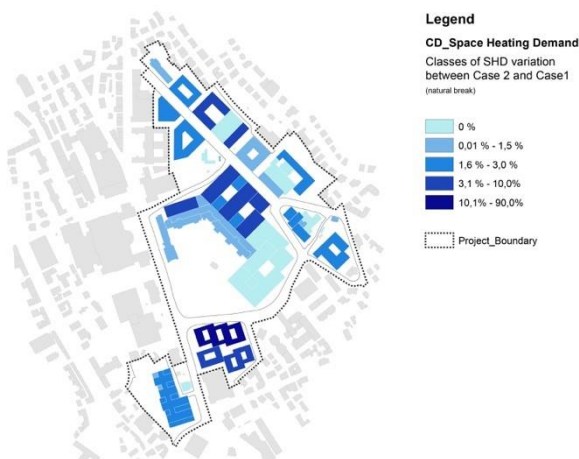


Fig.6. Percentage decreasing of space heating demand per square meter for the CD in Case 1 (compared with Case 2)

Due to the high level of insulation and the large internal gains in the buildings in the area, the space cooling demand in the HQ case is similarly significant,

with 11 kWh/m²-yr on average. The University Hospital's main building complex has the highest cooling demands at 14 to 22 kWh/m²-yr, whereas older buildings either had a lower demand or no cooling system at all. On the hottest day of the year, the average space cooling demand in the baseline case without microclimatic effects was 185 Wh/m². When microclimatic effects were considered, the overall demand in the area increased by 2%. The effect of microclimate on the peak cooling demand was more noticeable, with a 5% decrease in peak cooling power on the coldest day of the year.

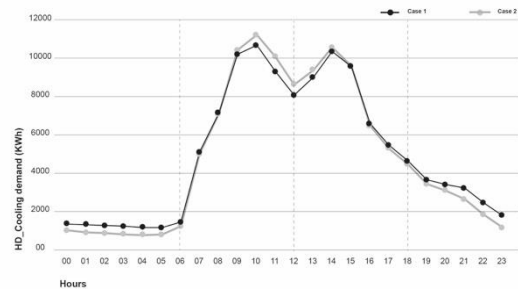


Fig.7. Comparison of the hourly cooling load in Cases 1 and 2 for the HD in a typical year.

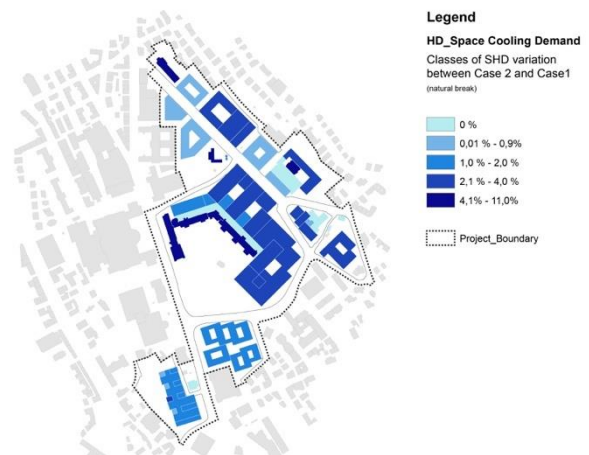


Fig.8. Percentage increasing of space cooling demand per square meter for the HD in Case 1 (compared with Case 2)

Older buildings showed a greater response to microclimate effects, while newer, highly insulated buildings had a much less significant effect in Case 1. For the cases including microclimate effects, the daily peak in the cooling demand is lowered for several buildings, however the higher night time temperatures cause several buildings to require cooling earlier than when microclimate effects are not accounted for. The new buildings of the University Hospital showed the greatest cooling power demand due to its high internal and solar gains and passive construction. Overall, the peak cooling power of the University Hospital's main

PLEA 2018 HONG KONG

Smart and Healthy within the 2-degree Limit

building decreased from 17.9 W/m² to 16.9 W/m² when microclimate effects were taken into consideration.

5. DISCUSSION AND CONCLUSIONS

The study outlines a method for quantitative analysis of district-scale energy consumption taking into account the microclimatic effects created by the design of open and built space. A coupling approach that links the simulation tools ENVI-met and CEA is employed in a case study where urban development processes are expected to change microclimatic conditions and consequentially the energy performance of buildings.

From the previous results some general conclusions can be drawn. First, from a microclimate perspective, an atmospheric urban heat island phenomenon is observed in the area. Compared to the measured data from the weather station, local temperatures are higher during the night and wind speed is mitigated for the two days analysed. Comparison between the two Cases analysed shows that the consideration of microclimatic patterns leads to a general increased building cooling demand on the hottest day and a lower building heating load during the coldest day.

The previous results indicate the capacity of the developed method to analyse the energy performance of a complex urban district considering reciprocal influences between urban fabric configuration and local climate. In addition, it can provide a more realistic description of building energy performance and help designers in comparing the energy impact of different design solutions.

6. ACKNOWLEDGMENT

This research is developed within the project SPACERGY, within the JPI Urban Europe research framework.

REFERENCES

World Energy Scenarios (2016). *The Grand Transition*, World Energy Council, 2016.

Bruse and Fleer, (1998). <http://www.envi-met.com/>

Fonseca, J., Thomas, D., Mosteiro-Romero, M., Hsieh, S., Happle, G., Sreepathi, B., Shi, Z., Schlueter, A. (2017). *City Energy Analyst 2.2*. Zenodo.

Ali-Toudert, F., & Mayer, H. (2006). Numerical study on the effects of aspect ratio and orientation of an urban street canyon on outdoor thermal comfort in hot and dry climate. *Building and Environment*, 41(2), 94–108. <https://doi.org/10.1016/J.BUILDENV.2005.01.013>

Ali-Toudert, F., & Mayer, H. (2007). Effects of asymmetry, galleries, overhanging façades and vegetation on thermal comfort in urban street canyons. *Solar Energy - SOLAR ENERGY*. 81. 742-754. [10.1016/j.solener.2006.10.007](https://doi.org/10.1016/j.solener.2006.10.007).

Taleghani, M., Kleerekoper, L., Tenpierik, M., & van den Dobbelsteen, A. (2015). Outdoor thermal comfort within five different urban forms in the Netherlands. *Building and*

Environment, 83, 65–78. <https://doi.org/10.1016/J.BUILDENV.2014.03.014>

Yang, X., Zhao, L., Bruse, M., & Meng, Q. (2012). An integrated simulation method for building energy performance assessment in urban environments. *Energy and Buildings*, 54, 243–251. <https://doi.org/10.1016/J.ENBUILD.2012.07.042>

Carnielo, E., & Zinzi, M. (2013). Optical and thermal characterisation of cool asphalts to mitigate urban temperatures and building cooling demand. *Building and Environment*, 60, 56–65. <https://doi.org/10.1016/J.BUILDENV.2012.11.004>

Fonseca, J. A., & Schlueter, A. (2015). Integrated model for characterization of spatiotemporal building energy consumption patterns in neighborhoods and city districts. *Applied Energy*, 142, 247–265. <https://doi.org/10.1016/j.apenergy.2014.12.068>

International Organization for Standardization, ISO (2008). *Energy performance of buildings – calculation of energy use for space heating and cooling (ISO 13790:2008)*. Geneva, Switzerland.

International Organization for Standardization, ISO (2017). *Energy performance of buildings - Energy needs for heating and cooling, internal temperatures and sensible and latent heat loads - Part 1: Calculation procedures (ISO 52016-1:2017)*. Geneva, Switzerland.

Happle, G., Fonseca, J.A., and Schlueter, A. (2017). Effects of air infiltration modeling approaches in urban building energy demand forecasts. *Energy Procedia* 122, 283–288.

Stadt Zürich (2016). *Masterplan Energie der Stadt Zürich. Energiebeauftragter*, Stadt Zürich, Switzerland.

Baudirektion Kanton Zürich (2014). *Masterplan Hochschulgebiet Zürich-Zentrum September 2014*. Kanton Zürich, Baudirektion. Zurich, Switzerland.

Meteotest (2013). *Meteonorm 7.0*.

Evaluating Computer Aided Design Tools for Building Performance: Trusting and Defining the Predetermined Automated Inputs

E.R. NEWMARCH¹, N. BAKSHI¹, M. DONN¹

¹Victoria University of Wellington, New Zealand.

ABSTRACT: BIM use is on the rise in New Zealand with popular software packages, including Revit and ARCHICAD, adopting a semi-automated simulation platform. This allows architects and designers to calculate the thermal and energy performance of their designs. This paper identifies the strengths and weaknesses of these semi-automated simulation platforms. The objective is to investigate how accurate their assumptions are in determining a reliable output for use in achieving compliance with Clause H1 of the New Zealand Building Code. To achieve this, this paper reports a comparative study that examines the program's ability to calculate construction R-values, interpret thermal properties and simulate energy performance. The results from this study show that if used as delivered there is a significant difference between the simulation results of the two software packages, due to the assumptions built into the default settings. It also identifies the disadvantages of the inbuilt construction R-value calculators and explores a potential path to resolving this through redefining the inputs of thermal properties.

KEYWORDS: Energy Simulation, BIM, Efficiency, Residential

1. INTRODUCTION

The fourth annual BIM Benchmark Survey in a 5-year series completed as part of a BRANZ (Building Research Association New Zealand) study, identifies that 57 per cent of all construction projects adopt the Building Information Modelling (BIM) approach over traditional methods [1]. This percentage is expected to rise following the exponential implementation trend over recent years [1]. The widely-used software packages within the construction industry, that support the BIM methodology, are ArchiCAD and Revit [2]. Their BIM functionality converts them into semi-automated building energy performance simulation platforms that aim to eliminate inappropriate human intervention that could cause results to be untrustworthy [3]. Instead of early design performance prediction based upon rules of thumb developed using predetermined prototypical performance they offer performance simulation inputs that are automatically assigned to increase workflow productivity. This paper investigates these simulation inputs and the accuracy of building energy performance simulation from these different widely used BIM software packages. This paper specifically focuses on how such BIM packages could be used to evaluate energy and building performance for producing evidence for compliance documentation. This is a major area of investigation yet to be explored because building energy performance simulation is, to date, one of the least used assets of these software packages, with only 14 per cent of the industry using BIM for this purpose, compared to 91 per cent which use it for 3D coordination [1]. Current trends also

identify a significant decline in the number of projects that use BIM to demonstrate code compliance, down to 0 per cent in 2017 from 9 per cent in 2016 [1]. There appears to be a significantly underutilised potential for a BIM based workflow in the New Zealand Industry.

The focus is the viability of BIM adoption in the residential market, where architects and designers are the target users. In this context, architects and designers are often solely responsible for ensuring the energy and thermal performance of the building meets the minimum building code, as there is rarely the money nor time available to out-source this task. Furthermore, the New Zealand Building Code [4] offers three potential methods of compliance: schedule, calculation and modelling methods. The first two disconnect the project from the BIM workflow as they both require a manual calculation of the thermal performance of each individual building component (floors, walls, roof etc.). The modelling method, however, presents the opportunity to remain within the BIM workflow and has the potential to achieve higher efficiency in demonstrating code compliance. The parameters of this method form the basis for the assessment of the ability of BIM-enabled software to demonstrate this compliance with a good measure of accuracy.

2. BACKGROUND

The interest and importance of simulating energy and building performance has grown in the architectural design industry due to the increased awareness of energy usage on building life cycle costs and the impact of indoor environment conditions [5]. However,

PLEA 2018 HONG KONG

Smart and Healthy within the 2-degree Limit

the ability to complete these predictions is weakened through simplistic and optimistic calculations prescribed by the building code to accommodate architects and designers. Sophisticated software, outside the BIM approach, has had the capability to create accurate predictions of building energy performance for decades. This software has not been widely adopted by practitioners in building design for many reasons [6]. Instead it is more commonly used for academic research [5]. Alternatively, BIM has become a promising development for the future of architecture, engineering, and construction. It has the advantage of creating a virtual (digital) version of the proposed building that has a wide variety of uses from planning to operation of the building. Yet, as a developing workflow, it also has issues getting practitioners to incorporate energy and building performance methodologies.

A paper investigating a library for energy and building performance in BIM, suggests that the BIM enabled interoperability between architectural design and energy simulation actually prevents energy analysis becoming an efficient process in the early stages of design [7]. The paper proposes an Object Orientated Physical Modelling (OOPM) approach that could produce component level simulation results which allow direct feedback to the designer of the impact on energy performance of building design decisions about individual building components. The benefit is the ability to visually link the results from the energy and building simulation directly to the virtual design, showing potential for implementation within practice. Another paper identifies numerous sources that suggest building energy performance simulation is seldom implemented in practice due to the associated labour intensive and costly processes [2]. In contrast, the semi-automated processes adopted by various CAD packages may reduce such costs. For these automated inputs to be trusted, their outputs need to be validated against known information. To be used for Code Compliance in the NZBC, Clause H1 “Energy Efficacy for housing and small buildings” these outputs also need to be converted into a format that is accepted and recognised by district councils, so that they can contribute as evidence for compliance.

3. METHODOLOGY

The NZBC “Modelling Method” requires submission of a compliance report comparing the performance of a simulated model with a reference model. The reference model is built to the compliance requirements outlined in NZS 4218. This model applies the minimum construction R-values for the relative climate zone and is considered the minimum level of performance.

To investigate the consistency of common BIM-enabled software packages, this paper adapts this

process and presents the building energy performance results of a reference model, a proposed model and a model using software inputs. As a measure of quality assurance all models use the same geometry and glazing ratio.

The “Reference Model” uses the simple R-values specified in the NZS4218 Standard [8]. The “Proposed Model” applies construction R-values calculated using the “isothermal planes” method specified in NZS 4214 [9]. These R-values account for the thermal bridging of the actual materials used in the building structure. They are therefore the targets for determining the accuracy of the software. The “Software Input Model” models’ results are compared to the Proposed and Reference models.

In both software packages, models were built using material descriptions that align closely with the building’s consent specifications. For example, Pink Batts®, a glass fibre batt insulation product commonly used in New Zealand construction, has been matched with the glass fibre batt insulation option in both ARCHICAD and Revit. Additionally, the default occupancy schedules and heating/cooling loads of a typical residential building were used to examine the difference in assumptions made by both software packages.

To test the ability of the inbuilt construction R-value calculator in each property, construction assemblies were made using materials present within the inbuilt library. Each material layer was given the same thickness to match the case study construction specification. However, as both inbuilt calculators were homogenous, for heterogeneous layers the most prevalent material properties were taken. In the context of this case study, in an insulated timber wall with a timber structure and insulation infill between the vertical timber studs, a single insulation material “layer” was defined. As a combination of the two materials’ R-values. The methodology for R-value inputs for the reference and proposed models differ slightly in each software due to their interface and settings. These are differences are outlined in the following sections.

3.1 Modelling in ARCHICAD

For the reference and proposed simulations, the construction R-values were input using the override setting within the energy model evaluation settings and the appropriate “Structure Heat Storage Mass” was applied [10].

3.2 Modelling in Revit

For the reference and proposed simulations, the construction R-values were input by creating a new material with thermal properties that generated the reference and proposed construction R-values.

PLEA 2018 HONG KONG

Smart and Healthy within the 2-degree Limit

4. INVESTIGATED BUILDING TYPE

The standalone single family housing is the most dominant housing typology (~80%) throughout New Zealand [11]. For this reason, a standalone typology has been selected for this research.

As the focus is on how well the software interprets and calculates the specification of building, a simplified case study has been selected. Construction assemblies represent the most common used systems in New Zealand residential construction. Walls and roofs are framed with timber + pre-nail manufacturing. Floor on ground is a concrete slab with polystyrene insulation (insulation under slab is increasingly more common in the south).

Detached single family houses have historically been the dominant housing typology in the Queenstown Lakes District. However, more recently there has been increasing demand for more affordable housing. The common answer, applied nation-wide, is to look towards medium density housing, to provide a lower upfront cost to the housing market. Yet, a recent housing preferences survey revealed that standalone housing scored consistently higher than attached, medium density, and high rise living, on perceived factors including; value for money, neighbours that are safe, have an enjoyable lifestyle, a good sense of community, and are visually appealing [12]. This strong desire to continue living in standalone, sole ownership, housing is feeding the rise of an increasingly popular typology of a main house and guest house on a single property title. Derived from a multi-family housing model, this typology has been edited to create a house and income model, which allows the owner to rent out the guest house to pay the mortgage on the full property. As Queenstown is a high tourism area, popular business apps such as AirBnB and HelpX, enable this housing typology's success and attractiveness. For these reasons a house and guest typology has been selected for this study.

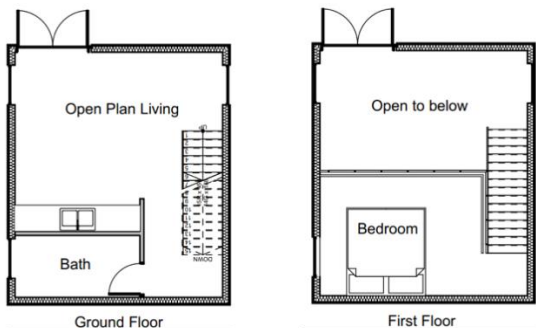


Figure 70: Case Study Floorplans

5. RESULTS

Initial simulations suggested that there is a significant identifiable difference between the outputs of each CAD package. These results drew attention to the

assumptions made by the automated inputs to the software. This study found that certain defaults have an appropriate place within the semi-automated simulation process, however, other pre-set inputs within the software could be improved to more adequately respond to New Zealand's building regulations, conditions, and climates. The end of this study examines the various observations between real world figures and the simulation findings of both the simulation methods explored, identifying variations in the semi-automated processes used by each CAD package that informed the numerous inputs.

5.1 Results - Building Component Construction Inputs

In energy simulation, it is essential to have reasonably accurate inputs for the thermal properties of the building's external envelope. These inputs are important as they can greatly impact the building's heat loss as well as the annual energy consumption.

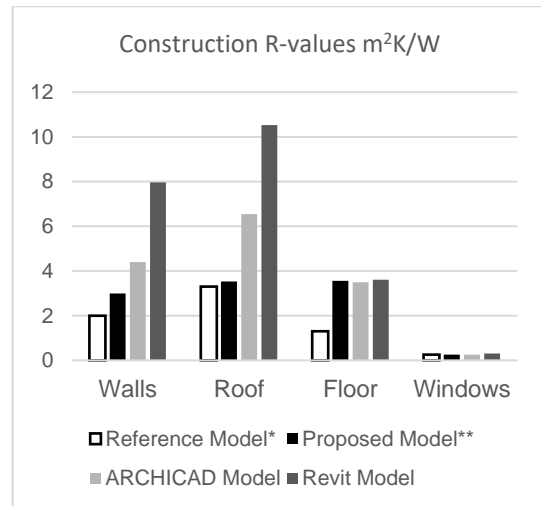


Figure 71: Construction R-value Calculations

*Minimum R-values based on Table 2 in NZS4218 for Climate zone 3

**Construction R-values calculated using the approved Isothermal planes method outlined in NZS 4214. These figures are considered a target for testing the software ability to calculate R-value's accurately.

The calculations shown in Figure 2 identify that there is significant variation in the software's ability to calculate accurate construction R-values for the walls and roof. Yet, there is consistency shown in the results for the floors and roof. This identifies that, such a simulation process is limited to only homogenous construction build means that the calculation can only account for a single material per layer.

This is an issue because the most common types of construction in New Zealand have at least one heterogeneous layer that is host to insulation placed in-between the timber structure. It is understandable that both the semi-automated simulation software packages would simplify the construction R-value

PLEA 2018 HONG KONG

Smart and Healthy within the 2-degree Limit

calculation to only include a homogenous build up due to the manual requirement of setting the appropriate percentages. However, by not allowing this flexibility in the calculation the results are unreliable and optimistic. This level of optimism can be costly as it gives a false representation to the architect or designer which could lead to compliance being awarded incorrectly. Ultimately, making generous assumptions in the simulation stage of a project only decreases the quality of the built product. Material libraries in both programs do not include materials that are within an acceptable range to be considered an accurate representation of the true material.

A potential solution would be either create a material library that is included in the software package for New Zealand. Alternatively establishing a format where products can supply a schedule that can be imported into the software could also be an opportunity for improvement. Creating construction elements, i.e. walls, floor, roof, etc. within either BIM enabled software is too simplistic to accurately account for heterogeneous construction layers. This is due to the construction assembly editing tool in both software packages only offering a basic homogenous construction build up. A potential way around this would be to create pre-set layers that included pre-calculated defaults for structural and insulation percentages. However, a weakness of this solution would be the quantity required to represent an appropriate range of structural configurations to gain a reasonably accurate percentage range.

This study also found that windows were the most accurately and consistently represented across all models. This is likely to be because there is very little room for variation compared to walls, roofs and floors. Additionally, thermal properties for windows are a well-recognised standard.

5.2 Results – Whole Building Energy Simulation

As expected the energy performance of the model using the software defaults is lower across both software packages. However, there is a significant gap between these two trends. This gap may potentially be caused by the difference between the default schedules and heating/cooling loads assigned to the model in each software according to its building types.

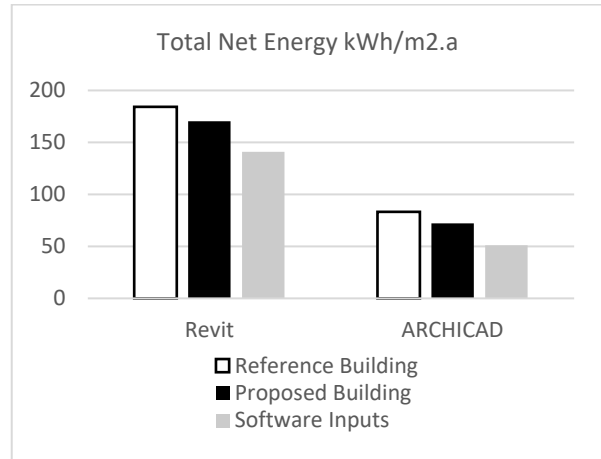


Figure 72: Whole Building Simulations in Revit and ARCHICAD

5.3 Material Properties comparison

In this case study, the software packages produced greater construction R-values compared to the proposed model, for the roof and wall elements which contained heterogeneous layers. However, as the difference between these R-values being so great, it is unlikely to be caused by the limitation of a homogenous calculation method alone. Instead, this difference has identified that the thermal properties of the materials that matched the description from the case study specification were significantly higher than the true thermal properties of the material used in New Zealand.

Table 11: Thermal Properties Glass Fibre Batts

	Conductivity (W/mk)	Density (kg/m ³)
Wall - Glass Fibre Batt		
Specified True Material	0.0388	14.0
Revit Material	0.19	32.0
ARCHICAD Material	0.033	50.0
Roof – Glass Fibre Batt		
Specified True Material	0.0487	8.1
Revit Material	0.19	32.0
ARCHICAD Material	0.033	50.0

Table 1 above shows that ARCHICAD had a closer thermal conductivity to the true material compared to Revit, however, Revit had a closer density. In both cases the thermal properties were not close enough to be considered an adequate representation of the true material.

5.4 Redefining the Inputs: Formulae for Calculating New Thermal Properties.

To compensate for the built-in R-value calculator being homogenous in both software packages, new material layers were calculated using the thermal properties of both insulation and wood. The new properties were calculated to account for the different ratios of each material that were prescribed in the proposed building

PLEA 2018 HONG KONG

Smart and Healthy within the 2-degree Limit

where the R-values were calculated using the Isothermal Planes calculation method required by NZS 4214.

Equations one and two demonstrate how new thermal properties were calculated. These were based off the principles of calculating isothermal planes. Fundamentally the purpose is to calculate an average of two properties that do not have an equal ratio.

In this study, equation 1 and equation 2 were used to redefine the thermal properties for the wall and roof heterogeneous layers. However, they could also be applied to the floor and any other part of the building that has a heterogeneous layer of any material type which needs to be converted into a format that can be used as an input for construction R-value calculations in ARCHICAD or Revit.

(1)

$$TC_n = \frac{1}{\left[\left(\frac{R_T}{TC_T}\right) + \left(\frac{R_I}{TC_I}\right)\right]}$$

(2)

$$D_n = \frac{1}{\left[\left(\frac{R_T}{D_T}\right) + \left(\frac{R_I}{D_I}\right)\right]}$$

Where...

- R_T Ratio of Timber (%)
- R_I Ratio of Insulation (%)
- TC_N Thermal Conductivity of New Material (W/mk)
- TC_T Thermal Conductivity of Timber (W/mk)
- TC_I Thermal Conductivity of Insulation (W/mk)
- D_N Density of New Material (kg/m³)
- D_T Density of Timber (kg/m³)
- D_I Density of Insulation (kg/m³)

New Material Properties

Description	Thermal Conductivity	Density
Wall Timber 18.7% Insulation 81.3%	0.0444	17.10
Roof Timber 12.1% Insulation 87.9%	0.0525	9.19

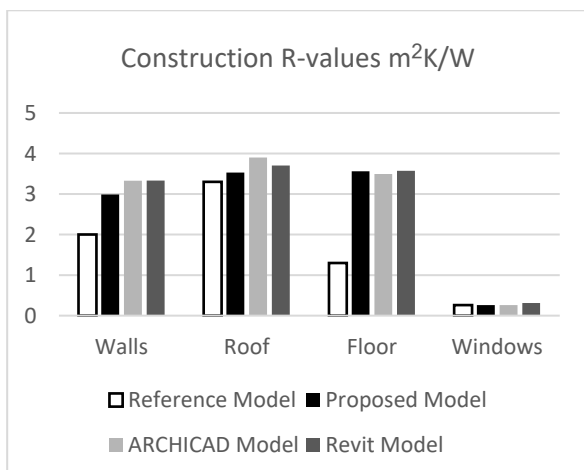


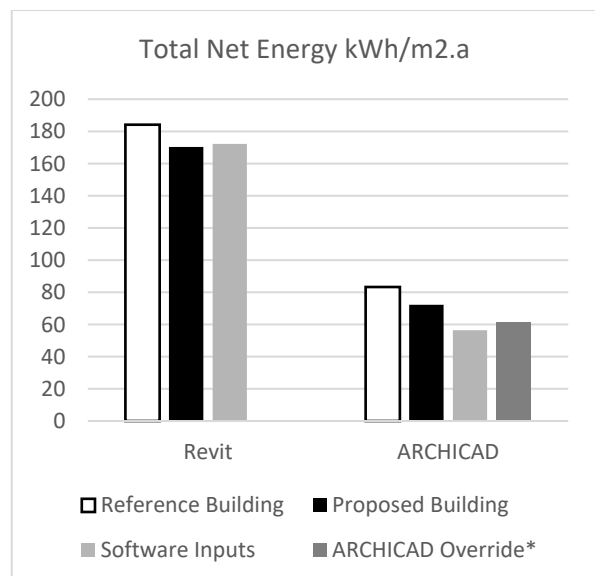
Figure 73: Updated Construction R-value calculations compared

Figure 4 shows that both ARCHICAD and Revit R-value calculators achieved a much closer result to the proposed R-value in both the wall and roof elements. This proves that defining a layer with the appropriate timber to insulation ratio and using thermal properties from New Zealand construction materials achieves a more reliable result.

5.5 Impact of the New Materials on Whole Building Simulation

Iterative simulations, shown in Figure five, simulate the case study with the updated construction R-values. These suggest that results now very closely match the proposed R-values. The simulation completed in Revit demonstrates the expected outcome, where the results from the updated model closely match the proposed model. However, the ARCHICAD simulation did not follow the same expected outcome, even though it's built in R-value calculator achieved results very close to the proposed R-values (Figure 4).

To examine the behaviour of the software, the R-value override function was used within ARCHICAD's energy evaluation settings (The same override function that was used for the reference and proposed simulations). The same R-value was put in and the "Structure's Heat Storage Mass" was assigned to the most appropriate option, i.e. "Timber Structure" for walls and roof. This simulation produced results closer to the proposed model, even though the same R-values were used. This suggests that in ARCHICAD there are other variables that are impacting the results that do not have the same impact in Revit. This is an interesting observation as both software packages claim validation through the ASHRAE 140 standard for international modelling software, yet, they respond to the same input differently. This is an area that merits further research.



PLEA 2018 HONG KONG

Smart and Healthy within the 2-degree Limit

Figure 74: Whole Building simulations completed with the updated construction R-value calculations

6. CONCLUSION

This study has identified that in both of the software packages examined the thermal properties of core construction materials are not an accurate representation of those used in New Zealand.

Although a homogenous construction R-value calculators, are built into both ARCHICAD and Revit, has the benefit of simplifying the calculation process, these values produce very optimistic results. This is due to the forced assumption of only a single material per layer. This is not an appropriate or accurate way of representing a timber framed house because the insulation is installed between the structural elements. This paper tested a potential way to account for the thermal bridging of the timber structure, however, this method required external calculation and input. This removes the benefit of a semi-automated simulation platform as it requires the user to externally research the relevant materials, combine them using the formulae written into this paper and then create a new material within the software. This requires an expertise in energy modelling that is well above what is expected of an architect or designer in practice.

However, the results in this study indicate that there may be a potential to create a pre-set material library that is customised to the thermal properties of New Zealand materials that are combined using ratios that are relative to New Zealand construction techniques. A pre-set library of this kind has the potential to be loaded into software for both architects and designers alike, to achieve a more accurate and reliable simulation result of energy performance. Any pre-set library will need to be tailored for each software package and is an area that merits further investigation.

It should be noted that this research is not without its limitations:

The simulation results from Revit and ARCHICAD, identify that there are significant differences in the default assumptions each software package incorporates. These default assumptions include occupancy schedules and heating and cooling loads.

To test each software package for its accuracy, without the expertise of an energy analyst, default settings of the occupation profiles or building schedules were used. These differ for both software packages. The accuracy of these results based on these varying schedules is an area that merits further research.

The case study examined in this paper used relatively simple materials. A subsequent study may potentially develop a wider range of pre-set materials that take into account of the materials available in New Zealand and their relative ratios with respect to the common timber framed construction methods used in New Zealand.

Finally, this study does not take into consideration different microclimate conditions within New Zealand. These could potentially be used to establish how accurately the automated inputs predict differences in heating and cooling energy use requirements.

REFERENCES

- Rosevear, M., & Curtis, M. (2017). Physical characteristics of new houses 2015. Wellington: BRANZ.
- Thompson, K. (2012, August/September). Making the most of BIM. *BUILD*, 39.
- Bazjanac, V. (2008). IFC BIM-Based Methodology for Semi-Automated Building Energy Performance Simulation. *CIB-W78 25th International Conference on Information Technology in Construction*. Santiago, Chile: Lawrence Berkeley National Lab.
- New Zealand Building Code (NZBC). (2007).
- Laine, T., Hanninen, R., & Karola, A. (2007). Benefits of BIM in the Thermal Performance Management. *Proceedings of the Building Simulation*. Helsinki.
- Attia, Shady. (2013) Tool for design decision making: Zero energy residential buildings in hot humid climate ; 13th Conference of the International Building Performance Simulation Association IBPSAA: Chambéry.
- Bum Kim, J., Jeong, W., Clayton, M. J., Haberi, J. S., & Yan, W. (2015). Developing a physical BIM library for building thermal energy simulation. In M. J. Skibniewski, *Automation in Construction* (Vol. 50, pp. 16-28). USA: Elsevier.
- NZS 4218 (2009). Thermal insulation – housing and small buildings.
- NZS 4214 (2006). Methods of determining the total thermal resistance of parts of buildings.
- GRAPHISOFT. (2017). *Energy Evaluation Workflow: Overview*. Retrieved 2018.
- Page, I.C, and Fung, J. BRANZ SR214 (2009) Housing life cycle and sustainability Part One I.
- Bryson, K. (2017). The New Zealand Housing Preferences Survey: Attitudes towards medium-density housing. Wellington: BRANZ.

Indoor air Quality and Its Effects on Health in Urban Houses of Indonesia: A case study of Surabaya

TETSU KUBOTA¹, HANIEF ARIEFMAN SANI¹, USEP SURAHMAN², SOPHIA HILDEBRANDT³,
HAMIDIE RONALD DANIEL RAY², BETA PARAMITA²

¹Graduate School for International Development and Cooperation, Hiroshima University, Higashi-Hiroshima, Japan

²Universitas Pendidikan Indonesia (UPI), Bandung, Indonesia

³Institute for Infrastructure and Resources Management, Leipzig University, Leipzig, Germany

ABSTRACT: *There is a possibility that the sick building syndrome has already spread widely among the newly constructed apartments in major cities of Indonesia. This study investigates the current conditions of indoor air quality, focusing especially on formaldehyde and TVOC, and their effects on health among occupants in the urban houses located in the city of Surabaya. A total of 471 respondents were interviewed and 82 rooms were measured from September 2017 to January 2018. The results indicated that around 50% of the respondents in the apartments showed some degrees of chemical sensitivity risk. More than 60% of the measured formaldehyde levels in the apartments exceeded the WHO standard, 0.08 ppm. The respondents living in rooms with higher mean formaldehyde values tended to have higher multiple chemical sensitivity risk scores.*

KEYWORDS: *Indoor air quality, Sick building syndrome, QEESI, Formaldehyde, Developing countries*

1. INTRODUCTION

Indoor air quality (IAQ) and its effects on health of occupants have been studied in many parts of the world over the last several decades [1]. In developing countries, however, most of the IAQ studies focused on the issues of exposure to biomass combustion, and thus there are relatively few studies investigating IAQ in urban houses [2]. Nevertheless, in response to rapid population growth and urbanization, the construction of urban houses using modern building materials is thriving in developing countries – but without sufficient standards or regulations for the building materials as well as minimum ventilation rates. This study investigates the current conditions of IAQ, focusing especially on formaldehyde and TVOCs, and their effects on health among occupants in urban houses of Indonesia. This paper presents the results of a case study conducted in the city of Surabaya in 2017-2018.

2. METHODOLOGY

Field investigations consisting of face-to-face interviews and measurements were conducted in five high-rise apartments, including low-medium cost apartments and condominiums, and five unplanned residential neighbourhoods, the so-called Kampongs from September 2017 to January 2018 (Table 1). This period includes part of dry season (Sep to Oct) and wet season (Nov to Jan). A total of 471 respondents were interviewed and 82 rooms were measured. The Kampongs comprise dense unplanned landed houses (approximately 11-53 years old) without proper urban

Table 1: Number of samples

	Kampongs	Apartment	Total
Questionnaire	298 (63%)	173 (37%)	471
IAQ measurement	42	40	82
Spirometer test	46	21	67



Figure 1: Views of (a) Kampongs and (b) apartment

infrastructure, whereas the apartments are high-rise buildings of about 20-storey or more (Fig. 1). These apartments were newly constructed since 2010 (see Table 4).

The interviews were conducted using a questionnaire form comprising the Quick Environmental Exposure and Sensitivity Inventory (QEESI[®]) developed by Miller & Prihoda [3] and several additional questions, amongst others: cleaning habits, window-opening behaviour and socio-economic factors. Formaldehyde (FMM-MD, Shinyei) and TVOCs (ToxiRAE Pro, RAE Systems) were measured on top of air temperature and RH for approximately three days in master bedroom and living room of respective houses. The interval time of measurement was 1 min for TVOC and 30 min for the other parameters. In addition, lung capacity of occupants was measured by the spirometer test.

PLEA 2018 HONG KONG

Smart and Healthy within the City

Table 2: MCS risk criteria [3]

Degree to which MCS is suggested	Symptom Severity Score	Chemical Intolerance Score	Masking Score
Very suggestive	≥ 40	≥ 40	≥ 4
Very suggestive	≥ 40	≥ 40	< 4
Somewhat suggestive	≥ 40	< 40	≥ 4
Not suggestive	≥ 40	< 40	< 4
Problematic	< 40	≥ 40	≥ 4
Problematic	< 40	≥ 40	< 4
Not suggestive	< 40	< 40	≥ 4
Not suggestive	< 40	< 40	< 4

Multiple chemical sensitivity (MCS), which was recommended to replace idiopathic environmental intolerance (IEI) in the World Health Organization/International Programme on Chemical Safety (WHO/IPCS) workshop, is defined as an acquired disorder with multiple recurrent symptoms, as being associated with diverse environmental factors tolerated by the majority of people, and as not being explainable by any known medical or psychiatric disorder [4]. Miller & Prihoda [3] developed the QEESI to differentiate between chemically sensitive people and normal people.

The QEESI consists of the following five scales [3]: chemical intolerance (to what extent certain odor or exposures make one sick); other intolerances (to what extent a variety of other exposures make one sick); the severity of symptoms (to what extent one experiences certain symptoms); the masking index (whether there is ongoing exposure from routinely used products); and life impact (to what extent the sensitivity affects certain aspects of life). Each scale is composed of ten questions, and each question is scored from 0-10, except for the masking index, which is scored as 'yes: 1' or 'no: 0'. Miller & Prihoda [3] suggested ranges for the scales and interpretation guidelines. The criteria for the risk criteria (degree to which MCS is suggested) are shown in Table 2.

3. RESULTS AND DISCUSSION

3.1 Multiple chemical sensitivity (MCS) risk

The final calculated results of MCS were analysed by respective housing types (Fig. 2). As shown, only 21.9% of respondents show some degrees of intolerances in Kampongs, but the percentage of problematic respondents is significantly higher in the apartments, which is 48.8% ($p < 0.01$). The percentage of problematic and very suggestive respondents in the apartments are more than twice than Kampongs. Fig. 3 shows the detailed results from QEESI. As illustrated in Fig. 3a, the respondents show high degrees of intolerance particularly to tobacco, diesel/gas, insecticide and paint. Overall, the magnitudes of intolerance in the apartments are significantly higher than those in Kampongs in most kinds of chemicals ($p < 0.01$). Nevertheless, if only problematic respondents of which MCS risks range from 'problematic' to 'very suggestive' are analysed

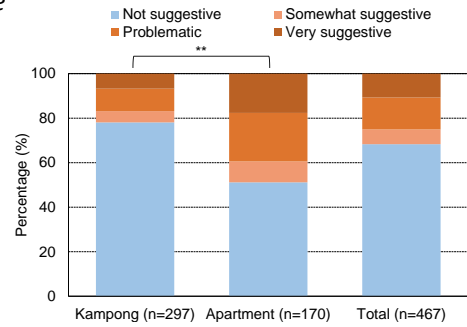
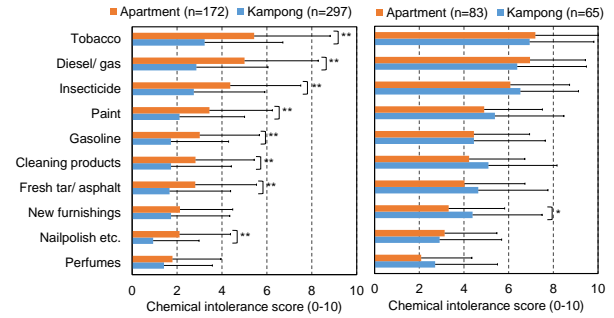
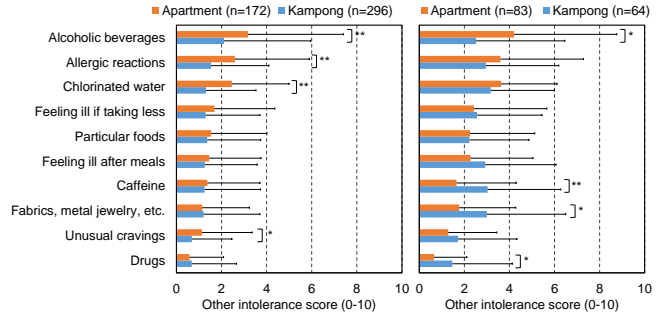


Figure 2: Results of MCS risk

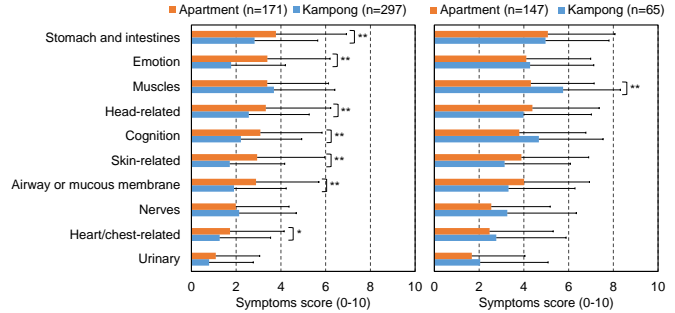
(a) Chemical intolerance score



(b) Other intolerance score



(c) Symptoms score



(d) Masking index

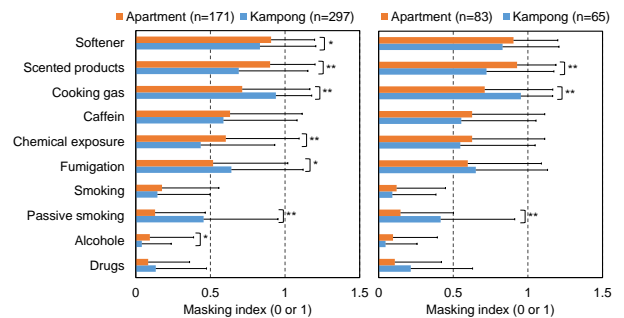


Figure 3: Results of QEESI. The left figure shows those of all samples and the right indicates those of only problematic respondents (MCS risk: 'Problematic' to 'Very suggestive'). The error bar indicates a standard deviation, and, hereafter, * shows 1% significant level, whereas ** indicates at 5% level.

PLEA 2018 HONG KONG

Smart and Healthy within the 2-degree Limit

(i.e. the right figures of Fig. 3), the magnitudes of intolerance in the apartments are not higher than those of Kampongs (Fig. 3a). Rather, the intolerance to new furnishings is higher in Kampongs than that in the apartments. Meanwhile, the degrees of intolerance to other chemicals are not as high as previous items, and some of them, including alcoholic beverages, allergic reactions and chlorinated water, present significant differences between Kampongs and apartment (Fig. 3b).

On average, symptoms scores (Kampongs/apartments) are high in terms of stomach and intestines (2.8/3.8), emotion (1.8/3.4), muscles (3.7/3.4), head-related (2.6/3.3), cognition (2.2/3.1), skin-related (1.7/2.9) and airway or mucous membrane (1.9/2.9). Significant differences between the two groups can be seen in most of the items, except for muscles. The average symptoms score for the muscles in Kampongs is significantly higher than that of apartments even among the problematic respondents ($p < 0.01$).

As described before, the masking index assesses whether there is ongoing exposure from routinely used products [3]. Among the problematic respondents, the average index score for scented products in the apartments is higher than that of Kampongs, whereas those for cooking gas and passive smoking in Kampongs are higher than the apartments (Fig. 3d).

The above results imply that although most of the factors affecting MCS risk are similar among problematic respondents of both Kampongs and apartments, a few different factors also can be seen in the two groups, such as intolerance to new furnishings, symptoms on muscles, masking factors of scented products, cooking gas and passive smoking.

3.2 Factors affecting MCS risk

We conducted correlation analyses to identify the factors affecting MCS risk scores in Kampongs and apartments respectively using the Spearman's test or Chi-square test depending on types of variable. Table 3 summarises the surveyed personal attribute variables and their relations to the MCS risk scores respectively. First, it is found that the female respondents tend to obtain higher MCS risk scores in the apartments ($p < 0.05$). In contrast, the increases in age and household income tend to increase the MCS risk in Kampongs ($p < 0.05$, $p < 0.01$). Second, the occupation of respondents has significant relationship with MCS in Kampongs: in particular, government officers and retired respondents tend to have higher MCS risk scores. The increase in stress level increases MCS risk scores in both groups. Meanwhile, those who have a medical history of asthma, eczema and other kinds of allergy tend to have higher MCS risk scores in Kampongs.

Table 3: Personal attributes and their relations to MCS risk

Variables	Kam- pongs	p	Apart- ment	p	Total	p
Gender [%]		.474		.032		.146
Male	35.5		42.1		37.9	
Female	64.5		57.9		62.1	
Age [%]		.068		.809		.115
<20	14.3		16.0		14.9	
20-29	13.0		68.0		33.1	
30-39	17.7		5.9		13.4	
40-49	27.0		4.7		18.8	
>50	28.0		5.3		19.7	
Income [%]		.000		.496		.000
<150US\$	24.8		10.5		18.3	
150-450	56.4		49.2		53.1	
450-750	9.4		14.5		12.1	
>750	9.4		25.8		16.5	
Occupation [%]		.001		.778		.001
Government	4.0		7.0		5.1	
Private	21.9		14.5		19.2	
Entrepreneur	21.5		6.4		16.0	
Student	19.2		66.3		36.5	
Housewife	24.6		3.5		16.8	
Retired	6.7		0.6		4.5	
Others	2.0		1.7		1.9	
Stress [0-10]	2.1	.000	4.3	.004	2.9	.000
Asthma [%]	12.8	.041	17.4	.740	14.5	.080
Eczema [%]	25.3	.000	36.0	.055	29.3	.000
Allergy [%]	31.6	.031	36.5	.117	33.4	.007

Table 4: Building attributes and their relations to MCS risk

Variables	Kam- pongs	p	Apart- ment	p	Total	p
Age of building [years]	31.7	.146	4.5	.750	25.2	.880
Duration of living [years]	25.3	.405	1.9	.474	15.2	.000
No. of windows in bedroom [%]		.004		.924		.049
0	12.5		7.0		10.1	
1	67.7		73.4		70.1	
>1	19.8		19.6		19.7	
No. of windows in living room [%]		.000		.280		.000
0	3.0		5.3		3.8	
1	75.9		47.4		65.6	
>1	21.2		47.4		30.6	
Duration of opening windows [hrs/day]						
Bedroom	13.6	.416	6.5	.141	9.9	.000
Living room	12.8	.773	7.3	.853	10.5	.008
HVAC ownership [%]						
Air-conditioner	20.9	.007	99.2	.608	57.6	.000
Fan	99.3	.509	29.5	.526	66.9	.001
Exhaust fan	10.6	.888	51.6	.133	29.9	.085
Modification [%]	71.1	.017	25.2	.987	50.2	.394
Water leakage [%]	69.8	.387	27.6	.143	50.4	.065
Furniture [mean units]		.003		.322		.087
Living room	3.8		5.1		4.4	
Bedroom	3.1		3.3		3.2	
Cleaning rooms [%]		.006		.626		.016
1/month or less						
Every 2-3 weeks	0.0		5.4		2.5	
Every week	0.0		6.2		2.8	
Every 2-5 days	2.6		32.3		16.3	
Everyday	7.8		27.7		17.0	
Cleaning	89.6		28.5		61.4	
Cleaning bathrooms [%]		.689		.061		.011
1/month or less	2.4		17.4		9.3	
Every 2-3 weeks	9.8		13.8		11.6	
Every week	36.9		43.7		40.1	
Every 2-5 days	28.6		18.6		23.9	
Everyday	22.3		6.6		15.0	

PLEA 2018 HONG KONG

Smart and Healthy within the 2-degree Limit

Table 4 presents the surveyed building attribute variables and their relations to the MCS risk scores. As shown, overall, the duration of living in the present houses has a significant relationship with MCS risk ($p < 0.01$), but the relationships are seen neither in each of the groups. Meanwhile, the increases in number of windows in both master bedroom and living room increase the MCS risk in Kampongs ($p < 0.01$). Nevertheless, the duration of opening windows obtains a significant relationship with MCS risk only for all samples ($p < 0.01$). Furthermore, in Kampongs, the ownership level of air-conditioning ($p < 0.01$), the history of modification ($p < 0.05$), the number of furniture in the living room ($p < 0.05$) and the frequency of cleaning rooms ($p < 0.05$) have significant relationships with MCS risk.

Table 5 indicates the surveyed indoor air quality sensations and their relations to the MCS risk scores. As shown, those who feel some smell and mold growth in their houses of Kampongs tend to obtain higher MCS risk scores ($p < 0.05$).

3.3 Indoor air quality (IAQ) measurement

Outdoor weather conditions differed between dry and wet seasons. As shown in Fig. 4, during the dry season, the outdoor air temperature ranges from 25.1-36.3°C with an average temperature of 29.9°C, whereas the RH ranges from 34-86% with an average of 64%. Meanwhile, the average outdoor temperature dropped to 28.1°C while the average RH increased up to 77% during the wet season.

In the dry season, the measured indoor air temperatures range from approximately 29-32°C in Kampongs, while those in apartments ranges from 27-31°C. As shown, air-conditioning was used in most of the rooms in the apartments unlike in Kampongs. The indoor RH does not exceed 70% even in Kampongs during most of the period in the dry season partially due to the increased indoor air temperatures. In

Table 5: Indoor air quality and their relations to MCS risk

Variables	Kampongs	p	Apartment	p	Total	p
Smell/Odor [%]	51.0	.024	60.5	.160	55.4	.064
IAQ [%]		.893		.056		.324
(Rather) Clean	42.1		42.3		42.2	
Neutral	46.7		43.8		45.4	
(Rather) Dirty	11.2		13.8		12.4	
OAQ [%]		.089		.148		.027
(Rather) Clean	38.8		33.8		36.5	
Neutral	43.4		54.6		48.6	
(Rather) Dirty	17.8		11.5		14.9	
Humidity [%]		.051		.128		.307
(Rather) Dry	31.3		30.7		31.0	
Neutral	42.7		48.0		45.1	
(Rather) Humid	26.0		21.3		23.8	
Mold [%]	42.4	.005	37.0	.660	39.9	.296
Mite [%]	6.0	.921	18.1	.107	11.5	.007

contrast, indoor RH maintained very high values, up to 87% in Kampongs during the wet season, while the indoor air temperatures were decreased to approximately 27-29°C.

The mean and maximum formaldehyde and TVOCs during the measurement periods were illustrated respectively in Fig. 5. These values were calculated based on the measured 30 min temporal average values, and therefore even the maximum values over the measurement period can be comparable with major international/domestic standards on IAQ. Overall, the average values of both formaldehyde and TVOCs are higher in the apartments than those in Kampongs except for the average maximum values of TVOCs, although a significant difference is found only for the mean values of formaldehyde ($p < 0.01$). For example, the maximum values of formaldehyde range up to approximately 0.172 ppm with an average of 0.081 ppm in Kampongs, while those in the apartments range from approximately 0.048-0.183 ppm with an average of 0.115 ppm, which is higher than the WHO standard, 0.08 ppm. Meanwhile, the maximum values of TVOCs range up to approximately 5.21 mg/m³ with an average of 2.59 mg/m³ in Kampongs, while those in apartments range up to

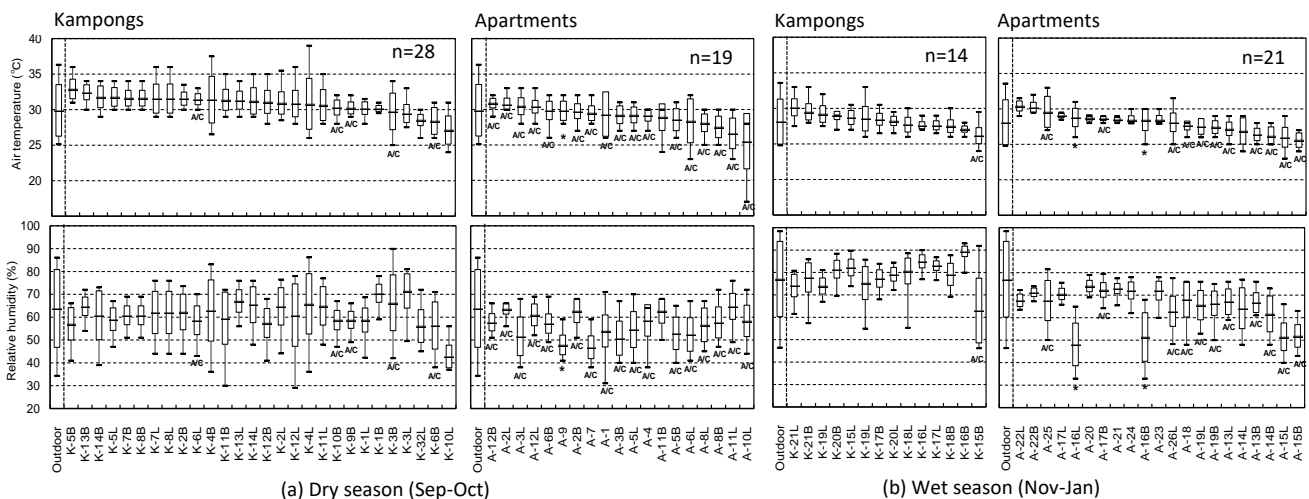


Figure 4: Statistical summary of outdoor and indoor air temperature and RH. 'AC' indicates rooms equipped with air-conditioning and * shows unknown. Hereafter, the box charts indicate the mean, the mean \pm standard deviation and the maximum/minimum values.

PLEA 2018 HONG KONG

Smart and Healthy W.

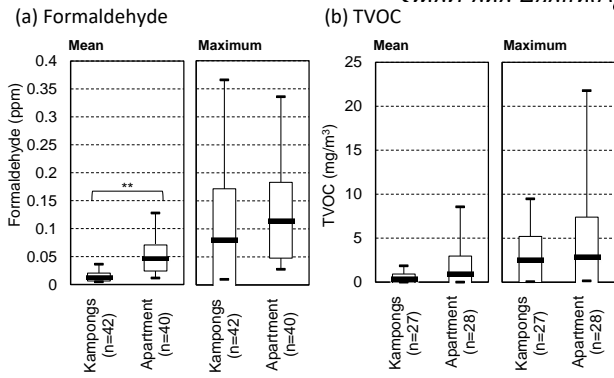


Figure 5: Statistical summary of IAQ measurement results.

approximately 7.40 mg/m^3 with an average of 2.90 mg/m^3 .

Figs. 6-7 present cumulative frequencies of formaldehyde and TVOCs respectively. As shown in Fig. 6, overall, the formaldehyde concentrations are higher in the apartments than those of Kampongs especially in terms of mean values. It should be noted that extremely high maximum values of formaldehyde were, however, obtained in both groups (Fig. 6b). This means that the background formaldehyde concentrations are apparently higher in the apartments than Kampongs as expected, but there are some exceptional cases even in Kampongs in which the formaldehyde levels are intermittently very high. Nevertheless, the result indicates that a large proportion of occupants in the apartments are routinely exposed to a high concentration of formaldehyde. As shown in Fig. 6b, more than 60% of the measured formaldehyde levels in the apartments exceed the WHO standard, whereas about 20% exceed the standard in Kampongs.

As shown in Fig. 7, the measured TVOC levels are not so different between Kampongs and apartments. Overall, the measured TVOC levels are divided into two opposites. Although approximately 60% of the rooms obtain relatively low TVOC levels with mean values of less than $400 \text{ } \mu\text{g/m}^3$, the rest of the rooms obtain high values, up to $8,000 \text{ } \mu\text{g/m}^3$ on average. Both Kampongs and apartments contain several extreme cases in which the maximum values range from $8,000$ up to $21,800 \text{ } \mu\text{g/m}^3$.

3.4 Influence of IAQ levels on MCS risk

We analysed the differences of mean values of formaldehyde and TVOCs respectively between the two different MCS risk groups: 'not suggestive' and 'problematic' to 'very suggestive' (Figs. 8-9). As shown in Fig. 8, significant differences are found in terms of formaldehyde in both Kampongs and apartments for mean and maximum values respectively. As expected, the respondents living in rooms with higher formaldehyde values tend to have higher MCS risk scores. Nevertheless, the opposite tendency can be seen for the maximum formaldehyde values in Kampongs. This is probably because there were some

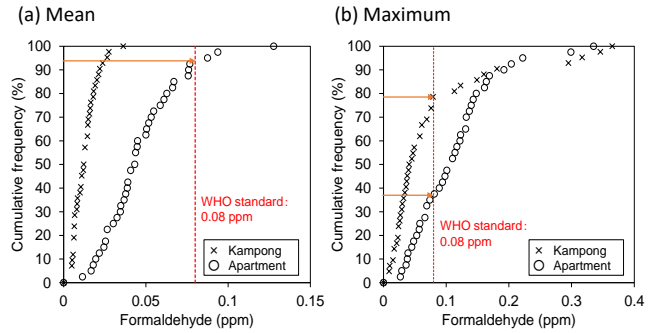


Figure 6: Cumulative frequency of the measured formaldehyde.

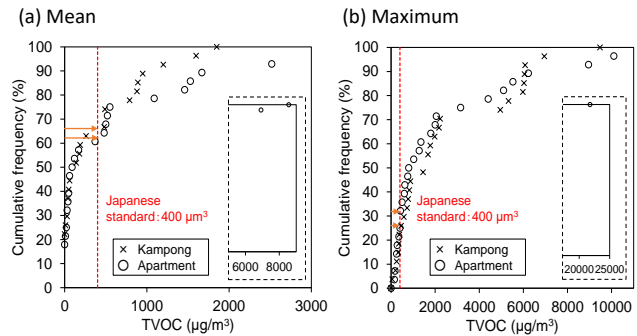


Figure 7: Cumulative frequency of the measured TVOCs.

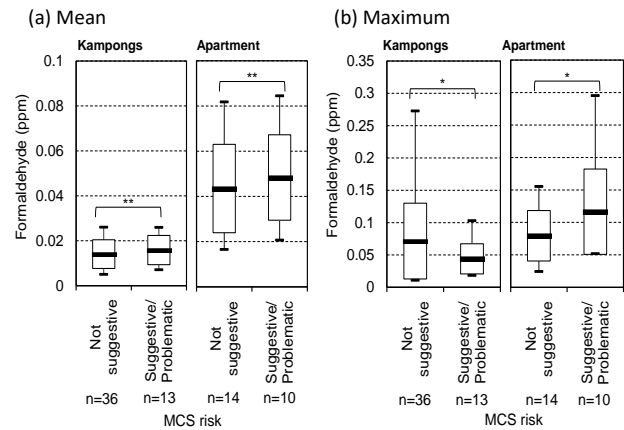


Figure 8: Formaldehyde levels by different MCS risk groups.

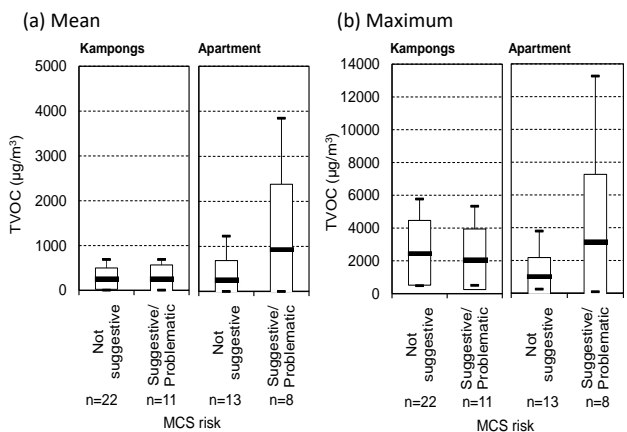


Figure 9: TVOC levels by different MCS risk groups.

exceptional cases in Kampongs in which the formaldehyde levels were intermittently very high as discussed before. In other words, this result implies that the long-term routinely exposure to formaldehyde would be more influential to the

PLEA 2018 HONG KONG

Smart and Healthy within the 2-degree Limit

occupants' chemical intolerance than by the intermittent but high exposures.

In contrast, significant differences cannot be seen in the TVOC results (Fig. 9). However, basically, the higher TVOC level is the higher the MCS scores would be, except for the maximum values in Kampongs.

3.5 Results of spirometer test

The FEV1% values were calculated based on the measured force expiration volume over a second (FEV1) compared with Indonesian standard values proposed in [5]. The above standard values are determined depending on the respondent's age and gender [5]. The FEV1%, which assesses the respondent's FEV1 levels compared with the required standard values in percentage, is an important measure of pulmonary function. As shown in Fig. 10, more than 55% of the respondents in Kampongs are considered less than normal respiratory conditions, while more than 85% in the apartments are considered the same. A significant difference was not found in mean values between the two groups ($p=0.108$), but overall, the respondents in the apartments show further worse conditions than Kampongs. Further analysis is needed to identify the factors causing these worse respiratory conditions in both groups.

4. CONCLUSIONS

This research is probably the first attempt to assess the IAQ conditions and their effects on health in urban houses of Indonesia. The key findings from the case study of Surabaya are as follows:

(1) There was a significant difference in mean values of MCS risk between Kampongs and the newly constructed apartments. Around 50% of the respondents in the apartments showed some degrees of chemical sensitivity risk, indicating possible spread of sick building syndrome.

(2) On the other hand, significant differences were not found in the results of TVOC measurement as well as spirometer tests between Kampongs and apartments. This implies that there are other IAQ problems even in Kampongs, which cannot be measured by the degree of chemical intolerance.

(3) Although most of the factors affecting MCS risk were similar among the problematic respondents of both two groups, there were a few different factors on the other hand. The chemical intolerance to new furnishings, symptoms on muscles, masking factors of cooking gas and passive smoking were higher in Kampongs, whereas the masking factor of scented products was higher in the apartments instead.

(4) Various kinds of personal and building attributes were found to affect MCS risk scores, but the influential factors were quite different between Kampongs and apartments, except for the degree of stress. For example, in Kampongs, the increases in age and household income increased MCS risk scores.

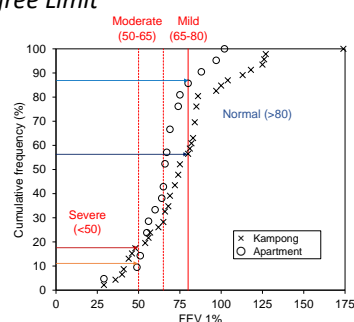


Figure 10: Cumulative frequency of FEV1%.

Moreover, those who have a history of allergic diseases tended to record higher MCS risk. In contrast, in the apartments, the female respondents tended to obtain higher MCS risk. In Kampongs, more factors are associated with personal and building attributes than the apartments.

(5) The average maximum values of formaldehyde were 0.081 ppm in Kampongs and 0.115 ppm in the apartments, which are higher than the WHO standard, 0.08 ppm. It was found that the background formaldehyde levels were apparently higher in the apartments than Kampongs, but there were some exceptional cases even in Kampongs in which the formaldehyde levels were intermittently very high. On the other hand, the measured TVOC levels were not so different between the two groups, ranging very widely up to 22 mg/m³ in maximum value.

(6) The respondents living in rooms with higher mean formaldehyde values tended to have higher MCS risk scores. It was suggested that the long-term routinely exposure to formaldehyde would be more influential to the occupants' chemical intolerance, which was particularly seen in the apartments, than by the intermittent but high exposures.

ACKNOWLEDGEMENTS

This research was supported by a grant from Panasonic Corporation and KAKENHI (JP15KK0210). We also would like to thank Dr. I Gusti Ngurah Antaryama and Dr. Sri Nastiti of Institut Teknologi 10 Nopember Surabaya (ITS) and the students who kindly supported our survey.

REFERENCES

1. Tham, K.W., (2016). Indoor air quality and its effects on humans-A review of challenges and developments in the last 30 years. *Energy and Buildings*, 130: p. 637-650.
2. Joshi, SM., (2008). The sick building syndrome. *Indian J. of Occupational and Environmental Medicine*, 12: pp. 61-64.
3. Miller, C.S., Prihoda, T.J., (1999). The environmental exposure and sensitivity Inventory (EESI): a standardized approach for measuring chemical intolerances for research and clinical applications. *Toxicology and Industrial Health* 15: pp. 370-385.
4. Heo, Y., Kim, S.H., Lee, S.K., Kim, H.A., (2017). Factors contributing to the self-reported prevalence of multiple chemical sensitivity in public facility workers and the general population of Korea. *J. of UOEH*, 39(4): pp. 249-258.

PLEA 2018 HONG KONG

Smart and Healthy within the 2-degree Limit

5. Alsagaff, H., Mangunegoro, H., (1993). Nilai normal faal paru orang Indonesia pada usia sekolah dan pekerja dewasa berdasarkan rekomendasi. *American Thoracic Society (ATS) 1987*. Surabaya: Airlangga University Press. pp. 26-122.

Study on the Thermal Performance of Office Spaces in the Tropics: A case study in Singapore

STEVE KARDINAL JUSUF¹, MASAYUKI ICHINOSE², YUTA FUKAWA², SATTAYAKORN SUTIDA³

¹Engineering Cluster, Singapore Institute of Technology, Singapore

²Department of Architecture and Building Engineering, Tokyo Metropolitan University, Tokyo, Japan

³Faculty of Architecture, Kasetsart University, Bangkok, Thailand

ABSTRACT: Commercial and office buildings often have problems on the aspects of indoor thermal environment and energy performances. The actual performance of these types of buildings, most of the time, are different from the desired performance. A data collection was conducted in an office space of a university building in Singapore as part of the ongoing study, measuring the environmental performance of office buildings across Southeast Asian countries. The objective measurement on the thermal condition shows that most measurement points across office space is at the colder side of the comfort zone. This finding is supported by the survey results where only about 65% of occupants voted for "slightly cool", "neutral" and "slightly warm" and about 22% of occupants showed "cold" related symptoms on their legs, hands and body at the end of working hours. The calculated neutral temperature range was generally from 24°C to 26°C, while the measured room temperature was mostly below 24°C.

KEYWORDS: Thermal performance, office space, Tropics, Singapore

1. INTRODUCTION

Southeast Asian cities are undergoing rapid development due to the population growth and economic development. Commercial and office buildings often have problems on the aspects of indoor thermal environment and energy performances. The actual performance of these types of buildings, most of the time, are different from the desired performance. The possible causes can be described as the followings; excessive capacity or inappropriate operation of mechanical system, less internal heat generation, and so on. Overall, this research aims to construct detailed database of indoor climate and energy consumption at large-scale buildings in the tropics of Asia.

This paper presents a small part of the ongoing study, measuring the environmental performance of office buildings across Southeast Asian countries. A data collection was conducted in the office of a university building in Singapore.

Located between latitudes 1°09'N and 1°29'N and longitudes 103°36'E and 104°25'E, Singapore can be classified as having hot humid climate. Uniform high temperatures, humidity and rainfall throughout the year characterize the climate. The diurnal temperature variations are small with the range for minimum and maximum temperatures of

23°C to 26°C and 31°C to 34°C respectively. The mean annual temperature was 27.4°C between the periods of 1982 to 2001⁴. The relative humidity is generally high and although it invariably exceeds 90 percent in the early hours of the morning just before sunrise; it frequently falls to 60 percent during the afternoons when there is no rain. During prolonged heavy rains, the relative humidity often reaches 100 percent. Between the periods of 1982 to 2001, the mean annual relative humidity was 83.5 percent. Due to the tropics climate condition, buildings are found to be uncomfortably hot and humid at certain times. Higher velocity of wind flow over the human body is required to increase the efficiency of sweat evaporation. Due to these climate characteristics, to achieve thermal comfort in buildings, HVAC system uses about 60% of total building energy use [1].

Based on several literatures [2, 3], some important definitions regarding thermal comfort are:

Thermal comfort: condition of mind, which expresses satisfaction with the thermal environment.

Acceptable thermal environment: an environment, which at least 80% of the occupants would find thermally acceptable.

⁴ Based on metrological data on 1982-2001, National Environmental Agency, Singapore.

PLEA 2018 HONG KONG

Smart and Healthy within the 2-degree Limit

Thermal sensation: a conscious feeling commonly graded into the categories of cold, cool, slightly cool, neutral, slightly warm, warm, and hot.

There are four factors that contributes to the occupants' TC perception, i.e. physiology, psychology, climatology and design factors [4]. Physiology and psychology are the two human factors, which interact dynamically in responding toward environment perception through the thermal sensation. Climatology covers wide range of natural setting of climate, which cannot be controlled or modified by human. But on the other hand, Climate can influence the planning of towns, buildings, and settlement designs, and can evoke strategies to promote the efficiency of thermal comfort for both outdoors and indoors [5].

2. METHODOLOGY

To measure and evaluate the actual performance of the building, there are five parameters that were measured are as follows: outdoor climate, indoor climate, energy consumption of the building, occupants' sensation and building management. For parameters 1-3, continuous measurement was conducted. Meanwhile, occupants' survey through questionnaire was conducted to measure occupants' sensation. By collecting and analyzing these data, it is possible to evaluate comprehensive actual building performance.

Table 12: Measurement schedule

Date	Measurement		No of Survey Respondents
29 Oct 2017	Installation		
30 Oct 2017	Installation		
31 Oct 2017	Automatic measurement	Manual measurement	26 (Male: 6, Female: 26)
1 Nov 2017	Automatic measurement & Removal	Manual measurement & Removal	24 (Male: 7, Female: 17)

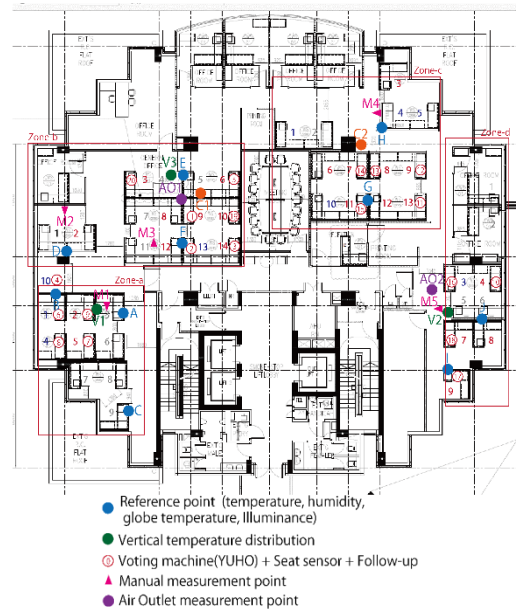


Figure 75: Measurement points layout plan

In this study, a typical fully air-conditioned office space was chosen for the evaluation and the measurement was conducted on 30 October – 1 November 2017, see Table 12. The number of occupants participated in the survey is 26 and 24 occupants on 31 October and 1 November 2017 respectively.

To understand thermal environment of this office space, sensors were installed at 15 points across the space as shown in Figure 75. The corresponding locations of air-conditioning diffusers and luminaires can be seen in Figure 76. Questionnaire survey was conducted at four different timings: short after the occupants reached office at around 9am, at 11 am, at 3pm and when the occupants were about to leave office, at around 6pm.

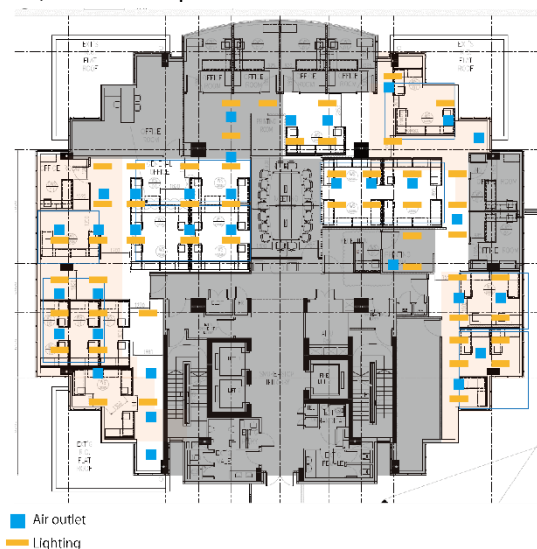


Figure 76. Layout of air-conditioning diffusers and luminaires

Points B, C, D, H, I and J are located at the perimeter zone, i.e. an area within 5 meters distance from the

PLEA 2018 HONG KONG

Smart and Healthy within the 2-degree Limit

building perimeter. Meanwhile, points A, E, F and G are located at interior zone. The measurement devices used in the study include T&D TR-74, TR-52+Globe ball to measure air temperature, globe temperature, relative humidity and illuminance; T&D MCR4+ thermocouple to measure vertical temperature distribution; and TR-76Ui to measure air temperature, relative humidity and CO₂ concentration.

The electricity power consumptions of artificial lighting and power outlets were measured at the corresponding distribution panel, while the air-conditioning power consumption was measured at the distribution panel in the corresponding level's AHU room (air-side). HIOKI clamp power loggers PW3360 on sensor 9661 and 9669 were used in the measurement.

3. RESULTS AND DISCUSSION

During the measurement period of 31 October – 1 November 2017, the weather conditions were mainly cloudy, especially on 31 October when the peak solar radiation reached only at less than 300W/m². The air temperature ranges from low of 25.8°C to high of 29.5°C, while the absolute humidity ranges from 19.8g/m³ to 22.7g/m³.

The indoor air temperature and operative temperature distributions at different locations during working hours (08:00 – 18:00 hours) are shown in Figure 78 and Figure 79 respectively. The temperature ranges between 22°C and 25°C. The median of room temperature at point A, C, D, G and H was around 24°C. The highest temperature distributions is at point B, with median value of 24.5°C, which was under the influence of radiant heat from the building envelope, i.e. northwesterly orientation. In the interior zone, the median of temperature was around 23.5°C at point E and F.

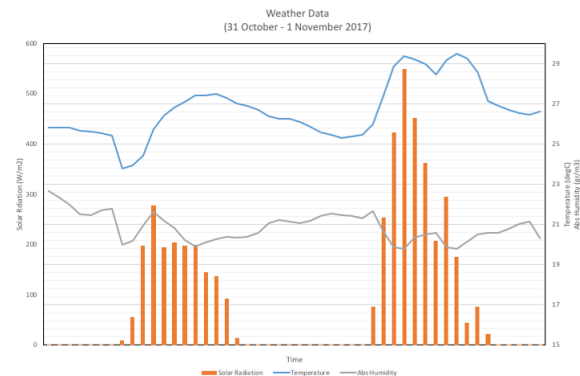


Figure 77. Weather condition on 31 October – 1 November 2017

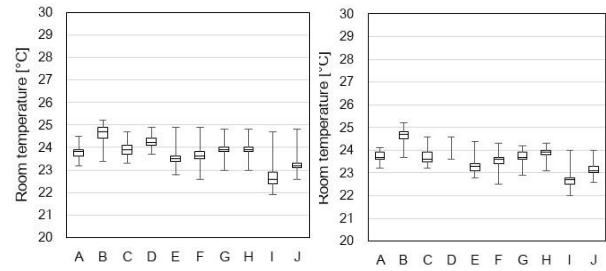


Figure 78: Frequency distribution of room air temperature on 31 October (Left) and 1 November 2017 (Right)

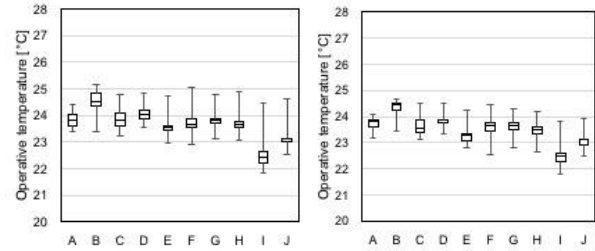


Figure 79: Frequency distribution of operative temperature on 31 October (Left) and 1 November 2017 (Right)

Figure 80 shows the operative temperature and absolute humidity on psychrometric chart and comfort zone based on ASHRAE standard 55-2013 for winter and summer. As Singapore is a hot humid tropical climate, the indoor condition should fall within the comfort zone for summer condition. The figure shows that most points is at the colder side of the comfort zone, while only Point B that falls within the comfort zone most of the time.

During the survey, the occupants' office outfit were ranging from long sleeve and long pants for male occupants to blouse and skirts and jacket for female occupants. The average clothing insulation is 0.5 clo, with metabolic rate of 1.2 met for office work activity. Comparing the results from the objective measurement with subjective measurement, i.e. thermal sensation vote, the number of occupants who voted for "slightly cool", "neutral" and "slightly warm" constitutes approximately 73%, 63% and 65% of the total votes on 31 October, 1 November 2017 and both days respectively (Figure 81). "Slightly cool", "neutral" and "slightly warm" votes are considered as thermally acceptable. The remaining occupants said to have colder thermal sensation which falls within the range from "very cold" to "cool". By correlating their survey responses, profile and seating positions, they feel colder because of sitting directly under the diffuser as well as the age of the occupants. Older female occupants tend to feel colder.

PLEA 2018 HONG KONG

Smart and Healthy within the 2-degree Limit

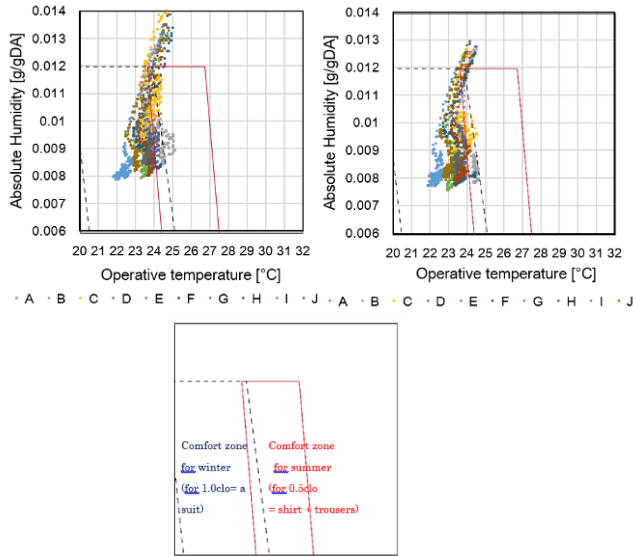


Figure 80: Psychrometric chart on 31 October (Above left), 1 November 2017 (Above right) and comfort zone legend based on ASHRAE Standard 55-2013 [1]

Despite that, the thermal acceptance votes (Figure 82) show that almost all of the occupants accept the temperature conditions.

When the occupants were asked whether they would like to change the temperature condition, about 40-50% of occupants prefer “no change”, while about both 20% of occupants prefer to be “warmer” and “cooler” (Figure 83). The remaining 10% of occupants did not state their preferences.

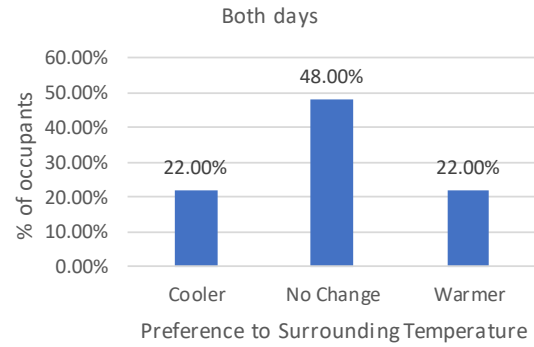


Figure 83: Occupants' preference vote on both days 31 October and 1 November 2017

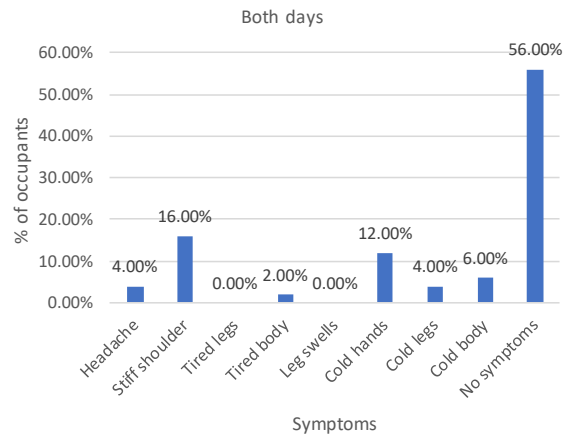


Figure 84: Symptoms at the end of working hours on both days 31 October and 1 November 2017

The occupants were also asked their symptoms after the working hours, as shown in Figure 84. The symptoms related to the coldness of the environment are “cold hands”, “cold legs” and “cold body”. If these symptoms are combined, the percentage of occupants felt cold in their body are 22% both days respectively. Despite that, more than 80% of them answered that the thermal environment was “acceptable” to them. This is apparent that though the occupants feel cold, they were still able to tolerate it, which leads to acceptance. Similarly, a little discomfort does not warrant an “unacceptable” rating from the occupants. The result highlights that the occupants have adapted to the cold thermal condition in their workspace.

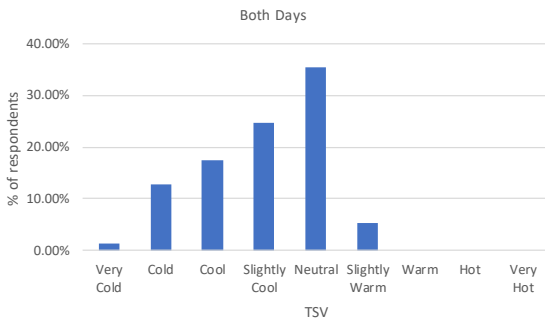


Figure 81: Thermal sensation vote on both days 31 October and 1 November 2017

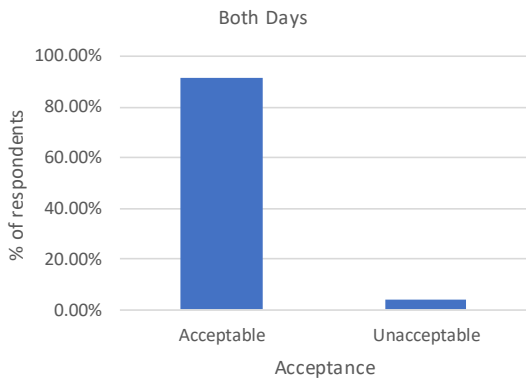


Figure 82: Thermal acceptance vote on both days 31 October and 1 November 2017

Figure 85 shows the distribution of neutral room temperature calculated by Griffith's method on 31 October, 1 November and combined both days. Interquartile ranges of neutral temperature were generally from 24°C to 26°C. Comparing with the room temperature measurement shown in Figure 78, where most of room temperature were below 24°C, this result indicated that it is necessary to change room temperature higher in order to make occupants' thermal sensation neutral state.

PLEA 2018 HONG KONG

Smart and Healthy within the 2-degree Limit

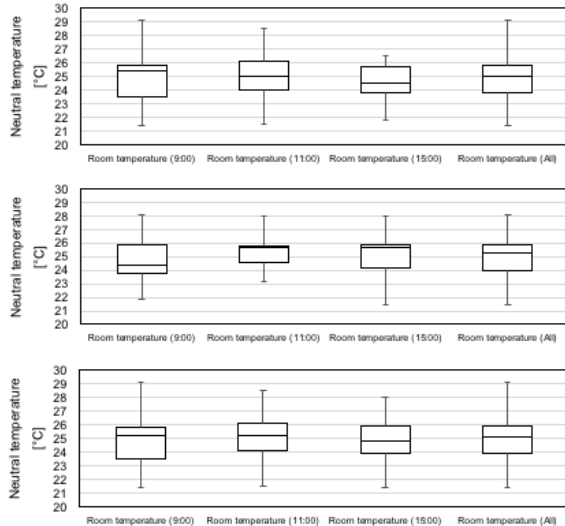


Figure 85. Box plot of neutral room temperature on 31 October (Above), 1 November 2017 (Centre) and both days (Below)

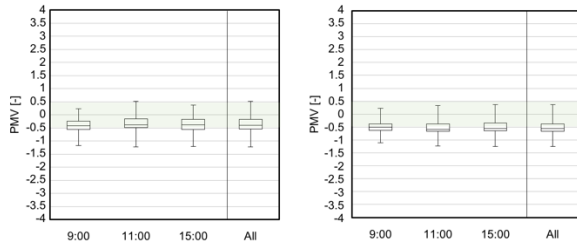


Figure 86. Box plot of PMV on 31 October and 1 November 2017

Figure 86 shows frequency distribution of PMV at 31st October and 1st November. PMV was calculated using air temperature, mean radiant temperature, wind velocity, relative humidity, clothing insulation and estimated value of metabolic rate (1.1 met). Overall, median of PMV was from -0.2 to -0.7. Thus, indoor thermal environment was not within the comfort zone based on ISO7730 in some cases. Meanwhile, Figure 87 shows frequency distribution of gaps between TSV and PMV on 31 October and 1 November 2017. Overall, median of these gaps was around 0.25. Thus, it confirms the subjective responses from the occupants that they felt cold.

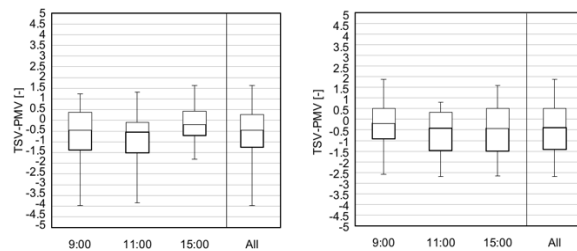


Figure 87. Box plot of gaps between TSV and PMV on 31 October and 1 November 2017

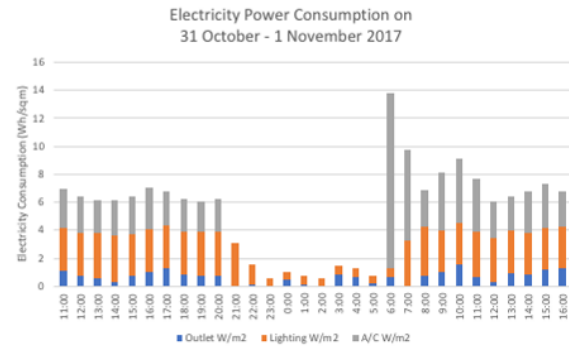


Figure 88. Electricity power consumption on 31 October and 1 November 2017

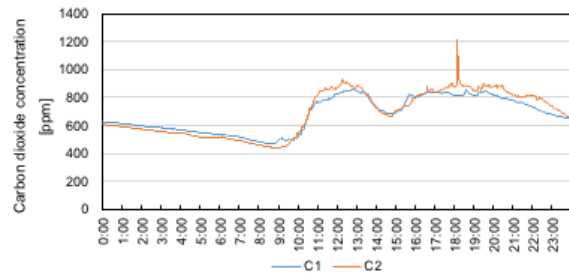
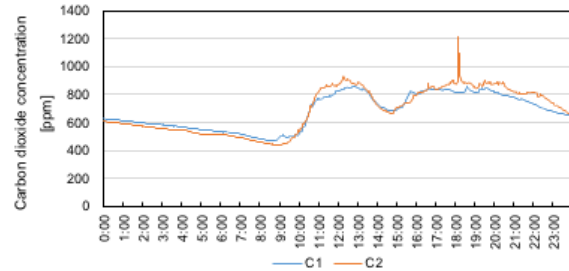


Figure 89. CO₂ concentration on 31 October (Above) and 1 November 2017 (Below)

The measured electricity power consumption from 31 October 2017 at 11am to 1 November 2017 at 4PM is shown in Figure 88. The graph shows that total power consumption started going down at late morning around 11am before it went up again after lunch time at 1-2pm. It also shows that AHU was turned off after 8pm and turned on at 6am, 2.5 hours before the official working hours started at 8.30am. It is observed that the air-conditioning power consumption is slightly lower than the lighting power consumption on 31 October 2017. Most probably, it is because the weather condition was much cooler and cloudy. Hence, it used less energy to cool down the office space. Figure 89 shows carbon dioxide (CO₂) concentration around point E and H on 31 October and 1 November 2017. The CO₂ concentration was less than 1000ppm. Acceptance criteria concentration is generally at 1000ppm. Thus, there is no issue on high CO₂ concentration for occupants' health during the working time.

4. CONCLUSION

This paper presents measurement results conducted in an office building of a university building in

PLEA 2018 HONG KONG

Smart and Healthy within the 2-degree Limit

Singapore. This study is one of the measurements done in office buildings across southeast Asian countries to measure its environmental performance. The objective measurement on the thermal condition shows that most measurement points across office space is at the colder side of the comfort zone. This finding is supported by the survey results where only about 65% of occupants voted for "slightly cool", "neutral" and "slightly warm" and about 22% of occupants showed "cold" related symptoms on their legs, hands and body at the end of working hours. Despite that more than 90% of occupants accepted the thermal condition and only 20% of them would like to have the space to be warmer. These findings show that the occupants have adapted to the cold temperature condition in their office space. The calculated neutral temperature range was generally from 24°C to 26°C, while the measured room temperature was mostly below 24°C. Therefore, it is recommended that the air temperature can be increased by 1°C in order to improve occupants' comfort and reduce the amount of air-conditioning energy consumption.

ACKNOWLEDGEMENTS

This research is supported by research fund of Tokyo Metropolitan Government; the title is "Platform for promoting economic exchange". The representative researcher is Masayuki Ichinose, Tokyo Metropolitan University.

REFERENCES

1. Chua, K.J., Chou, S.K., Yang, W.M. and Yan, J. (2013). Achieving better energy-efficient air conditioning – a review of technologies and strategies. *Applied Energy*, 104, 87-104.
2. American Society of Heating, Refrigerating and Air-Conditioning Engineers. (1992). ASHRAE - Standard 55, Thermal Environment Conditions for Human Occupancy. Atlanta, GA: American Society of Heating, Refrigerating and Air-Conditioning Engineers.
3. International Organization for Standardization. (2005). ISO 7730: Ergonomics of the Thermal Environment - Analytical Determination and Interpretation of Thermal Comfort using calculation of the PMV and PPD indices and Local Thermal Comfort Criteria. Geneva, Switzerland: International Standard Organization.
4. Feriadi, H. (2003). Thermal Comfort for Naturally Ventilated Residential Building in Tropical Climate. PhD-Thesis. National University of Singapore, Singapore.
5. Thompson, R.D., & Perry, A. (1997). *Applied Climatology*. London, United Kingdom: Routledge.

Estimating Impact of Green-Blue Infrastructure on Air Temperature Using Remote Sensing: Case study of Sabarmati Riverfront, Ahmedabad, India

PARTH BANSAL¹

¹Graduate School of Environmental Studies, Seoul National University, Seoul, Korea

ABSTRACT: With the availability of high quality remote sensing data, the phenomena of urban heat island has been well documented over the past two decades. Various mitigation measures, including changes to urban form, construction material, etc. have been suggested; however, these factors tend to be static and have a long gestation period. Water and forest body have higher specific heat compared to urban built up and thus have a lower surface temperature during the afternoon, when the temperature generally peaks. Many indigenous civilizations have used this 'cooling effect', but the effectiveness of water and forest bodies on cooling is poorly understood. This study uses remote sensing data, specifically, thermal imagery from Landsat 7 and 8 satellites to calculate the quantity and range of cooling due to the combined presence of water body and green strip along the water's shore. The study finds that in the studied area, the cooling effect ranges from 1.1 to 3.9° C but with a maximum effective range of 360 meters under the favourable wind conditions. The short range of cooling effect raises questions if green-blue infrastructure can be an effective way to combat UHI in the dense urban area where land is scarce and expensive.

KEYWORDS: Urban Heat Island, Green Blue Infrastructure, Sabarmati Riverfront

1. INTRODUCTION

Increase in paved surface and reflective material in dense urban areas has been documented to causes hikes in ambient temperature as compared to rural surroundings. The annual mean air temperature of a city with one million or more people can be 1.8 to 5.4°F warmer than its surroundings [1]. Even smaller cities and towns will produce heat islands, though the effect often decreases as city size decreases [2].

This increase in temperature not only increases energy requirements of the buildings, but also increases human discomfort in climate uncontrolled areas. Priyadarsini, 2011 [3] Arifwido and Chandrasiri, 2015 [4] have documented an increase in cooling requirement of building due to urban heat island (UHI) in different geographical settings and building uses. Green-Blue infrastructure has been used by indigenous civilization and its impact on reducing the UHI effect has been studied by many scholars [5]. However, there is a lack of simpler methodology which can be deployed by urban designers and planners using which impact of such green-blue infrastructure can be estimated. If a regression equation estimated using past projects in a given homogenous region can estimate impact based upon size, intensity and other parameters of the project, better intangible benefit calculations will be possible.

2. STUDY AREA

Located in the city of Ahmedabad, in the western part of India, Sabarmati was a seasonal river which

remained dry for the most part of the year and its shores were encroached upon by slums. Construction of project started in 2005 and since 2012 parts of the riverfront have been opened at regular interval. The area has a semi-arid climatic condition with maximum temperature exceeding 40°C in summer. Dominant wind flow is from west to east, 9° towards north, from March to July.

Figure 1 shows the typical condition of the river and surrounding encroachment around the banks in May 2003. Figure 2 shows the condition of the river in May 2017. The grid represents the pixel size and the location of the satellite imagery used. Figure 3 shows the typical dimension of the green-blue features of the project. The variety of shape, composition and 'before-after' comparison provides an opportunity to investigate how these parameters impact UHI.



Figure 90: River and surrounding area in May, 2003

PLEA 2018 HONG KONG

Smart and Healthy within the 2-degree Limit

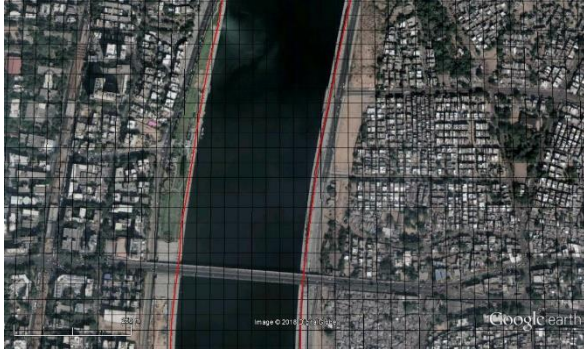


Figure 2: River and surrounding area in May, 2017

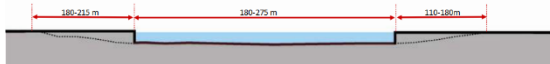


Figure 3: Typical dimension of Green-Blue Body.

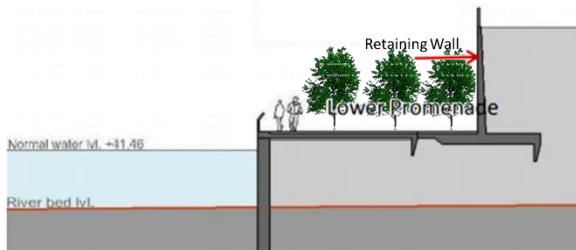


Figure 4: Typical interaction of blue-green-urban form [6]

The green feature along the shores varies from 180 - 215 m on the western side and 110 - 180 m on the eastern side. River body is narrower towards north (180 m) and reaches a maximum width of 275 m towards the southern end. Additionally, the water diversion raised the average water level by 3.84 m and 3 to 5 meter retaining wall forms barrier between green space and urban built-up as shown in figure 4 [6].

3. METHODOLOGY

Hung et. al, 2006 [7] in their empirical verification of reliability of thermal imagery have found it to be the accurate indicator of UHI if pre-processing for stray light correction is done. Thus, this research uses thermal band from Landsat 7 and 8 imageries which record the surface temperature at the interval of 8 days at 10 AM and 10:11 AM (± 15 minutes) respectively. The Landsat program consists of a series of satellite collecting imagery from 1970s and is administered by the United States Geological Survey. Each imagery set consists of a number of images showing individual band which records surface reflectance in the specified spectral range. For details on spatial, temporal and spectral resolutions of Landsat program, see [8].

Manteghi et. al, 2015 [9] in the meta analysis found that while the multiple studies confirmed the cooling effect of water bodies, the empirical relationship between the water body and degree of cooling is not clear. On the other hand, Nastran et. al (2018) [10]

have found degree of cooling from green area to depend upon landscape features, but a clear empirical relationship has not emerged. This study thus uses the geometry of green-blue body and distance as key independent variables and tries to isolate their pure effect on ambient temperature using multiple regression.

3.1 Data Processing

Landsat 7 ETM+ (Band 6) for Feb 01/2002 and May 15/2003 and Landsat 8 TIRS (Band 10) for May 18/2017, were acquired from USGS data portal. Note that for Landsat 8, band 10 was used instead of band 11 despite closer correspondence with Landsat 7's Band 6 due to higher error rate caused due to stray light in band 11 [11]. All the sets of imagery were processed through Fast Line-of-Sight Atmospheric Analysis of Hypercubes (FLAASH) module in ENVI 5.3 to account for stray light and other atmospheric corrections. For detailed accuracy assessment of FLAASH and comparison with other modules see Nazeer et. al, 2014 [12] which found the FLAASH to be most suitable model when the site was heterogeneous; with surface reflectance recorded by in-situ instrument and after correction Landsat imagery differing by 0 to 10%.

Surface temperature data were derived by converting DN to At-Satellite Temperature using equation (1) in ENVI 5.3. Environment for Visualizing Images (ENVI) is a geospatial imagery processing software provided by Harris Geospatial Solutions.

$$T_{AS} = K_2 / \ln (K_1/L_1 + 1) \quad (1)$$

Where:

T_{AS} = at-satellite brightness temperature in degrees Kelvin

K_2 = Band-specific thermal conversion constant from the metadata

K_1 = Band-specific thermal conversion constant from the metadata

L_1 = product of the Radiance formula

The surface temperatures were then converted to air temperature using equation (2) developed by Malaret et al. 1995 [13]. Note that the conversion tends to produce an error, however with pre-processing prescribed by Kawashima et. al, 2000 [14], standard error tends to limited between 1.4 - 1.5° K.

$$T_s = 219.972 + 0.5259 * T_{AS} \quad (2)$$

Where:

T_s = Air Temperature at 1.5 meter from satellite datum level.

3.2 Data Analysis

1.4° C was added to the 2003 data to account for the difference in weather condition reported by local meteorological station. Then, to establish that

PLEA 2018 HONG KONG

Smart and Healthy within the 2-degree Limit

difference in temperature pre and post project was statistically significant, paired two-sample t-test was performed. 2610 pixels, from the rough centreline of the river to 700 M on both sides were randomly selected for this test.

Once the difference in temperature was found to be statistically significant, using ArcMap 10.2, buffers from 0 to 700 m at the interval of 30 m were created; parallel to the river centreline, on both sides. 5 perpendicular lines were drawn at 300 meter interval, labelled as site A to E on the eastern side and site F to J on the western side of river and temperature were noted. Note that the temperature observations were average of 900 m² area since the spatial resolution of Landsat 7 and 8 imagery is 30 by 30 m.

4. RESULTS

The results of paired two-sample t-test are shown in table 1, based upon:

$$H_0: \mu_{2003} = \mu_{2017} \text{ And } H_A = \mu_{2003} > \mu_{2017}$$

Table 13: T-Test - Paired Two Sample for Means

	Temp_2017	Temp_2003
Mean	26.240	27.480
Variance	0.517	0.714
Observations	2613	2613
Pearson Correlation	0.856	
Hypothesized Mean	0	
df	2612	
t Stat	-145.155	
P(T<=t) one-tail	0	
t Critical one-tail	1.645	
P(T<=t) two-tail	0	
t Critical two-tail	1.960	

Since P value is less than 0.01, it is concluded that the mean air temperature was higher in 2003 as compared to 2017 (after taking into account prevailing weather condition). Note that the difference in mean in this table should not be considered as the expected impact of the green-blue project as it includes pixels from beyond the cooling range calculated in following sections.

The variation in air temperature at 5 sites along the eastern and western shore has been shown in figure 5 and 6 respectively. As specified before, the dominant wind flow direction during the measurement period is from west to east, i.e. figure 5 and 6 shows a typical condition in windward and leeward scenarios respectively. Note that the specified air temperatures are for the height of 1.1 to 1.7 meters from surface. This inconsistency arises due to the terrain and the curvature of the earth and the fixed datum level of the satellite. While it would be possible to homogenize the height using high resolution elevation model, this

study has assumed air temperature to be static with respect to distance from the ground.

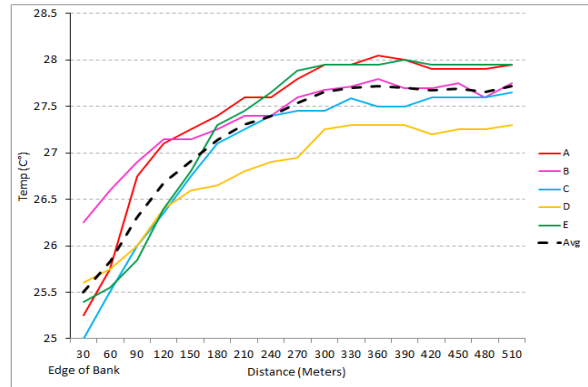


Figure 5: Air Temperature w.r.t distance from river bank on eastern (windward) side.

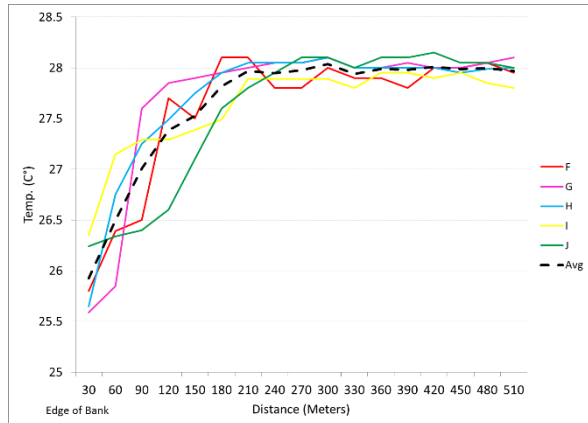


Figure 6: Air Temperature w.r.t distance from river bank on western (leeward) side.

To verify that this variation in temperature was in fact due to the installation of Green-Blue infrastructure, it was necessary that temperatures before the project construction are obtained. Feb 01, 2002 was chosen as a suitable date for collecting baseline temperature due to similar weather service reported temperature ($\pm 0.2^\circ$ C). The 'cooled temperature' is defined as average temperature from the shore till effective range and the range is defined as distance after which the variation is less than 1° C for the next 500 meters. The results of the comparison are shown in Table 2 and 3 for eastern and western sides respectively.

Table 14: Degree and range of cooling effect on eastern (windward) side

Site	Cooled Temp (°C)	Baseline Temp (°C)	Degree of Cooling effect (°C)	Range of Cooling Effect (M)
A	26.94	30.84	3.9	360
B	27.07	29.77	2.7	330
C	26.53	27.63	1.1	300
D	26.40	28.7	2.3	270
E	26.69	28.89	2.2	270

PLEA 2018 HONG KONG

Smart and Healthy within the 2-degree Limit

Table 3: Degree and range of cooling effect on western (leeward) side

Site	Cooled Temp (°C)	Baseline Temp (°C)	Degree of Cooling effect (°C)	Range of Cooling Effect (M)
F	27.60	29.9	2.3	210
G	27.71	30.11	2.4	270
H	27.70	29.4	1.7	300
I	26.63	28.03	1.4	210
J	27.56	29.66	2.1	270

Using SAS 9.3, level-log multivariate regression analysis was conducted so as to derive equations which can form a rule of thumb when estimating the degree of impact of green-blue infrastructure. Level-log regression was used over linear regression due to nature of the curve (decreasing slope along x axis) and consistent higher values of coefficient of determination. For depended variable Y and independent variable X, level-log regression coefficient (β_1) is interpreted as; increase in X by 1% increase Y by $\beta_1/100$ units of Y.

For Degree of Cooling:

$$Y_1 = 0.212 + 0.527\ln(X_1) + 0.025\ln(X_2) - 0.227\ln(X_3) + 0.462*Z \quad (3)$$

$$R^2 = 0.76$$

$$P = 0.013$$

± 1.09°C at 95% Prediction Interval

For Range of Cooling

$$Y_2 = 154.7 + 7.3\ln(X_1) + 1.3\ln(X_2) + 54.25*Z \quad (4)$$

$$R^2 = 0.69$$

$$P = 0.009$$

± 37.42 meter at 95% Prediction Interval

Where,

Y_1 : Degree of cooling (°C)

Y_2 : Range of cooling (M)

X_1 : Width of stream (M)

X_2 : Width of green area (M)

X_3 : Distance from bank (M)

Z= Dummy variable for wind profile (0 for leeward, 1 for windward)

5. DISCUSSION

Table 1 shows that for an area about the size of 2 km², air temperature reduction was observed when green-blue infrastructure was introduced into the urban fabric. Additionally, Figure 5 and 6 further strengthen the hypothesis that green-blue infrastructure has a significant impact in reducing air temperature and can be a viable tool for reducing UHI effect.

However, it is observed that the impact is dependent on the wind flow regime with significantly less cooling on the leeward side. In the case of windward side

(eastern shore in this case), air temperature was reduced by 1.1° C to 3.9° C with an average maximum range of 306 meters. On the leeward side, the reduction ranged between 1.7° C to 2.4° C with an average maximum range of 252 meters. Keeping the width of blue-green area constant, this translates into leeward sides, at the same distance from shore having an average of 0.46° C higher temperature. Additionally, the reduction in cooling range by 54 meters means that the reduced benefits are more spatially limited. A comparison of figure 5 and 6 also points out that on the leeward side, reduction in air temperature is concentrated around the shores and the temperature rises far more steeply as compared to the windward site.

While the observed reduction in temperature is significant, in the sense of their impact on outdoor human comfort and energy consumption by buildings, the impact extends, on average, only 306 and 252 meters for windward and leeward side respectively. This raises the question if the green-blue infrastructures, specifically linear ones, are economically feasible and land-use compatible for most cities as UHI control measures. None the less, equation (3) and (4) are handy expressions when trying to reduce the UHI effect at district level, especially in city centers where high concentration of paved surface and glass reflectance has been known to cause severe UHI and more benefits from limited range can be derived due to higher density of population and floor space. With planning stage design parameters, effective range and expected reduction in temperature can be calculated and design can be modified so as the results meet the expected outcomes. Since the results show that the effective reduction in temperatures varies with range, there is also scope for by-law modification in hotter climatic regions to promote more natural ventilation friendly buildings in the vicinity of green-blue infrastructure while mandating airtight structures in zones beyond effective range.

6. LIMITATIONS AND CONCLUSION

The research is a foundation for being able to numerically calculate the impact of various suggestive remedies of UHI. The paper considers both green-blue infrastructures combined and links expected range and temperature reduction, but failed to incorporate design aspects such as the difference in the elevation of water body, green field and built form, as in this case, shown in figure 4. Urban form is another important measure missing, with a growing literature suggesting that aggregated building forms at block/neighborhood level can have a significant impact on area's microclimate. This is reflected in unexplained variances, indicating the absence of the other independent variable.

PLEA 2018 HONG KONG

Smart and Healthy within the 2-degree Limit

Stewart and Oke, 2012 [15] have developed a simplified but comprehensive classification of urban form for the measurement of microclimate. As more research is done in future to populate each class with microclimate data, inclusion of urban form in these UHI studies will be possible. Additionally, it is very important to recognize that the regression coefficients have been calculated for single weather condition and geophysical region. This would mean that the equation would need calibration for application in other areas which could be difficult if no similar intervention have been made in past two decades.

None the less, the method enables planners and community on deciding effectiveness and cost vs. benefits when deliberating upon investing in such infrastructures.

REFERENCES

Oke, T.R. 1997. Urban Climates and Global Environmental Change. In: Thompson, R.D. and A. Perry (eds.) Applied Climatology: Principles & Practices. New York, NY: Routledge. pp. 273-287.

Oke, T.R. 1982. The Energetic Basis of the Urban Heat Island. Quarterly Journal of the Royal Meteorological Society. 108:1-24. <https://doi.org/10.1002/qj.49710845502>

Priyadarsini, R. 2011 Urban Heat Island and its Impact on Building Energy Consumption. Advances in Building Energy Research, pp. 3-1 261-270 <https://doi.org/10.3763/aber.2009.0310>

Arifwidodo S., and Chandrasiri O., 2015, Urban Heat Island and Household Energy Consumption in Bangkok Thailand, Energy Procedia, 79, pp. 189-194 <https://doi.org/10.1016/j.egypro.2015.11.461>

Gunawardena, K., Wells, M. and Kershaw, T. 2017. Utilising green and bluespace to mitigate urban heat island intensity. Science of The Total Environment, 584-585, pp.1040-1055. <https://doi.org/10.1016/j.scitotenv.2017.01.158>

Sabarmati Riverfront Development Project: A Multidimensional Environmental Improvement and Urban Rejuvenation Project, 2016, Project Report by KPMG.

Hung, T., Uchihama, D., Ochi, S., 2006. Assessment of satellite data of the urban heat island effect in Asian mega city, International Journal of Applied Earth Observation and Geoinformation 8-1, pp 34-48 https://www.usgs.gov/faqs/what-are-band-designations-landsat-satellites-0?qt-news_science_products=7#qt-news_science_products

Manteghi, G., Remz, D., 2015. Water Bodies an Urban Microclimate: A Review, Modern Applied Science, 9-6, <http://dx.doi.org/10.5539/mas.v9n6p1>

Nastran, M., Kobal, M., Eler, K., 2018. Urban heat islands in relation to green land use in European cities, Urban Forestry & Urban Greening <https://doi.org/10.1016/j.ufug.2018.01.008>

How are the Thermal Infrared Sensor (TIRS) thermal bands aboard Landsat 8 used. <https://landsat.usgs.gov/how-are-thermal-infrared-sensor-tirs-thermal-bands-aboard-landsat-8-used>

Majid Nazeer, Janet E. Nichol & Ying-Kit Yung (2014): Evaluation of atmospheric correction models and Landsat

surface reflectance product in an urban coastal environment, International Journal of Remote Sensing, <https://doi.org/10.1080/01431161.2014.951742>

Malaret, E., Bartolucci, L.A., Lozano-García, D., Anuta, P.E. & McGillem, C.D.. 1985. Landsat-4 and Landsat-5 Thematic Mapper data quality analysis.. Photogrammetric Engineering & Remote Sensing. 51, pp. 1407-141.

Kawashima, S., Ishiba, T., Minomura, M. & Miwa, T., 2000, Relationship between Surface Temperature and Air Temperature on a Local Scale during winter night, Journal of Applied Meteorology and Climatology, 39, pp 1570-79

Stewart, I. and Oke, T. 2012, Local Climate Zones for Urban Temperature Studies,

Bulletin of the American Meteorological Society. <https://doi.org/10.1175/BAMS-D-11-00019.1>

Development of the Adaptive Thermal Comfort Model for Sustainable Housing Design in Japan

HOM B. RIJAL¹, KAZUI YOSHIDA², MICHAEL A. HUMPHREYS³, J. FERGUS NICOL³

¹Faculty of Environmental Studies, Tokyo City University, Yokohama, Japan

²Tokyu Fudosan R&D Center Inc, Tokyo, Japan

³School of Architecture, Oxford Brookes University, Oxford, UK

ABSTRACT: In order to quantify the seasonal differences in the comfort temperature and to develop a domestic adaptive model for highly insulated Japanese dwellings, thermal measurements and a thermal comfort survey were conducted for more than one year in the living room of 3 condominiums in Tokyo and Yokohama areas of Japan. We have collected 19,081 thermal comfort votes from 94 residents of 69 flats. The results suggest that the residents are highly satisfied with the thermal environment of their dwellings. People are highly adapted to the thermal condition of the dwellings, and that the comfort temperature has large seasonal variation. An adaptive model for housing was derived from the data to relate the indoor comfort temperature to the prevailing outdoor temperature. Due to the high insulation of the condominiums, the seasonal differences of comfort temperature and the regression coefficient of the adaptive model are smaller than those of detached houses. Adaptive building design and adaptive thermal comfort of people are important for the energy saving building design.

KEYWORDS: Japanese dwellings, Field survey, HEMS, Comfort temperature, Adaptive model

1. INTRODUCTION

The use of an adaptive approach to thermal comfort is important for sustainable building design. Firstly, buildings are adapted to the climate and culture. In traditional vernacular buildings, thermal insulation, shading and ventilation are good examples of the adapted building design [1]. Such passive building design needs to be applied in modern buildings. Secondly, people adapt to the outdoor and indoor climates. We need to provide adaptive opportunities in buildings to allow for their active thermal adjustments. So, how we design the building is directly related to adaptation and energy use in buildings. If adaptative actions are successful, we can save energy used in heating and cooling. In addition, about 10 % of heating energy used in winter can be saved by a reduction of 1K in indoor temperature [2].

The variation of energy use and indoor air temperature is related to the insulation level of the building. Generally, the insulation level of the Japanese detached houses is lower than that of the condominium. In addition the detached houses stand individually, and thus the heat loss in winter and gain in summer are higher than that of the condominium. In the previous research focused in the ordinary Japanese detached houses, and clarified the seasonal comfort temperature and the adaptive model [3, 4]. However, it is not known whether the comfort temperature and adaptive actions are different in the condominium and the detached houses. The indoor air temperature might be more stable in the condominiums than in the detached houses, and so

effect to the comfort temperature and the adaptive response of the inhabitants.

In order to record seasonal differences in the comfort temperature and to develop a domestic adaptive model for HEMS condominiums, thermal monitoring and a thermal comfort survey were conducted in the living rooms in the Tokyo and Yokohama areas of Japan.

2. FIELD INVESTIGATION

The thermal comfort survey and thermal measurements were conducted in 3 condominiums in Tokyo and Yokohama areas of Japan from 2015 to 2016 (Table 1). The indoor air temperature and the relative humidity were measured in the living rooms, away from direct sunlight, at 2 to 10 minute intervals using a data logger (Figure 1). These devices were installed in all flats [5, 6]. The accuracy of the sensor for air temperature measurement was not high ($\pm 2^{\circ}\text{C}$), and thus they were calibrated using high accuracy sensors ($\pm 0.3^{\circ}\text{C}$ and $\pm 0.5^{\circ}\text{C}$). Detailed calibration methods are given in previous research [7]. There were 46 male and 48 female subjects. Respondents completed a questionnaire (Table 2) several times a day in the living rooms.

The ASHRAE scale is frequently used to evaluate the thermal sensation, but the words "warm" or "cool" imply comfort in Japanese, and thus the modified thermal sensation scale (mTSV) is used to evaluate the thermal sensation [8]. We have collected 19,081 thermal comfort votes. Outdoor air temperature and relative humidity were obtained from the nearest meteorological station.

PLEA 2018 HONG KONG

Smart and Healthy within the 2-degree Limit

Table 1: Description of the thermal comfort survey.

Area	Bldg. code	Survey period	No. of family	No. of male (M) and female (F) subjects			No. of votes Living
				M	F	Total	
Yokohama	G	2015/6/13~2016/10/15	7	4	4	8	1,211
	H	2015/6/6~2016/8/18	16	9	8	17	859
Tokyo	K	2015/9/9~2016/10/31	46	33	36	69	17,011
Total			69	46	48	94	19,081



Figure 1: Detail of the measurement and thermal comfort survey: (a) Instrument and (b) web survey image.

Table 2: Scales for modified thermal sensation vote (mTSV) and thermal preference (TP).

No.	mTSV	TP
1	Very cold	Much warmer
2	Cold	A bit warmer
3	Slightly cold	No change
4	Neutral	A bit cooler
5	Slightly hot	Much cooler
6	Hot	
7	Very hot	

3. RESULTS AND DISCUSSION

The data were divided into three groups: the FR mode (free running, no heating or cooling used), CL mode (during cooling by air conditioning) and HT mode (during heating). First we have determined that the CL and HT modes are based on actual cooling and heating used. Some in these categories used window opening to provide ventilation. All data that were in neither the CL or the HT mode were classified as being in the FR mode. The mixed mode (MX) includes all of these modes.

3.1 Outdoor and indoor air temperature

Figure 2 and Table 3 show the seasonal mean indoor and outdoor air temperature. Seasonal variation is found in both indoor and outdoor air temperature. The Japanese government recommends an indoor

temperature of 20 °C in winter and 28 °C in summer. The results showed that the mean indoor temperatures during heating and cooling were slightly lower than the recommendation. Figure 3 shows the relation between indoor (T_i) and outdoor air temperature (T_o). We have obtained the following equations.

$$\text{FR mode } T_i = 0.375T_o + 16.8 \quad (1)$$

($n=6,866$, $R^2=0.75$, $S.E.=0.003$, $p<0.001$)

$$\text{CL mode } T_i = 0.109T_o + 24.3 \quad (2)$$

($n=788$, $R^2=0.11$, $S.E.=0.011$, $p<0.001$)

$$\text{HT mode } T_i = 0.160T_o + 18.5 \quad (3)$$

($n=4230$, $R^2=0.11$, $S.E.=0.007$, $p<0.001$)

n is number of sample, R^2 is coefficient of determination, $S.E.$ is standard error of the regression coefficient and p is significant level of regression coefficient. Due to the high thermal insulation of these condominiums, the regression coefficients is lower than the detached houses and condominiums (FR=0.587, CL=0.183 and 0.220) [4].

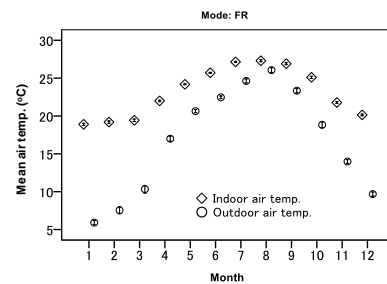


Figure 2: Variation of indoor and outdoor air temp.

Table 3: Indoor and outdoor air temp.

Mode	Items	N	T_o (°C)		T_i (°C)	
			Mean	S.D.	Mean	S.D.
FR	Winter	1,659	7.8	4.3	19.4	1.7
	Spring	1,906	18.1	5.3	22.9	2.1
	Summer	1,748	23.7	3.2	26.4	1.2
	Autumn	1,553	17.3	5.2	23.8	2.7
	All	6,866	16.8	7.3	23.1	3.2
CL	All	788	27.4	3.6	27.3	1.2
HT	All	4,230	8.3	4.4	19.9	2.1

N: Number of sample, T_o : Outdoor air temp., T_i : Indoor air temp., S.D.: Standard deviation

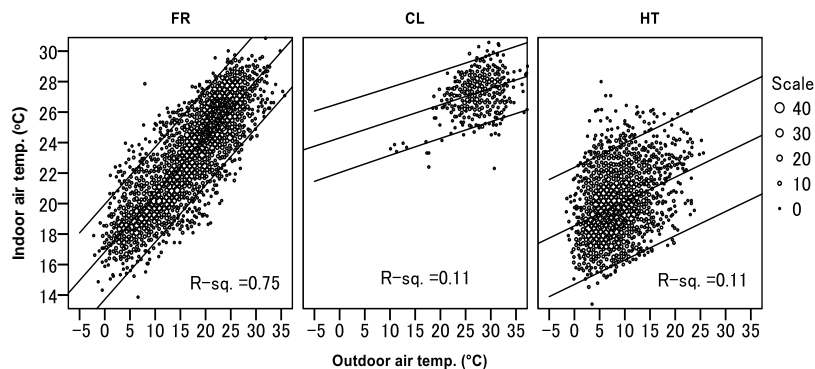


Figure 3: Relation between indoor and outdoor air temp.

PLEA 2018 HONG KONG

Smart and Healthy within the 2-degree Limit

3.2 Thermal sensation vote

Table 4 shows the percentage of each thermal sensation vote cast in each mode. Even when residents used the heating or cooling, they sometimes felt “cold” or “hot”. As there are a majority of “4 neutral” votes, it can be said that residents were generally satisfied in the thermal environment of the dwellings. This shows the adaptation of the residents to the local climate, buildings and culture.

Table 4: Percentage of thermal sensation in each mode.

Mode	Item	Thermal sensation							Total
		1	2	3	4	5	6	7	
FR	N	15	19	106	9768	124	37	24	12,689
	P	0.1	1.5	8.4	77	9.8	2.9	0.2	100
CL	N	2	-	24	867	166	40	1	1,100
	P	0.2	-	2.2	78.8	15.1	3.6	0.1	100
HT	N	14	12	910	4,129	104	5	2	5,292
	P	0.3	2.4	17.2	78	2	0.1	0	100

N: Number of sample, P: Percentage (%)

3.3 Thermal comfort zone

The thermal comfort zone is considered to be votes 3, 4 and 5 on the subjective scale. To locate the thermal comfort zone, Probit regression analysis was conducted for the thermal sensation vote (mTSV) categories and the temperature for FR mode. The analysis method is Ordinal regression using Probit as the link function and the temperature as the covariate. The results of the Probit analysis is shown in Table 5. The temperature corresponding to the median response (Probit = 0) is calculated by dividing the constant by regression coefficient. Thus, the mean temperature of the first equation will be $0.4/0.166 = 2.4$ °C (Table 5). The inverse of the Probit regression coefficient is the standard deviation of the cumulative Normal distribution. Thus, the standard deviation of air temperature of the FR mode will be $1/0.166 = 6.024$ °C (Table 5). These calculations are fully shown in Table 5. Transforming the Probits using the following function into proportions gives the curves of Figure 4 (a). The vertical axis is the proportion of votes.

$$\text{Probability} = \text{CDF.NORMAL}(\text{quant}, \text{mean}, \text{S.D.}) \quad (4)$$

where “CDF.NORMAL” is the Cumulative Distribution Function for the normal distribution, “quant” is the indoor air temperature (°C), the “mean” and “S.D.” are given in the Table 5.

Table 5: Detail of the Probit analysis.

Equation*	Mean	S.D.	N	R ²	S.E.
$mTSV(\leq 1)=0.166T_i-0.4$	2.4	6.024	6,872	0.13	0.006
$mTSV(\leq 2)=0.166T_i-1.5$	9.0				
$mTSV(\leq 3)=0.166T_i-2.3$	13.9				
$mTSV(\leq 4)=0.166T_i-5.1$	30.7				
$mTSV(\leq 5)=0.166T_i-6.0$	36.1				
$mTSV(\leq 6)=0.166T_i-7.4$	44.6				

*: All regression coefficients are significant ($P < 0.001$), $mTSV(\leq 1)$ is the Probit of proportion of the votes that are 1 and less, $mTSV(\leq 2)$ is the Probit of the proportion that are 2 and less, and so on., T_i : Indoor air temp. (°C), S.D.: Standard deviation, N: Number of sample, R²: Cox and Snell R², S.E.: Standard error of the regression coefficient.

The highest line is for category 1 (very cold) and so on successively. Thus, it can be seen that the temperatures for thermal neutrality (a probability of 0.5) is around 25 °C (Figure 4 (a)).

Reckoning the three central categories as representing thermal comfort, and transforming the Probits into proportions gives the bell-curve of Figure 4(b). The result is remarkable in two respects. The proportion of people comfortable at the optimum is very high, only just less than 100%, and the range over which 90% are comfortable is wide—from around 18 to 30 °C. This may be because people in their own dwellings are free to clothe themselves according to the room temperature, with fewer constraints that are apt to apply at work.

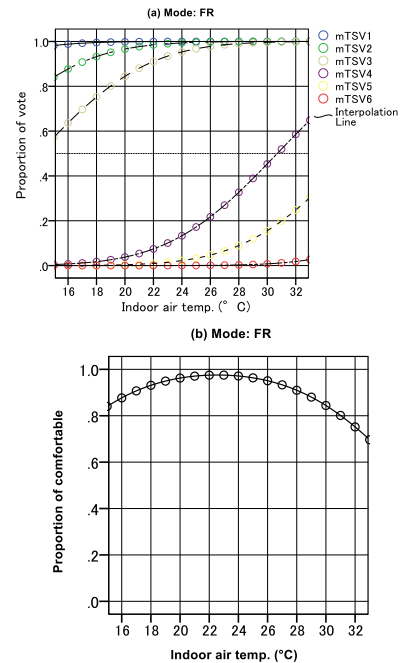


Figure 4: Proportion of mTSV or comfortable for indoor air temp.

3.4 Comfort temperature

3.4.1 Regression method

A regression analysis of the thermal sensation on indoor air temperature was conducted to estimate the

PLEA 2018 HONG KONG

Smart and Healthy within the 2-degree Limit

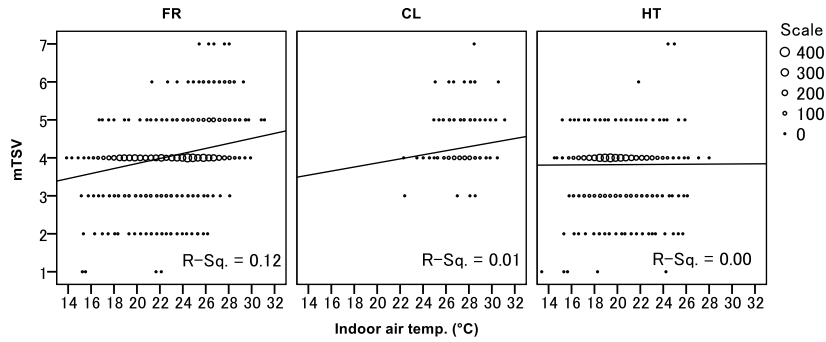


Figure 5: Relation between the thermal sensation and indoor air temperature.

comfort temperature (Figure 5). The following regression equations are obtained.

$$\text{FR mode } mTSV=0.066T_i+2.5 \quad (5)$$

(n=6,872, R²=0.12, S.E.=0.002, p<0.001)

$$\text{CL mode } mTSV=0.054T_i+2.8 \quad (6)$$

(n= 788, R²=0.01, S.E.=0.017, p<0.001)

The equation for HT mode is not statistically significant. When the comfort temperature is estimated by substituting “4 neutral” in the equations, it would be 22.7 °C in the FR mode and 22.2 °C in the CL mode. The comfort temperature is low in CL mode compared to mean indoor air temperature (Table 3). This might be due to the problem of using regression method in the presence of adaptive behaviour. Previous research has found it can be misleading when used to estimate the comfort temperature [3, 4]. So to avoid the problem the comfort temperature is estimated using the Griffiths method in next section.

3.4.2 Griffiths method

The comfort temperature is estimated by the Griffiths’ method [9-11].

$$T_c = T_i + (4 - mTSV) / a \quad (7)$$

T_c is comfort temperature by Griffiths’ method (°C) and a is rate of change of thermal sensation with room temperature, or Griffiths constant [2, 11]. In applying the Griffiths’ method, Nicol et al. [10] and Humphreys et al. [11] investigated the effect of using various values for ‘a’ (0.25, 0.33 and 0.50). We have done the same for these data. The mean comfort temperature with each coefficient is similar (Table 6 and Figure 6), and if the mean value of TSV is close to 4 it matters little which of these three values is used. We choose the value 0.50 for further analysis.

The mean comfort temperatures by the Griffiths’ method is 23.0 °C in FR mode, 26.8 °C in CL mode and 20.2 °C in HT mode (Table 6, Figure 6). The correlation between the comfort temperature and indoor air temperature is high in FR mode (Figure 7), showing

that fundamentally the people had adapted to a large extent to the temperatures that were provided.

Table 6: Comfort temperature by regression coefficients

Mode	Regression coefficient	Comfort temp. (°C)	
		Mean	S.D.
FR (N=6,872)	0.25	22.9	3.2
	0.33	23.0	3.0
	0.50	23.0	3.0
CL (N=788)	0.25	26.3	2.4
	0.33	26.5	1.9
	0.50	26.8	1.5
HT (N=4231)	0.25	20.6	2.8
	0.33	20.4	2.5
	0.50	20.2	2.3

N: Number of sample, S.D.: Standard deviation

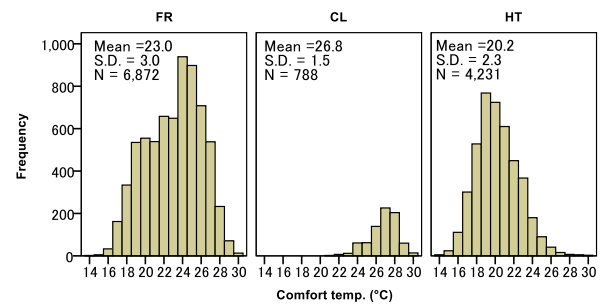


Figure 6: Comfort temperature by Griffiths’ method.

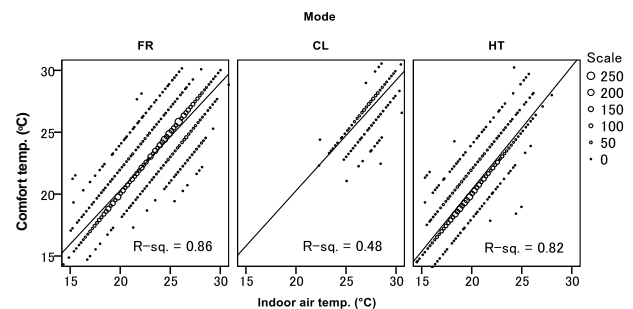


Figure 7: Comfort and indoor air temperatures.

3.4.3 Seasonal difference in comfort temperature

In this section, to clarify the seasonal difference, the comfort temperature for each month and season is investigated. The results showed that the comfort temperature changes according to the season (Figure

PLEA 2018 HONG KONG

Smart and Healthy within the 2-degree Limit

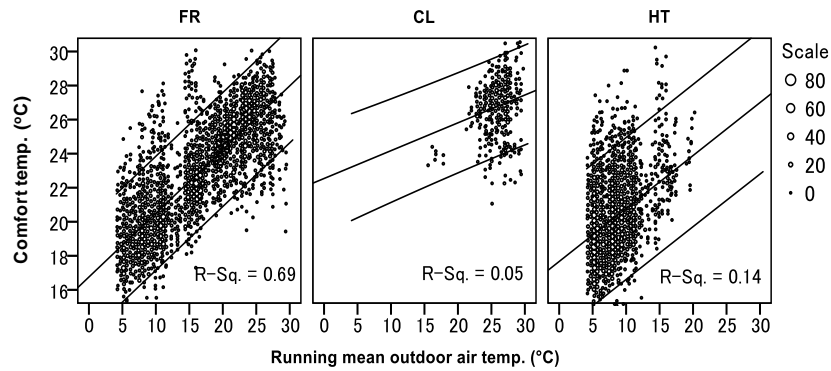


Figure 10: The adaptive model for each mode. 95% data points are within the band.

Table 8: Comparison of adaptive model with previous studies.

References	Location	Building	Mode	Equation*	n	R ²	S.E.
This study	Japan	Condominium	FR	$T_c=0.374T_{rm}+16.8$	6,872	0.67	0.003
			CL	$T_c=0.163T_{rm}+22.5$	788	0.05	0.027
			HT	$T_c=0.311T_{rm}+17.7$	4,231	0.14	0.012
			CL&HT	$T_c=0.360T_{rm}+17.3$	5,019	0.60	0.004
			All	$T_c=0.369T_{rm}+17.1$	11,891	0.66	0.002
Rijal et al. [3]	Japan	Detached	FR	$T_c=0.531T_{rm}+12.5$	13,471	0.68	0.003
			CL	$T_c=0.297T_{rm}+18.8$	1,955	0.06	0.026
			HT	$T_c=0.307T_{rm}+16.5$	5,240	0.11	0.012
Rijal et al. [4]	Japan	Detached & condominium	FR	$T_c=0.480T_{rm}+14.4$	25,177	0.70	0.002
			CL	$T_c=0.180T_{rm}+22.1$	6,528	0.02	0.014
			HT	$T_c=0.193T_{rm}+18.3$	3,582	0.05	0.014
			All	$T_c=0.432T_{rm}+15.4$	35,287	0.68	0.002
Rijal et al. [8]	Japan	Offices	FR	$T_{cg}=0.206T_{rm}+20.8$	422	0.42	0.012
			CL&HT	$T_{cg}=0.065T_{rm}+23.9$	4,236	0.10	0.003
Humphreys [12]	Worldwide	All types	FR	$T_c=0.534T_{om}+11.9$	-	0.97	-
ASHRAE [13]	Worldwide	Offices	NV	$T_c=0.31T_{om}+17.8$	-	-	-
CIBSE [14]	Europe	Offices	CL&HT	$T_c=0.09T_{rm}+22.6$	-	-	-
CEN [15]	Europe	Offices	FR	$T_c=0.33T_{rm}+18.8$	-	-	-

*: Regression coefficient of this research is statistically significant ($p < 0.001$), n: Number of sample, R²: Coefficient of determination, S.E.: Standard error of the regression coefficient (°C), FR: Free running, CL: Cooling, HT: Heating, NV: Naturally ventilated, T_c : Comfort temp. (°C), T_{cg} : Indoor comfort globe temp. (°C), T_{rm} : Daily running mean outdoor air temp. (°C), T_{om} : Monthly mean outdoor air temp. (°C).

8), and this may be related to the changes in indoor and outdoor air temperature (Figure 9). As shown in the Figure 8 and Table 7, the seasonal difference of the mean comfort temperature in FR mode for this study is 5.8 K which is lower than the detached houses (10.5K) or detached houses and condominium (9.4K) [3, 4]. This might be related to the high thermal insulation of the condominiums. In summer, the mean comfort temperature in the CL mode of this study is 0.3K lower than the detached houses (Table 7). In winter, the mean comfort temperature in the HT mode of this study is 1.9K higher than the detached houses (Table 7) which might be possible due to high thermal insulation of the condominium. The indoor temperature and the comfort temperature vary systematically with the outdoor air temperature (Figure 9).

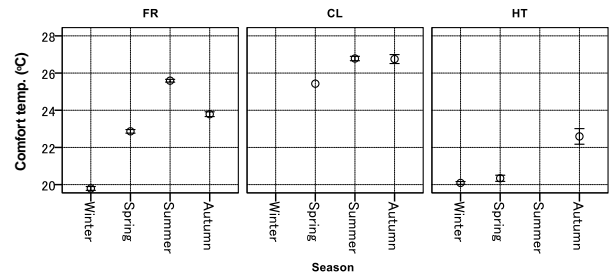


Figure 8: Seasonal variation of comfort temperature with 95% confidence intervals (mean $2 \pm S.E.$).

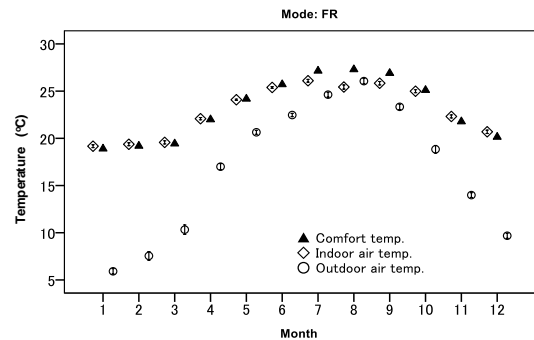


Figure 9: Monthly mean temperatures with 95% confidence intervals (mean $2 \pm S.E.$).

PLEA 2018 HONG KONG

Smart and Healthy within the 2-degree Limit

Table 7: Seasonal differences of the comfort temperature

Study	Mode	Mean comfort temperature (°C)				Seasonal diff. (K)
		Winter	Spring	Summer	Autumn	
This study	FR	19.8	22.9	25.6	23.8	5.8
	CL	-	***	26.8	26.8	0
	HT	20.1	20.3	-	22.6	2.5
Rijal et al. [3]*	FR	15.6	20.7	26.1	23.6	10.5
	CL	-	***	27.1	27.5	0.4
	HT	18.2	19.3	-	20.6	2.4
Rijal et al. [4]**	FR	17.6	21.6	27.0	23.9	9.4
	CL	-	25.2	27.1	26.7	1.9
	HT	19.5	20.9	-	20.4	1.4

*: Japanese detached houses, **: Japanese detached houses & condominiums, ***: Less than 5 sample is excluded.

3.5 The adaptive model

An adaptive model relates the indoor comfort temperature to the outdoor air temperature [12 -15]. Figure 10 shows the relation between the comfort temperature calculated by the Griffiths' method and the daily running mean outdoor temperature (T_{rm}). The regression equations are compared with other studies in Table 8.

The regression coefficient and the correlation coefficient in the FR mode are higher than in the CL and HT modes (Table 8). The regression coefficient in the FR mode (0.374) is higher than that in the CEN standard (0.33). The regression coefficient in the CL or HT or HT&CL mode is also higher than that in the CIBSE guide (0.09). The CEN standard or CIBSE guide is based on the field investigation in the office buildings, and therefore may not apply to dwellings, where residents have more freedom to adapt. It is interesting to note that the regression coefficient of HT&CL and MX mode is almost same.

Figure 11 shows the comparison of the adaptive model for FR mode with previous studies. The regression slope of this study (0.374) is shallower than the detached houses (0.531) or detached houses and condominium (0.480).

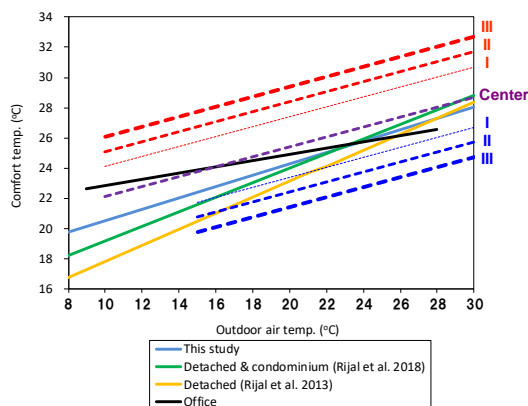


Figure 11: Comparison of the adaptive models in dwelling and office buildings in FR mode.

4. CONCLUSIONS

A thermal comfort survey of the residents of the Tokyo and Yokohama areas of Japan was conducted in living

rooms of the condominiums. The following results were found:

The residents were highly satisfied with the thermal environment of their dwellings, as indicated by the high proportion of 'neutral' responses.

The seasonal difference in comfort indoor temperature was 5.8 K which was lower than that of the detached houses.

Due to the highly insulated condominiums, the regression coefficient of the adaptive model (comfort temperature and running mean outdoor air temperature) (0.374) is lower than that of detached houses (0.531).

A known adaptive relation between the comfort temperature indoors and the outdoor air temperature can be a tool for predicting comfort temperature and for informing control strategies.

ACKNOWLEDGEMENTS

We would like to thank the households who participated in the survey.

REFERENCES

- Rijal, H.B. (2012). Thermal improvements of the traditional houses in Nepal for the sustainable building design, *Journal of the Human-Environment System*, 15 (1): pp.1-11.
- Nicol, J.F., M.A Humphreys and S. Roaf, (2012). Adaptive thermal comfort: Principles and Practice, Routledge.
- Rijal, H.B., M. Honjo, R. Kobayashi and T. Nakaya, (2013). Investigation of comfort temperature, adaptive model and the window opening behaviour in Japanese houses. *Architectural Science Review*: 56(1), pp. 54-69.
- Rijal, H.B., M.A. Humphreys and J.F. Nicol, (2018). Adaptive mechanisms for thermal comfort in Japanese dwellings, Proceedings of 10th Windsor Conference: Rethinking Thermal Comfort, pp. 703-719, Cumberland Lodge, Windsor, UK, 12-15 April 2018. London: Network for Comfort and Energy Use in Buildings, <http://nceub.org.uk>
- Rijal, H.B. and K. Yoshida, (2017). Development of the adaptive model for thermal comfort in HEMS condominium, The 17th Conference of the Science Council of Asia, pp. 153-159, Philippines, 14-16 June, 2017.
- KC, R., H.B. Rijal, K. Yoshida and M. Shukuya, (2016). Feasibility study on the use of HEMS for thermal comfort and energy saving in Japanese residential buildings, *International Journal of Civil, Environmental, Structural, Construction and Architectural Engineering*, 10 (9): 1098-1103.
- KC, R., H.B. Rijal, K. Yoshida, M. Shukuya, (2018). An in-situ study on occupants' behaviors for adaptive thermal comfort in a Japanese HEMS condominium, *Journal of Building Engineering*, 19: 402-411.
- Rijal, H.B., M.A. Humphreys and J.F. Nicol, (2017). Towards an adaptive model for thermal comfort in Japanese offices, *Building Research & Information*, 45(7), pp. 717-729.
- Griffiths, I.D., (1990). Thermal comfort in buildings with passive solar features: Field studies. Report to the Commission of the European Communities. EN3S-090, UK: University of Surrey Guildford.
- Nicol, F., G.N. Jamy, O. Sykes, M. Humphreys, S. Roaf and M. Hancock, (1994). A survey of thermal comfort in Pakistan

PLEA 2018 HONG KONG

Smart and Healthy within the 2-degree Limit

toward new indoor temperature standards. Oxford Brookes University, Oxford England.

Humphreys, M.A., H.B. Rijal and J.F. Nicol, (2013). Updating the adaptive relation between climate and comfort indoors: new insights and an extended database. *Building and Environment*: 63, pp. 40-55.

Humphreys, M.A., (1978). Outdoor temperatures and comfort indoors. *Building Research and Practice (Journal of CIB)*, 6(2): pp. 92-105.

ASHRAE Standard 55 (2004). Thermal environment conditions for human occupancy. Atlanta, Georgia, American Society of Heating Refrigeration and Air-conditioning Engineers.

CIBSE (2006). Environmental Design. CIBSE Guide A, Chapter 1, Environmental criteria for design. London: Chartered Institution of Building Services Engineers.

Comité Européen de Normalisation (CEN) (2007). EN 15251: Indoor Environmental Input Parameters for Design and Assessment of Energy Performance of Buildings Addressing Indoor Air Quality, Thermal Environment, Lighting and Acoustics., Brussels.

Development of an Affordable Sensing and Monitoring System for Post-Occupancy Building Performance Evaluation

JAIN ARIHANT¹, APTE MICHAEL G.¹, MANU SANYOGITA¹, DIXIT MAAZ¹

¹CEPT University, Ahmedabad, India

ABSTRACT: The building footprint is likely to increase five-fold by 2030. These buildings consume a large chunk of energy in the form of electricity for running systems like air conditioning, artificial lighting, and equipment to name a few. The energy consumption in the building sector can be decreased. This can be done by carrying out building performance evaluation studies, which will help in understanding the energy losses inside a building. This research focuses on developing an affordable monitoring and sensing system for building performance evaluation studies. Different hardware and software platforms are explored, and the component selection was done after comparative analysis based on various aspects. The aspects considered for selection include: specifications, the ease of use, cost, and complexity of the system. The expected outcome is a methodology tailored for custom needs of the user, and a prototype for building performance evaluation studies.

KEYWORDS: Wireless sensor networks, Building performance evaluation, Affordable, Open source, Sensors, Data collection, Indoor environment, Arduino

1. INTRODUCTION

In India, as of 2010, the building footprint was projected to increase by about 2.3 billion square meters by 2030. The buildings consume 33% of the total energy, and it is increasing at 8% per annum [1]. Energy efficient buildings are of vital importance for all future construction in India. According to recent studies, there has been an increase in the number of certified buildings in India. However, less effort is made to make sure these buildings deliver the performance as promised.

Therefore, to conserve energy, improve and to evaluate the building performance, a thorough evaluation and feedback is essential. Other than that, monitoring of energy use and indoor environmental conditions is also important.

The energy performance of a building can be demonstrated by building performance evaluation. Research shows that the performance of a building is not the same as the intended performance. To reduce this gap between the intended performance and the actual performance of buildings, building performance evaluation is essential. Learn-BPE is a collaborative project between CEPT University and Oxford Brookes University which aims to develop new knowledge, tools, and skills amongst researchers, postgraduate students and practitioners of engineering and architecture, to evaluate the actual performance of (green) buildings from a technical and occupant perspective [2]. Proper measurement and verification help in measuring the economic and environmental benefits of energy efficient projects in a cost-effective manner.

The Open Source Data Logger (OPENSDDL) developed through this research was compared against a HOBO

U12-012 data logger. The commercially available counterpart system can measure 3 parameters-temperature, RH, and illuminance, and has one external channel for other sensor types. A different sensing device would be required for measurement of any other parameter. A HOBO U12-012 costs ₹14,794 (\$212), whereas the OPENSDDL costs ₹4,605 (\$66), which is one-third the price of the commercial counterpart.

Arduino has been often used by several researchers for developing custom environmental monitoring systems due to its ease of use, low cost, ease of integration, and open-source hardware and software. Thus, it is the best viable option to select an Arduino based microcontroller unit for prototyping a system. Different sensor options were explored in different research studies, but a new set of sensors were selected for BPE studies.

Along with Arduino, the XBEE is the most commonly used wireless networking module due to its low cost, low power consumption, easy integration with Arduino and an effective communication range for BPE studies. But a different wireless module was used for the development of OPENSDDL system for its low cost, low power consumption, and small size.

The aim of this study is to find an affordable path for doing field measurements for BPE within budget while still maintaining the necessary accuracy and precision of the devices that meet the scientific goals of the research. This paper proposes a methodology and a prototype using open source software and hardware. It can be used for creating a wireless sensing network which is customizable and affordable. The proposed device is limited to measurement of air temperature, relative humidity, and illuminance levels. The goal of

PLEA 2018 HONG KONG

Smart and Healthy within the 2-degree Limit

the study was to develop a platform for sensor and data logger development that had the following features:

- Affordable (cheaper than commercial counterpart),
- Developed using open-source HW/SW,
- Easy to build for a novice user,
- Extensible to multiple sensor types,
- Accurate and precise for BPE studies,
- Data storage and timekeeping feature,
- Live stream data that can be seen online.

2. METHODOLOGY

Identifying the intent of monitoring of environmental parameters is crucial, and this methodology can be customized as per needs. The methodology for developing the system is divided in following steps-

2.1 Accuracy and Precision requirements

Before developing the OPENSDDL system, accuracy and precision required for BPE studies were explored. The Learn-BPE measurement protocol [3], developed by Oxford Brookes University, has some recommended levels of resolution and accuracy for logging and monitoring of indoor environmental parameters. This helped in deciding the specifications of the sensors that were suitable for this study.

Other standards like the International Performance Measurement and Verification Protocol (IPMVP) and ASHRAE Standard-55 [4,5] were referred. ASHRAE Standard-55 focuses mainly on thermal comfort studies and provides recommendations suitable for the same. Similarly, Learn-BPE measurement protocol was used for this study as it focuses more on BPE studies. Also, IPMVP provided a generic methodology and different recommendations related to specifications and placement of loggers, and other important criteria for monitoring purposes. The comparison of each of them is given in Table 1.

Table 15 Specifications as per different standards and

Parameter	Standard	Temp (°C)	RH (%)	Light (lx)
Measurement Range	ASHRAE - 55	10 – 40	25 to 95	--
Accuracy	ASHRAE-55	± 0.2	± 5	--
	IPMVP	±0.25	± 5	--
	Learn - BPE	± 0.5	± 10	± 0.5
Resolution	Learn - BPE	0.1	1	

measurement protocols

2.2 The OPENSDDL platform

This section describes the various open source hardware components, which include the microcontroller, data storage, real-time clock, wireless module, and sensors. The various aspects for selecting





the components were: ease of use, complexity of the system, cost and reliability.

2.2.1 Microcontroller (MCU)

The hardware and software of the OPENSDDL are based on the Arduino platform, which is open source. There were several options in selecting the platform, and a comparative analysis was done to choose the most suited MCU for this system. Apart from the above-mentioned aspects, the system specifications were also explored. The specifications of each of the MCU products are given in Table 2.

The system had to be connected to multiple sensors, read the sensor values, transmit those values to the Internet and lastly store them on an SD card. It does not require any processing of data. Thus, an MCU with a clock speed of as low as 16MHz was adequate. The communication protocol used for this project was I²C (Inter-Integrated Circuit), which does not require many general-purpose input-output pins. The RAM (Random Access Memory), stores the machine code used to run the controller. Apart from that, some of the sensor values can be stored in the RAM temporarily before writing them to SD card to save battery. Thus, larger RAM would help in this project. Arduino Uno has the least RAM; thus, the program must be as short as possible to keep space for storage. Apart from the technical aspects, the cost is one of the major selection criteria.

Table 16 Comparative analysis of different microcontrollers

	Arduino Uno	Raspberry Pi Zero W	Teensy 3.2	Nodemcu Esp8266
				
Clock Speed	16 MHz	1 GHz	72 MHz	80 MHz
Operating Voltage	7V – 12V	4.75V – 5.25V	1.7V – 3.6V	2.5V – 3.6V
Input/Output Pins	20	40	34	17
RAM	2 KB	512 MB	64 KB	50 KB
Flash Memory	32 KB	--	256 KB	512 KB
Cost (INR)	₹ 450	₹ 885	₹ 2,162	₹ 350
Cost (USD)	\$ 7	\$ 13	\$ 32	\$ 5

2.2.2 Sensors

As multiple sensors were to be connected to one MCU, I²C protocol for communication was chosen. This protocol allows multiple slave-type chips to be connected with one or more master-type chips. Another alternative was to use a serial peripheral interface (SPI) connection. The SPI connection needs

PLEA 2018 HONG KONG

Smart and Healthy within the 2-degree Limit

more number of signal lines, whereas the I²C protocol needs only two pins, which is why I²C was preferred. Different temperature and RH sensors were compared to select the most appropriate sensor. The comparison was done in terms of aspects like accuracy, precision, measurement range, response time, and cost. The BME-280 temperature and RH sensor by Bosch was chosen for its accuracy and precision and a fast response time at a reasonable cost. The DHT-22 appeared to be a great option but it was found to be unreliable [6]. Also, this chip provides both the temperature and RH sensors on the same printed circuit board (PCB), which helps in packaging, and limits the hassle of extra pins/wires required to connect temperature and RH sensor separately. The specifications of BME-280 are given in Table 3.

Table 17 Specifications of BME-280 sensor

Parameter (T & RH)	BME-280
Accuracy	±0.5 & ±3%
Precision	0.01 & 0.01%
Measurement Range	-40 to 85 & 0 to 100%
Response Time	1 second
Cost (INR & USD)	₹ 560 (\$ 8.25)

Similarly, a comparative analysis was done for the illuminance sensor. The light dependent resistors (LDR) type photoresistors are used in a variety of applications, where dark and light conditions have to be observed. However, they are not good for measuring the exact light intensity. The TSL2561 was chosen over any other type as it is more sensitive and accurate. It also provides more precise lux calculations by measuring both infrared and full visible spectrum of light, thus giving a wider range of wavelength. This wider analysis of wavelength of light approximates the response of the human eye, resulting in accurate measurements as compared to conventional LDR.

2.2.3 Data storage & real-time clock

Separate real-time clock and storage breakout boards were also available, but for ease of packaging and fabricating the system, a data logger shield was preferred. The clock on the shield was DS1307, which was considered accurate for data logging purposes. The internal processor clock on the Arduino was tested for reliability and it was observed during the test that the Arduino is capable of timekeeping, however, it was not very accurate, and it lags the actual time. Hence, a separate clock on data logger shield was preferred. So, even when the power goes off for the Arduino, the clock on the board would still work. Thus, it made the OPENSDDL more self-reliable.

2.2.4 Wireless Module

A few wireless modules for extracting data from sensors at different floors was explored. An ESP-01 Wi-Fi module and an XBEE chip were the two options for wireless data transfer. The ESP-01 is available at one-fifth the cost of the XBEE chip (\$3 and \$15 respectively). The ESP-01 was chosen for its lower cost, low power consumption, and commonly used Wi-Fi protocol. The OPENSDDL was developed to work either on SD card data storage or on wireless connectivity. It can be developed further to work on both modes simultaneously.

2.3 Monitoring plan

A monitoring plan was made in which the location of the sensors was decided. It was a crucial aspect as the number of sensors per system was decided after preparing a building monitoring plan. The number of sensor nodes required was dependent on this. The considerations done while developing building monitoring plan are discussed in data gathering methods.

2.4 Fabrication

After completing the selection of all the components, the tasks of MCU programming and overall device fabrication was done. The packaging also helped in shielding the system from electromagnetic radiations from other electronic devices, which can hinder the performance of the OPENSDDL units.

Operationally, a peripheral connector panel was developed to connect the sensors with the Arduino. Wires coming from the SCL and SDA pins are soldered on a vector board, and these solder joints are further connected to multiple four-contact 4P4C female (telephone-style connector) sockets. The vector board has multiple 4P4C plugs soldered onto it. The sensors require a total of 4 pins, two for I²C communication (SDA & SCL), and two for power (3.3V & GND), and the four-contact 4P4C plug has 4 pins for connection. A similar connection was made with the 4P4C female plug and the 4 wires of the sensor.

A 3-D printed casing for the sensors was developed using Polyactic Acid (PLA) material. A rectangular opening was created in the casing for temperature, RH sensor, where the 4P4C connector would fit in snugly. At the top of this sensor case, some perforations were provided so that the air can circulate inside the casing for accurate measurements.

Similarly, a casing for the illuminance sensor was developed with PLA material. A circular acrylic transparent watch cover was used for covering the light sensor to protect it from dirt and dust.





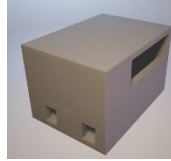

The casing for MCU was developed by laser cutting a medium density fibreboard (MDF). A 3D printed MCU case required 6 hours of 3D printing, whereas a case developed by laser cutting took less time (about half an hour) for cutting the entire sheet of A2 size, hence

PLEA 2018 HONG KONG

Smart and Healthy within the 2-degree Limit

MCU case was laser cut. Table 4 shows 3D and actual models.

Table 18 Different casing for sensors and microcontrollers

Component	Model	Real
Temperature and RH casing		
Illuminance sensor casing		
Micro-controller casing		

2.5 Programming

The program used consists of different pieces of codes put together. Different pieces of programs were used for programming the temperature & RH sensor (BME280), the illuminance sensor (TSL2561), the data logging and time keeping shield (data logger shield), the Wi-Fi chip (ESP-01), etc. These all different programs are freely available online and were customized.

The different program was used for different modes of the OPENSDDL units; the wireless mode and the local storage mode. The complete program for both the modes are available on the GitHub page.

2.6 Calibration

The process of calibration was a crucial matter. The accuracy of the OPENSDDL could be verified only after the calibration process. The temperature and RH calibration were performed in NABL (National Accreditation Board for Testing and Calibration Laboratories) accredited laboratory. The system was calibrated by analyzing the deviation in the OPENSDDL and comparing it with the reference measurements.

The calibration services for this project was provided by a local calibration company. A temperature-controlled calibration chamber was used for calibrating the sensors for temperature values. A Testo 735 calibrated temperature sensor with an accuracy of 0.2°C was used as a reference thermometer. A Rotronic RH sensor with an accuracy of 1.5% was used as a reference hygrometer, and the BME280 was calibrated against this in an Indecon RH control chamber.

The BME280 was calibrated by using multiple calibration points: 10°C, 20 °C, 30 °C, 40 °C, and 25%, 50%, 70% for RH. These calibration values were chosen as they lie within the environmental conditions where the sensors were to be used. When the specified temperature and RH values were reached, the time was noted. This time stamp helped in identifying the temperature and RH values of the BME280 sensor.

The illuminance sensor was compared against a Testo 540 Light Intensity meter which comes with a certificate of conformity from National Metrology Institute of Germany (PTB). This equipment, being factory calibrated, was used to compare the lux levels with the TSL2560 sensors. A box with black surfaces and a light source was used for comparing the lux levels. The distance between the light source and the sensor was varied- 0.5m, 0.6m, 0.7m, and 0.8m. In this box, the illuminance levels were measured with both- the sensor and the Testo equipment.

Table 19 Measured temperature readings from one of the sensors and a reference temperature sensor

Temperature from sensor 4 (°C)	Temperature from Master Sensor - (°C)
40.2	39.8
30.7	30.2
21.5	20.1
11.8	9.9

On plotting the data from Table 5 for temperature values, we get the results for temperature sensor 4 as shown in Figure 1. An $R^2 \geq 0.999$ indicates that the relation between both the sensor readings is linear, and hence, the equation- $y=1.0501x-2.6965$ was used in the program. Same steps were followed for other sensors.

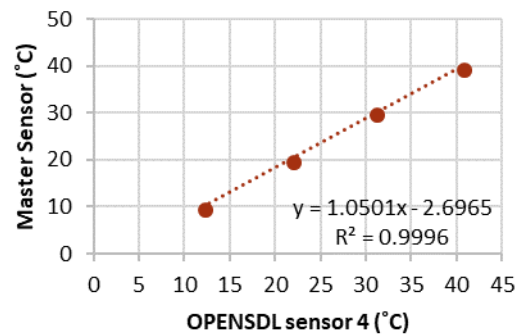


Figure 1 Correlation of OPENSDDL sensor 4 and master sensor

3. DATA GATHERING METHODS

While performing the field test, there are some aspects which were considered. These help in deciding the location of the sensors. These includes:

- Location of sensors
- Occupant density
- Number of floors
- Location of HVAC indoor units

PLEA 2018 HONG KONG

Smart and Healthy within the 2-degree Limit

The data collection frequency (continuous or periodic) was determined by the variability in the readings of the measured parameters, the monitoring intent. Appropriate standards like ANSI/ASHRAE-55 and IPMVP were referred for data collection methods. Some limitations apply to these standards to avoid tampering of the sensors inside the building.

Two sensors were placed on each floor where one temperature and RH sensor were placed on typical space for each floor, and another sensor was placed on the sitting space just under the HVAC indoor unit to understand the impact of the AC unit on that specific seating. The illuminance sensors were placed on the ground, first and second floors only. So, the points in the space with the lowest daylight levels were considered for monitoring of illuminance levels. While monitoring the building, HOBO data loggers were deployed along with the OPENSDDL units for comparing the data. The loggers were placed at inaccessible locations for security reasons. As the main purpose of monitoring was just comparing the data against HOBO U12-012 data logger, the location of sensors was not a major concern apart from security. No OPENSDDL units were placed outside the building as they were fabricated for indoor usage.

4. FIELD TESTING

The developed system was deployed in the University library building for field testing and performance validation. The area of the building was approximately 1500 sq.m. The building has 6 floors: 3 floors above ground, and 3 basement floors.

Figure 2 and 3 show the average hourly data from OPENSDDL and HOBO data logger for temperature, RH and illuminance measurements at each floor. The graphs have a similar pattern, indicating that the sensors are observing the same temperature variations, but with some margin of error. The maximum deviation observed in temperature measurements was of 2°C and 3% for RH. This deviation for RH is acceptable, as the OPENSDDL RH sensor has an accuracy of ±3%, whereas the temperature varied by about 2°C, which is not acceptable.

It should be noted that the HOBO data loggers were not checked for calibration and maybe not be calibrated for temperature measurements, whereas the OPENSDDL sensors were calibrated by using the NABL accredited reference sensors in controlled conditions. The graphs shown below for temperature and RH have some lines interrupting in the middle of the timeline. This is due to the on-site OPENSDDL installation problems, which were troubleshoot later while inspecting these loggers. Two OPENSDDL systems stopped working due to technical glitches.

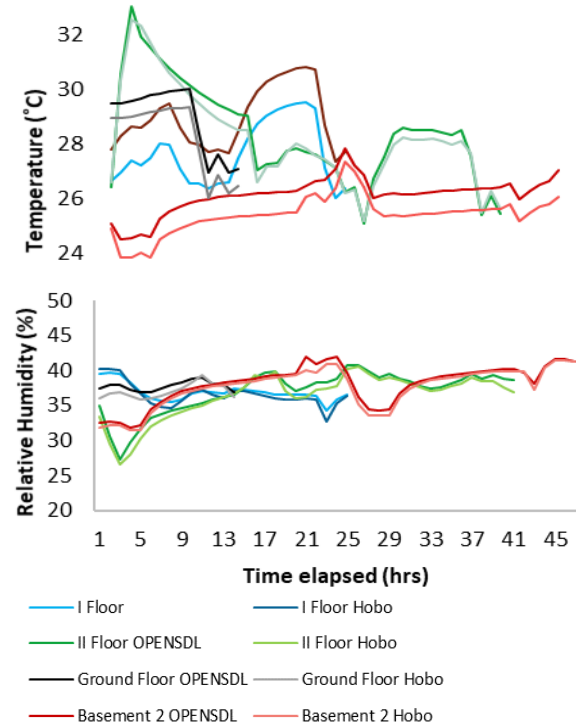


Figure 2 Average hourly data from OPENSDDL and HOBO data loggers for all floors (T & RH)

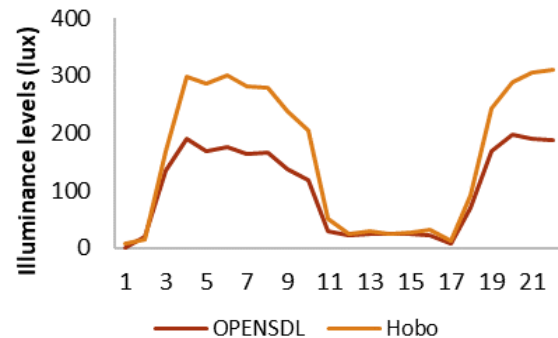


Figure 3 Average hourly data from OPENSDDL and HOBO data loggers for all floors (Illuminance)

5. COSTING

The cost breakdown of the OPENSDDL is given below in Table 6. This cost is for the developed system with only 3 sensors- temperature, relative humidity sensor, and one illuminance sensor. This is the same configuration as of the HOBO U12-012 data logger, which also comes with temperature and relative humidity sensor, and illuminance sensor. All the comparisons, including costs, are made with this specific HOBO model only. While doing this project, a stipend of ₹100/hour (\$1.4/hr) was paid. About 67 hours were spent working on the fabrication and packaging of the whole system. If we divide 67 by 5 (as 5 OPENSDDL were developed), one OPENSDDL takes about 13.4 hours for fabrication, which leads to a labor amount of ₹1,340 (\$19).

PLEA 2018 HONG KONG

Smart and Healthy within the 2-degree Limit

The calibration was done by a professional company, hence the charges for the same are included in the estimate. A total budget of ₹8,000 (\$114) was allotted from the Learn-BPE project for development of multiple OPENSDDL units, and it was developed well within the budget.

Table 20 Cost estimation of OPENSDDL unit with HOBO U12-012 like configuration

Component	Quantity	Price per unit	Cost (INR)	Cost (USD)
T & RH Sensor (BME280)	1	560	560	8
Illuminance sensor (TSL 2561)	1	450	450	6.45
Arduino Uno MCU	1	450	450	6.45
Data logger shield	1	350	350	5
Vector board	1	15	15	0.2
RJ-9 female connector	2	20	40	0.6
3D printing (Sensor case)	2	100	200	2.9
Laser Cutting (MCU)	1	200	200	2.9
Calibration	1	500	500	7.2
Wire	2	10	20	0.3
RJ-9 male connector	2	5	10	0.15
Battery holder	1	150	150	2.15
Batteries	8	40	320	4.6
Labour	13.4 hrs	100	1340	19.2
Total			4,605	66

6. CONCLUSION

The outcome of this research is a design, methodology and a prototype for developing a low-cost measurement system. This system is capable of measuring temperature, RH, and illuminance. This methodology can be used by various stakeholders like owners, architects, consultants, energy analysts, researchers, students etc. for study of environmental parameters inside a building.

The results from the field testing after the deployment of OPENSDDL with the commercial counterpart demonstrate that the OPENSDDL has the basic functionality but needs further improvements. This includes improving the solder joints on the custom shield, the casing design, the loose connectors, and the custom shield developed could be made into a printed circuit board (PCB). After all these mentioned

refinements, the device will become more reliable and can be used for building monitoring applications.

Other parameters of measurement like CO₂, wind speed, noise, power metering, etc. can be integrated into the OPENSDDL unit, thus expanding the usability and functionality of the system, making it more suitable for BPE studies. The unit as tested is affordable, but not reliable for BPE studies. Although it can still be used for educational, and training purposes. The illuminance sensor of the OPENSDDL needs proper calibration in controlled conditions.

The unique selling point of the OPENSDDL was that it is based on an open-source platform, which is customisable, and inexpensive. The OPENSDDL unit as compared to HOBO U12-012 data logger and is 69% cheaper. As the system developed is based on an open-source platform, it provides a huge possibility for upgrading and customizing the hardware and software of the system tailored for different applications. A DIY and other project details can be found on this GitHub page (<https://github.com/arihant93/OPENSDDL>).

ACKNOWLEDGEMENTS

The authors gratefully acknowledge the support of the Newton Fund through the Royal Academy of Engineering (RAEng) Industry Academia Partnership Programme for financially supporting the Learn-BPE project [Grant number IAPPI\74].

REFERENCES

1. Kumar, S., Sarraf, S., Seth, S., Pandita, S., Walia, A., Kamath, M., & Deshmukh, A. (2010). Performance Based Rating And Energy Performance Benchmarking For Commercial Buildings In India. Third German-Austrian IBPSA Conference, (pp. 447-454). Vienna.
2. Learn-BPE. (2018). Project Summary. Retrieved from Learn-BPE.org: <https://lcbgroup.wixsite.com/learnbpe/about>
3. National Institute of Standards and Technology. (2017, June).
3. Gupta, R., & Gregg, M. (2017). Review of building performance evaluation methods used in the UK. Oxford.
4. Efficiency Valuation organization. (2017). International Performance Measurement and Verification Protocol (IPMVP). Retrieved January 2018, from <https://evo-world.org/>: <https://evo-world.org/en/products-services-mainmenu-en/protocols/ipmvp>.
5. ASHRAE Standards Committee. (2013). ANSI/ASHRAE Standard 55 Thermal Environmental Conditions for Human Occupancy.
6. Smith, R. (2017, March). Testing Various Low-Cost Hygrometers. Retrieved from www.kandrsmith.org: <http://www.kandrsmith.org/RJS/Misc/hygrometers.html>

An Empirical Investigation of the Link between Indoor Environment and Workplace Productivity in a UK Office Building

RAJAT GUPTA¹, ALASTAIR HOWARD¹

¹Low Carbon Building Research Group, School of Architecture, Oxford Brookes University, Oxford, United Kingdom

ABSTRACT: Most studies on indoor environments and productivity have been conducted in controlled, static conditions often not representative of the real world. This paper uses a case study-based, real-world approach to empirically investigate the relationship between the indoor environment and workplace productivity in a mechanically-ventilated office environment in southern England. Evidence gathered during a baseline period is used to implement an intervention (limiting peak temperature) with the aim of improving productivity. Environmental parameters (temperature, relative humidity and CO₂) were monitored continuously. Transverse and longitudinal surveys recorded occupant perceptions of their working environments, thermal comfort and self-reported productivity, while performance tasks objectively measured productivity. Although the building was operating within narrow temperature, RH and CO₂ bands, workplace productivity was perceived to decrease when occupants were thermally uncomfortable and when they perceived the air as stuffy. Correlations with perceived changes in productivity were stronger for the perceived environment than for the measured environmental conditions. In addition, median scores were 16% lower for tests conducted when CO₂ levels were in the 1000-1200ppm range compared to those conducted below 800ppm. Insights from the study can be used to optimise indoor office environments to improve staff productivity.

KEYWORDS: Productivity, office, survey, indoor environment, comfort

1. INTRODUCTION

Productivity in the workplace has become a major concern, particularly in the UK where research suggests UK productivity is around 16% lower than the G7 average [1]. Improvements in the working environment could reduce this deficit by around 3% [2] - hugely significant in financial terms.

This paper uses a case study-based real-world approach to empirically investigate the link between indoor environment and workplace productivity in a mechanically-ventilated office environment in southern England. It uses a *baseline (observation)* and *intervention* approach, where a range of environmental parameters (indoor air temperature, relative humidity (RH) and CO₂ levels) are monitored continuously, alongside outdoor temperature and RH for six months (March-August 2017) in the *baseline* period and for one month (October-November 2017) in the *intervention* period. During these two periods, longitudinal online surveys record occupant perceptions of their working environment, thermal comfort and self-reported productivity, while performance tasks are designed to objectively measure productivity. In addition, a transverse Building Use Studies (BUS) survey [3] was conducted in April 2017 to gather occupants' perception of their working environment.

2. EVIDENCE TO DATE

CEN standard EN15251 acknowledges that the indoor environment affects occupant productivity, health and comfort [4] and limits were therefore set to optimise performance. Negative factors related to productivity (e.g. temperatures or CO₂ concentrations being too high) were often more obvious than positive factors (i.e. finding the optimal environment to increase productivity). Studies have therefore sought to understand these relationships more fully, although many of these have been conducted in controlled, static conditions which minimise or eliminate the myriad of potential influencing factors present in dynamic real world offices.

The effect of temperature on health and comfort has been widely researched and it is broadly recognised as an important indoor environment factor. The recommended limits for Category II mechanically ventilated office buildings are 20-26 °C, implying that within this range there is no direct risk to occupants' health and comfort. Tham [5] found that indoor temperature significantly influences workers' productivity, and Fang et al. [6] identified a link between temperature, RH and performance at different ventilation rates. Lan et al. [7] found that performance decreased in warmer conditions, but the results from the study imply that optimum thermal comfort and optimum productivity may not occur at the same temperatures – a finding supported by

PLEA 2018 HONG KONG

Smart and Healthy within the 2-degree Limit

others [8]. Seppänen et al's meta-analysis [9] suggests the temperature range for optimum performance is close to the optimum range for comfort, particularly for mechanically ventilated buildings in winter.

An indoor CO₂ concentration upper limit of 1500 ppm is specified for office spaces in order to maintain comfort air quality. In studies by Allen et al. [10], Satish et al. [11] and Kajtar et al. [12], performance was found to decrease as CO₂ concentration was increased. These studies indicate every-day CO₂ levels within the current recommended standards can have significant negative impacts on worker performance.

Innovate UK's national research programme on building performance evaluation (BPE) undertook case study investigations of 50 low energy non-domestic buildings located across the UK. Meta-analysis of the occupant surveys showed 12 out of 21 workspaces reporting an increase in perceived productivity due to the environmental conditions perceived by the occupants [13]. When occupants were satisfied with the indoor temperature, noise and lighting, perceived productivity increased; conversely, when indoor air was perceived as stuffy and smelly, perceived productivity decreased.

It is evident that research suggests a growing recognition of a link between indoor environment and perceived productivity in workplaces. This paper uses a case study office building in the south of England to investigate this link empirically.

3. CASE STUDY AND METHODS

The case study building selected is a modern office building in Southern England. It is a typical representation of a modern office building in the UK [14]. Construction of the building was completed in 2006. The facilities are managed by an on-site external facilities management company using a BMS system, with mechanical ventilation and non-openable windows. The second-floor work space in block B was selected as the case study office environment. The gender mix of occupants in this workspace (approximately 57% male, 43% female), and the distribution of age groupings (approximately 10% under 30 years, 90% 30 years and over) was representative of a typical working office.

The methodology adopted in the study has a three-pronged approach: (1) *Physical monitoring of indoor and outdoor environment* using data loggers; (2) *Occupant survey* (transverse and longitudinal) and (3) *Performance tasks* (productivity tests) which act as a proxy for productivity. Three different sets of performance tasks were selected from those used in previous research studies. They are designed to represent tasks typical of those conducted in the case-study office: *Numerical tests* (to solve simple mathematical questions), *Proof reading* (to identify spelling errors in a paragraph of text) and *Stroop test*

(an interference test, differentiating between the colour of the text and the word). Both the test score and time taken to complete the task were recorded.

4. BASELINE PERIOD: RESULTS

Physical monitoring from March 2017 to August 2017 showed that during occupied hours (8am-6pm, Monday-Friday) indoor temperatures were relatively warm, staying within 22-24°C for the majority of the time (Fig. 1). During the non-heating months (May-August) the range of temperatures increased.

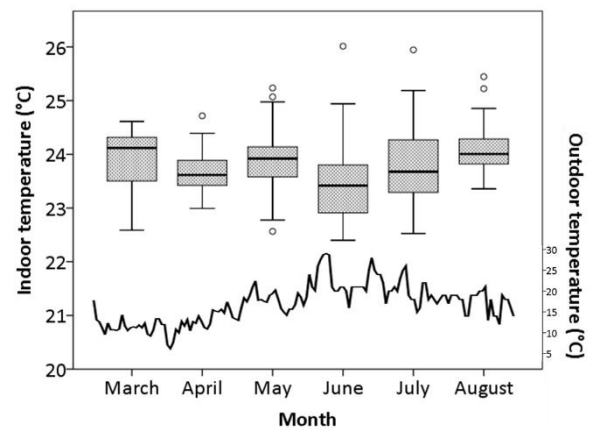


Figure 1: Boxplot of monthly indoor air temperatures (with daily average outdoor temperatures shown on secondary y-axis)

As the windows within the working area were not openable, CO₂ concentrations were not affected by windows being opened in warmer weather. Median CO₂ levels remained fairly stable (around 800 ppm) throughout the baseline period. RH within the office was close to the low end of the recommended range (40-60%) throughout both the baseline and intervention periods. RH levels increased in the summer months when indoor heating was used less.

4.1 Perceived productivity

The BUS survey (n: 69) provided a snapshot of occupant perception of their working environment during summer and winter and self-reported change in productivity. Occupants were asked "Please estimate how you think your productivity at work is decreased or increased by the environmental conditions in the building?", with responses on a scale from "-40% or less" to "+40% or more" in 10% increments. Occupants estimated that their productivity decreased by a mean of 5% due to the indoor environmental conditions. Interestingly when occupants perceived the environment to be uncomfortable (air quality, thermal comfort), their perceived productivity decreased (e.g. stuffy smelly air results in a decrease in perceived productivity).

PLEA 2018 HONG KONG

Smart and Healthy within the 2-degree Limit

The first round of the online (longitudinal) survey was conducted from 11 May to 24 May 2017 and the second round was from 11 July to 17 July 2017 (total n: 950). In both rounds, a link to the questionnaire was sent to the occupants three times a day. The responses were time stamped so concurrent indoor environmental measures could be identified. Thermal sensation votes, thermal preference votes, perceived air quality votes and overall comfort votes all received close to normal distributions. Notably, perceived air quality was slightly skewed toward stuffy rather than fresh, whereas overall comfort was slightly skewed towards comfortable rather than uncomfortable. As these surveys were investigating occupants' experience at a particular moment in time, the wording of the productivity question was adapted to "At present, please estimate how you think your productivity has decreased or increase by the environmental conditions in the building". The response scale was also adapted to be from "-20% or less" to "+20% or more" in 5% increments.

The following boxplots show visually the correlations between occupant perceptions of their environment and changes in their perceived productivity. About 73% of the responses were thermally comfortable (scoring 3-5 on the thermal sensation vote). When thermally comfortable, occupants perceived their productivity to be neutral (Fig. 2). At both ends of the scale, though more so at the warm end, occupants perceive their productivity to be reduced. Notably, occupants perceived their productivity to be more positively affected when they were comfortably cool than neutrally comfortable or comfortably warm.

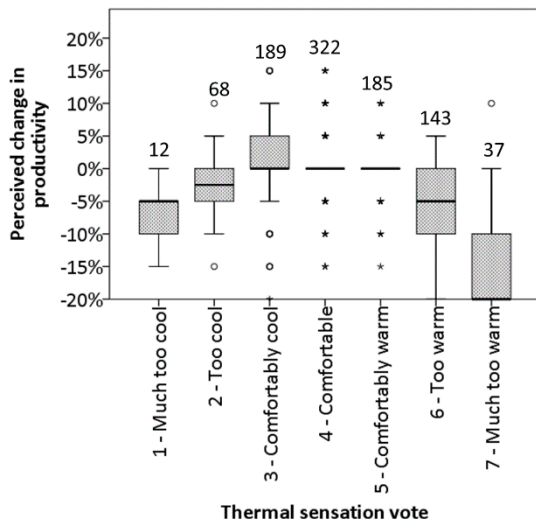


Figure 2: Baseline distribution of perceived change in productivity grouped by thermal sensation vote (with N shown). Note: Upper and lower quartiles for '4-Comfortable' and '5-Comfortably warm' were 0%

Similarly, the distribution of results for different thermal preference votes indicates that when

occupants would prefer to be much warmer or cooler, they perceive their productivity to be negatively affected (Fig. 3). 92% of responses voted neutral (a bit cooler, no change or a bit warmer).

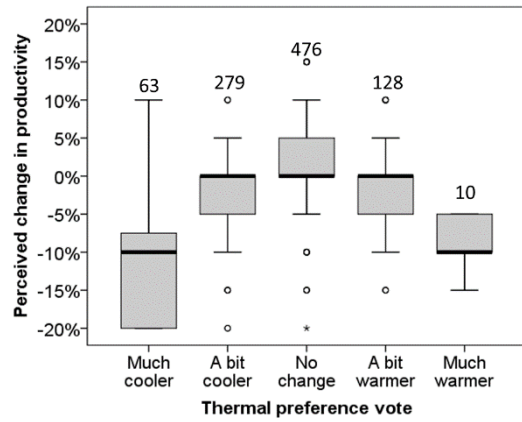
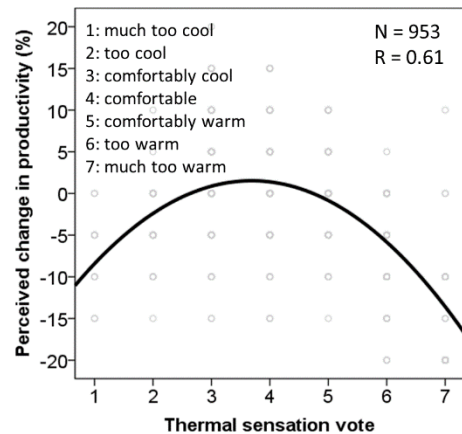


Figure 3: Baseline distribution of perceived change in productivity grouped by thermal preference vote (N shown for each vote)

Interestingly, occupants' perceived change in productivity had a stronger correlation with their thermal sensation votes (fig. 4) than with the measured indoor temperature. Indeed, statistical analysis of variance (comparing perceived change in productivity with measured temperature) indicated no statistical difference at the $p < 0.05$ level: the subjective thermal comfort of the occupants was more important in terms of perceived productivity than the objective temperature in which they were working. A temperature of 23°C, for example, was perceived by some occupants as being too warm and by others as being too cool. Thermal comfort depends on a combination of factors in addition to temperature, including RH and air movement. However, neither RH or air movement showed any statistically significant correlation with either thermal sensation votes or occupants' perceived change in productivity.



PLEA 2018 HONG KONG

Smart and Healthy within the 2-degree Limit

Figure 4: Scatter plot with quadratic trend line showing correlation between perceived change in productivity and thermal sensation vote.

The distribution of perceived change in productivity for different overall comfort votes (Fig. 5) showed that when respondents felt comfortable overall (voting 6 or 7) they perceived their productivity to be positively affected. A neutral perception of their change in productivity correlated with an overall comfort vote of 5. Overall comfort votes of 4 or lower correlated with an increasingly negative perception of change in productivity.

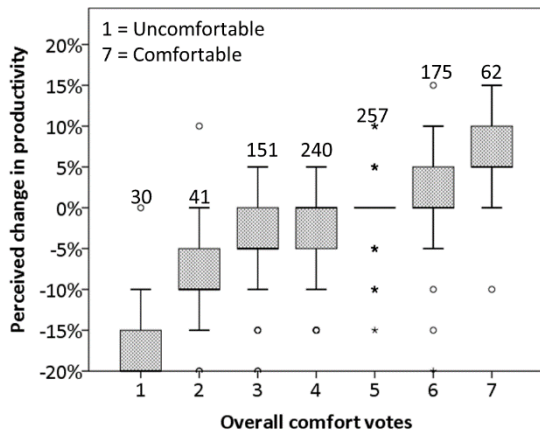


Figure 5: Baseline distribution of perceived change in productivity grouped by overall comfort vote (N shown for each vote) Note: Upper and lower quartiles for 5 were 0%

4.2 Measured productivity

The first round of the performance tasks was conducted from 5 June - 9 June, 2017 and the second round from 24 July - 28 July 2017 (total n: 285). As the tasks were time stamped, concurrent indoor conditions were recorded.

Indoor temperatures when tasks were conducted fell within a narrow band (predominantly 22-25°C), making it difficult to identify significant correlations. The direction of the trendline indicated that as indoor temperature increased, the proportion of correct answers decreased (Fig. 6). However, statistical analysis indicates this correlation is very weak and not statistically significant ($p > 0.05$).

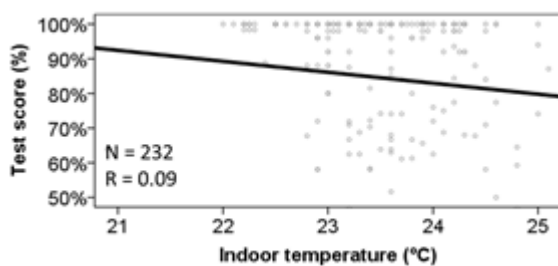


Figure 6: Scatterplot and linear trendline comparing scores from all baseline tests to concurrent indoor temperatures.

5. INTERVENTION PERIOD: RESULTS

Based on the findings from the baseline period, the BMS was used to control the temperature set-points (21.5°C, 22.0°C, 22.5°C and 23.0°C for each week) over a 4-week intervention period (23 Oct to 17 Nov 2017). During this period, online survey and performance tasks were repeated and time stamped.

5.1 Perceived productivity

The online (longitudinal) surveys were conducted three times a day on Mondays and Tuesdays. Responses indicated that the occupants were fairly satisfied with their thermal sensation (70% of thermal comfort responses voting neutral: 3-5) and with their thermal preference (91% of responses voting neutral: A bit warmer, no change or a bit cooler). Interestingly, these figures were slightly lower than the neutral responses at baseline (73% and 92% respectively). When occupants were thermally comfortable, they perceived their productivity to be unaffected, but when they were too cool or (more significantly) too warm, they perceived their productivity to be negatively affected. These results concurred with findings from the baseline study (Fig. 7).

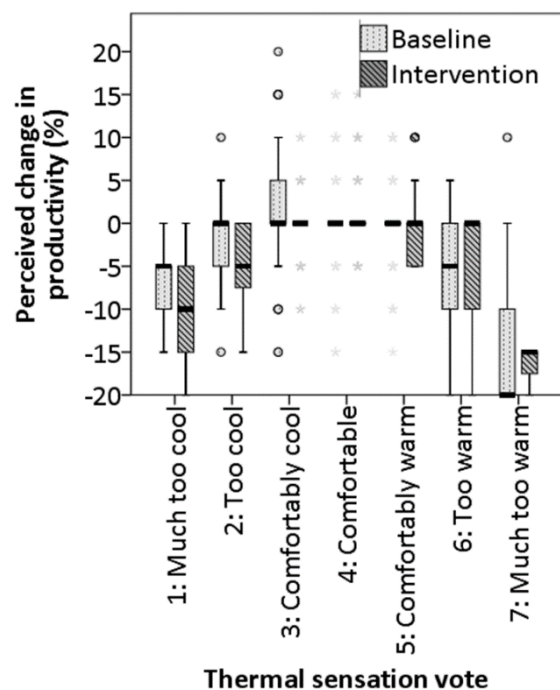


Figure 7: Baseline and intervention period distribution of perceived change in productivity grouped by thermal sensation vote (N shown for each vote). Note: Upper and lower quartiles for '3-Comfortably cool' and '4-Comfortable' were 0%.

PLEA 2018 HONG KONG

Smart and Healthy within the 2-degree Limit

Furthermore as thermal preference gets further from the neutral “no change”, the perceived change in productivity decreases. Again, these results concur with those in the baseline (Fig. 8).

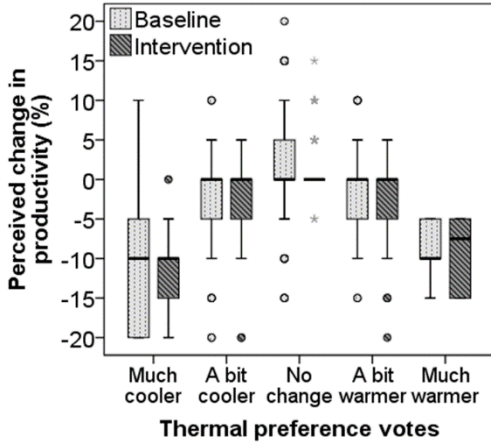


Figure 8: Baseline and intervention period distribution of perceived change in productivity grouped by thermal preference vote. Note: Upper and lower quartiles for intervention ‘No change’ were 0%

In summary, when comparing survey responses and the correlations between perceived change in productivity and the different environmental perceptions, the trends are very similar during the baseline and intervention periods.

5.2 Measured productivity

Online tasks were conducted twice daily from Wednesday to Friday during the intervention period, and were scheduled so that each type of task was conducted an equal number of times in the morning and afternoon to reduce any unintentional bias. As with the baseline, the indoor temperatures concurrent with the times the tasks were conducted covered a fairly narrow band (21-25°C). However, the intervention gave a more even spread of temperatures within this band. Again, the correlation between test scores and corresponding indoor temperatures was very weak ($R = 0.09$) and not statistically significant ($p > 0.05$). A stronger and more significant correlation was found between perceived productivity and thermal sensation vote (Fig. 9).

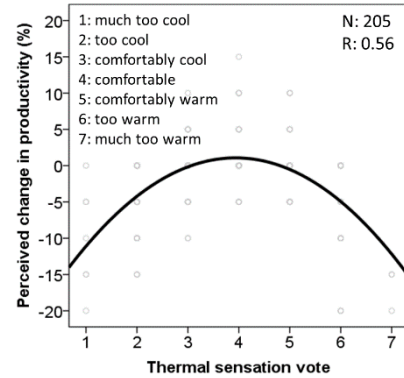


Figure 9: Scatterplot and quadratic trendline comparing perceived change in productivity to thermal sensation votes

Furthermore, when comparing test scores grouped by the concurrent levels of CO₂, it was evident that higher levels of CO₂ correlated with lower test scores, with the median score in the ‘1000-1200 ppm’ grouping 16% lower than the median score in the ‘less than 800 ppm’ grouping (Fig. 10 and table 1). Somers’ D test was run to determine the association between CO₂ concentration and test scores. The correlation was weak ($d = -0.16$) but statistically significant ($p = 0.03$). Although the recommended upper limit of CO₂ in offices is 1500 ppm in the UK, results from the study indicate that there may be productivity benefits to having CO₂ concentrations significantly lower than this.

Table 21: Descriptive statistics for intervention period test scores grouped by concurrent CO₂ concentrations

Statistic	Less than 800 ppm	800-1000 ppm	1000-1200 ppm
N	49	39	10
MEAN (%)	88	76	66
MEDIAN (%)	92	83	76
SD (%)	12	26	26
Q1 (%)	82	63	58
Q3 (%)	100	96	80

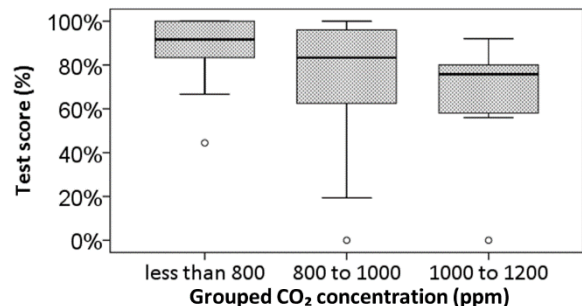


Figure 10: Boxplot showing intervention period distribution of test scores conducted within three bands of CO₂ concentration.

6. DISCUSSION

PLEA 2018 HONG KONG

Smart and Healthy within the 2-degree Limit

The present study has discovered interesting results through monitoring, surveys and tests in the case study, during the baseline and intervention periods. The workplace operated within fairly narrow bands of temperature (22-25 °C), RH (40-60 %) and CO₂ concentration (below 1200 ppm) for the majority of working hours. Consequently, correlations between measured indoor environment (particularly temperature and RH) and both perceived and measured productivity were very weak and not statistically significant.

Occupant feedback indicated that the majority of occupants were content with their indoor environment (thermal comfort, air quality, overall comfort). However, a significant proportion of occupants expressed discomfort due to feeling too cool, too warm, or the air feeling too stuffy. These responses corresponded to perceptions of productivity being decreased.

Stronger correlations were found between perceived changes in productivity and thermal sensation than actual measured temperature. Likewise, stronger correlations were found between perceived changes in productivity and perceived air quality than either measured RH or measured CO₂ concentration. These results indicate that how an occupant subjectively feels can have a greater impact on their perceived productivity than the objective environment they are in.

In addition to the perceived changes in productivity, measured changes in test score (used as a proxy for productivity) were observed which correlated with changes in the indoor environment. Both higher temperatures and higher CO₂ concentrations correlated with a decrease in average test score. Throughout the study, no statistically significant differences were found between gender (all surveys and tasks) or for respondents in different age categories (BUS survey).

7. CONCLUSION

This study has provided interesting results through continuous physical monitoring, surveys and performance tasks in a case-study working environment in the south of England.

Conducting this research in a real-world working office environment posed a number of challenges, particularly in terms of occupant engagement and data gathering. It also allows a great deal of 'noise' in the data, as a myriad of mitigating factors may influence the results.

Nevertheless, despite these challenges, this study has found empirical evidence that suggests elements of indoor environment (specifically CO₂ concentration) are related to workplace productivity, suggesting that by managing the indoor environment effectively, there is potential to improve productivity.

ACKNOWLEDGEMENTS

The authors would like to thank EPSRC (Grant ref: EP/N509000/1) and Innovate UK for funding the WLP+ research project. The authors are grateful to LCMB (lead industry partner) and NATS (project partner) for their efforts with occupant engagement.

REFERENCES

1. ONS (2018). International comparisons for UK productivity (ICP), final estimates: 2016. Available: <https://www.ons.gov.uk/economy/economicoutputandproductivity/productivitymeasures/bulletins/internationalcomparisonsofproductivityfinalestimates/2016> [25 May 2018]
2. BCO (2017). *Defining and measuring productivity in offices*.
3. BUS Methodology, [Online], Available: www.busmethodology.org.uk [9 Jan 2018]
4. CEN (2007). *Standard EN15251: Indoor environmental input parameters for design and assessment of energy performance of buildings addressing indoor air quality, thermal environment, lighting and acoustics*. Bruxelles: European committee for Standardisation.
5. Tham, K.W. (2004). *Effects of temperature and outdoor air supply rate on the performance of call center operators in the tropics*. *Indoor Air, Supplement*, 14(7), pp 119–125.
6. Fang, L. et al. (2004). *Impact of indoor air temperature and humidity in an office on perceived air quality, SBS symptoms and performance*. *Indoor Air*, 14(7), pp 74–81.
7. Lan, L. et al. (2011). *Effects of thermal discomfort in an office on perceived air quality, SBS symptoms, physiological responses, and human performance*. *Indoor Air*, 21(5), pp 376–390.
8. Al Horr, Y. et al. (2016). *Occupant productivity and office indoor environment quality: A review of the literature*. *Building and Environment*, 105, pp 369-389.
9. Seppänen, O. et al. (2006). *Effect of Temperature on Task Performance in Office Environment*. Lawrence Berkeley National Laboratory. [online] Available at: <https://indoor.lbl.gov/sites/all/files/lbnl-60946.pdf> [Accessed: 13th Dec. 2017].
10. Allen, J.G. et al. (2015). *Associations of Cognitive Function Scores with Carbon Dioxide, Ventilation, and Volatile Organic Compound Exposures in Office Workers: A Controlled Exposure Study of Green and Conventional Office Environments*. *Environmental Health Perspectives*, 124(6), pp 805-812. [Accessed: 13th Dec. 2017].
11. Satish, U. et al. (2012). *Is CO₂ an indoor pollutant? Direct effects of low-to-moderate CO₂ concentrations on human decision-making performance*. *Environmental Health Perspectives*, 120(12), pp 1671–1677.
12. Kajtár, L. et al. (2003). *Examination of influence of CO₂ concentration by scientific methods in the laboratory*. *Proceedings of Healthy Buildings*, 2003(3), pp 176-181.
13. Gupta, R. et al. (2016). *Desktop investigation to examine the relationship between indoor environmental conditions and productivity in work spaces*. SEEDS Proceedings 2016, pp 189-201
14. Korolija, I. et al (2013). *UK office buildings archetypal model as methodological approach in development of regression models for predicting building energy*

PLEA 2018 HONG KONG

Smart and Healthy within the 2-degree Limit

consumption from heating and cooling demands, Energy and Buildings, 60 (May 2013), pp 152-162.

The Impact of Urban Form on Summer Time Air Temperature and Energy Demand: A Case Study at Dhaka, Bangladesh

MD MASUDUL ISLAM¹

¹Bhumijo, Dhaka, Bangladesh

ABSTRACT: Cities are experiencing intensified urban heat island effect and rising energy demand because of urbanization. Dhaka, Bangladesh, is such an example with heat stress and energy crisis. This study investigates the role of different elements of urban form (vegetation, water body, building height and built-up area) in reducing urban energy demand by mitigating the urban heat island effect. First, two study sites were selected based on their land use; second, ENVI-met, a Computational Fluid Dynamics (CFD) tool was used to calculate localized air temperature; Onsite measurement was collected from one site to evaluate the simulation result; lastly, the energy simulation software UMI was used to simulate daily and hourly building energy use. The study results showed that vegetation, water body and building height can reduce the air temperature which can reduce the building cooling load during summer. Most significant cooling effect was observed because of vegetation by 1.22 C (maximum), which lowered the daily cooling energy load by 2.5%. On the other hand significant heating effect was observed because of increased built-up area by 1.54 C (maximum), which increased the daily cooling energy load by 5.38%. This research aims to facilitate environment sensitive planning and design in Bangladesh.

KEYWORDS: Urban heat island (UHI), Energy demand, Urban form

1. INTRODUCTION

In recent years, countries in hot-humid climate zones are experiencing rapid rates of urbanization (1). In less than sixty years (1950-2010), the hot – humid tropical region are transformed from predominantly rural to predominantly urban (1,2) while Europe took two hundred (mid 1700 to early 1900) years to do so (1, 3). This rapid urbanization has brought many changes in air and water quality and the microclimate (4). Many cities are transforming in natural vegetation and water bodies to create new site for development, which contributes to the urban heat island (UHI) effect (2, 5). Lack of water bodies and vegetation in urban areas reduces evapotranspiration and changes contributing to temperature increase in cities (5, 6, 7). As a result of increased heat cities are facing increased rate of energy consumption, compromised human health and comfort, and intensified carbon dioxide emissions (5). Increased urban temperatures have a direct effect of the energy consumption of buildings during the summer by increasing cooling load and proportion of carbon dioxide and other pollutants (8).

Until recently, changes in energy and human comfort caused by urbanization have received very little attention in urban design and urban planning practice in tropics where urbanization is at its peak. Policies and regulation for future development as well as modifications of current development should be formulated based on study of environmental impacts. The environmental performance should interact with technical, functional and economic reality, otherwise

environment sensitive design will be a failure (9). Dhaka, Bangladesh, is an example featuring unplanned rapid urbanization and various environmental problems including heat stress and energy demand. Taking this into account this study investigates the role of water bodies, vegetation and building form on summertime air temperature and energy demand. The key questions for the research are
What is the impact of different elements of urban form (vegetation, water body, building height and built-up area) on localized air temperature during summer?
What is the impact of localized air temperature on building cooling energy demand during summer?

2. METHODOLOGY

Two study sites were selected based on their land use, built form and growth pattern. The site at Gulshan, Dhaka (Site 01) is a commercial area with offices and shopping malls. Another site at Uttara, Dhaka (Site 02) is mainly a residential area beside a canal. ENVI met3.1, a Computational Fluid Dynamics (CFD) tool was used to simulate the impact of water body, vegetation, building height and density on summertime air temperature.

PLEA 2018 HONG KONG

Smart and Healthy within the 2-degree Limit

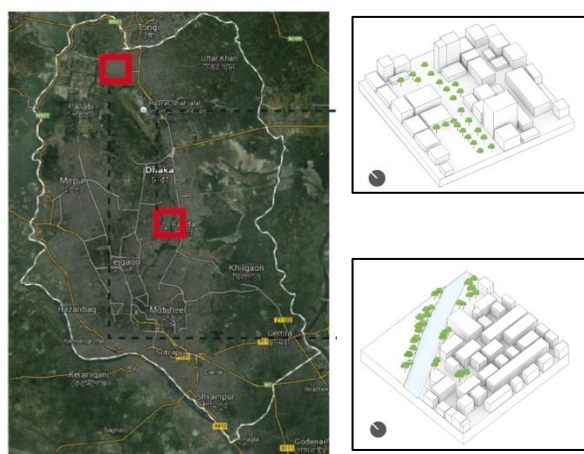


Figure 1: Study sites within Dhaka city

The first step in ENVI-met simulation is to create 3D model using ENVI met editor. The model with 225 m x 225 m area had 90 x 90 grid in xy direction with 2.5 m each grid for both sites. The z direction for site 02 had 20 grids with 2.5 m each while because of the higher building height site 01 had 28 grids with each 4m. To avoid calculation error at the boundaries of the model 6 nesting grid were used which added 67.5 m area to the model. The simulation was done using typical summer day using data from epw weather file. Simulation was done from 6:00 am – 21:00 (15 hours), but the data of 1st hour was not used to avoid error during initiation. Soil layer consisted of asphalt (for road), loamy soil, pavement and water. The cloud coverage was set to 0 in order to have the simulations in clear sunny day. To calculate the microclimate at any specific point several receptors were set.

To evaluate the ENVI-met simulation On-site measurements were collected at Uttara, Dhaka (Site 02) on May 27 (which can be considered as typical summer day). Using hygro thermometer the measurement was taken from 7:00 am to 21:00. The measuring device was placed at 15 m height outside of a building which is similar to the receptor position for simulation. On the day of onsite measurement, the sky was relatively clear and the average relative humidity was 61% which is close to the simulation condition (Humidity for simulation was 55%).

Based on the output data from Envi-met, energy simulation was done using UMI (Urban modelling Interface) to understand the impact of localized air temperature on cooling energy demand. Three scenarios were selected for building energy simulation, energy demand for 1) existing temperature, 2) reduced temperature and 3) increased temperature. A 3D model of 225 m x 225 m area for each site was created in Rhino. The basic epw file for Dhaka was downloaded from Energyplus website. All the building in both sites used the same building properties except building size and number of stories. ASHRAE 90.1 zone

5A as building template and 35% window/wall ratio was assigned. Shedding type for all faced was .5m overhang.

Parameters	Value	Source
Duration	14 hours	7:00 – 21:00
Wind Speed [m/s] (at 10 m ab. Ground)	2.6 m/s	Energyplus (epw)
Wind Direction (0:N..90:E..180:S..270:W)	180 °	Energyplus (epw)
Roughness Length z0 (at Reference Point)	0.1	ENVI met default
Initial Temperature Atmosphere [K] (at 2500 m height)	296.5	Laing, A., and J. L. Evans, 2011 (10)
Specific Humidity in 2500 m (g Water/kg air)	7	Laing, A., and J. L. Evans, 2011 (10)
Relative Humidity in 2m [%]	55	Energyplus (epw)
Temperature inside building (K)	293	ENVI met default
Heat Transmission Walls [W/m ² K]	1.94	ENVI met default
Heat Transmission Roofs [W/m ² K]	6	ENVI met default
Albedo Walls	0.2	ENVI met default
Albedo Roofs	0.3	ENVI met default

Figure 2: ENVI-met input data

3. RESULTS

3.1 Air Temperature

Simulation of localized air temperature in different scenarios using ENVI-met 3.1 was done to understand the impact of different variables like vegetation, water body, building height and built-up area on air temperature. This section first describes the results for the scenario with existing set-up (based on Google image and site observation), then the comparison of different scenarios with the existing set-up scenario has been discussed. After that comparison between all scenarios has been discussed to understand which variable has the most significant impact on temperature increase or decrease.

Scenario with Existing Urban Form

Site 01: Commercial area (Gulshan 01, Dhaka)

Figure 3 shows the existing urban form and air temperature profile of the area at 14:00 pm on the simulation day. The area was composed of primary (25m) and secondary streets running in north-south and east-west direction, building height varied from 54 m to 6m. Most of the buildings were used as commercial office spaces. Trees were present along main road and some of the empty plots. There was no existing water body in this area. The temperature map shows that the hotter zones were along the main road. The diurnal average temperature profile in Figure 4

PLEA 2018 HONG KONG

Smart and Healthy within the 2-degree Limit

shows that the temperature increases till 15:00 pm and starts decreasing afterwards.

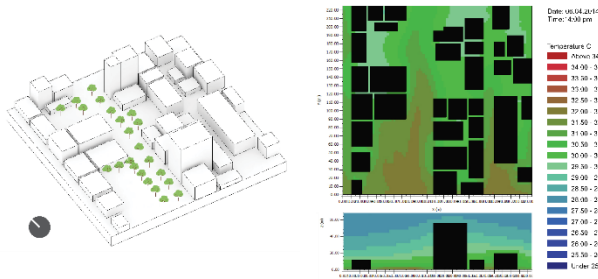


Figure 3: Existing urban form and air temperature (Site 01)

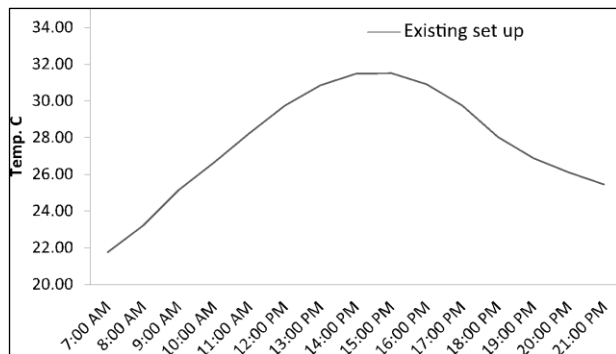


Figure 4: Existing simulated air temperature profile (Site 01)

Site 02: Residential area (Uttara, Dhaka)

Figure 5 shows the existing urban form and air temperature profile of the area at 14:00 pm on the simulation day. The area was composed of roads with an average width of 6 m running in north-south and east-west direction, building height varied from 24 m to 6m. Most of the buildings were used as residences. Northern part of the site was bounded by a 25 m wide lake. Trees were present along the existing water body and some of the empty plots. The temperature map shows that air temperature cooler above water and areas adjacent to water body. The temperature profile in Figure 6 shows that the temperature increases till 15:00 pm and starts decreasing afterwards.

Onsite measurement at site 02 (Uttara, Dhaka)

Figure 6 shows the comparison of simulation temperature and onsite measured temperature for site 02. At 7:00 am the onsite temperature was 30.2 C which has gradually increased till 16:00 pm reaching 35.9 C. After 16:00 pm the temperature decreases and reaches 33.1 at 21:00 pm. The average relative humidity has been observed 61%.

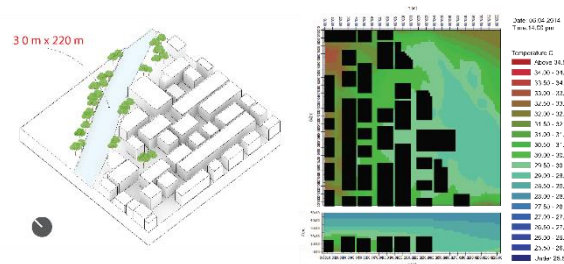


Figure 5: Existing urban form and air temperature (Site 02)

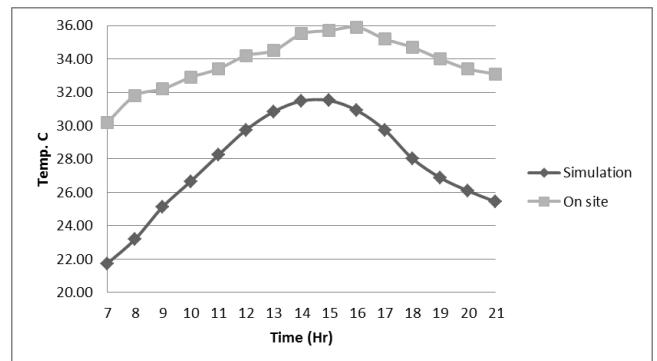


Figure 6: Existing simulated and onsite measurement air temperature profile (Site 02)

Site 01: Commercial area (Gulshan 01, Dhaka)

Scenario 1: Increased Vegetation

The amount of vegetation was increased at un-built plots of the study area. The amount of vegetation increase was 6% (3375 sq m) of the total area (50625 sq m). The result shows that air temperature was reduced all over the site because of additional vegetation cover. Areas with vegetation had more cooling effect. The cooling effect of vegetation gradually increased with time and the reduction of 1.22 C was observed at 16:00 pm. The cooling effect was also significant at night.

Scenario 2: Increased Water Body

Water bodies were created at some of the un-built plots. The total amount of area converted from loamy soil to water body was 3375 sq m, which is 6% of the total site. The result shows that air temperature was slightly reduced all over the site because of additional water body, but areas in close proximity to water showed more cooling effect. The temperature profile was similar with existing urban form. Temperature reduction of 0.1 C was observed at 15:00 pm which is not very significant.

Scenario 3: Increased Building Height

The existing urban form had building height of 54 m, 30 m, 18 m, 15 m, 10 m, 6 m, with height to width (H:W) ratio of maximum 1 : 2.5 and minimum 1:0.5. In the increased building height scenario all the building heights along the 25 m main road was increased to 54 m (H:W ratio of 1:0.5) and all the building heights along secondary road of 8m was increased to 30 m

PLEA 2018 HONG KONG

Smart and Healthy within the 2-degree Limit

(H:W ratio of 1:0.25).The result shows that air temperature was reduced all over the site because of increased building height. The decrease of temperature is mainly because of increased shadows casted by heightened buildings. The cooling effect of increased height gradually increased with time and the maximum reduction of 1.11 C was observed at 14:00 pm. The cooling effect was also significant at night.

Scenario 4: Increased Built-Up Area

The amount of built-up area was increased by removing the existing un-built plots and vegetation. The total site area covered by new buildings was 4,500 sq m, which is 10% of the total site area. All the new building heights along the main road was 54 m and along the secondary road was 30 m. The result shows that air temperature was increased all over the site because of additional built-up area cover. The area along the roads where most of the area was paved showed higher increase in temperature. The heating effect of increased built-up area started to increase form 7:00 am and during afternoon temperature increase rate was less. The maximum increase of 1.54 C was observed at 21:00 pm.

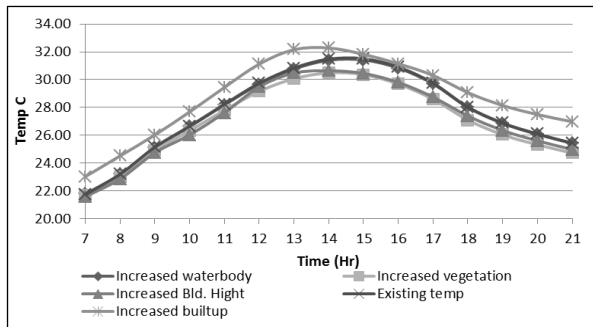


Figure 7: Comparison of average temperature profiles (Site 01)

Site 02: Residential area (Uttara, Dhaka)

Scenario 1: Increased Vegetation

The amount of vegetation was increased by removing the existing water body. The amount of vegetation increase was 10% (5500 sq m) of the total area (50625 sq m). The result shows that air temperature was reduced all over the site because of additional vegetation cover. Areas with vegetation had more cooling effect. The cooling effect of vegetation gradually increased with time and the reduction of 0.72 C was observed at 16:00 pm. The cooling effect was also significant at night time. The cooling effect was less than the cooling effect of site 01 because of the reduction of the water body.

Scenario 2: Increased Water Body

The amount of water body was increased by removing the existing vegetation along the northern edge of the existing water body. The existing water body with 30

m width was increased to 50 m. The total additional area converted to water body was 4000 sq m which is 8% of the total area. The amount of vegetation cover reduce was 8% of the total site. The result shows that air temperature was only reduced above the water body. The average diurnal temperature was slightly increased in this scenario. The reduction of vegetation might be the reason for this.

Scenario 3: Increased Building Height

The existing urban form had building height of 24 m, 21 m, 18 m, 15 m, 9 m and 6 m with height to width (H:W) ratio of maximum 1 : 1 and minimum 1:0.25. In the increased building height scenario all the building heights was increased to 24 m (H:W ratio of 1:0.25). The result shows that air temperature was reduced all over the site because of increased building height. The decrease of temperature is mainly because of increased shadows casted by heightened buildings. The cooling effect of increased height gradually increased with time and the maximum reduction of 0.75 C was observed at 14:00 pm. The cooling effect was not significant at night.

Scenario 4: Increased Built-Up Area

The amount of built-up area was increased by removing the existing un-built area, water body area and vegetation cover. The total site area covered by new buildings was 10,000 sq m, which is 20% of the total site area. All the new building was 24 m. The result shows that air temperature was increased all over the site because of additional built-up area cover. The heating effect of increased built-up area started to increase form 7:00 am and during afternoon temperature increase rate was less. The maximum increase of 1.25 C was observed at 19:00 pm.

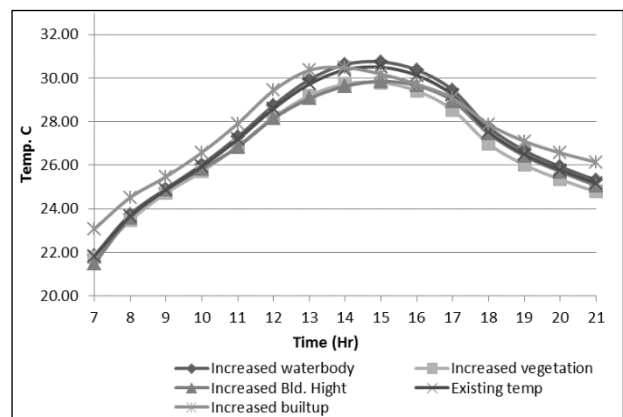


Figure 8: Comparison of average temperature profiles (Site 02)

3.2 Building Energy Demand

Building energy simulation using UMI (Urban modelling Interface), was carried out to understand the impact of localized air temperature on cooling

PLEA 2018 HONG KONG

Smart and Healthy within the 2-degree Limit

energy demand of building. Based on the output data from Envi-met simulation three scenarios were selected for building energy simulation. The scenarios are building energy demand for cooling 1) existing air temperature, 2) reduced air temperature and 3) increased air temperature. ENVI met simulation showed that the increased vegetation had most significant impact on lowering the temperature for both sites. So for calculating the cooling load at reduced temperature the data of from increased vegetation was used to modify the epw file. Similarly ENVI met simulation showed that the increased built-up area had most significant impact on increasing the temperature for both sites. So for calculating the cooling load at increased temperature the data of from increased built-up area was used to modify the epw file.

Site 01: Commercial area (Gulshan 01, Dhaka)

Total 25 buildings were simulated. Default shading search of 125 m was used to cover all the buildings within simulation boundary (225 m x 225 m). For increased temperature the total cooling load for all 25 building was increased from 18126 Kwh (for exg temp.) to 19102 Kwh (for heigh temp.). The amount of increased temperature was 976 Kwh, which is 5.38% higher than energy use during existing temperature. For reduced temperature the total cooling load for all 25 building was decreased from 18126 Kwh (for exg temp.) to 17666 Kwh (for heigh temp.). The amount of increased temperature was 460 Kwh, which is 2.5% lower than energy use during existing temperature.

Site 02: Residential area (Uttara, Dhaka)

Total 38 buildings were simulated. Default shading search of 125 m was used to cover all the buildings within simulation boundary (225 m x 225 m). For increased temperature the total cooling load for all 38 building was increased from 15688 Kwh (for exg temp.) to 16299 Kwh (for heigh temp.). The amount of increased temperature was 611 Kwh, which is 3.80% higher than energy use during existing temperature. For reduced temperature the total cooling load for all 38 building was decreased from 15688 Kwh (for exg temp.) to 15301 Kwh (for heigh temp.). The amount of increased temperature was 387 Kwh, which is 2.5% lower than energy use during existing temperature.

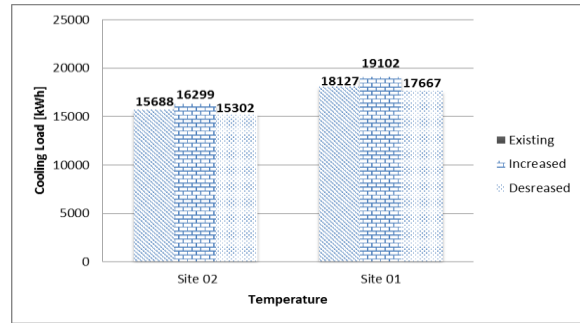


Figure 9: Comparison of cooling load for increased and decreased temperature scenario (Site 01 and 02)

3. DISCUSSIONS

The onsite measurement was taken at site 02 during a hot summer day with a similar humidity and sky cover condition of simulation. The highest temperature of 35.9 C has been observed at 16:00 pm and the lowest was 30.2 C at 7:00 am. An average temperature difference of 6 C has been observed between the simulation temperature and onsite temperature. But both the simulation and the onsite measurement temperature profile showed similarity.

Simulation creating scenario was done to understand the impact of different elements of urban form (vegetation, water body, building height and built-up area) on localized air temperature during summer. Because of increased vegetation air temperature was reduced in both the sites, but at site 01 (Commercial area) the cooling effect was more significant than site 02(residential area). The cooling effect gradually increased with time and was also significant at night time. At site 01, an increase of 6% vegetation caused the maximum temperature reduction of 1.22 C at 16:00 pm, while at site 02 an increase of 10% vegetation caused the maximum temperature reduction of 0.72 C at 16:00 pm. Because of increased water body air temperature was not changed significantly at any site, but the areas above water body and very close to water body was cooler than other areas. The diurnal temperature profile was similar with existing urban form. At site 01, an increase of 6% water body area caused the maximum temperature reduction of 0.1 C at 15:00 pm, while at site 02 an increase of 8% water body caused no temperature reduction. It should be considered that 8% vegetated area was reduced at site 02 which may have influenced the cooling effect. Another possible reason of less cooling effect of water body at both the sites may have caused because of the underestimation of evaporative cooling by water body in ENVI-met simulation process. Because of increased building height, air temperature was reduced in both the sites, but at site 01 the cooling effect was more significant than site 02. The cooling effect gradually increased with time and was also significant at night time. At site 01, an increase of building height caused the maximum temperature reduction of 1.11 C at 14:00 pm, while at

PLEA 2018 HONG KONG

Smart and Healthy within the 2-degree Limit

site 02 the maximum temperature reduction was 0.75 C at 14:00 pm. It should be considered that, ENVI-met simulation was unable to calculate the anthropogenic heat gain because of increased number of floors. So, the actual cooling effect because of increased building height might be less in reality. Because of increased built-up area air temperature was increased in both the sites, but at site 01 the heating effect was more significant than site 02. The heating effect started to increase from 7:00 am and during afternoon temperature increase rate was less, which went higher again at night. At site 01, an increase of 10% built-up area caused the maximum temperature increase of 1.54 C at 21:00 pm, while at site 02 an increase of 20% built-up area caused the maximum temperature increase of 1.25 C at 19:00 pm. It should be considered that, ENVI-met simulation was unable to calculate the anthropogenic heat gain because of increased number of buildings. So, the actual increase would be higher. The temperature increase caused by 10% increase in built-up area, increased the daily cooling load by 5.38% (976 Kwh extra need because of the same number of buildings) for site 01 while for the other site 20% increase of built-up area, increased it by 3.80% (611 Kwh extra need because of the same number of buildings). The daily cooling energy load was reduced because of decreased air temperature for both sites. The temperature decrease caused by 6% increase in vegetation area, decreased the daily cooling load by 2.5% (460 Kwh saving/day) for site 01 while for the other site 10% increase of built-up area, increased it by 2.5% (387 Kwh saving/day).

4. CONCLUSION

The simulation study results showed that vegetation, water body and building height could reduce the air temperature, which can reduce the building-cooling load during summer. The comparison between simulated temperature and the onsite measured temperature showed similar profile with consistent temperature difference. Therefore, it can be argued that the impact result from simulation will be close to real condition. Most significant cooling effect was observed because of vegetation by 1.22 C (maximum), which lowered the daily cooling energy load by 2.5%. On the other hand significant heating effect was observed because of increased built-up area by 1.54 C (maximum), which increased the daily cooling energy load by 5.38%. ENVI-met 3.1 considered water bodies as a type of soil, and the processes are limited to the transmission and absorption of shortwave radiation (11). It also considers as a still body without water turbulence mixing. Anthropogenic heat gain was not considered in ENVI-met3.1. These may have contributed to some limitations in understanding, many of which have been improved at updated version of the software. With the economic growth,

Bangladesh is having a rapid urbanization. The outcome of the work can inform the planning, design and development practice of the country.

REFERENCES

1. Emmanuel, M. R. (2005). An urban approach to climate-sensitive design: strategies for the tropics: Taylor & Francis.
2. Jauregui, E. (1997). Heat island development in Mexico City. *Atmospheric Environment*, 31(22), 3821-3831.
3. Landsberg, H. E. (1981). *The urban climate* (Vol. 28): Academic press.
4. Oke, T. R. (1987). *Boundary layer climates* (Vol. 5): Psychology Press.
5. Sun, R., & Chen, L. (2012a). How can urban water bodies be designed for climate adaptation? *Landscape and Urban Planning*, 105(1-2), 27-33. doi: 10.1016/j.landurbplan.2011.11.018
6. Patz, J. A., Campbell-Lendrum, D., Holloway, T., & Foley, J. A. (2005). Impact of regional climate change on human health. *Nature*, 438(7066), 310-317.
7. Patz, J. A., Campbell-Lendrum, D., Holloway, T., & Foley, J. A. (2005). Impact of regional climate change on human health. *Nature*, 438(7066), 310-317.
8. Santamouris, M. (2001). *Energy and climate in the urban built environment*. London: James and James Science Publishers.
9. Lippiatt, B. (1998). Building for environmental and economic sustainability (BEES). Paper presented at the Construction and the environment, CIB World Congress on, in Gävle, Sweden June.
10. Laing, A. and Evans, J.L. (2011). Introduction to tropical meteorology. Educational material from The COMET Program.
11. Bruse, M., (2007). Particle filtering capacity of urban vegetation: A microscale numerical approach. *Berliner Geographische Arbeiten*, 109, pp.61-70.

Effect of Intra-Climate Variation in Thermal Performance of Public Housing in a Composite Climate Of India

VAIBHAV GUPTA¹, KRISHAN UPADHYAY¹, RAJASEKAR ELANGO VAN¹, ASHOK KUMAR²

¹Indian Institute of Technology, Roorkee, India.

²Central Building Research Institute, Roorkee, India.

ABSTRACT: This paper deals with the effect of intra-climate diversity of composite climatic zone of India on the thermal performance of the naturally ventilated public housing buildings. This study is an attempt to improve the accuracy of the existing prescriptive benchmarks. The study has two objectives (a) to analyse the thermal severity variation within the composite climate of India and develop a tiered stratification of locations (b) analyse the impact of the thermal severity variation on the performance of representative public housing projects. The scope of the study is limited to naturally ventilated residential typology. Data for 162 locations were obtained from the Indian Meteorological Department (IMD) and statistically analysed in order to classify them based on thermal severities. A review of housing designs of low-income group housing being implemented by governmental agencies was reviewed and three representative designs are selected. A short-term thermal performance monitoring is conducted in these residences. The data is used to compare the thermal performance variations as well as to face validate the virtual models developed in Energy Plus software tool. The buildings are simulated for their performance at locations with high, moderate and low thermal severities within a composite climate zone. A comparative analysis is carried out with that of NBC prescribed thermal performance guidelines. A set of scaling factors is determined after performing local thermal optimizations at representative locations. The factors are validated with location-specific simulations performed for other locations.

KEYWORDS: Climate diversity, Composite Climate, Thermal Performance Index, Thermal Damping, Tropical Summer Index.

1. INTRODUCTION

This paper deals with the effect of intra-climate zone diversities on the thermal performance of public housing within the composite climate zone of India. According to the National Building Code of India, Indian climate has been divided into five major climate zones namely hot and dry, warm humid, temperate cold and a subgroup -composite climate zone. The composite climate zone is spread over 16 states and 2 union territories in India. Composite climate zone has been defined as a climate zone which does not receive any season more than 6 months[1]. NBC prescribes thermal performance benchmarks for building envelope for each climate zone. As the Composite climate zone is a sub group devised along with the climate zones, a common building regulation/standard cannot comply with different locations within it. A study by Rijildas and Rajasekar, 2016 show a significant variation in the energy consumption of buildings when constructed at different locations within the composite climate zone [2].

Thermal performance of buildings:

Thermal performance of the building is primarily driven by the climate and modulated by spatial design, thermo-physical properties of the building envelope and usage patterns[3]. It depends upon the wisdom of a designer to incorporate the climate responsive

features into the building at the design stage. However, the intra-climate zone variations within the composite climate pose a challenge in generalizing the potential strategies and their effectiveness. This study is an attempt to improve the accuracy of the existing prescriptive benchmarks. The study has three objectives (a) to analyse the thermal severity variation within the composite climate of India and develop a tiered stratification of locations (b) analyse the impact of the thermal severity variation on the performance of representative public housing projects. The scope of the study is limited to naturally ventilated residential typology.

2. METHODOLOGY

Meteorological data for 162 cities within composite climate zone of National Building Code, 2016[1] for a period of 30 years (1981-2010) was collected from Indian Meteorological Department (IMD), Pune and statistically analysed to classify them based upon thermal severities. A review of housing designs of economic weaker section (EWS) low-income group (LIG) and mid-income group (MIG) housing being implemented by governmental agencies were reviewed and three representative designs were selected respectively. A short-term thermal performance monitoring was conducted in these residences. The data was used to compare the

PLEA 2018 HONG KONG

Smart and Healthy within the 2-degree Limit

thermal performance variations as well as to face validate the virtual models developed in Energy Plus software tool. The thermal models of buildings were simulated for their performance at locations with high, moderate and low thermal severities within a composite climate zone. A comparative analysis was carried out with that of NBC prescribed thermal performance guidelines with existing cases. A set of scaling factors were determined after performing local thermal optimizations at representative locations. The factors were validated with location-specific simulations performed for other locations.

3. INTRA-CLIMATE DIVERSITY ASSESSMENT

To ascertain the Intra-climate diversity among the cities of composite climate, the meteorological data consisting of 98 percentile average maximum temperature for the Summer period (March, April, May, June, July), 98 percentile average minimum temperature for winter period (November, December, January, February) and annual average relative humidity was processed for this study.

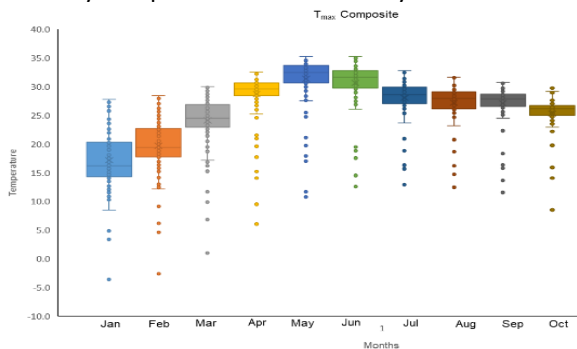


Figure 91: Box plot of Temperature Maximum for Composite Climatic Zone of India

In Figure 1, monthly variation within the zone is witnessed, the post-monsoon period is showing more variation in comparison to other seasons.

A statistical analysis of the IMD data enabled us to classify the cities. Three groups were formed namely G1 (>0.75) upper range, G2 (0.25-0.75) medium range, and G3 (<0.25) lower range (Table 1).

Table 22: Classification of the identified cities in the composite climatic zone of India.

Season	No. of cities	G1	G2	G3
Summer	162	72	34	26
Winter	162	62	42	28

Composite climate spans over 12 million square kilometres of area which is 36.5% of total geographic area of the country. The summer average maximum temperature ranges from 34.6 °C to 46.4 °C.

Also, the winter average minimum temperature ranges from -23.60 °C to 19.5 °C. The annual average

relative humidity ranges from 48% to 79%. The solar radiation intensity is very high in summer and low with predominantly diffuse radiation during monsoon.

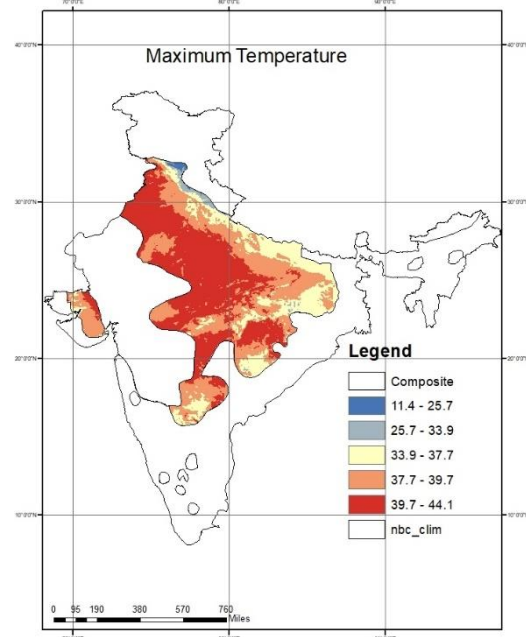


Figure 2: Summer average Maximum temperature (98 percentile)

The maximum daytime temperature usually ranges from 32 – 43°C and night time temperature ranges from 27 to 32°C in summers. Similarly, the daytime mean temperature ranges from 10 to 25°C and at night 4 to 10°C in winters.

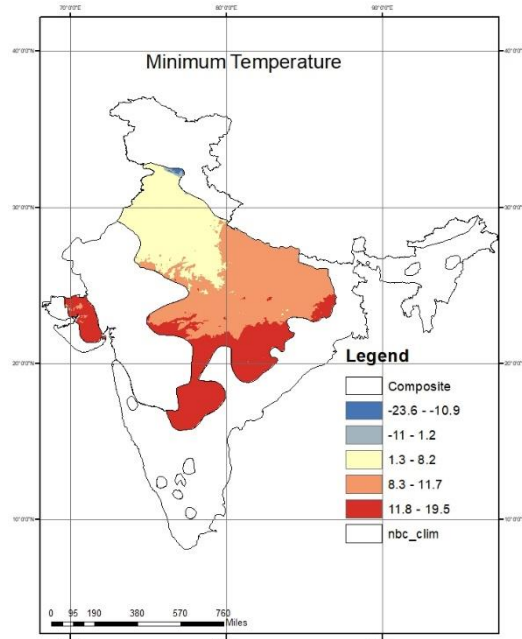


Figure 3: Winter average Minimum temperature (98 percentile)

PLEA 2018 HONG KONG

Smart and Healthy within the 2-degree Limit

Relative humidity varies around 20 – 25 % during the dry periods while in wet periods, it ranges from 55 – 95 %.

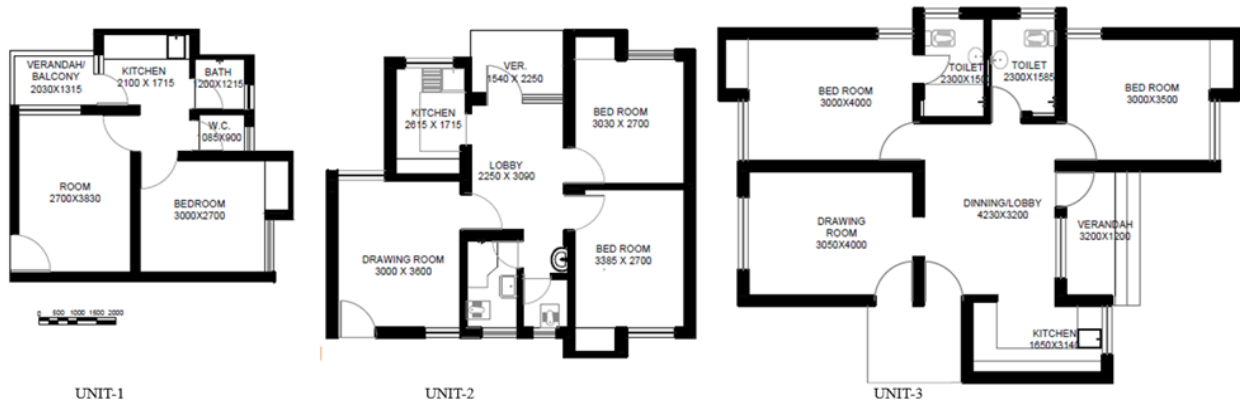


Figure 4: Representative Housing units (Source: UPPWD)

Figure 2, exhibits the variation of summer average maximum temperature range (98 percentile) by ArcGIS software, where the Punjab, Haryana, south-west Uttar Pradesh (Bundelkhand region) experiences most severe summers while cities like Dalhousie, Dharamshala, and Jammu experience comparatively comfortable summers whereas, the cities of southern India and Gujrat are relatively less warm than northern India.

Figure 3, exhibits the variation of winter average minimum temperature range (98 percentile) were Punjab, Himachal Pradesh, Haryana, Uttarakhand experience severe cold winters while southern India was relatively warm.

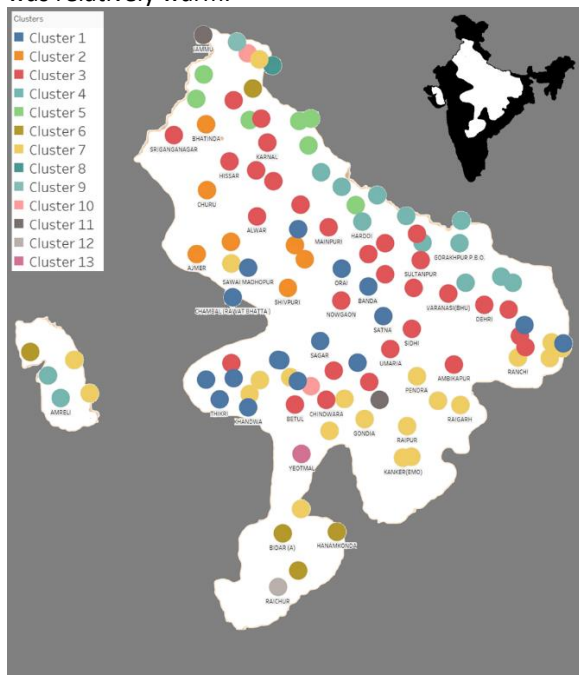


Figure 5: Cluster map for cities in Composite climate
The geospatial tool was used to classify the cities into 13 clusters[4] by applying K-means cluster analysis

method, inputs used for clustering were monthly temperature maximum and minimum data. Figure 5 shows that the cities within the same state exhibit regional scale climate diversity where cities form small pockets of similar climate characteristics.

Based on the above method, representative cities were identified as Agra, Lucknow and Gorakhpur in the Composite climatic zone which represent each group respectively.

Selection of Representative Housing Typology

A total of 57 building designs from Central Public Works Department (CPWD), Uttar Pradesh Public Works Department (UPPWD), and Uttar Pradesh Awam Vikas Parishad were studied. This sample included Type-1 housing for the Economic weaker section (EWS), Type-2 housing for Low Income Group (LIG) and Type-3 housing for Medium Income Group (MIG). The sample also included designs ranging from G+2 to G+13, constructed within the composite climate zone of India.

4. EVALUATION OF THERMAL PERFORMANCE

Real-Time field data collection

UNI-T 330B humidity/ temperature data logger was calibrated to record data at an interval of 10 minutes and placed inside the respective spaces[5]. It can record the temperature for a range of -40°C ~ 80°C, with accuracy of ±1°C (-30°C ~ 0°C, 40°C ~ 70°C) and relative humidity for a range of 0% ~ 100%, with accuracy of ± 5% (0%~20%, 80%~100%).

The data was recorded in the month of April (16th April to 23 April) which represent a typical summer day.

PLEA 2018 HONG KONG

Smart and Healthy within the 2-degree Limit

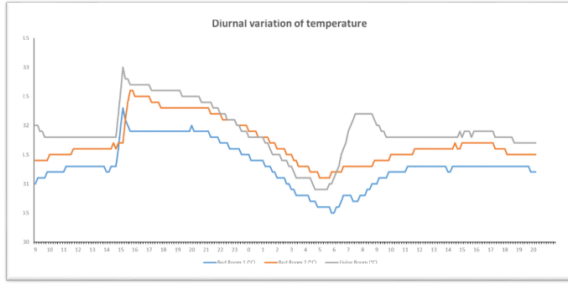


Figure 6: Diurnal variation of ambient temperature (Bedrooms, Apartment 1) for different units in Lucknow.

Temperature and Relative Humidity data are measured for two apartments for the duration of one day, for apartment no. 1 (Figure 6), peak temperature for bedroom 1 is 32.3 degrees C and lowest temperature is 30.5 degrees C, the time lag for bedroom 1 is 14 hours. Peak temperature for bedroom 2 is 32.6 degrees C and lowest temperature is 30.5 degrees C, the time lag for bedroom 2 is 13 hours. Peak temperature for the Living room is 33 degrees C and lowest temperature is 30.9 degrees C, the time lag for the living room is 14 hours.

Comparison of Real-time data

In figure 7, the graph show comparison of real-time recorded data and simulation data variation in indoor air temperature of dwelling unit type- 3 among the three cities Agra, Gorakhpur and Lucknow.

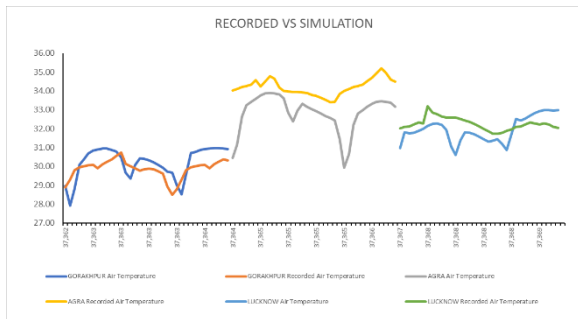


Figure 7: Master Bedroom- comparison of indoor air temperature.

The accuracy of the thermal model is $\pm 0.81^{\circ}\text{C}$ in Gorakhpur, $\pm 0.93^{\circ}\text{C}$ in Agra and $\pm 0.96^{\circ}\text{C}$ in Lucknow. Both the simulation as well as real-time data shows variations in the thermal performance of similar residential buildings for Gorakhpur, Agra and Lucknow which are different cities of Uttar Pradesh.

Comparison of thermal performance

Thermal performance Index (TPI) Thermal damping (D) and Tropical Summer Index (TSI) was calculated for each apartment unit type using weather file of Agra, Gorakhpur and Lucknow city.

Thermal Performance Index (TPI) is an indicator of the relative thermal performance rating of the

structure[6], TPI value $>75-125<$ is considered as acceptable.

$$\text{TPI} = (\text{Tis} - 30) / 8 * 100$$

where Tis is inside temperature range in $^{\circ}\text{C}$

TPI values compared in terms of cities have shown that Lucknow is exhibiting a better TPI and Agra is showing higher values than acceptable range. In terms of orientation, the south façade is showing better results than west façade.

Table 23: Thermal performance index and Thermal damping values for different spaces

		THERMAL PERFORMANCE INDEX			THERMAL DAMPING
		Space	SOUTH FAÇADE	WEST FAÇADE	
AGRA	UNIT-1	LIVING	151	152	52
		BEDROOM	147	160	45
	UNIT-2	LIVING	151	152	46
		BEDROOM	160	160	44
	UNIT-3	LIVING	159	173	46
		BEDROOM	157	170	48
GORAKHPUR	UNIT-1	LIVING	127	125	60
		BEDROOM	128	141	63
	UNIT-2	LIVING	141	154	54
		BEDROOM	138	138	61
	UNIT-3	LIVING	140	153	56
		BEDROOM	137	150	60
LUCKNOW	UNIT-1	LIVING	88	88	73
		BEDROOM	89	101	66
	UNIT-2	LIVING	100	152	69
		BEDROOM	100	99	63
	UNIT-3	LIVING	101	119	66
		BEDROOM	97	110	70

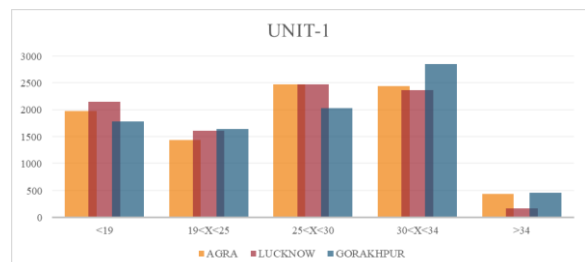


Figure 8: Annual comfort & Discomfort hours based on Tropical Summer Index

Thermal damping (D) is the decreased temperature variation; it is a characteristic dependent on the thermal resistance of the materials used in the structure[6].

$$D = ((\text{Tout} - \text{Tin})) / \text{Tout} * 100$$

PLEA 2018 HONG KONG

Smart and Healthy within the 2-degree Limit

Lowest 'D' is exhibited by Unit 2 Bedroom in Agra (Table 2), and highest value is exhibited by Unit 1 living room in Lucknow.

Tropical summer index was calculated for each dwelling unit in Agra, Lucknow and Gorakhpur respectively. The comfort and discomfort hours were calculated based upon the comfort and discomfort range mentioned in IS: SP: 41 (1987) i.e.- <19°C represent cold discomfort, ≥19°C & <25°C represent slightly cold, ≥25°C & <30°C represent comfort range and 27.5°C comfort temperature, ≥30°C & <34°C represent slightly warm and lastly, >34°C represent heat discomfort[6].

$$TSI = 0.308 T_w + 0.745 T_g - 0.206 \sqrt{V} + 0.841$$

where, T_w is wet bulb temperature in °C, T_g is globe temperature in °C and V is wind speed in m/s.

In figure 8, the graph shows maximum cold discomfort hours in dwelling unit-1 in Lucknow followed by Agra and Gorakhpur. While maximum heat discomfort hours in Gorakhpur followed by Agra and Lucknow. Maximum comfort hours were found in Agra followed by Lucknow and Gorakhpur. The graph also shows almost 24 days in a year experience hot as the TSI exceeds 34°C.

Comparison of Real-time data and validation of the virtual model

For validation purpose, 3000X3000X3200 sized bedroom was modelled resembling identified unit's bedroom using 230 mm thick brick wall and simulated using Energy Plus software to validate the field results.

Table 24: Variation in Thermal performance

Variables	Agra	Lucknow	Gorakhpur
T_{min}	5%	8%	-9%
T_{max}	7%	4%	26%
Difference	10%	-2%	47%

The accuracy of the virtual thermal model is ±0.81°C in Gorakhpur, ±0.93°C in Agra and ±0.96°C in Lucknow. Both the simulation as well as real-time data shows variations in the thermal performance of similar residential buildings for Gorakhpur, Agra and Lucknow which are different cities of Uttar Pradesh.

5. OPTIMIZATION FOR LOCAL CONTEXT

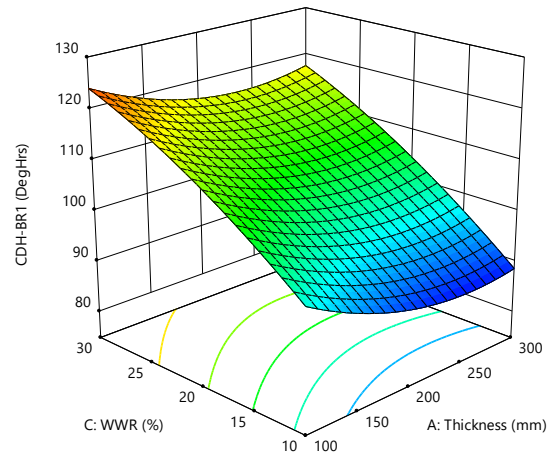


Figure 9: Optimization graph for Agra

In Agra, optimization suggests, optimum wall thickness to be 200 mm and 10 percent window to wall ratio (WWR) and cooling discomfort hours is 88 (deg. hours).

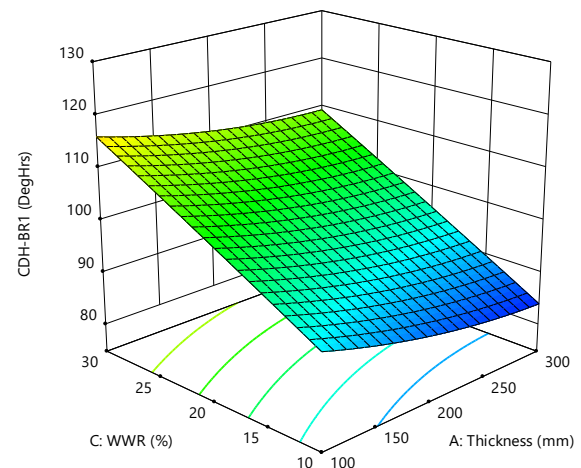


Figure 10: Optimization graph for Lucknow

In Lucknow, optimum wall thickness comes to be 300 mm and 10 percent window to wall ratio (WWR) and cooling discomfort hours is 85 (deg. hours).

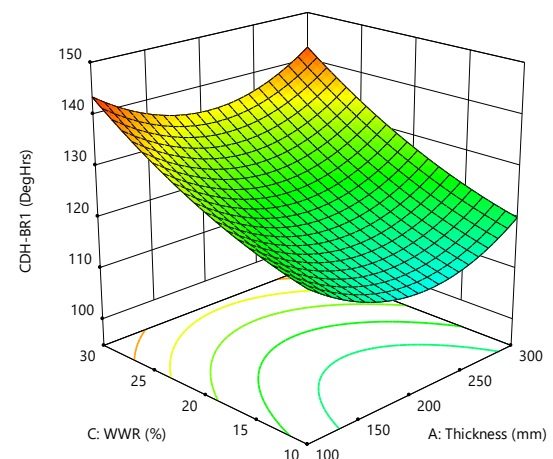


Figure 11: Optimization graph for Gorakhpur

PLEA 2018 HONG KONG

Smart and Healthy within the 2-degree Limit

In Gorakhpur, optimum wall thickness comes to be 300 mm and 10 per cent window to wall ratio (WWR) and cooling discomfort hours is 120 (deg. hours).

6. DISCUSSION AND CONCLUSION

Composite climate spread over 36.5% of the total geographic area of the country. Within the composite climate zone, summer average maximum temperature range has difference of 10 °C amongst the identified locations. Also, the winter average minimum temperature range have a difference of 30 °C and the annual average relative humidity range have a difference of 32% amongst the identified locations.

Statistical analysis of weather data obtained from Indian Meteorological Department shows that within composite climate, 13 clusters found of different climate severity.

Dwelling units' experience maximum heat discomfort during the month of May and June followed by April and July while the cold discomfort in January. Also, February and November were comfortable months for all the three cities.

Computational analysis showed a difference of 1°C and it goes up to 2.4°C in the internal temperature when simulated for different orientations. Also, within a dwelling unit, internal spaces towards the corridor/ staircase/ lift lobby experience less heating discomfort in comparison to the spaces with exposed walls.

Comparison of real-time data showed that the dwelling units' experience different thermal discomfort in Agra, Lucknow and Gorakhpur. This proves the hypothesis of having a difference in thermal performance of public housing when constructed at a different location within a composite climate zone. Also, validate the statistical analysis for different thermal severity. Comparison of computational analysis data shows extreme heat and cold discomfort in Gorakhpur followed by Lucknow and Agra respectively.

The results of the pilot study revealed that the composite climate could be further subdivided according to the clusters as cities in the same region exhibit the similar climate characteristics.

ACKNOWLEDGEMENT

We offer our sincere appreciation for assistance in grant to the IIT Roorkee and CBRI Roorkee from Indo-US Science & Technology Forum (Project no. IFU-1047-APD). We are also thankful to the Indian Meteorological Department (IMD) Pune, for providing the climatological data.

REFERENCES

Bureau of Indian Standards, "National Building Code of India 2016," vol. 1, 2016.

T. V Rijildas and E. Rajasekar, "Effect of location specific climatic diversities on comfort and energy consumption: A study on India's composite climate zone," *Mak. Comf. Relev.*, no. April, pp. 7–10, 2016.

E. Rajasekar, A. Udaykumar, R. Soumya, and R. Venkateswaran, "Towards dynamic thermal performance benchmarks for naturally ventilated buildings in a hot-dry climate," *Build. Environ.*, vol. 88, pp. 129–141, 2015.

R. G. Fovell and M. Y. C. Fovell, "Climate zones of the conterminous United States defined using cluster analysis," *Journal of Climate*, vol. 6, no. 11. pp. 2103–2135, 1993.

UNI-T, "UT330A.B.C.pdf." .

BIS, "SP 41 (1987) Handbook on Functional Requirements of Buildings (Other than Industrial Buildings)," 1987.

Assessing the Glare Potential of Complex Fenestration Systems: A Heuristic Approach Based on Spatial and Time Sampling.

Luis Santos¹, Luisa Caldas²

¹ UC Berkeley, Center for the Built Environment, United States of America

² UC Berkeley, College of Environmental Design, Department of Architecture, Lawrence Berkeley National Laboratory, USA

ABSTRACT: This paper proposes a new heuristic to simulate and study the visual comfort aspect in the designing of Complex Fenestration Systems. The goal of the heuristic is two-folded, (i) provide useful and simple visualization tools for preliminary glare assessments of indoor spaces, (ii) reduce the computational overhead of extremely expensive annual glare simulations by reducing the number of simulations necessary in the study of glare. The work demonstrates that through a spatial and temporal sampling of annual Vertical Illuminance data it is possible to map the potential glare POVs and to find the critical hours to conduct more detailed simulations. The authors applied the proposed heuristic in a comparative study of 3 different fenestration schemes for 3 annual sky types, a typically overcast (London, UK) and clear sky (Phoenix, AZ, USA), and an intermediate sky (Oakland, CA, USA). In sum, the results of the work show that the proposed heuristic yields a high potential to be used in design procedures that currently are based on expensive glare simulations.

KEYWORDS: Glare Simulation, Visual Comfort, Daylight Performance, Complex Fenestration Systems

1. INTRODUCTION

The main purpose of Light-redirecting Complex Fenestration Systems (LRCFS) is to redirect and evenly distribute daylight in deep plans. However, most of LRCFS are highly specular, yielding thus a high visual discomfort risk. Designers use climate-based daylight modeling (CBDM) to simulate the daylight performance of LRCFS. To study annual horizontal illuminance (E_h) of LRCFS different metrics such as Daylight Autonomy (DA), Spatial Daylight Autonomy (sDA), Annual Sun Exposure (ASE) [1], and Useful Daylight Illuminance (UDI) [2] have been proposed along with specific modeling methods. Regarding annual visual comfort, the most refined assessment method consists in calculating the Daylight Glare Probability index (DGP) by analyzing a time series of High Dynamic Range (HDR) images with evalglare [3]. Albeit annual DGP (aDGP) fully addresses the temporal aspect of the phenomenon it still holds a considerable computational overhead. Glare simulations also depend on location and on point-of-view (POV), posing thus a more intricate spatial problem when compared with E_h simulations. In sum, the simulation and assessment of visual comfort based on glare simulations still poses the following challenging question: *When (if representative point-in-time simulations are desired to replace aDGP), where, and where to look at?*

The work presented in this paper proposes a new heuristic approach based on the relation between glare and vertical illuminance at the eye level (E_v)

reported in [4]. The heuristic samples annual E_v results in different locations with the goal of describing the annual visual discomfort potential of a space without the use of expensive aDGP simulations.

A computational tool implements the heuristic to both display preliminary visual comfort information and automatically provide the necessary information to conduct more detailed and accurate point-time DGP simulations for the most critical POVs and hours.

Although the main object of the heuristic is LRCFS, the proposed computational tool is also able to assess the visual comfort of more common fenestration designs. This paper demonstrates the applicability of the tool in a simple scene with two windows facing South and West.

2. RELATED WORK

DGP was introduced by Weinold in [5] and it is the most advanced method available to assess visual comfort since it is able to cope with large glare sources such as the sun [6]. This was a considerable breakthrough because until then no glare metric was able to fully address the impact of direct daylight. Nevertheless, because DGP is based on the analysis of HDR images through evalglare, its use in simulation entails a considerable computational overhead since it requires the calculation of a full HDR image typically using Radiance [7].

To accelerate DGP simulations, a simplification was proposed under the name of DGPs [7]. DGPs is based on E_v but it assumes that no direct sun - or any specular

PLEA 2018 HONG KONG

Smart and Healthy within the 2-degree Limit

reflection of it - reaches the eye, thus, is not suitable in the glare assessment of either designs that are highly exposed to direct sun or of highly specular LRCFS. Despite this limitation, the experiments conducted by Wienold and Christoffersen [4] shows that an E_V threshold has potential to be used as a binary indicator for glare events but not to infer DGP levels. Recently, Jones and Reinhart [8] used Graphical Processing Unit (GPU) parallelization techniques to accelerate DGP simulations. Although the remarkable improvements in simulation time though GPU parallelization full aDGP simulations are still slow for parametric or metaheuristic-based optimization studies. This approach also limits designers and lighting analysts to use specific graphics cards.

Another way to study glare and visual comfort avoiding expensive DGP simulations is to correlate annual E_h metrics, such as UDI, with glare phenomena. However, there is no consensus about the use of UDI and its illuminance upper threshold as a proxy to glare and visual discomfort. Mardaljevic et al. [9] report some promising correlations between UDI and DGPs but because the study used DGPs a full correlation between E_h and DGP is hard to establish. In a field-based study, Konis [10] concludes that E_h is context specific and that it should be complemented with luminance-based metrics in visual comfort studies. Recently published work [11] shows that even with a conservative UDI overlit illuminance threshold (> 2000 lux), UDI is insufficient to fully assess the glare performance of a LRCFS corroborating, thus, the recommendations of [10]. ASE is another annual E_h based metric that is been used to assess visual discomfort potential. However, because it only contemplates direct light it falls short in assessing the glare performance of highly specular LRCFS.

Considering the limitations of the current metrics and simulation methods it is reasonable to assume that point-in-time DGP analyses at critical events is a suitable approach for quicker annual visual comfort evaluations. However, there are no guidelines on POV location and on hour-of-the-year (HOY) selection.

3. HYPOTHESIS AND RESEARCH GOALS

Based on the work of [4, 9] the main hypothesis is that it is possible to use annual E_V data for preliminary visual comfort assessments and to find events with high glare potential. To accomplish this the paper proposes a heuristic based both on time and spatial sampling. The main goal is to use a simpler and faster CBDM simulation (when compared with aDGP) to both indicate the POV and time periods that have a higher glare risk. The outcome is an interactive computational tool that samples, maps, and visualizes annual E_V data to provide a preliminary visual comfort performance assessments solution and to detect the relevant locations, POVs, and time events for full point-in-time

DGP simulations necessary in the assessment and optimization of LRCFS.

4. METHODS

The research entails 3 parts: 1) verification of annual E_V applicability to find time events that report glare; 2) development and implementation of the proposed heuristic; 3) application of the heuristic in 3 different experiments. The description and methods used in each part are summarized below.

4.1 Annual E_V as a tool to detect potential glare events

To test if E_V is able to capture glare events, based on [4] the authors set the E_V threshold to ≈ 2700 lux, to label an event as a potential glare one, and applied to a previous LRCFS study in [11]. The same study [11] [11] reports aDGP results for two locations; Phoenix (a tendentially clear annual sky) and London (a tendentially overcast annual sky). The investigated LRCFS was previously optimized for Daylight Factor (DF) and it is positioned on the top of the South Façade in a $4 \times 7.5 \times 3$ m test cell. The known aDGP results were compared with annual $E_V \geq 2700$ lux using the same POV, assumptions and simulation method, Radiance's 3-phase method [12]. Figure 1 and 2 compares the two metrics, aDGP and $E_V \geq 2700$ lux for Phoenix and London respectively. The top of both figures there is an aDGP heatmap, at the bottom a heatmap traces the events where $E_V \geq 2700$ lux, and the middle heatmap reports the error events, i.e. when $E_V \geq 2700$ lux missed to report glare events ($DGP \geq 0.35$). If we consider the whole year daylight period, $E_V \geq 2700$ lux matches the DGP results in 96% of the hours in both locations.

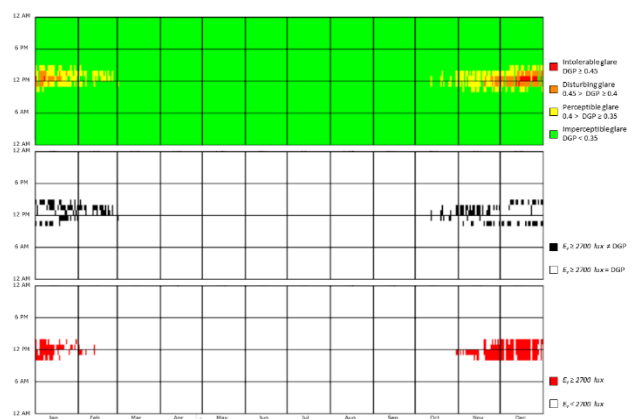


Figure 1: Comparison of DGP (top), $E_V \geq 2700$ lux (bottom), and error events of $E_V \geq 2700$ lux (middle) for the LRCFS reported in [11] under the annual Phoenix sky matrix.

PLEA 2018 HONG KONG

Smart and Healthy within the 2-degree Limit

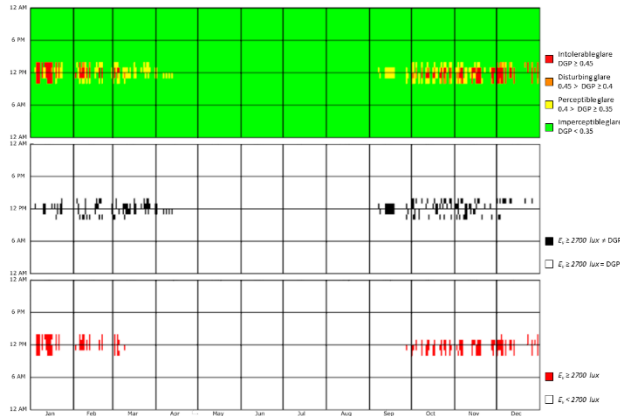


Figure 2: Comparison of DGP (top), $E_v \geq 2700$ lux (bottom), and error events of $E_v \geq 2700$ lux (middle) for the LRCFS *Lazy_S* reported in [11] under the annual London sky matrix.

However, a closer analysis of Figures 1 and 2 shows that $E_v \geq 2700$ lux simulation is more robust to predict disturbing and intolerable glare events. If we only consider the events that register $DGP \geq 0.35$, $E_v \geq 2700$ lux detects 47% of the events in Phoenix and 50.4% in London.

If we exclude the DGP events that reported perceptible glare ($0.4 > DGP \geq 0.35$), $E_v \geq 2700$ lux detects 92% of the events in Phoenix and 85% in London. In sum, although $E_v \geq 2700$ lux has difficulties to detect perceptible glare events, the results indicate that is possible to query annual E_v data for a heuristic that aims to select relevant to worst case scenarios events to conduct full point-in-time DGP simulations.

Heuristic description and implementation

The proposed heuristic encompasses 3 main phases: simulation, data post-processing, and data visualization and query. Each phase entails several tasks detailed below.

Simulation: (i) definition of an analysis sensor grid; (ii) for each point the heuristic considers an n ($n \geq 8 \wedge n \in \mathbb{N}$) cardinal-based POV; (iii) for each POV an annual E_v simulation is conducted.

Data post-processing: (iv) for each POV all the hours are labelled as susceptible to glare ($E_v \geq 2700$ lux) or non-susceptible to glare ($E_v < 2700$ lux). As mentioned above this threshold is based on field studies reported in [4] that showed a reasonable linear correlation between E_v and the percentage of disturbed persons ($R = 0.77$). The 2700 lux threshold corresponds to 35% of disturbed person, considering the linear regression presented in [4]. Based on the labelling, the procedure calculates the frequency of events susceptible to glare.

Data visualization and query: (v) in each point a radar graph displays the frequencies of events susceptible to glare of each direction for a specific period. By default, this period corresponds to the entire year, but it can be set to seasonally or monthly time intervals. This visualization indicates which are the POVs more

susceptible to glare. Although the user can visualize and query the data of each sensor the heuristic automatically selects the POVs with a frequency which deviation is within $\pm 10\%$ of the maximum frequency. (vi) Finally, in each grid point, the user can select any of the 8 POV to obtain feedback about the period that yields a higher glare potential. Once more, for each of the automatically selected POVs, the heuristic identifies by default which HOY should be used to conduct a full point-in-time DGP simulation by finding the hour that yields the highest E_v of the largest set of consecutive pair day/hour susceptible to glare.

The heuristic is implemented in Rhinoceros 3D/Grasshopper via Python programming language. The resulting system uses Radiance's 3-phase method to simulate annual E_v . The point-in-time DGP simulations for the selected samples resort to Radiance's *rpict* routine, to produce the hdr image, and to evalglare, to estimate the DGP. To ensure that the hdr image reflects the sky condition considered in the E_v calculation, the system uses Radiance's *gendaylit* subprogram to generate an accurate Perez all-weather sky given a specific hour, location, and Typical Meteorological Year (TMY) data.

4.3 Experiments

As a proof of concept, the authors tested the heuristic in a test cell that represents a hypothetical office room of a commercial building with a typical 5 x 7.5 m structural grid. The 9.8 x 7.2 x 2.7 m (Width x Length x Height) room faces both South and West. The South and the West façade have windows that start at 1.1 m height and stop at the ceiling. A six-point 4.2 x 3.2 x 1.5 m grid defines the spatial location of the different POVs. The sensor grid is centered relatively to the room and its spacing is based in a typical office layout. The system generated 8 POVs per point, each one facing a different cardinal direction. Table 1 describes the optical properties of the opaque surfaces of the test cell.

Table 1: Opaque surfaces properties of the test cell.

Surface	Reflectance
Ground	20%
Floor	40%
Ceiling	80%
Interior Walls	60%
Other	35%

Figure 3 describes the overall geometry of the test cell through two axonometries (SE and NW). Figure 4 shows the sensor grid overlaid over a hypothetical office furniture layout, in dashed line.

PLEA 2018 HONG KONG

Smart and Healthy within the 2-degree Limit

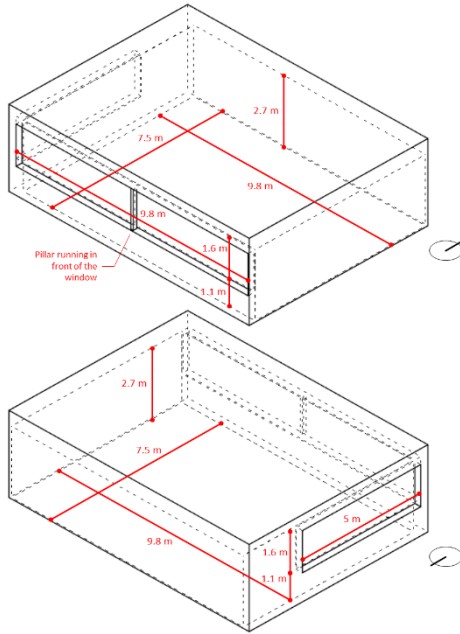


Figure 3: Test cell used in the experiments. Top: Southeast axonometry. Bottom: Northwest axonometry.

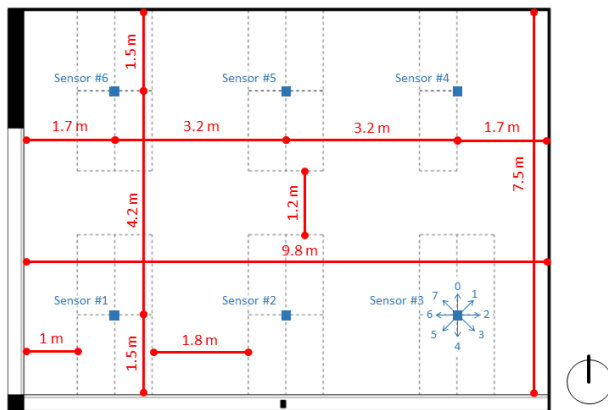


Figure 4: Sensor grid (in blue) and hypothetical room layout (in dashed line). Sensor 3 (bottom right) illustrates the 8 POV directions considered in each sensor.

The authors conduct 3 experiments using this office room model to compare 3 different fenestrations assemblies' schemes under 3 different annual sky conditions. The first fenestration scheme (Scheme #1) defines a baseline by resorting to a double clear glazing with a VT of 65%. Scheme #2 combines the double clear glazing (West window) with a glazing assembly based on a macroscopic LRCFS optimized for DF, illustrated in Figure 5, and described in [11] (South window). The LRCFS is a set of equally spaced highly specular/reflective blinds (99.3% of reflectance) placed between two clear glass panes (VT of 65%). The third fenestration scheme (Scheme #3) applies the LRCFS based glazing assembly to both windows. Experiment #1 compares the 3 schemes in a typical overcast annual sky condition represented by the TMY data of London, UK (Gatwick airport, latitude - 51.15° N, longitude - 0.18° E). Experiment #2 compares the

schemes in a typical annual clear sky, characterized by TMY data collected in Phoenix Sky Harbor International Airport, AZ, USA (33.45° N, 112° W). Finally, Experiment #3 conducts the comparison in an intermediate annual sky situation by using Oakland, CA, USA, TMY data (37.72° N, 122° W).

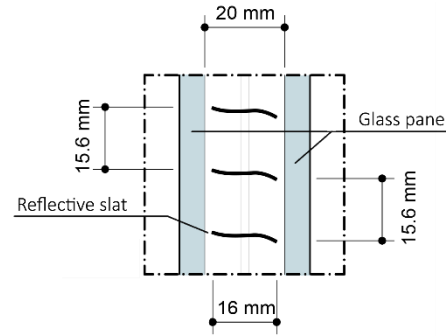


Figure 5: Section detail of the LRCFS used in this research and previously optimized in [11].

In each experiment the proposed heuristic runs a climate-based annual E_v , visualizes the frequency of events susceptible to glare per direction, selects the critical POV/HOY pairs, for the first row and second row of sensors separately, to then run a full DGP analysis. To better compare the results of each fenestration scheme, the proposed tool overlays the different radar graphs in each experiment.

The simulation parameters used in the 3-phase method annual simulations follow the LM-83 standard recommendations [1]: ambient bounces (-ab) is set to 6, ambient division (-ad) to 1000, and the direct threshold (-dt) to 0. With -dt equal to 0, Radiance is forced to test all light sources samples for shadow calculation [13]. The parameters of the DGP simulations are well above the commercial LRCFS recommendations [14]: -ab 6, -ad to 50,000.

5. RESULTS AND DISCUSSION

Figure 6, 7, and Table 2 present the results of the 3 experiments. Figure 6 shows the visualization output of the implemented heuristic, i.e. the radar graphs per sensor point mapping the frequency of the events susceptible to glare for each POV direction. The frequencies are normalized for the number of daylight hours: 4400 hours in London, 4399 hours in Phoenix, and 4392 hours in Oakland.

Table 2 presents a summary of the relevant information used by the proposed tool in selecting the POV/HOY pairs that yield high glare potential to then conduct a full point-in-time simulations. The last row of the table already shows the DGP results for each pair POV/HOY selected. Finally, Figure 7 assembles the images analyzed by evalglare, delivering information on the location of glare sources location, position of the circumsolar region, reflections, and other details.

PLEA 2018 HONG KONG

Smart and Healthy within the 2-degree Limit

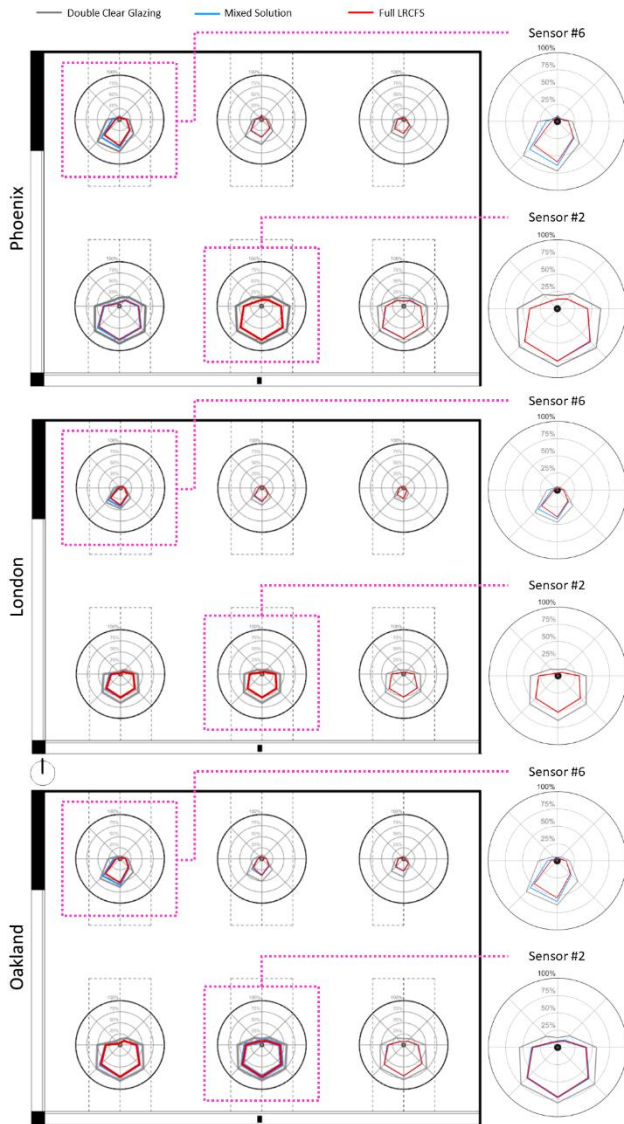


Figure 6: Visualization output of the implemented heuristic for the 3 locations.

Table 2: Results per sensor of the proposed procedure.

Experiment #1 - Phoenix						
Scheme	Sensor #2			Sensor #6		
	#1	#2	#3	#1	#2	#3
Dir. [x,y,z]	[0,-1,0]	[0,-1,0]	[0,-1,0]	[0,-1,0]	[0,-1,0]	[0,-1,0]
Date [m.d.h]	1.5.15	12.30.14	12.30.14	11.27.14	12.30.14	12.30.14
Date (lux)	4057	3982	3752	8008	8468	7965
Freq. ($E_v \geq 2700$ lux)	84%	76%	76%	72%	64%	59%
DGP	1.0	1.0	1.0	0.84	0.81	0.65
Experiment #2 - London						
Scheme	Sensor #2			Sensor #6		
	#1	#2	#3	#1	#2	#3
Dir. [x,y,z]	[0,-1,0]	[0,-1,0]	[0,-1,0]	[0,-1,0]	[0,-1,0]	[0,-1,0]
Date	1.15.13	1.7.14	1.21.12	1.12.15	1.12.15	1.12.15
Date (lux)	10403	6986	7878	18599	15538	16840
Freq.	65%	53%	53%	47%	42%	39%
DGP	1.0	1.0	1.0	1.0	1.0	1.0
Experiment #3 - Oakland						

Scheme	Sensor #2			Sensor #6		
	#1	#2	#3	#1	#2	#3
Direction	[0,-1,0]	[0,-1,0]	[0,-1,0]	[0,-1,0]	[0,-1,0]	[0,-1,0]
Date	11.19.10	12.22.14	12.22.14	12.22.12	8.1.13	8.1.13
Date (lux)	4339	4755	4302	9974	7858	7828
Freq. ($E_v \geq 2700$ lux)	81%	73%	72%	64%	59%	54%
DGP	1.0	1.0	1.0	0.36	0.44	0.45

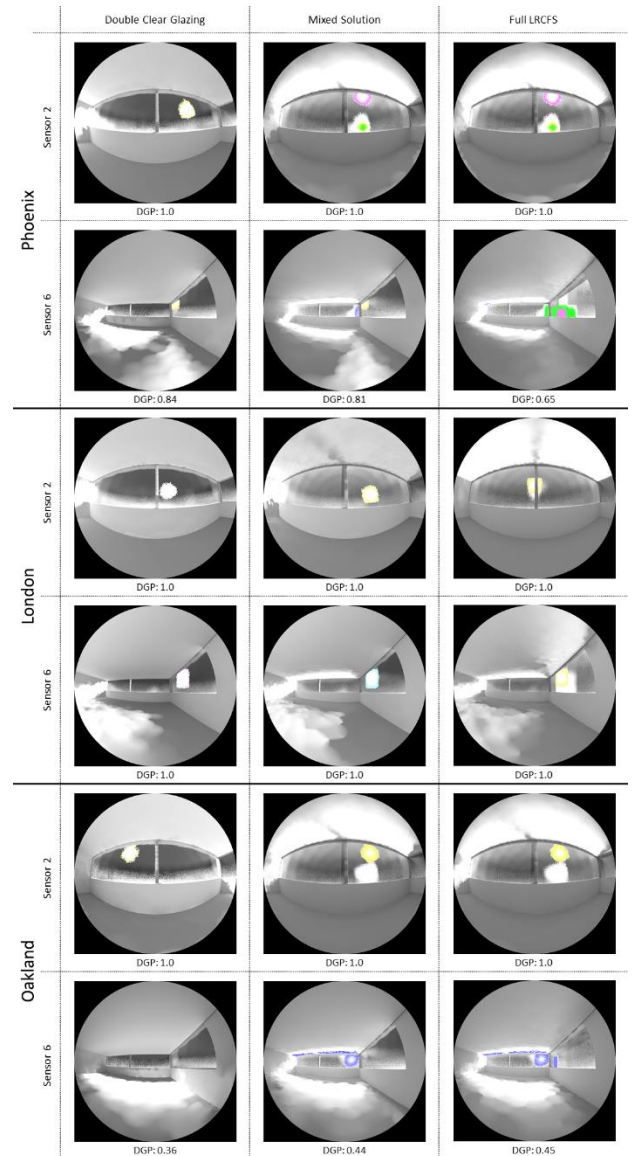


Figure 7: Full DGP analysis for the POV/HOY pairs determined by the heuristic.

When compared with Phoenix, London has a lower frequency of potential glare events. Table 2 and Figure 7 show that the selected events for London yield both a higher DGP and vertical illuminance levels. The analysis of the renders in Figure 7 indicate that one of the reasons for this is the higher latitude and a more frequent presence of the circumsolar region in the South quadrant. Oakland results follow a similar trend to Phoenix but with the lowest DGP values. Sensor #6 at at 2 pm of the 22nd of December reports a DGP of

PLEA 2018 HONG KONG

Smart and Healthy within the 2-degree Limit

0.36, a value close to the threshold that separates perceptible from imperceptible glare ($DGP < 0.35$). Figure 6 shows an expected pattern: the South window is the largest daylighting contributor, the Northeast corner is the darkest because it is the less exposed, and sensor #6 has an asymmetric distribution of potential glare events due to the impact of the West window in its field-of-view (FOV). Although sensor #1 and #2 have similar results, the system selected the south direction of the latter because it was the most consistent POV of the 3 experiments. In the second row of sensors the system selected the South direction of sensor #6 as the representative POV because it yields both the higher frequency of potential glare events and the highest E_V . The system also selected the Southwest direction of sensor #2, however, due to space limitations, that direction was not considered in this study. The radar graphs also show the shading impact of adding a LRCFS to the windows. Both the frequencies and illuminance values lower when the LRCFS is added to the South window. Nevertheless, adding the LRCFS to the West window does not produce a relevant impact in the frequency of events susceptible to visual discomfort. The main reason is that the LRCFS was optimized in [11] for a South window.

Finally, a closer analysis of Figure 7 and the E_V values reported in Table 2 shows that the proposed heuristic is able to capture critical events. However, in all those events the circumsolar region has a considerable weight in the FOV, indicating that there is a bias towards low sun angles and clear skies (all the selected HOY correspond to clear skies). A further refinement of the heuristic should contemplate strategies that address events with high potential for glare in hazier skies and/or with higher sun angles.

6. CONCLUSION

This paper demonstrates that by spatial and temporal sampling annual E_V data it is possible to (i) conduct preliminary assessments on glare performance of any type of fenestration (ii) find the relevant POV/HOY pairs to conduct full point-in-time DGP analysis, and (iii) reduce the number of expensive DGP simulations in LRCFS visual comfort studies. Although the proposed heuristic was able to find critical events, it showed a bias for low sun angles of bright and clear skies. The authors intend to refine the heuristic to find events with high glare potential in a wider range of skies by adding/modifying the HOY selection rules. For example, a second application of the heuristic could be done on hours where the circumsolar region is not visible. Finally, the work presented in this paper shows that this heuristic has a high potential to be used in automated search procedures for daylight-based design since it improves the simulation overhead by effectively reducing the number of expensive simulations used in annual visual comfort studies.

ACKNOWLEDGEMENTS

Work presented in this paper was partially supported by Portuguese national funds through Fundação para a Ciência e a Tecnologia (FCT) under the PhD scholarship SFRH/BD/98658/2013.

REFERENCES

1. IESNA (2012). LM-83-12 IES Spatial Daylight Autonomy (sDA) and Annual Sunlight Exposure (ASE). New York, NY, USA: IESNA Lighting Measurement.
2. Nabil, A. and J. Mardaljevic (2006). Useful daylight illuminances: A replacement for daylight factors. *Energy and buildings*, vol. 38, no. 7, pp. 905–913.
3. Wienold, J. (2004). Evalglare - A new RADIANCE-based tool to evaluate daylight glare in office space. In *3rd International RADIANCE workshop*.
4. Wienold, J. and J. Christoffersen (2006). Evaluation methods and development of a new glare prediction model for daylight environments with the use of CCD cameras. *Energy and buildings*, vol. 38, no. 7, pp. 743–757.
5. Wienold, J. and J. Christoffersen (2005). Towards a new daylight glare rating. In *Lux Europa*, Berlin, pp. 157–161.
6. Suk, J. Y., M. Schiler, and K. Kensek (2013). Development of new daylight glare analysis methodology using absolute glare factor and relative glare factor. *Energy and Buildings*, vol. 64, pp. 113–122.
7. J. Wienold, J. (2009). Dynamic daylight glare evaluation. In *Proceedings of Building Simulation*, pp. 944–951.
8. Jones, N. L. and C. F. Reinhart (2017). Experimental validation of ray tracing as a means of image-based visual discomfort prediction. *Building and Environment*, vol. 113, pp. 131–150.
9. Mardaljevic, J., M. Andersen, N. Roy, and J. Christoffersen (2012). Daylighting metrics: is there a relation between useful daylight illuminance and daylight glare probability. In *Proceedings of the building simulation and optimization conference (BSO12)*. Loughborough, UK, vol. 1011.
10. Konis, K. (2014). Predicting visual comfort in side-lit open-plan core zones: results of a field study pairing high dynamic range images with subjective responses. *Energy and Buildings*, vol. 77, pp. 67–79.
11. Santos, L., A. Leitão, and L. Caldas (2018). A comparison of two light-redirecting fenestration systems using a modified modeling technique for Radiance 3-phase method simulations. *Solar Energy*, vol. 161, pp. 47–63.
12. McNeil, A. and E. S. Lee (2013). A validation of the Radiance three-phase simulation method for modelling annual daylight performance of optically complex fenestration systems. *Journal of Building Performance Simulation*, vol. 6, no. 1, pp. 24–37.
13. Ward, G., "RPIC," [Online]. Available: http://radsite.lbl.gov/radiance/man_html/rpict.1.html [1 June 2018].
14. LightLouver LLC, LightLouver daylighting system, [Online]. Available: <http://lightlouver.com/design-information/cad-files/>. [30 May 2018].

A Comparative Study of Hygrothermal Simulations for a Bamboo Wall System with Natural Wool Insulation

Z.M. GOULD¹, G. REICHARD¹

¹Virginia Polytechnic and State University, Blacksburg VA, USA

ABSTRACT: The modern building industry sends products all over the world to improve building envelope performance. Though there are existing standards and tools to evaluate hygrothermal behavior of wall sections in different climates, they are often based on different assumptions and provide development teams with different insights. This paper attempts to compare the capabilities and limitations of three hygrothermal analysis tools: Ubakus, HT Flux, and WUFI. An engineered bamboo wall section with wool insulation that was recently built in Washington D.C. is used as a case. The results from the various tools are compared for the different climate zones where constituent parts of the building envelope were manufactured as well as the location of final assembly. Ubakus and HT Flux results proved remarkably similar with predicted condensation accumulations in the Munich climate of .33 and .32 kg/m², respectively. WUFI results were consistently higher (1.06 kg/m² in Munich) because of differences in computational methods and additional moisture migration factors considered in their model. All the applied simulation tools suggest a sufficient potential for dry-out periods within the studied climate regions.

KEYWORDS: Hygrothermal Simulation, Condensation Risk, Sustainable Materials, Bamboo, Green Building

1. INTRODUCTION

In a globalized economy, new sustainable assemblies developed and tested in one climate zone are often employed in new markets and environments without sufficient hygrothermal evaluation [1]. Thermally better performing envelopes with substantially higher volumes of insulation are key components of zero-energy buildings (ZEBs), the global market for which is projected to hit 1.3 trillion US dollars by 2035 [2]. As certain insulated wall cavities get wider, the temperature change that occurs inside the wall section increases and can lead to a higher risk of damage from condensation [3]. This paper compares three simulation tools and approaches that can be employed to identify hygric behavior in wall cavities and assesses their effectiveness in determining wall system suitability in new climates. As an example and case study a pre-fabricated bamboo (BamCore™) wall system filled with wool insulation is modelled and analyzed in three different software applications, namely Ubakus, HTflux, and WUFI.

2. BACKGROUND

The design basis of our chosen simulation case study is from the Grass House in Washington D.C. - a two story carriage house built with a BamCore shell and wool insulation. It is the first BamCore structure on the east coast of the US and currently the only one built outside of California. The walls were built based on a typical 2x6 stud wall cavity dimensions (140mm). However, the structural strength of the bamboo panels allows for almost stud-less construction and therefore significantly reduces thermal bridging. All interior wall cavity volumes, except for window

framing, electrical conduit, and some wood blocking to fasten the walls to the foundation, are filled with wool insulation as shown in Figure 1.



Figure 1: Real wall section cut-out from the Grass House showing interior BamCore wall with natural wool insulation.

There have been several other comparative studies in the literature looking at different building simulation tools but few of them focus on hygrothermal simulation specifically. Crawley et al. present an overview of twenty different building energy simulation programs of which only BSIm mentions condensation risk [4]. Delgado et al. wrote a book on the application of hygrothermal simulation tools in building physics and mention various iterations of the WUFI software and several suites that employ the Glaser method [5]. Current trends in hygrothermal modelling lean towards the integration of artificial intelligence in co-simulations that improve accuracy and speed up computation rates [6]. This paper focuses on more user-friendly tools that could

PLEA 2018 HONG KONG

Smart and Healthy within the 2-degree Limit

be helpful in both industry and classroom settings alike. The work presented here will build upon these existing studies by applying hygrothermal simulations to the natural building materials required for green building certifications.

3. METHODOLOGY

For the purposes of modelling, a simplified wall section of 32mm BamCore panels on both sides of a 140mm cavity filled with wool insulation with identical material properties was used across all simulations. All units are provided in SI format for consistency. In the most recent version of WUFI Pro 6.2, the BamCore Prime Wall System comes pre-loaded in the default material library. Havelock™ loose-fill insulation was used in Grass House construction. As fibrous, air-open insulation, its hygrothermal properties can be assumed similar to other wool insulation, such as Tirol Wool ISO™, which was in the WUFI material library and used instead. Furring strips, rain screen, and interior/exterior finishes were all left out of the simulation. Material property values used in the simulations are listed in Table 1.

Table 1: Material property inputs to hygrothermal simulations.

Material	λ (W/mK)	C_p (J/kgK)	μ	ρ (kg/m ³)
BamCore	0.114	1400	73	551
TirolWool	0.036	1650	1.8	26.2

where:

- λ ... the thermal conductivity in [W/m·K]
- C_p ... the thermal capacity in [J/kg·K]
- μ ... the water vapor diffusion resistance factor [dimensionless]
- ρ ... the density in [kg/m³]

Simulations were run for three different climates starting with regional climates of locations of material development and fabrication (Santa Rosa, California and Tyrol, Austria) as well as the site of final assembly (Washington D.C.). Washington D.C.'s mixed-humid climate was approximated with existing data from Baltimore, Maryland that was already present in the WUFI database. Santa Rosa's climate and Tyrol's, climate were approximated with Fresno, California and Munich, Germany weather data, respectively. For Ubakus and HT Flux, which are based on steady-state boundary conditions, the 10-year average annual temperatures and relative humidity of each region during the three winter months (December, January, and February) and the three summer months (June, July, and August) were identified using historical data from the Weather Underground database. The corresponding average relative humidity was calculated using the average dew point temperature

and the elevation above sea level. The -5°C and 80% relative humidity conditions are the standard values employed for Germany and surrounding climates under DIN 4108-3 standards and were left unchanged for steady state analysis of the Munich climate. Cold-year weather files from the WUFI database were selected for Munich, Fresno and Baltimore and utilized directly as inputs for transient analysis.

Table 2: Temperature (T) and relative humidity (RH) values used in steady state simulations for respective climate zones for winter and summer seasons.

Input	Munich	Fresno	Baltimore
Winter T/RH	-5°C/80%	10°C/70%	0°C/60%
Summer T/RH	15°C/70%	28°C/32%	25°C/65%

Interior temperatures and humidity conditions for WUFI simulations were set according to ASHRAE Standard 160 for a house with heating only in Munich and for houses with heating and air conditioning with dehumidification in Fresno and Baltimore. For Ubakus and HT Flux, static interior temperatures of 20 °C and 50% relative humidity, which are equivalent to A/C controlled interior conditions, were used as per the default European standards.

4. RESULTS

Results across all simulation tools identified a higher risk of condensation on the interior side of the exterior BamCore panel during winter months. The reporting and consequent evaluation of condensation risks and an eventual capacity of dry out during summer months differed across platforms.

Overall the hygrothermal performance of this simplified building envelope performs quite well. This can be attributed primarily to the vapor retarding qualities of the BamCore panels. In terms of reporting, Ubakus reports the hypothetical condensation amount in kg/m² (due to vapor diffusion only) based on the set boundary conditions for 90 days, which is the standard procedure to comply with German codes. However, HT Flux reports the daily amount of condensation assessed in a defined region. This allows to compare different areas of risk in a 2-dimensional (2-D) setting. To compare results to Ubakus, the measured area amounts must be converted to equivalent amounts per m² and then multiplied with 90 (days). Lastly, WUFI does not directly provide amounts of condensation but rather reports the water content in different positions of the construction. While it is possible to estimate the condensate amounts from WUFI results by comparing the water content changes over seasons, the process is not straight forward as users must read out graphs across different periods of time. Furthermore, it must be noted that WUFI goes beyond vapor diffusion to also

PLEA 2018 HONG KONG

Smart and Healthy within the 2-degree Limit

consider capillary action, wetting from rain, and other processes, utilizing a transient and not a steady state simulation model. Table 3 provides a summary of results to demonstrate how changes in climate affect the predicted accumulation of moisture in a given wall section, and how the effect of changing climate varies across different simulation tools.

Table 3: Summary of accumulated condensation predicted by various hygrothermal simulation tools. Ubakus and HT Flux values are 90-day steady state accumulations.

Software	Munich	Fresno	Baltimore
Ubakus	0.33 kg/m ²	0.00 kg/m ²	0.01 kg/m ²
HT Flux	0.32 kg/m ²	0.00 kg/m ²	0.09 kg/m ²
WUFI	1.06 kg/m ² *	0.54 kg/m ² *	0.80 kg/m ² *

* Values from WUFI are peak accumulations above BamCore's 66 kg/m³ built-in moisture and not directly comparable to condensation accumulation in other tools.

Ubakus results show the Fresno climate region, where BamCore is manufactured, as having the lowest potential for moisture accumulation, and the Munich climate region, where Tirol Wool ISO is manufactured, as having the highest risk of condensation problems. There was zero risk of condensation accumulation in the Fresno climate using the Ubakus tool. HT Flux also showed zero condensation in Fresno, almost identical results in Munich, and a slightly higher amount of accumulated moisture in Baltimore. Values from WUFI are peak moisture content accumulations above BamCore's 66 kg/m³ built-in moisture content from the material database. They are figures specific to the external BamCore panel and converted from kg/m³ to kg/m² by multiplying by BamCore's .032m panel thickness. Though the moisture content is higher it does not translate directly to condensation risk. A moisture content of 66 kg/m³ in the BamCore panel corresponds to an 80% relative humidity. Values above this level from November through March present risk of condensation but summer dry out periods compensate and the year over year moisture content is shown to decrease across all three climate zones showing the drying potential.

The following sections will go into more detail on the set-up of each simulation in the various software suites, the corresponding results, and the notable functionalities and limitations that affect their overall utility as hygrothermal modelling tools.

4.1 Ubakus

Of the three tools discussed in this paper, Ubakus is the only one accessible through a web application. Despite some lingering issues with German to English translation (mostly in the included material libraries and pop-up dialog boxes), it is by far the easiest to pick up and quickly start learning from. Ubakus is based on

the 1-D steady state solution of thermal flux and vapor flux through building enclosures and follows the calculation model set forward in ISO EN DIN 6949 (U value), DIN 4108-3 (moisture protection) and DIN 68800-2 (drying potential).

The bamboo wall section of the Grass House was first modelled for the Munich climate assuming the default steady state winter season of 90 days, which when following DIN 4108-3 is to be assumed with a temperature of -5°C. The thermal gradient of this construction is shown in Figure 2.

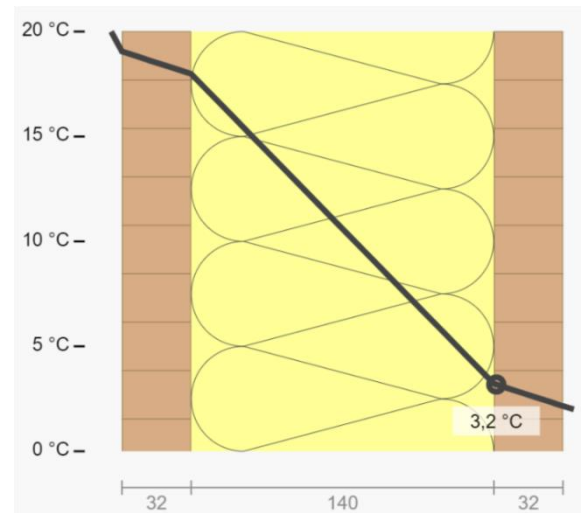
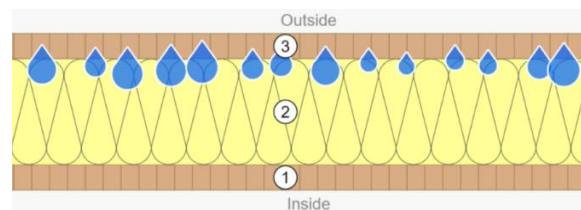


Figure 2: Ubakus simulation results showing dimensional inputs and temperature profiles in a Munich, Germany climate. These temperatures become the boundary conditions for hygrothermal analysis. The thickness of each component material is displayed in mm on the bottom.

The graphic results of the Ubakus hygrothermal simulation for Munich are shown in Figures 3 and 4. The size of the water droplets changes with the predicted amount of condensation at a given material interface. The 0.33 kg/m² predicted condensation during winter is the highest amongst modelled climates but still well below the 1 kg/m² limit set forth in DIN 4108-3. The straightforward graphical representation of the condensation risk makes the information more accessible for designers and architects who may not be accustomed to deciphering gradient maps or isopleths. It is immediately obvious that there is a risk for condensation as well as some indicator for the magnitude and location of the risk.



PLEA 2018 HONG KONG

Smart and Healthy within the 2-degree Limit

Figure 3: Glaser water vapor diffusion results from Ubakus for a Munich, Germany climate with areas of winter condensation risk marked by blue water droplets.

Ubakus also provides estimates for the drying potential of the modelled assembly. As Ubakus follows DIN standards the drying potential again assumes 90-day steady state summer conditions, and in our case assesses a drying period of 48 days (Drying season according to DIN 4108-3:2014-11). It also comments on the compliance with DIN 4108-3, which sets the maximum allowable amount of condensate at 1.0 kg/m² if all affected condensation layers are capillary open, otherwise it limits the total condensation amount with 0.5 kg/m² (e.g. concrete).

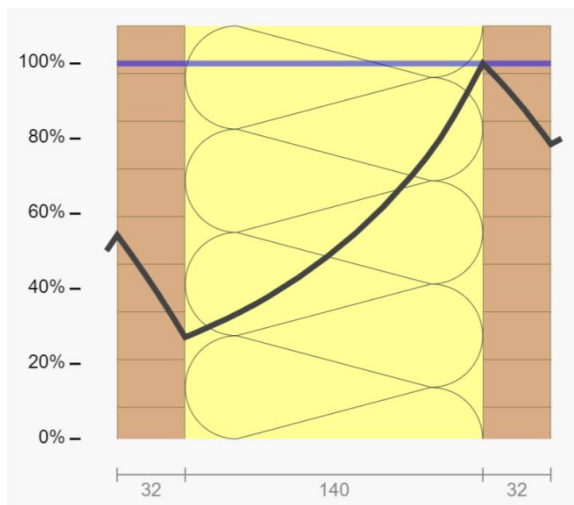


Figure 4: Ubakus simulation results showing dimensional inputs and relative humidity profiles in a Munich, Germany climate. The condensation risk is shown on the interior side of the exterior panel where the air saturates. Thicknesses are displayed in mm on the bottom.

Similar to the previous process when calculating condensation amount, we cannot use DIN default values for the US climate. Average temperatures and humidity calculated in Baltimore summer conditions (25°C and 65% relative humidity) result in a very different vapor pressure differential than the DIN summer conditions automatically assumed in Ubakus (which can be compared to 15°C and 70% relative humidity). Though drying to the exterior still appears to be possible in Baltimore summers, it would likely be much less. Potential condensate would still be able to diffuse inward to the air-conditioned side of the wall as 20°C at 50% RH represents a vapor pressure around 1200 Pa. Furthermore, any engineer using Ubakus in other climates must also consider the risk of summer condensation and cannot use baseline results.

4.2 HT Flux

HT Flux introduces a second dimension to vapor diffusion simulation, which opens it up to the

modelling of more complex geometries of interface details. Some interfaces can be areas of concern for condensation and moisture build up. In these cases, the added 2-D functionality can be valuable. See Figure 5 demonstrating the 2-D capabilities of HT Flux on a window detail.

HT Flux also presents additional functionality through a numerical measurement tool assessing minima and maxima of results in regions as well as flux accumulations, which can be used to measure condensate amounts. As seen in Figure 5, the areas of condensation risk are hatched on top of the blue region that shows 100% relative humidity. By defining a condensation measurement region, the program can compute the total amount of predicted condensation in that region in grams per day. First, the 2-D simulation shows that the condensation amounts on the exterior BamCore panel in area close to the window sill increase to 8 g/m²-d, which comes to 0.72 kg/m² over the winter season. While this is more than double the amount calculated in the standard regions of the wall, it is still an amount that can be absorbed and released by the adjacent materials. Second, the 2-D simulation also shows an area of condensation on the bottom of the window. While the amounts are not critical, designers will know to use proper materials.

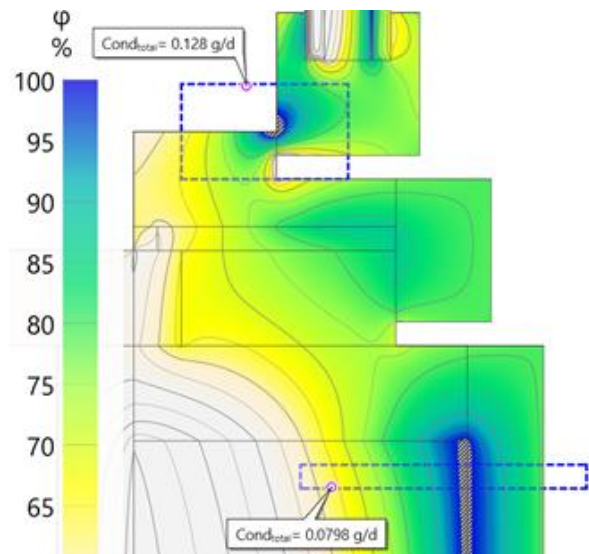


Figure 5: Window simulation in a Munich climate displaying Glaser 2D water vapor diffusion results from HT Flux with total condensation displayed in problem areas.

In general HT Flux provides more control over the simulation process and treats the model less like a black box than Ubakus. The user must run the thermal model first before proceeding to the Glaser 2D simulations, which emphasizes the importance of understanding the thermal behavior of the envelope before attempting to model vapor diffusion.

PLEA 2018 HONG KONG

Smart and Healthy within the 2-degree Limit

4.3 WUFI

WUFI (the authors used version Pro 6.2) introduces a transient functionality to the hygrothermal modelling process that allows a user to better investigate the condensation and drying out behavior of a wall section over time. Using weather file inputs from a database included in the software, WUFI can provide deeper insights of how a design will perform in the long run even when temporary condensation is occurring during certain months. Modelling at least two full years (the default is set to three years) allows users to predict if a wall with mild to moderate winter condensation risk will fully dry out during summer months. A fully sinusoidal curve that returns annually to its original values is a good thing, whereas a total moisture curve that gradually (or rapidly) rises in value is cause for concern. As seen in Figure 6, the bamboo/wool envelope of the Grass House will be exposed to significant moisture but the evaporation potential in the summer months provides adequate drying through evaporation. There is no accumulation of moisture year over year but rather a gradual annual decrease in water content.

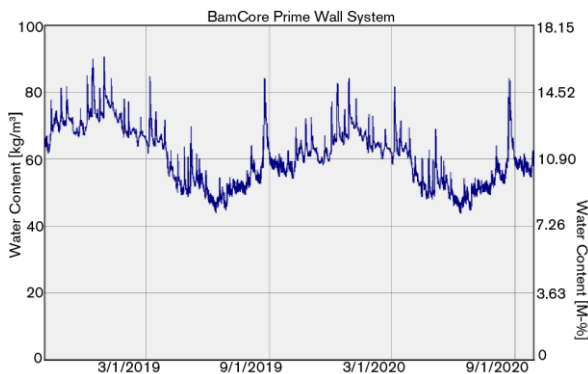


Figure 6: Water content in the exterior BamCore panel over a two-year period for the Grass House envelope conducted in WUFI Pro 6.2 in a Baltimore climate.

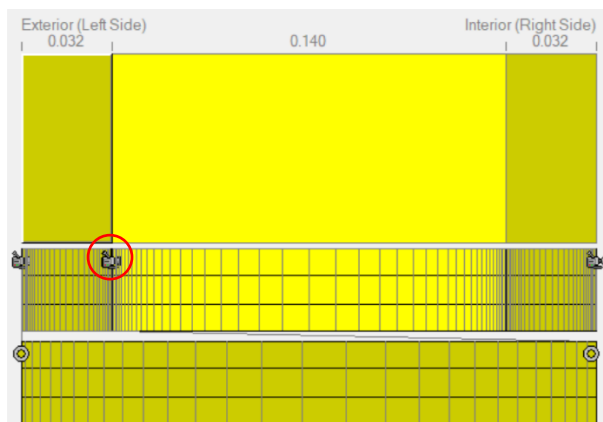


Figure 7: Additional monitoring capabilities are available in WUFI Pro 6.2. Monitor circled here is placed at the point of highest condensation risk.

WUFI essentially conducts a temporal iteration automatically by following long-term averaged weather input files and displaying several years of dynamic moisture results in a given climate. This eliminates the need to run separate seasonal simulations. WUFI also allows specific property monitoring at distinct parts of the wall section. As shown in Figure 7, additional result monitors were placed at the interface of the Tirol Wool ISO and the interior side of the exterior BamCore panel. This allows a much more in depth understanding of the material behavior at specific areas of concern. Figure 8 displays the local temperatures and relative humidity on the monitored inner edge of the exterior BamCore panel.

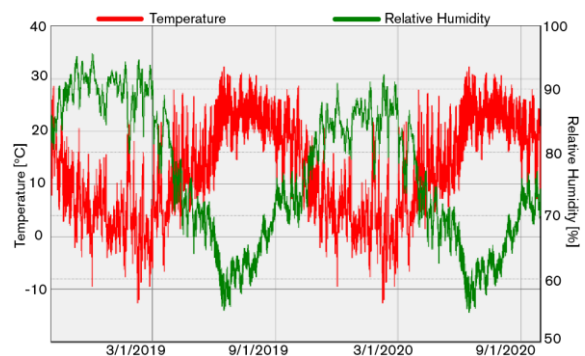


Figure 8: Temperature and relative humidity profiles monitored at the interior edge of the exterior BamCore panel in a Baltimore climate. The initial humidity is high but is shown to decrease with summer drying.

5. DISCUSSION

The fact that many of BamCore's current projects are in a similar climate zone as their fabrication facility in Santa Rosa, California—where there is less risk for interstitial condensation—could make it very easy to underestimate the importance of the material's hygrothermal performance. Fortunately, BamCore has put an emphasis on testing their product for moisture performance and ensuring that the relevant material properties are included in the WUFI database.

The simulations performed here suggest that important lessons can be learned through hygrothermal modelling that can help prevent material damage from moisture and condensation. Ubakus is the easiest to use model and interface. Though the modelling process is simplified, it alerts users immediately about potential condensation risks. However, users outside Germany, who may want to utilize the tool in other climate zones, must have a thorough understanding of the underlying boundary conditions and assessment assumptions (i.e. the correlated ISO and DIN Standards) to make correct conclusions about condensation and evaporation risks. This requires a thorough reading of background information, which may not be easy to find and may be even harder to comprehend for users new to vapor

PLEA 2018 HONG KONG

Smart and Healthy within the 2-degree Limit

diffusion processes. Ubakus can help to design envelope assemblies to avoid condensation risks from vapor diffusion completely, however, there are climates and assemblies that may never be without risk. It is important to understand the limitations of the tool which calculates the drying time and drying reserve based on a bulk method for a German climate. Extrapolations of what these amounts mean for other climates are possible as shown in this paper but require a thorough understanding of the underlying physical processes.

HT Flux has a considerably steeper learning curve but offers some interface features such as layering of drawing components, which can speed up comparative assessments. More importantly, due to its 2-D capabilities it is designed specifically to tackle interface regions, such as windows and corners, which can have heightened condensation risk due to the impact of thermal bridges. In this respect, HT Flux becomes an educational tool as it engages the user by providing numerical results that then require interpretation and reflection on the underlying model and assumptions.

When it comes to transient analysis needs, WUFI can be considered the most comprehensive tool with its ability to run simulations in many different climate zones using multiple years of weather data. WUFI allows designers to assess total water content and its inherent risks for each material. This can give engineers and architects an important edge when dealing with new material compositions in modern wall assemblies that have not yet undergone long term testing in the field.

6. CONCLUSION

In general, the dependence on vapor diffusion methods in hygrothermal modelling is a concern for the sustainable building industry. Tightly sealed envelopes in cold climates like Austria and Germany where PassivHaus standards were first developed can introduce higher risks for condensation. The lower heat flux through these enclosures also reduces the drying potential in summer months. It should be emphasized, that hygrothermal simulation only comes into full consideration when enclosure systems are built to high standards, i.e. air tight and highly insulated as vapor diffusion happens on a much smaller and slower rate than uncontrolled bulk movement of vapor laden air through cracks. Openings such as windows and controlled ventilation are different, as they can change the moisture load on the interior but typically do not create interstitial condensation issues within the enclosure.

Other areas of concern in transferring simulation tools across regions are language barriers and numerical unit conversions. Though all these tools have English language translations, all three of them were

developed in German speaking countries and translations are not always perfect.

Current methods for approximating weather conditions also rely too heavily on historical data. In an era when climate is changing rapidly, and extensive research is being conducted to predict changes in climate, predictive climate models should be available as inputs to both steady state and transient hygrothermal simulations. For sustainable building designs to meet long term performance goals, architects and engineers need to understand not only how the envelope will behave in the present but also how it is likely to behave in forecasted future conditions.

The last important issue to acknowledge is the general lack of hygrothermal material property information available for simulation input. For example, the actual manufacturer of the loose-fill, natural wool insulation used in Grass House construction did not have any metrics for their product's hygrothermal performance. This is often because the sales and marketing of envelope materials are dominated by cost and thermal performance. A greater emphasis on hygrothermal characteristics from policy and code/standard perspectives may be needed to force manufacturers to conduct proper moisture performance testing and give engineers the information they need to confidently avoid long term damage from condensation—regardless of the climate in which final construction will take place.

ACKNOWLEDGEMENTS

The authors of this paper would like to acknowledge the support from HT Flux and WUFI for non-commercial software licenses, Marcus Bianci from Owens Corning for sharing his insights on the current practice of hygrothermal analysis, and Teresa Hamm at Virginia Tech for assistance in the initial modelling process.

REFERENCES

1. Delgado, J. M. P. Q. (2016). "Hygrothermal Simulation Applied to Energy Efficiency Improvement." *Defect and Diffusion Forum*, 371, 97–101.
2. Bloom, E. (2012), "Net Zero Energy Buildings: Global Market, Regulatory, and Technology Analysis for Energy Efficiency and Renewable Energy in Commercial and Residential Buildings." Pike Research LLC, Q1 2012 Report, 3.
3. Cascione, V., Marra, E., Zirkelbach, D., Liuzzi, S., and Stefanizzi, P. (2017). "Hygrothermal analysis of technical solutions for insulating the opaque building envelope." *Energy Procedia*, ATI 2017 - 72nd Conference of the Italian Thermal Machines Engineering Association, 126, 203–210.1
4. Crawley, D. B., Hand, J. W., Kummert, M., and Griffith, B. T. (2008). "Contrasting the capabilities of building energy performance simulation programs." *Building and Environment, Part Special: Building Performance Simulation*, 43(4), 661–673.

PLEA 2018 HONG KONG

Smart and Healthy within the 2-degree Limit

5. Delgado, J. M. P. Q., Barreira, E., Ramos, N. M. M., and Freitas, V. P. de. (2012). *Hygrothermal Numerical Simulation Tools Applied to Building Physics*. Springer Science & Business Media.
6. Berger, J., Mazuroski, W., Oliveira, R. C. L. F., and Mendes, N. (2018). "Intelligent co-simulation: neural network vs. proper orthogonal decomposition applied to a 2D diffusive problem." *Journal of Building Performance Simulation*, 0(0), 1–20.

Particulate Concentrations in Bedrooms in Airtight Dwellings Findings from Eleven Dwellings in Scotland

FILBERT MUSAU¹

¹Mackintosh School of Architecture, Glasgow School of Art, Glasgow, United Kingdom

ABSTRACT: Occupant exposure to unhealthy Particulate Matter (PM) in naturally ventilated air-tight dwellings is not fully understood. In the UK, past studies have not investigated PM in bedrooms. Yet, PM is considered the most toxic pollutant and affects more people than any other pollutant; and bedrooms are the spaces that people typically occupy for the longest cumulative periods of their lifetime; with little or no control of ventilation during sleep. This paper evaluates monitored PM₁₀ and PM_{2.5} in the context of occupant health in bedrooms of eleven dwellings across Scotland. It focuses on PM_{2.5}, the size associated with greatest impact on health. PM and window operation were monitored concurrently. Air-tightness, smoke tests, dwelling inspections, occupant surveys, questionnaires, and interviews were also conducted. The results indicate that PM_{2.5} concentrations were generally above the recommended limits by WHO; and potentially unsafe in all the dwellings in the context of the EU-ESCAPE study. Bedtime mean concentrations were significantly lower than the 24hr mean, but would also have potentially negative health impacts based on the ESCAPE study. This suggests possible health burdens of particulates in bedrooms, with continuing construction of air-tight dwellings. Further work is needed on a larger sample of dwellings across different seasons.

KEYWORDS: Particulate matter, air-tight dwellings, bedrooms, occupant health

1. INTRODUCTION

Although appropriate provision of natural ventilation could address recent concerns on general indoor air quality in naturally ventilated air-tight dwellings, occupant exposure to unhealthy indoor particulates in such dwellings is not fully understood. In the UK, past studies have focussed on comparison between particulates in smoking and non-smoking traditional homes, which are less airtight; and homes that use solid fuels or gas for heating and cooking [1, 2]. Studies looking at Indoor Environmental Quality in bedrooms have focussed on CO₂, RH%, temperature, and mould conditions [3, 4, 5]; and left out Particulate Matter (PM). Yet, PM is considered the most toxic and affects more people than any other pollutant [6, 7]; and bedrooms are the spaces that people typically occupy for the longest cumulative periods of their lifetime [8], with little or no control of ventilation during sleep [9]. We spend around one-third of our lives sleeping, yet little is known as to how human exposure to indoor air pollutants during sleep impacts human health and sleep quality [10]. Based on a review of the state-of-knowledge on human exposures to pollutants in sleep microenvironments as at 2017, Boor *et al.* recommend that this area should get more attention; and future research is needed to fully understand how sleep exposures affect human health and sleep quality [10]. Outdoor PM_{2.5} levels in Scotland are relatively lower than most regions, but they have been associated with significant loss of life. A study on the effects on annual mortality of anthropogenic PM_{2.5} pollution [11], showed that in 2010, the deaths of people aged 25+ in

Scotland, Glasgow City, and Highlands Council were: 53,800 (1.47%); 6,508 (1.59%); and 2,296 (1.43%) respectively. The mean anthropogenic PM_{2.5} concentrations were 6.8, 8.3, and 4.3 µg/m³ respectively. Another study modelled PM levels based on measured levels at the nearest stations. It reported PM_{2.5} levels for Glasgow and Inverness as 10-12.5 µg/m³ and 5-10 µg/m³ respectively [12]. The two cities represent the higher and lower sides of the spectrum of PM concentrations across Scotland's urban areas. With such low outdoor PM_{2.5}, the "build tight-ventilate right" approach advocated by Perera and Parkins in 1992 [13], would be expected to result in low indoor PM levels in Scotland. But how do you "ventilate bedrooms right" in the predominantly cold and windy climate of Scotland, while asleep? A study of 109 dwellings showed that majority of people in Scotland sleep with their bedroom windows closed in winter, and occupants cited weather as the main reason for this. 75% of them never opened bedroom windows at night, and of them 73% gave the predominant reason being weather [14].

What has the Scottish govt. done to regulate and enforce the "build tight" and "ventilate right" parts of the approach? For the "build tight" part, Scottish regulations specify a minimum airtightness for new houses of 10 m³/(h.m²) @50 Pa; recommend a level of 5m³/(h.m²), and require Mechanical ventilation if airtightness is below 5m³/(h.m²). For the "ventilate right" part, the Scottish Building Standards require CO₂ monitors to be installed in the main bedroom in all new dwellings since 2015. According to the Scottish

PLEA 2018 HONG KONG

Smart and Healthy within the 2-degree Limit

Government's Technical Handbook of 2015, most residents have no idea what the air quality in their home is, or should be, and don't know that they need to open a window, hence the need for CO₂ monitors. The impact of such monitors is not known.

There are no regulated standards for indoor PM in Scotland and no health-based standards for most Indoor Air Pollutants (IAPs) in homes [1]. The most relevant guidance available is by the Dept. for Health Committee on the Medical Effects of Air Pollutants (COMEAP), Guidance on the Effects on Health of IAPs (Dept. of Health, 2004). It provides guidance on NO₂, CO, Formaldehyde, Benzene and Polycyclic Aromatic Hydrocarbons; but none for indoor PM. The evaluation in this paper is, therefore, based on UK, EU and WHO guidelines on PM [15, 16]; and the EU 2013 ESCAPE study, which assessed the health impacts of every 10% increase in PM levels [17]. The study involving 312,944 people in nine EU countries revealed that there was no safe level of particulates, and that for every increase of 10 µg/m³ in PM₁₀, the lung cancer rate rose 22%. For PM_{2.5} there was a 36% increase in lung cancer per 10 µg/m³. In a 2014 meta-analysis of 18 studies globally including the ESCAPE study data, for every increase of 10 µg/m³ in PM_{2.5}, the lung cancer rate rose 9% [18]. The relative impacts of PM sources and window control on PM concentrations is expected to vary across meteorological conditions and across homes with different airtightness and user actions. Scotland is wetter and colder region than the rest of the UK; and arguably the windiest country in Europe. The objective of the current study was to explore PM_{2.5} and PM₁₀ levels in recently built air-tight and naturally ventilated bedrooms in Scotland, in the context of occupant health. This paper discusses the PM_{2.5} results only.

2. METHODOLOGY

2.1 Case Study Dwellings

Eleven dwellings (D1 to D11 in Figure 1) were selected from four developments, all completed between 2010 and 2012, with a total of 191 dwellings – representing diverse demographics, house types, geographical spread, and characteristics (Table 1). Development A has 20 houses for rent/low cost ownership and 32 for the open market. Development B has 34 Sheltered housing flats for the elderly (aged 60+). Its Mainstream housing has 18 two-storey terraced houses, 54 flats; and 11-flats for residents with mental health needs. Development C has 16 flats for older people, while D has six 1.5-storey houses for older people.

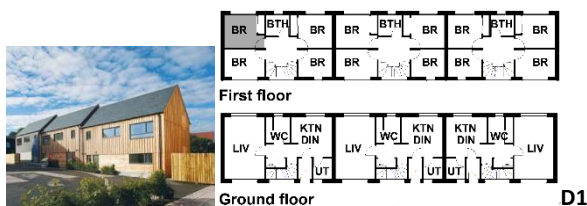


Figure 1: Views and floor plans of the case study dwellings. The monitored bedrooms are shaded in grey.

2.2 Collection of Household Data and Monitoring of Indoor Air Quality

A Standard Protocol was used for each dwelling and measurement. It included recording of the property address and time of arrival. Dwelling information was then recorded: (1) Type of Dwelling: Detached, Semi-Detached, Flat, Numbers of Storeys, units, Bedrooms, Occupants, and Construction Type; (2) Room Measurements: Length (mm), Width (mm), Height (mm), and Volume (m³); (3) Drawings of the shape and recording of positions of doors and windows; and (4) Photography of: windows and doors – including vents, undercuts and obstructions.

Indoor air quality was monitored concurrently with window operation in the bedrooms - all naturally ventilated. A portable GrayWolf monitoring kit set (Figure 2) was used. Temperature, relative humidity, CO₂, formaldehyde, CO and PM levels were recorded. The monitoring per dwelling was approx. 72 hours

PLEA 2018 HONG KONG

Smart and Healthy within the 2-degree Limit

during weekdays; and conditions were recorded every 5 minutes. Window opening/closing patterns were monitored with wireless contact sensors installed at windows, and linked via broadband.

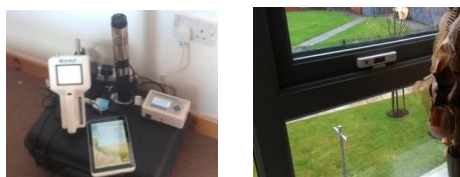


Figure 2: Portable monitoring apparatus and installed t-mac wireless contact sensors at windows

Residents were informed that: (1) the aim of the study was to measure the conditions in the bedroom under typical occupation so there was no need to alter their normal behaviour; (2) that the equipment would measure temperature, humidity, carbon dioxide, particulate matter and formaldehyde levels only; and (3) there was no noise or video recording. The following instructions and questions were issued: Windows should remain closed for the duration of the monitoring. This represented the typical case of windows in Scotland remaining mainly closed at bedtime, from late autumn through to early spring. Trickle vents should not be adjusted for the duration of the monitoring.

Doors should remain closed as often as possible, especially when the bedroom is occupied (to represent the typical sleep time closed status [3]).

Please do not switch off or unplug the recording equipment that has been placed in the bedroom.

When complete, after 48 hours (unless otherwise instructed), we will return to collect equipment.

How many people will occupy the room? Morning, Afternoon, Evening, Night.

If doors can't remain closed throughout, confirm preference in the: Morning (Yes/No); Afternoon (Yes/No); Evening (Yes/No); and at Night (Yes/No).

2.3 Air Permeability Testing

The testing was carried out in accordance with ATTMA (Air Tightness Testing and Measurement Association) TS1 (Technical Standard for air permeability testing of dwellings) which is broadly based on BS EN 13829:2001. The following points summarise the methodology for each test:

The building was measured to determine floor area, building envelope area, and volume.

All trickle vents, windows, and external doors were closed; none were sealed.

Table 1: Characteristics of households & occupancy patterns

	Dwelling/Households**									
	D1	D2	D3	D4	D5	D6	D7	D8	D9	D10
House type										

Semi Detached		✓		✓	✓					
Terraced	✓						✓			
Flat/Apartment			✓					✓	✓	✓
Householders										
Children (00-14 yrs.)	4	0	0	1	0	0	0	1	1	0
Youth (15-24 yrs.)	1	2	2	0	1	0	0	0	0	0
Adults (25-64 yrs.)	1	1	0	2	2	0	1	2	2	0
Elderly (65 + yrs.)	0	0	0	0	0	2	1	0	0	1
Occupancy patterns*	d	A	b	e	b	d	e	a	e	d
Fuel										
Gas cooking				✓	✓					
Electricity cooking	✓	✓	✓			✓	✓	✓	✓	✓
Gas heating - water	✓	✓		✓	✓	✓	✓			
Electr. heating- water								✓	✓	✓
Solar heating - water						✓	✓	✓	✓	✓
CHP heating - water										✓
Communal biomass heating - water			✓							
Gas heating - space (in D3, gas is back-up)	✓	✓	✓	✓	✓	✓	✓			
Electr. heating - space								✓	✓	✓
Communal biomass heating - space			✓							
Ventilation										
Windows	✓	✓	✓	✓	✓	✓	✓	✓	✓	✓
Trickle vents				✓	✓					
Extracts										
Kitchen	✓			✓	✓					
Bathroom				✓	✓					
Smoking	✓			✓						
Pets (cat = c, dog = d)	c	D		d						

*Typical domestic occupancy categories in UK [19]: (a) Short Occupancy A: Adults working externally and sch. age children. Weekday: All absent-08:30-16:00 Weekend: All absent-10:30-16:00; (b) Short Occupancy B: Adults working externally / all with full time jobs. All absent - 08:30 - 18:00 (4 days a week) or 08:30 to 21 (3 days a week). House partially occupied when at home; (c) Partial Occupancy: One or more residents with part time jobs. House unoccupied 09:00-13:00; or House unoccupied 13:00- 18:00. House partially occupied when at home; (d) Home stay A: Retired (over 65) / Family with small children. House occupied all day. All areas of occupied when at home: (e) Home stay B: 2 adults one stays at home during the day. House occupied all day. House partially occupied all day. **Dwelling 10 not included, has 1 adult householder and pattern (d)

Internal doors were propped open.

Mechanical ventilation was sealed and switched off where applicable.

A portable fan and frame were installed in the front entrance door, creating an airtight seal.

Infrared thermography was undertaken to detect areas where infiltration paths could exist.

The building was depressurised to an internal/ external pressure difference of at least 50Pa.

Infrared thermography was undertaken to detect possible infiltration paths.

PLEA 2018 HONG KONG

Smart and Healthy within the 2-degree Limit

A series of air flow measurements were recorded at varying indoor/outdoor pressure differentials. The fan was set to pressurise the building to an internal/external pressure difference at 50Pa. A series of air flow measurements were recorded at varying indoor/outdoor pressure differentials. The results were computed through regression analysis of the recorded measurements.



Figure 3: Air Pressure Testing fan in dwelling door (left); and air leakage smoke tests at windows, pipe routes etc.



Figure 4: All trickle air vents, mechanical air vents, and kitchen hoods were sealed off; mechanical ventilation air ingress and egress points were also sealed and the systems switched off before air pressure and air leakage tests.

3. RESULTS AND DISCUSSION

The air tightness results confirmed that the dwellings were tight enough to rely on windows as the main ventilation route. Five dwellings (6 for the second test) had tightness below $5\text{m}^3/(\text{h}\cdot\text{m}^2)$ - the threshold below which a whole house mechanical ventilation should be installed under current Scottish Standards. Of the five, D4 & D5 were designed to be less airtight. The designers thought these dwellings didn't require Mechanical Ventilation. The airtightness results, however, suggest that their natural ventilation using background ventilators is insufficient.

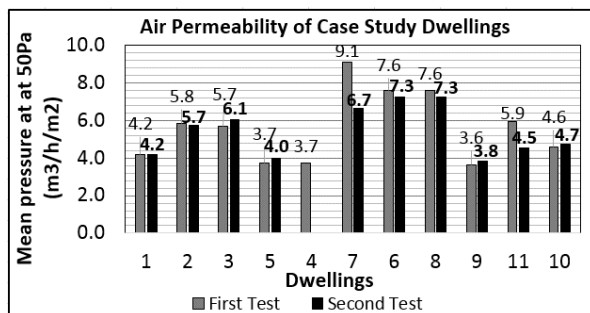


Figure 5: Comparison of first and second air permeability test results at 50Pa ($\text{m}^3/(\text{h}\cdot\text{m}^2)$) across dwellings.

In the context of the ESCAPE study, the $\text{PM}_{2.5}$ concentrations in majority of the eleven monitored dwellings would affect occupant health negatively. In

the context of the WHO guidelines, seven had mean $\text{PM}_{2.5}$ concentrations above the recommended 24-hr mean ($25\mu\text{g}/\text{m}^3$). For sensitive groups (children & the elderly), of the five dwellings with elderly householders, two had $\text{PM}_{2.5}$ concentrations over $25\mu\text{g}/\text{m}^3$, one with exactly $25\mu\text{g}/\text{m}^3$, and two had over $50\mu\text{g}/\text{m}^3$ (Figures 6 & 7). Three dwellings with children had $\text{PM}_{2.5}$ levels above the WHO guidelines. The analysis focusing on bedtime concentrations, when occupants were sleeping, shows concentrations of $\text{PM}_{2.5}$ below WHO guidelines (Figures 6 & 7). However, their concentration levels would have negative health impacts in the context of the ESCAPE study. WHO also states that there is no established threshold for safe levels of $\text{PM}_{2.5}$. All dwellings had some level of $\text{PM}_{2.5}$ and none could therefore be said to be safe. This is against the relatively low background outdoor $\text{PM}_{2.5}$ (Table 2) measured at Scottish Air Quality monitoring sites nearest to case study dwellings [20]; and calculated $\text{PM}_{2.5}$ using the Pollution Climate Mapping model [21]. For 2014, the year of monitoring the dwellings, the mean background $\text{PM}_{2.5}$ in Scotland calculated with the model was $5.9\mu\text{g}/\text{m}^3$. All levels across the sites, except for Feb. at Broxburn, meet the target upper limit of $10\mu\text{g}/\text{m}^3$ set by the Scottish Government.

Table 2: Mean monthly outdoor $\text{PM}_{2.5}$ concentrations in $\mu\text{g}/\text{m}^3$ at sites near the case study dwellings (averaged data from 2007 to 2018 available at scottishairquality.co.uk [20].

Dwelling	Nearest Site(s)	Jan	Feb	Mar	Apr	May	Jun	Jul	Aug	Sep	Oct	Nov	Dec
D1 to D3	Inverness	8	8	8	6	5	5	5	4	5	6	7	8
D4 & D5	Broxburn	9	10	9	8	7	8	5	3	6	5	7	8
D6 & D7	Waulkmillglen	6	6	6	6	6	7	4	3				
D8 to D11	Byres road	9	8	9	8	9	9	6	5				8
D8 to D11	Townhead	8	7	8	8	8	7	6	6	9	8	7	7

When plotted together, the air permeability and $\text{PM}_{2.5}$ results suggest a potential relationship between the extent of uncontrolled air leakage (infiltration) through the building fabric with the concentrations of $\text{PM}_{2.5}$. They show that, generally, the leakier the dwelling, the less the $\text{PM}_{2.5}$ concentrations (Figure 6).

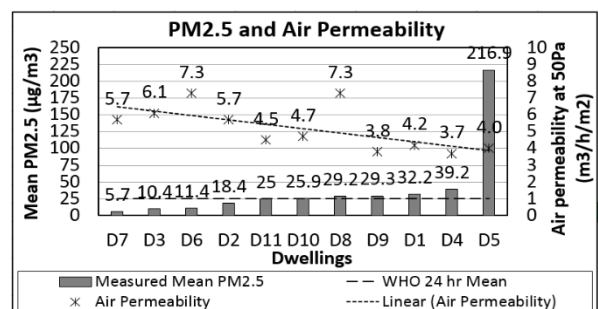


Figure 6: Air permeability and mean $\text{PM}_{2.5}$ concentrations for the monitored period.

PLEA 2018 HONG KONG

Smart and Healthy within the 2-degree Limit

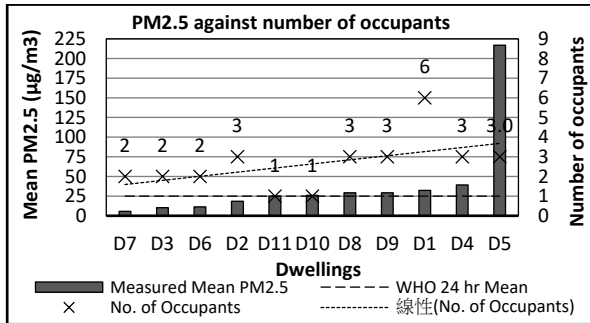


Figure 7: PM_{2.5} concentrations and number of householders per dwelling for the monitored period.

The number and age of householders, and consequently the level of human activity, seem to have the greatest influence on indoor PM_{2.5}. In all but one of the dwellings with over two householders, PM_{2.5} levels were above the WHO guidelines. Two dwellings located within one development, one with a couple in their sixties and the other with a couple in their seventies, were within the guideline levels. Only one dwelling (D10) with a single householder had concentrations above the guideline levels, and this is only slightly above. It is a flat located along a busy road. This suggests that such a location has the potential to contribute to higher indoor PM_{2.5}.

Dwelling D11, on the same block and location as D10, was monitored after being vacant for some time; to test the impact of being unoccupied and window operation. Windows were left closed for the first half of the monitoring period, and then opened for the second half. The results (Figure 8), show that its PM_{2.5} concentrations increased and became more variable when the window was opened. Even then, its peaks did not reach the WHO guideline (25µg/m³); and overall, had the lowest PM_{2.5} across all dwellings (Figure 9). Although proximity to the busy road may influence PM levels, overall, there seems to be a stronger association between the number of householders and indoor PM_{2.5} levels than between proximity to the road and indoor PM_{2.5} levels. PM₁₀ varied more than PM_{2.5} when windows were open.

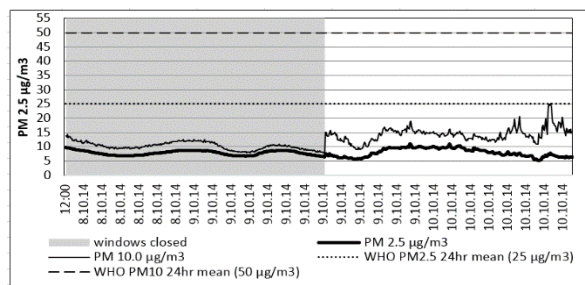
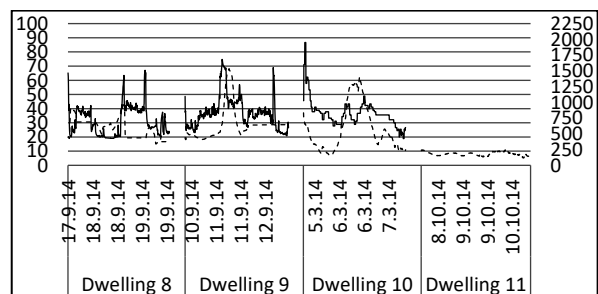
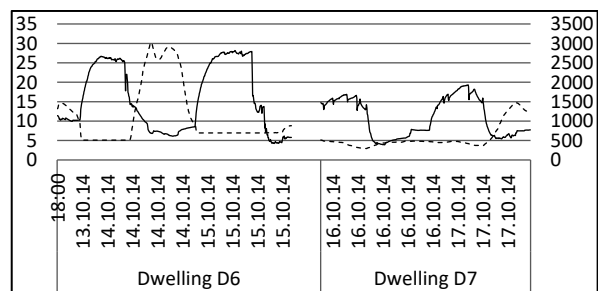
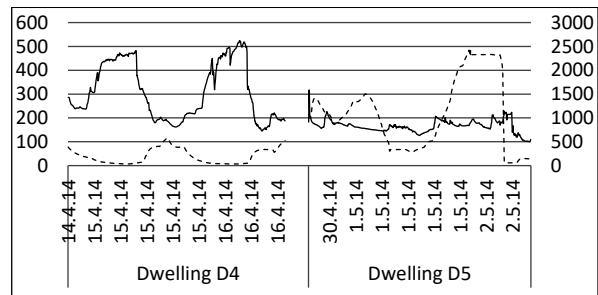
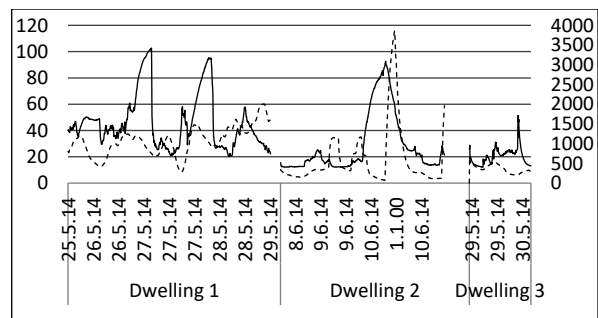


Figure 8: PM_{2.5} concentrations in unoccupied bedroom with windows left closed (shaded) and then left open.

The patterns of particulate levels measured across the dwellings suggest indoor and outdoor sources of PM_{2.5}. When CO₂ is considered as an occupancy indicator,

there was no clear evidence to determine whether the presence of occupants in bedrooms increased PM_{2.5}. An inverse relationship between CO₂ levels and PM_{2.5} concentrations appears to happen at night in some dwellings. A rise in CO₂ is accompanied by a drop in PM_{2.5}, when occupants have slept - presumably when the particles have settled. This was the case in dwellings D4, D5, and D6; but there was no clear relationship in the other dwellings (Figure 9). This suggests that, although CO₂ may predict ventilation and indicate occupancy, it may be a poor predictor of PM_{2.5} in bedrooms. Although PM_{2.5} was measured in series instead of concurrently, Figure 9 shows the potential for dwellings in one location to have significantly different levels of indoor PM_{2.5}.



..... PM 2.5 µg/m³ — Carbon Dioxide ppm

PLEA 2018 HONG KONG

Smart and Healthy within the 2-degree Limit

Figure 9: CO₂ against PM_{2.5} levels. Dwellings at each site are plotted together. CO₂ is also an indicator of ventilation for the monitored period.

In the context of Scotland, a wet and windy country with cold climate, it may be more important to control exposure to internal than external PM_{2.5}. While Scotland's rainy weather and dispersion by wind may partly explain the low outdoor PM_{2.5} at the sites in Table 2, it's many hills and valleys could also impede PM_{2.5} dispersions. Scotland's high rainfall and low annual temperature keep people indoors for much longer than outdoors, with closed windows. Yet, the government focuses on exterior PM_{2.5} reduction, despite meeting it's target outdoor mean PM_{2.5} of 10µg/m³ at most of the monitoring sites e.g. in Table 2. There are no set targets for indoor PM_{2.5}.

4. CONCLUSIONS

PM_{2.5} levels in the eleven dwellings were generally above the set limits by WHO; and not safe in all the dwellings in the context of the EU ESCAPE study. With PM_{2.5} in over half of the dwellings exceeding the WHO 48hr mean standard, the results suggest that the health burden of PM_{2.5} in bedrooms could be significant. Since the dispersion of external PM_{2.5} is expected to be high in Scotland, indoor PM_{2.5} levels may be higher in less windy contexts. The bedtime levels were significantly lower than the 24hr mean levels, suggesting that using a 24hr mean may be misleading, if occupancy patterns are not taken into account. The bedtime indoor PM_{2.5} levels were higher than the typical outdoor PM_{2.5} across Scotland. Since the influence of outdoor PM_{2.5}; and disturbance of settled indoor PM_{2.5} by occupants is expected low at bedtime, this suggests a need to commit efforts in the control of sources and levels of indoor PM_{2.5}; and to review regulations and enforcement of existing airtightness and ventilation standards. The results suggest clearer relationships between the number of householders and PM_{2.5}; and between air tightness and PM_{2.5}; than between occupancy and PM_{2.5}. Further work is needed on: (i) how indoor PM_{2.5} could be managed; (ii) how occupants could be informed of indoor PM_{2.5} – an invisible pollutant; (iii) measures that architects could integrate in the design and planning of dwellings to control bedroom PM_{2.5}; and (iv) monitoring a larger sample of dwellings, with repeat measurements at different seasons.

REFERENCES

1. Semple, S., Garden, C., Coggins, M., Galea, K., Whelan, P., Cowie, H., Ayres, J. (2012). Contribution of solid fuel, gas combustion or tobacco smoke to indoor air pollutant concentrations in Irish and Scottish homes. *Indoor Air*, 22(3): p. 212–223.
2. Semple, S., Apsley, A., Azmina I., Turner, S., & Cherrie, J. (2015). Fine particulate matter concentrations in smoking households: Just how much second hand smoke do you breathe in if you live with a smoker who smokes indoors?. *Tobacco Control*. 24: e205-e211.
3. Sharpe, T., Farren, P., Howieson, S., McQuillan, J. and Tuohy, P., (2015). Occupant Interactions and Effectiveness of Natural Ventilation Strategies in Contemporary New Housing in Scotland, UK. *International Journal of Environmental Research and Public Health*. 12: p. 8480-8497.
4. Howieson, S., Sharpe, T., and Farren, P. (2013). Building tight - Ventilating right? How are new air tightness standards affecting indoor air quality in dwellings? *Building Services Engineering Research and Technology*. 35: p. 475-487.
5. Building Research Establishment (1985). Surface condensation and mould growth in traditionally built dwellings. *Digest 297*. BRE Press, Garston.
6. Harrison R., Giorio C., Beddows D., Dall'Osto M. (2010). Size distribution of airborne particles controls outcomes of epidemiological studies. *Sci. Total Environ*. 409 p. 289-293.
7. WHO, (2014). *Ambient (outdoor) air quality and health*. World Health Organization. Fact sheet No 313.
8. Leng, Y., Wainwright, N., Cappuccio, F. (2014). Self-reported sleep patterns in a British population cohort. *Sleep Medicine*. 15(3): p. 295-302.
9. Canha, N., Lage, J., Candeias, S., Alves, C., and Almeida, S. (2017). Indoor air quality during sleep under different ventilation patterns. *Atmospheric Pollution Research*. 8(6): p. 1132-1142.
10. Boor, B., Spilak, M., Laverge, J., Novoselac, A., and Xu, Y. (2017). Human exposure to indoor air pollutants in sleep microenvironments: A literature review. *Building and Environment*. 125: P. 528-555.
11. Gowers AM, Miller BG and Stedman JR, (2014). 'Estimating Local Mortality Burdens associated with Particulate Air Pollution' Report number PHE-CRCE-010, Public Health England Centre for Radiation and Chemicals in the Environment, Didcot, Oxfordshire.
12. Brookes, D. M., Stedman, J. R., Kent, A. J., *et al* (2013). Technical report on UK supplementary assessment under the Air Quality Directive (2008/50/EC), the Air Quality Framework Directive (96/62/EC) and Fourth Daughter Directive (2004/107/EC) for 2012. Ricardo-AEA. Report Ricardo-AEA/R/3380, Issue 1.
13. Perera, E. and Parkins, L. (1992). Build tight – ventilate right. *Building Services*. Chartered Institution of Building Services Engineers, London. P. 37-38.
14. McGill G. (2018). Occupant interaction with ventilation in systems in dwellings. Unpublished report and paper in production. MEARU, Mackintosh School of Architecture.
15. WHO, (2006). Air quality guidelines for particulate matter, ozone, nitrogen dioxide and sulphur dioxide Global update 2005.
16. WHO, (2014). Guidelines for indoor air quality: household fuel combustion.
17. Raaschou O. *et al.* (2013). Air pollution and lung cancer incidence in 17 European cohorts: prospective analyses from the European Study of Cohorts for Air Pollution Effects (ESCAPE), *The Lancet Oncology*. 14 (9): p. 813–22.
18. Hamra B., Guha N., Cohen A.; *et al.* (2014). Outdoor Particulate Matter Exposure and Lung Cancer: A Systematic Review and Meta-Analysis. *Environmental Health Perspectives* 122 (9).
19. University of Southampton (2016). Occupancy Patterns Scoping Review Project. Final Report.

PLEA 2018 HONG KONG

Smart and Healthy within the 2-degree Limit

20. Scotland government. *Air Quality in Scotland*, [Online]. www.scottishairquality.co.uk/ [26 August 2018].
21. DEFRA, UK govt. *Pollution Climate Mapping Model*. [Online]. <https://uk-air.defra.gov.uk/research/air-quality-modelling?view=modelling> [26 August 2018].

Impact of Apartment Room Layout in Reducing Unwanted Temperature-Rise in Rooms Adjacent to Kitchen: A case from Dhaka city

SAIFUL ISLAM¹

¹North South University, Bangladesh

ABSTRACT: In urban apartment buildings in hot humid climate, kitchen heat causes unwanted temperature-rise in the surrounding rooms. This paper aims to identify effective apartment room layout patterns that help to reduce this unwanted temperature-rise. After reviewing more than hundred floor plans of apartment buildings in Dhaka city, the following common patterns have been identified – bed room and kitchen are separated either by a common wall or by a buffer space; dining room those are next to kitchen either has cross-ventilation, single-sided ventilation or no ventilation at all. Three apartment buildings have been identified where all these patterns exist. Both field measurements and computer simulations were carried out to study these buildings. This study initially assumed that, compared to a common wall, a buffer space would perform better in reducing the unwanted temperature-rise. However, no significant difference has been identified in this study. This study found that the unwanted temperature-rise in the dining room is minimized when it is cross-ventilated. The unwanted temperature-rise in dining room is highest when it is surrounded by other rooms. The unwanted temperature-rise in dining room stays in-between the previous two levels when the dining room has single-sided ventilation.

KEYWORDS: Kitchen, Temperature-rise, Ventilation, EnergyPlus

1. INTRODUCTION

Previous Research has found that kitchen air temperature can get more than 5.5°C above the comfort level [1]. In urban apartment units, due to compact room layout, this additional heat causes unwanted temperature-rise in adjacent rooms. Existing literature states that to exhaust kitchens' heat and pollutant, a kitchen should be a detached component of a house. It also admits that this detachment is not pragmatic in urban apartments due to space scarcity [2]. Unfortunately, literature regarding alternative options for placing kitchens in urban apartments is scarce.

The literature review done for this paper could not identify such researches yet. The majority of the researchers studied kitchen mostly in terms of air quality [3 & 4], pollution control [5], health hazard [2], ventilation strategies [4], and thermal comfort within the kitchen itself [6]. None of these researches had the scope or intention to study the impact of room layout pattern in reducing unwanted temperature-rise in adjacent rooms due to their close proximity to kitchen. Therefore, research on "layout pattern of kitchen and adjacent rooms for apartment design" requires much attention.

2. RESEARCH OBJECTIVES

The primary objective of this study is to identify effective apartment room layout strategy to minimize unwanted temperature-rise in rooms those are

adjacent to kitchen. In particular, dining room and bed room have been the subjects of the investigation.

3. METHODOLOGY

This study aims to achieve its objective through the following three steps – a) identify kitchen and adjacent room layout typologies among existing apartments in Dhaka city, b) for each type, for a brief period of time, record temperature data in representative apartment unit using HOBO data logger, c) perform room temperature simulations for the selected apartment units using EnergyPlus simulation tool. The measured and simulated data are then examined to identify effective strategies for layout of kitchen and adjacent rooms in an apartment unit. In the following paragraphs, each step is discussed.

For the first step, a total of one hundred 3-bedroom-apartment plans have been collected. It has been done through an open call to the student body of North South University Architecture department. It allowed covering apartments from almost all corners of the city. However, out of these hundred plans, fifty five plans found to have enough details for further review. It has been found that kitchens are invariably surrounded by at least a bed room and dining room. For bed rooms, two major typologies have been identified from these plans – i) in thirty four plans, kitchen and bed room are separated by a buffer space like toilet or store room, and ii) in twenty one plans, kitchen and bed room are separated by a common wall. For dining room, three layout strategies have been identified – i) dining room

PLEA 2018 HONG KONG

Smart and Healthy within the 2-degree Limit

entirely surrounded by kitchen and other rooms that is dining room with no ventilation; ii) dining room with single-sided ventilation, and iii) dining room with cross ventilation.

For the second step, all fifty five apartment units were approached to get permission for field measurement. Due to security and privacy issue, only eleven apartment units' owners allowed the author to perform the measurements. For each of these apartment units, three U12-013 HOBO Temp/RH/2 External Channel Data Loggers were employed to record temperature data simultaneously. One was set close to the gas burner, at five feet height on the wall and the other two were set at the similar height on a dining room wall and a bed room wall. The walls were selected based on their close proximity to the kitchen. During recording field measurement, it was observed that the studied apartments varied in terms of number of occupants as well as the gas burner operating hours. For these reasons, EnergyPlus simulation found to be an effective alternative to the field measurements where the selected apartment units could be simulated and compared for a consistent context.

For the third step, out of the eleven units, three representative units were chosen for simulation. Plan-A (Figure 1), Plan-B (Figure 2) and Plan-C (Figure 3) are the selected apartment units for EnergyPlus simulations. EnergyPlus uses Airflow Network model for natural ventilation simulation. According to Lixing Gu (2007), EnergyPlus's airflow network model was validated against measured data from both the Oak Ridge National Laboratory (ORNL) and the Florida Solar Energy Center (FSEC) (Gu, 2007). Although Computational Fluid Dynamics simulation is a much more rigorous approach for ventilation simulation, this study chose not to use it due to unavailability of such tools. The selected simulation parameters are stated in Table 1.

Table 1: Some selected simulation parameters for all three apartment units

Parameter	Descriptions
Solar distribution	Full exterior and interior
Ext. Wall	10 inch brick with both side plaster
Int. Wall	5 inch brick with both side plaster
Window	6mm single pain clear glass window
Reporting schedule	April 5 th , the hottest day in the weather file used by EnergyPlus.
Occupants schedule	Five persons for dining room, two for kitchen and two for bed room. Their detailed schedules are not attached.
Kitchen gas-burner schedule	Until 7:00 – 0, Until 9:00 – 1, Until 11:00 – 0, Until 14:00 – 1, Until

19:00 – 0, Until 22:00 – 1, Until 24:00 – 0

Electric Lighting schedule: For dining room with no ventilation: Until 24:00 – 1. For all other spaces: Until 6:00 – 0.05, Until 8:00 – 1, Until 17:00 – 0.05, Until 24:00 - 1

Ventilation schedule: Through: 3/31, until 24:00 – 25.55; Through: 10/31, until 24:00 – 21.11; Through: 12/31, until 24:00 – 25.55;

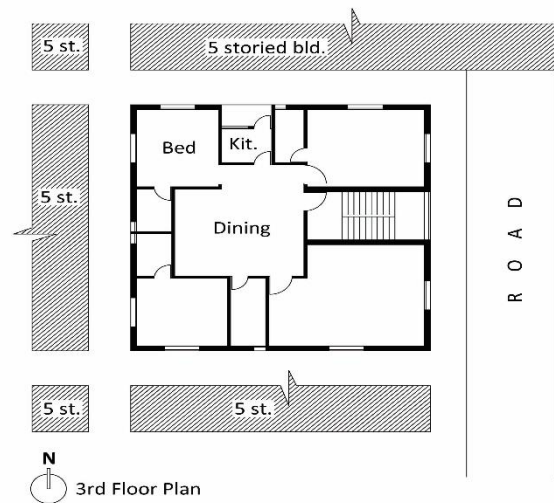


Figure 1: Plan-A where dining room has no direct ventilation and bed room is next to kitchen without any buffer space

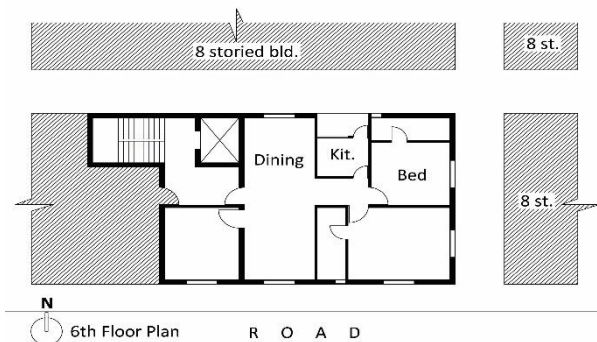


Figure 2: Plan-B where dining room has cross ventilation and bed room is next to kitchen without a buffer space

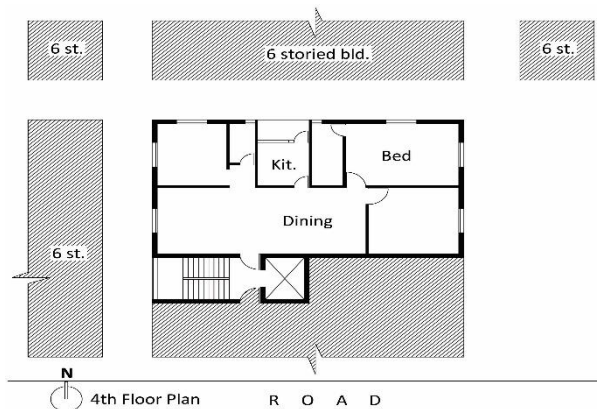


Figure 3: Plan-C where dining room has single-sided ventilation and bed room and kitchen are separated by a buffer space

PLEA 2018 HONG KONG

Smart and Healthy within the 2-degree Limit

4. RESULTS

Out of the three representative apartment units mentioned above, field measurement data of Plan-A was unable to retrieve from one of the data loggers. Data measured in Plan-B and Plan-C are also not comparable as they were measured on different dates. To accommodate the apartment owners' convenience, Plan-B was measured on November 15 and Plan-C was measured on April 4. However, temperature difference measured in kitchen, bed room and dining room within an individual unit depicts specific patterns. It is evident in Figure 4.

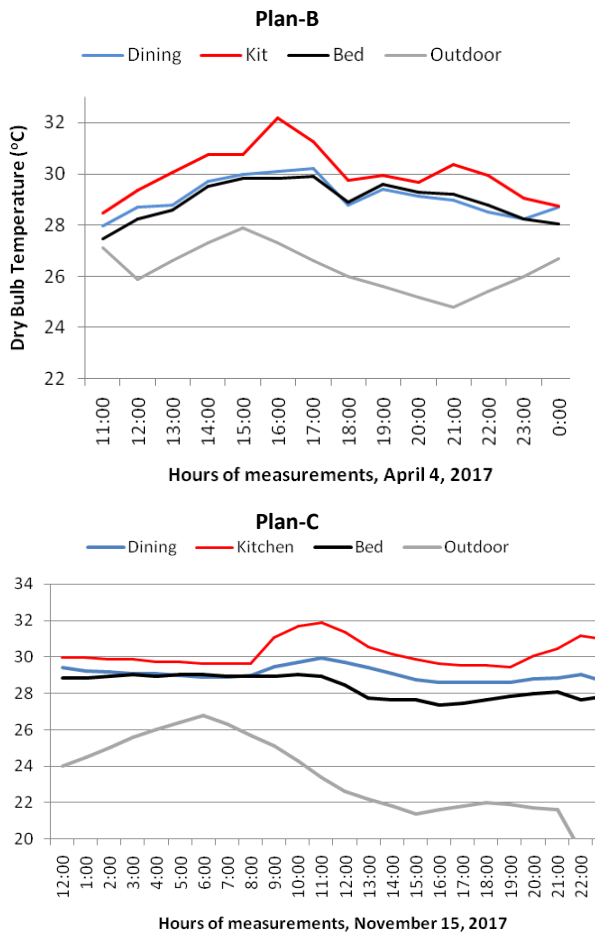


Figure 4: Field measurement of dry bulb temperature (°C) in Plan-B (top) & Plan-C (bottom)

Figure 4(top) shows the temperature difference observed in Plan-B. It shows that temperature difference between kitchen and dining room is almost similar to the temperature difference between kitchen and dining room. Figure 4(bottom) shows the temperature difference observed in Plan-C. Here, the bed room experiences lower temperature than that of the dining room.

In Plan-B (Figure 2), both bed room and dining room are separated from kitchen by common walls. In Plan-C (Figure 3), dining room is separated from kitchen by

a common wall but bed room is separated from kitchen by a buffer space. Therefore, results shown in Figure 4 could be used to make the following argument – temperature-rise in the kitchen-adjacent room is minimized when kitchen and the room are separated by a buffer space.

However, to critically examine the cases, other variables like weather, uniform gas burner operation schedule had to be considered. For this purpose, all these three cases were simulated in EnergyPlus. The simulation results are shown in Figure 5. It represents indoor temperature of April 5th as well, the hottest day of the year according to the used weather file.

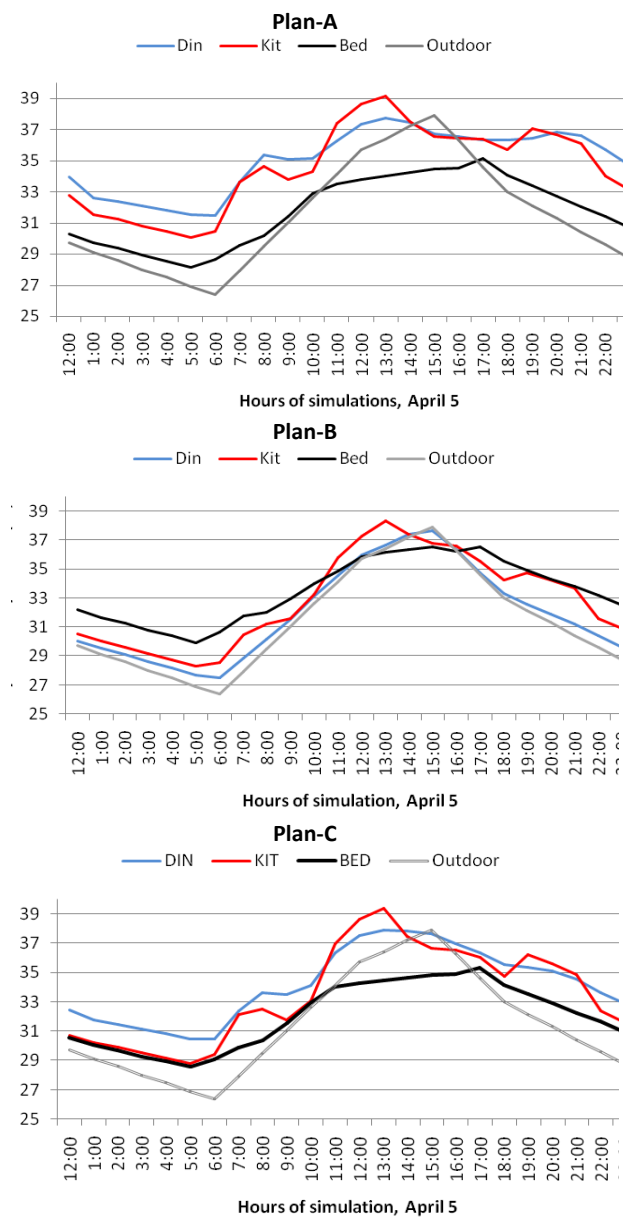


Figure 5: Temperature (°C) simulation results of Plan-A(top), Plan-B(middle) & Plan-C(bottom)

From Figure 5(top), it is clearly evident that in Plan-A (Figure 1), the dining room which has no ventilation potential, experiences same temperature swing as it is

PLEA 2018 HONG KONG

Smart and Healthy within the 2-degree Limit

evident in the adjacent kitchen. Moreover, its temperature is most of the time higher than the kitchen. Surprisingly the bed room next to kitchen, although having no buffer space in between, experiences better temperature pattern all day long. One assumption was that cross ventilation opportunity of the bed room due to its bilateral windows helped in reducing its temperature.

Figure 5(middle) shows temperature pattern in Plan-B (Figure 2). Both the bed room and the dining room are separated from kitchen through common walls. None of them have buffer space in between. Therefore both were expected to have similar temperature pattern like the kitchen. However, for the majority of time, the bed room experiences higher temperature than both the dining room and the kitchen. The single-sided ventilation of the bed room might be the reason for it. Surprisingly, both dining room and the kitchen experiences lower temperature pattern like the outdoors. The cross ventilation potential might be the reason for it. From the weather data, it is found that on the studied day, air flows from south all day long. Therefore, the dining room is expected to have cross ventilation from south to north end; the kitchen is expected to have cross ventilation from its south facing door through its north facing window.

Figure 5(bottom) shows that the bed room experiences better temperature compared to the other two. It might be because of its separation from the kitchen by a buffer space and it has cross ventilation potential from its bilateral windows. The dining room is separated from kitchen through a common wall. Besides it has only single-sided ventilation potential. Therefore, it experiences higher temperature than the other two. However, it is not clear why kitchen, although having single-sided ventilation opportunity, experiences lower temperature than the dining room.

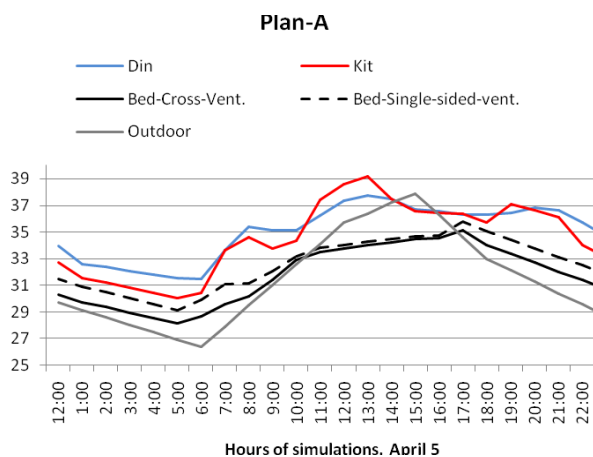
To examine the expected impact of cross ventilation mentioned above, all the plans had to be simulated further.

Figure 6: Comparison of bed room temperature between cross-ventilated and single-sided ventilated situation

First, benefit of cross-ventilated bed room in Plan-A was studied. Two sets of simulations were carried out. In one simulation, both bed room windows were kept open; in another simulation, only one bed room window was kept open. The results compliment with the assumption made in previous paragraphs. Bed room experiences lower temperature when it is cross ventilated. It experiences bit higher temperature when it has single-sided ventilation. It is shown in Figure 6. A temperature-rise of 1.5°C has been observed when one of the windows were kept closed. The simulations referred in Figure 5 were performed with bed room doors being closed from the dining room. It was intended to simulate times when privacy is ensured. However, bed room doors are seldom kept open towards dining room especially when dining room has no exterior walls to have ventilation. To examine such situation, Plan-A, where dining room has no exterior wall, was again simulated with bed room doors being kept open. The results are shown in Figure 7 (top).

Figure 7 (Top) shows that when bed room door is closed, the bed room is cooler and the dining room is warmer. The situation reverses when the door is opened. While bed room door is closed, the dining room does not have ventilation option other than through kitchen door. Therefore, dining room experiences the highest temperature, even sometimes higher than the kitchen. At the same time, bed room remains cooler since it is not getting any convective heat transfer from kitchen via the dining room. A close review of the data reveals that the bed room gets up to 2.7°C warmer when the door is opened towards the dining room. Similarly, the dining room also gets up to 2.8°C warmer when the dining room has limited ventilation option due to bed room door being closed. This same investigation was performed for Plan-B and Plan-C to see the temperature pattern in dining room under both cross ventilated and single-sided ventilation situations. Plan-B simulation results (Figure 7-middle) shows that temperature in dining room remain unchanged whether bed room door is closed or not. It is because the dining room is cross ventilated. However, when the bed room door is open, the bed room gets much warmer due to possible convective heat transfer from the kitchen. Up to 2.2°C temperature-rise has been observed.

Plan-C has dining room that has single-sided ventilation option. Besides, its bed room is separated from kitchen by a buffer space. Figure 7 (bottom) shows that bed room experiences lower temperature when the door is closed. If the door is opened up towards dining room it gets up to 1.7°C warmer. The dining room gets benefitted when the door is open.



PLEA 2018 HONG KONG

Smart and Healthy within the 2-degree Limit

Compared to a closed bed room door situation, open door situation allows up to 0.9°C lower temperatures. However, this temperature reduction is not as significant as it is in Plan-A since temperature is already reduced due to its single-sided ventilation option. Therefore, it is evident that dining room must have cross ventilation or at least one exterior wall to have single-sided ventilation opportunity. Otherwise, the bed room has to leave its door open which would result in unwanted temperature-rise in the bed room.

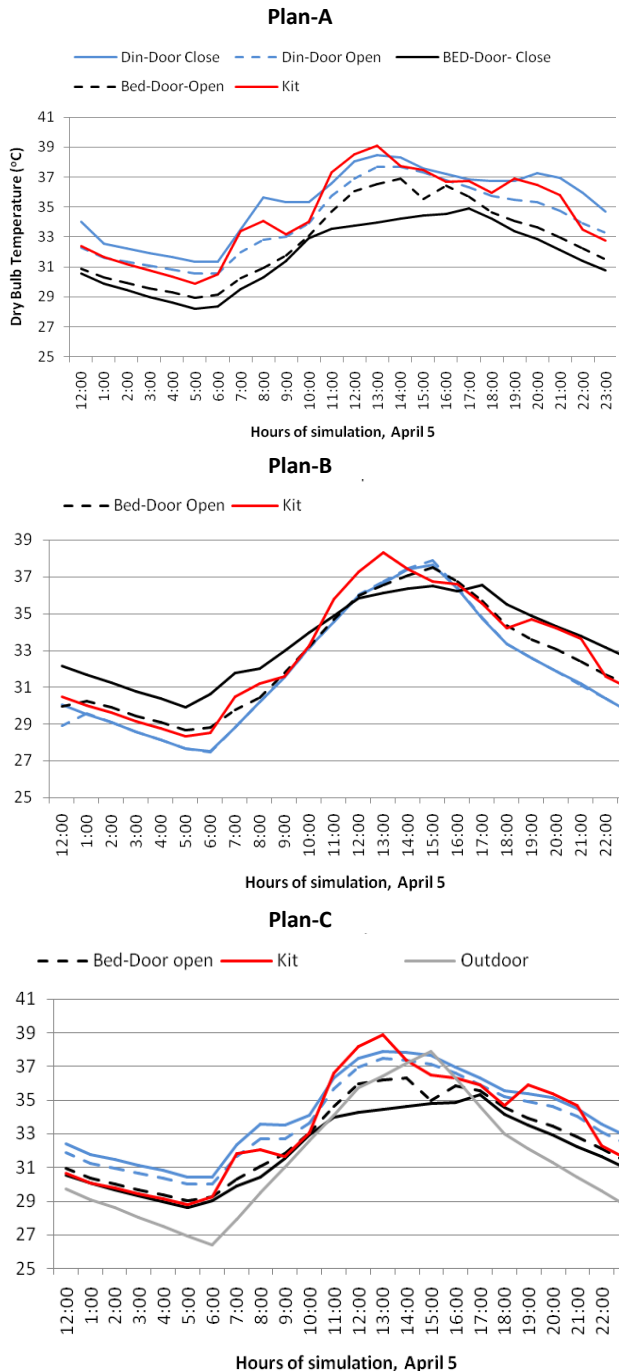


Figure 7: Comparison of temperature (C°) in all three plans for two situations – doors kept open & close

5. DISCUSSION

Examination of the above mentioned results could be summarised like the following. Dining rooms are more vulnerable to kitchen heat than bed rooms. It is because, in all the studied plans, it is directly connected to kitchen through both a common wall and a common door. A cross ventilated dining room found to be the best strategy to address this difficulty. Dining room without ventilation to outside is the worst case. It has been observed in Figure 7 (Top) which represents Plan-A. Single-sided ventilation found to be a better option than a no-ventilation case but it is not as effective as cross-ventilation.

The results for bed room are not what it was expected. Bed room's proximity or its separation strategy from kitchen found to be insignificant in terms of kitchen heat transfer. Rather bed rooms' physical connection to kitchen heat through door opening found to be significant. An in-between buffer space was assumed to be a better strategy than an in-between common wall. However, plan-A and Plan-B simulation results show that the common wall between kitchen and the studied bed room have least impact when door is closed. When door is open, bed room in Plan-A gets higher temperature but the bed room in Plan-B is unchanged. It is because, in Plan-A, kitchen heat is trapped in the unventilated dining room hence the heat enters into the bed room. On the other side, kitchen heat did not get a chance to stay in the cross-ventilated dining room hence no heat entered through the bed room door.

So, this study concludes that during apartment design, caution should be taken in providing dining room in the plan. Cross-ventilated dining room should be the first target. If not, at least single-sided ventilation option must be there. In no case, dining room should be surrounded by other rooms.

6. CONCLUSION

This paper investigated kitchen and surrounding room layout of apartment design to identify effective ways to mitigate kitchen generated heat. Reviewing more than hundred apartment plans, the following patterns have been identified – bed rooms are separated from kitchen either by a common wall or a buffer space; dining room next to kitchen have either cross-ventilation, single-sided ventilation or no ventilation. Three apartment buildings were identified where all the patterns exist. Both field measurements and computer simulations have been carried out. A buffer space between kitchen and bed room was assumed to be a better option but the study results do not agree to it. The common wall found not to be the reason for temperature rise in bed room rather temperature rises when bed room door is open. Impact of kitchen heat is minimized when dining room has cross ventilation option. In no case, dining room should be surrounded

PLEA 2018 HONG KONG

Smart and Healthy within the 2-degree Limit

by other rooms. If not, at least single-sided ventilation option must be there.

7. LIMITATION & FUTURE WORK

The selected apartments were simulated following their original orientation. Orientation variation has not been explored and will be carried out in future research. Due to unavailability of CFD tool and access to powerful computational resources, both temperature and air flow patterns have not been examined. Upon receiving such resources, this will be carried out in future.

ACKNOWLEDGEMENTS

The author acknowledges the monetary support awarded by the North South University as its 2017-18 NSU Research Grant.

REFERENCES

1. Li, A., Zhao, Y., Jiang, D., & Hou, X. (2012). Measurement of temperature, relative humidity, concentration distribution and flow field in four typical Chinese commercial kitchens. *Building and Environment*, 56, 139-150. doi: <https://doi.org/10.1016/j.buildenv.2012.03.001>
2. Nyström, M. (2003). Kitchen design: energy and health in the eyes of the beholder. *Energy for Sustainable*

- Development, 7(3), 8-29. doi: [https://doi.org/10.1016/S0973-0826\(08\)60361-0](https://doi.org/10.1016/S0973-0826(08)60361-0)
3. Saha, S., Guha, A., & Roy, S. (2012). Experimental and computational investigation of indoor air quality inside several community kitchens in a large campus. *Building and Environment*, 52, 177-190. doi: <https://doi.org/10.1016/j.buildenv.2011.10.015>
 4. Debnath, R., Bardhan, R., & Banerjee, R. (2016). Investigating the age of air in rural Indian kitchens for sustainable built-environment design. *Journal of Building Engineering*, 7, 320-333. doi: <https://doi.org/10.1016/j.jobee.2016.07.011>
 5. Gu, L. (2007, September) Airflow network modeling in EnergyPlus. Paper presented at the Building Simulation, Beijing, China.
 6. Zhou, B., Chen, F., Dong, Z., & Nielsen, P. V. (2016). Study on pollution control in residential kitchen based on the push-pull ventilation system. *Building and Environment*, 107, 99-112. doi: <https://doi.org/10.1016/j.buildenv.2016.07.022>
 7. Wei, P., Zhou, B., Tan, M., Li, F., Lu, J., Dong, Z., . . . Xiao, Y. (2017). Study on Thermal Comfort under Non-uniform Thermal Environment Condition in Domestic Kitchen. *Procedia Engineering*, 205, 2041-2048. doi: <https://doi.org/10.1016/j.proeng.2017.10.084>

PLEA 2018 HONG KONG

Smart and Healthy within the 2-degree Limit

Breaking the Glass Box:

Strategies to reduce the Energy Consumption in 24/7 IT Offices in Delhi NCR

GUNVEER SINGH¹, JORGE RODRÍGUEZ-ÁLVAREZ¹

¹Architectural Association School of Architecture, London, United Kingdom

ABSTRACT: This paper focuses on the trends of 24/7 occupied IT offices in the Northern part of India. The rise of the IT Industry in India has resulted in an adaptation of the office spaces to the international trends of constructing glass box with deep plans and high glazing ratios coupled with aluminium composite panels with less considerations to the environmental and occupant needs. Such buildings are invariably dependant on air conditioning which results in huge energy expenditure. Fieldwork and Survey conducted for analysis illustrate the trends of the building typology which can be used as a basis for potential design solutions for IT offices being constructed in Delhi NCR by understanding the factors affecting the high energy demands and the spatial relationships.

KEYWORDS: Energy Use Intensity (EUI), Occupancy, Cooling Set point, Equipment, IT Office

1. INTRODUCTION

Post Globalization, India has experienced a tremendous growth of the tertiary sector, which burgeoned the demand for new office spaces. The Information and Technology (IT), Industry has been at the fore front of the demands with about 70% of the offices that are being developed are occupied by them. [1] As per the report published by BEE (Bureau of Energy Efficiency, Government of India), the building sector is growing rapidly in India. Offices are developing at a rate of 8% annually and it is projected to reach approximately 20000 million sqm by 2030.[2] Moreover, Gurgaon and Delhi NCR have the highest preference for the development of IT and SEZ spaces, accounting for almost 60% of the total spaces.

Setting up global companies and the drive to compete with developed nations, glass boxes with deep plans have become synonymous with the IT industry. Such a drive to achieve visual cohesion and standardized indoor environment for a workspace has resulted in a heavy reliance on mechanical conditioning and artificial lighting, to maintain a reasonable operating condition, which results in higher energy demands. The extensive financial capabilities of the IT firms usually condone the dearth of consideration of energy consumption by the designers.

Green rating systems plays a crucial role in the design of IT offices. Designers and developers seek a certification merely for its cachet, rather than designing to achieve occupancy driven design. For instance, The DLF Infinity Towers in Gurgaon is a LEED Silver certified building. However, the building scores extremely low for its Indoor Environmental Quality,

due to lack of provision of thermal or lighting control to the occupants. Even in terms of daylighting the building does not meet the benchmark. [3] Such facts, stimulate a sceptical view on the approach towards sustainability.

In India, IT industry is dominated by two major components: IT services and business process outsourcing (BPO). Majority of the companies are from United States, Japan and United Kingdom. This requires a 24-hour operation of the office to cater to the different time zones. Various offices have different considerations for specifying their schedules and thus, this diversity in the scheduling is a challenging aspect for environmental considerations.

A 24/7 IT office is structured into 2 main operational divisions known as the Off-shore Development Centre (ODC) and the financial centre. The morning shift has operations in the ODC and the financial centre. The intermediate and night shifts have operations primarily in the ODC space. The ODC spaces are typically designed with an extremely high occupancy, resulting in high internal loads as these are usually accompanied by excessive equipment usage. Figure 1 shows the layout of a floor space occupied by Infosys in DLF building 6, Gurgaon.

PLEA 2018 HONG KONG

Smart and Healthy within the 2-degree Limit

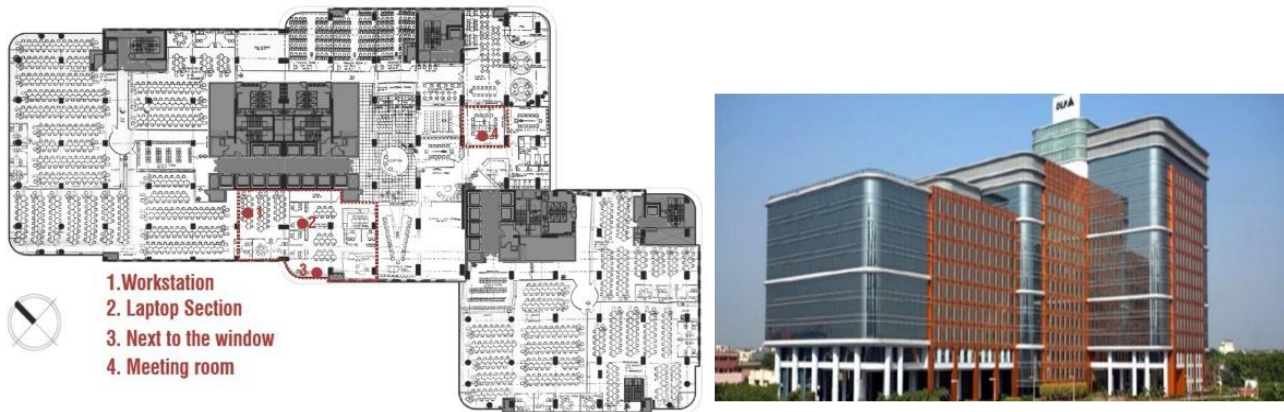


Figure 1: Floor Plan of Infosys [source: Acquired from Management] and exterior view in DLF Building 6, Gurgaon [source: www.dlfcybercity.com]

Methodology

The starting point of the research was the fieldwork and a pilot survey to understand the behaviour and comfort of the occupants in the IT offices. Energy bills were acquired and compared with the benchmark that was set by the Bureau of Energy efficiency in India. Further analysis was carried out by generating a thermal model for one of the office spaces that was calibrated against fieldwork data. The model was manipulated to infer the impact of various corrective measures, such as the cooling set point, density of occupation, and material specifications on the overall cooling loads of the office spaces.

The next step was to check the impact of glazing ratios and orientations in terms of daylight levels and thermal performance through computer simulations. Radiance and Honeybee software were used for daylight simulations, with OpenStudio and Energy Plus for thermal simulations. Based on the analytical work, a design proposal has been developed with passive strategies to accommodate a 24/7 operating culture with a lower Energy usage.

2. FIELDWORK AND SURVEY

A survey was conducted to observe the work environment and Indoor Environment Conditions as per the occupants. The survey conducted was primarily focused on 3 parameters:

Office Size

Operational Hours and Occupancy Pattern

Equipment usage

2.1 Office Size

The size of an IT office depends on the kind of the space it is occupying. On an average the size of an IT office is about 300 employees, with 35% of the responses stating the number of employees being less than 200. But, there are companies that take up a bigger office space as well and from the survey about 9% of the responses stated that their offices to have more than 800 employees.

2.2 Operational Hours and Occupancy Pattern

The survey revealed that in an IT office, the employees usually work for 9 hours, 5 days a week. (Figure 2). One important factor is the break timing. The US Department of Energy(DOE) suggests a fixed break timing for an hour from simulation purpose. But, from Figure 2, we can understand that not all occupants have a same duration of break and it was also observed that in IT offices, one can take their break within a time range. Thus, there need to be flexibility in terms of the occupancy pattern. The survey data was used to formulate an occupancy pattern by developing a script on grasshopper, as shown in Figure 2. The CIBSE guidelines combined them with the pilot survey, resulted in a shift in the maximum occupancy ratio. The night shifts usually have a lower overall occupancy, as certain departments run just single shift during the day. The maximum occupancy ratio during the night was considered 0.5. Understanding the occupancy pattern is significant to recognize its impact on the internal loads during the operational time. A Critical point is observed during the change of shift.

2.3 Equipment Usage

Gunay et al. [4] stated that the most common plug-in equipment in office buildings are computers and monitors, photocopier, printers, and network equipment. Computers and monitors are responsible for about 70% of the plug-in equipment electricity use in ICT related office buildings.

The occupancy pattern specified earlier can help in defining the operational characteristics for the equipment, such as:

T-arrival (Shift time): Standard arrival time

T-Departure (Shift time): Standard departure time

T-arrival (Extended): Early arrival

PLEA 2018 HONG KONG

Smart and Healthy within the 2-degree Limit

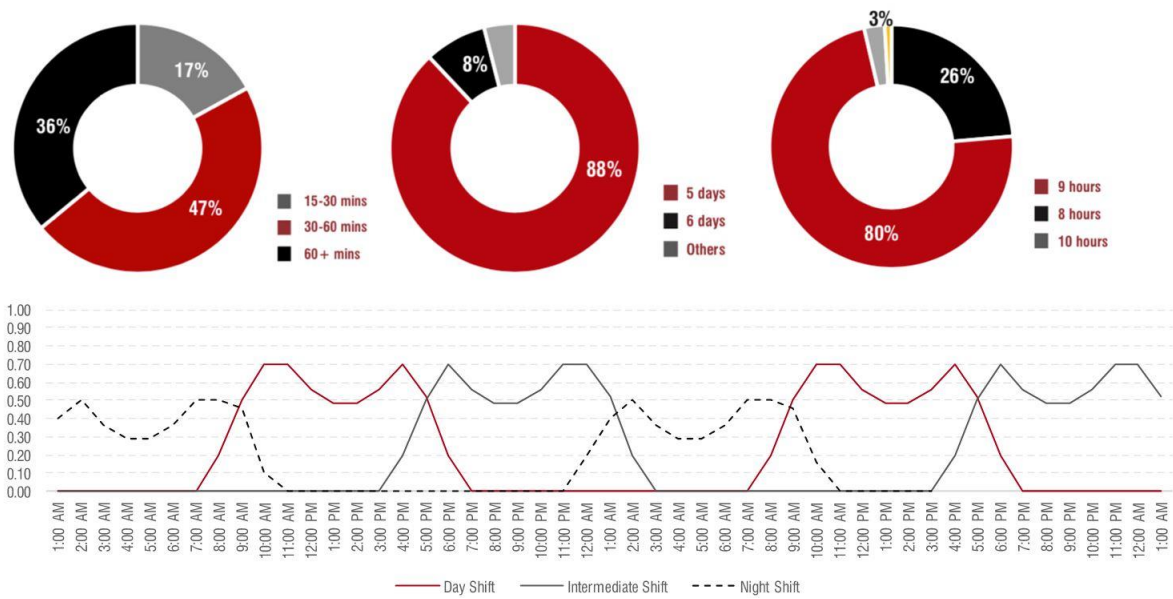


Figure 2: Survey results for: Duration of Break during the operational timing (top left), Number of Working Days in a da (top centre), Hours of operation/shift duration (top right). Occupancy Pattern Generated using the survey results (bottom).

T-Departure (Extended): Late departure

Based on the Pilot survey conducted, variations can be observed in the Internal Gains based on the occupancy type, ranging from 140 W/person in case of a hot desk to 210 W/person in case of individual cabin spaces.

2.4 Energy Usage Intensity (EUI)

The EUI for 'three-shift commercial office buildings' is benchmarked at 350 kWh/m²/year in the ECO III project.[5] The main reason associated with such a high number could be the operational schedule of these office spaces. Apart from the study conducted by the ECO III project, Bureau of Energy Efficiency, India (BEE) also has its own benchmarking that is based on the climatic condition the building is designed in and the percentage of space that is air conditioned. They have divided the commercial sector into 5 different categories, i.e., IT parks, offices, hotels, hospitals and retail shopping centres. In case of 24/7 operating offices, the benchmarking is based on the hours of operation of an office space. This is known as the "Average Annual Hourly Energy Performance Index'(AAHEI). The unit is Wh/m² and the minimum AAHEI should be 52 Wh/m². If the value is compared with other standards with a consideration of 24/7 operation, the EUI is about 450 kWh/m²/yr.[2]

A field survey was conducted to collect the annual energy bills for the IT offices that run 24/7 in IT parks in the Delhi NCR region and the tri-city around Chandigarh. As shown in table 1, the offices surveyed exceeded the benchmark set by the Bureau of energy efficiency, as highlighted. The high EUI for the analysed

offices could be due to high cooling demands and 100% space cooling without significant occupant control.

Table 25: Energy Usage from seven IT offices compared against benchmark

	kWh/m ² /yr
BEE Benchmark	350-450
Reliance communication, Chandigarh	615
Baseware corp. Office 2, Chandigarh	780
Infosys, Chandigarh	650
Baseware corp., Chandigarh	800
Trigma, Chandigarh	610
Concentrix, Chandigarh	1070
Infosys, Building 6, Gurgaon	830

2.5 Case study

Out of the buildings surveyed for the Occupant comfort and compared with the benchmarks, Infosys DLF Building 6 in Gurgaon was considered for installation of data loggers to measure the occupied space (Figure (3)).

As shown in Figure (1), the data loggers were placed in 4 different places with different equipment usage and occupancy patterns. The lower cooling set-points result in a minor temperature fluctuation in the spaces which doesn't account for the occupant adaptability. Most of the spaces run at temperatures lower than the adaptive comfort range, thus, providing potential for operational changes for air conditioning and testing of other measures for reducing the energy consumption.

PLEA 2018 HONG KONG

Smart and Healthy within the 2-degree Limit

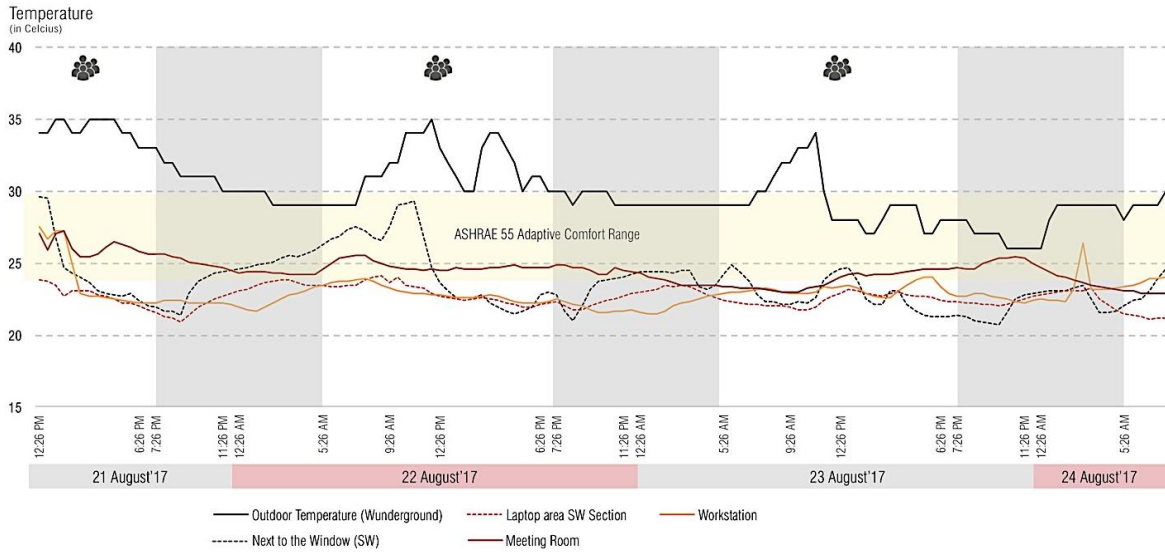


Figure 3: Indoor air temperature in of the Infosys in DLF Building 6, Gurgaon during the monitored period

3. BASE CASE CALIBRATION AND BASIC ENERGY SAVINGS

3.1 Climate

In Gurgaon, the daily thermal swing is a key factor for understanding the climate. The year is divided into four periods: Summer, Monsoon/Transitional period, winters and spring. The highest temperatures occur during the summer months (i.e. from April - June end), with a diurnal variation between the range of 9.5K to 13.5K. Mid May to June end observes the hottest period with the temperatures going up to 45°C during certain times of the day and the coldest period is observed between the December and February with an average diurnal variation of 12K and an average temperature ranging between 14°C to 17°C. The monsoon period/transitional period i.e. July to Sept end has a very low diurnal variation. The monthly mean relative humidity ranges from 39% in April to 74% in August. The summer period has very low humidity level with the relative humidity between 39% to 57%. Whereas, the winter months have a higher humidity levels, averaging approximately 69%.

3.2 Base case and potential savings

Based on the fieldwork, an office space from the DLF building 6, Gurgaon was considered for analysis. The base model was calibrated according to the fieldwork (Figure 3), to understand the parameters effecting the cooling loads and subsequently analysing the reduction potential by retrofitting the building or changing the program of the space as shown in Figure 4.

For analytical purpose, the ODC (Off-shore Development Centre) was simulated. This space is an open plan space with a very high density of 4.5 m²/person. The office space operates at a set point between 21-24°C. The analysis showed that: The base case has an overall energy consumption of

962.4 Kwh/m²/yr. with a cooling load of **727.6 Kwh/m²/yr.** A low Set point of 21°C coupled with high internal gains and occupancy density, results in a cooling load density of 84W/m².

Changing the cooling set point to 24°C with similar internal loads, a reduction in the cooling load density from 84 W/m² to 65 W/m² is observed, reducing the EUI to **891.3 Kwh/m²/yr.** If the set point was set to 26°C, a further reduction can be observed in the EUI to **809 Kwh/m²/yr.**

High density of the occupied space of 4.5 m²/person results in higher equipment load density of 30 W/m². If the office space is occupied at 6 m²/person, the equipment load density reduces to 25 W/m², significantly reducing EUI to **752.2 Kwh/m²/yr.** along with cooling load density down to 54 W/m².

As per ECBC compliance [6], retrofitting the wall assembly to achieve a thermal conductance of 0.4 W/m²-K and providing a double glazed window with the SHGC of 0.3 and thermal conductance of 2.1 W/m²K, reduces EUI to **693.6 Kwh/m²/yr.,** in case of 24°C set point and a further reduction to **608 Kwh/m²/yr.** with 26°C set point.

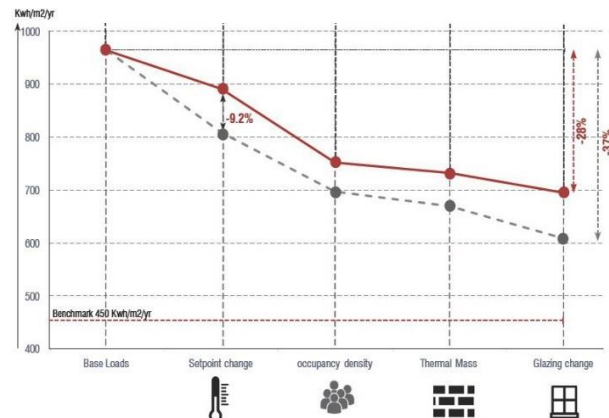


Figure 4: Potential savings by optimization

PLEA 2018 HONG KONG

Smart and Healthy within the 2-degree Limit

	Out-Source Development Center	Training Room	Projection Room	Meeting Rooms	Security Check Area	Printer room	Locker Room	Finance center	Breakout Spaces	Restaurants/Cafeteria	Server Rooms	Circulation Cores	Reception Area
ENVIRONMENTAL													
Daylight	■	■	■	■	■	■	■	■	■	■	■	■	■
Natural Ventilation	■	■	■	■	■	■	■	■	■	■	■	■	■
Solar Access	■	■	■	■	■	■	■	■	■	■	■	■	■
Acoustic Isolation	■	■	■	■	■	■	■	■	■	■	■	■	■
Individual Thermal Control	■	■	■	■	■	■	■	■	■	■	■	■	■
Mechanical Cooling	■	■	■	■	■	■	■	■	■	■	■	■	■
OTHER													
Privacy	■	■	■	■	■	■	■	■	■	■	■	■	■
Glare Control	■	■	■	■	■	■	■	■	■	■	■	■	■
Security	■	■	■	■	■	■	■	■	■	■	■	■	■

Figure 5: Design matrix for Spatial and Environmental aspects

4. DESIGN STRATEGIES FOR LOW ENERGY OFFICES

4.1 Design Concept

The measures analysed so far have considered materials, occupancy and the impact of cooling set point on the EUI to achieve Thermal comfort. The following stage of the investigation addresses design aspects, not least the built form and proportion of glazing to provide alternatives to the archetypical IT office.

First, most contemporary IT parks are vertically stacked office spaces with offices of multiple shifts operating on different floors. The occupants are not afforded any control over the cooling set points. The first design concept to be explored was the splitting of the office spaces in separate towers, based on operational timing. This results in horizontal expansion of the built spaces rather than vertical stacking of office space.

Secondly, the IT offices are completely air conditioned which led to continuous supply of cooling to areas that are not even occupied at a given point time. Thus, segregation based on spatial and occupancy was done. The spaces with high internal gains and occupancy were considered for air conditioning, while the spaces with variable occupancy patterns and less internal gains were labelled as non-air-conditioned spaces or

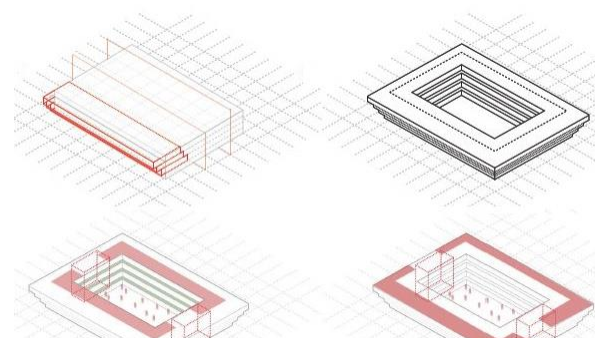


Figure 6: Design stages. From top left, clockwise: stepping, final form with a landscaped courtyard passively cooled, mixed mode and free running spaces facing the courtyard with the cores on the opposite ends, ODC and Finance centre which will be air conditioned placed outward.

under mixed-mode operation, reducing the overall air-conditioned space to 70%. For understanding the spatial context, a sustainability design matrix was graphed to highlight the services that are critical for a designed space and the ones which are not important for consideration as shown in Figure 5.

Finally, a climate responsive built form should provide protection from the strong solar radiation while allowing sufficient daylight to reduce solar and artificial lighting gains. A shallow plan with a vegetated courtyard and stepped floors on the perimeter was the design concept to be explored. This arrangement would divide the floors in passive and active areas. The provision of 2 separate circulation cores on the opposite ends of the floor space allowed a horizontal expansion and formation of a courtyard within the typology (see Figure 6).

4.2 Energy saving potential

Thermodynamic models were designed to analyse the impact of the proposed strategies:

The first step was to **reduce the air conditioned area**. The office support areas (like: locker room, security areas, print rooms etc.) were grouped and left in a free running mode, whereas other spaces have time driven and variable occupancy patterns (like meeting rooms, conference rooms). It was found that only the Off-shore development centre (ODC), finance centre and training room requires the air conditioning due to maximum occupancy during the day. This resulted in reducing the overall air conditioned space to 70%. In terms of cooling loads and EUI, a reduction of 39% was observed with a set point of 26°C, compared to the optimized base case .

The design proposal of **40% Window-to-Wall (WWR)** throughout **with a double glazing with 6mm air fill and "stepping back" of the facades** to create self-shading for the exterior surfaces was analysed for not just the daylight performance but thermally helped reduce the energy consumption by a further 15%.

Subsequently **the impact of the thermal conductance of the wall constructions** was tested. In a composite climate with higher degree of dry days, the rigid insulation performed well as compared to a capacitive insulation. A variety of wall constructions were tested to understand the impact of on cooling loads. Based on the analysis, a cavity wall with 325 mm of polystyrene insulation and U-value of 0.4 W/m²-K was selected.

The benchmark set for a 24/7 IT office is 450 Kwh/m²/yr. The proposal with the specified design specifications and reduced air conditioned space, the office space was entirely occupied and running on 24/7 occupancy had an EUI of **322 Kwh/m²/yr**. BEE specifies that, in case of 24/7 operating office spaces, the EPI is in terms of Average Annual Hourly Energy Performance Index' (AAHEPI). The unit is Wh/hr/m². [7]

PLEA 2018 HONG KONG

Smart and Healthy within the 2-degree Limit

Based on the values specified for composite climate, the AAHEPI for the design ranges between 26 Wh/m² to 30 Wh/m² depending on the case of occupancy (Fig. 7).

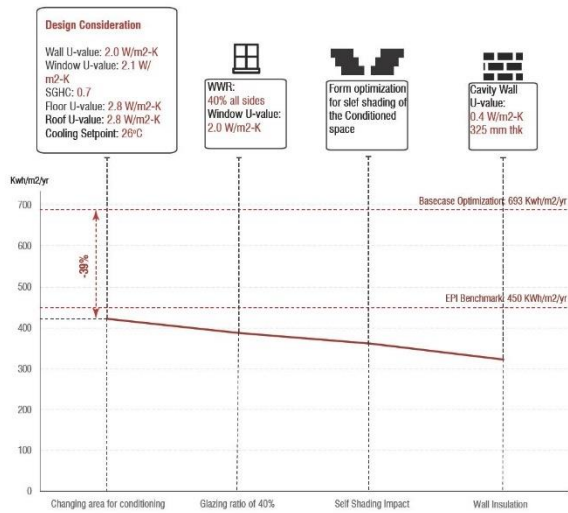


Figure 7: Design optimization and savings potential

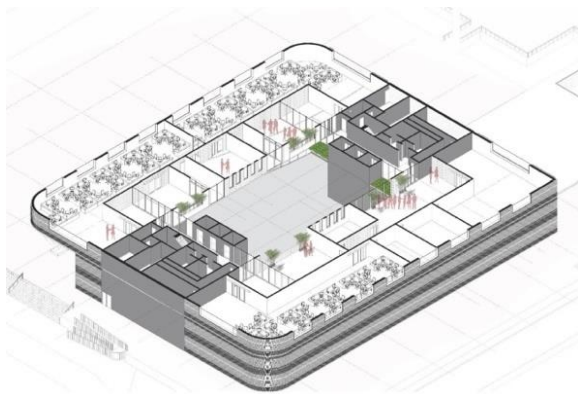


Figure 8: Optimized office layout for a 24/7 low energy office

5. CONCLUSIONS

The paper illustrated the trends of office size, occupancy density, equipment usage and the Energy Use Intensity through results from survey and fieldwork. The spaces in case of a core and shell building typology have shown higher energy consumptions, especially the cooling loads. The high internal gains due to high occupancy and equipment usage coupled with poorly insulated glass boxes with least consideration to the orientation and climate have been the main culprits for extremely high cooling load densities and Energy Use Intensities.

The calibrated base case provided a better understanding about the impact of the occupancy density and equipment usage on the overall energy usage. A possible reduction of 28% in the EUI was observed in case of office spaces designed for 6 m²/person density and a cooling set point of 24°C and approximately 37% reduction with a set point of 26°C. But, even with approximately a third in reduction of the EUI, the overall consumption was very high

because of deep plans and 100% conditioned space. The design proposal (Figure 8) firstly focuses on the spatial programming and environmental parameters which are critical for given space type.

The climatic conditions forced the design typology to be introvert with the passively cooled or mixed-mode operating spaces facing towards the courtyard being formed and the ODCs or the air conditioned spaces facing outwards with a stepping out concept to self-shade the lower floor. The above mentioned strategies itself resulted in a reduction of 39% from the optimized base case.

The window to wall ratio of 40% coupled with insulated exposed walls with a thermal conductance of 0.4 W/m²K resulted in a further reduction of EUI to 322 Kwh/m²/yr. The resulted values are lower than the specified benchmark of 455 KWh/m²/yr but are still considerably high because the occupancy density for the simulation of the conditioned ODC was taken as 4.5 m²/person which affected the equipment usage. Finally, this work aims to go beyond the theoretical sphere. The proposal is technically and spatially feasible and hence is aimed to meet the demands of a 24/7 operating IT office more efficiently.

ACKNOWLEDGEMENTS

The paper produced is based on the research conducted for a dissertation for MArch in Sustainable Environmental Design program at Architectural Association School of Architecture. I would also extend my gratitude to the institute and the offices that provided valuable information for the research.

REFERENCES

- Nasscom Report. (2012): "The IT-BPO Sector in India: Strategic Review 2012". [Online], <http://www.nasscom.org/domestic-itbpo>
- Building Code and Rating in India [Online], https://www.rehva.eu/fileadmin/events/eventspdf/REHVA_ACREX_2013_Seminars/REHVAISHRAE_EC_BEE_seminar_S_Kumar_Deepa_.pdf
- LEED Buildings Scorecard [Online], <http://www.gbig.org/activities/leed1000039978/dashboard>
- H.B Gunay, W O'Brien, I Beausoleil- Morrison, S Gilani, Modelling plugin equipment load patterns in private office spaces
- Benchmarking Energy Use in Buildings and Cleanrooms [Online] http://www.iesaonline.org/presentations/vs2011/Dr.%20Satish%20Kumar_Schneider.pdf
- ECBC Guidelines [Online], energysavers.co.in/wpcontent/uploads/2014/12/ECBC-User-GuidePublic.pdf
- Details of the scheme for rating the building-BPO [Online] <https://beeindia.gov.in/sites/default/files/BEE%20star%20Rating%20for%20BPO.pdf>

Integrating Hydroponics into Office Buildings: Model and presentation of the impacts of edible plants on the indoor environment on occupants

MELANIE JANS-SINGH¹, HELEN GILLARD¹, REBECCA WARD¹, RUCHI CHOUDHARY¹

¹University of Cambridge, Cambridge, United Kingdom

Integrating plants into our built environment could help reduce temperatures and improve air quality, and thus reduce the need for ventilation, heating and air conditioning. Hydroponics allow to grow a high density of plants with little maintenance, weight and water use. The aim of this paper is to determine the potential advantages and viability of integrating numerous hydroponic modules in an office building. It presents in a first part the implementation of 50 hydroponic modules in an office building in Cambridge. The second part discusses the qualitative and quantitative monitoring of the impact of plants on the office. Finally, a model of interactions between the plants and the building environment is presented, and initial results of running a plant module in building energy simulation software TRNSYS are shown. Creating the model alongside the implementation project allowed to gain further insights into the impacts on environmental conditions, building energy use, and occupants of integrating a large density of plants into a building.

KEYWORDS: Energy efficiency, Urban farming, hydroponics, occupants

1. INTRODUCTION

Almost 4 billion people are living in cities around the world, representing 54% of the global population [1], and the built environment accounts for over half global CO₂ emissions. Global urban population is set to rise by 2.6 billion by 2050, which will continue to put pressure on the energy supply of cities, where demand is dominated by building energy use [2]. Thermal comfort is the driver behind building energy consumption in developed cities [3], and energy used for cooling is expected to rise by up to 30% by 2050 [4]. This research paper presents the concept of using a modern technology, hydroponics, to improve building air quality, energy use and occupant well-being. Growing plants with hydroponics helps reduce the mass and water volume of growing a high density of plants compared to growing in soil. The objective is to evaluate plant-air interaction on air temperature, humidity and CO₂ levels in buildings, thereby impacting on the need for mechanical ventilation, heating and cooling of buildings. By focusing on the implementation of hydroponic modules in an office building, the aim is to present the effects of a large density of plants in buildings, both practically and through a “plant module” model to be incorporated in building energy simulation.

First, this paper will present the setup and design of 50 hydroponic modules in the James Dyson Building (JDB) at the University of Cambridge. In a second part, the qualitative and quantitative monitoring put in place to record the effects of the plants on the building environment and social network will be discussed. The

third section presents how a “plant module” has been developed to be integrated with traditional building energy simulation software TRNSYS [4]. Initial results from modelling the third floor of the JDB with varying levels of plants will be presented.

As plants in buildings may have a ground-breaking impact on indoor and façade building design in the future, the results of this paper will highlight how on-going monitoring of the building environment can be used to setup future projects, both through simulation and in practice.

2. SETUP OF HYDROPONICS IN AN OFFICE BUILDING

2.1 Hydroponic modules

Hydroponic systems offer an efficient method for intensively growing plants in controlled environments, with plant roots suspended in nutrient rich water, with minimal inputs of resources compared to conventional methods [6]. Two systems were installed in the building: 45 hydroponic modules from IKEA (Tragger/Vaxer, [7], Fig. 1) on windowsills by the glass



Figure 92: IKEA module with white cabbage [7]



Figure 93: Aponic unit with basil [8]

facades and on desks, and 4 Aponic [8] vertical aeroponic modules along building columns and in the communal area (Fig. 2).

PLEA 2018 HONG KONG

Smart and Healthy within the 2-degree Limit

The IKEA units are 40x23x6 cm water reservoirs, with a perforated lid which can take up to 8 pots of plants (Fig. 1). The seedling is grown in rockwool, and transplanted into mesh pots, where the rockwool pod is supported by inert and porous growing media, such as perlite, vermiculite, clay balls or coconut coir. The modules need to be watered once a week with approximately 1.5 L of water, and 10 mL of nutrient solution.

The Aponic units consist of three vertical tubes, which each hold up to 25 plants vertically, over a surface area of 100x90x15 cm. The interface between the rockwool seedling and the tube is green foam, and the roots are exposed inside the tube. The roots are sprayed every 15 minutes, for 10 seconds, from a pump linked to the reservoir beneath, with an estimated requirement of 10 L/month of water with 15 mL of nutrients.

The location of the plant modules across three floors in the JDB is illustrated in Fig. 3 below. In total there were 280 edible plants growing in the modules in the building at the time of writing.

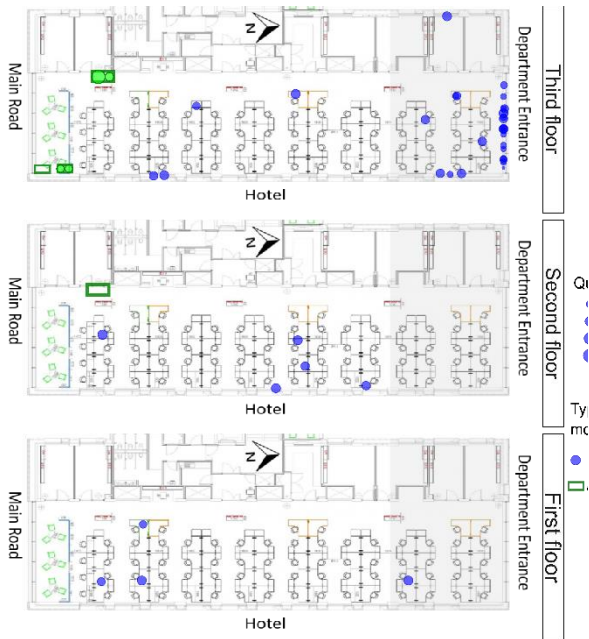


Figure 94: Map of location of plant modules over the floorplan as of 07/06/2018 in the JDB. The point size indicates the number of plants in the module.

2.2 Urban farming community

To maintain the project, 25 volunteers have signed up to be part of a “Community of Growers”, where they have engaged to water, prune, harvest the edible plants grown in the office. Workshops, posters, emails and word of mouth have led the community to grow, and it is expected the size of the community will double by the end of the year, now that the plant modules have been procured.

Leafy edible plants were chosen such as basil, lettuces and cabbage for their high leaf area index (LAI, ratio of

leaf area over planted area), easiness to grow, and to frame the project under an urban farming perspective. Due to popular demand, tomatoes and chilis are also being grown, and ornamental plants will be included in the future.

3. MONITORING THE IMPACT OF PLANTS IN THE OFFICE

3.1 Temperature, Humidity and CO₂

Sensors spaced at regular intervals all over the buildings record CO₂ levels, temperature, and mechanical ventilation rates [9]. Additional CO₂-temperature-humidity-light sensors will be installed closer to the plant modules, and to verify the building management data.

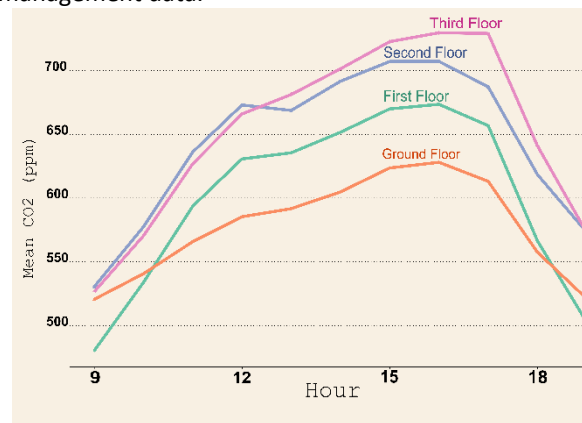


Figure 95: Average CO₂ over a year in the Dyson Building between 9am and 8pm on weekdays.

The ventilation is activated at CO₂ levels of 850 ppm according to the Breathing Buildings operations manual [9]. The monitored data shows that the JDB’s high occupancy rates lead to high CO₂ levels (Fig. 4) and ambient conditions (20-25°C, 50-80% humidity) which are ideal for productive plant growth [6]. Table 26 shows that the CO₂ levels tended to be much higher in winter and varied over the three monitoring years as number of occupants increased.

Table 26: Average number of hours/day environmental thresholds were reached on weekdays and triggered ventilation (Monday-Friday)

For the	April-May 2016 (first occupied)	April-May 2017	April-May 2018	December 2016-Feb 2017
3 rd Floor				
More than 850 ppm	0.51	0.58	0.74	3.21
More than 600 ppm	1.18	5.03	2.3	7.68

3.2 Qualitative assessment: individuals

A questionnaire was given to community members before the plants were introduced in the building in November 2017, and after in June 2018. The second

PLEA 2018 HONG KONG

Smart and Healthy within the 2-degree Limit

questionnaire was divided between active participants in the plants project, and passive participants, who simply enjoyed having a greener office or would like to participate in the future. The ease of maintenance, crop growth, and distribution of the modules is continuously being recorded as the project is being set up.

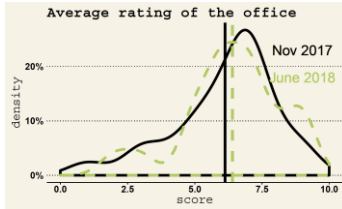


Figure 96: Rating of the office environment in November 2017 (black line), and in June 2018 (dashed green line). The vertical lines represent the average rating.

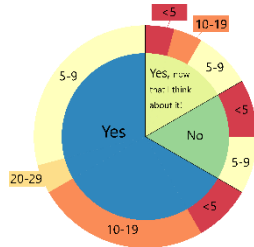


Figure 97: Answer to the question "Do you wish there was more interaction across the floor?"

Knowledge of plant growth: At the start of the project, participants interested in joining the community had a good grasp about how plants grew, and the nutrients required for healthy growing but would not feel confident about which month to harvest or sow seeds for typical crops such as strawberries or lettuce. Six months later, active participants in the scheme were much more confident at answering the ideal conditions for crop growth, compared to colleagues who do not grow plants.

Harvesting: Respondents tended to think favourably to eating the harvest from the office (65% responded they definitely or probably would), yet only 30% had eaten the produce yet.

Community: Most respondents wanted more interaction with other occupants of the office, yet some did not (Fig. 6 inner circle), and regularly interacted with less than 10 people. It was perceived that an office initiative such as the Community of Growers could provide an opportunity for increased interaction. The main reasons for participating were for improved quality of breaks, the opportunity to grow food, and to support the new office initiative.

Perceived quality of space: The overall ranking of the office slightly improved in between the two measured periods (Fig. 5), possibly due to people liking that there was an office initiative and enjoying the increased amount of plants. Occupants on floors with less plants wanted more, and occupants on the third floor tended to be happy with the level of plants in the office, as there were more plants (see Fig. 3).

3.3 Record keeping of plants growing in an office

Record keeping of crop growth, harvesting, watering and location of plant modules can be tricky in an open plan office, maintained by volunteers. After setup of the modules, the volunteers only need to regularly

update the average height and length of leaf, and number of plants growing in the module.

The average plant height was 17.05 cm, and leaf length was 5.22 cm for all the plants growing, from 7 months to 1 months old. Table 27 shows how the LAI [16] could be estimated with this information, the relationship will be refined with a larger dataset per crop type and stage of growth. The average LAI found was 0.775, which gave a total leaf area of 4.9 m², compared to a planted area of 6.9 m².

Table 27: Estimated values of LAI

Plant height	Leaf length	LAI
>0 cm	>0	0.2
>5 cm	>3cm	0.8
>10 cm	>3cm	1
>15 cm	>5cm	1.5
>15 cm	>10cm	2

4. PLANT MODULE FOR BUILDING SIMULATION

4.1 Theoretical model

The physiological nature of plant growth leads to CO₂, moisture and heat exchange with the environment. Modelling of plant growth so far has been limited towards horticultural commercial sites [10], or building-integrated greenhouses [11]. The plant-air interaction module is adapted from the model developed by Ward et al. (2017) [12] to simulate the environmental conditions in an underground farm called Growing Underground (GU). The model had initially been designed for a greenhouse in Kew Gardens [13], based on [14-15], and modified to model temperature, CO₂, and humidity of a four-layer hydroponic system under artificial lighting for GU. The change in temperature, humidity and CO₂ can thus be modelled by the heat and mass transfers described in the following equations, and schematically illustrated in Fig. 7. Fig. 8 shows how the plant module interacts with the existing flows in the building.

(1) **Sensible heat:** exchange of heat by convection, radiation and conduction between the "plant module" and the surrounding environment. Measured by change in temperature, given by Eq. 1, it is dependent on material properties of the plant elements and the building materials.

$$\frac{dT_j}{dt} = \frac{A_g}{m_j c_j} \sum_i q_{i,j} \quad (1)$$

Where A_g is the surface area (m²), and each layer j has a temperature T_j (K), mass m_k (kg), heat capacity (J/kgK). The change in temperature is due to the sum of the effect of each heat transfer process i (conduction, radiation, convection) defined by q_i between each layer.

$$\frac{dC_a}{dt} = \frac{A_g}{h_{fg}V} \sum_k q_k \quad (2)$$

PLEA 2018 HONG KONG

Smart and Healthy within the 2-degree Limit

(2) **Mass and latent heat:** exchange of water vapour, dominated by plant transpiration. As plants draw up nutrient-rich water through their roots, moisture evaporates from the leaves which releases latent heat and thus has a cooling effect (Eq.2).

$$\frac{dC_a}{dt} = \frac{A_g}{h_{fg}V} \sum_k q_k \quad (2)$$

Where C_a is air moisture content (kg/m^3), and each layer h_{fg} is the latent heat of condensation of water (J/kg), V is the volume of the unit (m^3). The change in air moisture content is due to the sum of the effect of each possible heat transfer process q_k (see Fig. 3) such as condensation and transpiration. Transpiration is based on the Penman-Monteith equation, and is a function of LAI, temperature differential, aerodynamic resistance r_a and mostly the stomatal resistance r_s to water vapour transfer [11].

(3) **CO₂ and O₂:** exchange of gases between leaf and the environment as part of the photosynthesis process. Eq. 3 shows the different components affecting the change in mass of carbon MC over time, based on the commonly used Farquhar-von Caemmerer-Berry model of the leaf photosynthesis process [18].

$$\frac{dMC}{dt} = MC_{supp} - MC_{i \rightarrow e} - MC_{i \rightarrow v} + \sum_{org} MC_{m \rightarrow i} + \sum_{org} MC_{v \rightarrow i} \quad (3)$$

The change in the mass of carbon MC is determined in greenhouse models by the additional CO₂, MC_{supp} , the losses due to ventilation ($MC_{i \rightarrow v}$), the net rate of CO₂ assimilation by the plant ($MC_{i \rightarrow v}$), the CO₂ contribution due to maintenance growth ($MC_{m \rightarrow i}$) and respiration ($MC_{v \rightarrow i}$). These processes are dependent on light intensity (particularly Photosynthetically Active Radiation PAR), temperature, and CO₂ levels, as well as plant specific parameters [12,19].

4.2 Modelling plants in the third floor

To integrate the plant module (Fig. 7) with the heat and mass flows in the building (Fig. 8), a simplified model of the third floor of the Dyson Building was developed in TRNSYS [19].

4.2.1 The TRNSYS model of the building

The building energy simulation software, TRNSYS [5] can calculate building energy use, temperatures and humidity of a building for a defined geometry, occupancy, equipment, ventilation and infiltration schedules, and a weather file input including solar radiation. For this first model, it was decided only to simulate the third floor, as this was where most of the plants were to be initially installed (see Fig. 3). The

building geometry was drawn in Google SketchUp (Fig. 9), and the material properties were defined in TRNBUILD. The weather data used was from Meteororm for Cambridge, UK.

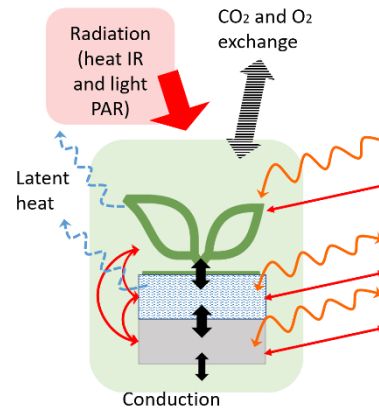


Figure 98: Schematic of heat and mass transfer process for a "plant module".

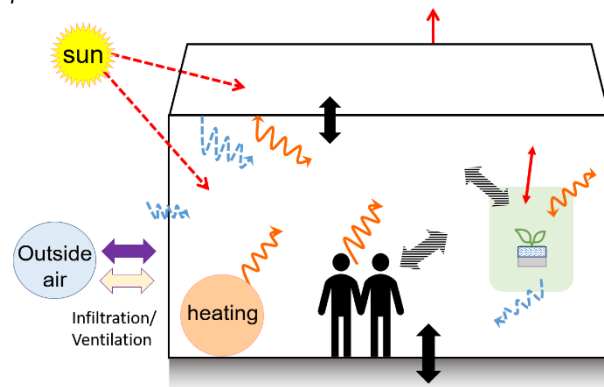


Figure 99: Integration of plant module into building energy model. The key is the same as for Fig. 7.

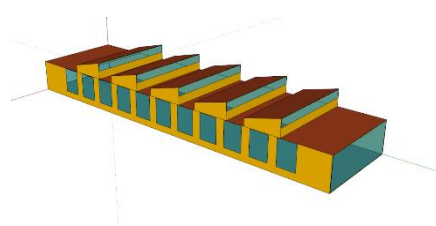


Figure 100: SketchUp drawing of the Third Floor of the Dyson Building [19].

4.2.2 Inputs

The material parameters (Table 28) were taken from the building manuals [9,17], national guidance [21] and architectural drawings. The internal gains were defined using CIBSE guidelines and based on observation and are summarised in Table 29.

Table 28: Material parameters of building components

Building component	Thermal conductance ($\text{W}/\text{m}^2\text{K}$)	Solar absorptance (-)	Heat transfer coefficient ($\text{kJ}/\text{hour m}^2\text{K}$)

PLEA 2018 HONG KONG

Smart and Healthy within the 2-degree Limit

External walls	0.16	0.6	11 (front of wall) 60 (back of wall)
Internal walls	0.16	0.6	11 (front of wall) 89 (back of wall)
Window material (insulating argon)	1.4	0.589	NA
Internal floor material (Bestest Heavyweight – floor)	0.04	0.6	11 (front of wall) 89 (back of wall)
Roof material (Bestest Heavyweight – floor)	0.04	0.6	11 (front of wall) 89 (back of wall)

Table 29: Internal heat gains in TRNSYS model

Internal Gains	Heat Gains	Schedule
People	35 people	50%: 8-10h and 16 to 20h 100%: 10-16h
Computers	140W/person	50%: 8-10h and 16 to 20h 100%: 10-16h
Artificial lighting	8 W/m ²	40%: 8-10h and 18 to 22h 100%: 10-18h

Heating was set to 22°C between 8am and 6pm, and with a maximum power of 140 kJ/h. External shading was in place only on the south facing windows with constant shading factor of 0.3. Internal shading was allocated to all windows but North facing, equal to total incident South face radiation divided by 3400 kJ/hour m², modified with shading factors along different surfaces [5]. To mimic the mechanically assisted passive ventilation [9] processes, two schedules were set: 5 ACH between 4 and 6pm, and an additional “summer ventilation” when temperatures exceeded 26°C in the summer months.

4.3. Plugging in the “plant module” into TRNSYS

Since building energy simulation models currently do not include plants, the plant model developed for GU [12] was adapted by Gillard (2018) [19] to use the building energy simulation as inputs at each time step, and integrated with the TRNSYS model using the object type 155.

Since the plants would receive daylight as well as artificial lighting the following equation was used for PAR reaching the canopy PAR_{plants} . Sunlight was input from radiation calculations in TRNSYS.

$$PAR_{plants} = \frac{A_p}{A_f} PAR (1 - \rho_v)(1 - \exp(-k LAI)) \quad (4)$$

Where PAR and NIR were taken as 50% each of incident solar radiation according to [20], ρ_v is the far-IR reflectivity of the leaf and k is the extinction coefficient (taken as 0.85 for light in visible range). Furthermore, the plants in the Dyson Building can be represented by single layer modules, therefore the shape factors were modified to calculate correct estimates of incident radiation.

The CO₂ input was fed directly into the MATLAB model from the monitored data, and not from the building energy simulation. The change in temperature and humidity from the plant model was then fed back into TRNSYS for the next time step through a delay component Type 661. This component also stored in between each time step the data output in MATLAB only used in the plant model and not necessary for TRNSYS, such as CO₂ and plant cover temperature.

4.4 Model results

Integrating the “plant module” into the building energy simulation for the third floor allowed to model CO₂ change with planted area compared to the data monitored over a year. Fig. 10 shows promising drops in CO₂ levels as planted area increases. Improvements in the model parameterisation and increase in actual planted area would allow verification of these values. Furthermore, the model showed that temperature could decrease by up to 3 °C for a 399 m² planted area, as the time series in Fig. 11 illustrates, which would decrease the need for ventilation in summer but perhaps increase the need for heating in winter, although only for very large plant coverage. Not shown here, but a slight increase in humidity would also be observed.

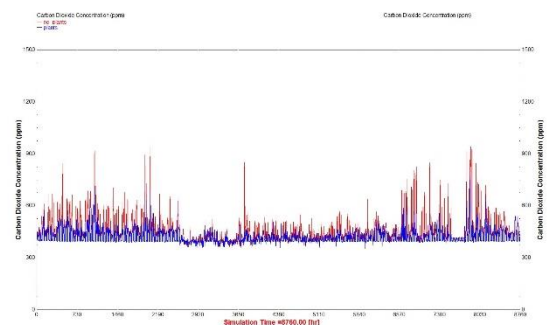


Figure 101: CO₂ levels monitored vs with 200m² of plants [19]

PLEA 2018 HONG KONG

Smart and Healthy within the 2-degree Limit

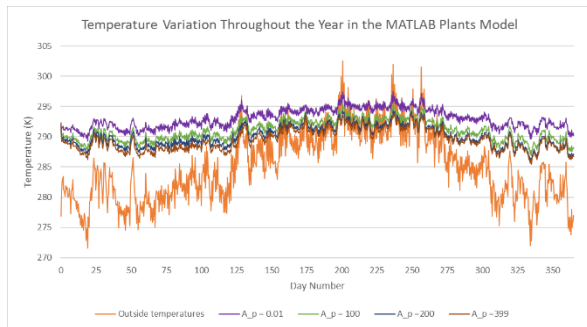


Figure 11: Temperatures in the office over a year for different planted areas

5. CONCLUSIONS AND IMPLICATIONS

This paper has presented an initial study into how hydroponics could be incorporated into office buildings

by considering both occupants and environmental conditions. The aim was to quantify the impact of significant planting schemes on building energy demand and provide tools for further adoption.

Using a combined building energy simulation and plant-air interaction model, the results demonstrate that temperature falls, and humidity increases due to the cooling effect of plants through transpiration. Creating a model alongside the implementation gave the opportunity to test how a validated model of plants in a tunnel could be applied for an office and gain further insights of the impact of hydroponics in a building. This first attempt provides a basis for modelling the effects of adding plants to a conventional office on temperature, humidity and CO₂ concentration, using typical building energy software, show plants have an impact, albeit limited at times. Future work will improve the parametrisation of the model and continue implementing the plants in the office to present a holistic impact of plants in an office. The results will aim to be validated with published data of CO₂ assimilation rate of edible plants. As the plant modules will be installed in different spaces, the next step of this research will be to compare CO₂ levels over different floors and years. Control environmental data of photosynthesis rates of the office crops from a Plant Science lab will also be used. Furthermore, including qualitative surveying and making use of monitoring of the building allowed for a more holistic view of the impacts of plants and how to take the project further.

ACKNOWLEDGEMENTS

We would like to acknowledge the “Energy and Carbon Reduction Project” scheme from the University of Cambridge who are funding this project. Thanks also to the Planit Green team and community & Roger Ling for help accessing the building data. Congratulations and thanks extend to Helen Gillard for being part of the Planit Green Team this year.

REFERENCES

1. United Nations, (2015). World Population Prospects: The 2015 Revision (DESA - Population Revision Key Findings No. ESA/P/WP.241). United Nations, New York.
2. Pérez-Lombard, L., Ortiz, J., Pout, C., (2008). A review on buildings energy consumption information. *Energy and Buildings*, 40, 394–398.
3. Yang, L., Yan, H., Lam, J.C., (2014). Thermal comfort and building energy consumption implications – A review. *Applied Energy*, 115, p. 164–173.
4. Kolokotroni, M., Ren, X., Davies, M. and Mavrogianni, A. (2012). London's urban heat island: Impact on current and future energy consumption in office buildings. *Energy and Buildings*, 47, p.302-311.
5. Klein S., (2017). TRNSYS 18: A Transient System Simulation Program, [Online], Available: <http://sel.me.wisc.edu/trnsys> [20 January 2018].
6. Kozai T., Niu G., Takagaki M. (eds), (2016). Plant Factory - An Indoor Vertical Farming System for Efficient Quality Food Production. *Elsevier Inc*, Oxford, UK .
7. IKEA. (2018). *Indoor Growing Kits & Cultivators – IKEA*, [online], Available: <http://www.ikea.com/gb/en/products/> [31 January 2018].
8. Aponic Ltd Aeroponic. (2018). *Aquaponic Hydroponic Vertical Soilless Growing Systems*. [online], Available: www.aponic.co.uk/ [31 January 2018].
9. Breathing Buildings (2016). Operation & Maintenance Manual, CUDE, Fen Causeway, Cambridge.
10. Boulard T., Roy J.C., Pouillard J.B., Fatnassi H., Grisey A., (2017). Modelling of micrometeorology, canopy transpiration and photosynthesis in a closed greenhouse using computational fluid dynamics. *Biosystems Engineering*, 158, p.110–133.
11. Graamans L., van den Dobbelsteen A., Meinen E., Stanghellini C., (2017). Plant factories; crop transpiration and energy balance. *Agricultural Systems*, 153, p.138–147.
12. Ward, R., Jans-Singh, M. and Choudhary, R., (2017). Chapter 26: Quantifying environmental and energy benefits by use of urban environment to grow food. In: *Next Generation Plant Factory*. Elsevier. Tokyo, Japan. Manuscript submitted for publication.
13. Ward, R., Choudhary, R., Cundy, C., Johnson, G., McRobie, A., (2015). Simulation of Plants in Buildings; Incorporating Plant-Air Interactions in Building Energy Simulation. In *14th Conference of International Building Performance Simulation Association*. Hyderabad.
14. Vanthoor, B. (2011). A model-based greenhouse design method. PhD Thesis. Wageningen University.
15. De Zwart, H. F. (1996). Analysing energy saving options in greenhouse cultivation using a simulation model. PhD Thesis. Wageningen University.
16. Sonnentag, O., Talbot, J., Chen, J. and Roulet, N. (2007). Using direct and indirect measurements of leaf area index to characterize the shrub canopy in an ombrotrophic peatland. *Agricultural and Forest Meteorology*, 144(3-4), p.200-212.
17. Imtech Engineering Services Central Ltd. (2016). O&M Manual for Cambridge University James Dyson Building.
18. Farquhar, G., von Caemmerer, S. and Berry, J. (1980). A biochemical model of photosynthetic CO₂ assimilation in leaves of C3 species. *Planta*, 149(1), p.78-90.

PLEA 2018 HONG KONG

Smart and Healthy within the 2-degree Limit

19. Gillard, H. (2018). Simulating plants in buildings. MEng Thesis. University of Cambridge.
20. Monteith, J. (1966). The Photosynthesis and Transpiration of Crops. *Experimental Agriculture*, 2(1), p.1-14.
21. Ministry of Housing, Communities & Local Government. (2018). Conservation of fuel and power: Approved Document L. Statutory Guidance.

Recycled Materials Impact on Thermal Comfort of Low-Cost Housing in Latin America

Case study: Bogota D.C, Colombia

ANDRES MORENO SIERRA¹, WALTER TORRES²

¹King Abdulaziz University, Jeddah, Saudi Arabia

²Universidad Católica, Bogotá, Colombia

ABSTRACT: Construction of low-cost housing in Colombia is one of the greatest social challenges of the country. Due to Bogotá's climate conditions at 8500 ft. of altitude and non-adapted materials to local conditions, the temperature of these state-subsidized dwellings is usually below optimum comfort standards. This research analyses the impact on temperatures using certain types of materials, comparing the effect of some traditional building skins— composed by brick and concrete - with a new wall envelope made of recycled elements. A comparative study was carried out by housing typologies, based on a work of measurement of the temperatures inside 16 individual dwellings.

Thermal simulations were made to compare the traditional brick envelope material vs a compacted plastic brick, and the results suggest that the construction of dwellings with traditional materials such as brick blocks and prefabricated concrete blocks may not provide the best conditions of thermal comfort. However, alternative materials made of recycled plastic can represent a cheaper, ecological and comfortable solution. Findings could be of interest for construction stakeholders for low-cost housing programs in resilient cities, within the framework of a new plastics economy.

KEYWORDS: Social housing, thermal comfort, envelope, architecture, recycled materials, energy efficiency.

1. INTRODUCTION

In Latin America, a large number of communities have been marginalized by poverty conditions and political conflicts. In the case of Colombia, after the peace treaty between official government and illegal guerrilla groups (FARC), the United Nations High Commission for Refugees has registered more than 5 million people - mostly Afro-Colombian and indigenous populations - that has been affected by the violence and have been displaced from 1997 to 2013 [1]. Most of these populations moved to peripheral areas on the south of Bogotá and started informal settlements, constructing dwellings by themselves.

Despite the government initiatives to promote the construction of new housing programs, economic considerations have prevailed above quality criteria and have not yet integrated technical aspects related to temperature conditions. According to a study carried out between 2006 and 2015, new social housing units in Bogota only meet 47% of 108 quality indicators [2].

Due to the high mountain climate conditions in Bogota, the temperature of these dwellings is usually below optimum comfort standards [3]. This research focuses on building envelopes of informal settlements, through case studies of low-income self construction housing projects.

The study analyses internal houses temperatures by comparing a traditional building skin made of brick/concrete with a wall composed by modular units

of recycled plastic as a low-cost, high-standard sustainable bricks.

A detailed study was carried out based on data collection of physical measurements, structured surveys of a representative number of dwellings and digital simulations. The objective is first to establish if traditional construction materials of these dwellings are adapted to the particular conditions of the tropical humid cold climate, and then compare its behaviour with new materials made of recycled elements.

2. CASE OF STUDY

The city of Bogota D.C requires urgent mitigation actions for the new urban settlements, frequently exposed to poverty conditions and generally non adapted to environmental conditions. The research focused on these particular cases.

2.1 Climate conditions

Informal settlements in the city are usually located above 8530 - 8600 ft. of altitude, registering outdoor average temperatures close to 14°C [Fig. 1].

PLEA 2018 HONG KONG

Smart and Healthy within the 2-degree Limit

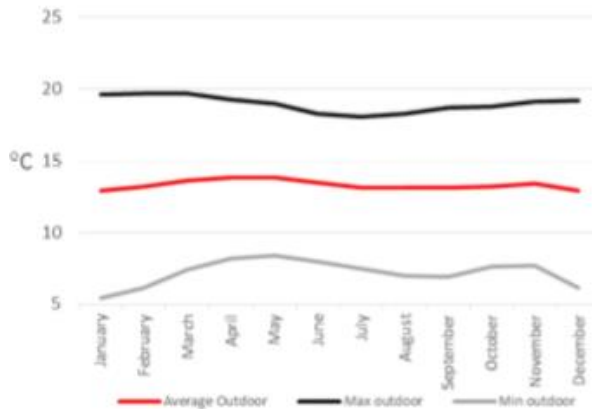


Figure 1: Average temperatures in Bogota, D.C.

Although thermal conditions may be affected by insulation, ventilation and air renewal, several studies show that indoor spaces in this type of dwellings are generally outside a temperature comfort zone, more than 50% of the year [3].

Thermal comfort represents then a crucial aspect for the quality of these settlements. In terms of habitability, low indoor temperatures prompt condensation and dampness and may be associated to health risk and respiratory problems [3].

Based on the in-situ measurements, the driven hypothesis of this study states that traditional construction materials of these dwellings (Brick and concrete) are not adapted to the particular conditions of the tropical humid cold climate.

2.1 Description of dwellings

Informal settlements are usually living in conditions of extreme poverty and there are exposed to environmental risks as natural hazards and high levels of pollution. First temporary individual houses are spontaneously built with brick walls and recycled materials, from simple wood tables to zinc roof slates as a common practice to build a refugee (Fig.2)



Figure 2: case of study / self-constructed dwellings

The study was carried out on the site of San Cristobal at the south of Bogota (latitude: 04-31N, longitude: 74-

05W, elevation 9000 ft.), and focuses on a low-income housing neighbourhood close to the “Juan Rey / Arboleda Santa Teresita” site. For the research, 16 representative case study houses were selected. These permanent constructions were composed by concrete roof / floor slabs and standard brick block walls with small single-glazed (4mm) fenestrations and wood doors. Each 90 sq.m house (for 2 families) was divided in three thermal zones by floor corresponding to rooms, living zones and storage/bathroom areas (Fig.3). Buildings were classified in four groups of six elements, according to its orientation and topography.

3. METHODS AND TOOLS

Source data was collected in two categories. First, physical measurements of the internal temperatures were performed. In each of the houses studied, 2 USB type hygrothermal sensors (datalogger) were installed inside the dwelling (in the social area and without direct solar radiation on the sensor) and 2 sensors were placed outside (under shade conditions) in order to measure climate conditions. The equipment recorded and memorized 16,000 temperature and humidity measurement points over a period of 4 months between august and November 2016.

In a second instance, surveys were carried out with inhabitants. A thermal comfort diary was designed and provided to the head of household or spouse, who were instructed to record their thermal perception of comfort twice a day at 8 am and 6 pm in the living room and master bedroom for periods of 7 consecutive days.

3.1 Predicted Mean Vote

There are different tools and methods to measure thermal comfort conditions, and these are related to different factors [6,9] such as physical and socio cultural aspects [12].

The PMV index was performed using the equation derived from Fanger [8] based on experiments in climatic chambers. The PMV required input variables were derived as follows: The feeling of thermal comfort has been evaluated through a survey with a Predicted Mean Vote to measure the thermal comfort perception with greater probabilities of being experienced by a group of people in a given environment under a stationary condition [11].

Inhabitants were asked to define their thermal comfort feeling based on a range of seven points: Very cold (-3), cold '(-2), cool' (-1), 'comfortable' (0), 'comfortable' Warm '(1), hot' (2) and 'too hot' (3). The index of numerical values was assigned according to the convention of ISO 7730. The users were asked to record in a daily comfort diary their thermal feeling in every zone. The following information was recorded: date of data collection, entry and exit times,

PLEA 2018 HONG KONG

Smart and Healthy within the 2-degree Limit

temperature feeling in the living room and bedroom, dress habits and occupants' activity level.

3.2 Thermal comfort standards

The ASHRAE 55 Standard [4] also incorporates an optional standard known as the "variable" model, specifically designed to predict thermal comfort in naturally ventilated buildings. This model compensates for the limited efficiency of the heat balance model, in predicting the range of more extensive comfort often observed in naturally ventilated buildings. The adaptive models use the outside temperature as the key variable to predict the comfort range.

3.1 Digital simulations

Based on to the characteristics of the dwellings, different models were elaborated according to their general conditions, user profiling and space zoning (Fig.3)



Figure 3: Outdoors temperature and humidity

In order to compare the behaviour and conditions of the real dwellings with a new building envelope, four different three-dimensional thermal models were made of the studied cases (Fig.4).

Thermal conditions were analysed through Design Builder software, a Dynamic thermal simulation software using Energy Plus models (Fig 3). According to ISO 7730, air velocity was defined at 0.1 m/s.

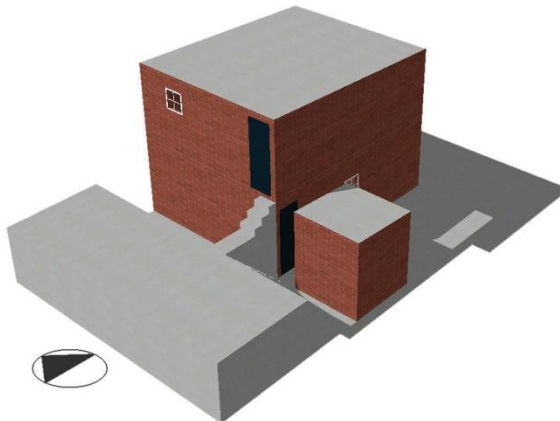


Figure 4: Thermal 3D building models in Design Builder.

Thermal conductance values were used as follows (Tab.4):

Table 1: Thermal conductance values for digital simulations

Table 1. Thermal conductance values for digital simulations	
Zone	Conductance W/(m2K)
Concrete slabs (floor/roof/intermediate)	1.60
Brick block (external walls)	0.65
Prefabricated Concrete block	1.63
Prefabricated Plastic brick	0.16
Partitions (brick block)	0.70
Roof tiles	0.90
Doors (wood panels)	0.15
Glazed Windows (4mm)	5.90

3.2 Data analysis

Data of recorded measures was analysed comparing outdoor/indoor temperatures in different moments of several journeys [10].

3.2.1 Outdoor temperatures

According to the measures, Outdoor temperatures fluctuate significantly (Fig.5). It is observed a Delta of 16°C during the day, with a minimum registered of 6.2°C at 3:00 am, and a maximum of 21°C at 13:00 pm, recording an average of 13.2°C. Relative humidity varies from 50 to 90%.

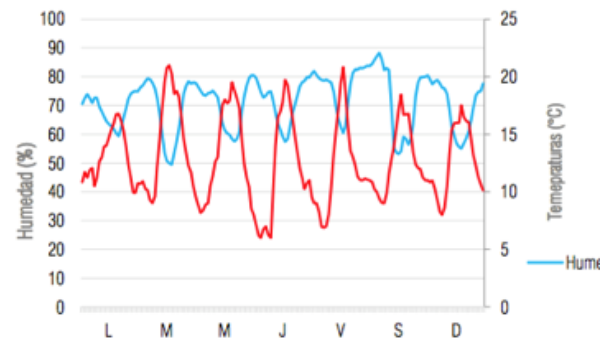
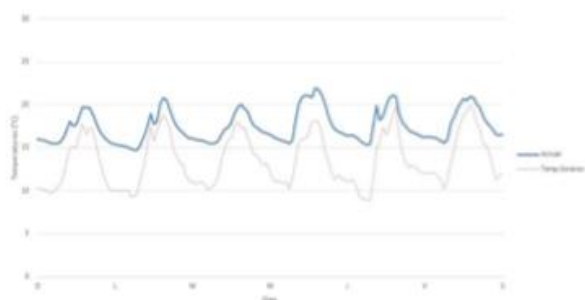


Figure 5: Outdoors temperature and humidity

3.2.1 Indoor temperatures

Indoor temperatures in the existing dwellings correspond to an average of 17.4°C (Fig. 6). Maximum peaks of 22°C and minimum peaks of 15°C have been registered. 16 thermal comfort journals were distributed and compared with the information of more than 16000 points measured simultaneously in



PLEA 2018 HONG KONG

Smart and Healthy within the 2-degree Limit

each dwelling. Most of households provided data and completed 75% of the journals for the 7-day periods.

Figure 6: Indoor Vs. Outdoor temperatures

4. RESULTS

The resulting temperatures - in a range of 15 ° C to 21°C (Fig.6) – were compared to thermal perceptions. Over the recorded data in diaries by users, 60% presented unfavourable conditions of thermal comfort. The feeling of comfort registered by the users has a strong tendency to the feelings of Cold and Too Cold (Table 2).

Table 2: PMV Results. Inhabitants surveys

QUESTION	COMFORT FEELING				
	COLD		COMFORTABLE		WARM
1. Please describe the temperature in the house	28.9%	31.5%	36.4%	3.2%	0%
	too cold	cold	comfortable	comfortable warm	very warm

4.1 Thermal comfort perception of existing dwellings

Traditional materials have a medium thermal inertia behaviour, which influence the ambient temperature conditions inside the dwellings.

Average temperatures of 17.1°C have been associated to a “too cold” comfort feeling by its inhabitants even in conditions of adaptation to their environment.

It is suggested that the quality of the envelope’s insulation and ventilation effects, increase the relative humidity percentage and decrease the temperature, generating comfort problems and risks to human health [13].

The registered temperature perceptions scored by inhabitants according to the PMV scale, show a discomfort feeling inside the studied cases, related to recorded temperatures (Fig.7).

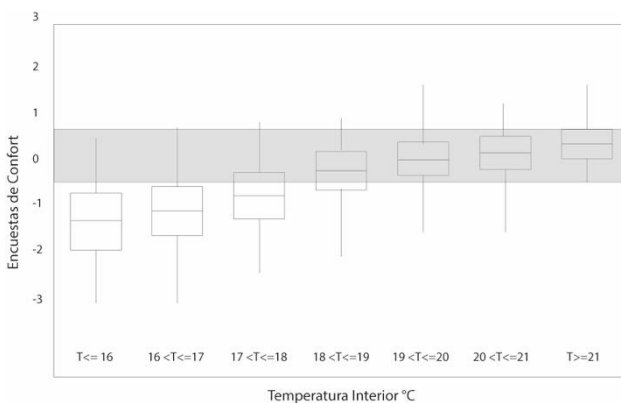


Figure 7. Standard deviation of comfort temperatures registered in existing dwellings.

It is hypothesized to increase the average interior temperature by reducing the rate of energy loss through the envelope. Closed walls with higher internal surface temperatures, may reduce discomfort caused by asymmetry between the radiant

temperature and the air temperature that occurs when hot air touches cold surfaces. By improving the uniformity of temperature distribution inside the houses, the impact of "thermal stress" associated with sudden changes in temperature is reduced.

4.1 Thermal comfort of simulated dwellings

In a second research stage, Dynamic thermal simulation models presented better results.

Indoor temperatures of simulated buildings after the replacement of the building’s envelope by a modular plastic brick, register more favourable comfort conditions. The results obtained on the improved houses, correspond to average temperatures of 19.5 ° C, which represents picks of 2.1°C above the previously recorded values (Fig. 5).

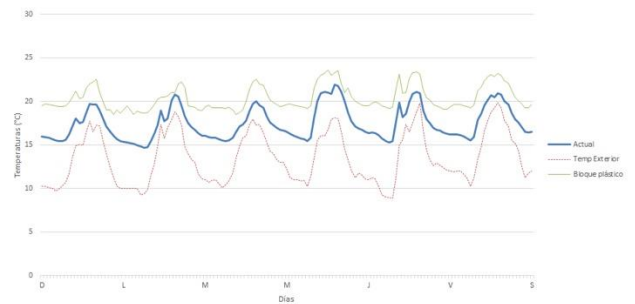


Figure 8. Simulated temperatures with plastic bricks

The use of plastic bricks for the houses’s envelope has increased indoor temperatures and the level of average comfort raised close to neutrality (CV = -0.05 CI, 95%: -0.11 to 0.02). The increase of temperatures represents an evolution in the variation of the feeling of thermal comfort from 36.4% to 62.3 (Table 3). By consequence, thermal comfort is associated to an average increase of the interior temperature of 1.19°C.

Table 3: PMV Results. Inhabitants surveys

SIMULATION	COMFORT FEELING BASED ON TDS - PMV				
	COLD		COMFORTABLE		WARM
2. Thermal feeling of temperatures	16.6%	21.1%	62.3%	0%	0%
	too cold	cold	comfortable	comfortable warm	very warm

Some variations have been registered in the PMV scale from "uncomfortable" - to the "Comfortable" or "comfortable-warm" perception. The increasing insulation properties of plastic bricks, benefits the reduction of heat loss, and directly influence over the internal temperature (Fig.8)

The increase of the thermal inertia and the reduction of the heat transfer through the envelope improves thermal isolation of the building skin, reducing energy losses and optimizing the comfort conditions. The improvements in temperature and thermal comfort

PLEA 2018 HONG KONG

Smart and Healthy within the 2-degree Limit

clearly demonstrate the adaptation process associated with the thermal comfort of the building.

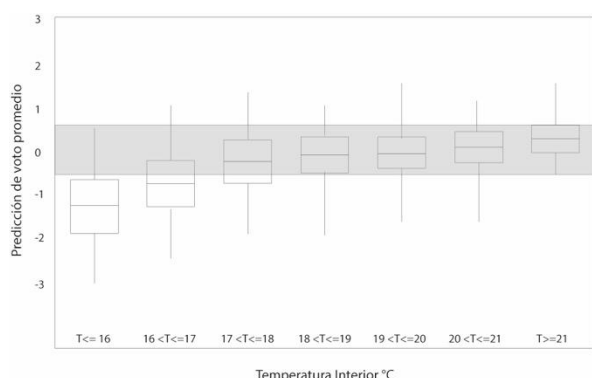


Figure 9. Standard deviation of comfort temperatures registered in existing dwellings.

5. DISCUSSION AND CONCLUSIONS

Self constructed and informal settlements do not include any insulation. Due to the inherent inertia of the standard brick, thermal comfort is directly related to outside temperature, resulting in low indoor temperatures.

It is exposed that there is an improvement on thermal comfort conditions with the use of a compacted plastic brick for the building's envelope, instead of traditional materials. The alternative materials analysed show a better response to the climate and low temperature conditions at Bogota.

It is suggested that actual samples of social housing projects currently developed are not adapted to cold climates. Alternative materials made of recycled elements show a better performance in local conditions of tropical humid cold climate and may improve habitability.

The construction of dwellings with traditional materials such as brick blocks and prefabricated concrete blocks may not provide the best conditions of thermal comfort and may be even uncomfortable. Alternative materials made of recycled elements show a better performance in local conditions of tropical humid cold climate and may improve habitability conditions for the development of new housing programs.

The results suggest that recycled plastic can represent a cheaper, ecological and comfortable solution. Findings could be of interest to construction stakeholders for the low-cost housing construction in resilient cities, within the framework of a new plastics economy.

ACKNOWLEDGEMENTS

This project is the first part part of a research of thermal comfort in Tropical humid climates developed in King Abdulaziz University, Jeddah, Saudi Arabia.

REFERENCES

- UNHCR, 2013, 2015
- Escallón, C., & Rodriguez, D. (2010). Who asks the questions about housing quality? Who answers them? *UNIANDÉS dearq*, 6, 6-19.
- Agudelo, C.A. (2014). Effect of wall and window materials in thermal and lighting comfort for social housing in Bogotá. *Los Andes U.*
- Humphreys MA. (1978). The dependence of comfortable temperatures upon indoor and outdoor climates.
- ANSI/ASHRAE Standard 55. (2004). Thermal environmental conditions for human occupancy. American National Standards Institute (ANSI) and American Society of Heating, Refrigerating and Air-Conditioning Engineers (ASHRAE).
- Brager GS (1998), de Dear RJ, Thermal adaptation in the built environment: a literature review, *Energy and Buildings* 1998; 27:83-96.
- Dear RJ, Brager (2002) GS, Thermal comfort in naturally ventilated buildings: revisions to ASHRAE Standard 55. *Energy and Buildings* 2002; 34:549-61.
- Fanger PO (1970). Thermal comfort. Malabar, FL: Robert E. Krieger;
- HSE, (2016). Thermal comfort, the six basic factors, Health and Safety Executive website. Retrieved from: <http://www.hse.gov.uk/temperature/thermal/factors.htm>
- Humphreys MA. (1978). The dependence of comfortable temperatures upon indoor and outdoor climates. In: Cena, Clarke, editores. *Bionegineering, thermal physiology and comfort*. London: Elsevier; 1978.
- Hunt D, Gidman M. (1982) A national field survey of house temperatures. *Building and Environment*; 17(2): 107-24.
- Mishra, A. K. & Ramgopal, M. (2013). Field studies on human thermal comfort: An overview. *Building and Environment*, 64, 94-106.doi: 10.1016/j.buildenv.2013.02.015.
- Nicol. F. (1993) *Thermal comfort: a handbook for field studies toward an adaptive model*. UK: University of East London; 1993.
- Shin, J. (2016). Toward a theory of environmental satisfaction and human comfort: A process-oriented and contextually sensitive theoretical framework. *Journal of Environmental Psychology*, 45, 11–21.
- Schnieders J, Betschart W (2002). Room air current in the passive house: measurement and simulation. *HLH 03* 2002:61.
- UNIANDÉS. (2015). Observatorio de calidad de vivienda nueva. Retrieved from: <http://observatoriodevivienda.uniandes.edu.co/>

Innovative RES Solutions for Isolated Territories: Hydrogen as a Storage Medium Integrated with Renewable Energy Sources

BARBARA WIDERA¹

¹Faculty of Architecture, Wrocław University of Science and Technology, Wrocław, Poland

ABSTRACT: The first aim of this paper is to analyse the potential for application of hydrogen production and storage systems integrated with renewable energy sources, aimed to provide safe, efficient and stable energy solutions for building and transportation on isolated territories. The value of this concept will be checked on the examples of pilot and demonstration facilities developed for distant European islands. Several archipelagos belonging to different European countries were selected as case studies. The purpose of such choice is to investigate various climatic, geographic and legislative conditions determining the new opportunities that may bring benefits to cleaner and more sustainable environment. The second goal of this study is to check if/how European Union Framework Programmes contributed to the development of increased energy efficiency, independence and renewability in the isolated European territories.

KEYWORDS: Energy, hydrogen, storage, RES, fuel cells, climate

1. INTRODUCTION

In the light of the Paris Agreement it is extremely important to provide the proper balance of resources and to control carefully the adequacy of various activities towards tackling climate change. Development of increased energy efficiency, independence and renewability in the European islands and isolated territories became particularly significant and actual issue. A lot of islands, located within a longer distance from the mainland, suffer from dependence on fossil fuels imported from the continent. This generates increased fuel costs and higher environmental pollution. While a lot of EU energy actions were focused on the continent, only few addressed isolated territories. On the other hand, these small and distant islands may strongly affect global climate, especially in case of lack of proper energy policy, which may lead to uncontrolled events.

2. HYDROGEN STORAGE SYSTEMS INTEGRATED WITH RENEWABLE ENERGY SOURCES

Distantly located European islands often struggle with high costs of energy. In case of non-renewable energy this is related both to the transportation and production expenses. Renewable energy should be perceived as the appropriate long term solution, justified by environmental and economic reasons. However, in purpose to take advantage of renewable energy sources typically available on the islands, such as solar, wind and hydro energy, it is necessary to deal with their intermittency. Adequate storage systems must be developed and properly integrated with the local energy network. Moreover, this approach can contribute to cleaner environment, circular economy and tackling climate change through lower emissions.

2.1 Limits and opportunities of hydrogen storage

While heat energy is relatively easy to store, the storage of electricity is more difficult. Nowadays the most efficient systems are the ones based on reversible hydro and hydrogen storage [1]. However, sustainable reversible hydro systems, where water is pumped into the upper reservoir, may be applied solely in places with a natural altitude difference. Such concept has been tested in 2016 on El Hierro (Canary Islands, Spain) [2] and was proposed also for Corvo island (Azores, Portugal) [1]. Other interesting proposals address the combination of renewable hydrogen production and storage with the second generation biofuels [3].

Some of the most actual and efficient renewable energy systems dedicated for islands, combine wind energy with hydrogen storage. The excess of energy from wind turbines is converted to hydrogen by electrolysis process. Hydrogen is stored and used as fuel e.g. for public transportation when the electricity demand is low. In the hours of high energy demand, electricity is produced from hydrogen with the fuel cell or internal combustion engine. Batteries can be used for electricity storage in small power systems.

A hydrogen - electric power station can also deliver electricity to the local research/education facilities, harbour industries or nearest dwellings. Warm water from cogeneration system may be used either in these industries or at tourist facilities (e.g. for salt water ocean swimming pools) for pleasure and the visitors' awareness [3].

Among the identified challenges of hydrogen production and storage systems there are technological limitations related to low efficiency, poor performance and short lifetime of electrolyzers

PLEA 2018 HONG KONG

Smart and Healthy within the 2-degree Limit

and fuel cells [4]. Appropriate wind conditions, understanding and supportive local community, a back-up system in place, a high degree of failsafe and the access to service personnel are also very important.

3. ANALYSIS OF PILOT CASE STUDIES, METHODOLOGY

Following pilot and demonstration projects were selected for analysis: Utsira, El Hierro, Corvo, Terceira, Shapinsay and Eday. The scenarios checked:

Technology readiness and technical feasibility

System efficiency

Costs and other economic aspects

Reduction of CO₂ emissions

Other environmental impacts

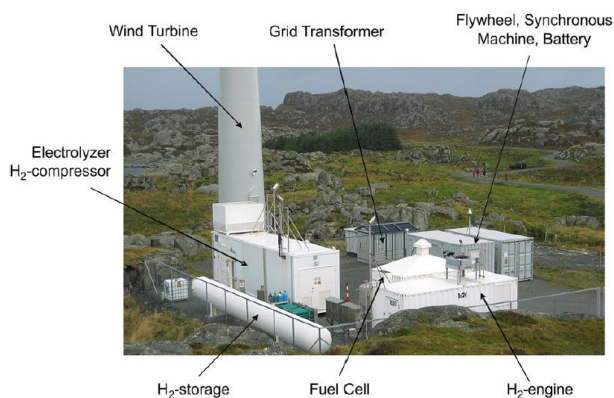


Figure 1: Utsira Wind Power & Hydrogen Plant (2004-2008) by Statoil ASA & Enercon GmbH. Demonstration plant [4].

3.1 Utsira (Norway)

Utsira is a small Norwegian island with wind and weather conditions difficult for transportation but perfect for wind energy production. This is why the location was selected for the world's first full-scale combined wind power and hydrogen plant (Fig. 1). Utsira Wind Power and Hydrogen Plant project was launched in 2004 by Statoil ASA & Enercon GmbH and was aimed to demonstrate how renewable energy can provide a safe, continuous, and efficient energy supply to distant areas [5]. The distinguishing feature of the project was that the facility was remotely operated from the mainland control center. In the period 2004-2008 ten houses were supplied exclusively by the energy generated from two Enercon E40 wind turbines installed at Utsira, 600 kWh each. Hydrogen was produced in the Hydrogen Technologies electrolyser (10 Nm³/h) on windy days when the power production would exceed the households' demands. Hydrogen was compressed with the Hofer compressor (5 kW) and stored in a 200 bar tank with capacity of 2400 Nm³ to provide continuous power supply to the houses on windless days or when the wind was too strong. In such cases the 55 kW MAN hydrogen internal combustion engine and a 10 kW IRD fuel cell would use the stored hydrogen to produce electricity.

The project was successful, with the good power quality and high level of customers' satisfaction. However, some technical problems also appeared, especially related to the low durability of the fuel cell (less than 100 hours) as well as leaking of the coolant fluid, damage to the voltage monitoring system during assembly, and frequent false grid failure alarms [5]. Also the wind energy utilization was only 20% and the project leaders concluded that there is a need to develop high-performance electrolyser (more efficient, with small footprint) and to improve the hydrogen-electricity conversion efficiency [4]. Another conclusion was that future projects should include more than one renewable energy source [5].

3.2 El Hierro (Canary Islands, Spain)

Small Spanish island El Hierro belongs to the Canary Islands being an active volcanic island with a population of about 10.000 habitants. Energy system on El Hierro was totally dependent from fossil fuels transported by the sea to power electricity generators (6600 tons of diesel fuel per year) [6]. The location was selected due to the very good wind conditions (wind capacity factor of 49%) and topography allowing for the combination of wind farm (11,5 MW) and hydro power plant with upper (500.000 m³) and lower (150.000 m³) reservoir (Fig. 2 a-b). Five wind turbines (Enercon E70) were installed, 2,3 MW each. When production exceeded demand, wind energy was used to pump water up into a natural volcanic crater. When there was not enough wind, the water was released down through a pipe connecting the two reservoirs through turbines, which generated hydro-power. Renewable energy penetration was aimed at 80% [7]. The project of El Hierro Wind & Pumped Hydro System was inaugurated in 2014 with EU financial support and the test operation was launched in 2015 with aim to increase gradually the renewable energy penetration rate without endangering grid stability and security of supply [2]. At the beginning of 2016 the diesel power plant was switched off for the first time for 16 hours [8] (Fig. 3 a-b). The final results from the demonstration plant revealed that the wind and hydro power penetration in the electric grid reached 34.6% (less than half of the initial assumptions), while the hydro power contribution over the testing year period was only 3.9% of total energy [2].

PLEA 2018 HONG KONG

Smart and Healthy within the 2-degree Limit



Figure 2: El Hierro Wind & Pumped Hydro System (2014-2016): a) The upper reservoir, in an inactive volcanic crater [8]
b) The lower reservoir of the hydro plant [8]

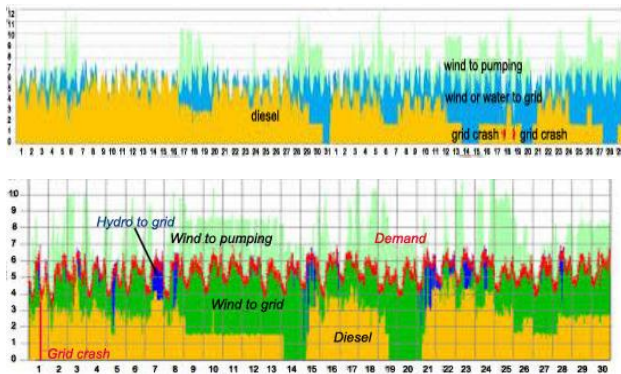


Figure 3: El Hierro Wind & Pumped Hydro System (2014-2016): a) Energy generation in MW – January and February 2016. Yellow – diesel, blue – wind or water to pumping, green – excessive wind to pumping, red – demand and grid crash [2] b) Wind Park Production as 10 min averages in MW – June 2016 [2]

Observations of Fig. 3a revealed that during the period when the diesel power plant was switched off, on 31st January and 20th February, when the wind dropped below the current grid load, the tests were stopped. The initial estimations were that the water storage should cover the energy demands for at last 4 days with worse wind conditions [2]. The energy generation graph from Jan./Febr. 2016 shows that this system did

not work properly (or was not used in line with the previous assumptions).

Another surprising remark from Fig. 3 a-b is that during the diesel-off tests the excess wind power was still used for water pumping, while the test should start with a full upper reservoir (to have the stored hydro power as a backup if the wind drops). This leads to the conclusion that the problems with grid stability were the reason for the short periods of RES operation with diesel plant off [2]. This issue was related to the insufficient energy storage capacity and therefore the hydrogen storage is actually considered.

3.3 Corvo (Azores, Portugal)

On Corvo Island energy is produced mainly from fossil fuels, namely oil transported by waterway. The security of supply is very low due to the long distance from the land and bad weather conditions frequently occurring. The island has high potential to use wind and hydro energy, while reversible hydro and hydrogen may be used for storage. The analysis of Corvo case study shown that the cost of energy can be significantly reduced by utilizing a combination of hydrogen storage and RES. This will also allow for RES high level penetration [1,9]. The lessons learnt from El Hierro project also confirmed the validity of this concept. Assessment of technical feasibility of various options for integrated energy and resource planning was carried out under RenewIslands project (2002-2004) financed by EU Framework Programme 5.

3.4 Terceira (Azores, Portugal)

In terms of the number of inhabitants Terceira is the second island of Azores archipelago. The Azorean energy system depends almost entirely on fossil fuels imported from Portugal mainland. In 2004 only 3% of the global energy consumed in the region would come from local renewable production [3]. In 2008 the comprehensive scenario and detailed calculations for Renewable Electricity and Hydrogen Facilities Scheduled for Terceira were presented by Alves [3]. Serra do Cume Campus and Praia da Vitória were selected for the hydrogen and oxygen production from wind and ocean wave energy. Hydrogenopolis in Praia da Vitória included demo/research subunits such as:

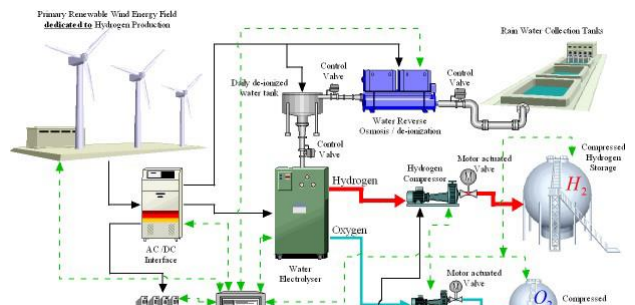


Figure 4: Global Flow Diagram for hydrogen production from wind energy. Components Design for the Terceira Hydrogenopolis [3]

PLEA 2018 HONG KONG

Smart and Healthy within the 2-degree Limit

hydrogen-electric power station, hydrogen vehicle filling station, research laboratory, a demo park and hydrogen and oxygen stationary storage (Fig. 4). The expected average hydrogen production through electrolysis in both locations was assumed as 2200 Nm³ H₂/h (with the oxygen production of 1100 Nm³ H₂/h). A half of the hydrogen/oxygen should be used for the electricity generation with a hydrogen-oxygen boiler and a steam CoGen turbine with Rankine Reheat-Regenerative Cycle. Additionally, Hydrogen Internal Combustion Engines and Hydrogen Fuel cells should be installed to generate electricity (expected efficiency of 35%) and produce CoGen warm water (expected efficiency of 45%). Biogas generation unit with methane purification was also proposed in purpose to evaluate opportunities and optimise strategies for a joint use of Hydrogen and Natural Gas (a blend mixing usually known as hythane) [3].

Although the concept of Renewable Electricity and Hydrogen Facilities Scheduled for Terceira was very well developed, it was not introduced so far. In 2014 about 17% of electricity was generated on a 12.6 MW wind farm, 0,2% of electricity would come from three hydroelectric power stations and 82.7% electricity was still generated on an oil-based thermal power station [10, 11]. In 2017 new scenarios for Terceira Pump Hydro System were proposed, in the combination with bio-waste and geothermal energy storage. Another option taken into account was the usage of NaS and Li-ion batteries [10]. In this case the authors did not consider any hydrogen storage.

3.5 Shapinsay and Eday (Orkney Archipelago, Great Britain)

The issue of integrated RES for islands was addressed again by the project BIG HIT Building Innovative Green Hydrogen Systems in an Isolated Territory: a Pilot for Europe. The project is currently financed from Horizon 2020 and was selected by the FCH 2 JU (The Fuel Cells and Hydrogen 2 Joint Undertaking) as the only hydrogen project of its kind to receive funding. The BIG HIT was launched in May 2018. This world leading pilot and demonstration project aims to put in place a fully integrated model of hydrogen production, storage, transportation and utilisation for low carbon heat, power and transport. The concept combines energy from community-owned wind turbines, located on two islands of the Orkney archipelago: Shapinsay and Eday, with hydrogen production and storage. The otherwise curtailed capacity is used to produce low carbon hydrogen and oxygen with a 1MW Polymer-Electrolyte-Membrane (PEM) electrolyser. BIG HIT will enable the deployment of 10 electric vans, fitted with a hydrogen fuel cell range extender, and the construction of a hydrogen refuelling station. In order to demonstrate the potential scope hydrogen also has for heating purposes in Orkney, BIG HIT will install two

hydrogen-powered boilers at suitable premises to provide zero carbon heat for the local school building [12].



Figure 5: BIG HIT Building Innovative Green Hydrogen Systems in an Isolated Territory: a Pilot for Europe (2016-2020). The schedule shows the combination of wind energy with hydrogen production and storage [12]

Ongoing BIG HIT project already produced social, environmental and economic impact:

- Increased innovation and research: development of solutions integrating intermittent renewable energy supply (RES), fuel cell (FC) and hydrogen infrastructure to promote RES and innovative decentralized power systems penetration in islands.
- Energy independence: contribution to the market penetration of new energy systems combining fuel cells (FC), renewable energy sources (RES) and hydrogen (H₂) in islands and remote regions in EU.
- Innovation and technological development: innovative technologies related to hydrogen production and storage on islands, such as the first Polymer-Electrolyte-Membrane (PEM) Electrolyser and Hydrogen Storage which was installed on Eday in November 2016.
- Fostering the efficient use of resources (renewable & non-renewable): overcoming the limitation of the renewable energy sources since hydrogen is utilized as a storage medium integrated with intermittent RES such as wind, wave and solar. Hydrogen storage in islands is associated with more effective use of installed renewable technology capacity, as it makes use of otherwise wasted renewable energy at times when electricity demand is low.
- Governance and good administration: impact on policy documents (preparation for system change), i.e. project contributed to establishment of HFC Roadmap (Sept 2016) which sets out key opportunity areas for next 10-15 years in UK, namely: Road Transport Roadmap, H₂ Supply for Transport, Portable FC Applications, HFC Services to Energy Network, Large Scale Stationary, Small Scale Stationary, Non-Road Transport, Bulk Hydrogen Production and links with

PLEA 2018 HONG KONG

Smart and Healthy within the 2-degree Limit

CCU & CC, Liquid Fuels and Industry, Hydrogen Pipelines [12].

4. DISCUSSION: THE ROLE OF EU FRAMEWORK PROGRAMMES IN DEVELOPMENT OF INTEGRATED RENEWABLE ENERGY SOLUTIONS FOR ISOLATED TERRITORIES

EU Framework Programmes from FP4 to H2020 consequently support transition from traditional fossil fuels to RES. Newly created funding possibilities were used in purpose to help overcoming the barriers of energy production and storage, with a special focus on the use of hydrogen as a storage medium integrated with renewable energy sources such as wind, solar, tidal etc. To enhance coherent policy in the field of clean energy in the whole Europe, growing attention is given to isolated territories such as islands. Under FP5 and H2020 some particular initiatives dedicated to energy issues of isolated territories, including islands, were undertaken. Various activities covered the research, technological development and demonstration programmes oriented towards tackling technological and non-technological barriers (e.g. policy regulations) for Hydrogen/FC/RES integrated solutions. Four of five projects described above received support from EU funds. These pilots demonstrated the feasibility of combining renewable energy and hydrogen in remote locations and opened new opportunities for the application of electrolysers and hydrogen fuel cells in future energy systems [9]. Consequently, undertaken actions should contribute to the development of integrated RES solutions for isolated territories. Presented projects produced significant economic, environmental, social and scholar impacts. Expected impact is related to further development of hydrogen and fuel cells technologies and their practical application such as building hydrogen systems, ramping up deployment of hydrogen vehicles and fuel cells, gas grid conversion as well as increased use of hydrogen in buildings, transportation and industry. This should produce consequent economic and environmental impacts such as reducing GHG emissions and other environmental pollution, fostering the efficient use of resources, technological development and energy independence of islands and other isolated territories. It is worth to note that although the case studies shortly presented in this paper were tailor made for specific energy issues of particular islands, the developed solutions can be multiplied also in different locations.

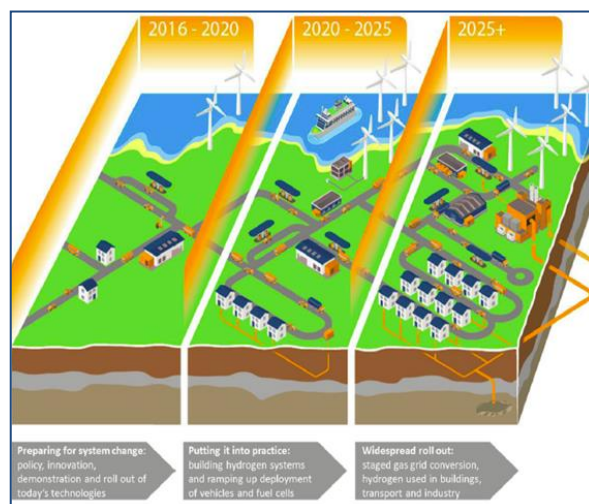


Figure 6: BIG HIT Building Innovative Green Hydrogen Systems in an Isolated Territory: a Pilot for Europe.

2016-2020 Preparing for the system change: policy, innovation, demonstration and roll-out of FC/Hydrogen/RES integrated technologies.

2020-2025 Practical application: building hydrogen systems, ramping up deployment of hydrogen vehicles and fuel cells.

From 2025 Widespread roll out: stage gas grid conversion, hydrogen used in buildings, transport and industry [12].

4. CONCLUSIONS

This paper provided the short overview of the research which proved that the combination of hydrogen storage with RES may significantly contribute to more stable, efficient and sustainable energy systems for isolated territories. Hydrogen storage can be successfully integrated with building and transportation network. Such solutions can maximize the value of RES, decrease fuel dependency, reduce emissions and allow for duplication [9]. Described case studies were the examples of pilot and demonstration facilities developed for different European islands, belonging to Norway, Spain, Portugal and Great Britain. Analyzed scenarios as well as pilots and demonstrations confirmed the technology readiness and technical feasibility for renewable energy generation and storage systems (including hydrogen production and storage) dedicated for remote islands and isolated territories. While all the presented pilot projects were successful, some detailed conclusions address technical problems and indicate suggestions for the future actions. Most of the reported issues were related to the low system efficiency which increased the operating costs and finally resulted with rather poor cost-effectiveness. Three projects: Utsira Wind Power and Hydrogen Plant, Renewable Electricity and Hydrogen Facilities Scheduled for Terceira and BIG HIT Building Innovative Green Hydrogen systems in an Isolated Territory: a Pilot for Europe, which combined wind energy with hydrogen production and storage, brought up the most promising results (although this conclusion is not final

PLEA 2018 HONG KONG

Smart and Healthy within the 2-degree Limit

for on-going BIG HIT while Terceira scenario was not tested in practice). Both launched projects (Utsira and BIG HIT) received a lot of support from local community and authorities, and with good information campaigns managed to overcome some general concerns about the safety of hydrogen storage. Technical problems observed in Utsira involved low durability of the fuel cell, coolant fluid leaking, voltage monitoring system damage during assembly and frequent false grid failure alarms. At the end, the wind energy penetration in Utsira electric grid reached only 20%. More efficient high-performance electrolyser should contribute to the increased utilization of wind energy and improved productivity of hydrogen-electricity conversion.

The other two projects, dedicated for El Hierro and Corvo, were focused on the combination of wind energy and pumped hydro system. Demonstration facility of El Hierro Wind & Pumped Hydro System revealed issues with grid stability that significantly shortened RES operation periods with diesel plant off. The wind and hydro energy penetration in grid reached 34,6% (with hydro power contribution of 3,9%). To overcome problems related to the insufficient energy storage capacity the hydrogen storage is considered in the future. This remark is in line with the general conclusion from all the projects that the most effective systems should include more than one renewable energy source.

The analysis confirmed the importance of EU Framework Programmes for the development of presented solutions. Methodology proposed in this research was applied to analyse particular islands cases as specific examples of isolated territories. However, the same methodology may be applied also to other places, where the integration of renewable energy sources with hydrogen used for energy storage should bring about positive effects.

ACKNOWLEDGEMENTS

A part of this study was carried out within the activities related to the work of EC "Expert group on evaluation methodologies for the interim and ex-post evaluations of Horizon 2020". The author wishes to thank European Commission for this opportunity and declares that solely publicly available open access materials were used for this paper.

REFERENCES

1. Duic' N. et al. (2008). RenewIslands methodology for sustainable energy and resource planning for islands. In: Renewable and Sustainable Energy Reviews 12 (2008) p. 1032–1062. DOI:10.1016/j.rser.2006.10.015
2. Jargstorf B. (2017). An Independent Evaluation of the El Hierro Wind & Pumped Hydro System. <http://euanmearns.com/an-independent-evaluation-of-the-el-hierro-wind-pumped-hydro-system/> [6.04.2018].

3. Alves M. (2008). Hydrogen Energy: Terceira Island Demonstration Facility. In: Chemical Industry & Chemical Engineering Quarterly 14 (2) 2008, p. 77–95. DOI:10.2298/CICEQ0802077A
4. Harg K. (2005). Utsira – demonstrating the hydrogen society on renewable terms [6.04.2018] <http://www.hydrogenambassadors.com/hm05/conference/utsira.pdf>
5. IPHE (2011). Utsira Wind Power and Hydrogen Plant. <http://www.statoil.com/en/NewsAndMedia/Multimedia/features/Pages/HydrogenSociety.aspx> [11.11.2017].
6. Frayer L. (2014). Tiny Spanish Island Nears Its Goal: 100 Percent Renewable Energy. <https://www.npr.org/sections/parallels/2014/09/17/349223674/tiny-spanish-island-nears-its-goal-100-percent-renewable-energy> [7.04.2018].
7. Suárez, S., (2009). Overcoming RES - Storage barriers on the Spanish Islands: the Case of the Canary Islands. <http://marjan.fesb.hr/~fbarbir/PDFs%20Obnovljivi%20izvorij/pdf> [11.11.2017].
8. Andrews R. (2016). El Hierro – 16 hours of 100% renewables generation. <http://euanmearns.com/el-hierro-16-hours-of-100-renewables-generation/> [8.04.2018]
9. Center for Renewable Energy Sources and Saving (2010). Maximization of the Penetration of Res in Islands. https://ec.europa.eu/energy/intelligent/projects/sites/iee-projects/files/projects/documents/stories_maximization_of_the_penetration_of_res_in_islands.pdf [11.11.2017].
10. Rodrigues A., Machado D., Dentinho T. (2017). Electrical Energy Storage Systems Feasibility; the Case of Terceira Island. In: Sustainability 2017, 9, 1276. www.mdpi.com/2071-1050/9/7/1276/pdf [9.04.2018]. DOI:10.3390/su9071276
11. Eletricidade dos Açores (2014). Procura e Oferta de Energia Eléctrica, EDA: Ponta Delgada, Portugal http://www.eda.pt/Mediateca/Publicacoes/Producao/ProducaoConsumo/POEE%20dezembro_2014.pdf [30.07.2015].
12. Olsen K. (2016). Hydrogen and Fuel Cell Activities in Scotland & the Orkney Islands, Highlights & Next Steps, CFA-ITM Power, Scottish Fuel Cell and Hydrogen Association [26.10.2016] http://www.scandinavianhydrogen.org/wp-content/uploads/2016/11/1_Kristoffer-Olsen.pdf